U.S. DEPARTMENT OF ENERGY | Energy Efficiency & Renewable Energy

2010 annual progress report

Energy Storage R&D

U.S. Department of Energy
1000 Independence Avenue, S.W.
Washington, D.C. 20585-0121

FISCAL YEAR 2010
ANNUAL PROGRESS REPORT FOR
ENERGY STORAGE R&D

January 2011

Approved by

David Howell, Hybrid Electric Systems Team Lead

Vehicle Technologies Program, Energy Efficiency and Renewable Energy

Table of Contents

I. INTRODUCTION 1

I.A Vehicle Technologies Program Overview 1

I.B Energy Storage Research & Development Overview 1

I.B.1 Programmatic Structure 1

I.B.2 Some Recent Highlights 3

I.B.3 Organization of this Report 4

II. AMERICAN RECOVERY & REINVESTMENT ACT (ARRA) OF 2009 9

II.A Integrated Battery Materials Production, Cell Manufacturing, and Battery Assembly Facilities 10

II.A.1 Domestic advanced battery industry creation project (Johnson Controls, Inc.) 10

II.A.2 Vertically Integrated Mass Production of Automotive Class Lithium-ion Batteries (A123Systems) 13

II.A.3 Accelerating the Electrification of U.S. Drive Trains: Ready and Affordable Technology Solutions for Domestically Manufactured Advanced Batteries (Exide Technologies) 15

II.A.4 PHEV Battery Development (East Penn Manufacturing Co., Inc.) 18

II.B Battery Cell and Pack Assembly Facilities 19

II.B.1 Cell and Battery Manufacturing Facility in Michigan to Support the EV and HEV Markets (Kokam/Dow, Midland Battery Park) 19

II.B.2 Development of High-Performance PHEV Battery Pack (LG Chem Michigan Inc. – formerly known as Compact Power, Inc.) 21

II.B.3 Lithium-ion Cell Production and Battery Pack Assembly (EnerDel) 24

II.B.4 Li-Ion Battery Pack Manufacturing (GM) 26

II.B.5 Lithium-ion Cell Production and Battery Pack Assembly (Saft America, Inc.) 29

II.C Battery Materials Production Facilities 31

II.C.1 Manufacturing Facilities Initiative for Lithium-Ion Battery Separators (Celgard) 31

II.C.2 Advanced Cathode Materials Production Facility (Toda America Inc.) 34

II.C.3 Domestic Production of Lithium Carbonate and Lithium Hydroxide (Chemetall Foote) 37

II.C.4 High-Volume Manufacturing of $LiPF_6$ – A Critical Lithium-ion Battery Material (Honeywell) 40

II.C.5 Construction of a Li-ion Battery Cathode Production Plant (BASF) 42

II.C.6 Nanoengineered Ultracapacitor Material (EnerG2, Inc.) 43

II.C.7 Expansion of Novolyte Capacity for Lithium-Ion Electrolyte Production (Novolyte) 45

II.C.8 Establish and Expand Commercial Production of Graphite Anode Batteries for High Performance Production of Li-ion Batteries (FutureFuel) 47

II.C.9 Battery Materials Production Facilities (Pyrotek Incorporated) 49

II.C.10 Manufacture of Advanced Battery Components (HTTM LLC, H&T, Trans-Matic) 51

II.D Battery Recycling Facilities 53

II.D.1 Next-Generation Lithium-Ion Battery Recycling Facility (Toxco) 53

II.E Battery Research Facilities 56

II.E.1 Prototype Cell Fabrication Facility (ANL) 56

II.E.2 Material Scale Up Facility (ANL) 58
II.E.3 Post-test Laboratory Facility (ANL) 60
II.E.4 High-Energy Battery Testing Facility (INL) 62
II.E.5 Batery Thermal Test Laboratory (NREL) 63
II.E.6 Battey Abuse Test Facility (SNL) 65
III. ADVANCED BATTERY DEVELOPMENT, SYSTEMS ANALYSIS, AND TESTING 69
III.A Advanced Battery Development 70
III.A.1 High Energy/PHEV Systems 72
III.A.1.1 Advanced High-Performance Batteries for Plug-In Hybrid Electric Vehicle Applications (JCI-Saft) 72
III.A.1.2 Development of High-Performance PHEV Battery Pack (LG Chem, Michigan) 75
III.A.1.3 Nano-phosphate for PHEV Applications: A Multi-Generational Approach (A123Systems) 78
III.A.2 High Power/HEV Systems 81
III.A.2.1 A Novel Nano-phosphate-based Li-ion Battery for 25 kW Power-assist Applications (A123Systems) 81
III.A.2.2 Battery Abuse Testing and Ultracapacitor Development (NSWC) 84
III.B Advanced Materials and Processing 87
III.B.1 HTMI Separator Development (Celgard, LLC) 87
III.B.2 Highly Filled and/or Crosslinked Li-Ion Battery Separators for HEV/PHEV Applications (Entek) 89
III.B.3 Advanced Cathode Materials with High Energy, Power, and High Thermal Stability for PHEV Applications (3M) 93
III.B.4 Advanced Negative Electrode Materials for PHEV Li-Ion Batteries (3M) 100
III.B.5 Stabilized Li Metal Powder (FMC) 103
III.B.6 Develop and Improve Lithium Sulfur Cells for EV Applications (Sion Power) 107
III.B.7 High Volume, Low-cost Manufacturing Techniques for Cathode Materials (BASF) 110
III.B.8 Hybrid Nano Carbon Fiber/Graphene Platelet-Based High-Capacity Anodes for Lithium-ion (Angstron) 112
III.B.9 New High-Energy Nanofiber Anode Materials (NCSU) 118
III.B.10 Chemical Shuttle Additives in Lithium-ion Batteries (EnerDel) 123
III.B.11 Internal Short Circuits in Lithium-Ion Cells for PHEVs (TIAX, LLC) 129
III.B.12 High Throughput Fabrication of 10 Year PHEV Battery Electrodes (A123Systems) 131
III.B.13 Small Business Innovative Research Projects (SBIR) 133
III.C Systems Analysis 135
III.C.1 PHEV Battery Cost Assessments (Tiax) 135
III.C.2 Battery Pack Requirements and Targets Validation (ANL) 138
III.C.3 Battery Life Trade-Off Studies (NREL) 144
III.C.4 Battery Lease Analysis - Battery Ownership Model (NREL) 149
III.C.5 PHEV Battery Secondary Use Study (NREL) 154
III.C.6 Battery Recycling (ANL) 158
III.C.7 Low Energy HEV Requirements Analysis (NREL) 162

III.D Battery Testing Activities....166
III.D.1 Battery Performance and Life Testing at ANL....166
III.D.2 Smart Battery Status Monitor (INL)....169
III.D.3 Battery Performance and Life Testing (INL)....173
III.D.4 Battery Abuse Testing at SNL....176
III.E Computer Aided Engineering of Batteries (CAEBAT)....180
III.E.1 Computer Aided Engineering of Batteries - CAEBAT (NREL)....180
III.E.2 Computer Aided Engineering of Batteries Effort (ORNL)....186
III.E.3 Battery Thermal Analysis and Characterization Activities (NREL)....190
III.E.4 Lithium-Ion Abuse Model Development (NREL)....195
III.F Energy Storage R&D Collaborative Activities with the International Energy Agency (IEA)....198
IV. APPLIED BATTERY RESEARCH FOR TRANSPORTATION....203
IV.A Introduction....203
IV.B Materials Research....205
IV.B.1 Cell Components and Composition....205
IV.B.1.1 Screen Electrode Materials and Cell Chemistries (ANL)....205
IV.B.1.2 Streamlining the Optimization of Li-Ion Battery Electrodes (ANL)....209
IV.B.1.3 Scale-Up of BATT Program Materials for Cell-Level Evaluation (LBNL)....214
IV.B.2 Applied Battery Research on Anodes....218
IV.B.2.1 Developing a New High Capacity Anode with Long Life (ANL)....218
IV.B.2.2 Develop Improved Methods of Making Inter-metallic Anodes (ANL)....221
IV.B.2.3 Lithium Metal Anodes (ANL)....225
IV.B.2.4 New High Power $Li_2MTi_6O_{14}$ Anode Material (ANL)....229
IV.B.3 Applied Battery Research on Cathodes....232
IV.B.3.1 Engineering of High Energy Cathode Material (ANL)....232
IV.B.3.2 Developing New High Energy Gradient Concentration Cathode Material (ANL)....236
IV.B.3.3 Design and Evaluation of Novel High Capacity Cathode Materials (ANL)....239
IV.B.3.4 Development of High-Capacity Cathode Materials with Integrated Structures (ANL)....243
IV.B.3.5 Evaluation of Li_2MnSiO_4 Cathode (ANL)....247
IV.B.4 Applied Battery Research on Electrolytes....250
IV.B.4.1 Novel Electrolytes and Electrolyte Additives for PHEV Applications (ANL)....250
IV.B.4.2 Develop Electrolyte Additives (ANL)....252
IV.B.4.3 High Voltage Electrolytes for Li-ion Batteries (ARL)....258
IV.B.4.4 Development of Novel Electrolytes for Use in High Energy Lithium-Ion Batteries with Wide Operating Temperature Range (JPL)....261
IV.B.4.5 Novel Phosphazene-Based Compounds to Enhance Electrolyte Safety and Stability for High Voltage Applications (INL)....265
IV.C Calendar and Cycle Life Studies....269
IV.C.1 Diagnostics and Modeling....269
IV.C.1.1 Electrochemistry Cell Model (ANL)....269

IV.C.1.2 Diagnostic Studies on Li-Battery Cells and Cell Components (ANL) 273
IV.C.1.3 Structural Investigations of Layered Oxide Materials for PHEV applications (ANL) 276
IV.C.1.4 Electrochemistry Diagnostics of Baseline and New Materials (LBNL) 279
IV.C.1.5 Investigate Mechanical Fatigue in Cycled Electrodes (ORNL) 283
IV.C.1.6 Mechanistic, Molecular, and Thermodynamic Modeling/Diagnostics in support of ABR Cell Performance and Aging Studies (INL) 286
IV.C.2 Cell Fabrication and Testing 290
IV.C.2.1 Fabricate PHEV Cells for Testing & Diagnostics (ANL) 290
IV.C.2.2 Baseline PHEV Cell Life Testing (ANL, INL) 294
IV.D Abuse Tolerance Studies 297
IV.D.1 Abuse Diagnostics 297
IV.D.1.1 Diagnostic Studies supporting Improve Abuse Tolerance (BNL) 297
IV.D.1.2 Internal Short Circuit Test Development (SNL) 303
IV.D.2 Abuse Mitigation 307
IV.D.2.1 Develop & Evaluate Materials & Additives that Enhance Thermal & Overcharge Abuse (ANL) 307
IV.D.2.2 Impact of Materials on Abuse Response (SNL) 311
IV.D.2.3 Overcharge Protection for PHEV Cells (LBNL) 316
IV.E Applied Research Facilities 319
IV.E.1 Battery Materials Pilot Production Facility 319
IV.E.1.1 Process Development and Scale up of Advanced Cathode Materials (ANL) 319
IV.E.1.2 Process Development and Scale up of Organic Electrolyte Components (ANL) 321
V. FOCUSED FUNDAMENTAL RESEARCH 325
V.A Introduction 325
V.B Cathode Development 327
V.B.1 First Principles Calculations and NMR Spectroscopy of Electrode Materials (MIT, SUNY) 327
V.B.2 Cell Analysis, High-energy Density Cathodes and Anodes (LBNL) 332
V.B.3 Olivines and Substituted Layered Materials (LBNL) 336
V.B.4 Stabilized Spinels and Nano Olivines (University of Texas) 341
V.B.5 The Synthesis and Characterization of Substituted Olivines and Layered Manganese Oxides (SUNY) 345
V.B.6 Low Cost SiO_x-Graphite and Olivine Materials (HQ) 348
V.B.7 The Role of Surface Chemistry on the Cycling and Rate Capability of Lithium Positive Electrode Materials (MIT) 351
V.B.8 Characterization of New Cathode Materials using Synchrotron-based X-ray Techniques and the Studies of Li-Air Batteries (BNL) 356
V.B.9 Layered Cathode Materials (ANL) 361
V.B.10 Development of High Energy Cathode (PNNL) 366
V.B.11 High-Energy Cathodes - Performance and Safety of Olivines and Layered Oxides (LBNL) 370
V.C Anode Development 375

V.C.1 Nanoscale Composite Hetero-structures: Novel High Capacity Reversible Anodes for Lithium-ion Batteries (University of Pittsburgh) 375
V.C.2 Interfacial Processes - Diagnostics (LBNL) 380
V.C.3 Nanostructured Metal Oxide Anodes (NREL) 384
V.C.4 Search for New Anode Materials (University of Texas) 389
V.C.5 Intermetallic Anodes (ANL) 392
V.C.6 Nano-structured Materials as Anodes (SUNY) 397
V.C.7 Development of High Capacity Anodes (PNNL) 400
V.C.8 Advanced Binder for Electrode Materials (LBNL) 405
V.C.9 Executive Summaries of New Anode Projects for FY 2010 (Various) 408
V.D Electrolyte Development 410
V.D.1 Polymer Electrolytes for Advanced Lithium Batteries (University of CA, Berkeley) 410
V.D.2 Interfacial Behavior of Electrolytes (LBNL) 413
V.D.3 Molecular Dynamics Simulation Studies of Electrolytes and Electrolyte/Electrode Interfaces (University of Utah) 417
V.D.4 Bi-functional Electrolytes for Lithium-ion Batteries (CWRU) 421
V.D.5 Advanced Electrolyte and Electrolyte Additives (ANL) 424
V.D.6 Inexpensive, Nonfluorinated (or Partially Fluorinated) Anions for Lithium Salts and Ionic Liquids for Lithium Battery Electrolytes (NCSU) 427
V.D.7 Development of Electrolytes for Lithium-ion Batteries (URI) 431
V.E Cell Analysis and Modeling 435
V.E.1 Electrode Fabrication and Failure Analysis (LBNL) 435
V.E.2 Modeling—Thermo-electrochemistry, Capacity Degradation and Mechanics with SEI Layer (University of Michigan) 440
V.E.3 Intercalation Kinetics and Ion Mobility in Electrode Materials (ORNL) 443
V.E.4 Investigations of Electrode Interface and Architecture (LBNL) 446
V.E.5 Analysis and Simulation of Electrochemical Energy Systems (LBNL) 450
V.E.6 Carbon Fiber and Foam Current Collectors (ORNL) 453
V.E.7 Positive and Negative Electrodes: Novel and Optimized Materials (LBNL) 456
V.E.8 Modeling - Predicting and Understanding New Li-ion Materials Using Ab Initio Atomistic Computational Methods (LBNL) 459
V.F Energy Frontier Research Centers 462
V.F.1 Energy Frontier Research Center at ANL 462
V.F.2 Emerging Frontiers in Research Center – Novel *in situ* Diagnostics Tools for Li-ion Battery Electrodes (LBNL) 465
V.G Integrated Lab-Industry Research Program (ANL, LBNL) 468
Appendix A: American Recovery and Reinvestment Act (ARRA) Awards 471
Appendix B: List of Contributors and Research Collaborators 473
Appendix C: Acronyms 479

List of Figures

Figure II- 1: American Recovery and Reinvestment Act (ARRA) 2009 grants distribution for battery and electric drive manufacturing. 9
Figure II- 2: Photos of the A123Systems Livonia Facility 14
Figure II- 3: Saft Factory of the Future under Construction 30
Figure II- 4: Conceptual design of the Toda Facility 34
Figure II- 5: Toda America Inc. Battle Creek Facility construction in progress. 35
Figure II- 6: Interior construction and equipment installation in progress. 35
Figure II- 7: LiPF6 is Required in all Li-ion Batteries 40
Figure II- 8: Schematic plan view of post-test facility. 61
Figure II- 9: Plan view of improved laboratory layout, showing placement of major equipment. The VersaProbe (X-ray photoelectron spectroscopy) will be purchased with non-ARRA funds. 61
Figure II- 10: Bitrode Battery Testing Equipment at NREL's New Battery Thermal Test Facility 64
Figure II- 11: Environmental Chambers at the ARRA-sponsored NREL's Facility 64
Figure II- 12: The Equipment Bought from Several Different Suppliers across U.S. 64
Figure II- 13: CT image of an 18650 lithium-ion cell with a large defect in the roll. 66

Figure III- 1: C/2 cycling at 45°C compares performance improvement to previous (Gen 0) testing and other NMC materials. 73
Figure III- 2: Preliminary prismatic cell mechanical design. 73
Figure III- 3: Preliminary prismatic cell mechanical design. 74
Figure III- 4: Preliminary prismatic cell mechanical design (Another view). 74
Figure III- 5: Baseline PHEV 10-mile development system being tested at Argonne National Labs 74
Figure III- 6: Baseline PHEV system-available energy at 1500 cycles. 74
Figure III- 7: Cycle-life comparison of the three generations of cells developed in this program. 76
Figure III- 8: Comparison of the calendar-life of PLG0 and PLG1 cells at 60°C and SOC=90%. 76
Figure III- 9: Comparison of the calendar-life of PLG1 and PLG2 cells at 30, 40 and 50°C and SOC=80%. 76
Figure III- 10: Comparison of the cooling characteristics of liquid-cooled and a refrigerant-to-air cooled Li-ion packs during cycling 77
Figure III- 11: Picture of a Li Ion battery pack comprising a refrigerant-to-air cooling system and delivered to National Labs. 77
Figure III- 12: Charge Depleting Cycle Life 79
Figure III- 13: Gen 1.5 Cell Power vs Gen 1 Calendar Life 80
Figure III- 14: Calendar life regime for Gen 1 Prismatic Cells 80
Figure III- 15: Calendar life regime for Gen 1 Prismatic Cells 80
Figure III- 16: 25Wh Cycle Life Capacity - 32113 Gen 1 and Gen 2 Cells 82
Figure III- 17: 25Wh Cycle Life Available Energy - 32113 Gen 1 and Gen 2 82
Figure III- 18: USABC Gen 2 Calendar Life Data and Life Extrapolations 82
Figure III- 19: A123Systems 10-cell Module Design 83
Figure III- 20: Thermogravimetric analysis of several steam- activated and KOH-activated carbons. 85
Figure III- 21: The open circuit voltage of a 3,000 F symmetric C/C capacitor obtained from Maxwell Technologies (top), a 5 Ah $Li_4Ti_5O_{12}$/C asymmetric capacitor containing a lithium reference (middle) and a 5 Ah Li_xC_6/C asymmetric capacitor containing a lithium reference (bottom). 86
Figure III- 22: The effect of temperature on the capacity of 500 F lithium-ion capacitors. Cells were cycled at the 10C rate. 86
Figure III- 23: Hot tip test setup 88
Figure III- 24: Hot ER test setup 88
Figure III- 25: TMA test setup. 88
Figure III- 26: 18650 cells 90
Figure III- 27: Cycle life test results, unfilled control separators 90
Figure III- 28: Cycle life test results, Silica filled separators 90
Figure III- 29: Calendar life test results, control separators 90
Figure III- 30: Calendar life test results, silica filled separators 91
Figure III- 31: Capacity vs. storage time. 91
Figure III- 32: Shutdown test results 91
Figure III- 33: Coextruded tri-layer film 91
Figure III- 34: MNC-OH 1/1/1 produced in the 300L pilot reactor. The MNC-OH size varies from 3 to 25um. 94

Figure III- 35: Discharge / regen power capability from HPPC tests on the 18650-size cell after every 250 CDC (Charging Depleting Cycles) 94
Figure III- 36: SEMs of MNC-OH Precursor Produced in 600L Pilot Reactor 95
Figure III- 37: Rate Evaluation Data Summary (2.8V Cutoff) 96
Figure III- 38: Rate Evaluation Data Summary (2.0V Cutoff) 97
Figure III- 39: HPPC Behavior for 18650 Cells 97
Figure III- 40: Coin half-cell rate capability tests of L-20772 alloy, L-19725 alloy and high power graphite (HPG). 101
Figure III- 41: 160C Hotblock test results for 18650's all having NMC-type cathodes. 102
Figure III- 42: Range of statistically-optimal mixture designed experiment for electrode formulation. 102
Figure III- 43: Plan-view SEM images showing the drastic improvement in dispersion from replacing 30wt% of the liquids in the slurry with IPA. 102
Figure III- 44: Yasui coater set up to use the micro-gravure method to apply SLMP onto a substrate. 105
Figure III- 45: (a) SLMP coated onto a substrate using micro-gravure method. (b) Prefabricated anode sheet with SLMP transferred onto it. 105
Figure III- 46: (a) Effect of SLMP on irreversible capacity improvement for MCMB/$LiMn_2O_4$ system. (b) Effect of SLMP on the cycle performance of MCMB/$LiMn_2O_4$ system. 105
Figure III- 47: Effect of SLMP on delivered capacity for hard carbon/$LiMn_2O_4$ system. 105
Figure III- 48: Li anode cycling behavior in 250 mAh experimental cells 108
Figure III- 49: Thermal behavior of Li-S laboratory cells with and without the dual phase electrolyte system. 109
Figure III- 50: BASF NCM 111 Lot Comparisons 111
Figure III- 51: BASF NCM 523 Lot Comparisons 111
Figure III- 52: BASF NCM 424 Lot Comparisons 111
Figure III- 53: A custom-designed lab-scale electro-spinning equipment 113
Figure III- 54: Large-format PAN nanofiber mat prepared by the new electrospinning machine 113
Figure III- 55: (a) Highly aligned carbon nanofibers (b) Randomly arranged carbon nanofibers 113
Figure III- 56: Lab-scale CVD system for Si-coating process 114
Figure III- 57: Four-tube CVD system for silicon coating 114
Figure III- 58: The chemical composition of Si coated carbon fiber analyzed by EDS 114
Figure III- 59: (a) Carbon fiber web (b) Si coated carbon fiber web XRD spectra results 114
Figure III- 60: The SEM images of Si coating on CNFs 115
Figure III- 61: Si particle size vs. varied processes 115
Figure III- 62: The morphology of Si coating (a) 8K X (b) 130K X (c) 120K X 115
Figure III- 63: The SEM images of the electrode surface (a)The electrode ready for CVD (b) Electrode surface before Si coating (c) Si-coated electrode 116
Figure III- 64: Button cells prepared at Angstron 116
Figure III- 65: Updated half-cell performance of the Si-coated electrode 116
Figure III- 66: Schematic of Composite Nanofiber Anode. 119
Figure III- 67: Elmarco's Nanospider™ Electrospinning Production Line (A), and High-Speed Electrospinning Process of Nanospider™ (B). 119
Figure III- 68: Typical SEM (A) and TEM (B) Images of Si/PAN Precursor Nanofibers. 119
Figure III- 69: Typical SEM (A) and TEM (B) Images of Si/C Nanofibers. 119
Figure III- 70: WAXD patterns of C (a) and Si/C (b) Nanofibers. 120
Figure III- 71: Raman spectra of C (a) and C/Si (b) Nanofibers. 120
Figure III- 72: Charge-discharge curves of Si anode. 120
Figure III- 73: Charge-discharge curves of Si/C nanofibers. 120
Figure III- 74: Cycling performance of Si/C nanofibers. 120
Figure III- 75: SEM images of Si/C nanofibers from Si/PAN precursors without (A) and with (B) 0.01 mol/L SD surfactant. 121
Figure III- 76: Cycling performance of Si/C nanofiber anodes made from Si/PAN precursors with and without surfactant. 121
Figure III- 77: 18650 cells containing Si/C nanofibers as anodes. 121
Figure III- 78: Discharge curves of Si/C nanofibers in 18650 cells. 121
Figure III- 79: Thermal stability of Si/C nanofibers in 18650 cells. 121
Figure III- 80: Cyclic voltammograms of 1 mM BDB in electrolyte #1. 124
Figure III- 81: Cyclic voltammograms of 1 mM BDB in electrolyte #2. 124
Figure III- 82: Cyclic voltammograms of 1 mM DDB in electrolyte #1. 124
Figure III- 83: Cyclic voltammograms of 1 mM DDB in electrolyte #2. 125
Figure III- 84: Cyclic voltammograms of 1 mM Li2B12F12 in electrolyte #1. 125

Figure III- 85: Cyclic voltammograms of 1 mM Li2B12F12 in electrolyte #2. 125
Figure III- 86: Cyclic voltammograms of freshly prepared electrolyte containing DDB and after 1 month of storage. 127
Figure III- 87: Cyclic voltammograms of 1 mM BDB and 1% water added to electrolyte #2. 127
Figure III- 88: Expanded region of the first cycle of cyclic voltammograms of BDB without LiF (blue) and with LiF (red). Scan range 3 to 0 V at 1 mV/s. Working electrode is graphite. 127
Figure III- 89: Cyclic voltammograms of BDB without LiF (blue) and with LiF (red). Scan range 3 to 0 V at 1 mV/s. Working electrode is graphite. 128
Figure III- 90: Predictions of real world vs. rated charge depletion distances for several plug-in electric vehicles 140
Figure III- 91: 2009 estimates of $/kWh for PHEV battery packs, holding pack kW at 60, and increasing kWh 140
Figure III- 92: 2010 $/kWh estimates for HEV, PHEV, and E-REV battery packs, in different narrow kW brackets, as kWh rises 140
Figure III- 93: Percent decline in LMO-G pack cost vs. scale of manufacture beyond 10,000 battery packs per year. 141
Figure III- 94: Incremental Benefit to Cost Ratio of Powertrains in Comparison to the Split HEV (red dotted line) at $5/gallon. (Cross group comparisons are not valid) 142
Figure III- 95: Fitting of life model to Saft VES-140 dataset for geosyncronous satellite application (Hall, 2006). (a) Cycling-related resistance growth dependence on depth-of-discharge. (b) Comparison of final global model with data. 146
Figure III- 96: Comparison of life model with vehicle battery aging data. (a) JCS HP12LC cell tested under HEV cycle (Belt, 2008). (b) JCS VL41M cell tested under PHEV cycle (Gaillac, 2009). 146
Figure III- 97: Battery cost and useable depth-of-discharge at beginning-of-life for PHEV batteries sized for various years life and temperature. Each case is optimized to select a power-to-energy ratio that minimizes cell cost. 147
Figure III- 98: Overview of the battery ownership model with its nine sub- modules 150
Figure III- 99: Comparing levelized cost per mile from various sources with the results of the battery ownership model 151
Figure III- 100: Range of vehicle levelized cost ratio 152
Figure III- 101: Sensitivity of vehicle levelized cost ratio to design variables 152
Figure III- 102: Value and market potential for the use of li-ion batteries in grid applications 156
Figure III- 103: Present value of secondary use for first generation EVs 156
Figure III- 104: Present value of secondary use for later generation EVs (additional results) 156
Figure III- 105: Recycled Materials Enter Varying Production Stages 159
Figure III- 106: The Impact of Recycling and Reuse on Future US Lithium Demand 159
Figure III- 107: Where Recycled Materials Could Enter Battery Production 159
Figure III- 108: Energy Use for Battery Production Steps 160
Figure III- 109: PA-HEV Available Energy Requirement of 300 Wh Leads to 425 Wh Energy Window for Vehicle Use. 163
Figure III- 110: Simulation Results over the US06 Driving Cycle. 163
Figure III- 111: Energy Used in Production HEV During Various Drive Cycles. 163
Figure III- 112: Distribution of Power Pulses vs. Duration (dashed purple lines indicates the largest energy and highest DOH HEV case over the US06 drive cycle). 164
Figure III- 113: LEESS Energy Window for Vehicle Use of 165 Wh Leads to 26 Wh of Available Energy where Charge and Discharge Requirements are Simultaneously Met for 10 sec Pulses. 164
Figure III- 114: Resistance vs. cycle count for two cells in an accelerated screening test. 167
Figure III- 115: C/1 capacity vs. cycle count for two cells in an accelerated screening test. 167
Figure III- 116: Resistance at 50% SOC vs. cycle count for Groups A and B. 167
Figure III- 117: C1 Capacity Data 167
Figure III- 118: Input current for *in situ* impedance detection. 170
Figure III- 119: Hardware for *in situ* impedance measurement. 170
Figure III- 120: Control software graphical user interaface. 171
Figure III- 121: Comparison between EIS and HCSD measurements. 171
Figure III- 122: Comparison between HPPC and impedance measurement techniques. 171
Figure III- 123: PHEV Operation Philosophy 173
Figure III- 124: Typical power and energy capability for PHEV cells under test. 173
Figure III- 125: CD and CS Available Energies 174
Figure III- 126: JCS 344-Volt Battery Pack 174
Figure III- 127: Typical affect of temperature on lithium-ion battery resistance rise. 174
Figure III- 128: CPI 400-Volt Battery Pack 175
Figure III- 129: Altairnano Charge Depleting Energy Summary 175
Figure III- 130: Formation cycling a $LiCoO_2$ 18650 cell at a 200 mA C/D rate. 177
Figure III- 131: Cell voltage and cell exterior temperature for a 4A overcharge of a $LiCoO_2$ 18650 cell. 177
Figure III- 132: Cell voltage and temperature as a function of time during a thermal ramp (5 C/min) of a $LiCoO_2$ 18650 cell. 178

Figure III- 133: Cell heating rate (C/min) calculated from the thermal ramp for a $LiCoO_2$ cell showing the onset to thermal runaway at ~150°C followed by a high order runaway at 200°C. 178
Figure III- 134: Test setup for the blunt rod test on an 18650 cell. 178
Figure III- 135: Cell voltage and applied load (lbf) as a function of time during a blunt rod test of a $LiFePO_4$ 18650 cell. 178
Figure III- 136: Applied current and cell voltage as a function of time during a blunt rod test of a $LiFePO_4$ 18650 cell. 178
Figure III- 137: Four Elements of the Computer Aided Engineering for Batteries (CAEBAT) Activity. 181
Figure III- 138: Muti-scale physics in battery modeling from molecular modeling to pack and system level modeling. 181
Figure III- 139: Sub-elements of the Computer Aided Engineering for Batteries (CAEBAT) Activity and Industry Collaboration. 183
Figure III- 140: Modularized hierarchy of model structure in NREL's MSMD approach 184
Figure III- 141: Example results of battery modeling multi-physics interaction for 40 Ah prismatic cells with terminals on the same side; after 2 minutes of 200 A constant discharge (compare it with the next figure) 184
Figure III- 142: Example results of battery modeling multi-physics interaction for 40 Ah prismatic cells with terminals both sides; after 2 minutes of 200 A constant discharge (compare it with the previous figure) 185
Figure III- 143: Schematic of the modeling framework and interactions with other tasks within the CAEBAT program and external activities. 187
Figure III- 144: Dual foil case study: flow diagram 188
Figure III- 145: IPS framework layout 189
Figure III- 146: An example IPS application structure 189
Figure III- 147: IPS execution environment 189
Figure III- 148: Data management – simulation tree layout 189
Figure III- 149: Efficiency and heat generation comparison between the Gen 2B0.1 and Gen 2 B1.0 HEV cells. 191
Figure III- 150: Infrared thermal image of the CPI PLG1 Pouch Prismatic Cells under US06 cycling. 191
Figure III- 151: Thermal image of the EnerDel HEV cell under US06 cycling 192
Figure III- 152: CPI refrigeration system cools down the cell temperatures after a high temperature soak condition 192
Figure III- 153: Macroscopic design parameters used for this optimization study; with fixed conditions for $\delta_{Al} = 1.6 \times \delta_{Cu}$, 20 Ah capacity, electrode loadings, and electrode thicknesses. 193
Figure III- 154: Comparison of model prediction with measured data for voltage response of CPI PLG2 cell at 30°C during USABC charge depleting cycle. The model fits good overall, but it under-predicts heat generation by about 14%. 193
Figure III- 155: Relation between steady state cell temperature and contact resistance factor f at 5W per cell heat generation condition (top); Temperature and external heat transfer coefficient relation with and without Kapton layer, when excessive thermal contact resistance (f=0.02) is caused by Kapton wrap. 194
Figure III- 156: Integrated Multi-Physics Internal Short-Circuit Model 196
Figure III- 157: Concept sketch of the ISC instigater that could be implanted inside a Li-ion cell. 196
Figure III- 158: Modelig strategy 2D modeling geometry and boundary conditions, the modeling domain assigned near the ISC instigator inside a jellyroll: current merging into the ISC instigator is considered as a constant current boundary condition in the present model. 196
Figure III- 159: Modeling results: Note that the aspect ratio of the figures is adjusted for clear vision (a) electric potential contour, (b) current density contour 197

Figure IV- 1: Task and subtask breakdown for the Applied Battery Research Program 204
Figure IV- 2: Specific capacity requirements for anode and cathode electrode of lithium-ion battery 206
Figure IV- 3: Voltage profile of Li/ $LiNi_{0.8}Co_{0.15}Al_{0.05}O_2$ cell 207
Figure IV- 4: Rate performance of MAG10/ $LiNi_{0.8}Co_{0.15}Al_{0.05}O_2$ cell 207
Figure IV- 5: $Li/Li_{1.05}(Ni_{4/9}Co_{1/9}Mn_{4/9})_{0.95}O_2$ cell Voltage profile 207
Figure IV- 6: $MAG10/Li_{1.05}(Ni_{4/9}Co_{1/9}Mn_{4/9})_{0.95}O_2$ cell Rate performance 207
Figure IV- 7: DSC results of fully charged NCA and NCM. 208
Figure IV- 8: Schematic diagram of streamlining the optimization of electrode 210
Figure IV- 9: Conductivity measurement using nano probe SEM 210
Figure IV- 10: Interaction between particle and PVdF binder 211
Figure IV- 11: Schematic diagram of carbon coating by Hosokawa 211
Figure IV- 12: Uncoated (left) and coated (right) NCM particels 211
Figure IV- 13: Powder conductivity of carbon coated NCM 211
Figure IV- 14: 4 probe conductivity of electrode on substrate polyester (top) and (bottom) aluminum. 212
Figure IV- 15: SEM images of electrode with no carbon coating (left) and with 3% carbon coating on the particles. 212

Figure IV- 16: SEM images of BCF oxdide film. 212
Figure IV- 17: Plot of capacity versus C-rate for the baseline LFP material and the same material synthesized by a less expensive process. 215
Figure IV- 18: (left) MIT material; (right) LBNL duplicate. 217
Figure IV- 19: Photograph of MIT material in pellet form. 217
Figure IV- 20: Scanning electron microcopy images of the TiO_2 precursor. 219
Figure IV- 21: Cycling behavior of the silicon-based composite. 219
Figure IV- 22: Charge and discharge voltage profile of Cu_6Sn_5 versus lithium. 221
Figure IV- 23: Volumetric capacity density of Cu_6Sn_5-based intermetallic alloys compared against graphite. 222
Figure IV- 24: Photo of rectangular bars cast from various intermetallic alloys used for mechanical property studies. 223
Figure IV- 25: SEM photo of optimum Cu_6Sn_5 powder based on mechanical properties for discharge to Li_2CuSn. 223
Figure IV- 26: (left) Thin film formed on lithium metal electrode dip-coated with 1-vinyl imidazole. After 200 cycles (right) polymeric layer has decomposed leaving the lithium surface unprotected and having the general appearance of the uncoated control sample. Scale bar is 100 um for both micrographs. 226
Figure IV- 27: Capacity (normalized) vs. cycle number for two different silanes is shown versus an uncoated lithium control. 226
Figure IV- 28: Surface structure of clean lithium on 20sec exposure to electrolyte (1.2 M $LiPF_6$, EC:EMC 30:70) 227
Figure IV- 29: Surface structure of clean lithium on 5 min exposure to electrolyte (1.2 M $LiPF_6$, EC:EMC 30:70) 227
Figure IV- 30: X-ray diffraction powder patterns of $MLi_2Ti_6O_{14}$ prepared by sol-gel method. 230
Figure IV- 31: Charge/discharge voltage profiles of $SrLi_2Ti_6O_{14}$ (top) and $Na_2Li_2Ti_6O_{14}$ (bottom) cycled between 0.5 and 2 V under 10 mA/g. 230
Figure IV- 32: Cyclability of $MLi_2Ti_6O_{14}$ performed between 0.5 and 2 V at 10 mA/g. 231
Figure IV- 33: Rate capability of $MLi_2Ti_6O_{14}$ cycled between 0.5 and 2 V. 231
Figure IV- 34: Rate capability of $LiMn_2O_4/SrLi_2Ti_6O_{14}$ cycled between 1.5 and 3.8 V. 231
Figure IV- 35: Charge and discharge capacity variation with lithium concentration in high-energy composite electrode with and without Co doping. 233
Figure IV- 36: SEM images of $Li_{(1+x)}Ni_{0.25}Co_{0.15}Mn_{0.6}O_{(2.25+x/2)}$ ($0.225 < x < 1.65$). (Left side: secondary particles, 5µm scale bar; right side: primary particles, 1 µm scale bar. 233
Figure IV- 37: Cycling performance of a cell made of $Li_{(1+x)}Ni_{0.25}Co_{0.15}Mn_{0.6}O_{(2.25+x/2)}$ ($x = 0.225$) vs. lithium metal at C/3 rate 234
Figure IV- 38: SEM of cross section of AlF_3-coated and uncoated $Li_{(1+x)}Ni_{0.25}Co_{0.15}Mn_{0.6}O_{(2.25+x/2)}$ ($x = 0.225$) 234
Figure IV- 39: Alternating current impedance of a cell made of a 2 wt% AlF_3-coated and uncoated $Li_{(1+x)}Ni_{0.25}Co_{0.15}Mn_{0.6}O_{(2.25+x/2)}$ ($x = 0.225$) 234
Figure IV- 40: Cycling performance of the AlF_3-coated and the uncoated $Li_{(1+x)}Ni_{0.25}Co_{0.15}Mn_{0.6}O_{(2.25+x/2)}$ ($x = 0.225$) at 25°C 234
Figure IV- 41: Cycling performance of the AlF_3-coated and the uncoated $Li_{(1+x)}Ni_{0.25}Co_{0.15}Mn_{0.6}O_{(2.25+x/2)}$ ($x=0.225$) at 55°C 235
Figure IV- 42: Experimental setup for making concentration gradient material (CGM). 237
Figure IV- 43: Capacity of CGM cathode at 4.3, 4.4, and 4.5 V under 0.2 C rate. 237
Figure IV- 44: Cycling performance of CGM cathode at 4.3, 4.4, and 4.5 V at 0.2 C rate and room temperature. 237
Figure IV- 45: Cycling performance of CGM cathode at 4.3, 4.4, and 4.5 V at 0.2 C rate and 55°C. 237
Figure IV- 46: Cycling performance of CGM-material/graphite and core-material/graphite cells at 55°C and 1 C rate. 238
Figure IV- 47: Nail penetration test of CGM-material/graphite cell and core-material/graphite cells. 238
Figure IV- 48: First galvanostatic charge voltage profile of Li/LFO at a slow rate current density of 7 mA/g. 240
Figure IV- 49: 1st galvanostatic discharge voltage profiles of C/LFO-MnO_2 electrode. 240
Figure IV- 50: 1st and 30th galvanostatic discharge voltage profiles of Li/LVO and Li/Al_2O_3-coatedLVO 241
Figure IV- 51: Rate performance study – coated LVO vsrsus uncoated. 241
Figure IV- 52: 40 cycles at 1.3C cycling - coated LVO versus uncoated. 241
Figure IV- 53: XRD patterns for (top) $Li_{5.6}Fe_{0.4}Co_{0.6}O_4$, and (bottom) $Li_5Fe_{0.4}Co_{0.6}O_4$. 241
Figure IV- 54: First charge-discharge voltage profile for Li/LFO and Li/LFCO cells. 242
Figure IV- 55: *Ex situ* XRD patterns from chemically delithiated LFO; x values represent each equivalent of Li removed. 242
Figure IV- 56: Voltage profiles of Li/$Li_xMn_{0.75}Ni_{0.25}O_Z$ cells discharged from open circuit voltage after assembly 244
Figure IV- 57: Discharge voltage profiles of Li/$Li_xMn_{0.75}Ni_{0.25}O_Z$ cells cycled at 2.0-4.95 V, 10 mA/g (a), and 2.0-4.6 V, 15 mA/g (b). Capacity variations during cycling are given in the insets. 244
Figure IV- 58: Discharge capacity vs. current density plot of Li/$Li_xMn_{0.75}Ni_{0.25}O_Z$ cells. The cells charged to 4.6 V at 15 mA/g and discharged to 2.0 V at various current rates. The dotted line denotes 1C rate line. 244
Figure IV- 59: Capacity variations of Li/$Li_{1.2}(Mn_{0.75}Ni_{0.25})_{1-y}Co_yO_z$ cells cycled between 2.0 and 4.95 V. 245
Figure IV- 60: TEM pictures of pristine $Li_{1.2}Mn_{0.75}Ni_{0.25}O_z$ sample. 245
Figure IV- 61: (a) Ni- and (b) Mn K-edge spectra of pristine and cycled $Li_{1.2}Mn_{0.75}Ni_{0.25}O_z$ electrodes. 245
Figure IV- 62: DSC profile of charged $Li_{1.2}Mn_{0.75}Ni_{0.25}O_z$ electrode. 246

Figure IV- 63: X-ray patterns of Li_2MnSiO_4 prepared at 700°C, under reducing atmosphere. Calculated pattern also shown at top. 248
Figure IV- 64: Typical voltage profile of Li/C-Li_2MnSiO_4 248
Figure IV- 65: Typical cycling bahavior of Li/C-Li_2MnSiO_4 248
Figure IV- 66: PDF analysis of Li_2MnSiO_4 charged to 4.8V and discharged to 1.5 V. 249
Figure IV- 67: Voltage profile and cycling data of $Li_2Mn_{0.5}Fe_{0.5}SiO_4$ and Li_2FeSiO_4. 249
Figure IV- 68: Preparing the methyl ester version of GC. 251
Figure IV- 69: NCA(+)//Gr(-) cell cycling in GCAc:DMC (1:8, by wt.) + 1.2M $LiPF_6$ eelctrolyte. Voltage range: 3-4.3V. 251
Figure IV- 70: CV profiles of 1M LiTFSI sulfones (left) and their ambient conductivities (right). 253
Figure IV- 71: Specific cathode charge/discharge capacities of cells for LTO/$LiMn_2O_4$ (left) with 1M LiTFSI sulfones and LTO/$LiNi_{0.5}Mn_{1.5}O_4$ (right) with 1M $LiPF_6$ sulfones. 254
Figure IV- 72: Differential capacity profiles of Li/MCMB with 1.2M $LiPF_6$ EC/EMC 3/7+2% additive. 254
Figure IV- 73: Plots of normalized discharge capacity vs cycle number for MCMB/NCM cells with and without additives. 254
Figure IV- 74: Nyquist plots of the MCMB/NCM cells with and without LTFOP or LTOP before (top) and after 200 cycles (bottom) at 55°C at open-circuit voltage of 3.8 V. 255
Figure IV- 75: Capacity retention of the MCMB negative electrode (top) and NCM positive electrode (bottom) vs the aging time at 55°C. 255
Figure IV- 76: DSC profiles of the fully lithiated MCMB mixed with nonaqueous electrolytes with and without LTFOP. 256
Figure IV- 77: Differential capacity profiles of MCMB/NCM cells with 1% additive in 1.2M $LiPF_6$ EC/EMC 3/7. 256
Figure IV- 78: Capacity retention of MCMB/NCM cells cycled between 2.7 and 4.2V at 55 ◦C with electrolyte of 1.2M $LiPF_6$ EC/EMC 3/7 with and without addtive. 256
Figure IV- 79: Voltage profiles of a $LiNi_{0.5}Mn_{1.5}O_2$/Li half cell in 1 M $LiPF_6$/EC:EMC(3:7 w/o) versus capacity at different cycles cycled between 3.5 and 4.9 V at room temperatures. 259
Figure IV- 80: Voltage profiles of a $LiNi_{0.5}Mn_{1.5}O_2$/Li half cell in 1 M $LiPF_6$/SL/EC:EMC(1.5:1.5:7 w/o)+1 wt% ARL3 versus capacity at different cycles cycled between 3.5 and 4.9 V at room temperatures. 259
Figure IV- 81: A comparison of capacity retention of $LiNi_{0.5}Mn_{1.5}O_2$/Li half cells in 1 M $LiPF_6$/EC:EMC(3:7 w/o) with and without 1 wt% ARL3 versus cycle number. The cells were cycled between 3.5 and 4.9 V at room temperature. 260
Figure IV- 82: A comparison of capacity retention of $LiCoPO_4$/Li and m-$LiCoPO_4$/Li half cells in 1 M $LiPF_6$/EC:EMC(3:7 w/o) with and without 1 wt% ARL3 versus cycle number. 260
Figure IV- 83: The discharge energy obtained with MCMB-$LiNiCoAlO_2$ cells at -40°C, using 5C discharge rates. 262
Figure IV- 84: The cycle life performance (100% DOD) of MCMB-$LiNiCoAlO_2$ cells containing wide operating temperature electrolytes at 50°C 263
Figure IV- 85: AC impedance (Nyquist) plots of $LiNi_XCo_{1-X}O_2$ electrodes in MCMB-$LiNi_XCo_{1-X}O_2$ cells containing 1.0M $LiPF_6$ EC+EMC (50:50 v/v %) electrolyte with and without additives after being subjected to 20 cycles at 60°C. 263
Figure IV- 86: Discharge capacity of MCMB-$LiNi_XCo_{1-X}O_2$ cells containing 1.0M $LiPF_6$ EC+EMC+MB (20:20:60 vol %) electrolytes with and without additives at - 40°C. 264
Figure IV- 87: Tafel Polarization measurements of the cathodes of MCMB-$LiNi_XCo_{1-X}O_2$ cells containing 1.0M $LiPF_6$ EC+EMC+MB (20:20:60 vol %) electrolytes with and without additives at - 30°C. 264
Figure IV- 88: Heterocyclic phosphazene structure 266
Figure IV- 89: Results of Stability Testing 267
Figure IV- 90: Electrolyte Viscosity Comparison 267
Figure IV- 91: Electrolyte Conductivity Comparison 267
Figure IV- 92: SEI Formation Capacity and Maintenance Rates 267
Figure IV- 93: SM4 and SM5 Comparisons 267
Figure IV- 94: Slow discharge curve of MCMB graphite negative electrode showing tinted single phase regions. 271
Figure IV- 95: Lithium concentration distribution in particle for each phase. The tinted regions are the stable concentration ranges for each stage (red for Stage 1, blue for Stage 2, and green for Stage 3). 271
Figure IV- 96: Graphite MCMB electrode volume fraction of each Stage during a C/50 discharge. 271
Figure IV- 97: Graphite MCMB electrode volume fraction of each Stage during a C/10 discharge. 271
Figure IV- 98: Graphite MCMB electrode volume fraction of each Stage during a C/1 discharge. 272
Figure IV- 99: SEM images of the PHEV baseline positive and negative electrodes. 274
Figure IV- 100: First few cycles on a PHEV baseline cell, 30°C. 274
Figure IV- 101: RE cell data (after formation cycling) showing positive and negative electrode voltage changes when the full cell voltage changes from 3 to 4.1V at a C/10 rate. 274
Figure IV- 102: EIS (Full Cell) data showing decreasing impedance with increasing cell temperature. 275
Figure IV- 103: HPPC (Full Cell) 18s discharge pulse (various magnitudes) data showing cell impedance at 30°C. 275
Figure IV- 104: Initial aging data showing capacity fade (calculated at 30°C) of a cell that completed 3000 C-rate cycles between 3.6 to 4.0V at 45°C. 275

Figure IV- 105: HAADF-STEM micrographs and SAED patterns of high purity Li_2MnO_3 showing the $Li_{1/3}Mn_{2/3}$ plane stacking sequence. ..277
Figure IV- 106: HAADF-STEM micrograph of high purity Li_2MnO_3 showing the structure of the $Li_{1/3}Mn_{2/3}$ planes. ..278
Figure IV- 107: HREM micrograph of high purity Li_2MnO_3 showing stacking faults corresponding to local rotations of the monoclinic lattice about the $Li_{1/3}Mn_{2/3}$ plane stacking direction. ..278
Figure IV- 108: $Li_{1.2}Co_{0.4}Mn_{0.4}O_2$ HAADF image showing Li-TM-TM contrast akin to earlier Figures Figure IV- 105(a) and (c) ..278
Figure IV- 109: Surface Raman maps of the ID/IG ratio from 48μm×74μm area at ca. 0.7μm resolution of (a) pristine graphite electrode, and (b) electrode cycled between 1 and 0.18V vs. Li/Li+ ..280
Figure IV- 110: Schematic diagram of structural stress induced into grapite upon Li+ intercalation ..281
Figure IV- 111: Schematic view of the *in situ* AE-XRD cell design used to study LIBs during cycling. ..284
Figure IV- 112: *in situ* AE-XRD experimental setup showing the cell connected to an AE sensor and current leads and sitting in the X-ray beam path ..284
Figure IV- 113: Cumulative AE and cycling voltage of *in situ* AE-XRD cell containing a composite silicon electrode. ..284
Figure IV- 114: Lattice strain in the crystalline region of silicon particles and voltage as a function of time. ..284
Figure IV- 115: a and c lattice strains in NMC materials cycled in an *in situ* AE-XRD cell. ..284
Figure IV- 116: INL Essential Modeling Tools ..287
Figure IV- 117: Temperature Profiles per Thermal Cycle ..288
Figure IV- 118: Electrochemical cell modeling parameters ..288
Figure IV- 119: Conductance fade profile over time ..288
Figure IV- 120: Capacity fade profile over time ..289
Figure IV- 121: Interim results from PPD discharge impedances ..289
Figure IV- 122: PHEV baseline 18650 cells. ..292
Figure IV- 123: Winder/stacker used to assemble lithium-ion pouch cells in Argonne's cell fabrication facility. ..292
Figure IV- 124: Electrolyte-filling vacuum chamber and heat sealer for lithium-ion pouch cell fabrication at Argonne. ..292
Figure IV- 125: 18650 cell making equipment in Argonne's cell fabrication facility. ..293
Figure IV- 126: Relative ASI vs. calendar time. ..295
Figure IV- 127: Relative C/1 capacity vs. calendar time. ..295
Figure IV- 128: Relative C/25 capacity vs. calendar time. ..296
Figure IV- 129: EIS from a PH1C cell. ..296
Figure IV- 130: EIS from a Gen2 baseline cell. ..296
Figure IV- 131: TR-XRD of charged $Li_{0.33}Ni_{0.8}Co_{0.15}Al_{0.05}O_2$ (Gen2) during heating ..298
Figure IV- 132: R-XRD of charged $Li_{0.33}Ni_{1/3}Co_{1/3}Mn_{1/3}O_2$ (Gen3) during heating ..298
Figure IV- 133: *In situ* XAS spectra of charged $Li_{0.33}Ni_{0.8}Co_{0.15}Al_{0.05}O_2$ (Gen2) and $Li_{0.33}Ni_{1/3}Co_{1/3}Mn_{1/3}O_2$ (Gen3) during heating ..299
Figure IV- 134: Edge position changes with heating temperature of Gen2 and Gen3 cathode materials ..299
Figure IV- 135: TR-XRD of bare overcharged $Li_{0.33}Ni_{0.8}Co_{0.15}Al_{0.05}O_2$ (Gen2) during heating ..299
Figure IV- 136: TR-XRD of ZrO_2 coated overcharged $Li_{0.33}Ni_{0.8}Co_{0.15}Al_{0.05}O_2$ (Gen2) during heating ..299
Figure IV- 137: *in situ* soft XAS results of bare overcharged $Li_{0.33}Ni_{0.8}Co_{0.15}Al_{0.05}O_2$ (Gen2) by PEY mode (surface) during heating ..300
Figure IV- 138: *In situ* soft XAS results of ZrO_2 coated overcharged $Li_{0.33}Ni_{0.8}Co_{0.15}Al_{0.05}O_2$ (Gen2) by FY mode (bulk) during heating ..300
Figure IV- 139: The HRTEM image of overcharged Gen2 cathode particle at room temperature. The spinel and rock-salt structures observed only at high temperatures by XRD were observed at the surface and edge of the particle at room temperature ..300
Figure IV- 140: The *in situ* HRTEM image of overcharged G2 cathode particle at 100°C. The Spinel and rock-salt structures were growing into the bolk from the surface and edge of the particle. ..301
Figure IV- 141: The *in situ* HRTEM image of overcharged G2 cathode particle at 200°C. The Spinel and rock-salt phases continued to grow larger and larger with raising temperature in the expense of layeed structure. ..301
Figure IV- 142: The *in situ* HRTEM image of overcharged G2 cathode particle at 300°C. The Spinel and rock-salt phases became the dominating phases. ..301
Figure IV- 143: The *in situ* HRTEM image of overcharged G2 cathode particle at 400°C. The majority of the particle changed into the rock-salt phases. ..301
Figure IV- 144: Normalized AC impedance of a separator sheet rolled between two copper foil electrodes. Each of the four traces represents replicate samples. The electrodes are shorted together using a Bi/Sn/In alloy with a melting temperature of 60°C. ..304
Figure IV- 145: Cell voltage as a function of temperature for NMC coin cells that are shorted using a Bi/Sn/In alloy with a melting temperature of 60°C. The red, black, gray, and navy traces are cells built with the alloy between the anode and cathode and the blue trace is for a cell built with the alloy between the two current collectors. ..304
Figure IV- 146: Ambient temperature charge/discharge cycling of an NMC 18650 cell with a metal alloy defect showing "normal" cell behavior. ..304
Figure IV- 147: Cell OCV as a function of temperature for an NMC 18650 cell that develops a short circuit as a result of a metal alloy trigger at 68°C. ..305

Figure IV- 148: Ambient temperature charge/discharge cycling of an NMC 18650 cell post-ISC triggering clearly showing evidence of soft shorting. 305
Figure IV- 149: X-ray image of an 18650 cell with an internal heater. 305
Figure IV- 150: Internal short circuit of an 18650 cell with an internal heater at 115°C. 305
Figure IV- 151: DSC profile of different cell components showing that the SEI decomposition is the bottleneck for battery safety. 308
Figure IV- 152: DSC profiles of different lithiated carbons with non-aqueous electrolyte. 309
Figure IV- 153: Charge (red) and discharge (blue) capacity of a $Li_{1.1}[Mn_{1/3}Ni_{1/3}Co_{1/3}]_{0.9}O_2$/C lithium-ion cell during the overcharge test using $Li_2B_{12}F_9H_3$ based electrolyte containing 5 wt% 2-(pentafluorophenyl)-tetrafluoro-1,3,2-benzodioxaborole and 1 wt% lithium difluoro(oxalato)borate. 309
Figure IV- 154: Cyclic voltammogram of a newly synthesized redox shuttle tested in Pt/Li/Li three-electrode electrochemical cell. The structure of the redox shuttle is shown as an inet. 309
Figure IV- 155: Voltage profile of an MCMB/$Li_{1.2}Ni_{0.15}Co_{0.1}Mn_{0.55}O_2$ lithium-ion cell during overcharge test. 310
Figure IV- 156: Charge/discharge capacity of an MCMB/$Li_{1.2}Ni_{0.15}Co_{0.1}Mn_{0.55}O_2$ lithium-ion cell during overcharge test. 310
Figure IV- 157: ARC profiles for Hitachi $LiFePO_4$ cells with N-7b, N-20, and Ns-15f anode materials. 312
Figure IV- 158: ARC profiles for three Hitachi $LiFePO_4$/N-7b cells: two cells with VC (VC2, red and green trace) and one cell without VC (VC0, blue trace). 312
Figure IV- 159: ARC profiles for NMC (red trace) and AlF_3-coated NMC cells (blue, navy, and green traces). 313
Figure IV- 160: Total STP gas volume as a function of temperature during an ARC experiment for NMC (red trace) and AlF_3-NMC (navy trace) 18650 cells. Gas evolution shown during heating, themal runaway and cooldown. 313
Figure IV- 161: Discharge capacity of NMC cells with 1.2 M $LiPF_6$ EC:EMC (3:7) (black trace) and 1.0 M LiF/ABA EC:EMC (3:7) (blue trace) electrolytes. 314
Figure IV- 162: STP gas volume during an ARC experiment for NMC cells with 1.2 M $LiPF_6$ EC:EMC (3:7) (black trace) and 1.0 M LiF/ABA EC:EMC (3:7) (blue trace) electrolytes. 314
Figure IV- 163: Discharge capacity of a 2.0 Ah NMC cell where the electrodes were coated and the cell was built at SNL 314
Figure IV- 164: ARC profiles for a 1.04 Ah $LiNi_{0.4}Mn_{0.3}Co_{0.3}O_2$ cell at 4.3 V (red trace) and a 0.94 Ah $Li_{1.1}(Ni_{1/3}Mn_{1/3}Co_{1/3})_{0.9}O_2$ (Gen3) cell at 4.1 V (blue trace). 315
Figure IV- 165: Rate performance of an overcharge-protected $Li_{1.05}Mn_{1.95}O_4$ - Li cell with a) "sandwich" configuration and b) parallel configuration. 317
Figure IV- 166: Low-temperature performance of an overcharge-protected $Li_{1.05}Mn_{1.95}O_4$ - Li cell with a) "sandwich" configuration and b) parallel configuration. 317
Figure IV- 167: Potential profiles across P3BT composites prepared by a) solution impregnation in Celgard separator and b) electrodeposition in AAO template. 318

Figure V- 1: BATT Overview 325
Figure V- 2: ^{7}Li NMR spectra of metallic lithium (a 1-3), as a function of time in a $LiCoO_2$ cell, for one charge-discharge cycle. Measured voltage and the applied current (C/10 rate) are plotted in (b) and (c). The measured Li metal intensity ($I_{exp}(t)$) is shown as a solid black line in (d), where the signal (S(t)) has been normalized to the signal at t=0, to give $I_{exp}(t) = [S(t)-S(t=0)]/S(t = 0))$. Theoretical values of I(t), calculated under various assumptions are shown for comparison: (i) no skin depth issues $I_{vol}(t)$ (blue dashed line), (ii) all of lithium is smoothly deposited $I_{SD}(t)$ (red dotted line), (iii) all of lithium deposited/stripped forms micro-structure $I_\mu(t)$ (blue circles; equation 16). Only $I_\mu(t)$ provides a good fit to the experimental data, the small deviation being due to a small amount of smoothly deposited lithium. $I_{exp}(t)$, in combination with total mass of Li deposited or stripped $M_{Li}(t)$ (extracted from the electrochemistry), can be used to calculate the mass of deposited Li, $M_{SD}(t)$ and Li microstructures $M_\mu(t)$, taking into account of the skin-depth problem (e). 328
Figure V- 3: The pair distribution function (PDF) (G(r)) of silicon following 1 cycle, obtained from diffraction data. The 1st two dominant correspond to directly bound Si and Si within a tetrahedra. 329
Figure V- 4: Calculated phase diagram of $Li_xFe_{0.5}Mn_{0.5}PO_4$ 329
Figure V- 5: Schematic illustration of immobile point defects obstructing fast 1D Li diffusion. 330
Figure V- 6: O_2 evolved versus temperature for delithiated MPO_4 (M = Fe, Mn) 330
Figure V- 7: Voltage vs. thermal stability for thousands of compounds (calculated). 330
Figure V- 8: First two cycles of pre-lithiated Sn electrode. 333
Figure V- 9: Comparison of irreversible capacities and cycling stability of (a) untreated and (b) pre-lithiated Si/C electrodes. 333
Figure V- 10: (a) Charge-discharge curves for Si electrode; (b) DSC traces at points marked in (a). 333
Figure V- 11: Crystal structures of (a) α-$NaCoPO_4$; (b) $NaCuPO_4$. 334

Figure V- 12: (a) Electrode cross section; state of charge distribution following charging to 50 % SOC at: (b) C/8, (c) 18 C; and (d) simulated charge distribution at 20 C (V. Srinivasan). 334
Figure V- 13: State of charge distribution in the plane of an electrode following charging to 50 % SOC at 12 C. 335
Figure V- 14: Schematic of one of the spray pyrolysis setups used to produce cathode materials. 337
Figure V- 15: Li/Li[$Ni_{0.45}Co_{0.1-y}Al_yMn_{0.45}$]$O_2$ (y=0, 0.025, 0.05, 0.075, and 0.1) cells charged and discharged at 0.1 mA/cm^2 between 4.3 and 2.0V. The inset shows dQ/dV plots derived from the data. 337
Figure V- 16: Discharge capacity as a function of cycle number for Li/Li[$Ni_{0.45}Co_{0.1}Mn_{0.45}$]$O_2$ and Li/Li[$Ni_{0.45}Al_{0.05}Co_{0.05}Mn_{0.45}$]$O_2$ cells discharged at 0.1 mA/cm^2. 337
Figure V- 17: Relative changes in c-axis parameters as a function of state-of-charge in Li_{1-x}[$Ni_{0.45}Co_{0.1}Mn_{0.45}$]$O_2$ and Li_{1-x}[$Ni_{0.45}Al_{0.05}Co_{0.05}Mn_{0.45}$]$O_2$ electrode materials. 337
Figure V- 18: Discharge profiles of lithium cells containing Li[$Ni_{0.33}Co_{0.33-y}Ti_yMn_{0.33}$]$O_2$ compounds, discharged at 0.1 mA/cm^2 between 4.7 and 2.0V. 338
Figure V- 19: Capacity as a function of cycle number for Li/Li[$Ni_{0.33}Co_{0.33}Mn_{0.33}$]$O_2$ and Li/Li[$Ni_{0.33}Co_{0.3}Ti_{0.03}Mn_{0.33}$]$O_2$ cells cycled between 4.7 and 2.0 V at 0.1 mA/cm^2. 338
Figure V- 20: SEM images of a) nanoporous $LiFePO_4$/C spheres; b) a single 3D nanoporous $LiFePO_4$/C sphere; c, d) broken 3D nanoporous $LiFePO_4$/C spheres, showing the 3D nanoporous microstructure.. 339
Figure V- 21: a) EDS maps of Fe, P, O, and C on single $LiFePO_4$/C spheres and b) HR-TEM image of a fractured surface, showing the carbon coating. 339
Figure V- 22: Rate capability of $LiFePO_4$/C sample produced by spray pyrolysis. 339
Figure V- 23: Cyclability of $LiMn_{1.5}Ni_{0.5}O_4$ and the Fe-substituted samples. 342
Figure V- 24: Comparison of the rate capabilities of $LiMn_{1.5}Ni_{0.5}O_4$ and the Fe-substituted samples. 342
Figure V- 25: EIS plots of $LiMn_{1.5}Ni_{0.5}O_4$ and the Fe-substituted samples. 342
Figure V- 26: Charge-discharge profiles and cycle life of Li2MSiO4/C. 343
Figure V- 27: Capacity as a function of discharge rate for $LiNi_{0.4}Mn_{0.4}Co_{0.22}O_2$, on a carbon nanotube mesh grid. 346
Figure V- 28: Morphology of $LiFePO_4$ substituted with 5 wt% V. 346
Figure V- 29: TGA in O_2 of $Li_2Mn_{1-y}Fe_yP_2O_7$. 347
Figure V- 30: Cycling of $Li_2Mn_{1-y}Fe_yP_2O_7$. 347
Figure V- 31: Reversible capacity and efficiency of Li/ SiOx:Gr cells in EC-DEC-$LiPF_6$. 349
Figure V- 32: Ragone plot of Li/SiOx:Gr cells in EC-DEC-$LiPF_6$ with # carbons. 349
Figure V- 33: Reversible capacity and efficiency of Li/ SiOx:Gr cells in EC-DEC-$LiPF_6$. 349
Figure V- 34: 1st cycles of Li/$LiMnFePO_4$ cells in EC-DEC 1M $LiPF_6$ at 25°C. 350
Figure V- 35: Reversible capacity and energy density of cycles 1 and 2 of Li/$LiMnFePO_4$ cells in EC-DEC 1M $LiPF_6$ at different ratios of Fe/Mn. 350
Figure V- 36: Voltage capacity profiles for "$AlPO_4$" coated $LiCoO_2$ electrodes cycled in lithium cells with $LiPF_6$ and $LiClO_4$ in EC:DMC. 352
Figure V- 37: ARXPS of O 1s region for pristine bare and "$AlPO_4$" coated $LiCoO_2$ and after 20 cycles in $LiPF_6$ and $LiClO_4$ in EC:DMC. Electrodes were analyzed without washing by the solvent unless otherwise indicated by "(W)". 352
Figure V- 38: Depth profile spectra of the Co 2p region of coated $LiCoO_2$ electrodes after 20 cycles in $LiPF_6$ and $LiClO_4$. 353
Figure V- 39: ARXPS of Ni and Mn 2p spectra for $LiNi_{0.5}Mn_{0.5}O_2$ electrodes cycled in $LiPF_6$ electrolyte before and after washing by the solvent. 354
Figure V- 40: TEM micrographs of pristine and cycled $Li_{1.2}Ni_{0.25}Mn_{0.75}O_y$. 354
Figure V- 41: Carbon coated new olivine type $LiFe_{1-x}Mn_xPO_4$ cathode materials with nano-pore structure.synthesized by the Institute of Physics, Chinese Academy of Sciences. 357
Figure V- 42: Rate capability of carbon coated new olivine type $LiFe_{1-x}Mn_xPO_4$ cathode materials with nano-pore structure. 357
Figure V- 43: Charge and discharge curves and *in situ* XRD spectra of carbon coated $LiFe_{0.8}Mn_{0.2}PO_4$ sample during charge-discharge cycling. 357
Figure V- 44: Charge and discharge curves and *in situ* XRD spectra of carbon coated $LiFe_{0.6}Mn_{0.4}PO_4$ sample during charge-discharge cycling. 357
Figure V- 45: Charge and discharge curves and *in situ* XRD spectra of carbon-coated $LiFe_{0.4}Mn_{0.6}PO_4$ sample during charge-discharge cycling. 358
Figure V- 46: Charge and discharge curves and *in situ* XRD spectra of carbon coated $LiFe_{0.2}Mn_{0.8}PO_4$ sample during charge-discharge cycling. 358
Figure V- 47: Charge and discharge curves and *in situ* XAS spectra at Ni K-edge of $Li_{1.2}Mn_{0.6}Ni_{0.2}O_2$ sample during charge-discharge cycling. 358
Figure V- 48: Charge and discharge curves and *in situ* XAS spectra of $Li_{1.2}Mn_{0.6}Ni_{0.2}O_2$ sample at Mn K-edge during charge-discharge cycling. 358

Figure V- 49: Potentiodynamic for O_2 reduction at pristine and MnO_2-loaded UMB4 and UMB5 activated carbon materials. Surface area of pores with size larger than 15Å was used to calculate the current density. Scan rate: 0.5mVs^{-1}. 359
Figure V- 50: Catalytic activity (the slope of potentiodynamic reduction curves as shown in Figure V- 49) as a function of R value. 359
Figure V- 51: Electrochemical data of uncoated and $Li_{3-2x}Ni_xPO_4$-coated $0.5Li_2MnO_3$● $0.5LiNi_{0.44}Co_{0.25}Mn_{0.31}O_2$ electrodes. 363
Figure V- 52: Initial two cycles of: (a) cathode-limited TiO_2-C/ANL-NMC100, 3.25-0.05 V, (b) anode-limited TiO_2-C/ANL-NMC125, 3.5-0.05 V, and (c) cycling performance of anode- vs. cathode-limited cells. 363
Figure V- 53: Simulated layer termination atomic arrangement of a reconstructed (111) surface in which the Mn ions (green squares) are coordinated in distorted square planar complexes, with mutual edge and corner sharing. The Li-ions (black circles) are three-fold coordinated. (Red dots are oxygen.) 364
Figure V- 54: Synthesis of $LiMnPO_4$ in a molten hydrocarbon 367
Figure V- 55: (a,b,e) FESEM and (c,h) HRTEM images of $LiMnPO_4$ nanoplates, (d) Rietveld refinement of $LiMnPO_4$, (f) simulated diffraction pattern parallel to [100], (g) nanobeam diffraction pattern, and (h) orientation of $LiMnPO_4$ grown using a molten hydrocarbon process 367
Figure V- 56: a) Voltage profiles of $LiMnPO_4$ at various discharge C rates; b) rate performances of $LiMnPO_4$; c) Ragone plot comparison of $LiMnPO_4$ to $LiFePO_4$. All the cells were constantly charged at C/25. 367
Figure V- 57: a) XRD patterns and b) cycling performances of Li_xMnPO_4 ($0.5 \leq x \leq 1.2$) 368
Figure V- 58: a) Voltage profiles and b) *cyclability* of Li_2CoPO_4F 368
Figure V- 59: Electrochemical reactions of PAQS as a cathode material during charge and discharge processes 368
Figure V- 60: a) Voltage profiles of PAQS and b) cycling stability of PAQS in different electrolytes. Current density: 50 mA/g. 369
Figure V- 61: a) XRD patterns of heat-treated $Li_xMg_xMn_{1-x}PO_4$ crystals, b) DSC profiles of $Li_xMg_xMn_{1-x}PO_4$ in the presence of the electrolyte, and c) the relationship between the heat evolved and the Mn content in the phosphates. 371
Figure V- 62: SEM images of $Li_{1.14}(Ni_{0.33}Mn_{0.33}Co_{0.33})_{0.86}$ crystals synthesized at 850°C in a $0.88LiNO_3$-0.12LiCl eutectic mixture, a) R=4 and b) R=40. 372
Figure V- 63: a) TEM and [001] zone axis electron diffraction patterns, and b) XRD patterns of $Li_{1+x}(Ni_{1/3}Mn_{1/3}Co_{1/3})_{1-x}O_2$ (x=0 and 0.14). 372
Figure V- 64: a) relationship between the amount of NO_2BF_4 used and the residual Li in the delithiated $Li_{1.14}(Ni_{0.33}Mn_{0.33}Co_{0.33})_{0.86}O_2$ crystals and b) Lattice parameters and crystallite size of the crystals. 373
Figure V- 65: SEM images of fresh and delithiated $Li_{1.14}(Ni_{0.33}Mn_{0.33}Co_{0.33})_{0.86}O_2$ crystals. 373
Figure V- 66: Lattice parameters and crystallite size of delithiated $LiNi_{0.33}Mn_{0.33}Co_{0.33}O_2$ crystals. 373
Figure V- 67: (a) HR-TEM image of nc-Si/CNT. EELS spectra of (b) CNT, (c) interface and (d) Si. 377
Figure V- 68: Discharge/charge capacity plot of *nc*-Si/CNT. 377
Figure V- 69: Variation of specific capacity and coulombic efficiency *vs*. cycle number of *a*-Si/C thin film anode. 377
Figure V- 70: XRD patterns of *a*-Si/Gr nanocomposite after 5h of MA and after thermal treatment at 773K and 1073K. 378
Figure V- 71: variation od specific capacity vs. cycle numbers of *a*-Si/C composite cycled at C/3 rate. 378
Figure V- 72: Anodic current-time responses observed in compartment B for different Al thicknesses. 381
Figure V- 73: Raman images of a $LiMnPO_4$ electrode displaying areas with strong $LiMnPO_4$ (red) and $Li_4P_2O_7$ (blue) peak intensities a) after an O_2 plasma etch, b) followed by a full charge, and c) full discharge. 382
Figure V- 74: Electrochemical performance of 70:20:10, MoO_3:PVdF:AB electrodes: bare, coated with ~ 8Å ALD Al_2O_3 and MoO_3 particles coated prior to electrode fabrication for a) cycling stability and b) rate capability. 385
Figure V- 75: Cycling performance of ANL Li-excess and Al_2O_3-coated MoO_3 full cell, with a capacity of ~ 160 mAh/g. 386
Figure V- 76: Optical images of damage caused by nanoscratching with a load of 80 mN for a) bare and b) 4-Al_2O_3 ALD coated MoO_3 composite electrodes. 386
Figure V- 77: a) Colorized SEM image of Fe_2O_3 nanoparticles (yellow/blue) suspended in an SWNT net (white) and b) durable high-rate capability. 387
Figure V- 78: a) TEM image of SWNTs conformally following $LiNi_{0.4}Mn_{0.4}Co_{0.2}O_2$ particles b) NMCCNT rate capability. 387
Figure V- 79: Performance of $TiNb_2O_7$ versus Li^+/Li with 1M $LiPF_6$/EC +DMC (1:1) half cell 390
Figure V- 80: The first discharge and charge curves for the pure distilled water and Fe^{3+} / Fe^{2+} redox couples dissolved in water 390
Figure V- 81: (a) Discharge/charge curves of Li/$Fe(NO_3)_3$ within a closed-cathode cell; (b) Hydrolysis of the $Fe(NO_3)_3$ and $Fe(NO_3)_2$ in aqueous solution. 390
Figure V- 82: X-ray diffraction pattern of a Cu-Sn-Sb multi-component electrode. 393
Figure V- 83: The electrochemical properties of a Cu-Sn-Sb multi-component electrode. 393
Figure V- 84: Cu_2Sb electrodes deposited on Cu foil under various conditions. 394
Figure V- 85: Electrochemical performance of 2-D and 3-D Cu_2Sb electrodes deposited under various conditions 394
Figure V- 86: HRTEM image of a carbon-coated SnO_2 nanoparticle produced by an autogenic reaction 394
Figure V- 87: Electrochemical profiles of the first two cycles of a lithium cell with (a) C-coated SnO_2 electrode, and (b) SnO_2 electrode after burning off the carbon coating. 395
Figure V- 88: Lithium insertion and delivery rates from the Sn-Co amorphous material (top to bottom is a-d in discussion). 398

Figure V- 89: Cycling capacity of an Al-M-C material at 0.5 mA/cm^2. 398
Figure V- 90: Cycling capacity of an Al-Si alloy at 0.5 mA/cm^2....399
Figure V- 91: Cycling capacity of a Si-C material at 0.5 mA/cm^2. 399
Figure V- 92: Cycling capacity of a Si-C material at 0.5 mA/cm^2. 399
Figure V- 93: Self-assembly process for TiO_2/graphene composites....401
Figure V- 94: (a) Charge/discharge profile of anatase TiO_2 and anatase TiO_2/graphene composite. (b) Rate performance of anatase TiO_2 and anatase TiO_2/graphene composite. (c) Cycling stability of anatase TiO_2 and anatase TiO_2/graphene composite at 1C rate...401
Figure V- 95: Formation process for porous Si/graphene composites 401
Figure V- 96: TEM images of (a) porous Si particles with selected area electron diffraction pattern (insert). (b) Cross-sectional image of porous Si/graphene nanocomposite. 402
Figure V- 97: Cycling stability of porous Si/graphene hybrid electrode at 0.1C rate 402
Figure V- 98: Cycling stability of micron-sized Si with different carbon additives 402
Figure V- 99: Si cycling stability at high current density (400 mA/g) and shallow (0.17 V to 0.9 V) cycling conditions....403
Figure V- 100: SEM images of the surface structure of porous Cu/SnO_2 composite anode sheets with Cu:SnO_2 weight ratios of 8:2 403
Figure V- 101: Battery cycling performance of macroporous Cu/SnO_2 composite anode sheets with Cu/SnO_2 at weight ratios of 95:5, 9:1, 85:15, and 8:2, along with a comparison of nano-sized SnO_2 powder coated on Cu foil. 403
Figure V- 102: a. TEM image of commercial Si nanoparticles. b. SEM image of the surface of the composite Si/conductive polymer electrode. 406
Figure V- 103: The lithium-ion doping process of the conductive polymer. 406
Figure V- 104: Cycling performance of the Si.conductive polymer composite electrode. 406
Figure V- 105: Improve 1st cycle coulombic efficiency by SLMP doping of the Si/conductive polymer anodes. 407
Figure V- 106: Salt diffusion coefficient and conductivity of symmetric PS-PEO block copolymers as a function of the molecular weight of the PEO block at 90^{o}C. 411
Figure V- 107: Impedance measurements on iodine doped polyphenylene vinylene- polyethylene oxide block copolymer. Top: No lithium salt. Bottom: With lithium salt. 411
Figure V- 108: Conductivity of PS-PE-PS and conventional Celgard separators as a function of void fraction. The caption shows the molecular weights of the blocks in kg/mol. The average pore width increases with molecular weight: 11, 22, and 25 nm and is nearly independent of void fraction. 412
Figure V- 109: Preparation of Network Single ion Conductor. 414
Figure V- 110: New salts synthesized and tested in FY10. 415
Figure V- 111: Conductivities of Li slats in PEIO as a function of temperature. 415
Figure V- 112: Exchange current densities for lithium salts in PEO as a function of temperature. 415
Figure V- 113: Conductivity of Borate salts in liquid solvents. 415
Figure V- 114: Comparison of cycling behavior of two lithium salts in EC/EMC solvents in full cells ($LiNi_{0.8}Co_{0.2}O_2$:MCMB). 416
Figure V- 115: SEI components from the reduction of EC and VC as predicted by ReaxFF MD simulations. 418
Figure V- 116: Snapshot of a simulation of an EC/DMC/$LiPF_6$ electrolyte between graphite electrodes at high potential difference between the electrodes. 418
Figure V- 117: Conductivity of EC:DMC/LiFSI electrolytes from MD simulations and experiments. *Abouimrane et al. J. Power Sources 2009, 189, 693.* 418
Figure V- 118: Scheme 1. Synthesis of (THF)Li(C2O4)(O2PPh2)2, 1. 422
Figure V- 119: ORTEP diagrams of 1 showing monomer (upper figure, THF and hydrogen atoms omitted for clarity) and dimeric association (lower figure, hydrogen atoms, phenyl rings, and THF omitted for clarity. 422
Figure V- 120: TGA analysis of solid 1. 422
Figure V- 121: Charge/Discharge Curves with and without 1 in a 2032-type coin cell (see test for details. The cells were filled directly from septum type electrolyte container without using a glove box. 423
Figure V- 122: Photograph of the cell for *in situ* ATR-FTIR measurements. 423
Figure V- 123: Structure of adsorbed Li_2CO_3 dimer at graphite defect site. 425
Figure V- 124: Calculated structure of the tetramer of LiDFOB. 425
Figure V- 125: Sample organoborate salt structure 428
Figure V- 126: :Portion of crystal structure of the $(EC)_{3/2}$:LiBOB solvate (Li: purple, B: tan, O: red) 428
Figure V- 127: Crystal structure of $LiBF_2Ox$ (Li: purple, B: tan, O: red, F: green) 428
Figure V- 128: Crystal structure of the $(DMC)_{3/2}$:$LiBF_2O_x$ solvate (Li: purple, B: tan, O: red, F: green): (a) unit cell and (b) Li+ and anion coordination - note that the central DMC molecule in (b) is disordered over two positions....429
Figure V- 129: Lithium dicyanotriazolate (LiDCTA) structure....429
Figure V- 130: DSC heating traces of the crystallized ionic liquids (5°C/min). 429

Figure V- 131: Cycling performance of lithium-ion batteries (MCMC/$LiNi_{0.8}Co_{0.2}O_2$) before (initial formation cycles) and after thermal storage at 65˚C for 2 weeks with 1 M $LiPF_6$ and 1 M $LiPF_4(C_2O_4)$ electrolytes. 432
Figure V- 132: FTIR-ATR spectra of cathodes stored at different potentials with EPDM as the binder. 432
Figure V- 133: Capacity retention of the Li/$Li_{1.17}Mn_{0.58}Ni_{0.25}O_2$ cells cycled from 2.0 to 4.9 V containing 1 M $LIPF_6$ in 1:1:1 EC/DEC/DMC with and without additives. 433
Figure V- 134: Cycling performance of graphite/ $LiNi_{1/3}Co_{1/3}Mn_{1/3}O_2$ cells with PC electrolytes. 433
Figure V- 135: RT cycling performance of coin cells made of $LiFePO_4$ cathode with different electrolytes. 433
Figure V- 136: Measure of viscosity of five slurries of identical composition but differing by order in which the constituents were combined. 436
Figure V- 137: SEMs of an electrode made from the solids process and the glue process. 436
Figure V- 138: Young's modulus and Ultimate Strain before breaking of five laminates from starting materials combined five different ways. 437
Figure V- 139: Cycling results, of cycling at a C/1 discharge and C/2 charge rate in coin cells against an NCM cathode, of anodes of differing processing steps. 437
Figure V- 140: SEMs of the anodes after cycling. On the left is an electrode from the glue process and on the right is an electrode from the solids process. 437
Figure V- 141: Cycling results of Graphite/NCM cells with the baseline electrolyte (left) and the high-voltage electrolyte (right). 438
Figure V- 142: The average shift in capacity per cycle as a result of the side reactions with the baseline electrolyte and the high voltage electrolyte when stepping up in voltage. 438
Figure V- 143: The average shift in capacity per cycle as a result of the side reactions with the baseline electrolyte and the high voltage electrolyte when stepping down in voltage. 438
Figure V- 144: Long-term cycling of full cells with HVE to an upper cut-off voltage of 4.4V. One of the cells was first cycled to 4.6 V for seven cycles. 438
Figure V- 145: Reaction current density via (a) electrochemical model and (b) thermo-electrochemical model. 441
Figure V- 146: Heat generation via thermo-electrochemical model. 441
Figure V- 147: Time history of (a) reaction current density and (b) heat generation via thermo-electrochemical model. 441
Figure V- 148: SEI layer formation via phase field model 441
Figure V- 149: TEM image of $LiMn_2O_4$ 442
Figure V- 150: (a) Surface morphology and (b) modulus mapping of $LiCoO_2$. 442
Figure V- 151: Thin film $LiCoO_2$ cathode annealed at (a) 700°C and (b) 800°C. 444
Figure V- 152: FIB machined pillar. 444
Figure V- 153: Relative vertical displacement of FIB micro-machined cylinders. 444
Figure V- 154: FEM modeling of $LiCoO_2$ micro-pillar. 444
Figure V- 155: ESM of $LiCoO_2$ grains: (a) amplitude; (b) hysteresis loops at different locations 445
Figure V- 156: Model experimental comparison for base-line (Srinivasan and Newman) and high-rate (Kang and Cedar) data 447
Figure V- 157: Extent of % State-of-Discharge disparity between small and large particles at the porous electrode/separator interface as a function of particle size distributions with an average particle size being 50 nm for a discharge process at 5C rate 447
Figure V- 158: Maximum charge capacity that can be obtained before formation of $Li_{15}Si_4$ at different applied current densities for cells cycled to 1,000; 2,000; and 3,578.6 mAh/g 448
Figure V- 159: Rate capability of cells cycled to 1000, 2000, and 3000 mAh/g with the capacity matched to a NCA cathode of 180 mAh/g capacity, 80 µm thick, 35% porosity, and 3.6 mAh/g loading 448
Figure V- 160: Stress in graphite and PVdF binder at the end of discharge as a function of rate of discharge. 448
Figure V- 161: Decrease in stress in graphite with and without open circuit. 449
Figure V- 162: Dimensionless current density along the anode/separator interface at the beginning of discharge at a 0.1 C-Rate 451
Figure V- 163: Dimensionless change in the lithium metal interface after a full cycle (discharge then charge) at various rates and a 25% depth of discharge. The dimensionless difference is calculated by dividing the change in the position of the Li after a full cycle by the average change in position after half of the cycle. 451
Figure V- 164: Current vs. time for the reduction of 1.0 M $LiPF_6$ in EC:DEC. The decreased current with time shows that products are passivating the surface, while collapsing curves for different trials show reproducibility. 451
Figure V- 165: Kinetic current i_K versus voltage for electrode after 10, 30, and 60 minute holds at 0.6 V. Increased film formation time reduces the amount of ferrocene reduction for the same overpotential. 452
Figure V- 166: Replacement of standard particle coating on a metal foil (left) with a composite of particles carbon-bonded to highly conductive carbon fibers (right). Active cathode is red, organic binder green, and carbon fibers and binder, gray. 454
Figure V- 167: Specific energy and power performance of $LiFePO_4$ cathodes prepared with Toray carbon papers of 0.11 and 0.37 mm thickness. Values are normalized for the total cathode weight, including the fibers. The solids loading of the slurry and the source of $LiFePO_4$ powder are given in the legend. 454

Figure V- 168: Rate performance from C/10 to 50C for a composite prepared of $LiFePO_4$(HQ) with loose carbon fibers and 5wt% carbon from mesophase pitch. Capacity is normalized to weight of the $LiFePO_4$ alone. 454
Figure V- 169: Thermal diffusivity measured through thin pellets with compositions shown in the legend. 455
Figure V- 170: SEM pictures of $LiNi_{0.5}Mn_{1.5}O_4$ made from MnO_2, $MnCO_3$ and hydroxide precursors. 457
Figure V- 171: Electrochemical performance of $LiNi_{0.5}Mn_{1.5}O_4$ samples cycled in Li batteries at C rate (BM=exOH). 457
Figure V- 172: ^{6}Li MAS-NMR spectra of NiO electrodes at different states of charge and discharge. 458
Figure V- 173: Representative TEM images for Sn nanoparticles. 458
Figure V- 174: Li slab space as a function of state of charge in $Ni_{1/3}Mn_{1/3}Co_{1/3-x}Al_xO_2$. 460
Figure V- 175: Li mobility barriers in $Ni_{1/3}Mn_{1/3}Co_{1/3-x}Al_xO_2$ as a function of Li slab space. 460
Figure V- 176: Li chemical diffusivity as a function of Li content in graphite, from first-principles calculations and kinetic Monte Carlo simulations. 461
Figure V- 177: Real part of Ni EXAFS data and a preliminary fit to the data of a Ni-coated electrode structure. 464
Figure V- 178: Microscope setup and principles of data processing for 3D XANES microscopy. 466
Figure V- 179: Reconstructed 3D XANES tomography data of a sample of NiO reduced halfway. 467
Figure V- 180: Tomography of a fully cycled NiO electrode. 467

List of Tables

Table II- 1: List of Milestones for the EnerDel Manufacturing Project. 25
Table II- 2: EnerG2 Nanoengineered Ultracapacitor Project Milestones. 44
Table II- 3: Cell Prototype Fabrication Facility Equipment Budget. 57
Table II- 4: List of Key Equipment for the Battery Abuse Test Facility Upgrade. 66
Table II- 5: Remaining Schedule for the Battery Abuse Test Facility Upgrade. 66

Table III- 1: Summary Requirements for PHEV Batteries 70
Table III- 2: Energy Storage Targets for Power Assist Hybrid Electric Vehicles. 71
Table III- 3: Details of Cell Chemistry Optimization Studies. 76
Table III- 4: Gap Analysis for 10 Mile (Minimum) PHEV Cell 79
Table III- 5: Gap Analysis for 40 Mile (Minimum) PHEV Cell 79
Table III- 6: 6S3P Module Abuse Test Results 80
Table III- 7: Gap Analysis for Gen 1 and 2 32113 Cells 82
Table III- 8: USABC Abuse Test Results 83
Table III- 9: Gap Analysis for 6 Ah Prismatic HEV Cell 83
Table III- 10: Material Process Robustness Verification Runs 95
Table III- 11: Summary of Characterization Data from Large-scale Simulation Runs. 95
Table III- 12: Electrode Preparation Summary. 96
Table III- 13: Thermal Ramp test Reproducibility 96
Table III- 14: Thermal Runaway Threshold Data 96
Table III- 15: BSF Results for 18650 Cells 97
Table III- 16: Electrode Preparation Summary Table. 98
Table III- 17: Summary Table for 18650 Fabricated Cells 98
Table III- 18: Results of Internal, Nail Tip and External Voltages for the 18650 Cells Prepared with BC-618 Benchmark 98
Table III- 19: Results for 160 ºC Hot Block Abuse Testing 98
Table III- 20: Average Discharge Pulse Resistance Results for Cycled Cells 99
Table III- 21: Available Energy Results for Cycled Cells 99
Table III- 22: Improved dispersion quantities from sonication and IPA. 102
Table III- 23: Theoretical Cost Analysis for NCM Compositions 111
Table III- 24: Electrical conductivity of electro-spun carbon nano-fibers produced by Angstron 113
Table III- 25: Redox potentials and diffusion coefficients for DDB, BDB, and $Li_2B_{12}F_{12}$ in various electrolytes at 25°C (first two are literature values). 125
Table III- 26: Moisture and HF content of electrolytes with DDB and BDB. 126
Table III- 27: Datasets used for fitting NCA/graphite Li-ion life model. 145

Table III- 28: Design Variables Examined in this Study 151
Table III- 29: Survey of existing battery modeling capabilities at the DOE National laboratories 188
Table III- 30: Dual foil case study: analyzing input and output.....188

Table IV- 1: Investigators and Materials Status.....216
Table IV- 2: Fracture Toughness Obtained via a Single Edged Notched Bend (SENB) test.....223
Table IV- 3: Optimum particle sizes for lithiation halfway (to Li_2CuSn) and one for full lithiation (to $Li_{17}Sn_4$). 223
Table IV- 4: Viscosity of Selected INL Phosphazene Additives at Room Temperature with and without Salt.....266
Table IV- 5: Salt Saturation Limits ($LiPF_6$) in INL Phospazenes at Room Temperature.....266
Table IV- 6: Electrode composition and constitution 274
Table IV- 7: Final composition of electrodes for the PHEV cell build 291
Table IV- 8: Cell distribution 295
Table IV- 9: Initial values from cells used in the calendar life test. 295
Table IV- 10: Physical and chemical properties of carbon anodes.....308
Table IV- 11: Anode description for 2% VC cells 312

Table V- 1: ICP results and initial discharge capacities at C/50 for Li_xMnPO_4 ($0.5 \leq x \leq 1.2$) 368
Table V- 2: Thermal Events, Temperature, and Mass Loss Assignments based on the data in Figure V- 120 422

I

Introduction

A. Vehicle Technologies Program Overview

B. Energy Storage Research & Development

I. INTRODUCTION

In 2010, the U.S. continued a slow recovery from the severe recession of 2009. As part of that recovery, sales of U.S. light duty vehicles rebounded slightly to approximately 12 million from less than 10 million in 2009. Sales of hybrid electric vehicles (HEVs) remain in the two to three percent range. The U.S. government continued its strong R&D support of electric drive vehicles (EDVs), including HEVs, plug-in hybrid electric vehicles (PHEVs), and pure electric vehicles (EVs). In 2010, the United States Department of Energy (DOE) also completed all contract negotiations with the recipients of the American Recovery and Reinvestment Act (ARRA) grants announced earlier[1] for the construction of advanced battery and battery component manufacturing facilities. A description of the battery manufacturing grants is presented in Chapter II.

An important step for the electrification of the nation's personal transportation and for the continued success of the new domestic Li-ion battery manufacturing factories is the development of more cost-effective, long lasting, and abuse-tolerant Li-ion batteries. DOE's continuing R&D into advanced batteries for transportation offers the possibility of reducing our dependence on foreign oil and the negative economic impacts of crude oil price fluctuations. It also supports the Administration's goal of deploying 1 million PHEVs by 2015. During the fiscal year (FY) 2010, battery R&D work continued its focus on high-energy batteries for PHEVs and EVs.

I.A Vehicle Technologies Program Overview

The DOE's Vehicle Technologies (VT) Program develops advanced transportation technologies that would reduce the nation's use of imported oil. Technologies being supported by VT include hybrid drive technologies, advanced energy storage devices (batteries and ultracapacitors), power electronics and motors, advanced structural materials, and advanced combustion engines and fuels[2].

DOE works with industry, universities, and national laboratories under the FreedomCAR and Fuels Partnership. Collaboration with automakers enhances both the relevance and the potential for success of these programs. DOE works with the U.S. automakers through the United States Council for Automotive Research (USCAR)—an umbrella organization for collaborative research among Chrysler LLC, Ford Motor Company, and General Motors Company[3]. This partnership is focused on funding high-reward/high-risk research that promises improvements in critical components needed for more fuel efficient and cleaner vehicles.

I.B Energy Storage Research & Development Overview

I.B.1 Programmatic Structure

The energy storage research and development effort within the VT Program is responsible for researching and improving advanced batteries and ultracapacitors for a wide range of vehicle applications, including HEVs, PHEVs, EVs, and fuel cell vehicles (FCVs). Over the past few years, the emphasis of these efforts has shifted from high-power batteries for HEV applications to high-energy batteries for PHEV and EV applications.

The energy storage effort includes multiple activities, from focused fundamental research, to applied R&D, to hardware development with industry. The activities begin by establishing technical requirements for the energy storage technologies in cooperation with industry. Next, commercially available batteries are evaluated against those requirements. If requirements are unmet, additional R&D takes place, which involves either short-term directed research (applied research) by commercial developers and national laboratories, or exploratory research, generally spearheaded by the national laboratories. Thus, there are three major inter-related and complementary program elements, namely:

- Advanced Battery Development, System Analysis, and Testing.

[1] http://www.whitehouse.gov/the-press-office/24-billion-grants-accelerate-manufacturing-and-deployment-next-generation-us-batter

[2] See http://www1.eere.energy.gov/vehiclesandfuels/ for more information.

[3] For more information, please see http://www.uscar.org/guest/view_partnership.php?partnership_id=1.

- Applied Battery Research (ABR)
- Focused Fundamental Research, or Batteries for Advanced Transportation Technologies (BATT)

The *Advanced Battery Development, System Analysis, and Testing program*'s goal is to support the development of a U.S. domestic advanced battery industry whose products can meet electric drive vehicle performance targets. This includes battery and materials development projects, systems analysis, and testing. The technologies include lithium-ion batteries, ultracapacitors, and separators (since the separators contribute significantly to the total system cost). The activity takes place in close partnership with the automotive industry, through our cooperative agreement with the United States Advanced Battery Consortium (USABC). In FY 2010, the USABC initiated cost-shared contracts with eight developers to further the development of batteries for EVs, PHEVs, and new low-cost, low-energy HEVs. DOE also works directly with industry battery and material suppliers via National Energy Technology Laboratory (NETL) contracts – nine of which were active in FY 2010. Benchmark testing of emerging technologies is performed to remain abreast of the latest industry developments. Battery technologies are evaluated according to USABC Battery Test Procedures Manuals for the relevant EDV applications[4,5,6]. Additional R&D involves thermal management issues for battery systems, which need to be addressed to avoid degradation in battery performance, and reduced life when encountering a greater likelihood of abusive conditions.

The *Applied Battery Research* (ABR) assists industrial developers of high-energy/high-power lithium-ion batteries meet the FreedomCAR long-term battery-level PHEV energy density (~200 Wh/kg) goal, while simultaneously meeting the cost, life, abuse tolerance, and low-temperature performance goals. The ABR projects cover materials development, calendar and cycle life studies, and abuse tolerance studies. ABR utilizes the expertise of six national laboratories, industry, and several universities. There is general agreement on major barriers to using lithium-ion batteries in PHEVs. Those include:

- Inadequate energy density and specific energy to meet the "charge-depleting" energy requirement, within the weight and volume constraints, for the 40-mile all-electric-range mid-size passenger PHEV.
- Insufficient cycle life stability to achieve the 3,000 to 5,000 "charge-depleting" deep discharge cycles.

The *Focused Fundamental Research* activity, also called the Batteries for Advanced Transportation Technologies (BATT) activity, addresses fundamental issues of chemistries and materials associated with lithium batteries. It attempts to gain insight into system failures, develops models to predict failure and to optimize systems, and researches new and promising materials. It emphasizes the identification and mitigation of failure modes, coupled with materials synthesis and evaluation, advanced diagnostics, and improved electrochemical models. Battery chemistries are monitored continuously with periodic substitution of more promising components based on advice from within this activity, from outside experts, and from the assessments of world-wide battery R&D. The work is carried out by a team headed by the Lawrence Berkeley National Laboratory (LBNL) and involves several other national labs, universities, and commercial entities. BATT currently carries out investigations into three baseline systems:

- A high-energy cell with $LiNi_{1/3}Mn_{1/3}Co_{1/3}O_2$ cathode, $LiPF_6$-EC-DEC electrolyte, and carbon-coated graphite anode.
- A low-cost and abuse-tolerant $LiFePO_4$ system to develop significantly improved materials using liquid or gel electrolytes. This is regarded as a moderate-energy, low-voltage system that is inherently stable and has low cost.
- A low-cost high-power cell, with high-rate spinel system, aiding work in Applied Battery Research

Small business innovation research (SBIR) contracts are also supported by VT, in addition to the R&D described above. SBIR projects have been the source of new ideas and concepts over the years. Currently active Phase I and Phase II energy storage SBIR contracts represent a value of over $8 million, utilized at the rate of $2 – $3 million per year. These SBIR projects are focused on the development of new battery materials and components.

Coordination within DOE and with other government agencies is a key attribute of the VT energy storage R&D effort. VT coordinates efforts on energy storage R&D with the DOE Office of Science, the DOE Office of Electricity, and the Advanced Research Projects Agency – Energy (ARPA-E). VT also has established extensive and comprehensive ongoing coordination efforts with other government agencies in energy storage R&D. Such efforts include membership and participation in the Chemical Working Group of the Interagency Advanced Power Group (IAPG), active participation in

[4] United States Advanced Batteries Consortium, USABC Electric Vehicle Battery Test Procedure Manual, Rev. 2, U.S. Department of Energy, DOE/ID 10479, January 1996.
[5] U.S. Department of Energy, PNGV Battery Test Procedures Manual, Rev. 2, August 1999, DOE/ID-10597.
[6] United States Council for Automotive Research, RFP and Goals for Advanced Battery Development for Plug-in Electric Vehicles, http://www.uscar.org/.

program reviews and technical meetings sponsored by other government agencies, and coordinating the participation of representatives from other government agencies in the contract and program reviews of DOE-sponsored efforts. Recent attendees have included representatives from such agencies as the U.S. Army – Tank-Automotive Command (TACOM), the U.S. Army – Communications-Electronics Research, Development, and Engineering Center (CERDEC), the National Reconnaissance Office (NRO), the Central Intelligence Agency (CIA), the Office of Naval Research (ONR), the Naval Surface Warfare Center (NSWC), the National Aeronautics and Space Administration (NASA), and the Jet Propulsion Laboratory (JPL). DOE also coordinates with the Department of Transportation/National Highway Traffic Safety Administration (DOT/NHTSA), the Environmental Protection agency (EPA), and with the United Nations Working Group on Battery Shipment Requirements. Additional international collaboration occurs through a variety of programs and initiatives. These include: the International Energy Agency's (IEA's) Implementing Agreement on Hybrid Electric Vehicles (IA-HEV), the eight-nation Electric Vehicle Initiative (EVI), and the Clean Energy Research Center (CERC) bilateral agreement between the US and China.

I.B.2 Some Recent Highlights

This section contains brief summaries of a few key technical accomplishments in FY 2010 resulting from the Energy Storage R&D and associated efforts. These accomplishments were selected from the many active projects and each represents a significant degree of accomplishment within the project, or the completion of a significant milestone, or a significant breakthrough of another kind that took place during the year.

- **DOE-supported technologies move to commercial applications.** Several technologies, developed partially under VT-sponsored projects, have moved into commercial applications. Hybrid electric vehicles on the market from BMW and Mercedes are using lithium-ion technology developed under projects with Johnson Controls–Saft (JCS). Lithiuim-ion battery technology developed partially with DOE funding of a USABC project at Compact Power Inc. (CPI) is being used in GM's Chevrolet Volt extended-range electric vehicle and has been selected for the upcoming Ford Focus EV battery. Eaton announced that it would use batteries from that CPI plant for future Eaton hybrid drive heavy vehicles. Johnson Controls-Saft began supplying lithium-ion battery packs to Azure Dynamics for electric delivery vans built on the Ford Transit Connect platform. A123Systems was selected to develop and produce lithium-ion battery systems for the Navistar Modec Electric trucks. A123Systems will supply lithium-ion batteries for use in the Fisker Karma luxury EV.
- **Recovery Act Facilities Projects Initiated and Production Underway.** All projects for battery and materials manufacturing facilities funded by the American Recovery and Reinvestment Act were initiated. Production began at several facilities, including separator material production at Celgard LLC in Charlotte, NC, cell and pack at A123Systems in Livonia, MI and battery pack assembly at the General Motors facility in Brownstown, MI and at Johnson Controls–Saft in Holland, MI.
- **Nanophosphate Technology for HEV Applications.** A123Systems developed a 32113 cylindrical cell which meets USABC FreedomCAR targets for power, energy, and cycle life. These cells underwent HEV cycle life testing through 360,000 cycles, and projections indicate that more than 450,000 cycles will be achieved prior to a 20% capacity fade. Cells were tested using standard USABC abuse test protocols and they achieved European Council for Automotive R&D (EUCAR) safety ratings of 3 or lower.
- **Novel Battery Thermal Management System.** LG Chem, Michigan (previously called Compact Power, Inc.) developed a unique battery thermal management system which incorporates a pack-internal refrigerant loop to cool the air within the battery pack slowly circulated around the cells. The large temperature gradient between the air and the cells facilitates efficient heat transfer without the need for high velocity air circulation. This system also obviates the need for complex coolant manifolds within the pack. During 2010, 6 battery packs were delivered for testing.
- **Nickel-Manganese-Cobalt (NMC) Prismatic Cell for PHEVs.** Johnson Controls-Saft (JCS) combined Saft cell technology with Johnson Controls, Inc. (JCI) automotive system expertise. During 2010, JCS transitioned from Saft-developed, Nickel-Cobalt-Aluminum (NCA)-graphite, cylindrical cells to a new JCS-designed, NMC-graphite, rigid prismatic cell. Hundreds of prismatic cells were fabricated in new facilities at the JCS Milwaukee Technical Center. The new prismatic design provides a significant improvement in volumetric energy density, with a projected system volume of 65 liter for a 20-mile all-electric-range PHEV system.
- **Nanophosphate Prismatic Cell for PHEVs.** A123Systems developed a 19-Ah prismatic cell which is projected to meet the USABC FreedomCar power and energy targets for 10-mile and 40-mile PHEV applications. Improvements in cell performance enabled a 23% reduction in the battery size factor (BSF) and significantly reduced the system

cost. Safety and abuse tests resulted in EUCAR ratings of up to 4. During 2010, prototype and process development were completed, and a US production facility opened in Livonia, MI.

- **Advanced Cathode Material for PHEVs.** 3M Corporation developed advanced cathode materials made from $Li[Ni_xMn_yCo_{1-x-y}]O_2$ with $x \neq 1/3$ (advanced NMC) that provide 10% higher energy (Wh/kg) and 15% lower raw material cost compared to the baseline NMC $Li[Ni_{1/3}Mn_{1/3}Co_{1/3}]O_2$, while maintaining comparable or higher thermal stability and cycle life performance.
- **Inorganic-Filled Separators for HEV/PHEV Applications.** Entek Membranes, LLC developed separators with an interconnected three-dimensional inorganic network that prevents high temperature shrinkage and internal shorts. Entek produced 20-30 microns thick, inorganic-filled separators that shrank less than 3.3% after heating in an inert atmosphere for one hour at 200°C. The excellent stability of the separator at high temperature is expected to improve abuse tolerance of Li-ion cells (e.g. internal short circuit).
- **High-Temperature Melt Integrity (HTMI) Separator.** Celgard, LLC determined that three tests on battery separator materials are critical to understanding thermal failure modes: hot tip, hot electrical resistance, and thermomechanical analysis. Celgard used these tests as a standard methodology to rapidly screen materials for their potential HTMI behavior. Using this technique, Celgard successfully developed an HTMI lithium-ion battery separator that maintains structural integrity at temperatures where typical shutdown mechanisms can fail.
- **Pre-lithiating graphite and Sn anode materials, reducing first cycle irreversible capacity-loss.** First-cycle loss is a significant issue for many high-energy anode materials, including Si, Sn, and intermetallic materials. Lawrence Berkeley National Laboratory (LBNL) discovered that lithium-nitride metathesis is useful in preparing partially-lithiated anode-materials, including graphite, Si, Al, and tin. The open circuit voltage of a prelithiated anode is much lower than that of the untreated material, substantially reducing the Li lost during the first charge. The reactions can be carried out in the presence of carbon black so that subsequent mixing is unnecessary.
- **Surface-coated, high-energy cathode material with good cycling capability and a capacity of 190 mAh/g.** Argonne National Laboratory (ANL) improved the power capability of their high capacity, layered-layered cathode by applying a nickel phosphate coating. Structurally-integrated electrode materials, such as 'layered-layered' $xLi_2MnO_3 \bullet (1-x)LiMO_2$ systems in which M is predominantly Mn, Ni and Co, yield high capacities (240-250 mAh/g) when discharged at relatively low rates (C/10), but exhibit much lower capacities at higher rates. The charge/discharge reactions of '$LiNiPO_4$'-coated electrodes were 100% efficient, delivering improved capacities of 184 – 193 mAh/g when cycled at the 1C rate between 4.6 and 2.0 V.
- **New Additive for Li-ion and Li-Air Electrolytes.** Brookhaven National Laboratory (BNL) developed a new electrolyte for high voltage Li-ion batteries and Li-air batteries. This research has resulted in a new boron-based additive with combined molecular structure with functionalities of both anion receptors (BBAR) and stable SEI film formation capability. A provisional patent application was submitted.
- **Development of Rapid, *in situ* Impedance Measurement Technique.** Idaho National Laboratory collaborated with the University of Montana and Qualtech Systems, Inc. to develop an inexpensive and rapid technique of measuring the impedance of a battery. Laboratory impedance measurements typically require costly equipment (costing up to $50,000), have to be performed in a lab environment, and typically take ~60 minutes. The newly developed technique measures impedance quickly (in about 10 seconds) using low-cost hardware (costing $50 or less) that can be embedded in the battery while in the vehicle. Impedance determination is a crucial step in establishing the battery state-of-health. The technique has been validated and the results closely matching standardized impedance spectroscopy measurements when the battery is at rest.

I.B.3 Organization of this Report

This report covers all the projects currently ongoing or starting as part of the energy storage R&D effort within the Office of Vehicle Technologies. Chapter II contains information on the projects which are funded under the American Recovery and Reconstruction Act (ARRA) of 2009 (the Recovery Act). A list of the ARRA grant recipients is provided in Appendix A. Chapter III focuses on the battery development program. Chapter IV lists all the projects which are being conducted under the Applied Battery Research activity in which ANL has a leading role. Similarly, Chapter V lists all the projects which are part of the Focused Fundamental Research activity with a leading role by LBNL. A list of the individuals who contributed to this annual progress report or otherwise are collaborating with the energy storage R&D effort appears in Appendix B. A list of acronyms is provided in Appendix C. An electronic version of this report can be accessed at http://www1.eere.energy.gov/vehiclesandfuels/resources/fcvt_reports.html.

We are pleased with the progress made during the year and look forward to continued work with our industrial, government, and scientific partners to overcome the remaining challenges to delivering advanced energy storage systems for vehicle applications.

David Howell
Team Lead, Hybrid and Electric Systems
Vehicle Technologies Program

Tien Q. Duong
Manager, Exploratory Technology Research
Vehicle Technologies Program

Peter W. Faguy
Manager, Applied Battery Research
Vehicle Technologies Program

Brian Cunningham
Lead, Battery Testing, Analysis and Design
Vehicle Technologies Program

II

AMERICAN RECOVERY & REINVESTMENT ACT (ARRA) OF 2009

A. Integrated Battery Materials Production, Cell Manufacturing, and Battery Assembly Facilities

B. Battery Cell and Pack Assembly Facilities

C. Battery Materials Production Facilities

D. Battery Recycling Facilities

E. Battery Research Facilities

II. AMERICAN RECOVERY & REINVESTMENT ACT (ARRA) OF 2009

The American Recovery and Reinvestment Act of 2009 (ARRA) (Public Law 111-5) is an economic stimulus package enacted by the 111th United States Congress in February 2009. This Act of Congress is based largely on proposals made by President Obama early during his Administration and is intended to provide a stimulus to the U.S. economy in the wake of an economic downturn. The measures are nominally worth $787 billion and include federal tax cuts, expansion of unemployment benefits and other provisions, including domestic spending in education, health care, and infrastructure, including that in the energy sector.

As part of ARRA implementation, on August 5, 2009 President Obama announced $2.4 Billion in manufacturing grants to accelerate the manufacturing and deployment of the next generation of U.S. batteries and electric vehicles – by funding 48 new advanced battery and electric drive components manufacturing and electric drive vehicle deployment projects – including PHEV and EV demonstration and education projects – in over 20 states. The grantees were selected through a competitive process conducted by DOE and are intended to accelerate the development of U.S. manufacturing capacity for batteries and electric drive components as well as the deployment of electric drive vehicles to help establish American leadership in developing the next generation of advanced vehicles. The new awards included $1.5 billion in grants to U.S. based manufacturers to produce batteries and their components and to expand battery recycling capacity, distributed over all parts of the country. As shown in Figure II- 1, these grants cover a range of manufacturing areas including those associated with material supply, cell components, cell fabrication, pack assembly, and recycling. The amounts for the individual grants are tabulated in Appendix A.

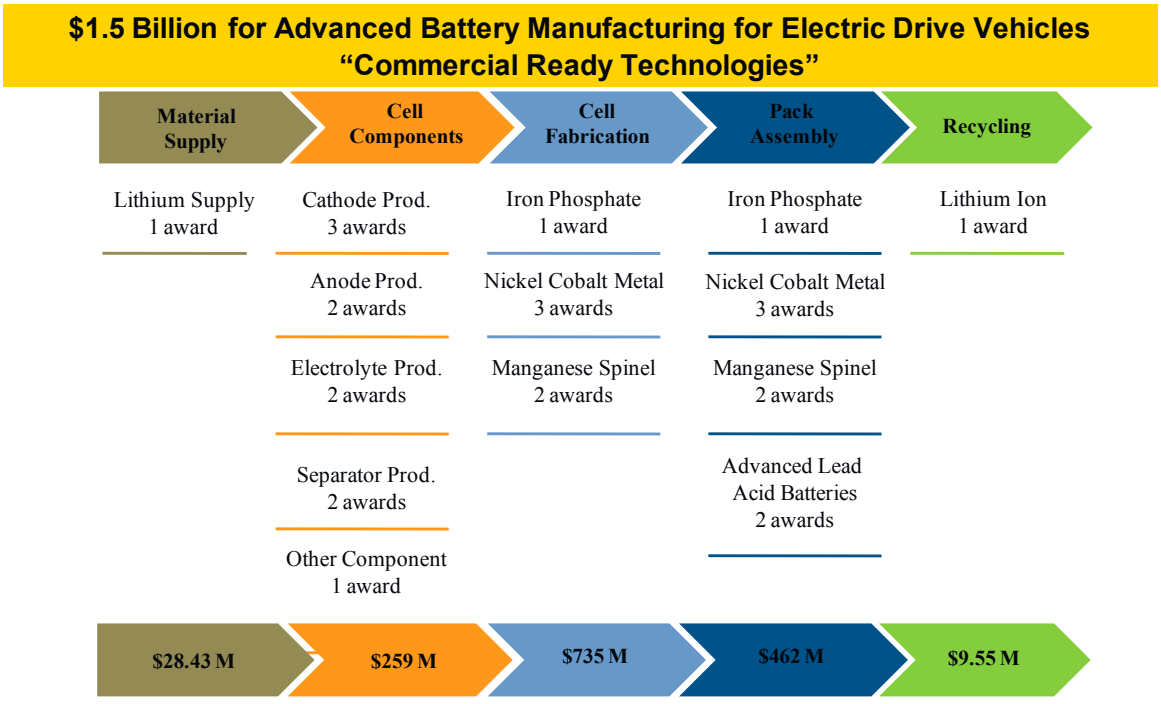

Figure II- 1: American Recovery and Reinvestment Act (ARRA) 2009 grants distribution for battery and electric drive manufacturing.

The rest of this section presents a brief summary of the individual ARRA grants.

II.A Integrated Battery Materials Production, Cell Manufacturing, and Battery Assembly Facilities

II.A.1 Domestic advanced battery industry creation project (Johnson Controls, Inc.)

Christopher Johnson (NETL Project Manager)
Grant Recipient: Johnson Controls, Inc.

Eric Ellerman
5757 N. Green Bay Ave.
Milwaukee, WI 53209
Phone: (414) 524-27080
E-mail: eric.j.ellerman@jci.com

Start Date: July 2009
Projected End Date: October 2012

Objectives

- Stand up a domestic advanced battery industry scaled to be globally competitive
- Build a demand base
- Manufacture battery cells and systems
- Create jobs
- Build a domestic supply chain
- Accelerate the deployment of charging infrastructure

Technical Barriers

Addressing market demand vs. capacity barriers: Market demand for advanced energy vehicle batteries is projected to lag manufacturing capacity

Addressing the domestic supply chain barrier: Nearly all the batteries for hybrid electric vehicles and plug-in electric vehicles, along with the materials and equipment to manufacture them, are made in Pacific Rim countries

Addressing the barriers to domestic technology development: The U.S. needs to reestablish our position as the world leader in transferring innovation into commercially successful products that are made in the U.S.

Technical Targets

Johnson Controls' goals

- Invest in America
- Invest in people
- Deliver successes
- Install state-of-the-art equipment
- Reduce costs
- Ensure employee safety

American Reinvestment and Recovery Act (ARRA) Goals

- Create new jobs and save existing ones
- Spur economic activity and invest in long-term growth
- Foster unprecedented levels of accountability and transparency in government spending

DOE Vehicle Technologies Program Goals

- Develop energy efficient and environmentally friendly highway technology
- Use less petroleum
- Increase mobility
- Promote energy security
- Lower cost and reduced impact on environment

Accomplishments

Accomplishments towards Johnson Controls goals – overview:

- Investing in America
  - We are making an investment in the U.S. to build an advanced energy industry
  - Developing and bringing advanced products to market

- Investing in people
  - We are hiring engineers, technicians, and an experienced manufacturing workforce in the U.S.
- Delivering successes
  - Vehicles that use our batteries, like the Ford Transit Connect Electric, are reaching the public with great interest and success
  - We are building a domestic supply base, as well as anchoring foreign suppliers in the U.S.
  - Our plant is has already begun domestic production of complete advanced battery systems this year, full ramp-up next year

Accomplishing Johnson Controls goals – manufacturing excellence

- Installing state-of-the-art equipment to deliver:
  - Automotive quality product
  - High volume capability
  - Significantly reduced cost
  - Minimized environmental impact
  - Processing efficiency
- Reducing costs
  - Domestic production will allow us to reduce shipping and duty costs from our European plant
  - Domestic sourcing
  - Design optimization
  - Manufacturing process optimization
  - Johnson Controls operational excellence, Best Business Practices, and continuous improvement

Accomplishing Johnson Controls' goals – sustainability:

- Certified LEED® factory
  - Our plant performs more efficiently with less impact on the environment
- Cooling for free
  - Our plant's cooling towers relieve significant pressure from our facility's chiller plant
  - As a result, the plant will have more consistent operating costs throughout the year
- Recovering heat
  - Heat from the battery formation process is captured and used in other areas of battery manufacturing
- Reclaiming what would have been wasted
  - We have designed our processes to reclaim materials used in manufacturing to save time, cost and energy

Accomplishing Johnson Controls' goals – employee safety:

- At Johnson Controls, maintaining a safe, clean and sustainable environment for our employees is our top priority. Our safety plan is explicit:
  - Equipment must provide adequate protection from hazards or safety risks to the operators or to those who are working on or in the area during normal operation, standing alone or during its non-production functions (e.g., manual cycles, set up modes, re-work modes, etc.). Servicing and Maintenance for equipment must be user friendly, safe, and convenient. In order that these goals may be met, Johnson Controls has compiled this specification, which represents Johnson Controls' interpretation of applicable standards and laws. Johnson Controls must authorize all deviations from this specification.

Accomplishments towards ARRA goals:

- Employing people – high quality jobs are being created
  - In the previous quarter, this project has directly resulted in 100.4 FTE jobs in the U.S.
  - The Holland, Michigan plant will employ 98 workers by the end of next year. 303 permanent full time jobs will be created when at full capacity
- Spurring economic activity
  - $66.7M has been spent on customer programs, materials, equipment and service suppliers; 95% of that has been with U.S.-based suppliers
- Growing for the long-term
  - We are building a sustainable business model that does not rely on Government subsidies
- Defining accountability
  - Meeting all reporting requirements of the ARRA and the DOE
  - Our program office proactively self monitors and self audits internal processes and procedures to ensure uncompromised integrity in the use of tax payer dollars

Accomplishments towards DOE Vehicle Technology goals

- Energy efficient and environmentally friendly highway technology
  - Vehicles powered by our Li-ion batteries, including Daimler, BMW, Azure Dynamics, and Ford, produce fewer emissions and get better fuel

economy than conventional internal combustion engines

- Reduced petroleum consumption
  - Our combination of HEVs, PHEVs, and EVs reduce or eliminate petroleum usage
- Freedom of mobility
  - Battery technology gains in cycle life and energy density are providing Americans with extended all-electric range vehicles to eliminate range anxiety
- Energy security
  - Domestic advanced energy products improve energy security by reducing petroleum imports and minimizing the possibility of a foreign battery cartel
- Lower cost and reduce impact on environment
  - Batteries manufactured at our facility are optimized for cradle-to-cradle product lifecycle, including recycling and the recovery of key materials

Introduction

The $299 million grant by the United States Department of Energy under the American Recovery and Reinvestment Act (ARRA) is designed to build domestic manufacturing capacity for advanced batteries for hybrid and electric vehicles. This award represents approximately half of Johnson Controls' total planned investment of $600 million in domestic advanced battery manufacturing capacity and infrastructure development.

Approach

The $299 million grant by the United States Department of Energy under the American Recovery and Reinvestment Act (ARRA) is designed to build domestic manufacturing capacity for advanced batteries for hybrid and electric vehicles. This award represents approximately half of Johnson Controls' total planned investment of $600 million in domestic advanced battery manufacturing capacity and infrastructure development. Towards that objective, Johnson Controls has been specifying manufacturing equipment and analyzing equipment quotes, hiring plant management, preparing on-boarding and training procedures for new plant employees, and putting the plant system infrastructure in place. Other work includes business development, forming partnerships and alliances, and the program work necessary to build this industry.

Results

Johnson Controls is meeting our internal goals, plus the goals of the American Reinvestment and Ecovery Act and those of the DOE Vehicle Technologies program.

Conclusions and Future Directions

Currently:

- Our Holland, Michigan plant is assembling battery packs and shipping them to our customers
- We are delivering market-derived solutions to transportation needs

In the remainder of the project:

- Our Holland, Michigan plant will begin to manufacture advanced Li-ion cells
- We will be assemble complete battery packs with domestically produced cells
- Accelerate market demand to support the full capacity of our plant
- Continue to win production contracts to produce xEVs
- Continue to develop our technology roadmap to maintain Johnson Controls leadership position

Takeaways

- Market demand will only increase when the economics are equal or better than internal combustion engines. Johnson Controls is leveraging our position as a technology leader and investigating the electrification of our fleet
- Johnson Controls, with ARRA matching grant funding as a catalyst, is developing a domestic supply base. We are sourcing all major components of our cells domestically.
- The ARRA matching grant has knocked down the barrier to building manufacturing domestically. The matching grant solidified Johnson Controls' decision to expand advanced battery production in the US versus Europe or Asia.

FY 2010 Publications/Presentations

1. 2010 DOE annual merit review poster session

II.A.2 Vertically Integrated Mass Production of Automotive Class Lithium-ion Batteries (A123Systems)

Ralph Nine (NETL Project Manager)
Grant Recipient: A123Systems

Andy Chu
321 Arsenal Street
Watertown MA 02472
Phone: (617) 778-5700; Fax: (617) 924-8910
E-mail: jalvarez@a123systems.com

Start Date: December 3, 2009
Projected End Date: December 2, 2012

Objectives

The overall objective of this project is to establish the manufacturing capability in the US to produce at least 500 MWh of automotive lithium-ion batteries per year by the end of 2012. A123Systems will build a vertically-integrated automated factory capacity that encompasses the full production process, including: the manufacturing of cathode powder, electrode coatings, cell fabrication, module fabrication, and the assembly of complete battery pack systems ready for vehicle integration. Design and production validation will also be performed under this program, ensuring that the process transfer is optimized, the products meet customer specifications, and that the production lines conform to standard automotive practice.

Technical Barriers

The manufacturing scale-up requires the design, installation, and qualification of many different processes, resulting in products that must meet stringent automaker performance and quality standards In addition, A123Systems is transferring our existing processes from our Asian facilities into the US plants as fully automated operations.

Technical Targets

- Produce 500 MWh of automotive lithium-ion batteries per year by the end of 2012

Accomplishments

- In less than one year, A123Systems has designed, installed, qualified, and started production of automotive batteries in the Livonia facility.
- A123Systems has started the construction phase of the Coating plant in the Romulus facility
- With the excellent progress on this program, in addition to the strong customer demand, A123Systems has accelerated the manufacturing plan, which is now scheduled to reach 30 cells per minute (cpm) by the end of 2011. This is equivalent to 1 million cells per month of cell output that will be used to manufacture battery packs. Each pack has between 250 – 500 cells.

Approach

The general philosophy of manufacturing expansion is to cost-effectively meet the rapidly escalating customer volume needs while managing operational risk. This approach began with transferring our existing low-risk, mature process technologies from Asia, improving the processes and level of automation, and systematically increasing throughput and lowering costs over time. The first portion of the build-out involves the rapid deployment, using a "Copy Improve" approach wherein the initial Livonia cell and module/pack factory capacity will be installed with the same processes and equipment currently used in A123Systems' Asian factories, while increasing the level of automation for material movement and process control to increase output and boost productivity. This work will mostly occur in 2010.

The second portion of the build-out uses nearly identical equipment as what is used in the Liovnia production factory, but with increased throughput at specific operations that are at low risk. This "Factory of the Future" approach for high volume manufacturing (HVM) capacity will further reduce cost and headcount through additional automation, data collection and improved manufacturing execution platforms. Although this design work starts in 2010, the production facilities will not be operational until 2011, with additional capacity being brought online in 2012. This approach will be used as A123Systems brings up the Coating and Powder operations at the Romulus campus.

Results

Project 1 – Livonia – Cell Assembly/Module & Pack

- Dry Rooms have been completed and comissioned

- Cell Assembly equipment delivered, installed, and qualified
- Formation and Aging automated equipment installed and qualified
- Lot Q and DVP&R areas completed
- Automated Module and Pack Assembly lines are being installed and qualified

Project 2 – Romulus – Powder & Coating

Design completed and bid packages issued for Dry Rooms and long Lead items

- Dry rooms and major utilities being installed
- Coater 1 installation and qualification has begun
- Coater 2 in transit
- Started discussions for 2nd Romulus facility
- Powder facility design concept started

Project 3 – Romulus – Cell Assembly & Module/Pack

- Negotiating leases and potential timing of construction

Photos of the Livonia facility are included in Figure II- 2.

Conclusions and Future Directions

A123Systems will continue to increase the manufacturing capability for cell, module, and pack production in Livonia. The Romulus Coating facility will be qualified and operational in 2011. The Romulus expansions will continue thru 2012.

FY 2010 Publications/Presentations

1. 2010 DOE Annual Peer Review Meeting Presentation

Figure II- 2: Photos of the A123Systems Livonia Facility

II.A.3 Accelerating the Electrification of U.S. Drive Trains: Ready and Affordable Technology Solutions for Domestically Manufactured Advanced Batteries (Exide Technologies)

Bruce W. Mixer (NETL Project Manager)
Grant Recipient: Exide Technologies

Bob Kuhlke
13000 Deerfield Pkwy Ste 200
Milton, GA 30004
Phone: (678) 566-9023; Fax: (678) 566-9613
E-mail: bob.kuhlke@exide.com

Start Date: December 3, 2009
Projected End Date: December 2, 2012

Objectives

- This project covers the expansion of Exide Technologies' manufacturing capacity for producing advanced batteries in existing U.S.-based battery plants.
  - The project plan is to implement a combined increase in yearly production capacity of 1.5 million additional units at two of Exide's current manufacturing locations:
    - Columbus, Georgia
    - Bristol, Tennessee
  - These advanced battery technologies are targeted to have an accelerated near-term impact (in high volume) for micro-hybrid vehicles, idle reduction commercial vehicles, and other strategic market segments.

Description

This manufacturing expansion project involves two of Exide's global technologies: a Spiral Wound Absorbed Glass Mat (AGM) design and a Flat Plate AGM design, both of which will be manufactured with advanced carbon technology as required by customer specific advanced vehicle applications.

The Exide Advanced Battery Expansion Project Addresses Key Program Targets - ARRA and VT Program.

- $70M in direct economic activity in two domestic locations over the 3 year scope of the project
- 320 manufacturing jobs in areas hit hard by the economic downturn
  - 200 jobs in Columbus GA
  - 120 jobs in Bristol TN
- When installed in vehicles incorporating energy management technologies, these advanced batteries enable a savings potential of
  - 75 million gallons of fuel per year, or more than $200M at the pump
  - 3 million barrels reduction of imported oil per year
  - 600,000 metric tons of CO_2 per year in reduced emissions

Targets and Technical Barriers

- Advanced Battery (Domestic) Production Capacity - to Enable Advanced Vehicles
  - Improved Energy Efficiency
  - Reduced Dependence on Foreign Oil
  - Reduction in Greenhouse Gasses
  - Enhancing National Security
- ARRA Targets
  - Stimulate Economy
  - Increase Domestic Employment

✧ ✧ ✧ ✧ ✧

Introduction

The Exide project covers the expansion of Exide Technologies' manufacturing capacity for producing advanced batteries in existing U.S.-based battery plants. With 34 plants and operations in over 80 countries, Exide is a global leader in stored electrical energy solutions, manufacturing more than 40 Gigawatt-hours of battery energy per year used in transportation, motive power, network power, and military applications. The project plan is to implement a combined incremental increase in yearly production capacity of 1.5 million additional units at two of Exide's current manufacturing locations: Columbus, Georgia, and Bristol, Tennessee. This expansion will occur at these facilities on property that is currently owned or controlled by the Company.

These advanced battery technologies are targeted to have an accelerated near-term impact (in high volume) for

micro-hybrid vehicles, idle reduction commercial vehicles, and other strategic market segments. This expansion involves two of Exide's global technologies: a Spiral Wound Absorbed Glass Mat (AGM) design and a Flat Plate AGM design, both of which will be manufactured with advanced carbon technology as required by customer specific advanced vehicle applications.

The spiral wound battery product is currently in production at an Exide battery plant in Europe. When the planned technology transfer to the United States takes place, which will be accelerated by the federal grant, the Tennessee Exide production operation will be the only Spiral Wound lead acid battery "made in America" that is focused on the transportation market segment. Furthermore, this production capacity will serve both an existing market of 2 million units, and will also enable development of advanced spiral wound designs for upcoming new micro-hybrid and mild hybrid applications. Thus, the Exide project fulfills both the job creation goals of the advanced battery program, as well as promoting the enhanced use of hybrid vehicles, thereby achieving the energy saving goals of the program as well.

These expansion projects will create approximately 320 new U.S. manufacturing jobs and will set the stage for retaining existing jobs by enhancing the advanced technology base at the designated production sites. The project will also create additional jobs in the supply chain thereby generating a job multiplier effect which will further advance the economic stimulus goals of the advanced battery grant program. The Exide proposal will also result in the creation of many construction jobs at the project sites in Tennessee and Georgia during the 3-year project period.

Approach

This project is being carried out in four major project phases at each location over the 3-year life of the project.

- Project Phases
  - Design Project and Arrange Funding
  - Procurement & Installation
  - Shakedown & Qualification
  - Production Ramp-up & Market Deployment

  The project deployment plan - key items
- Project Task Areas
  - Pre-Agreement Planning
    - Prepare documents for NEPA EA
    - Preliminary product engineering planning
    - Order long lead time equipment
  - Project Management and Execution
    - Product design and planning
    - Order remaining equipment
    - Environmental Permitting
    - Receive, Install and Debug Equipment
    - Deliver to the DOE of 18 batteries manufactured from each completed manufacturing facility from low rate initial production for validation purposes
  - Production Scale-up including Hiring and Training of New Manufacturing Employees
  - Achieve Production and Product Performance Targets
- Project Management Organization Structure – A formal organization has been implemented
  - High-level Steering Committee was formed with corporate officer leadership and direction
    - Periodic meeting schedule - established & on track
  - Functional teams were formed with experienced leaders
- Project Management - Implementation team established
  - System software decisions and upgrades
  - Special refresher training completed
    - PMBOK Principles
    - Common deployment across project sites
  - DOE EVM spreadsheet
    - Verified conformance
    - Training for key team members

Results

The Exide ARRA Battery Project has made significant progress into the Procurement and Installation Phase During FY10.

- Successful DOE negotiation period to achieve Cooperative Agreement (Aug '09 – Dec '10)
- Successful NEPA Environmental Assessment (EA) resulting in Finding of No Significant Impact (FONSI) for both project sites (Sep '09 – Mar '10)
- Successful DCAA Audit report regarding financial systems and controls (Sep '09 – Mar '10)
- Full time Project Managers hired for both production sites
- Formal Project Management software system implemented
- Capital equipment procurement on track
- Facility prep for production areas progressing to plan

Project Deployment – Columbus GA Site ~ Flat Plate AGM.

- Full time Project Manager hired to run project

- Weekly *Columbus Update* meetings
  - cross functional team members
  - executive staff from commercial divisions
- Bi-weekly Columbus team meetings
  - Focused meetings to follow status of key equipment
- Major process technical reviews
  - Ongoing and structured to achieve needs
- Critical Path Equipment Ordered and on track
  - Specification and procurement planning
  - Layout decisions and implementation schedule
- Facility site prep and infrastructure for new production area is nearing completion
  - Multiple pieces of equipment have been received and installed; some in debug stage
- There has been no slippage in projected timing from the date of the CA, no changes that would impact either the scope or cost of the project, and no foreseen problems that would prevent a successful completion of the project

Project Deployment – Bristol TN Site ~ Spiral Wound AGM.

- Full time Project Manager hired to run project
- Coordination of the Orbital Project continues
  - Weekly Implementation Team conference calls
  - Monthly All Day On-Site events
  - Major equipment/process technical reviews
- Product design, equipment procurement, and facility improvement areas continued to progress through the period
- Equipment procurement activities on track
  - All major equipment on order
  - Vendor visits for design reviews / progress updates
- Advanced Product Quality Planning ongoing
  - DFMEA & PFMEA accomplished
  - Product/Process specifications documented
- There has been no slippage in projected timing from the date of the CA, no changes that would impact either the scope or cost of the project, and no foreseen problems that would prevent a successful completion of the project

Conclusion and Future Directions

- Major Progress Planned for FY11
- Both sites scheduled for heavy front loaded spending during the coming period
  - ~53% of total project spending scheduled in FY11
- Production line sites will continue to be readied and most major equipment will be installed in FY11
  - Several items were received and installed in FY10
- Hiring will continue, but will lag rate of spending through most of FY11 – long lead times on many major capital items

II.A.4 PHEV Battery Development (East Penn Manufacturing Co., Inc.)

John G. Tabacchi (NETL Project Manager)
Grant Recipient: East Penn Manufacturing Co., Inc.

Robert P. Flicker
Deka Road
Lyon Station, PA 19536
Phone: (610) 682-6361; Fax: (610) 682-1650
E-mail: rflicker@dekabatteries.com

Start Date: December 3, 2009
Projected End Date: December 2, 2012

Objectives

The expansion of production capacities to manufacture high volumes of Advanced VRLA (Valve Regulated Lead-Acid) batteries and the UltraBattery, both proven commercially viable technologies. East Penn will use a recently constructed manufacturing plant that will be populated and fully developed with specialized battery manufacturing equipment.

Technical Barriers

No technical barriers have been encountered at this time. Product development is continuing as planned. Marketing growth and interest in VRLA and UltraBattery technology is solid. Numerous potential applications are being considered and investigated due to ARRA funding exposure.

Technical Targets

- Battery cell pack cost testimates
- OEM specification test plan
- Performance/abuse tests and test report
- Delivery of VRLA batteries to DOE for validation

All milestone dates currently met or exceeded.

Accomplishments

- Purchased two Cast On Strap/Assembly machines, one operational
- Electrode Formation and Rectifiers for the 6th Ninth are being installed and the 7th Ninth is on order
- East Baghouse is functional. The South East and West Baghouses are on order and in the process of installation
- Five Injection Molding machines are operational at this point with two others being installed and two on order
- Active Material Mixing is being installed
- Electrode Curing Phase I is being installed
- The Strip Caster/Puncher equipment (Phase I) is on order
- Concast #1 has been delivered

✧ ✧ ✧ ✧ ✧

Introduction

To achieve the project's objectives, the acquisition of specialized battery manufacturing equipment and related auxiliary equipment will be purchased, installed, and commissioned in a recently constructed 739,000 square foot manufacturing plant. The manufacturing plant will be equipped with electrode formation, current collector and cell assembly equipment (suitable for both Advanced VRLA batteries and the UltraBattery), battery assembly equipment, and equipment for electrolyte filling, finishing, conditioning, and testing. Also, component production (containers and covers) and distribution facilities will be expanded to support the additional production capacities.

Approach

East Penn is proceeding with the project in an accelerated and aggressive manner. It continues to purchase and install equipment to maintain our goal of producing the VRLA and UltraBatteries.

Results

Project scope, equipment purchasing, installation and start up is consistent with the SOPO. Product development along with job creation/retention proceeding as planned.

Conclusions and Future Directions

The project objectives, total project costs and cost share have been sustained through this fiscal year. All reporting requirements required of East Penn Mfg. have been maintained. The DOE should have a high level of confidence the Statement of Project Objectives (SOPO) will be maintained and adhered to.

FY 2010 Publications/Presentations

1. 2010 DOE Annual Peer Review Meeting Presentation

II.B Battery Cell and Pack Assembly Facilities

II.B.1 Cell and Battery Manufacturing Facility in Michigan to Support the EV and HEV Markets (Kokam/Dow, Midland Battery Park)

Ralph Nine (NETL Project Manager)
Grant Recipient: Kokam/Dow, Midland Battery Park.

John Pham
2125 Ridgewood Drive
Midland, MI 48642
Phone: (989) 698-3304
E-mail: jpham@dowkokam.com

Start Date: December 9, 2009
Projected End Date: December 8, 2011

Objectives

- to design, construct, and commission a facility in Michigan to manufacture cells and batteries to power electric and/or hybrid electric vehicles,
- to advance the battery manufacturing and development processes to make the battery affordable, safer, more reliable, and longer lasting, and
- to support the Nation's goal of promoting less dependence on foreign oil for the transition to petroleum or emission free vehicles.

✧ ✧ ✧ ✧ ✧

Approach

To accomplish the Project objectives above, the Recipient will execute a three phased approach. The three phases and their objectives are:

PHASE I (DESIGN, ENGINEERING & PLANNING) OBJECTIVES:

1. Identify appropriate site and secure rights to construct facility;
2. Design a facility and manufacturing process that will manufacture cells and batteries to power electric or hybrid electric vehicles;
3. Complete the detailed construction drawings; and
4. Obtain all required related permits sufficient to begin construction.

PHASE II (PROCUREMENT, CONSTRUCTION & EQUIPMENT STARTUP) OBJECTIVES:

1. Prepare site for construction;
2. Procure manufacturing equipment;
3. Construct the manufacturing plant;
4. Install all manufacturing process equipment;
5. Hire staff plant operations and maintenance; and
6. Commission manufacturing process.

PHASE III (OPERATIONS & MAINTENANCE) OBJECTIVES:

1. Train operators and maintenance staff;
2. Manufacture cells and batteries in accordance with OEM specifications; and
3. Continuously improve upon battery and manufacturing processes.

Description & Approach

The Recipient will execute the three phased approach in order to successfully accomplish the Project's objectives. These three phases incorporate the functions and steps necessary to bring the Project from the planning stages to full scale production. Each phase is very unique and its proper execution will be critical to the overall success of the Project.

Design, Engineering, & Planning is the first of the three phases and will include the preliminary and conceptual efforts of the Project team. During this Phase, the Project team will form a site selection committee to review available sites to ensure the selected location meets Project requirements. Engineering teams will also be formed to review equipment specifications and determine throughput configurations to optimize manufacturing operations. The process engineers and construction management will collaborate to design an efficient manufacturing facility and work with Federal, State, and local Agencies, as necessary, to obtain the required construction and operational permits.

Phase two activities include construction of the facility and the procurement and start up of the equipment. The construction team will engage the proper experts necessary to perform testing (subsurface utility investigation, geotechnical, etc.) of the site to ensure the location meets constructability requirements. Competitive bids will be obtained from multiple contractors, where applicable, for the construction of the building and procurement of equipment. The Project management team will work closely with the construction and development

team to ensure all construction milestones are met. Great care will be taken to synchronize the construction of the facility and the delivery of all equipment. The Recipient will work closely with equipment manufacturers and process engineers to install and commission all manufacturing equipment and will utilize the local labor force, where applicable, when staffing the manufacturing and administrative positions.

The final phase, Operations and Maintenance, will be a very important step in ensuring the longevity of the business and equipment used in the operations. During this phase, the manufacturing and maintenance employees will be properly trained by the equipment specialists on how to use and care for each piece of machinery. This training will cover the manufacturing equipment, as well as the facility systems necessary to support all operations of the building. Another aspect of this phase will be the validation and implementation of programs for advancing battery and manufacturing techniques. Having these programs in place will help position the Recipient as a key competitor in battery industry for years to come.

Introduction

Dow Kokam was established in 2009 to develop and manufacture technologically advanced and economically viable battery solutions for the transportation, defense, industrial and medical industries. Dow Kokam is owned by The Dow Chemical Company, TK Advanced Battery LLC and Groupe Industriel Marcel Dassault (Dassault).

Uniting the three companies creates the first battery and energy management systems manufacturer to combine the viable, scalable, large-format battery technology with the market franchise, manufacturing expertise and market knowledge necessary to become the clear partner of choice across industries.

Results

- Preparations for full scale construction, that included designing the facility and then the clearing and grading of the site over an eight month period, were completed.
- A highly publicized Ground Breaking ceremony was held on the Midland Battery Park site on June 21st. It was attended by Vice President Biden, Senators Levine and Stabenow, and Governor Granholm along with 500 other attendants from the Midland area.
- Major equipment system purveyors were selected.
- Comprehensive and extensive engineering of major equipment systems is well underway and continuing, to optimize equipment specifications and advance technology transfer.
- 22% or $71 million of the Grant budget has been expended, primarily for process equipment engineering, technology licensing and early phases of construction.

Conclusion and Future Directions

The project is on schedule and we do not foresee problems or delays in bringing this state of the art scalable, large-format lithium advanced battery manufacturing facility on line for mid-year 2012. The project will advance battery manufacturing and development processes, make the battery affordable, safer, more reliable, and longer lasting, and will support the Nation's goal of promoting less dependence on foreign oil for the transition to petroleum or emission free vehicles. When completed, this advanced battery manufacturing facility will have a target capacity of 600 million watt hours per annum with an estimated employment of 320 people.

II.B.2 Development of High-Performance PHEV Battery Pack (LG Chem Michigan Inc. – formerly known as Compact Power, Inc.)

Samuel Taylor (NETL Project Manager)
Grant Recipient: LG Chem, Michigan, Inc.

Kee Eun
10717 Adam Street
Holland, MI 49423
Phone: (248) 291-2377
E-mail: kEun@compactpower.com

Start Date: February 17, 2010
Projected End Date: February 16, 2013

Objectives

This project is designed to directly address our interest in Cell and Battery Manufacturing Facilities. The completion of this effort would result in validated production capability for advanced Lithium-Ion battery cells in an all-new US facility.

The overall objectives of this project are to:

- Construct a new plant that will be fully equipped with state of the art processes, machinery and equipment.
- Replicate production of Li-Ion battery cells from Ochgan, South Korea into a new manufacturing facility in Holland, MI.
- Begin manufacturing operations in 2012.
- Reach full scale, integrated production of over eighteen million battery cells annually by the end of 2013.

Description

The start of production of Li-ion battery cells in the Holland plant will involve construction of a new facility, the installation of new equipment and staffing the plant with operators, engineers and administrative staff. The building construction will be done in two phases, the first in 2011 to begin assembly operations, and the second in 2012 as an expansion to accommodate high volume electrode manufacturing as well as more than doubling assembly capacity.

In the first phase of the project, to meet customer timing requirements, two assembly lines will begin operation in the 2nd quarter in 2012 utilizing electrodes made in LGC's Korean based plant to produce 5 million cells in 2012. This permits timely supply and also provides an opportunity for experienced technical experts to fully develop the manufacturing equipment and processes that will ultimately be duplicated in Michigan. Concurrent with the start of assembly production, the new building will be expanded to accommodate new electrode manufacturing and added assembly equipment that will bring the capacity to 18 million cells per year by the end of 2013. This project could bring valuable technology, manufacturing capability and jobs to the U.S. to serve the automotive industry and potentially many other future applications.

Technical Barriers

Customer- Overcapacity from failure to acquire new customers or securing sufficient production volume after significant manufacturing investment.

- Supplier- An investment boom in battery cell manufacturing driven by Govt. stimulus or other grants from the government leading to high demand in the market, emergence of lower quality products, delay in delivery from equipment suppliers, component supplier production or quality issues causing disruption of LG Chem ("LGC")'s production.
- Technology- Failure to protect intellectual property permitting reduced barriers for competitive entry to LGC's market(s). Failure to protect the commercialization technology of the automotive lithium-ion product.
- Production- Substantial quality issues in early production phase, failure to reach target yield rate or failure to obtain required cycle times after running initial production.
- Labor- Failure to hire skilled and experienced work force causing loss in productivity.
- Financial- Worsening of external financial environment from changes in money/currency markets or weakened financial structure inside of New Co.
- Regulations- As foreign origin company, LGC might have less understanding of local legal and regulatory restrictions.
- Culture- LGC has limited experience in US labor culture.

✧ ✧ ✧ ✧ ✧

Introduction

LGC is, at its roots, a chemical company. Where most battery making competitors have emerged from the electronics industry, LGC has developed an understanding of the underlying science of batteries and, over the last fifteen years, has applied its knowledge of chemistry to develop and mass-produce a number of increasingly advanced LI-Ion battery cell types including cylindrical, prismatic and laminated packaged with various chemistries tailored for different applications, becoming one of the world's largest suppliers of product and technology.

Through a complex and challenging development project with GM, LGC prepared a unique, high power and energy, abuse tolerant, laminated battery cell. In October 2008, LGC was awarded the production supply contract for use in the Chevrolet Volt, the first volume production PHEV/EREV in the US. Successful commercialization of this vehicle now depends to a very large extent on LGC's product. To meet quality and cost, project activity was begun for production launch in LGC's plant in Ochang, Korea.

With the potential for incentives from the US DOE, an earnest assessment was made to determine the possibility and advantages of moving the manufacture of the new automotive cells to the US. LGC now feels that this funding opportunity creates very real potential to make near-term investments in a US Li-Ion Polymer cell manufacturing facility that would be mutually beneficial to the efforts of the DOE and to LGC. It presents a viable path for ensuring that this growing technology business will have a strong foundation in Michigan in support of its automotive economy.

Having the know-how and partnering with domestic and global automobile manufacturers in and outside the United States, LGC's US operations will assume a leadership role in this important evolution of automobiles. It will provide an enhanced capability to take the product into new commercial and non-automotive markets for a long-term, sustainable business.

Approach

Technical feasibility of the project, including both the ability to complete the facility and to deliver a commercial ready product within 3 years or less of award.

LGC/LGCMI has started its project in Holland, MI by acquiring building approvals in the 2nd Q of 2010 although preparations for site selection and facility design will be conducted in 2009. And, it will continue to work through 2012 and into 2013 to facilitate integrated production and expansion for more US and international business.

Our plant in Holland, MI will make battery cells. The cells will be supplied to GM to build into battery packs and full battery systems. More than 250 LGC cells are required for each system. In full production, over 18 million cells will be required.

In our experience, it typically takes 2 years to reach stable production in terms of productivity, operator's skill and high levels of product quality control. For this reason, in the first phase of production, it is essential that all production be done in an established plant location. This allows LGC to leverage all possible existing resources, know-how and expertise in our small-cell manufacturing until confidence in production capability and product quality is ensured. LGC will not sacrifice quality of product by putting a start-up facility in the demanding new product launch process.

LGC has a lithium-ion battery manufacturing operation in Ochang, South Korea, which has been fully validated and stabilized. Based on such success, LGCMI in Holland is setting up the identical processes in Holland, Michigan. By choosing to set up the identical processes, LGCMI anticipates the least disruption of supply and minimized trial and error when the facility begins operation as stated earlier.

Having started three high volume manufacturing plants in the last 11 years, LGC is well prepared to start another operation in Michigan. Consequently, it will take LGC/LGCMI less time than its competitors to complete the equipment and line setup, run trials and prove out production since the specific processes required to make the GM qualified battery for the Volt have already been developed and are operational in LGC's Korean operations.

LGC has a business plan that commits significant levels of resources to both this product development and to building a Michigan based manufacturing facility.

Both in terms of experience in establishing new facilities and technical readiness of the product for commercialization, LGC/LGCMI's solid plan supports the achievement of a successful operation for cell manufacturing in Michigan. Moreover, support from our partners such as General Motors, Ford, and the State of Michigan will further ensure success of this project.

Results

- LGC/LGCMI selected a facility location in Holland, MI.
- The groundbreaking took place on June 1, 2010. On July 15, 2010, LGCMI held an official groundbreaking ceremony at the project site, in

which President Obama attended and celebrated the event.

- LGC/LGCMI has completed mobilization on June 14, 2010.
- LGC/LGCMI has begun the site work and is currently on schedule.
- Foundation and structure phases have begun and are on schedule at present.

Conclusion and Future Directions

The project would meet this objective and provide a foundation for the emergence, growth and success of electric and hybrid electric Vehicles in the U.S. automobile market. When in full production, the proposed facility will create more than 300 jobs and will produce over 18 million cells (3.75V, 15Ah) annually. After starting assembly operations in 2012, an expansion of production capability will continue through 2013 with the addition of a mega-electrode manufacturing line and more assembly lines.

This project is designed to directly address our interest in Cell and Battery Manufacturing Facilities. The completion of this effort would result in validated production capability for advanced Lithium-Ion battery cells in an all-new US facility.

The overall objectives of this project are to:

- Construct a new plant that will be fully equipped with state of the art processes, machinery and equipment.
- Begin operations in 2012.
- Reach full scale, integrated production of over eighteen million battery cells annually by the end of 2013.

II.B.3 Lithium-ion Cell Production and Battery Pack Assembly (EnerDel)

Christopher Johnson (NETL Project Manager)
Grant Recipient: EnerDel

Casey Butler
8740 Hague Road, Building #7
Indianapolis, IN 46256
Phone: (317) 585-3400 Fax: (317) 585-3444
E-mail: cbutler@enerdel.com

Start Date: January 29, 2010
Projected End Date: January 28, 2013

Objectives

- To expand the US based manufacturing capacity for automobile-grade lithium-ion batteries.
- Position the Recipient as a Tier 1 auto parts supplier
- Enhance Supply Chain and Promote Cost Competitiveness of Base Materials.
- Develop competitive mass production and engineering capability

Approach

The project is comprised of tasks associated with acquisition and upgrade of manufacturing facilities, acquisition and upgrade of manufacturing equipment, integration of manufacturing lines to provide high-volume output, selection of material suppliers, and recipient certification as a tier I auto parts supplier.

Tasks

Task 1.0 Purchase and expand the Recipient's existing site locations and equipment capacity.

- EnerDel is optimizing existing sites for cell manufacturing and pack assembly. We have acquired a third site for pack assembly, warehousing and cell manufacturing. We have and will enhance existing equipment capabilities and purchase new equipment at the sites as required.

Task 2.0 Develop competitive mass production and engineering capability.

- EnerDel is enhancing our engineering capability to address multiple automotive requirements via a high-volume, high-speed automated production line for cell manufacturing. We are currently validating and implement a high-volume, lean-manufacturing production line for battery system assembly by establishing a prototype production line, optimizing it, and then deploying similar production lines in order to meet customer capacity requirements. We have hired the necessary talent to support mass production battery output.

Task 3.0 Enhance Supply Chain and Promote Cost Competitiveness of Base Materials.

- EnerDel has identified key suppliers and materials for domestic sourcing. We are currently conducting the qualification process for suppliers and materials for Lithium-Ion Battery manufacturing. We are utilizing this strategy to prioritize the selection of domestic suppliers whenever feasible within pricing, supply, and quality standard requirements.

Task 4.0 Position the Recipient as a Tier 1 auto parts supplier.

- EnerDel has implemented strategies, achieve standards, and complete certifications required to become a tier I auto parts supplier. This includes ISO certification and PPAP manufacturing.

Technical Barriers

Schedule – Equipment lead times and production create considerable resource and management issues for our project. We are mitigating these risks with time contingencies and by working with vendors throughout the acquisition process. The acquisition process involves equipment specification writing and design freezes which allow the manufacturer to build equipment based upon an agreed set of specifications. Success will be based upon having the equipment arrive on time (and on budget). This is tracked through purchase requisitions based upon agreed terms and conditions with the vendors and suppliers.

Budget – EnerDel still currently operates the only high volume, large format lithium-ion battery facility in the United States. This puts EnerDel in the unique position of having access to historical data associated with costing profiles of manufacturing lines and equipment. The information allows EnerDel to create detailed budgets based upon historical data and such data is not available to other companies. Since this battery industry sector is a new industry in the United States, there are still unknowns concerning costs and lead times. EnerDel has hedged against these unknowns by building contingencies into project costs and using actual costs from previous equipment acquisitions. The success of the budget will be judged against the budget timeline and will be considered a successful project if it the total costs meet the proposed budget.

Quality – Quality is always in issue when purchasing equipment, certifying suppliers and construction. With a new industry, there can be significant technical and resource management issues. Currently, the United States has a dearth of qualified chemical suppliers for lithium-ion battery production. In addition, there are very few vendors that supply the needed manufacturing equipment. EnerDel currently utilizes many off-shore suppliers for quality equipment and supplies, but under this project, we have committed to help develop a domestic supply chain. Quality success will be judged on receiving quality and chemical supplies, as well as manufacturing equipment that can obtain the yields and speeds that are required to meet our ORM commitments. Currently, EnerDel is evaluating many domestic vendors and working with foreign vendors to set up domestically. An example is Kureha; they have recently finished negotiations with West Virginia to set up a manufacturing facility.

Safety and environmental – EnerDel is committed to being an industry leader regarding our safety and environmental practices, and we have a strong record in this area. Our business is, and will continue to be, operated in a manner that protects the environment and promotes the health and safety of our employees, our customers and the public.

Accomplishments

- Acquired a new facility and received NEPA compliance at all three facilities.
- Started production of the THINK battery pack. The manufacturing process is fully PPAP.
- Fully outfitted the Hague Road facility with another coater line, electrode cutting line and several electrode stacking lines.
- Expanded the Hague Road facility dry room
- Developed and implemented new manufacturing technology in every step of the process.
- Added over 150 jobs since 2009.

Milestone Status

Table II- 1 contains a list of milestones accomplished by EnerDel during FY 2010. We accomplished our manufacturing installation goals, but validation has been delayed. Validation will continue into 2011 and will be completed in Q1.

Table II- 1: List of Milestones for the EnerDel Manufacturing Project.

Milestone	Milestone Title	Completed
1	Grant Documentation Signed	X
2	NEPA/FONSI Approved	X
3	Start of Production for Think Pack	X
4	Hired an additional 50 people from start date.	X
5	Purchase and Install Equipment for 20 EV cell coating capacity	X
6	Phase II Mt. Comfort Design Complete	
7	Hired an additional 100 people from start date.	X
8	Phase III Mt. Comfort Design Complete	
9	Purchase and Install Equipment to 40 EV pack capacity	
10	Hired an additional 500 people from start date.	
11	Hired an additional 1000 people from start date.	
12	Purchase and Install Equipment to 60 EV pack capacity	
13	Project Completion	

✧ ✧ ✧ ✧ ✧

Conclusions and Future Directions

EnerDel has successfully implemented several manufacturing processes that are state of the art and will help the US to become the world's leading manufacturer of lithium-ion battery technology.

The following are the results of this implementation:

- Development of a new business sector through the grid energy storage sector.
- Continual success with our existing and potential customer based.
- Signed Volvo, Toro and FSK supply contracts.
- Developed relationships with local, state and federal institutions.

2010 was a great year for EnerDel. We moved forward and solved many manufacturing and logistics problems that arose. 2011 will be a bigger year for EnerDel. There are many customers in the pipeline which will be announced in Q1/Q2 of 2011. With these announcements, EnerDel will establish itself as a world leader in lithium-ion battery technology.

Additionally, in 2011, EnerDel plans on acquiring and utilizing the other half of the Mt. Comfort facility along with starting the phase II manufacturing plan as it lines up with customer demand.

II.B.4 Li-Ion Battery Pack Manufacturing (GM)

Samuel Taylor (NETL Project Manager)
Grant Recipient: General Motors

Linda M. Trumm
GM Manufacturing Engineering
30001 Van Dyke, Mail Code 480-735-810
Warren, MI 48090
Phone: (248) 240-8324 Fax: (586) 492-3534
E-mail: linda.trumm@gm.com

Start Date: August 2009
Projected End Date: September 2013

Objectives

- Deliver domestically produced, affordable, and environmentally sound energy sources to substantially reduce petroleum consumption.
- Aid in the nation's economic recovery by creating U.S.-based manufacturing jobs.
- Develop reliable, quality battery packs that can be cost-effectively produced in high volume.

Technical Barriers

- Consumer acceptance and new technology implementation
- Product cost

Technical Targets

- Establish and validate production capability for GM Li-Ion Battery Pack Manufacturing operations.
- Provide specialized workforce training in advanced battery pack manufacturing technology
- Provide continuous improvement and innovation cycles to move battery pack technology down the cost curve

Accomplishments

- Production equipment has been designed, built, and installed for use in manufacturing General Motor's 2011 Model Year Volt EREV battery pack.
- Validation of production processes has been ongoing. Process and equipment refinements and adjustments have been identified and implemented based on learnings from manufacturing validation activities.
- New production team members have been hired and trained in advanced battery pack manufacturing processes.
- Volt EREV battery pack components have achieved PPAP Saleable status.
- Brownstown Battery Assembly Plant has received Landfill-Free status.
- Volt EREV battery pack refurbishment operations have been established.
- Battery packs have been shipped for testing confirmation and assembly into Volt vehicles at GM's Detroit Hamtramck assembly plant.
- Future battery pack manufacturing process planning is ongoing. Preproduction builds for batteries is underway, manufacturing learnings are being collected and incorporated into process plans.
- Plans for preproduction build processes have been completed and initial equipment orders have been issued. Preproduction equipment & tool design, layouts and process flows are underway.
- Training in the key areas of Health and Safety, Global Manufacturing Systems (GMS), Technical Maintenance, and Production Operations continues according to the training plan.

✧ ✧ ✧ ✧ ✧

Introduction

The project will create and retain jobs in at least four areas: 1) manufacturing of preproduction battery packs; 2) design, construction, and installation of production machinery and equipment, tooling, and supporting operations; 3) process and quality improvement during the product lifecycle; and 4) manufacturing jobs in the ongoing operation.

This project will deliver production capability for GM's Li-ion battery packs to serve electric drive vehicles. It will design, construct, install, and validate machinery, equipment, tooling, and facilities. It will also establish a capable workforce to support battery pack manufacturing programs and the manufacturing operation.

The Volt's battery pack design is directly coupled with the vehicle design to assure complete integration between the battery pack and the vehicle. This integrated approach assures both performance and efficiency of the overall vehicle, to meet final customer expectations.

Approach

Program Management and Planning involves the program leadership team and the office of program management which will utilize proven, industry-standard and GM internal processes for product launch and manufacturing validation. Standardized processes for review and corrective action are in place to ensure adequate controls to maintain cost, quality and schedule performance.

Each ***Battery Pack Manufacturing*** program involves a cross functional team with resources from product and manufacturing engineering, suppliers, production operations, purchasing, quality, and after-market service. Battery pack manufacturing programs begin with preproduction builds to confirm manufacturability and production processes and document initial production standardized work. Critical tooling and equipment concepts are also validated. Preproduction builds will be used to obtain data on process capability in battery pack manufacturing operations. This validation activity during preproduction provides critical learning and is important to successful high volume production.

Once preproduction builds are complete, the cross functional team continues the work to deliver a fully validated production system. Production equipment and tooling will be installed and validated. All elements of the process, including people, equipment, tooling, material, environmental, communication and control systems will be integrated and validated during a series of in-plant builds prior to start of regular production. Refurbishing and recycling operations will be defined, installed and validated. Standardized work for all operations will be created and implemented.

Workforce training, continuous improvement and innovation cycle phase has two distinct parts. The first, workforce training, includes specialized classes and hands-on training in launch processes and battery manufacturing technology. The second, continuous improvement & innovation cycles, involves focused projects using engineering analysis and process testing on critical areas to improve quality, manufacturing flexibility, and cost.

Results

- Engineering and Plant teams staffed.
- Total cumulative project jobs retained or created based on ARRA guidelines: 67.7 FTE
- Battery pack manufacturing processes are defined and standardized work documented.
- Manufacturing process equipment and tools have been designed, constructed and installed at Brownstown.
- Preproduction and manufacturing validation builds are completed. Saleable Builds are underway.
- Container designs and validation are complete.
- Material scheduling systems and logistics plans have been defined and confirmed for key battery pack components.
- Refurbishment processes and equipment have been installed and validation is underway.
- Workforce training is being completed to plan.
- Initial process planning and preproduction builds for future battery pack programs are underway.
- Continuous improvement is underway in the areas of:
    - Joining Manufacturing and Quality Processes
    - Battery Design For Assembly
    - Battery Assembly Process Variation Reduction
    - Assembly Tooling Durability
    - Battery Charging & Diagnostic Testing

Conclusions and Future Directions

Investment in this project will drive innovation cycles and move the battery pack technology down the cost curve. The project will accelerate U.S. manufacturing capabilities for commercially viable extended-range electric drive vehicles; and create U.S. leadership in automotive applications of new generation battery technologies. The project will expand the U.S. workforce trained in automotive battery pack manufacturing technologies, creating and retaining green jobs at GM and its suppliers.

The project will contribute to national goals for reducing petroleum dependence and improving carbon footprint. It will enable high-volume production of electric drive vehicles (EDVs) and strengthen U.S. contribution to global CO_2 reduction. This capacity will significantly contribute to the Administration's goal of having one million plug-in EDVs by 2015.

General Motors is committed to the success of Electric Vehicles.

2010 and 2011 Future Direction:

- Complete the manufacturing validation and production launch for the 2011 Model Year Chevrolet Volt EREV battery pack.
- Implement continuous improvement project results into production processes.
- Complete the validation of refurbishment processes and equipment.
- Establish preproduction build capabilities at the Brownstown site.

- Conduct preproduction and manufacturing validation builds for Chevrolet Volt battery pack model year enhancements.
- Provide increased Chevrolet Volt battery pack capacity as needed for market demand, increase plant staffing as required.
- Continue manufacturing process design and early validation builds for future battery pack programs.

II.B.5 Lithium-ion Cell Production and Battery Pack Assembly (Saft America, Inc.)

Samuel Taylor (NETL Project Manager)
Grant Recipient: Saft America, Inc.

Peter J. Denoncourt
6196 Lake Gray Blvd., Ste. 108
Jacksonville, FL 32244
Phone: (904) 861-1504; Fax: (904) 772-1463
E-mail: peter.denoncourt@saftbatteries.com

Start Date: December 2009
Projected End Date: May 2013

Objectives

- Construct a 235,000 square foot Li-ion Factory of the Future in Jacksonville, FL for high volume production of batteries for military hybrid vehicles, smart grids, renewable energy storage, broadband and aerospace application.
- Provide a showcase of environmentally friendly and energy efficient design concepts
- Employ hundreds of U.S. workers in well-paid jobs
- Produce lithium-ion cells, modules, and battery packs at a competitive cost to enable renewable energy storage systems, Smart Grid, broadband systems, military hybrid vehicles and aviation, thereby achieving significantly reduced carbon emissions and fuel savings.

✧ ✧ ✧ ✧ ✧

Introduction

Saft is using its considerable experience in building factories for lithium-ion cell and battery manufacturing and expertise in lithium-ion technology to build a Factory of the Future capable of manufacturing and delivery of high quantities of lithium-ion cells, modules and batteries to the military hybrid vehicle, industrial energy, eledtric drive and aerospace markets.

Approach

Saft is investing immediately, along with DOE, in establishing the factory and manpower to support manufacturing which will be used in delivery of lithium-ion cells and batteries in high volumes. Saft is creating at least 280 jobs within 5 years of beginning the project, with the first year job creation starting at 106 new jobs. Saft is using lean manufacturing techniques to ensure that the factory is established with consideration for cost savings. Also, Saft is employing risk mitigation and risk management practices which will assure being able to provide on-time schedule and technical performance.

Saft is using the Earned Value Management System of assigning and managing project costs in respect to the financial objectives of the program. It is using LEED® green factory initiatives in the buildings, power usage and waste management; all of which are complemented by its recycling plan for batteries once used. The decision to use LEED® techniques in designing the Factory of the Future is consistent with the markets intended to be addressed, which are green energy related.

Accomplishments

Factory Design and Equipment Specification. The factory design was contracted to The Haskell Company in January 2010 as part of a design-build contract. The design was completed in April 2010 with completion of a 100% design review. The design is consistent with LEED® Silver requirements.

Equipment specifications for all schedule critical equipment have been completed. Saft is currently in process of completing specifications for non-critical equipment items. This task should be completed by October 2010.

Factory Construction and Equipment Procurement. Construction of the factory began with site preparation starting in February 2010. A formal groundbreaking was conducted on 15 March 2010. The site preparation was completed in May 2010 and building construction started immediately. The building is currently under construction and is approximately 60% complete, as shown in Figure II- 3.

Figure II- 3: Saft Factory of the Future under Construction

Procurement of all schedule critical equipment is complete, and most equipment design reviews have been conducted and approved. All equipment fabrication is proceeding on schedule.

Equipment Installation. This task is not scheduled to begin until December 2010.

Process and Product Qualification. This task is not scheduled to begin until May 2011.

Program Management. The Program Management Plan and Statement of Program Objectives have been submitted to DOE and updated quarterly as required. A Risk Assessment is currently being conducted as part of the Risk Management Plan. Quarterly progress reports, Earned Value Management reports and ARRA progress reports have been submitted on time and are current.

EVMS indicators: SPI=1.00 indicating the program is on schedule overall. Projected completion date for the project is 31 May 2013. CPI=1.15 indicating spending below projections. At this time Saft believes this indicator is artificially high due to the way the costs are incurred in our software earlier than they are actually invoiced by our contractor. Saft is projecting completion of the program on budget. The program is approximately 24% complete at end-September 2010.

Conclusions and Future Work

The Saft Factory of the Future program is proceeding on budget and meeting its goals. There are currently 180 construction workers employed on the factory site, plus 38 Saft employees in Jacksonville dedicated to the program. The factory design is consistent with LEED Silver requirements and should be certified in 2011.

In 2011, Saft anticipates completion of the factory construction, installation of one complete production line, qualification, start of production and commencing sales of products from the first production line. Furthermore, Saft anticipates commencing procurement of equipment and installation of equipment for a second production line during 2011-2012.

FY 2010 Publications/Presentations

1. 2010 DOE Annual Peer Review Meeting Presentation.

II.C Battery Materials Production Facilities

II.C.1 Manufacturing Facilities Initiative for Lithium-Ion Battery Separators (Celgard)

Bruce W. Mixer (NETL Project Manager)
Grant Recipient: Celgard

Gerry Rumierz
13800 South Lakes Drive
Charlotte NC 28273-6738
Phone: 704-587-8538
Email: gerryrumierz@celgard.com

Start Date: December 2009
Projected End Date: May 2013

Objectives

Celgard will use the DOE grant funding to accelerate investments in production capacity and create jobs in North Carolina in preparation for increasing demand from the Electric Drive Vehicle (EDV) market.

The primary objectives of the Celgard U.S. Manufacturing Facilities for Advanced Battery Separators Project are as follows:

- Develop domestic battery separator manufacturing capacity in support of the DOE Advanced Battery Manufacturing Initiative
- Create long-term American manufacturing jobs starting within three (3) months of the project grant award
- Install phased separator production capacity to match domestic lithium battery market requirements
- Minimize project risks by utilizing:
  - Qualified and trained personnel
  - Proven processes for manufacturing lithium battery separators

Technical Barriers

Product Design and Manufacturing

- Celgard's use of proven separator technology greatly reduces any risk in product design and manufacturing know-how.
- The project's use of existing manufacturing resources allows for rapid knowledge transfer of manufacturing and quality systems.
- Celgard has established skill definitions and recruiting systems in place to ensure manufacturing and support positions are staffed appropriately.

Product Qualification and Commercialization

- Celgard will manage the risk of installing significant new manufacturing capacity by replicating existing technology to produce proven EDV products.
- Celgard has the ability to easily share expertise between its Charlotte, NC and Concord, NC facilities (45 minutes apart).
- Global sales and logistics systems are already in place and well-established.

Equipment Design, Sourcing, Installation

- Celgard has successfully executed three previous expansions at the Charlotte, NC site.
- Celgard has established relationships with key equipment vendors, which minimizes risks associated with design and supply issues.

Investments, Funding

- The cost-share funds have been fully secured from Celgard's parent company, Polypore International, Inc.

Technical Targets

- The project is being implemented in phases, with the entire production capacity on target to be completely installed and qualified by the U.S. EDV industry by 2012. The first jobs associated with this project were created in October 2009.

Accomplishments

- See "Results".

✧ ✧ ✧ ✧ ✧

Introduction

Celgard, LLC, a leading supplier of separators for the lithium battery industry, was awarded a grant from the U.S. Department of Energy (DOE) under the Funding Opportunity DE-FOA-0000026 (FOA), Area of Interest 2. The DOE grant is part of the American Recovery and Reinvestment Act of 2009 (ARRA) that provides federal stimulus funding to support the creation of American jobs while promoting the development of U.S.-based advanced battery production for the Electric Drive Vehicle (EDV) market.

Celgard is a leading global supplier of separators used in lithium batteries and is one of the largest participants in the U.S. lithium battery supply chain. Celgard supplies separators to lithium battery manufacturers whose battery packs are in multiple EDV models on the road today, as well as others that will launch between now and 2013.

Celgard® brand separators are highly-engineered microporous membranes. They are primarily used in rechargeable lithium batteries for personal electronics devices such as notebook computers, mobile phones, digital cameras, power tools, reserve power and electricity grid storage systems, and now, EDVs. These separators play a critical role in the performance, life, and safety of lithium battery cells by providing a barrier between the positive and negative electrodes – preventing short circuits while controlling the exchange of lithium-ions from one side of the battery to the other.

Celgard has more than 40 years of experience in the design, production, and distribution of high-performance membranes, with the first Celgard® products developed in the mid- 1960s. By the mid-1970s, Celgard® products enjoyed commercial success as a key component in blood oxygenation devices commonly used in heart bypass surgery.

Celgard's first entry into the lithium battery industry came in the early 1980s and the company has reliably supplied separators to the battery industry ever since from its manufacturing facilities in Charlotte, North Carolina.

Approach

Celgard will implement its lithium battery separator capacity expansion in a two-phase approach to meet market needs. In the first phase, Celgard will add capacity at its existing Charlotte, North Carolina facility. In the second phase, Celgard plans to build a facility in nearby Concord, North Carolina.

- Phase 1: Expand existing Charlotte, NC facility to meet commercial scale operation starting in mid-2010
- Phase 2: Develop new manufacturing site in Concord, NC to meet increasing commercial demand starting in mid-2012

The expansion will significantly increase Celgard's lithium battery separator production capacity in the U.S. by 2012. It is expected to create more than 200 North Carolina jobs within Celgard and provide more than 1000 jobs among Celgard's contractors and suppliers.

Total investment for the expansion project is approximately $100 million, more than half of which will be funded by Polypore International, Inc., Celgard's parent company.

Results

Phase 1 – Charlotte, NC

- The phase 1 capacity installation is on target for 100% installation by the end of 2010 and full product qualification by Q2 2011.
- In April 2010, Celgard welcomed President Barack Obama to its Charlotte facility for a tour of the expansion area.
- All equipment has been installed and qualifications are in process.
- Staffing is complete and fully trained.

Phase 2 – Concord, NC

- Celgard celebrated its groundbreaking for phase 2 on September 2nd, 2010.
- Building construction has begun and is on schedule.
- Resource planning is active with initial management personnel in place.

Product Qualification

- Celgard® products have already been adopted in commercialized EDV applications, including the Mercedes S400 Hybrid and Hyundai Avante.

Job Creation

- Job creation from this project currently stands at 100 full-time employees and is on target to achieve the original estimate of 251 jobs created by 2012.
- Local project management and construction resources are employed on the project resulting in many additional project-related jobs.

Conclusions and Future Directions

Celgard has a long history of supplying membrane separators for leading-edge battery applications and is recognized industry leader delivering outstanding product performance, reliable supply, technical solutions, and global business support.

Celgard understands the dynamic nature of the lithium battery market, and has continuously demonstrated its dedication to the industry through capacity expansions, acquisition of additional manufacturing facilities, and the development of new products and technologies in anticipation of customer needs.

With this project, Celgard is expanding capacity at its manufacturing operations in Charlotte, North Carolina and building a new manufacturing facility in Concord, North Carolina to support increasing demand in the EDV market. The expansion is supported in part by $49 million in grant funding from the U.S. DOE Electric Drive Vehicle Battery and Component Manufacturing Initiative, as well as significant investments by Polypore International, Inc., Celgard's parent company.

The expansion project will significantly increase Celgard's lithium battery separator production capacity in the U.S. and is expected to add more than 200 jobs within Celgard and more than 1,000 jobs among Celgard's suppliers by 2012.

FY 2010 Publications/Presentations

1. None.

II.C.2 Advanced Cathode Materials Production Facility (Toda America Inc.)

Samuel Taylor (NETL Project Manager)
Grant Recipient: Toda America, Inc.

Yasuhiro Abe
4750 W. Dickman Road
Battle Creek, MI 49037
Phone: 269-962-0353; Fax:
Email: abe@todaamerica.com

Start Date: February 2010
Projected End Date: December 2013

Objectives

- Design, build, and operate a U.S. production facility for advanced cathode materials to meet the needs of Toda's current Li-ion battery manufacturer customers and emerging players in the rapidly growing U.S. battery and electric drive vehicle industry.
- In 2 Phases, implement a total of 4 production lines with 2 lines in each Phase. Establish capacity for a total production volume of 4,000 tons of cathode materials per year. Complete first line and achieve initial production by 1Q2011.

Challenges

A significant challenge is the very compressed schedule – first line production within less than 12 months of start of project. The construction of the facility, sourcing and installation of the equipment, recruiting and training personnel, and successful product validation must all be accomplished within this tight timeframe. A fast-track customer certification process must be employed, which leverages process validation data from Toda Kogyo Corporation(Toda)'s existing facilities in Japan supplemented with local process validation in the newly built facilities in Battle Creek, Michigan.

Technical Targets

- Produce $LiNiCoAlO_2$ (LNCA) and $LiNiCoMnO_2$ (LNCM), and other cathode materials as required by demand, to deliver the quality, performance, and cost requirements as a premier supplier to the U.S. market.

Accomplishments

- Acquired 18-acre brownfield site in Battle Creek, Michigan; and completed remediation and obtained all regulatory approvals to proceed with construction of a cathode materials manufacturing facility. The conceptual design is shown in Figure II- 4.
- Phase 1 buildings are constructed with over 65% completion as of September 2010. Equipment installation for Line 1 is substantially completed with expected full completion by December 2010.
- Recruiting and training is underway, with commissioning of Phase 1 Line-1 expected in December 2010. Project is on schedule as planned.

Figure II- 4: Conceptual design of the Toda Facility

✧ ✧ ✧ ✧ ✧

Introduction

Advanced Cathode Material Production Facility. Toda is a cathode materials supplier to Li-ion battery manufacturers worldwide. In this project, the principal objective is to establish Toda America Inc. as a high voume cathode materials production facility to become a strong and supportive strategic supplier partner to the U.S. advanced battery industry. ITOCHU Corporation, a diversified global trading company, actively engaged in the chemicals and energy sectors, has partnered with Toda in this U.S. joint venture.

As a first step, Toda is investing an estimated $70+ million (total capital investment) to establish its U.S. plant, as part of a long term U.S. commitment. This facility will develop and produce oxide cathode materials to serve both existing Toda customers and emerging players in this industry. Phase 1 and 2 will each contain two lines for a total of four lines for this U.S. facility. Phase 1 will be built-out and equipped in two steps; Step-1 outfitted with the first line will be completed first, followed by Step-2 where the second line will be installed in sequence. Total production capacity at this facility will be 4,000 tons of cathode materiasl per year when completed, which is

sufficient to supply batteries for around 450,000 HEV's or 125,000 PHEV's. In addition, Toda has robust R&D capabilities, and is currently working to commercialize the next-generation Li-ion cathode materials using the latest technology licensed from Argonne National Laboratory (ANL). Toda already produces several cathode material products using proprietary Li-metal oxide combinations and technologies, serving the transportation, consumer electronics, and industrial tool markets worldwide.

Approach

The facility that will be used for this project is being built in Battle Creek, Michigan, in close proximity to its battery and vehicle OEM customers and its nearby input material supply operations. It will incorporate facility designs and equipment substantially identical to that currently being used in Toda's cathode manufacturing facility in Japan. Production of cathode material for shipment to customers is scheduled to start in 1Q11, approximately 18 months after the award was granted and about 12 months after the award was finalized.

Toda's existing U.S. customers purchasing cathode materials from its Japanese plant have committed to buy cathode material from its Battle Creek plant. Due to the existing customer relationships and product quality experience with currently certified product, Toda America is working closely with customers to speed up the product certification process for cathode material production in the Battle Creek facility.

Results

Figure II- 5: Toda America Inc. Battle Creek Facility construction in progress.

Building Construction. As of September 2010, over 65% of the planned construction activities for Phase 1 Step-1 are completed, with expected full completion by December 2010. On an 18 acre site, the building complex consists of plant, warehouse, office, utilities, and wastewater treatment facilities. The Phase 1 building provides for capacity for installation and operation of Lines 1 and 2. (See Figure II- 5)

Equipment Installation. As of September 2010, equipment procurement and delivery is 80% completed for Phase 1 Step-1. This includes continuous flow kiln, mixer and crusher, conveyor, electrical controls, piping, Quality Control equipment, and wastewater treatment equipment. All equipment for Phase 1 Step-1 are expected to be installed by December 2010. (See Figure II- 6)

Figure II- 6: Interior construction and equipment installation in progress.

Operations. Managerial staffing for the U.S. operation is in place, and technical operations staff for Phase 1 Step-1 are being hired and trained, with expected completion in 4Q10. Project is on track for commissioning in December 2010, with first production validation targeted for 1Q11.

Conclusions and Future Directions

Toda America's plans for the U.S. cathode materials production facility is progressing as planned. The construction of the facility has been quite manageable despite its compressed schedule. What is less controllable is the pace with which the U.S. market will develop, and the adoption rates of the various cathode material products. Therefore, Toda America must monitor the market and assess carefully the anticipated product demand and mix in order to plan effectively with the right processing capacity at the right time. Market analysis will determine exact timing and technology details as Toda America completes its step-wise capacity implementation plan for this project.

Toda America is planning for substantial further investment in the U.S. over the next 10-15 years, paced with the expected growth of the U.S. battery manufacturing industry. Toda America intends to collaborate closely with federal, state, and local stakeholders and to engage in creative industrial partnering options and is poised to serve as a key contributor in the development of a robust advanced battery manufacturing industry in the U.S.

FY 2010 Publications/Presentations

1. 2010 DOE Annual Merit Review Meeting Presentation.

II.C.3 Domestic Production of Lithium Carbonate and Lithium Hydroxide (Chemetall Foote)

Christopher Johnson (NETL Project Manager)
Grant Recipient: Chemetall Foote Corp.

John Groves
348 Holiday Inn Drive
Kings Mountain, NC 28086
Phone: (704) 739-2501; Fax: (704) 734-2692
E-mail: john.groves@chemetall.com

Start Date: April 2010
Projected End Date: May 2013

Objectives

The overall objective of this project is to provide a competitive domestic source of lithium for the US battery industry by expanding lithium carbonate production in Silver Peak, Nevada by 100%, converting the main electrical source at that location to geothermal energy which will reduce operating costs of the plant, and in Kings Mountain, NC expanding the company's capability to produce lithium hydroxide by more than 100%. This will sustain the only domestic source of lithium compounds, create permanent jobs and provide the US automotive battery makers with a high quality local source of raw materials.

Technical Barriers

Chemetall Foote Corp. (the Company) has successfully implemented similar projects for more than 50 years. The process technology is well known and has been practiced throughout the company for years. The company holds many patents on lithium brine processing, lithium carbonate and lithium hydroxide production. There is little or no risk of technical failure since this is for the most part a duplication of currently used technology.

The Company's Geothermal Power Plant project shares risks common to all geothermal projects: uncertainty regarding the location, performance and sustainability of the underground geothermal resource.

Technical Targets

The three major parts of the project are: a) expand the existing Lithium Carbonate Plant in Silver Peak, NV by drilling new production wells and expanding the solar evaporation system; b) convert Silver Peak to geothermal power by construction of a 3.5MW (net output) binary cycle geothermal power generating plant in close proximity to the lithium carbonate processing plant in Silver Peak, NV and c) build a 5000 MT/yr lithium hydroxide plant in Kings Mountain, NC. The existing Kings Mountain site will provide the basic infrastructure for a new lithium hydroxide plant which will use conventional technology reacting lithium carbonate with lime and purifying, drying and packaging the product for sale to the battery industry.

Accomplishments

Lithium Carbonate.

- Completed +/- 15% cost estimate
- Completed acquisition of a drill rig, semi-tractor, drill pipe, drill pipe trailer and backhoe to support the well field drilling program. The drill rig will require minor modifications and repainting to ensure suitability and reliability. Drill rig and support equipment are expected to be available for use in November 2010
- Issued a purchase order for a salt harvester with delivery expected in early to mid-November 2010. The salt harvesting support vehicles are planned to be on-site by mid-November as well
- Completed salt removal activities in three out of five ponds to prepare the pond system for additional brine capacity
- Received the Finding of No Significant Impact (FONSI) and Final Environmental Approval

Geothermal Power Plant.

- Completed +/- 20% cost estimate
- Environmental assessment (EA) work has been divided into three sections to facilitate achieving 2010 spending and activity schedules. Section 1 has been completed as a categorical exclusion allowing geophysical survey work to be conducted on an area of land adjacent to the Chemetall Foote Corp.'s Silver Peak site. Section 2 will include a categorical exclusion allowing temperature gradient holes to be drilled at targeted locations, as well as an EA to enable drilling geothermal wells. Section 3 will include a full EA for construction and operation of the geothermal power plant
- Geophysical survey activities conducted by Auckland University are progressing as scheduled. A final

geophysical report and 3-D model of the targeted resource is expected in December 2010

- Initiated the exploration plan development activities with target completion by February 2011

Lithium Hydroxide.

- Completed +/- 10% cost estimate
- Engaged an engineering firm to develop the detailed design of the plant. The detailed design is expected to be completed by the end of May 2011
- Placed purchase orders for 16 out of 24 major equipment packages
- Completed demolition of idle piping, electrical wire, conduit and cable tray in the existing building which will be utilized as the basic infrastructure for construction; began re-routing existing pipe lines out of the construction area
- Evaluated vendor quotes for demolition of the existing building's siding, tankage and structural steel
- Received a Finding of No Significant Impact (FONSI) and Final Environmental Approval
- Received an approved air permit for the project from the State of North Carolina.

✧ ✧ ✧ ✧ ✧

Introduction

The company already supplies some battery customers with lithium carbonate and lithium hydroxide from its existing operations. There are shortfalls in some areas of product quality / purity that will be addressed by these projects. Battery customers are sensitive to metal contamination and impurities such as calcium, sodium and potassium. Materials of construction will be specified to reduce risk of metal contamination. Additionally, a metal detector system will be utilized to scan the final product and reduce any chance of metal contamination. The other impurities such as sodium and calcium will be removed in the crystallization step.

With this expansion, the company will be able to meet the predicted needs of the US automotive market for lithium carbonate and lithium hydroxide through the year 2020 with domestic sourced materials.

The projects will provide a secure domestic source of lithium carbonate and lithium hydroxide for the US automotive battery industry. It will create 60+ permanent jobs and over 200 construction jobs during the peak of implementation.

Approach

Lithium Carbonate. Excessive buildup of unwanted salts in the solar evaporation pond complex would otherwise hinder achievement of production levels targeted by this project. Earth-moving/civil contractors will complete near-term removal of these salts along with improved contouring of the ponds. Near-term salt removal activities are ~60% complete at this time and will be concluded in 2010.

The acquisition of a custom built salt harvester and associated equipment will enable Chemetall Foote Corp. to self perform long-term salt removal activities and maintain optimal performance in the brine ponds. Delivery of the salt harvester and associated equipment is scheduled for November 2010 and long-term salt removal activities will initiate this winter.

Acquisition of a well drilling rig and associated equipment, along with assembly of a well drilling team, will enable the site to develop a robust drilling program and increase lithium brine flow rates to the pond system. Several pieces of drilling equipment have been purchased including the drill rig itself. The remaining ancillary components will be acquired in 2010 and well drilling activities will commence at a rate of one well per month throughout 2011.

Geothermal Power Plant. A phased approach to this project has been adopted to minimize financial risk to the Company and the Department of Energy. These risks are a result of uncertainty regarding the location, performance and sustainability of the underground geothermal resource.

Phase 1, the exploration phase, is currently underway and includes geophysical and geological survey activities to map the underground resource, drilling of temperature gradient holes to map the heat flow through the targeted well field, and drilling a deep observation well to log flow, pressure, temperature and chemistry of the resource. Geophysical survey activities will be completed in November of this year and a final report will be available in December 2010. A report of the observation well's data analysis is expected to be available for review in May 2011.

Phase 2, the resource development phase, includes design and development of a resource well field. At present, two resource wells and one re-injection well are planned to be drilled to resource depth (2,200 – 4,000 feet). Depending on the temperature of the resource, a sustainable flow rate of 3,000 – 5,000 gpm will be required to achieve the targeted 3.5MW (net output). Phase 2 will begin in May 2011 and is anticipated to conclude in March 2012. Resource well field drilling activities will occur during the final months of Phase 2 during the second half of 2011.

Phase 3, scheduled to begin in 2012, includes the production/equipment phase, including site preparation, well field pipeline construction, design/build/construct and commissioning of the power plant, full load performance testing and separation from the Nevada power grid.

Operational hand-off of the power plant is scheduled for August 2013.

Lithium Hydroxide. Chemetall Foote put together an in-house project team and contracted with BE&K (KBR) to develop the 30% and the 10% cost estimates for the Lithium Hydroxide Project.

BE&K is an engineering firm located in Birmingham, Alabama and was chosen for their engineering experience in similar process design (Chorli-Alkali). Upon completion of the 10% cost estimate, BE&K was contracted to perform the Detail Design Engineering. During detail design, long lead equipment will be competitively bid and placed on order.

The construction work packages developed in detailed design will be placed for bid as well. A construction manager will be contracted to review the bid packages and work with the subcontractors on construction of the Lithium Hydroxide Plant. Construction is scheduled to begin in the second quarter of 2011 and be completed for start-up in the first quarter of 2012.

Results

Chemetall Foote Corp. anticipates having the results no earlier than 2nd quarter of 2012 for the Lithium Hydroxide and Lithium Carbonate Expansion, and 2nd quarter of 2013 for Geothermal Power Plant project.

Conclusions and Future Directions

Drilling activities throughout 2011 will steadily increase lithium brine flows until both the well field and pond complex are performing at targeted rates. Full (targeted) throughput of lithium brine will be achieved during 1st quarter of 2012.

The phased approach to the geothermal power plant project will minimize the risks typical of such projects by allowing the Company and Department of Energy the opportunities at key junctures to review developmental progress and determine if proceeding to subsequent phases of the project is warranted. Geological and geophysical data collected to date continues to look promising and support early opinions that the Silver Peak site is a viable target for geothermal exploration. A full report of geological and geophysical findings will be available for review in December 2010.

Chemetall is working with BE&K on ordering the long lead equipment for the Lithium Hydroxide project. Equipment is scheduled to arrive beginning February 2011. Detailed Engineering is to be completed in the 2nd quarter of 2011. Construction is scheduled to start in the 2nd quarter of 2011 and to be completed by the 4th quarter of 2011. Plant commissioning and testing of the new equipment will be completed in the 1st quarter of 2012.

FY 2010 Publications/Presentations

1. 2010 DOE Annual Merit Review and Peer Evaluation Meeting Presentation.

II.C.4 High-Volume Manufacturing of $LiPF_6$ – A Critical Lithium-ion Battery Material (Honeywell)

Bruce W. Mixer (NETL Project Manager)
Grant Recipient: Honeywell International, Inc.

Brian O'Leary
20 Peabody Street
Buffalo, NY 14210-1523
Phone: (973) 455-5700
E-mail: Brian.Oleary@honeywell.com

Start Date: October 2009
Projected End Date: September 2010

Objective:

Honeywell is building a U.S. manufacturing facility to produce a critical Li-ion battery material – lithium hexafluorophosphate, $LiPF_6$. Honeywell's $LiPF_6$project directly supports the DOE's objective to build and validate production capability of battery materials in the U.S. This project will result in the first U.S. manufacturing facility for $LiPF_6$, establish a secure domestic supply for this critical material in the Electric Drive Vehicle (EDV) supply chain, and form the foundation of a sustainable domestic Li-ion battery industry.

Project Description:

All Li-ion batteries require $LiPF_6$ (Figure II- 7), a material that is not currently made in the U.S. and was in short supply in 2008. Leveraging our capabilities as the world's largest HF manufacturer, the Honeywell team developed a novel process to prepare high-purity $LiPF_6$ as demanded for high-quality lithium-ion batteries. Our project will create 151 direct engineering and construction jobs to build the facility, as well as additional jobs with American equipment suppliers. Honeywell will also add 34 long-term professional and manufacturing jobs to manufacture this strategic Li-ion battery material. Most importantly, the project will help ensure the success of American battery manufacturing and electric vehicle initiatives that are expected to create tens of thousands of jobs.

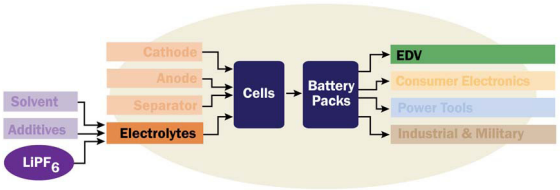

Figure II- 7: $LiPF_6$ is Required in all Li-ion Batteries

✧ ✧ ✧ ✧ ✧

Introduction

Honeywell's experience in developing manufacturing processes and facilities, combined with its history in the industry and relationships with battery customers, ensure that the project will be both a technical and commercial success and therefore advance the national objective to increase the availability and affordability of EDVs. Our project will leverage significant existing assets and knowhow, which enables us to bring $LiPF_6$ to market quickly. It is imperative that the U.S.-based Li-ion battery industry have secure access to the highest quality $LiPF_6$ to avoid disruptions in supply and/or quality from foreign sources.

This project will help enable the successful commercialization of EDVs by providing a secure, reliable supply of $LiPF_6$ to the U.S. market. Honeywell's manufacturing process is environmentally sound, eliminating a hazardous by-product typically produced in alternative processes. All domestic Li-ion battery manufacturers, and their EDV customers, will benefit from this secure and cost-effective supply of $LiPF_6$.

Approach

The objective of this project is to support the EDV Battery Manufacturing Initiative by commercializing the $LiPF_6$ process into an operating Commercial Plant. Using an integrated and systematic approach, Honeywell will complete the engineering design, construction, and commissioning of both the Sample and Commercial Plants. The program has been divided into two phases to meet the expedited timeline required under this FOA. The first phase is the construction and operation of a $LiPF_6$ Sample Plant. This will allow customers to qualify product in their process quickly while the Commercial Plant is under construction. These customer samples will be integrated into batteries, tested and qualified for full

scale battery production. In the second phase of the project, a Commercial Plant will be built, which will be the first U.S. $LiPF_6$ production plant.

In 2010, Honeywell began construction of a plant in Buffalo, New York and will begin sampling customers in 2011. Honeywell will produce sufficient quantifies of $LiPF_6$ to enable our customers (and their customers) to begin the material qualification process.

Results

The award was finalized on April 16th, 2010 and the following results were achieved during the year ended September 2010:

- NEPA Finding of No Significant Impact issued in September 2010
- DCAA Audit was completed in June as scheduled
- Project Management & Planning was completed under Task 1
- Milestone 1 (basic engineering package development) was achieved in June as scheduled; this was the only milestone due during the year
- Procurement & Construction is in process and all equipment has been ordered under Task 2
- Operations Staffing is in process under Task 3.1

Conclusion

The project is progressing on schedule and will help enable the successful commercialization of EDVs by providing a secure, reliable supply of $LiPF_6$ to the U.S. market.

II.C.5 Construction of a Li-ion Battery Cathode Production Plant (BASF)

John Tabacchi (NETL Project Manager)
Grant Recipient: BASF

Joe DiCarlo
39 Veronica Avenue
Somerset, NJ 08873
Phone: (732) 545-5100 ext: 4119; Fax: (732) 249-0271
E-mail: joe.dicarlo@basf.com

Start Date: February 2010
Projected End Date: June 2014

Objective

Construct a lithium-ion cathode production plant capable of supplying cathode materials for more than 100,000 plug in hybrid electric vehicles (5kWh each). The materials to be manufactured are based on technology licensed from Argonne Nathanial Lab.

Technical Barriers

The challenge for the construction of this facility is in the scale up of our pilot operations from Beachwood, Ohio facility currently capable of producing cathode materials in the 10 ton per year quantity to our Elyria facility. The design of our Elyria facility will be flexible enough to manufacture several cathode materials yet efficient enough to produce these materials at competitive price.

Technical Targets

- Conceptual Planning of Production Facility
- Extended Conceptual Planning of Facility
- Implementation (Construction of Facility)

Accomplishments

- Completion of Conceptual Planning Phase.
- Scheduled ground breaking for October 2010 (five months ahead of original schedule).

✧ ✧ ✧ ✧ ✧

Introduction

BASF has made a commitment to become a major lithium-ion cathode producer in the US as well as on a global scale. Prior to making this commitment, BASF secured a license from Argonne National Lab for the portfolio of cathode materials in the lithium nickel, cobalt, manganese phase space. These materials are currently the materials of choice by many cell manufacures for the automotive market due to their superior performance, cost and safety properties. Also of high importance to BASF's commitment was the US Govermenment's investment in building the infrastructure (lithium-ion battery value chain) in the US. A third factor that led to BASF's commitment was favorable feedback from some of our target customers on the performance of our cathode materials supplied by our US based pilot facility. These three factors, along with BASF's technical competence in scale up of inorganic oxide materials, formed the base of our commitment for our investment in a US cathode production facility.

Approach

BASF is doing most of the detailed design for the cathode facility itself due to the intricate nature of the cathode production process; however, BASF plans to outsource the construction contracts to US based companies. In addition, BASF is in the process of procuring both domestic and international equipment for the production of cathode materials. BASF uses a very fair and competitive process to select vendors for both construction and equipment.

Results

BASF has completed the conceptual planning phase of the cathode production facility and has scheduled the ground breaking for the facility in October 2010. BASF is also well underway in providing pilot plant samples of our NCM cathode materials to many global manufactures of lithium-ion batteries.

Conclusions and Future Directions

BASF is well underway on the construction of a lithium-ion cathode facility in Elyria, Ohio. BASF hopes to complete the construction phase of our project by next October and have the cathode facility operational in 2012.

FY 2010 Publications/Presentations

1. No Publications/Presentations in 2010

II.C.6 Nanoengineered Ultracapacitor Material (EnerG2, Inc.)

John G. Tabacchi (NETL Project Manager)
Grant Recipent: EnerG2, Inc.

Eric Luebbe
Morgantown Campus
3610 Collins Ferry Road, PO Box 880
Pittsburgh, PA 15236
Phone: (412) 386-7298; Fax: (412) 386-5835
E-mail: john.tabacchi@netl.doe.gov

Start Date: April 2010
Projected End Date: March 2012

Objectives

EnerG2, Inc. will build the first facility in the world dedicated to the commercial scale production of synthetic, high-performance carbon electrode material and the only U.S. facility to manufacture electrode materials for ultracapacitors (a market currently dominated by Japanese suppliers). Our product, the NC-Series Electrode Carbon, will result in a next generation ultracapacitor with significantly higher power density and much lower cost per kW. This achievement will enable the combination of ultracapacitors and batteries in electric drive vehicles to reduce battery replacement costs, improve mileage efficiency, and increase vehicle road performance. The new plant will produce enough NC-Series electrode carbon to supply production of 60,000 EDVs annually.

Leading international ultracapacitor manufacturers are already evaluating this material and will purchase our electrode material to make these energy storage devices available to a broad array of EDV manufacturers. In relation to DOE objectives, this U.S. plant based on American nanotechnology will spur a strategic shift away from pure battery packages to optimized battery/ultracap systems for EDVs. The project will exclusively utilize an American raw material feedstock similar to resins used in the wood products industry and create a minimum of 50 construction jobs and 35 manufacturing jobs in Albany, OR - a rural community hard hit by unemployment.

✧ ✧ ✧ ✧ ✧

Introduction

The premise of the project is that, based on existing technologies, a combined battery-ultracapacitor energy storage system can be built that is fundamentally superior to an all-battery system for electric drive vehicle applications. However, before such a combined system can be produced, the cost-performance profile of ultracapacitors must be improved. The only viable path to such improvements can come from enhancements to the carbon electrode materials that comprise the most important ingredient in an ultracapacitor.

The DOE has funded EnerG2 to build the first facility in the world dedicated to the large-scale production of synthetic, high-performance carbon electrode materials for ultracapacitors. The plant will be turned up on a 23-month fast track by early 2012 and will produce NC-Series electrode carbon for use in ultracapacitors for EDV energy storage systems. This project addressed DOE's Vehicle Technologies Program Area of Interest 2. The total project costs will be $28.4M.

Approach

EnerG2 has achieved a breakthrough with its proprietary engineered carbons for ultracapacitor electrodes. The company's nanomaterials will be the needed catalyst for new battery-ultracapacitor applications in EDV systems and a new round of rapid industry expansion beyond transportation. The EnerG2 research team has developed and commercialized a low cost process for synthesizing high-performance pure carbon materials using sol-gel processing nanotechnologies. Through precision control of the molecular self-assembly of the materials from basic chemical inputs, these processes optimize the key physical characteristics of the resultant material:

- Ultra-high surface area
- Carefully optimized surface structures
- Near perfect purity

The project, when complete, will fully migrate these commercialization efforts from small-scale outsourced manufacturing to large-scale internal manufacturing operations.

Project Goals

The project has been compartmentalized into four overlapping project phases:

- Phase I Process Design – This phase established the project management system and confirmed roles among team members, confirmed building site selection and saw the consummation of the real property transaction for the site, finalized building and process design specifications, selected many

subcontractors, started equipment procurement of long lead time items and conducted testing for environmental permitting.

- Phase II Equipment Procurement – Work during this phase will involve equipment procurement, manage initial stages of building construction, and file all environmental permits with appropriate authorities.
- Phase III Construction – This phase will focus on completion of the required upgrades to the building, installation of all equipment, utility connections, and environmental hazard, chemical hygiene, security, and fire safety systems. All environmental permits are secured. Plant personnel required for startup are recruited and trained and HR systems fully implemented. Plant operating and QA/QC procedures fully established.
- Phase IV Startup – This phase consists of testing and integrating all equipment and control systems, generating first batches of finished product, and process optimization to meet all specifications. Final operating personnel are also hired and trained.

EnerG2 is currently in Phase II of the project, as defined by the phase durations established and confirmed in Phase I. Phase III is expected to commence and ramp up in early 2011 and will involve and estimated 50 construction jobs in the Albany, Oregon area. Phase IV will begin in fall of 2011. By the end of Phase IV, the project will have created 35 permanent, high quality jobs.

Milestones

EnerG2 is in the early stage of the project and has recently begun Phase II of the project. Several milestones have been completed, as listed in Table II- 2.

Table II- 2: EnerG2 Nanoengineered Ultracapacitor Project Milestones.

Milestone Title	Planned End Date
DOE Contract Signed	March 2010
NEPA Assessment Complete	April 2010
E/P/CM Notice to Proceed	June 2010
Process Design Complete	August 2010
Ground Breaking Ceremony	August 2010

Next Steps

With the conclusion of Phase II of the project, EnerG2 will commence construction of the physical facilities within an existing converted warehouse in Albany, Oregon. Processing equipment will be designed, ordered, manufactured, delivered and installed. Throughout most of 2011, EnerG2 and project subcontractors will be working to establish an integrated manufacturing line, based on EnerG2's proprietary manufacturing processes, to meet the carbon electrode demands of 60,000 EDVs per year.

FY 2010 Publications/Presentation

None

II.C.7 Expansion of Novolyte Capacity for Lithium-Ion Electrolyte Production (Novolyte)

Christopher Johnson (NETL Project Manager)
Grant Recipent: Novolyte

Ralph Wise
8001 East Pleasant Valley Road
Independence, Ohio
Phone: (216) 867-1064; Fax: (216) 867-1089
E-mail: wiser@novolyte.com

Start Date: May 2010
Projected End Date: September, 2015

Objectives

- This is a two phase $40 M plant expansion project. The objective of the first phase of the project is to increase Novolyte's electrolyte manufacturing capacity at its Zachary, LA facility from 1500 metric tons (MT) to 4,500 MT.
- The objective of the second phase of the project is to increase plant capacity from 4,500 MT to 10,000 MT intersecting with forecast demand for large lithium-ion batteries for the adoption of electric drive vehicles.

✧ ✧ ✧ ✧ ✧

Introduction

The project retains existing employees while creating new employment opportunities by expanding an existing electrolyte manufacturing facility in Zachary, Louisiana, while targeting and supplying a rapidly growing strategic industry, electric drive vehicles. Once completed, this expanded facility will have enough capacity to supply the volume of electrolyte necessary to support a xEV penetration of an estimated domestic demand of 10% of the forecast global electric drive market in 2015, with Novolyte serving 50% of the domestic market share.

The expansion component of the proposed project will consist of the installation of approximately 60,000 square feet of new buildings, bulk chemical storage, materials handling, purification, mixing and reaction vessels in order to efficiently manufacture electrolyte solutions, a key component of lithium batteries, lithium-ion batteries and ultracapacitors. In addition, packaging, handling and quality control/quality assurance capabilities consistent with current and expected market requirements will be adopted and installed as part of the project.

Approach

Phase 1 utilizing approximately $6M in capital to 2012 consists of installing 3,100 square feet for building upgrades, adding bulk chemical storage, expanding materials handling, adding purification and mixing capability, increasing reactor capacity and upgrading support and ancillary equipment including utilities. Process development and manufacturing related activities in this scope of work include handling and manufacturing lithium salts, upgrading organic solvent handling, producing electrolyte mixture formulations, purchasing storage, shipping, and handling (cleaning) equipment, purchasing and testing reusable electrolyte shipping containers and implementing further quality control measures by upgrading the laboratory as well as installing additional utility infrastructure and environmental compliance and support.

The scope of work for Phase 2, utilizing $34 M in capital and set to begin in 2013, increases manufacturing capacity from 4,500 MT to 10,000 MT. This phase of expansion will consist of the installation of approximately 60,000 square feet of new buildings, bulk chemical storage, materials purification, mixing and reactors in order to efficiently safely manufacture electrolyte solutions.

Results

Novolyte was officially put under contract by the DOE on April 30th, 2010. Plant expansion activities since that date have focused on upgrading quality control measurement equipment, testing and implementing new processes and systems as well as installing low to medium volume sampling and handling equipment. To insure high quality, a gas chromatograph/mass spectrometer and an ion chromatograph were purchased and installed. New quality checks and audits to adhere to the demanding quality needs of the automotive industry were implemented. Designs, upgrades and new piping were installed for a 150 gallon sample reactor. Additional shipping vessels and an electrolyte sump pump were also purchased and installed.

A significant development for Novolyte that occurred in September 2010, and that will interact with the goals of this project was the signing of a joint venture agreement by Novolyte and Foosung, a Korean manufacturer of lithium

hexaflourophosphate ($LiPF_6$) the critical salt in lithium-ion electrolytes. It should be stressed that no ARRA DOE expansion funds will support the development of Foosung's existing or future Korean assets.

Conclusions and Future Directions

FY 2011 work continues with site construction activities that will further increase electrolyte manufacturing capacity with improvements in utility, logistical and transportation infrastructure as well as the purchase of large scale holding and reactor tanks and control systems.

FY 2010 Publications/Presentations

None

II.C.8 Establish and Expand Commercial Production of Graphite Anode Batteries for High Performance Production of Li-ion Batteries (FutureFuel)

John Tabacchi (NETL Program Director)
Grant Recipient: FutureFuel Chemical Company

Gary McChesney
2800 Gap Road / P.O. Box 2357
Batesville, Arkansas 72501
Phone: (870) 698-3000; Fax: (870) 698-3000
E-mail: GaryMcChesney@ffcmail.com

Start Date: August 2010
Projected End Date: February 2012

Objectives

- Design and construct a manufacturing plant to produce 10,000,000 pounds per year of graphite anode material for high performance lithium-ion batteries
- Checkout, commission, and start up a manufacturing plant to produce 10,000,000 pounds per year of graphite anode material for high performance lithium-ion batteries
- Qualify anode material for use in high performance lithium-ion batteries

Technical Targets

- Produce graphite anode material with performance equivalent to graphite anode material produced in semi-works facility
- Produce 10,000,000 pounds per year of graphite anode material

Accomplishments

- Engineering contractor hired and engineering started – August 2010
- 43% of process equipment purchased as of September 30, 2010
- Construction started – September 2010

✧ ✧ ✧ ✧ ✧

Introduction

FutureFuel Chemical Company (FFCC) will design, install, and operate a commercial-scale plant to produce an Intermediate Anode Powder exclusively for ConocoPhillips (COP). FFCC has a specialty chemical and biofuel manufacturing facility located in Batesville, Arkansas. The Intermediate Anode Powder is a coated petroleum coke powder that is an intermediate for ConocoPhillips CPreme® Anode Materials.

An existing FFCC manufacturing plant in Batesville, Arkansas, will be retrofitted to produce Intermediate Anode Powder, based on patented technology and proprietary manufacturing processing methods developed by COP. This technology has been demonstrated in COP's Ponca City, Oklahoma, research and semi-works facility. The FFCC plant will be at least ten times the scale of COP's semi-works facility.

By leveraging existing manufacturing assets, infrastructure, and environmental permits, FFCC will complete the Intermediate Anode Powder plant for a fraction of the capital cost of a new facility, and will commence commercial production at a 10,000,000 pound-per-year rate as early as the first quarter of 2012.

The FFCC manufacturing plant to be reconfigured includes 70% of the major process equipment and 60% of the pumps required. Construction of additional manufacturing building floor space will not be required for the completion of the project. Site utility systems have adequate capacity to supply the requirements for the Intermediate Anode Powder plant except for a required expansion of air separation. The new air separation equipment will provide nitrogen for tank blanketing and inerting of the dryer system. Only minor modifications to FFCC's Title V air permit are required to initiate production of the Intermediate Anode Powder.

The plant will be designed with the capability to produce Intermediate Anode Powder used in all commercial and developmental CPreme® Anode Materials. When completed in 2012, the facility will have the capacity to process 10,000,000 pounds per year of Intermediate Anode Powder, sufficient for supplying over 2,000,000 hybrid-electric vehicles.

Approach

A project management system including the following components will be used to manage the project:

Front-end Planning. The project scope is defined and the initial budget estimate is developed. The estimate is based on current equipment lists, quotes from equipment vendors, and use of a historical database. The work

breakdown structure and engineering deliverables are defined.

Detailed/Appropriation Estimate. This estimate will be prepared based upon the goals, project description, procurement, and constructions plans, and design criteria. .The estimate will include direct accounts associated with specific project deliverables and indirect accounts for engineering, project management, and miscellaneous field charges.

Scheduling. An engineering, procurement,, and construction schedule will be developed based on the work breakdown structure and detailed estimate. Microsoft Project scheduling software will be used. Durations will be assigned to activities, imposed dates (constraints) will be identified, and resource requirements will be input to the schedule. A baseline schedule will be set to monitor all future progress.

Monitoring. Actual status of engineering, procurement, and construction progress are noted and input into the scheduling system on a biweekly basis. After each update cycle, the schedule will be reviewed and any problems identified by examining negative or low float paths. Actual costs and progress of engineering and construction productivity will be input to cost systems.

Reporting & Analysis. Biweekly generated reports will be used to contrast actual schedule/cost data against baseline schedule/cost data. Variation from the baseline plan indicating areas of potential concern will be addressed. Project management will react to schedule/cost variances, adjusting the schedule to minimize the impact of variances.

Forecasting. Based on the current status of the project schedule/cost, forecasts will be made to estimate date and cost of project completion.

Justification of Schedule for Completion. The appropriation estimate and baseline schedule will be compared/benchmarked to help predict project outcome. A project evaluation system, using a set of statistical models, can evaluate project outcomes in a number of key areas including cost and schedule. Cycle time duration (project definition through mechanical completion) and execution duration (detailed engineering through mechanical completion) will be compared to industry averages and historical data for similar sized projects.

A formal project change order process will be implemented to control cost. The originator of a change must estimate its cost and schedule impact, and identify other areas of the project that will be affected by the change. Approval is required by other members of the project team. If the change is an estimating variance or a variance within scope, it is considered to be a control type change order. If the change is a scope change, it is considered to be a design change order and a memorandum of change will be initiated to acquire additional approvals.

Schedule slippage will be controlled by reviewing the schedule after each biweekly update cycle. Negative or low float paths will be reviewed with the discipline involved; engineering, procurement, or construction to resolve the problem by schedule compression or by logic revisions to bring the schedule back on track.

Gated Company Work Process to Execute Project. Checklists will be used for the following gates/stages of project execution:

- Final Appropriation. Includes estimate, approved P&I drawings, equipment list, environmental permit requirements, project schedule.
- Start-up/Readiness. Includes systems turnover, system checkout, safety reviews.
- Closing. Includes punch list certified complete, all orders closed, engineering drawings released, and documents archived.

Results

As of September 30, 2010, the project has been underway for two months. The engineering contractor is working, a significant quantity of long-lead time equipment has been purchased, and construction has started on one portion of the plant.

Conclusions and Future Directions

The project is on schedule, on budget, and expected to achieve all objectives and technical targets.

FY 2010 Publications/Presentations

None

II.C.9 Battery Materials Production Facilities (Pyrotek Incorporated)

John Tabacchi (NETL Project Manager)
Grant Recipient: Pyrotek Incorporated

Michael J Sekedat
Kevin Scott
2040 Cory Road
Sanborn, NY 46256
Phone: (716) 731-3221; Fax: (716) 731-4943
E-mail: kevsco@pyrotek-inc.com

Start Date: October 2009
Projected End Date: December 2011

Objectives

Pyrotek utilizes proprietary furnaces and processes to heat treat materials to extremely high temperatures, known as graphitization. We utilize our services to graphitize material from one of our customers, ConocoPhillips, to produce a superior anode material for the production of lithium-ion batteries. The DOE Award under Funding Opportunity DE-FOA-0000026 has provided a grant to support our expansion of our Sanborn, NY plant and our graphitization operation. There are three objectives associated with this project:

- Increase anode material production capacity at the Sanborn plant to meet higher projected EV, PHEV and HEV demands.
- Decrease processing costs to ultimately provide a lower priced material to the lithium-ion battery manufacturers.
- Meet the objectives of ARRA2009 by creating and preserving construction and manufacturing jobs within the United States.

Technical Barriers

The graphitization/heat treatment service that is provided by Pyrotek utilizes a proven furnace technology that has been in use by Pyrotek for more then forty (40) yrs. This furnace technology along with our customer's proprietary raw material preparation techniques, have proven to produce an anode material that is superior to that of any other on the global market. Pyrotek is and has been supplying this specific heat treatment service to our customer for more than two (2) years, so although there are ongoing efforts to achieve technical advancements and production efficiencies, our equipment and processes are already proven to be successful at producing a superior anode material.

Technical Targets

- Increase capacity to meet the forecast demands for lithium-ion battery anode material, by increasing plant size and production equipment.
- Increase capacity via improved processing methods to maximize equipment throughput, thus increasing overall plant capacity and reducing production costs.

Accomplishments

- Award was finalized in March 2010.
- Facility engineering has been completed, and site work and construction was started on July 15, 2010.
- Long lead time equipment purchases have begun. As of the end of September 2010, over seventy percent (70%) of the Purchase Orders have been issued to vendors for all facility and equipment acquisitions associated with this expansion project.

✧ ✧ ✧ ✧ ✧

Introduction

Pyrotek, Incorporated ("Pyrotek") is a privately owned US based company that was founded in 1956, in Spokane, WA. Metaullics Systems, a Division of Pyrotek, provides graphitization services with proprietary furnaces and processes within our Sanborn, NY plant. Due to the high demand for electricity in this process, our plant utilizes the low cost hydro-power available from Niagara Falls, as allocated by the New York State Power Authority.

Pyrotek is a strategic partner of ConocoPhillips in the production of a high performance anode material, marketed and sold by ConocoPhillips as CPreme® Anode Material (CPreme®). Our role in the production of this high performance anode material is to graphitize specially treated material provided by ConocoPhillips. This is the final step in producing CPreme®.

ConocoPhillips is presently the only domestic producer of anode material for lithium-ion batteries. They use patented technologies and proprietary processes to produce their anode raw material. This anode is superior to other materials available in the global market, because of its high power capability and efficiency, excellent charge capacity, and thermal characteristics. The lower priced hydro-power electricity effectively lowers the overall processing cost at the Sanborn plant, which equates to lower priced lithium-ion batteries.

Our involvement with this anode production makes us a key member of a domestic supply chain for lithium-ion batteries for the automotive, load leveling, power tool and defense industries.

Approach

This project will add an additional ninety-three thousand square feet (93,000 sq ft) to an existing Pyrotek plant. Seventy-five thousand square feet (75,000 sq ft) will be used to increase the processing capacity. This will also include the acquisition of additional material handling equipment, and twelve (12) new graphite furnaces that are scheduled to be built and brought online by the end of CY2011, as needed to meet the projected volume demands. As of September 30, 2010, Pyrotek has contracted with three main vendors to handle the facility expansion, the electrical infrastructure and the mechanical/piping infrastructure. Pyrotek is managing these vendors to ensure the expansion schedule is met (barring any uncontrollable winter weather interruptions). At this time, the new facility occupancy is targeted for the end of February, 2011.

A data collection/bar code system will track all material by lot numbers, keeping track of inventory and processing metrics. Material quality testing will be performed after completing processing steps to ensure the desired anode material properties are achieved and provided to the battery manufacturers. The network will automate much of the material tracking (which will be necessary as the volumes continue to grow over the next few years), while also providing a direct link into our MRP System to avoid duplicate data recording. At present, Pyrotek is graphitizing an increasing volume of material within our existing Graphitization Department. The end product quality consistently meets our customer (and their battery manufacturer customers') requirements.

Post award volume forecasts suggest the facility will be brought to full capacity at a faster pace than originally scheduled. As noted, seventy-five thousand square feet (75,000 sq ft) of the expansion will be utilized for the initial production increase. The remaining eighteen thousand square feet (18,000 sq ft) will be used as a storage area for equipment spare parts, as well as for material storage, as needed. After this expansion project is completed, and the final draws from the DOE Award have been made, it is expected that the storage area will be utilized to house an additional six (6) new graphite furnaces, in response to the forecasted, growing material demand levels.

Results

At this point, the site work and facility construction is underway, and the procurement of the specialized and proprietary equipment has begun. The project is on schedule, as we have been very fortunate with an excellent string of good weather days. As more of the project budget is finalized, we have now determined that we will be slightly over budget. When the award application was submitted in April, 2009, the expansion size and equipment needs were based on production volumes known at that time. Since then, material costs have dramatically increased, and the overall size of the project has grown to accommodate the higher production forecasts now being provided by the entire supply chain. The total project budget contained within our award application was $22,669,303. At this point, we have adjusted our budget up to $23,328,900.

Conclusions and Future Directions

As noted, the anode material that Pyrotek completes is a superior product. Specifically, this anode material is more stable, which equates to a longer battery life. In addition, the anode material provides a higher discharge rate, which resultisin a smaller, lighter battery for HEVs, and it has a higher thermal stability for a safer battery. Lastly, this material provides the ability to develop ultra high power anodes for other challenging applications.

In response to the future forecasted demand for anode material that will far exceed the full capacity of our completed plant expansion, our long term plans include adding furnaces to bring the total up to (18) furnaces within the new plant. Beyond that, we expect to either initiate a second expansion project on our adjacent (12) acre parcel in Sanborn, NY, or to pursue expansion options within other states, where comparable low cost hydro power is available.

Concurrently, our customer has informed us of their future plans to expand the product line to target a wide spectrum of automotive lithium-ion battery chemistries, and to scale-up their own raw material production levels to meet the growing demand and drive costs lower. All the while, we will continue to jointly work on optimizing the production processes to lower costs further while being able to accommodate all newly developed products aimed at growing the lithium-ion battery adaptation.

FY 2010 Publications/Presentations

1. 2010 DOE Annual Peer Review Meeting Presentation.

II.C.10 Manufacture of Advanced Battery Components (HTTM LLC, H&T, Trans-Matic)

John Tabacchi (NETL Project Manager)
Grant Recipients: HTTM, LLC, H&T, Trans-Matic

Dan Moffa
H&T Waterbury, Inc.
984 Waterville Street
Waterbury, CT 06704
Phone: (203) 596-3329
dan.moffa@ht-group.com

Robert Stander
HTTM General Manager
300 East 48th St.
Holland, MI 49423
Phone: (616) 820-2456
bstander@transmatic.com

Start Date: September 2009
Projected End Date: September 2015

Objectives

- Design and engineer unique U.S.-based product development and manufacturing processes which will produce metal outer shell containers, covers, and other components and assemblies for sustainable lithium-ion battery products for automotive and other applications;
- Develop and expand a highly skilled technical workforce through hiring & training several new professional, semi-skilled and skilled technicians; and,
- Install the designed processes at the Holland, Michigan facility and begin production.

Technical Barriers

Given the nature and ultimate operating use of the battery container components and other associated parts, the choice of base materials is critical, along with the manufacturing process. Normal commercial grade materials do not often have the consistency of gage and physical properties required for this application. This is especially important in the areas of cleanliness and safety vent design. Safety vent consistency and predictability is directly proportional to the base material consistency and the tooling precision and process capability.

In addition to the tight control of base material properties, the level of residual particulate matter present on the components after fabrication is critical. The low particle count and surface finish requirements as specified by battery OEMs are well beyond normal manufacturing protocol. In each case plans are developed to address these issues including primary lubricants and coolants, handling of raw materials and components during fabrication and assembly, final cleaning equipment and processes, inspection and automated packaging systems and dunnage.

Technical Targets

- Develop a cell containment system to meet OEM technical, quality, durability and cost objectives.
- Design and install a manufacturing process to produce consistent hermetically sealable container components that can be assembled automatically by the customer. Design and produce a safety vent feature with an operating bursting range of 8 to 12 bar.
- Create and implement an in-tool automated vent feature measurement system that provides accurate and dynamic feedback on 100% of the parts produced.
- Provide components that comply with class 100 cleanliness specifications, or other specification as determined by OEM customers.

Accomplishments

- Successful simulation, development, and prototyping of both cylindrical and prismatic deep drawn and impact extruded cell cases.
- Successful design and development of vent design features in cell cases that maintain a statistically valid bursting range within 4 bar.
- Designed and built burst testing equipment to provide a controlled and repeatable bursting test in order to validate the production process used to create the vent feature in cell cases.
- Developed a cover assembly terminal component using a lower cost manufacturing method.
- Development of an integral termination feature for cell covers as a future value engineering change for additional cost reduction.
- Pre-production cell cases and cover assemblies have been produced and delivered to customers on time.

✧ ✧ ✧ ✧ ✧

Introduction

HTTM via its parent companies and affiliates is a global industry leader providing engineered components, mechanical assemblies and proprietary products to diverse markets. The company specializes in producing deep drawn and stamped precision metal components and assemblies. Over the past several years there has been a strategic focus on the development and supply of containers, components, and cover assemblies to the global market for advanced energy storage cells.

Current HTTM capabilities were adapted to provide stainless steel, steel and aluminum cylindrical and prismatic containers with integral safety vents using deep drawn, progressive, and impact extrusion processes. Covers/lids and other components of various materials were also developed, produced and then assembled utilizing laser welding, integral termination, swaging, threading, and helium leak testing processes.

Approach

HTTM offered many advantages and capabilities to its OEM advanced battery customers:

- With over 100 years of combined technical, tooling and manufacturing experience, HTTM has the capabilities needed to produce the tight tolerance sophisticated cell container components and assemblies;
- HTTM chose to vertically integrate beyond component fabrication and also invest in assembly, cleaning and testing capability as to offer "turnkey" services to OEM customers.
- Through the utilization of its parent companies, HTTM has facilities in the US, Europe and China and therefore is able to scale up and supply to the Global OEM Advanced Battery System Producers.
- The internal innovation, development, design and prototyping capabilities of HTTM go well beyond run of the mill stamping companies. HTTM engineers offer design and processing expertise that is not resident within the advanced battery OEM's and HTTM experts become an extension of OEM engineering groups through the use of joint development agreements.
- HTTM, through its parents, has a long history of production of consumer battery components as well as components for other energy storage devices such as high energy capacitors.
- The financial strength of HTTM and its parent companies along with the DOE ARRA grant funding has enabled HTTM to procure and implement state of the art equipment and processes to meet the increasingly rigorous technical requirements for storage cell container systems.

Results

HTTM (H&T and Trans-Matic) have been successful in working with OEM advanced battery customers to provide the expertise, products and processes needed to be successful in the advanced energy storage market.

HTTM is currently working with several OEM cell producers to provide cell containers and cover assemblies for various cylindrical and prismatic battery cell systems. Prototype, pre-production and production containers and cover assemblies have been produced and shipped to OEM customers as required.

Tooling and processing equipment design and fabrication are on schedule and on budget for the projects. Facility preparations are underway to accommodate high volume production in mid 2011.

HTTM has been successful in establishing itself as a subject matter and manufacturing expert for the development and production of advanced battery container components. HTTM utilizes its capabilities on a global basis and has delivered specialized development expertise and flexible manufacturing centers to create high quality and cost effective solutions for its customers.

Conclusions and Future Directions

HTTM through H&T and Trans-Matic has taken its successful core businesses and technologies and effectively applied these to this new advanced energy storage market. With existing relationships with several of the key OEM players, HTTM has won the trust of the OEM producers and will continue to deliver turnkey solutions for battery containerization. As the industry and market evolve with technology and ultimate customer needs, HTTM will remain in a leadership position through confidential joint development work with its key customers and through continued independent research and development.

Publications/Presentations/Exhibitions

1. 2010 Business of Plugging in Conference – Detroit, MI
2. 2010 Fabtech Exposition – Atlanta, GA
3. 2010 Euroblech Exposition – Hannover, Germany

II.D Battery Recycling Facilities

II.D.1 Next-Generation Lithium-Ion Battery Recycling Facility (Toxco)

Bruce W. Mixer (NETL Project Manager)
Grant Recipient: Toxco

Hector Morales
Electricore, Inc.
27943 Smyth Drive, Suite 105
Valencia, CA 91355.
Phone: (661) 607-0286; Fax: (317) 607-0264
E-mail: hector@electricore.org

Start Date: September 2009
Projected End Date: September 2015

Objectives

Toxco Incorporated proposes a comprehensive project to establish the domestic recycling capacity for large format advanced Li Ion batteries used in advanced electric drive vehicles (EDVs), including plug-in hybrid electric vehicles (PHEV) and hybrid electric vehicles (HEV), by designing and building an advanced, innovative recycling facility to operate in conjunction with our existing hybrid and electric vehicle battery recycling facility in Ohio. Successful completion of this project will provide lithium battery quality cathode and anode material plus purified electrolyte solvents and raw materials to the battery OEM's and ensure the proper environmental management of the end of life batteries.

Technical Barriers

There are disadvantages associated with any specific type of battery beyond its useful life and many used batteries need to be disposed of according to applicable EPA requirements.

Technical Targets

The following are the technical objectives for each phase of the proposed work:

- Phase One (Year 1):
  - Define customer requirements
  - Environmental assessment and permitting complete
  - Complete process and facility designs
  - Validate recycle and refurbish process on a lab scale
  - Complete facility build
  - Install the Lithium Cobalt and NiMH processing line
- Phase Two (Year 2):
  - Conduct pilot operation of the Lithium Cobalt and NiMH line
  - Install the Lithium Mixed Metal Oxide processing line
  - Install battery refurbishing process line
  - Conduct pilot operation of the battery refurbishing process line
- Phase Three (Year 3):
  - Conduct pilot operation of the Lithium Mixed Metal Oxide line
  - Install the Lithium Iron Phosphate Processing line
  - Conduct pilot operation of the Lithium Iron Phosphate line
  - Validate recycle processes (all lines) on a production scale
  - Validate refurbish process on a production scale

Accomplishments

- Lithchem Energy successfully tested some of the recovery processes for the lithium process lines
- The groundbreaking took place on November.
- Toxco has begun the site work and is currently on schedule.
- Foundation phases have begun and are on schedule at present.
- DCAA compliance has been established and Toxco is now awaiting audit.

✧ ✧ ✧ ✧ ✧

Introduction

When reviewing the technical feasibility of the proposed U.S. advanced battery recycling facility, past history and current activities show that Toxco is

uniquely qualified to bring this project to an assured conclusion. In 1993, Toxco, Inc., designed, and built a facility with the expressed purpose of managing and recycling highly reactive primary lithium batteries in Canada. Today, the recycling of lithium batteries remains Toxco Inc.'s primary activity at the Trail location. As the development of lithium batteries gained momentum in the 1990's, Toxco added to the facility's capabilities with the addition of secondary processing lines to manage rechargeable lithium-ion batteries.

Toxco Inc's Canadian facility is generally recognized as a world leader in the field of lithium recycling as they currently recycle both primary and secondary lithium batteries from a broad range of power applications. Toxco currently works with a multitude of battery manufacturers, as well as automobile manufacturers throughout North America. Toxco has developed technologies and recycling capabilities to handle a variety of lithium battery systems at their facility in Trail, British Columbia, Canada.

It is Toxco's intentions, through the DOE funding opportunity DE-FOA-0000026, to enhance and modify the existing secondary lithium-ion recycling technologies and, relying on Toxco's years of experience within the battery recycling industry, build an improved operation in the United States.

As a result of Toxco's longevity within the battery recycling industry, and as our experience shows, Toxco is certain that the system outlined in the technical discussion is with merit and is technically feasible. In addition, the risks associated with this project are well known by Toxco and will be actively managed throughout the project and as part of the company's ongoing operations.

Approach

Toxco will build a 50,000 sq ft building with the required extensive permitting for the new LIB recycling plant on its property adjacent to its current lead acid, NiMH, and NiCad battery recycling plant in Lancaster, OH. This facility will have access to truck and rail siding. Toxco is expecting three basic LIB cathode chemistries for advanced EDV batteries and is therefore planning on the three segregated parallel processing lines in order to maximize the ability to eliminate cross contamination of the cathode components and potentially other unique battery components as technology develops. Although Toxco has identified the currently expected HEV/PHEV/EV lithium-ion battery cathode chemistries, the three segregated lines can be adjusted to any new LIB developments and more than one type of LIB can be run on any of the lines when there is a clean out between runs. These chemistries are NiMH, Lithium Cobalt, Lithium Mixed Metal Oxide and Lithium Iron Phosphate. Additionally, Toxco has identified the need to process and refurbishes these chemistries at end of life.

Lithium Cobaltate. This is a valuable cathode material which must be kept pure (segregated) if the lithium cobaltate is to be reused for LIB application or even if it must be extracted out of the cathode/anode carbon filter cake as the cobalt cation. This has been the predominant cathode material for LIB.

Lithium Iron Phosphate. This is the cathode material of choice for higher power long life batteries and has been selected for the Toyota Prius and various planned Chrysler models (A123Systems). These LIB batteries must be held separate from the other LIB cathode chemistries if the others are to be recycled. This is because the iron is a diluent and destroys the performance of the other cathode materials. The value of lithium iron phosphate is the highest if it can be reclaimed as an intact high performing cathode material. It has little or no value if acid is extracted from the anode carbon/cathode filter cake which is an added cost. Toxco will work on reclaiming it as an intact cathode material for direct reuse in batteries.

Lithium Nickel Cobalt Aluminum Oxide. This is the cathode material selected by Saft for the HEV/PHEV/EV. This is one of many mixed oxide type cathode materials. It also has the highest value on recycling if it can be obtained as the intact cathode material. This dedicated line will be used for all mixed oxides since simple clean up between mixed metal oxide types should be sufficient for maintaining adequate purity for these materials since they are not sensitive to trace amounts of other related metallic cation impurities. Another reason at this time for using a dedicated line for the Saft battery is the fact that they plan to use methyl butyrate in their electrolyte. Toxco has had very unpleasant experiences in recycling batteries containing this noxious smelling ester (derivative of butyric acid) at its Trail facility (OSHA concern due to inducing feelings of nausea in some people). Toxco has changed the process flow diagram somewhat on line 3 to try to isolate and counteract the strong noxious odor from the electrolyte containing this material. (Adding LiOH at the start of the process to promote hydrolysis of the ester to the lithium butyrate and not recovering the solvents until the methyl butyrate and probably some of the dissolved solvents are reacted.)

Toxco currently manages lithium-ion (including small consumer batteries and prototype large format automotive EDV batteries), nickel metal hydride and lead acid batteries at their Trail, British Columbia and Lancaster, Ohio facilities. Toxco recycles the lithium, nickel and lead batteries and can refurbish lead acid batteries through their Battery Power of Ohio

(Baltimore, OH) operation. This corporate experience is one of the keys to the feasibility of the proposed project. Toxco's proposed process is built on tremendous knowledge of the battery recycling and refurbishing industry as well as the chemistry and manufacture of lithium-ion battery salts, electrodes, cathode material and cells.

Specifically, Toxco has had over 16 years experience in the commercial operation of a recycling line for primary lithium batteries and a separate line for lithium-ion batteries (LIBs). The current process for LIBs was designed and improved based on operating experience for small LIBs consisting of many different chemistries and with a volume greater than 1 M lbs a year of LIB. However, Toxco has actual experience in recycling large lithium-ion automotive batteries on this LIB line and has gained very valuable information from this. Additional hands-on experience has also been acquired in recycling NiMH and lead acid batteries and refurbishing lead acid automotive batteries at its Lancaster, OH facility. This facility is also currently crushing and recycling large industrial lead acid and NiCd batteries commercially.

LithChem Energy, the research and development organization for Toxco, has gained a thorough understanding of the manufacturing and chemistry of the lithium-ion battery through ongoing LIB development programs both on LIB component materials including cathode materials, electrolytes, lithium salts, and cell construction. (A list of key Toxco personnel patents is provided in this proposal.) Other development programs in LIB recycling, lead acid battery recycling and ultra capacitor recycling have given Toxco a broad and comprehensive view of the process technologies that can be applied to large volume and large size LIB(HEV/PHEV/EV) recycling. Based on this advanced LIB materials, cell development and unequalled hands-on LIB recycling experience, Toxco is proposing to build the most advanced practical LIB recycling line in the world which will recover the maximum amount of LIB battery components for direct reuse in the manufacture of LIBs. Toxco will build upon their extensive experience to design and build a comprehensive large format lithium-ion recycling facility. This section will discuss our current processes at Trail and Lancaster and propose a novel process for handling large format Lithium batteries for EDVs.

Included in the Facility Appendix and the Project Management Plan are the proposed schematics of the proposed building as well as a time frame in which it is to be completed.

The overall expected cost of the proposed Toxco facility is $19.1 million dollars. This investment shows Toxco's commitment to the existing and developing U.S. HEV/PHEV market and the anticipated growth of U.S. lithium battery manufacturing. These costs are realistic and based on:

- Current bids for the facility construction
- Toxco operational history for facility, utilities, and material costs
- Historic pricing and current bids for new equipment
- Known labor market costs
- Currently owned land

The cost is significantly lower than other new proposed facilities because Toxco currently owns the land and operates a facility at the proposed Lancaster, OH location. This will save both time and money to acquire and permit new land. Additionally, Toxco has all necessary utilities on site as well as existing relationships with the State and Local governments as well as regulatory agencies.

Results

- Lithchem Energy successfully tested some of the recovery processes for the lithium process lines
- The groundbreaking took place on November.
- Toxco has begun the site work and is currently on schedule.
- Foundation phases have begun and are on schedule at present.
- DCAA compliance has been established and Toxco is now awaiting audit.

Conclusions and Future Directions

Three years is an ample and reasonable time frame to complete the proposed project should the Toxco facility be chosen by the DOE for expansion and development. Toxco is confident that within this time period the development of the facility will be completed and equipment will be in place to accommodate the anticipated future and current needs of the HEV/PHEV vehicle market.

FY 2010 Publications/Presentations

None

II.E Battery Research Facilities

II.E.1 Prototype Cell Fabrication Facility (ANL)

Dennis W. Dees
Argonne National Laboratory (ANL)
9700 South Cass Avenue
Argonne, IL 60439-4837
Phone: (630) 252-7349; Fax: (630) 972-4520
E-mail: dees@anl.gov

Contributors:
Andrew Jansen, ANL
Bryant Polzin, ANL
Ilias Belharouak, ANL
Wenquan Lu, ANL
John Vaughey, ANL
Zonghai Chen, ANL
Sun-Ho Kang, ANL

Start Date: April 2010
Projected End Date: January 2011

Introduction

Equipment is being purchased in this project to support the establishment of a prototype cell fabrication facility at Argonne to fabricate advanced lithium-ion cells for use in its applied R&D program. A new state-of-the-art dry room is now operational, and equipment for fabricating prototype cells has been acquired for implementation in the dry room. The equipment being purchased in this project includes electrochemical cycle testers (for forming and evaluating newly fabricated cells), environmental chambers (for use in extreme temperature testing of these cells), a multi-channel impedance analyzer (for conducting in-depth electrochemical studies on selected cells), an accelerating rate calorimeter (for quantifying thermal abuse characteristics of selected cells), a new controlled-atmosphere glove box (for use in filling the cells with electrolyte), and a new X-ray diffraction unit (for use in quality control of cathode powders that will be used in these cells).

The total funding for this project is $1M. Two milestones and deliverables have been established. First, the equipment is expected to be identified and ordered by the end of August 2010. Second, the equipment is expected to be delivered and installed by the end of December 2010. The project is scheduled to finish by the end of January 2011.

Relevance

If the nation is to move forward with the use of lithium-ion batteries in transportation applications, improvements in life, cost, abuse tolerance, and performance must be achieved before their full potential can be realized. To that end, advanced materials are currently under development in academia, national laboratories, and industry. The first step to getting advanced lithium-ion chemistries and components into production is their incorporation into prototype cells that can be easily evaluated by battery developers. The Electrochemical Energy Storage Department in the Chemical Sciences and Engineering Division of Argonne National Laboratory has been developing the capability to produce small batches of high-quality prototype cells, utilizing advanced lithium-ion chemistries, as part of the DOE-EERE Applied Battery Research for transportation Program.

While Argonne is well on its way to developing the capacity to produce small batches of prototype lithium-ion cells, funding for additional equipment to support this effort is lacking. Basic cycling and characterization instruments are needed to complement the cell fabrication equipment and allow us to conduct in-depth diagnostic studies on advanced prototype cells, as well as their constituent components and materials.

In this project, Argonne will purchase several key pieces of equipment that will greatly enhance our ability to conduct vital diagnostic studies on the advanced prototype lithium-ion cells. With DOE's support, the Electrochemical Energy Storage Department at Argonne has had a long history of battery technology research and development. Further, Argonne is a recognized world leader in the development and study of advanced lithium-ion chemistries. We regularly work cooperatively with universities and other national laboratories on various lithium-ion battery projects. Argonne has established relationships with battery developers and other industrial sponsors. These funds will support our ability to promote to battery developers advancements in lithium-ion cell technologies, thus creating a conduit for academia, national laboratories, and industry to get their new battery materials and components into production.

Technical Accomplishments & Progress

All major pieces of equipment (X-ray diffraction unit, battery cyclers, impedance characterization equipment,

accelerating rate calorimeter, and glove box) and almost all the smaller items (ovens, chambers, etc.) were identified (see Table II- 3) and the orders placed before the end of August. The total orders placed represents approximately 97% of the total funding. The original estimates and actual purchase costs for the equipment are given in Table II- 3. An equipment order for the remaining funds is on hold to insure that adequate funds will be available to cover the existing orders. The X-ray diffraction unit and impedance characterization equipment, representing approximately 35% of the total funding, have arrived and are being installed.

Future Work

The remaining pieces of equipment are anticipated to arrive in October and should be operational by the end of the calendar year. An order for equipment to fully utilize the approved funds will be placed in October and should also arrive before the end of the calendar year. Thus the project will effectively meet both its milestones and deliverables, in addition to finishing on schedule.

Table II- 3: Cell Prototype Fabrication Facility Equipment Budget.

Equipment	Estimated Cost ($K)	Actual Cost ($K)
Electrochemical Impedance Equipment	70	93.5
Ovens and Environmental Chambers	60	70.8
Cell Electrochemical Formation and Cycling Equipment	300	301.7
X-Ray Powder Diffractometer	280	259.9
Accelerating Rate Calorimeter (ARC)	140	155.7
Inert Atmosphere Glove Box	150	84.2
Total Requested Funds	1000	965.8

II.E.2 Material Scale Up Facility (ANL)

Gregory Krumdick

Argonne National Laboratory
9700 South Cass Ave.
Argonne, IL 60439
Phone Number: (630) 252-3952
Email: gkrumdick@anl.gov

Start Date: April 2010
Projected End Date: September 2012

Introduction

The objective of this project is to design and set up a laboratory-scale battery materials production facility (Materials Engineering Facility or MEF) to rapidly scale up battery chemistries developed on the bench scale and produce bulk quantities of the materials for evaluation in prototype cells to enable quick turnaround validation of the materials chemistries.

This project consists of two tasks,

a) Construction of the MEF and

b) Specifying and ordering equipment for the facility.

Construction budget = $3.3M

Milestone 1: Complete full facility design (10/1/2010).

Milestone 2: Award full facility construction contract (2/1/2011).

Deliverable 1: Open interim facility (9/30/2010).

Deliverable 2: Complete full facility construction (2/1/2012).

Deliverable 3: Open full facility (3/31/2012).

Equipment budget = $2.5M

Milestone 1: Interim facility equipment purchased & installed (12/31/2010).

Milestone 2: Production scale-up facility (MEF) equipment purchased & accepted (12/31/2011).

Deliverable 1: Interim facility open (9/30/2010).

Deliverable 2: Full facility open (3/31/2012).

Relevance

The proposed Materials Engineering Facility (MEF) will provide a new capability to Argonne's existing battery facilities, capabilities, and expertise. While the MEF will support Argonne's R&D program in batteries and ultra-capacitors, it will be an open facility and access will be available to other organizations, including other national laboratories, universities, and industry, for the validation of new materials and materials processing schemes. The new facility will also support strategic Argonne partnerships to enable a domestic battery manufacturing industry, such as the Kentucky-Argonne Battery Manufacturing R&D Center. As such, the MEF will enable substantial progress to be made in the development, validation, and ultimate commercial implementation of advanced battery-materials chemistries. Such a facility is a key missing link between the bench-scale development of battery technology and high-volume manufacturing of large-format advanced batteries for transportation applications.

Technical Accomplishments & Progress

Construction task. Jacobs Engineering has completed the conceptual design report, completing construction milestone 1 (8/19/2010). The construction contract is currently out for bids; therefore milestone 2 is on track (2/1/2011).

While the MEF is being prepared, an interim facility consisting of three labs for initiating R&D has been established and Deliverable 1 has been met (9/17/2010). Two full-time employees have been hired to staff the electrolyte interim lab, equipment has been installed and this lab is functional. One part-time employee has been hired to staff the cathode materials interim lab, much of the equipment has been installed and this lab is also functional. One full-time employee has been hired to staff the cathode analytical lab and equipment has been ordered and is not expected to be delivered until early 2011. Candidates are being interviewed to fill two additional positions in the cathode materials interim lab.

Equipment task. Milestone 1 is on track (12/31/2010), the majority of equipment required for the electrolyte interim lab has been ordered, as is most of the analytical equipment for the cathode analytical interim lab. Equipment for the cathode material interim lab is in the process of being ordered. Once the MEF is complete, this equipment will be moved to the MEF.

Current funding is inadequate to complete milestone 2 (12/31/2011). The entire equipment budget of $2.5M is needed to fund the process and analytical equipment for scaling electrolytes and cathode materials on the 1-10 kg scale in the interim labs. To achieve process scale up to the 10-100 kg scale, additional funding of $3-5M will be required in FY11.

Future Work

Upon awarding the design/build contract for the MEF, the final design will be completed and construction will begin. Site preparations have already begun with the removal of unused equipment at the site.

Orders for the remainder of the equipment for the interim facilities will be placed and equipment will be installed upon its being received.

Initial process scale-up work on initial battery material chemistries will continue in the electrolyte/additives lab, and will begin in the cathode materials lab, upon completion of staffing the lab.

II.E.3 Post-test Laboratory Facility (ANL)

Ira Bloom

Argonne National Laboratory
9700 South Cass Ave.
Argonne, IL 60439
Phone Number: (630) 252-4516
Email: ira.bloom@anl.gov

Start Date: April 2010
Projected End Date: December 2011

Introduction

Batteries are routinely tested according to standard test procedures to learn how they perform. From these data, failure modes can sometimes be deduced. More often, only tear-downs and physical analyses will provide the needed information. To answer this need, a post-test analysis (PTA) facility is being built at Argonne in support of DOE's and USABC's battery development programs. Here, the experience and techniques developed in DOE's applied battery R&D program would be used in a standardized manner, similar to what is done in the testing area. This facility would be used to identify failure modes within a given technology and, perhaps, across technologies.

This project consists of two efforts, laboratory modification and equipment purchases. The milestones and budgets for these efforts are given below.

Laboratory modification (Budget: $300K)

- Complete design for post-test construction – 7/30/2010 (complete)
- Start construction of post-test laboratory – 9/30/2010 (complete)

Deliverable: Construction complete 3/31/2011

Equipment (Budget: $1.7M)

- Post-test equipment identified – 7/30/2010 (complete)
- Issue solicitation for glovebox and analytical equipment – 9/30/2010 (complete)
- Deliverable: Complete construction of facility 12/31/2011

Relevance

Standardized post-test examination procedures and techniques would be expected to accelerate battery development. Here, the well-understood techniques are expected to produce diagnostic information which, in turn, can be readily used to understand the failure modes in operation. With an understanding of the failure modes, the given battery technology can be improved. Thus, the developer would know how to more efficiently improve the technology. As a result, battery development would accelerate. With better batteries, electric cars would become more economical and the nation, as a whole, progress toward obtaining energy independence.

Technical Accomplishments & Progress

The approach to this project includes establishment of a laboratory which contains a large, multi-purpose glove box (see Figure II- 8) and the purchase of necessary equipment. All cell-opening and component-manipulation activities would be performed in an inert atmosphere. The box will be arranged and equipped so that most of the characterization techniques can be performed inside the box or very close to it, minimizing the exposure of moisture and/or air-sensitive cell components to the ambient atmosphere.

In addition to equipment needed to open cells, the glove box will house the following instruments: Raman spectrometer, a thermo-gravimetric analyzer coupled to a gas chromatograph/mass spectrometer, an optical microscope, and a transfer chamber to an X-ray photoelectron spectrometer. The box has two distinct areas, one for sample preparation (cell opening, disassembly, and metallography) and another for characterization. The sample preparation area will be under a nitrogen atmosphere and the characterization areas, under an inert gas, such as argon. The two areas will be separated by an antechamber. The atmospheres are arranged so that the highly sensitive surface characterization can be performed in a very clean environment. Since the sample can be characterized without leaving the glove box, the surface characteristics, which are key in lithium-ion batteries, would be unchanged, providing better understanding of failure modes.

The first milestone was to use the concept shown in Figure II- 8 to design a practical laboratory, optimizing floor and glove box space. After considering how materials will flow from one work area in the box to another, the layout shown in Figure II- 9 was designed.

It should be noted that the Fourier transform infrared (IR) spectrometer is no longer in the glove box. There was no practical way to interface the optical probe to the box because the IR-transparent materials were too brittle for this task. Instead, it will be located nearby, in its own inert-atmosphere glove box. Thus, the glove

box design contains areas for cell opening/sample preparation, electrochemical characterization, spectroscopy and thermogravimetric analysis.

Future Work

Construction is expected to start in October 2010. The necessary analytical equipment and the glove box will be ordered. Their deliveries will be timed to arrive approximately when the laboratory construction phase is near complete in December 2010. The equipment will be installed and tested. The facility will be qualified then using commercially-available lithium-ion batteries to design techniques and procedures.

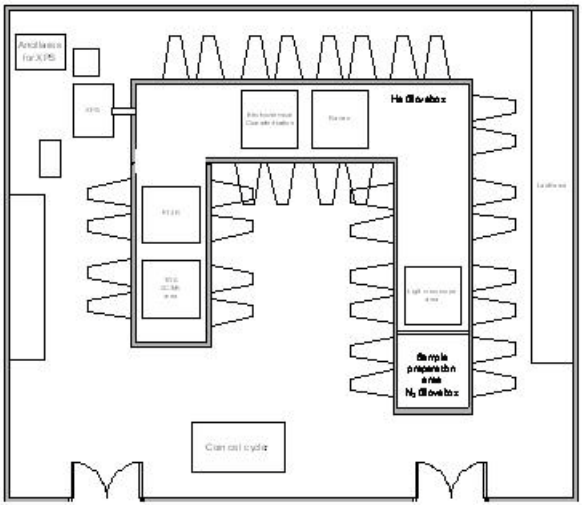

Figure II- 8: Schematic plan view of post-test facility.

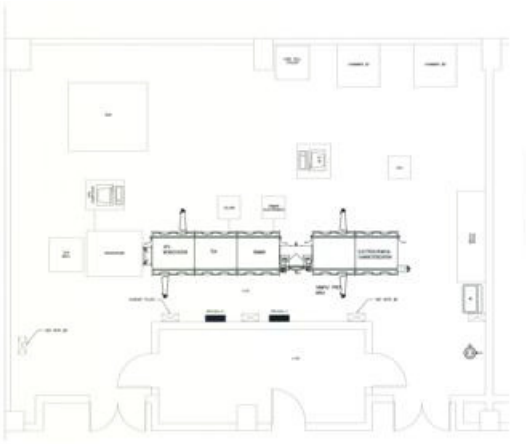

Figure II- 9: Plan view of improved laboratory layout, showing placement of major equipment. The VersaProbe (X-ray photoelectron spectroscopy) will be purchased with non-ARRA funds.

II.E.4 High-Energy Battery Testing Facility (INL)

Timothy C. Murphy

Idaho National Laboratory
PO Box 1625
Idaho Falls, Idaho 83415-2209
Phone Number: (208) 526-0480
Email: timothy.murphy@inl.gov

Start Date: March 2010
Projected End Date: September 2012

Introduction

This project is for equipment and facility upgrades needed to fully operate the new Idaho National Laboratory (INL) High Energy Battery Test Facility that will be constructed at the INL.

- Project Time Line: 03/01/10 – 09/30/12.
- Funding: $5.0M received to date from DOE.

Relevance

Supporting the nation's economic recovery by creating U.S. based national laboratory jobs; the INL is building a new 10,000 sq. ft. high energy battery test facility. .

The INL project is in response to an identified capability shortfall within the DOE-EERE battery test facility complex. The DOE lead test facilities at the national laboratories current capability to test full size high voltage battery systems will not be able to meet the testing demand in support of DOE EERE battery development and manufacturing projects over the next five to ten years. Several DOE/USABC development contracts are scheduled to deliver full-size vehicle battery systems in the next several years. These currently include deliverables from A123Systems, CPI/LG Chem, Johnson Controls/Saft, and many others.

The requested equipment funding will enable electrical performance testing of 10 additional full-size battery systems. This new capability also will enable expanded exposure by DOE battery developers to the testing operations, increasing overall quality and reducing costly procedural errors. In addition, the creation of a new test facility focused on high voltage systems will allow existing facilities to expand capability for testing cells and module size deliverables. Lastly, this capability expansion will greatly enhance the INL mission focus on diagnostic testing, providing cradle-to-grave analysis of cells, modules, and full systems, targeting mechanistic-level knowledge that will enable determination of failure mechanisms and subsequent technology improvement and optimization for the intended automotive applications.

Technical Accomplishments & Progress

The facility groundbreaking has experienced minor delays due to financial approvals required before construction can begin. The current target for groundbreaking is December of 2010. However the scheduled completion of January 2012 remains as the target for construction to be completed. As a result, the scheduled project completion date of September of 2012 is still valid for operation. All equipment installations and facility upgrades under this project are expected to be completed by this project completion date.

Spending authority for this project was granted to the INL on 03/01/2010. As of 09/30/2010 a total of $810,392.00 has been obligated or paid against equipment orders. The April 2010 modified spending plan called for $600,000.00 in costs in Fiscal Year 2010. Actual INL costs against this goal were not met primarily due to long lead item delivery delays. However, costs are expected to close this gap in FY 2011. Once construction of the new facility progresses, cost and schedule variances will be reduced significantly.

Items ordered or received in FY 2010 were the first high voltage test system, two complex calibration systems, a high capacity vibration test system and support hardware items. Equipment will be staged or stored in existing facilities until it is possible to move items into the new facility.

Future Work

2011 plans involve working directly with the facility builder in order to integrate thermal management and power system upgrades into the construction process and manage to cost of those modifications. Additional long lead items, specifically high voltage test channels will be ordered by June of 2011. Staging arrangements are required as equipment will continue to be delivered before the facility can be occupied.

II.E.5 Batery Thermal Test Laboratory (NREL)

Matt Keyser & Ahmad Pesaran

National Renewable Energy Laboratory
1617 Cole Blvd, Golden, CO 80401
Phone: (303) 275-3876, (303) 275-4441

Email: Matthew.Keyser@nrel.gov
ahmad.pesaran@nrel.gov

Start Date: April 2010
Projected End Date: June 2012

Introduction

To facilitate and accelerate the commercialization of advanced energy storage technologies by the U.S. industry, the Department of Energy awarded the National Renewable Energy Laboratory (NREL) $2M to expand and upgrade its battery thermal facility under the 2009 American Recovery and Reinvestment Act (ARRA). Proper thermal design and performance are critical in achieving desired battery life, performance and cost targets. In this facility, NREL will perform thermal evaluation and characterization for batteries developed by U.S battery developers to aid them in understanding the thermal characteristics of batteries to improve thermal design. The project was funded in April of 2010 and it is anticipated to be completed in June of 2012.

The milestones in FY10 and FY11 for this effort are as follows:

1. Progress report on acquisition of equipment and facility modifications – June/2010 (This milestone completed on time and a report was delivered to DOE)
2. Acquire all major pieces of equipment identified in the SOW – December/2010 (More that 90% of the major pieces of equipment was acquired by the end of September 2010 - Complete)
3. Complete facility modifications and install and calibrate equipment - June/2011 – (Anticipated completion date of March/2011)

Relevance

Temperature is a critical parameter in obtaining the desired performance and life of all batteries impacting life-cycle cost. In DOE program-funded work, NREL has measured thermal properties of cells and batteries with different chemistries by measuring heat generation and heat capacity; obtained infrared thermal images; performed performance thermal testing of battery and ultracapacitor modules and packs; analyzed the thermal performance of cells and modules; and developed thermal models.

NREL performs thermal testing, analysis, and modeling for two purposes: (1) assisting DOE and United State Advanced Battery Consortium (USABC) battery developers in designing cells/modules/packs for improved thermal performance, and (2) benchmarking and validating the thermal performance of cell/module/pack deliverables from DOE/USABC battery developers and suppliers.

Benchmarking cells, modules, and packs being developed has been critical for integration of battery systems in advanced vehicles. NREL's current thermal test facilities identify areas of thermal concern as well as characterizing the efficiency and heat generation of cells (with different chemistries) and sub-modules under various drive profiles and at various temperatures. NREL's equipment can also benchmark how changing the design of the cell using a different cathode, anode, current collector, electrolyte, or separator affects the overall performance of the cell.

The information garnered from these tests helps battery and car manufacturers design thermal management systems that reduce the life-cycle cost of battery systems in advanced vehicles. Because DOE's energy storage program has expanded over the past year, we have a backlog in thermal characterization and testing of prototypes, particularly in heat generation measurement. With the anticipated growth in the DOE program and an increase in the number of batteries coming from domestic battery manufacturing facilities under the ARRA funding, we plan to add capacity and enhanced capability by adding new equipment and additional space in our existing facilities. We will add calorimeters, thermal conductivity measuring instruments, pack thermal evaluation equipment, environmental chambers, and high-power cell and module battery cyclers.

Technical Accomplishments & Progress

To enhance and expand the NREL thermal characterization and testing capabilities, we need to identify, acquire, and install the latest equipment. The primary focus of FY10 was placed on acquiring the capital equipment identified in the ARRA SOW. The equipment acquired in FY10 includes: many cell/module/pack battery testing units (cyclers) (Figure II- 10), several environmental chambers (Figure II- 11), a Xenon Flash thermal conductivity meter, a bulk thermal conductivity meter, a coin cell calorimeter and a glove box. The total cost of the equipment purchased was about $1M (Figure II- 12).

In additional of identifying and acquiring the equipment, NREL has also concentrated on expanding its laboratory space for the new equipment. NREL management provided an additional 1000 ft^2 of office space adjacent to our present energy storage laboratory facilities. During FY10, we converted the office space into laboratory space and are

presently upgrading the utility infrastructure for the new equipment under the ARRA task. The infrastructure upgrades include expanding the electrical service, plumbing chilled water to the new environmental chambers, and adding compressed-air drops to the expanded space. Furthermore, we are updating the ventilation and safety features in the laboratory.

We have identified the need for a cell and small module calorimeter based on the design of NREL's large volume isothermal calorimeter. We have interacted with several companies to build this calorimeter for us, but their initial cost estimates have been too high and we are pursuing other approaches. In order to evaluate thermal performance of the battery pack management system, we have identified the need to design and build a set up to for a "thermal management in the loop testing apparatus."

Future Work

In FY11, we anticipate bringing the newly acquired equipment on-line – this includes calibration and verification to confirm that the equipment meets the manufacturer's performance specifications. We will start to develop new test procedures for measuring the thermal parameters of batteries and these parameters will be fed into our performance and life models of battery systems in support of the US battery industry.

We will continue the laboratory facility modifications with the ARRA funds. The electrical and chilled water improvements are anticipated to be completed in January 2011.

We will complete the design for a cell calorimeter and interact with an outside manufacturer to build the unit. We will also initiate the design process for a "thermal management in the loop testing apparatus." This thermal management in the loop testing capability will enable the testing of energy storage devices and their thermal management control systems within the context of actual real-time interaction with an advanced vehicle. The equipment will also be used to integrate prototype systems into actual vehicles for testing both on-road and with a chassis dynamometer. This approach will demonstrate the ultimate fuel use impact of different thermal management strategies, and guide development of strategies that deliver the best trade-off between enhanced battery life and realized fuel savings.

Figure II- 10: Bitrode Battery Testing Equipment at NREL's New Battery Thermal Test Facility

Figure II- 11: Environmental Chambers at the ARRA-sponsored NREL's Facility

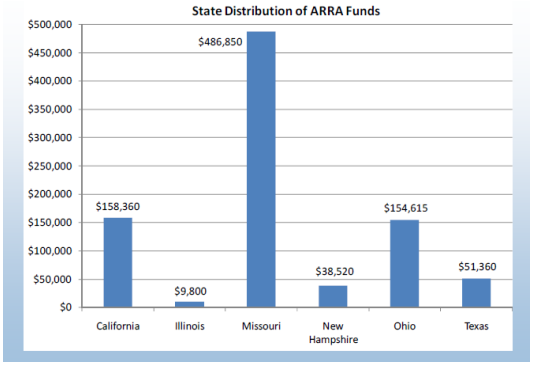

Figure II- 12: The Equipment Bought from Several Different Suppliers across U.S.

II.E.6 Battey Abuse Test Facility (SNL)

Christopher J. Orendorff and William A. Averill

Sandia National Laboratories
P. O. Box 5800, MS-0614
Albuquerque, NM 87185-0614
Phone: (505) 844-5879; Fax: (505) 844-6972
E-mail: corendo@sandia.gov

Start Date: April 2010
Projected End Date: March 2012

Objectives

- Recapitalize and upgrade the Sandia Battery Abuse Test Facility.
- Update our testing equipment, add testing/characterization and analytical capabilities, increase our testing throughput, and upgrade the safety features of the facility to accommodate testing lager PHEV and EV battery packs.

Accomplishments

- 60% Design goal met in June 2010 and 90% design goal met in October 2010 for the construction phase
  - 40% of the equipment for the facility is purchased in FY10, 3 months ahead of schedule
- Installation and staging of new equipment beginning in September 2010.

✧ ✧ ✧ ✧ ✧

Introduction

In 2010, Sandia National Laboratories was awarded funding through the American Reinvestment and Recovery Act (ARRA) for facility upgrades to the Battery Abuse Testing Laboratory. Upgrades to the facility are focused on improving the safety engineering controls and systems required to accommodate abuse testing of PHEV and EV sized battery packs, improving our testing efficiency and throughput, and updating laboratory equipment and systems to facilitate the growing demand for safety testing.

With the upcoming widespread commercialization of PHEVs and EVs using lithium-ion batteries, the demand for testing the safety and reliability of these systems by the battery developers and auto manufacturers will increase. Sandia has developed a unique testing and characterization facility for these systems over the past decade and the upgrades to the facility outlined in this project will advance our capabilities to meet the needs of our customers now and well into the future. Safety system and facility improvements include, upgrading the laboratory power and relocating power out of the hardened test bays for safer operation, fire/explosion proofing test bays (lighting, equipment panels, etc.), and adding fire suppression capabilities for large test articles. We also aim to upgrade the exhaust/scrubber systems in the facility to ensure safe testing of large scale battery modules and packs.

Our equipment recapitalization reflects the growing demand for larger scale batteries (> 5 kWh) as well as our vision for adding capabilities to support our testing and R&D programs. Equipment upgrades include high voltage/high current power supplies and battery cyclers, analytical characterization equipment, updated battery calorimetry instrumentation, mechanical test equipment large enough for full PHEV and EV pack testing, large thermal test chambers, and an X-ray computed tomography system for failure analysis. In addition, we will be completely renovating our data acquisition systems and software to allow for fully integrated (data, video, audio), parallel testing which will significantly improve our efficiency and throughput.

Progress Update

Facility Renovation. Funding was received in April 2010 for the facility upgrade. The first three months were spent on laboratory design, identifying key equipment needs, obtaining instrument specifications/estimates, and facility design. The 60% facility design includes:

- Mechanical: removal of unused utilities, relocation of process gases and building exhaust to accommodate new calorimetry/glove box equipment, upgrading the scrubber system, increasing and rebalancing test bay exhaust, redesign common space floor plan to maximize efficiency and usable area.
- Electrical: Complete laboratory redesign and upgrade in power to accommodate large testers (>500V), relocation of power for safer operations
- Fire protection: explosion proof lighting, explosion proof equipment panels, relocation of power outside test bays, CO_2 fire suppression systems for module and pack tests

To date, the scope of the construction phase is on budget and elements of the construction phase will begin ahead of schedule in November 2010 (utilities, equipment installations).

Equipment Upgrades. Equipment identified for the facility has been identified and the procurement process initiated. In fact, > 40% of the instrumentation (by dollar amount) was received and costed in FY10; three months ahead of schedule. Equipment was chosen to support our core testing programs as well as to expand our testing/characterization capabilities. Key equipment are listed in Table II- 4.

Table II- 4: List of Key Equipment for the Battery Abuse Test Facility Upgrade.

Equpiment for Battery Abuse Test Facility Upgrade
Electrical Test Equipment
Battery Cycler
Cell Level Tester
Pack Level Tester
Analytical Equipment
IR spectrometer
Mass spectrometer
Thermal Test Equipment
Thermal Chambers
Pack Thermal Chamber
Mechanical Abuse Equipment
Hydraulic Press and Controller
Calorimetry and Characterization Tools
IR laser diagnostic platform
X-Ray CT
ARCs (2)
Cell Reaction Calorimeter
Microcalorimeter
Glove Box

The cyclers and testers will facilitate Charge/Discharge cycling, overcharge abuse, and overdischarge abuse testing of vehicle scale, high energy batteries (>15 kWh). The upgrades to the spectroscopy tools (mass spectrometer and IR spectrometer with heated transfer lines) will facilitate real-time quantitative gas analysis for degradation products from the abuse of these batteries. Additional accelerating rate calorimeters (ARCs, one large and one small volume) will improve our testing throughput of materials, 18650 cells, and will also allow us to perform additional ARC experiments on large format PHEV and EV cells for our DOE programs. The X-ray CT system gives full CT images with resolution on the order of tens of microns (Figure II- 13). This will expand our capabilities to performing failure analysis/forensics on cells and even modules post-test. This will give us some insight *in situ* into failure mechanisms for these systems (e.g. internal short circuit, etc.)

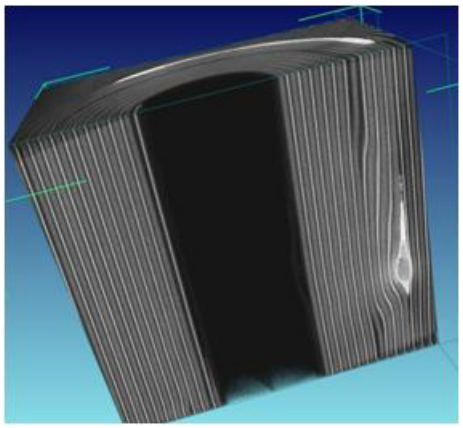

Figure II- 13: CT image of an 18650 lithium-ion cell with a large defect in the roll.

Future Work

An overview of the remaining schedule for this project is lised in Table II- 5.

Table II- 5: Remaining Schedule for the Battery Abuse Test Facility Upgrade.

Schedule Overview for the Battery Abuse Test Facility Upgrade	
October 2010	Design completed
November 2010	Construction phase begins
June 2011	Construction completed
July 2011	Installation of new equipment
March 2012	Project completed

The final design of the facility will be completed in October 2010. Preliminary elements of the facility upgrade will begin in October 2010 and the bulk of the construction project will begin in November 2010. The facility modifications are currently scheduled to be completed in June 2011. Installation of new equipment will begin in July 2011 and the facility is scheduled to be 100% operational by March 2012.

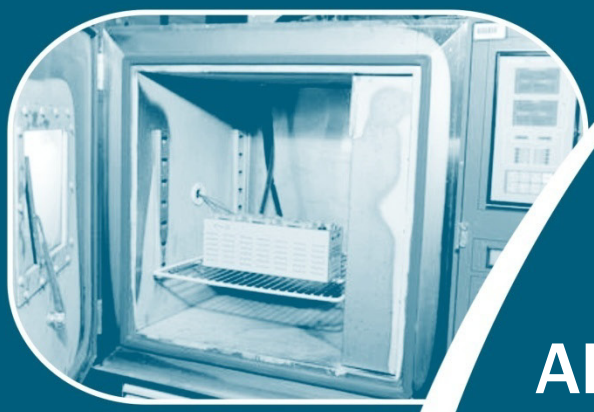

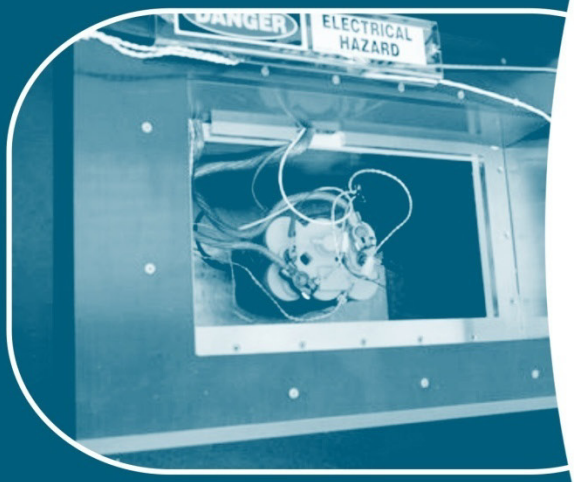

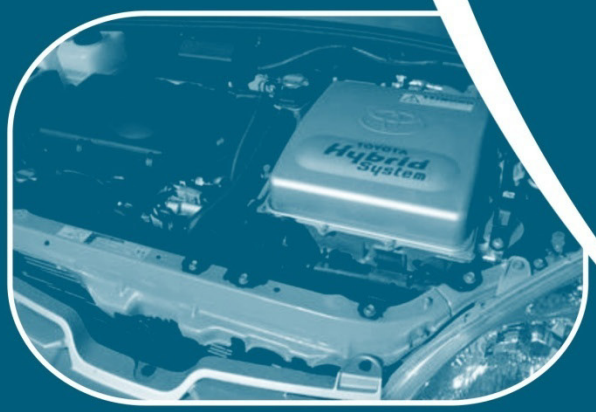

III

ADVANCED BATTERY DEVELOPMENT, SYSTEMS ANALYSIS, AND TESTING

A. Advanced Battery Development

B. Advanced Materials and Processing

C. Systems Analysis

D. Battery Testing Activities

E. Computer Aided Engineering of Batteries

F. Energy Storage R&D Collaborative Activities

III. ADVANCED BATTERY DEVELOPMENT, SYSTEMS ANALYSIS, AND TESTING

One of the primary objectives of the Energy Storage effort is the development of durable and affordable advanced batteries and ultracapacitors for use in advanced vehicles, from start/stop to full-power HEVs, PHEVs, and EVs. The battery technology development activity supports this objective through projects in several areas:

- System and materials development of full battery systems and advanced materials for those systems,
- Systems analysis which includes thermal analysis and simulation, various simulations to determine battery requirements, life modeling, recycling studies and other studies,
- Testing of batteries being developed with DOE support and of emerging technologies to remain abreast of the latest industry developments and to validate developer claims,
- International activities which DOE supports in order to remain abreast of technology and policy developments around the world, and
- Small Business Innovative Research (SBIR) to fund early-stage R&D for small businesses/entrepreneurs.

III.A Advanced Battery Development

Objectives

- By 2014, develop a PHEV battery that enables a 40 mile all-electric range and costs $3,400

Technical Barriers

- **Cost** – The current cost of Li-based batteries is approximately a factor of two-three too high on a kWh basis for PHEVs and approximately a factor of two too high on a kW basis for HEVs. The main cost drivers being addressed are the high costs of raw materials and materials processing, cell and module packaging, and manufacturing.
- **Performance** – The performance advancements required include the need for much higher energy densities to meet the volume and weight requirements, especially for the 40 mile PHEV system, and to reduce the number of cells in the battery (thus reducing system cost).
- **Abuse Tolerance** – Many Li batteries are not intrinsically tolerant to abusive conditions such as a short circuit (including an internal short circuit), overcharge, over-discharge, crush, or exposure to fire and/or other high temperature environments. The use of Li chemistry in the larger (PHEV) batteries increases the urgency to address these issues.
- **Life** – A 15-year life with 300,000 HEV cycles or 5,000 EV cycles is unproven.

Technical Targets

- Focus on the small-scale manufacture of cells, batteries, and advanced materials for high-power applications (HEVs and 42 Volt start/stop systems) and high-energy applications (e.g., PHEVs).
- Attempt to meet the summary requirements for PHEVs, HEVs, and Lower-energy energy storage systems (LEESS) developed with industry as shown in Table III- 1 and Table III- 2.

Table III- 1: Summary Requirements for PHEV Batteries[7]

Characteristics at End of Life (EOL)		High Power/Energy Ratio Battery	Moderate Energy/Power Ratio Battery	High Energy/ Power Ratio Battery
Reference Equivalent Electric Range	miles	10	20	40
Peak Pulse Discharge Power (2 sec/10 sec)	kW	50/45	45/37	46/38
Peak Regen Pulse Power (10 sec)	kW	30	25	25
Available Energy for CD (Charge Depleting) Mode, 10 kW Rate	kWh	3.4	5.8	11.6
Available Energy in CS (Charge Sustaining) Mode	kWh	0.5	0.3	0.3
CD Life / Discharge Throughput	Cycles/MWh	5,000/17	5,000/29	5,000/58
CS HEV Cycle Life, 50 Wh Profile	Cycles	300,000	300,000	300,000
Calendar Life, 35°C	year	15	15	15
Maximum System Weight	kg	60	70	120
Maximum System Volume	Liter	40	46	80
System Recharge Rate at 30°C	kW	1.4 (120V/15A)	1.4 (120V/15A)	1.4 (120V/15A)
Unassisted Operating & Charging Temperature	°C	-30 to +52	-30 to +52	-30 to +52
Survival Temperature Range	°C	-46 to +66	-46 to +66	-46 to +66
Maximum System Price @ 100k units/yr	$	$1,700	$2,200	$3,400

[7] For more details and for additional goals, see http://www.uscar.org/guest/view_team.php?teams_id=11.)

Table III- 2: Energy Storage Targets for Power Assist Hybrid Electric Vehicles.

Characteristics	Lower Energy Energy Storage System (LEESS)	Minimum value	Maximum value
Pulse discharge power (kW)	20 (10 s)	25 (10 s)	40 (10 s)
	55 (2 s)		
Maximum regenerating pulse (kW)	30 (10 s; 83 Wh)	20 (10 s; 55 Wh)	35 (10 s; 97 Wh)
	40 (2 s; 22 Wh)		
Total available energy (kWh)	0.056 (Discharge)	0.3	0.5
	0.083(Regenerative)		
	0.026 (Both)		
	0.165 (Total vehicle window)		
Cycle life (cycles)	300k	300k 25-Wh cycle (7.5 MWh)	300k 50-Wh cycle (15 MWh)
Cold-cranking power at−30ºC (kW)	5 (after 30 day stand at 30 ºC)	5 (three 2-s pulses, 10-s rests between)	7(three 2-s pulses, 10-s rests between)
Calendar life (years)	15	15	15
Maximum weight (kg)	20	40	60
Maximum volume (liters)	16	32	45
Production price @ 100k units/year ($)	400	500	800
Operating temperature (ºC)	−30 to +52	−30 to +52	−30 to +52
Survival temperature (ºC)	−46 to +66	−46 to +66	−46 to +66

Accomplishments

- The PHEV research and development activity remains fully underway with multiple systems development contracts being conducted, and numerous advanced materials and components contracts through the National Energy and Technology Laboratory (NETL). All system development for light duty vehicles is conducted in collaboration with industry through the USABC. All of the USABC subcontracts are awarded competitively and are cost-shared by the developer at a minimum of 50 percent.
- The following subsections highlight the battery and materials development activities for FY 2010.

III.A.1 High Energy/PHEV Systems

III.A.1.1 Advanced High-Performance Batteries for Plug-In Hybrid Electric Vehicle Applications (JCI-Saft)

Renata Arsenault (USABC Project Manager)
Subcontractor: Johnson Controls-Saft, Inc.

Scott Engstrom
5757 N. Green Bay Road
Glendale, WI 53209
Phone: (414) 524-2357; Fax: (414) 524-2008
E-mail: scott.engstrom@jci.com

Start Date: June 16, 2008
Projected End Date: April 29, 2011

Objectives

- Develop a prismatic battery cell which will meet program gap chart targets at system and cell levels.
- Develop and build a PHEV battery system capable of a 20-mile all-electric drive using cells developed for this program.
- Develop and deliver a design study for a 40-mile all-electric range PHEV battery system using the 20-mile cell.

Technical Barriers

- Improving pack level volumetric and gravimetric energy density while providing adequate thermal management
- Cycle-life in charge-depleting and charge-sustaining modes
- Characterization and improvement of the abuse tolerance behavior in large energy cells
- Meeting performance goals without compromising the financial target

Technical Targets

- Available energy in charge depleting mode: 5.8 kWh for 20-mile system and 11.6 kWh for 40-mile system
- Specific Energy: 83 Wh/kg for 20-mile and 97 Wh/kg for 40-mile system
- Energy Density: 126 Wh/L for 20-mile and 145 Wh/L for 40-mile system
- 20-Mile System Cost: $2,200

Accomplishments

- Selected Nickel-Manganese-Cobalt (NMC) material for first generation cells based on evaluations of various NMC mix configurations (including alternate anode material, carbons and electrolyte) from competitive suppliers.
- Proof-of-concept prismatic hard-shell mechanics were built into cells at SAFT. Improvements were made to address assembly issues, a subsequent cell build was performed in Milwaukee.
- Continued evaluation of alternative high temperature separators; improvements have been noted.
- Abuse testing for overcharge, short-circuit and nail penetration conducted on first prismatic cells and cylindrical surrogate cells with NMC showing improvement.
- Final cell size was determined and seems to be aligned with global OEM standardization initiatives.
- PHEV system development effort was kicked off and first module build was completed in September.
- Overcharge testing on both wound and stacked electrodes in prismatic cells were successful (EUCAR 4 ratings) at 200% SOC.
- Evaluation of a baseline 10-mile AER PHEV system (cylindrical cells) delivered in 2008 continues at Argonne National Lab.
- Low-volume stacking and cutting equipment was designed and built. This is now in use to build prototype stacked prismatic cells in Milwaukee.
- Builds of cylindrical and prismatic cells using NMC were completed in lieu of November deliverables to the National Labs for validation testing. Similar cells are currently undergoing similar validation testing.
- Based on HPPC testing of A-sample cells, data was forwarded to Argonne National Labs for the system BSF calculation.

✧ ✧ ✧ ✧ ✧

Introduction

Following a major scope change from cylindrical to prismatic cells, the major focus over the previous year has

been on cell development. The change includes development of a new chemistry (to JCS) and the extension of all electric PHEV range from 10 to 20 miles. Over the past year, JCS has shifted its scope from packaging an existing cylindrical cell toward development of a new prismatic cell, which will be packaged into a deliverable system.

Approach

The general approach was to first develop the cell and then focus on system optimization. In the early stages, both wound and stacked electrodes have been considered, developed, built and evaluated. In the short term, as equipment specific to stacked-electrodes was not readily available, JCS partner SAFT executed initial builds using their stacking equipment. The cell size was limited by that equipment. The resulting size has now been further validated via customer feedback and that size will continue to be developed.

The second phase of this development will be to optimize the electrode geometry and mechanics to the chosen prismatic size factor.

The JCS system approach has been to leverage and reuse existing system components wherever possible and optimize improvements to existing sub-assemblies and technology assembly to reduce costs. PHEV software and core battery management system components will be reused. JCS will deliver a system intended for bench test, only. A white-paper design will reflect the commercial-intent system design.

JCS is now developing an NMC cathode technology to minimize the pressure on large prismatic faces, relative to NCA technology. NMC from various selected suppliers has been evaluated over the past year using both a prismatic form factor and other surrogate cell packaging (cylindrical and pouch). In addition to NMC material, JCS is evaluating electrolytes, anode coatings, and high temperature separators to improve performance and abuse tolerance.

JCS has developed low-volume stacking and winding equipment in its Milwaukee lab to provide cells for the material evaluations. The need exists for more advanced, flexible equipment to provide a greater quantity of evaluation cells.

Results

NMC Cathode Development: Prior to submitting the program change proposal to USABC, JCS began work to develop NMC cathode technology in 2008 using pouch packaging. In fact, JCS's partner SAFT has studied NMC technology over the past ten years and much of that knowledge was leveraged as a starting point. Cylindrical cells have now been built for evaluation and JCS has been working with multiple suppliers of advanced cathode materials toward selecting the appropriate formulation. Figure III- 1 shows the cycling relationship between different material suppliers, as well as the improvement in capacity relative to first evaluations.

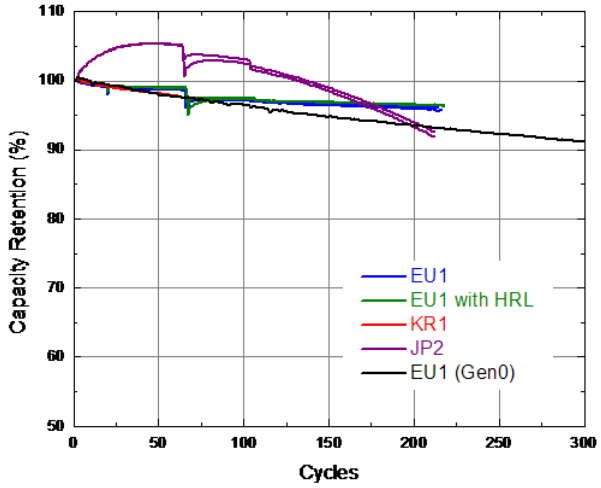

Figure III- 1: C/2 cycling at 45°C compares performance improvement to previous (Gen 0) testing and other NMC materials.

Cell Mechanical Design: Cell mechanics were first designed in the third quarter of 2009 and built into cells over the following two quarters, Figure III- 2. Over the course of the year, issues noted during the builds have been addressed in the design, most notably to improve the welding of electrode collectors and to seal the lid onto the can. With improved welding equipment to be installed in December, JCS will be able to further optimize the design to associated cost, while maintaining product integrity.

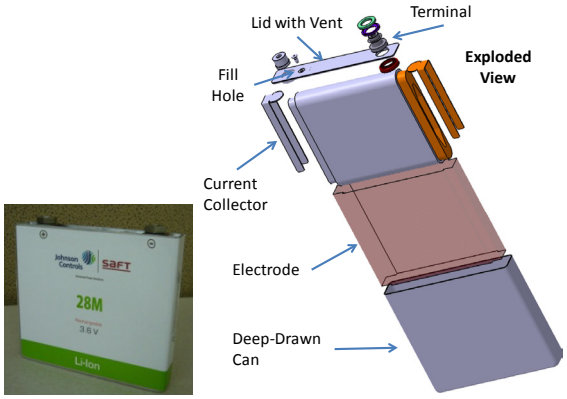

Figure III- 2: Preliminary prismatic cell mechanical design.

Abuse Tolerance Testing: Abuse tolerance testing was conducted on prismatic cells and on cylindrical-surrogate cells to evaluate various NMC and electrode materials. Ceramic-filled, ceramic-coated and higher melting-point materials have been tested. Not only have stacked prismatic cells yielded better abuse tolerance results, but they also exhibit better thermal management at

the cell level by conducting heat away from hot spots more readily. It has also been demonstrated that overcharging these cells to 200% SOC produces acceptable results of EUCAR 4 or less.

Prismatic System Packaging: Once the cell size was determined, system development work in conjunction with thermal analysis began, Figure III- 3 and Figure III- 4. Among the benefits to packaging prismatic cells are improved packaging efficiency, thermal management and reduced system height. Thermal simulations were run using the chosen cell size to understand the best approach to minimize the temperature gradient within the module. JCS is now evaluating cells in a module to validate the simulations. The system being designed for the USABC hardware deliverable will be for a bench test only system. Studies have recently begun toward a commercial-intent design via optimized packaging.

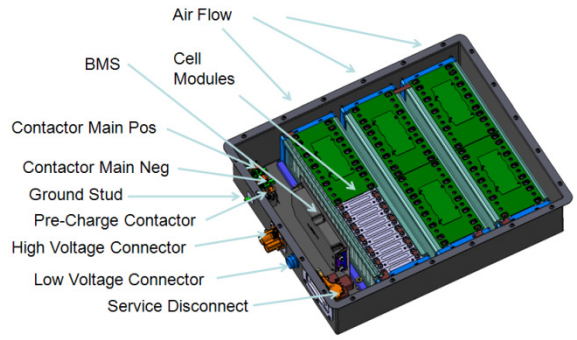

Figure III- 3: Preliminary prismatic cell mechanical design.

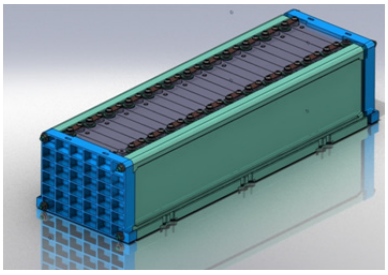

Figure III- 4: Preliminary prismatic cell mechanical design (Another view).

PHEV Baseline System Characterization: An 88-cell 10-mile AER baseline system (Figure III- 5) was delivered to Argonne National Labs in 2008. Life cycle testing continues and is reported quarterly. The characterized baseline unit is still meeting the target DOE target for available energy after 1500 cycles, Figure III- 6.

Conclusions and Future Directions

In the near-term, JCS will finalize the NMC electrochemical 1st Generation design. Once the cathode active material was selected, cylindrical cells were built for National Lab evaluation and comparison. These cells along with prismatic baseline cells will be submitted over the next year of the program. Based on early evaluation results and lessons learned during the cell builds, improved prismatic cells will be delivered by the end of the program.

Figure III- 5: Baseline PHEV 10-mile development system being tested at Argonne National Labs

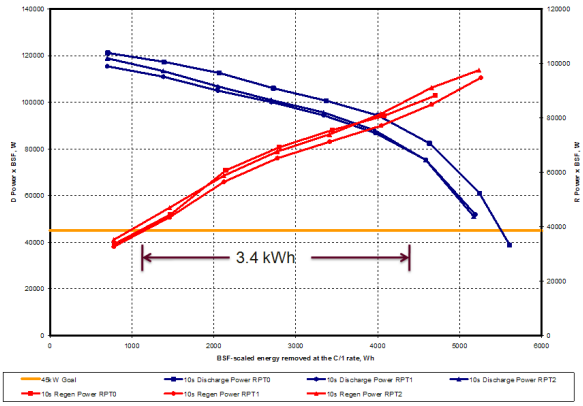

Figure III- 6: Baseline PHEV system-available energy at 1500 cycles.

PHEV system development of a 20-mile all-electric range is progressing toward a late March, 2011 hardware deliverable. The final BSF of the system will be confirmed by the end of October. Prismatic cells produced on JCS development equipment will be built into a first prototype system by December to provide an opportunity to address any assembly related issues. A thermal evaluation using the prototype system and baseline cells is just underway. The design study to produce a commercial-intent system for both 20 and 40-mile PHEV has recently started to identify areas of opportunity for improvements.

This development program runs through the end of April, 2011.

FY 2010 Publications/Presentations

1. Presentation to the 2010 DOE Annual Peer Merit Review Meeting (June 8, 2010).

III.A.1.2 Development of High-Performance PHEV Battery Pack (LG Chem, Michigan)

Harshad Tataria (USABC Project Manager)
Contractor: LG Chem, MI (Compact Power, Inc.)

Mohamed Alamgir
1857 Technology Drive
Troy, MI 48083
Phone: (248) 291-2375; Fax: (248) 597-0900
E-mail: alamgir@compactpower.com

Subcontractor: LG Chem, Seoul, South Korea

Start Date: January 1, 2008
Projected End Date: March 31, 2010

Objectives

- This was a 27 month program aimed primarily at developing and demonstrating a Li-ion cell for PHEV applications which will meet the energy, power and life requirements of the USABC program. A 15-yr calendar-life and 5000 cycles are the targets for this cell. While addressing these key issues, attention was also given on evaluating the abuse-tolerance and low-temperature performance of these cells.
- The above cell work was supplemented by studies related to modules leading to the development, testing and delivery of packs to the USABC. These studies were directed at finding a design solution that maximizes the effectiveness of the enclosed cells in terms of performance, life and abuse tolerance, while minimizing system weight, volume, and cost. In order to achieve these goals, the proposed pack development work involved analysis, design and test of a pack that is scalable and efficient with respect to manufacturing and validation.

Technical Barriers

The project focused on addressing the following technical barriers.

(A) Demonstrate Cycle-life of over 5000 cycles

(B) Demonstrate Calendar-life of over 15 years

(C) Cold-cranking power of 7kW

(D) Develop a pack that is efficient mechanically, electrically as well as meets the USABC cost target of $1,700.

Technical Targets

- Our objective for this project was to demonstrate the cell cycling capability of over 5000 cycles.
- Show data to demonstrate 15 years of calendar-life.
- Develop a novel cooling system that is electrically and mechanically efficient.
- Develop a pack design that is modular, easy to manufacture and is close to the cost target of USABC.

Accomplishments

- We have demonstrated that our high power baseline HEV cell is capable of meeting the 5000 cycle-life as well as the 15-year calendar-life target of the USABC under the PHEV cycling conditions.
- Two generations of high specific energy PHEV cells have been fabricated which allowed us to identify design factors critical for the life of these cells. These results have now been incorporated into the design of cells to be delivered to and tested at the National Labs.
- The cells have been characterized thermally at National Renewable Energy Labs (NREL). Thanks to laminated/plate design, the cells demonstrate lower and uniform heating during cycling.
- Abuse-tolerance tests have been carried out at Sandia National Labs showing attractive results.
- We have developed a pack that is thermally efficient using an advanced cooling system.
- Packs and modules were built and delivered to INL, Sandia and NREL for performance and abuse-testing.

✧ ✧ ✧ ✧ ✧

Introduction

Development of a cost-effective, high performance battery is a prerequisite for the successful introduction of PHEVs and EVs. With that objective in mind, we

have been working to develop a spinel-based Li-ion battery using laminated packaging.

Approach

To achieve the USABC objective, we have developed a cell chemistry based on spinel, our patented Safety Reinforcing Separator (SRS) and a laminated packaging design. The objective was to optimize the mixed cathode, anode and electrolyte compositions in order to meet the USABC targets for cycle- and calendar-life. Evaluation of other critical factors such as anode to cathode ratios, effect of binders and electrolyte additives was also an important task. In addition, compositions of the various components were altered to improve the cold-cranking power of the cells.

We have developed a pack design which is mechanically, electrically and thermally efficient. Since our cells are based on laminated packaging, work was focused on developing unique cell restraint and interconnect mechanism, especially involving welding. To achieve an efficient thermal system, a new type of cooling system was also designed.

Results

Optimizing cell chemistry. A considerable amount of effort was dedicated toward optimizing the cathode (spinel to layered cathode ratios), the anode (graphite to amorphous carbon blend) and the electrolyte (solvent ratios as well as additives). Details of these studies were described in our previous reports and important features of these cells are given in Table III- 3.

Table III- 3: Details of Cell Chemistry Optimization Studies.

Component		PLG0	PLG1	PLG2
Cathode		$LiMn_2O_4$/layered	$LiMn_2O_4$/layered	Same as PLG1
Anode		Graphite	Graphite/Amorphous carbon	Same as PLG1
Electrolyte			• New solvent/additive compositions	• Same as PLG0
Feature	Cold-cranking Power	• Does not meet at EoL	• Higher cold-cranking power than PLG0.	• Similar power to PLG1
	Calendar life	• Poor	• Significantly better than PLG1	• Significantly better than PLG1 • Being validated
	Cycle life	• Meets target	• Does not meet target	• Expected to meet target • Being validated

Life. Both the anode and the electrolyte compositions played critical roles in the determining the life and cold-cranking power of the cells. This is illustrated by the data in Figure III- 7 which compares the cycle-life characteristics of the three generations of cells we developed in course of this Program.

For example, the PLG0 cells showed good cycleability but inferior calendar-life, and a change in the anode composition to augment calendar-life caused considerable deterioration of cycle-life. A readjustment in the electrolyte composition in the PLG2 cells, however, improved the cycle-life and we expect to achieve the USABC target cycle-life with this cell. The poor calendar-life of the PLG0 cells vs. the PLG1 cells is shown in Figure III- 7 and Figure III- 8.

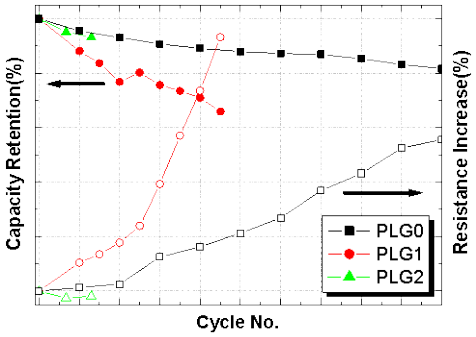

Figure III- 7: Cycle-life comparison of the three generations of cells developed in this program.

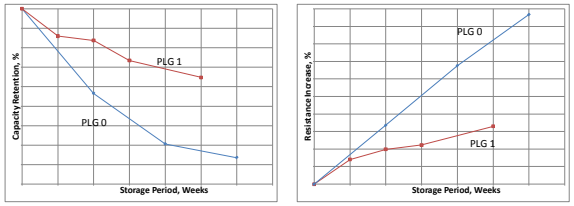

Figure III- 8: Comparison of the calendar-life of PLG0 and PLG1 cells at 60°C and SOC=90%.

The PLG2 cells showed calendar-life characteristics very similar to that of the PLG1 cells. The relative performance of these cells at the three different temperatures of 30, 40 and 50°C is shown below (Figure III- 9).

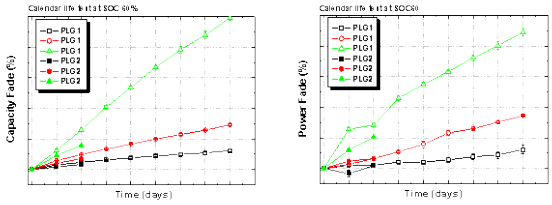

Figure III- 9: Comparison of the calendar-life of PLG1 and PLG2 cells at 30, 40 and 50°C and SOC=80%.

Abuse-Tolerance Characteristics. The cells have been subjected to a number of key abuse-tolerance tests such as short-circuit, nail-penetration, thermal stability and overcharge. The data demonstrate the efficacy of our proprietary separator in preserving high degree of abuse-tolerance for these high energy PHEV cells.

Development of Pack. Considerable effort was directed at developing a mechanically robust pack design. This involved developing an optimum cell restraint system for the laminated cell as well as fabrication procedures for interconnect system, especially terminal-to- terminal welding.

Development of an efficient cooling system. A focus of our pack development work was the development of an efficient cooling system. From a careful analysis of a total of 10 potential cooling systems using key matrices such as the ability to remove heat from cells, uniform performance across all the cells in the pack, energy required to run the cooling system, simplicity of manufacturing and cost, we decided on the refrigerant-to-air method as the cooling system of choice.

Tests were carried out to compare the cooling efficiency of refrigerant-to-air system with that of a liquid cooled system when a prototype Li-ion battery pack is cycled. The data show that an optimally designed refrigerant-to-air cooling system can be as efficient as a liquid-cooled thermal system (Figure III-10). One apparent benefit of refrigerant-cooled system is its faster response time.

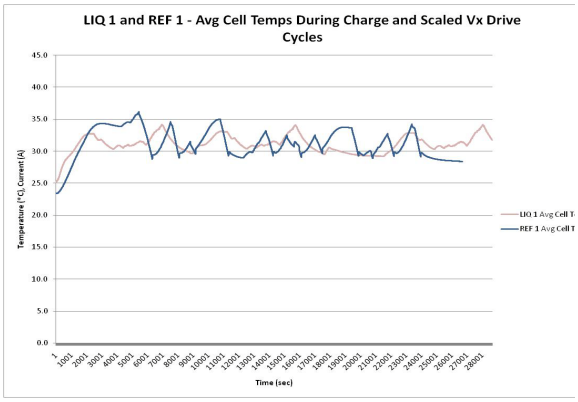

Figure III- 10: Comparison of the cooling characteristics of liquid-cooled and a refrigerant-to-air cooled Li-ion packs during cycling.

A total of 6 packs and 8 modules were manufactured and delivered for testing at INL, Sandia and NREL. The testing consists of performance and life at INL, abuse-tolerance at Sandia as well as thermal characterization at NREL. Picture of a pack delivered to the National Labs is given below (Figure III- 11).

Figure III- 11: Picture of a Li Ion battery pack comprising a refrigerant-to-air cooling system and delivered to National Labs.

Conclusions and Future Directions

Considerable optimization studies have been carried out to identify especially anode and electrolyte compositions which result in improved cycle- and calendar-life. Extensive abuse-testing of the cells and modules have also been carried out with attractive results. A number of design iterations have led to the development of a new refrigerant-to-air cooling system which has been incorporated into the Li-ion battery we have fabricated and delivered to the USABC. The packs are now being tested at the National Labs.

FY 2010 Publications/Presentations

1. Presentation at the 2010 DOE Annual Peer Review Meeting, Washington, DC, June 2010.
2. Presentation at FL International Seminar on Li batteries, Ft Lauderdale, March 2010.

III.A.1.3 Nano-phosphate for PHEV Applications: A Multi-Generational Approach (A123Systems)

Ron Elder (USABC Project Manager)
Subcontractor: A123Systems

Leslie Pinnell,
321 Arsenal Street
Watertown, MA 02472
Phone: (617) 778-5577; Fax: (617) 778-5749
E-mail: lpinnell@a123systems.com

Start Date: March 2008
Projected End Date: March 1, 2011

Objectives

- Design, build and test cells and modules for 10 and 40 mile PHEV hybrid battery systems that will achieve the DOE / USABC FreedomCAR performance and cost targets.
- Develop and demonstrate performance and cost impact from innovative smart materials.

Technical Barriers

This project addresses the following technical barriers for performance and cost:

- Cycle Life
- Calendar Life
- System Weight and Volume
- System Cost

Technical Targets

- Demonstrate cell performance which can meet FreedomCAR targets for both 10 mile (minimum) PHEV and 40 mile (maximum) PHEV targets.
- Develop technology which enables achievement of USABC cost targets of $1,700 / 10 mile PHEV system and $3,400 / 40 mile PHEV system.
- Demonstrate calendar life performance consistent with 15 years at 35°C.

Accomplishments

- Consistent improvements in cell performance characteristics have enabled a 7% reduction in the battery size factor (BSF) for the 10 mile PHEV pack, 8% for the 40 mile PHEV pack versus Q1'10 estimates.
- The lower BSF will reduce system weight and volume, which will now meet the 10 mile PHEV weight target and narrow the gap on the 40 mile PHEV targets. The reduced BSF will also result in significantly lower cost compared to estimates provided in Q1'2010.
- A123Systems' Gen 1 PHEV cell has completed 6 RPT's of charge depleting cycle life testing. Testing of the Gen 1.5 production cell will be initiated in October, 2010.
- Calendar life testing has been conducted on Gen 1 cells at five temperatures, from 15 – 55°C and five states of charge, from 20 – 80%. Cells have reached RPT 7, and testing is ongoing. Gen 1.5 cells are expected to start calendar life testing in October, 2010.
- GEN 1.5 PHEV cells have completed USABC abuse tolerance testing, with no test exceeding a EUCAR 4 response
- Cell deliverables to the National Labs are on track for October, 2010. Module and pack deliverables are on track for January, 2011.

✧ ✧ ✧ ✧ ✧

Introduction

Achievement of USABC FreedomCAR goals requires cells and battery modules which successfully deploy technologies with high energy and efficient design. The most significant challenge in meeting 10 and 40 mile PHEV goals is cost. Cost estimates for both 10 mile and 40 mile PHEV systems dropped from 2008 to 2009, and have been reduced again from 2009 to 2010, by 30 and 30% respectively. This reduction was partially due to an improved materials pricing structure, but was also impacted by improved performance with the Gen 1.5 cell design, enabling a lower BSF for both the 10 mile and the 40 mile PHEV application. The Gen 1.5 cell is currently in production at A123Systems' new facility in Livonia, Michigan.

Approach

A123Systems has developed a 19Ah prismatic cell which has power and energy projected to meet most of

the USABC FreedomCAR targets. Continued challenges lie in ongoing and aggressive cost reduction, demonstration of cycle and calendar life, and cold crank performance. The development approach to close the gaps on performance objectives has been to improve electrode design for longer life and continue to incrementally increase energy and power for lower BSF and cost per watt hour. Module design has been optimized to further enhance cycle and calendar life by adopting a low volume compression system to ensure continuous and optimal pressure on each cell.

Results

10 Mile (Minimum) PHEV. End of program estimates for the 10 mile PHEV modules show that many FreedomCAR goals can be achieved or exceeded based on preliminary Gen 1.5 results**,** as shown in Table III- 4. The A123Systems nanophosphate system strength is in power capability, therefore, the focus has been on optimizing energy and life through improved materials and design.

Charge depleting cycle life and calendar life testing has been conducted for benchmarking purposes, using Gen 1 cells. Updated methods for calculating available energy for charge depleting and charge sustaining mode affected early performance on Gen 1 cells by decreasing the overlap between CD and CS energy, requiring an increased BSF. The improved power and energy in the Gen 1.5 cells made up the difference, and allowed for a BSF below that reported in Q1'10. Testing of the Gen 1.5 cells vs. FreedomCAR charge depleting cycle life and calendar life regimes will start in October, 2010. The cold crank estimate has increased from last year and is just shy of the 7 kW target.

Table III- 4: **Gap Analysis for 10 Mile (Minimum) PHEV Cell**

A123 PHEV packs vs. FreedomCAR Energy Storage System End-of-Life Performance Goals
10 Mile PHEV System

Characteristics	Units	USABC Goals	Projected EOL
2s Discharge Pulse Power	kW	50	
10s Discharge Pulse Power	kW	45	
10s Regen Pulse Power	kW	30	
Available Energy for CD Mode	kWh	3.4	
Available Energy for CS Mode	kWh	0.5	
Min Round Trip Energy Efficiency	%	>90	
Cold Crank power at -30°C	kW	7	
Charge Depleting Cycle Life	Cycles	5000	
Charge Sustaining Cycle Life	Cycles	300k	
Calendar Life, 35°C	year	15	
Maximum System Weight	kg	60	
Maximum System Volume	Liter	40	
Selling Price / System @ 100k/yr)		$1,700	
Maximum Operating Voltage	V	≤ 400	
Minimum Operating Voltage	V	≥ 0.55 V	
Self Discharge	Wh/day	50	
System Recharge Rate at 30°C	kW	1.4	
Operating Remperature Range	°C	-30 to 52	
Survival Temperature Range	°C	-46 to 66	

System level cost estimates have been reduced by 30% during the last 12 months of this project, due to decreasing pack BSF, continued reduction of materials costs and internal processing improvements.

40 Mile (Maximum) PHEV. End of program estimates for the 40 mile PHEV application generally meet or exceed FreedomCAR goals, as shown in Table III- 5. Cycle life and calendar life are expected to be challenging, based on earlier benchmarking of the Gen 1 design. Testing of Gen 1.5 cells for the 40 Mile PHEV system are scheduled to start in October, 2010.

Efforts to decrease cost on a cell and module basis have resulted in a reduction of approximately 20% during the last 12 months of the program. Continued efforts to decrease cost to within 1.5 times the goal is focused on development of more innovative, but slightly longer-term materials concepts.

Table III- 5: Gap Analysis for 40 Mile (Minimum) PHEV Cell

A123 PHEV packs vs. FreedomCAR Energy Storage System End-of-Life Performance Goals
40 Mile PHEV System

Characteristics	Units	USABC Goals	Projected EOL
2s Discharge Pulse Power	kW	46	
10s Discharge Pulse Power	kW	38	
10s Regen Pulse Power	kW	25	
Available Energy for CD Mode	kWh	11.6	
Available Energy for CS Mode	kWh	0.3	
Min Round Trip Energy Efficiency	%	>90	
Cold Crank power at -30°C	kW	7	
Charge Depleting Cycle Life	Cycles	5000	
Charge Sustaining Cycle Life	Cycles	300k	
Calendar Life, 35°C	year	15	
Maximum System Weight	kg	120	
Maximum System Volume	Liter	80	
Selling Price / System @ 100k/yr)		$3,400	
Maximum Operating Voltage	V	≤ 400	
Minimum Operating Voltage	V	≥ 0.55 V	
Self Discharge	Wh/day	50	
System Recharge Rate at 30°C	kW	1.4	
Operating Remperature Range	°C	-30 to 52	
Survival Temperature Range	°C	-46 to 66	

Cycle Life. Cycle life testing (Figure III- 12) was run on Gen 1 PHEV cells as a preliminary assessment of progress until the Gen 1.5 cells were available. Testing was completed through RPT6, meeting available energy requirements.

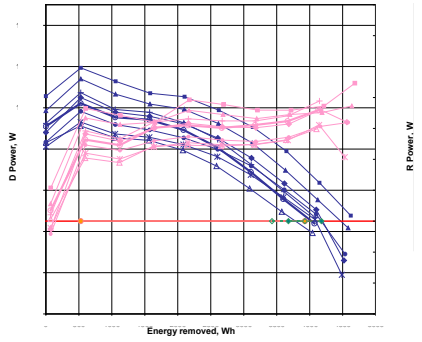

Figure III- 12: Charge Depleting Cycle Life

Testing initiated on Gen 1.5 cells shows significantly improved discharge and regen power, Figure III- 13, leading to the reduction in BSF. Based on non-standard USABC test results, cycle life is expected to improve upon results observed in Gen 1 cells.

Calendar life testing is in progress on Gen 1 prismatic cells, across five temperatures and states of charge. Testing at 90% SOC, at 35C has reached RPT 9 and is ongoing, Figure III- 14, pending initiation of Gen 1.5 tests.

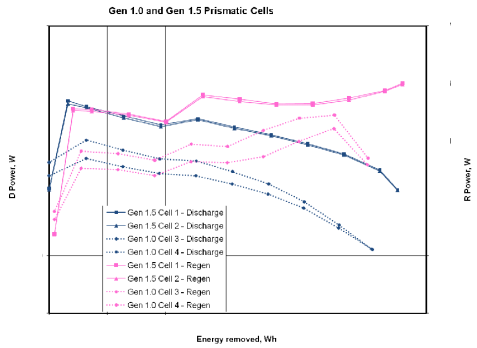

Figure III- 13: Gen 1.5 Cell Power vs Gen 1 Calendar Life

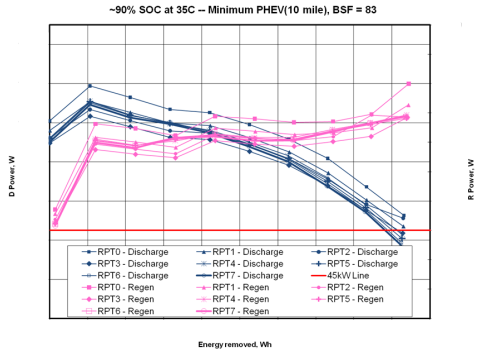

Figure III- 14: Calendar life regime for Gen 1 Prismatic Cells

PHEV Module Design. The module development program objective is to evaluate optimal configurations for PHEV modules which accommodate different series-parallel configurations and minimizes design and manufacturing costs. Effort has been increasingly focused on creating a flexible, modular structure to meet a wide range of customer applications with a standard set of design elements. Technical challenges include managing the tradeoff between volumetric energy density and cooling, cell to cell thermal management and SOC balancing, and assembly simplicity for lowest cost.

UT DOT abuse testing was completed at the module level, on three different configurations. Tests conducted were

- Altitude Simulation
- Thermal Test
- Vibration
- Shock
- External Short Circuit
- Overcharge

The modules achieved ≤ EUCAR 2, see Table III- 6.

Small modules with Gen 1 PHEV cells were cycled at 1C charge and either 2C or 4C discharge at 100% depth of discharge and have achieved over 3,000 cycles to date.

Table III- 6: 6S3P Module Abuse Test Results

Checks	Voltage (V)	Mass (g)	Leak (Y/N)	Vent (Y/N)	Rupture (Y/N)	Dissasemble (Y/N)	Fire (Y/N)	Results (EUCAR)
Pre-T1 (Altitude Simulation)	20.06	12010.2	N	N	N	N	N	
Post-T1	20.06	12009.5	N	N	N	N	N	
% Change	0.0%	0.0%						0
Pre-T2 (Thermal Cycling)	20.06	12009.5	N	N	N	N	N	
Post -T2	20.03	12006	N	N	N	N	N	
% Change	0.1%	0.0%						0
Pre-T3 (Vibration)	20.03	12005.6	N	N	N	N	N	
Post-T3	20.03	12003.7	N	N	N	N	N	
% Change	0.0%	0.0%						0
Pre-T4 (Shock)	20.03	12003.7	N	N	N	N	N	
Post-T4	20.01	12005.5	N	N	N	N	N	
% Change	0.1%	0.0%						0
Pre-T5 (Short Circuit)	NA	NA	NA	NA	NA	NA	NA	
Post -T5	NA	NA	NA	NA	N	N	N	
% Change	NA	NA	NA	NA	N	N	N	2

Conclusions and Future Directions

A123Systems' PHEV program is on track for delivering 55 test samples of Gen 1.5 19 Ah prismatic cells by October, 2010, three 1P modules by December, 2011, eight 3P modules by January, 2011, and one pack by February, 2011

Cycle life and calendar life have not yet been determined on this product generation using USABC-protocol tests, therefore these goals cannot be estimated until interim results are available, in Quarter 1 or 2 of next year, see Figure III- 15. Cost is the most challenging target, and has received heightened focus, with significant reductions achieved. Development and eventual implementation of Smart Materials in this project have the capability of significantly reducing overall system cost, and closing the gap between current estimates and FreedomCAR goals. Although these materials have not been incorporated into the current Gen 1.5 product, the development effort expended within this program will be leveraged in future programs.

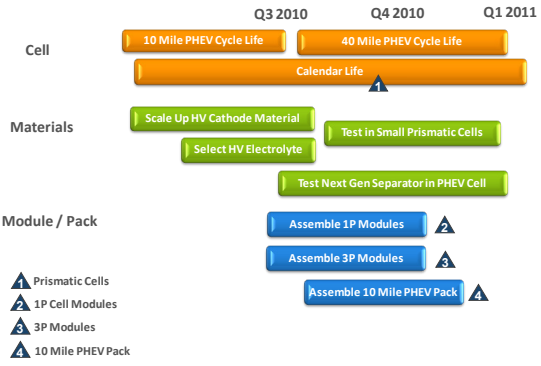

Figure III- 15: Calendar life regime for Gen 1 Prismatic Cells

FY 2010 Publications/Presentations

1. Presentation to the 2010 DOE Annual Peer Review Meeting.

III.A.2 High Power/HEV Systems

III.A.2.1 A Novel Nano-phosphate-based Li-ion Battery for 25 kW Power-assist Applications (A123Systems)

Ron Elder (USABC Project Manager)
Subcontractor: A123Systems

Terri Sacco/Leslie Pinnell
321 Arsenal Street
Watertown, MA 02472
Phone: (617) 393-4124; Fax: (617) 924-8910
E-mail: tsacco@a123systems.com

Start Date: December 2006
Projected End Date: December 2010

Objectives

- Design, build, and test cells and modules for HEV hybrid battery systems that will achieve the DOE / USABC performance and cost targets.
- Develop and demonstrate performance and cost impact from innovative, smart materials and designs.

Technical Barriers

This project addresses the following technical barriers for performance and cost:

- Cycle Life
- Calendar Life
- System Weight and Volume
- System Cost

Technical Targets

- Demonstrate cell performance which can meet FreedomCAR HEV targets.
  - Improved Calendar Life
  - Increased Cycle Life Capability
  - Increased Power
  - Abuse Tolerance at Cell Level
- Develop technology which enables achievement of USABC cost targets of $500 system production price @ 100,000 systems/yr

Accomplishments

- Exceeded FreedomCAR HEV targets for 25 Wh cycle life target of 300K cycles on 32113 Gen 1 cells, Cycle life is currently at 360k, and cells have not yet reached an end of life condition.
- Gen 2 32113 cells are on target to meet FreedomCAR HEV targets, having achieved more than 280k cycles to date. Cells are still on test and have not yet reached an end of life condition.
- Ten 10S1P HEV modules were assembled and shipped to National Labs for testing.
- A 32113 paper pack design was completed and submitted to USABC, including
  - Thermal management system
  - Electronics and Controls
  - Estimated Cost
- Thirty 6Ah prismatic prototype cells were assembled and delivered to USABC and the National Labs for testing.
- A no cost extension was granted to develop a 3D Electrochemical / Thermal modeling program to use as a tool to evaluate cell designs and electrode characteristics vital to optimizing performance in future HEV cell generations.

✧ ✧ ✧ ✧ ✧

Introduction

Achievement of USABC FreedomCARgoals requires cell and battery module technologies with high power and efficient design. The most significant challenge in meeting FreedomCAR goals is cost. Cost estimates have dropped significantly since the beginning of the program due to higher energy and lower cost materials and designs, enabling reduction of the BSF. Cost estimates at the beginning of the HEV program were almost three times the USABC target. Currently, the 6 Ah prismatic cell provides an opportunity to decrease the cost to within 10 – 30% of target.

Approach

A123Systems developed a 32113 cylindrical cell which meets most of the USABC FreedomCAR performance targets. Current gaps include cost and cold crank performance. The development approach to close the gap on these objectives was to optimize the materials and design for the cylindrical cell, while simultaneously developing a new, high power prismatic cell with lower BSF and much lower cost.

Results

32113 Cell Cycle Life. The Gen 1 cell design has now successfully achieved all FreedomCAR HEV targets with the exception of cold crank and cost. The cell design has been improved to a Gen 2 design, with higher capacity and power. The Gen 2 cell design enabled a reduction in the BSF while still meeting the USABC power and energy requirements, resulting in decreased system cost. The cycle life projection of the Gen 2 product is somewhat lower than Gen 1, due to the lower BSF and resulting higher power requirements per cell, see Table III- 7.

Table III- 7: Gap Analysis for Gen 1 and 2 32113 Cells

A123 HEV Pack vs FreedomCAR End of Life PerformanceGoals
32113 Gens 1 and 2

Characteristics	Units	USABC Goals	Projected EOL Gen 1	Projected EOL Gen 2
10s Discharge Pulse Power	kW	25		
10s Regen Pulse Power	kW	20		
Total BOL Available Energy	kWh	0.30		
Min Round Trip Energy Efficiency	%	> 90		
Cold-Cranking Power at -30 deg C	kW	5		
25 Wh Cycle Life	Cycles	300k		
Calendar-life (At 35 deg C)	Years	15		
Maximum System Weight	kg	<<40		
Maximum System Volume	Liter	<<32		
Selling Price/System @ 100k/yr)	$	500		
Maximum Operating Voltage	Vdc	≤ 400		
Minimum Operating Voltage	Vdc	≥ 0.55 V_{max}		
Self-discharge	Wh/day	50		
Operating Temperature Range	°C	-30 to 52		
Survival Temperature Range	°C	-46 to 66		

The Gen 1 cycle life projections based on 360k completed cycles indicate that >450k cycles will be achieved prior to 20% capacity fade. The Gen 2 cells have already provided over 280k cycles, and the cycle life projection indicates that the FreedomCAR target can be met at 300k cycles, prior to 20% capacity fade, Figure III- 16.

Available energy is still well above target, at 300k cycles for Gen 1, and 260k cycles for Gen 2, Figure III- 17.

32113 Cell Calendar Life. Calendar life testing has been completed through 225 days for Gen 2 32113 cells. The capacity fade at elevated temperatures is showing the characteristic shape observed for nanophosphate technology. USABC testing was conducted on cells stored at 23˚C, 45˚C and 65˚C, then the data was interpolated to develop a predictive curve for 35C (the middle curve in the chart below). The current projection based on observations to date indicates that the USABC calendar life target shows an eight year life to 20% capacity fade and a 17 year life to 30% fade, Figure III- 18.

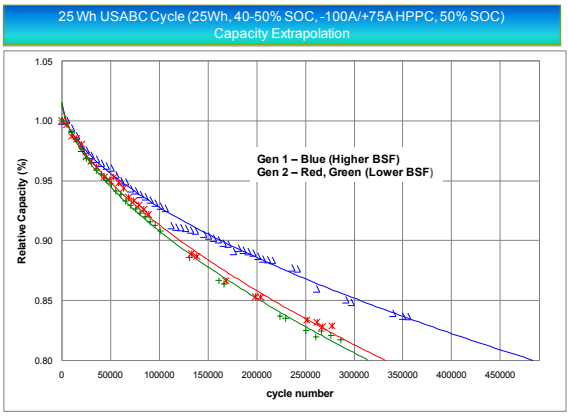

Figure III- 16: 25Wh Cycle Life Capacity - 32113 Gen 1 and Gen 2 Cells

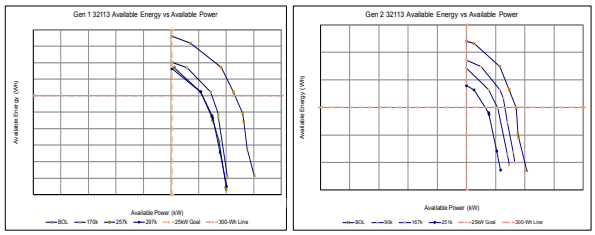

Figure III- 17: 25Wh Cycle Life Available Energy - 32113 Gen 1 and Gen 2

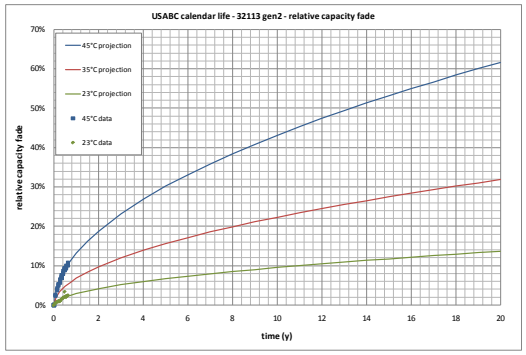

Figure III- 18: USABC Gen 2 Calendar Life Data and Life Extrapolations

Abuse Test Results. Standard USABC abuse test protocols were completed for Gen 1 and Gen 2 HEV 32113 cells, with EUCAR ratings of 4 or less. Gen 2 cells were tested with EUCAR ratings of 3 or lower, see Table III- 8.

Table III- 8: USABC Abuse Test Results

Test	Gen 1 Results	Gen 2 Results
Nail penetration	EUCAR 3	EUCAR 3
External Shorting	EUCAR 4	EUCAR 2
Overcharge	EUCAR 2	EUCAR 2
Thermal Stability	EUCAR 2	EUCAR 2
Crush	EUCAR 2	EUCAR 2
Overdischarge	EUCAR 2	EUCAR 2
Mechanical Shock	EUCAR 2	EUCAR 0

6Ah HEV Prismatic Cell. Samples of A123Systems' new 6 Ah prismatic cell were provided to the National Labs for performance and abuse testing. These are early prototypes designed to demonstrate HEV capability, and to support development of a Gap Analysis using a prismatic form factor. Initial performance tests have proven this to be a very high power cell capable of a much lower BSF, resulting in a projected cost that closes the gap v.s. the USABC goal. Cost is driven by the current limit of 300A; if the current limitation can be eliminated, cost will be within 10 – 30% of target. This cell is projected to meet all other USABC FreedomCAR HEV targets, see Table III-9.

Table III- 9: Gap Analysis for 6 Ah Prismatic HEV Cell

Characteristics	Unit	USABC Goal	Projected EOL
10s Discharge Pulse Power	kW	25	
10s Regen Pulse Power	kW	20	
Total BOL Available Energy	kWh	0.30	
Min Round Trip Energy Efficiency	%	> 90	
Cold-Cranking Power at -30 deg C	kW	5	
25 Wh Cycle Life	Cycles	300k	
Calendar-life (At 35 deg C)	Years	15	
Maximum System Weight	kg	<<40	
Maximum System Volume	Liter	<<32	
Selling Price/System @ 100k/yr)	$	500	
Maximum Operating Voltage	Vdc	≤ 400	
Minimum Operating Voltage	Vdc	≥ 0.55 V_{max}	
Self-discharge	Wh/day	50	
Operating Temperature Range	°C	-30 to 52	
Survival Temperature Range	°C	-46 to 66	
Capacity			

HEV Module Design. A 10s1P (10 cells in series, 1 cell in parallel) module prototype was developed and samples were provided to USABC/ National Labs for testing. Figure III- 19 shows a schematic of the module.

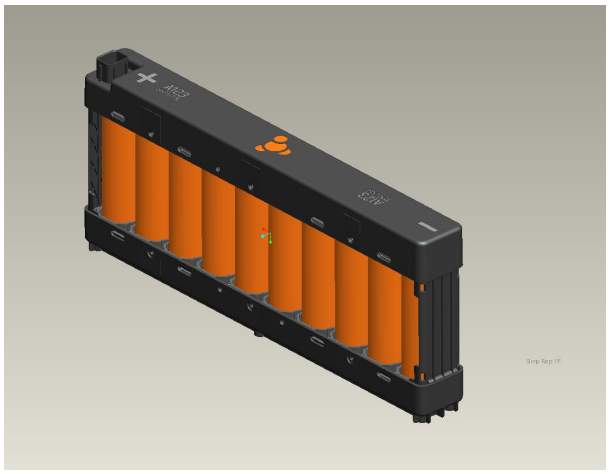

Figure III- 19: A123Systems 10-cell Module Design

Conclusions and Future Directions

A123Systems' HEV 32113 Gen 2 cells have proven to meet the energy and power USABC goals outlined at the beginning of the program. Cycle life and calendar life testing on the 32113 cells are close to completion and the cells are on track to pass long-term USABC targets. All abuse tolerance tests were passed with EUCAR ratings of 3 or less for the Gen 2 design. Ten-cell module prototypes were made and forwarded to USABC testing in April, 2010.

Moving forward, cost is the most challenging target. The 6Ah Prismatic cell was developed to overcome this challenge and provide a more compelling cost alternative to HEV FreedomCAR goals. Prototypes of this cell were delivered to USABC for evaluation. A no cost extension has been provided until December 31, 2010 to allow for completion of a 3D Electrochemical Thermal model to improve cell design capability for future cylindrical HEV cells.

III.A.2.2 Battery Abuse Testing and Ultracapacitor Development (NSWC)

Patricia H. Smith

Naval Surface Warfare Center (NSWC)
9500 MacArthur Blvd
West Bethesda, MD 20817-5700
Phone: (301) 227-4168; Fax: (301) 227-5480
E-mail: patricia.h.smith1@navy.mil
Naval Surface Warfare Center (NSWC), Bethesda, MD

Collaborators:
Thomas Jiang, NSWC
Thanh Tran, NSWC
Steven Dallek, Spectrum Technology Group
Deyang Qu, University of Massachusetts, Boston
Linda Zhong, Maxwell Technologies

Start Date: March 2008
Projected End Date: September 2012

Objectives

- Develop electrode/electrolyte materials that will enable an ultracapacitor to meet the USABC power assist and regenerative breaking goals.

Technical Barriers

There are several obstacles that must be overcome before an ultracapacitor can provide value to the automotive industry. These include:

- Low Energy Density: It must be increased with a minimum sacrifice to power capability and cycle life.
- High Self Discharge: It must be lower than today's conventional ultracapacitors.
- Safety Hazards: Must be determined.
- High Cost: Electrode and electrolyte materials must be affordable and available.

Technical Target

At the cell level:

- Gravimetric Energy Density: 15 to 20 Wh/kg
- Power Density: 650 W/kg
- Operational Temperature: -30°C to 50°C
- Cycle Life: 750,000 - 1,000,000 cycles
- Survivability Temperature: -46°C to 65°C

Accomplishments

- Evaluated the effect of temperature on lithium-ion (Li_xC_6/C) capacitor cell performance. Identified the need for better low temperature electrolytes.
- Demonstrated that the shelf discharge of lithium-ion capacitors (1-7%) is lower than that of conventional ultracapacitors (17%).
- Initiated the safety evaluation of lithium-ion capacitor electrode/electrolyte materials and cells.

✧ ✧ ✧ ✧ ✧

Introduction

Ultracapacitors (also referred to as supercapacitors or electrochemical capacitors) display certain characteristics that may be of value to electric and hybrid vehicles. In contrast to batteries which store energy in the bulk of the electroactive materials, capacitors store energy electostatically at the surface of the electrode electrolyte interface. As a consequence, ultracapacitors can deliver quick bursts of energy. This high power capability would be beneficial when the vehicle is accelerating and the demand for power assist is great.

Ultracapacitors can accept charge quickly which allows them to easily convert the kinetic energy of a braking vehicle into stored energy. They have excellent cycle life in comparison to other energy storage approaches and they may not need replacement during the lifetime of the vehicle. In addition, ultracapacitors operate well at low temperature, which is an excellent characteristic for starting engines during the winter months. They are, however, not without limitations. While their energy density is high compared to electrostatic and electrolytic capacitors, it is still significantly lower than batteries and fuel cells.

Recently asymmetric configurations, where a battery electrode replaces one of the activated carbon electrodes, have been investigated for their higher working voltages and energy densities. One example is the lithium-ion capacitor. Lithium-ion capacitors were first developed by Glenn Amatucci using a Li-intercalation negative electrode based on nano-structured $Li_4Ti_5O_{12}$ and an activated carbon as electrical double-layer positive electrode. More recently other lithium-ion capacitors using carbonaceous materials (graphite, hard/soft carbons) have been studied. Lithium-ion capacitors can reach energy densities of 10-15 Wh/kg. Greater energy densities could be obtained if

higher capacitance carbons and electrolytes with wide stability potential windows could be identified.

Approach

We will develop an asymmetric capacitor utilizing a lithium-ion intercalation negative electrode. Asymmetric designs offer the promise of achieving cell energy densities significantly greater than those observed with conventional carbon/carbon ultracapacitors (3-5 Wh/kg). Our focus will be to advance the technology of the carbon electrode and the electrolyte solvent system.

Activated carbons have much lower capacities than traditional lithium intercalation anode materials (~30-40 mAh/g versus ~120-160 mAh/g). Investigations will therefore be undertaken to identify higher capacitance activated carbons. Improvements in this area will result in a reduction to the amount of positive carbon required for a balanced cell design and lead to an increase in gravimetric and volumetric energy density. Various types of activated carbon materials and their corresponding electrodes will be assessed in terms of surface area, pore size distribution, capacitance and cell resistance.

The capacitor's energy density is proportional to the square of the cell voltage. The cell voltage is the key to obtaining an appreciable increase in energy density. Our efforts will focus on identifying an electrolyte solvent system that is stable over a wide potential window. This may be particulary challenging as the surface area of the activated carbons range from 1000 to 2000 m^2/g. Attention will be paid to achieving good low temperature performance and excellent cycle life. There is opportunity to reap the benefits of the extensive studies directed toward the development of advanced electrolytes for lithium-ion batteries. This project will keep abreast of emerging efforts in this area and identify solutions that may assist the development of a high performance capacitor.

Historically, capacitors have had the reputation of being safer than lithium batteries. However, the proposed asymmetric capacitor is in many respects similar to a lithium-ion battery. It must therefore be assumed that there are potential safety issues that need to be identified. A comprehensive safety analysis will be conducted on the lithium-ion capacitor electrode materials and prototype cells.

Results

NSWC continued to investigate newly emerging activated carbons being developed by academia and industry. Higher capacitance was achieved with carbons activated by potassium hydroxide (KOH) (150F/g, 80F/cc) than for those activated by steam. Carbons activated by KOH typically have higher oxygen content. Preliminary experiments revealed a correlation between the carbon weight loss and cell capacitance (Figure III- 20). We theorized that, between 100°C and 550°C, differences in weight loss result from the amount of functional groups located on the edges of the graphene sheets. The greater the number of functional groups, the greater the amount of gaseous species evolved from their decomposition in this temperature range. Since KOH-activated carbons have a higher degree of functional groups, they would be expected to have a greater weight loss. We attribute weight loss differences above 600°C to surface area. The electrochemical performance of candidate carbon materials may be predicted from TGA data.

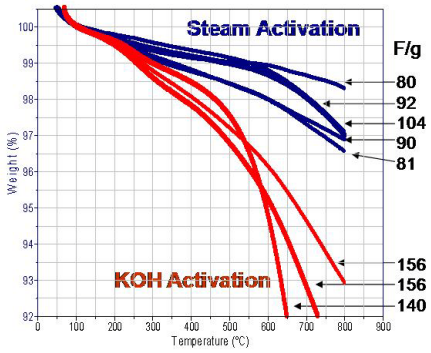

Figure III- 20: Thermogravimetric analysis of several steam-activated and KOH-activated carbons.

Ultracapacitors have a much higher self discharge than batteries. This behavior can be a limitation if capacitors are required for standby use. The self discharge characteristics of asymmetric capacitors utilizing either a lithium titanate or a carbonaceous anode were investigated and compared to a 3,000 Farad symmetric ultracapacitor (Maxwell Technologies). The open circuit voltages of fully charged cells stored at ambient temperature (~25°C) were monitored for three days. The asymmetric cells were found to have a lower self discharge rate (1-7%) compared to that of traditional ultracapacitors (17%, Figure III- 21).

For automotive applications, it is important that a capacitor not suffer from a high loss of performance when cycled at low temperatures. It is also necessary that the capacitor be capable of surviving periodic high temperature extremes. Capacitors were evaluated at temperatures ranging from -30°C to 65°C. The cells exhibited excellent high-temperature performance but displayed significant degradation at low temperatures (Figure III- 22).

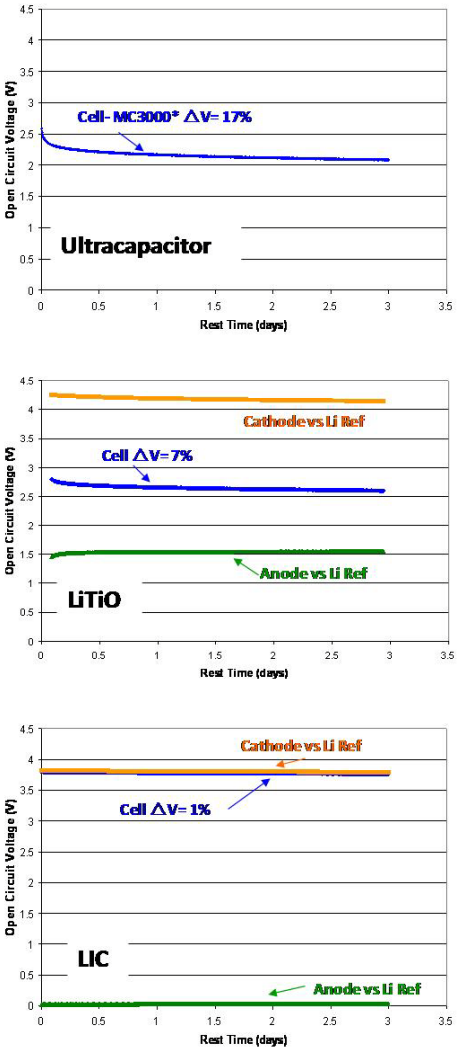

Figure III- 21: The open circuit voltage of a 3,000 F symmetric C/C capacitor obtained from Maxwell Technologies (top), a 5 Ah $Li_4Ti_5O_{12}$/C asymmetric capacitor containing a lithium reference (middle) and a 5 Ah Li_xC_6/C asymmetric capacitor containing a lithium reference (bottom).

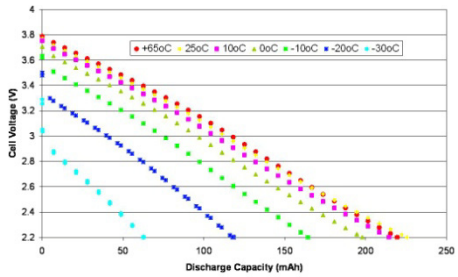

Figure III- 22: The effect of temperature on the capacity of 500 F lithium-ion capacitors. Cells were cycled at the 10C rate.

Conclusions and Future Directions

We are developing lithium-ion asymmetric capacitors that offer the promise of higher energy densities than their their conventional symmetric (C/C) counterpart. Several high-surface-area activated carbons were investigated to identify a material that could deliver high capacitance in Li^+ electrolyte solutions. Prototype cells utilizing either $Li_4Ti_5O_{12}$ or graphitic anode materials were fabricated and evaluated at various discharge rates and tempeatures. Results confirmed previous reports that the graphite system delivers greater energy density because of its higher operating voltage. There are safety concerns for this system that are being examined at both the material and cell level. Differential scanning calorimetry (DSC) experiments are underway to identify and quantify potential exothermic reactions among cell components. The asymmetric lithium-ion design displays low self-discharge at ambient temperature. Future efforts will examine self-discharge characteristics when the cells are charged to various voltages at different temperatures. Efforts will also include a low temperature electrolyte investigation.

FY 2010 Publications/Presentations

1. 2010 DOE Annual Peer Review Meeting presentation.
2. Gourdin, T. Jiang, P. Smith, D.Y. Qu, "Comparison of Post-Stress Response of Various Porous Carbon Electrodes in Supercapacitors", Electrochemical Society Meeting, April 25-30, 2010, Vancouver, Canada.
3. D.Y. Qu, G. Gourdin, P. Smith, T. Jiang, "The Investigation of Activated Carbon Electrodes in Non-Aqueous Electrolyte", Electrochemical Society Meeting, May 24-29, 2009, San Francisco.

III.B Advanced Materials and Processing

III.B.1 HTMI Separator Development (Celgard, LLC)

Amy Paik (USABC Project Manager)
Subcontractor: Celgard, LLC

Kristoffer Stokes
13800 South Lakes Dr.
Charlotte, NC 28078
Phone: (704) 587-8807; Fax: (704) 588-5319
E-mail: kstokes@celgard.com

Start Date: October 1, 2008
End Date: September 30, 2010

Objectives

- Develop a test methodology to provide rapid screening of potential high temperature melt integrity (HTMI) battery separator materials.
- Create an HTMI separator that can validate the screening protocol.

Technical Barriers

The major technical barrier to this project is the need for HTMI materials to validate the test methodology. These are not part of Celgard standard product lineup and must be rationally designed and developed from the ground up.

Technical Targets

- Create a test, or series of tests, that can give an indication of performance within a battery at high temperatures. The tests should mimic particular failure modes at elevated temperatures.
- Validate the testing protocols by creating HTMI separators that can withstand temperatures of greater than 200°C

Accomplishments

- An HTMI test suite has been developed to correlate film behavior to properties within a battery application.
- Materials that pass the film tests have been developed and successfully tested within batteries.

✧ ✧ ✧ ✧ ✧

Introduction

Delivering both the necessary power and capacity as well as thousands of recharge cycles with minimal degradation, lithium-ion battery technology has been identified as an ideal technology for use in electric drive (EDV) or hybrid electric (HEV) vehicles. Typically, lithium-ion batteries are manufactured as a sandwich of a graphitic anode, a lithium metal oxide cathode and some form of separator. The job of the separator is exactly as described: separation of the two oppositely charged electrodes. A solid membrane, however, is unsuitable for this application. Microporosity is required so that the internal electrical circuit can be completed, and lithium-ions can flow between the electrodes during charge-discharge cycles. Celgard has been an industry supplier to the lithium-ion battery market since its inception. In recent years, Celgard has developed technology that has tremendously enhanced the performance of lithium-ion cells through the use of its trilayer “shutdown” microporous materials. These shutdown enabled separators physically close their pores when a programmed temperature is exceeded, creating an open circuit within the cell. Ideally, this happens before other chemical events occur which exceed the temperature rating for the separator. If the programmed shutdown is unable to halt the thermal runaway behavior, the separator material completely melts exposing the electrodes, and leading to an internal short and failure.

Celgard high temperature melt integrity (HTMI) battery separator technology represents a new and substantial leap forward in technology. While the previously mentioned shutdown mode is sufficient for a narrow temperature range, this further thermal degradation of the separator material presents an opportunity to build in another safety feature. Maintenance of the separator structure under high temperature conditions is imperative in the prevention of this failure mode. USABC and Celgard have worked together in the past to provide necessary steps toward not only a technologically viable HTMI separator, but also one that is cost effective for use in the large scale needed for the EDV market.

Approach

Together with USABC, Celgard is working to define the performance characteristics of the next generation of lithium-ion separator materials. A

packaged test suite to screen future promising separators has been developed. Meanwhile, potential HTMI separators have been developed to validate the testing protocols and to deliver the first step towards a truly low cost HTMI solution.

Results

HTMI Test Suite. One of the two major tasks that Celgard identified in the creation of an HTMI separator was the need for a standard methodology to rapidly screen materials for their potential HTMI behavior without the need of building a complete battery. This tactic allows for the quick production of prospective materials on a small scale. Then, with little extra time, the samples can be validated against these standard tests outside of the battery system. Under a previous contract, Celgard determined that there are three tests which simulate conditions within a hot battery that can focus efforts on important thermal failure modes.

Hot Tip – One failure mode is a point failure where the electrodes short in a very limited area. Nearly instantaneously, the localized temperature will increase to greater than 400°C. Hot tip testing is an attempt to mimic the ability of the separator to mitigate the short. The hot tip test is fairly straightforward: a pointed tip (typically ~0.5 mm diameter) is heated to 450°C, and placed in contact with a separator (Figure III- 23). Once the tip contacts the negative electrode, it is held in place for 10 seconds then retracted.

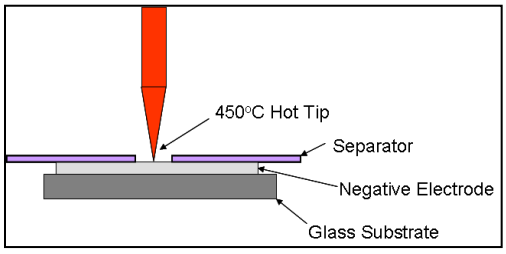

Figure III- 23: Hot tip test setup

Analysis of the film is done by measuring the resulting hole. A film that fails the test retracts from the tip to a great extent, further exposing the electrode. In a live battery, any amount of retraction exposes more potential short locations which leads to failure propagation throughout the separator.

Hot Electrical Resistance (ER) – Another way to test a hot short is through the hot ER test. In this setup, two electrodes are placed on either side of a separator in a model electrolyte solution (Figure III- 24). The separator electrical resistance is continually monitored as the temperature is raised by 10°C/min. Passing films will maintain some resistance, either high or low, as the temperature is raised. Failure is defined as a material that allows the electrodes to short at elevated temperatures.

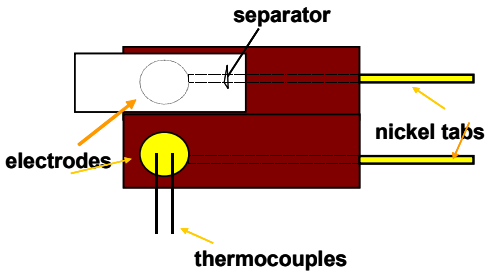

Figure III- 24: Hot ER test setup

Thermomechanical Analysis (TMA) – Thermal dimensional stability is important in a battery application for similar reasons to the hot tip test. While the hot tip test is specifically applied to point defects, TMA tests the whole film for dimensional stability under heat and stress.

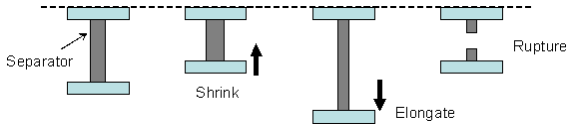

Figure III- 25: TMA test setup.

A separator is placed in a TMA under a small stress at room temperature. As the sample cell temperature is raised, the strain in the system is measured. Standard materials experience three different behaviors under these test conditions (Figure III- 25). Shrinkage occurs first, indicated by a negative dimension change, as the microvoids collapse upon themselves. Further heating leads to increased molecular motion of the polymer chains and a loss of film coherence. This behavior is manifested in elongation (gradual increase in dimension change) and eventually rupture (sudden, large increase in dimension change) of the separator. Passing HTMI separators do not demonstrate this behavior. Instead, the shrinkage region tends to be much smaller than standard separator as well as the complete lack of rupture below 200°C.

Conclusions and Future Directions

Celgard has successfully developed a testing methodology and validated it with HTMI separator materials. Using these techniques, rapid HTMI property screening can be completed on a variety of separator compositions before incorporation into a battery system.

Further development of HTMI separators will be performed with performance characteristics molded by the results of the testing suite.

III.B.2 Highly Filled and/or Crosslinked Li-Ion Battery Separators for HEV/PHEV Applications (Entek)

Ion Halalay (USABC Project Manager)
Subcontractor: ENTEK Membranes, LLC

Richard W. Pekala
250 N. Hansard Ave.
Lebanon, OR 97355
Phone: 541-259-3901, Fax: 541-259-8016
E-mail: rpekala@entek-membranes.com

Start Date: February 1, 2010
Projected End Date: April 30, 2011

Objectives

- Identify optimum formulations and manufacturing process conditions for lithium-ion battery separators with high inorganic filler loadings that exhibit excellent high temperature melt integrity, with or without shutdown functionality.
- Deliver separator roll stock to a domestic Li-ion battery maker for 18650 cell builds. Cells will undergo cycle life and calendar life testing at Entek.

Technical Barriers

The project addresses conflicting separator requirements, technical barriers and material cost issues.

(A) Thermal stability and minimum puncture requirements trend in opposite directions with filler contents: high thermal stability requires high inorganic phase contents (> 50 wt %), while high puncture strength requires high polymeric phase contents.

(B) Implementation of a shutdown capability in single layer separators in hindered by the high filler loading required for increased thermal stability.

(C) Producing defect free precursor films for biaxial stretching with good uniformity in machine and cross machine direction thickness as well as low polymer crystallinity.

Technical Targets

- Thickness: less than 25 µm
- Permeability: MacMullin Number less than 11
- Wettablity: wets out in electrolytes
- Pore Size: less than 1 µm
- Puncture Strength: greater than 300 gf / 25.4 µm
- Thermal Stability at 200°C: less than 5% shrinkage
- Tensile Strength: Less than 2% offset at 1000 psi
- Versions with and without high temperature shutdown.
- No adverse affects on cell performance due to presence of fillers in the separator

Accomplishments

- Six sets of 18650 cells were built (one with an unfilled control and five with ceramic-filled separator fromulations). The controls and the first experimental set have completed 700 cycles at 1C. The cumulative fade for the controls is 11.1% and for the first experimental set 7.5%.
- Accelerated (60°C) calendar life test: the first set of cells with experimental separators has a more stable OCV and lower rate of capacity fade than controls.
- The first iteration of a coextruded three layer separator showed significant increase in resistance during shutdown testing.

✧ ✧ ✧ ✧ ✧

Introduction

For small commercial lithium-ion cells under abuse conditions, such as external short circuit or overcharging, the separator is required to shutdown at temperatures well below the temperatures at which thermal runaway can occur. Shutdown results from collapse of the pores in the separator due to softening or melting of the polymer, which slows down or stops the ion flow between the electrodes. Nearly all Li-ion battery separators contain polyethylene as part of a single- or multi-layer construction so that shutdown begins at ~130°C, the melting point of polyethylene. After shutting down, residual stress and reduced mechanical properties above the polymer melting point can lead to shrinkage, tearing, or pinhole formation.

For larger cells such as those used in hybrid, plug-in hybrid and battery electric vehicles (HEV, PHEV, BEV), shutdown may or may not be required, depending on specific application and system design. For power cells in HEV applications much of the safety and abuse tolerance for failure modes in which separator shutdown might play

a role is handled at a system level. For this reason high temperature melt integrity is considered more important than shutdown. For energy cells in PHEV and BEV applications both shutdown and high temperature melt integrity may be important.

The goals of this project are (i) a separator for power cell applications with low impedance and excellent high temperature, mechanical and dimensional stability and (ii) a separator for energy applications with the addition of shut down functionality.

Approach

For applications with no shutdown requirement the following approaches will be used: (1) incorporation of inorganic fillers into a polyolefin separator at high loading levels during extrusion (filled separators) and (2) annealing of biaxially-oriented, highly filled separators above the melting point of the polymer matrix, to reduce residual stress while maintaining high porosity.

The following approaches will be used making separators for applications with shutdown requirement: (1) co-extrusion of multilayer films with filled and unfilled layers; (2) reduction of film thickness by chilled roll casting or biaxial orientation.

Results

Six sets of 18650 cell builds. The initial cell build, in April 2010, consisted of ten control cells with an unfilled 20µ Teklon Gold XP separator and ten experimental cells with a 20µ silica filled separator, Figure III- 26. The cells were built and formed at American Lithium Energy Corp. in San Marcos, CA, using commercial NMC positive and graphite negative electrodes. These cells have completed 700 cycles and ~ 150 days on 60°C storage (or calendar) life test.

A second cell build took place in August. These cells were built with four different experimental separators with different fillers and filler blends. These cells have completed initial reference performance tests and have begun cycle life and 60° C storage life testing. The five sets of experimental separators do not have shut down functionality.

Figure III- 26: 18650 cells

Cycle Life: The cycle life test consisted of the following sequence to test steps: (i) charge at 1.2A to 4.2V; (ii) discharge at 1C rate to 3.0V; (iii) rest 1 hr. between charge and discharge at ambient temperature; (iv) repeat 5 cycles per day. Four cells from each group are on cycle life testing. The controls and the silica filled experimental have completed 700 cycles. The cells with the control separator have lost 11.1% of their initial capacity, while the cells with the experimental separators have lost 7.2% of their initial capacity, see Figure III- 27 and Figure III- 28.

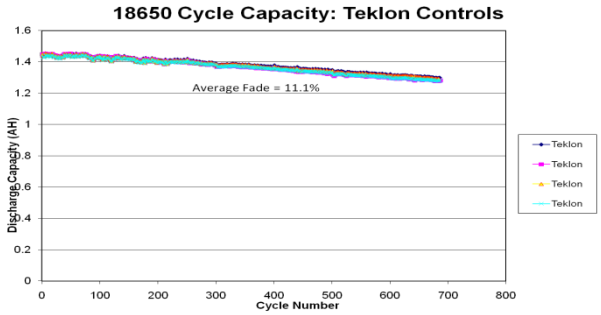

Figure III- 27: Cycle life test results, unfilled control separators

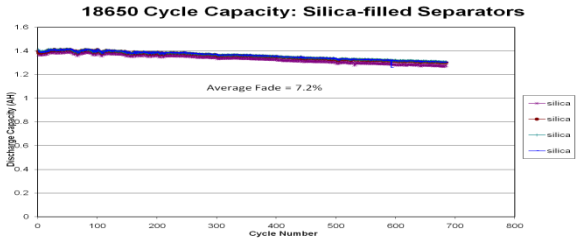

Figure III- 28: Cycle life test results, Silica filled separators

Accelerated (60°C) Storage Test: Cells are stored at 100% SOC and 60° C. Standard capacity and HPPC tests are repeated every 28 days at 30°C. OCV during storage is measured once a day. The cells with the silica filled experimental separators have a more stable OCV (lower rate of self discharge) than the controls, see Figure III- 29 and Figure III- 30.

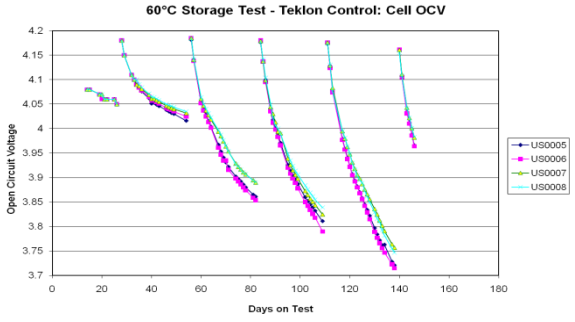

Figure III- 29: Calendar life test results, control separators

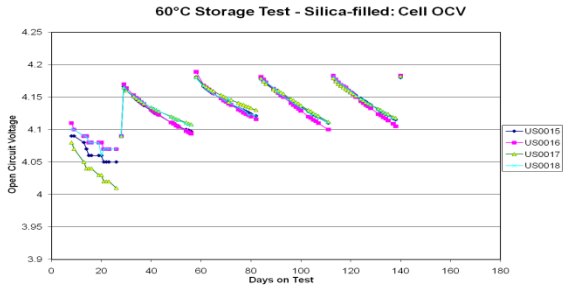

Figure III- 30: Calendar life test results, silica filled separators

Both groups have experienced a loss of capacity at 30°C. The rate of loss is greater for the controls and less for the cells with silica-filled separator. At 20 weeks the controls have retained 63% of initial capacity while the cells with the silica filled separator have retained 82% of initial capacity, Figure III- 31.

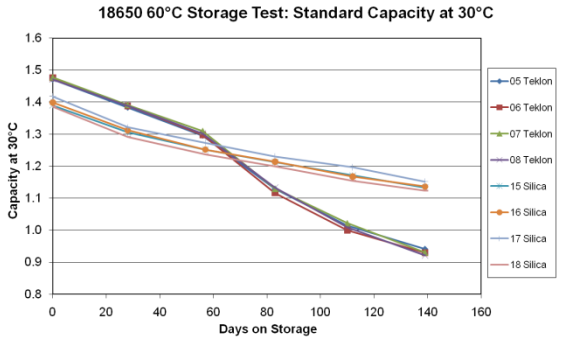

Figure III- 31: Capacity vs. storage time.

High Temperature Shut Down. Shutdown testing is conducted on a separator that is wetted out with an electrolyte. The sample is placed between two wetted carbon electrodes that are positioned between two metal platens which are heated at a constant rate of 50°C/min. The separator impedance at 1 kHz is continuously measured using a LCR meter, while the temperature is ramped from 25°C to 200°C. The impedance at 100°C is noted and the temperature at which a 1000 fold increase over the recorded value occurs represents the shutdown temperature of the separator.

Figure III- 32 shows shutdown curves for an un-filled polyethylene separator (black squares), and a blank consisting of electrolyte only (green line) and a coextruded tri-layer separator (red circles).

This coextruded tri-layer film (unfilled / filled / unfilled) shown in Figure III- 33 is a first iteration and, at 417 µm, is too thick for a practical separator.

While resistance does begin to increase at about 140°C, the tested film does not meet the technical definition of shutdown representing a 1000-fold increase in resistance. Co-extrusion presents a cost advantage in that all three layers are formed at the same time rather than being laminated in a separate step. In the remainder of the program we will work on reducing thickness, reducing initial electrical resistance and reducing the shutdown onset temperature.

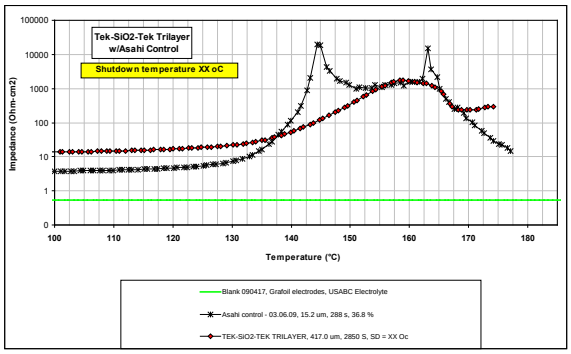

Figure III- 32: Shutdown test results

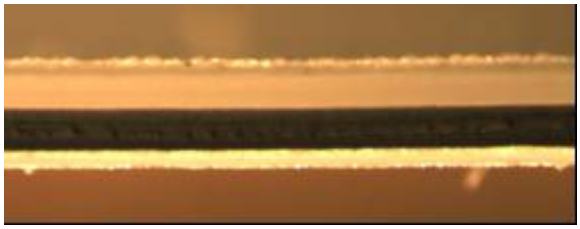

Figure III- 33: Coextruded tri-layer film

Conclusions and Future Directions

Highly filled battery separators for use in high power lithium-ion batteries for HEV applications have been produced. These separators have:

- High ceramic filler contents (60 to 70 wt% inorganic phase);
- High porosities (in the range of 80%);
- Very low MacMullin number (approx. 3);
- Good wet-out in the electrolyte;
- Good thermal stability (<5% shrinkage at 200°C);
- No high temperature shut down;
- Less than 2% offset at 1000 psi.

The work done so far on the project indicates that both the thermal stability and tensile properties can be improved by heat treatment.

Six sets of 18650 cells have been built (1 set of cells with unfilled control separator and 5 sets of cells with experimental ceramic-filled separators). After 700 cycles the first set of cells with a ceramic-filled separator is outperforming the controls.

The first coextruded tri-layer film with potential shutdown functionality has been produced.

During the remainder of the project Entek will focus on optimizing both the non-shutdown and shutdown

separators, will optimize the separator formulations and will gain additional experience with scale-up in a production environment.

III.B.3 Advanced Cathode Materials with High Energy, Power, and High Thermal Stability for PHEV Applications (3M)

Adam Timmons (USABC Project Manager)
Subcontractor: 3M

Jamie P. Gardner, Technical Manager
3M Electronics Markets Materials
3M Center, Building 209-1W-13
St. Paul, MN 55144
Phone: (651) 737-1478; Fax: (651) 733-2312
E-mail: jpgardner@mmm.com

Start Date: March 1, 2009
Projected End Date: April 1, 2011

Objectives

- Design and optimize a new cathode material that has better performance and lower cost than commercial $LiNi_{1/3}Co_{1/3}Mn_{1/3}O_2$ material.
- Demonstrate the manufacturing capability of the new cathode material in 3M pilot plant (~ 100kg level) and through the superior performance in 18650-size cell.

Technical Barriers

This project addresses the following technical barriers:

(A) High cost of cathode materials (the most expensive part of high energy, Lithium-ion cells)

(B) Insufficient energy density for 40 mile PHEV

(C) Abuse tolerance of high energy Li-ion cells

Technical Targets

- New material with around 5 ~ 10% capacity improvement compared to commercial $LiNi_{1/3}Co_{1/3}Mn_{1/3}O_2$ material.
- Approximately 10% cost reduction.
- Similar or higher thermal stability than commercial $LiNi_{1/3}Co_{1/3}Mn_{1/3}O_2$ material.

Accomplishments

1. Completed the optimization and 1000 Charging Depleting Cycles (CDC) on 18650-size cell with benchmark and advanced cathode material (MNC 111)
2. Systematically screened MNC material according to its physical property, electrochemical performance, and thermal stability and finally two MNC compositions were chosen
3. Successful designed and set up the 600L pilot reactor, which enables 3M to produce around 25kg of MNC-OH precursor per batch
4. Made several successful trials on both MNC candidates and verified pilot production of USABC compositions meet basic physical and electrochemical expectations of this project
5. Verified pilot process robustness and costs in line with current NMC process costs
6. Built 18650 cells of both USABC compositions. Conducted abuse and performance testing of 18650 cells showing no significant difference between cells with USABC compositions and baseline NMC.
7. Developed quantitative method for determining secondary particle crushing during electrode calendaring process.
8. Evaluated material preparation process resulting in process “P2” yielding higher secondary particle integrity during calendaring.
9. Prepared large scale cathode coatings of BC-618 and USABC Compositions 1 and 2 prepared by “P2” process as well as anode coatings to construct 18650 cells.
10. Conducted nail penetration and hot-block Abuse testing on 18650 cells finding that USABC Composition 2 cells show significantly less or comparable thermal activity than baselinecells.
11. Initiated Cycling evaluation of cells with new hardware containing Compositions 1 and 2 (both process “P0” and “P2” and BC-618 and 90 and 95% active levels.)

Introduction

Achieving the USABC cathode goal will require that the new material have a capacity around 165mAh/g at 4.3V. In order to meet the cost reduction by ~10%

compared to the basline $LiNi_{1/3}Co_{1/3}Mn_{1/3}O_2$ material, the Co composition in the new cathode material needs to be as low as possible, since the Co price heavily influences the material cost in Li-Ni-Co-Mn-O layered cathode materials. The new cathode material needs to have high capacity, low cost, and also high thermal stability, which will be potentially ideal for automotive applications.

Approach

To meet the USABC-3M capacity target of 5 ~ 10% capacity improvement compared to $LiNi_{1/3}Co_{1/3}Mn_{1/3}O_2$, we need to improve the Ni and Co content, since they are both electrochemically active. In order to meet the cost reduction of ~10%, we need a lower amount of Co than 20%.

Based on the above considerations, we planned to characterize 12 different compositions of cathode material, where Co is ~10% or 20% with Ni ranging from 25% ~ 75% and Mn ranging from 10% ~ 40%.

Results

1. We optimized the 18650-size cell designs (electrode loading, density, current collector, tab numbers, electrolyte additives, etc.) with commercial MNC 1/1/1 material. The final optimized cell gave low cell impedance of ~ 40mΩ. By using an additive, we significantly improved the CDC life from 200 cycles to above 1000 cycles. The power capability of the cell stabilized in around 600 cycles with the power fading around 22%.
2. We systematically studied 15 different MNC materials and finally chose two promising MNC compositions. These two compositions showed high capacity, high thermal stability, and also low raw materials cost. The small batch experiments showed that both materials met our program target.
3. We successfully set up a 300L pilot reactor to control the MNC-OH precursor morphology. Figure III- 34 shows the different sizes (3 to 25um) of MNC-OH 1/1/1 produced in the 300L pilot reactor. The size controlling capability at the pilot scale is the key to design the MNC oxide with different morphologies for PHEV applications, which requires high energy density and good power.
4. We produced kilogram quantities of both optimized MNC materials in a 10L reactor at different synthesis conditions. The initial coin cell data show excellent performance for both materials, which match the data from small batch experiments in Phase 1.
5. We optimized the 18650-size cell designs (electrode loading, density, current collector, tab numbers, electrolyte additives, etc) with commercial MNC 1/1/1 material. The final optimized cell gave low cell impedance ~ 40mΩ. By using electrolyte additives, we significantly improved the charging-depleting cycling life from 200 cycles to above 1250 cycles. Figure III- 35 shows the discharge / regen power capability from HPPC tests on the 18650-size cell after every 250 CDCs (Charging Depleting Cycles). The cell available energy decreased ~17% after 1250 cycles and the cell impedance only increased approximately 6% with the additives in the electrolyte. The data show excellent performance of cycling with the benchmark MNC 111 material in 18650-size cells.

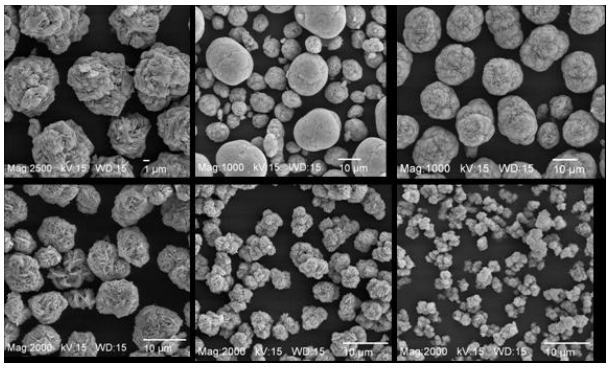

Figure III- 34: MNC-OH 1/1/1 produced in the 300L pilot reactor. The MNC-OH size varies from 3 to 25um.

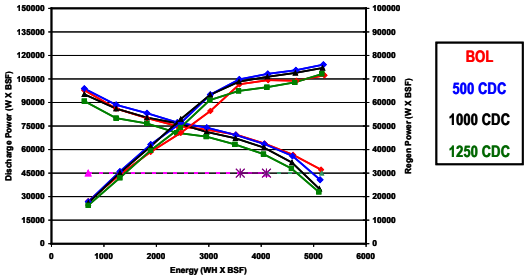

Figure III- 35: Discharge / regen power capability from HPPC tests on the 18650-size cell after every 250 CDC (Charging Depleting Cycles)

6. We systematically studied the impact of reaction parameters (such as pH value, reaction temperature, reactant concentration, flow speed, etc) on the morphology of MNC-OH precursor during the co-precipitation process in 2L and 20L reactor, respectively. We then transferred the knowledge to the 600L pilot plant to control the MNC-OH crystal growth. Figure III- 36 shows that we can effectively

control the MNC-OH precursor morphology including the density, size, and spherical shape. The precursor density ranges from 1.0 ~ 2.1 g/cc and the average size (D50) from 3 to 15 um. The success of the pilot co-precipitation reactor setup is the key for us to produce ~ 25kg level MNC oxide after the composition and process optimizations.

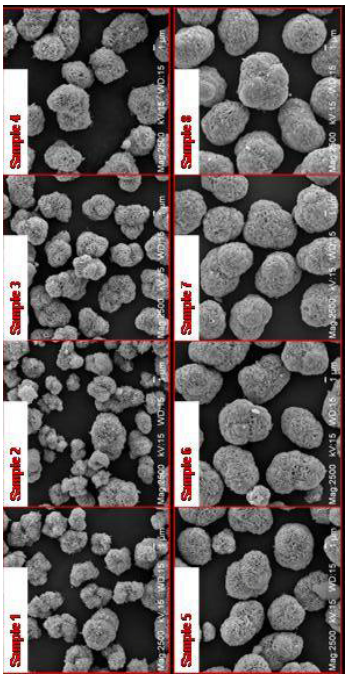

Figure III- 36: SEMs of MNC-OH Precursor Produced in 600L Pilot Reactor

7. We finished ~ 5 trials for each of the MNC candidates in the 600L reactor to tune the co-precipitation process. We achieved excellent performance of both MNC candidates in terms of physical properties and electrochemical performance. The specific discharge capacity of both MNCs are ~ 170mAh/g at 4.3 V vs. Li metal, compared to ~ 155mAh/g of MNC 111 benchmark. The raw material cost saving of both MNC candidates vs. MNC 111 benchmark is over 10%. The new MNC performance data from the pilot plant confirmed the initial data from the smaller scale of 2L reactor and met the USABC-3M cathode program goal.

8. Co-precipitation runs were made in order to identify sources of potential variance and overall process robustness. Three items were identified as major potential contributors to process variation. Limits and procedures for these factors have now been set and verification of process control is indicated in Table III- 10.

Table III- 10: Material Process Robustness Verification Runs

	Composition 1		Composition 2	
Test	Tap Density	PSD [D50]	Tap Density	PSD [D50]
Run V1	1.92	8.25	1.95	7.47
Run V2	1.90	8.24	2.00	8.35
Run V3	1.92	8.31	2.01	7.46
Average	1.91	8.27	1.99	7.76
Range	0.01	0.04	0.04	0.59
% Err	0.52%	0.48%	2.01%	7.60%
Std Dev.	0.01	0.03	0.03	0.42

9. Careful characterization of material from multiple large scale verification runs was conducted relative to initial small/lab scale reactions. The data is summarized in Table III- 11.

Table III- 11: Summary of Characterization Data from Large-scale Simulation Runs.

Requirement	BC618 Benchmark	Target	Comp. 1 Lab Scale	Comp.1 Pilot Scale	Comp. 2 Lab Scale	Comp. 2 Pilot Scale
Tap Density (g/ml)	2.25	1.80 ± 1	1.35	1.89	1.38	1.81
PSD [D50] (µm)	11.0	8 ± 1	9.89	8.14	10.2	7.81
Surface Area/BET (m^2/g)	0.27	≥ 0.3	1.05	0.41	1.10	0.38
Irreversible Capacity at 30°C	9.9%	≤15%	9.4	8.9	5.7	8.8
Capacity C/10 at 30°C (mAh/g)	156	≥172	168	173	172	174
Capacity C/2 at 30°C (mAh/g)	146	≥ 161	160	164	163	162
Capacity 2C at 30°C (mAh/g)	135	≥ 149	149	154	152	150
DSC Onset (°C)	273	≥ 273± 5	261	270	272	270
DSC Peak Max (°C)	317	≤ 317 ± 3	321	318	315	310
DSC Delta Heat (J/g)	700	≤ 700 ± 50	825	760	750	800
DSC Delta Heat / Capacity (J/mAh)	4.45	≤ 4.45	4.91	4.39	4.36	4.60
Raw material Cost ($/kg)	11.9	≤ 10.7	9.6	9.6	8.6	8.6

10. Electrode coating is a key aspect to cell and material performance. Multiple coating runs were conducted with the 2 compositions of interest to 3M and USABC. After initial trials to establish basic coating parameters, systematic optimization was initiated and 70-100 electrodes of the conditions described in Table III- 12 were coated.

Table III- 12: Electrode Preparation Summary.

Ctg	3M ID	Active	Active %	Binder %	Conductive %
C1	233C	Comp # 2	95	2.5	2.5
C2	234C	Comp # 2	90	5.0	5.0
C3	235C	Comp # 1	95	2.5	2.5
C4	236C	Comp # 1	90	5.0	5.0

Electrodes were characterized by SEM, bend testing, resistance and half cell electrochemical evaluations. They were found to be suitable for materials comparison and fabricating 18650 cells.

11. 18650 cells were fabricated with both composition 1 and 2 materials according to the design principles of maintaining cathode composite capacity. This principle allows the best comparison between materials keeping the anode coating constant. Additionally, for material comparison purposes electrodes C1 and C3 were selected because the baseline electrode was formulated at 95/2.5/2.5. The binder and conductive agent utilized in all coatings is equivalent and the electrolyte used in all cells is the standard electrolyte with equivalent amounts of additives A and B.
12. We measured the thermal stability of cells, through tests such as smart nail penetration, oven test, overcharge test, etc. During the nail penetration process, both the cell surface and nail tip temperature are measured. USABC recommended that 3M focus on thermal ramp stability in addition to nail penetration. Working with SNL, a final test method was established. After finalizing the method, experimental reproducibility was determined utilizing industrial quality $LiCoO_2$ cells and 3M prepared cells containing the Baseline BC 618 material. The results of this work are summarized in Table III- 13.

Table III- 13: Thermal Ramp test Reproducibility

18650	Thermal Runaway Temperature (ºC)	Std Dev (± ºC)
BC-618	227	2
Comp 1	226	2
Comp 2	229	2

The results show that the 3M evaluation method is reproducible and that it can differentiate between different classes of material.

The thermal ramp method established above was then applied to 18650 cells containing baseline and USABC composition materials. A thermal runaway threshold was set at a temperature increase of 20ºC/ min. The data is summarized in Table III-14.

Table III- 14: Thermal Runaway Threshold Data

Cell Type	Number of Cells	Average Onset	Standard Dev
Commercial 18650 - $LiCoO_2$	**4**	**187** ºC	± 3ºC
3M 18650 – NMC BC618	**4**	**225** ºC	± 5ºC

The results show that 18650 cells containing composition 1 and 2 do not have a significant difference in thermal behavior relative to the baseline cells containing BC618. This is consistent with the project's objectives.

13. The signature curve method was validated and then utilized to determine the rate capability of 18650 cells prepared with both USABC compositions and the baseline cell. Measurements were taken at 30ºC with a cutoff voltage of 2.8V at rates of 2.5C, 2C, C, C/2, C/5, and C/10. The data from the evaluations is presented below (Figure III- 37).

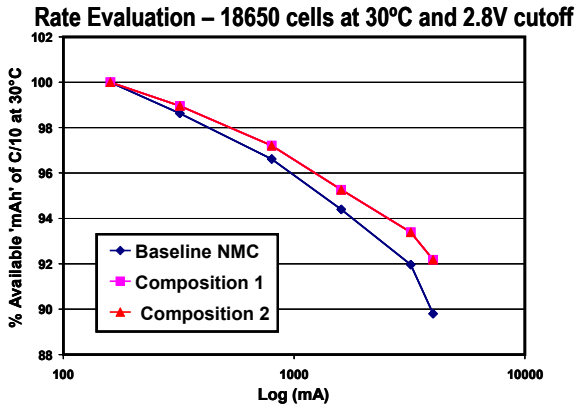

Figure III- 37: Rate Evaluation Data Summary (2.8V Cutoff)

The data clearly shows rate performance advantages of the USABC compositions over the baseline composition at 30ºC. This result is consistent with the projects objectives.

The signature curve method was also utilized to determine the rate capability of 18650 cells prepared with both USABC compositions and the baseline cells at -30ºC. Cells were allowed to equilibrate for 3 hours before evaluation and rest for 2 hrs between discharges. Measurements were taken at -30ºC with a cutoff voltage of 2.8V and 2.0V at rates of 2.5C, 2C, C, C/2, C/5, and C/10. The data shows that with a 2.8 V cutoff the baseline cells perform better than cells with the USABC compositions and that USABC composition 1

performs better than USABC composition 2. Utilizing a 2.0V cutoff, however, allows differentiation of the material's capabilities while still exceeding the USABC's minimum voltage guideline. When a of 2.0V cut-off is utilized composition 1 demonstrates superior rate capability performance to both composition 2 and the baseline cells. This result is consistent with the projects objectives. The data is presented below (Figure III-38).

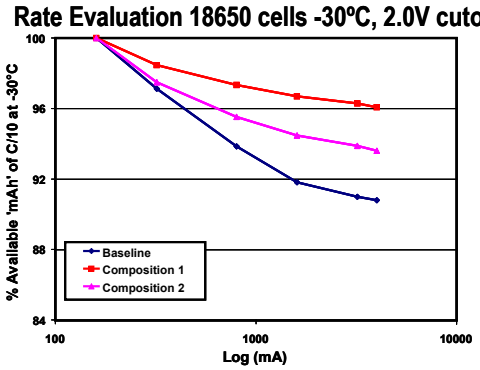

Figure III- 38: Rate Evaluation Data Summary (2.0V Cutoff)

14. 18650 Cells containing USABC compositions 1 and 2 were evaluated according to USABC HPPC protocols. The data is shown graphically below (Figure III- 39).

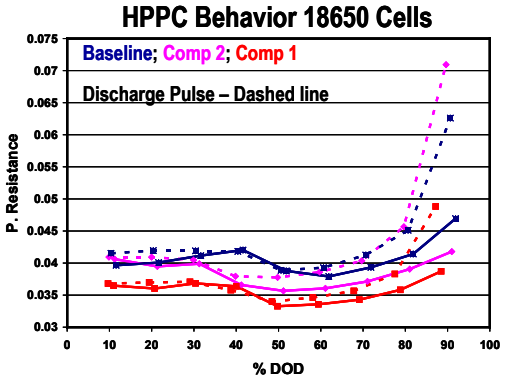

Figure III- 39: HPPC Behavior for 18650 Cells

15. 18650 cells with USABC composition 1 demonstrated the lowest pulse resistance. From the HPPC data standard USABC methods were utilized to calculate the Battery Size Factor (BSF). The results from the calculations (with standard deviations in parentheses) are shown in Table III-15.

Table III- 15: BSF Results for 18650 Cells

Cathode Material	BSF	
	Energy Limited	Power Limited
Baseline BC 618	1155 (32)	907 (11)
Comp 2	1095 (42)	860 (10)
Comp 1	1190 (32)	830 (40)

In all cases the BSF is energy limited. The USABC compositions demonstrate lower power limited BSFs vs. baseline cells. No substantial improvements in energy limited BSF would be expected and given the precision of method no significant differences are observed.

16. It was observed that the secondary particles of the USABC composition positive electrode material appeared to fracture during the electrode fabrication process to a greater extent than the benchmark material. Although the impact of this on cell cycle life is unknown – determining a method to characterize the difference and the cause was undertaken.
An analysis method was developed for dissolving a calendared coating in NMP, centrifuging, washing residual solids in acetone and then analyzing particle distribution in a Horriba La-910 PSD analyzer. This method was utilized to confirm that calendaring was causing the secondary particle fracturing and that more particle fracturing occurred with USABC compositions than with the benchmark material.
A material process design was undertaken on USABC composition 2 to determine if altering the preparation process could reduce secondary particle fracture without compromising electrochemical performance.
The materials that resulted from seven process conditions were analyzed for secondary particle integrity. The lower the volume fraction of < 2µm particles after calendaring the more fracture resistant the particle. Based on the data, process "P2" was identified as the optimum process for improving secondary particle robustness while maintaining necessary electrochemical properties.

17. 15. Multi kg quantities of USABC composition 1 and 2 were prepared in order to fabricate electrodes of 18650 cells. The specific electrodes and approximate quantities coated are summarized in Table III- 16.

Table III- 16: Electrode Preparation Summary Table.

Cathode Material	Approx Number of Electrodes	
	90 wt% Cathode	95 wt% Cathode
BC-618K	>70	>150
Comp 1 - P0	>70	>70
Comp 2 - P0	>70	>70
Comp 1 - P2	>70	>70
Comp 2 - P2	>70	>70
Anode - MAGE-92%	>300	

Electrodes were characterized by SEM, bend testing, resistance and half cell electrochemical evaluations. They were found to be suitable for materials comparison and fabricating of 18650 cells.

18. 18650 cells were fabricated with both materials, processes and at 90 and 95% active levels according to the design principles of maintaining cathode composite capacity. This principle allows best comparison between materials keeping the anode coating constant. The cells fabricated are summarized in Table III- 17.

Table III- 17: Summary Table for 18650 Fabricated Cells

Cathode Material	Number of Cells	
	90 (wt%) Cathode	95 (wt%) Cathode
BC 618K	10	15
Comp 1 – P0	5	4
Comp 2 – P0	5	10
Comp 1 – P2	13	9
Comp 2 – P2	11	11

19. Cycling imitated in July with cells containing Composition 1 and 2 was terminated due to cell hardware leakage which caused cell failure. Root cause was determined to be mismatch of new lot of PTC headers with the can being used to assemble the cells.
20. 18650 cells prepared with BC-618 benchmark and USABC Composition 2 materials were utilized for nail penetration abuse testing. Cells were prepared to have the same capacity, formed, and charged to 4.2V. Internal, nail tip and external skin temperature as well as voltage are measured during the penetration. The results are summarized in Table III- 18.

Table III- 18: Results of Internal, Nail Tip and External Voltages for the 18650 Cells Prepared with BC-618 Benchmark

Requirement	BC618 Benchmark	USABC Comp 2
Nail Penetration Result	*Venting/ Smoke and Combustion*	*Venting/ Electrolyte Boiling*
Max Temperature (ºC)	***425***	***183***

Nail penetration testing of the cells found at least comparable stability between 18650 cells fabricated with the benchmark BC618 and the USABC Composition 2 materials.

21. 18650 cells prepared with BC-618 benchmark and USABC Composition 2 materials were also utilized for 160 ºC Hot Block abuse testing. Standard cells were prepared for each of these conditions, with same capacity, were formed and charged to 4.2V. Hot block testing was performed by dropping cells into an aluminum block maintained at 160 ºC and monitoring cell temperature. Table III- 19 summarizes the results.

Table III- 19: Results for 160 ºC Hot Block Abuse Testing

Requirement	BC618 Benchmark	USABC Comp 2
Hot Block Result/Description	*Venting/ No smoke*	*Venting/ No smoke*
Max Temperature (ºC)	***163***	***166***

Hot-Block testing of the cells found comparable behavior between 18650 cells fabricated with the benchmark BC618 and the USABC Composition 2 materials.

22. Cycling was initiated on all of the cell designs. Table III- 20 and Table III- 21 show the average discharge pulse resistance and available energy at 125 cycles for these cells.

Table III- 20: Average Discharge Pulse Resistance Results for Cycled Cells

HPPC Avg Discharge Pulse Resistance of Cells Studied

Cathode Material	Avg Discharge pulse resistance (mΩ ± 4)	
	90 (wt%) Cathode	95 (wt%) Cathode
BC 618K	41	45
Comp 1 – P0	49	46
Comp 2 – P0	62	42
Comp 1 – P2	40	36
Comp 2 – P2	50	39

Due to the limited cycle life data it is not possible to draw significant conclusions about the relative performance of the materials and cells being studied. Data collection is ongoing.

Table III- 21: Available Energy Results for Cycled Cells

Available Energy (AE) Margin after 125 Charge Depleting Cycles. BOL AE Margin = 30%

Cathode Material	% Available Energy	
	90 (wt%) Cathode	95 (wt%) Cathode
BC 618K	28	29
Comp 1 – P0	27	26
Comp 2 – P0	21	29
Comp 1 – P2	Cycle life testing in progress	
Comp 2 – P2		

Conclusions and Future Directions

The objectives for increased capacity and decreased raw materials costs whilst not adversely affecting thermal abuse tolerance and power capability were accomplished. Experiments are underway to characterize the cycle and calendar lives in addition to power capability and internal resistance rise with cycling and calendar time. USABC and 3M have chosen to move forward with composition 2 for the cell builds for Argonne life and Sandia abuse tolerance testing that will begin in Q1 2011.

Tasks ongoing or outstanding (taken from the no-cost extension SOW):

Internal Evaluation of Cells.

Complete the following electrochemical and abuse evaluations of the 18650 cells

- Rate performance at 30ºC and -30 ºC
- HPPC and BSF determination
- Cold crank capability
- Initiate CD cycling
- Thermal ramp evaluation
- Nail penetration

Cell Assembly for National Lab Sampling

- Assemble 20 cells of one selected USABC composition and 20 cells of baseline composition.
- Ship cells to Argonne and Sandia National Laboratories

Assemble Final Report

- Complete and summarize data
- Author and submit project report

III.B.4 Advanced Negative Electrode Materials for PHEV Li-Ion Batteries (3M)

Christopher Johnson (NETL Project Manager)
Subcontractor: 3M

Kevin Eberman (Principal Investigator)
3M Electronics Materials Marketing Division
3M Center
St. Paul, MN 55144-1000
Phone: (651) 733-4958; Fax: (651) 736-7478
E-mail: kweberman@mmm.com

Start Date: Jan 5, 2009
Projected end date: June 22, 2012

Objectives

- Identify, synthesize, and characterize new high energy density alloy anode material for use in advanced lithium-ion batteries for PHEVs.
- Optimize alloy manufacturing processes to demonstrate scalability.
- Use 18650 test cells to optimize alloy coating formulations, electrolyte formulations and cell designs for PHEV electrochemical performance and abuse tolerance.

Technical Barriers

This project addresses the following technical barriers associated with the use of alloy negative materials:

(A) Low cycle life

(B) High irreversible capacity, leading to low overall cell energy density

(C) High manufacturing costs associated with the production of nanostructured alloys

(D) Accommodation of the large volume expansion of alloy negative materials in electrochemical cells

(F) Thermal stability issues associated with the use of alloy anodes.

Technical Targets

- Enable a 15-20% improvement in energy density over conventional cells containing graphite anodes.
- Enable at least 300 cycles with 20% fade when cycled with a capacity swing of 70%.
- Demonstrate manufacturability on a pilot scale (>3 kg).
- Demonstrate thermal stability: (150ºC hot block test, no thermal runaway, <5°C overshoot).
- Demonstrate a rate capability of 2C/0.2C > 90%.

Accomplishments

- Demonstrated that a new material, L-20722, meets all technical targets of this program and offers some advantages for PHEV applications over the material of last year's effort, L-19725 which also met all technical targets of this program.
- Developed method to accelerate discovery of improvements to capacity retention (Subtask 2)
- Demonstrated power-capability equal to that of high-power graphite in full-cells (Subtask 4)
- Showed excellent thermal stability in 18650's (Subtask 5)
- Optimized formulation of alloy-graphite blend electrodes for high capacity-retention (Subtask 7)
- Advanced methods to improve alloy-graphite dispersion, an approach to quantify this, and the ultimate effect of improved capacity-retention (Subtask 7).
- Discovered a new class of alloy-anode materials that show the promise of increased capacity-retention and reduced SEI growth, while maintaining low irreversible-capacity, high reversible-capacity, high power, and low cost (Subtask 9).

Introduction

The main focus of this DOE funded research is to develop anode materials that can increase the energy density of PHEV power sources significantly beyond what current Li-ion technology can provide. All aspects of the L-20772 material developed in this program meet the technical targets of this program, including >80% capacity retention at 300 cycles. However, we believe further reduction in fade is probably necessary for viability in a PHEV power source. This has been the over-all focus of the work this year.

Approach

The purpose for this research program is to develop practical anode materials for PHEV power sources. Therefore in addition to the performance requirement objectives of this project there are other restrictions that need to be met in order for the materials developed in this

program to have practical use. Specifically, the following approach towards materials development was taken:

- Raw materials cost must be kept low.
- Inexpensive existing manufacturing processes that can result in high-volume production should only be considered.
- Coatings should preferably be from aqueous slurries and must be coated using existing slurry coating procedures.
- Cell assembly must be performed using existing manufacturing procedures.

Without meeting the above specifications it is our opinion that the likelihood of adoption of any new battery materials technology is low.

It is widely recognized that Si or Sn-based alloys are the only alloy materials that can deliver significant gains in energy density over graphite. With the above guidelines in mind research in this project focused on Si-based alloys, since the raw-materials cost of Sn-based alloys was deemed too high for PHEV applications. The design of the alloy was based on the active/inactive alloy concept described in reference 1, with a target volumetric capacity of 1500 mAh/cc. At this capacity the alloy is expected to have a volumetric expansion of 100% during lithiation and increase the energy density of a lithium-ion cell by 15-20%, depending on the cathode formulation.

Results

Subtask 1.1-3: Initial Characterization. These tasks were successfully completed and reported in 2009.

- Initial Characterization
- Manufacturing/Viability Analysis
- 18650 Cell Performance testing

Subtask 2 - Electrolyte Optimization. This task was 90% completed and reported in 2009. It was found that at least 40% FEC content was required in the electrolyte for good cycling to be obtained.

This year a method was developed for accelerating the fade measurement and for quantifying the resulting SEI. We showed that by cycling at 60C we can more quickly determine the impact on reducing fade from any modification we make to the material or electrolyte. By disassembling a fully delithiated anode from a cell cycled at 60C, we found that measuring the Li content by ICP gave sufficiently precise value to allow us to track the SEI growth. It appears that the SEI on alloy materials grows thicker and thicker each cycle. Efforts to address this issue are reported under Subtask 9 below.

Subtask 3 - Cell Development for the Accommodation of Anode Volume Expansion. The primary goals of this task were completed in 2009. However, because of the important discovery of continuous volume expansion with the cycling of alloys, work related to this task will continue under the heading of Subtast 9.

Subtask 4 - Cell Development for Power Characteristics. Figure III- 40 shows the results of initial rate capability tests of L-20772 alloy compared to L-19725 large particle size alloy (an earlier generation alloy) and a high-power graphite (HPG) material used in PHEV cells. As shown in the figure L-20772 alloy has nearly identical rate performance up to 20C rates as high power graphite. Such performance is extremely impressive for an alloy material and further demonstrates L-20772 alloy's potential for use in PHEV applications.

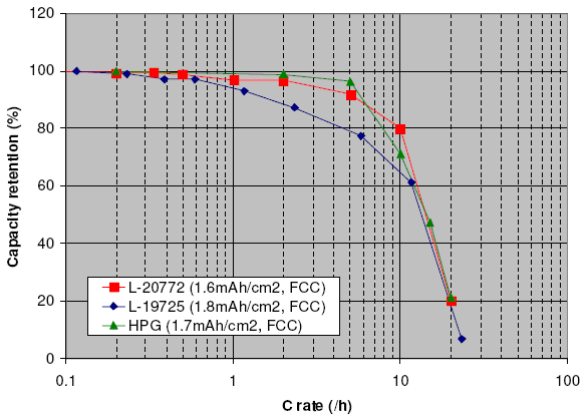

Figure III- 40: Coin half-cell rate capability tests of L-20772 alloy, L-19725 alloy and high power graphite (HPG).

Subtask 5 - Abuse Tolerance. DSC and initial 18650 thermal abuse testing has demonstrated very promising results for the alloy anode materials. Figure III- 41 shows the results of hot-block tests comparing alloy/graphite blend cells to pure graphite cells. The cathodes are all 3M NMC materials (BC-618 and Advanced NMC). In this test the cell introduced directly into a slot in a block of metal that has already been heated to 160C. A thermo-couple on the cell monitors the temperature over-shoot. A cell fails the test if it goes into thermal run-away. Despite the fact that over-shoot is primarily driven by the energy of the cell, the 2.6Ah alloy-based cell passes the test and has only slightly greater over-shoot than the graphite-based cells.

Subtask 6 - Anode Behavior during PHEV Cycling Protocols. Taking advantage of the USABC cathode program, in which 18650's have been built using advanced MNC cathodes, an initial set of cell has been built using MNC cathodes and L-20772. PHEV-type HPPC testing is scheduled for the next months.

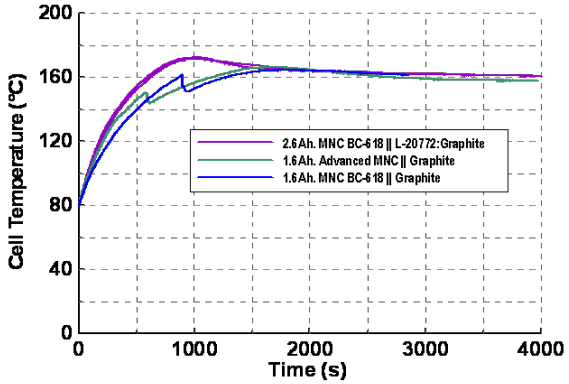

Figure III- 41: 160C Hotblock test results for 18650's all having NMC-type cathodes.

Subtask 7 - Anode Composite Development. Tremendous progress was made this quarter in developing an improved electrode using the alloy anode. Figure III- 42 shows the design spaced examined for maximum capacity retention, which was correlated to power-performance. An optimal composition was of L-20772:Graphite:Carbon-Black:Binder was determined which is expected to increase cycle life by 30 %. Additonal studies identified an optimal graphite for blending with the alloy in electrode preparation which also had a positive effect on cyclign of X % relative to the prior graphite.

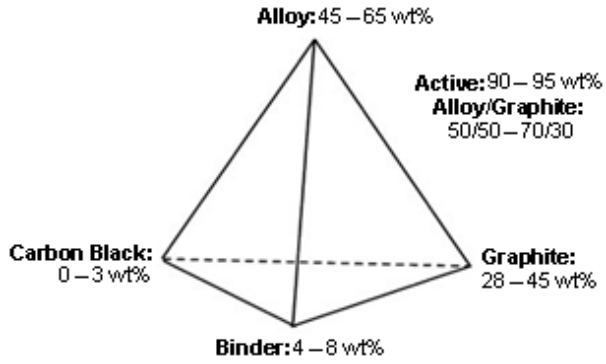

Figure III- 42: Range of statistically-optimal mixture designed experiment for electrode formulation.

An important discovery, that retention is greatly increased with improved dispersion of the graphite and alloy in the electrode, was made using image analysis. Figure III- 43 shows qualitatively how the dispersion is improved progressively by sonicating the slurry and by replacing 30wt% of the water in the slurry with isopropyl alcohol (IPA). Table III- 22 shows quantitatively the degree of improvement. The fraction gives percent of the area that is black, which should be constant for equivalent formulations, regardless of the dispersion quality. The count of the particles increases with greater dispersion. The average, standard deviation, and maximum of the particle area and all decrease with greater dispersion.

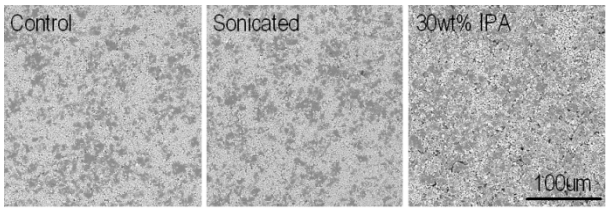

Figure III- 43: Plan-view SEM images showing the drastic improvement in dispersion from replacing 30wt% of the liquids in the slurry with IPA.

Table III- 22: Improved dispersion quantities from sonication and IPA.

	Fraction [%]	Ave. [µm²]	Std. Dev. [µm²]	Max. [µm²]
Control	32.6	27.0	147	3504
Sonicated	31.5	24.2	128	3484
IPA	32.4	28.7	92	1160

Subtask 8 - Cathode Composite Development. A first set of 18650's have been made using 3M BC-618. 3M has made significant progress developing several other advanced cathode materials in the last year. Some of these will be selected to provide an improved 18650 in the next two quarters.

Subtask 9 - Electrolyte Development. The goal of this task is to further reduce capacity fade, continuous volume expansion, and SEI growth (which are synonymous). To address the issues of this task more effectively, focus has shifted to developing a new class of anode materials. These new materials contain one or more XRD-amorphous or nanoscopic phases that are components of each particle. The process used to make these uses the same approach as L-20772, and is therefore also expected to be manufacturable at large-scale at a similar low-cost. Work in this area is early on, and will be the primary focus of the next phase of this project. A full compositional design space remains to be screened, however, preliminary results indicate the compositions of interests have the ability to match the capacity retention of graphite cells as measured by accelerated testing, and an approach has been devised to reduce the irreversible capacity to levels at or below that of L-20772 while maintaining overall capacity. We believe that these materials could significantly improve the performance of alloy materials for PHEV applications.

FY 2010 Publications/Presentations

2010 DOE Annual Peer Review Meeting Presentation

III.B.5 Stabilized Li Metal Powder (FMC)

Christopher Johnson (NETL Project Manager)
Subcontractor: FMC Corporation

Marina Yakovleva
FMC Corporation, Lithium Division
Seven LakePointe Plaza
2801 Yorkmont Road, Suite 300
Charlotte, NC 28208
Tel: 704-868-0891, Fax: 704-868-5496
E-mail: Marina.Yakovleva@fmc.com

Start Date: May 1, 2009
Projected End Date: April 30, 2012

Objectives

- Objective 1: Develop a process and prototype unit for the commercial production of dry stabilized lithium metal powder (SLMP).
- Objective 2: Develop a process and design commercial unit to scale-up the production of SLMP dispersion.
- Objective 3: Explore the use of alternative pilot scale unit to produce dry SLMP powder directly from battery-quality lithium metal.
- Objective 4: Integrate SLMP Technology into the Li-ion cell for PHEV application.

Technical Barriers

This project addresses the following technical barriers from the Financial Assistance Funding opportunity Announcement, U. S. Department of Energy

National Energy Technology Laboratory, FY 08 Vehicle Technologies Program, Wide FOA, Funding Opportunity Number: DE-PS26-08NT01045-00, CFDA Number: 81.087 Renewable Energy Research and Development.

(A) Develop PHEV Technologies capable of 40 mile electric range

(B) Substantial petroleum displacement

(C) Improved air quality

Technical Targets

- Make available commercial quantities of SLMP, an independent source of lithium that will enable higher energy, safer, environmentally friendlier and lower cost lithium batteries.
- Expedite the development of cost-effective manufacturing processes for SLMP to support high volume production of Li-ion batteries.
- Evaluate, design and acquire pilot-scale unit for alternative production technology to further decrease the cost of production by cutting the number of process steps and increasing the volume of production by using a continuous process.
- Develop process technology for the integration of Stabilized Lithium Metal Powder into Li-ion battery systems and demonstrate the benefits relative to a state-of-the-art baseline.

Accomplishments (10/01/09-09/30/10)

- The Prototype Unit for Dry Powder Production has been installed and commissioned. An experimental program explored the effects of the key process variables. An optimized production scheme was determined.
- The commercial-scale unit for production of lithium dispersion was designed, installed and commissioned. The initial SLMP dispersion batches from this scaled-up process produced a smaller particle size product than the pilot-scale system could at the same conditions.
- The engineering design has been completed for the alternative pilot-scale unit to produce dry SLMP directly from battery-quality lithium metal.
- Demonstration of the benefits of the SLMP Technology using graphite/$LiMn_2O_4$ system has been completed and work is in progress for the hard carbon/ $LiMn_2O_4$ system. Significant progress was achieved in developing application technique to implement SLMP Technology into manufacturing of Li-ion batteries using micro-gravure method.

✧ ✧ ✧ ✧ ✧

Introduction

Achieving the DOE technical and cost targets for the HEV/PHEV batteries will require development and use of the new electrode materials. SLMP Technology provides an independent source of lithium for Li-ion systems breaking the current limitation that all lithium has to come from the cathode and, thus, allowing the use of non-lithium providing cathode materials with potentially larger capacities. These new cathode materials are expected to be

more overcharge tolerant and could be used with high capacity advanced anodes with high irreversible capacities.

Approach

It is very difficult to satisfy safety, cost and performance requirements for the PHEV and EV applications. As the initial step in SLMP Technology introduction, industry can use commercially available $LiMn_2O_4$ or $LiFePO_4$, for example, that are the only proven safer and cheaper lithium providing cathodes available on the market. Unfortunately, these cathodes alone are inferior to the energy density of the conventional $LiCoO_2$ cathode and, even when paired with the advanced anode materials, such as silicon composite material, the resulting cell will still not meet the energy density requirements. However if SLMP Technology is used to compensate for the irreversible capacity in the anode, the efficiency of the cathode utilization will be improved.

Based on the current trend of oil prices, we believe the demand for PHEVs will be ahead of the technology development. In other words, the launch of PHEVs will be mainly limited by the technology development cycle, which will likely require another 5 years. The main hurdle is still safety, followed by cost and calendar life. To satisfy the critical national need of reducing our dependence on imported oil, it is critical to develop and validate revolutionary technologies, such as SLMP Technology, and to establish the manufacturing base for the production of the advanced battery materials to meet the nation's needs.

Results

The processes to produce SLMP have been scaled-up. The vendor fabricated and delivered our Prototype Unit for Dry Powder Production. This unit was installed and commissioned as per schedule. Following an extensive experimental study and with the assistance of mathematical modeling, the optimized production schemes have been determined. The commercial-scale unit for producing SLMP dispersions was designed, fabricated and delivered. This unit has been installed and commissioned.

Lithium metal is a flammable solid that reacts violently with moisture to create flammable hydrogen and corrosive lithium hydroxides. Molten lithium is especially reactive and given that its auto ignition point is essentially the same as its melting point, it can spontaneously ignite in air. The reactivity of lithium increases with temperature and surface area. Therefore, molten metals or dispersions require special care in handling. The special coating on SLMP that provides stability for handling in a dry room will increase the safety of handling these high surface area particles but SLMP is still 98% lithium so care must be taken. Therefore, a significant effort was made during the design and installation of the scaled-up equipment to ensure that the safety requirements would be met.

Five variables were identified to investigate during the filtration and washing experiments. Over fifty experiments were completed to study the filtration, washing and drying steps used to produce dry SLMP from dispersion in mineral oil.

The optimization of the process to make dry SLMP is based on the cost of production so it is not readily determined experimentally. A mathematical model was developed based on the experimental results to predict the washing conditions required to meet the desired SLMP quality and to estimate the equipment and labor times required. The total cost of each SLMP production scheme was calculated from the raw materials used, labor required and waste generated. Two different optimized schemes to filter, wash and dry SLMP were identified based on different SLMP production rates. Potential process improvements for cost savings were proposed.

Screening experiments suggest that the commercial-scale SLMP dispersion system produces SLMP that is comparable to or even better than in terms of particle size distribution material produced in the pilot-scale unit. The experimental design for the commercial-scale SLMP dispersion system is nearly complete. The previous results from the pilot-scale runs were analyzed and the statistically significant variables were determined.

A pilot-scale unit to produce dry SLMP powder directly from battery-quality lithium metal was purchased. We have customized the design of the electrical components to meet the higher rating required for equipment that operates in areas with the potential for flammable atmospheres. The vessels have been fabricated and assembly of the system has begun.

We have completed coating trials using the micro-gravure method to apply SLMP to a substrate. SLMP slurry was coated onto the substrate using a Yasui coater. Very uniform coated film has been produced. The loading of SLMP on the film is $0.25 mg/cm^2$. In order to be able to coat in a range below and above the level achieved in conducted trials, modifications to the coater will be required. Efforts are underway to address the issues identified and to find alternative solutions. Figure III- 44 below shows the Yasui coater that was set up to use the micro-gravure method to apply SLMP onto a substrate and Figure III- 45(a) shows a picture of the substrate with SLMP applied onto it. Figure III- 45(b) shows a picture of the electrode to which SLMP was transferred: the uniformity of the SLMP distribution was preserved.

Figure III- 44: Yasui coater set up to use the micro-gravure method to apply SLMP onto a substrate.

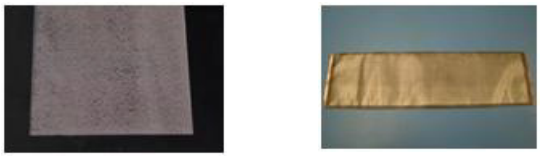

Figure III- 45: (a) SLMP coated onto a substrate using micro-gravure method. (b) Prefabricated anode sheet with SLMP transferred onto it.

The effect of SLMP on the performance of MCMB/$LiMn_2O_4$ system was evaluated. The spinel electrode formulation used was $LiMn_2O_4$ (90%) + carbon black (5%) + PVdF (5%); the graphite anode formulation was MCMB-25-28 (90%) + carbon black (3%) + PVdF (7%). The surface application technique was used to apply SLMP in p-xylene slurry onto the prefabricated anode sheets. The MCMB electrodes were calendered at 200 lbs/cm^2. The MCMB/$LiMn_2O_4$ pouch cells were assembled and 1M $LiPF_6$/EC+DEC (1:1) from Ferro Corporation was used as the electrolyte. The cells were pre-conditioned at room temperature for 5 hours and then cycled using the following test protocol: constant current charge at 0.25 mA/cm^2 to 4.3 V, constant voltage charge at 4.3 V for 7 hours; constant current discharge at 0.25 mA/cm^2 to 3.0 V.

Figure III- 46(a) shows the improvement in the cell's irreversible capacity due to SLMP incorporation. The 1st cycle coulumbic efficiency for the baseline cell is about 82%. In comparison, the 1st cycle coulumbic efficiency for the SLMP-incorporated cell is about 91%. The irreversible capacity significantly decreases as a result of the SLMP incorporation.

Figure III- 46(b) shows the effect of SLMP on the pouch cell cycle performance; the capacity was normalized based on the 1st charge capacity. The SLMP-incorporated cell showed improved cyclability: after fifty cycles, the baseline cell has lost 14.3% of the first discharge capacity while the SLMP-incorporated cell has lost only 1.3%.

We have initiated work to demonstrate benefits of the SLMP Technology on hard carbon/$LiMn_2O_4$ system. Hard carbon/$LiMn_2O_4$ pouch cells were assembled using machine-coated electrodes. The pouch cell size was 7 cm × 7 cm. The cathode electrode formulation was $LiMn_2O_4$ (90%) + carbon black (5%) + PVdF (5%) and the anode formulation was Carbotron P S(F) (90%) + carbon black (3%) + PVdF (7%). 1M $LiPF_6$ /EC+DEC (1:1) from Novolyte Corporation was used as the electrolyte. The cells were pre-conditioned for 5 hours and then cycled using the following test protocol: constant current charge at 0.25 mA/cm^2 to 4.3 V, constant voltage charge at 4.3 V for about 7 hours; constant current discharge at 0.25 mA/cm^2 to 3.0 V.

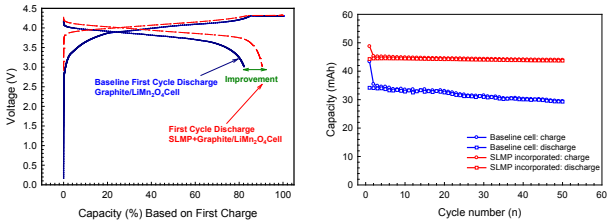

Figure III- 46: (a) Effect of SLMP on irreversible capacity improvement for MCMB/$LiMn_2O_4$ system. (b) Effect of SLMP on the cycle performance of MCMB/$LiMn_2O_4$ system.

Figure III- 47 shows the effect of SLMP on the cell's deliverable capacity. In the 1st charge process, both cells have similar capacity: ~68 mAh. However, the coulombic efficiency has been significantly improved (about 50%) by incorporating SLMP: the 1st cycle coulombic efficiency for the baseline cell is about 61% vs. about 92% for the SLMP–incorporated cell. The irreversible capacity decreases significantly as a result of SLMP incorporation. SLMP Technology clearly shows more value for the materials with high reversible and high irreversible capacities.

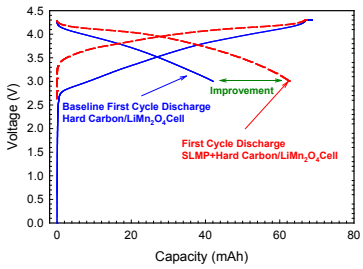

Figure III- 47: Effect of SLMP on delivered capacity for hard carbon/$LiMn_2O_4$ system.

Conclusions and Future Directions

We have completed all the tasks scheduled for the past 12 months of this project.

We have designed and purchased a prototype unit for the commercial production of dry stabilized lithium metal powder (SLMP). We completed an extensive set of experiments from which we developed an optimized process for producing SLMP at different rates. More importantly, we identified a couple process modifications

with the potential to save costs which should be examined in the future.

We have designed, purchased, installed and commissioned a commercial-scale unit for the production of SLMP dispersion. The experimental program for making SLMP dispersions in the new commercial-scale unit is being designed and it will be completed during the upcoming year. The results will be analyzed statistically and the optimum dispersion conditions determined.

We are expecting the delivery of the pilot-scale unit for dry SLMP production directly from battery-quality lithium metal in late 2010, followed by installation and commissioning of the unit in January 2011. We will then explore this alternative technology for SLMP production according to the proposed plan.

We have successfully demonstrated benefits of the SLMP Technology using graphite/spinel and hard carbon/spinel systems. We will continue our efforts towards developing application processes to enable commercialization of the SLMP Technology as well as demonstration of the benefits of this technology using advanced battery materials.

FY 2010 Publications/Presentations

1. Marina Yakovleva, Yangxing Li, Brian Fitch, Chris Woltermann, and Y. Gao, “Stabilized Lithium Metal Powder (SLMP®) – Material and Application Technologies for High Energy Li-ion Batteries,” IBA/PPSS Meeting, January 2010 (invited talk)
2. Brian Fitch, Yangxing Li, Marina Yakovleva, and Yuan Gao, “Stabilized Lithium Metal Powder (SLMP®) as a Performance Enhancer for Graphite/$LiMn_2O_4$”, the 217th ECS Meeting, April 2010
3. Yangxing Li, Brian Fitch, Marina Yakovleva, and Y. Gao, "SLMP® and LMCF: A Solution to the Lithium-Ion Battery Challenges of the Future", 15th International Meeting on Lithium Batteries in Montreal, Canada, June 2010, Abstract Number # 765
4. Marina Yakovleva, Yangxing Li, Brian Fitch, Scott Petit, Terry Arnold, Prakash Palepu, Mike Barr, Yuan Gao, and Christopher Woltermann “SLMP®, Enabling Material and Revolutionary Technology for High Energy Li-ion Batteries,” DOE AMR 2010, Abstract EC011.
5. Yangxing Li, Brian Fitch and Marina Yakovleva “SLMP®—Its Capacity and Incorporation into Carbonaceous Materials”, the 218th ECS Meeting, October 2010, Abstract #1090.

III.B.6 Develop and Improve Lithium Sulfur Cells for EV Applications (Sion Power)

Adrienne Riggi (NETL Project Manager)
Subcontractor: Sion Power

Yuriy Mikhaylik (Project Manager)
Sion Power Corporation
2900 East Elvira Rd
Tucson, AZ 85756
Phone: (520) 799-7609; Fax: (520) 799-7501
E-mail: ymikhaylik@sionpower.com

Start Date: October 1, 2009
Projected End Date: September 30, 2012

Objectives

- Phase 1 Applied Research. Develop metallic lithium anode stabilized with dual-phase electrolyte system and demonstrate whole anode electrode specific capacity exceeding 650 mAh/g over 50 full charge-discharge cycles in the laboratory scale Li-S cells.
- Phase 2 Technology Development. Develop large format prototype Li-S cells with lithium anode stabilized with dual-electrolyte system and demonstration of higher energy >350 Wh/kg and longer cycle life at USABC test conditions.
- Phase 3 Technology Validation. Large format production cells manufacturing, full scale USABC test performance evaluation and abuse tolerance test and improvement demonstration by making the cell more thermally stable – increasing the runaway temperature to >165°C.

Technical Barriers

This project addresses the following technical barriers:

(A) Materials for dual-phase electrolyte sufficiently inhibiting detrimental side reactions on the Li anode

(B) Gel-polymer coating for dual-phase electrolyte compatible with high speed production.

(C) Hardware for dual-phase electrolyte components coating.

(D) Hardware for dual-phase electrolyte experimental and large format prototype cells manufacturing and test.

Technical Targets

- Optimization of Dual-Phase System Constructs
- Selection of Method to Create a Dual-Phase System in the Cell
- Dual-Phase Electrolyte Formulation and Mass Balance Optimization
- Laboratory Scale Cells Design, Manufacturing and Test: Demonstration of Anode Unit Specific Capacity to exceed 650 mAh/g and achieving over 50 full charge/discharge cycles.
- Gel Polymer Mixing/Coating Hardware System Development
- Large Format Cell Design, Optimization and Cell Manufacturing
- Large Format Production Cell Manufacturing, Test & Evaluation- full scale USABC test performance evaluation and abuse tolerance test

Accomplishments

- We have accomplished and exceeded objectives for the Phase 1 project:
  - Twice longer vs. targeted cycle life demonstrated for Li anode unit with dual phase electrolyte.
  - Twice bigger vs. targeted specific capacity demonstrated for anode unit with dual phase electrolyte.
  - Protection of Li anode with dual phase electrolyte eliminated thermal runaway for half of the laboratory 0.25 Ah rechargeable Li-S cells.
- Modeling of large format 2.5 Ah Li-S accomplished: optimal electrodes sizes, metalized substrates thickness and active cathode and anode materials loading selected.
- Large scale Gel Polymer Mixing/Coating Hardware System has developed and produced gel-polymer coated anodes.

✧ ✧ ✧ ✧ ✧

Introduction

Achieving the DOE cell performance targets for electric vehicle application will require improved Li anode chemical stability (safety), cycle-ability and capacity. It also requires higher cell-level specific energy and ability to be manufactured at high volume.

Approach

To meet the DOE targets SION Power is developing a unique electrolyte providing two liquid phases having good Li+ conductivity, self-partitioning and immiscibility, serving separately the cathode and anode electrodes. Self-partitioning multi-phase electrolyte will enable us to tailor electrolyte composition at each electrode to provide the optimum chemical stability.

This innovative approach was applied to develop stabilized high energy metallic lithium anode. While this approach could be generally applied to any Li metal or Li Ion rechargeable cell, SION Power uses a Lithium-Sulfur rechargeable battery system to apply two liquid phases concept.

Requirements for "Anode" and "Cathode" phases of dual phase electrolyte working in the Li-S cell are below.

"Anode" Liquid 1:

- Immobilized within polymeric gel applied to anode.
- Stable with lithium preventing side reactions and dendrite growth.
- Immiscible with Phase 2 electrolyte and does not dissolve polysulfides.
- Polymeric gel can serve as coated separator.

"Cathode" Liquid 2:

- Tailored to improve high energy Sion Power sulfur cathode performance.
- Immiscible with Phase 1 electrolyte.
- High ion conductivity

Results

Materials for dual-phase electrolytes. The main components of dual-phase electrolyte system are solvents with self-partitioning or immiscibility and gel-polymers to immobilize immiscible anode solvent. We have identified over 10 solvents exhibiting desired properties. We also identified several polymers forming gel-electrolytes with ionic conductivity exceeding $3*10^{-4}$ S/cm. These polymers are web-coating compatible and can be formed during monomers polymerization on the anode surface or can be coated from polymer solution.

Dual phase electrolyte optimization included lithium salt concentration optimization as well as polysulfide repelling solvent concentration optimization. Li salt and polysulfide repelling solvent amounts have been balanced to achieve formation of two immiscible electrolytes when the first minimal polysulfides concentrations were generated in the cell. The polysulfide repelling solvents also have been screened to provide acceptable ionic conductivity in the presence of lithium salt. The dual phase electrolyte optimization process resulted in two formulations containing low and high viscosity polysulfide repelling solvents: ethylal and butyl ether. We have found also that butyl ether formed immiscible liquids at lower polysulfide concentrations compared with ethylal. Higher viscosity butyl ether had the lowest polysulfide solubility but lower ionic conductivity as well. Both electrolyte formulations were tested in the experimental Li/S cells.

Experimental cells test. Gel-polymer coated anodes have been combined with sulfur cathodes in the experimental 250 mAh cells filled with electrolyte forming two immiscible liquid phases at presence of polysulfides.

250 mAh cells with butyl ether containing electrolyte formulation demonstrated high Li anode specific capacity above 1,000 mAh/g over 100 cycles thus exceeding Phase 1 objective. Li anode cycling performance is shown in Figure III- 48.

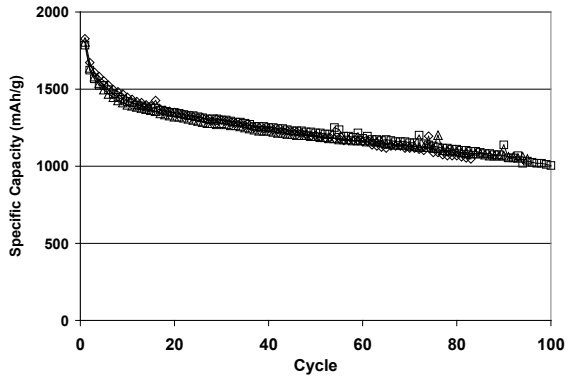

Figure III- 48: Li anode cycling behavior in 250 mAh experimental cells

Gel-polymer anode coating also substantially improved small experimental Li-S cells thermal stability with runaway temperature exceeding 165°C. Thermal behavior of 250 mAh Li-S laboratory cells is shown in Figure III- 49. The cells presented in Figure 2 have been tested at 100% state of charge after 10 full charge-discharge cycles. Cells without dual phase electrolyte protection experienced thermal runaway at the lithium melting point (181°C). Half of the cells protected with the dual phase electrolyte system did not experience significant thermal events above the lithium melting

point and up to 240°C. Example of the thermal behavior of such cells is shown in Figure 2 Another half of cells with dual phase electrolyte experienced a reduced form of runaway. All these data suggest that thermal runaway can be mitigated in the Li-S rechargeable battery.

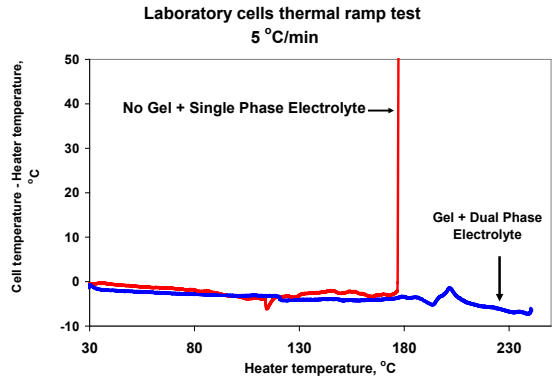

Figure III- 49: Thermal behavior of Li-S laboratory cells with and without the dual phase electrolyte system.

Gel Polymer Mixing/Coating Hardware System Development Gel-polymer mixing hardware system was upgraded and allowed producing up 4 gallons of polymer/monomer mixture. Polymer mixing/coating optimization resulted also in much smoother coating than previously anticipated. The key factor affecting coating smoothness was method of dispersing silica filler in the polymer coating slurry. Arithmetic average roughness of gel-polymer films was reduced to 0.05 µm.

Gel-polymers films were coated with Sion Power pilot gel-coater at web speed 1-1.5 m/min. Two coating techniques have been explored: gravure coating and slot die coating. Both techniques produced very uniform smooth films. Solution delivery systems worked satisfactory for both techniques.

Better gel-polymer film uniformity or smoothness played a substantial role in protection of Li anode with dual phase electrolyte. Starting with uniform dry polymer films formed higher quality and defect free gel electrolytes after swelling in the liquid electrolyte media. It also led to better current distribution over the Li anode surface.

Large Format Cell Design, Optimization and Cell Manufacturing. Modeling of large format 2.5 Ah Li-S components was accomplished: optimal electrodes sizes, metalized substrates thickness and active cathode and anode materials loading selected. Analysis of current distribution uniformity on resistive substrate at Li-S cell environment lead to selection of optimal electrodes sizes of ~10 x10 cm. Electrodes stack design and manufacturing of 2.5 Ah cells with optimized electrodes are in progress.

Conclusions and Future Directions

We have accomplished and exceeded objectives for the Phase 1 project:

- Twice longer vs. targeted cycle life demonstrated for Li anode unit with dual phase electrolyte.
- Protection of Li anode with dual phase electrolyte substantially increased Li-S cells thermal stability.

Viability of dual phase electrolyte approach has been successfully demonstrated for the Li-S system for laboratory scale cells. Materials selected, new hardware and coating techniques developed, optimal electrodes sizes modeling and selection paved the way for designing and manufacturing of 2.5 Ah dual phase electrolyte protected cells.

Future steps include:

- Finalizing of 2.5 Ah cell design.
- Production of optimal size coated cathodes and gel-polymer coated anodes.
- Adjusting of supporting tooling for assembling of 2.5 Ah cells.
- 2.5 Ah cells experimental samples manufacturing.
- Cells electrolyte and electrodes mass balance optimizations.
- 2.5 Ah cells performance evaluations under USABC test conditions.

III.B.7 High Volume, Low-cost Manufacturing Techniques for Cathode Materials (BASF)

Christopher Johnson (NETL Project Manager)
Subcontractor: BASF

Anthony M Thurston (Project Manager)
BASF Catalysts, LLC
23800 Mercantile Road
Beachwood, OH 44122
Tel: 216-360-5043; Fax: 216-464-5780
E-mail: anthony.thurston@basf.com

Subcontractor:
Farasis Energy, Hayward CA

Start Date: September 15, 2009
Projected End Date: February 25, 2012

Objectives

- Successfully produce two low cost cathode materials, suitable for PHEV application.
- Validate that quality targets are achieved through cell testing and battery pack testing
- Work closely with a Tier 1 auto supplier and/or automotive OEM.

Technical Barriers

This project addresses the following objectives of the Vehicle Technology Program for Renewable Energy Research and Development

(A) Development of LIB cathode materials for PHEV application

(B) Scale up of manufacturing process for LIB cathode material

(C) Reduction of production costs

(D) Achieve USABC target and quality requirements

Technical Targets

- Synthesis of NMC in semi-batch laboratory scale process
- Production of NMC at the Pilot Plant level to fully address scalability issues
- Production Trials for NMC at a Production Plant level to validate process, quality and cost targets are achieved.
- Development of a secondary LIB cathode material through the Pilot Plant level

Accomplishments

- Increased Electrochemical Applications testing capability and capacity by addition of new equipment.
- Successful testing of samples at both coin cell and pouch cell levels.
- Successful synthesis of NMC at the laboratory level that meets currently available NMC material targets for quality and performance.
- Evaluation of various process parameters to reduce processing time and production costs while maintaining a consistent and acceptable product quality and performance
- Demonstrated reproducible production of quality cathode material at a full Pilot Plant scale capacity with quality equal to Lab produced samples.
- Increased customer sampling program from small kilogram samples to several hundred kilograms samples.

✧ ✧ ✧ ✧ ✧

Introduction

The production of low cost cathode materials is dependent upon the proper selection of raw materials coupled with a cost effective production process. This alone is however not enough; there are also many specific requirements for chemical purity, physical characteristics and electrochemical performance that must be achieved and can not be sacrificed. The optimum cathode composition would be one that is low in Cobalt and high in Manganese due to the cost difference between these two metals, it would use readily available lithium compounds and most importantly – Deliver the Target Performance for successful launch into the Electric Vehicle Program.

Approach

To meet the USABC targets BASF will use a systematic approach in the development and scale up for the production of cathode materials using its background and knowledge of materials chemistry and expertise.

The effort will be focused on minimizing or eliminating expensive starting materials and the incorporation of low cost processing steps that do not require exotic conditions such as high pressure, expensive solvents, or aggressive processing steps.

Results

With NCM based cathode materials one of the best ways to reduce the cost of the cathode material is to minimize the Cobalt and Nickel percentage in the target material. This is not simple because of the requirements of the customer may not be fully met by simply adjusting the formula. Table III- 23 demonstrates a potential cost savings by simply adjusting the composition. The values are based on the assumption that the process for all compositions would remain constant. The reality is that adjusting the composition requires changes from the selection of raw materials to equipment and process modifications that can easily offset any theoretical savings. NCM 111 is used a base price and NCM 622 and NCM 226 are shown as extremes in formulation.

Table III- 23: Theoretical Cost Analysis for NCM Compositions

	NCM 111	NCM 523	NCM 424	NCM 622	NCM 226
% Ni	21.3%	32.0%	25.7%	38.3%	12.97%
% Co	21.4%	12.9%	12.9%	12.8%	13.02%
% Mn	19.9%	18.0%	24.1%	11.9%	36.42%
Raw Material Cost	-	-12%	-18%	-7%	-28%

Cost based on 07/10 Metals Market Price

To date BASF has been able to consistently produce NCM 111 cathode materials at the pilot plant scale that meet or exceed current specifications (Figure III- 50) and has supplied several prominent LIB automotive cell producers with multiple samples of increasing size which are currently being evaluated and qualified. BASF's work to expand its NMC product line has shifted much of the work to the development of NCM 523 and NCM 424. Results from the initial Design of Experiments program have been utilized to identify the major key elements that are critical for the end product performance as well as identifying independent variables.

Work with NCM 523 and NCM 424 has progressed to the pilot plant stage. BASF has demonstrated that with its existing equipment it can successfully produce the NCM 523 consistently with minimal lot variation (Figure III- 51). However, the process modifications necessary to achieve high quality NCM 424 consistently have not been fully completed and additional work is required (Figure III- 52). BASF will focus on precursor improvements and calcination profile modifications in order to improve the reproducibility of the NCM 424. It is important to note that the advantage of moving away from NCM 111 has to be based on electrochemical performance enhancements and not only on theoretical savings because process modifications can offset the theoretical raw material cost savings.

Conclusions and Future Directions

Future work will be devoted to refining the critical process parameters for NCM 424 and further enhancements for NCM 523 in an effort to reduce processing time and processing steps while maintaining total product quality and reproducibility.

Further cost reduction by lowering the cobalt and nickel content is anticipated to be evaluated in the lab with transfer to the pilot scale in the coming year.

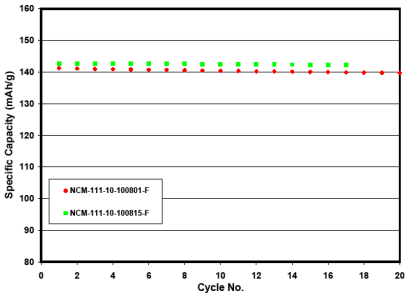

Figure III- 50: BASF NCM 111 Lot Comparisons

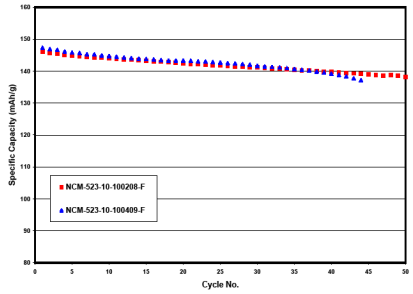

Figure III- 51: BASF NCM 523 Lot Comparisons

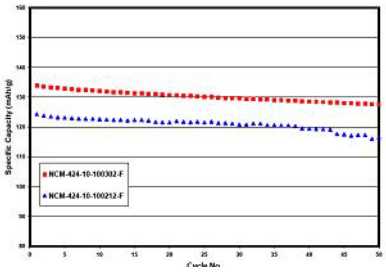

Figure III- 52: BASF NCM 424 Lot Comparisons

III.B.8 Hybrid Nano Carbon Fiber/Graphene Platelet-Based High-Capacity Anodes for Lithium-ion (Angstron)

Bruce W. Mixer (NETL Project Manager)
Subcontractor: Angstrom Materials

Aruna Zhamu (Principal Investigator)
C.G.Liu, James D. Hodge
Angstron Materials, Inc
1240 McCook Avenue
Dayton, OH 45404-1059
Phone: (937)331-9881
E-mail: Aruna.Zhamu@Angstronmaterials.com

Objective

- To develop and commercialize a Si-coated NGP/CNF anode technology that will speed the development and deployment of advanced lithium-ion batteries for plug-in hybrid (PHEVs) and other types of electric vehicles.

Approach

- To determine optimized Si-coated NGP/CNF blends that exhibit the best performance/cost ratios.
- To develop a process for cost-effective production of these compositions.

Accomplishments

- Developed a process for preparing carbon nano-fibers by a low-cost electro-spinning method (ES-CNFs, as opposed to vapor-grown CNFs).
- Installed a lab-scale CVD system for Si deposition. A uniform Si coating has been successfully deposited on the anode electrode directly. Designed a larger lab-scale CVD system for cost-efficient production of Si coated NGP anode materials.
- Characterized the morphology, crystal structure, and chemical composition of Si coating by using SEM, XRD and EDS.
- Developed a lamination process of making anode electrodes, which can be highly advantageous as compared with the conventional coating process. A graphene based conductive adhesive has been developed for making the anode.
- Continued to evaluate the cycle stability of the developed anodes by using button shape half-cells.

The life cycle test has been achieved for >45 cycles (cycle test continuing). After 45 cycles, the specific capacity is still over 1,100 mAh/g with over 98% columbic efficiency. A high efficiency is important for the good cycling life.

Introduction

The intent of this DOE project is to develop a new anode technology that will speed the development and deployment of advanced Lithium-ion batteries for plug-in hybrid electric vehicles (PHEVs). The proposed work will also commercially exploit a dramatic improvement in Li-ion battery technology, having the power to extend the mileage range of hybrid electric vehicles (HEVs) and all electric vehicles (EVs) to a range competitive to current internal combustion engines. In addition, this new anode technology will further enhance the acceptance of Li-ion batteries for electric vehicle use by dramatically improving charge/discharge rates by reducing the internal heat build up and limiting Li-ion diffusion paths to nanometer scales.

Approach

The key to this new technology is the ability to capture the highest charge capacity allowed with silicon over extended charge/discharge life, using highly conductive yet inexpensive nano graphene platelets (NGPs) and/or carbon nano-fibers (CNFs). The approach of coating Si nano particles with conductive CNF web developed by researchers at Angstron Materials and Nanotek Instruments, includes: (1) Optimization of Si-supporting CNF-NGP blend compositions; (2) Development and optimization of processes for mass-producing Si-coated CNF-NGP blends; and (3) Performance evaluation of Li-ion batteries featuring this new anode technology.

Results

Preparation of electrically conductive mats. A conductive nano-fiber mat, coated with Si, is used to support active materials (Si) in the electrode structure. Carbon nanotubes (CNTs) and vapor-grown carbon nanofibers (VG-CNFs) are superior materials for building highly conductive network structures. However, the high costs of CNTs and VG-CNFs have severely limited their

application for lithium-ion battery electrodes. Electro-spinning is herein investigated as an alternative way to produce carbon nano-fibers from precursor polymer solutions. Currently, there are several commercially available, large-scale electro-spinning systems that are capable of mass-producing electro-spun fibers at low costs. The proposed approach is scalable and highly suitable for the production of lithium-ion battery anode materials.

As shown in Figure III- 53, a custom-made electro-spinning system has been built for this project at Angstron. This electro-spinning system is based on a needle-less, multi-channel technique capable of producing polymer nano-fibers at a high rate. With the current rotating sample collecting apparatus, nanofiber mat with over 12"x24" can be readily prepared. Two large format PAN nanofiber mat samples are shown in Figure III- 54.

Figure III- 53: A custom-designed lab-scale electro-spinning equipment

Figure III- 54: Large-format PAN nanofiber mat prepared by the new electrospinning machine

Herein we have demonstrated that several polymers can be used as carbon precursors to prepare carbon nanofibers. We have been able to prepare both highly aligned carbon fibers Figure III- 55(a) and randomly arranged carbon nano-fibers Figure III- 55(b). Angstron's graphene can be incorporated into the carbon fibers during the electro-spinning process to increase the strength and electrical conductivity of the mats.

(a)

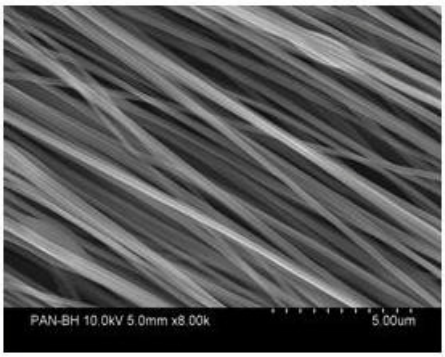

(b)

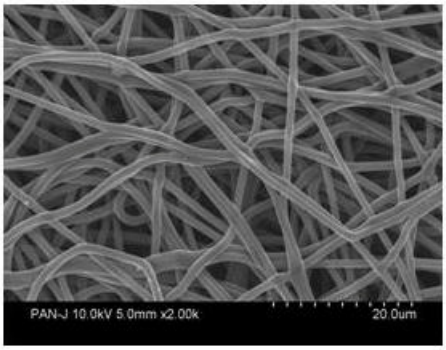

Figure III- 55: (a) Highly aligned carbon nanofibers (b) Randomly arranged carbon nanofibers

Table III- 24 shows the electrical conductivity of this conductive mat produced by Angstron Materials. Compared to the VG-CNFs/CNTs mat prepared by a conventional paper-making process, the electrical conductivity of this new conductive mat is 6.5 times higher, and the density is also higher (0.40g/cm^3, as opposed to 0.25g/cm^3 for VG-CNF/CNT mats).

Table III- 24: Electrical conductivity of electro-spun carbon nano-fibers produced by Angstron

Conductive mat	Conductivity (S/cm)
Highly aligned carbon nanofiber mat	9.15
Randomly arranged carbon nanofiber mat	11.7
CNFs/CNTs mat	1.8

CVD system for Si deposition. The lab-scale CVD Si coating system contains a heating system, a 3-channel gas delivery system with flow rate control, a pressure control module (down to 10-4 Torr), and a safety protection system. This system can achieve a significantly higher deposition rate and a more flexible chamber design, and enables roll-to-roll manufacturing.

In order to guarantee lab safety and environmental control, Angstron has been working with two local industrial gas companies on the procedures and apparatus for safely using siliane. As shown in Figure III- 56, a lab-scale CVD system has been delivered to and installed at Angstron.

Figure III- 56: Lab-scale CVD system for Si-coating process

The original plan was to build a larger scale CVD system to speed up silicon coating process. A four-tube CVD system (Figure III- 57) has been designed and will be installed at Angston.

Figure III- 57: Four-tube CVD system for silicon coating

The above mentioned CVD system, although being able to process larger quantities of samples, has some limitations: 1) with samples (either powder type or fiber type) laid inside the tubes, silicon coating will be more likely occur on the surface where exposed to silane gas. The fibers underneath the skin layers will have less chance to be coated due to the limited diffusivity of silane gas into the sample. A dynamic CVD system is being designed to obtain uniform Si coating across the thickness of the mats.

Composition and microstructure analysis of Si. Figure III- 58 shows the chemical composition of Si coated carbon fiber as analyzed by EDS. The film prepared is pure silicon.

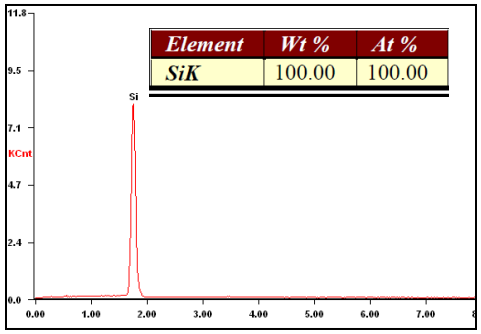

Figure III- 58: The chemical composition of Si coated carbon fiber analyzed by EDS

Figure III- 58(b) is the XRD spectra results of Si coated carbon fiber web, compared with the uncoated substrate as shown in Figure III- 59(a). It can be seen that no obvious crystal structure change was observed. These results indicate that the deposited silicon film is amorphous.

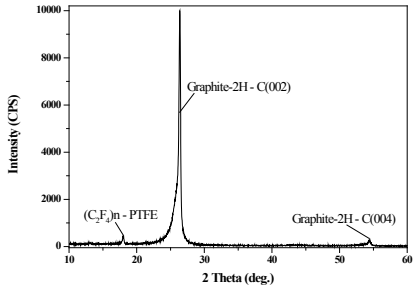

(a)

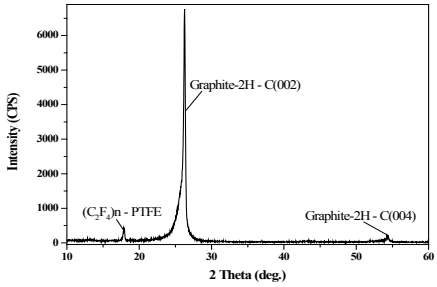

(b)

Figure III- 59: (a) Carbon fiber web (b) Si coated carbon fiber web XRD spectra results

Characterization of the morphology of Si coating. The effects of SiH_4 flow rate, deposition temperature and time on Si morphology and Si particle size were studied. The particle size can be changed from 200 nm to 500 nm

by varying process parameters, such as temperature, gas flow rate and process duration time. Figure III- 60 shows the SEM image of Si particles deposited on surface of ES-CNFs.

The effects of different processing parameters on the morphology of Si coating are summarized in Figure III-61.

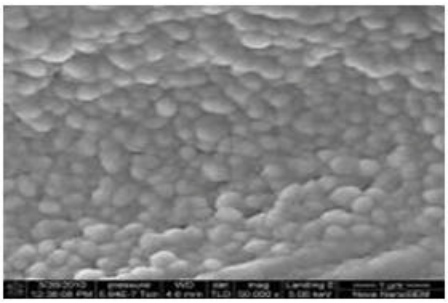

Figure III- 60: The SEM images of Si coating on CNFs

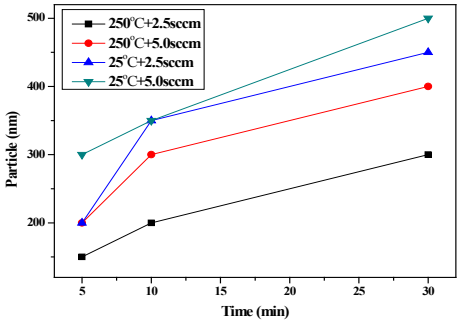

Figure III- 61: Si particle size vs. varied processes

According to the calculated results in our proposal, the thickness of Si coating preferably should be less than 200 nm (further preferably < 100 nm), so that the distance that lithium-ions have to travel is extremely short as compared to current anode materials. The electrodes can quickly store or release lithium and, hence, the battery can be discharged or re-charged rapidly. These are highly beneficial features for a battery that is intended for electric vehicle applications, where a fast discharge rate capability (e.g., during acceleration) is required. In all battery applications, a fast re-charge rate is clearly a highly desirable feature.

Proper process parameters have been identified to deposit Si around the e-spun carbon nano fiber web. Figure III- 62 shows the morphology of Si coated e-spun conductive web. A uniform Si coating with a thickness of about 200 nm was obtained; the results met the technical target which was stated in this DOE proposal.

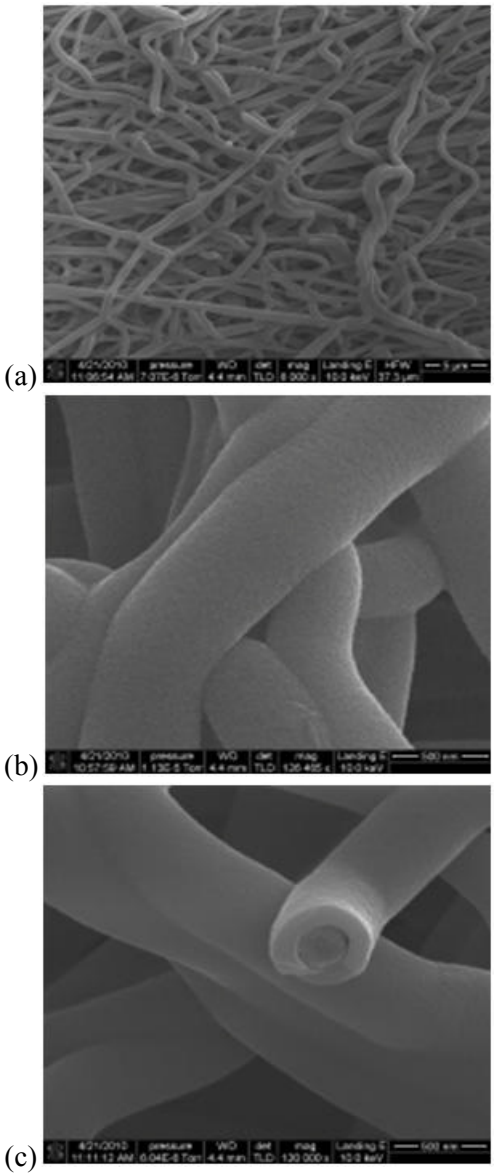

Figure III- 62: The morphology of Si coating (a) 8K X (b) 130K X (c) 120K X

Performance evaluation of small-scale cells. For preparation of button cells, the carbonized NGP/ nanofiber mat was attached onto copper foil current collector with a NGP based conductive ink. As shown in Figure III- 63, the electrode was then cut into desired size for Si coating.

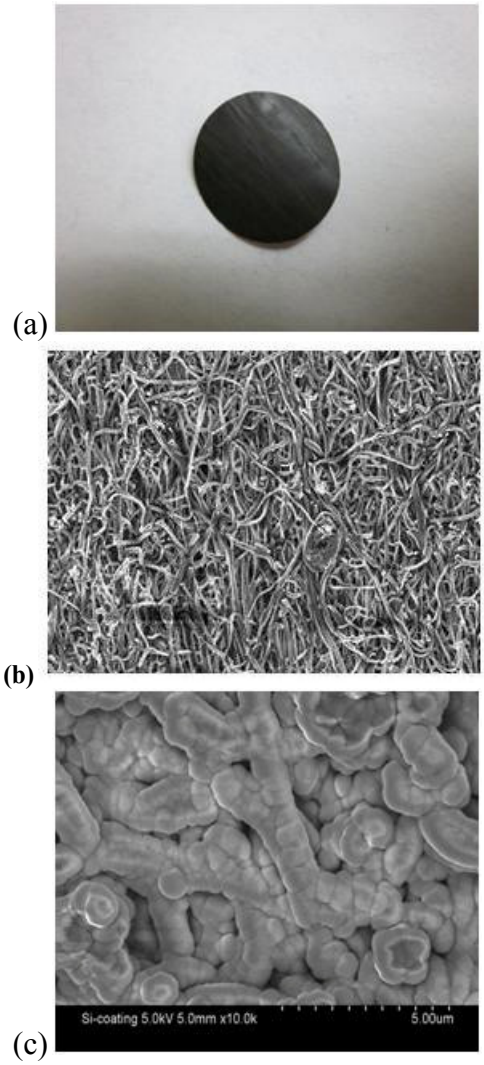

Figure III- 63: The SEM images of the electrode surface (a)The electrode ready for CVD (b) Electrode surface before Si coating (c) Si-coated electrode

For the battery development described in this DOE project, button cells (Figure III- 64) with a half cell configuration were evaluated by using this new Si alloy anode material. The purpose of the preliminary battery test is to evaluate the viability of further mass production.

During the sample preparation process, this web-shaped anode electrode exhibits a good binding behavior with the copper foil collector as compared to the traditional electrode fabrication processes.

As shown in Figure III- 65, good capacity and first cycle efficiency was obtained from the half-cell evaluation results. The specification of this Si-alloy anode and test status are shown as follows:

- Si Loading: < 15 wt%
- Specific surface area: < 2.0 m^2/g
- Tap density: >1.2 g /cm^3
- Charge / Discharge rate: 0.2C

More cycles have been finished on the silicon coated carbon fiber electrode and the result looks good. After 45 cycles, the specific capacity is still over 1,100 mAh/g with over 98% columbic efficiency. A high efficiency is important for the good cycling life.

Figure III- 64: Button cells prepared at Angstron

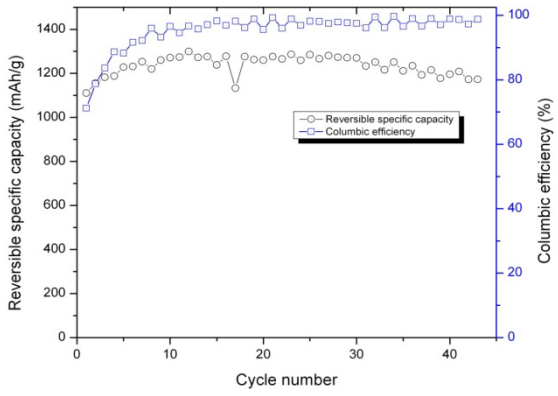

Figure III- 65: Updated half-cell performance of the Si-coated electrode

Commercialization Activities

The early and continued success has motivated us to begin pro-actively engaging in commercialization activities. Examples of these activities are given as follows:

1. We visited Company A (Canada and Taiwan), which is a leader in the EV battery technology, having implemented its Li-ion batteries in 400+ BMW automobiles currently operating in California.
2. Company B (China), a large Li-ion producer in China, will work with Angstron for anode material evaluations.

3. Company C (USA) develops and manufactures rechargeable Li-ion battery systems based on the intrinsically safe cathode material - lithium iron phosphate (LFP). Company C will perform battery anode material evaluation and battery testing, and share this information with us.
4. Company D (USA) is a developer and producer of large-format and layered Li-ion polymer electrolyte batteries, which provide superior safety and reliability.
5. Company E (USA), a strategic customer of Angstron and Nanotek, is interested in assisting us to commercialize the high-capacity anode materials in Li-ion batteries for light EV applications.

Conclusions

A process window to manufacture low-cost and highly electrically conductive supporting substrate for Si coating has been developed. Compared to the CNF/CNT-based conductive mats produced by the conventional paper-making process, the electro-spun fiber mat exhibits significantly higher electrical conductivity and higher density. The electro-spinning process parameters can be easily adjusted to produce nano-fibers of various diameters and nano-fiber mats of various porosity levels to enable uniform deposition of CVD Si as a high-capacity anode active material.

A demonstration sample of the anode electrode has been obtained, and Si has been successfully coated by CVD. The coating particle size is from 50 nm to 500 nm. The properties of this Si coating have been tested: this Si-coated conductive web is composed of up to 60.76 wt% Si element.

The preliminary evaluation of Si-alloy anode materials has been finished. With a Si loading of 15wt%, a good specific capacity and high first cycle efficiency has been obtained from the half-cell evaluation results.

This new anode composition and electrode preparation processes provide a versatile platform technology for producing high-capacity and low-cost anode materials that can be used for next generation EV batteries.

Future Directions

Improve the cost-effectiveness of Si-coating processes. Further optimize the lab-scale electro-spinning system. A nano-fiber web with x-y dimensions of 12’’x12” will be produced by using this system.

FY 2010 Publications

1. Publications
   As required by DOE, we presented a technical paper at DOE Annual Merit Review of the Hydrogen and Vehicle Technology Programs in Washington, DC (June 2010).
2. Web site or other Internet sites that reflect the results of this project.
   www.AngstronMaterials.com has been updated to include information related to this on-going project.
3. Inventions/Patent Applications.
   Aruna Zhamu and Bor Z. Jang, “Anode Compositions for Lithium Secondary Batteries,” US Pat. Appl. No. 12/655,746 (01/07/2010).

III.B.9 New High-Energy Nanofiber Anode Materials (NCSU)

Bruce W. Mixer (NETL Project Manager)
Subcontractor: North Carolina State University

Xiangwu Zhang, Peter S. Fedkiw, Saad A. Khan, Alex Q. Huang (Principal Investigators)
North Carolina State University
Raleigh, NC 27695-8301
Phone: (919) 515-6547; Fax: (919) 515-6532
E-mail: xiangwu_zhang@ncsu.edu

Subcontractor: Jiang Fan, American Lithium Energy Corp, San Marcos, CA 92069

Start Date: September 15, 2009
Projected End Date: August 15, 2012

Objectives

- Use electrospinning technology to integrate dissimilar materials (silicon and carbon) into novel composite nanofiber anodes, which simultaneously have large energy density, high powder capability, reduced cost, and improved abuse tolerance.
- Demonstrate 18650 cells containing high-energy anode materials that achieve specific capacities greater than 1,200 mAh/g and cycle life longer than 5,000 cycles of ~70% state of charge swing with less than 20% capacity fade.

Technical Barriers

This project addresses the following technical barriers on materials and manufacturing technologies of high-energy lithium-ion battery anodes:

(A) Electrode Material Manufacturing

(B) Energy Capabilities

(C) Cost and Life

(D) Abuse Tolerance

Technical Targets

- Phase One: Deliver anodes capable of initial specific capacities of 650 mAh/g and achieving ~50 full charge/discharge cycles in small laboratory scale cells (50 to 100 mAh) at the 1C rate with less than 20 percent capacity fade;
- Phase Two: Assemble, cycle, and evaluate 18650 cells using proposed anode materials, and demonstrate practical and useful cycle life (750 cycles of ~70% state of charge swing with less than 20% capacity fade) with at least twice improvement in the specific capacity than conventional graphite electrodes;
- Phase Three: Deliver 18650 cells containing proposed anode materials, and achieve specific capacities greater than 1200 mAh/g and cycle life longer than 5000 cycles of ~70% state of charge swing with less than 20% capacity fade.

Accomplishments

- Constructed electrospinning devices that are suitable for producing nanofiber anodes.
- Produced silicon/carbon (Si/C) nanofiber anodes by using the electrospinning method.
- Examined the structure of Si/C nanofibers.
- Assembled coin-type cells using Si/C nanofiber anodes and evaluated their performance.
- Assembled 18650 cells and evaluated their performance.

✧ ✧ ✧ ✧ ✧

Introduction

Achieving the DOE anode targets for advanced lithium-ion batteries (LIBs) will require novel material manufacturing technologies that can lead to anodes with large energy density, high power capability, reduced cost, and improved abuse tolerance. In this work, electrospinning technology was used to integrate dissimilar materials (silicon and carbon) into novel composite nanofiber anodes to meet DOE targets.

Approach

Graphite is the most utilized anode material for lithium-ion batteries due to its low and flat working potential, long cycle life, and low cost. However, the most lithium-enriched intercalation compound of graphite only has a stoichiometry of LiC_6, resulting in less-than desirable theoretical charge capacity (370 mAh/g). Silicon can incorporate large amounts of lithium, and hence have high theoretical capacity (4200 mAh/g). The major problem associated with use of Si anodes is the mechanical failure brought about by large-volume changes during lithium insertion/extraction.

We use electrospinning technology (combined with carbonization) to synthesize a novel type of Si/C composite nanofiber anode (Figure III- 66) combining the

advantageous properties of silicon (high storage capacity) and carbon (long cycle life). The nanofiber structure can allow the anode to withstand repeated cycles of expansion and contraction. Si/C composite nanofibers are electronically conductive and can provide high electronic conductivity in electrodes. In addition, composite nanofibers can form a desirable porous electrode structure, thereby leading to fast Li-ion transport. As a result, anodes made of Si/C composite nanofibers can have large energy density, high power capability, reduced cost, and improved abuse tolerance.

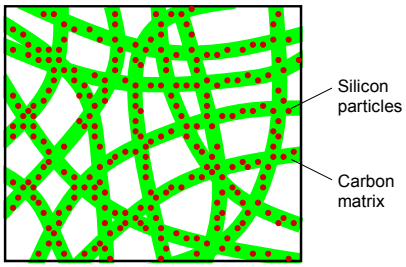

Figure III- 66: Schematic of Composite Nanofiber Anode.

One unique aspect of the project is to utilize a scalable electrospinning approach to fabricate Si/C nanofiber anodes. Compared with most nanotechnologies, electrospinning is a relatively low-cost process, and is being used in many industries. Figure III- 67 shows an example of Elmarco's Nanospider™ electrospinning production line. In addition to Elmarco, several other companies, including MECC, Fuence, Yflow, and ANSTCO, provide large-scale electrospinning machines for mass production of nanofibers. The availability of large-scale electrospinning machines can speed up the commercialization process of electrospun Si/C nanofiber anodes.

Figure III- 67: Elmarco's Nanospider™ Electrospinning Production Line (A), and High-Speed Electrospinning Process of Nanospider™ (B).

Results

Preparation of Si/C Nanofibers. Precursor nanofibers were first electrospun from dispersions of Si nanoparticles in polyacrylonitrile (PAN)/N,N-dimethylformamide (DMF) solutions. Figure III- 68 shows SEM and TEM images of Si/PAN precursor nanofibers. It is seen that the diameter of Si/PAN nanofibers ranges from 300 to 500 nm. Si nanoparticles are distributed along nanofibers.

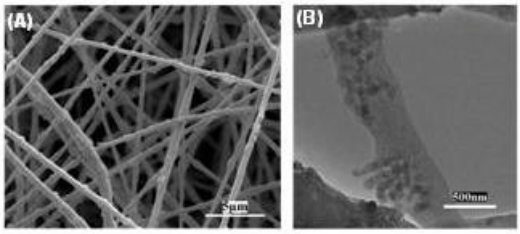

Figure III- 68: Typical SEM (A) and TEM (B) Images of Si/PAN Precursor Nanofibers.

Electrospun Si/PAN precursor nanofibers were carbonized in an electric heat-treating furnace to form Si/C nanofibers. First, electrospun Si/PAN fibers were heated to 280°C (heating rate of 5°C /min) in an air environment and this temperature was maintained to stabilize PAN for 5.5 hours. The temperature was then increased from 280°C to at least 700°C (heating rate of 2°C/min) in a high-purity argon atmosphere. The nanofibers were held at the final temperature for 1 hour in order to complete the carbonization process.

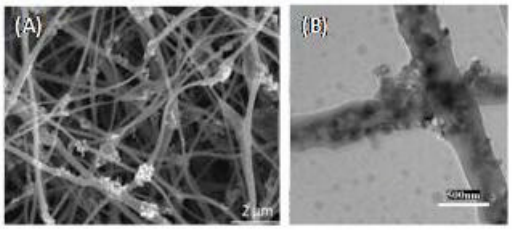

Figure III- 69: Typical SEM (A) and TEM (B) Images of Si/C Nanofibers.

Figure III- 69 shows SEM and TEM images of the prepared Si/C nanofibers. It is seen that the nanofiber structure is maintained after the carbonization process. XRD pattern of Si/C composite nanofibers is shown in Figure III- 70. Si/C composite nanofibers present diffraction peaks at 2θ of about 28.4°, 47.4°, 56.2°, 69.2°, 76.5° and 88.1°, which are ascribed to the (111), (220), (311), (400), (331) and (422) planes of Si crystals in nanofibers, respectively. Figure III- 71 shows Raman spectra of Si/C composite nanofibers. The peak centered near 1350 cm^{-1} (D band) can be explained as structure defect- and disorder-induced features in the graphene layers of carbon materials, while the peak centered near 1600 cm^{-1} (G band) is indicative of the high-frequency E_2g

first-order graphitic crystallites of the carbon. The presence of the strong D band suggests that the carbon matrix in nanofibers has low crystallinity and graphitization and is typical of disordered graphitic material with two Raman bands. The structure of the carbon matrix can be changed to have higher crystallinity and graphitization by modifying the carbonization process, such as by increasing the carbonization temperature.

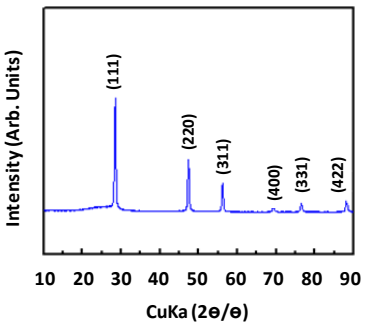

Figure III- 70: WAXD patterns of C (a) and Si/C (b) Nanofibers.

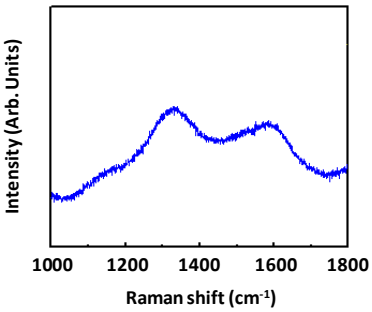

Figure III- 71: Raman spectra of C (a) and C/Si (b) Nanofibers.

Performance of Si/C Nanofibers in Coin Cells. The electrochemical performance of Si/C nanofiber anodes was first investigated in coin-type cells by carrying out galvanostatic charge-discharge tests at a constant current density of 50 mA/g between 0.01 and 2.8 V. Figure III- 72 and Figure III- 73 show the charge-discharge curves of pure Si and Si/C nanofiber anodes, respectively. The Si anode was prepared by using the traditional powder electrode method, i.e., mixing 80 wt % of Si nanoparticles with 10 wt % of polyvinylidene fluoride binder and 10 wt % of carbon black conductor. It can be seen in Figure III- 72 that during the discharge of Si anode, a potential plateau appears approximately at 0.2 V with a charge capacity up to 3300 mAh/g. However, the high Li packing density results in a large volume change during the insertion process, which results in anode cracking and therefore a total loss of the capacity. As a result, the actually charge capacity of Si anode is only 113 mAh/g. However, Si/C nanofibers show relatively good capacity retention during cycling. As shown in Figure III- 73, at the first cycle, Si/C nanofibers show a specific charge capacity of approximately 1095 mAh/g and discharge capacity of 850 mAh/g, which are significantly greater than the theoretical capacity (370 mAh/g) of graphite. Due to the fact that Si has a high Li-storage capacity while carbon has a long cycle life, the electrochemical performance of lithium-ion battery anodes has been improved by embedding Si nanoparticles into carbon nanofibers. Figure III- 74 shows the cycling performance of Si/C nanofibers. It is also seen that with increase in cycling number, the capacity of Si/C nanofibers remains relatively constant, indicating that these anode nanofibers have good cycling stability.

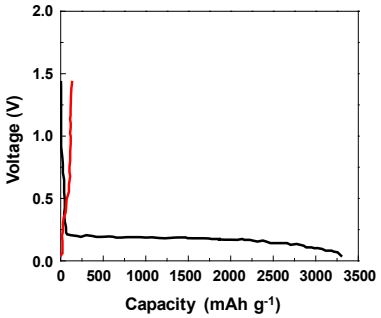

Figure III- 72: Charge-discharge curves of Si anode.

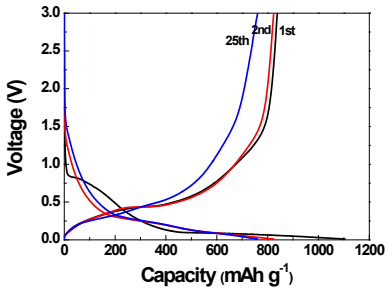

Figure III- 73: Charge-discharge curves of Si/C nanofibers.

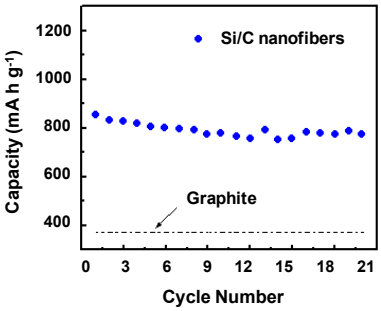

Figure III- 74: Cycling performance of Si/C nanofibers.

The electrochemical performance of Si/C nanofibers can be further improved by modifying the Si particle dispersion using a surfactant. A surfactant, sodium dodecanoate (SD, $CH_3(CH_2)_{10}COONa$), was added in Si/PAN precursor solution to modify the surface of Si nanoparticles and improve the dispersion of Si in the resultant nanofibers. The concentration of SD added was 0.01 mol/L. Figure III- 75 shows SEM images of Si/C nanofibers prepared from Si/PAN precursors with and

without SD surfactant. It is seen that the addition of SD surfactant in the precursor can reduce the agglomeration of Si nanoparticles.

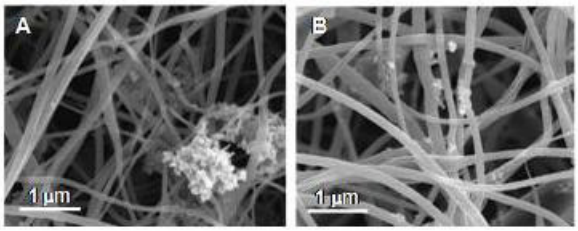

Figure III- 75: SEM images of Si/C nanofibers from Si/PAN precursors without (A) and with (B) 0.01 mol/L SD surfactant.

Figure III- 76 compares the discharge capacities of Si/C nanofibers prepared from precursors with and without surfactant. It is seen that after the addition of surfactant, the capacity of Si/C nanofibers increases due to the enhanced dispersion of Si nanoparticles in the nanofiber matrix. It is also seen in Figure III- 76 that with increase in cycle number, the capacity of Si/C nanofibers remains relatively constant, indicating that these anode nanofibers have good cycling stability. These results demonstrate that the Phase 1 Technical Target has been achieved.

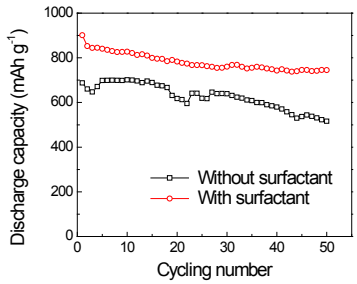

Figure III- 76: Cycling performance of Si/C nanofiber anodes made from Si/PAN precursors with and without surfactant.

Performance of Si/C Nanofibers in 18650 Cells. Si/C nanofibers have been assembled into 18650 cells (Figure III- 77). Figure III- 78 shows the preliminary result on the discharge capacities of Si/C nanofibers in 18650 cells. It is seen that, in the first 5 cycles, the discharge capacities of the Si/C nanofibers are around 600 mAh/g. Although this capacity value is still lower than those obtained in coin-type cells, the result shows that it is feasible to use Si/C nanofiber anodes in 18650 cells. Based on this baseline performance, future work will focus on the enhancement of the electrochemical performance of 18650 cells using structurally-improved Si/C nanofibers.

Figure III- 77: 18650 cells containing Si/C nanofibers as anodes.

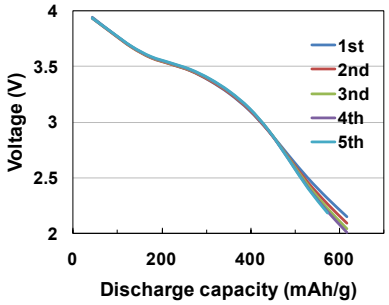

Figure III- 78: Discharge curves of Si/C nanofibers in 18650 cells.

The thermal stability of Si/C nanofiber anodes in 18650 cells was also examined, and the result is shown in Figure III- 79. It is seen that cell voltage can maintain at 4.15 V until 150°C. This exceeds the UL standard and meets the requirement of most applications.

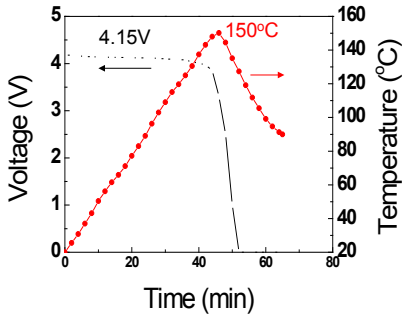

Figure III- 79: Thermal stability of Si/C nanofibers in 18650 cells.

Conclusions and Future Directions

Si/C nanofibers have been prepared through electrospinning Si nanoparticles dispersed in PAN/DMF solutions, followed by the carbonization of electrospun Si/PAN precursor fibers. The electrochemical performance of Si/C nanofibers has been evaluated in coin-type cells and 18650 cells. Results demonstrate that the Phase 1 Target has been achieved.

Future work in Phase Two will focus on:

- Establish guidelines for controlling the nanofiber anode performance by selectively adjusting the processing and structures of the nanofiber anodes;

- Assemble nanofiber anodes into both coin cells and 18650 cells, and improve the cell performance by selectively adjusting the processing and structures of the nanofiber anodes;
- Demonstrate practical and useful cycle life (750 cycles of ~70% state of charge swing with less than 20% capacity fade) with at least twice the specific capacity of conventional graphite electrodes.

FY 2010 Publications/Presentations

1. Xiangwu Zhang, "Nanofiber-Based Energy Storage and Conversion", COT Research Open House, Raleigh, NC, April 2010.
2. Mataz Alcoutlabi, Liwen Ji, Bingkun Guo, Shuli Li, Ying Li, Shu Zhang, Ozan Toprakci and Xiangwu Zhang, "Electrospun Nanofibers for Energy Storage", 2010 AATCC International Conference, Atlanta, Georgia, May 2010.
3. Xiangwu Zhang, Ozan Toprakcim, and Su Zhang, "Electrospun Nanofibers for Energy Storage", Techtextil North America 2010 Symposium, Atlanta, Georgia, May 2010.
4. Xiangwu Zhang, Peter Fedkiw, Saad Khan, and Alex Huang, "New High-Energy Nanofiber Anode Materials", 2010 U.S. Department of Energy Hydrogen Program and Vehicle Technologies Program Annual Merit Review and Peer Evaluation Meeting, Washington, DC, June 2010.
5. Xiangwu Zhang, Mataz Alcoulabi, Liwen Ji, Bingkun Guo, Shuli Li, and Ozan Toprakci, "High-Performance Lithium-Ion Batteries Based on a Novel Nanofiber Technology", 14th Annual Green Chemistry & Engineering Conference, Washington DC, June 2010.
6. Xiangwu Zhang, "Electrospun Nanofibers for Advanced Energy Storage and Conversion", Oak Ridge National Lab, Oak Ridge, TN, July 2010.
7. Xiangwu Zhang, "Electrospun Nanofibers for Energy Storage", Nanofibers for the 3rd Millennium 2010 (N3M2010) Conference, Raleigh, August 2010.

III.B.10 Chemical Shuttle Additives in Lithium-ion Batteries (EnerDel)

Christopher Johnson (NETL Project Manager)
Subcontractor: EnerDel

Adam J. Hunt (Principal Investigator)
EnerDel, Inc.
8740 Hague Road, Bldg. 7
Indianapolis, IN 46256
Phone: (317) 585-3464; Fax: (317) 585-3444
E-mail: ahunt@enerdel.com

Subcontractor: Argonne National Laboratory

Start Date: October 1, 2009
Projected End Date: March 31, 2013

Objectives

- Develop a chemical shuttle agent with a redox voltage in the range of 4.4 to 4.6V to use in hybrid electric vehicles, plug-in hybrid electric vehicles, and electric vehicles to increase safety and potentially simplify and lessen the role of the battery management system electronics.
- Characterizing the redox shuttle additive in coin cells, bag cells, jelly roll cells, large cells, and multi-cell battery packs.
- Assessing the redox shuttle additive's effectiveness in terms of safety and reducing the need for a battery management system.
- Assessing the effect that the redox shuttle additive has on the cell electrochemical performance parameters.
- Characterizing the effect of the presence of the redox shuttle additive on the cell components.

Technical Targets

- The goal is to increase the safety of the lithium-ion battery, while making the battery lighter, smaller, and more inexpensive.

Technical Barriers

The addition of redox shuttle compounds to lithium-ion batteries is a relatively new concept that has not been tried in large format batteries. Among the potential technical challenges are:

(A) chemical stability of the redox shuttle additive

(B) electrochemical stability of the redox shuttle additive

(C) the redox shuttle additive may affect the performance of the battery adversely

(D) the diffusion coefficient of the redox shuttle additive must be high enough so that a large current density can be tolerated, averting overpotential

(E) some redox shuttle additives attack the copper current collector of the anode

(F) too much heat may be generated during the redox process

Accomplishments

- We have received an additional 10 g of the initial redox shuttle additive (2-(pentafluorophenyl)-tetrafluoro-1,3,2-benzodioxaborole, or BDB) from Argonne National Laboratories.
- The redox potential, diffusion coefficient, and window of electrochemical stability were evaluated using cyclic voltammetry (CV) in different electrolytes
  - $Li_2B_{12}F_{12}$,
  - 2-pentafluorophenyl-tetrafluoro-1,3,2-benzodioxaborole (BDB)
  - 2,5-di-tert-butyl-1,4-dimethoxybenzene (DDB)
- The effect of moisture in electrolyte containing BDB was examined by CV.
- CV was also used to determine the reduction potential of BDB with and without the addition of LiF against graphite and whether or not it may be involved in SEI film formation
- During literature review, no prior art was found that interfered with a new class of compounds that might be useful as high voltage redox shuttles.
- Two representatives from EnerDel attended an XPS (X-ray photoelectron spectroscopy) training course at the Birck Nanotechnology Center at Purdue University.

✧ ✧ ✧ ✧ ✧

Introduction

The redox shuttle additive will be characterized by electrochemical testing such as cyclic voltammetry. Cell testing will begin with small coin cells and will culminate in testing of larger multi-cell battery packs. Materials characterization using various analytical techniques will also be performed to examine the effect of the presence of the redox shuttle on the battery components.

Approach

We will select the anode and cathode materials for the first experiments using the redox shuttle additive. We will also select an appropriate electrolyte.

We will determine the effect of the redox shuttle additive on the capacity, rate capability, cycleability, calendar life, and temperature performance of the cells. The anode and cathode materials will be examined with tools such as scanning electron microscopy and X-ray photoelectron spectroscopy to characterize any differences that may occur as a result of exposure to the redox shuttle additive. Inductively coupled plasma spectrometry will be employed to determine if the redox shuttle additive is changing the concentration of metal ions in the electrolyte. Gas chromatography-mass spectrometry will be used to examine the organic compounds in the electrolyte, including the redox shuttle additive and any potential decomposition products. The electrode surfaces will be examined using Fourier transform infrared spectrometry to assess any differences in the materials upon exposure to the redox shuttle additive.

Abuse testing will also be performed. Cells containing the redox shuttle additive will intentionally be overcharged to assess the effectiveness of the additive. The maximum current density at a particular overcharge potential that can be tolerated will be determined. External short circuiting and nail penetration testing will eventually also be performed.

Results

Diffusion coefficient and maximum charge rate. We have continued to evaluate BDB and also are evaluating $Li_2B_{12}F_{12}$, and DDB. Both $Li_2B_{12}F_{12}$ and DDB have been previously reported as redox shuttles for Li-ion batteries.[1,2] The diffusion constant was measured in two different standard electrolytes because the solvent viscosity can impact the diffusion coefficient, which ultimately determines the maximum current that can be shuttled.

Using Equation 1, the diffusion coefficient may be calculated after measuring the peak current at various scan rates during a cyclic voltammetry experiment.

$$I_p = 2.69x10^5 \cdot n^{3/2} \cdot A \cdot D^{1/2} \cdot v^{1/2} \cdot C \quad \text{Eq 1}$$

The cyclic voltammograms of 1 mM BDB (Figure III- 80 and Figure III- 81), DDB (Figure III- 82 and Figure III- 83), and $Li_2B_{12}F_{12}$ (Figure III- 84 and Figure III- 85) in the electrolytes 1.2 M $LiPF_6$ in 30/70 EC/DEC (electrolyte #1) and 1.2 M $LiPF_6$ in 25/5/70 EC/PC/EMC (electrolyte #2) are shown below. The scan rates used were 5, 10, 20, 30, 40, 50, and 100 mV/s.

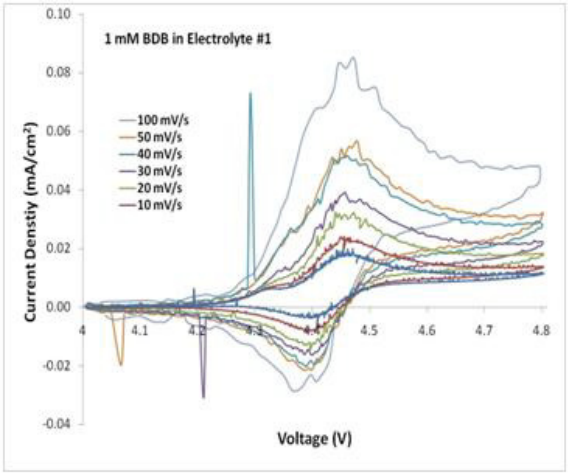

Figure III- 80: Cyclic voltammograms of 1 mM BDB in electrolyte #1.

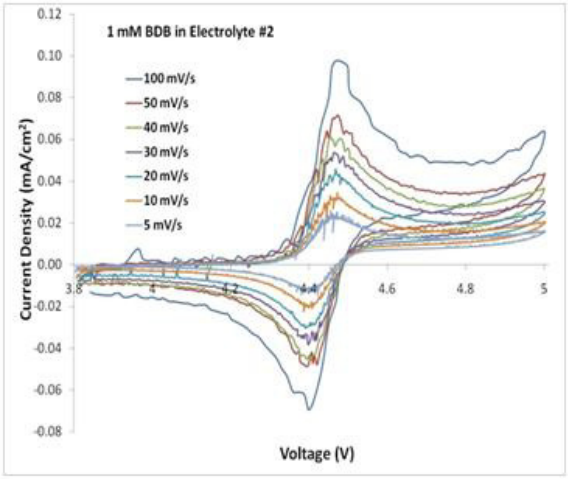

Figure III- 81: Cyclic voltammograms of 1 mM BDB in electrolyte #2.

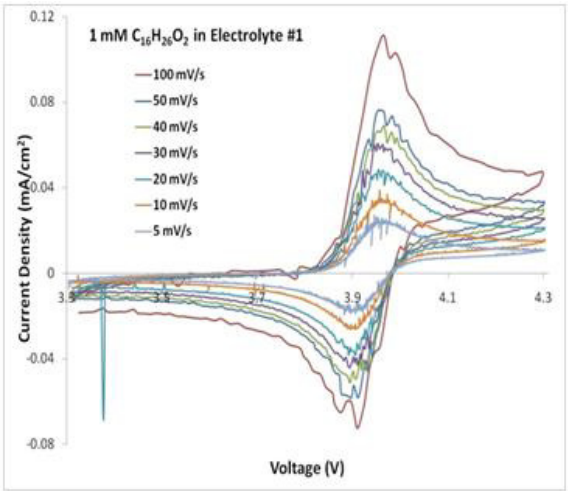

Figure III- 82: Cyclic voltammograms of 1 mM DDB in electrolyte #1.

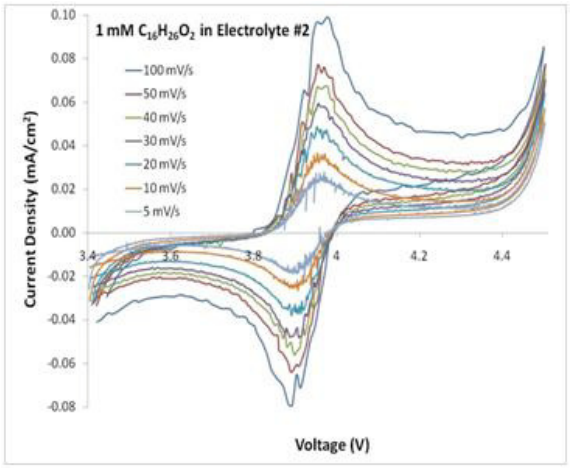

Figure III- 83: Cyclic voltammograms of 1 mM DDB in electrolyte #2.

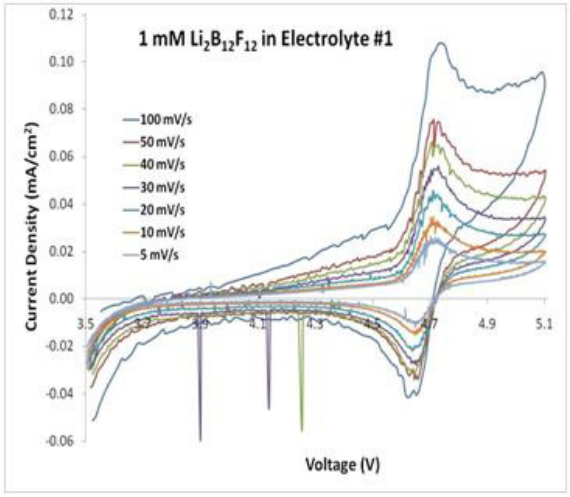

Figure III- 84: Cyclic voltammograms of 1 mM $Li_2B_{12}F_{12}$ in electrolyte #1.

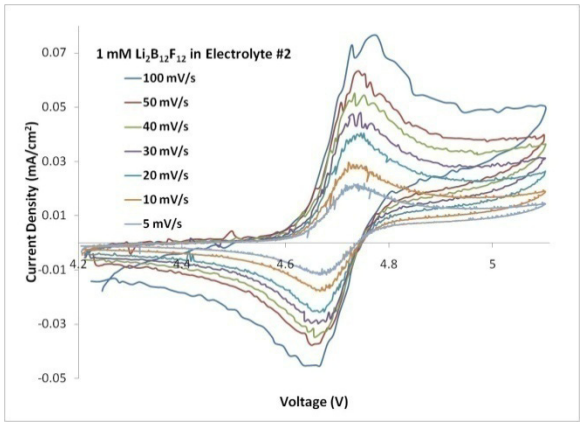

Figure III- 85: Cyclic voltammograms of 1 mM $Li_2B_{12}F_{12}$ in electrolyte #2.

A summary of the redox potential and diffusion coefficient for these three redox shuttles is shown in Table III- 25.

Table III- 25: Redox potentials and diffusion coefficients for DDB, BDB, and $Li_2B_{12}F_{12}$ in various electrolytes at 25°C (first two are literature values).

Redox Shuttle	Electrolyte Composition	Average Redox Oxidation Potential, V	Diffusion Coefficient, cm^2/sec
$Li_2B_{12}F_{12}$	1M $LiPF_6$ in 3:7 EC:EMC	4.6	2.1×10^{-6}
DDB	0.5 M LiBOB in 1:2:1:2 PC:DMC:EC:DMC	3.95	1.6×10^{-6}
$Li_2B_{12}F_{12}$	#2	4.72	9.76×10^{-7}
$Li_2B_{12}F_{12}$	#1	4.70	1.55×10^{-6}
DDB	#2	3.96	1.35×10^{-6}
DDB	#1	3.95	1.69×10^{-6}
BDB	#2	4.47	1.12×10^{-6}
BDB	#1	4.45	1.08×10^{-6}

The redox potential of the shuttle should be about 0.1 to 0.3 V above the maximum potential that the cathode reaches during normal charging. If the oxidation potential of the redox shuttle molecule is too low, the shuttle will be oxidized during normal charging. This would cause inefficient and incomplete cell charging because some of the charging current would be consumed by the oxidation of the redox shuttle molecule. If the oxidation potential of the redox shuttle molecule is too high, damage to the cell may occur and significantly shorten its life. In an extreme case, the shuttle would provide no protection at all. Based on this consideration, cells with layered oxide cathode materials that operate at 4.1 to 4.2 V should employ a redox shuttle with an oxidation potential in the range of about

4.2 to 4.5 V. The oxidation potential of $Li_2B_{12}F_{12}$ at about 4.7 V is too high but this material might be suitable for high voltage cathodes. The DDB has an oxidation potential of about 3.95V that is too low for mixed oxide cathodes but might be useful for $LiFePO_4$. The BDB has a redox potential in the desired range for mixed oxide cathodes but thus far it has not provided effective overcharge protection in full cells with NMC cathodes and hard carbon anodes (please see previous reports).

The diffusion coefficient of the redox shuttles varies with the electrolyte and in large part is influenced by the viscosity of the solution. For $Li_2B_{12}F_{12}$ and DDB, the diffusion coefficient is higher in electrolyte #1. For BDB, the diffusion coefficient is slightly higher in electrolyte #2 than electrolyte #1. This difference might because of an interaction between the BDB which is a Lewis acid and the carbonate solvents which are Lewis

bases. This could also explain the lower diffusion coefficient for BDB compared to $Li_2B_{12}F_{12}$ which has a similar molecular mass.

The diffusion rate of the redox shuttle governs an upper limit on the charge current that may be shuttled once the redox potential of the shuttle is reached. A cell charged above this rate would enter into overcharge in spite of the presence of the redox shuttle molecule. The maximum charge current density in A/cm^2 may be calculated from the diffusion coefficient, D (cm^2/sec), using equation 2 where n is the number of electrons removed in the oxidation (dimensionless), F is Faraday's constant (96485 coulombs/mole), C is the concentration (mol/cm^3), and L is the distance between the electrodes (cm).

$I_{max}/A = nFDC/L$ Equation 2

In terms of C-rate, the maximum charge current varies depending on the cell capacity. For high energy cells such as that would be used in EV applications, the maximum C-rate is about 1 to 2C. For high power applications, in which the cells have smaller capacity but similar geometry, the maximum current corresponds to about a 2 to 4 C rate. Since high power applications demand C rates above 4C, redox shuttles are unlikely to be applicable for high power cells.

Electrolyte stability and the effect of moisture. During the course of testing, the solutions of some of the electrolytes were observed to become yellow over time in the presence of DDB and BDB, while control solutions of electrolyte alone remained colorless. The yellowing of electrolyte solutions is thought to be related to organic compounds formed after the breakdown of $LiPF_6$ as shown in Scheme 1. The HF concentration is higher in the DDB solution with the more intense yellow color as shown in Table III- 26. It is not clear why the DDB or BDB should cause the yellowing of the electrolyte solution. The DDB or BDB may be involved in the decomposition of $LiPF_6$

$$LiPF_6 \rightleftharpoons LiF + PF_5$$

$$PF_5 + H_2O \rightarrow POF_3 + 2HF$$

by shifting the equilibrium in the top reaction of Scheme 1 to the right. Also, trace contaminants or other decomposition products may be involved.

Table III- 26: Moisture and HF content of electrolytes with DDB and BDB.

Electrolyte	Average Moisture Concentration, ppm	Average HF Concentration, ppm
Electrolyte #2	7.12	---
Electrolyte #1	3.35	---
1 mM DDB in #2 (very yellow)	5.72	74
1 mM DDB in #1 (slightly yellow)	4.87	48
1 mM BDB in #2	3.91	---
1 mM BDB in #1	2.94	---

Electrolytes with BDB had lower water content than electrolytes without BDB. BDB is a Lewis acid and may shift the equilibrium of the decomposition of $LiPF_6$ shown in Scheme 1 to the right by abstracting fluoride ion to form a new Li salt. The abstraction of fluoride from $LiPF_6$ yields PF_5 which readily reacts with water to form HF. POF_3 has been shown to catalyze the decomposition of organic carbonate solvents.[3] This could explain the lower measured water content and yellowing of the solution. Further, it is thought that BDB reacts with water to form the starting materials of the synthetic reaction, namely TFC (3,4,5,6-tetrafluorocatechol) and pentafluorobenzene boronic acid. Both of these reactions may explain the lower concentration of water in the electrolyte solutions after the addition of BDB.

The reactions that result in the yellow color of the electrolyte also appear to be responsible for the irreversible oxidation of the redox shuttle. Electrolyte with DDB that was stored for one month that had a yellow color did not have a reversible peak at 3.95 V as it did when the electrolyte was freshly prepared as shown in Figure III- 86. Also, the addition of water to electrolyte containing BDB produces an irreversible oxidation peak at 4.45 V, as shown in Figure III- 87. This is important since a by-product of BDB synthesis is water (condensation reaction) and water could be an impurity. Further, water enters cell packaging that is not hermetically sealed. Water may react with BDB to form the starting materials.

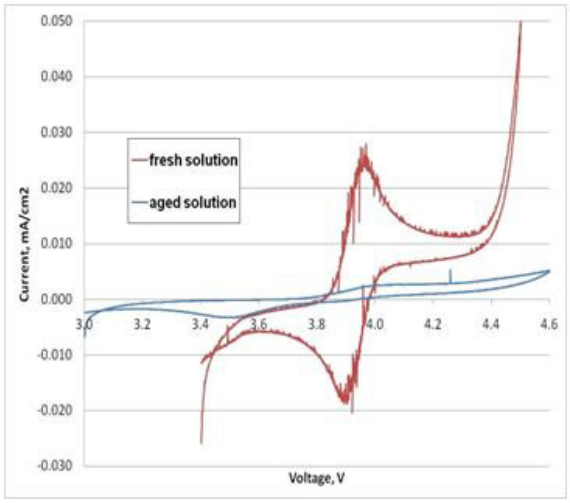

Figure III- 86: Cyclic voltammograms of freshly prepared electrolyte containing DDB and after 1 month of storage.

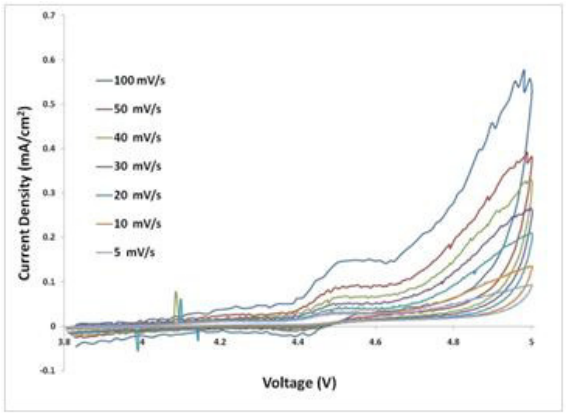

Figure III- 87: Cyclic voltammograms of 1 mM BDB and 1% water added to electrolyte #2.

Effect of LiF and SEI film formation. As previously stated, BDB is a Lewis acid. It has a 3-coordinate boron center that may accept a Lewis base such as F^-. It has been suggested by Argonne National Laboratory that the addition of LiF will stabilize the BDB. The fluoride ion complexes to the BDB, forming an anion. This anion is expected to be less susceptible to hydrolysis and would be less likely to abstract fluoride from the PF_6^- anion.

Cyclic voltammetry of the BDB with and without the addition of LiF also shows that there are differences in the reduction potential at a graphitic electrode. Without the addition of LiF, there is a reduction peak at 1.3 V during the first scan from 3 to 0 V, as shown in Figure III- 88. With the addition of LiF, the reduction peak at 1.3 V is not present. Also, the peak at about 0.6 V which is attributed to solvent reduction is suppressed in the electrolyte of the BDB without LiF. Without the addition of LiF, the BDB has an electron deficient three coordinate boron center that is likely easily reduced. Addition of LiF not only fills the boron atom's shell with eight electrons but also forms an anion which could be more stable than a neutral species.

The BDB without LiF therefore appears to be involved in the formation of the SEI layer on the graphite surface. Continued reduction of BDB does not appear to occur as the reduction peak at 1.3 V is not present on subsequent cycles as shown in Figure III- 89. Also, the suppression of the peak at 0.6 V suggests that there are less solvent reduction products in the SEI. The lithium intercalation into the graphite is shifted to more negative potentials and its deintercalation is shifted to more positive potentials. This suggests that the film formed from the BDB without LiF may be more resistive than films formed with BDB and LiF or standard electrolytes. The cyclic voltammogram of electrolyte with BDB and LiF resembles that of electrolyte alone; the cyclic voltammogram of electrolyte with only BDB is different as explained above.

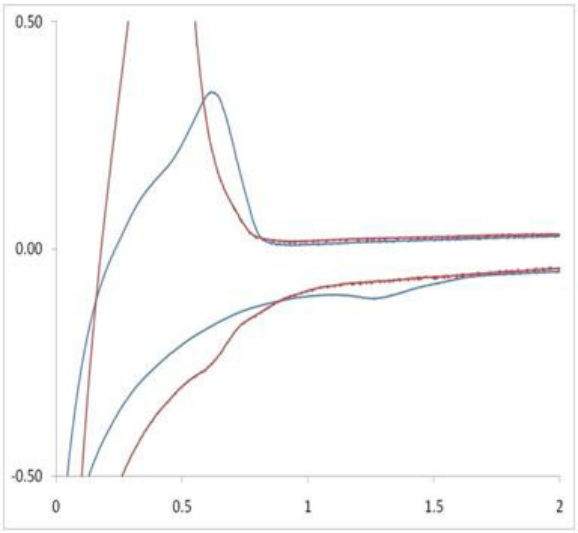

Figure III- 88: Expanded region of the first cycle of cyclic voltammograms of BDB without LiF (blue) and with LiF (red). Scan range 3 to 0 V at 1 mV/s. Working electrode is graphite.

New redox shuttle materials. We have reviewed the literature and found no prior art that interfered with a new class of compounds that could be useful as high voltage redox shuttles. We are in the process of applying for patents and plan to have the materials synthesized at an outside source. Following their synthesis we plan to evaluate the materials.

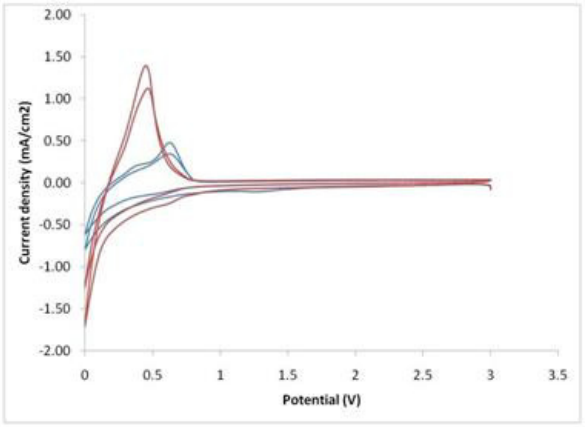

Figure III- 89: Cyclic voltammograms of BDB without LiF (blue) and with LiF (red). Scan range 3 to 0 V at 1 mV/s. Working electrode is graphite.

XPS Training. Two representatives from EnerDel (M.L. Patterson and M. Taggougui) attended the XPS Introductory Workshop at the Birck Nanotechnology Center at Purdue University on September 22-23, 2010. XPS will be a vital tool to aid in the understanding of the SEI layer on the anode in the presence and absence of redox shuttle molecules.

FY 2010 Publications/Presentations

1. Chen, J. Liu, A.N. Jansen, G. GirishKumar, B. Casteel, K. Amine Electrochem. Solid-State Lett. 134) A39 (2010)
2. Buhrmester, J. Chen, J. Jiang, R.L. Wang, J.R. Dahn, J. Electrochem. Soc. 152 (2005) A2390–A2399. 3 C.L. Campion, W. Li, B.L. Lucht, J. Electrochem. Soc. 152 (2005) A2327.

III.B.11 Internal Short Circuits in Lithium-Ion Cells for PHEVs (TIAX, LLC)

Christopher Johnson (NETL Project Manager)
Subcontractor: TIAX, LLC

Suresh Sriramulu
Richard Stringfellow
TIAX LLC
35 Hartwell Avenue
Lexington, MA 02421
Phone: (781) 879-1240; Fax: (781) 879-1209
E-mail: sriramulu.suresh@TIAXLLC.com

Start Date: May 2010
Projected End Date: May 2012

Objectives

- Develop an improved understanding of the conditions under which a thermal runaway will occur in a Li-ion cell.
- Use modeling to determine the threshold conditions for thermal runaway following an internal short circuit.
- Assess how the generation and growth of internal short circuits capable of inducing thermal runaway occurs with respect to the timing and duration of the short generation process, and its dependence on a variety of cell conditions.
- Identify design factors that can reduce propensity for thermal runaway.
- Identify and analyze opportunities for prevention of internal short circuits, or intervention/mitigation before they can cause thermal runaway.

Technical Barriers

On rare occasions, Li-ion cells can experience thermal runaway during normal charge/discharge cycles because of internal short-circuits; we term such failures as field-failures. Even though such incidents are rare, the potential consequences can be very serious. Safety technologies currently employed in Li-ion cells, such as PTC, CID, shut-down separators, etc., have not prevented thermal runaway due to internal shorts in commercial Li-ion cells. Development of new safety technologies is hindered by the rarity of field-failures in Li-ion cells, and the current incomplete understanding of field-failures. In this program, we will fabricate Li-ion cells with various means to stimulate or develop appropriate internal shorts in order to study the effect of cell design variables, and cell-level materials choices. This improved understanding will help develop select and test technologies that enhance the safety of PHEV Li-ion batteries.

Technical Targets

- Develop guidelines that will enable the development of technologies for a safe battery pack.
- Establish an experimental facility that will permit testing the efficacy of technologies developed to mitigate safety incidents that occur in the field at a rate of one failure in 1-10 million cells produced.
- Establish a facility for fabricating Li-ion cells to study the effect of cell materials and cell design parameters on thermal runaway, and to compare to model predictions.
- Using model and experimental data, select and test technologies to enhance Li-ion battery safety, and experimentally evaluate the benefits of such technologies.

✧ ✧ ✧ ✧ ✧

Introduction

Concerns regarding the safety of Li-ion batteries could severely limit their use in PHEVs, and undermine the prospects for realizing the appealing benefits of PHEVs. Recent highly publicized safety incidents and the ensuing widespread recalls of Li-ion batteries used in laptops and cell phones have elevated such concerns. In these safety incidents, called field-failures, Li-ion batteries operating under otherwise normal conditions undergo what appear to be spontaneous thermal runaway events with violent flaming and extremely high temperatures. These field-failures cause significant damage to cells, packs and devices, and sometimes to their surroundings. Because a typical PHEV pack would be significantly larger than a typical laptop pack, the consequences of a field-failure in a PHEV pack could be far more severe than would be the case for a laptop pack, and may occur more far more frequently.

Although it is well-recognized that the commercial viability of Li-ion technology in PHEVs is dependent on avoiding spontaneous occurrence of such incidents on board vehicles, it is clear but less well-recognized that the safety technologies currently employed in commercial Li-ion batteries for portable electronic applications are inadequate. For example, the many millions of cells recalled in the last few years due to safety incidents all came from lots that passed all industry-standard safety tests. Furthermore, there are

currently a variety of standard safety-related technologies to guard against abuse of the Li-ion battery; electronic controls, current interrupt and positive temperature coefficient devices, shutdown separators, etc., are intended to counter potential hazards due to inadvertent overcharge, failure of protection circuits, exposure to high temperatures, external short circuits, etc. However, field-failures have occurred despite the presence of these technologies in cells and packs. There is no adequate test for the type of field-failure that presents the basic safety issue for Li-ion.

Given that field-failures occur in a manner that is not effectively addressed by any of the standard safety measures currently used in Li-ion batteries, and that there is no test currently available that can identify these cells before they undergo field-failure, it is clear that a fundamentally new approach is required to develop technologies that will prevent these rare but profoundly destructive safety incidents caused by internal short circuits in PHEV cells.

Approach

TIAX is integrating testing of experimental Li-ion cells incorporating deliberately introduced internal short circuits with numerical simulations, in order to develop guidelines for lithium-ion cell design and for internal short circuit prevention and/or mitigation. This work is intended to eliminate or reduce the propensity for lithium-ion PHEV cells to undergo internal short circuit-induced thermal runaway.

As one key element of its approach, TIAX is enhancing an existing modeling tool that is able to predict the propensity for any given Li-ion cell chemistry/design to undergo internal short circuit-induced thermal runaway. As a second key component of its approach, TIAX is creating a flexible Li-ion cell prototyping facility to enable construction of cells with "implanted" shorts, cells incorporating short prevention or mitigation technologies, and cells with broadly varied design parameters. Testing of cells having a broadly varied range of chemistry and design will enable us to better understand what factors contribute to or detract from a cell's propensity to undergo internal short circuit-induced thermal runaway, and will provide important feedback and validation for the internal short circuit model. These types of flexibly-designed cells cannot be produced at battery companies with typical manufacturing equipment.

By combining, in this program, the ability to make and test Li-ion cells having any desired chemistry and design with the ability to generate internal short circuits at any location within the cell "on demand", TIAX aims to generate guidelines for design of Li-ion cells and develop internal short circuit prevention and mitigation technologies that enable PHEV battery manufacturers to design field-failure-safe Li-ion batteries. This same capability to make varied cells with implanted internal short circuits will also support and validate development of a modeling tool that can run simulations of even more varied cell parameters.

III.B.12 High Throughput Fabrication of 10 Year PHEV Battery Electrodes (A123Systems)

Ralph Nine (NETL Project Manager)
Subcontractor: A123Systems

David P. Ventola
A123Systems, Inc.
321 Arsenal Street
Watertown, MA 02472
Phone: (617) 393-4142; Fax: (617) 924-8910
E-mail: dventola@a123systems.com

Start Date: October 1, 2009
Projected End Date: September 30, 2011

Objectives

- On lab scale, define:
  - CTQ metrics for PHEV electrodes.
  - Key manufacturing process parameters
  - Scalable manufacturing process
- Demonstrate in manufacturing higher throughput (line speeds) for manufacture of PHEV electrodes to significantly reduce manufacturing costs.

Technical Barriers

This project addresses the following technical barriers to increasing line speeds for PHEV electrodes:

(A) Slurry stability

(B) Scale-up from lab to production

(C) Increased drying rate

(D) Electrode uniformity

(E) Process controls to meet CTQs

Technical Targets

- 60 – 100% increased throughput of electrodes
- Process model to predict production conditions for efficient scale-up
- 50% reduction in electrode process costs

Accomplishments

- Ordered & installed production equipment in Romulus, MI plant designed to meet project objectives
- In production facility in Asia, demonstrated increased line speeds that provide foundation for additional improvements.
- Built cost model to capture cost and guide continued improvement efforts.
- Completed Lab trials for each of the key new process tools to increase line speed.
- Completed first draft of process model for scale-up

Introduction

Achieving the increased throughput targets will require changes to or improvements in several process parameters in PHEV battery electrode production. This project will define on lab scale the processes required and scale to manufacturing operation.

Approach

To meet the objective for increased throughput in manufacturing the team will work to 1) optimize slurry formulation and rheology to include study of alternative binders, 2) optimize slurry manufacturing process, 3) improve the drying process, and 4) define more rigorous scale-up procedures to include modeling of the key process variables.

While we have long term goals, we are focused on as step-wise improvement of throughput where incremental increases in throughput will be qualified over time.

Results

Slurry Formulation. The formulation of PHEV battery electrode slurries was studied to optimize product performance as well as manufacturability. This study included an assessment of various binder systems. Composition of matter was chosen in order to meet CTQ performance metrics.

Slurry Make Process. In parallel with the product design (selection of composition of matter), the team studied various approaches to slurry manufacture. The slurry manufacturing process was chosen based to match composition of matter and meet CTQ performance metrics.

Improved Drying Process. The current rate limiting step is the drying process for battery electrodes. During the equipment design and selection process,

additional tools and process controls were specified to provide the capability to increase drying rate, characterize the process, and meet product performance criteria.

In addition a drying model has been developed as a tool to define constraints in production speed, and to quantify the scale-up from lab to production.

Finally some initial scoping trials for the additional tools for drying have been completed prior to the start-up of new factory in Michigan.

Scale-up Procedures. The focus has been to define tools and models that can fully characterize critical process levers at the lab scale. Using these tools and models, production conditions can be predicted. Then final optimization is performance on the production lines.

Cost Model. Constructed a cost model for PHEV battery electrode production. The model drives specific throughput targets, as well as guides decisions for equipment specification and procurement.

Results from Production. During 2010 the new factory in Michigan was in design & construction, so the team performed some initial work and data gathering at the A123Systems production facility in Asia. This has resulted in significant learning toward the project objectives. For both PHEV battery electrodes, incremental improvement in increased line speeds have been tested and implemented to begin the process of incremental improvements. These trials have strengthened the foundation on which further increases can be completed.

Conclusions and Future Directions

The initial work in the lab as well as production facility in Asia demonstrates that increasing throughput of electrodes is achievable. The short term goals are clearly achievable: 60% improvement in throughput. The validity and value of the model and scale-up tools have been tested and confirmed.

In order to meet the longer term goal of 100% increase in throughput, testing on the new production equipment in Michigan is required. During the remainder of the project period, these tests will be conducted. The equipment will be ready in Q1 2011 to continue work toward the long term goal.

FY 2010 Publications/Presentations

No publications or presentations were made.

III.B.13 Small Business Innovative Research Projects (SBIR)

Brian Cunningham
EE-2G, U.S. Department of Energy
1000 Independence Ave., SW
Washington, DC 20585
Phone: (202) 287-5686; Fax: (202) 586-2476
E-mail: Brian.Cunningham@ee.doe.gov

Start Date: Continuing Effort
Projected End Date: September 30, 2011

Objectives

Use the resources available through the Small Business Innovation Research (SBIR and Small Business Technology Transfer (STTR) programs to conduct research and development of benefit to the Energy Storage effort within the Vehicle Technologies Program Office.

Introduction/Approach

The Energy Storage effort of the Vehicle Technologies Program Office supports small businesses through two focused programs: Small Business Innovation Research (SBIR) and Small Business Technology Transfer (STTR). Both of these programs are established by law and administered by the Small Business Administration. Grants under these programs are funded by set aside resources from all Extramural R&D budgets; 2.5% of these budgets are allocated for SBIR programs while 0.3% for STTR grants. These programs are administered for all of DOE by the SBIR Office within the Office of Science. Grants under these programs awarded in two phases: a 6-9 month Phase I with a maximum award of $100K and a 2 year Phase II with a maximum award of $750K. Both Phase I and Phase II awards are made through a competitive solicitation and review process.

The Energy Storage team participates in this process by writing a topic which is released as part of the general DOE solicitation. A typical topic focuses on a broad area and will contain several focused sub-topics. The Energy Storage sub-topics are written to address technical barriers associated with the successful commercialization of advanced energy storage systems for use in electric drive vehicles within the scope of the SBIR process.

The grant process places the following constraints on the drafting of these sub-topics:

- The scope of work must be appropriate for a small business.
- The sub-topic must be broad enough to attract five to seven proposals.
- The sub-topic must be narrow enough to attract no more than twelve to fifteen proposals.
- The scope of work must be appropriate given the funding limitations of the SBIR/STTR programs.

Phase II Awards Made in FY 2010. Under the SBIR/STTR process, companies with Phase I awards that were made in FY 2009 are eligible to apply for a Phase II award in FY 2010.

The FY 2009 subtopics were:

(A) Technologies to Assess the Behavior of a Lithium-Ion Cell Containing an Internal Short Circuit

(B) Development of Asymmetric Electrochemical Capacitors

(C) Development of Lithium-ion Cells that Do Not Require the Positive Electrode to Provide the Lithium that Is Cycled

(D) Additives to Reduce the Flammability of Materials Vented from a Lithium-Ion Cell

Three Phase II grants were awarded in the summer of FY 2010 from seven Phase I grants that were conducted in FY 2009.

Subtopic A: Implantation, Activation, Characterization and Prevention/Mitigation of Internal Short Circuits in Lithium-Ion Cells (Tiax, LLC. 35 Hartwell Avenue, Lexington, MA 02140). This project will develop technology to improve the safety of lithium-ion batteries for PHEVs and HEVs, making these vehicle technologies more commercially viable, and thus increasing the likelihood that they will yield their potential environmental, economic and political benefits.

Subtopic B: 3-D Nanofilm Asymmetric Ultracapacitor (Ionova Technologies, Inc., 182 Thomas Johnson Drive Suite 204L, Frederick, MD 21702). This project will apply advances in nanotechnology to create a new ultracapacitor capable of storing significantly more energy, of scaling to the voltage needs of important new applications and of providing improvements in safety, cost, and environmental impact. This will eliminate the issues of low energy density, cost, and safety concerns that plague current generation ultracapacitors.

Section C: Novel High Performance Li-ion Cells (Farasis Energy, Inc., 23575 Cabot Blvd. Suite 206, Hayward, CA 94545). This project will develop a novel approach to increasing the performance and capacity of Li-ion cells. Use of the technology could accelerate the adoption of efficient distributed power

systems and EVs by greatly increasing the life of the battery systems.

Phase I Awards Made in FY 2010. Subtopics in FY 2010 were:

(A) Technologies that Allow the Use of a Lithium Metal Negative Electrode in a Rechargeable Cell

(B) Multi-Electron Redox Materials for High Energy Batterie

(C) Technology to Allow the Recovery and Reuse of "High-Value" Materials from Used Lithium-Ion Batteries

(D) New Electrolytes for Lithium-Ion Cells

Five Phase I grants were awarded in the Summer of FY 2010.

Topic B.

High Energy Density Battery with Multi-Electron Redox Couple (CFX Battery, Inc., 1300 W Optical Drive Suite 300, Azusa, CA 91702). This project will develop a fluoride ion rechargeable battery technology that has significantly higher energy storage capability than the current lithium-ion systems and, since it's a lithium free technology, the safety will be considerably improved compared to the existing batteries. This technology will reduce dependence on foreign oil, diminish environmental pollutions, and revolutionize the way automobiles are powered.

Inexpensive Carbon Matrix for High Performance Lithium Sulfur Batteries (TDA Research, Inc., 12345 W. 52nd Ave, Wheat Ridge, CO 80033). This project will develop new electrode materials for lithium-sulfur batteries resulting in capacities at least twice that of state of the art lithium-ion batteries. Patented carbon technology will be uses to make conductive containment for the sulfur active materials.

The Sol-Gel Derived Novel High Capacity Cathode Materials for Li-ion Batteries (Chemat Technology Inc., 9036 Winnetka Avenue, Northridge, CA 91324). This project will develop novel high capacity cathode materials for Li-ion batteries to achieve high power and high energy densities, due to rigorous weight and volume constraints of HEV and PHEV. The new cathode materials will be based on the multi-electron redox mechanism and fabricated by the sol-gel nano process. The chemical precursors and processing conditions will be determined and the special functional nano-coatings will be applied to the nano-materials for Li-ion cathodes. The resulted materials are expected to have high energy, low cost, green and long cycle life.

Topic D.

New Electrolytes for Lithium-ion Cells (Leyden Energy, 46840 Lakeview Blvd, Fremont, CA 94538). This project will develop a new electrolyte that will significantly improve the performance and safety of conventional lithium-ion batteries. These improved batteries are required for applications with severe operating conditions, including automotive: hybrid, plug-in hybrid and electric vehicles.

Non-flammable and High Voltage Electrolytes and No Carbonates (Versatile Dynamics, Inc., 4 Nicholas Lane, Sandwich, MA 02563). The project addresses the marriage of high voltage stability, non-flammable electrolytes, under development with lithium battery manufacturing capabilities. This project will result in a practical, rechargeable lithium battery with voltage capabilities that significantly exceed state of the art batteries.

FY 2010 Publications/Presentations

1. Presentation to the 2009 DOE Annual Peer Review meeting.

III.C Systems Analysis

III.C.1 PHEV Battery Cost Assessments (Tiax)

Brian Barnett
Jane Rempel
TIAX LLC
35 Hartwell Avenue
Lexington, MA 02421-3102
Phone: (781) 879-1249; Fax: (781) 879-1202
E-mail: barnett.b@tiaxllc.com

Start Date: April 24, 2008
Projected End Date: September 30, 2011

Objectives

- Assess battery cost implications of selected cathode material chemistries being considered for PHEV applications.
- Identify factors with significant impact on cell/pack costs; develop insight into the relative benefits of alternative cathode chemistries; identify areas where more research could lead to significant reductions in battery cost.
- Assess cost implications of employing prismatic rather than cylindrical cell designs.
- Develop initial cost estimates for lower energy-energy storage system (LEESS) batteries.

Technical Barriers

- Not applicable

Technical Targets

- Not applicable

Accomplishments

- Estimates were developed for the high volume manufacturing cost of lithium-ion PHEV batteries employing five different cathode active materials, and one alternative anode material at three electrode loading levels, and two fade levels.
- Factors with significant impact on cell costs were identified and quantified.
- Areas where more research could lead to significant reductions in battery cost were identified.
- Cost projections and an initial sensitivity analysis were developed for batteries broadly conforming to the recently defined USABC requirements for End of Life for LEESS power assist HEV.

✧ ✧ ✧ ✧ ✧

Introduction

TIAX's established cost model for PHEV batteries assumes a vertically integrated manufacturing process from cell fabrication through completed battery system. For cell production, the TIAX cost model yields estimates for the cost of goods sold (COGS), i.e., manufacturing cost, including capital cost. Materials and manufacturing cost estimates were based on production of cylindrical format cells in high volume and modified as appropriate for consideration of prismatic form factor cells. All supplied materials, e.g., cell materials, packaging components, are treated as outside-purchased and include supplier mark-ups. No supplier mark-up is included in in-process goods, e.g., cells to be assembled into packs.

The TIAX cost model was used to assess the implications to cost of a 5.5 kWh-usable Li-ion PHEV battery pack for the following cost modeling factors and conditions:

- Cathode materials (5): $LiNi_{0.8}Co_{0.15}Al_{0.05}O_2$ (NCA), $LiNi_{1/3}Co_{1/3}Mn_{1/3}O_2$ (NCM), $LiFePO_4$(LFP), $LiMn_2O_4$(LMO) and the emerging layered-layered NCM (LL-NCM).
- Anode material (2): graphite and lithium titanate
- Electrode loading (3): low (1.5 mAh/cm^2), medium (2.25 mAh/cm^2)and high (3.0 mAh/cm^2)
- Fade (2): 0%, 30%

These cost modeling factors produced a matrix of different scenarios to be considered. Each scenario was based on an assumed SOC range of 80%. Costs were to be estimated at a production volume of 5,000,000 cells/year.

Approach

For PHEV modeling, TIAX employed a parametric approach in which TIAX's cost model was applied many times with different sets of input parameters. Inputs included:

- Pack energy required (20 mile range)

- Nominal battery pack voltage
- Fade
- Battery chemistries
- SOC range
- Electrode loadings
- Material costs
- Equipment costs
- Equipment throughput and labor requirement.

Individual cost input variables were identified and a likely range of values established for each. Cell designs were built up from specific electrode properties. Since Li-ion batteries of the size and design considered in this study have not been manufactured and tested, key assumptions were made about battery performance, including:

- Power output: peak power (40 kW for 2 seconds, or 20 kW for 100 seconds) is available from the battery across the full range of SOC assumed (see below). Low temperature performance was not considered.
- Power input: the battery can be recharged at the peak rate (30 kW) except when the battery is at a high SOC.
- SOC range: 10-90%, i.e., battery size is 6.9 kWh nominal to deliver 5.5 kWh usable.

It should be noted that it is not certain that target power and fade levels can actually be met at the electrode loadings modeled and over the SOC range modeled for all cathode active material chemistries.

Both single and multi-variable sensitivity analyses were performed for the purpose of identifying key factors influencing costs, particularly those factors with potential high leverage to reduce battery cost.

For LEESS the TIAX model was adjusted to consider a range of design and operating conditions. Candidate operational energy window ranges were investigated (as % nominal) and the consequences were evaluated for selected chemistries. Selected alternative chemistries and electrode thicknesses were characterized experimentally to provide perspective on appropriate energy window ranges over which the goals could be met.

Results

The PHEV battery configurations modeled in this study resulted in battery costs (COGS) ranging from \$264kWh to \$710/kWh, or \$1,452 to \$3,905 for 5.5 kWh usable power when employing graphite anodes and cathode materials initially considered, namely NCA, NCM, LFP and LMO. Modeled PHEV battery costs ranged from \$325 to \$700/kWh for LL-NMC/graphite and from \$575 to \$1225/kWh for LL-NMC/LTO. Using LTO in place of graphite led to an across the board increase in material and process costs, though it should be pointed out that certain attractive aspects of the use of LTO anode materials are not quantified in this analysis.

Cost of cathode active material is a somewhat less important factor in battery system cost than might have been thought. There is significant overlap in battery costs among the five cathode classes evaluated, with wider variation within each chemistry than between chemistries.

Upfront cell design is a critical factor in battery cost. Electrode loading (i.e., electrode length) seems to be more significant than cathode active material cost within the ranges evaluated. Manufacturing process speed also has a significant impact on battery cost.

The projected costs for PHEV batteries in this study are consistent with what might be expected from consideration of 18650-based Li-ion battery costs. 18650 cells are a standardized Li-ion design currently produced in volumes approaching one billion cells/year worldwide, using the most highly automated processes currently available in the industry. This production volume corresponds to about 10 GWh/year, or enough volume in terms of materials and electrode area to yield about one million PHEV batteries/year. Current Li-ion OEM 18650 cell costs are in the \$200-\$250/kWh range.

Prismatic cell designs result in higher costs than were obtained for cylindrical cells due especially to the fact that certain operations, such as winding or stacking, are slower. PHEV batteries based on wound prismatic cells exhibited a pack level cost in the range of 3-5% higher than for cylindrical cells. When stacked prismatic cells are employed, the pack level costs are 8-17% higher.

For LEESS batteries, initial results indicated that weight and volume requirements could probably be met with chemistries now under consideration, but cost targets appear much more difficult. This work is on-going as of submission of this summary.

Conclusions and Future Directions

The PHEV battery configurations modeled in this study resulted in battery costs (COGS) ranging from \$264/kWh to \$710/kWh, or \$1,452 to \$3,905 for 5.5 kWh usable energy. There is significant overlap in battery costs among the five cathode classes evaluated, with wider variation within each chemistry than between chemistries.

Doubling the speed of all manufacturing processes noticeably decreased battery cost in most scenarios. Separator cost and coater speed are significant factors in battery system cost.

The ability to utilize a wide SOC range contributes significantly to reducing energy storage costs. Lower fade and wider SOC range both reduce cost by resulting in lower required nominal battery energy and hence smaller battery size. Therefore, materials that support a wide SOC range should help to reduce overall battery costs.

Other specific areas of research with potential to yield reductions in battery cost include materials that provide minimal fade, impedance growth and calendar aging. Also, chemistries and/or electrode designs that permit shorter, thicker electrodes while meeting target requirements for power and energy should yield cost reductions in the battery. In general, chemistries and designs that enable lower overall electrode area per battery and minimize battery size will reduce cost. Fundamentally different electrode preparation processes could result in favorable battery manufacturing cost impact, both capital and operating. Also, identification and adoption of advanced processing technologies to increase coater speed and/or other unit operations significantly are a potential source of cost reduction. Cell formation and aging, anode and cathode coating and drying, and winding together account for as much as 70% of the total processing costs and represent the most fruitful targets for future process improvement and cost reduction.

For LEESS batteries, a major issue is the extent to which the battery must be over-sized with respect to energy in order to deliver the required power (and life). The performance requirements that most directly impact battery sizing are being evaluated as well as the sensitivity to these factors.

FY 2010 Publications/Presentations

1. Presentation at the 2010 DOE Annual Peer Review Meeting.

III.C.2 Battery Pack Requirements and Targets Validation (ANL)

Danilo J. Santini
Argonne National Laboratory
9700 South Cass Avenue
Argonne, IL 60439
Phone: (703) 678 7656; Fax: (630) 252-3443
E-mail: dsantini@anl.gov

Subcontractor: Electric Power Research Institute
Project lead: Argonne
Partner: IEA HEV & EV Implementing Agreement

Start Date: Oct. 2006
Projected End Date: Sept. 30, 2011

Objectives

- Examine li-ion electric drive battery chemistries
- Evaluate parallel, split and series powertrains
- Evaluate li-ion alternatives for electric drive – EVs, E-REVs, PHEVs, and HEVs
- Determine cell power and energy cost trade-offs, by chemistry (4+)
- Determine best electric drive system attributes to maximize U.S. electricity-for-gasoline substitution, and fuel use reduction, including HEVs.
- Estimate representative real world fuel & electricity use by electric drive vehicles.
- Determine likely early U.S. market for plug-in electric drive vehicles.
- Estimate WTW emissions and energy use by electric drive vehicle type and pattern of use.
- Work with the IEA HEV& EV Implementing Agreement to disseminate, reevaluate, and revise study results in an international context.

Technical Barriers

This project addresses the following technical barriers in the choice of battery chemistry and battery pack configuration in support of maximum market success of electric drive.

1. Initial costs of providing various mixes of power and energy in plug-in hybrid and electric vehicle batteries
2. Establishing a cost effective balance/mix of mechanical and electric drive in PHEVs
3. Achieving battery life cycle net benefits, given probable U.S. gasoline prices, considering trade-offs among:
   - Initial cost
   - Cycle life
   - Calendar life
   - Energy and power densities

Technical Targets

- Maximization of net present value benefits per kWh of grid electricity used. Evaluate chemistries, powertrains, pack kW and kWh, by target market.
- Determination of cost effectiveness of battery power and kWh energy storage relative to charging infrastructure costs (high kWh per pack and few charges/day vs. less kWh per pack with more charges)
- Determination of fuel saved per kWh used during charge depletion, by chemistry and powertrain type

Accomplishments

Draft and published information from the study to date includes estimates supporting the following points:

- To successfully market electrification of drivetrains, PHEVs and E-REVs are far superior to EVs.
- Car (or small crossover)-based parallel or split PHEVs with moderate power (50-70 kW) and energy (~ 6-10 kWh) are most cost effective options examined
- Suburbs appear to be the best target market for personal use electric drive vehicles.
- The perspective on economic viability of electric drive vehicles may be distorted (negatively) by present test protocols and resulting public information.
- PHEVs, E-REVs and EVs should be compared to conventional drivetrains in suburban driving conditions, as well as to HEVs.
- For personal use vehicles EVs are generally not economically attractive as “city cars”.
- Drivetrain electrification via blended mode PHEVs rather than E-REVs can most cost effectively reduce GHGs and extend fuel resources (enhance sustainability).
- EVs must be intensively utilized. EVs must deplete & recharge daily to be cost effective.

- Plug-in electric drive may never be universal, will take time to cut oil use.
- Best li-ion chemistries will likely vary across EVs, E-REVs, PHEVs, and EVs by pack volume and pack W/Wh ratio required.
- Very significant production volumes (hundreds of thousands) for battery packs will be necessary for li-ion based electric drive to occasionally be cost effective at present gasoline and electricity prices. Cost reductions via increased volume continue into the millions of units.

✧ ✧ ✧ ✧ ✧

Introduction

Achieving currently stated DOE cost and technical performance targets for electric drive (HEVs, PHEVs, EVs) may be sufficient to support cost effective near-term introduction of electric drive. However, by examining the market into which the various kinds of battery packs will "fit" (powertrain type, charge depletion strategy, vehicle size and function, driving behavior of probable purchasers, charging costs and availability), the advisability of adjusting cost and technical targets is investigated.

Approach

There are five candidate battery chemistries under evaluation to achieve DOE technical and cost targets for near-term use in light duty passenger vehicles.

(1) $LiNi_{0.8}Co_{0.15}Al_{0.05}O_2$/graphite (NCA-G),

(2) $LiFePO_4$/graphite (LFP-G)

(3) $Li_{1.06}Mn_{1.94}O_4/Li_4Ti_5O_{12}$ (LMO-TiO) and

(4) $Li_{1.06}Mn_{1.94}O_4$/graphite (LMO-G).

(5) $Li_{1.05}(Ni_{4/9}Mn_{4/9}Co_{1/9})_{0.95}O_2$/graphite (NMC-G)

This study includes development of a production cost model for these chemistries.

There are several powertrain options under development for plug in hybrid electric drive. Among these are: (1) power split, (2) parallel, (4) dual mode, and (3) series range extender. In this discussion, we label any plug-in electric hybrid which shares use of internal combustion and stored grid electric power during charge depletion a PHEV, while labeling any plug-in hybrid which normally operates all electrically during charge depletion an E-REV. Generally, the first three powertrain options readily become PHEVs while the fourth is well suited to be an E-REV. Nevertheless, for each it is possible to configure the powertrain to operate in charge depletion mode with varying shares of stored grid electric energy and on-board internal combustion power. This study includes assessment of production costs for alternatives among these powertrain options, taking into account the battery pack cost trade-offs identified in the battery cost model, and considering different choices of power and energy in battery packs installed in these powertrains. In addition, this study is also evaluating both hybrid (HEV) and battery electric vehicles (BEVs).

For near-term introduction, the charging infrastructure is divided into three categories, level 1 (ubiquitous 120 V, 15 amp AC circuits), level 2 (240 V, 20-80 amp AC circuits), and level 3 (480V, 80+ amp AC circuits). This study primarily considers the benefits of designing PHEVs to make the greatest use of level 1 charging, taking into consideration the potential to upgrade to level 2. Level 3 charging for electric vehicles is a secondary concern.

This study takes into account level 1 "plug availability" in proximity to parked vehicles (garage & carport locations) and the related patterns of vehicle use by households with readily accessible level 1 charging.

Results

Target Market for PHEVs. In general, it had been estimated that the market advantage for PHEVs in comparison to EVs and HEVs is at an average driving speed faster than for these powertrains. When combined with considerations of household income and garage/carport ownership, this implied that PHEVs will be most competitive in relatively low density suburbs.

For HEVs the dominant powertrain type is the split hybrid. The parallel HEV powertrain has a much smaller share of hybrids in light duty vehicles, but is the standard HEV technology in medium duty trucks. PHEV "spin-offs" of such HEVs are anticipated to be designed to have a power capability sufficient for all electric neighborhood and city core driving, but otherwise operate in "blended mode". In prior year evaluations of such PHEVs, simulation predicted that the distance to depletion will generally increase as driving speed and aggressiveness increase. Such behavior is being confirmed in field tests of Prius conversion PHEVs by Idaho National Laboratory. However, these conversion Prius PHEVs have far lower battery pack power than PHEVs previously simulated.

During this year, simulations of similarly sized PHEV passenger cars with battery pack power levels of 50-65 kW predict that consumer realized distances to charge depletion in real world driving will decrease significantly from rated values developed from dynamometer tests used for Corporate Average Fuel Economy ratings (Figure III-90). The predicted percentage decline was greater in simulations of E-REVs, which had battery pack peak power ratings of 148-158 kW and used only electricity during depletion. Initial presentation of results was made in early June, including a prediction of 25 miles of "real world" range for an E-REV40, and 64 for a BEV100. Coincidentally, following this presentation automakers

changed public statements about range, including values similar to these.

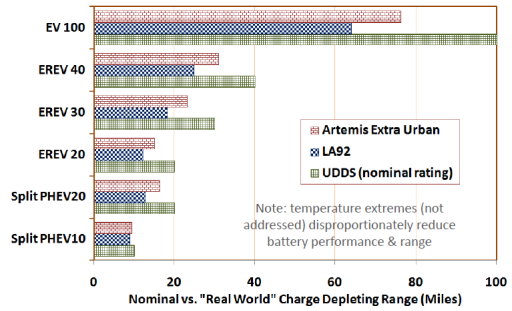

Figure III- 90: Predictions of real world vs. rated charge depletion distances for several plug-in electric vehicles

Battery pack costs: HEVs, PHEVs, E-REVs, EVs. In 2009, in our initial paper on battery cost modeling, we did not link vehicle simulation to the packs characterized, having used a constant kW rating for packs while altering kWh (presented at EVS24, May 2009). The National Academy of Sciences (NAS) subsequently published a prediction that the $/kWh for a PHEV10 and PHEV40 pack would be the same, at about $1000/kWh, while our constant kW results implied a sharp drop from a $1,000/kWh value for an HEV pack, based on cylindrical cells. A preliminary presentation was made in January 2010 at the Transportation Research Board Meeting to explain why our results looked so dramatically different. A known key reason was that the powertrain technologies being compared in the NAS study were very different, one being a short range PHEV (labeled PHEV10) and the other a long-range E-REV (labeled PHEV40 in the NAS study). In a forthcoming EVS25 paper [1] the link of battery pack cost and energy densities to powertrain type and attributes has been made. Other important changes to the cost model were made, including a switch to simulation of large format prismatic cells, adjustment of materials costs, and improved modeling of chemistries. Our 2009 $/kWh plot (Figure III- 91) is retained from last year to aid in understanding the changes.

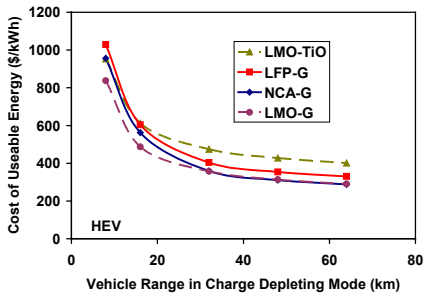

Figure III- 91: 2009 estimates of $/kWh for PHEV battery packs, holding pack kW at 60, and increasing kWh

Our considerably more comprehensive and complex plot of $/kWh costs for PHEVs and E-REVs follows (Figure III- 92). Major differences from the 2009 estimates are:

- Consistently lower $/kWh cost predictions
- Separation (downward) of LMO-G costs from other chemistries examined
- Chemistry limitations prevent use of two nickel based chemistries in a higher power/energy ratio HEV pack than evaluated in 2009
- The vehicle simulations no longer assume it is reasonable to include a PHEV40 design.

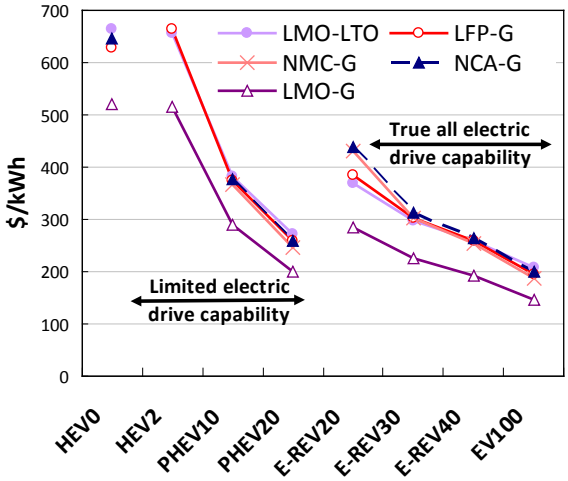

Figure III- 92: 2010 $/kWh estimates for HEV, PHEV, and E-REV battery packs, in different narrow kW brackets, as kWh rises

Unchanged is the prediction that the $/kWh cost of a pack for a plug-in hybrid with 40 miles of rated range will be considerably less than for one with 10 miles of range, despite the fact that the power for the former is over twice that of the latter. An unknown is whether or not the NAS study assumed liquid thermal management for the E-REV40 in comparison to air thermal management for the PHEV10. Estimates above assume air thermal management in both cases. Coming E-REVs do use liquid thermal management. Liquid thermal management will be examined in 2011.

Another very important source of variation in predicted cost incorporated into the battery pack cost model is production volume. For the LMO-G chemistry, Figure III- 93 shows how a choice to assume a production volume of 10,000 packs per year could cause much higher cost estimates than if our modeled values of 100,000 packs per year were used.

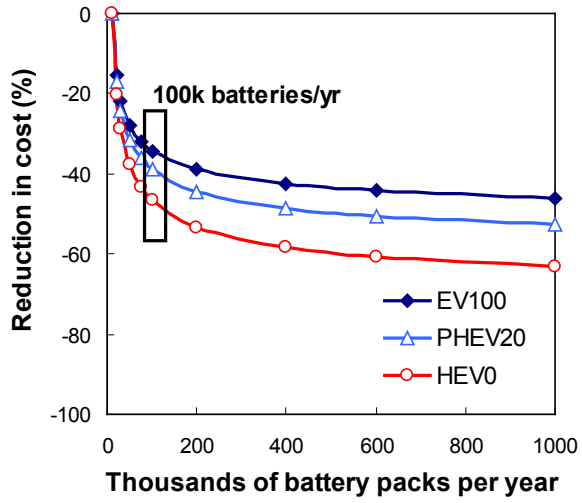

Figure III- 93: Percent decline in LMO-G pack cost vs. scale of manufacture beyond 10,000 battery packs per year.

As is evident, a number of the changes implemented to the battery pack cost model resulted from review of the 2009 version. Because of the 2009 paper, the U.S. Environmental Protection Agency (EPA) asked about the status of improvements and updates to the model. The study team provided copies of the model and a user's guide that were being developed in support of the overall project. Among models available to it, EPA concluded that this model was the most transparent and detailed, with the advantage that prismatic cells are characterized. Since the model was used by EPA as a reference point in conjunction with other information, the National Highway Transportation Safety Administration, working with EPA on future vehicle regulation, also requested and obtained a copy of the model. Other copies were provided as a courtesy to analysts evaluating battery pack costs for the California Air Resources Board, a governmental body also having authority to set standards based on best available information on the potential of electric drive options using future generations of lithium-ion batteries. EPRI was also provided a copy.

The model has benefitted from peer review and was adapted as a result. Additional comments from analysts that have been provided a copy of the model have been requested. The model will be documented and made generally available in FY 2011, later than anticipated.

During the year, a request was received from the sponsor to conduct a focused evaluation of HEV packs with higher power to energy ratios than had been examined in the FY 2009 analyses. A focused investigation was requested, related to HEV pack goals. This analysis was conducted and internal reports were provided to the sponsor. Although there are no immediate plans for separate documentation of that work, the focused investigations of various chemistries has led to modifications of the battery cost model, which have been incorporated, and will be included in the version documented. While this diverted effort that could have otherwise been used to complete the synthesis evaluation of simulated vehicles and packs, it should lead to a better characterization of incremental costs of implementing the plug in option in HEV powertrains in 2011.

Potential for Electric Drive Options vs. Gasoline. The technical potential to substitute miles driven electrically via PHEVs was estimated in 2009, also (as in the case of battery cost) based on rough approximations of hypothetical PHEVs. Investigation of patterns of daily use of vehicles for placement of chargers was included. This work was presented in a 2009 paper at the 88th Transportation Research Board Meeting, which was subsequently published in the Transportation Research Record [2]. The paper was awarded the Barry McNutt prize for best paper submitted to the Energy and Alternative Fuels Committees.

Costs of vehicles were not included in the 2009 investigation of technical potential. This year we begin to evaluate the cost effectiveness potential for electric drive based on the vehicle simulations constructed by EPRI, and on the retail price estimates for various powertrains constructed by EPRI. A paper was also submitted for possible presentation at the 90th TRB Meeting [3]. It is under revision in response to reviews, and is likely to be presented. Although these are simulations, several of the simulations are reasonable approximations of a coming short range PHEV, an E-REV40, and a BEV.

The National Household Travel Survey (NHTS) pattern of daily vehicle use continues to be utilized. In this paper the market was divided into vehicles traveling less than and more than 50 miles per day, which departed and returned to the same dwelling unit. About half of the total miles of travel were in each group. Average speeds (22, 39mph) and time of operation (0.9 and 2.6 hours/day) for vehicles in the two groups were contrasted, and real world driving appropriate to the speeds was simulated. The incremental benefit to cost ratio of choosing a specified vehicle instead of a reference split HEV was estimated for average operations of each set of vehicles.

For the vehicles driven at an average of 39 mph for 2.6 hours per day, plug-in electric drive begins to be broadly desirable relative to a hybrid if gasoline prices are $5/gallon (Figure III- 94). The hybrid, in turn, is far more desirable than the conventional gasoline powertrain. However, for the far more numerous vehicles that are driven 22 mph for 0.9 hours per day, the conventional gasoline powertrain remains more desirable than any electric drive option. The critical fact is that the high costs of the electric drive powertrains require very intensive daily use to pay back the original investment. Accordingly, in terms of number of vehicles for which electric drive powertrains are justifiable, the market is a

(big) niche market. However, given the intensive use of the vehicles for which benefits may exceed costs, the national fuel savings potential represents a much larger share of the fuel market than does the share of plug-in vehicles within the vehicle market.

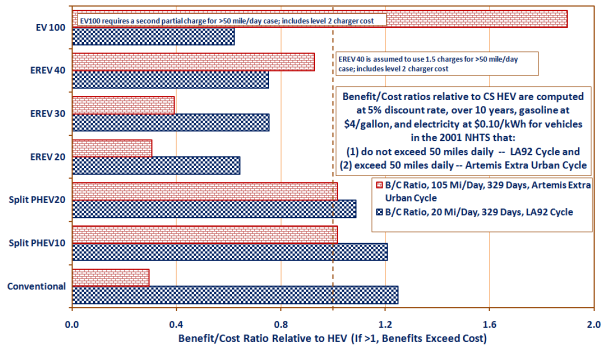

Figure III- 94: Incremental Benefit to Cost Ratio of Powertrains in Comparison to the Split HEV (red dotted line) at $5/gallon. (Cross group comparisons are not valid)

Although the common wisdom is that the EV is a city car, when compared to PHEV10s, PHEV20s, and E-REV40s, it is estimated to be the least desirable option in consistent slow speed urban driving. This is the case even without considering limitations of range and charging locations on days when the vehicle does not return to the dwelling unit at night.

At $3/gallon the split HEV is the most cost effective powertrain in the high daily use group. A manufacturer that pursues this option in the near term for the high use group can use it as a basis for future "spin-off" of PHEV10s and PHEV20s. As gasoline prices rose, these plug-in powertrains would be the first plug in electric drive option to become attractive for the low daily use group.

A judgmental interpretation is that the personal use EV could be attractive on a financial basis in suburban locations where the vehicle returns to the house during the day for a second charge, thereby avoiding the cost of a second charge point. High daytime electricity rates sought in conjunction with smart charging strategies would discourage this option. It would also be desirable for the EV to be a part of a set of vehicles that allowed the owner to use other vehicles for inter-city travel, thereby ameliorating concern over availability fast charging infrastructure between cities.

The cost analysis completed to date relies on a retail battery pack cost model chosen by EPRI and based on the nickel-metal hydride chemistry. 2007 evaluations in an MIT study included a generic plot of nickel metal hydride pack costs vs. lithium-ion costs as a function of production volume, going into the millions. Nickel metal hydride and lithium-ion pack costs intersected at a few hundred thousands, with lithium-ion dropping below nickel metal hydride thereafter. Accordingly, the battery retail price estimates here, which are for about a hundred thousand packs per year, are probably not significantly different than they will be when lithium-ion retail prices are estimated. The present model estimates wholesale, not retail prices.

In FY 2011, a retail price battery pack cost model based on lithium-ion chemistries will be developed. The implications of the comparison of retail vehicle price predictions with lithium-ion vs. nickel metal hydride will be investigated. It is quite possible that the important attributes of lithium-ion packs are found in the flexibility to provide power and energy in smaller, lighter packs, rather than packs of less $/kWh cost. Of particular interest is the cost and value of power, which the 2010 lithium-ion battery pack model addresses.

GHG emissions and sustainability. An observation made this year is that the top selling hybrids, which use body designs that lower aerodynamic drag and that reduce tire rolling resistance are not available with gasoline powertrains. The standard of comparison for scientific/academic analyses conducted to date has been to assume that both gasoline and electric drive are available in the same bodies and with the same tires. Attention is turning toward "real world" effects of implementation of electric drive. It may be more legitimate for a significant fraction of cases to compare gasoline powertrains in conventional bodies against electric drive powertrains in "lower load" bodies since this low load package appears to be what will continue to be offered in many cases. This issue was raised in the Santini et al presentation at Plug-in 2010 [7]. It is anticipated that vehicle simulation investigations to isolate the magnitude of the "real world" fuel saving and GHG reduction effect in the actual marketplace will be conducted next year.

With respect to GHG emissions results, some inherent conflicts between smart charging goals and GHG reduction goals were noted in a webinar presentation [9].

Note:

Thanks to the efforts of the team of analysts contributing to this project, on January 29 at the Society for Automotive Engineers' (SAE) Government/Industry Meeting in Washington DC, Dr. Santini was given the SAE Barry D. McNutt award for Excellence in Automotive Policy Analysis "His nomination focused primarily on his technical analysis and leadership in the PHEV arena; and his technical expertise has contributed directly to more effective federal R&D policy for PHEVs." Though also named in honor of Barry D. McNutt, this is a separate award from the TRB paper award mentioned elsewhere. Dr. Santini is more an interpreter of excellent technical analysis done by team members than an originator of such analysis. The award is clearly a credit to

those named in publications generated by this project, and the project itself.

Conclusions and Future Directions

Appropriate evaluation of the financial merits of electric drive requires prediction of the driving behavior of most probable owners. The near-term target market for personal light duty HEVs, PHEVs, E-REVs and EVs is the suburbs, for consumers who drive more than two hours a day. Despite conventional wisdom, the EV does not appear to be an attractive "city car" for U.S. consumers, due to a rate of vehicle utilization too low to recover high capital costs. It appears more likely that the "sticky" EV market niche would be in a multi-vehicle household, providing local trips, particularly if the intensity and pattern of use can support more than one charge per day at the house. For a given amount of battery capacity per vehicle, if all consumers were to purchase vehicles with electric drive from plugging into the grid, the most miles electrifiable per kWh produced would be obtained if the packs were in PHEVs and E-REVs rather than EVs. Between PHEVs and E-REVs, 2010 evaluation implies that PHEVs of 10-20 miles of range look more attractive financially than E-REVs of 20-40 miles of range. Battery pack costs per kWh drop very sharply when one compares a PHEV to an HEV, but drop much less sharply when one compares an EV to a PHEV. According to this year's estimates, the costs of providing adequate battery pack power to assure all-electric drive rather than blended mode operation during charge depleting operation has a negative effect on the financial viability of E-REVs. This result is preliminary. It depends on the cost and fuel saving value of battery pack power (regenerative braking effects). Costs of power may be more favorable with some of the lithium-ion chemistries than presently modeled by EPRI. This will be investigated further next year.

The lithium-ion battery pack cost model will receive further review and will be documented for general use early next calendar year. This year's financial effectiveness results by powertrain type (prepared by EPRI) will be documented. Results will then be re-evaluated and extended in conjunction with international consultations under the IEA HEV and EV Implementing Agreement's study of Plug-in Hybrid Electric Vehicles (Annex XV). These revised investigations will make use of the first release of the battery pack cost model. Infrastructure costs (charge circuit upgrades, charge point installations) will be incorporated in greater detail.

FY 2010 Publications/Presentations

Publications

1. Santini, D.J., K.G. Gallagher, and A.P. Nelson. *Modeling of Manufacturing Costs of Lithium-Ion Batteries for HEVs, PHEVs, and EVs*. The 25th World Battery, Hybrid and Fuel Cell Electric Vehicle Symposium and Exhibition (EVS-25). Shenzhen China Nov. 5-9, 2010.
2. Vyas, A., D. Santini and L. Johnson. *Plug-In Hybrid Electric Vehicles' Potential for Petroleum Use Reduction: Issues Involved in Developing Reliable Estimates. Paper and poster presentation* Transportation Research Record 2139 pp. 55-63 (past conference publication republished in TRR and awarded Barry D. McNutt prize by the Energy and Alternative Fuels Committees).
3. Santini, D.J., A. Vyas, D. Saucedo, and B. Jungers. *Where Are the Market Niches for Electric Drive Vehicles?* Submitted Aug. 1 2010 to be considered for presentation in the 2011 90th Annual Meeting of the Transportation Research Board, January, Washington DC.
4. Santini, D.J. *Highway Vehicle Electric Drive in the United States: Current Status and Issues*. Argonne National Laboratory Report, forthcoming.

Presentations

5. Santini, D. Cost Effective PHEV Range: Battery Costs vs. Infrastructure Costs. Presented at the 89th Annual Meeting of the Transportation Research Board. Washington DC. Jan. 12, 2010.
6. Vyas, A. and D. Santini. On the Cost Effectiveness of Electric Drive in Suburbia. Presented at the TRB Environment and Energy Research Conference, Raleigh, NC, June 7, 2010
7. Santini, D.J., A. Vyas, Saucedo, D. and B. Jungers. Market Implications of Synergism Between Low Drag Area and Electric Drive Fuel Savings. Presented at Plug-in 2010. San Jose CA. July 28, 2010.
8. Saucedo, D. Vehicle Systems Modeling: What's in the numbers? Presented at Plug-in 2010. San Jose CA. July 28, 2010.
9. Santini, D. Regulatory Influences That Will Likely Affect Success of Plug-in Hybrid and Battery Electric Vehicles. Clean Cities Quarterly Webinar on Electric Drive. Sept. 16, 2010

III.C.3 Battery Life Trade-Off Studies (NREL)

Kandler Smith
National Renewable Energy Laboratory
1617 Cole Blvd
Golden, CO 80401
Phone: (303) 275-4423
E-mail: kandler.smith@nrel.gov

Start Date: FY08
End Date: on-going

Objectives

- Develop techno-economic models that quantify battery degradation over a range of real-world temperature and duty-cycle conditions.
- Develop physically-based, semi-empirical battery life prediction models for the life-trade off studies.
- Identify systems solutions and controls that can reduce the overall lifetime cost of electric-drive-vehicle batteries.
- Identify impact of alternative business models (e.g. battery leasing/swapping) and use scenarios (e.g. vehicle-to-grid cycles) on battery life and cost.

Technical Barriers

- Achieving 10-15 year battery life in disparate thermal/geographic environments and duty-cycles
- Appreciable cost of PHEVs and EVs driven by conservative battery designs employed in order to reduce warranty risk
- Lack of models and methods to perform economic and engineering analyses related to battery life.

Technical Targets

- 10-15 years calander life for batteries used in electric drive vehicles suchs as HEVs, PHEVs, and EVs.
- Develop strategies to enable 10-15 year PHEV and EV battery life in challenging thermal and duty-cycle environments
- Develop models and analysis tools to understand impact of real-world duty-cycles and scenarios on battery life.
- Validate battery life models using both accelerated laboratory and real-world data.

Accomplishments

- Compiled a composite dataset from multiple laboratories describing graphite/nickel-cobalt-aluminum (NCA) Li-ion battery degradation over various temperatures and cycling conditions.
- Based on degradation mechanisms reported in DOE Gen II and other studies, formulated a physically-justified, semi-empirical life model that describes the full composite dataset.
- Coupled battery life and cost models to develop guidelines for PHEV battery sizing for specified years life under various thermal and cycling conditions.
- Quantified battery degradation under challenging scenarios, including operation in hot climates.
- Quantified the value of battery thermal management by equating incremental improvements in thermal management design to reducing overall battery cost.

Introduction

Electric-drive vehicle (EDV) batteries face significant challenges to achieve long life on par with conventional vehicles. Unlike consumer batteries, automotive batteries reside in a severe thermal environment and face challenging duty cycles. HEV NiMH batteries presently achieve 10+ years of life by only using a small portion, less than 25%, of their total energy. An HEV battery's long life is thus achieved with a four-fold mark-up in cost. To achieve electric-only drive capability, PHEV batteries contain greater than 10 times the useable energy of HEV counterparts. Clearly, over-sizing a PHEV battery similar to the present HEV practice would result in unreasonably large battery packs and expensive vehicles. For PHEVs to be accepted into the market, it is critical to optimize batteries for minimum size and cost but still achieve 10+ years of life in a variety of demanding hot and cold environments.

For successful introduction of EDVs, worst-case real-world conditions for battery aging must be quantified and understood, as these conditions drive the need to oversize batteries. In some cases, systems solutions and controls can be added to lessen the impact of the stressor on battery wear. Ultimately, battery life and cost are intimately related. The cost of any additional system to extend battery life must outweigh the savings that can be realized by implementing a smaller battery in a given vehicle.

In FY10, the life model was expanded and fit to additional graphite/nickel-cobalt-aluminum (NCA) Li-ion datasets beyond FY09, including results from vehicle battery tests conducted at National Laboratories to ensure realistic life predictions. While the FY09 model considered cycling-effects only or temperature-effects only, the FY10 model has full flexibility to consider any arbitrary temperature and duty-cycling scenario. Combined with simple cost and performance models, FY10 trade-studies quantified battery life/cost benefits of various types of active cooling (e.g. air vs. liquid), standby cooling and thermal preconditioning systems. In FY11, NREL will fit the life model to additional Li-ion chemistries, initiate validation studies with real-world vehicle fleets, and perform statistical analyses to quantify design margin necessary to meet warranty requirements for various real-world duty cycles.

Approach

Based on degradation mechanisms reported in DOE/ATD/ABR Gen II (Christophersen, 2006; Abraham, 2007) and other studies, NREL formulated a physically-based, semi-empirical battery life model. The model is readily fit to laboratory-accelerated and real-time aging data. It considers separate terms for mechanical stress related to electrode cycling and chemical/ electrochemical stress related to time accumulated at various temperatures and voltages.

Calendar-driven fade is attributed to growth of a resistive solid-electrolyte interface (SEI) layer at the electrode surface. SEI growth increases cell resistance and consumes cyclable Li from the system. Calendar resistance growth and capacity fade are assumed to be proportional to the square-root of time, $R_{SEI} \sim a_1 t^{1/2}$, $Q_{Li} \sim b_1 t^{1/2}$.

Cycling-driven fade is predominantly attributed to mechanical expansion/contraction of electrodes resulting in stress and fracture. This mechanical stress causes loss of electrode active sites, reducing capacity and increasing resistance. Cycling resistance growth and capacity fade are assumed to be proportional to the number of cycles, $R_{sites} \sim a_2 N$ and $Q_{sites} \sim c_1 N$.

The correlation of acceleration factors accounting for various stressors is a unique feature of the model that enables interpolation/extrapolation to scenarios other than those tested by experiment. Formulas for the various acceleration factors are taken from the literature and seen to agree well with the data. Temperature dependence is described with an Arrhenius formula, voltage dependence is described with a Tafel formula, and cycling-related depth-of-discharge stress is described with a Wöhler power-law formula. The afore-mentioned rate constants a_1, a_2, b_1, c_1 thus have functional dependence on T, V and ΔDoD. A model fit to parametric aging data for various T, V and ΔDoD stress levels can thus make predictions for other arbitrary scenarios.

Results

Life Model Fitting. The model was fit to datasets for the NCA Li-ion chemistry shown in Table III- 27, leveraging existing studies from multiple labs. For vehicle batteries, end-of-life is typically defined when power and energy fades to 70% to 80% of initial beginning-of-life performance. In this region, performance fade is relatively graceful. As degradation proceeds beyond 70% fade, often a "knee" in the curve is reached, beyond which battery degradation becomes quite rapid. With the expectation that properly designed vehicle batteries will operate in the graceful-fade region, only that region was used for fitting the present model.

Table III- 27: Datasets used for fitting NCA/graphite Li-ion life model.

	Test	Source	Temperature	End-of-Chg. or Storage Voltage	Depth-of-Discharge	Cycles/day
Fitted Data	Resistance Growth	Broussely (Saft), 2007	20,40,60°C	3.6,4.1V	Storage	0
		Hall (Boeing), 2006	20°C	3.9,4.0,4.1V	20,40,60,80%	1,4
	Capacity Fade	Smart (NASA), 2009	10,23,40,55°C	3.6V	Storage	0
		Broussely (Saft), 2001	20°C	3.6,4.1V	Storage	0
		Hall (Boeing), 2006	20°C	3.9,4.0,4.1V	20,40,60,80%	1,4
Validation Cases	HEV combined cycling + calendar	Belt (Idaho Nat. Lab.), 2008	30,45,53°C	3.6V	1.5%	95,290,500
	PHEV accelerated cycling	Gaillac (S. Calif. Edison), 2009	25°C	4.0V	75%	4

An example of model fitting is shown in Figure III-95, using data from a study of Saft VES-140 cells tested for geosyncrounous satellite application by Boeing (Hall, 2006). First, resistance growth trajectories from eight different cycling conditions were separately fit with models $R = a_1 t^{1/2} + a_2 N$. Next, functional dependence of a_1 and a_2 on T, V, and ΔDoD were determined. Figure III-95(a) shows that, once each fade rate is corrected for different voltage exposure using a Tafel model, the growth of relative resistance per cycle, a_2, can be readily correlated with ΔDoD using a Wöhler power-law model. With just a few coefficients capturing the effect of voltage and ΔDoD stressors, a single global model readily reproduces all eight test conditions shown in Figure III-95(b).

Comparing Model with HEV & PHEV Technologies. Aging studies used for model-fitting were from cells designed and tested for aerospace applications. To ensure the model is consistent with present-day vehicle battery technology, the model was also compared with two vehicle battery aging datasets.

Figure III- 96(a) shows the model compared to data from Idaho National Laboratory (Belt, 2008) where a JCS HP12LC NCA-chemistry HEV cell was shallowly cycled (1.5% ΔDoD) at various temperatures and with different number of cycles per day. It can be seen that the

temperature dependence from other NCA datasets also describes this dataset well. Model agreement worsens at high temperatures >45°C, indicating a separate high temperature fade mechanism may exist that is not captured by the present model.

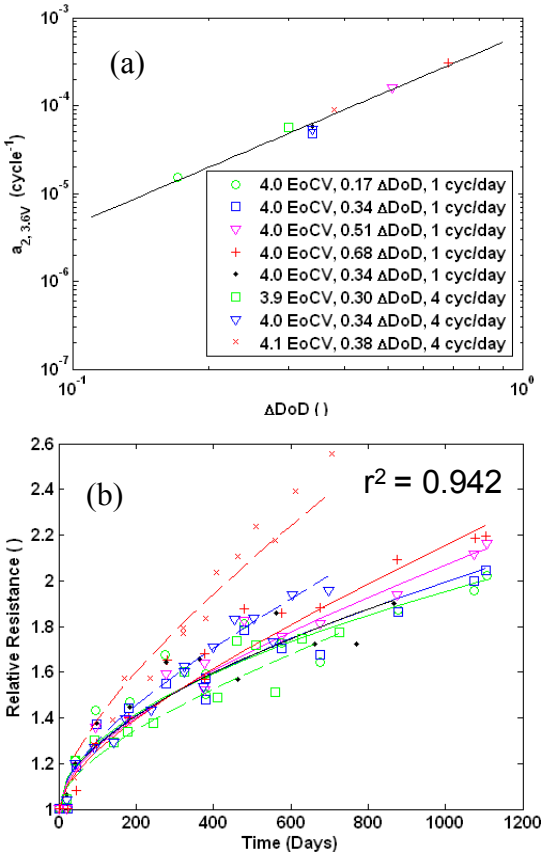

Figure III- 95: Fitting of life model to Saft VES-140 dataset for geosyncronous satellite application (Hall, 2006). (a) Cycling-related resistance growth dependence on depth-of-discharge. (b) Comparison of final global model with data.

Figure III- 96(b) shows the model compared to data from Southern California Edison (Gaillac & Pinsky, 2009) where a 40 Ah JCS VL41M NCA-chemistry PHEV cell was deeply cycled (75%ΔDoD) at 25 °C using a dynamic stress-type power profile repeated four times per day. Unlike the shallowly cycled HEV cell, the PHEV cell shows a more linear fade trajectory. The life model predicts electrode site loss dominates capacity fade under this test condition. If cycling were less frequent, say one deep cycle/day, the life model predicts Li loss would control capacity fade. So while the accelerated cycling tests may be useful in validating life for cycling-intense applications, there is some question how well suited they are to extrapolate years-life for a typical PHEV/EV consumer that cycles their battery just once per day.

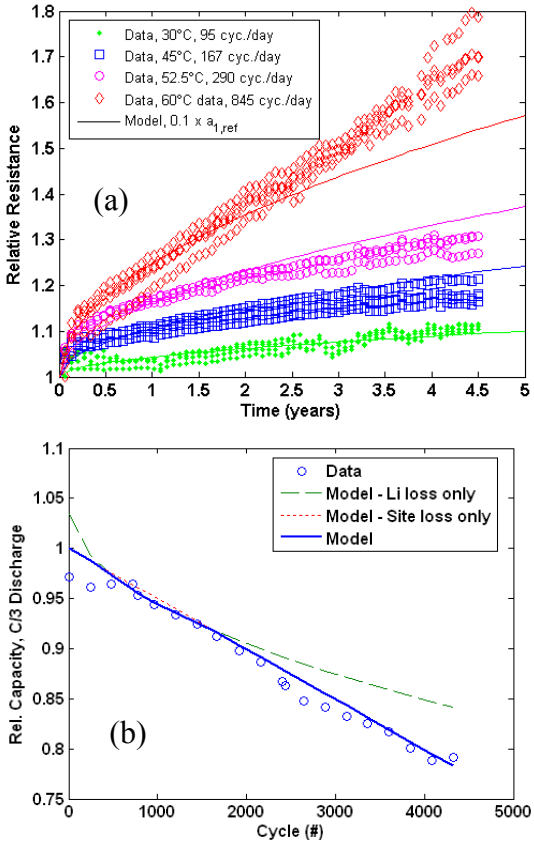

Figure III- 96: Comparison of life model with vehicle battery aging data. (a) JCS HP12LC cell tested under HEV cycle (Belt, 2008). (b) JCS VL41M cell tested under PHEV cycle (Gaillac, 2009).

Trade-off studies. NREL used the life model to develop a procedure for sizing a battery based on power and energy requirements at the end-of-life. Either a power-optimized design or an energy-optimized cell design can satisfy a given life/performance requirement, though the two designs will need different amounts of beginning-of-life energy and power margin to meet the requirement. Compared to a low power battery, a high power battery can better access energy at the bottom-of-discharge, meaning that charge sustaining operation can be achieved at very low SOCs, which can be especially important at end-of-life when a battery has faded. For the same energy content, the high power battery is slightly more expensive, however. Combining a simple cost model with the life model, we are able to identify optimum power-to-energy ratios that result in a minimum cost battery for a given application. When designing a battery, it is preferable to oversize on power rather than energy, by selecting a cell with slightly higher power-to-energy ratio than might be needed. Oversizing on energy means expensive active matieral goes unused. Oversizing on power means more energy is accessible at low states-of-charge and the battery generates less heat while driving.

Figure III- 97 shows the cost of various batteries optimized for 1 deep cycle/day operation at various temperatures and sized to last for 5, 10, or 15 years. The simple cost model

$/pack = 11.1*kW + 224.1*kWh + 680

reflects high-volume production cost to manufacturer. The $320-$440/kWh cost predictions in Figure III- 97 are perhaps half of today's low-volume-production battery costs. Figure III- 97(b) shows that the incremental cost of sizing a battery for one additional year of life is small, just 1% to 1.5%. This indicates that sizing a battery slightly larger to achieve a few extra years of life is preferable to periodically replacing a smaller battery, say every 5 years. The incremental cost of temperature exposure is larger, with battery cost increasing 3.5% to 5% as the battery is resized for each 5°C in battery storage/operating temperature. This indicates that sizing a battery for hot climates, and/or oversizing a battery to compensate for poor thermal control can be expensive.

The life model was also used in a trade-study to investigate the impact of different battery thermal management techniques on PHEV20 battery size and cost to achieve 10 years life in Phoenix, Arizona (Smith, 2010). Under an assumed duty-cycle, battery pack size and cost varied as much as 10% depending on whether liquid cooling, air cooling, or no cooling was used to reduce battery temperature excursions while driving. A hypothetical low impedance cell was also considered, as such a cell is sometimes proposed to reduce heat generation rate and temperature rise. The low impedance/high power cell has a high upfront cost, however. The air-cooled, low-impedance battery design was found to be more costly than a nominal-impedance system with no active cooling (sized with more cells to accommodate its faster degradation). The conclusion is that effective thermal management is cheaper than sizing a battery with substantial excess power to reduce heat generation rate.

To achieve a long-life low-cost battery, active thermal management while driving is only one part of the solution. Battery calendar aging takes place all 24 hours of the day – not just during the one hour or so of daily driving. Provided an EV or PHEV is grid-connected while parked, battery standby cooling and thermal preconditioning (prior to driving) can also be effective methods to reduce battery average and peak temperatures. A preconditioning study found that EV battery capacity fade could be reduced by ~5% in a Pheonix-like environment by using a preconditioning system that lowers battery temperature by 8°C in the 20 minutes prior to driving (Barnitt, 2010).

Conclusions and Future Directions

Optimizing a battery system for long life and low cost requires (i) understanding of battery life under worst-case

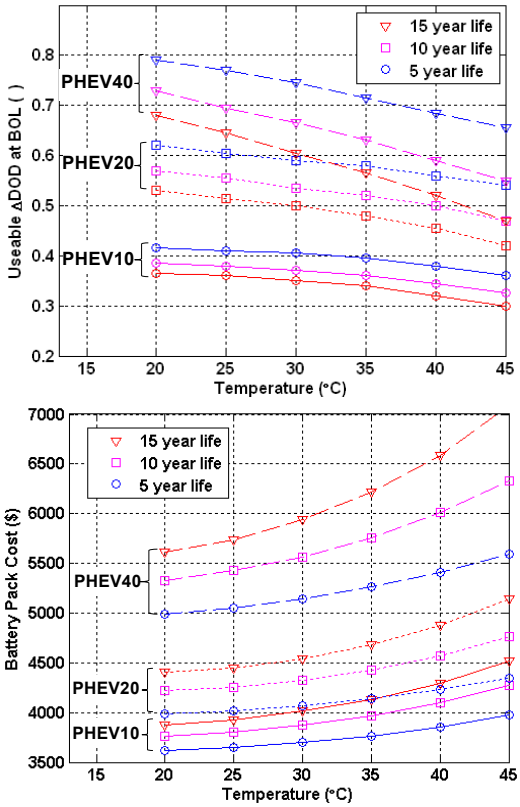

Figure III- 97: Battery cost and useable depth-of-discharge at beginning-of-life for PHEV batteries sized for various years life and temperature. Each case is optimized to select a power-to-energy ratio that minimizes cell cost.

aging conditions and (ii) development of systems that can minimize the effect of those conditions. Battery life models are useful for interpretation of multiple aging datasets and enable trade-off comparison of battery life under various scenarios. Calendar fade is often a dominant factor in determining whether an automotive Li-ion battery can last 10-15 years. Attributed to Li-loss from the system, this calendar fade may also be coupled with cycling as the SEI layer is fractured and regrown. Going forward, identification of the correct physical model for life-prediction is critical to enable proper extrapolation of accelerated cycling and calendar test results to real-world temperature and duty-cycle conditions.

FY10 trade-studies quantified excess power and excess energy to meet various years-life requirements at minimum battery cost. The incremental cost of upsizing a battery to achieve a few extra years life is small, indicating that replacing a battery halfway through a vehicle's life is not warranted. To accommodate uncertain aging conditions, it is preferable to slightly oversize a cell on

power rather than energy as excess active material is expensive. Effective thermal management appears to be a cheaper solution for achieving long life compared to drastically oversizing a battery on power to reduce heat generation rate. Thermal management systems that can draw temperature slightly below ambient, including while the vehicle is parked will be cost-effective in meeting battery life requirements with a cheaper, smaller battery.

In future work, NREL will expand the present NCA-chemistry life model to other Li-ion chemistries. NREL will also work to validate the life model with real-world data collected from vehicle fleets and test data from other National Labs. In conjunction with the DOE Computer-Aided Engineering of Batteries (CAEBAT) program, NREL will use more sophisticated physics-based degradation models to increase the fidelity of life predictions and help reduce the experimental burden of battery life validation.

FY 2010 Publications/Presentations

1. T. Markel, K. Smith, A. Pesaran, "Improving petroleum displacement potential of PHEVs using enhanced charing scenarios" Chapter 8 in *Electric and Hybrid Vehicles,* G. Pistoia ed., Elsevier, 2010.
2. K. Smith, A. Pesaran, "Opportunities for improving thermal design of electric-drive vehicle batteries," EV Battery Technology Conference, Troy, MI, Sept. 2010.
3. K. Smith, T. Markel, G.-H. Kim A. Pesaran, "Design of electric vehicle batteries for long life and low cost: Robustness to geographic and consumer-usage variation" IEEE Accelerated Stress Testing and Reliability Workshop, Denver, CO Oct. 2010.
4. R. Barnitt, A. Brooker, L. Ramroth, J. Rugh, K. Smith, "Analysis of off-board powered thermal preconditioning in electric drive vehicles" 25th Electric Vehicle Symposium, Shenzhen, China, Nov. 2010.

III.C.4 Battery Lease Analysis - Battery Ownership Model (NREL)

Ahmad Pesaran (Principal Investigator)
Michael O'Keefe
Jeremy Neubauer

National Renewable Energy Laboratory
1617 Cole Boulevard, Golden, Colorado 80401-3393
Phone: (303) 275-3084
E-mail: Jeremy.Neubauer@nrel.gov

Start Date: FY2009
Projected End Date: FY2012

Objective

- Continue the analysis of the technical and economic feasibility of various battery ownership business approaches including the battery lease-and-swap concept for accelerating the affordability of electric vehicles.
- Understand how battery performance, life, and usage affect cost and other engineering parameters over various vehicle powertrain types, business scenarios, geographic locations, and price forecasts.

Technical Barriers

There are many proposal, strategies, and activities taking place around the United States and the world to use electric traction drive powertrain vehicles together with various degrees and types of charging infrastructure: fast charging, distributed level 1 and/or 2 charging, and battery swap stations. Lack of a robust techno-economic analysis tool hinders evaluation of technical and economical merits of various approaches. This barrier is addressed by this activity involve using systems approaches with infrastructure and opportunity charging to explore the use of these approaches to reduce the sensitivity of total end-user cost to today's battery cost, life, and performance.

Technical Targets

This project is ultimately related to the cost and performance targets for batteries for hybrid, plug-in hybrid, and pure-electric vehicles. We use the technical targets within our analysis to determine if there are system benefits to be had from the electric vehicle charging infrastructure.

Accomplishments

At the end of FY09, we had constructed a working model and had performed a preliminary comparison of the costs of operating an EV to the costs of operating other types of vehicles. In FY10, the model was significantly updated as follows:

- Service provider financial model refined
- Vehicle and battery resale model revised
- Optimization algorithm improved
- Hawaii specific driving profiles and forecasts for gasoline and electricity price added

Following the above updates the following completed:

- The model was thoroughly scrutinized and revalidated against available real world data.
- New parametric runs performed to find the sensitivity of the results to the input parameters, particularly to the local specifics of State of Hawaii.
- The capabilities of the model and these results were documented in a peer reviewed technical paper at the 25th Electric Vehicle Symposium (EVS-25) in November, 2010.

✧ ✧ ✧ ✧ ✧

Introduction

Wide-scale consumer acceptance of alternatives to conventional gasoline-powered vehicles (CVs) such as hybrid electric vehicles (HEVs), plug-in hybrid electric vehicle (PHEVs), and pure electric vehicles (EVs) will depend on their cost-effectiveness and their functionality, including driving range and ease of refueling.

A number of technical and business strategies have been proposed and/or deployed to enable the transition to these alternative powertrain technologies affordable. These include: the electric utility utilization of the vehicle batteries as a distributed resource; battery leasing by a service provider who takes on the risk and upfront cost of battery ownership; public infrastructure development to recharge electric vehicles while parked; fast-charge and/or battery swap stations that effectively extend EV range; and alternative car ownership models that allow users to own an EV but rent other vehicles for long-distance excursions. Each strategy has unique implications to the vehicle design, local fuel and electricity cost structure, operating characteristics, and battery life. Accordingly, it can be

challenging to compare different strategies system options on a consistent basis.

To address this issue, the U.S. Department of Energy's (DOE's) National Renewable Energy Laboratory (NREL) has developed a computer tool called the *Battery Ownership Model* (BOM). We will briefly describe the tool here and give an example of its use.

Approach

The purpose of the battery ownership model (BOM) a techno-economic evaluation tool is to calculate the cost of vehicle ownership under various scenarios of vehicle and component cost, battery and fuel price forecasts, driving characteristics, charging infrastructure cost, financing, and other criteria. The vehicle economics that are considered include vehicle purchase, financing, fuel, non-fuel operating and maintenance costs, battery replacement, salvage value, and any costs passed on by a third-party such as a service provider to account for the installation, use, and availability of infrastructure.

There are many reasons why an individual car buyer chooses one vehicle over another. Economics is an important factor for individual consumers, but there are many other factors that impact the purchasing decision as well. For end-users such as fleet owners, economics is one of the top factors for purchasing. In addition, the economics of technologies can aid policy makers in decision-making. Thus, there is a strong motivation to look at the economics of vehicle technologies to see how they compare against each other. As such, the primary output of the BOM provides an economic indicator of end-user net present costs called "levelized cost per mile" (LCPM). The LCPM economic metric is defined as follows:

$$LCPM = \frac{\sum_{i=1}^{N} c_i \cdot d_i}{\sum_{i=1}^{N} vmt_i \cdot d_i} \qquad (1)$$

The variable *c* is the cost to the end user during the given period, *i*. The discount factor for the given period is *d*. Finally, the vehicle miles traveled for the given period is *vmt*. The total number of periods is represented by *N*. The BOM consists of nine modules as shown in Figure III- 98. The model is currently written in Microsoft Excel.

Figure III- 98: Overview of the battery ownership model with its nine sub- modules

The nine modules are: Location-Specific Data Module; Vehicle Performance and Sizing Module; Vehicle Component Cost Module; Battery Cycle Life Module; Electricity Usage Module; Infrastructure Requirements Module; Service Provider Economics Module; Greenhouse Gas Accounting Module; and Driver Economics Module.

Results

The following provides example results to show the utility. All currency reported in the results section is in year 2007 United States dollars.

Levelized Cost per Mile Validation. As a means of validation, we compared our LCPM prediction for various CVs with existing data sources. This comparison appears in Figure III- 99. The reference gasoline forecast case for U.S. average conditions is assumed along with 5 years of ownership. The data labeled as "AAA" is referenced from online documentation [1]. The Ward's data [2] were adjusted to the U.S. average annual VMT of 12,375 miles/year in 2005 [3]. Data listed as "IRS mileage reimbursement" correspond to the federal reimbursement rate of 55 cents per mile (in 2008) used to calculate the deductible costs of operating an automobile for business, charitable, medical or moving purposes when filing tax returns [4].

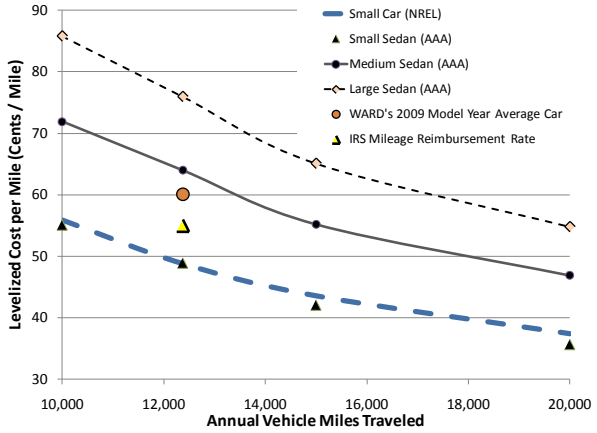

Figure III- 99: Comparing levelized cost per mile from various sources with the results of the battery ownership model

The NREL-predicted LCPM compares well with the data provided by AAA for a small car. Depending on the type of vehicle driven and how far it is driven each year, LCPM can vary significantly. At the 2005 U.S. average VMT of 12,375 miles/year, LCPM varies between $0.49 per mile and $0.76 per mile, depending of the vehicle driven. It is noteworthy to compare the cost of advanced technology vehicles against the range of what people spend for conventional transportation.

Scenario Analysis. In this section, we present an example demonstrating some of the capabilities of our model. A midsize car is assumed to be owned by one owner for 15 years. Four powertrain options for this vehicle are examined: a gas power conventional vehicle (CV), HEV, a PHEV with 40 miles of electric range (PHEV40), and an EV with 100 miles of electric range (EV100). The EV is directly owned by the end user and assumed to be charged once per day at home. Due to time and space constraints, an EV with a service provider option is not addressed. The components in each vehicle powertrain are sized by the program to yield equivalent acceleration performance: 0 to 60 mph in ~10 seconds. Note, however, that the EV100 does not have the same utility as the other vehicles due to the lack of a service provider infrastructure such as fast charging or battery swap for extended range operation. For all powertrain options, we assume the vehicle owner makes a down payment of 20% of the upfront purchase costs with a total sales tax rate of 7% and finances the balance over 5 years at a loan rate of 8%. Inflation is assumed at 2.5%. The end user is assumed to value money at an annual 8% discount rate. Seven design variables (D*i*) are examined as shown Table III- 28.

Table III- 28: Design Variables Examined in this Study

Variable	Min	Max
D1: GHG Market Cost (2007 U.S. Dollars/Ton CO_2e-Year)	0.00	28.53
D2: Federal Tax Incentive (2007 U.S. Dollars)	0	7,500
D3: Gasoline Cost Forecast	EIA Reference Oil-Price	EIA High Oil-Price
D4: Annual Distance Driven (Miles/Year)	9,059	15,691
D5: Vehicle Auxiliary Load (W)	700	2,200
D6: Battery Energy Cost Coefficient (2007 U.S. Dollars / kWh)	350	700
D7: Battery Life Coefficient	86 (low cycle life)	433 (high cycle life)

The design variables include cost for GHG emissions in dollars per ton of CO_2 equivalent emitted per year, the amount of federal tax incentive offered to buyers of the EV100 and PHEV40, the EIA gasoline forecast scenario used: reference or high-oil price case [5], the annual VMT per year, the magnitude of accessory loads on the vehicle from 0.7 to 2.2 kW, the battery energy cost coefficient, and finally, the battery life coefficients representing different battery life curves [6].

Over the range of design variables examined, the model predicts fuel economy to be between approximately 26 and 32 mpg for the CV and 35 and 44 mpg for HEV. The PHEV40 has aggregate fuel consumption between 54 and 74 mpg gasoline and 103 to 128 Wh/mile electricity, while the EV100 consumes between 248 and 353 Wh/mile. Accessory load is a major driving factor behind the change in fuel consumption rate of electric traction drive vehicles as has been observed elsewhere [7].

The range of variation in vehicle levelized cost ratio over the full factorial of all simulated runs is given in Figure III- 100. Vehicle *levelized cost ratio* is the vehicle's LCPM divided by the CV LCPM for a given scenario. The majority of the EV100's cost is due to the cost of the battery pack. Therefore, it is not surprising that the EV100 shows a large variation in *cost ratio* over the design variables examined. All vehicles, including the EV100, may achieve a cost ratio below 1.0 over some of the scenarios (the minimum EV100 cost ratio is 0.99).

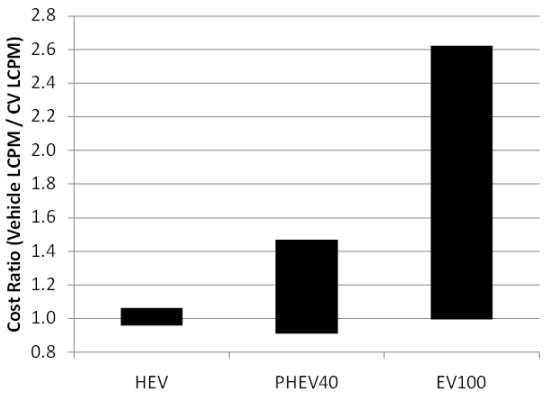

Figure III- 100: Range of vehicle levelized cost ratio

Figure III- 101 shows the sensitivity of the vehicle levelized *cost ratio* to the design variables listed in Table III- 28. Sensitivity to a given design variable is calculated from the full factorial levelized *cost ratio* results by first taking the absolute value of the difference between the average *cost ratio* at the high and low settings of the design variable. All sensitivity values were then divided by the largest of all sensitivities seen to normalize the maximum sensitivity to a value of one. The sensitivity of vehicle levelized *cost ratio* to design variable interactions with each other is not plotted.

The EV100 vehicle levelized *cost ratio* is most sensitive to battery costs, but also shows considerable sensitivity to battery cycle life. After that, the presence of a federal tax incentive, assumptions on gasoline cost, annual distance driven, and magnitude of vehicle auxiliary loads all have approximately equal effect on the EV100 levelized cost ratio. GHG market cost does not seem to be a large economic driver in and of itself over the range of assumptions examined.

Conclusion and Future Directions

Multiple new powertrain configurations, infrastructure options, and business strategies are being suggested for future electric drive vehicles. To comparatively investigate these business approaches, NREL developed a new techno-economic model called the *Battery Ownership Model*. The model uses the present value metric of levelized cost per mile of owning and operating an EV under various business strategies and compares it with those of CV, HEV, and PHEVs. This paper focused on giving an overview of the model and illustrated some of the model inputs. We also presented an example analysis that investigated the sensitivity of vehicle levelized cost ratio to seven design variables. The vehicle levelized cost ratio for an EV with a 100-mile range was found to be most sensitive to battery cost and cycle life with accessory loads, annual distance traveled, the existence of a tax incentive, and gasoline cost assumptions all having a secondary though approximately equal effect over the range of design variables examined.

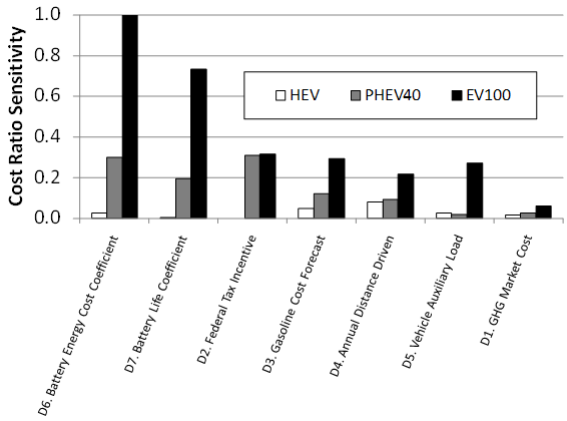

Figure III- 101: Sensitivity of vehicle levelized cost ratio to design variables

In future work, we plan to use our model to further explore the techno-economic trade-offs of EV technologies, including consideration of service provider infrastructure options, markets such as taxis or long-distance commuters, alternative vehicle ownership scenarios, optimal EV range in the presence of infrastructure, optimal battery life and replacement schedules, larger vehicle size classes, further depth and emphasis on battery costs and associated projections, and vehicle usage and recharging strategies (e.g., opportunity charging). The present model currently has the capability to analyze all of these. In addition, since the battery is such a critical element for this model, we would like to enhance our battery cycle life model to better predict when batteries will fail and what residual value they will have at end of life. One area that the BOM is omitting is *non-monetary* and *societal* benefits to the driver such as reduction in petroleum dependence, reduced GHG emissions, pride of driving green technology, reduction in the number of visits to gas stations, and the instant torque response of EVs. Inclusion of these externalities increases the value proposition of EVs to the driver over and above what we see from pure economics.

In summary, NREL's *Battery Ownership Model* was constructed to calculate the present value of costs to the end user of advanced electric traction drive vehicles and related infrastructure on a consistent basis over multiple scenarios. The results of the model show that there are scenarios where HEVs, PHEVs, and even EVs can be less expensive than CVs, and it also highlights which parameters have the largest influence over the vehicle levelized cost per mile. Furthermore, the BOM is equipped to answer many pressing questions that drivers, third party service providers, EV marketers, and policymakers have as they turn a transportation electrification system into reality.

FY2010 Publications/ Presentations

1. M. O'Keefe, A. Brooker, C. Johnson, M. Mendelsohn, J. Neubauer, "Technical and Economic Evaluation of Various EV Battery Ownership Concepts," NREL Milestone to DOE, August 2010.
2. M. O'Keefe, A. Brooker, C. Johnson, M. Mendelsohn, J. Neubauer, and A. Pesaran. (2010). "Battery Ownership Model: A Tool for Evaluating the Economics of Electrified Vehicles and Related Infrastructure". Presented at *the 25th International Electric Vehicle Symposium and Exposition*. Nov. 5-9, 2010. Shenzhen, China.

References

1. AAA, "Your Driving Costs: 2008 Edition," AAA Exchange.com, 2008 Edition, Heathrow, FL. [Online] www.aaaexchange.com/main/Default.asp?CategoryID=3&SubCategoryID=9&ContentID=23. [Accessed: Aug. 8, 2010].
2. Ward's Automotive Yearbook, Ward's Communications, 2009.
3. S.C. Davis, S.W. Diegel, and R.G. Boundy, "Transportation Energy Data Book: Edition 26," U.S. Department of Energy, Oak Ridge, TN. 2007.
4. U.S. Federal Government Internal Revenue Service, "Revenue Procedure 2008-72," in Part III Administrative, Procedural, and Miscellaneous. Rev. Proc. 2008-72, 2008, 30 pages. [Online]. [Accessed: Aug. 9, 2010].
5. U.S. Department of Energy, "Annual Energy Outlook." www.eia.doe.gov/oiaf/aeo, [Accessed: May 2009].
6. M. Duvall, "Batteries for Plug-In Hybrid Electric Vehicles," presented at The Seattle Electric Vehicle to Grid (V2G) Forum, June 6, 2005.
7. R. Farrington and J. Rugh, "Impact of Vehicle Air-Conditioning on Fuel Economy, Tailpipe Emissions, and Electric Vehicle Range," NREL/CP-540-28960, October 31, 2000. Golden, CO: National Renewable Energy Laboratory [Online]. www.nrel.gov/docs/fy00osti/28960.pdf. [Accessed: Sep. 1, 2010].

III.C.5 PHEV Battery Secondary Use Study (NREL)

Jeremy Neubauer

National Renewable Energy Laboratory (NREL)
1617 Cole Blvd.
Golden, CO 80401
Phone: (720) 989 1919
E-mail: Jeremy.neubauer@nrel.gov

Start Date: February 2009
Projected End Date: October 2013

Objectives

- Identify, assess, and verify profitable applications for the second use of PHEV/EV Li-Ion traction batteries after their end of useful life in a vehicle to reduce the cost and accelerate adoption of PHEV/EVs.

Technical Barriers

- Currently the cost of batteries is too high for mass of electric drive vehicles. Re-using EV/PHEV batteries in secondary applications and avoiding sending them to recycling prematurely is of a lot of interest.
- Applications best suited for used EV/PHEV batteries, their value and market potential, have not yet been identified. Grid based applications – those typically discussed as most appropriate – are often complicated by uncertain electrical demands, complex and difficult to assess revenue streams, and regulatory structures prohibitive to energy storage technology.
- Battery degradation, both in automotive and secondary service, is notoriously difficult to ascertain, yet has a strong impact on the potential profitability of secondary use strategies. Further, it is envisioned that accurate degradation forecasting will be necessary to meet warranty requirements on second use batteries. However, sufficiently capable and accurate degradation models have yet to be developed, representative testing not yet performed, and used automotive batteries for such testing are in extremely short supply at present.
- Profitable second use applications may require significant reconfiguration of automotive batteries, and/or the integration of a large number of disparate (both in design and age) automotive batteries into a single system. Further, it is as of yet unclear what thermal and electrical management systems from the donor automobile will be supplied with each used battery. Thus, identifying the hardware and approach necessary to meet performance and safety targets while minimizing cost is a significant challenge.

Technical Targets

- Identify profitable and sustainable second use applications for PHEV/EV Li-Ion traction batteries
- Devise optimized use strategies for automotive traction batteries to facilitate their second use, maximizing their value and reducing cost to the automotive consumer and also prevent premature recycling of otherwise useable batteries.

Accomplishments

- Composed and released a request for proposals and associated statement of work soliciting a detailed techno-economic analysis, supply of used automotive PHEV/EV Li-ion traction batteries, and long term testing of said batteries in identified high-value second use applications. Proposals were received and reviewed, and an awardee selected.
- Identified major technical barriers for second use strategies.
- Completed a preliminary analysis of grid based energy storage needs to identify likely high value second use applications. It was shown that uses including area regulation, electric service power quality and reliability, and transmission and distribution upgrade deferral could offer significant value for second use batteries.
- Extended the analysis to assess possible discounts for automotive consumers resulting from secondary use. Based on the considerable value of possible second use application identified today, it is speculated that the price of new batteries in the future will be a major factor in the value of used batteries.
- Share the second use analysis with reprrentative of Environmental Protection Agency and a Workgroup within USCAR.

✧ ✧ ✧ ✧ ✧

Introduction

Accelerated market penetration of Plug-In Hybrid Electric Vehicles (PHEVs) and Electric Vehicles (EVs) is presently limited by the high cost of lithium-ion (Li-Ion) batteries. In fact, it has been estimated that more than a 50% reduction in battery costs is necessary to equalize the

current economics of owning PHEVs/EVs and conventionally fueled vehicles.

One means of reducing battery costs is to recover a fraction of the battery cost via reuse in other applications after it is retired from service within the vehicle, where it may still have sufficient performance to meet the requirements of other energy storage applications. By extracting additional services and revenue from the battery in a post-vehicle application, the total lifetime value of the battery is increased. This increase could be credited back to the automotive consumer, effectively decreasing automotive battery costs.

There are several current and emerging applications where EV/PHEV battery technology may be beneficial. For example, the use of renewable solar and wind technologies to produce electricity is growing, and their increased market penetration can benefit from energy storage, mitigating the intermittency of wind and solar energy. New trends in utility peak load reduction, energy efficiency, and load management can also benefit from the addition of energy storage, as will smart grid, grid stabilization, low-energy buildings, and utility reliability. Such application of used and new automotive traction batteries has been investigated before, but due to the use of outdated application and battery assumptions, these studies are in need of revision.

Approach

This effort investigates the application of new and used li-ion PHEV/EV batteries to modern utility and other applications with the goal of reducing the cost to automotive consumers. The major technical barriers to success of such efforts have been identified as second use application selection, long term battery degradation, and cost and operational considerations of certifying and repurposing automotive batteries.

To address these barriers, NREL is conducting a detailed techno-economic analysis to develop optimal use strategies for automotive batteries – inclusive of second use application identification. The results of this analysis will be in part verified via the acquisition of used automotive batteries and their long term testing in second use applications. Success of the project is measured by the completion of long term testing and the determination of used battery value. In order to facilitate and speed up the acquisition of second use batteries and their long-term testing in a potential second-use applications, we decided to identify partners interested in second use application by issuing a request for proposals (RFP) for a collaborative project. In addition, we collaborated with others interested in second use of end-of life EV batteries. These included Environmental Protection Agency, and United State Council of Automotive Research (USCAR).

Results

A preliminary analysis was conducted to assess the value and market potential of possibly grid based secondary use applications. This analysis combined the results of Eyer and Corey's 2010 Sandia report titled "Energy Storage for the Electricity Grid: Benefits and Market Potential Assessment Guide" with the limitations of typical Li-ion batteries to provide the revenue possible on a dollars per kilowatt-hour basis as seen in Figure III-1 below. These results suggest that area regulation, electric service power quality and reliability, and transmission and distribution upgrade deferral offer considerable value – possibly enough to justify using new Li-ion batteries at today's prices.

However, the scale of such markets is important to note. Figure III- 102 reveals that for most of the high value applications, the total *ten year* market potential is less than or only marginally exceeds 5 GWh. This market potential is about the estimated target a*nnual* battery production of in the US to be generated in factories funded by the Recovery Act of 2009. This implies that the high value second use markets will quickly saturate, even with limited EV/PHEV penetration (~1% of the 2010 light vehicle fleet). Both the growth of these high value markets and the adoption rate of EV/PHEVs over the coming decade are uncertain, though, providing an opportunity for use of batteries in early EVs.

Assuming that applications of such considerable value are present in the future, it becomes reasonable to assume that the value of used batteries will be set not by the value of the application, but of competing technology. Assuming the competition for used li-ion batteries to be new li-ion batteries, second use value then becomes a strong function of future battery prices.

Accounting for the anticipated future decline in battery prices, degraded battery health at automotive retirement, the cost or repurposing, a used product discount factor, and the time value of money, the possible first purchase discount was calculated and presented in Figure III- 103 and Figure III- 104. In each figure, two different health at retirement factors were considered (K_h = 40% and 80%).

Figure III- 103 is indicative of a first generation EV reuse scenario, where initial battery cost is $1000/kWh, but new battery prices decline by 70% prior to repurposing. This combined with relatively high repurposing costs and used product discount factor results in quite small initial purchase discounts.

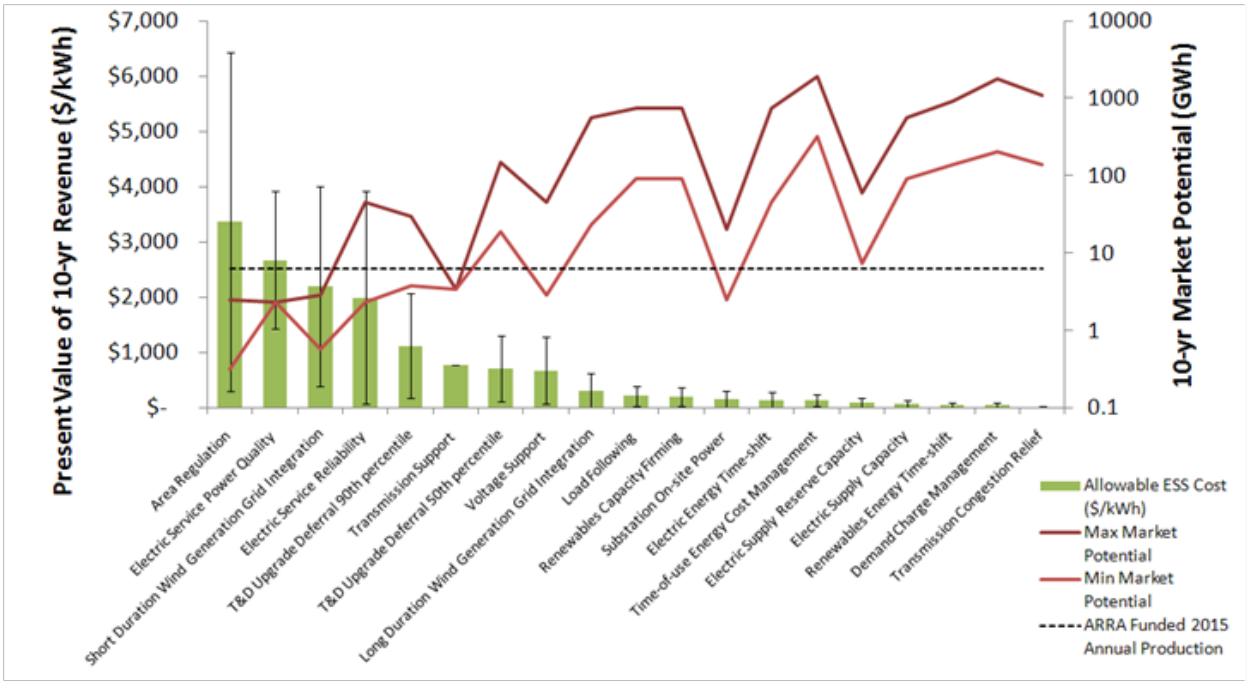

Figure III- 102: Value and market potential for the use of li-ion batteries in grid applications

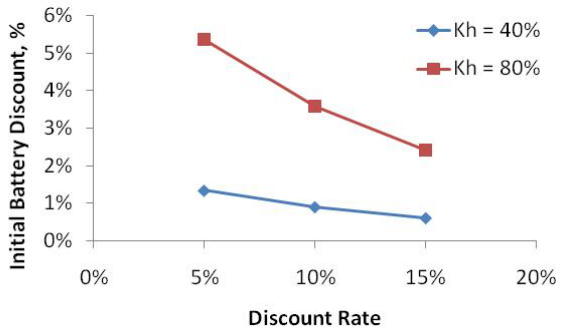

Figure III- 103: Present value of secondary use for first generation EVs

Figure III- 104 is representative of a later generation EV reuse scenario, where battery prices only decline by 30% between purchase and repurposing, and second use has been considered from the outset to minimize repurposing costs. The results show that second use can be of considerable value once EVs and their batteries have altered.

Request for Proposals. One major strategy and approach for this work was to collaborate with others who are interested in EV/PHEV secondary battery use. One of our interests was to enter into a cost-shared collaboration with others to acquire second use batteries, identify potential second-use applications with high value, and then perform their long term testing under the profiles of these applications. To support this strategy, we prepared a technical statement of work and issued a Request for Proposal (RFP) seeking a 50%-50% cost shared projects with three tasks: 1. Analysis to Identify 2nd use applications, 2. Securing used EV/PHEV batteries, and 3.

Characterization and long term testing of the secured batteries per identified applications. The RFP was issued in May 2010. We received proposals by the end of June 2010 and reviewed, scored and ranked them in July. In August, we seeked clarifications regading the approach and cost of the top proposer. In Spetember, we idendified the winning proposal and contacted the proposer team and entered into subcontract negociations. We inticipate the subcontract to be awarded and the work begin in 1st quarter of FY11.

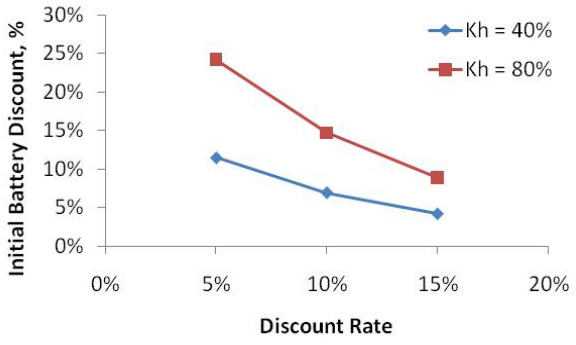

Figure III- 104: Present value of secondary use for later generation EVs (additional results)

Collaboration with Others. In addition, we collaborated with others interested in second use of end-of life EV batteries. These included Environmental Protection Agency (EPA), and United State Council of Automotive Research (USCAR). W had a few conference calls with EPA representatives and filled some questions regarding our analysis and finding for 2nd use of EV batteries. EPA is interested in learning about the 2nd use to minimize the environmental impact of EV adoption related to batteries. We provided a summary write-up discussing our analysis and finding. We also worked with a USCAR workgroup investigating the potential of second use batteries in high value and sustainable applications and how this could impact the design of the battery packs and cars. We had a conference call and a face to face meeting in USCAR, Southfield, MI in September of 2010.

Conclusions and Future Directions

NREL has completed a preliminary analysis on the second use of PHEV/EV Li-Ion traction batteries. The results of this study indicate that several high value grid based energy storage applications exist today, though the size of their markets relative to the expected available supply of second use batteries is questionable. Further analysis has shown that the value of second use will be strongly impacted by future battery prices; thus, second use may have little ability to impact the cost of first generation EVs, but could be a significant factor in the value equation for latter generation EVs once the technology has matured.

These preliminary results encourage further study. NREL is currently in the process of selecting a subcontractor to perform a more detailed techno-economic analysis of the second use question, as well as to procure used li-ion batteries and conduct long term testing to verify predictions. Others such as EPA and USCAR are interested in the subject of 2nd use of batteries and we will continue to collaborate with them.

FY 2010 Publications/Presentations

1. Neubauer, J. and Pesaran, A., "PHEV/EV Li-Ion Battery Secondary-Use: Opportunities and Challenges," *Advanced Automotive Battery Conference*, , Orlando, FL, May 2010
2. Neubauer, J. and Pesaran, A., "NREL's PHEV/EV Li-Ion Battery Secondary-Use Project," *Meeting with USCAR Battery Second Use Workgroup,* Southfield, MI, September 2010.
3. Neubauer, J. and Pesaran, A., "PHEV/EV Li-Ion Battery Secondary-Use," NREL Milestone Report, Golden, CO, June 2010.

III.C.6 Battery Recycling (ANL)

Linda Gaines

Center for Transportation Research
Argonne National Laboratory
9700 S. Cass Ave.
Argonne, IL 60439
Phone: 630/252-4919, Fax: 630/252-3443
E-mail: lgaines@anl.gov

Start: spring 2008
Projected Completion: fall 2011

Objectives

- Estimate material demands for Li-ion batteries
  - Identify any potential scarcities
- Calculate theoretical potential for material recovery
- Evaluate real potential for recovery using current recycling processes
- Determine potential for recovery via process development
- Characterize ideal recycling process
- Develop improved process to maximize material recovery

Barriers

- Scarcity could increase costs for battery materials
  - Recycling could increase effective material supply and keep costs down
  - Current processes recover cobalt, use of which will decline
  - Recycling economics in doubt because of low prices for lithium and other materials
- Process data are not published

Technical Goals

- Characterize current battery recycling processes
- Determine current production methods for other materials
- Estimate impacts of current recycling processes
- Estimate energy use/emissions for current material processes
- Estimate energy use/emissions for current battery processes
- Evaluate alternative strategies for additional material recovery
- Develop improved recycling processes

Accomplishments

- Selected promising battery chemistries
- Designed battery packs for each chemistry and vehicle type
- Estimated materials use for optimistic EV demand scenario
- Compared US and world lithium demand to reserves and determined sufficiency past 2050
- Presented lithium demand estimates and recycling technology comparison at battery and plug-in vehicle conferences
- Determined current production methods for lithium and batteries
- Characterized current and developing methods for recycling Li-ion batteries
- Began battery production and recycling lifecycle analysis to compare impacts and identify ideal recycling processes.

✧ ✧ ✧ ✧ ✧

Introduction

Recycling of material from spent batteries will be a key factor in alleviating potential material supply problems. We are examining battery recycling processes that are available commercially now or have been proposed. The processes are being compared on the basis of energy saved and emissions reductions, suitability for different types of feedstock, and potential advantages. We are comparing the potential of several recycling processes to displace virgin materials at different process stages (Figure III- 105), thereby reducing energy and scarce resource use, as well as potentially harmful emissions from battery production. Although few automotive batteries have been produced to date, work is under way to develop the best processes to recycle these batteries when they are no longer usable in vehicles. Secondary use of the batteries could delay return of material for recycling, thus increasing the demand for virgin materials and the resultant life-cycle impacts (seeFigure III- 106).

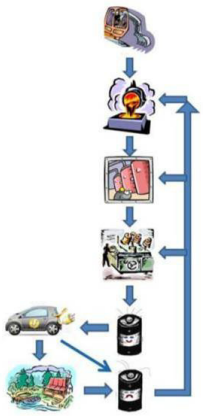

Figure III- 105: Recycled Materials Enter Varying Production Stages

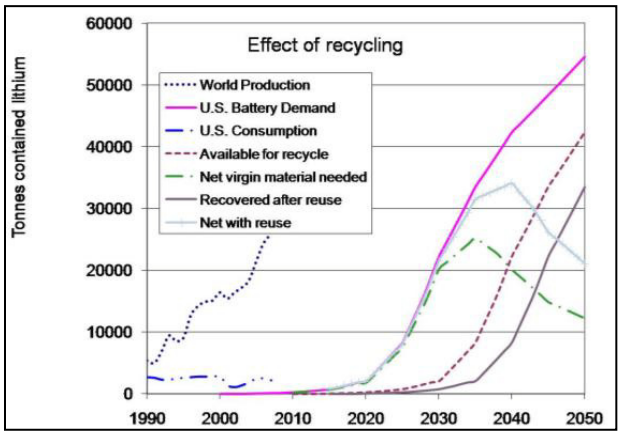

Figure III- 106: The Impact of Recycling and Reuse on Future US Lithium Demand

Approach

We answered these questions to address material supply issues.

- How many electric vehicles will be sold in the U.S. and world-wide?
- What kind of batteries might they use?
  - How much lithium would each use?
- How much lithium would be needed annually?
- How does the demand compare to the available resources?
  - How much difference can recycling make?
  - What recycling processes are available?
  - Could other materials become scarce?

Now, lifecycle analysis, based on detailed process data, will be used to compare energy savings and emissions reductions enabled by different types of recycling processes.

Results

Battery Production-- Roughly half of battery mass consists of materials (copper, steel, plastics, aluminum) that have been extensively documented in previous analyses. Therefore, we focus on the active battery materials that are not as well-characterized. Production steps are shown schematically in Figure III- 107.

The cathode (positive electrode) material is a metal oxide, with lithium-ions inserted into the crystal structure. Commercial electronics batteries generally use cobalt, but oxides containing nickel, manganese, and other elements are being developed for vehicle batteries. Both cobalt and nickel are smelted from sulfide ores, leading to significant sulfur dioxide emissions, even from plants with extensive controls. Lithium carbonate is produced from salars (large brine lakes), mostly in Chile. Brines are concentrated in ponds for over a year, then treated with soda ash. The carbonate precipitates, and is filtered out and dried. Active cathode compounds are made from lithium carbonate and metal salts by chemical replacement reactions in solution. High temperature treatment may be required to produce the desired configurations.

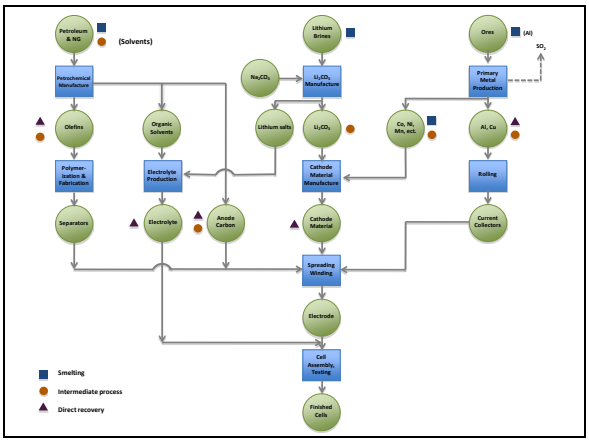

Figure III- 107: Where Recycled Materials Could Enter Battery Production

The anode (negative electrode) is generally made of graphite. To eliminate detrimental oxygen-containing species on the surface, it is baked at 2,000°F (1,100°C) in a reducing or inert atmosphere. Additives are mixed in to make the anode paste. The electrode materials are spread onto thin metallic foil substrates, which also serve as the current collectors. For the cathode, aluminum foil (about 20 µm thick) is used, and for the anode, copper (about 14 µm thick).

Separators for Li-ion batteries are typically made from polyolefins using 3- to 8-µm layers (PP/PE/PP or else just PE). The porous film keeps the electrodes apart, and if the cell becomes too hot, melts and closes off the pores, thereby shutting off the cell current. The electrodes and

separator are rolled up together and placed in cans before addition of the electrolyte, which is usually a dilute solution of a fluorine-containing lithium salt in an organic solvent. Assembled cells are conditioned and tested.

Recycling Processes. Recycling can recover materials at different production stages, from basic building blocks to battery-grade materials. The chart in Figure III- 106 is marked with symbols to show where 3 current recycling processes can actually recover materials. Impacts from all process steps above the symbols are avoided.

At one extreme are smelting processes that recover basic elements or salts. These are operational now on a large scale and can take just about any input, including different battery chemistries (including various Li-ion, Ni-MH, etc.), or mixed feed. Smelting takes place at high temperature, and organics, including the electrolyte and carbon anodes, are burned as fuel or reductant. The valuable metals (Co and Ni) are recovered and sent to refining so that the product is suitable for any use. The other materials, including lithium, are contained in the slag, which is now used as an additive in concrete. The lithium could be recovered by using a hydrometallurgical process, if justified by price or regulations.

At the other extreme, recovery of battery-grade material has been demonstrated. Such processes require as uniform feed as possible, because impurities jeopardize product quality. The components are separated by a variety of physical and chemical processes, and all active materials and metals can be recovered. It may be necessary to purify or reactivate some components to make them suitable for reuse in new batteries. Only the separator is unlikely to be usable, because its form cannot be retained. This is a low-temperature process with a minimal energy requirement. Almost all of the original energy and processing required to produce battery-grade material from raw materials is saved.

The third type of process is between the 2 extremes. It does not require as uniform a feed as direct recovery, but recovers materials further along the process chain than does smelting.

Comparison of Recycling to Primary Production. In Figure III- 108, we see that a large percentage of the battery production energy is consumed during assembly and testing and cannot be recovered by recycling. If the battery can be used again, however, the energy use and emissions per use are divided among service lives. Once the battery is no longer usable, it can still be recycled, although some of the materials may be more degraded after two uses and therefore require more processing. Metals illustrate the benefits of recycling, as the percent reduction in energy consumption ranges from about 25% for steel to 75% for aluminum and nickel. Advanced batteries will likely require high grade materials for their components, so it will be important to understand the quality of the output from recycling processes. A closed-loop battery recycling process would produce materials that could be used in the production of new batteries, while an open-loop recycling process would produce materials that would be used in another product.

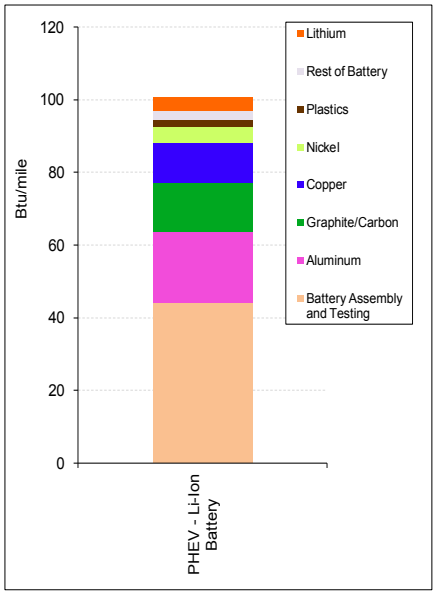

Figure III- 108: Energy Use for Battery Production Steps

Enablers of Recycling and Reuse. Material separation is often a stumbling block for recovery of high-value materials. Therefore, design for disassembly or recycling would be beneficial. Similarly, standardization of materials would reduce the need for separation. In the absence of material standardization, labeling of cells would enable recyclers to sort before recycling. Standardization of cell design, at least in size and shape, would foster design of automated recycling equipment. Standardization would also be beneficial to reuse schemes, where cells from various sources would be tested and repackaged in compatible groups for use by utilities or remote locations.

FY 2010 Publications/Presentations

Presentations

1. *Lithium-ion Batteries: Examining Material Demand and Recycling Issues*, TMS 2010 Annual Meeting & Exhibition, Seattle, WA, February 14-18, 2010.
2. *Recycling Processes for Lithium-ion Batteries*, 27th International Battery Seminar & Exhibit, Ft. Lauderdale, FL, March 15 - 18, 2010.
3. *Battery Materials Availability and Recycling*, Building a US Battery Industry for Electric Drive Vehicles: Progress, Challenges, and Opportunities

(NAS Review), Livonia, MI, July 26-27, 2010 (invited).
4. *Lifecycle Analysis for Lithium-Ion Batteries*, Plug-In 2010, San Jose, CA, July 26-29, 2010, and US China Battery Meeting, Argonne National Laboratory, August 30-31, 2010 (invited)

Papers

1. *Lithium-ion Batteries: Examining Material Demand and Recycling Issues*, TMS 2010 Annual Meeting & Exhibition, Seattle, WA, February 14-18, 2010.
2. *A Review of Battery LCAs: State of Knowledge and Critical Needs*, Argonne National Laboratory Draft Report August 2010

III.C.7 Low Energy HEV Requirements Analysis (NREL)

Ahmad Pesaran and Jeff Gonder
National Renewable Energy Laboratory (NREL)
Address 1617 Cole Blvd. Golden, CO 80401
Phone: (303) 275-4441 and (303) 275-4462
E-mail: Ahmad.Pesaran@nrel.gov, and
Jeff.Gonder@nrel.gov

Start Date: April 2007
Projected End Date: September 2013

Objectives

- Evaluate the relationship between the energy storage system (ESS) capabilities in a hybrid electric vehicle (HEV) and the vehicle fuel consumption.
- Support the United States Advanced Battery Consortium (USABC) Alternate HEV ESS Workgroup in establishing lower energy ESS targets relative to the current set of requirements for power-assist (PA) HEVs.

Technical Barriers

Technical targets and goals that are too aggressive and not attainable could lead to unreasonable expectations that could impede progress. This project addresses technical concerns raised in the Electrochemical Energy Storage (EES) Technical Team Technology Development Roadmap as they related to the existing targets: does the available energy requirement for PA-HEV ESS result in a battery with ambitious efficiency, weight, volume and affordability goals?

This project was aimed at establishing new targets to provide reasonable and clear goals for energy storage developers and research community.

Technical Targets

In collaboration with USABC and FreedomCAR Technical Team, this work resulted in developing new technical targets:

- 2 sec | 10 sec discharge pulse power:55 kW | 20 kW for the new targets (previously 25 kW for 10 sec)
- 2 sec | 10 sec regen pulse power: 40 kW | 30 kW for the new targets (previously 20 kW for 10 sec)
- Energy over which both power requirements simultaneously met: 26 Wh (previously 300 Wh)
- Energy window for vehicle use: 165 Wh (previously 425 Wh)
- Selling system price @ 100k/yr: $400 (previously $500)

Accomplishments

- Used simulation to show that most HEV fuel savings can be realized with ESS energy windows for vehicle use ≤165 Wh. Chassis dynamometer test data confirmed the analysis for production HEVs.
- Determined the ESS pulse power performance (over standard tests) required to satisfy the HEV power demands on the ESS during driving.
- Provided consultation to USABC and the EES Technical Team's Alternate HEV ESS Workgroup, which recommended establishing a new set of ESS requirements for PA-HEV called lower-energy ESS.
- USABC issued a request for proposal information (RFPI) in early 2010 to initiate development of ES systems satisfying the LEESS targets.
- Educated various audiences about the new requirements by presenting on the development of LEESS targets at battery and vehicle conferences in 2010.

✧ ✧ ✧ ✧ ✧

Introduction

The USABC ESS performance goals for power-assist HEVs were last published in November 2002. Those goals call at a minimum for an HEV ESS to possess 300 Wh of "available" energy over which the ESS charge and discharge power requirements are simultaneously met. Adding the energy swept by the 10-second charge and discharge power requirements to either end of this simultaneously met region results in an energy window for vehicle use of 425 Wh as shown in Figure III- 109. This large of an energy requirement has been found to increase the cost of HEV energy storage. In order to evaluate any cost-saving opportunities, the USABC formed the Alternate HEV ESS Workgroup in 2009 to look into setting a new set of requirements and requested NREL to investigate the relationship between HEV fuel use and the ESS in-use energy window.

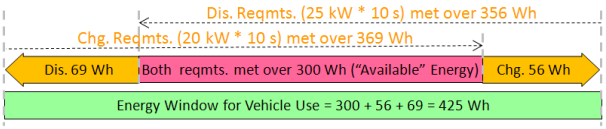

Figure III- 109: PA-HEV Available Energy Requirement of 300 Wh Leads to 425 Wh Energy Window for Vehicle Use.

Approach

As indicated in last year's annual report, NREL modeled a generic midsize parallel HEV using the DOE-managed Powertrain System Analysis Toolkit (PSAT) software program. The modeling included three different degrees of hybridization or DOH cases (ratio between the power of the electric motor and the engine in the HEV). For each DOH case the ESS energy content was swept over six cases from a high to a low. Simulating each configuration over multiple drive cycles revealed trends in fuel consumption and ESS usage between the various designs. In order to isolate the impact of the ESS on the vehicle fuel use, the vehicle mass and all other platform characteristics were held constant for all of the configurations.

To provide verification for the simulation results, the study also analyzed data from controlled testing on production hybrid vehicles and observed the ESS in-use energy window over standard drive cycles.

Results

Fuel Consumption Trends from Simulations. Figure III- 110 shows some of the simulation results over a US06 drive cycle. The vertical axis on the figure shows the vehicle fuel use (lower on the figure is better). The horizontal axis on the figure shows the in-use energy window for the ESS during the drive cycle. The point that falls on the left axis (with an energy window of zero Wh) represents the fuel use of a comparable conventional vehicle. All the other data points in the figure represent a different HEV configuration. Each of the three sets of colored lines represents a different DOH, with the higher DOH (higher electric motor power and smaller engine) cases resulting in lower fuel use. This is largely due to the fact that the smaller engine is able to operate at high efficiency levels a greater amount of the time relative to a larger engine.

In addition to showing a fuel savings benefit from higher electric motor/ESS power, the figure shows a fuel savings trend with increasing ESS energy window. Across all three DOH cases, significant fuel savings occur in the first roughly 50 Wh, with additional albeit tapering fuel savings thereafter. Most additional fuel savings appear to occur with energy windows out about 165 Wh.

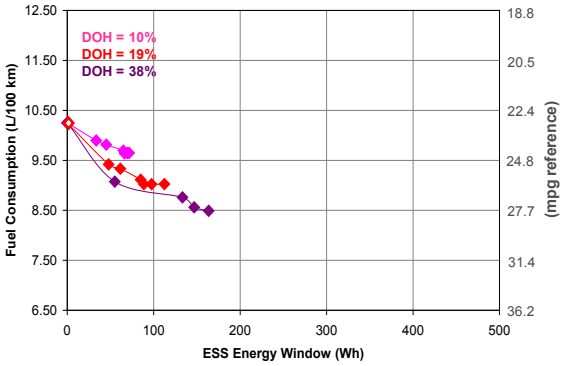

Figure III- 110: Simulation Results over the US06 Driving Cycle.

Comparison with Production HEV Test Data
Figure III- 111 presents a similar graph based on analysis of production HEV test data over standard drive cycles. This analysis confirms the ability of existing HEVs to operate using energy windows within roughly 165 Wh.

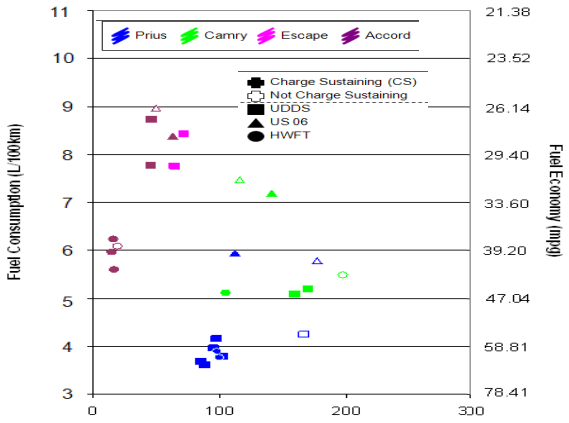

Figure III- 111: Energy Used in Production HEV During Various Drive Cycles.

Power Pulse Analysis Next we determine the desired pulse power capability of the lower energy ESS device. This was done by examining the pulse power characteristics of the different simulated HEV configurations over the standard city-type drive profile as well as a high speed and acceleration drive cycle. Ultimately, the power pulse characteristics of the most aggressive case (the largest DOH vehicle operating on the high speed and acceleration US06 drive cycle) were selected for establishing the new targets. Figure III- 112 shows the envelope for various pluses during the US06 drive cycle with respect to each pulse's duration in seconds and magnitude in kW. The recommendation from the EES Tech Team was to use the 2 sec and 10 sec values as the basis for the power goals: for discharge (+55 kW for two seconds and +20 kW for ten seconds) and charge, such as from HEV regenerative braking (-40 kW for two seconds and -30 kW for ten seconds). The corresponding in-use

energy window for the US06 cycle was 165 Wh and was recommended as a new target for the LEESS. This in-use energy window is the same as the term "energy window for vehicle use."

LEESS Requirements and Goals Based on the results of NREL analysis, the USABC Alternate ESS Workgroup recommended selecting the pulse power capabilities and energy window for vehicle use discussed above as the initial set of requirements for the LEESS.

The "energy window for vehicle use" is a new term introduced and for testing purposes we needed to relate that to the traditional term of "available energy." We used the following approach as depicted in Figure III- 113 to relate these two terms:

- Begin with the stated "energy window for vehicle use" (i.e., 165 Wh)
- Calculate energy for pulse requirements
  - Discharge (i.e., 10 sec x 20 kW → 56 Wh)
  - Charge (i.e., 10 sec x 30 kW → 83 Wh)
- Subtract pulse energy from ends of vehicle use energy (i.e., 165 Wh – 83 Wh – 56 Wh = 26 Wh)
- This gives "available energy over which pulse power requirements must be met" (i.e., perform ES size factor analysis with≥ 26 Wh bounded by 10 s ec power requirements)
- Repeat if needed for other pulse power levels (e.g., if energy from 2 sec power requirements happens to be greater than that from the 10 sec power requirements)

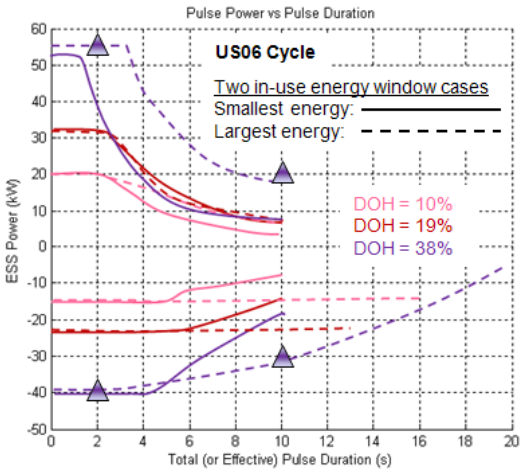

Figure III- 112: Distribution of Power Pulses vs. Duration (dashed purple lines indicates the largest energy and highest DOH HEV case over the US06 drive cycle).

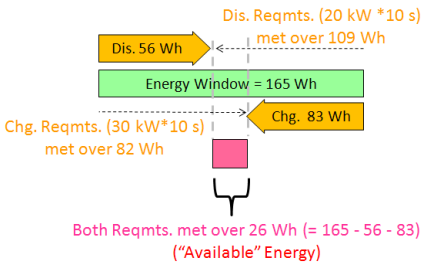

Figure III- 113: LEESS Energy Window for Vehicle Use of 165 Wh Leads to 26 Wh of Available Energy where Charge and Discharge Requirements are Simultaneously Met for 10 sec Pulses.

Based on several discussions at the EES Technical Team and USABC Management Committee meetings, other requirements for calendar life, cycle life, cold cranking, round trip efficiency, weight, volume, and cost were identified. Most of these requirements are consistent with the power-assist HEV requirements, except for efficiency which was 95% for LEESS and cost which was $400/system. The end of life requirements for LEESS was earlier included in Table III- 2. Please note that definition for "cold cranking" for LEESS is slightly different than the previous USABC definitions. For LEESS, "cold cranking power is at -30C after the system stands for 30 days at +30C. The justification for the stand at +30C is for a higher self discharge than at colder temperatures. Please note that with this definition, there was no need to define a self-discharge requirement as previously defined for power-assist HEVs.

Conclusions and Future Directions

Based on the analysis described here, the USABC established a new set of lower-energy ESS targets for power-assist HEVs, which are hoped to support development of cost-effective, fuel saving HEVs. Systems satisfying the new targets could be based on symmetric or asymmetric capacitors, batteries or some other device. USABC issued a request for proposals and received several proposals. After reviewing the proposals USABC and DOE awarded 3-4 companies with contracts to develop LEESS.

In FY11, we are proposing to turn a production full HEV into a test platform for evaluating various LEESS prototypes that will be delivered later by USABC developers. This includes taking the batteries out of a PA-HEV and replacing them with various LEESS such as supercapacitors or very high power batteries.

FY 2010 Publications/Presentations

1. Gonder, J., Presentation to the FreedomCAR Vehicle Systems Analysis Technical Team, VSATT. (Nov 2009)

2. USABC issued Request for Proposal Information: uscar.org/commands/files_download.php?files_id=219. (Dec 2009)
3. Gonder, J., Pesaran,A., Lustbader, J. and Tataria H., " Hybrid Vehicle Comparison Testing Using Ultracapacitor vs. Battery Energy Storage", *SAE 2010 Hybrid Vehicle Technologies Symposium;* San Diego, CA. (Feb 2010)
4. Gonder, J.; Pesaran, A.; Howell, D.; Tataria, H. "Lower-Energy Requirements for Power-Assist HEV Energy Storage Systems—Analysis and Rationale." *Proceedings of the 27th International Battery Seminar and Exhibit;* Fort Lauderdale, FL. (Mar 2010

III.D Battery Testing Activities

III.D.1 Battery Performance and Life Testing at ANL

Ira Bloom (Principal Investigator)
John Basco
Panos Prezas
Lee Walker
Argonne National Laboratory
9700 South Cass Avenue
Argonne, IL 60439
Phone: 630 252 4516; Fax: 630 252 4176
e-mail: ira.bloom@anl.gov

Start Date: September 1976
Projected End Date: Open

Objectives

- Provide DOE, USABC, and battery developers with reliable, independent and unbiased performance evaluations of cells, modules and battery packs.
- Benchmark battery technologies which were not developed with DOE/USABC funding to ascertain their level of maturity.

Technical Barriers

This project addresses the following technical barriers as described in the USABC goals [1, 2]:

- Performance at ambient and sub-ambient temperatures
- Calendar and cycle life

Technical Targets

- 15-year calendar life
- 300,000 HEV cycles
- 5,000 PHEV charge-depleting cycles
- End-of-life target of 25 kW at 300 Wh (HEV) or 45 kW at 500 Wh / 3.4 kWh charge-depleting energy (PHEV)
- 5-kW cold cranking power at -30°C

Accomplishments

Tested battery deliverables from many developers:

- HEV batteries: Test battery technologies from A123Systems (still in progress), Johnson Controls-SAFT
- PHEV batteries: Test contract deliverables from Johnson Controls-SAFT (still in progress)
- Benchmark battery technologies for vehicle applications. Test deliverables from SK Energy, G4 Synergetics, Mitsui Mining and Smelting, Samsung, Firefly Energy, Lightening Energy, DowKokam (still in progress).

✧ ✧ ✧ ✧ ✧

Introduction

Batteries are evaluated using standard tests and protocols which are transparent to technology. Two protocol sets are used: one that was developed by the USABC [1, 2], and another which provides a rapid screening of the technology.

Approach

The batteries are evaluated using standardized and unbiased protocols, allowing a direct comparison of performance within a technology and across technologies. For those tested using the USABC methods, the performance of small cells can be compared to that of larger cells and full-sized pack by means of a battery scaling factor [1, 2].

The accelerated screening test protocols were designed to accrue many cycles on a battery quickly and to work with high-energy and high-power cells. The point of these tests is to determine how stable the performance of the battery is in a short amount of time. It should be noted that these are not USABC hybrid-electric or plug-in hybrid-electric vehicle tests.

Results

The battery technology from a developer was benchmarked using accelerated screening protocols. Two cells were used for this work. The test consisted of an initial characterization using C/1 capacity measurements and the hybrid pulse-power characterization test at the low-current value (HPPC-L) at 25°C and 100% DOD cycling at the C/1 rate at 50°C. After every 50 cycles, the battery was re-characterized at 25°C in terms of the C/1 capacity and HPPC-L tests. Both cells successfully completed 500 cycles and testing was voluntarily terminated.

The changes in cell resistance vs. cycle count from the HPPC-L tests are shown in Figure III- 114. As can be seen from the figure, the cell resistance increases with cycle count in both cases. A preliminary kinetic analysis of the data from both cells indicates that the resistance data seems to depend on t^2. Since the regression coefficients, 0.90 and 0.92, are less than 0.95, other time-dependencies are possible. Additionally, the scatter in the data may obscure the true nature of the dependence on time.

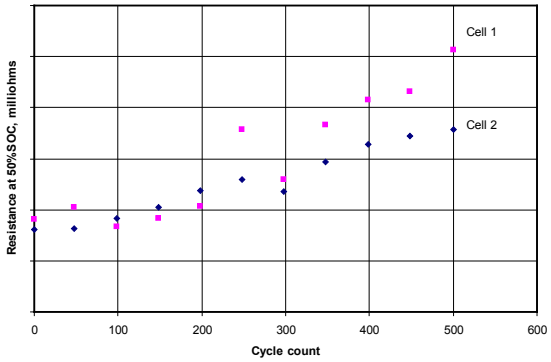

Figure III- 114: Resistance vs. cycle count for two cells in an accelerated screening test.

A plot of the C/1 data (at 25°C) versus the square root of cycle count is shown in Figure III- 115. The data from both cells yield reasonably straight lines, implying that the C/1 fade data are consistent with a diffusion-limited mechanism.

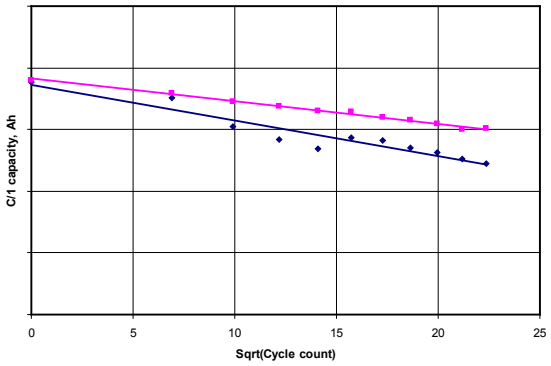

Figure III- 115: C/1 capacity vs. cycle count for two cells in an accelerated screening test.

In another experiment, the effect of the cycling voltage limts on cell life was measured. Here, there were two groups. Group A was cycled between 4.2 and 2.7 V and Group B, between 4.1 and 3.1 V. All characterization tests were performed at 30°C and were carried out at the beginning of testing and after every 50 cycles. Cycling was performed at 40°C.

The changes in cell resistance vs. cycle count for both groups are shown in Figure III- 116. As can be seen from the figure, there was a strong dependence of resistance on the cycling limits, with the group with Group A showing a greater resistanc rise.

Similar effects were seen in the C/1 capacity data (Figure III- 117). Here, Group A displayed greater capacity fade.

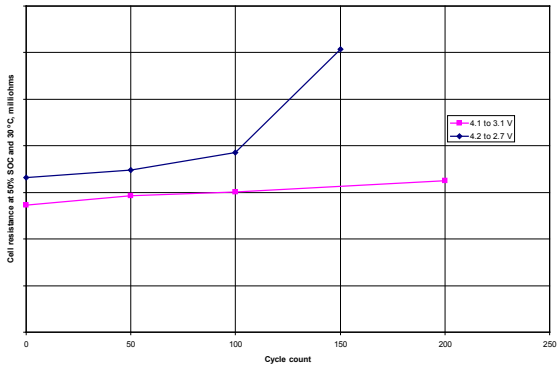

Figure III- 116: Resistance at 50% SOC vs. cycle count for Groups A and B.

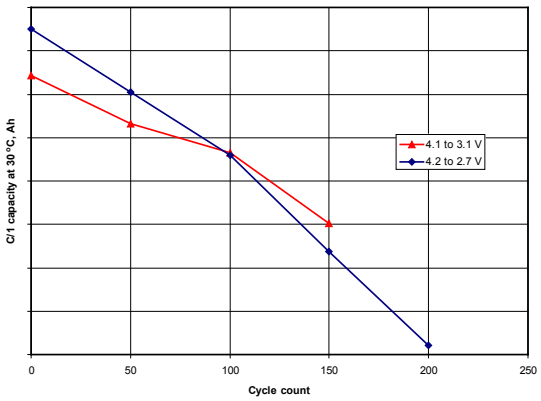

Figure III- 117: C1 Capacity Data

Conclusions and Future Directions

Accelerated screening testing has been shown to be a useful way to gauge the state of a developer's technology and to determine the effect of cycling parameters.

For the future, we plan to:

- Continue testing HEV contract deliverables
- Continue testing PHEV contract deliverables
- Continue acquiring and benchmarking batteries from non-DOE sources
- Aid in refining standardized test protocols
- Upgrade and expand test capabilities to handle increase in deliverables

- Explore the possibilities for test protocol comparison and, perhaps, standardization with Europe, Japan and China

FY 2010 Publications/Presentations

1. *Technology Life Verification Testing (TLVT)*, J. P. Christophersen, I. Bloom, E. V. Thomas, V. S. Battaglia, US-China Electric Vehicle and Battery Technology Workshop, Argonne National Laboratory, August 20-September 1, 2010.
2. *Battery Testing in the US*, I. Bloom, US-China Electric Vehicle and Battery Technology Workshop, Argonne National Laboratory, August 20-September 1, 2010.
3. *Differential Voltage Analyses of High-Power Lithium-Ion Cells 4. Cells Containing NMC*, Ira Bloom, Lee K. Walker, John K. Basco, Daniel P. Abraham, Jon P. Christophersen, and Chinh D. Ho, J. Power Sources, 195 (2010) 877-882.

References

1. FreedomCAR Battery Test Manual for Power-Assist Hybrid Electric Vehicles, DOE/ID-11069, October 2003.
2. FreedomCAR Battery Test Manual for Plug-In Hybr id Electric Vehicles, June 2010.

III.D.2 Smart Battery Status Monitor (INL)

Jon P. Christophersen

Idaho National Laboratory
P.O. Box 1625
Idaho Falls, ID 83405
Phone: (208) 526-4280; Fax: (208) 526-0690
E-mail: jon.christophersen@inl.gov

Collaborators:
Chet Motloch, ETEC
John Morrison, Montana Tech
William Morrison, Qualtech Systems, Inc.

Start Date: October, 2008
Projected End Date: Ongoing

Objectives

The objective of this work is to develop a Smart Battery Status Monitoring system that successfully identifies state of health through:

- Passive observations (voltage, current, temperature),
- Active measurements (*in situ* impedance), and
- Battery models, databases, and expert learning-software tools.

Technical Barriers

No industry standard has yet been adopted for battery state-of-health due to the complex nature of the problem. Present techniques tend to be based on direct measurements from which the capacity or state-of-charge are estimated. However, this is an incomplete assessment of battery health since information about impedance, resistance, and power capability are also required. With both active impedance measurements and passive observations, combined with battery models and expert prognostic software tools, a standardized smart battery system can be established for all industries that rely on expensive energy storage devices.

Technical Targets

- Develop hardware and software for *in situ* impedance measurements that can be applied to cells, modules, and packs.
- Validate *in situ* impedance measurement technique as a viable prognostic tool.
- Design an embedded impedance measurement system for field testing (long term goal).
- Design and build the overall smart battery status monitoring system with passive observations, active measurements, and expert learning software tools (long term goal).

Accomplishments

- Designed and built a ruggedized, portable demonstration Impedance Measurement Box.
- Developed ruggedized control software for portable demonstration hardware.
- Initiated long-term validation testing of the novel *in situ* impedance measurement technique using Sanyo SA cells.

✧ ✧ ✧ ✧ ✧

Introduction

Robust, *in situ* state-of-health assessment techniques remain a critical need for the successful and widespread implementation of battery technologies for various applications (automotive, military, space, telecommunications, etc.). Due to the complexity of the problem, however, no industry standard for battery state-of-health (SOH) estimation has yet been adopted. Typical SOH techniques tend to based on direct measurements (i.e., voltage, current, and temperature) from which the capacity, energy, or state-of-charge can be inferred. Additionally, these SOH techniques are very specific to the particular chemistry or application. However, passive observations do not provide a complete picture of the overall battery health.

Another significant aspect of battery health is found in the impedance, resistance, and power capability. However, heretofore, rapid *in situ* measurements have not been possible because of the lack of a robust measurement system. The resistance and power are typically determined from charge-depleting pulses that result in lower available energy or state-of-charge swings that degrade battery performance. A benign alternative is Electrochemical Impedance Spectroscopy (EIS) since it operates on low-level, charge neutral input signals to determine the impedance spectra over a broad range.[8] EIS, however,

[8] J. P. Christophersen, C. D. Ho, C. G. Motloch, D. Howell, and H. Hess, "Effects of Reference Performance Testing during Aging Using

requires expensive and delicate laboratory equipment, and the measurements can take between 10 minutes to an hour to complete depending on settings. Consequently, EIS measurements are also impractical for *in situ* applications.

The Idaho National Laboratory has been collaborating with Montana Tech of the University of Montana and Qualtech Systems, Inc. on developing a rapid, *in situ* impedance measurement technique. Information determined from onboard impedance measurements, when combined with other passive measurements, models, and expert learning software, enable the development of an overall Smart Battery Status Monitor (SBSM) that will be relevant to all industries that utilize expensive or mission-sensitive battery systems.

Approach

Harmonic Compensated Synchronous Detection (HCSD)[9,10] is an *in situ* impedance measurement technique that is based on a low-level, charge neutral input signal. The input signal consists of a bandwidth limited octave harmonic (i.e., frequencies increasing by 2^k, where k is an integer) sum-of-sines current signal with a duration of one period of the lowest frequency. Figure III- 118 shows a representative sum-of-sines input current signal with a starting frequency of 0.1 Hz (shown by the thick, sinusoidal line) and an RMS current of 0.5 A. The cumulative capacity removed for this example 10-s signal (one period of the lowest frequency) is 567.7 μAh.

The magnitude and phase at each frequency of interest are then synchronously detected from the voltage response of the battery. There is no cross-talk error between the responses at each frequency since they are separated by octave harmonics. However, if higher resolution data are desired (i.e., 1.5^k instead of 2^k harmonics), then the synchronously detected voltage response must be corrected for the cross-talk error effects. This is accomplished by reassembling the time record of the voltage response with each frequency except for the one of interest, and subtracting it from the measured voltage response. This new signal is synchronously detected again at the desired frequency to determine the compensated magnitude and phase response.

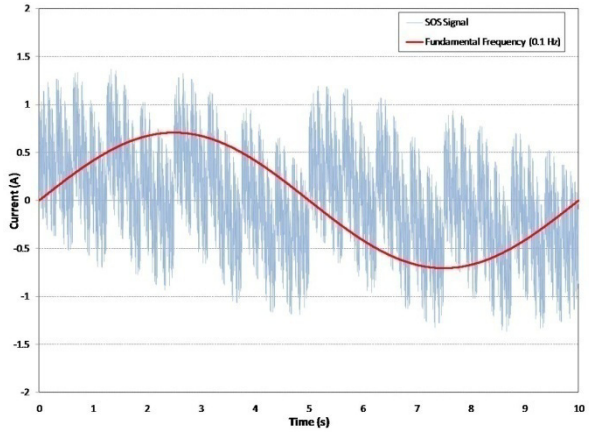

Figure III- 118: Input current for *in situ* impedance detection.

Results

Hardware. Figure III- 119 shows the second generation Impedance Measurement Box hardware system for *in situ* measurements. The chassis has been designed as a portable unit (17"x14"x4") that is laptop controlled and USB-driven. Presently, the device can only measure single cells (≤ 5 V), but a system capable of measuring module-level batteries (≤ 50 V) is also under development.

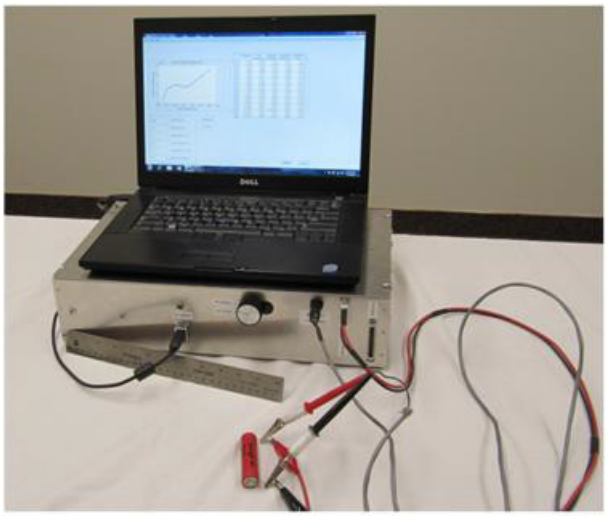

Figure III- 119: Hardware for *in situ* impedance measurement.

Software. Figure III- 120 shows a representative graphical user interface of the control software. The user determines the range by selecting the lowest frequency and the number of frequency lines assuming an octave harmonic input. The sample rate, input RMS current, voltage range, and number of periods of the lowest frequency are also user inputs. After a successful test, the results are displayed graphically in the upper-left window with either a Nyquist or Bode plot. The results will also be displayed numerically in the upper-right hand side.

Commercial Lithium-Ion Cells," *J. Electrochem Soc.*, 153, A1406-A1416 (2006).

[9] J. P. Christophersen, C. G. Motloch, J. L. Morrison, I. B. Donnellan, and W. H. Morrison, "Impedance Noise Identification for State-of-Health Prognostics," *Proceedings from the 43rd Power Sources Conference* (2008).

[10] J. L. Morrison and W. H. Morrison, "Method of Detecting System Function by Measuring Frequency Response," U.S. Patent No. 7,395,163 B1, July 1, 2008.

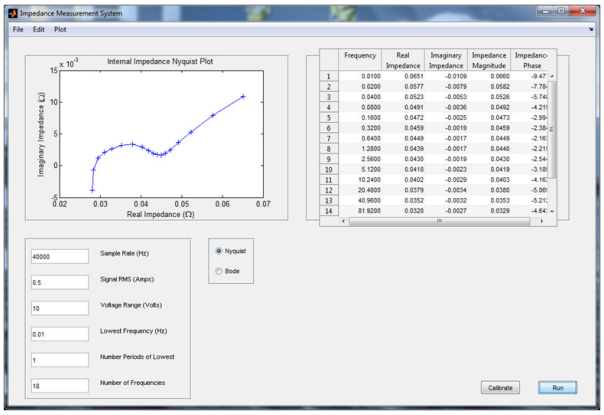

Figure III- 120: Control software graphical user interaface.

Validation Study. The *in situ* impedance measurement technique was initially verified with three Sanyo SA cells. These cells were subjected to PHEV charge sustaining cycle-life test profiles at 60% state-of-charge and 50°C with reference performance tests (RPTs) every two weeks. The reference performance tests consisted of a low-current Hybrid Pulse Power Characterization (HPPC), EIS, and HCSD measurement.

Figure III- 121 shows a comparison between the EIS and HCSD measurements for a representative Sanyo cell through six RPTs. The real impedance was shifted to the right with each RPT to visually separate and clarify the comparisons. For the key, mid-frequency range, the HCSD impedance spectra matches very well the corresponding EIS spectra. Note that each EIS measurement took approximately ten minutes to complete, whereas each HCSD measurement only took ten seconds. For the high and low frequency regions (left and right sides of the spectra, respectively), the HCSD results deviate somewhat from the EIS measurements, and these differences may be due to calibration effects from the HCSD. Improved HCSD calibration methods are presently under development.

Despite the differences at high and low frequency, the growth of the charge transfer resistance in the mid-frequency region is nearly identical between HCSD and EIS. It has previously been shown that EIS measurements correlate very well with independently determined pulse resistance data from standardized HPPC tests.[11] The same comparison was made for the Sanyo cells using the measured data at the semicircle trough just before the start of the low-frequency Warburg impedance tail, and the results are shown in Figure III- 122. Both EIS and HCSD show a strong correlation to the growth in HPPC discharge resistance determined at the same state-of-charge through six reference performance tests. These data demonstrate that HCSD yields comparable data to EIS, and further indicate that it is an efective, *in situ* impedance measurement technique which will be utilized to drive the Smart Battery Status Monitor.

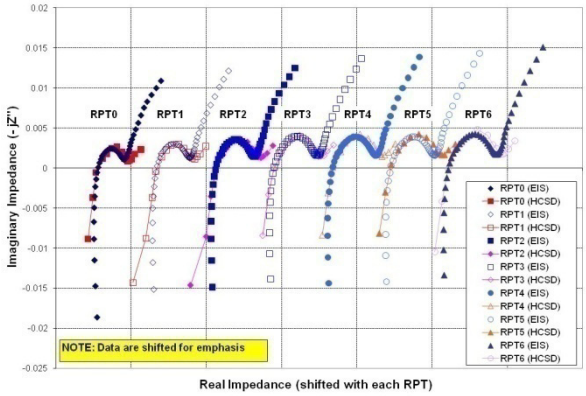

Figure III- 121: Comparison between EIS and HCSD measurements.

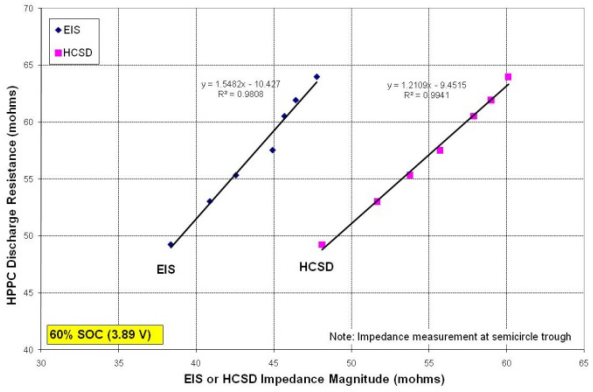

Figure III- 122: Comparison between HPPC and impedance measurement techniques.

Conclusions and Future Directions

Harmonic Compensated Synchronous Detection enables low-cost, embedded, rapid, and *in situ* impedance measurements that address a significant need in the battery market that is presently unsatisfied. This technology, when combined with passive monitoring (i.e., voltage, current, and temperature), battery models, and expert learning prognostic tools, forms the development of an overall smart battery status monitor that will be relevant to all industries that rely on expensive energy storage devices.

The second generation prototype hardware system has been developed to provide demonstrations for various industries that may benefit from this technology, including the U.S. automotive manufacturers, in FY 2011. Additionally, the next phase of this work is to upgrade the

[11] J. P. Christophersen, D. F. Glenn, C. G. Motloch, R. B. Wright, C. D. Ho, and V. S. Battaglia, "Electrochemical Impedance Spectroscopy Testing on the Advanced Technology Development Program Lithium-Ion Cells," *IEEE Trans. Veh. Technol.*, 56(3), 1851-1855 (2002).

hardware system to successfully measure the impedance of module-size batteries.

FY 2010 Publications/Presentations

1. J. P. Christophersen, C. G. Motloch, J. L. Morrison, and W. Albrecht, "Method and Apparatus for *in situ* Characterization of Energy Storage and Energy Conversion Devices," U.S. Patent No. 7,675,293 B2, March 9, 2010.
2. J. L. Morrison, W. H. Morrison, J. P. Christophersen, and C. G. Motloch "Method of Determining Battery Health Using Impedance Spectrum," Patent Application (2010).
3. J. L. Morrison, W. H. Morrison, J. P. Christophersen, and C. G. Motloch "Method of Detecting System Function By Measuring Frequency Response," Patent Application (2010).
4. J. L. Morrison, W. H. Morrison, J. P. Christophersen, and C. G. Motloch " *in situ* Real Time Electrochemical Impedance Identification System," Patent Provisional Application (2010).
5. J. L. Morrison, W. H. Morrison, J. P. Christophersen, and C. G. Motloch "Time Domain System Detection to Measure Frequency Response," Patent Provisional Application (2010).
6. J. P. Christophersen, C. G. Motloch, J. L. Morrison, W. H. Morrison, "Onboard Impedance Monitoring for Battery State-of-Health Assessment," 81st Meeting of the Lithium Battery Technical/Safety Group Meeting, Key West, FL, February 9-10, 2010.
7. J. P. Christophersen, C. G. Motloch, J. L. Morrison, W. H. Morrison, " *in situ* Impedance Measurements for Smart Battery Status Monitor Technology," USCAR Tech Team Meeting, Detroit, MI, August 19, 2010.

III.D.3 Battery Performance and Life Testing (INL)

Jeffrey R. Belt (Primary Contact)
Taylor Bennett, Chinh Ho, Clair Ashton
Idaho National Laboratory
PO Box 1625, Idaho Falls, Idaho 83415-2209
Phone: (208) 526-3813, Fax (208) 526-0690
Email: Jeffrey.belt@inl.gov

Start Date: FY 2009/2010
Projected End Date: Open task

Objectives

The purpose of this activity is to provide high-fidelity performance and life testing, analyses, modeling, test procedures and methodologies development, reporting and other support related to electrochemical energy storage devices under development by the Department of Energy's Vehicle Technologies Program.

Technical Barriers

This project supports all of the primary technical barriers; performance, life, abuse tolerance and cost.

Technical Targets

- Target applications include power-assist hybrid electric vehicles (HEVs), Plug-in Hybrid Electric Vehicles PHEVs, and Battery Electric Vehicles (BEVs).
- See "Technical Targets"

Accomplishments

- 472 cells, 7 modules, and 5 vehicle system level lithium-ion battery packs were tested during the FY2009/2010 reporting period.
- Revision 1 of the Battery Test Manual for Plug In Hybrid Electric Vehicles, INL-EXT-07-12536 was published in September 2010.

Introduction

The development of advanced batteries for automotive applications requires that developmental, diagnostic and validation testing be performed to support development goals and to characterize performance against Technical Targets established for HEV's (including Ultracapacitors), PHEV's, BEV's, and other high energy electric drive system applications.

Approach and Results

Several changes in methodology required a revision of the Battery Test Manual For Plug-In Hybrid Electric Vehicles, INL/EXT-07-12536. Revision 1 was issued September 2010. The original PHEV operational philosophy was modified as shown in Figure III- 123. Figure III- 124 shows the typical power and energy capability for a PHEV cell.

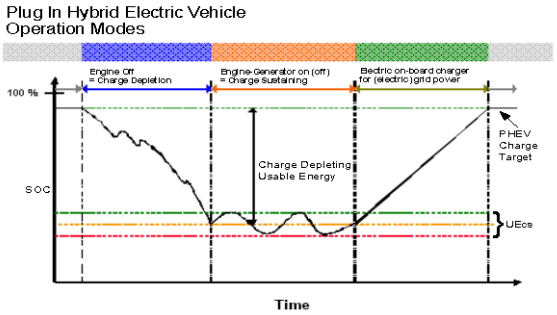

Figure III- 123: PHEV Operation Philosophy

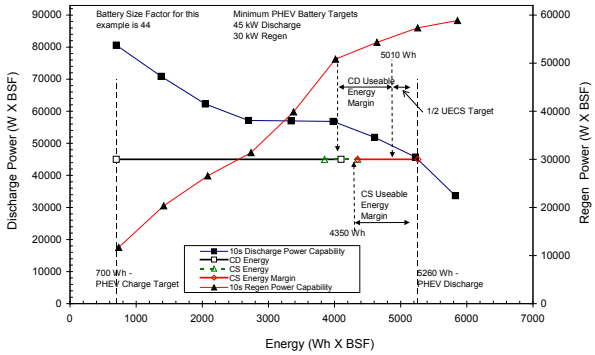

Figure III- 124: Typical power and energy capability for PHEV cells under test.

Figure III- 125 shows the new relationship between the Charge Depleting Available Energy and the Charge Sustaining Available Energy and Power.

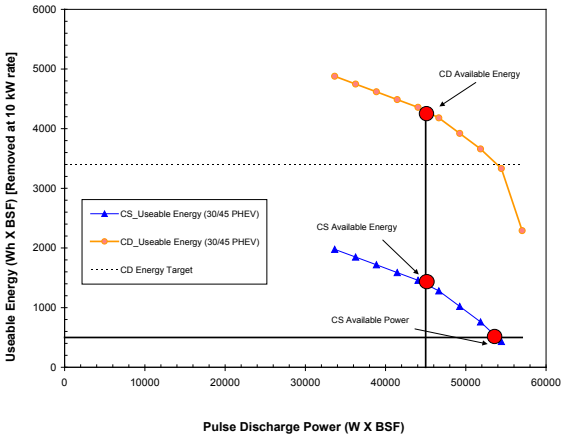

Figure III- 125: CD and CS Available Energies

Deliverables tested at INL are detailed for each of three DOE development programs assigned to the INL. In addition, status information is provided on benchmark test hardware.

Two sets deliverables were tested from Johnson Controls - Saft. The first set of deliverables consists of a 24-cell study that focused on combined calendar/cycle life testing that was initiated in FY2001. The lithium-ion cells were designed for the Power Assist Hybrid Electric Vehicle application.

The second set of deliverables consists of two VL7P battery packs that focused on cycle life testing. The 344-Volt lithium-ion packs were designed for the Maximum Power Assist Hybrid Electric Vehicle application (Figure III- 126). Four sets of deliverables are being tested from Enerdel. The first set of deliverables consists of a 20 cell study that is focused on calendar and cycle life testing.

Figure III- 126: JCS 344-Volt Battery Pack

The lithium-ion cells were designed for the Minimum Power Assist Hybrid Electric Vehicle application. The second set of deliverables consists of a 3-cell study that focused on cycle life testing. The lithium-ion cells were designed for the Maximum Plug-In Hybrid Electric Vehicle application. The third set of deliverables consists of a 6-cell and 6-module study that focused on cycle life testing. The lithium-ion cells were designed for the Minimum Power Assist Hybrid Electric Vehicle application. The fourth set of deliverables consists of one dual module that was designed for the Electric Vehicle application.

Three sets of deliverables were tested from Compact Power. The first set of deliverables consists of a 20-cell study that focused on calendar and cycle life testing from a large battery manufacturer of the FY2008 technology. The lithium-ion cells were designed for the Minimum Power Assist Hybrid Electric Vehicle application.

General results from the above projects suggest some lithium-ion designs exhibit an increase in power at 30°C. This secondary mechanism generally diminishes after a year of calendar life testing. However, the general trend as shown in Figure III- 127 for lithium-ion chemistry tends to show increased power fade with increased temperature. Diagnostic testing on specific technologies will further elucidate the mechanisms involved in temperature related power and capacity fade.

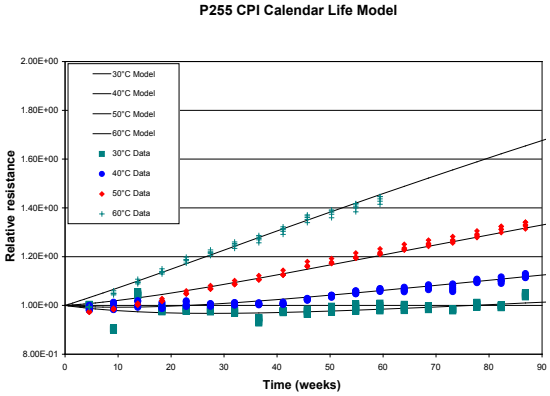

Figure III- 127: Typical affect of temperature on lithium-ion battery resistance rise.

The second set of deliverables consists of a 40-cell study that focused on cycle life testing. The lithium-ion cells were designed for the Maximum Plug-In Hybrid Electric Vehicle application (Figure III- 128). The third set of deliverables consists of three full size battery systems that have thermal management systems incorporated into the design.

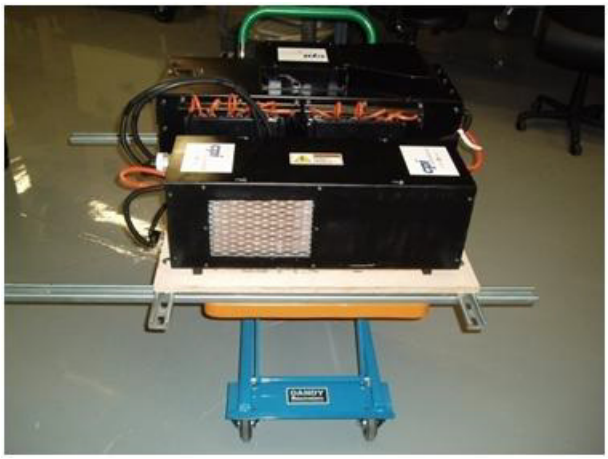

Figure III- 128: CPI 400-Volt Battery Pack

The DOE also supports an INL benchmarking program, wherein various electrochemical energy storage devices are tested to evaluate their performance and potential for focused development activities. The INL tested several devices during FY 2009/2010. A commercial vendor provided 350 18650-size cells of various power and energy capabilities for calendar and cycle life testing that are applicable to Power Assist and Plug-In Hybrid Electric Vehicle Designs. The results indicate that no rest time is needed during accelerated charge depleting cycling. These cells are capable of performing 5000 CD cycles with 20% energy fade. Additionally, energy fade during charge sustaining cycle life tests and calendar life tests at 30% SOC is much lower than at 60% and 90% SOC. C-rate cycling indicates that a state of charge swing of 100 to 0% causes ten times the energy fade compared to a reduced range of 90 to 30% SOC for the same energy throughput. Additional tests are planned this fiscal year to evaluate this trend. The large number of test cells has allowed several focused diagnostic studies aimed at identifying performance limiting mechanisms.

Envia provided three lithium-ion cells using novel materials for Electric Vehicle applications. The cells are currently undergoing cycle life testing to validate their performance. EIG provided three lithium-ion cells using an iron phosphate cathode for charge depleting cycle life testing for PHEV applications. Additionally, the Axion Power provided 16 modules, a unique lead acid-carbon electrode configuration aimed at potential micro-hybrid applications for calendar life testing.

Altairnano provided lithium-ion cells using novel materials for both the Power Assist and Plug-In Hybrid Electric Vehicle Designs. One set of cells consists of 20 3.5-Ah cells that are undergoing calendar and cycle life testing at various temperatures for HEV applications. Another set of 20 cells are undergoing charge depleting cycle life testing for PHEV applications. Figure III- 129 shows the energy fade over the course of 5000 Charge Depleting Cycles.

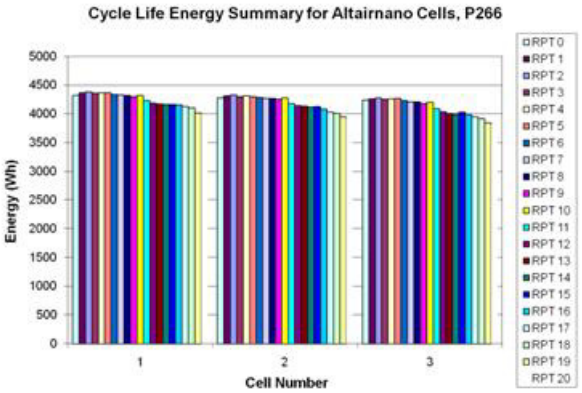

Figure III- 129: Altairnano Charge Depleting Energy Summary

INL continues to collaborate with ANL, SNL, and LBNL for Technology Life Verification Testing. This work focuses on accelerated testing and modeling for life prediction Testing in support of this project and will continue in FY 2011. The INL has begun a new collaboration with SNL to perform abuse testing on aged and new cells supplied by a commercial vendor.

Conclusions and Future Directions

Testing has identified the technologies that suffer from temperature dependent power and capacity fade. Focused diagnostic testing will further help to identify the mechanisms responsible for the accelerated fade at higher temperatures. Testing has also established baseline performance and helped to track improvements made during the development programs.

Publications/Presentations

1. M. Conte, F. Valerio Conte, I. D. Bloom,
2. K. Morita, T. Ikeya, and J. R. Belt "Ageing Testing Procedures on Lithium Batteries in an International Collaboration Context," EVS-25 Shenzhen, China, Nov. 5-9, 2010
3. J. R. Belt, C. D. Ho, "Altairnano PHEV Lithium-ion Cell Test Results," Electrochemical Society, October 2010
4. J. R. Belt, "FreedomCAR Battery Test Manual For Plug-In Hybrid Electric Vehicles." Rev 1, INL/EXT-07-12536, September 2010.
5. J. R. Belt, "Energy Storage Testing and Analysis, Accelerated Life Testing," International Meeting On Life Testing, INL/CON-10/17616, January 2010.

III.D.4 Battery Abuse Testing at SNL

Christopher J. Orendorff (Principal Investigator)
E. Peter Roth
William A. Averill

Sandia National Laboratories
PO. Box 5800, MS-0614
Albuquerque, NM 87185-0614
Phone: (505) 844-5879; Fax: (505) 844-6972
E-mail: corendo@sandia.gov

Start Date: October 1, 2009
Projected End Date: September 30, 2010

Objectives

- Serve as an independent abuse test laboratory for DOE and USABC
- Abuse tesing in accordance with the USABC test manual and SAE J2464
- Sucessful testing of all deliverables from developers under USABC contracts

Technical Barriers

- Abuse tolerance of energy storage devices is identified as a barrier in USABC and DOE battery development programs
- The failure modes for lithium-ion batteries are complex and need to be evaluated for all types of chemistry, design, packaging and systems for PHEV/EV applications

Technical Targets

- Perform abuse testing and evaluation of cells and modules delivered from contractors to USABC
- Report results to DOE, the USABC Tech Team, and contractors to USABC

Accomplishments

- Completed abuse tesing of all cell and module deliverables from the developer through USABC contracts including:
  - EnerDel (16 HEV cells and 7 HEV modules)
  - A123Systems (6 HEV cells and 4 HEV modules)
- Compact Power-LG Chem (12 PHEV cells and 7 PHEV modules)

✧ ✧ ✧ ✧ ✧

Introduction

Abuse tests are designed to determine the safe operating limits of full HEV\PHEV energy storage devices. The tests are performed to yield quantitative data on cell\module\ pack response to allow determination of failure modes and help guide developers toward improved materials and designs. Standard abuse tests are performed on all devices to allow comparison of different cell chemistries and designs. New tests and protocols are developed and evaluated to more closely simulate real-world failure conditions.

Approach

Abuse tolerance tests are performed which evaluate the response to expected abuse conditions.

- Test to failure of energy storage device.
- Documentation of conditions that cause failure.
- Evaluate failure modes and abuse conditions using destructive physical analysis (DPA)
- Provide quantitative measurements of cell/module response.
- Document improvements in abuse tolerance.
- Develop new abuse test procedures that more accurately determine cell performance under most likely abuse conditions

Possible tests that can be performed cover three main categories of abuse conditions:

- Mechanical Abuse: Controlled crush, penetration, drop, water immersion, mechanical shock and vibration
- Thermal Abuse: Thermal stability, simulated fuel fire, elevated temperature storage, rapid charge/discharge, thermal shock cycling
- Electrical Abuse: Overcharge/overvoltage, short circuit, overdischarge/voltage reversal, partial short circuit

The core abuse tests that are typically performed under this program include:

- Overcharge: 1C, 3C, or 32 amp rate (depending on test article size)
- Flammability: with or without external ignition source

Monitor heat generation, cell strain (pressure), and gas evolution

- Short circuit:
  - Hard short (1 mΩ)
  - Intermediate short (applied load comparable to cell or module internal impedance, e.g. 10 mΩ)
  - Monitor heat generation, cell strain (pressure), and gas evolution
- Thermal Ramp
  - Ramp to 250°C or article failure (5°C/min rate)
  - Vary the state of charge (50-100% SOC)
  - Flammability: with or without external ignition source
  - Monitor heat generation, cell strain (pressure), and gas evolution
- Mechanical crush
  - Crush to 25% of the unit height
  - Crush to 50% of the unit height or 8000 lbf
  - Flammability: with or without external ignition source
  - Monitor heat generation and gas evolution
- Blunt rod
  - < 1 mm/s stroke rate
  - Depress blunt rod into the battery until a change in voltage or temperature are observed
  - Monitor heat generation and gas evolution
- Separator shutdown integrity
  - Heat to temperatures > separator shutdown temperature and hold
  - Apply external voltage (20 V) and monitor separator breakdown
  - Repeat at 10°C increments until failure

Results

The actual USABC testing results are Battery Protected Information and prohibited from public release. However, representative data is shown below for 18650 test cells that have either been fabricated in our lithium-ion cell fabrication facility.

Cell Overcharge Test. An 18650 cell is prepared with a $LiCoO_2$ cathode, MCMB carbon anode, and 1.2 M $LiPF_6$ in EC:EMC (3:7) electrolyte. The cell is formation cycled at 200 mA C/D cycles (Figure III- 130). After formation cycling, the cell is subjected to overcharge abuse by first charging the cell to 100% SOC (4.1 V), then continuing to charge the cell at 4A (3C rate, 20 V compliance voltage) until failure. Figure III- 131 shows the cell voltage and cell skin temperature as a function of time. The cell voltage increases to ~5 V and holds relatively constanstant for 12 minutes, while the temperature increases steadily at a rate of ~8 C/min. At 12 minutes, the internal impedance of the cell increases and the cell reaches the compliance voltage of 20 V. When the cell reaches the compliance voltage, the temperature rise rate increases significantly. When the cell reaches 135°C, the spiral roll is ejected from the 18650 can, ignites, burns, and the test is terminated.

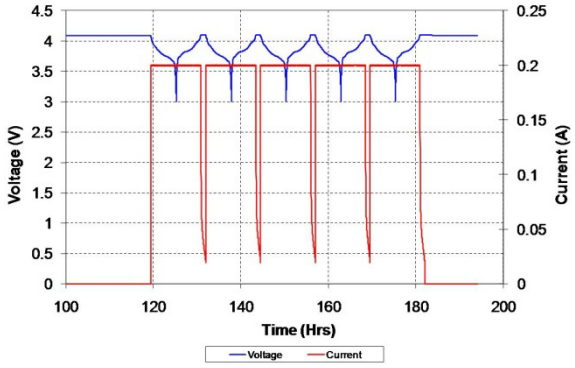

Figure III- 130: Formation cycling a $LiCoO_2$ 18650 cell at a 200 mA C/D rate.

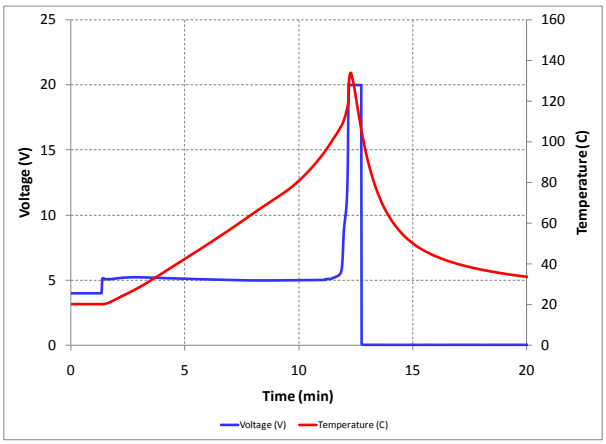

Figure III- 131: Cell voltage and cell exterior temperature for a 4A overcharge of a $LiCoO_2$ 18650 cell.

Cell Thermal Ramp Test. The thermal ramp procedure involves heating a cell in an insulated copper heating block at a rate of 5 C/min up to 250°C and hold for 30 min (or until cell failure). Cell skin temperature, block temperature, and cell OCV for an 18650 cell ($LiCoO_2$ cathode) during the course of a thermal ramp test are shown in Figure III- 132. The cell temperature tracks the block temperature up to 150°C. At 150°C, the cell voltage drops and begins to self-heat at a slightly higher rate (2-5 C/min), shown in Figure III- 133 (referred to as the onset of thermal runaway). The cell heating rate continues to increase until the cell temperature reaches 200°C and the cell goes into a high rate thermal runaway. The peak runaway temperature is measured to be 525°C.

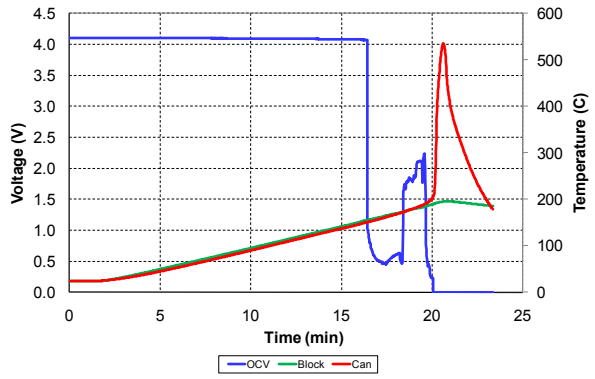

Figure III- 132: Cell voltage and temperature as a function of time during a thermal ramp (5 C/min) of a $LiCoO_2$ 18650 cell.

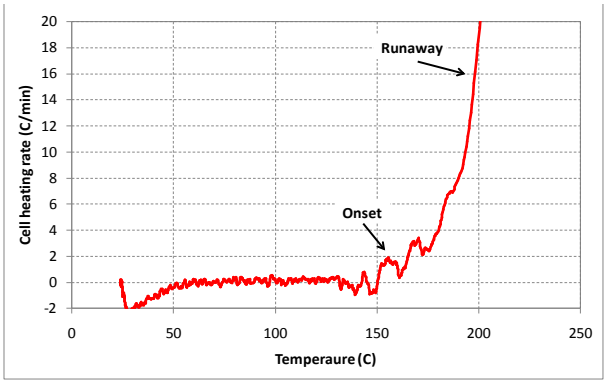

Figure III- 133: Cell heating rate (C/min) calculated from the thermal ramp for a $LiCoO_2$ cell showing the onset to thermal runaway at ~150°C followed by a high order runaway at 200°C.

Blunt Rod Test. During a blunt rod test, a 3 mm diameter steel rod is depressend into a cell (cylindrical or prismatic) at a rate < 1 mm/sec in an effort to short the cell internally. As an example, Figure III- 134 shows a $LiFePO_4$ 18650 cell charged to 3.65 V at 100 mA (C/10). The current tapers (with a 100 mA limit) as a 3 mm diameter steel rod with a rounded tip is depressed into the center of the cell can at a rate of 0.1 mm/sec (Figure III- 135).

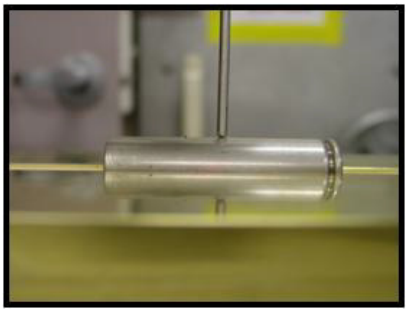

Figure III- 134: Test setup for the blunt rod test on an 18650 cell.

The blunt rod is continually depressed into the cell can until the cell shorts internally; the voltage drops (520 s, 215 lbf) and the cell draws 100 mA current (Figure III- 135 and Figure III- 136) at which point the rod is stopped. The current limit is increased (to 1 A) and the cell draws 550 mA to maintain the 3.65 V, shown in Figure III- 136. There are several variations of this approach, however, we have found that testing a cell that is drawing current gives more information on the severity of the internal short (~6.6Ω short in this example) in an effort to quantify the cell response.

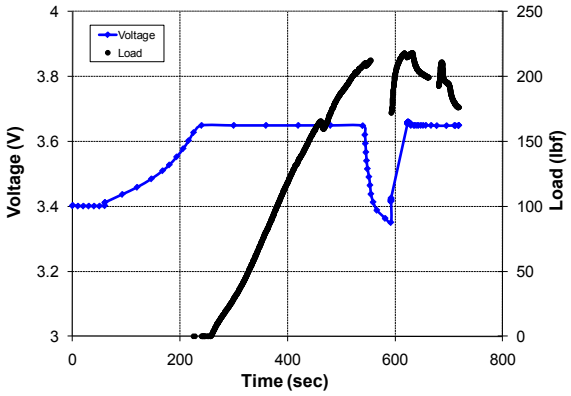

Figure III- 135: Cell voltage and applied load (lbf) as a function of time during a blunt rod test of a $LiFePO_4$ 18650 cell.

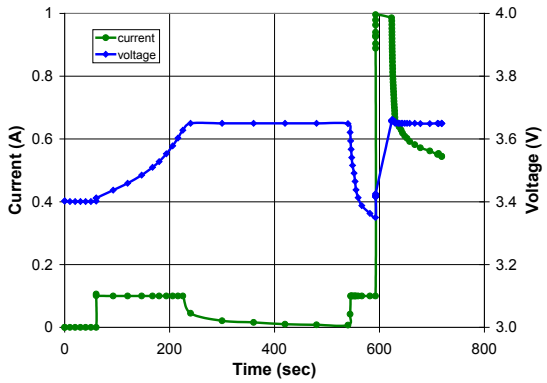

Figure III- 136: Applied current and cell voltage as a function of time during a blunt rod test of a $LiFePO_4$ 18650 cell.

Conclusions and Future Directions

Testing of the larger format cells, modules and packs has required development of several unique, custom testing fixtures and testing procedures. These larger scale tests require careful control and monitoring of high energy release abuse events while recording detailed cell data to allow determination of the failure modes. This cell and module abuse testing has provided critical information to the USABC cell developers that has aided in development of improved abuse tolerant cell and module designs. This information is necessary for an objective evaluation of these cells and designs by the DOE and the US automobile manufacturers.

Testing in FY11 will follow on with additional HEV and PHEV cells, modules and packs along with deliverables from materials development contractors including separators and active materials for cell-level evaluation.

FY 2010 Publications/Presentations

The information produced for the USABC is protected and cannot be published or presented in an open public forum. Presentation of the testing results is limited to quarterly Tech Team meetings consisting of the car manufacturers and DOE personnel.

1. E. P. Roth and C. J. Orendorff "Sandia Abuse Test Support for EnerDel" USABC Tech Team Meeting, February 2010
2. C. J. Orendorff and E. P. Roth "On Demand ISC Update" USABC Tech Team Meeting, February 2010
3. C. J. Orendorff, E. P. Roth, and W. A. Averill "Abuse Response of CPI PHEV Cells" USABC Tech Team Meeting, May 2010
4. C. J. Orendorff, E. P. Roth, and W. A. Averill "Abuse Response of A123Systems Prismatic HEV Cells" USABC Tech Team Meeting, August 2010
5. C. J. Orendorff, E. P. Roth, and W. A. Averill "Abuse Response of CPI PHEV Modules" USABC Tech Team Meeting, August 2010
6. C. J. Orendorff "Triggering ISCs in 18650 Cells" USABC Tech Team Meeting, August 2010

III.E Computer Aided Engineering of Batteries (CAEBAT)

III.E.1 Computer Aided Engineering of Batteries - CAEBAT (NREL)

Stephen Goguen (VT Project Manager)
Subcontractor: National Renewable Energy Laboratory

Ahmad Pesaran
National Renewable Energy Laboratory
1617 Cole Blvd.
Golden, CO 80401
Phone: 303-275-4441
E-mail: ahmad.pesaran@nrel.gov

Start Date: April 2010
Projected End Date: September 2015

Objectives

- Develop battery cell, pack and system modeling tools to enhance understanding of battery performance, life, and safety to enable development and manufacture of cost-effective batteries for electric drive vehicles.
- Collaborate among National Labs and support the U.S. industry to develop battery modeling tools to simulate and design cells and battery packs in order to accelerate development of improved batteries for hybrid, plug-in hybrid and electric vehicles.

Technical Barriers

- Life (calendar and cycle), high performance at all temperatures, cost, and safety are barriers for major adoption of lithium-ion batteries in electric drive vehicles (EDV).
- Large investment and long lead time in cell and pack research, design, prototyping, and testing cycle - and then repeating the cycle many times even with some minor changes - increase production costs.

Technical Targets

- Develop suite(s) of software tools that enable automobile manufactures, battery developers, pack integrators, and other end-users the ability to simulate and design cells and battery packs in order to accelerate development of energy storage systems that meet the requirements of the electric drive vehicle.

Accomplishments

- NREL Supported DOE with preparing an initial draft of a planning document as a basis for a Project Plan for CAEBAT.
- We interacted with six other National Labs through face to face meetings for obtaining input for the draft planning document.
- NREL prepared a statement of work and issued a request for proposals (RFP) on July 30, 2010 seeking industry partners to develop computer aided design tools for automotive batteries with a 50%-50% cost sharing.
- We received several proposals in September 2010 and reviewed them with help of external experts including other National Labs.
- NREL selected the top proposals meeting the technical and cost requirements of the RFP.
- We continued our electrochemical-thermal modeling of cells through the multi-physics, multi-scale, multi-dimensional (MSMD) platform for CAEBAT.

✧ ✧ ✧ ✧ ✧

Introduction

Currently, battery and pack developers tediously experiment with many different cell chemistries and geometries in an attempt to produce greater cell capacity, power, battery life, thermal performance and safety. A typical manufacturing cycle spans over many months and thus, the process of testing new materials in multiple cell sizes, in multiple battery pack designs, and over many months is extremely time consuming and expensive. By introducing battery simulations and design automation at an early stage in the battery design life cycle, it is possible to significantly reduce the product cycle time and cost and thus significantly reduce cost of the battery. In the past few years, NREL has initiated development of an electrochemical-thermal model f lithium-ion cells with 3-dimentioanl geometries.

Despite the extensive modeling efforts in the past by National Laboratories, Universities, private companies and other institutions to capture the electrochemical performance, life, thermal profiles and cost of batteries, ultra-capacitors and the like, the battery industry (cell

developers) has not been comfortable to implement the model-based design approach. One major impediment to this process is that the models developed are often very specific and tailored to the respective entity's specific needs – thereby making it difficult to combine the independent efforts into widely used design packages. Another reason is the lack of validation and verification for the developed models. Further development and validation of existing models that simulate electrochemical and thermal performance and abuse behavior of cells and their integration into common Computer Aided Engineering (CAE) are needed to create full battery design suites. Such modeling tools will support the design of new materials, cells, and packs, ultimately accelerating development of batteries for EDVs. In many industries, including automotive and combustion engine development, CAE tools have been the proven pathway to:

- Improve performance by resolving relevant physics in complex systems;
- Shorten product development design cycle, thus reducing cost; and
- Provide an efficient manner for evaluating parameters for robust design.

CAE for battery industry needs to mature at par with modeling tools for internal combustion engines, conventional drive trains and the like in order to make batteries competitive and affordable for use in advanced vehicles. Recognizing this need, in April of 2010, DOE announced a new program activity called Computer-Aided Engineering of Electric Drive Vehicle Batteries (CAEBAT) to develop software tools for battery design, R&D, and manufacturing. The objective of CAEBAT is to incorporate existing and new models into battery design suites/tools with the goal of shortening design cycles and optimizing batteries (cells and packs) for improved performance, safety, long life, and low cost.

The CAEBAT program is broken down into four elements, as shown in Figure III- 137.

- Material and component level models,
- Cell level models,
- Pack level models, and
- Open architecture software for interfacing all models.

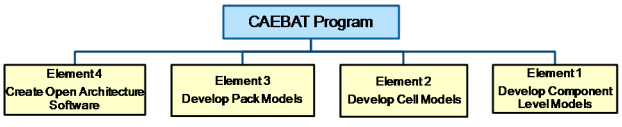

Figure III- 137: Four Elements of the Computer Aided Engineering for Batteries (CAEBAT) Activity.

Approach

For several years, DOE Energy Storage R&D program have supported battery modeling and simulation the Focused Fundamental Research (i.e. BATT), Applied Battery Research (ABR), and Battery Development activities at national laboratories and universities. The battery modeling under BATT has been focused on understanding the behavior of materials, electrochemistry, electrolyte, stress propagation, and degradation physics. The battery modeling under ABR has been focused on life prediction, abuse reaction-thermal models, internal short circuit simulations, and cost projects. The battery modeling under Battery Development program activity has been focused on thermal, electrical, electro-thermal and electrochemical modeling of cells and more recently with 3-D geometries, thermal and fluid flow analysis of multi-cell module and packs using CAE design tools. The scale of these modeling varied from nanometers to meters as shown in Figure III- 138. The links between various physics (electrochemistry, chemistry, thermal, electrical, mechanical, etc. and scales (material, cell, module, pack) have been limited and for specific cases. After a comprehensive review of battery-related modeling and simulation efforts at national labs, universities, and industry, DOE has focused the CAEBAT program on linking the relevant battery models, and to initiate stronger collaborations between Labs and industry and academia, and to make these simulation tools readily accessible and available as design tools for the industry and other end-users.

Each of these elements of the CAEBAT program will be accomplished by collaboration between national laboratories, academia, industry, and other interested organizations. To oversee the successful execution of the CAEBAT program, DOE has designated NREL as the Overall Program Coordinator.

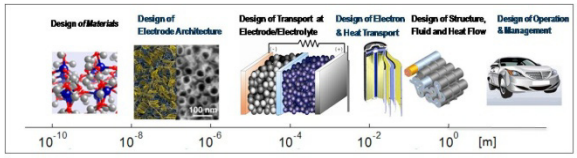

Figure III- 138: Muti-scale physics in battery modeling from molecular modeling to pack and system level modeling.

The *Material/Component Level Modeling* will be mostly performed by national labs with LBNL as the coordinator. The *Cell Level Modeling* and *Pack Level Modeling* will be performed by industry, national laboratories, and academia coordinated through NREL. The *Open Architecture Software* element will be performed by the national laboratories to be coordinated by ORNL. The *Cell Level Modeling* and *Pack Level Modeling* by the industry will conducted by sub-

contractors chosen through a competitive procurement process. NREL will coordinate the industry participation.

To support the activities of the CAEBAT, NREL needed to perform the following:

- Interact with DOE program mangers, other national laboratories with battery modeling background, universities, and industry to understand the state of battery models to develop a draft planning document for eventual preparation of a Project Plan.
- Write a statement of work for request for proposals from industry for participation in CAEBAT to develop software suits that included battery design tools.
- Continue further enhance and develop its multi-physics multi-scale, multi-domain battery models and disseminate results.

Results

Coordination of CAEBAT. Based on the strategy provided by DOE Energy Storage program mangers, NREL drafted an overview project description plan to discuss with other national labs and industry. Since this a new activity, the strategy included understanding the battery modeling capabilities at national laboratories, universities, and battery developers, software companies, and others and also identifying initial gaps in models. It was found out that a number of models are available at components, electrode, and cell levels, most were dealing with fundamental understanding of battery behavior without capturing the realistic 3-dimentioanl geometry of cells. The pack level models are limited in scope and not linked to cell level electrochemical-thermal models. After NREL's initial planning meeting with DOE Energy Storage program managers, discussion with other national laboratories including ANL, INL, LBNL, LLNL, ORNL, and SNL was initiated. In addition, NREL's CAEBAT coordinator introduced the CAEBAT program to the public (battery and car industry, universities, and others organizations) by presenting a talk at the Advanced Automotive Batteries Conference in June 2010 in Orlando, FL.

The coordination activities between National Labs continued with discussion with representative(s) from the Idaho National Laboratory (INL) and Sandia National Laboratory (SNL) vesting NREL in June. NREL principals visited Lawrence Berkeley National Laboratory (LBNL) and Lawrence Livermore National Laboratory (LLNL) in July. Representatives from Argonne National Laboratory visited NREL in September and we had a conference call with Oak Ridge National Laboratory (ORNL). These visits and discussions further enhanced the understandings of the capabilities and expertise of each Lab in modeling area so a more integrated and synergistic program plan and task activities could be defined. Based on input received from DOE and all the Labs and the above discussions, a draft project plan was assembled. The project plan includes the following sections:

1. Introduction
2. Executive Summary
3. Background
4. Program Overview
5. Program Critical Functions
6. Stakeholders and Partners
7. Technology Research and Development Pan
   - 7.1 Electrode/Component Level Modeling
   - 7.2 Battery Cell Level Modeling
   - 7.3 Battery Pack Level Modeling
   - 7.4 Open Architecture Software
   - 7.5 Interactions with BATT and ABR
   - 7.6 Industry Collaboration through an RFP
8. Program Administration

Appendices

The draft planning document is a working document and will be distributed for review among the program participants to be further finalized. One of the major element of the Technology Development Plan was collaboration with industry, academia and others was through competitive procurement process, i.e. Request for Proposals (RFP). Figure III- 139 outlines the structure of sub-elements of CAEBAT identifying Elements 2 and 3 as the activities that require active participation of the industry through and RFP.

Request for Proposals to Develop Battery Design Tools. The goal of the CAEBAT activity is to "develop suite(s) of software tools that enable automobile manufactures, battery developers, pack integrators, and other end-users the ability to simulate and design cells and battery packs in order to accelerate development of energy storage systems that meet the requirements of the electric drive vehicle." So involvement of industry (car makers, battery developers, and pack integrators) in CAEBAT activity particularly for Elements 2 and 3 (Development of Cell and Pack Models) is essential. DOE's major strategy was to solicit active participation of industry in developing cell and pack software suit(s) for design of batteries. In support of this goal, NREL work to issue a Request for Proposals (RFP) to seek collaboration for development of the cell and pack battery design tools for a period of 3 years with 50%-50% cost sharing.

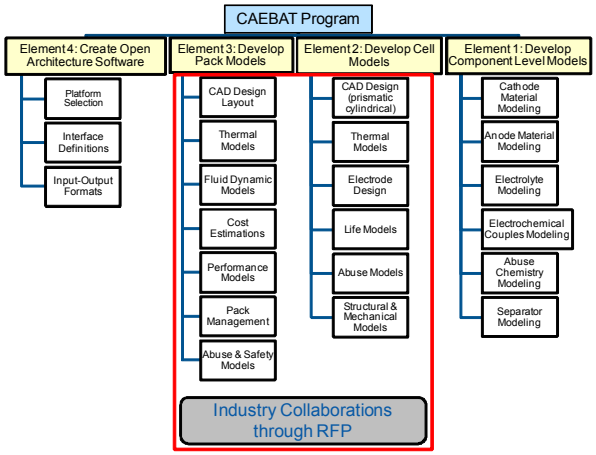

Figure III- 139: Sub-elements of the Computer Aided Engineering for Batteries (CAEBAT) Activity and Industry Collaboration.

In June 2010, NREL prepared a Statement of Work (SOW) titled "Development of Computer Aided Design Tools for Automotive Batteries," with the following Tasks:

Task 1. Battery Cell Level Modeling
Subtask 1.1. Identify what End-Users Need in a Cell CAE tool.
Subtask 1.2. Enhance Physics Linkage -Expandability
Subtask 1.3. Enhance Solver Modules - Fflexibility);
Subtask 1.4. Validation, Verification, and Demonstration;
Subtask 1.5. User Interface Development

Task 2. Battery Pack Model Development
Subtask 2.1 Identify End-User Needs for a Pack CAE Tool
Subtask 2.2 Models, Codes and Algorithms Development
Subtask 2.3 Validate, Verify, and Demonstrate Models
Subtask 2.4 User Interface Development

Task 3. Interface Development to Interact with CAEBAT Open Architecture Software (OAS)
Subtask 3.3.1 Interactions with CAEBAT OAS Workgroup
Subtask 3.3.2 Develop Interfaces for CAEBAT OAS

The SOW also identified review meetings, travel requirements, deliverables, and stage-sates reviews. After review internal and later by DOE energy storage program mangers, a request for proposal was prepared outlining: project description, terms and conditions, cost sharing requirements (50%-50%), period of performance (up to three years), best value selection process, and price (cost) evaluation for best value selection. The qualitative merit criteria for best value selection were: *technical approach (45%); project plan (20%); capabilities and facilities (15%), and experience and past performance (20%).*

The RFP was released to the public y sending emails and issuing a press release on July 30, 2010. Questions by interested parties were answered by August 15. Several proposals were received by September 24th. A Source Evaluation Team consisting of internal and external reviewers was assembled to review and recommend top proposals that meet the objectives and requirements of the RFP. The SET voting members included members from the NREL's Center for Transportation Technologies and Systems and external experts from ANL, LLNL, and ORNL. The none-voting members of the SET were from DOE, Advanced Engineering Solutions, and NREL's Business/Contract Services and Legal Office. The review process ended in October of 2010 by SET selecting top proposals. This selection was made based on criteria established under the RFP, the SET's assessment of the proposals submitted in response to the RFP, the terms and conditions, and the capabilities, expertise, and technical approach in fulfillment of the objectives of the program. DOE Energy Storage program mangers concur with the selection of the winning team and based on the availability of funding. Subcontracts will be placed in winter of FY11 after negotiations with the teams submitting the winning proposals. The work will begin soon after the subcontracts are agreed by all parties.

Development of Multi-Physics Battery Models. NREL has developed a battery model captures that three dimensional aspect of a cell while modeling electrochemistry as proposed by Dr. John Newman's group. The Newman's model captures lithium diffusion dynamics and charge transfer kinetics in porous media; predicts current/voltage response of a cell; and provides design guide for thermodynamics, kinetics, and transport across electrodes. The equations cover Charge Transfer Kinetics at Reaction Site; Species Conservation; Charge Conservation and Energy Conservation. Although the model has been very successful for small cells, it is difficult to resolve heat and electron current transport in large cell systems. Newman's model is often appropriate to predict the behavior of small cells. In large cells, particularly for automotive applications, however, working potential and temperature are non-uniform throughout the cell. NREL has developed a modeling framework for predictive computer simulation of lithium-ion batteries, namely the Multi-Scale Multi-Dimension (MSMD) model, which addresses the interplay among the various battery physics in varied scales. At NREL we have extended Newman's model to thermal-electrochemical 3D model using the multi-scale multi-dimensional (domain) model approach.

The MSMD model approach has achieved computational efficiency for resolving multi-physics interactions occurring over wide range of length scales by introducing separate solution domains for particle physics, electrode-scale physics, and cell-scale physics. In addition, the MSMD approach provides a modularized framework enabling model flexibility by providing multiple sub-model solver options with various physical/ computational complexities and expandability to add new physics of interest or to drop physics of insignificance or indifference. The MSMD model, the successfully developed integrated

multi-scale model, would expand knowledge on the interplay of different scale battery physics to help fast development of high performing, long lived, and safe lithium-ion batteries for electrified vehicles. Figure III- 140 shows the modularized hierarchy of structure in NREL's MSMD model.

As shown in the Figure III- 140, this modularized approach allows the end-user to pick and choose the desired physics and cod for particle, electrode, or cell modeling. The solution technique in each domain depends on the accuracy and fidelity desired. The MSMD approach applies to any electrochemistry, cell shape (cylindrical or prismatic), and electrode configuration (rolled or stacked) with 3-dimensional geometries.

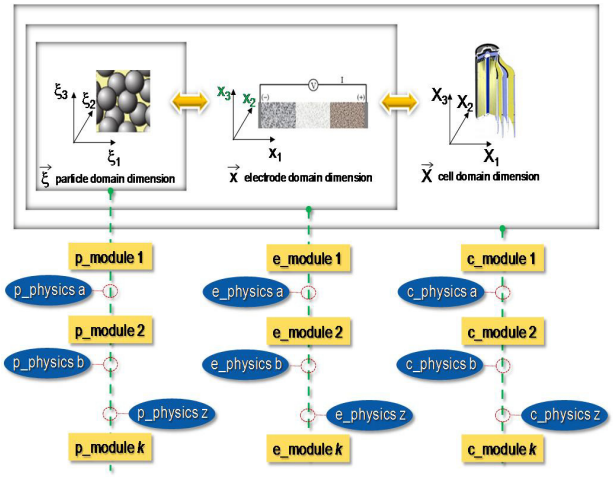

Figure III- 140: Modularized hierarchy of model structure in NREL's MSMD approach

To show the utility of battery computer aided engineering for designing cells, an example for impact of tab location for a large stacked prismatic cell is provided in this section for a lithium-ion battery with nickel-cobalt-aluminum (NCA) cathode and graphite anode. Figures III.E.1.5 and III.E.1.6 show the example results of multi-scale, multi-domain model of NREL to a 40 Ah stacked cell design with prismatic configuration after discharging the cell at constant current rate of 200 A for 2 minutes. Two cases were studied, one with positive and negative terminals on the same end (Figure III- 141) while the other with terminals on both ends (Figure III- 142). The model predicts the working potential, electrochemical current production, and the resulting temperature. In this case, the temperature near the tabs of the cell with terminals on both sides is about 4-5°C higher than the other cell.

The temperature distribution in the cell with terminals on both ends was much more uniform and thus provides a better way to cool. This stems from the differences in working potential that leads to a different current production and thus temperature distribution, which in turn results in difference in sate of the charge (SOC) of each cell. Having these non-uniformity in temperature, current distribution, and SOC in a cell over the many years and cycles expected from the large format cells could lead to non uniformity of usage of the active material and thus the areas close to the tabs in the cell with terminal on the same side can have more usage and thus potentially could degrade faster as has shown by Smith, et.al.

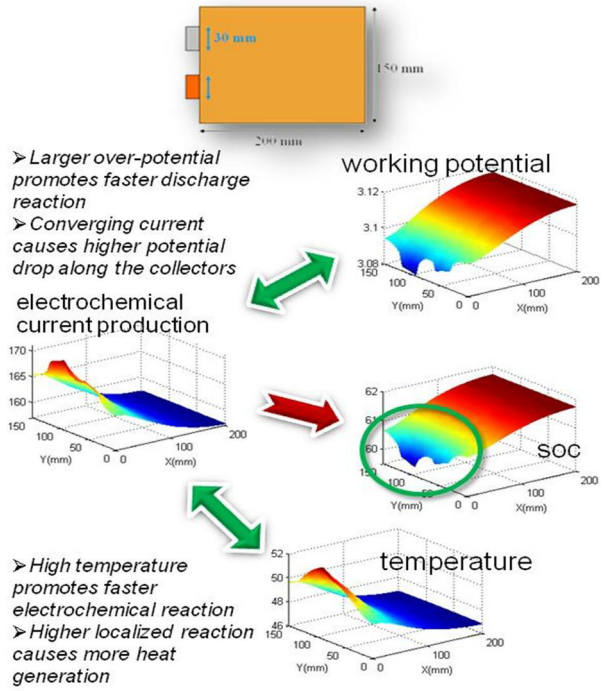

Figure III- 141: Example results of battery modeling multi-physics interaction for 40 Ah prismatic cells with terminals on the same side; after 2 minutes of 200 A constant discharge (compare it with the next figure)

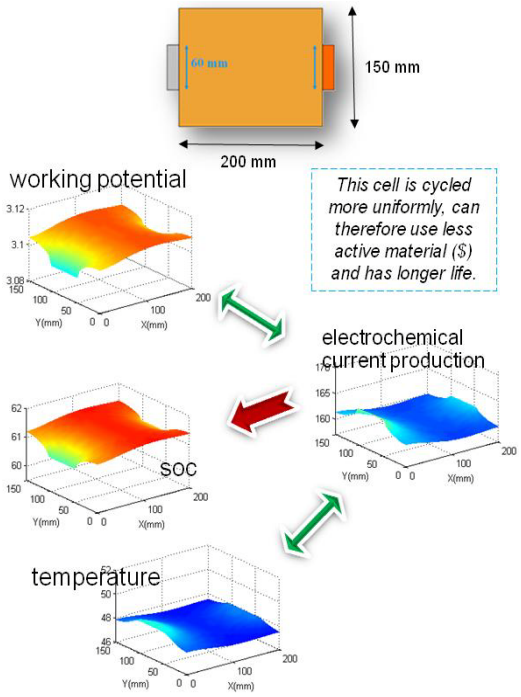

Figure III- 142: Example results of battery modeling multi-physics interaction for 40 Ah prismatic cells with terminals both sides; after 2 minutes of 200 A constant discharge (compare it with the previous figure)

Conclusions and Future Directions

NREL has initiated supporting DOE's Energy Storage program by coordinating the new activity called Computer-Aided Engineering of Electric Drive Vehicle Batteries (CAEBAT). NREL prepared an initial draft of a planning document for this activity. We interacted with six other National Labs (ANL. LBNL, INL, LLNL, ORNL, and SNL) through face to face meetings to obtain input for the draft planning document. We prepared a statement of work and issued a request for proposals (RFP) on July 30, 2010 for seeking industry partners to develop computer aided design tools for automotive batteries with a 50%-50% cost sharing. We received several proposals in September 2010 and reviewed them with help of external experts including other National Labs. NREL selected the top proposals meeting the technical and cost requirements of the RFP. We continued our electrochemical-thermal modeling of cells through the multi-physics, multi-scale, multi-dimensional (MSMD) platform for CAEBAT.

In FY11, NREL will execute the following activities:

- Negotiate with the teams submitted the winning proposals to sign a subcontract so the work could begin in the winter of FY11.
- Monitor technical performance of the CAEBAT subcontracts with industry per agreed schedule.
- Revise the CAEBAT planning document per DOE's guidance and working with the National Labs in the Program to identify gaps in support of the CAEBAT industry subcontractors.
- Continue the multi-physics MSMD modeling of batteries to support of CAEBAT partners.
- Organize an industry and Lab working meeting to enhance the collaboration between stakeholders on the subject of battery computer aided engineering.

FY 2010 Publications/Presentations

1. K.A. Smith, A. Vlahinos, G.-H. Kim, A. Pesaran, "Computer-Aided Optimization of Macroscopic Design Factors for Lithium-Ion Cell Performance and Life," *217th ECS Meeting*, April 29, 2010, Vancouver, Canada
2. Pesaran, G.-H. Kim, and K.A. Smith, " Accelerating Design of Batteries Using Computer Aided Engineering Tools," *The 25th Battery, Hybrid and Fuel Cell Electric Vehicle Symposium & Exhibition,* Shenzhen, China, November 5-9, 2010.
3. Kim, G. H.; Smith, K.; Pesaran, A.; Howell, D., "Computer-Aided Engineering of Automotive Batteries." NREL Report No. PR-540-48145 and *Proceedings of the Advanced Automotive Battery Conference*, Orlando FL, June 2010.
4. Pesaran, "CAEBAT Project Plan," NREL working draft document sent to DOE, June 2010 Milestone Report.
5. K. Roque, A. Pesaran, "Development of Computer Aided Design Tools for Automotive Batteries," NREL Request for Proposal, RCI-0-40497, Issued on July 30, 2010.

III.E.2 Computer Aided Engineering of Batteries Effort (ORNL)

Stephen Goguen (VT Project Manager)

Subcontractor: Oak Ridge National Laboratory

John A. Turner (Project Manager)
Computational Engineering and Energy Sciences Group
Oak Ridge National Laboratory
Office: (865) 241-3943
Cell: (865) 201-1849; Fax: (865) 241-4811
E-mail: turnerja@ornl.gov

Collaborators: S. Pannala, P. Mukherjee, S. Allu, W. Elwasif, and D. Bernholdt

Start Date: July 2010
Projected End Date: September 2013

Objectives

- Develop a flexible and scalable computational framework that can integrate multiple physics models at various scales (battery pack, cell, electrodes, etc.), and provide a predictive modeling tool under the auspices of the CAEBAT program.
- Coordinate with partners across the program on requirements and design of the framework so as to preserve the investment in existing models.
- Ultimately, the detailed simulation capability will model coupled physical phenomena (charge and thermal transport; electrochemical reactions; mechanical stresses) across the porous 3D structure of the electrodes (cathodes and anodes) and the solid or liquid electrolyte system while including nanoscale effects through closures based on resolved quantities.
- The simulation tool will be validated both at the full-cell level and at the battery-pack level, providing an unprecedented capability to design next-generation batteries with the desired performance and the safety needs for transportation.

Technical Barriers

Given the complex requirements for development of electrical energy storage devices for future transportation needs, a predictive simulation capability which can guide rapid design by considering performance and safety implications of different chemistry and materials choices is required. This capability must leverage existing investments and integrate multiple physics models across scales in order to (1) provide feedback to experiments by exploring the design space effectively, (2) optimize material components and geometry, and (3) address safety and durability in an integrated fashion. Such models do not currently exist.

Technical Targets

Develop the computational framework that will integrate existing models across the battery pack, modules, cells, etc. to provide an integrated design tool to battery manufacturers to optimize performance and safety in an accelerated fashion.

Accomplishments

- Polled all the national labs for modeling capabilities available at their institution and summarized these capabilities. A detailed report which contains the survey of models along with gap-analysis is under development.
- We have identified the Python-based Integrated Plasma Simulation (IPS) framework developed for fusion, SWIM (Simulation of RF Wave Interactions with Magnetohydrodynamics), to serve as our initial skeleton. Modifications are underway to accomodate CAEBAT requirements. The available source files are being integrated into this framework.

✧ ✧ ✧ ✧ ✧

Introduction

Computational tools for the analysis of performance and safety of battery systems are not currently predictive, in that they rely heavily on fitted parameters. While there is ongoing experimental research at various length scales around the world, computational models are primarily developed for the lower-length scales (atomistic and mesoscopic), which do not scale to the system-level. Existing models at the macroscopic or system-level are based on electrical circuit models or simple 1D models. The 1D models are limited in their ability to capture spatial variations in permeability or conductivity or able to handle multidimensional structure of recent electrode and solid electrolyte material. There have been some recent extensions to 2D and 3D and this is still an active area of development. Currently there is no design tool for batteries that can leverage the significant investments in modeling efforts across DOE and academia. An open and flexible computational framework that can incorporate the diverse

existing capabilities can provide a foundation for a predictive tool for the rapid design and prototyping of batteries.

Approach

We will develop a flexible, robust, scalable open-architecture based framework that can integrate models of coupled multiphysics phenomena (charge and thermal transport; electrochemical reactions; mechanical stresses) across the porous 3D structure of the electrodes (cathodes and anodes) and the solid or liquid electrolyte system while obtaining inputs from the nanoscale processes through closures based on resolved quantities. The schematic of such a framework is given in Figure III- 143.

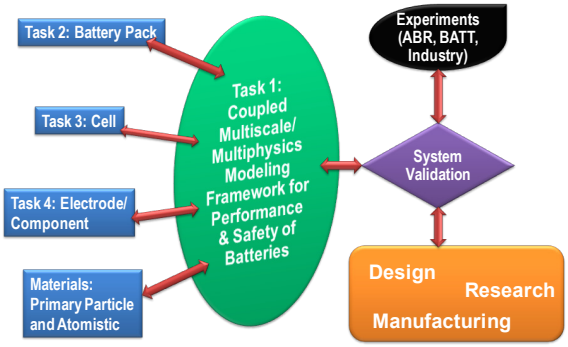

Figure III- 143: Schematic of the modeling framework and interactions with other tasks within the CAEBAT program and external activities.

This framework will allow for integration of the following coupled phenomena critical to develop a predictive simulation capability for modeling battery performance and safety:

- Mass Transport
  - Lithium/electron transport through cathode, anode and electrolyte materials, binder material, carbon etc.
  - Account for spatiotemporal variations in material properties
- Thermal Transport
  - Thermal transport through various battery materials as a function of space and time
- Electrochemistry
  - Primary and secondary reactions
  - Interfacial reactions
- Mechanical behavior
  - Linear and nonlinear mechanics
    - Stress/strain relationships
  - Fracture at primary and secondary particle levels

The short-term goal is to create a light-weight extensible software infrastructure that can support multiple modeling approaches for the various physical phenomena and here are some of the guiding principles for the design of this framework:

- Flexible
  - language-agnostic
  - multiple modeling approaches
  - combine appropriate component models for problem at hand
  - support integrated sensitivity analysis and uncertainty quantification
- Extensible
  - ability to add proprietary component models
- Scalable from desktop to HPC platforms
  - hardware architecture-aware

This framework will also be linked to a general purpose C++ PDE/ODE solver that can enable other task members to easily simulate mass/charge/electron/thermal transport, electrochemical reactions and mechanics. This would be similar to capabilities offered in COMSOL but specific to the needs of the CAEBAT program while leveraging development efforts from other DOE offices such as NE, ASCR and NNSA. This will give the users access to the best algorithms to do fully implicit, semi-implicit or explicit integration of the governing equations for modeling batteries.

In addition, the long-term goal is to develop the mathematical and computational infrastructure to be able to carry out multiscale and multiphysics simulations with the ability to transfer information across different models in a mathematically / physically consistent fashion for both spatial and temporal variations.

The eventual goal is to create a thoroughly-tested (verified), well-documented, highly-scalable (parallel), portable, flexible (extensible and easily-modified), maintainable software that leverages best existing open-source software framework that other CAEBAT tasks can easily integrate their models and validate against experiments to produce a software that industry can use for rapid prototyping and design of batteries.

We envision this framework to have a highly-modular design with well-defined interfaces, carefully-designed data structures, and a lightweight Python backplane. The interfaces will be defined with input from all the stake holders (national lab researchers, industry users, independent software vendors, academia, etc.). The design will be primarily driven by collecting user requirements from all these stake holders. Some of the specific tasks related to this activity are:

- Form working groups in each software-module area to collect existing models and standardize interfaces.

Identify gaps in existing models for future development.

- Define module interfaces, document, and circulate within working groups for review.
- Develop open architecture to link user-selected modules for coupled analysis.
- Define software modules necessary for CAE open architecture to perform trade-off analysis of battery performance, life, cost and safety from the material-to-pack scale.
- Demonstrate new capability of open architecture platform in Cell and Pack areas.
- Deliver beta version of open architecture software to CAEBAT program participants, industry, and academic partners for evaluation and comment.

Results

The CAEBAT activities at ORNL for FY2010 centered primarily around two milestones: a) Survey of existing models at partner institutions and initial modeling framework to integrate transport and thermal models and b) Incorporate existing models into common software repository and development of scalable computational framework. As part of the first activity, we have conducted a detailed analysis of existing computational software at various national laboratories and the survey summary is reported in Table III- 29. A more detailed report of this survey with gap analysis will be distributed soon for input from other laboratories and DOE.

Table III- 29: Survey of existing battery modeling capabilities at the DOE National laboratories

Institution	Code(s) / Model(s)	Features	Language(s)	Requirements	CAEBAT Element(s)
LBNL	DualFoil / COMSOL and ab-initio tools	Pseudo-2D and 2D models for cell	Fortran 77 & COMSOL (?)	BANDJ, DASSL	Element 3
NREL	Kinetics, Short-circuit, MSMD, Life-Predictive Model	Charge (1D), thermal (3D), chemical kinetics, empirical battery system life models	MatLab, Fluent (?)		Elements 1,2,3
ORNL	AMPERES	Full 3D meso-macroscopic model (transport, thermal, chemistry and mechanics)	C++	Trilinos, Sundials	Elements 1,2,3
ANL	Battery design and electrochemistry models	Several capabilities developed over the years	Excel / Fortran / MatLab (?)		Elements 3
INL	POL, AEM, Kinetics	Cell capacity, cell conductance, electrolytes	Fortran		Elements 1,2,3
SNL	Cantera and other detailed sub-continuum models	Detailed Electrochemicalkinetics	C++ / Python	Trilinos	Elements 1,2,3
LLNL	ALE3D	General purpose FEA with ALE algorithm	Fortran / C (?)	Meshing software (such as TruGrid)	Elements (?)

In addition, detailed analysis of commonly used Dual Foil software for battery cell modeling has been performed and Table III- 30 provides the input and output related to this software and Figure III- 144 provides the flow diagram. We are performing similar analysis with other available software so that we can identify the inputs and outputs to the various components in order to define standard interfaces. We are also in the process of binning this input and output into five major categories: Geometry, Runtime, Initial Conditions, Boundary Conditions, and Properties and Coefficients so that appropriate classification can be done for the files which will handle the various inputs and outputs. This should also aid in standardizing these different variables needed for the simulation software.

Table III- 30: Dual foil case study: analyzing input and output

Variables	Description
iim	limit on number of iterations
h1	thickness of negative electrode (microns)
h2	thickness of separator (microns)
h3	thickness of positive electrode (microns)
hcn	thickness of negative electrode current collector (microns)
hcp	thickness of positive electrode current collector (microns)
n1	number of nodes in negative electrode
n2	number of nodes in separator
n3	number of nodes in positive electrode
T	temperature (K)
xs(1, n1+2)	initial concentration (mol/m3)
csx	initial stoichiometric parameter for negative
csy	initial stoichiometric parameter for positive
tmmax	maximum time step size (s)
dfs1(1)	diffusion coefficient in negative solid (m2/s)
dfs3(1)	diffusion coefficient in positive solid (m2/s)
Rad1	radius of negative particles (microns)
Rad3	radius of positive particles (microns)
ep1	volume fraction of electrolyte in negative electrode
epp1	volume fraction of polymer phase in negative electrode
epf1	volume fraction of inert filler in negative electrode
ep2	volume fraction of electrolyte in separator
epp2	volume fraction of polymer phase in separator
ep3	volume fraction of electrolyte in positive electrode
epp3	volume fraction of polymer phase in positive electrode
epf3	volume fraction of inert filler in positive electrode
sig1	conductivity of negative matrix (S/m)
sig3	conductivity of positive matrix (S/m)
rka1(1)	reaction rate constant for negative reaction
rka3(1)	reaction rate constant for positive reaction
re	density of electrolyte (kg/m3)
rf	density of inert filler (kg/m3)
rpl	density of polymer phase (kg/m3)
rs	density of separator material (kg/m3)
rcn	density of negative current collector (kg/m3)
rcp	density of positive current collector (kg/m3)

Variables	Description
ranode(1)	anode film resistance (ohm-m2)
rcathde(1)	cathode film resistance (ohm-m2)
htc	heat-transfer coefficient with external medium (W/m2K)
dUdT	temperature coefficient of EMF (V/K)
Cp	heat capacity of cell (J/kg-K)
residm	residual mass (kg/m2)
Tam	ambient temperature (K)
ncell	number of cells in a cell stack
iht	0 users htc 1 calcs htc 2 isothermal
nside	side reaction flag
ii1	1 for long print-out 0 for short print-out
ii2	prints every ii2 th node in long print-out
ii3	prints every ii3 th time step in long print-out
imp	0 for no impedance 1 for impedance
cspp1	capacitance of negative material (F/m2)
cspp3	capacitance of positive material (F/m2)
icurs	number of current changes

Output (can be a function of t, x, and y):

Cell voltage
Uocp (open circuit potential)
Electrolyte potential
Electronic potential
Li concentration in solid
Li concentration in electrolyte
Current density
Temperature
Heat generation

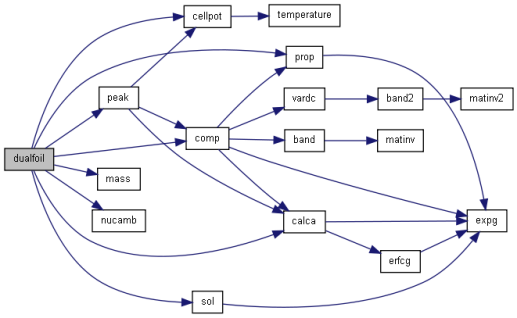

Figure III- 144: Dual foil case study: flow diagram

After detailed review of the framework options available for linking of existing software, we have selected a Python-based architecture. In particular, we have identified the IPS framework, developed for the fusion SWIM project. The IPS framework has the following design features which made it attractive for the CAEBAT effort:

- Component-based approach
  - *Extensibility*, V&V, independent development.
- Common solution (battery) state layer
  - Data repository.
  - Conduit for inter-component data exchange.
- File-Based data exchnage
  - No change to underlying codes.
  - Simplify *"unit testing"*
- Scripting Based Framework (Python)
  - Rapid Application Development (RAD).
  - Adaptability, changeability, and flexibility.
- Simple component connectivity pattern
  - Driver/workers topology.
- Codes as components:

- Focus on code-coupling vs physics-coupling as first step.

- Simple unified component interface
- init(), step(), finalize().

The framework layout is given in Figure III- 145 and a sample IPS structure for a CAEBAT application (using Dual Foil, Cantera for chemistry and Sundials for time integration) is given in Figure III- 146. The framework can launch parallel jobs but also create several instances (such as parameter sweeps) on a parallel cluster. The IPS execution environment is shown in Figure III- 147 and the data management architecture is shown in Figure III- 148 where the different config, input, logs, work, and results files reside.

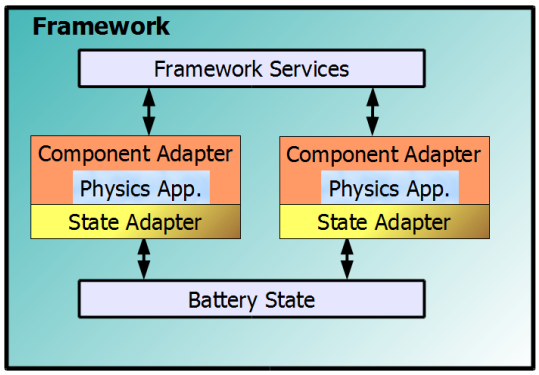

Figure III- 145: IPS framework layout

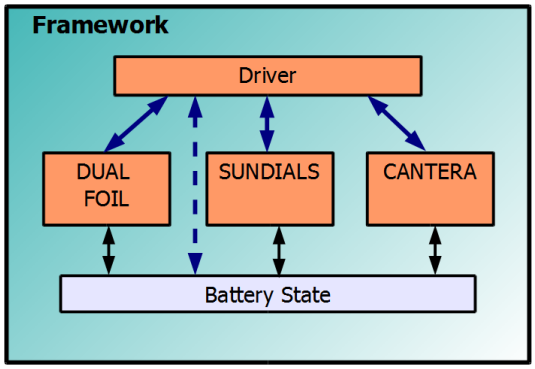

Figure III- 146: An example IPS application structure

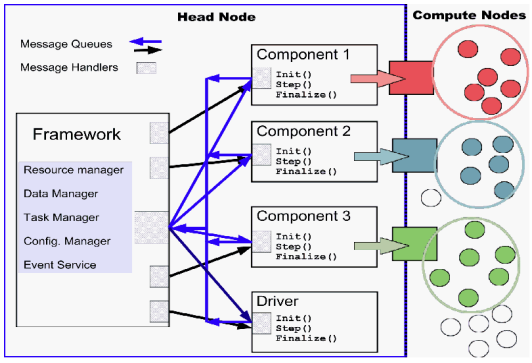

Figure III- 147: IPS execution environment

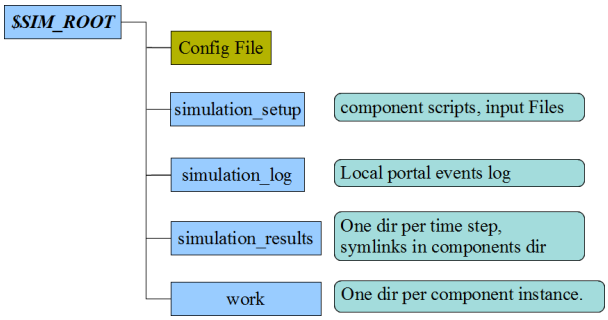

Figure III- 148: Data management – simulation tree layout

Conclusions and Future Directions

ORNL has identified the major software components from the DOE national laboratories that need to be linked in the CAEBAT framework. In addition, we are in the process of adapting an existing Python-based framework to integrate these software components to perform simulations of various battery components and systems.

In the coming year, ORNL will execute the following tasks:

- Convene working groups to standardize interfaces (file as well as data) to all the major software components
- Deliver the survey report, along with gap-analysis
- Demonstrate the framework on sample problems
- Initial validation at various levels (cell, module and battery pack) using existing experimental data

FY 2010 Publications/Presentations

1. "Modeling and Simulation for Batteries," Presentation to Ed Owens, Brian Cunningham, and Steve Goguen, EERE VT program, ORNL, Aug. 5, 2010.
2. "Modeling and Simulation for Batteries," Presentation to Ted Miller, Ford Research, ORNL, Aug. 23, 2010.

III.E.3 Battery Thermal Analysis and Characterization Activities (NREL)

Matt Keyser and Gi-Heon Kim

National Renewable Energy Laboratory
1617 Cole Boulevard
Golden, Colorado 80401
Phone: (303) 275-3876; Fax: (303) 275-4415
E-mail: matthew.keyser@nrel.gov
gi-heon_kim@nrel.gov

Start Date: October 2009
Projected End Date: September 2013

Objectives

- Use NREL's unique test equipment to thermally test and evaluate PHEV and HEV cells and modules developed by FreedomCAR/USABC developers.
- Support FreedomCAR/USABC developers with electro-thermal analysis of energy storage devices for assessing and improving the thermal design of their electrochemical devices for enhanced life and performance.

Technical Barriers

This project addresses the following Energy Storage Research and Development technical barriers as identified by the Vehicle Technologies Program:

- Cost – The current cost of Li-based batteries system (the most promising chemistry) is approximately a factor of three-five too high on a kWh basis. Thermal management and packaging add cost to the system and need to be optimized.
- Performance – The performance barriers include the need for much higher energy densities to meet the volume/weight requirements and to reduce the number of cells in the battery (thus reducing system cost). Improved thermal management is essential.
- Life – The ability to attain a 15-year life, or 300,000 HEV cycles (at 30C), or 5,000 EV cycles (at 35C) are challenging and difficult to attain. Specifically, the impact of temperature over the life of the battery in a vehicle, even when the car is parked must be evaluated and overcome.

Technical Targets

- By 2010, develop an electric drive train energy storage device with a 15-year life at 300 Wh with a discharge power of 25 kW for 18 seconds and a cost of $20/kW.
- Develop hardware with thermal management for specific applications that can be tested against respective performance targets and used for subsystem benchmarking.

Accomplishments

- Thermally and electrically evaluated the
  - A123Systems Gen 2 B0.1 and Gen 2 B1.0 HEV (iron phosphate) cylindrical cells;
  - CPI PHEV PLG1 and PLG2 (spinel with hard carbon) cell, the
  - EnerDel HEV and PHEV ($LiMnO_2$) cells, and
  - CPI PHEV battery pack (refrigerant cooled).
- Initiated testing of the A123Systems HEV 6.3 Ah prismatic cell, the A123Systems HEV 32113 module, and the EnerDel HEV module.
- Performed a thermal analysis using a computational design tool of a large format stacked prismatic cell using NREL's multi-physics MSMD model.
- Created a simple Li-Ion cell model, based on FreedomCAR model, capable of capturing basic electric and thermal behavior.
- Performed an analytical & numerical investigation to evaluate the impacts of additional Kapton layer on thermal response for a JCS cell design.

✧ ✧ ✧ ✧ ✧

Introduction

The operating temperature is critical in achieving the right balance between performance, cost, and life for both Li-ion batteries and ultracapacitors. At NREL, we have developed unique capabilities (such as calorimeter and thermal imaging) to measure the thermal properties of cells including. We calibrated and have begun using NREL's new large calorimeter to measure the heat generation of large PHEV cells and modules. We also use our electro-thermal lithium-ion battery models to analyze the thermal performance of battery systems in order to aid battery developers with improved thermal designs.

Approach

Using NREL's unique calorimeters and infrared thermal imaging equipment, we obtain thermal characteristics (heat generation, heat capacity, and thermal fingerprints) of batteries and ultracapacitors developed by

FreedomCAR developers and other industry partners. In the last several years, NREL have created a framework for predictive computer simulation tool for batteries, the multi-physics, Multi-Scale Multi-Dimensional (MSMD) model, addressing various physics in relation with battery performance, safety, durability, and interactive coupling of multi-physics in varied scales. We performed a demonstration of a computational design optimization of a large format stacked prismatic cell using NREL's MSMD model. NREL supported the FreedomCAR Electrochemical Energy Storage Technical Team by participating in various work groups such as the JCS, CPI, A123Systems, and EnerDel Work Groups. For CPI, we developed a Li-Ion heat generation model based on a simple lumped capacitance. For JCS, we performed thermal analysis to evaluate the impact of additional Kapton layer placed in a cell for improving safety response of a JCS large format cylindrical cell.

Results

Thermal Evaluation of the A123Systems Gen 2 B0.1 and Gen 2 B1.0 HEV cells. NREL evaluated the heat generation and efficiency of the A123Systems Gen 2 B0.1 and Gen 2 B1.0 HEV cells at -15°C, 0°C, and 30°C. The difference between the two design was that B0.1 version was can neutral, while the B1.0 version had can positive design.

Figure III- 149 compares and contrasts the two generations of the HEV cells containing iron phosphate cathodes. Essentially, the efficiency and heat generation between the two generations of cells are equivalent. It should be noted that the cells have the same volume and package style – 32113. Under the 25 Wh HEV cycle at 30°C, the cells have an efficiency of greater than 96 %; whereas the efficiency decreases to approximately 94.0% under the 50 Wh HEV cycle at the same temperature.

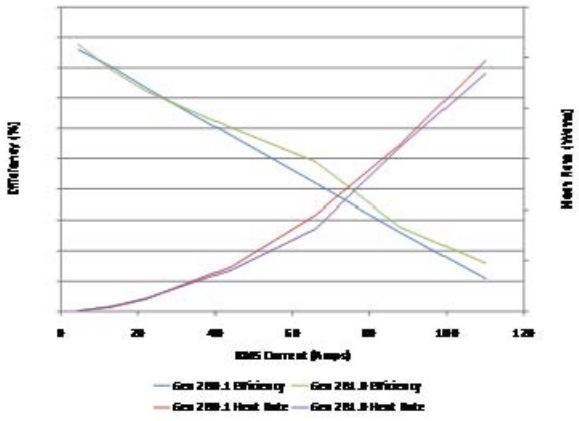

Figure III- 149: Efficiency and heat generation comparison between the Gen 2B0.1 and Gen 2 B1.0 HEV cells.

Thermal Evaluation of the CPI/LG Chem PLG1 and PLG2 Pouch Cell. In FY10, NREL tested the PLG1 and PLG2 pouch cell from Compact Power, Inc., US subsidiary of LG Chem of South Korea. The cells were designed and evaluated for a PHEV10 application. Prototype cells were built at LG Chem (spinel cathode) and tested by CPI and DOE under the USABC program. NREL performed thermal characterization testing of the deliverable cell. Tests included thermal imaging of the cells under high rate discharge and aggressive vehicle power profile (US06) cycling – shown in Figure III- 150. The cells showed reasonable thermal uniformity, with no significant hot spots of concern. In PHEV 10 application, maximum temperature is reached at the end of charge depletion, EV-type cycling. Charge sustaining, HEV-type cycles generate far less heat and thus require less cooling from the thermal management system to maintain desired battery temperature. Heat generation measurements were conducted using NREL's calorimeter at -15°C, 0°C and 30°C for a range of constant current discharge/charge and vehicle power profiles. The PLG1 and PLG2 cells have equivalent efficiencies and heat generation at 30°C.

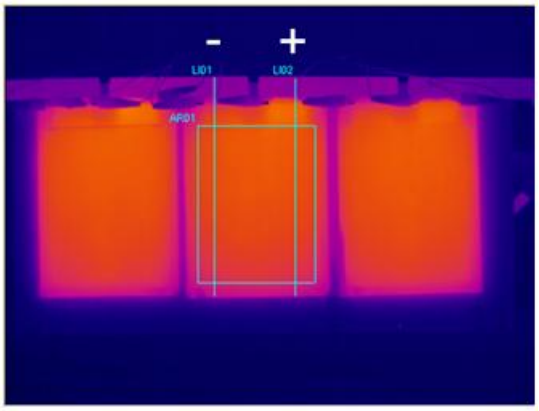

Figure III- 150: Infrared thermal image of the CPI PLG1 Pouch Prismatic Cells under US06 cycling.

EnerDel HEV and PHEV Cells. NREL electrically and thermally evaluated the EnderDel HEV cell (lithium manganese). The HEV cell was electrically evaluated by capacity cycling the cell and performing an HPPC on the cell. The cell was then thermally imaged under various high current discharge cycles as well as the US06 driving profile. The cell showed good thermal uniformity during US06 cycling of the cell – see Figure III- 151. The cell was also thermally evaluated with NREL's calorimeter at 30°C and -15°C. The cell was greater than 98% efficient under the US06 cycle at 30°C.

NREL also performed an initial electrical and thermal evaluation of the EnerDel PHEV $LiMnO_2$ cell. However, the cells were sent back to EnerDel for further design modifications before the cells were rigorously tested at NREL.

Thermal Evaluation of the CPI PHEV Lithium-ion Battery Pack. NREL thermally evaluated performance of the CPI/LG Chem PHEV battery pack. The cell consisted of PLG2 cells from LG Chem with spinel cathodes.

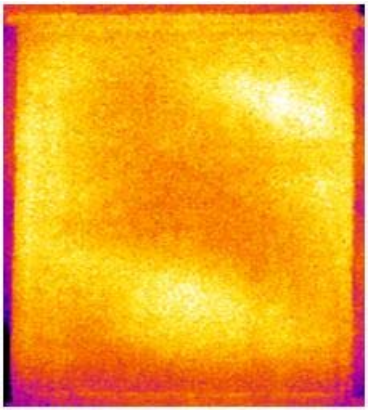

Figure III- 151: Thermal image of the EnerDel HEV cell under US06 cycling

The cells were prismatic pouch with about 20 Ah capacities. The battery pack is engineered with an independent vapor compression cooling system. The cells were cooled by this dedicated external refrigeration loop by flowing coolant in a plate with cell in thermal contacts with it. CPI installed many thermocouples between various cells (Figure III- 152). We measured the temperature rise and difference between corresponding cells as well as the voltage of each cell within the pack. Testing was done at ambient temperatures of 30°C and -20°C using a modified Toyota Camry US06 power profile. During testing, the power draw from the vapor compression system as well as the BMS were recorded and evaluated. The battery pack showed good temperature uniformity from cell to cell during the NREL testing. Future tests include thermally evaluating the pack under a real world 24 hour cycle – driving + parked conditions. NREL will also investigate how standby thermal management can potentially reduce battery degradation due to high ambient temperatures while charging.

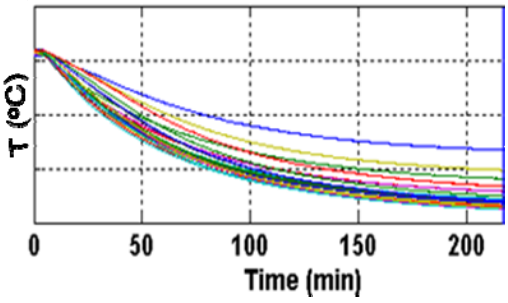

Figure III- 152: CPI refrigeration system cools down the cell temperatures after a high temperature soak condition

Computer-Aided Optimization of Macroscopic Design Factors for Lithium-Ion Cell Performance and Life. Battery development process of testing new materials in multiple cell sizes, in multiple pack designs, and over many months is extremely time consuming, expensive, and ad hoc. Large cells and batteries suffer from heat, current, stress issues not present in small configurations. NREL performed a demonstration of a computational design optimization of a large format stacked prismatic cell using NREL's MSMD model (Figure III- 153). The results were presented at an Electro Chemical Society meeting in FY10 and the 25th Electric Vehicle Symposium in China. Macroscopic design parameters of a 20 Ah stacked prismatic cell, such as aspect ratio, number of stacked layers, tap size, current collector foil thickness, were chosen for optimization with given materials and identical microscopic electrode structures. Energy density of a cell and the maximum local temperature in 3D cell geometry during PHEV10 US06 cycle were used for design evaluation criteria. Robust design CAE methods provide straight-forward process for optimization, so long as objectives & constraints are well-defined and physics and geometry are properly captured. Compared to baseline design, identified optimization of macroscopic factors decreases peak temperatures (fewer losses in cell) while increasing useable energy density.

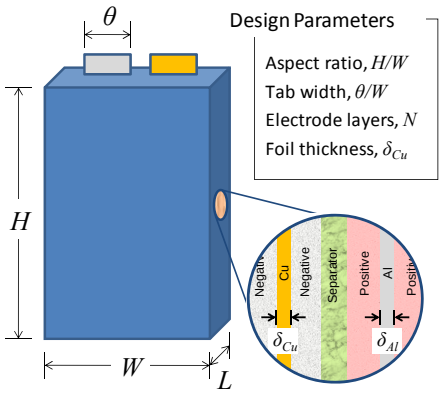

Figure III- 153: Macroscopic design parameters used for this optimization study; with fixed conditions for $\delta_{Al} = 1.6 \times \delta_{Cu}$, 20 Ah capacity, electrode loadings, and electrode thicknesses.

Cell Heat Generation Prediction using Lumped Parameter Model: CPI PLG2 15 Ah. Computationally-fast cell model with reasonable accuracy in thermal and electrical response prediction would be useful for multi-cell pack behavior prediction. A simple Li-Ion cell model, based on the Randles model discussed in the FreedomCAR Battery Manual, was created capable of capturing basic electrical and thermal behavior. From the developed model, heat generation prediction at 30°C shows 10-15% range average error, 10-25% error for driving cycles (Figure III- 154). Entropic heat (involving dV/dT term) not

yet considered but to be included in future, may improve prediction results.

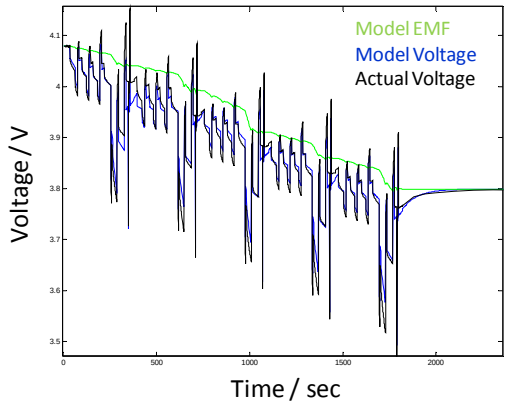

Figure III- 154: Comparison of model prediction with measured data for voltage response of CPI PLG2 cell at 30ºC during USABC charge depleting cycle. The model fits good overall, but it under-predicts heat generation by about 14%.

Impacts of Kapton Wrapping on Thermal Signature of Large Cylindrical Cells. Kapton film wrapping is considered between the outermost surface of jelly roll and the can inner wall to improve safety response of large format cylindrical cells for blunt nail tests.

However, the impacts of additional Kapton layer on thermal response of a cell should be evaluated. Therefore, an analytical & numerical investigation was performed. For uncertainty of quantifying thermal resistance at the contact interface between the parts, parametric formulation was developed. Portion of temperature change inside kapton film, $\Delta T_{internal}$, against the total temperature change, ΔT, including temperature discontinuity at interface was set as a parameter.

$$\Delta T_{internal} = f * \Delta T \qquad (0 <= f <= 1)$$

$$R_{therm} = \frac{l_{Kapton}}{k_{Kapton} \cdot f} + \frac{l_{Al}}{k_{Al}} + \frac{1}{h_\infty} \quad \left[\frac{^oC}{W/m^2}\right]$$

Kapton wrapping is not expected to impact significantly on thermal response of large capacity cylindrical cells in typical air cooling conditions (where h ~ 5 to 25 W/m^{2}K), unless it causes excessive thermal contact resistance as shown in Figure III- 155.

Conclusions and Future Directions

Although there is variation between lithium chemistries, the efficiency of these cells are typically greater than 90% at 30^{o}C under US06 cycling. As PHEV and EV packs come to the market, further research needs to be performed with regards to pack design to ensure that the cell to cell temperature difference is less than 2-3^{o}C to ensure a 15 year life. The data provided by NREL's unique test equipment aides in the development of innovative thermal designs to achieve this goal. In FY11, NREL will continue to thermally evaluate HEV, PHEV and EV cells from USABC and FreedomCAR (A123Systems, CPI, Maxwell, ActaCell, Quallion) to meet the Vehicle Technologies Program's goals and objectives.

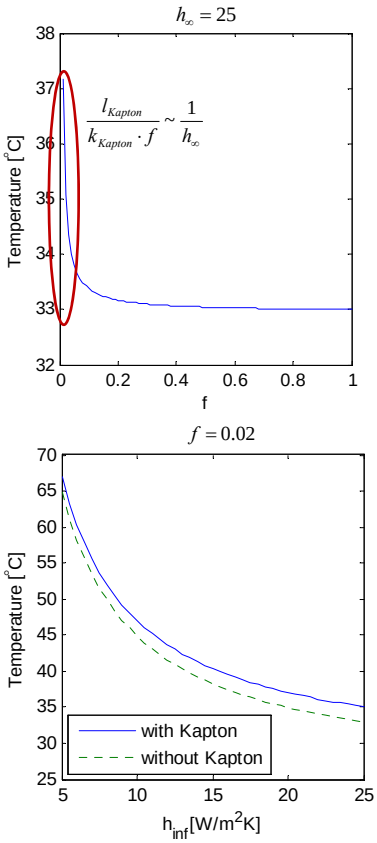

Figure III- 155: Relation between steady state cell temperature and contact resistance factor f at 5W per cell heat generation condition (top); Temperature and external heat transfer coefficient relation with and without Kapton layer, when excessive thermal contact resistance (f=0.02) is caused by Kapton wrap.

FY 2010 Publications/Presentations

1. K. Smith, A. Vlahinos, G.-H. Kim and A. Pesaran, "Computer-Aided Optimization of Macroscopic Design Factors for Lithium-Ion Cell Performance and Life", *217th Electrochemical Society Meeting*, Vancouver, Canada, April 29, 2010
2. Presentations to USABC and FreedomCAR Energy Storage Tech Team and its Working groups at JCS, CPI, A123Systems and EnerDel.
3. K. Smith, M. Keyser, D. Long, A. Pesaran, "Battery Thermal Evaluation Studies - CPI PHEV10 Module & Pack," *Milestone Report*, NREL, September 2010

4. G.-H Kim, K. Smith, D. Long, and J. Neubauer, "Thermal Modeling of Advanced Lithium-Ion Batteries," *Milestone Report*, NREL, June 2010,
5. M. Keyser, K. Smith, D. Long, "Thermal Characterization of Advanced Lithium Batteries," *Milestone Report*, NREL, June 2010.

III.E.4 Lithium-Ion Abuse Model Development (NREL)

Gi-Heon Kim
National Reneable Energy Laboratory
1617 Cole Blvd.
Golden, CO 80401
Phone: 303-275-4437
E-mail: Gi-Heon.kim@nrel.gov

Start Date: October 2008
Projected End Date: September 2013

Objectives

- Enhanced exsiting lithium-ion abuse models developed at NREL by adding internal short circuit modeling (ISCs)
- Develop a model of the "on-demand ISC instigator" device developed at National Renewable National Laboratory
- Understand working principles of NREL ISC instigator device and providing guidance for improving the design of the device.

Technical Barriers

Saftey concerns for lithium-ion batteries in electric drive vehicles (EDV) is one of the major barriers to wide-spread adoption of EDVs. Most of the safety concerns arise from the external instigators such as crush, overcharge, puncture, overheating that could lead to thermnal runaway. However one of the challenges in development of technologies for mitigating Li-ion battery safety concern is that of the mechanism of internal short circuit (ISC) evolution resulting in catastrophic themal reunaway. It is not well-understood due to the lack of well-defined experimental data while the ISC is a major cause for the most of safety incidents in field operations. The ISCs are hardly reproducible in experimental environments with plausible methods. Many researchers have tried to replicate field safety incidents by conducting overcharging, nail penentration, pinch test, crush test, oven tests, metal particle implantation, etc, but it seems that none of those methods appropriately simulate the ISCs. Therfore a new approach to investigate the ISC phenomina is required to fulfill battery safety.

Technical Targets

- Develop a numerical model of internal short circuits in the NREL's ISC instigator device.
- Evaluate impacts of design parameters of the ISC instigator.

Accomplishments

- Demonstration of electric current paths through cell parts and the ISC instigator.
- Calculation of electric resistances of the ISCs.
- Evaluation of impacts of metal patch thicknesses and diameters on electric resistance of the ISCs.

✧ ✧ ✧ ✧ ✧

Introduction

In FY09, we developed an integrated simulation tool for multi-physics, 3-dimensional modeling of internal short circuit of lithium-ion cells by combining NREL's electrochemical, electro-thermal, and abuse kinetics reaction models. This model was used extensively. This year we have used a part of the model to simulate NREL internal short cuircuit instigator device to improve its design.

NREL researchers have recently invented an ISC instigator device which can be implanted inside Li-ion cells with expected negiligible impacts on electrochemical performance. This device could be later activiated to trigger internal short circuits on demand that are relevant to field failures due to manufacturing defects and faults evolution. NREL has been working to improve this invention by stand-alone tests, tests in coin cells and recently test with 8 Ah prismatic li-ion cells. At the time, we were writing this report, we were also in the process of applying for a patent for this on-deman ISC. To protect the legality of our patent application, unfortunately, not much information on the details could be discussed in a publically-open document like this Annual Progress Report. Figure III- 156 shows that the NREL ISC instigator consists of several metallic pieces and a special material is placed between the metal pieces to prevent an immediate short and to allow the instigator triggering the short externally. NREL has conducted experimental verification and model development simultaneously for the ISC instigator device to understand physics of the ISC and to enhance the design of the ISC instigator.

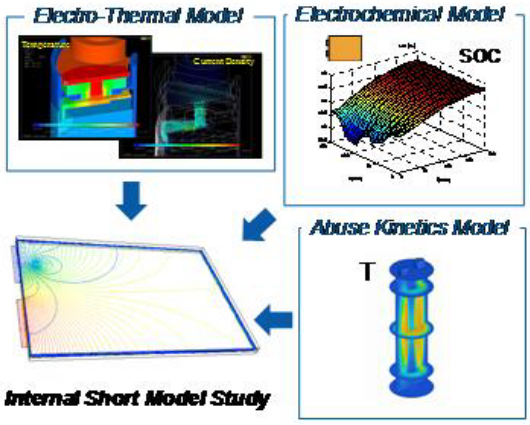

Figure III- 156: Integrated Multi-Physics Internal Short-Circuit Model

Electric resistance of the ISCs including the ISC instigators is the key factor determining wheather an ISC is followed by immediate thermal runaway or not. For small cells of up to 2-4 Ah capacitiy, it has been known that ISCs with electric resistance of 1~3Ω are likely to lead to thermal events. However there has not been an effective method to measure or control electric resistance of an ISC occuring inside a Li-ion cell yet. It is not proper to measure electric resistance of an ISC based on the resistance of the short itself (e.g. electric resistance through the ISC instigating device), because resistances of ISCs are determined not only by the nature of the short but also by the electrical configuration and materials and geometries of the component parts in a cell (Figure III- 157). Therfore a numerical model has been developed to solve current distribution and calculate electric resistance of ISCs through the invented device.

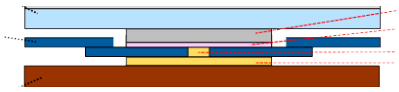

Figure III- 157: Concept sketch of the ISC instigater that could be implanted inside a Li-ion cell.

Approach

A two-dimensional axis symmetry is assumed in the present model. The simplified schematics diagram for the solution domain geometry is shown in Figure III- 158. Contact resistances are ignored assuming perfect contacts between the parts. In the actual cells with the ISC instigator, the short current generated from the cell is likely to flow towards the shorted region and eventually merge into the short as shown in the figure. The current boundary condition in the axis symmetry model domain is feasible to represent the current uniformely merging into the short.

We used design parameters and physical properties used for the model, but this will be not shown here for protection of patent application. To investigate impacts of design space, parametric studies were conducted with different parameters.

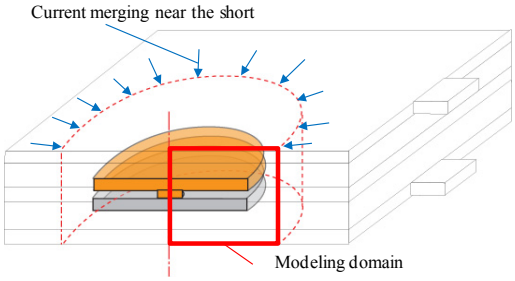

Figure III- 158: Modelig strategy 2D modeling geometry and boundary conditions, the modeling domain assigned near the ISC instigator inside a jellyroll: current merging into the ISC instigator is considered as a constant current boundary condition in the present model.

Results

Electrical characteristics of the ISCs. The modeling results of the reference case in Figure III- 159(a) show that the most of potential drop in the ISC occurs in the cathode electrode between metal piece and the positive current collector. It can be explained that the short current causes a large potenrial drop during passing through the cathode electrode layer because the cathode material is highly resistive.

In Figure III- 159(a), the current flow from the positive current collector to the metal piece of the device contacting cathode layer surface is evenly distributed in the cathode volume between the collector and metal piece forming a path minimizing electric resistance. Current density contour in Figure III- 159(b) presenting high current density in the whole area of metal pieces is consistant with the observation. This implies that the current is preferentially carried by conductive metal parts rather than the composite electrode matrices. Therfore current flows from the positive current collector to the metal piece and then merges into the the other metal piece. Current in the anode electrode goes in the same way but there is no large potential drop occurred because the anode material is less resistive than the cathode material.

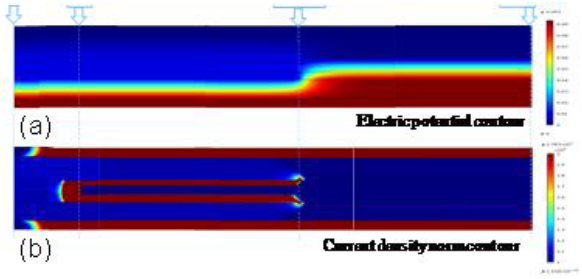

Figure III- 159: Modeling results: Note that the aspect ratio of the figures is adjusted for clear vision (a) electric potential contour, (b) current density contour

Impacts of design parameters. Primary design parameters of the ISC instigator are thicknesses and diameters of the metal pieces. To understand impacts of those parameters on electric resistance of the ISCs and to obtain design parameters able to bring low electric resistances of the ISCs, various cases with different paremeters were conducted. Electric resistance of the reference case, R_{ref}, is calculated as 0.0933Ω. Since the electric resistance of the ISC instigator itself is calculated very small in the model, the order of 10^{-7} Ω, the most of R_{ref} is contributed by the current paths through the resistive electrodes. Electric resistance of a case with no piece is 2.3188 Ω which is about 25 times larger than R_{ref}. When the metal pieces are removed from the ISC instigator, current should flow in the resistive electrode through a small area same with the area of the metal-piece resulting in a high electric resistance. High electric resistances due to small areas for current flows in electrodes are consistantely shown in modeling results of cases with small pieces (1.6219 Ω, 1700% of R_{ref}), small Al piece (1.1138Ω, 1100% of R_{ref}), and small Cu piece (0.2413 Ω, 260% of R_{ref}). Low electric resistance from the case with large metal pieces (0.0046 Ω, 47% of R_{ref}) also shows the consistency of the explanation. Size of the mteal pieces located in the cathode side has larger impacts on electric resistance than that of the other metal pieces in the anode side because the cathode material is more resistive than the anode electrode. Electric resistance of a case with thin pieces (0.0955 Ω, 103% of R_{ref}) implies that thicnkesses of the metal pieces do not influence electric resistance of ISCs much.

NREL continues to develop numerical models of the ISC instigator and to enhance its design. Improved ISC istigators will be used to test various safety devices for further validating study.

Conclusions and Future Directions

Electrical modeling of internal short circuits including NREL's unique ISC instigator is delveloped to investigate ISC characteristics and to estimate effects of design parameters. Modeling results show that the overall electric resistance of the formed short is determined at the resistive electrodes, espetially in the cathode electorde. The results of parametric studies present large metal patches having advantages to reduce electric resistance of an ISC with an ISC instigator.

FY 2010 Publications/Presentations

1. G.H. Kim, K.J. Lee, "Modeling Internal Short Circuit Instigator," Presentation to DOE by NREL, August 12, 2010.
2. M. Keyser, D. Long, A. Pesaran, "NREL Internal Short Circuit Simulator – Development Summary," *NREL Milestone Report to DOE*, March 2010.

III.F Energy Storage R&D Collaborative Activities with the International Energy Agency (IEA)

David Howell, Team Leader
Hybrid and Electric Systems
EE-2G, U.S. Department of Energy
1000 Independence Ave., SW
Washington, DC 20585
David.Howell@ee.doe.gov
202-586-3148

Alternate Point of Contact:
James A. Barnes
James.Barnes@ee.doe.gov
202-586-5657

Start Date: Continuing Effort

Objective

Use the resources available through the International Energy Agency's (IEA) Implementing Agreement on Hybrid and Electric Vehicles (IA-HEV) to facility the exchange of information on relevant technologies and governmental activities within the international community and to study relevant issues.

Introduction and Approach

The International Energy Agency (IEA) is an autonomous body that was established in November 1974 within the framework of the Organization for Economic Co-operation and Development (OECD) to implement an international energy program. It carries out a comprehensive program of energy co-operation among twenty-six of the OECD's thirty member countries. Much of the IEA's work is done through over 40 Implementing Agreements. The Hybrid and Electric Systems Team is very active in the IA-HEV. This IA has 15 member countries: Austria, Belgium, Canada, Denmark, Finland, France, Ireland, Italy, Netherlands, Spain, Sweden, Switzerland, Turkey, the United Kingdom, and the United States. Additional countries have applied and been invited to join the Agreement. The IA-HEV functions through seven annexes (working groups) that focus on relevant areas of interest. These include Information Exchange (I), Electrochemical Systems (X), Electric Cycles (XI), Heavy-duty Hybrid Vehicles (XII), Fuel Cells for Vehicles (XIII), Lessons Learned (XIV), and Plug-in Hybrid Electric Vehicles (XV). Annexes XIV and XII are scheduled to end in late 2010. Several new annexes including ones on system integration and battery testing are being discussed for 2011. The United States is a member of all of these annexes and provides organizational leadership for Annexes I, X, XIV and XV. The National Renewable Energy Laboratory (NREL) is very active in several of the annexes associated with vehicle systems. More information about the activities of the IA-HEV and its annexes may be found in its 2009 Annual Report; copies of this report are available from James Barnes; requests may be sent to the address at the beginning of this section.

Annex X: Electrochemical Systems. Annex X is most relevant to the focus of the Energy Storage effort within Vehicle Technologies. It functions by sponsoring informal, focused workshops to address technical or informational issues important to batteries for vehicles. In FY 2010, it held two workshops.

A meeting on the **Accelerated Life Testing of Batteries (Especially Lithium-ion Batteries) for Vehicles** was held in Waikoloa, Hawaii, USA on 15 – 17 January 2010. The location and time were chosen to allow the workshop to be held in conjunction with meetings of the International Battery Association and the Pacific Power Sources Symposium (PPSS).

The need for the workshop was based on the fact that automotive manufactures want batteries in electric drive vehicles to last the life of the vehicle, sometimes as much as 15 years; but that at the time of vehicle introduction; but that these manufacturers often have only 2 or 3 years of real-time data on a new battery technology. This meeting was to discuss how to predict the life of a battery in normal use based on experiments done in less than 2 years.

In order to allow for effective discussions, attendance at the workshop was limited. Invitations were sent to battery companies, vehicle manufacturers, and representatives of governments and universities. Attendees at the PPSS were also invited. Over 30 people pre-registered for the meeting and another 10 who were attending the PPSS asked if they could attend when they learned of the workshop. Attendees represented the following groups and companies:

- Governments and national laboratories: Austria, Canada, Italy (planned), Japan, Taiwan, USA
- Universities: Japan, Sweden, Taiwan, USA
- Battery manufacturers: A123Systems (US/China/Korea), DowKokam (US), E-One Moli Energy (Canada/Taiwan), FMC Lithium (US), IREQ (Hydro Quebec, Canada), Medtronic (US), TIAX (US)
- Vehicle manufacturers: GM (US/global), Volvo (Truck, Sweden)

Topics that were discussed included:

- The importance of Accelerated Life Testing
- Test procedures and approaches used by different organizations
  - Battery companies
  - Vehicle manufacturers
  - National laboratories
  - Universities

Preliminary conclusions included the following:

- There is broad interest in such testing.
- Each continent/nation has its own set of procedures.
  - These procedures are similar, but not identical.
- There are some major issues.
  - How complex a charge/discharge cycle is needed?
- There is interest in collaborating to produce a "standard" set of international test procedures.
  - In June, the IA-HEV decided to sponsor a separate annex on this subject to allow it to be addressed in significant depth. The preliminary Operating Agent for this new annex will be from Italy.

Annex X also sponsored a workshop on **Government Support for Vehicle Battery Manufacturing Facilities** in Valbonne, France on 27 – 28 September 2010. This meeting was hosted by the staff at ADEME, the French Environment and Energy Management Agency. The meeting was scheduled the same week as Batteries 2010 which was held in Cannes, France.

The basis of the meeting was that some governments have provided support for facilities to manufacture batteries for vehicles; other governments are providing other support to the electric drive vehicle market; and still other governments are considering providing such support. This meeting was held to allow an exchange of information and insights on these support activities.

As with other workshops sponsored by the annex, the meeting was "off the record;" but all of the presentations given at the meeting were distributed to those who attended. Attendees included a dozen people representing governments, national laboratories, and industry from Austria, France, Sweden, and the US.

The topics discussed included

- Programs of Government Support
- Aspects of These Programs that Had the most Effect
- Issues/Problems Associated with Aspects of These Programs
- Effects of These Programs on Industry
- Future Plans of Several Governments.

FY 2010 Publications/Presentations

1. 2009 Annual Report of the Implementing Agreement on Hybrid and Electric Vehicles, May, 2010.

IV

APPLIED BATTERY RESEARCH

A. Introduction

B. Materials Research

C. Calendar and Cycle Life Studies

D. Abuse Tolerance Studies

E. Applied Research Facilities

IV. APPLIED BATTERY RESEARCH FOR TRANSPORTATION

IV.A Introduction

The Applied Battery Research (ABR) for Transportation program is being conducted in support of the FreedomCAR and Fuel Partnership which is targeting more fuel-efficient light duty vehicles that can reduce U.S. dependence on petroleum, without sacrificing performance. There is an emphasis on developing and improving critical component technologies; and energy storage technologies are included among those critical components. In PHEVs, energy storage devices provide the primary power source for a number of "all-electric" miles, after which the vehicles again operate in the conventional HEV mode. They enhance the efficiency of the prime power source (currently an internal combustion engine) in HEVs by leveling the load and capturing regenerative braking energy. Better energy storage systems are needed to help expand the commercial markets for HEVs and to help make PHEVs commercially viable. The energy storage requirements for various vehicular applications were presented in Section III.

The ABR program is focused on materials and cell couples for high energy PHEV batteries for use in light-duty vehicles. The key barriers associated with PHEV batteries are:

- High cost
- Limited calendar and cycle life,
- Insufficient tolerance to abusive conditions,
- Insufficient energy density to meet 40-mile all-electric range, and
- Operation between -30ºC and +52ºC.

The program is seeking to develop higher energy materials, higher voltage electrolytes, and more optimal cell chemistries that are more chemically, structurally, electrochemically, and thermally stable in the cell environment; as well as possessing cost advantages over current materials. Conventional high-energy Li-ion batteries, of the type used in consumer electronics, employ sophisticated and relatively expensive electronic controls that limit their exposure to abusive conditions. The program has focused on both understanding and enhancing the inherent abuse tolerance of the individual materials, components, and cell chemistries, which will help reduce the level of sophistication of the electronic control system and thereby realize cost savings.

Six DOE national laboratories and two external laboratories are collaborating in the program. Argonne National Laboratory (ANL) provides coordination of the program activities for DOE. The other six participating DOE laboratories are Brookhaven National Laboratory (BNL), Idaho National Laboratory (INL), Lawrence Berkeley National Laboratory (LBNL), Oak Ridge National Laboratory (ORNL), and Sandia National Laboratories (SNL). The two additional laboratories are the Army Research Laboratory and the Jet Propulsion Laboratory. As part of this program, ANL researchers maintain close communications and (in some cases) collaborations with a large number of international material supply companies, through which they gain access to the latest advanced electrode and electrolyte materials for evaluation.

The Applied Battery Research for Transportation program is organized into three main tasks to address the issues associated with PHEV and HEV energy storage technologies:

Battery Cell Materials Development—focuses on research, development, and engineering of higher energy advanced materials and cell chemistries that simultaneously address the life, performance, abuse tolerance, and cost issues.

Calendar & Cycle Life Studies—deals with understanding the factors that limit life in different Li-ion cell chemistries, which are used as feedback to Task 1. This task also deals with the establishment of in-program cell fabrication capabilities for use in these life studies.

Abuse Tolerance Studies—deals with understanding the factors that limit the inherent thermal and overcharge abuse tolerance of different Li-ion cell materials, components, and cell chemistries, as well as developing approaches for enhancing their inherent abuse tolerance.

The subtask breakdown for the program is provided in Figure IV- 1.

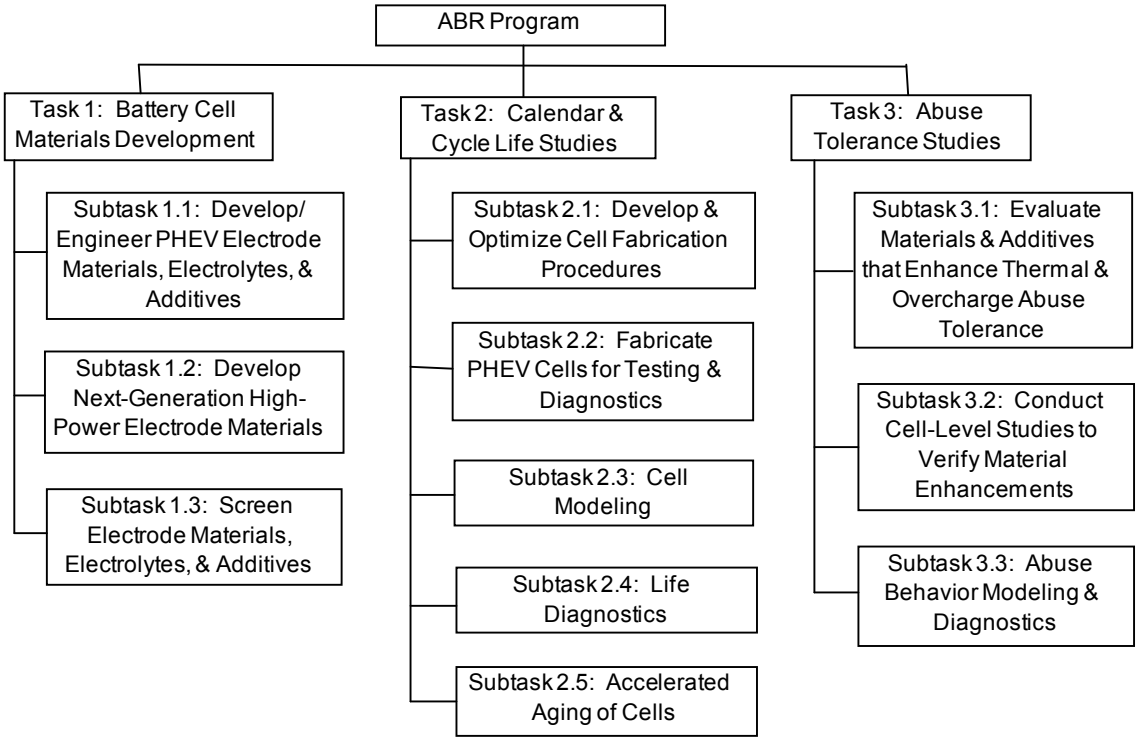

Figure IV- 1: Task and subtask breakdown for the Applied Battery Research Program

The remainder of this section provides technical highlights and progress on the Applied Battery Research program for FY 2010. The information provided is representative only and detailed information is available from publications cited in each project overview.

IV.B Materials Research

The objectives of the materials development effort are numerous. Researchers are screening new materials, optimizing Li-ion electrolytes, and working to develop and improve specific new materials. The goal is to enable affordable, safe 40 mile PHEV batteries that are free from many of the abuse tolerance shortcomings inherent in today's chemistries. In addition, researchers are looking for breakthrough high power materials to enable a revolutionary reduction in HEV cost.

IV.B.1 Cell Components and Composition

IV.B.1.1 Screen Electrode Materials and Cell Chemistries (ANL)

Wenquan Lu

Argonne National Laboratory
9700 South Cass Avenue
Argonne, IL 60439-4837
Phone: (630) 252-3704; Fax: (630) 972-4414
E-mail: luw@anl.gov

Collaborators:
Nathan Liu (ANL)
Andrew Jansen (ANL)
Sun-Ho Kang (ANL)
Dennis Dees (ANL)
Khalil Amine (ANL)
Gary Henriksen (ANL)
Electron Microscopy Center (ANL)

Subcontractor:
Illinois Institute of Technology, Chicago, IL

Start Date: October, 2008
Projected End Date: September, 2010

Objectives

- To identify and evaluate low-cost materials and cell chemistries that can simultaneously meet the life, performance, and abuse tolerance goals for plug-in HEV applications.
- To enhance the understanding of advanced cell components on the electrochemical performance and safety of lithium-ion batteries.

Technical Barriers

A large number of materials are being marketed by vendors for lithium-ion batteries. It is a challenge for battery developers to screen these materials and evaluate their value for PHEV applications.

There are no commercially available high energy materials that can meet the 40-mile all-electric-range (AER) within the weight and volume constraints established for PHEVs by DOE and the USABC. Identification of new high-energy electrode materials is the primary goal for this project.

Establishing the impact of formulation and processing on electrode performance for materials with a broad variation in chemical and physical properties is another major challenge.

Technical Targets

- Higher energy density materials identification and evaluation.
- Low cost cell components identification and characterization.

Accomplishments

The $LiNi_{0.8}Co_{0.15}Al_{0.05}O_2$ (NCA) cathode material from Toda was selected as a preliminary test chemistry for PHEV-40 application. The electrochemical performance of the highly loaded electrode was characterized. Coupled with a MAG10 anode, the cells exhibit both high energy and high power capability and are being used to understand the particulars of constructing a high energy (thick) electrode.

A member of Argonne's family of composite cathode materials, $(Li_{1.05}(Ni_{4/9}Co_{1/9}Mn_{4/9})_{0.95}O_2)$ was thoroughly investigated. In addition to its high energy density and high power capability, this material exhibits better thermal stability than NCA, due to the stable Li_2MnO_3 component in the structure. Also, less Ni and Co, compared to NCA, makes it less costly.

The effect of a fluorinated solvent from Daikin (Japan) on cell electrochemical and thermal stability was studied. Cyclic voltammetry indicates that the fluorinated electrolyte is stable to high voltage and it postpones the

on-set temperature and total heat generation during DSC tests using fully charged cathode materials.

Also, NCM cathode materials from other suppliers and other components, such as graphite, separators, carbon blacks, and current collectors, were characterized. The test results have been shared with the suppliers.

Introduction

The curves in Figure IV- 2 were calculated using Argonne's battery design model. The model indicates that one needs higher energy electrode materials than those commercially available in order to achieve the 40-mile AER within the weight and volume constraints established by DOE and the USABC. For example, if one uses a 20% margin for energy fade over the life of the battery, one would need a combination of anode and cathode materials that provide 420 mAh/g and 220 mAh/g respectively, at the beginning of life, assuming an average cell voltage of 3.6 volts. The search for new high energy density materials is the focus of this project.

In addition to high energy density electrode materials, other cell components continue to be evaluated to address the performance, safety, and cost issues.

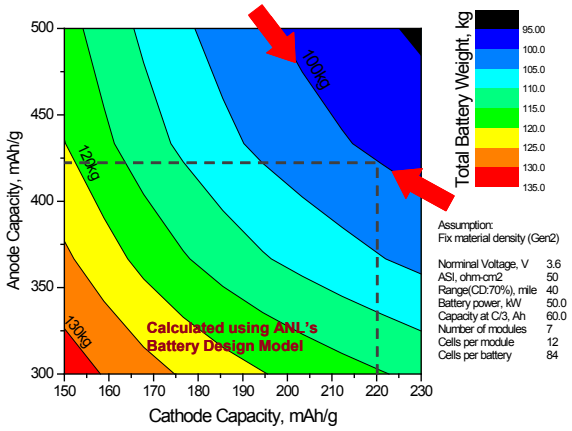

Figure IV- 2: Specific capacity requirements for anode and cathode electrode of lithium-ion battery

Approach

The search for new high-energy materials includes new commercially available materials, as well as new high energy density materials under development. During the search and evaluation process, the cost issue is always considered, e.g. avoiding the rare elements, expensive precursors, and/or elaborate processing.

The selected electrode materials are evaluated in controlled conditions following established protocols. The commonly used parameters, such as pulse power and charge depleting (CD) capacity tests are derived from the "Battery Test Manual for Plug In Hybrid Electric Vehicle" (Mar. 2008) issued by Idaho National Laboratory.

Coin cells (2032 size) are used for the initial screening studies. If promising results are obtained with coin cells, then larger laboratory cells such as the 32 cm² stainless steel planar test fixture or simple single-stack pouch cells, are used. Preliminary accelerated aging studies are performed at 55°C for promising materials to give a preliminary indication of life. Where appropriate, the thermal abuse response is studied using differential scanning calorimetry (DSC). Materials that show characteristics favorable to PHEV batteries are then recommended for further life evaluation in Task IV.C.2 cell fabrication and testing.

In addition to electrode materials, other cell components, such as separators, binders, current collectors, etc., are being secured and evaluated to establish their impact on electrochemical performance, thermal abuse, and cost. The test methods for different materials are separately defined.

Results

$LiNi_{0.8}Co_{0.15}Al_{0.05}O_2$ from Toda (Japan). NCA is one of higher energy density electrode materials currently available. The thicker electrode design used for PHEV cells will improve the energy density at the cell and battery levels compared to the thinner electrodes used for HEV cells. In this study, thicker electrodes were fabricated and studied. The electrode loading is as high as 18.9 mg/cm^2, which is more than 2 times higher than the loading of NCA electrode used in the previous ATD program. The impact of electrode thickness on cell performance, such as power capability and life, is being investigated as part of the ABR Program.

Figure IV- 3 shows the voltage profile of a Li/ $LiNi_{0.8}Co_{0.15}Al_{0.05}O_2$ half cell, which delivers about 163 mAh/g reversible capacity with cut-off voltages between 3.0V and 4.15V. The irreversible capacity loss (ICL) during the first formation cycle was 17%. At the C/10 rate, the energy density was calculated to be 618Wh/kg at an average cell voltage of 3.77 volts.

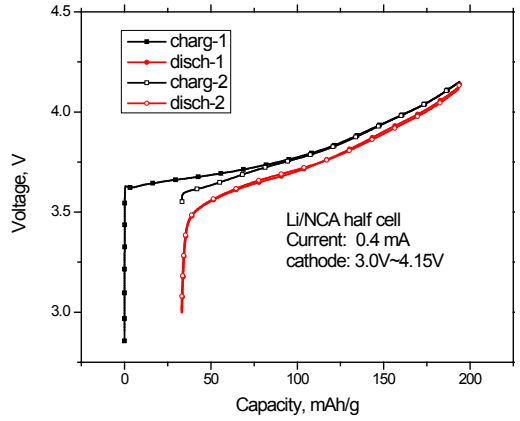

Figure IV- 3: Voltage profile of Li/ $LiNi_{0.8}Co_{0.15}Al_{0.05}O_2$ cell

Coupled with MAG10 graphite, the rate and cycle life were investigated for the NCA electrode. The rate performance of MAG10/$LiNi_{0.8}Co_{0.15}Al_{0.05}O_2$ cell is shown in Figure IV- 4. Almost 90% of its C/4 capacity can be obtained at the 1C discharge rate. However, the achievable capacity falls off dramatically (less than 50%) when discharged at the 2C rate. The power performance was also tested using hybrid pulse power characterization (HPPC) profiles. The 10-second area specific impedance (ASI) using the 2C pulse was about 30 ohm-cm^2. Therefore, the power requirement can be met using this MAG10/NCA couple.

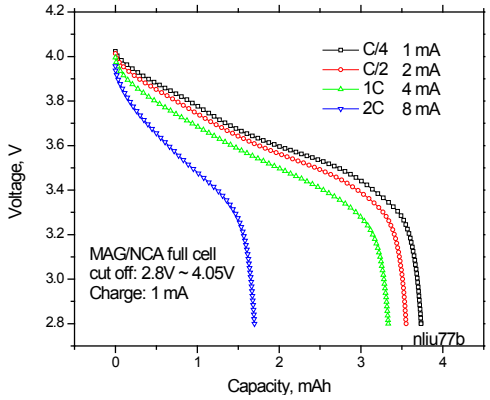

Figure IV- 4: Rate performance of MAG10/ $LiNi_{0.8}Co_{0.15}Al_{0.05}O_2$ cell

High Energy Density $Li_{1.05}(Ni_{4/9}Co_{1/9}Mn_{4/9})_{0.95}O_2$ (NCM). Argonne's composite structure cathode materials, of the type $Li_{1+a}(Ni_xCo_yMn_z)_{1-a}O_2$, are available in lab-scale quantities for evaluation. The composite structure allows operation at higher voltage and stable performance at a higher degree of delithiation. The $Li_{1.05}(Ni_{4/9}Co_{1/9}Mn_{4/9})_{0.95}O_2$, (one of these composite structure materials) was provided by S. H. Kang (ANL). This material has less Co than $Li_{1+x}(Ni_{1/3}Co_{1/3}Mn_{1/3})_{1-x}O_2$ and is made by the same process, so the cost should be lower. Also, this material exhibited enhanced electrochemical performance.

A cell using Li/$Li_{1.05}(Ni_{4/9}Co_{1/9}Mn_{4/9})_{0.95}O_2$ exhibited a specific capacity of close to 180mAh/g between 3.0V and 4.4V cut-off voltage at C/10 rate, as shown Figure IV- 5. The energy density was calculated to be 690Wh/kg with an average 3.9V operational voltage. In addition to its high energy density, it exhibited less than 10% irreversible capacity loss (ICL). This low ICL can further impove the energy density at the cell and battery levels via an optimized battery design.

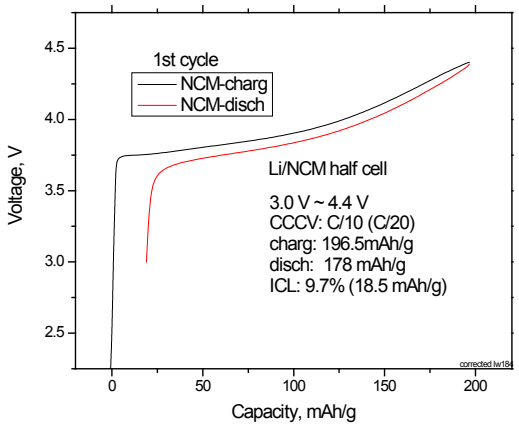

Figure IV- 5: Li/$Li_{1.05}(Ni_{4/9}Co_{1/9}Mn_{4/9})_{0.95}O_2$ cell Voltage profile

The power performance was evaluated for the $Li_{1.05}(Ni_{4/9}Co_{1/9}Mn_{4/9})_{0.95}O_2$ using MAG10 as the anode. It can be seen from Figure IV- 6 that there was more than 90% capacity available up to the 2C discharge rate. The ASI value obtained from the HPPC test for the MAG10/ $Li_{1.05}(Ni_{4/9}Co_{1/9}Mn_{4/9})_{0.95}O_2$ cell was ~30 ohm-cm^2, which is similar to the NCA cell with the thick electrodes. The high rate capability of $Li_{1.05}(Ni_{4/9}Co_{1/9}Mn_{4/9})_{0.95}O_2$ could be partially due to its lower electrode material loading (6.8 mg/cm^2). The electrode loading needs to be taken into consideration.

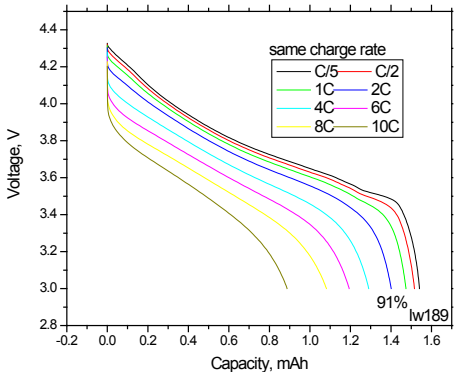

Figure IV- 6: MAG10/$Li_{1.05}(Ni_{4/9}Co_{1/9}Mn_{4/9})_{0.95}O_2$ cell Rate performance

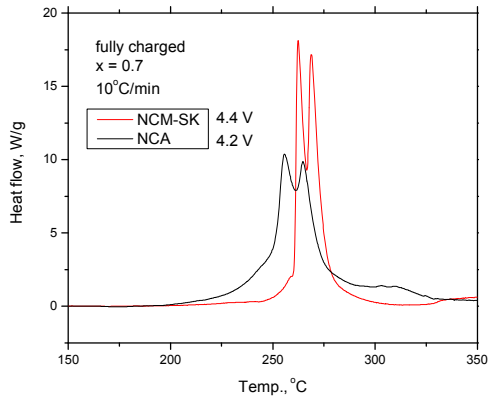

Figure IV- 7: DSC results of fully charged NCA and NCM.

The thermal stability of $Li_{1.05}(Ni_{4/9}Co_{1/9}Mn_{4/9})_{0.95}O_2$ was also studied using DSC. Figure IV- 7 shows the heat rate profiles of both fully charged NCM and NCA cathode materials. In order to make a fair comparision, the same amount of lithium was extracted from the structure, corresponding to 4.4V and 4.2V for NCM and NCA, repectively. The on-set temperature of NCM was postponed to 250°C compared to 200°C for NCA. Furthermore, the total heat generation of the NCM material at the fully charged state was calculated to be 1400J/g, less than the 1880J/g for the fully charged NCA.

The $Li_{1.05}(Ni_{4/9}Co_{1/9}Mn_{4/9})_{0.95}O_2$ cathode material demonstrated higher energy density, low irreversible capacity loss, good power capability, and better thermal stability than NCA, which makes it a promising candidate cathode material for AER PHEV applications.

Conclusions and Future Directions

$LiNi_{0.8}Co_{0.15}Al_{0.05}O_2$ (NCA) was selected as test case for the PHEV application. The high loading electrode was characterized and it was learned that electrode thickness has an impact on the cell power capability. The power requirement can be met by using 18.9mg/cm^2 loading.

A member of Argonne's composite structure cathode material family ($Li_{1.05}(Ni_{4/9}Co_{1/9}Mn_{4/9})_{0.95}O_2$) was investigated. Because of the stabilizing component in the crystal structure, this material can be charged to higher voltage (4.4V vs Li/Li^+), thereby delivering a higher energy density (690Wh/kg). Also, better thermal stability was observed from the DSC study.

In the future, the focus of this project will remain idntification and characterization of new high energy density cathode and anode materials. As for cathode materials, the composite materials will be intensively studied in terms of their rate capability, thermal stability and cycle life. In order to balance the high energy density cathode, high energy density anodes, such as silicon and silicon composites, will be obtained for investigation.

FY 2010 Publications/Presentations

1. Studies of Structural Changes for Cr and F Substituted Spinal Cathode Materials using *in situ* X-Ray Diffraction, X. Wang, K. Nam, Y. Zhou, W. Lu, A. Jansen, D. Dees and X. Yang, The 15th International Meeting on Lithium Batteries (IMLB 2010), June 28, 2010 Montreal Canada.
2. Overcharge Effect on Carbon Electrode for Lithium-Ion Batteries, W. Lu, C. López, A. Jansen and D. Dees, The 15th International Meeting on Lithium Batteries (IMLB 2010) June 28, 2010, Montreal Canda.
3. Electrolyte additive to improve performance of MCMB/$LiNi_{1/3}Co_{1/3}Mn_{1/3}O_2$ Li-ion cell, Y. Qin, Z. Chen, W. Lu, and K. Amine, J. Power sources, 195, 2010, 6888-6892.
4. 2010 DOE Annual Peer Review Meeting Presentation, Jun 7th-11th 2010, Washington DC.

IV.B.1.2 Streamlining the Optimization of Li-Ion Battery Electrodes (ANL)

Wenquan Lu and Sun-Ho Kang

Argonne National Laboratory
9700 South Cass Avenue
Argonne, IL 60439-3704
Phone: (630) 252-3704; Fax: (630) 972-4414
E-mail: luw@anl.gov

Collaborators:
Nathan Liu (ANL)
Dennis Dees (ANL)
Jansen Andrew (ANL)
Daniel Abraham (ANL)
Center for Nanoscale Materials (ANL)
Electron Microscopy Center (ANL)
Hosokawa micron powder system (USA)

Start Date: October, 2008
Projected End Date: September, 2010

Objectives

To establish the scientific basis needed to streamline the optimization of lithium-ion electrode processing.

- To identify and characterize the physical properties relevant to the electrode performance at the particle level.
- To quantify the impact of fundamental phenomena associated with electrode formulation and fabrication (process) on lithium-ion electrode performance.

Technical Barriers

Develop a cost-effective and abuse tolerant lithium-ion battery for a PHEV with a 40 mile all electric range that meets or exceeds all performance goals.

- The undocumented interdependence of lithium-ion electrode performance and the specifics of the electrode fabrication process.
- The complexity of the optimization process caused by the broad range of active materials, additives, and binders.

Technical Targets

- Correlate the electronic conductivity with the electrochemical performance of the electrode. 96 Wh/kg at the system level while delivering 5,000 deep discharge cycles.
- Develop a model to quantify the impact of electronic conductivity on cell performance.

Accomplishments

- Single particle conductivity was measured using nano probe SEM. The higher conductivity of $LiNi_{0.8}Co_{0.15}Al_{0.05}O_2$ measured by this technique indicates that the lower conductivity obtained using the conventional method was due to interfacial resistance.
- The binder effect on the particle conductivity was also investigaged using the nano probe SEM. The PVdF binder was found to form a film on the surface of graphite which makes the electrode less conducitive.
- Carbon coated $LiNi_{1/3}Co_{1/3}Mn_{1/3}O_2$ was prepared by Hosokawa.
  - The powder conductivity increased exponentially with increasing carbon coating.
  - The electrode conductivity with carbon coated particles was improved using an alumimum substrate.
  - Calendering can reduce the interfacial resistance, but not the electrode sheet resistance.

✧ ✧ ✧ ✧ ✧

Introduction

In general, the performance of a lithium-ion electrode is highly dependent on the specifics of the fabrication process. Furthermore, the broad range of active materials for both positive and negative electrodes (e.g. oxides, phosphates, graphites, carbons, and alloys), as well as polymer binders and conductive additives, compounds the complexity of the optimization process. The literally hundreds of variables associated with the fabrication of new active material electrodes generally require lengthy development efforts to be fully optimized. This sometimes causes promising materials to be discarded prematurely. Quantifying the impact on performance of the fundamental phenomena involved in electrode formulation and fabrication should greatly shorten the optimization process for new electrode active materials. The goal of this work is to establish the scientific basis needed to streamline the lithium-ion electrode optimization process for new materials.

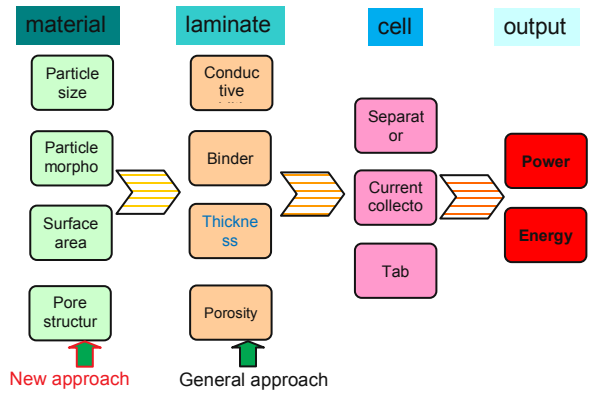

Figure IV- 8: Schematic diagram of streamlining the optimization of electrode

Approach

The conventional approach is to optimize the electrode by varying the amounts of conductive additive and binder to overcome the percolation threshold at the laminate level. New electrode materials are generally judged on their electrochemical properties. This method, generally adopted by industry, requires lengthy development efforts to fully optimize a single material and sometimes causes promising materials to be discarded. Our new approach in this project attempts to establish the scientific basis at the particle level. The focus is on the chemical and physical properties (e.g. primary particle size, secondary particle size and extent of agglomeration, as well as the surface characteristics, see Figure IV- 8), which, in most cases, can dictate the overall performance of the electrode.

Impedance phenomena in porous electrodes can be broken down into three types: (1) electronic effects (i.e. potential changes associated with getting electrons in and out of the electrode); (2) ionic effects (i.e. potential changes associated with getting ions in and out of the electrode); and (3) interfacial effects (i.e. potential changes associated with the electrochemical reaction and getting the ions and electrons across the SEI). Lithium-ion electrodes are designed and fabricated to minimize their overall impedance, which tends to be dominated by the interfacial effects. However, the electronic impedance phenomena can vary over several orders of magnitude, depending on many factors (e.g. particle-to-particle contact resistance, particle distribution, conductive additive properties, and the active material bulk electronic conductivity). Minimizing the impact of the electronic impedance effects is extremely important to optimizing the electrode design. Based on modeling work by Dennis Dees, it was determined that the electronic conductivity does not impact the electrode impedance once the effective electronic conductivity becomes much greater than the ionic conductivity of the electrode (>>0.01 S/cm). In order to examine electronic conductivity effects, the factors affecting the distribution of binder and conductive additives throughout the composite matrix are being systematically investigated at the particle level, as well as their effect on overall electrode performance. Modeling work is being conducted to help quantify the impact of fundamental phenomena on electrode performance.

Results

Single particle electronic conductivity measurement. Previously, powder conductivities of various electrode materials were investigated using an in-house developed apparatus. The results, presented in last year's report, were consistent with those reported in the literature. However, the contact resistance between particles was part of that measurement and this contribution is difficult to quantify. In order to obtain the true conductivity of the electrode particle, the 4 probe measurement on a single particle was carried out using Omicron UHV Nanoprobe (Germany) at Center for Nanoscale Materials (ANL), as shown in Figure IV- 9. The current was applied to the particle using two probes with about 70 nm diameters. The voltage difference on the other pair of tips was recorded. The conductivity of the particle was then calculated using the Dees model. It was determined that the obtained conductivity was higher than that reported in literature. In the meanwhile, the measured resistances are similar regardless of the pair of tips used for the current path. These observations indicate that the contact resistance between the tip and particle may be dominant. Therefore, it is fair to conclude that the true particle conductivity of the NCA is higher than that measured by conventional methods. The interface resistance needs to be addressed in the electrode optimization process.

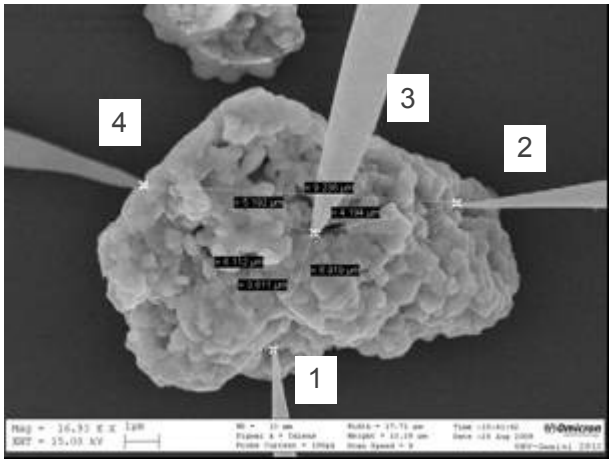

Figure IV- 9: Conductivity measurement using nano probe SEM

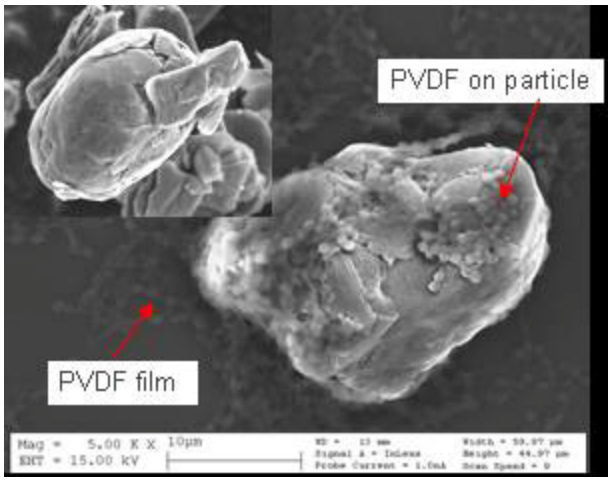

Figure IV- 10: Interaction between particle and PVdF binder

Furthermore, the effect of PVdF binder on the particle conductivity was investigated using nanoprobe SEM. In Figure IV- 10, the insert is the pristine graphite particle, which exhibits a clean and smooth surface. The small particle-like material on the surface of the graphite particle in the main image is PVdF binder. Using nanoprobe SEM, the resistance of the particle with PVdF film was measured and an extremely high resistance was obtained due to the poor conductivity of the PVdF binder. Therefore, the binder effect on the electronic conductivity of the electrode needs to be studied.

Carbon coated $LiNi_{1/3}Co_{1/3}Mn_{1/3}O_2$. The single particle investigation demonstrated that the interfacial resistance of electrode particles is a significant contributor to electrode resistance with fixed electrode materials. It is rational to expect that the conductive carbon coating can improve the electrode conductivity. However, carbon coating is generally completed under a reducing atmosphere, which is not applicable for metal oxides.

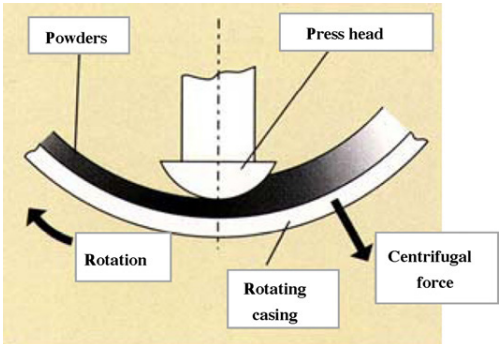

Figure IV- 11: Schematic diagram of carbon coating by Hosokawa

In this study, carbon coating of NCM particles was performed by Hosaka, using a novel carbon coating technology. As shown in Figure IV- 11, the powders are subjected to a centrifugal force and are securely pressed against the inner wall of a rotating casing. The powders are further subjected to various mechanical forces, such as compression and shear forces, as they pass through a narrow gap between the casing wall and the press head. As a result, smaller guest particles are dispersed and bonded onto the surface of the larger host particles without using binders of any kind.

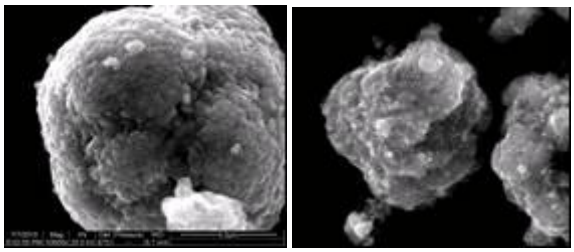

Figure IV- 12: Uncoated (left) and coated (right) NCM particels

Two different carbon coated NCM samples (1wt.% and 3wt.%) were prepared by Hosokawa. SEM images are provided in Figure IV- 12. Carbon paricles are clearly observed on the surface of NCM particles. TGA results confirmed the reported carbon composition at particle level. The powder conductivity was then measured and the data are provided in Figure IV- 13. It is observed that the electronic conductivity of the particles increase exponentially with increasing carbon content. This conductivity improvement is apparently caused by a reduced interfacial resistance resulting from the carbon coating.

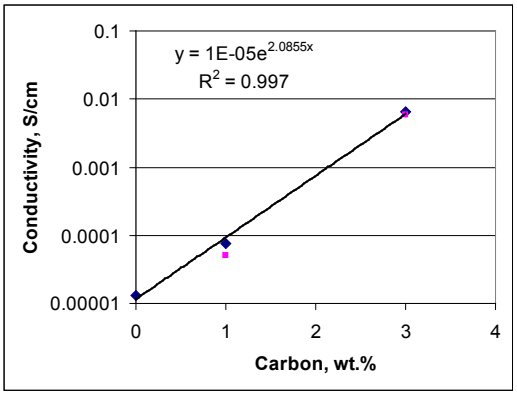

Figure IV- 13: Powder conductivity of carbon coated NCM

The conductivity of electrodes made with both uncoated and coated NCM particles were also investigated using the 4-point probe method. The coated carbon on the particle was taken into consideration when preparing the electrode slurry. For instance, only 2wt% additional carbon was added into composite when 5wt% cabon additive is the target and 3wt% carbon coated NCM particles were the starting material. The subtrates for the electrodes are either conductive aluminum foil or insulating polyester.

The electronic conductivity measured by the 4-point probe method is shown in Figure 7. When the insulating polyester substrate is used, the voltage difference in the plot refers to the resistance of the composite electrode

sheet. When the conducting aluminum sheet is used, the voltage difference refers to the resistance of the electrode in depth and interfacical resistance between the composite electrode sheet and the aluminum current collector. Surprisingly, it can be seen for the electrode on polyester substrate (Figure IV- 14) that the sheet resistance of the electrode with 3wt% carbon coating is higher. The electrode sheet resistance increases after calendering for both coated and uncoated samples. As anticipated, the resistance of the electrode with 3wt% carbon coating sample on aluminum foil shows less resistance than that without coating, and resistances of both electrodes decrease after calendering.

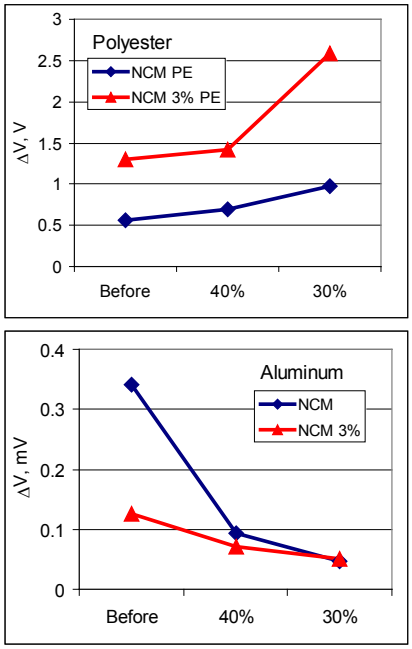

Figure IV- 14: 4 probe conductivity of electrode on substrate polyester (top) and (bottom) aluminum.

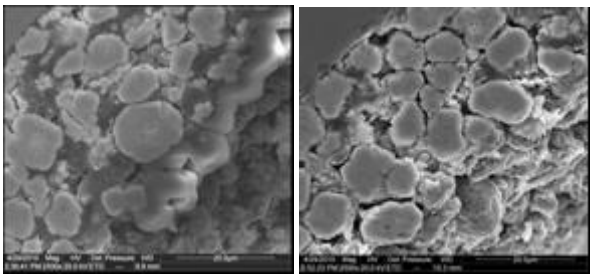

Figure IV- 15: SEM images of electrode with no carbon coating (left) and with 3% carbon coating on the particles.

In order to better understand the results of the 4-point probe measurement, SEM was carried out on electrodes employing both particles with and without carbon coatings (see Figure IV- 15). It can be clearly seen from images that less carbon additive is present in the matrix of the electrode made of NCM with 3wt% carbon coating. For this sample, the target carbon additive was 5wt%. Only 2wt% additional carbon was added to the composite since there was 3wt% coated carbon on the particle. According to the previous SEM image on carbon coated particles, the carbon was evenly distributed around the particle. Therefore, there was less carbon to form the conductive matrix in the composite, leading to higher electrode sheet resistance. Also, it was noticed for the electrode using polyester as the substrate that the resistance of the electrode increases after calendering. This was probably caused by the discontinuous conductive matrix. After calendering, the continuous carbon matrix might be separated by the low conductive NCM particles.

For the electrode with the alumimum substrate, the opposite trend was observed. The electrode resistance made of carbon coated particles had less resistance before calendering. We believe that the inferface resistance is dominant in this case. Before calendering, the carbon coated partical had better contact between the particles and substrate. The contact resistance between the particles and substrate would be further reduced with calendering.

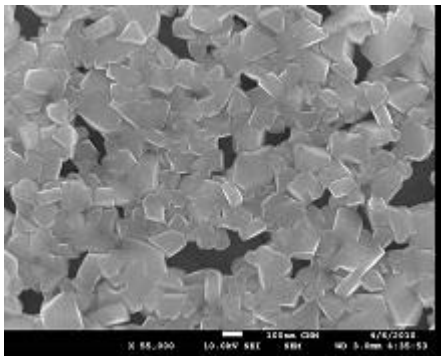

Figure IV- 16: SEM images of BCF oxdide film.

Binder and carbon free (BCF) oxide thin film. BCF oxide cathodes can provide useful insight into the correlation between active material particle characteristics and the electrode's electrochemical characteristics, without complication from the carbon or the binder.

Thin film $LiNiCoMnO_2$ electrodes were prepared using the sol-gel spin coating method and an SEM image is provided in Figure IV- 16. Approximately 100nm particle size was obtained. The electrochemical results are consistent with the layered character of this cathode material. Electrochemical impedance spectra have been measured and are in the process of being analyzed. Different microstructures (particle size) with the same active material loading will be investigated.

Conclusions and Future Directions

The conductivity measured using nanoprobe SEM is higher than that using conventional methods. Together with the binder effect on the couductivity of the particle, the interfacial resistances between particles and

particle/substrate are believed to be the key factors that affect electrode conductivity.

The conductivity of carbon coated NCM particles prepared, by Hosokawa, increases with increasing carbon coating due to reduced interfacial resistance. 4-point probe tests were conducted on electrodes made with uncoated and coated NCM particles. Surprsisingly, the electrode sheet conductivity of the electrode made of carbon coated particles is less than that of uncoated one. After calendering, the electrode sheet resistance increased. However, the electrode made with carbon coated particles exhibited lower infacial resistance, which is dominant in the electrode with the aluminum substrate, leading to lower overall electrode resistance.

The interactions between components of composite electrodes and the interfacical resistance between the particles and particle/substrate will be further investigated using BCF thin film electrodes. The modeling work will continue to better understand the interfacial phenomenon.

FY 2010 Publications/Presentations

1. Olivine electrode engineering impact on the electrochemical performance of lithium-ion batteries, Wenquan Lu, Andrew Jansen, Dennis Dees, and Gary Henriksen, J. Material Research, 25 (8) 2010, 1656-1660.
2. 2010 DOE Annual Peer Review Meeting Presentation, Jun 7th-11th 2010, Washington DC.

IV.B.1.3 Scale-Up of BATT Program Materials for Cell-Level Evaluation (LBNL)

Vince Battaglia (Principal Investigator)
M.S.70R0108B
1 Cyclotron Road
Berkeley, CA 94720
Phone: (510) 486-7172; Fax: (510) 486-4260
E-mail: vsbattaglia@lbl.gov

Start Date: June 2008
Projected End Date: September 2012

Objectives

- Identify materials in the BATT Program ready for full-cell analysis.
- Scale-up identified materials to 10 g if PI does not have the resources.
- Test materials in well-sealed full-cells with quality electrodes.
- Provide PIs with an independent analysis of their material.

Technical Barriers

The challenge to getting more electrified vehicles on the road is reducing the cost, which translates, technically, to improving battery energy density and life.

Technical Targets

- Develop a cell to meet the 40-mile PHEV goals:
- Improve the energy density of cells through the use of a new material with the goal of meeting the 207 Wh/l energy density target.
- Demonstrate improved life with new materials.

Accomplishments

- We tested seven materials from the BATT program.
- Many of the materials displayed poor first-cycle irreversible capacity.
- A design analysis indicates that a battery's size is directly related to the 1st cycleirreversible capacity loss.
- Ceder's iron phosphate material was scaled-up and tested. We found that the material is capable of high rates.
- We performed XPS of the surface and determined that the black color is not the result of carbon.
- We showed Ceder's group how to make better cells.
- Some analysis with researchers at the LBNL Molecular Foundry indicated that the black color of the material is a result of traps in the band gap.
- Stoichiometric material does not have the same rate capability as Ceder's non-stoichiometric material.

Introduction

The cost of batteries for automotive applications is too high (or the cost of gasoline is too low). Hybridized and all-electric vehicles will not become commonplace until the cost is reduced. Several researchers in the BATT program are developing new materials with improved energy density, lower cost, or improved safety. These researchers are experts at making materials but not necessarily at making electrodes. Making quality electrodes requires ~10 g of material, an effort that some researchers would prefer to avoid. These researchers also appreciate confirmation of their findings and a formalized comparison to the BATT baseline.

Approach

The first thing we do is contact all BATT PIs as to whether they expect to have a new material in the coming fiscal year and whether they will be able to supply 10 g of active material, 1 g of salt, or 15 cm^2 of finished electrode, or if we'll have to scale-up their material for them. Once we know of the PI's interest, we can plan accordingly.

Once we have the material in an appropriate form for electrochemical evaluation, it is first tested in a half cell. We measure the first-cycle reversible capacity and irreversible capacity, and its coulombic efficiency against Li. We then test its rate capability.

There are two comparisons we like to make. We first want to compare our results with the results the investigator collected in his/her own lab; based on the outcome of that evaluation, we would then like to make a comparison with the baseline. The best test would be to make electrodes of the thickness that approaches the optimum for the technology for which it is best suited. If this is a high-rate material, then perhaps an HEV electrode is most appropriate; if it is a high-energy

material or improved-safety material, then perhaps a PHEV 40 is best. If the results are favorable, we then test the material cycleability in full cells.

Full-cell testing is different than half-cell testing as the electrodes need to be matched in capacity. Problems arise when the material of interest results in a large first-cycle irreversible capacity. To compare against the baseline, there are two options: does one make the capacity of the cathode larger so that the electrodes are matched and cells of the same capacity are compared although only a fraction of the cathode is now being cycled, or does one accept the loss and cycle the cell with a lower reversible capacity, where the cathode is fully cycled but the anode is partially cycled? In 2009 to 2010 we avoided this issue by not cycling a material that had a large first-cycle loss because we believe this is too detrimental to the energy density and hence cost of the battery. For 2010 to 2011, we plan to cycle *via* the second approach. All results are shared with the PI and DOE, upon request. If the results look good and we can provide additional insight as to why, then we provide additional analysis.

Results

Materials Testing. Eight investigators responded to the call for materials evaluation, far more than we anticipated. However, most supplied the materials in the form of electrodes. The list of PIs and their materials are provided in Table IV- 1. The list includes five cathodes, two anodes, and a salt. We will now provide a brief description of the results of each test, saving the first one listed for last.

M. Thackeray sent us some of his newest Li_2MnO_3-stabilized NCM material in the form of powders. In our initial studies we sought to compare it with baseline $LiNi_{1/3}Co_{1/3}Mn_{1/3}O_2$, and made electrodes of the material in the same way we make electrodes of the baseline material. We spent several weeks making electrodes of this material as best as we could following the ANL recipe. We cycled it in full cells against graphite from 3.5 to 4.3 V, as this is the voltage we found ideal for cycling NCM. We found, overall, that this material did not cycle as well as the baseline. We believe this may be due to the electrode build and would have preferred to spend more time on the electrode fabrication process using some of the formulations that we developed.

N. Dudney sent us carbon fiber mat electrodes impregnated with $LiFePO_4$ which was sent to us in small disks suitable for coin cells. This electrode was 100 microns thick and not fully impregnated. We tested this material for rate capability and compared its performance to the baseline $LiFePO_4$ that we obtain from HydroQuebec. Because of the limited impregnation, Dudney's material did not compare well with the baseline $LiFePO_4$ electrodes made the traditional way with binder and conductive additive. We saw little value in determining whether this material cycled well and reported our results back to Dudney. To be fair, this electrode is meant to replace the copper current collector and therefore in operation this material should be tested sandwiched between two anodes. We cannot do this in a coin cell and therefore it is not a valid comparison. Dudney is going to revisit this and try to improve the packing density of $LiFePO_4$ and send us samples that can be tested in pouch cells. This requires her to develop carbon electrodes with tabs attached.

M. Doeff had been working on several NCM materials, two of which are showing promise. One is substituting Al for Co to obtain higher rate capability; the other is substituting Ti for Co to obtain higher capacity. We will work with her in the coming year to decide upon a material and will evaluate it for her.

P. Kumta sent us laminates of his *a*-Si/C anode material. We ran some initial characterization tests and found that it still had a 30% first-cycle irreversible-capacity loss. This is much more than the 20% that he expected. In the coming year, Kumta expects to send us some of his new material where the 1st cycle loss is closer 12%.

K. Zaghib sent us electrodes and powders of his newest $LiFePO_4$ material. This material was made from a new, lower-cost fabrication process intended to make the same types of material as the BATT baseline. SEMs indicated that the material appeared very similar to the baseline. We tested the electrodes and found that they did not perform as well as the electrodes we made from their material. With our electrodes of their material, we found that the new material is just as good as the old material, as seen in Figure IV- 17 in the Modified Peukert plot. We cycle life tested this material and found the cycle life to be comparable to the baseline LFP material.

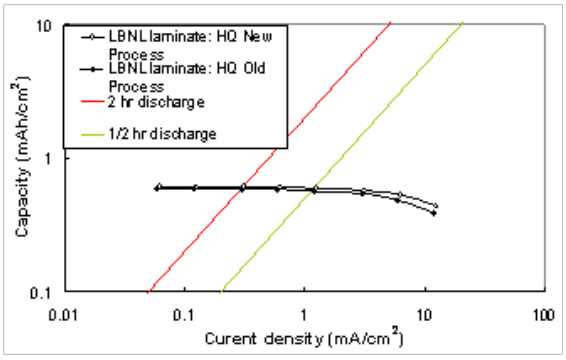

Figure IV- 17: Plot of capacity versus C-rate for the baseline LFP material and the same material synthesized by a less expensive process.

Table IV- 1: Investigators and Materials Status.

Investigator	Institution	Material	Barrier	Feedback	Status
Respondents in FY09					
G. Ceder	Massachusetts Inst. of Technology	High-rate $LiFePO_4$	High system cost	We made the material w/ their guidance	Rate tested
M. Thackeray	Argonne National Laboratory	High-capacity NCM material	Low energy density	Sent us materials and electrode formulations	Cycle life tested
N. Dudney	Oakridge National Laboratory	$LiFePO_4$ in carbon mat – no Cu cur. col.	High system cost	Sent us anodes	Tests complete (low cap. dens.)
M. Doeff	Lawrence Berkeley Nat. Laboratory	Al-doped NCM material	High material cost	We will make material w/ their guidance	To be initiated
P. Kumta	University of Pittsburgh	Si-C nanocomposite	Low energy density	Sent 1st gen anodes.	Tests complete (high 1st cycle ICL)
K. Zaghib	Hydro-Québec	Lower cost $LiFePO_4$	High cost	Sent 50 g of powder and laminates	Cycle life tested
A. Dillon	National Renewalble Energy Lab.	High capacity MoO_3 anode	Higher energy density	Sent us anodes	Tests complete (high 1st cycle ICL)
B. Lucht	University of Rhode Island	$LiPF_4C_2O_4$ thermally stable salt	Poor high temperature performance	Sent us 10 g of salt	Tests complete (high 1st cycle ICL)

B. Lucht sent us some of his electrolyte with $LiPF_4C_2O_4$. This salt is similar to $LiPF_6$ with the replacement of two fluorine atoms with an oxalate molecule. When we tested this salt in a half cell of graphite and lithium metal we saw a reduction reaction at *ca*. 1.7 V which led to a large first-cycle irreversible-capacity loss of *ca*. 30%. The equation for theoretical energy density is

$$E = \frac{q_a q_c}{q_a + q_c}\left(V_c - V_a\right)$$

If we assume that for the cathode the capacity is 180 mAh/g at an average voltage of 3.8 V and for the anode the capacity is 300 mAh/g and the voltage is 150 mV on discharge, then we get on discharge a theoretical energy density of 410 Wh/kg. If there is a first cycle inefficiency associated with the cathode and anode, and that of the cathode is less than that of the anode then the equation, with some approximation looks like

$$E = \frac{\left(1-\eta_c+\eta_a\right)q_a q_c}{q_a + \left(1-\eta_c+\eta_a\right)q_c}\left(V_c - V_a\right)$$

where η_c is the first-cycle efficiency of the cathode and η_a is the first-cycle efficiency of the anode. If we substitute a first-cycle efficiency of the cathode of 90% and a first-cycle efficiency of the anode as either 90 or 70%, the ratio of the energy density with and without Lucht's salt is 355/410 = 0.865. Since our initial tests, Lucht has developed salts with fewer impurities and claims he gets less 1st cycle irreversible capacity loss. We have since sent him some our laminates to confirm this result.

MIT High-Rate LFP. MIT had recently published a paper in Nature touting that they could make a cell with iron phosphate that could discharge at a rate of 400 C and invited us to come to their lab and learn to make the material. In Figure IV- 18 is shown an SEM of their material and an SEM of our repeat of their material.

Once we convinced ourselves we could make the powder it was just a matter of time before we were able to make good electrodes. Upon making good electrodes we found we could cycle them at the rates reported by MIT.

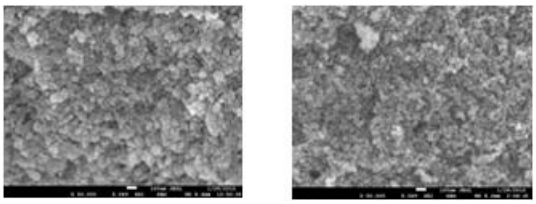

Figure IV- 18: (left) MIT material; (right) LBNL duplicate.

At this point we were satisfied by our results but were curious as to the mechanism for the high rate. We also noticed that the material was very black, see Figure IV- 19. We inquired about the color and MIT thought that the black may have been due to some residual carbon on the materials coming from the iron precursor. To confirm this, we sent the materials out for XPS analysis with ion sputtering. The XPS results indicated that there was a carbon film, but too thin to make the materials look this black. The group that performed the XPS analysis also confirmed that the materials remained black through the sputtering, indicating this was more than a surface phenomenon.

Figure IV- 19: Photograph of MIT material in pellet form.

The XPS analysis also revealed that the material was coated by a thin film (*ca*. 5 nm) of Li_3PO_4, and not $Li_4P_2O_7$, as previously reported. The $Li_4P_2O_7$ was originally reported to be the source of the high rate capability. It is now believed that the thin film on the surface helps to keep the material in nano form. Preliminary work with investigators at the Molecular Foundry at LBNL suggests that the source of the black color may be due to the presence of intermediate states in the band gap that may be the result of defects in the material as a result of making it with off-stoichiometry. We since made the MIT material but added the precursors stoichiometrically to make pure $LiFePO_4$ and were still able to make nano-materials; however, the material was not as black and we were not able to make electrodes with the same rate capability. We now intend to make the stoichiometric material but coat with carbon using a carbon coating procedure developed by HQ.

Conclusions and Future Directions

This year we evaluated several materials from the BATT program. The materials were designed for improved high energy density, safety, or rate capability. Most of the materials had improvements in some area but also resulted in a reduction in energy density. The results were shared with the PIs and several plan on sending improved materials in the coming fiscal year.

We performed a more exhaustive analysis of the MIT material as it seemed to perform as expected. There were conditions uncovered that led us to believe that the improvements reported were not the result of earlier explanations provided. XPS revealed that the material was coated in a ceramic, less-conductive film than was originally reported, and that the material was black but not as a result of residual carbon. Preliminary analysis suggested that the color of the material arose from trapped states in the band gap, which may have been responsible for improved conductivity of the bulk of the material.

Future work will entail revisiting the salt from the University of Rhode Island and the conductive carbon mat impregnated with LFP from Oakridge National Laboratory. We also expect to receive new Si-based materials from the University of Pittsburgh. We will also put out another inquiry for new materials from the other BATT PIs; we are especially interested in $LiNi_{1/2}Mn_{3/2}O_4$ materials being made in that program. Finally, we hope to make the MIT material with a stoichiometric chemistry and thin carbon coating and test this material for rate capability.

FY 2010 Publications/Presentations

1. 2010 DOE Annual Peer Review Meeting Presentation.

IV.B.2 Applied Battery Research on Anodes

IV.B.2.1 Developing a New High Capacity Anode with Long Life (ANL)

Khalil Amine

Argonne National Laboratory
9700 South Cass Avenue
Argonne, Il 60439
Phone: (630) 252-3838; Fax: (630) 252-4176
E-mail: amine@anl.gov

Collaborators:
Damien Dambournet (Argonne)
Ilias Belharouak (Argonne)
Ali Abouimrane (Argonne)
Dupont

Start Date: October, 2008
Projected End Date: September, 2010

Objectives

- Develop new anode materials that can provide very high gravimetric and volumetric energy densities for plug-in hybrid electric vehicle (PHEV) applications.
- Develop low-cost synthesis methods which provide control over particle morphology.
- Perform structural characterization and electrochemical evaluation of the prepared anode materials.
- Demonstrate the high capacity of these anodes in half and full cells.

Technical Barriers

This project aims to address the following technical barriers:

- Inherent safety-related issue of graphite
- Life span of existing lithium-ion batteries
- Energy requirements for the PHEV application

Technical Targets

- Develop two advanced anode systems:
  - Titania (TiO_2) having brookite structure as a potential 330 mAh/g anode material.
  - New high capacity silicon-based composites with less volume expansion.
- Test both anodes with advanced high-capacity cathode materials.

Accomplishments

- Developed a new synthesis method to prepare nano-structured TiO_2 brookite material with high surface area and high packing density.
- Investigated the mechanism of formation of TiO_2.
- Evaluated the electrochemical performance and investigated the lithium insertion mechanism of TiO_2 brookite.
- Developed of a new high-capacity and long-life silicon-based composite anode as the ultimate solution to overcome the capacity shortfall of TiO_2.

✧ ✧ ✧ ✧ ✧

Introduction

Beyond their wide use in small electronic devices, lithium-ion batteries are now facing the challenge of meeting the energy and power requirements of PHEVs and EVs. In this effort, our research is focused on the development of new electrode materials that could provide higher power or higher energy, longer cycle life, lower cost, and enhanced safety. Titanium-based oxide (titania) and silicon-based materials have been selected as an alternative to the graphite anode. Titania could provide 330 mAh/g capacity if fully lithiated. This capacity is slightly lower than graphite but could be, through densification, made comparable and safer. Silicon has a much higher capacity compared to graphite. In practice, this capacity is not realized due to mechanical constraints. Embedding silicon in a carbonaceous matrix can extend the life of the composite anode.

Approach

- TiO_2 having the brookite type structure was prepared by using a low cost synthesis involving two steps. The first consists of aqueous precipitation of a titanium oxalate $Ti_2O_3(H_2O)_2(C_2O_4)\cdot H_2O$, which is subsequently decomposed at low temperature (<400°C) to form TiO_2 brookite. The process is unique in that it allows monitoring the morphology and the size of particles by tuning the synthesis parameters (concentration, duration time, etc.).

- A new silicon-based composite was prepared by a scalable high-energy ball milling method.

Results

The morphology of the TiO_2 precursor was retained after the thermal treatment. The obtained nano-structured TiO_2 material has high surface area (~400 m^2/g), but high packing density, which can increase the volumetric energy density at the cell level.

Since the characteristics of the prepared TiO_2 brookite are dictated by those of the precursor, the aqueous precipitation process of the oxalate hydrate phase was studied. It was shown that the formation of the TiO_2 brookite occurred via different steps that are affected by the synthesis conditions, i.e., the oxalate source and the duration time. At first, in agreement with Ostwald's rule of stages, the formation of the oxalate phase implied a metastable intermediate that is a poorly crystallized TiO_2 phase. The pH of the solution was shown to influence the kinetics of transformation of this intermediate to the final compound. In the presence of alkali ions, the oxalate phase was shown to undergo a dissolution/etching process that is dependent upon the nature of the alkali ion used. The difference in adsorption ability of the alkali ions over the crystal planes of the titanium oxalate hydrate phase accounted for the variation of morphology. An example of the morphologies that can be obtained is shown in Figure IV- 20. It was proposed that the reaction was promoted by a coordination-assisted mechanism involving the complexing properties of the oxalate anions with the Ti^{4+} ions.

The morphology displayed by TiO_2 brookite appears to be of interest for lithium-ion batteries due to better dispersibility during the coating process, a high surface area, and high packing density.

By using an X-ray pair distribution function (PDF) analysis, we determined that the structure of TiO_2 brookite was stable upon a high degree of lithiation. Nevertheless, due to the insulating character of TiO_2, the material delivered a lower capacity than expected at high rate.

With regard to the silicon-based composite prepared by a scalable high-energy ball milling method, preliminary data showed that the material has a high packing density (1.7 g/cm^3) and promising electrochemical properties. Figure IV- 21 shows the excellent cycling behavior of the silicon composite in a lithium half cell.

Conclusions and Future Directions

Nano-structured, high surface area, and high packing density TiO_2 brookite has been made by an innovative method, reported for the first time here. X-ray PDF analysis has confirmed the stability of the brookite structure after lithiation. The electrochemical performance of the prepared TiO_2 brookite has been shown to be under the project's goals. Ways to improve the electrochemical performance can be applied. In addition, a high capacity and long life anode based on a silicon-composite system has been developed. Future work will mainly focus on this new silicon composite anode to further increase the capacity and lower the irreversible capacity loss, while maintaining good cycle life.

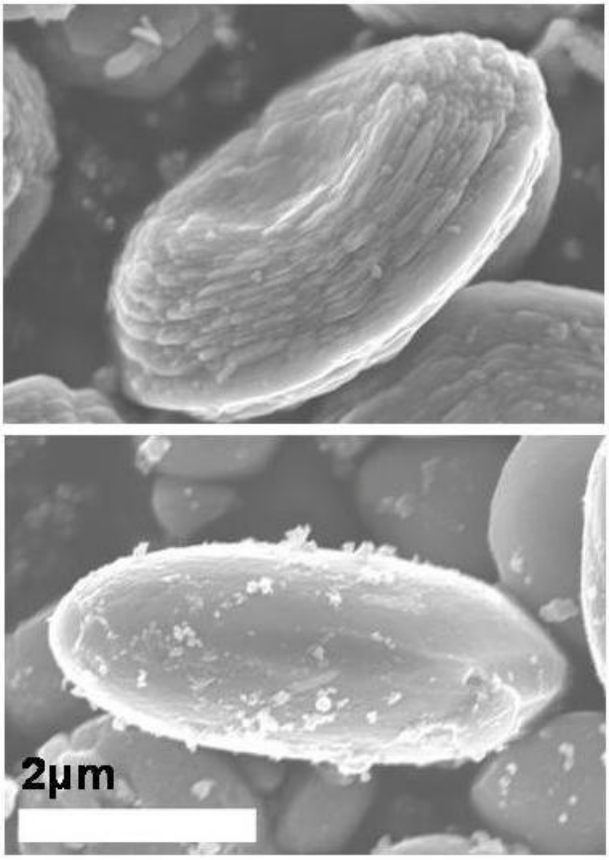

Figure IV- 20: Scanning electron microcopy images of the TiO_2 precursor.

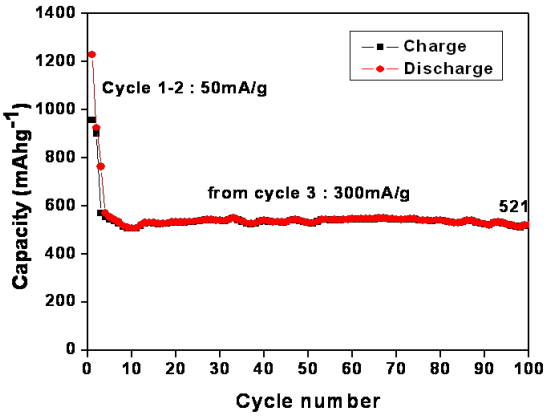

Figure IV- 21: Cycling behavior of the silicon-based composite.

FY 2010 Publications/Presentations

1. Oral presentation at the DOE Annual Peer Review Meeting, Washington, DC, 2010.
2. Dambournet, I. Belharouak and K. Amine, TiO_2 Brookite Anodes for Li-ion Batteries, Oral presentation at Materials Challenges in Alternatives & Renewable Energy, Feb 21-24, 2010, Cocoa Beach, Florida.
3. Dambournet, I. Belharouak and K. Amine, Tailored Preparation Methods of TiO_2 Anatase, Rutile, Brookite: Mechanism of Formation and Electrochemical Properties, *Chemistry of Materials*, 22, 1173 (2010).
4. D. Dambournet, I. Belharouak, J. Ma, and K. Amine, Toward High Surface Area TiO_2 Brookite with Morphology Control. Submitted.

IV.B.2.2 Develop Improved Methods of Making Inter-metallic Anodes (ANL)

Andrew N. Jansen

Argonne National Laboratory (ANL)
9700 South Cass Avenue
Argonne, IL 60439-4837
Phone: (630) 252-4956; Fax: (630) 972-4461
E-mail: jansen@anl.gov

Collaborators:
Jack Vaughey, ANL
Dileep Singh, ANL
Dennis Dees, ANL
Paul Nelson, ANL
Chris Joyce, ANL

Start Date: October, 2008
Projected End Date: September, 2014

Objectives

- Make electrodes based on intermetallic alloys such as Cu_6Sn_5 using a wide selection of binders with a particular emphasis on binders that are able to accommodate relatively large volume expansions.
- Develop methods to determine and control the optimum particle size, composition, and morphology of Cu_6Sn_5 based intermetallic alloys.

Technical Barriers

Plug-in Hybrid Electric Vehicles (PHEVs) need a high energy density battery to meet the 40 mile range target in 120 kg (80 L) battery size. Intermetallic alloys have the potential to be high capacity anode materials, but the following issues must be addressed

- Low cycle life
- Large volume expansion upon lithiation.

Technical Targets

- Determine the influence of binder on Cu_6Sn_5 cycle life.
- Explore methods of controlling particle size and morphology.
- Produce an intermetallic electrode with 200 cycles and 80% capacity retention.

Accomplishments

- Developed blending and coating process to make electrodes with varying thickness of Cu_6Sn_5 to establish baseline.
- Evaluated the influence of binders and inert additives to electrode powder mix.
- Expanded Argonne's Battery Design Model to assess the benefit of using intermetallic alloys in PHEV batteries.
- Measured mechanical properties of several intermetallic alloys to predict optimum particle size.
- Obtained tailor made intermetallic alloys of 0.5 micron particle size with promising morphology.

✧ ✧ ✧ ✧ ✧

Introduction

Previous work from the BATT program has shown that doped-Cu_6Sn_5 materials have reversible capacities similar to graphite. Their voltage profile (Figure IV- 22) is approximately 100 mV above graphite potential, which should enhance safety but not significantly affect energy. When their high material density is taken into account the volumetric capacities are nearly 3X that of an optimized graphite based electrode as can be seen in Figure IV- 23. This will enable the use of much thinner negative electrodes; smaller batteries for same energy.

Work on the Li_xSi system by 3M has shown that using binders more appropriate for the volume expansion of the Li_xSi system can greatly enhance cycle life. It is hoped that with proper binder selection, particle size, and morphology, Cu_6Sn_5–based materials will find success as lithium-ion anodes.

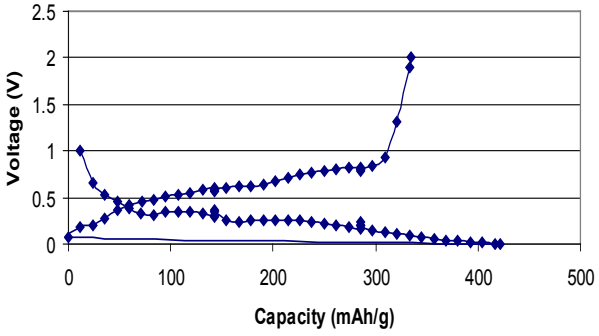

Figure IV- 22: Charge and discharge voltage profile of Cu_6Sn_5 versus lithium.

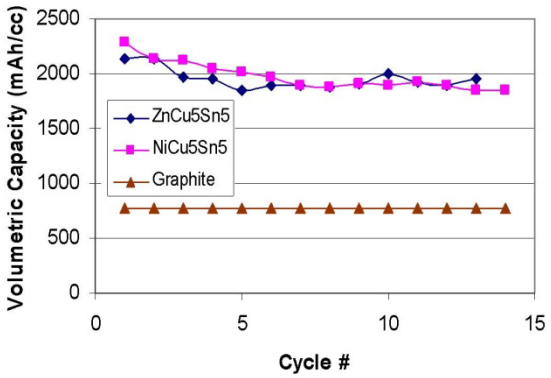

Figure IV- 23: Volumetric capacity density of Cu_6Sn_5-based intermetallic alloys compared against graphite.

Approach

The general approach in this subtask is to explore alternative methods of making electrodes based on intermetallic alloys such as Cu_6Sn_5. The goal is not necessarily to develop new classes of active materials but rather, to employ materials already being developed in the BATT program.

Success will be achieved upon development of an electrode that can accommodate the large volume expansion and contraction during deep discharge cycling, and can prevent the excluded metal (such as copper) from agglomerating into an inert mass during cycling. Likely solutions to these problems will involve the proper choice of binders and methods of controlling the particle size and morphology during production, and during repeated cycling.

Results

In FY09, several classes of commercial binders were evaluated with a commercially prepared sample of Cu_6Sn_5 (with 10 micron particle size) powder. The binders include PVdF-based polymers with functional groups tailored for anodes and cathodes over a range of molecular weights, and a few aqueous-based binders. Several methods of making electrode slurry were explored including an initial step of dry blending the Cu_6Sn_5 powder with acetylene black carbon and SFG-6 graphite on a roller mill.

The cycle life of each electrode was determined from coin cells, and was found to be only around 20 cycles. The choice of binder did not significantly affect the capacity fade of these electrodes. This result was not expected and a search was begun to determine the cause of this excessive capacity loss.

Electrodes were also made with Cu_6Sn_5 and acetylene black as the baseline mix, into which graphite, MgO, or alumina powder was added. It was hoped that this would help prevent the metal diffusion (Cu and its substitutes) away from the active tin. Unfortunately, the addition of metal oxide additives to the bulk electrode did not appear to prevent capacity fade in these thick electrode designs.

It became clear that the commercially obtained Cu_6Sn_5 baseline material was not ideal for use in a lithium-ion battery. No binder or inert additive was found that could compensate for the large volume expansion that occurs upon lithiation. Repeated cycling caused the particle to crack and split into smaller particles that were no longer connected to the conductive electrode matrix. Modeling work in literature suggests that the particle cracking problem can be avoided by starting with a particle that is less than a critical size.

In FY10, efforts were directed to determine the optimum particle size for Cu_6Sn_5 based on the model of Huggins and Nix[12]. They developed a simplified model based on the modulus and fracture toughness of the bulk Sn material. The results of this model can be represented by the following equation:

$$h_c \approx \frac{23}{\pi}\left(\frac{3K_{Ic}}{Be_T}\right)^2$$

where

h_c is critical size in μm
K_{Ic} is fracture toughness in MPa-m^{½}
B is elastic modulus in GPa
e_T is strain dilation (ΔV/V)

This opens up a new approach to searching for optimum intermetallic anode materials. Find metallic and intermetallic alloys that are capable of being lithiated and then determine their bulk mechanical properties to determine a critical particle size. If the particle size is too small then try to increase the fracture toughness and decrease the elastic modulus of the metal anode material through alloying with additional metals and phases.

The mechanical properties of $Li_xM_yCu_5Sn_5$ electrode materials are not published in the literature. Efforts were undertaken to determine these properties for Cu_6Sn_5 and its alloys. Recently, the mechanical properties of several intermetallic alloys were determined at Argonne and are listed in Table IV- 2. The elastic modulus was obtained using a Universal Materials Testing Machine (Instron). Measurements were made from stress strain plots obtained during four-point-bend tests using rectangular bars of the test material (Figure IV- 24). Outer fiber stress and associated strain were obtained from standard elastic beam

[12] R.A. Huggins and W.D. Nix, "Decrepitation Model For Capacity Loss During Cycling of Alloys in Rechargeable Electrochemical Systems", *Ionics* **6** (2000) p. 57-63.

theory. Slope of the stress vs. strain plot gave the elastic modulus of each alloy.

The fracture toughness was obtained via a Single Edged Notched Bend (SENB) test. A thin wafering blade was used to notch the samples such that the notch depth to sample thickness was ~0.5. Samples were tested in three-point bend loading configuration at a constant displacement rate. Fracture toughness was determined from the peak load at failure, sample dimensions, and a standard fracture mechanics relationship. Results are shown in Table IV- 2.

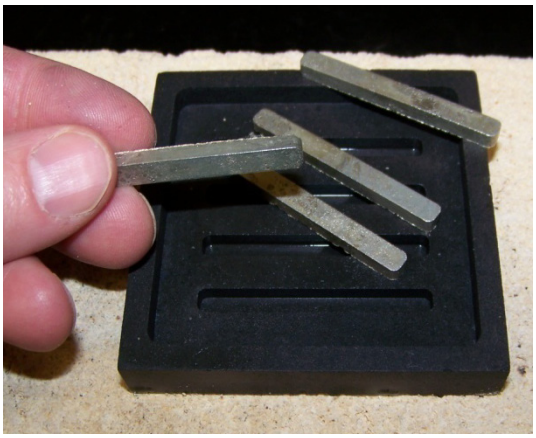

Figure IV- 24: Photo of rectangular bars cast from various intermetallic alloys used for mechanical property studies.

Table IV- 2: Fracture Toughness Obtained via a Single Edged Notched Bend (SENB) test

Alloy	Strength (MPa)	Modulus (GPa)	Fracture Toughness (MPa $m^{0.5}$)
Cu_6Sn_5	79 ± 14	41.1 ± 4.4	2.19 ± 0.54
$NiCu_5Sn_5$	41.0 ± 7.5	65.9 ± 8.5	1.32 ± 0.13
$ZnCu_5Sn_5$	93.0 ± 8.9	46.0 ± 6.2	2.56 ± 0.23
$FeCu_5Sn_5$	78.9 ± 7.0	52.19 ± 0.89	2.38 ± 0.15
Cu_6Sn_6	81	41	2.56
Li_2CuSn			

The measured mechanical properties were then used in the equation above from Huggins' model and the optimum particle size was calculated. Two optimum particle sizes were calculated – one for lithiation halfway (to Li_2CuSn) and one for full lithiation (to $Li_{17}Sn_4$). These results are shown in Table IV- 3. In general, the optimum particle size is near 0.5 microns for half lithiation, and near 50 nanometers for full lithiation for all of the alloys studied, except for the nickel based alloy, which required even smaller particles. It is no surprise that the efforts based on the commercial sample with 10 micron particle size met with little success as this is nearly two orders of magnitude larger than the 0.5 micron predicted particle size.

Table IV- 3: Optimum particle sizes for lithiation halfway (to Li_2CuSn) and one for full lithiation (to $Li_{17}Sn_4$).

Intermetallic Alloy	$10Li + MCu_5Sn_5 \leftrightarrow 5Li_2CuSn + M$		$85Li + 4MCu_5Sn_5 \leftrightarrow 5Li_{17}Sn_4 + 20Cu + 4M$	
	Critical Particle Size, µm (eT = 0.63)	Theoretical Capacity, mAh/g	Critical Particle Size, µm (eT = 1.8)	Theoretical Capacity, mAh/g
Cu_6Sn_5	0.47	257	0.058	507
$NiCu_5Sn_5$	0.067	258	0.0082	510
$ZnCu_5Sn_5$	0.51	256	0.063	507
$FeCu_5Sn_5$	0.35	259	0.042	511
Cu_6Sn_6	0.65		0.079	
Li_2CuSn				

A search was performed to find a new source for smaller particle size Cu_6Sn_5 based intermetallic alloys that led to Wildcat Discovery Technologies. They are a high throughput materials discovery company with specialty synthesis capabilities. Wildcat performed a high throughput screen to identify reaction conditions for the target particle size that Argonne provided. A variety of morphologies were induced, and a final selection was made for one synthesis method based on its resulting primary particle size and separation (see Figure IV- 25). Five 100-g alloys were then synthesized by Wildcat Discovery Technologies with the composition of MCu_5Sn_5, where M was Cu, Sn, Ni, Zn, and Fe with a controlled particle size near 0.5 microns.

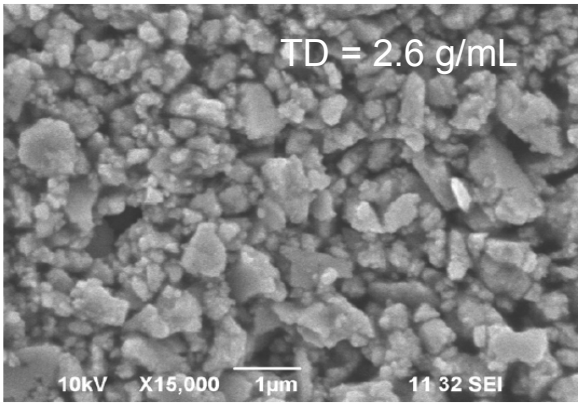

Figure IV- 25: SEM photo of optimum Cu_6Sn_5 powder based on mechanical properties for discharge to Li_2CuSn.

Conclusions and Future Directions

It became clear in this effort that engineering efforts alone cannot solve the problem of expansion and contraction during cycling. Success may be achieved if an intermetallic alloy can be made with an ideal composition and optimum particle size in an electrode configuration that can accommodate large volume changes of its active material.

FY11 efforts will center on electrochemically testing MCu_5Sn_5 alloys with 0.5 micron particle size from Wildcat Discovery Technologies. The most promising alloy will be used to revisit the influence of elastic binders and inert additives. New approaches to making electrode coatings may be needed in this work due to the small particle size. Key to this issue will be to monitor the energy density of various electrode designs to compare against graphite/carbon electrodes. Electrolyte additives that enhance SEI formation on MCu_5Sn_5 alloys will also be explored.

FY 2010 Publications/Presentations

1. Poster presentation at the DOE Vehicles Technology Program 2009 Annual Merit Review Meeting.
2. Oral presentation at the DOE Vehicles Technology Program 2010 Annual Merit Review Meeting.

IV.B.2.3 Lithium Metal Anodes (ANL)

John T. Vaughey

Chemical Sciences and Engineering Division
9700 S Cass Ave
Argonne National Laboratory
Lemont, IL 60439
Phone: (630) 252-8885
E-mail: vaughey@anl.gov

Collaborators:
Dennis W. Dees
Carmen Lopez

Start Date: October 1, 2007
Projected End Date: September 30, 2010

Objectives

- To overcome the well known problems with the metallic lithium electrode - stability, safety, and cycling efficiency - that continue to block its implementation into advanced lithium batteries for PHEVs.
- Characterize the morphological evolution of the lithium electrode on cycling
- Develop and characterize coating technologies that will withstand the lithium cell environment

Technical Barriers

This project addresses the following technical barriers from the Energy Storage section of the DOE Vehicle Technologies Program Multi-Year Research, Development and Demonstration Plan:

(A) 40 mile range for PHEVs

(B) Abuse tolerance

(C) Cell life

Technical Targets

- Synthesize, design and characterize polymer-alloy composite films deposited on the surface of a lithium electrode.
- Utilize characterization tools available at the National Electron Microscopy Center and Center for Nanoscale Materials to investigate the changes in morphology that occur on cycling for a lithium metal anode.
- Investigate new types of surface coatings with better surface adhesion.

Accomplishments

- Studied the morphological changes in the lithium electrode as a function of electrolyte exposure and time. We have identified new structures that form on contact with various electrolyte components and act as SEI nucleation points. This highlights one of the causes of the difference in SEI components between graphite and lithium.
- Showed that loss of electrolyte solvent to side reactions with the lithium metal was a key limiting factor in cell lifetimes. Demonstrated that re-filling the cell with fresh electrolyte resulted in a drop in cell resistivity to near initial levels.
- Loss of direct contact by the lithium with the current collector was a major factor in a dramatic rise in cell impedance seen at end-of-life.
- Demonstrated that early cycling history and surface conditioning was an important variable in extending lithium metal anode cycle life. Showed that current densities > 0.25 mA/cm^2 were required to suppress formation of surface structures generated by gas encapsulation.
- Extended silane-coating effort to a larger variety of materials. Was able to demonstrate that the type of coating was important although a more dominant factor was packing density of the side-chain alkyl groups.
- Materials with the densest packed surfaces had longest cycle life (set at loss of 20% initial capacity).
- Performed detailed study of common graphitic SEI formers and showed they lacked long term stability against lithium and were not acceptable as components of composite coatings.

✧ ✧ ✧ ✧ ✧

Introduction

Achieving the DOE 40 mile range target for PHEVs will require several improvements in current lithium-ion battery technology. For anode materials studies, the focus has been on safety, stability on cycling of the passivation (SEI) layer, and capacity – both gravimetric and volumetric. Whereas most anode evaluation and optimization studies have been done on graphitic or hard carbons, lithium metal has many intrinsic advantages, and recent advances in polymer science, diagnostics, and coatings technology, can make it a viable anode material. Advantages of lithium metal, including significant

increases in anode capacity, increased options for cathode materials, faster kinetics, and a factor of four reduction in coating volume, make lithium metal a promising alternative to graphite as new markets for lithium-ion batteries evolve. However, safety concerns have limited the appeal of lithium metal in commercial cells. Issues including poor electrodeposition characteristics and electrolyte instabilities must be addressed before industrial cell builders will introduce it into their processes and products.

Approach

To meet the DOE targets, we initiated a study of the morphological signatures that result from the common failure mechanisms of lithium metal anodes in order to develop a better understanding of the chemistry involved and to propose new solutions to make them a viable alternative to graphite for PHEV battery systems.

We are studying methods to establish a stable, dense, and uniform lithium/electrolyte interface exhibiting good electrochemical performance.

- Analyze the failure mechanisms of various Li-metal electrode coatings previously postulated in the literature to be stable for various lengths of time.
- Develop conformal stable coatings using newly developed solution-based silane chemistry.
- Evaluate nanocomposite polymer/Li-ion conductor coatings.
- Use some of the latest microscopic and spectroscopic characterization equipment to characterize the lithium/electrolyte interface.

Results

Lithium Metal Coatings Coating lithium metal has been a well studied approach to extending the life of this class of electrodes. Literature studies predominantly from the early 1990s were focused on electrolyte decomposition products and the effect of SEI-forming additives on performance. Some of the more notable successes of this approach were by Aurbach and co-workers who identified the electrolyte 1M $LiAsF_6$ in 1,3 dioxolane as stable under certain conditions to lithium metal. Systematic studies indicated that the active coating was in fact a composite of the Zintl phase Li_3As (from the salt) and a conductive PEO-like polymer derived from the solvent. The system was stable at rates below C rate but above that the polymer proved unstable. We previously studied analogues of this system using a variety of more conductive Zintl salts and other polymers identified by theoreticians and other experimental groups as forming stable coatings at the appropriate potentials.

In general it was found that the Zintl materials were easily incorporated into a variety of polymeric films at concentrations that could be controlled during the synthesis. Numerous combinations were evaluated and it was concluded that in all attempts the polymeric coating failed on cycling. Figure IV- 26 shows the before and after pictures of a lithium electrode coated with a 1-vinylimidazole.

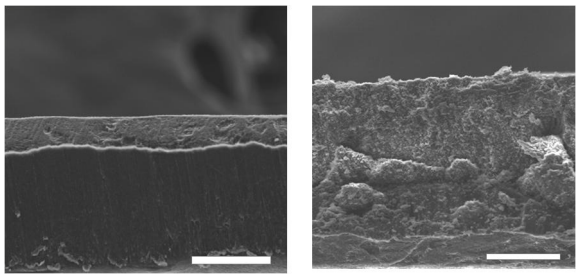

Figure IV- 26: (left) Thin film formed on lithium metal electrode dip-coated with 1-vinyl imidazole. After 200 cycles (right) polymeric layer has decomposed leaving the lithium surface unprotected and having the general appearance of the uncoated control sample. Scale bar is 100 um for both micrographs.

Conformal Coatings To better adhere the coating to the surface we have initiated studies on utilizing atomic layer deposition (ALD)-type chemistry utilizing simple silanes. In these studies we take advantage of the naturally hydroxlated surface of lithium metal and selectively react it with a small chain silane to produce a monolayer coverage of the desired material.

Previous studies of the coatings show them to be very stable in the battery environment and successful in protecting the lithium surface from electrolyte reactions in an uncycled state. This effort has been extended to show how the coatings that had the lowest initial impedance had the lowest fade rate ion cycling. The normalized capacity as a function of cycle number for two difference coatings is shown in Figure IV- 27.

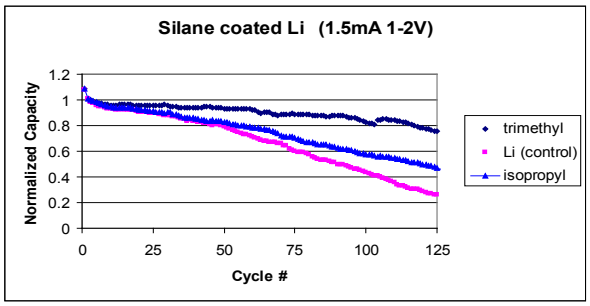

Figure IV- 27: Capacity (normalized) vs. cycle number for two different silanes is shown versus an uncoated lithium control.

Morphological Studies We previously reported on our extensive SEM study on the evolution of lithium metal and the surface of lithium metal on cycling. In this work we were able to show how initial cycling conditions affected the initial surface structure and how these conditions controlled the nucleation of dendrites and controlled long term electrode stability (cycle life). We

have extended this study to the stability of various layers formed on the electrode surface during cell assembly. A typical pre-cycled electrode is shown in Figure IV- 28.

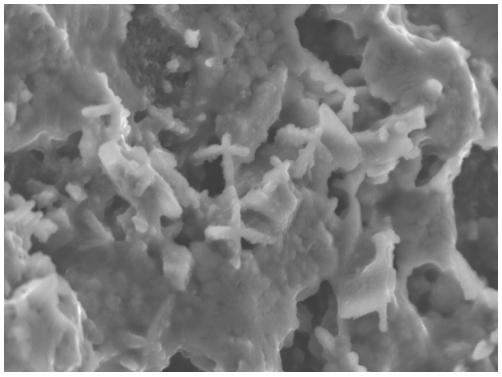

Figure IV- 28: Surface structure of clean lithium on 20sec exposure to electrolyte (1.2 M $LiPF_6$, EC:EMC 30:70)

Additional SEM studies of the electrode over time showed that within minutes the surface had been transformed as inorganic species (mainly salts) started to deposit and grow. A typical SEM of this is shown in Figure IV- 29.

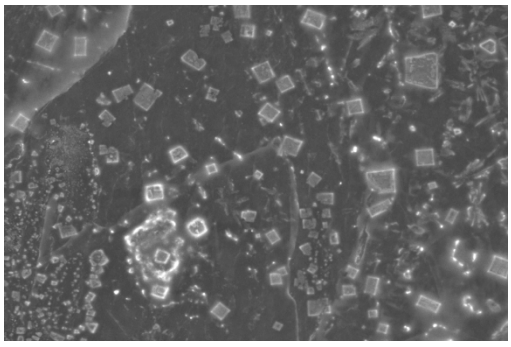

Figure IV- 29: Surface structure of clean lithium on 5 min exposure to electrolyte (1.2 M $LiPF_6$, EC:EMC 30:70)

These morphological observations on cycling have implications on SEI formation as it has been previously observed by Aurbach, Ross, and Edstrom that the SEI layer on lithium has a higher inorganic content than those found on graphitic or other carbon-based anodes. These initial decomposition products, which form on contact with the metal, form before an electrochemical SEI layer has formed and may introduce various structural weaknesses or points of lower lithium conduction into the layer.

Conclusions and Future Directions

- Zintl metal / composite polymer coatings (Li_xM / $(VEC)_x$; M = Ag, Sn, Al) show good stability and density on formation on a pre-cycled electrode. On cycling the polymerized VEC component breaks down and coating failure is observed.
- The stability of lithium metal in electrolyte was studied and various pre-cycling morphological changes were observed that may have some implication for the differences noted in SEI layer composition between graphite and lithium metal.
- Gradual loss of good contact between the porous lithium anode and the current collector results in a large impedance rise and eventual cell failure.
- Continue studies of silane and related materials coatings on lithium metal surface. Conformal coatings may have higher stability and extend cell lifetime.

FY 2010 Publications/Presentations

1. J. T. Vaughey, C. Lopez, D. Dees "Recent Advances in Understanding Lithium Metal Anodes" Department of Chemistry, Advanced Materials Research Institute, University of New Orleans, February, 2010.
2. C.M. Lopez "A Systematic Study of the Lithium Metal Anode", Invited Seminar, National Renewable Energy Laboratory / Colorado School of Mines, Golden CO, February, 2010.
3. C.M. Lopez "A Systematic Study of the Lithium Metal Anode", Invited Seminar, Accumulator Research Institute, University of Ulm, Ulm, Germany, March, 2010.
4. J. T. Vaughey "Lithium-ion Batteries: A Materials Chemistry Perspective" Departmental Colloquium, Department of Chemistry, Clemson University, Clemson, SC, September 2010.
5. J. T. Vaughey, C. M. Lopez, D. W. Dees "Morphological Evolution of Lithium Metal Anodes on Cycling" NEDO-Argonne Meeting on Lithium-Ion Batteries, Argonne, IL, October 2010.
6. J. T. Vaughey, C. M. Lopez, L. Trahey, D. W. Dees, M. M. Thackeray "Lithium and Lithium-Ion Battery Anode Materials" Gordon Conference on Solid State Chemistry, New London, NH, August, 2010.
7. M. Thackeray, C. Johnson, S. Kang, V. Pol, L. Trahey, J. Vaughey, H. Kung, D. Shin, C. Wolverton, L. Hardwick, P. G. Bruce "Designing Advanced Anode and Cathode Materials for Lithium-Ion Batteries" 213th Materials Research Society, Boston, MA. November, 2009.
8. Michael M. Thackeray, Mahalingam Balasubramanian, Christopher S. Johnson, Sun-Ho Kang, Swati Pol, Vilas Pol, Lynn Trahey, John T. Vaughey, Dongwon Shin and Chris Wolverton "Advances in the Design of Anode and Cathode Materials for Lithium Batteries" International Battery Seminar for Primary & Secondary Batteries, Fort Lauderdale, FL, March 2010
9. M. M. Thackeray, M. Balasubramanian, R. Benedek, C. S. Johnson, S.-H. Kang, V. G. Pol, S. V. Pol, L. Trahey, J. T. Vaughey "Designing Anode and Cathode Materials to Counter the Performance Limitations of Li-Ion Batteries" 15th International

Meeting on Lithium Batteries (IMLB), Montreal, Canada, June 2010.

10. Sun-Ho Kang, Carmen M. Lopez-Rivera, John Vaughey, Dongwon Shin, Christopher Wolverton, Michael M. Thackeray "Improved Rate Capability of High-Capacity (x) $Li_2MnO_3 \bullet (1\text{-}x)LiMO_2$ Electrodes by Li-Ni-PO_4 Surface Treatment" 216th Meeting of the Electrochemical Society, Vienna, Austria, October, 2009.

IV.B.2.4 New High Power $Li_2MTi_6O_{14}$ Anode Material (ANL)

Khalil Amine

Argonne National Laboratory (ANL)
9700 South Cass Avenue
Argonne, Il 60439
Phone: (630) 252-3838; Fax: (630) 252-4176
E-mail: amine@anl.gov

Collaborators:
Damien Dambournet (ANL)
Ilias Belharouak (ANL)

Start Date: September 1, 2008
Projected End Date: September 30, 2010

Objectives

- Develop new anode materials that provide very high power capability and outstanding safety.
- Explore ways for preparing pure and nanosized $Li_2MTi_6O_{14}$ with full capacity.
- Compare the electrochemical properties of $Li_2MTi_6O_{14}$ (M= Sr, Ba, or 2Na) materials.
- Investigate the applicability of $Li_2MTi_6O_{14}$ (M= Sr, Ba, or 2Na) as anodes for Li-ion batteries.

Technical Barriers

This project addresses the following technical barriers:

- Overcome the inherent safety-related issue of the graphite anode.
- Improve the power density of the Li-ion battery.
- Improve the cycle and life span of the Li-ion battery.

Technical Targets

- Develop safe and high power anode materials based on the open-structure $MLi_2Ti_6O_{14}$ materials with M=Sr, Ba, or 2Na.
- Develop a suitable anode material morphology to achieve high capacity.
- Develop Li-ion cell chemistries based on these new anodes for hybrid electric vehicles (HEVs).

Accomplishments

- Developed a sol-gel method to prepare pure $MLi_2Ti_6O_{14}$ with M=Sr, Ba, or 2Na.
- Completed a comparative study of $MLi_2Ti_6O_{14}$ based on structural and electrochemical characterizations.
- Identified a nano-structured Sr-based compound that delivers high capacity and rate capability.
- Demonstrated high power capability of these anodes in full cell tests with $LiMn_2O_4$ cathodes.

Introduction

Lithium-ion batteries are being considered to power a new generation of clean vehicles. Battery life span, cost, and safety are still major barriers. With regard to safety, the issues associated with the formation of the solid-electrolyte interface (SEI) at the graphitic electrode can be overcome through the development of alternative anodes that can operate within the electrochemical stability zone of conventional electrolytes. This region is generally known to be above the potential (~1 V) of SEI formation and below the potential (~4.3 V) of electrolyte oxidation. Tetravalent titanium-based materials such as $LiTi_2(PO_4)_3$, TiO_2, and $Li_4Ti_5O_{14}$ are promising anode materials. Their operating voltages are 2.5, 1.7, and 1.5 V, respectively, vs. metallic lithium. These variations are primarily due to the difference of structures and the iono-covalent character of the Ti-O bonds, though the Ti^{4+}/Ti^{3+} redox couple is common for these materials. In general, the energy of a given electrochemical couple can be tailored, based on structural considerations and the chemical bonding involved. A new Li-ion insertion anode, $MLi_2Ti_6O_{14}$ (M = Sr, Ba, or 2Na), exhibits lower operating voltage and lower resistivity compared to $Li_4Ti_5O_{14}$. The voltage of $MLi_2Ti_6O_{14}$ prevents the formation of the SEI layer and, hence, mitigates the safety concerns.

In general, this project aims to develop a high power anode for lithium-ion batteries, and $MLi_2Ti_6O_{14}$ compounds have been chosen for investigation based on the above properties.

Approach

We have developed a new synthesis route to prepare pure $MLi_2Ti_6O_{14}$ (M = Sr, Ba, or 2Na) compounds, using a sol-gel method. Lithium acetate hydrate, “M” acetate, and titanium isopropoxide are used as precursors and dissolved in a solution containing anhydrous ethanol and acetic acid. The formed gel is heated at 200°C overnight to complete the removal of the solvents. Finally, after grinding, the dry gel is annealed at 900°C for 12 h under air atmosphere.

The synthesized material was characterized by various analytical techniques and tested as an anode in coin cells.

Results

The X-ray patterns of the prepared $MLi_2Ti_6O_{14}$ (M = Sr, Ba, or 2Na) materials are shown in Figure IV- 30 and attest to the phase purity. The $MLi_2Ti_6O_{14}$ structure is built upon edge and corner sharing TiO_6 octahedra, resulting in a three-dimensional network. The lithium atoms are located in tetrahedral sites, forming tunnels within the structure. The main difference between the monovalent and bivalent cations is that Na atoms fully occupy the 11-fold available positions, which are only half-occupied in the case of Sr and Ba atoms. This results in a lowering of the unit cell symmetry from the Fmmm space group to Cmca space group within the orthorhombic system. Therefore, in terms of occupancy, $Na_2Li_2Ti_6O_{14}$ has less structural void compared to $SrLi_2Ti_6O_{14}$ and $BaLi_2Ti_6O_{14}$.

Concerning the material morphology, the solids consist of 500-nm primary particles that agglomerate in larger particles. Because $BaLi_2Ti_6O_{14}$ showed larger agglomerates, which have a negative impact on power and capacity, we will focus on the results for the Sr- and Na-based compounds.

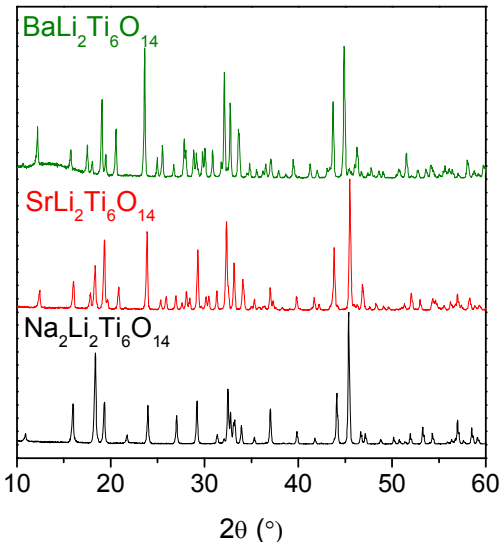

Figure IV- 30: X-ray diffraction powder patterns of $MLi_2Ti_6O_{14}$ prepared by sol-gel method.

Figure IV- 31 shows the voltage profile curves of the $SrLi_2Ti_6O_{14}$ and $Na_2Li_2Ti_6O_{14}$ materials in the voltage range between 0.5 and 2 V. These materials displayed an average voltage of 1.25 V (Na) and 1.4 V (Sr). The $SrLi_2Ti_6O_{14}$ showed higher capacity than $Na_2Li_2Ti_6O_{14}$. This finding is in good agreement with the structural characterization.

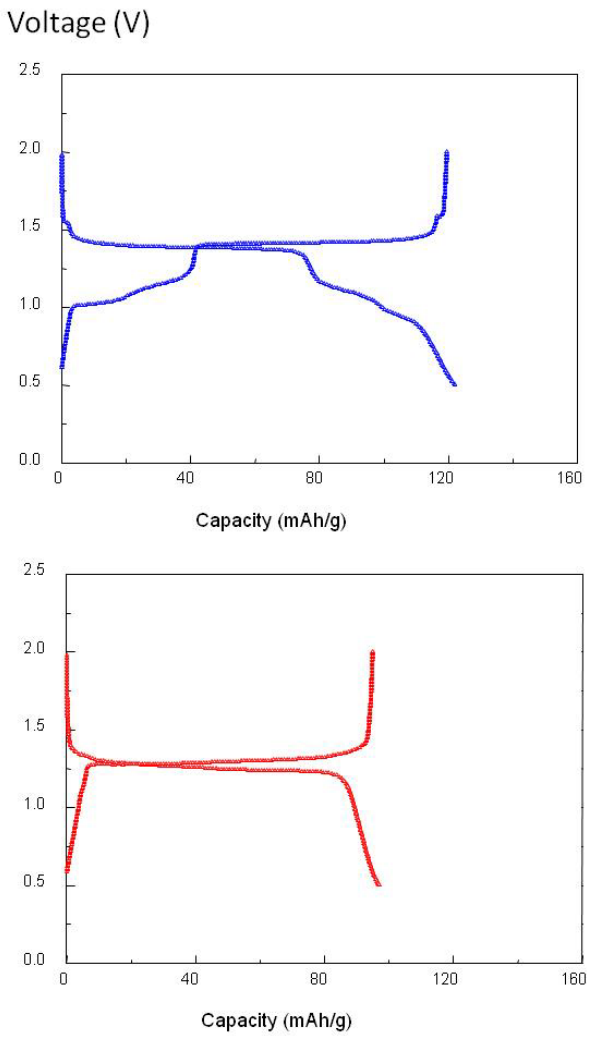

Figure IV- 31: Charge/discharge voltage profiles of $SrLi_2Ti_6O_{14}$ (top) and $Na_2Li_2Ti_6O_{14}$ (bottom) cycled between 0.5 and 2 V under 10 mA/g.

Figure IV- 32 shows the performance of the Li/$MLi_2Ti_6O_{14}$ half cell (M = Sr and 2Na) at a current density of 10 mA/g for 50 cycles. Both electrodes exhibited excellent capacity retention with a reversible insertion of 3 and 2 Li^+ ions for $SrLi_2Ti_6O_{14}$ and $Na_2Li_2Ti_6O_{14}$, respectively.

Figure IV- 33 shows the rate capability of the Sr- and Na-based materials cycled at 100, 200, 400, and 800 mA/g current density.

The Sr-based compound showed superior rate capability compared with $Na_2Li_2Ti_6O_{14}$. The $SrLi_2Ti_6O_{14}$ can deliver 92 mAh/g capacity within 15 min charge and discharge, *i.e.,* 800 mA/g current density.

The $SrLi_2Ti_6O_{14}$ anode was coupled with $LiMn_2O_4$, a 4-V cathode material, providing a 2.7 V cell. Figure IV- 34 shows the rate capability of the $LiMn_2O_4/SrLi_2Ti_6O_{14}$ full cell at the C/5, C/2, and 2C rates.

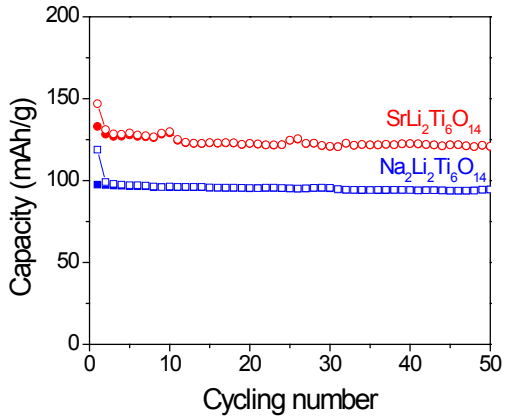

Figure IV- 32: Cyclability of $MLi_2Ti_6O_{14}$ performed between 0.5 and 2 V at 10 mA/g.

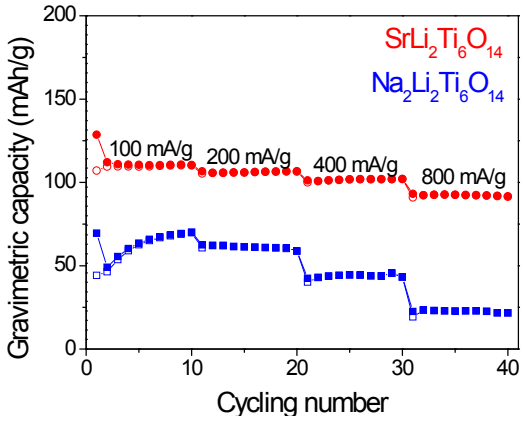

Figure IV- 33: Rate capability of $MLi_2Ti_6O_{14}$ cycled between 0.5 and 2 V.

Conclusions and Future Directions

The open-type-structure materials $MLi_2Ti_6O_{14}$ (M = Sr, Ba, or 2Na) have been synthesized by a sol-gel method. The incorporation of a monovalent (Na^+) or divalent (Sr^{2+}, Ba^{2+}) ion inside the structure affected the symmetry of the crystal as well as the lithium insertion mechanisms. The $SrLi_2Ti_6O_{14}$ electrode exhibited the best rate capability. The future plan for this work includes the following:

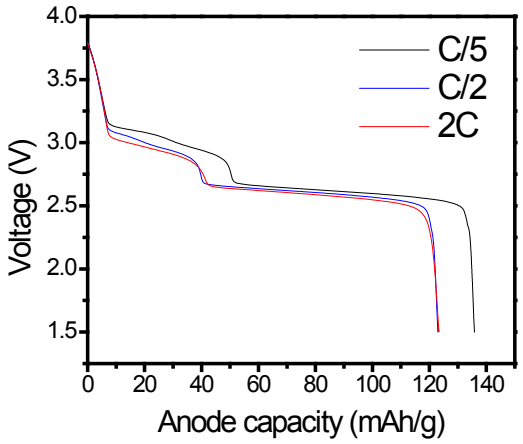

Figure IV- 34: Rate capability of $LiMn_2O_4/SrLi_2Ti_6O_{14}$ cycled between 1.5 and 3.8 V.

- Optimize the $SrLi_2Ti_6O_{14}/LiMn_2O_4$ cell design and evaluate its electrochemical properties for HEV applications.
- Complete *in situ* structural characterization of $SrLi_2Ti_6O_{14}$.
- Investigate the pulse-discharge and charge performance of the cell based on the $SrLi_2Ti_6O_{14}$anode through hybrid pulse power characterization (HPPC test).
- Increase the power performance of the $MLi_2Ti_6O_{14}$ electrode through new synthesis method and/or through nano-carbon coating.
- Investigate the potential use of $Na_2Li_2Ti_6O_{14}$as a high power anode.
- Investigate the safety and stability (vs. electrolyte,) of these materials.

FY 2010 Publications/Presentations

1. Oral Presentation at the DOE Annual Peer Review Meeting, Washington, DC, 2010.
2. Dambournet, I. Belharouak and K. Amine, $MLi_2Ti_6O_{14}$ (M = Sr, Ba, 2Na) Lithium Insertion Titanate Materials: A Comparative Study, *Inorganic Chemistry*, 49: 2822 (2010).

IV.B.3 Applied Battery Research on Cathodes

IV.B.3.1 Engineering of High Energy Cathode Material (ANL)

Khalil Amine

Argonne National Laboratory
9700 South Cass Avenue
Argonne, IL 60439
Phone: (630) 252-6551; Fax: (630) 972-4451
E-mail: amine@anl.gov

Collaborators:
Huiming Wu (ANL)
Ilias Belharouak (ANL)
Ali abouimrane (ANL)
Y. K. Sun (Hanyang University)
Xiao Qing Yang (BNL)

Start Date: October 1, 2008
Projected End Date: September 30, 2014

Objectives

- Enable the use of the Argonne high-energy composite layered cathode, $xLi_2MnO_3 \bullet (1-x)LiNiO_2$, in a plug-in hybrid vehicle (PHEV) with electric drive range of 40 miles
- Optimize cathode composition and engineer this material to improve its packing density and rate capability for PHEV applications
- Explore surface protection to enable high capacity and long cycle life at high voltage (4.6 V)

Technical Barriers

- Poor continuous charge and discharge rate capability
- High electrode impedance
- Low pulse power
- Low packing density, which translates to low volumetric energy density
- High reactivity with the electrolyte at high voltage

Technical Targets

- Improve the rate capability. Our target is to increase the rate capability from C/10 to 1C ~ 2C.
- Improve the packing density to 2~2.4 g/cc.
- Stabilize the surface of the particles to improve significantly the calendar and cycle life.

Accomplishments

- Developed a carbonate-based co-precipitation process that provides spherical particle morphology.
- Optimized the carbonate-based co-precipitation process and composition to obtain high packing density cathode materials with high reproducibility.
- Optimized the composition to obtain reproducible and highly pure materials.
- Validated the improvement of rate and cycling stability at high temperature using AlF_3 surface nano-coating.

✧ ✧ ✧ ✧ ✧

Introduction

The 40-mile electric-drive PHEV requires development of a very high-energy cathode and/or anode that offers 5,000 charge-depleting cycles, 15 years calendar life, and excellent abuse tolerance. These challenging requirements make it difficult for conventional cathode materials to be adopted in PHEVs. Here, we report on a very high-energy material based on a layered lithium-rich nickel manganese oxide composite electrode as a potential cathode for PHEV and all-electric vehicle applications. This material exhibits over 200 mAh/g capacity, relatively good stability, and improved safety characteristics.

Approach

- Develop a process that leads to very dense material to increase the electrode density and, therefore, the electrode capacity per unit volume.
- Investigate ways of obtaining spherical cathode particles with a high degree of homogeneity.
- Investigate nano-coating of the material with metal fluoride, phosphate, and oxide to reduce the initial interfacial impedance and stabilize the cathode interface in order to improve the cycle life at elevated temperature.
- Investigate the effect of making 3-µm secondary particle and 50-nm primary particles that are distributed in a dense configuration (limited pores) on the rate capability of the material.

- Investigate new ways of coating oxides with carbon to improve conductivity of the material.

Results

Effect of cobalt doping on scalability of composite electrode. In the past year, our focus was on developing high-energy cathodes based on the layered lithium-rich nickel manganese oxide composite with an optimum composition of $Li_{(1+x)}Ni_{0.25}Mn_{0.75}O_{(2.25+x/2)}$. This material shows a high packing density of 2.1 g/cc and a high capacity of 210 mAh/g at the 1C rate. The high rate capability of this material was attributed to the particle morphology (10-µm secondary particles and dense 80-nm primary particles), which reduces the lithium pathway diffusion. However, when attempting to scale up this material from the 50 g level to the 500 g to 1,000 g levels, we were not able to reproduce the performance of the smallest scale material. Figure IV- 35 shows the charge and discharge capacity of $Li_{(1+x)}Ni_{0.25}Mn_{0.75}O_{(2.25+x/2)}$, where $1 < x < 1.32$. In this case, the capacity of the material drops very quickly when $x > 1.1$. It is possible that when scaling up the materials to 1000 g, we were not able to completely wash out the Na from the $NaCO_3$ used as co-precipitating agent. As a result, the final stoichiometry of the material was slightly different from the targeted one. The performance of the material could not be reproduced because of the sensitivity of the capacity to the ratio of lithium, as shown in Figure IV- 35. However, when using a small amount of cobalt doping, we found that the charge and discharge capacities of the composite material were not affected much by excess lithium Figure IV- 35 (b). As a result, it was much easier to obtain reproducible data when scaling up this material.

Figure IV- 36 shows scanning electron microscopy (SEM) images of the cobalt-doped high-energy cathode, $Li_{(1+x)}Ni_{0.25}Co_{0.15}Mn_{0.6}O_{(2.25+x/2)}$ $(0.225 < x < 1.65)$. As in the case of the material without cobalt doping, reported last year, the primary particles that construct the secondary particles underwent significant size change after lithiation, namely, from around 100 nm ($x = 0.225$) to around 500 to 900 nm for samples with the highest lithium content ($x = 1.65$). The images also show that the primary particles that compose the surface of the samples with $x = 0.225$ form a much denser and smoother surface than the samples with high excess lithium. In this case, the packing density of the material was 2.1 g/cc.

Effect of cobalt doping on cycling performance of composite electrode. Figure IV- 37 shows the cycling performance of the nano-sized $Li_{(1+x)}Ni_{0.25}Co_{0.15}Mn_{0.6}O_{(2.25+x/2)}$ $(x = 0.225)$ vs. lithium metal as counter electrode. The material achieved 225 mAh/g capacity at C/3 during the initial cycling. However, the discharge capacity faded gradually with cycling and declined to 150 mAh/g after only 50 cycles. This result is different from the high energy composite without doping, which shows excellent cycling performance with no capacity fade after 200 cycles.

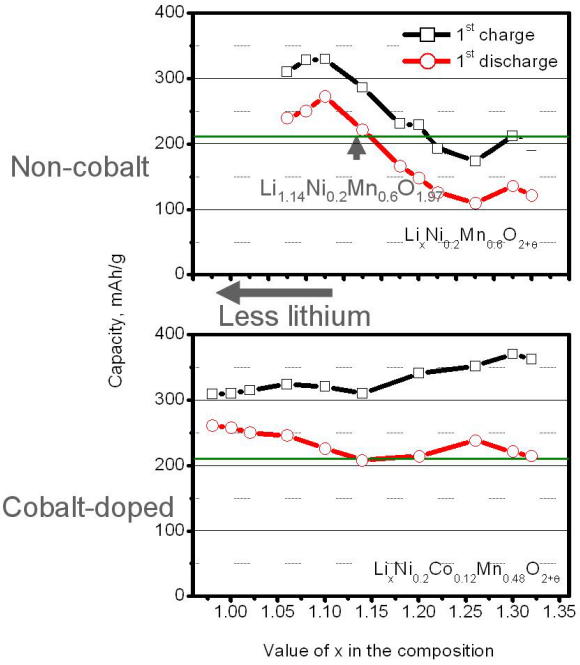

Figure IV- 35: Charge and discharge capacity variation with lithium concentration in high-energy composite electrode with and without Co doping

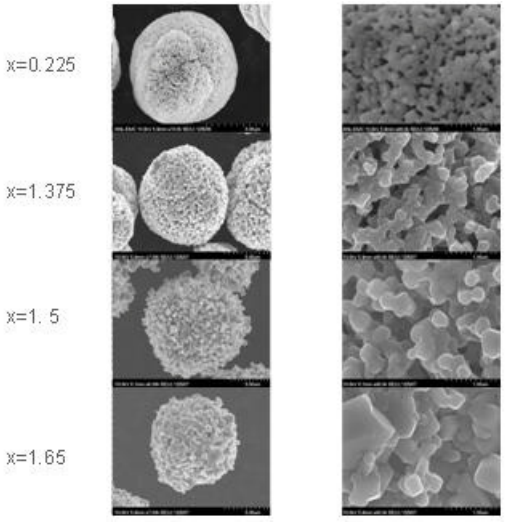

Figure IV- 36: SEM images of $Li_{(1+x)}Ni_{0.25}Co_{0.15}Mn_{0.6}O_{(2.25+x/2)}$ $(0.225 < x < 1.65)$. (Left side: secondary particles, 5µm scale bar; right side: primary particles, 1 µm scale bar.

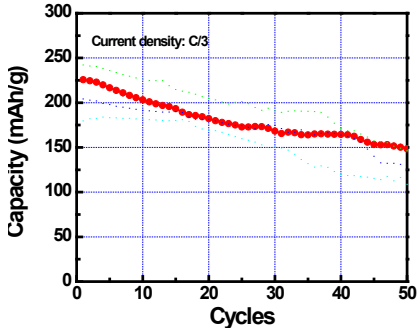

Figure IV- 37: Cycling performance of a cell made of $Li_{(1+x)}Ni_{0.25}Co_{0.15}Mn_{0.6}O_{(2.25+x/2)}$ (x = 0.225) vs. lithium metal at C/3 rate

Effect of AlF_3 coating on cycling performance of Co-doped composite electrode. To improve the cycling performance of the lithium-rich nickel manganese oxide composite electrode with cobalt doping, we investigated protecting each particle with a very stable coating that acts as a barrier against any reactivity between the charged electrode and the electrolyte. In this case, the composite electrode was charged to 4.6 V to achieve very high capacities. At this high voltage, the conventional electrolyte usually reacts easily, leading to a significant interfacial impedance rise and thus cell performance degradation. Figure IV- 38 shows an SEM image of a cross section of an uncoated particle and a particle that was coated with an AlF_3 thin layer. In this case, the coating thickness was less than 10 nm. The effect of the thin AlF_3 coating on the initial impedance of the cell is shown in Figure IV- 39. Because of the very thin coating, the initial impedance of the coated material was lower than that of the uncoated material after the initial formation cycle. This result indicates that the uncoated material reacts with the electrolyte during the initial formation cycles and forms a thicker coating, which results in a high initial impedance of the cell.

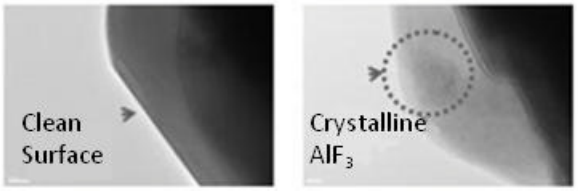

Uncoated **AlF_3 coated**

Figure IV- 38: SEM of cross section of AlF_3-coated and uncoated $Li_{(1+x)}Ni_{0.25}Co_{0.15}Mn_{0.6}O_{(2.25+x/2)}$ (x = 0.225)

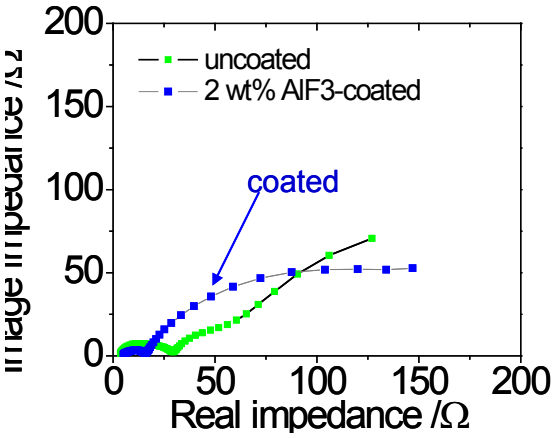

Figure IV- 39: Alternating current impedance of a cell made of a 2 wt% AlF_3-coated and uncoated $Li_{(1+x)}Ni_{0.25}Co_{0.15}Mn_{0.6}O_{(2.25+x/2)}$ (x = 0.225)

Figure IV- 40 shows the cycling performance of the AlF_3-coated and uncoated $Li_{(1+x)}Ni_{0.25}Co_{0.15}Mn_{0.6}O_{(2.25+x/2)}$ (x = 0.225). The cycling was carried out at room temperature and the C/3 rate. The coated material shows excellent cycling performance with no capacity fade after 100 cycles. By contrast, the uncoated material shows gradual fade in the capacity with cycling.

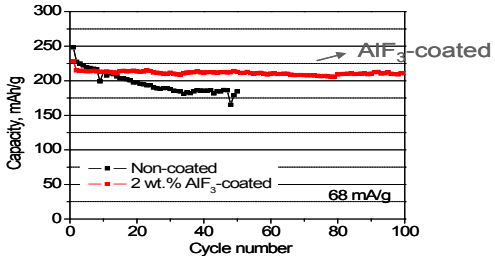

Figure IV- 40: Cycling performance of the AlF_3-coated and the uncoated $Li_{(1+x)}Ni_{0.25}Co_{0.15}Mn_{0.6}O_{(2.25+x/2)}$ (x = 0.225) at 25°C

Figure IV- 41 shows the cycling performance of the AlF_3-coated $Li_{(1+x)}Ni_{0.25}Co_{0.15}Mn_{0.6}O_{(2.25+x/2)}$ (x = 0.225) and uncoated material. This test was carried out at 55°C and the C/3 rate. The coated material achieved 240 mAh/g capacity and showed excellent cycling performance at the high temperature. This result indicates that protecting the surface of the composite active material may be necessary to improve its long-term cycling performance.

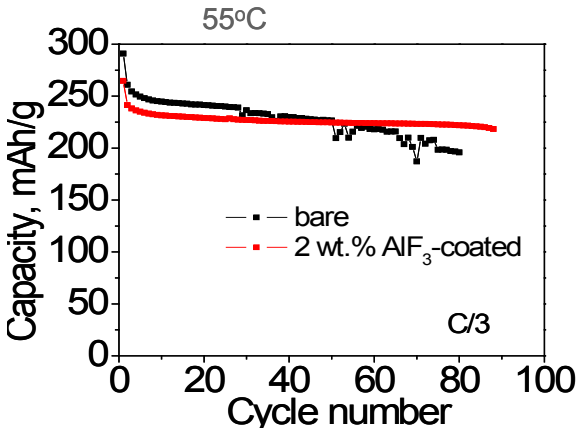

Figure IV- 41: Cycling performance of the AlF_3-coated and the uncoated $Li_{(1+x)}Ni_{0.25}Co_{0.15}Mn_{0.6}O_{(2.25+x/2)}$ (x=0.225) at 55°C

FY 2010 Publications

1. Deng, H.X., I. Belharouak, R.E. Cook, H.M. Wu, Y.K. Sun, and K. Amine, Nanostructured Lithium Nickel Manganese Oxides for Lithium-Ion Batteries, *Journal of the Electrochemical Society*, 157(4): A447-A452 (2010).
2. Myung, S.T., K.S. Lee, C.S. Yoon, Y.K. Sun, K. Amine, and H. Yashiro, Effect of AlF_3 Coating on Thermal Behavior of Chemically Delithiated $Li_{0.35}[Ni_{1/3}Co_{1/3}Mn_{1/3}]O_2$, *Journal of Physical Chemistry C*, 114(10): 4710-4718 (2010)
3. Deng, H.X., I. Belharouak, Y.K. Sun, and K. Amine, $Li_xNi_{0.25}Mn_{0.75}O_y$ ($0.5 \leq x \leq 2$, $2 \leq y \leq 2.75$) Compounds for High-Energy Lithium-Ion Batteries, *Journal of Materials Chemistry*, 19(26): 4510-4516 (2009).
4. Lim, J.H., H. Bang, K.S. Lee, K. Amine, and Y.K. Sun, Electrochemical Characterization of Li_2MnO_3-$Li[Ni_{1/3}Co_{1/3}Mn_{1/3}]O_2$-$LiNiO_2$ Cathode Synthesized via Co-precipitation for Lithium Secondary Batteries, *Journal of Power Sources*, 189(1): 571-575 (2009).

IV.B.3.2 Developing New High Energy Gradient Concentration Cathode Material (ANL)

Khalil Amine

Argonne National Laboratory
9700 South Cass Avenue
Argonne, IL 60439-4837
Phone: (630) 252-3838; Fax: (630) 252-4176
E-mail: amine@anl.gov

Collaborators:
Gary Koenig, Argonne
Ilias Belharouak, Argonne
Y-K. Sun, Hanyang University
ECPRO

Start Date: October, 2008
Projected End Date: September, 2010

Objectives

The objective of this work is to develop high-energy concentration-gradient cathode materials for a 40-mile plug-in hybrid vehicle (PHEV). The selected materials will have the following characteristics:

- Over 200 mAh/g capacity
- Good rate capability
- Excellent cycle and calendar life
- Improved abuse tolerance

Technical Barriers

The primary technical barrier is the development of a battery system with a 40 mile all-electric range for PHEV applications. This Li-ion battery system must offer:

- High energy density with targeted weight, volume, and affordability
- Intrinsic tolerance to abusive conditions

Technical Targets

- Optimize the process that provides Ni-Mn-Co-hydroxide precursors having gradient concentration.
- Validate the concept of high-energy concentration-gradient cathode materials in small quantities.
- Demonstrate the high capacity and good cycle life of concentration-gradient cathode materials.
- Demonstrate the improvement in the safety characteristics using differential scanning calorimetry (DSC) of the concentration-gradient cathode materials.

Accomplishments

- Developed a co-precipitation process that provides small quantities of a high-energy concentration-gradient precursor and cathode materials.
- Characterized the materials and demonstrated that they have a changing concentration of Ni, Mn, and Co within each particle.
- Demonstrated that the concentration-gradient cathode materials provide high capacity, good cycle life, and excellent abuse tolerance in small laboratory cells.

✧ ✧ ✧ ✧ ✧

Introduction

A variety of oxides of Li, Ni, and Mn have been investigated in efforts to produce desirable cathode materials. High capacities have been reported for nickel-enriched materials; however, these materials suffer from poor cycle life and high interfacial cell impedance, attributed to oxygen release and high concentrations of unstable Ni^{4+} ions. Relatively lower capacities have been reported for manganese-enriched materials, but these materials have demonstrated excellent cycle life and safety attributed to their stability when in contact with the battery electrolyte. Efforts have focused on combining these two attributes, high stability with high capacity, by engineering cathode particles with a core enriched in Ni for high capacity and a shell enriched in Mn for high stability and cycling performance (so-called “core-shell” materials).

Approach

Concerns over Li^+ diffusion across the core-shell interface within these cathode particles, as well as voids observed between the structurally and chemically distinct core and shell regions, led to a new particle design where a shell with a gradient in the chemical composition was grown onto the surface of a core material, which had a constant chemical composition. We have developed a novel high-capacity and safe cathode material in which each particle consists of bulk material, $Li[Ni_{0.8}Co_{0.1}Mn_{0.1}]O_2$, that provides over 200 mAh/g

capacity, surrounded by a concentration-gradient outer layer where nickel ions are gradually replaced with manganese ions to provide outstanding cycle life and safety.

Results

For synthesizing the concentration gradient particles, we used the following steps:

Step 1: We used a co-precipitation process schematically illustrated in Figure IV- 42. A solution of constant nickel and manganese concentrations was fed to a continuous stirring reactor (CGR) to prepare the $[Ni_{0.8}Co_{0.1}Mn_{0.1}](OH)_2$ core.

Step 2: We fed a solution with a high composition of Mn (Ni 0.08: Co 0.46: Mn 0.46) to a solution with a high composition of Ni (Ni 0.8: Co 0.1: Mn 0.1), which was then fed to the reactor to grow the concentration gradient shell. At the end of the feeding, the mixed solution in the reactor had a concentration of Ni 0.4: Co 0.3: Mn 0.3.

Step 3: We prepared $[Ni_{0.64}Co_{0.18}Mn_{0.18}](OH)_2$ with concentration gradient of Ni, Co, and Mn.

Step 4: We incorporated lithium at high temperature (~750°C in air), which formed $Li[Ni_{0.64}Co_{0.18}Mn_{0.18}]O_2$ with concentration gradient of Ni, Co, and Mn.

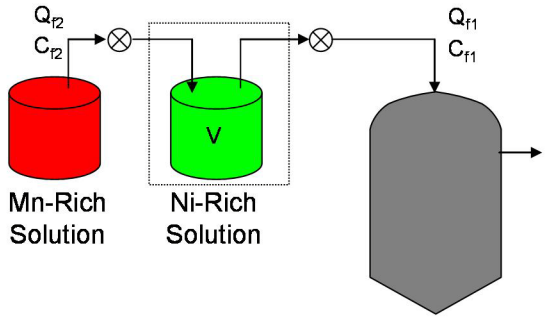

Figure IV- 42: Experimental setup for making concentration gradient material (CGM).

Figure IV- 43 shows the initial charge and discharge capacity of CGMs at different cut-off voltages in lithium half cells. At room temperature, more than 200 mAh/g capacity could be reached at 4.5 V cut-off voltage under the 0.2 C rate.

Figure IV- 44 shows the performance of the CGM material over 50 cycles at different cut-off voltages in lithium half cells at room temperature. The stability of the capacity is excellent at 4.3 V cut-off voltage, with a capacity retention of 182 mAh/g for over 50 cycles. The capacity increased at higher cut-off voltages (4.54 and 4.5 V); however, a slight decrease in capacity was noticed with cycling.

Figure IV- 45 shows the performance of the CGM material over 50 cycles at different cut-off voltages in lithium half cells at 55°C. Initially, the capacity at 4.3 V was 190 mAh/g, and less than 5% capacity fade was observed after 50 cycles. Despite the higher cut-off voltage, the cycling of the CGM material was quite good compared to the material that had the $LiNi_{0.8}Co_{0.1}Mn_{0.1}O_2$ core.

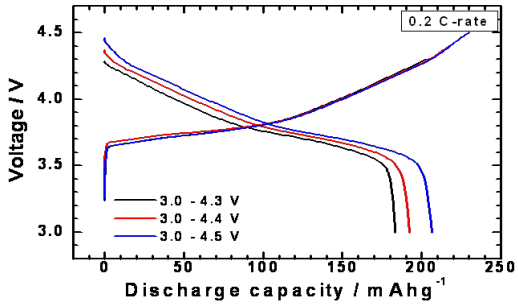

Figure IV- 43: Capacity of CGM cathode at 4.3, 4.4, and 4.5 V under 0.2 C rate.

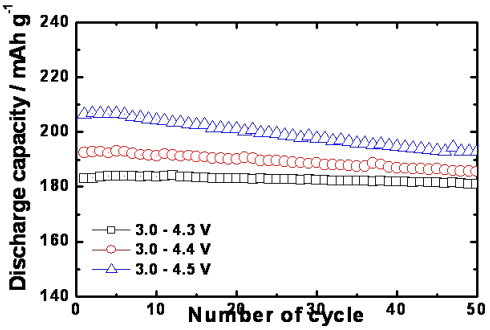

Figure IV- 44: Cycling performance of CGM cathode at 4.3, 4.4, and 4.5 V at 0.2 C rate and room temperature.

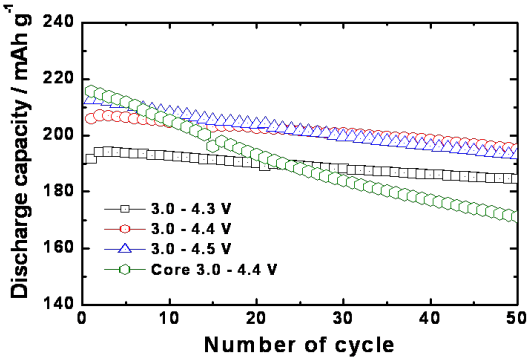

Figure IV- 45: Cycling performance of CGM cathode at 4.3, 4.4, and 4.5 V at 0.2 C rate and 55°C.

Figure IV- 46 shows the cycling performance of the CGM material in lithium full cells at 55°C. Graphite mesocarbon microbeads were used as the negative

electrode material. The cell was charged to 4.3 V at the 1C rate with a conventional electrolyte. In Figure 5, cycling behavior of the CGM-material/graphite couple is compared to that of the core-material/graphite couple. Capacity fade after 400 cycles was around 4% for the CGM-material/graphite cell and more than 15% for the core-material/graphite cell.

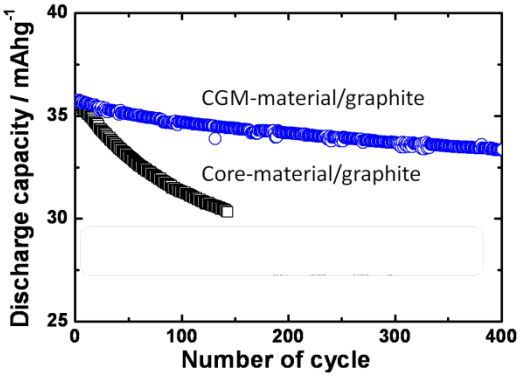

Figure IV- 46: Cycling performance of CGM-material/graphite and core-material/graphite cells at 55°C and 1 C rate.

Figure IV- 47 shows the thermal stability of a 100 mAh CGM-material/graphite cell as determined by the nail penetration test. The results are compared to those from a nail penetration test of a cell made of the core-material/graphite chemistry. The CGM-material/graphite cell took about 50 sec before a voltage drop occurred with a temperature increase to around 50°C. For the core-material/graphite cell, the voltage drop occurred in less 25 sec, the temperature increased to around 250°C, and fumes and signs of thermal runaway were observed. These safety tests clearly demonstrate that the cell with the CGM material showed better safety performance than the cell with core material.

Conclusions and Future Directions

The following conclusions were reached:

- New gradient concentration cathode material with very high capacity was developed.
- Scanning electron microscopy and electron probe micro-analysis of a cross section showed that each particle of the material has a bulk composition rich in Ni and an outer layer rich in Mn.
- The CGM achieved 209 mAh/g at 1 C rate when charged to 4.4 V.
- The CGM showed excellent cycling performance at 55°C, 4.4 V and 1 C rate.
- The CGM safety performance was excellent when compared to the bulk material.

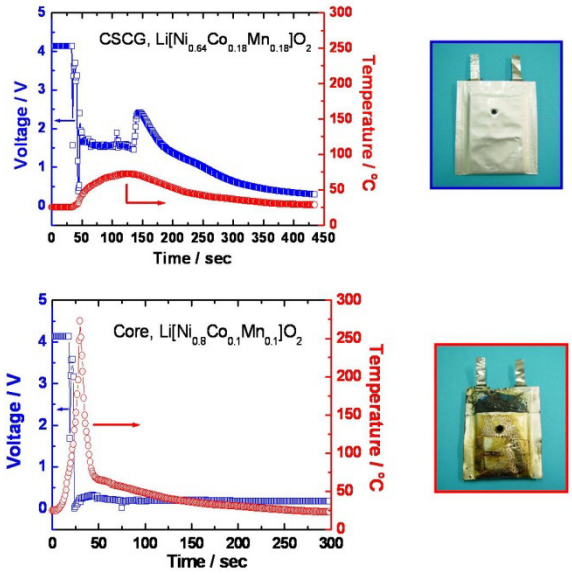

Figure IV- 47: Nail penetration test of CGM-material/graphite cell and core-material/graphite cells.

- We aim to achieve the following in the future:
  - Tune the synthetic process to obtain highly pure CGM in 100~500 g quantities to carry out extensive characterization and testing.
  - Further optimize the composition of the outer layer of the gradient concentration to maximize the surface stability of the material.
  - Further optimize the thickness of the outer layer of the gradient concentration to a minimum possible to further increase capacity while maintaining good surface stability.
  - Carry out calendar and cycle life testing of optimum CGM.
  - Carry out extensive safety test, including accelerating rate calorimetry and overcharge test.

FY 2010 Publications/Presentations

1. Sun, Y.K., S.T. Myung, B.C. Park, J. Prakash, I. Belharouak, and K. Amine, High-energy cathode material for long-life and safe lithium batteries. Nature Materials, 8(4): p. 320-324 (2009).
2. Sun, Y.K., D.H. Kim, C.S. Yoon, S.T. Myung, J. Prakash, and K. Amine, A Novel Cathode Material with a Concentration-Gradient for High-Energy and Safe Lithium-Ion Batteries. Advanced Functional Materials, 20(3): p. 485-491 (2010).
3. 2010 DOE Annual Peer Review Meeting Presentation.

IV.B.3.3 Design and Evaluation of Novel High Capacity Cathode Materials (ANL)

Christopher S. Johnson

Argonne National Laboratory
9700 South Cass Avenue
Argonne, IL 60439
Phone: (630) 252-4787 ; Fax: (630) 252-4491
E-mail: cjohnson@anl.gov

Collaborators:

M. M. Thackeay (ANL), S.-H. Kang (ANL),
M. Balasubramanian (ANL), S. V. Pol (ANL)

Start Date: October 1, 2008
Projected End Date: September 30, 2011

Objectives

The project objective is to design, evaluate and screen high-capacity cathodes that will provide high-energy for transportation batteries. Novel electrode materials are needed in order to advance the field and push the limits of state-of-art technology into new cathode systems. To satisfy the energy requirements of batteries for 40 mile all-electric mode in plug-in hybrid electric vehicles (PHEV), we are focusing on novel systems that can maximize the available energy density, but also try to utilize inexpensive materials, such as inherently safe oxides of Fe, V, and Mn that possess high-capacities, and operate at low voltage to promote long life.

Technical Barriers

- Low energy density
- High cost
- Low abuse tolerance

Technical Targets

- 96 Wh/kg, 316 W/kg (PHEV 40 mile requirement)
- Cycle life: 5000 cycles
- Calendar life: 15 years
- Improved abuse tolerance

Accomplishments

- Optimized synthesis of Li_5FeO_4 as a lithium-rich cathode precursor for loading the graphite anode or alternative high-energy Si anodes of lithium-ion cells with active lithium.
- Investigated structural changes in chemically-delithiated Li_5FeO_4 samples by X-ray diffraction methods, which, as previously reported by XAS, demonstrated that lithium extraction from Li_5FeO_4 was accompanied by oxygen loss (net loss = Li_2O) without any significant change to the Fe oxidation state.
- Initially demonstrated the use of MnO_2 (a charged cathode) in a Li-ion cell with graphite using Li_5FeO_4 as a cathode blended pre-lithiation precursor.
- Significantly improved capacity, energy, and rate performance of charged high-capacity LiV_3O_8 by coating with Al_2O_3.
- Synthesized Co-substituted $Li_yFe_{1-x}Co_xO_4$. The analysis of X-ray diffraction shows a solid-solution behavior, and electrochemistry results in a faster rate characteristics for release of lithium on the first charge.

✧ ✧ ✧ ✧ ✧

Introduction

High-energy Li-ion cells and batteries are needed for advanced transportation technologies, such as plug-in hybrid electric vehicles (PHEV) and, in the long-term, electric vehicles (EV). Cathode materials in Li-ion batteries contain a variety of 4 V oxides such as $LiCoO_2$ (LCO), $LiNi_{0.8}Co_{0.15}Al_{0.05}O_2$ (NCA), $LiNi_{1/3}Mn_{1/3}Co_{1/3}O_2$ (NMC) with layered structures, and $LiMn_2O_4$ (LMO) spinel or substituted spinels. Blends of cathode oxide materials also have been used in order to capture performance characteristics of both electrodes. In order to achieve an extended range all electric mode PHEV, new cathodes and anodes are required which possess higher energies than what is commercially available. Higher energy cells can be achieved when 'layered-layered' or 'layered-spinel' composite oxides with high capacities above 220 mAh/g are used. These electrodes consist of Li-rich layered oxides that in the presence of Ni and Mn form LiM_6 units resulting in ordered or disordered monoclinic Li_2MnO_3 components as nanosized domains in the electrode. To achieve the high-capacity, high voltages are needed to activate the Li_2MnO_3 component, which releases net Li_2O, leaving a reversible cycling MnO_2 component, but the oxygen loss negatively affects the rate capability.

The coupling of high-capacity cathodes with high-capacity anodes, such as Si composite materials, can provide a cell with high-energy. MnO_2, V_2O_5 and LiV_3O_8

are the commonly known materials that feature high-capacity, stability, and potentially low cost in volume production. These materials operate at lower-voltage, but feature practical capacities above 250 mAh/g. To implement such materials in Li-ion cells, however, a source of lithium is needed. Pre-lithiation components are necessary in order to load the anode with lithium during the first charge, and then discharge or insert lithium into the charged cathode (i.e. MnO_2, V_2O_5 and LiV_3O_8). Another method of introducing lithium to a cell is the application of stabilized lithium metal powder materials such as SLMP® (FMC Lithium) loaded in the anode. Through pre-SEI formation, this extra lithium counteracts irreversible capacity loss in the cell for high capacity anodes. SLMP® can also be used in conjunction with charged cathodes.

Approach

In this approach we utilize the high capacity MnO_2 (308 mAh/g) or $Li_{1.2}V_3O_8$ (372 mAh/g) cathode materials. A high lithium containing material, Li_5FeO_4 (LFO) is blended in the cathode, in contrast to SLMP® that is loaded in the anode. The LFO is used to prelithiate the anode during the first charge, which introduces lithium into the cell. When these cells are combined with high-capacity Si anode materials, then high-energy density cells are possible. Towards the demonstration of this concept, we have focused on optimizing LFO, the evaluation of dopants, and gaining a greater understanding of the release of lithium during the first charge. In addition, the electrochemistry of LiV_3O_8 (LVO) has been improved and tested in lithium half cells. The optimization of the charged LVO material is important to improve the energy density and power of the cathode. In addition, Co-substituted LFO materials were also synthesized and tested.

Results

In the last report for FY '09, we introduced LFO, discussed its structure, and demonstrated the release of 4 lithium cations below ~4.3 V during the first charge in a Li half cell. A representative first charge profile is shown in Figure IV- 48 at a slow rate. LFO was also blended with LVO and tested in a full cell with graphite. Although the capacity and voltage was low for such a cell, the concept was demonstrated.

While the ideal reaction of Li_5FeO_4 is release of $2.5Li_2O$ and $1/2Fe_2O_3$, in practice however, only 4 lithiums can be removed on charge in a practical voltage window. These 4 lithiums are, at the same time, inserted into the anode and a Li-ion cell is created with the blended charged cathode. Note that irreversible capacity associated with the anode, such as in a Si anode can be accounted for by the sacrificial extra lithium released by LFO in this method.

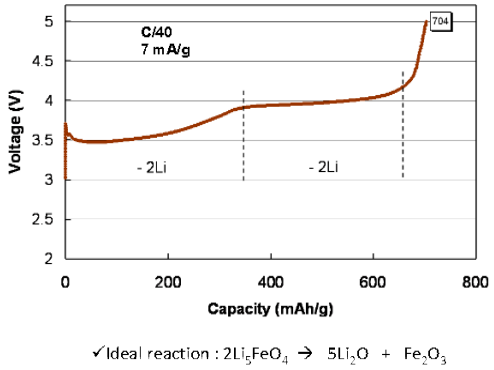

Figure IV- 48: First galvanostatic charge voltage profile of Li/LFO at a slow rate current density of 7 mA/g.

C/MnO_2-Li_5FeO_4 cell. The application of MnO_2 in Li-ion cells is prohibitive since there is no source of lithium in the cell. This is not a problem when the MnO_2 is co-blended with a high-Li containing prelithiation source such as LFO (i.e. 5Li/Fe). Therefore to demonstrate the principal, an electrolytic MnO_2 (EMD) was paired with LFO and run as a Li-ion cell against a graphite anode. The resultant voltage profile is shown in Figure IV- 49. The capacity from LFO on the first charge was 209 mAh/g, and on discharge the MnO_2 (and residual Fe_2O_3 (from Li_5FeO_4 decomposition)) showed 225 mAh/g. Therefore, this cell chemistry demonstrates a cell energy above 625 Wh/kg. Furthermore, this Li-ion chemistry features low cost, abundant and stable Fe and Mn compounds, and acceptable performance as a first demonstration.

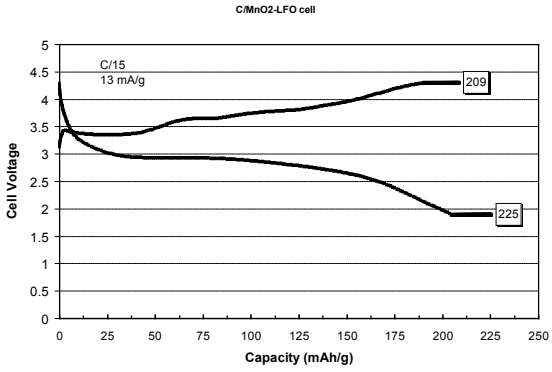

Figure IV- 49: 1st galvanostatic discharge voltage profiles of C/LFO-MnO_2 electrode.

LVO Optimization. In order to improve the Li/LFO-LVO blended cell performance, LVO powder should be optimized for better cycling and stability. An alumina (Al_2O_3) coating process was developed for LVO powders that consists of stirring the LVO in the presence of AlOOH

colloid (5 wt.%), followed by a light firing at 300°C which converts the AlOOH to Al_2O_3. As shown in Figure IV- 50, the Al_2O_3 coated LVO electrochemical performance was greatly improved in comparison to uncoated LVO. The impedance is lower, the capacity is greater and the retention of capacity is better. Initial capacity for coated LVO was 310 mAh/g compared to 288 mAh/g for uncoated. No dissolution of V in the electrolyte was detected for the coated LVO.

The rate performance of the Li/Al_2O_3-coated LVO versus uncoated Li/LVO cells is shown in Figure IV- 51. As is evident in the graph, the performance is much improved, and is about 2x the capacity of the uncoated LVO at high rates.

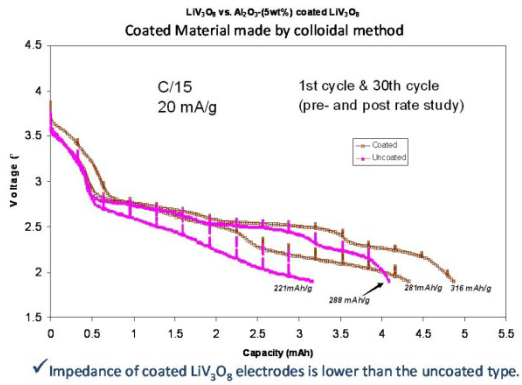

Figure IV- 50: 1st and 30th galvanostatic discharge voltage profiles of Li/LVO and Li/Al_2O_3-coatedLVO

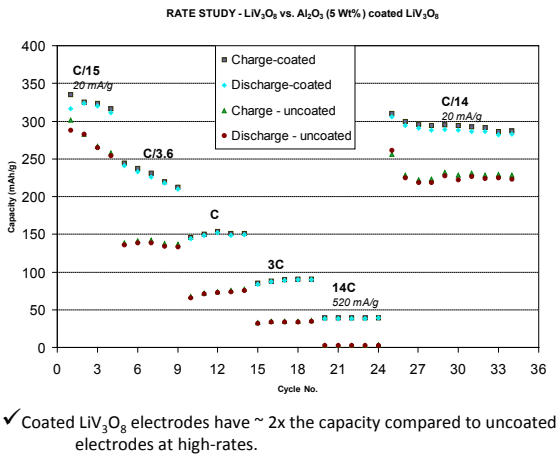

Figure IV- 51: Rate performance study – coated LVO vsrsus uncoated.

Continuous 1.3C cycling is shown in Figure IV- 52. Again the coated LVO performs much better, holding a capacity of about 140 mAh/g.

Co-substitution in $Li_yFe_{1-x}Co_xO_4$ (LFCO). The synthesis of LFO was optimized during this last reporting period. A balance of phase purity, time, temperature, and starting materials were determined. From the study, we found that the reaction is best done over 4 days, in nitrogen at 780°C, using lithium hydroxide and iron(III) oxide.

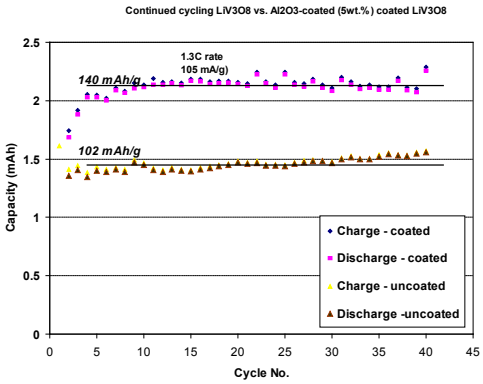

Figure IV- 52: 40 cycles at 1.3C cycling - coated LVO versus uncoated.

Importantly, the use of an alumina high-temperature boat or tray is not recommended. The best results came when a stainless steel or nickel crucible was used. For the Co-substituted material ($Li_5Fe_{0.4}Co_{0.6}O_4$; LFCO), the reaction included the addition of $CoCO_3$ in the appropriate amount. The following compositions were synthesized: $Li_{5.6}Fe_{0.4}Co_{0.6}O_4$ and $Li_5Fe_{0.4}Co_{0.6}O_4$. For the first composition, where the material is Li-rich (y = 5.6), then for charge balancing, the Co is divalent. For y=5 (stoichiometric), the Co is trivalent. The XRD pattern for both is shown in Figure IV- 53.

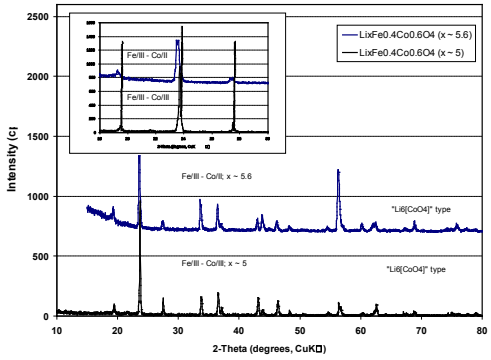

Figure IV- 53: XRD patterns for (top) $Li_{5.6}Fe_{0.4}Co_{0.6}O_4$, and (bottom) $Li_5Fe_{0.4}Co_{0.6}O_4$.

The unit-cell is slightly smaller for the Fe(III)-Co(III) material (bottom curve and inset) as compared to the Fe(III)-Co(II) material (top curve and inset), consistent with a smaller global Co(III)-O bond distance.

The comparison between Li/LFO and Li/LFCO cells are shown in Figure IV- 54. In this Figure, the current density was increased in order to evaluate the release of lithium from both materials. Up to 4.3 V, the LFCO yields about 550 mAh/g compared to ~ 430 mAh/g for LFO.

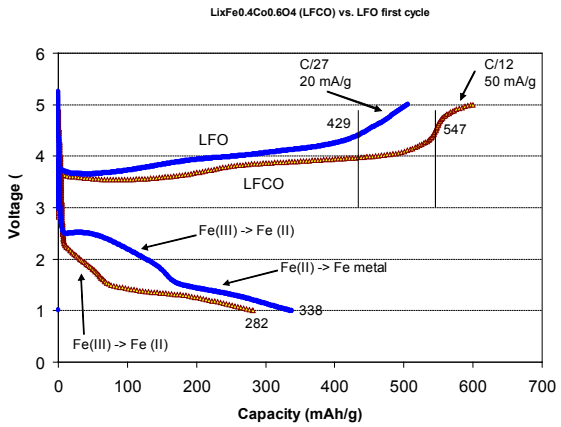

Figure IV- 54: First charge-discharge voltage profile for Li/LFO and Li/LFCO cells.

The Co-substitution appears to improve the impedance as well: the charge voltage is lower even at a higher current density. The charge capacity for LFCO indicates a combination of oxygen loss from the material that has a difference in the charged product; i.e. a Co-substituted Fe_2O_3, or a separate Co-oxide phase product, perhaps Co_3O_4. The mechanism of this reaction needs to be further studied.

The LFO clearly shows the Fe(III) to Fe(II) reduction on discharge in Figure IV- 54, but surprisingly the LFCO has a lower discharge capacity which may indicate that the Co-oxide formed on charge of LFCO is not electroactive on discharge. The Fe_2O_3 phase (hematite) was confirmed by *ex situ* XRD of oxidized LFO material that was chemically delithiated using NO_2BF_4, a strong oxidizing agent. This phase is marked by an arrow in Figure IV- 55 and increases with the amount of Li extracted from the LFO structure. Other LFO peaks remain present in the XRD pattern and show that the structure is somewhat robust to harsh chemical oxidation.

Conclusions and Future Directions

Additional experiments on Li_5FeO_4 (LFO) and Co-substituted $Li_5Fe_{0.4}Co_{0.6}O_4$ (LFCO) were completed. Due to the large amount of available lithium (5 Li/Fe), this material has promising features and characteristics as a very high-capacity (867 mAh/g), low cost, pre-lithiation precursor cathode material for lithium battery applications. Still, however, cell chemistry improvements will be necessary to make these materials ultimately viable as new cell chemistry for Li-ion batteries. The LFO material is intended to provide a different option and approach to use low-cost, safe materials consisting of Fe, V, and Mn elements in the electrode.

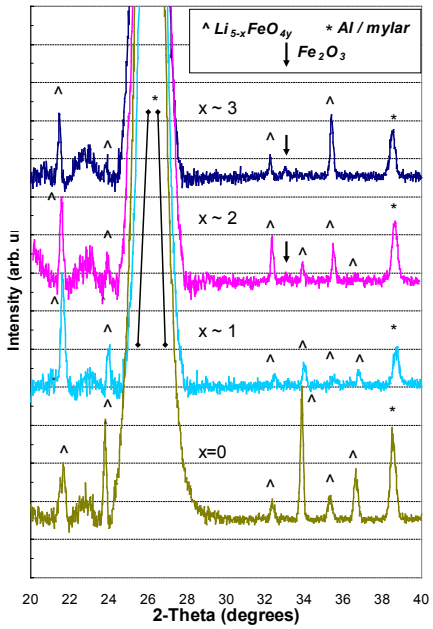

Figure IV- 55: *Ex situ* XRD patterns from chemically delithiated LFO; x values represent each equivalent of Li removed.

For the future directions, we plan to synthesize additional samples of LFO, doped or substituted with a focus on improving the electrochemical properties by optimizing morphology, particle size, surface area, and coatings. We will have completed cell-testing with blended charged cathodes using these new formulations in both lithium half cells and Li-ion full cells, including Si cells. Finally we will improve the properties of charged cathodes such as LVO, MnO_2, and high capacity V_2O_5 (442 mAh/g) coating processes, powder optimization and dopants. Using diagnostic methods, we hope to understand the rate-determining step for the LFO bond breakage and formation of oxygen gas from the structure collapse. From previous studies, we know that hematite is formed from LFO upon removal of two Li_2O units, but this condensation reaction mechanism is unknown. Once the mechanism is discerned, we will apply this knowledge to choose the right combination of particle morphology, particle size, surface area of the powder, and electrochemical conditions, in order to optimize the LFO for the Li_2O removal reaction, and to improve its reversibility on charge-discharge cycling in combination with an optimized charged cathode.

FY 2010 Publications/Presentations

1. "Li_2O removal from Li_5FeO_4 – a cathode precursor for lithium-ion batteries" C. S. Johnson et al. Chemistry of Materials; Vol. 22, 1263-1270 (2010).
2. Oral presentation to the 2010 DOE Annual Peer Review Meeting in Washington D.C.

IV.B.3.4 Development of High-Capacity Cathode Materials with Integrated Structures (ANL)

Sun-Ho Kang

Argonne National Laboratory
9700 South Cass Avenue
Argonne, IL 60439-4837
Phone: (630) 252-4212; Fax: (630) 252-4176
E-mail: sunho.kang@anl.gov

Collaborators:
Kevin Gellagher, Argonne National Laboratory
Donghan Kim, Argonne National Laboratory
Michael Thackeray, Argonne National Laboratory
Mali Balasubramanian, Argonne National Laboratory
Chris Carlton, MIT
Yang Shao-Horn, MIT

Start Date: October, 2008
Projected End Date: September, 2012

Objectives

Plug-in hybrid-electric vehicles (PHEVs) require lithium-ion batteries with higher energy density than those adopted in HEVs. Safety and cost also need to be improved because of the larger size of PHEV battery packs. The current commercial cathode materials, such as $LiCoO_2$, $LiNi_{0.8}Co_{0.15}Al_{0.05}O_2$, $LiNi_{1/3}Co_{1/3}Mn_{1/3}O_2$, $Li_{1+x}Mn_{2-x}O_4$, $LiFePO_4$, do not meet those requirements particularly for PHEVs with a 40-mile all-electric range (PHEV 40). The objective of this effort is to develop low-cost, high-energy, and thermally-stable cathode materials with acceptable power capability to meet the performance requirements for a PHEV 40.

Technical Barriers

The primary technical barrier is the development of a safe and cost-effective PHEV battery with a 40 mile all electric range that meets or exceeds all performance goals. Specific barriers for this project include:

(A) Low energy density

(B) High cost

(C) Thermal abuse limitations

Technical Targets

- Development of Mn-based oxide cathode materials with integrated structures
- Specific capacity of ~200 mAh/g at 1C rate

Accomplishments

- Studied and evaluated various lithium-to-transition metal ratio in $Li_xMn_{0.75}Ni_{0.25}O_z$, $1<x<1.5$ composition range to optimize chemical composition.
- Studied and evaluated the effects of Co substitution in $Li_{1.2}(Mn_{0.75}Ni_{0.25})1\text{-}yCo_yO_z$
- Carried out detailed structural study using analytic techniques (X-ray absorption and TEM) of pristine and cycled $Li_{1.2}Mn_{0.75}Ni_{0.25}O_z$ electrode material.
- Evaluated thermal stability of charged $Li_{1.2}Mn_{0.75}Ni_{0.25}O_z$ electrode by differential scanning calorimetry.

✧ ✧ ✧ ✧ ✧

Introduction

Li- and Mn-rich oxide electrodes with 'layered-layered' composite structure, $xLi_2MnO_3\bullet(1\text{-}x)LiMO_2$ (M=Mn,Ni, Co), are known to deliver high capacity (>200 mAh/g) when charged to high voltages (>4.4 V *vs.* Li^+/Li). In general, however, the materials are also known to suffer from high first-cycle irreversibility and poor rate capability especially when the materials do not contain cobalt. Additionally, it is expected that the oxide particle surface is damaged from repeated high-voltage cycling (4.6-4.8 V vs. Li/Li^+), leading to a poor ionic conductivity at the particle surface and, correspondingly, a high interfacial impedance.

To overcome those limitations of the Li- and Mn-rich oxide electrodes with 'layered-layered' composite structure, efforts have been made to create spinel components in the layered-layered structure. Compositional optimization and structural investigation using analytic techniques have been carried out.

Approach

Lithium metal oxides with a spinel-type structure are well known to exhibit fast Li-ion diffusion through a three-dimensional interstitial space. It is, therefore, anticipated that the rate performance of 'layered-layered' cathode materials could be enhanced, should a structurally-compatible spinel component be introduced into the intergrown structure. $LiMn_{1.5}Ni_{0.5}O_4$ (or $Li_{0.4}Mn_{0.6}Ni_{0.2}O_2$

with a spinel-type structure and $Li_{1.2}Mn_{0.6}Ni_{0.2}O_2$ with an integrated layered-layered structure have the same Mn-to-Ni ratio (Mn/Ni=3/1) but different lithium-to-transition metal (TM=Mn+Ni) ratios (Li/TM=0.5 and 1.5, respectively). Therefore, by simply varying the Li content, it is expected that electrode materials with different structures and electrochemical properties could be prepared. In this work, various Li contents between 1.0 and 1.5, while the Mn-to-Ni ratio was kept fixed, were evaluated. Effect of Co substitution was also examined. X-ray absorption spectroscopy and transmission electron microscopy were also adopted to study the layered-spinel feature of the synthesized materials.

Results

Electrochemical Properties of $Li_xMn_{0.75}Ni_{0.25}O_z$ with various Li contents. Figure IV- 56 shows initial discharge profiles of $Li/Li_xMn_{0.75}Ni_{0.25}O_z$ cells that were discharged from open-circuit voltage. As the lithium content (x) decreased, the initial discharge capacity increased with voltage plateaus developing at 2.7-3.0 V, indicating increased spinel content.

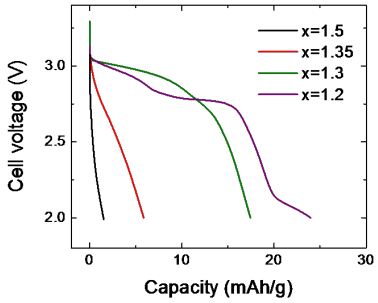

Figure IV- 56: Voltage profiles of $Li/Li_xMn_{0.75}Ni_{0.25}O_Z$ cells discharged from open circuit voltage after assembly

Discharge curves of a $Li/Li_{1.2}Mn_{0.75}Ni_{0.25}O_z$ cell cycled between 2.0-4.95 V (10 mA/g) and 2.0-4.6 V (15 mA/g) are given in Figure IV- 57 (a) and Figure IV- 57(b), respectively; capacity variations during cycling are given in the insets. When cycled between 2.0 and 4.95 V, the cells exhibited excellent cycling performance in spite of the extremely high upper cut-off voltage (4.95 V). However, the profiles suffered from severe shape changes, which is possibly due to structural changes during cycling. Significantly suppressed voltage shape change was observed by lowering the cut-off voltage as shown in Figure IV- 57(b). However, ~5 break-in cycles were needed to obtain high capacity.

Figure IV- 58 shows results of rate capability study of $Li/Li_xMn_{0.75}Ni_{0.25}O_z$ cells discharged at different rates from 4.6 V. The $Li_{1.2}Mn_{0.75}Ni_{0.25}O_z$ electrode showed excellent rate capability, delivering 200 mAh/g at 1C.

Effect of Co Subsitution. Capacity variations against cycle number of $Li_{1.2}(Mn_{0.75}Ni_{0.25})_{1-y}Co_yO_z$ electrodes in lithium cells are shown in Figure IV- 59. Further characterization is underway to explore the effect of Co on various electrochemical properties.

Structural Study of Pristine and Cycled $Li_{1.2}Mn_{0.75}Ni_{0.25}O_z$ electrode material. The TEM picture of pristine $Li_{1.2}Mn_{0.75}Ni_{0.25}O_z$ material is given Figure IV-60, which successfully shows intergrowth of layered and spinel structures at nanometer scale. Figure IV- 61(a) and Figure IV- 61(b) show Ni- and Mn K-edge XANES spectra, respectively, of pristine and cycled (2-4.95 V, 50 cycles) $Li_{1.2}Mn_{0.75}Ni_{0.25}O_z$ material. Ni spectra show negligible change after cycling; Mn spectra, on the other hand, indicate significant reduction of Mn ions after cycling.

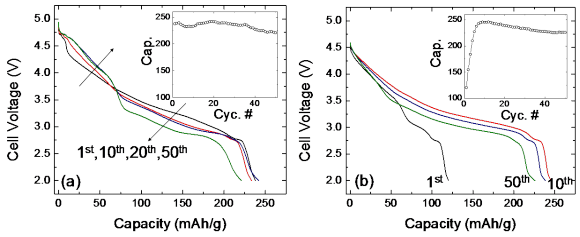

Figure IV- 57: Discharge voltage profiles of $Li/Li_xMn_{0.75}Ni_{0.25}O_Z$ cells cycled at 2.0-4.95 V, 10 mA/g (a), and 2.0-4.6 V, 15 mA/g (b). Capacity variations during cycling are given in the insets.

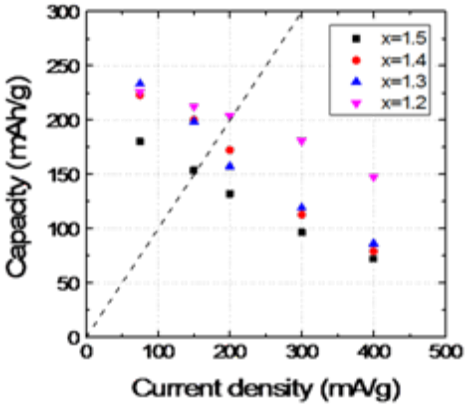

Figure IV- 58: Discharge capacity vs. current density plot of $Li/Li_xMn_{0.75}Ni_{0.25}O_Z$ cells. The cells charged to 4.6 V at 15 mA/g and discharged to 2.0 V at various current rates. The dotted line denotes 1C rate line.

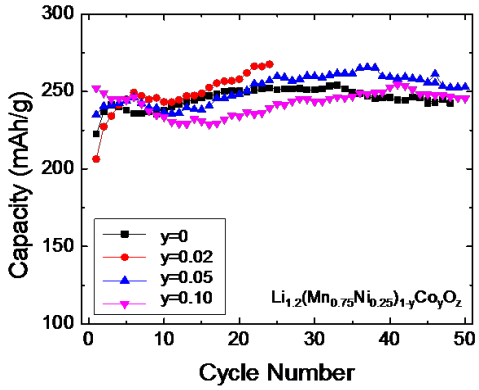

Figure IV- 59: Capacity variations of Li/$Li_{1.2}(Mn_{0.75}Ni_{0.25})_{1-y}Co_yO_z$ cells cycled between 2.0 and 4.95 V.

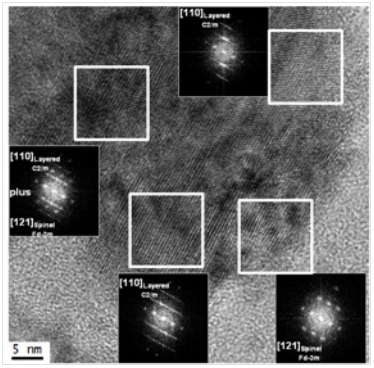

Figure IV- 60: TEM pictures of pristine $Li_{1.2}Mn_{0.75}Ni_{0.25}O_z$ sample.

Thermal Stability of Charged $Li_{1.2}Mn_{0.75}Ni_{0.25}O_z$ electrode. Thermal stability of charged the $Li_{1.2}Mn_{0.75}Ni_{0.25}O_z$ electrode was examined using differential scanning calorimetry. The electrode was cycled in a lithium cell between 2.0 and 4.8 V, twice and then between 2.0 and 4.6 V, three times. The electrode was then charged to 4.6 V before disassembly for DSC measurement. The charged electrode exhibited an onset temperature for the exothermic reaction at ~225 °C with an enthalpy of 829 J/g, Figure IV- 62.

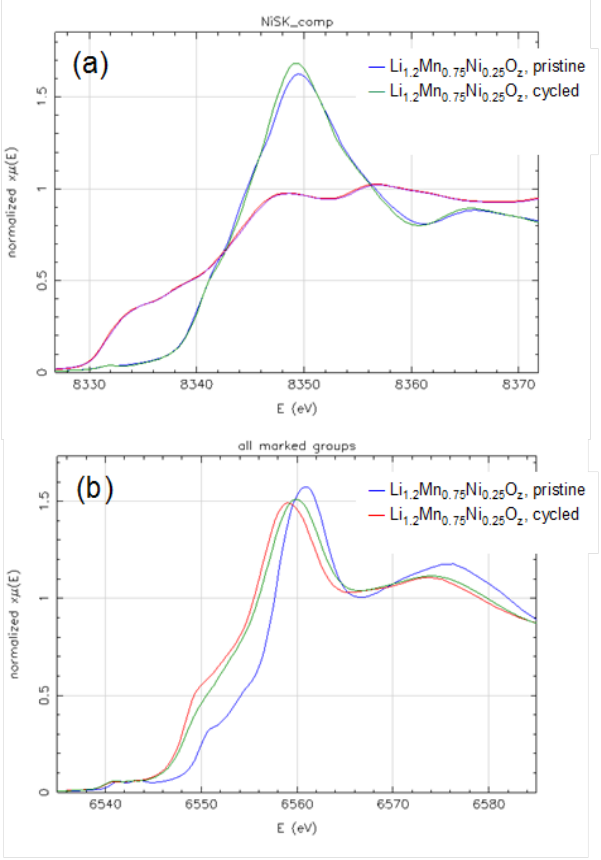

Figure IV- 61: (a) Ni- and (b) Mn K-edge spectra of pristine and cycled $Li_{1.2}Mn_{0.75}Ni_{0.25}O_z$ electrodes.

Conclusions and Future Directions

Cathode materials with three-component 'composite' structures have been synthesized. Initial cycling performance and rate capability study of the chemistry ($Li_{1.2}Mn_{0.75}Ni_{0.25}O_z$) at 2.0-4.95 V have been completed. In spite of the good cycling performance and rate capability (~200 mAh/g at 1C rate), severe voltage shape change during extended cycling was considered problematic. By allowing ~5 break-in cycle to the cells, high capacity (~250 mAh/g) and outstanding rate capability (>200 mAh/g at 1C rate) was also observed at 2.0-4.6 V. The $Li_{1.2}Mn_{0.75}Ni_{0.25}O_z$ electrode material exhibited good thermal stability at charged state. To further optimize the chemical composition, various Li- and Co contents have been studied; based on this study, optimum composition will be established. Furthermore, other electrode structures that can overcome the limitations of high-capacity layered-layered materials will also be investigated.

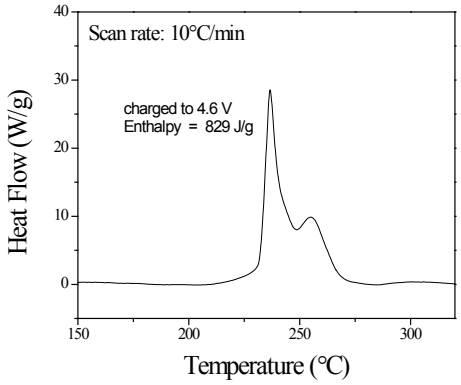

Figure IV- 62: DSC profile of charged $Li_{1.2}Mn_{0.75}Ni_{0.25}O_z$ electrode.

FY 2010 Publications/Presentations

1. 2009 DOE Annual Peer Review Meeting Presentation, June 7-11, 2010.
2. J. Cabana, S. –H. Kang, C. S. Johnson, M. M. Thackeray, C. P. Grey, "Structural and electrochemical characterization of Li-Mn-Ni-O electrodes with integrated layered-spinel structures for Li-ion batteries," *J. Electrochem. Soc.*, **156**, A730-736 (2009).
3. "Advanced high-capacity cathode materials for Li-ion batteries," Invited presentation, NREL, June 4,2009, Golden, CO
4. "Advanced cathode materials with integrated structure for high-energy Li-ion batteries," Invited presentation, The 3rd International Symposium on Functional Materials, June 15-18, 2009, Jinju, Korea
5. "Advanced Lithium Metal Oxide Electrode Materials with Integrated Structure for Lithium-Ion Batteries," Invited presentation, ICAM Workshop of Physics of Novel Energy Materials, Chinese Academy of Science, Beijing, China, May 31-June 3, 2010.
6. "Advanced high-capacity lithium metal oxide electrode materials for Li-ion batteries," Invited presentation, 2010 Spring Meeting of Korean Battery Society, Seoul, Korea, May 27-28, 2010.
7. "Advanced nano-composite lithium metal oxide electrodes for high energy lithium-ion batteries," Invited presentation, The 7th US-Korea Forum on Nanotechnology: Nanomaterials and Systems for Nano Energy, Seoul, Korea, April 5-6, 2010.

IV.B.3.5 Evaluation of Li_2MnSiO_4 Cathode (ANL)

Ilias Belharouak

Argonne National Laboratory
9700 South Cass Avenue
Argonne, IL 60439-4837
Phone: (630) 252-4450; Fax: (630) 972-4454
E-mail: belharouak@anl.gov

Collaborators:
A. Abouimrane, Argonne National Laboratory
D. Dambournet, Argonne National Laboratory
K. Amine, Argonne National Laboratory

Start Date: October, 2008
Projected End Date: September, 2010

Objectives

The objective of this work is to search for high energy density cathode materials for PHEV applications.

- Identify high-capacity (per kg), high-potential, and high packing density cathode materials.
- Identify materials that can exchange more than one lithium per unit formula.

Technical Barriers

The primary technical barrier is the development of a battery system with a 40 mile all electric range for PHEV applications.

- High energy density Li-ion battery systems with targeted weight, volume, and affordability
- Li-ion battery system that are intrinsically tolerant of abusive conditions.

Technical Targets

- Develop new preparation methods to synthesize high purity Li_2MSiO_4 (M = Mn, Fe) materials.
- Understand the structure of these materials at the local and bulk levels.
- Check whether these materials can reversibly cycle 2-lithium-ions per formula unit.
- Achieve an overall evaluation of these materials from structural and electrochemical standpoints with regard to their possible applicability in high-energy density Li-ion batteries.

Accomplishments

- Materials preparation and characterization
  - Introduced new preparation methods including solid state, Pechini, and sol-gel reactions to synthesize pure Li_2MnSiO_4
  - Carried out physical and structural characterizations in order to elucidate the impact of the morphological and atomic arrangement on the electrochemical properties of Li_2MnSiO_4.
  - Investigated the capacity fade observed for Li_2MnSiO_4.
  - Investigated of $Li_2(Mn_{1-x}Fe_x)SiO_4$ stabilized phases.
- Electrochemical performances.
  - Assembled positive electrodes made of Li_2MnSiO_4 with lithium anode and conventional electrolytes to check the capacity of the material.
- Materials optimization.
  - Carried out carbon coating, carbon nanotube integration, and ball milling to improve the electronic conductivity of Li_2MnSiO_4.

✧ ✧ ✧ ✧ ✧

Introduction

Increasing the overall energy density of Li-ion batteries by reducing the inactive materials at the battery pack level has been exhausted over the last decade. The only route to surmount the energy density shortfall is the development of high specific capacity, high potential, and high packing density active materials both at the positive and negative sides. The main reason is that when an NCA cathode electrode (150mAh/g, 100 µm-thick) combined with a high capacity anode (700mAh/g, 50µm-thick), the energy density increases approximately 30% compared to a cell with a standard anode (350 mAh/g). The silicate family (Li_2MSiO_4, where M = Fe, Mn, and Co) is attractive because its high theoretical capacity may be exploited if the transition metal ions can be oxidized and reduced reversibly from their lowest oxidation state (2+) to a higher oxidation state (4+). This condition requires the extraction/insertion of two lithium-ions from the host structure, with the generation of 333-mAh/g theoretical capacity. The manganese ($Mn^{2+/4+}$) redox couple is of particular interest because it exhibits a high potential (vs. Li^o), and resources to prepare the material are plentiful and

clean. The preparation of Li_2MnSiO_4 material is, however, not trivial due to the possible presence of mixed phases and/or impurities.

Approach

Li_2MnSiO_4 can be iso-structural to certain forms of Li_3PO_4. The extraction/insertion of 2-Li-ions will result in 333mAh/g capacity. Strong covalent Si-O bonds should be good for safety. New preparation methods including a sol-gel reaction had been adopted to synthesize pure Li_2MnSiO_4. Experiments using the pair distribution analysis upon lithium removal and uptake were conducted to understand the capacity fade observed for Li_2MnSiO_4. $Li_2(Mn_{1-x}Fe_x)SiO_4$ stabilized phases were investigated.

Results

Several materials were prepared, as follows:

- Batch 1: gelation occurred in acetic acid medium containing lithium, manganese, and silicon acetates followed by subsequent heat treatments up to 700°C.
- Batch 2: during gelation, high surface area carbon was added to be part a composite material.
- Batch 3: during gelation, cellulose, ethylene glycol, etc. were incorporated to yield a carbon coated material.

XRD patterns for these three batches are shown in Figure IV- 63. MnO impurity was observed for batch 2 and 3. Particle size reduction experiments using silica template and ball milling were carried out in order to prevent agglomeration. Also, carbon integration experiments using the implantation of carbon nanotubes and gas phase carbon coating were carried out to improve the electronic conductivity of the material.

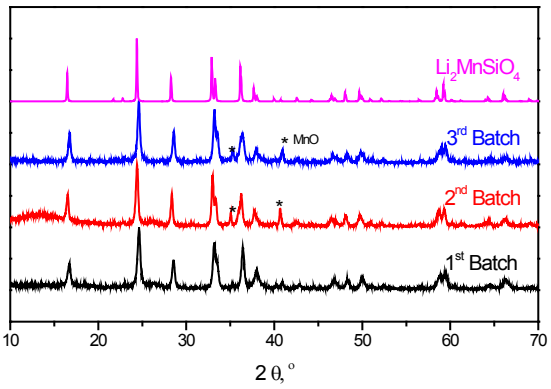

Figure IV- 63: X-ray patterns of Li_2MnSiO_4 prepared at 700°C, under reducing atmosphere. Calculated pattern also shown at top.

Figure IV- 64 shows a typical charge/discharge profile of the carbon coated Li_2MnSiO_4 cathode material in coin cells. The cells were assembled with lithium metal as the negative electrode and were tested in the voltage range of 1.5-4.8 V under a current density of 10 mA/g. Cells assembled with uncoated Li_2MnSiO_4 did not show a reasonable capacity.

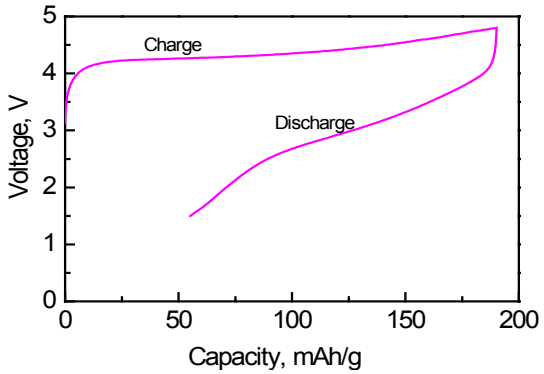

Figure IV- 64: Typical voltage profile of Li/C-Li_2MnSiO_4

Figure IV- 65 shows typical cycling behavior of Li/ Li_2MnSiO_4. Drastic capacity fade was observed starting from the first cycle. At the end of the first charge, Li_2MnSiO_4 material became amorphous according to X-ray data.

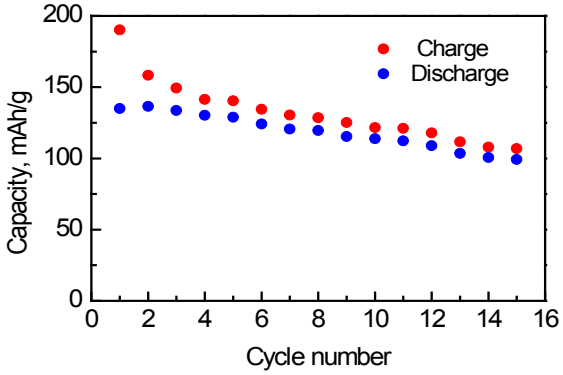

Figure IV- 65: Typical cycling bahavior of Li/C-Li_2MnSiO_4

Pair distribution function (PDF) analysis upon lithium removal and uptake was used to understand the amorphoziation that is believed to be responsible for the quick capacity fade of Li_2MnSiO_4. The radial pair distribution function G(r) gives direct information on interatomic distances (Figure IV- 66). G(r) is independent of orientation; it thus provides valuable structural information on amorphous materials. The radial PDF can be calculated directly from X-ray powder diffraction through the use of Fourier Transform. The following observation can be made:

- The local structure of Li_2MnSiO_4 is kept when the latter is fully charged or discharged. The long range structural order is disrupted.
- Evidence of lithium removal and uptake is seen through the shortening and elongation of the Mn-O bond.

Fe^{2+} ion incorporation experiments were carried out in order to stabilize the structure of Li_2MnSiO_4. $Li_2(Mn_{1-x}Fe_x)SiO_4$ stabilized phases were prepared by a sol/gel method. The X-ray patterns confirmed the structural order of Li_2MnSiO_4. Electrochemical data showed that the iron-based phases had much better capacity retention upon cycling. The trend is that the higher the concentration of iron content, the better the capacity is (Figure IV- 67).

Conclusions and Future Directions

- Amorphization is responsible for the capacity fade of Li_2MnSiO_4 upon lithium removal. Pair distribution function analysis confirmed that this is not a structural disintegration of Li_2MnSiO_4. It will be quite challenging to prevent this phenomenon from occurring.
- Stabilization of Li_2MnSiO_4 through iron incorporation has led to structure stabilization. $Li_2Mn_{1-x}Fe_xSiO_4$ materials have shown promise in terms of capacity retention

We aim to achieve the following in the future:

- Full understanding on the mechanistic reasons behind the amorphization of Li_2MnSiO_4 upon lithium removal.
- Continue the work on the stabilization of Li_2MnSiO_4 through iron incorporation.

FY 2010 Publications/Presentations

- 2010 DOE Annual Peer Review Meeting Presentation.

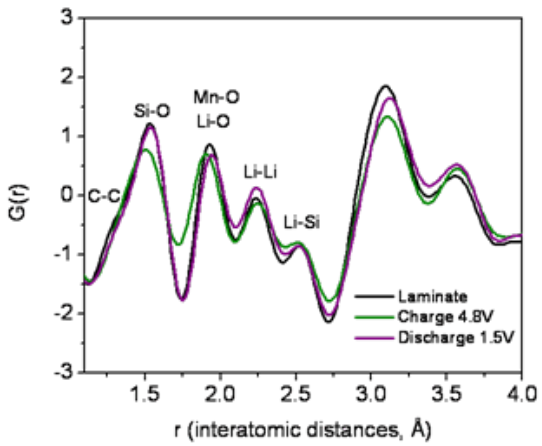

Figure IV- 66: PDF analysis of Li_2MnSiO_4 charged to 4.8V and discharged to 1.5 V.

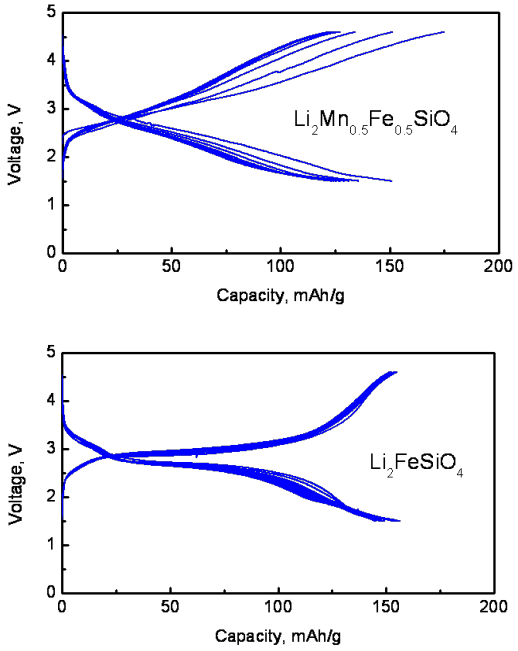

Figure IV- 67: Voltage profile and cycling data of $Li_2Mn_{0.5}Fe_{0.5}SiO_4$ and Li_2FeSiO_4.

IV.B.4 Applied Battery Research on Electrolytes

IV.B.4.1 Novel Electrolytes and Electrolyte Additives for PHEV Applications (ANL)

Daniel P. Abraham
Argonne National Laboratory
9700 South Cass Avenue
Argonne, IL 60439-4837
Phone: (630) 252-4332; Fax: (630) 972-4406
E-mail: abraham@anl.gov

Collaborators:
G. Cheng, Argonne National Laboratory
S. Trask, Argonne National Laboratory
B. Lucht, University of Rhode Island
A. Best, CSIRO, Australia

Start Date: October, 2008
Projected End Date: September, 2014

Objectives

The performance, calendar-life, and safety characteristics of Li-ion cells are dictated by the nature and stability of the electrolyte and the electrode-electrolyte interfaces. Desirable characteristics for these electrolytes include stability in the 0 to 5V vs. Li range, excellent lithium-ion conductivity, wide temperature stability range, non-reactivity with the other cell components, non-toxicity and low cost. Our goal is to develop novel electrolytes and electrolyte additives to meet the cost, calendar life and safety requirements of batteries for PHEV applications.

Technical Barriers

This project addresses the following technical barriers to the development of a PHEV battery with a 40 mile all electric range that meets or exceeds all performance goals.

- Cell performance
- Cell calendar and cycle life
- Cell abuse tolerance

Technical Targets

- Develop novel electrolytes with electrochemical stability in the 0 to 5V vs. Li voltage range.
- Develop additives to conventional electrolytes that improve cell shelf and cycle life by 50%. Cell performance and thermal abuse characteristics should stay the same or be enhanced by these additives.

Accomplishments

- Investigated of glycerol carbonate (GC)-based electrolytes.
  - Examined performance/cycling behavior of electrolyte mixtures containing various Li-salts
- Developed techniques to replace the H (in the OH of GC) with other species, and conducted experiments with these "GC-derivative" solvents.
  - Examined performance/cycling behavior of electrolyte mixtures
- Identified new electrolyte solvents and electrolyte additives that can enhance cell life
  - Effects on cell performance, life, and safety are being determined
- Performed electrochemical studies with ionic liquids
  - Examined electrode performance/cycling behavior

✧ ✧ ✧ ✧ ✧

Introduction

Recent advances in cathode and anode materials have refocused attention on electrolytes as the technological bottleneck limiting the operation and performance of lithium-batteries. Whereas, attributes such as cell potential and energy density are related to the intrinsic property of the positive and negative electrode materials, cell power density, calendar-life and safety are dictated by the nature and stability of the electrolyte and the electrode-electrolyte interfaces. A wide electrochemical window, wide temperature stability range, non-reactivity with the other cell components, non-toxicity, low cost, and a lithium-ion transference number approaching unity are, in general, desirable characteristics for lithium battery electrolytes. In addition, the electrolyte should have excellent ionic conductivity to enable rapid ion transport between the electrodes, and be an electronic insulator to minimize self-discharge and prevent short-circuits within the cell.

Approach

Our approach is to (i) develop novel electrolytes that include glycerol carbonate, and modifications thereof, (ii) examine electrolyte additives that can enhance cell life by protecting the electrode surfaces, (iii) investigate the use of ionic liquids, and mixtures of ionic liquids and carbonate solvents, to enable more abuse tolerant batteries. GC can be a low-cost substitute for currently used lithium-battery solvents. Our approach is to dry/purify GC obtained from a commercial manufacturer and examine its performance in lithium-ion cells. Furthermore, we've developed techniques to replace the H (in the OH) group of GC with other alkyl species to form methyl ethers, ethyl ethers, and oligoethylene oxide ethers that will be examined as solvents. The electrolyte additives to generate passivation films at the positive and negative electrode surfaces are being determined by theoretical (molecular orbital) calculations on the electrolyte components to examine oxidation and reduction voltages. Some of the ionic liquids under consideration are ones reported to show promise in the lithium-battery literature.

Results

In previous reports we have shown that graphite electrodes can be cycled in GC-based electrolytes. $Li(Ni_{0.8}Co_{0.15}Al_{0.5})O_2$ (NCA)-based electrodes can also be cycled in these GC electrolytes. In this case, however, significant lithium consumption occurs during the first cycle, but later cycles show reasonable stability. The Li-GC solvate apparently oxidizes during the first cycle (but not in subsequent cycles) forming a surface film on the oxide electrodes. Cycling behavior in NCA(+)/Gr(-) cells (3- 4.1V) is not good because lithium consumption during GC oxidation depletes Li-inventory in the cell.

Other compounds dervived from GC have been synthesized and tested. Figure IV- 68 shows a scheme for preparing the methyl ester version of GC, henceforth referred to as GCAc. Both graphite- and NCA- based electrodes can be cycled in cells containing GCAc:DMC (1:8, by wt.) + 1.2M $LiPF_6$ electrolyte. The NCA/Li cells do not show the significant Li consumption observed for GC-based electrolytes. Therefore, NCA(+)/Gr(-) cells show acceptable cycling behavior in these electrolytes (see Figure IV- 69). Capacity retention is better when cell upper voltage is limited to 4V, instead of 4.3V.

A new family of organic electrolyte solvents/additives has been identified – performance and life tests with these compounds are in progress, and will be reported in later reports. Ionic liquid electrolytes, tested so far, show good cyclability with either the positive or negative electrode in Li-metal cells. Compounds stable at both highly oxidizing and reducing potentials are yet to be identified. However, electrolyte additives appear to improve the cycling behavior of ionic liquid electrolytes; these data will reported at another time.

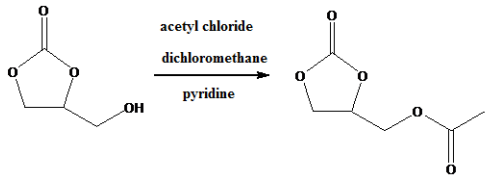

Figure IV- 68: Preparing the methyl ester version of GC.

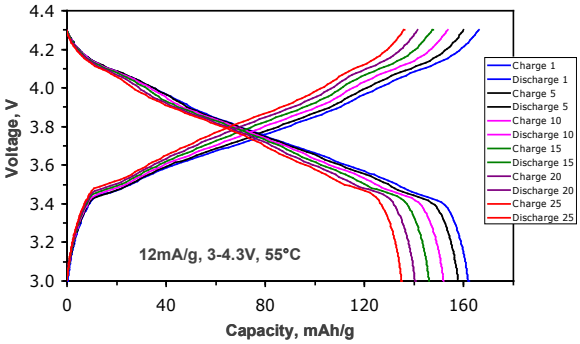

Figure IV- 69: NCA(+)//Gr(-) cell cycling in GCAc:DMC (1:8, by wt.) + 1.2M $LiPF_6$ eelctrolyte. Voltage range: 3-4.3V.

Conclusions and Future Directions

We will continue our investigations of novel solvents that include glycerol carbonate (GC), and modifications thereof, which includes (i) Preparation of compounds derived from GC, (ii) Performance/cycling behavior of various solvent-salt electrolyte mixtures, and (iii) Properties (electrochemical stability window, temperature stability, etc.) of "promising" electrolytes. We expect to develop criteria to identify new electrolyte additives that can enhance cell life by protecting electrode surfaces from reactions with the electrolyte. Our plan is to examine multifunctional additives that can simultaneously affect both positive and negative electrodes. Our studies on ionic liquids and on mixtures of ionic liquids and conventional electrolytes will continue. These studies include examining electrode performance/cycling behavior under PHEV conditions.

FY 2010 Publications/Presentations

1. 2010 DOE Annual Peer Review Meeting Presentation.
2. Electrolytes For Lithium And Lithium-Ion Batteries, Argonne Invention Report, ANL-IN-10-003
3. Electrolytes For Lithium And Lithium-Ion Batteries, Argonne Invention Report, ANL-IN-08-071

IV.B.4.2 Develop Electrolyte Additives (ANL)

Zhengcheng Zhang

Argonne National Laboratory (ANL)
9700 South Cass Avenue
Argonne, IL 60439-4837
Phone: (630) 252-7868; Fax: (630) 972-4440
E-mail: zzhang@anl.gov

Collaborators:
Khalil Amine, ANL
Yan Qin, ANL
Ali Abouimrane, ANL
Lu Zhang, ANL
Zonghai Chen, ANL

Start Date: FY09 (New project)
Projected End Date: September, 2014

Objectives

The objective of this work is to develop new electrolytes and associated additives that could bring additional features to the state-of-the-art lithium-ion battery electrolyte to meet the requirements of EV and PHEV applications.

- Screen and evaluate new electrolyte components (solvents and additives etc.) that could improve the electrolytes in any aspect of cell performance, especially on large electrochemical window, safety, and cycle & calendar life.
- Understand the connections between the chemical structures and cell performances, thus design new electrolyte components (solvents and additives etc.) tailored to specific properties.

Technical Barriers

The general technical barrier is the development of safe, cost-effective electrolytes for lithium-ion battery tailored to EV and PHEV applications that meet or exceed all performance goals. Specific barriers of the electrolyte development include:

- Insufficient voltage stability;
- High flammability, low safety;
- Poor cycle & calendar life;
- Surface reactivity with electrodes.

Technical Targets

- Develop new electrolyte components, such as solvents and additives, to improve the anodic stability and reduce the flammability of the electrolytes;
- Screen and evaluate novel electrolyte additives to improve the cycle & calendar life of lithium-ion cells;
- Characterize and analyze electrochemical properties of the cell system, including interface and surface reactions, that could be vital factors to the cell performance.

Accomplishments

- Sulfone based electrolyes were developed for high voltage lithium-ion battery.
  - Five sulfone based electrolyes were investaged in terms of ionic conductivity, electrochemical stability, flammability and cycle performance using different cell chemistries. Significant improvements were obtained including enlarged electrochemical window, reduced flammability and comparable cycle life.
- SEI additives were evaluated and optimized for lithium-ion battery with prolonged cycle life and improved safety.
  - Oxalato phosphate based additives were investageted to improve the cycle life of MCMB/NCM cells for high power applications. The addition of those additives improved the capacity retention of the cells as well as the thermal stability of the lithiated electrodes.
  - Succinic anhydride based additives were evaluated in the lithium-ion cells. The results indicated that those additives can significantly improve the cell cyclabiility and also the subtle difference in the chemical structures can result in large difference in cell performance.
  - Maleic anhydride based additives were also evaluated in lithium-ion cells. Significantly improved high temperature cyclability was obtained with the addition of these additives.

✧ ✧ ✧ ✧ ✧

Introduction

The electrolyte is a ubiquitous and indispensable component of lithium-ion batteries. Because it is sandwiched between the positive and negative electrodes, the electrolyte is in close interaction with both electrodes. Therefore, when new electrode materials emerge, the need for compatible electrolytes usually arises. Conventional carbonate based electrolyte has been used predominantly for the current lithium-ion battery industry; however, the flammability and anodic instability at high potential make it unsuitable for the high voltage cathode materials. With numerous high energy cathode materials emerging, the electrolyte must evolve to enable more abuse-tolerant operation and to become more stable without intervening with the electrochemical performance.

The interfaces between the electrolyte and the two electrodes often dictate the performance of the cell. Additives that stabilize those interfaces provide an efficient and economic method to improve the cell performance. The development of novel additives tailored to prolong cell cycle life and improve safety is the key in the lithium-ion battery technology. In particular, the interface between the anode and the electrolyte is a crucial factor affecting cell performance. A thin passivation layer, called SEI (solid electrolyte interface) is usually formed during the first charging process preventing further reactions of the electrolytes on the anode surface. For full cells utilizing carbon anodes, the formation process is potential dependant and stepwise, and is determined by the reactive components of the electrolytes that participate in the formation reactions. The SEI layer can be tuned to afford better cell performance through the use of advanced additives.

Approach

The development of novel electrolytes and additives consists of three phases. The first phase is to screen and evaluate novel electrolyte and additive candidates using DFT and relatively simple tests. Even though theoretical analysis and preditions are being actively conducted, the electrochemical preporties cannot be definitively predicted based only on chemical structures. We therefore need to screen a great number of different candidates to find the most promising ones. In this phase, some candidates may stand out with superior features. In the second phase, thorough evaluation and mechanism analysis will be conducted on the promising candidates to gain insights into their superior performance. Various measurements, including electrochemical, spectroscopic and computational methods, will be utilized to gather as much information as possible to help understand the connections between the chemical strutures and the cell performace. In this phase, better understanding should be obtained in terms of how the chemical compounds work in the cell. In the third phase, new design of promising electrolytes and additives will be proposed and organic synthesis will be used to make these compounds. Evaluations will provide feedback and lead to modifications and even more new designs. Our efforts this year have focused on screening and evaluating electrolyte and additive candidates in the first and second phases.

Results

Sulfone-based Electrolyte for High Voltage Lithium-ion Battery. The electrochemical stability of sulfone-based electrolytes was determined by cyclic voltammetry. Figure IV- 70(left) shows that among these solvents, tetramethylene sulfone (TMS) and ethyl methyl sulfone (EMS) exhibited the highest anodic potential, above 5.0V *vs* Li^+/Li, followed by 1-Fluoro-2-(methylsulfonyl)benzene (FS) (4.5V), butyl sulfone (BS) (4.2V), and ethyl vinyl sulfone (EVS) (4.2V). Conductivity measurements, Figure IV- 70(right), showed comparable values to their conventional counterparts.

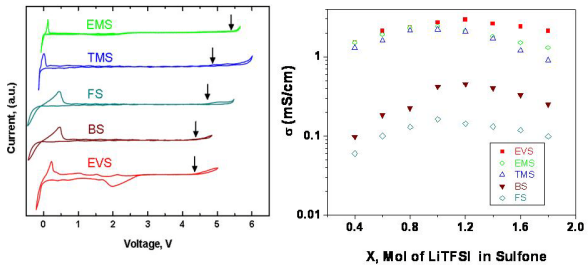

Figure IV- 70: CV profiles of 1M LiTFSI sulfones (left) and their ambient conductivities (right).

The cell performance of the sulfone electrolytes with LTFSI salt were first evaluated using an $Li_4Ti_5O_{12}$ (LTO)/ $LiMn_2O_4$ cell. Figure IV- 71(a-c) is the cycling data between 1.5 to 3V, indicating that the cells using EMS and TMS can deliver more than 80 mAh/g capacity at C/3 (33mA/g) with 99% capacity retention and maintain 100% coloumbic efficiency through the 100^{th} cycle. However, poor capacity retention is observed for FS electrolyte (Figure IV- 71(c)) probably due to its poor conductivity (0.14 mS/cm) and narrow electrochemical window.

The LTO/$LiNi_{0.5}Mn_{1.5}O_4$ cell with 1M $LiPF_6$ TMS electrolyte was cycled at a low rate (10mA/g) (C/12). Initially, the capacity of the cell increased from 108 (cycle 1) to 118 $mAhg^{-1}$ (cycle 6), and then decreased monotonically to 106 $mAhg^{-1}$ after 100 cycles (Figure IV-71 (d)). The improvement in the initial cell capacity probably resulted from the increased wettability at the interface between the electrodes and the fiber glass separator. The wettability increased with further cycling and led to more than 99% coloumbic efficiency. TMS solvent was blended with EMC (50:50 v/v) as a thinner

solvent to enhance the wettability and rate capability of the cell.

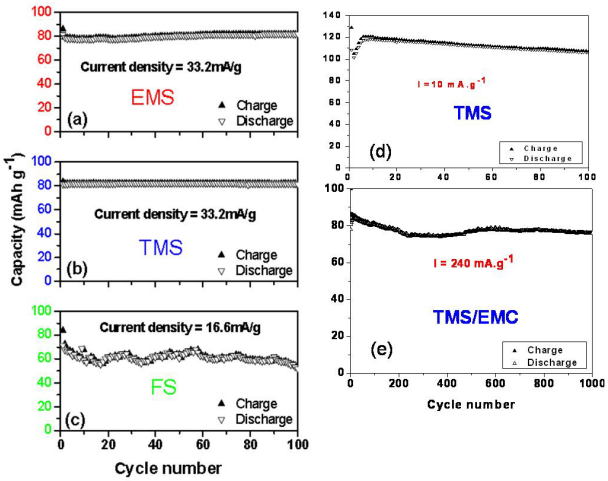

Figure IV- 71: Specific cathode charge/discharge capacities of cells for LTO/$LiMn_2O_4$ (left) with 1M LiTFSI sulfones and LTO/$LiNi_{0.5}Mn_{1.5}O_4$ (right) with 1M $LiPF_6$ sulfones.

As shown in Figure IV- 71(e), the cell exhibited outstanding cycle life for 1000 cycles at the 2C rate ($240mAg^{-1}$). Clearly, the sulfone-carbonate co-solvent system offers the electrochemical stability needed for a high-voltage cell system despite the high content of the EMC solvent that has a narrower electrochemical window.

SEI Electrolyte Additives to Improve the Performance of Lithium-ion Battery. I. Oxalate Phosphate Derivatives - Lithium tetrafluoro(oxalate) phosphate (LTFOP) and lithium tris(oxalato) phosphate (LTOP) were investigated as electrolyte additives to improve the cycle and calendar life of MCMB/$Li_{1.1}[Ni_{1/3}Co_{1/3}Mn_{1/3}]_{0.9}O_2$ (NCM) cells for high power applications. Reduction potentials of these additives are determined by charging the Li/MCMB half cell. In Figure IV- 72, reduction peaks at 1.7V and 2.1V are observed for LiTFOP and LTOP, respectively, indicating a new SEI formation prior to EC decomposition.

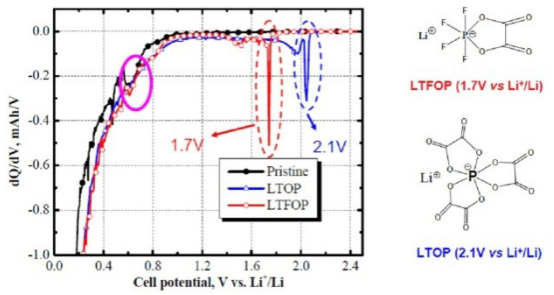

Figure IV- 72: Differential capacity profiles of Li/MCMB with 1.2M $LiPF_6$ EC/EMC 3/7+2% additive.

Figure IV- 73 shows cycling performance (55°C, between 3.0 and 4.0 V, with a constant current of 1C, or 2.0 mA) improvement with the new additives. Capacity retention after 200 cycles was improved from 80% for the pristine electrolyte to 87% by adding 1 wt % of LTFOP, 92% for 2 wt % of LTFOP, and 97% for 3 wt % of LTFOP electrolytes.

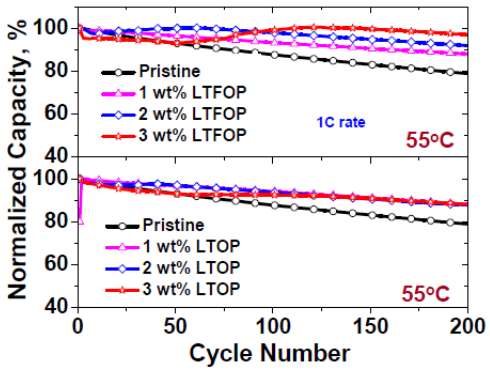

Figure IV- 73: Plots of normalized discharge capacity vs cycle number for MCMB/NCM cells with and without additives.

However for LTOP, higher concentration did not result in lareger improvements. This difference can be well explained by the impedance increase for LTOP in Figure IV- 74.

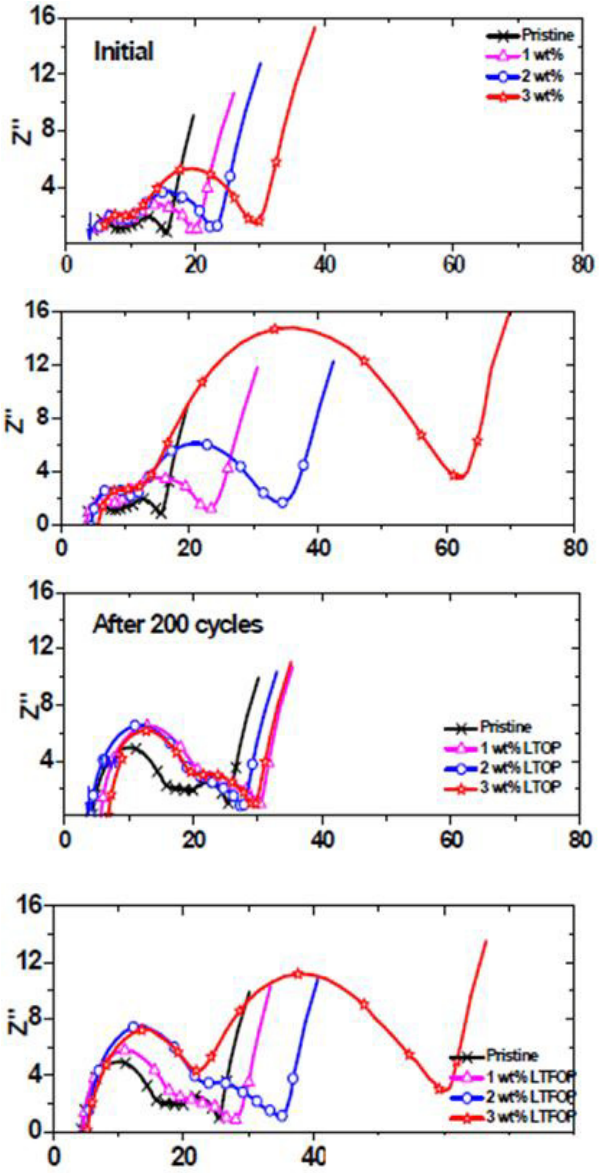

Figure IV- 74: Nyquist plots of the MCMB/NCM cells with and without LTFOP or LTOP before (top) and after 200 cycles (bottom) at 55°C at open-circuit voltage of 3.8 V.

The addition of LTFOP to the cells resulted in impedance growth with slow increasing rate, but for the case of LTOP, much larger impedance was observed which will affect the power of the cell.

Figure IV- 75 shows the ambient charge capacity of the MCMB negative electrode (top) and NCM cathode electrode (bottom) with different LTFOP concentrations in the electrolyte after the cell had been aged at 55°C for different periods of time. After being aged for 30 days at 55°C, the cell with a pristine electrolyte had only half of the initial reversible capacity left, and it lost all of its capacity after 40 days. The cells with 1, 2, and 3 wt % of LTFOP showed capacity retention of almost 100% even after more than 90 days of aging, and the concentration of LTFOP did not make any difference. Less improvement on the cathode material was observed for LTFOP Figure IV-75 (bottom). The aging results confirmed that the stabilization on MCMB surface of LTFOP is the main contributor of the improved cell performance.

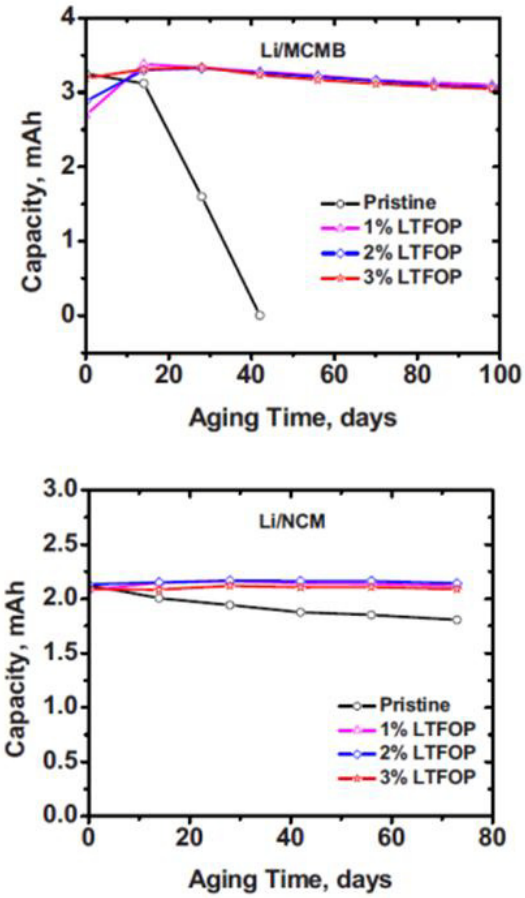

Figure IV- 75: Capacity retention of the MCMB negative electrode (top) and NCM positive electrode (bottom) vs the aging time at 55°C.

A further indirect evidence of the positive effect of LTFOP additive on the MCMB negative electrode is the thermal decomposition of the SEI layer. Figure IV- 76 shows a DSC profile of lithiated MCMB mixed with a nonaqueous electrolyte with and without LTFOP as the additive. When no LTFOP was added, an exothermal signal was observed at about 110°C, which is believed to be caused by the breakdown of the SEI layer on the MCMB surface. This initial breakdown of the SEI resulted in an unprotected surface area on the negative electrode, which led to a continuous reformation and breakdown of the secondary SEI. This observation is supported by the long exothermal plateau from 110 up to 220°C, as shown in Fig. 7. The energy generated from the continuous breakdown of the secondary SEI could be enough to trigger a thermal runaway in a large battery system. When

LTFOP was added, the onset temperature of the SEI decomposition increased to about 150°C, meaning a more stable SEI layer and higher activation energy for the decomposition reaction. Therefore, LTFOP electrolyte additive should also improve the thermal stability of the negative electrode.

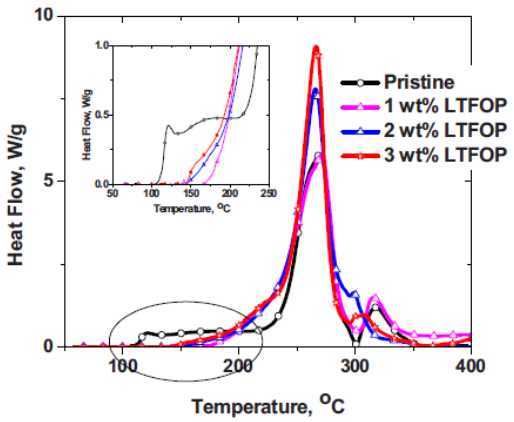

Figure IV- 76: DSC profiles of the fully lithiated MCMB mixed with nonaqueous electrolytes with and without LTFOP.

SEI Electrolyte Additives to Improve the Performance of Lithium-ion Battery - II. Maleic Anhydride and Succinic Anhydride Derivatives. Maleic anhydride based additives were also evaluated. Differential capacity profiles (Figure IV- 77) suggested that with the addition of maleic anhydride additives, EC reduction (0.6-0.8V vs Li^+/Li) may be depressed and additive 5 (1.12V vs Li^+/Li) and 6 (1.31V vs Li^+/Li) were involved in the SEI layer formation process prior to the formation of the conventional SEI.

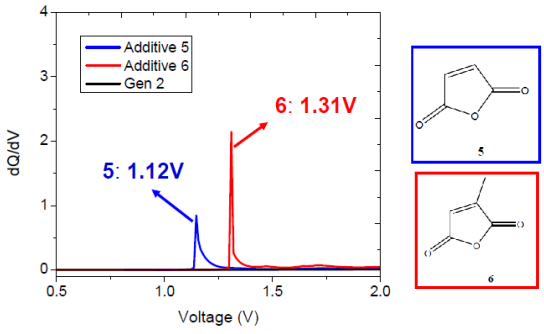

Figure IV- 77: Differential capacity profiles of MCMB/NCM cells with 1% additive in 1.2M $LiPF_6$ EC/EMC 3/7.

Figure IV- 78 shows the cycling performance at 55°C. It reveals a clear indication of the improvements by adding additive 5 and 6, additive 5 shows better capacity retention than additive 6. The new SEI provided better stability of the electrolyte/electrode interface.

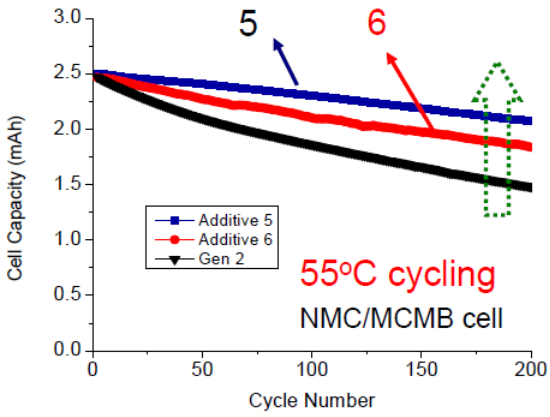

Figure IV- 78: Capacity retention of MCMB/NCM cells cycled between 2.7 and 4.2V at 55 ◦C with electrolyte of 1.2M $LiPF_6$ EC/EMC 3/7 with and without addtive.

Similar to maleic anhydrides, succinic anhydride based additives can also form an SEI on the anode surface. High temperature charge-discharge tests indicated an improved cycle life compared with electrolyte containing no succinic anhydride additive. The contribution of this improvement is under investigation.

Conclusions and Future Directions

Sulfones such as TMS and EMS are promising electrolyte systems that could enable their use with high-potential cathodes such as $LiNi_{0.5}Mn_{1.5}O_4$ in long-life lithium-ion batteries by providing large electrochemical window, comparable cyclability and improved flammability.

SEI additives have been investigated to improve the MCMB/NCM cell performance in terms of cycle life, high power, and safety property, including LTFOP, LTOP, succinic anhydride derivatives and maleic anhydride derivatives. The excellent cycling results can be obtained by adding certain amount of additives. Also, a thorough evaluation towards high power applications and safety was conducted using various techniques, including AC impedance, aging measurement, and DSC.

Furure directions on this project are two fold. First, we will continue to screen and evaluate different electrolyte and additive candidates for superior cell performance. Second, we will design new electrolyte and addtive candidates to explore the connection between the chemical structures and cell performance, enabling more opportunities for the development of next generation lithium battery electrolytes.

FY 2010 Publications/Presentations

1. Investigation of sulfone-based electrolytes with a titanate anode, Abstract #129, 215th ECS Meeting, 2009

2. Sulfone-based electrolytes for high-voltage Li-ion batteries, Electrochemistry communications, 11 (5),1073-1076, 2009
3. Lithium tetrafluoro oxalato phosphate as electrolyte additive for lithium-ion cells, Electrochemical and Solid-State Letters, 13 (2) A11-A14, 2010
4. Redox shuttle for overcharge protection for lithium-ion battery, US patent application with internal # ANL-IN-08-082
5. New electrolyte additive for lithium-ion battery, US patent application with internal # ANL-IN-09-108
6. 6. Non-aqueous electrolyte for lithium-ion battery, US patent application with internal # ANL-IN-10-082

IV.B.4.3 High Voltage Electrolytes for Li-ion Batteries (ARL)

Kang Xu, Arthur von Cresce, Jan L. Allen,
T. Richard Jow

Point of Contact:
T. Richard Jow/Kang Xu
U.S. Army Research Laboratory
2800 Powder Mill Road
Adelphi, MD 20783
Phone: (301) 394-0340/(301) 394-0321
Fax: (301) 394-0273
E-mail: taiguang.richard.jow@us.army.mil/
conrad.xu@us.army.mil

Start Date: August 15, 2008
Projected End Date: September 30, 2010

Objectives

- Develop high voltage electrolytes that enable the operation of Li-ion batteries with high voltage cathodes for enhanced energy density for plug-in hybrid electric vehicles (PHEV).

Technical Barriers

This project addresses the following technical barriers of today's Li-ion batteries:

- State of the art (SOA) electrolytes based on carbonate solvents decompose above 4.5 V; thus, high voltage cathode materials today do not have suitable high voltage electrolytes for realizing their capacity and achieving long cycle and storage life.
- Sulfone-based solvents showed anodic stability up to 5.8 V but:
  - SEI chemistry from the reduction of sulfones does not provide protection of graphitic anodes
  - Most sulfones such as dimethyl sulfone and sulfolane are viscous liquids with a melting point near RT.
- Lack of a reliable 5 V cathode as characterization platform.

Technical Targets

- Synthesize improved sulfone based solvents with and without unsaturated bonds and evaluate their electrochemical properties.
- Identify and synthesize additives for electrolytes based on sulfone solvents for Li-ion cells.
- Identify and synthesize additives for electrolytes based on carbonate solvents for Li-ion cells.
- Formulate, test and evaluate electrolytes containing synthesized additives in Li half cells.
- Select promising formulations, test and demonstrate in complete button cell or in prototype cell configurations.

Accomplishments

- Evaluated high voltage electrolytes using Li/$LiNi_{0.5}Mn_{1.5}O_4$ half cell as a test vehicle for cycling stability between 3.5 and 4.95 V.
- Replacing EC with sulfolane (SL) completely or partially in 1M $LiPF_6$/EC:EMC (3:7) as a control results in higher capacity retention but lower coulombic efficiency. With ethyl methyl sulfone (EMS) as an additive, coulombic efficiency was improved.
- Evaluated electrolytes with different additives including ARL1-5 in the baseline electrolyte, 1 M $LiPF_6$/EC-EMC (3:7 w/o), resulting in varied effectiveness in improving capacity retention and coulombic efficiency. The cycling of Li/$LiNi_{0.5}Mn_{1.5}O_4$ half cells in the electrolyte with ARL3 shows the most improved performance, 88% capacity retention over 200 cycles, comparing to that in the baseline electrolyte and electrolytes with other additives.
- Developed modified $LiCoPO_4$ (m-$LiCoPO_4$), a 4.8 V cathode material, through study of substitutional chemistry. The m-$LiCoPO_4$/Li cells showed substantial improvement in capacity retention compared with $LiCoPO_4$/Li when cycled in the baseline electrolyte.
- Demonstrated further improvement in charge retention of m-$LiCoPO_4$/Li cells when cycled in 1 M $LiPF_6$/EC:EMC(3:7 w/o) with 1 wt% ARL3.

✧ ✧ ✧ ✧ ✧

Introduction

Achieving higher energy density using the new generation of high voltage cathodes with voltages from 4.5 to 5.0 V such as $LiNi_{0.5}Mn_{1.5}O_2$ and $LiCoPO_4$ for Li-ion batteries for PHEVs will need compatible high voltage electrolytes. The state-of-the-art electrolytes made of $LiPF_6$ in carbonate solvent mixtures decompose at voltages above 4.5 V and are unable to realize the higher energy

density and achieve long cycle and storage life. The development of compatible high voltage electrolytes is urgently needed.

Approach

Instead of using the state-of-the-art carbonate based solvent systems, our approach is to explore the use of sulfone based solvent systems and the use of additives for both the sulfone based and the carbonate based solvent systems. The sulfone solvents with unsaturated bonds would also be good candidates as additives for both sulfone and carbonate based electrolytes. It has been reported that the electrolytes containing sulfone based solvents are anodically stable up to about 5.8 V. However, they lack the ability to form a protective SEI at the anode. Furthermore, the commercially available sulfones such as dimethyl sulfone and sulfolane are viscous. To allow the operation of high voltage cathode materials, we will develop electrolytes based on improved sulfone based solvents.

To improve the sulfone based and carbonate based solvent systems, our approaches include the following:

- Explore asymmetric sulfones with different functional groups for lower melting points and viscosity.
- Explore sulfone solvents with functional groups containing un-saturated bonds as solvents and as additives.
- Explore the use of other additives that have the ability for forming the protective layers on cathodes.

Results

Evaluation of Electrolytes Containing Additives in Sulfone/Carbonate Mixed Solvents. The electrolyte made of $LiPF_6$ in sulfolane (SL):EMC (30:70 w/o) was evaluated in $LiNi_{0.5}Mn_{1.5}O_2$/Li half cells. A number of electrolyte formulations containing additives including ethyl methyl sulfone (EMS) and ARL1-4 in 1 M $LiPF_6$ in SL:EC:EMC (15:15:70 w/o) solvent mixtures were also evaluated in $LiNi_{0.5}Mn_{1.5}O_2$/Li half cells. The results indicated that the coulombic efficiency and capacity retention of these cells were no better than those in the baseline electrolyte, 1 M $LiPF_6$ in EC-EMC (3:7 w/o), Figure IV- 79. The only standout was the electrolyte containing both EMS and ARL3: 1 M $LiPF_6$ in SL:EC:EMC (15:15:70 w/o) solvent mixtures, Fig 2, which resulted in substantial improvement in coulombic efficiency and capacity retention.

Evaluation of Electrolytes Containing Additives in Carbonate Solvents. $LiNi_{0.5}Mn_{1.5}O_4$ is a 4.7 V cathode material. The cycling of this material has been challenging. A steady loss of capacity is observed in cycling this cathode against Li anode between 3.5 and 4.9 V in our baseline electrolyte, 1 M $LiPF_6$ in EC:EMC (3:7), is shown in Fig. 3.

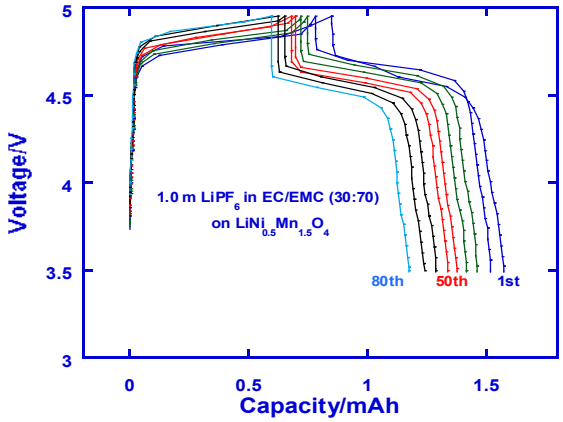

Figure IV- 79: Voltage profiles of a $LiNi_{0.5}Mn_{1.5}O_2$/Li half cell in 1 M $LiPF_6$/EC:EMC(3:7 w/o) versus capacity at different cycles cycled between 3.5 and 4.9 V at room temperatures.

However, the same $LiNi_{0.5}Mn_{1.5}O_4$ cathode could be cycled with low capacity loss when cycled in an electrolyte of 1.0 wt% ARL3 additive added to the baseline electrolyte. The voltage profiles of charge and discharge vs. capacity are shown inFigure IV- 80.

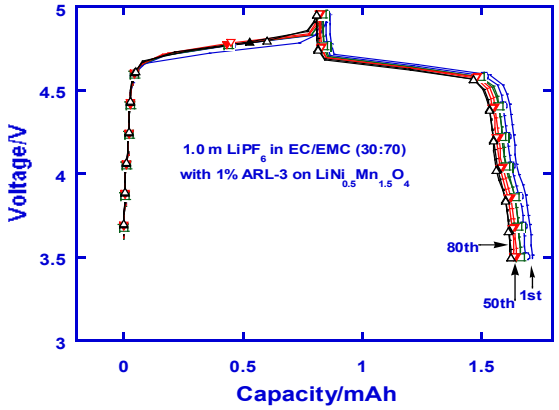

Figure IV- 80: Voltage profiles of a $LiNi_{0.5}Mn_{1.5}O_2$/Li half cell in 1 M $LiPF_6$/SL/EC:EMC(1.5:1.5:7 w/o)+1 wt% ARL3 versus capacity at different cycles cycled between 3.5 and 4.9 V at room temperatures.

The charge retention of the above two cells as a function of cycle number up to 200 was compared and plotted in Figure IV- 81.

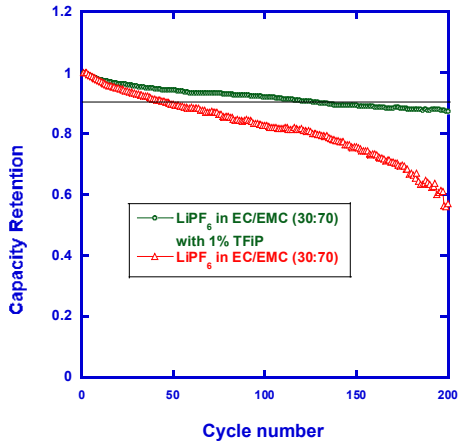

Figure IV- 81: A comparison of capacity retention of $LiNi_{0.5}Mn_{1.5}O_2$/Li half cells in 1 M $LiPF_6$/EC:EMC(3:7 w/o) with and without 1 wt% ARL3 versus cycle number. The cells were cycled between 3.5 and 4.9 V at room temperature.

Development of High Voltage $LiCoPO_4$ Based Cathode for the Evaluation of High Voltage Electrolyte. $LiCoPO_4$ is a 4.8 V cathode material with potentially 40% higher energy density than $LiFePO_4$ and is an ideal test vehicle for high voltage electrolytes. However, its relatively poor cycle life resulting from lack of structural stability plus compatible high voltage electrolytes became a challenge for using this material. We were able to modify $LiCoPO_4$, m-$LiCoPO_4$, through its substitutional chemistry. This is evidenced by improved charge retention as shown in Figure IV- 82. The charge retention of m-$LiCoPO_4$ could be further improved by using the electrolyte containing 1 wt% ARL3.

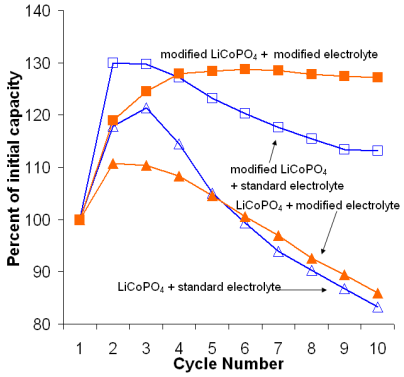

Figure IV- 82: A comparison of capacity retention of $LiCoPO_4$/Li and m-$LiCoPO_4$/Li half cells in 1 M $LiPF_6$/EC:EMC(3:7 w/o) with and without 1 wt% ARL3 versus cycle number.

Conclusions and Future Directions

We have identified additives for both the sulfone–based and carbonate based electrolyte formulations. With the addition of ARL3 in the baseline electrolyte, 1 M $LiPF_6$/EC:EMC(3:7 w/o), the charge retention of $LiNi_{0.5}Mn_{1.5}O_2$ and m-$LiCoPO_4$ cycled against Li could be substantially improved. Our works in progress include the following.

- The evaluation of the impact of ARL3 on anodes including graphite and Li alloys.
- The evaluation of ARL3 in full cells. We are in urgent need of reliable high voltage cathode with matched anode for reliable evaluation.
- The evaluation of ARL3 at elevated and low temperatures for stability and rate performance of Li-ion batteries.
- Understanding the mechanism of how ARL3 works for developing more effective additives.
- Adding computational efforts to develop a basic understanding of and potentially to provide guidance in materials development.

FY 2010 Publications/Presentations

1. "Differentiating contributions to "ion transfer" barrier at electrolyte/graphite interphase from Li+-desolvation and interphasial resistance", K. Xu, A. von Cresce, and U. Lee, *Langmuir*, 2010, **26**, 11538
2. "Electrolytes and Interphasial Chemistry in Li Ion Devices", K. Xu, Invited contribution to Special Issue on Lithium-ion Batteries, *Energies* 2010, **3**(1), 135.
3. "Electrolytes: Overview", K. Xu, In: Juergen Garche, Chris Dyer, Patrick Moseley, Zempachi Ogumi, David Rand and Bruno Scrosati, editors. *Encyclopedia of Electrochemical Power Sources*, Vol. 5, Amsterdam: Elsevier; Nov. 20the 09, pp. 51~70
4. "Electrolytes, SEI and Charge Discharge Kinetics of Li-ion Batteries", T. R. Jow, J. L. Allen, M. Marx, K. Nechev, B. Deveney, S. Rickman, *ECS Transactions*, 2010, **25** (36), 3.
5. "New Cathode Materials for Lithium-ion Batteries," J. L. Allen, J. Wolfenstine, T. R. Jow, *Proceedings of the 44th Power Sources Conference*, Las Vegas, NV, Paper 8.3, June 2010.

IV.B.4.4 Development of Novel Electrolytes for Use in High Energy Lithium-Ion Batteries with Wide Operating Temperature Range (JPL)

Dr. Marshall C. Smart

Electrochemical Technologies Group
Power and Sensor Systems Section
Jet Propulsion Laboratory
California Institute of Technology
4800 Oak Grove Drive, M/S 277-207
Pasadena, CA 91109-8099
(818) 354-9374 (Phone)
(818) 393-6951 (Fax)
E-Mail: Marshall.C.Smart@jpl.nasa.gov

Start Date: Oct 1, 2009
Projected End Date: September 30, 2014

Objectives

- Develop a number of advanced Li-ion battery electrolytes with improved performance over a wide range of temperatures (-30 to +60°C) and demonstrate long-life characteristics (5,000 cycles over 10-yr life span).
- Improve the high voltage stability of these candidate electrolyte systems to enable operation up to 5V with high specific energy cathode materials.
- Define the performance limitations at low and high temperature extremes, as well as, life limiting processes.
- Demonstrate the performance of advanced electrolytes in large capacity prototype cells.

Technical Barriers

This project addresses the following technical barriers associated with the development of PHEVs:

(A) Narrow operating temperature range

(B) Limited life

(C) Poor abuse tolerance.

Technical Targets

- The technology development program is focused on enabling 10 s discharge power, and is associated with a number of technical targets, including:
  - (a) 750 W/kg (10 mile) and 316 W/kg (40 mile)
  - (b) Cold cranking capability to -30°C,
  - (c) Cycle life: 5000 cycles (10 and 40 mile)
  - (d) Calendar life: 15 years (at 35°C);

Accomplishments

- Demonstrated improved performance with wide operating temperature electrolytes containing ester co-solvents (i.e., methyl propionate and ethyl butyrate) in Quallion prototype cells.
- At -40°C, a methyl propionate-based electrolyte was demonstrated to deliver over 60% of the room temperature capacity using a 5C rate.
- Investigated a number of electrolyte additives to improve the performance of methyl propionate and methyl butyrate-based blends in MCMB-$LiNiCoO_2$ cells.
- Formulations possessing mono-fluoroethylene carbonate (FEC), lithium bis(oxalato) borate (LiBOB), lithium oxalate, and vinylene carbonate (VC) have shown promise in experimental cells.
- Performed extensive electrochemical characterization to determine the degradation modes when subjected to extreme temperatures.
- Investigated the use of methyl butyrate and methyl propionate-based electrolyte containing additives in conjunction with $LiNi_{1/3}Co_{1/3}Mn_{1/3}O_2$ and $Li(Li_{0.17}Ni_{0.25}Mn_{0.58})O_2$ cathode materials in experimental cells.
- Investigated the use of lithium dinitramide (LiDNA) as a potential electrolyte additive. Preliminary results suggest efficient SEI formation is occurring with good reversibility.

✧ ✧ ✧ ✧ ✧

Approach

The development of electrolytes that enable operation over a wide temperature range, while still providing the desired life characteristics and resilience to high temperature (and voltage) remains a technical challenge. To meet the proposed objectives, the electrolyte development will include the following general approaches: (1) optimization of carbonate solvent blends, (2) use of low viscosity, low melting point ester-based co-solvents, (3) use of fluorinated esters and fluorinated carbonates as co-solvents, (4) use of novel "SEI

promoting" and thermal stabilizing additives, (5) use of novel non-fluorine based salts (with Materials Methods and LBNL). Many of these approaches will be used in conjunction in multi-component electrolyte formulations (i.e., such as the use of low viscosity solvents and novel additives and salts), which will be targeted at improved operating temperature ranges while still providing good life characteristics.

Electrolyte Characterization. The candidate electrolytes are characterized using a number of approaches, including ionic conductivity and cyclic voltammetry, and evaluating the performance characteristics in experimental ~ 400 mAh three electrode cells. Initially, cells will be fabricated with either (a) MCMB /$LiNi_{0.8}Co_{0.2}O_2$ or (b) graphite/$LiNi_{1/3}Co_{1/3}Mn_{1/3}O_2$ electrode couples. Other chemistries can be evaluated depending upon availability from collaborators. In addition to performing charge/discharge characterization over a wide range of temperatures and rates on these cells, a number of electrochemical characterization techniques will be employed, including: (1) Electrochemical Impedance Spectroscopy (EIS), (2) DC linear (micro) polarization, and (3) Tafel polarization measurements. The electrochemical evaluation in proven three electrode test cells enables electrochemical characterization of each electrode (and interface) and the identification of performance limiting mechanisms. Electrodes are easily harvested from these test cells and samples will be delivered to collaborators (i.e., URI and LBNL). In addition to evaluating candidate electrolytes in spirally wound experimental cells, studies will be performed in coin cells, most notably in conjunction with high voltage cathode materials.

Performance Demonstration. Performance testing of large capacity prototype cells containing candidate advanced electrolytes will be performed and evaluated under a number of conditions (i.e., assessment of wide operating temperature capability and life characteristics). JPL has on-going collaborations with a number of battery vendors and also has the capabilities to perform extensive testing. Typical prototype cells that will be considered include (i) Yardney 7 Ah prismatic cells, (ii) Quallion prismatic cells (0.300Ah size), and (iii) A123Systems 2.2 Ah cylindrical cells. Cells will be procured and obtained through on-going collaborations

Results

We have investigated a number of ester containing electrolytes, namely methyl propionate and methyl butyrate-based electrolytes, in conjunction with electrolyte additives, with the intent of providing improved low temperature performance while still delivering acceptable high temperature resilience. More specifically, we have focused upon formulations consisting of $LiPF_6$ in ethylene carbonate (EC) + ethyl methyl carbonate (EMC) + methyl propionate (MP) or methyl butyrate (MB) with and without electrolyte additives, including lithium oxalate, FEC, VC, and LiBOB. The identification of these esters, as well as the optimization of their concentrations in EC+EMC-based solutions, was based upon studies with MCMB-$LiNiCoO_2$ and $LiNiCoAlO_2$ systems.

As illustrated in Figure IV- 83, MCMB-$LiNiCoAlO_2$ prototype cells manufactured by Quallion, LCC containing electrolytes possessing ester co-solvents, such as methyl propionate, dramatically outperform all carbonate-based systems at low temperatures, such as the DOE baseline formulation consisting of 1.2M $LiPF_6$ in EC+EMC (30:70 vol %). As illustrated, nearly a five-fold increase in the delivered capacity at high rate (i.e., 5C) was obtained at low temperature (-40°C).

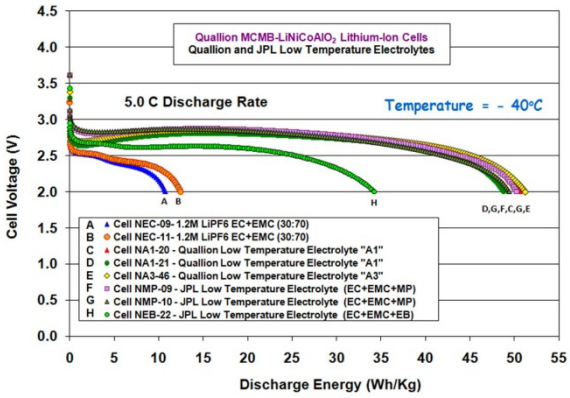

Figure IV- 83: The discharge energy obtained with MCMB-$LiNiCoAlO_2$ cells at -40°C, using 5C discharge rates.

The discharge rate performance was evaluated over a range of rates and temperatures, and improved low temperature performance was obtained to temperatures as low as -60°C. However, greater degradation was observed with the ester containing systems when subjected to high temperature operation. As shown in Figure IV- 84, when prototype cells were subjected to 100% DOD cycling at 50°C, increased capacity fade was observed for the ester-containing electrolytes. Variable temperature cycling, in which the cells are cycled intermittently between high and low temperatures (i.e., +50°C to -40°C), demonstrated that the low temperature capability of the cells also declines after being exposed to high temperature.

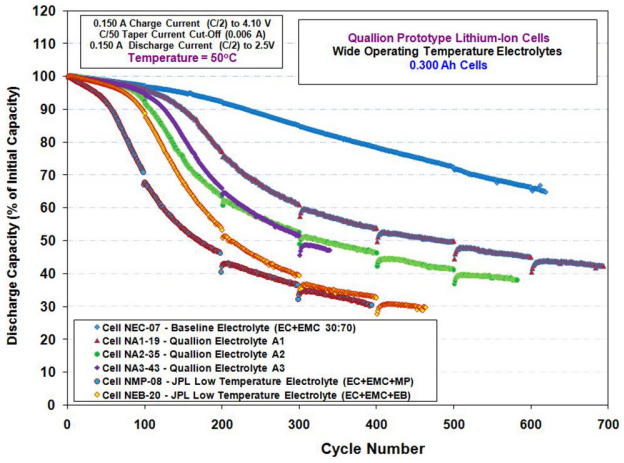

Figure IV- 84: The cycle life performance (100% DOD) of MCMB-$LiNiCoAlO_2$ cells containing wide operating temperature electrolytes at 50°C

To improve the high temperature resilience of such electrolyte systems, a number of additives were investigated with the intent of producing desirable electrode interfacial layers (i.e., SEI), at both the anode and the cathode. Initial efforts were focused upon investigating candidate additives in experimental MCMB-$Li_xNi_yCo_{1-y}O_2$ cells, which were exposed to temperatures as high as 80°C, namely VC, dimethyl acetamide (DMAc), FEC, and lithium oxalate, in an electrolyte solution anticipated to perform well at warm temperature (i.e., 1.0M $LiPF_6$ in EC+EMC (50:50 vol %). In addition to determining the capacity and power losses at various temperatures sustained as a result of high temperature cycling (cycling performed at 60° and 80°C), the three-electrode MCMB-$Li_xNi_yCo_{1-y}O_2$ cells (lithium reference) enabled us to study the impact of high temperature storage upon the SEI film characteristics on the carbon anodes (MCMB-based materials), the metal oxide cathodes, and the subsequent impact upon electrode kinetics.

After completing 20 cycles at 60°C, EIS measurements were performed on the $LiNi_XCo_{1-X}O_2$ electrodes, as shown in Figure IV- 85. As illustrated, all of the electrolytes containing the additives under evaluation provided a beneficial effect in terms of preserving low film and charge transfer resistances. The following trend was observed, expressed in terms of increasing impedance: 4% FEC < 2% FEC < 2% VC + 2% DMAc < lithium oxalate < 2% VC < baseline electrolyte (no additive). When EIS measurements were performed on the MCMB anodes after the formation cycling and before exposure to high temperatures, it was apparent that there is less differentiation between the spectra obtained as a function of electrolyte type, suggesting that the overall cell impedance was observed to be dominated by the contribution of the $Li_xNi_yCo_{1-y}O_2$ cathodes.

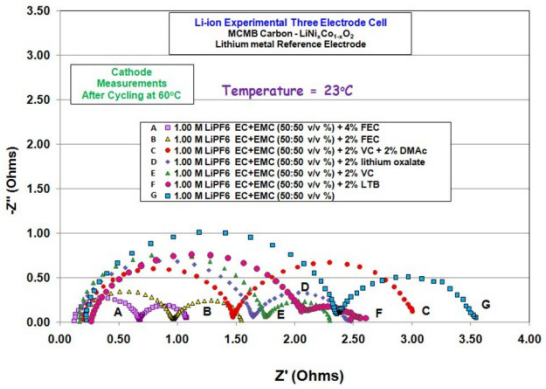

Figure IV- 85: AC impedance (Nyquist) plots of $LiNi_XCo_{1-X}O_2$ electrodes in MCMB-$LiNi_XCo_{1-X}O_2$ cells containing 1.0M $LiPF_6$ EC+EMC (50:50 v/v %) electrolyte with and without additives after being subjected to 20 cycles at 60°C.

Based upon these approaches, a number of methyl butyrate–based electrolytes were investigated with the anticipation that the high temperature resilience will be improved. Specifically we investigated: (1) 1.20M $LiPF_6$ in EC+EMC+MB (20:20:60 v/v %), (2) 1.20M $LiPF_6$ in EC+EMC+MB (20:20:60 v/v %) + 2% FEC, (3) 1.20M $LiPF_6$ in EC+EMC+MB (20:20:60 v/v %) + 4% FEC, (4) 1.20M $LiPF_6$ in EC+EMC+MB (20:20:60 v/v %) + lithium oxalate, (5) 1.20M $LiPF_6$ in EC+EMC+MB (20:20:60 v/v %) + 2% VC, and (6) 1.20M $LiPF_6$ in EC+EMC+MB (20:20:60 v/v %) + 0.10M LiBOB. These electrolytes have been shown to have improved performance in MCMB-$LiNiCoO_2$ and graphite-$LiNi_{1/3}Co_{1/3}Mn_{1/3}O_2$ experimental Li-ion cells, as described below.

Although the intention of utilizing the electrolyte additives was to improve the high temperature resilience of the systems, they also imparted greater low temperature rate capability. For example, methyl butyrate-containing formulations with a number of electrolyte additives were observed to outperform the baseline solutions (i.e., a MB-based solution without any additives) when discharged at -40°C, as shown in Figure IV- 86. The improved low temperature performance has been ascribed to the improved kinetics at the anode (especially in the case of FEC and lithium oxalate) and at the cathode (especially with VC and LiBOB), as shown in Figure IV- 87.

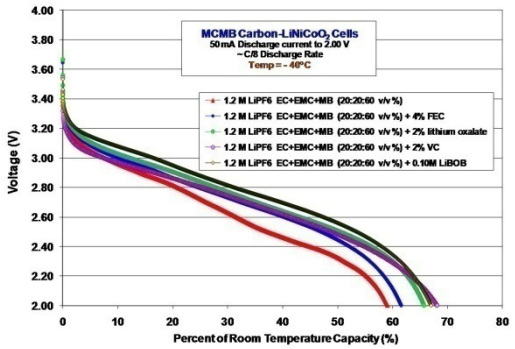

Figure IV- 86: Discharge capacity of MCMB-$LiNi_XCo_{1-X}O_2$ cells containing 1.0M $LiPF_6$ EC+EMC+MB (20:20:60 vol %) electrolytes with and without additives at - 40°C.

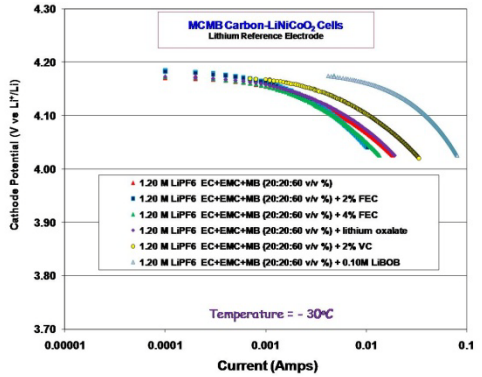

Figure IV- 87: Tafel Polarization measurements of the cathodes of MCMB-$LiNi_XCo_{1-X}O_2$ cells containing 1.0M $LiPF_6$ EC+EMC+MB (20:20:60 vol %) electrolytes with and without additives at - 30°C.

In summary, we have demonstrated improved performance with a number of wide operating temperature electrolytes containing ester co-solvents (i.e., methyl propionate and ethyl butyrate). In Quallion prototype cells we demonstrated over 60% of the room temperature capacity can be obtained at -40°C at a 5C rate. In addition, we demonstrated reasonable cycle life over a wide temperature range (-40 to +70°C).

We have also developed a number of methyl propionate and methyl butyrate containing electrolytes that contain various additives intended to improve the high temperature resilience. With these solutions, improved low temperature performance was obtained with many formulations, which has been attributed to improved low temperature electrode kinetics.

We have also studied the degradation modes of these systems when exposed to high temperature cycling. Formulations possessing FEC, LiBOB, lithium oxalate, and VC have shown promise in experimental cells. These electrolytes have been investigated with many chemistries (i.e., $LiNiCoO_2$, $LiNiCoAlO_2$, $LiNi_{1/3}Co_{1/3}Mn_{1/3}O_2$, $Li(Li_{0.17}Ni_{0.25}Mn_{0.58})$), with a current emphasis upon attempting to improve the life characteristics, especially at higher temperatures.

Future work will involve continuing the investigation of the use of additives in conjunction with ester-based wide operating temperature range electrolytes, with a focus upon (i) assessing other candidate additives, (ii) studying the high temperature and cycle life degradation modes, (iii) correlating electrochemical trends with performance, and (iv) identifying performance limiting aspects at extreme temperatures. These electrolytes will be investigated using a number of different chemistries, including high voltage systems. Effort will also be devoted to demonstrating these systems in prototype cells, such as in LiFePO-based cells (A123Systems) and $LiNiCoO_2$ cells (Yardney).

Collaborations

During the course of this program, we have collaborated with a number of institutions, including: (a) Univ. Rhode Island (Brett Lucht: perform analysis of harvested electrodes, on-going collaborator), (b) Argonne National Laboratory (Khalil Amine: source of electrodes, on-going collaborator), (c) Material Methods, LBNL (John Kerr) (evaluation of novel salt, *ex situ* analysis), (d) A123Systems, Inc. (electrolyte development, on-going collaborator), (e) Quallion, LCC. (electrolyte development, on-going collaborator), (f) Yardney Technical Products (electrolyte development, on-going collaborator), (g) Saft America, Inc. (collaborator, industrial partner under NASA program), and (f) NREL (Smith/Pesaran) (supporting NREL in model development by supplying data).

FY 2010 Publications

1. M. C. Smart, B. V. Ratnakumar, A. S. Gozdz, and S. Mani, *ECS Trans.* **25** (36), 37 (2010).
2. M. C. Smart, B. V. Ratnakumar, F. C. Krouse, W. C. West, and L. W. Whitcanack,2010 Space Power Workshop, Manhattan Beach, CA, April 22, 2010.
3. M. C. Smart, B. V. Ratnakumar, M. R. Tomcsi, M. Nagata, V. Visco, and H. Tsukamoto, 2010 Power Sources Conference, Las Vegas, NV, June 16, 2010.
4. M. Tomcsi, M. Nagata, H. Tsukamoto, M. C. Smart, and B. V. Ratnakumar, 2010 Space Power Workshop, Manhattan Beach, CA, April 22, 2010.
5. M. C. Smart, B. V. Ratnakumar, K. B. Chin, and L. D. Whitcanack, *J. Electrochem. Soc.,* in press.

IV.B.4.5 Novel Phosphazene-Based Compounds to Enhance Electrolyte Safety and Stability for High Voltage Applications (INL)

Kevin L. Gering, PhD

Idaho National Laboratory (INL)
2525 N. Fremont Ave.
Idaho Falls, ID 83415-2209
Phone: (208) 526-4173; Fax: (208) 526-0690
E-mail: kevin.gering@inl.gov

Collaborators:
Mason K. Harrup, Harry W. Rollins, Sergiy V. Sazhin, Fred F. Stewart, INL
Princess Energy Systems

Start Date: January, 2009
Projected End Date: ongoing

Objectives

Our focus is on producing electrolyte compounds resilient in both temperature and voltage regimes, while meeting a competitive baseline performance in transport properties and SEI characteristics. We seek compounds that will:

- enable the use of advanced higher-voltage electrode couples,
- promote better safety performance under abuse conditions,
- provide enhanced cell life.

Another objective is to gain understanding of molecular-scale interactions between phosphazenes and other electrolyte species and cell components.

Technical Barriers

Safety and longevity of Li-ion batteries continues to be an issue for future vehicular applications. This is complicated by the drive toward higher voltage cells (5V+) and some usage patterns and conditions that would cause batteries to operate at higher temperatures.

A viable alternative electrolyte for Li-ion batteries must simultaneously meet multiple criteria regarding transport properties, SEI film formation, voltage stability, flammability, aging mechanisms, chemical compatibility, etc. A fundamental challenge remains to reduce viscosity to competitive levels to maintain attractive transport properties, and some success has been had toward that goal.

Technical Targets

With regard to higher voltage systems, our targets are split between two veins of research:

- Phosphazenes as primary solvents (>50%) to greatly reduce electrolyte flammability. These must meet specific requirements in the resultant electrolytes to approach a competitive basis (e.g., room temperature viscosity of salted electrolyte less than 5 cP, conductivity greater than 6 mS/cm, and lithium salt solubility at least 0.7 M).
- Phosphazenes as additive solvents (<20%) to enhance chemical/thermal stability of the bulk electrolyte and improve SEI properties in terms of thermal runaway and stability over life.

Accomplishments

- Early generations of phosphazene solvents have been synthesized and characterized.
- More efficient and economical synthesis routes have been found for some classes of compounds to decrease electrolyte cost.
- Electrolyte blends for key phosphazenes have been characterized by multiple methods (conductivity, viscosity, CV, etc.), using a baseline system of EC:EMC (2:8) + 1.2M $LiPF_6$.
- We have determined that low amounts of phosphazenes greatly enhance the chemical/thermal stability of the baseline electrolyte, as evidenced in prolonged studies performed at 60°C.
- Coin cell testing has been performed for the most promising candidates to determine behavior of the phosphazenes within the cell environment and SEI characteristics.

✧ ✧ ✧ ✧ ✧

Introduction

Electrolytes play a central role in performance and aging in most electrochemical systems. As automotive and grid applications place a higher reliance on electrochemical stored energy, it becomes more urgent to have electrolyte components that enable optimal battery performance while promoting battery safety and longevity.

Safety remains a foremost concern for widespread utilization of Li-ion technology in electric-drive vehicles, especially as the focus turns to higher voltage systems. This work capitalizes on the long established INL expertise regarding phosphazene chemistry, aimed at battery-viable compounds that are highly tolerant to abuse. Various references document or relate to this work [1-6].

Approach

The general heterocyclic phosphazene structure is given in Figure IV- 88.

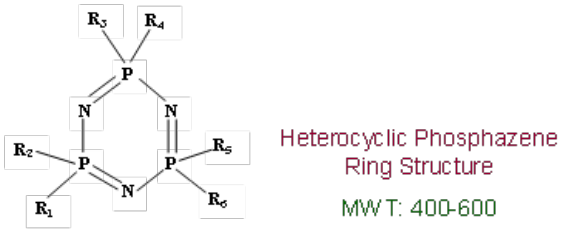

Figure IV- 88: Heterocyclic phosphazene structure

A change of chemical structure in the ring pendant arms has a strong influence on electrolyte properties, performance, and longevity in a higher-voltage system (5V+) and at higher temperatures. By customizing the pendant structures we seek to improve transport properties while increasing flash point and having acceptable SEI characteristics and cell aging. We are seeing progress in this fundamental challenge, and are aware of both the benefits and challenges tied to such compounds. Benefits include inherent stability and non-flammability, very low vapor pressure, good lithium salt dissolution, and choice of R groups (pendant arms) can be customized to precisely engineer properties. Challenges include high viscosity and the need to attenuate N:Li^+ attraction that occurs due to electron doublet transfer.

Our early generation compounds have been derived from the following four groups:

SM: employs ether groups attached to the phosphorus centers
AL: employs unsaturated analogues of the SM series
FM: employs fluorinated analogues of the SM series
AP: based on an ionic liquid structure.

Synthesis work continues to find efficient routes to several different phosphazene-based ionic liquid electrolyte solvents. The ionic liquid variant helps to mitigate some of the limitations seen with traditional cyclic phosphazenic solvents, such as N:Li^+ association that can adversely affect conductivity. Non-cyclic phosphazene compounds are also being targeted, and salts other than $LiPF_6$ are being considered.

Coin cells (type 2032) were used to test candidate electrolytes in an actual cell environment. The electrode pair consisted of a $LiCoO_2$ cathode and a carbon anode made by Piotrek, having an effective rated capacity of around 2.2 mAh/cm^2. Coin cell testing covers issues of formation, interfacial impedance, polarization testing, and aging. We continue to seek other ABR-relevant electrode pairs to test with our materials, and desire collaboration with ANL to achieve this objective.

Results

Based on the four groupings of compound structures, early generations of phosphazene solvents have been synthesized (AL4, AL5, SM4, SM5, SM6, SM7, FM1, FM2, AP1). Early characterization was performed to help screen the compounds and their electrolytes for the intended application within Li-ion cells. Cell testing has also been performed using selected compounds in the electrolyte to determine the effect of the compounds on the SEI formation process and rate of aging. Figure IV- 89 to Figure IV- 93, Table IV- 4, and Table IV- 5 provide examples of data and methods.

Table IV- 4: Viscosity of Selected INL Phosphazene Additives at Room Temperature with and without Salt

Recent SM compounds have reduced viscosity!

Formulation	Viscosity neat (cP)	Viscosity sat. w/$LiPF_6$ (cP)
AL-2	68	305
AL-3	46	440
SM-1	58	605
SM-2	39	1750
SM-3	27	640
SM-4	21	260
SM-5	18	45

Table IV- 5: Salt Saturation Limits ($LiPF_6$) in INL Phospazenes at Room Temperature

Formulation	Solubility limit (mM)
AL-2	n/a
AL-3	860
SM-1	950
SM-2	950
SM-3	880
SM-4	840
SM-5	660

An important finding in 2010 was that the presence of INL phosphazene additives promotes chemical stability of the baseline electrolyte, making it more tolerant to higher temperatures. In Figure IV- 89 the result of our stability testing is summarized for tests maintained at 60°C for a minimum of 60 days. The coloration of the baseline electrolyte over time is due to degradation processes, resulting in a thick, dark mass at 60 days, while the colors of the phosphazene containing samples were largely unchanged over the study.

Regarding transport properties, we closely monitor how the choice of pendant groups affects quantities such as electrolyte viscosity and conductivity. Figure IV- 90 and Figure IV- 91 provide a comparison between SM4, SM5, and FM1. The differences seen can be attributed to molecular-scale quantities and interactions.

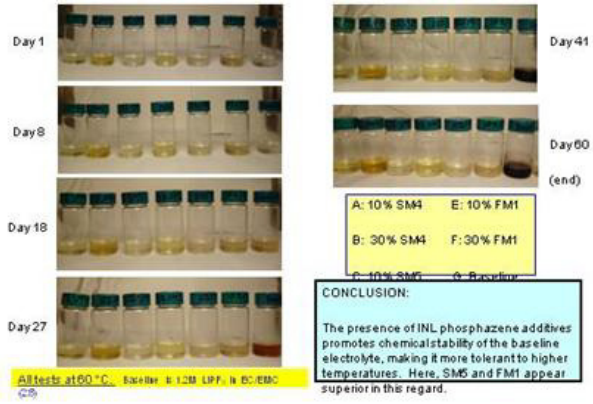

Figure IV- 89: Results of Stability Testing

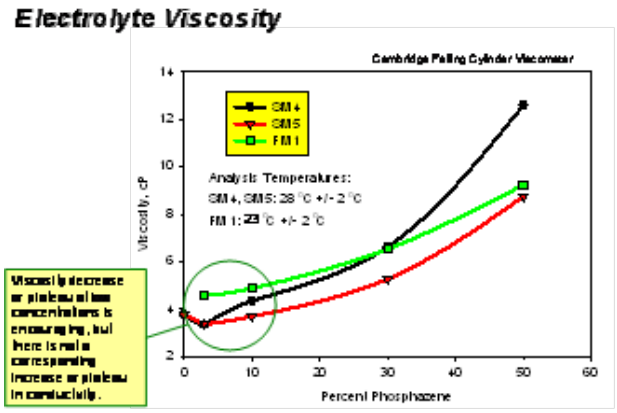

Figure IV- 90: Electrolyte Viscosity Comparison

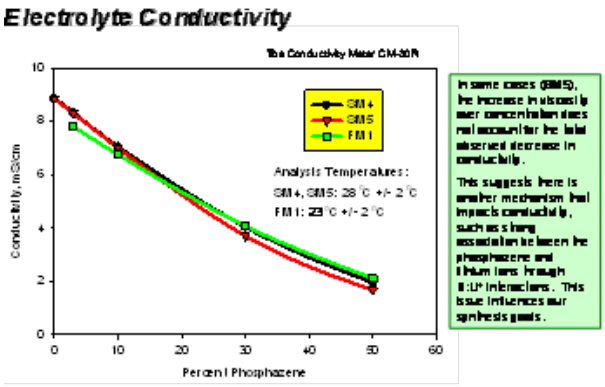

Figure IV- 91: Electrolyte Conductivity Comparison

In FY 2010 we developed and validated a new method and parameters for SEI and electrolyte characterization. The new parameters are SEI formation capacity and SEI maintenance rate, as denoted in Figure IV- 92. The method was presented at a recent meeting [2], and followed by a paper [3]. For example, SM4 and SM5 additives have a greater effect on the reductive stability at the negative electrode, compared to the baseline. This results in a more prolonged SEI formation process that will likely yield a higher interfacial impedance at the negative electrode. These additives act to moderate the oxidative processes at the positive electrode, and hence slightly enhance stability at higher voltages. Thus, if cell voltages are kept above OCV, then some overall benefit is seen with regard to voltage tolerance. SM5 is a good choice under these conditions, as seen in comparison of Figure IV- 93.

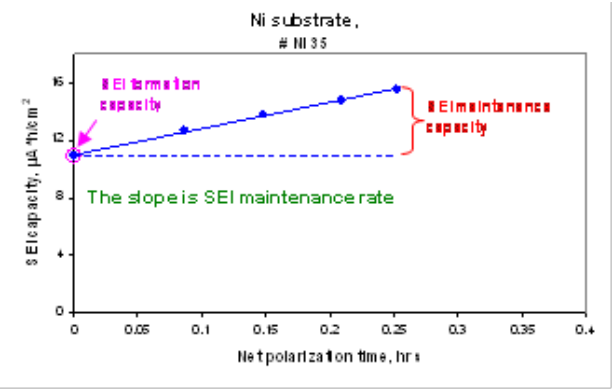

Figure IV- 92: SEI Formation Capacity and Maintenance Rates

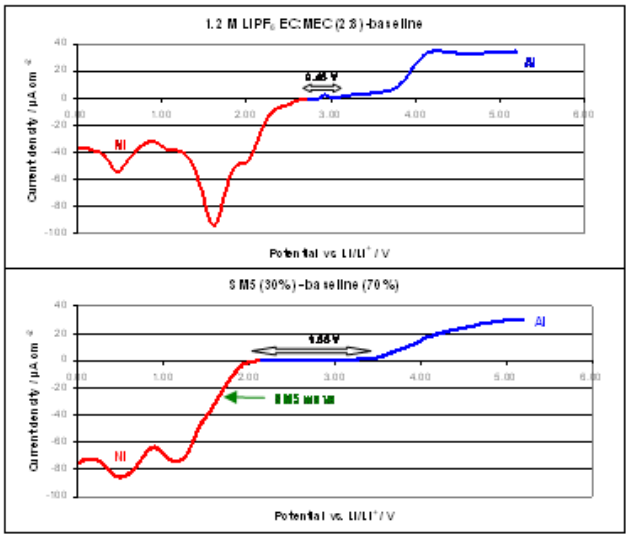

Figure IV- 93: SM4 and SM5 Comparisons

Later in 2010, activity was focused on expansion and refinement of the voltammetry method. A newer variation allows us to characterize SEI transport properties at OCV and under polarization. At OCV, the evaluating parameter

is SEI corrosion (degradation) rate. At polarization, the parameter is still SEI maintenance rate however under only potentiostatic polarization. Focus of the work was on improving the test protocol, experimental procedures, and overall accuracy and reproducibility of the new method variation. Validation of this version has started. After completion, a more precise and sensitive method will be available to characterize new electrolytes and their SEIs.

Lastly, in a small pass/fail study we are also looking at the feasibility of synthesizing complementary intercalative phosphazenic host materials. Such solid-state hosts will promote chemical compatibility between electrolyte and electrode materials, and could improve SEI performance. Results from this solid-state study are formative at this point, and we will work closely with DOE in tracking our progress in this area.

Conclusions and Future Directions

Early work with INL phosphazene materials has shown benefit toward enhanced electrolyte stability in terms of voltage and elevated temperature. We have seen how the choice of the pendant R groups can have a profound influence on electrolyte properties tied to fate and performance within Li-ion cells. Characterization is ongoing, and will indicate whether these compounds provide superior SEI-forming qualities and transport properties compared to other compounds. In future months a new vapor pressure analyzer will help determine how much phosphazenes suppress electrolyte vapor pressure. A new 600 MHz NMR spectrometer will allow for more detailed studies of molecular interactions in new and aged electrolyte formulations.

We will also explore electrolyte systems having mostly phosphazene solvents to exploit the inherent low flammability of these additives, wherein non-cyclic phosphazene compounds will be targeted to reduce viscosity. Newer compounds (e.g., FM and AP series) will indicate whether these structures provide superior benefit compared to other phosphazenes. Half-cell studies on SEI will be considered. More CV work is planned to look at specific interactions between phosphazene-based electrolytes and cell components such as ABR electrode active materials. Salts other than $LiPF_6$ will be considered (e.g., LiFBOB, LiTFSI), to avoid possible detrimental interactions between phosphazenes and anions over voltage. The best candidate electrolytes will be sent to SNL for abuse-tolerance testing.

FY 2010 Publications/Presentations and Other Relevant Citations

1. K. L. Gering, “Novel Compounds for Enhancing Electrolyte Stability and Safety of Lithium-ion Cells”, 2010 DOE-VTP Annual Merit Review Meeting Presentation, Project ES027.
2. S. V. Sazhin, M. K. Harrup, K. L. Gering, Characterization of Low-Flammability Electrolytes for Lithium-ion Batteries, International Battery Association Meeting and Pacific Power Source Symposium, January 11-15, 2010, Waikoloa, HI.
3. S. V. Sazhin, M. K. Harrup, K. L. Gering. Characterization of Low-Flammability Electrolytes for Lithium-ion Batteries. J. Power Sources, in press (journal ref – Power 13566).
4. M. K. Harrup, J. R. Delmastro, F. F. Stewart, T. A Luther, Safe Battery Solvents, U. S. Patent 7,285,362 B2, 2007.
5. M. K. Harrup, J. R. Delmastro, F. F. Stewart, T. A Luther, Safe Battery Solvents, U. S. Patent Application 2008/0096056 A1, 2008.
6. Invention Disclosure Record BA-342, “Phosphazene-based ionic liquids (PhIL) as candidate solvents for battery and capacitor electrolytes”, K. L. Gering, M. K. Harrup, and H. W. Rollins (Idaho National Laboratory).

IV.C Calendar and Cycle Life Studies

IV.C.1 Diagnostics and Modeling

IV.C.1.1 Electrochemistry Cell Model (ANL)

Dennis W. Dees

Argonne National Laboratory (ANL)
9700 South Cass Avenue
Argonne, IL 60439-4837
Phone: (630) 252-7349; Fax: (630) 972-4520
E-mail: dees@anl.gov

Collaborators:
Kevin Gallagher, ANL
Daniel Abraham, ANL
Sun-Ho Kang, ANL
Andrew Jansen, ANL
Wenquan Lu, ANL
Kevin Gering, INL

Start Date: October, 2008
Projected End Date: September, 2010

Objectives

The objective of this work is to correlate analytical diagnostic results with the electrochemical performance of advanced lithium-ion battery technologies for PHEV applications.

- Link experimental efforts through electrochemical modeling studies.
- Identify performance limitations and aging mechanisms.

Technical Barriers

The primary technical barrier is the development of a safe, cost-effective PHEV battery with a 40 mile all electric range that meets or exceeds all performance goals.

- Interpreting complex cell electrochemical phenomena.
- Identification of cell degradation mechanisms.

Technical Targets

- Complete development of the two-phase active material model.
- Initiate development of capacity loss model.
- Complete development of an efficient parameter fitting method.

Accomplishments

- Further development and evaluation of phase transition lithium diffusion transport model for two-phase electrode active materials (e.g. LiC_6, $LiFePO_4$, $LiMn_2O_4$, $Li_4Ti_5O_{12}$).
  - Model simulations indicate the coexistence of three phases (i.e. Stage 1, Stage 2, and Stage 3) in graphitic negative electrodes (MCMB, Gen 3) during normal cell operation.
  - Model was modified to account for coexistence of three phases and changes were integrated into full cell model.
  - Initiated study of second graphite negative electrode (Mag 10, PHEV baseline).
- Initiated development of capacity loss degradation model.
  - Conducted literature review and considered possible phenomena.
  - SEI model developed to examine growth mechanisms.
- Supported other development efforts in program.
  - Integrated improved electrode impedance and limiting current estimates into Argonne's Battery Design and Cost Model.
  - Developed spherical geometry four probe conductivity model for single particle conductivity measurements.
  - Initiated modeling studies on binder-carbon-free electrodes to examine primary-secondary active particle microstructure and interactions.

✧ ✧ ✧ ✧ ✧

Introduction

The electrochemical modeling effort is aimed at associating electrochemical performance measurements with post-test diagnostic studies conducted on lithium-ion cells. The methodology for the electrochemical model is

described in detail in the literature.[13,14,15] Two versions of the model are utilized in this effort. One version of the electrochemical cell model is used to simulate the cell response from Electrochemical Impedance Spectroscopy (EIS) studies, and the other model version is utilized for examining DC studies, such as controlled current or power cycling and diagnostic HPPC tests. The underlying basis for both models is the same, as well as their parameter set.

The general methodology for the electrochemical model follows the work of Professor Newman at Berkeley. Continuum based transport equations using concentrated solution theory describe the movement of salt in the electrolyte. Volume-averaging of the transport equations accounts for the composite electrode geometry. Electrode kinetics, thermodynamics, and diffusion of lithium in the active material particles are also included. The detailed theoretical description of the active material/electrolyte interface, commonly referred to as the solid electrolyte interphase, or SEI, is based on post-test analytical diagnostic studies. The SEI region is assumed to be a film on the active material and layer at the surface of the active material. The film is taken to be an ill-defined mixture of organic and inorganic material through which Li-ions from the electrolyte must diffuse to react electrochemically at the surface of the active material. The lithium is then assumed to diffuse through the surface layer and into the bulk active material in the particle. Capacitive effects are incorporated into the model at the electrochemical interfaces and a localized electronic resistance between the current carrying carbon and the oxide interface can also be included. The model can also accept multiple particle fractions with unique characteristics.

Approach

The approach for electrochemical modeling activities is to build on earlier successful HEV characterization and modeling studies in extending efforts to PHEV technologies. The HEV studies involved developing a model based on the analytical diagnostic studies, establishing the model parameters, and conducting parametric studies with the model. The parametric studies were conducted to gain confidence with the model, examine degradation mechanisms, and analyze cell limitations. Efforts this year have focused on expanding and improving the model's capabilities.

Results

Development has continued on the phase transition lithium diffusion transport model initiated last year for two-phase electrode active materials (e.g. LiC_6, $LiFePO_4$, $LiMn_2O_4$, $Li_4Ti_5O_{12}$). Early development of a modified shell-core two-phase active material model that focused on describing the graphite active material was able to adequately account for cell potential changes associated with the transport of lithium in the graphite, but the relatively slow phase transition rate suggested that the two-phase boundary may occur over a region rather than at an interface. Further, literature studies suggest that the shell-core model is not generally correct for lithium-ion active materials.[16]

The lithium transport model includes lithium diffusion in both phases of the active material and equilibrium at the interfaces between active phases. Volume averaged transport equations are used inside the particle and the well known Avrami phase growth equation[17] (see Equation 1) with a lithium concentration dependent rate constant (k in Equation 1) is used to describe the phase transition. In Equation 1, ε_S is the volume fraction of the phase, t is time, and n is related to the dimensionality of the phase change.

$$\varepsilon_{S2} = 1 - e^{-(kt)^n} \quad [1]$$

The Avrami, equilibrium, and diffusion equations were integrated into the full electrochemical cell model in such a way as to minimize the number of additional variables.

For the model, the open circuit voltage curve (shown in Figure IV- 94 for the Gen 3 MCMB graphite electrode) is used to establish the single and two-phase regions, as well as the lithium concentration equilibrium relationships between phases. The single phase regions are indicated by the tinted regions in Figure IV- 94. For simplicity, Stages greater than Stage 2 are treated as Stage 3.

[13] D. Dees, E. Gunen, D. Abraham, A. Jansen, and J. Prakash, *J. Electrochem. Soc.,* **152** (7) (2005) A1409.
[14] D. Abraham, S. Kawauchi, and D. Dees, *Electrochim. Acta,* **53** (2008) 2121.
[15] D. Dees, E. Gunen, D. Abraham, A. Jansen, and J. Prakash, *J. Electrochem. Soc.,* **155** (8) (2008) A603.
[16] J. Allen, R. Jow, and J. Wolfenstine, *Chem. Mater.* **19** (2007) 2108.
[17] *Phase Transformations in Metals and Alloys*, D. Porter and K. Easterling, New York: Van Nostrand Reinhold, 1981.

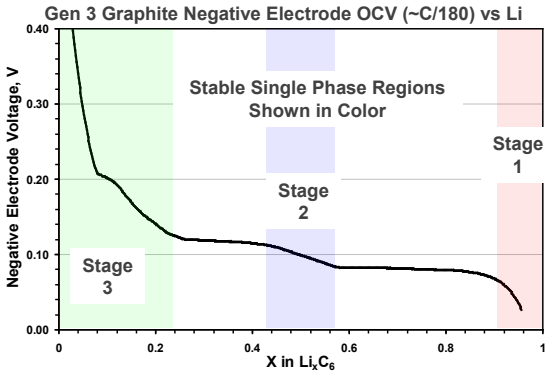

Figure IV- 94: Slow discharge curve of MCMB graphite negative electrode showing tinted single phase regions.

As the cell is discharged, the lithium concentration in each phase drops. When the lithium concentrations in each phase falls below its stability limit (i.e. outside the tinted single phase regions in Figure IV- 95) the lower concentration phase begins to form following the Avrami equation. As shown in Figure IV- 95, early modeling studies with the two-phase model on the graphite negative electrode indicated that the lithium concentration in both phases could drop below their stability limit. As a result, the phase growth model was modified to allow for the coexistence of three phases. Further, the changes were integrated into the full cell DC electrochemical model.

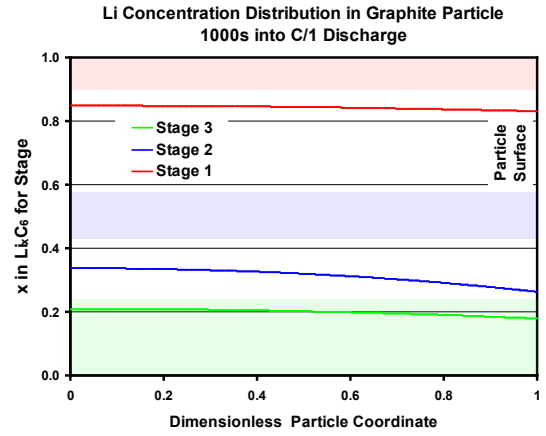

Figure IV- 95: Lithium concentration distribution in particle for each phase. The tinted regions are the stable concentration ranges for each stage (red for Stage 1, blue for Stage 2, and green for Stage 3).

Fast lithium diffusion through the graphite particles allows for high lithium transport rates (i.e. the electrode is able to support high current densities). This is illustrated by the relatively flat lithium concentration gradients shown in Figure IV- 95. However, the slow phase transition rate constant accounts for the electrode's apparent sluggishness to reach equilibrium as indicated by the MCMB graphite electrode's slow relaxation in the two-phase regions after a current pulse. The sluggishness of the electrode can also be seen in its hysteresis when cycling at very slow rates (e.g. C/50), which can at least qualitatively be accounted for by the electrochemical model.

As described above, a slow transition rate constant can allow for the coexistence of more than two phases during operation, as shown by Figure IV- 96, Figure IV- 97, and Figure IV- 98. Figure IV- 96 shows the change in volume fraction for each Stage of a fully charged MCMB electrode being discharged at a C/50 rate. While the region where all three stages coexist is relatively small, it does serve to indicate that the electrode is not fully at equilibrium, even at this slow rate. At a C/10 rate (see Figure IV- 97) the region where all three stages coexist is a significant fraction of the total discharge and it is even more extensive at a C/1 rate (see Figure IV- 98).

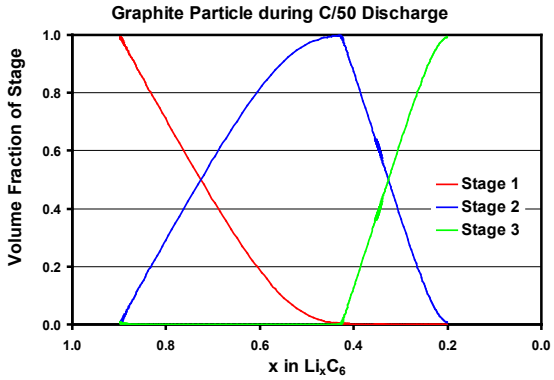

Figure IV- 96: Graphite MCMB electrode volume fraction of each Stage during a C/50 discharge.

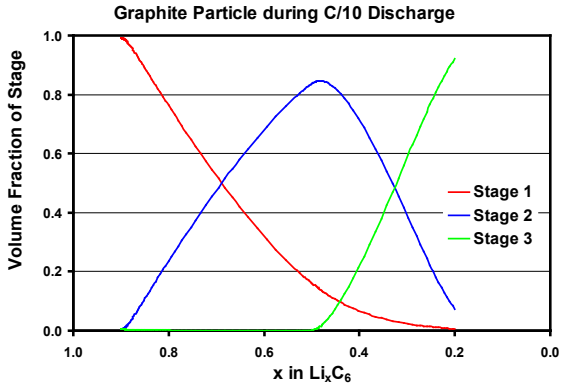

Figure IV- 97: Graphite MCMB electrode volume fraction of each Stage during a C/10 discharge.

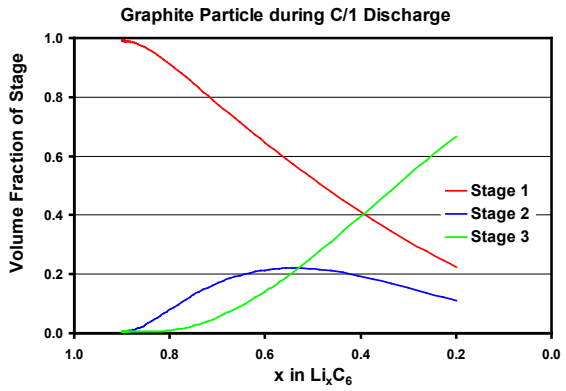

Figure IV- 98: Graphite MCMB electrode volume fraction of each Stage during a C/1 discharge.

Progress was also made in several other areas that will only be mentioned here. Development of a capacity loss degradation model was initiated. Specifically, an extensive literature review was conducted, producing a number of possible phenomena and mechanisms that were considered. Further, an SEI model was developed to examine various growth mechanisms. The modeling effort was also able to integrate improved electrode impedance and limiting current estimates into Argonne's Battery Design and Cost Model. In addition, a spherical geometry four probe conductivity model was developed and utilized for analysis of single particle conductivity measurements. Finally, a modeling study on binder-carbon-free electrodes to examine primary-secondary active particle microstructure and interactions was initiated.

The equivalent circuit interfacial model previously developed has greatly streamlined electrode parameter estimation for the full cell electrochemical model. However, a complete impedance model optimization program is needed to efficiently fit all the active material parameters, specifically the parameters associated with the low frequency impedance. Work on this effort has been suspended until an efficient parameter optimization software package could be identified that would easily interface to the EIS electrochemical model and data.

Conclusions and Future Directions

The phase transition lithium diffusion transport model for two-phase active materials adds much to the understanding of these materials while at the same time not increasing greatly the complexity of the complete cell electrochemical model. Further work needs to be done on developing an EIS version of the phase change electrochemical model. Finally, the model should be exercised on several lithium-ion battery technologies.

With most lithium-ion PHEV technology battery packs having excess power, the primary concern for performance degradation becomes capacity loss. Development of a capacity loss degradation model has been initiated and will be continued in the next fiscal year. The capacity loss degradation model will need to be integrated into the full cell electrochemical model. Further, continued development of PHEV technology electrochemical models is needed such as examining alternative materials, additives, and testing protocols.

Other ABR projects will be supported as needed. As an example, a multi-layer four probe conductivity model previously developed was improved to support the materials screening and electrode optimization efforts. There also remains needed improvements in the DC electrochemical model such as including non steady-state interfacial effects and adding the capability for multiple active material particle fractions.

FY 2010 Publications/Presentations

1. 2010 DOE Annual Peer Review Meeting Presentation, Jun 7th-11th 2010, Washington DC.

IV.C.1.2 Diagnostic Studies on Li-Battery Cells and Cell Components (ANL)

Daniel P. Abraham

Argonne National Laboratory
9700 South Cass Avenue
Argonne, IL 60439-4837
Phone: (630) 252-4332; Fax: (630) 972-4406
E-mail: abraham@anl.gov

Collaborators:
D. Dees, Argonne National Laboratory
A. Jansen, Argonne National Laboratory
G. Cheng, Argonne National Laboratory
S. Trask, Argonne National Laboratory
J. Bareño, Argonne National Laboratory
I. Petrov, University of Illinois at Urbana-Champaign
B. Lucht, University of Rhode Island

Start Date: October, 2008
Projected End Date: September, 2014

Objectives

The objective of this study is to identify factors that contribute to cell performance degradation (capacity fade, impedance rise) on long-term storage/cycling. Identifying sources of cell performance degradation is an important step towards modifying the cell chemistry to attain the 15 year life (for example, by electrolyte additives that modify the electrode surfaces).

Technical Barriers

This project addresses the following technical barriers to the development of a PHEV battery with a 40 mile all electric range that meets or exceeds all performance goals.

- Cell performance, life, and safety.

Technical Targets

Develop electrode couples and electrolytes that will meet the performance, life, and safety targets of cells for PHEV applications.

Accomplishments

- Completed studies on "Gen3" cells and cell constituents. These studies included cell disassembly, electrochemical and physicochemical characterization of harvested cell components, and determining sources of performance degradation.
- Initiated characterization of PHEV baseline electrodes and aging studies on cells with these electrodes.
  - Electrochemical cycling and impedance (EIS and HPPC) data were obtained on electrodes and full cells. Data obtained on these electrodes and cells are similar to those obtained for cells with ATD-Gen2 chemistry, which have a comparable chemistry.
- Examined the effect of impurities and moisture on LiBOB electrolyte performance in lithium-ion cells
  - Cycling, impedance, NMR, FTIR, and TGA data were obtained to identify impurities responsible for inconsistency in salt performance. Formulated reaction mechanisms based on the data

✧ ✧ ✧ ✧ ✧

Introduction

The performance and performance degradation of materials and cells being developed for PHEV purposes are being studied. These cells contain (a) electrode materials that are new or modified versions of current chemistries, (b) novel electrolytes, or additives to current electrolytes, to enhance cell performance and life, (c) changes in cell testing conditions that include wider voltage windows and greater state-of-charge (SOC) swings, etc. The degradation mechanisms associated with various cell chemistries and testing conditions will be identified to determine suitable electrode-electrolyte combinations that will meet the goals of PHEV batteries. We will also continue examination of electrode surface films after formation cycling in cells containing various electrolytes and electrolyte additives. Some of these experiments will be conducted on model electrodes, such as binder-free graphite electrodes and binder- and carbon-free oxide electrodes.

Approach

We typically employ electrochemical and physicochemical techniques for our diagnostic studies. Our electrochemical measurements are conducted in cells that include coin cells, pouch cells, and reference electrode cells to determine cell performance, performance degradation characteristics, and degradation sources. Our physicochemical examinations employ a combination of spectroscopy, microscopy, diffraction and chemical analysis techniques that include scanning and transmission electron microscopy, energy dispersive spectroscopy, electron energy loss spectroscopy, X-ray diffraction, X-ray

photoelectron spectroscopy, Fourier transform infrared spectroscopy (FT-IR) with attenuated total reflectance (ATR), and nuclear magnetic resonance (NMR) spectroscopy.

Results

Testing of sample PHEV electrode materials and cells is currently in progress. These cells contain a layered oxide based positive and a graphite based negative electrode (see Table IV- 6, and Figure IV- 99). The baseline electrolyte is 1.2 M $LiPF_6$ in 3EC:7EMC (by wt.); some cells contain 1 to 2 wt% vinylene carbonate (VC). The cells are aged under various conditions with periodic interruptions for reference performance tests to gauge cell capacity and impedance changes as a function of aging.

Table IV- 6: Electrode composition and constitution

	Cathode (+)	Anode (-)
Composition		
Active	84% LiNi0.8Co0.15Al0.05O2	95% Mag-10 graphite
	4 wt% SFG-6 graphite	
	4 wt% Super P	
Binder	8% PVDF (KF1120)	5% Binder (SBR+CMC)
Loading Density		
Coating	18.8 mg/cm^2	10.8 mg/cm2
Active Material	**15.8 mg/cm2**	**10.3 mg/cm2**
Thickness		
Current Collector	**Al - 22 µm**	**Cu - 10 µm**
Electrode Coating	**65**	**79**
Total	**87**	**89**

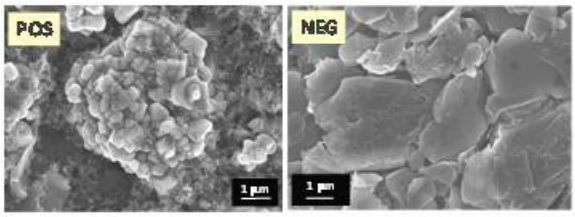

Figure IV- 99: SEM images of the PHEV baseline positive and negative electrodes.

Figure IV- 100 contains typical data that show the first few cycles on this PHEV cell. The electrochemical efficiency in the first cycle is ~86% (~C/10) and greater than 99.7% in subsequent cycles. The cells display a capacity of ~170 mAh/g (positive-limited) at 30°C in the 3-4.1V voltage window. Because the electrodes are thicker than typical HEV cell electrodes, "electrode-wetting" features are sometimes observed in the data.

Figure IV- 101 shows data from a cell that contained a Li-Sn reference electrode (RE). It is apparent from the figure that when the full cell is charged from 3 to 4.1V, the positive electrode voltage varies from 3.5 to 4.15V, whereas the negative electrode voltage varies from 0.5 to 0.05V. The discharge cycle data is a mirror image of the charge cycle data.

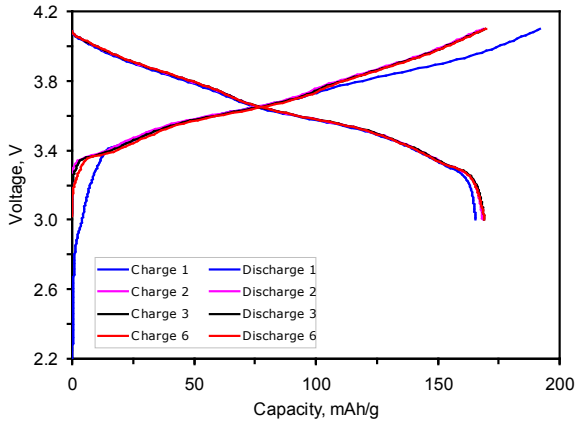

Figure IV- 100: First few cycles on a PHEV baseline cell, 30°C.

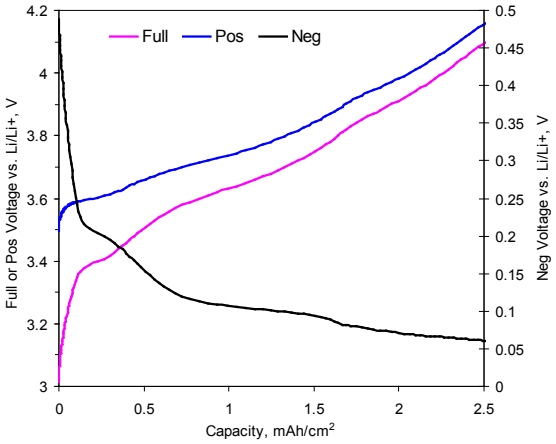

Figure IV- 101: RE cell data (after formation cycling) showing positive and negative electrode voltage changes when the full cell voltage changes from 3 to 4.1V at a C/10 rate.

Figure IV- 102 shows AC impedance data from a cell held at 30, 40 and 55°C. It is apparent that cell impedance decreases with increasing temperature. Furthermore, this impedance reduction is seen in the mid-frequency arc, which is often attributed to processes at the electrode-electrolyte interface. Data from a RE cell indicated that these decreases are at both positive- and negative-electrode electrolyte interfaces.

Figure IV- 103 shows 18-s pulse discharge data from an HPPC test conducted at 30°C. The data indicate that up to a 5C discharge pulse, the cell impedance is roughly constant (~27 ohm-cm^2) between 3.5 and 4.0V. For a 10C pulse, however, the area specific impedance (ASI) rises rapidly below 3.67V. Corresponding data from a RE cell (not shown) indicate that this impedance increase arises at the positive electrode. A small impedance increase is also observed at the negative electrode for the 10C pulse.

Figure IV- 104 **Cycles (10^3)**shows initial aging data from a cell that was cycled between 3.6 and 4.0V at 45°C. The cell impedance rise, calculated at 30°C, was about 16% after 3000 C-rate cycles (data not shown); the cells also lost about 16% of its initial C/1 capacity during aging. The origin and mechanisms associated with this capacity fade will be explored in the coming year.

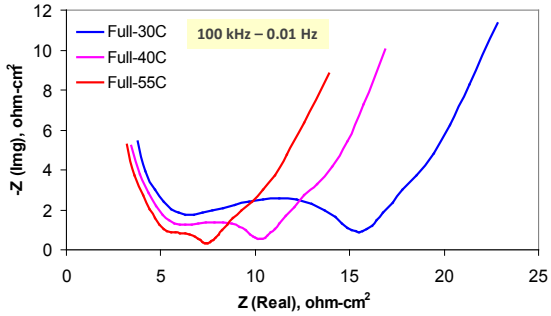

Figure IV- 102: EIS (Full Cell) data showing decreasing impedance with increasing cell temperature.

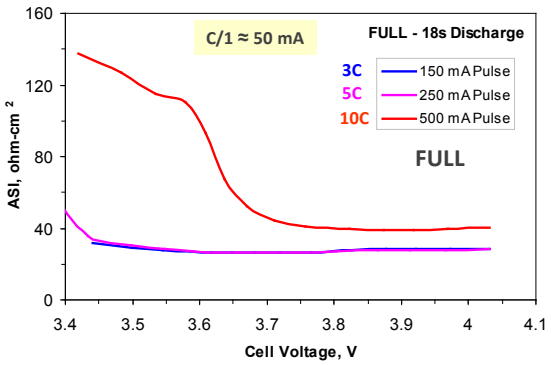

Figure IV- 103: HPPC (Full Cell) 18s discharge pulse (various magnitudes) data showing cell impedance at 30°C.

Conclusions and Future Directions

We've been studying the performance and performance degradation of sample PHEV cells. These cells contain a positive electrode with $Li(Ni_{0.8}Co_{0.15}Al_{0.5})O_2$, negative electrode with Mag-10 graphite, and 1.2 M $LiPF_6$ in 3EC:7EMC (by wt.) electrolyte. Initial data show that the cells are of low impedance and that the impedance rise is relatively slow during cycle-life aging at 45°C; the cells, however, display gradual loss of capacity.

In the coming year, we will examine performance and performance degradation of promising materials and electrochemical couples that have been identified by the ABR program. Cells containing these electrochemical couples will be examined and characterized under PHEV-battery relevant conditions.

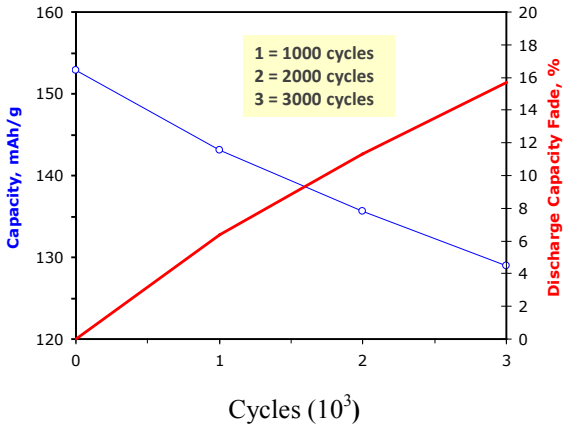

Figure IV- 104: Initial aging data showing capacity fade (calculated at 30°C) of a cell that completed 3000 C-rate cycles between 3.6 to 4.0V at 45°C.

FY 2010 Publications/Presentations

1. 2010 DOE Annual Peer Review Meeting Presentation
2. D.P. Abraham, D.W. Dees, J. Christophersen, C. Ho, A.N. Jansen, "Performance of High Power Lithium-Ion Cells under Pulse Discharge and Charge conditions", International Journal of Energy Research 34 (2010) 190.
3. L. Yang, M.M. Furczon, A. Xiao, B.L. Lucht, Z. Zhang, D.P. Abraham, **"**Effect of Impurities and Moisture on LiBOB Electrolyte Performance in Lithium-ion Cells", J. Power Sources 195 (2010) 1698**.**
4. A. Xiao, L. Yang, B.L. Lucht, S-H. Kang, D.P. Abraham, "Examining the Solid Electrolyte Interphase on Binder-Free Graphite Electrodes", J.Electrochemical Soc. 156 (2009) A318

IV.C.1.3 Structural Investigations of Layered Oxide Materials for PHEV applications (ANL)

Daniel P. Abraham

Argonne National Laboratory
9700 South Cass Avenue
Argonne, IL 60439-4837
Phone: (630) 252-4332; Fax: (630) 972-4406
E-mail: abraham@anl.gov

Collaborators:
J. Bareño, Argonne National Laboratory
S.-H. Kang, Argonne National Laboratory
M. Balasubramanian, Argonne National Laboratory
I. Petrov, University of Illinois at Urbana-Champaign
J.G. Wen, University of Illinois at Urbana-Champaign

Start Date: October, 2008
Projected End Date: September, 2014

Objectives

The structure and structural rearrangements in Li-bearing Mn-based layered oxides, which show anomalously high-capacities when cycled to high-voltages, have a significant effect on cell performance, calendar-life, and safety. The objective of this work is to obtain a detailed structural understanding of $Li_{1+a}(TM_{1-x}Mn_x)_{1-a}O_2$; TM=transition metal (Ni, Co, Cr, Fe, etc.). These oxides display significant differences between the long range crystal structure and local arrangements around individual atoms, which are important because the local atomic environments affect Li-ion transport, and hence the rate capability of the oxide.

Technical Barriers

This project addresses the following technical barriers to the development of a PHEV battery with a 40 mile all electric range that meets or exceeds all performance goals.

- Oxide/positive electrode/cell performance
- Cell calendar life
- Oxide stability/cell safety

Technical Targets

Our experiments are designed to answer various questions that include the following:

- What are the local atomic arrangements in the as-prepared oxides and how are these arrangements influenced by composition?
- What are the charge compensation mechanisms during oxide delithiation and lithiation, i.e., during electrochemical cycling?
- What phase transformations result on cycling/aging? How does this affect the oxide's capacity and rate performance?
- What are the correlations between the composition, structure, and performance for the various oxides?

Accomplishments

Detailed crystallographic data on high-quality Li_2MnO_3 material was obtained using a combination of experimental techniques. These experiments yielded the following information:

- Rietveld refinement indicated that the C2/m spacegroup provided the best fit for X-ray diffraction data.
- Electron diffraction patterns obtained along various zone axes, on defect-free oxide particles, could be uniquely indexed to the monoclinic structure.
- Electron microscopy images of defect-free grains showed a Li-Mn-Mn-Li arrangement (i.e., lithium ordering) in the transition metal planes.
- Low-magnification microscopy images occasionally revealed stacking defects within oxide particles that resulted in a trigonal local arrangement within the monoclinic sequence.

✧ ✧ ✧ ✧ ✧

Introduction

Lithium-bearing manganese-based layered oxides are promising positive electrode active material candidates to achieve high energy and power density lithium-ion batteries. However, the performance and calendar life of existing materials needs to be improved before widespread applications in plug-in hybrid (PHEV) and fully-electric vehicles (EV) can be realized. Despite considerable materials research over the last decade, the structure of common positive electrode materials, as well as its evolution upon cycling, and the atomistic mechanisms

responsible for these changes remains the subject of debate.

This project combines advanced structural characterization techniques, including X-ray diffraction, X-ray absorption spectroscopy (XAS), and analytical electron microscopy (AEM) to investigate atomistic rearrangements in lithium-bearing layered oxide materials during and after electrochemical cycling. Fundamental insights into the tradeoffs between oxide performance and stability will help define new design strategies for the next-generation of high-performance long-lasting batteries.

Approach

We have embarked on a multi-institution effort to synthesize, characterize, and model these complicated oxide structures. After oxide synthesis, structure examination by XRD, and initial electrochemical performance examination, we conduct both *ex situ* and *in situ* XAS measurements on the samples. These XAS studies, conducted at Argonne's Advanced Photon Source (APS), provide information on transition metal (TM) oxidation states, coordination characteristics around the TM atoms, and changes in these parameters during electrochemical cycling. Because the information obtained by XAS is an average over several grains, the data provides a snapshot of the oxide bulk that is used as a guide for analytical electron microscopy (AEM) study, which provides information on the local (<2 nm) structure and composition in the oxides. The AEM study includes electron diffraction and high angle annular dark field (HAADF) electron microscopy to examine the oxide's crystal structure at near-atomic spatial resolution and electron energy loss spectroscopy to examine composition variations in the 1 to 10 nm scale range.

Results

Structural studies of Li_2MnO_3 are of paramount interest because the compound represents one end member of the $Li_{1+a}(TM_{1-x}Mn_x)_{1-a}O_2$ family (x = 1, a = 1/3) of compounds, which are promising positive electrode materials because of their high capacity and thermal stability. Presently there is ongoing debate in the literature on whether these compounds form homogeneous solid solutions or contain ordered or partially disordered Li_2MnO_3 domains intergrown and integrated with the $LiTMO_2$ structure. We studied Li_2MnO_3 samples by electron microscopy to obtain structure standards that allow us to examine the possible presence of Li_2MnO_3 clusters in layered oxides of interest for PHEV applications.

Figure IV- 105(a) and Figure IV- 105(c) present experimental HAADF images of a Li_2MnO_3 sample recorded along two directions normal to the bonds in the hexagonal planes, henceforth referred to as A_1 or $[10\bar{1}0]$ (of the $R\bar{3}m$ structure) zone axis with the plane normal running vertical in the figure. The micrographs show, respectively, homogeneous parallelogram (P) and rectangular (R) patterns of bright and dark spots, originating from the projection of the sample structure as follows. In HAADF images the intensity in each pixel is, in general, proportional to the average atomic number. As light elements in Li_2MnO_3 contribute weakly to electron scattering at higher angles, HAADF images can be regarded as directly depicting atomic positions within the transition metal ($LiMn_2$) planes.

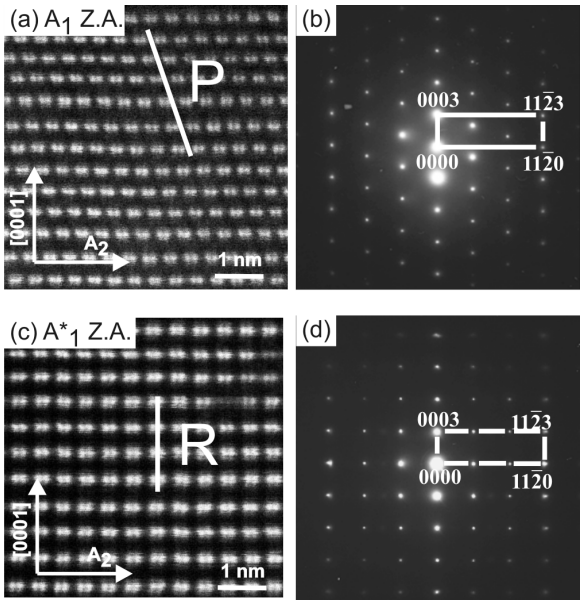

Figure IV- 105: HAADF-STEM micrographs and SAED patterns of high purity Li_2MnO_3 showing the $Li_{1/3}Mn_{2/3}$ plane stacking sequence.

Each row in Figure IV- 105(a) and Figure IV- 105(c) consists of a periodic sequence of two bright and one dark spot, which indicates a Li-Mn-Mn-Li arrangement (i.e., Li ordering) in the $LiMn_2$ planes.

The corresponding selected area electron diffraction (SAED) patterns, shown in Figure IV- 105(b) and Figure IV- 105(d), consist of very bright, sharp reflections indicating that the regular atomic ordering revealed in the micrographs is maintained over long distances within the sample. The white box drawn in these patterns indicates the reciprocal unit cell expected from the rhombohedral α-$NaFeO_2$ parent structure, while the presence of additional reflections at 1/3 $(11\bar{2}0)$ positions stems from the $\sqrt{3}\times\sqrt{3}-R\,30°$ ordering of the Li sublattice within $LiMn_2$ planes.

Figure IV- 106 presents a HAADF-STEM micrograph of high purity Li_2MnO_3 along the $[001]_M$ zone axis; i.e., 19° away from normal to $LiMn_2$ (001) planes. The micrograph shows a repeat motif consisting of a hollow hexagonal ring of sharp spots forming an overall

honeycomb pattern. The horizontal periodicity of the image is 0.47 nm, corresponding to the projection of the second-nearest neighbor interatomic spacing in the hexagonal planes. The spot spacing, measured along the undistorted [010] direction (vertical axis of the image), is 0.28 nm, corresponding to the nearest-neighbor distance within the hexagonal planes in Li_2MnO_3 (b/3 ≈ 0.284 nm).

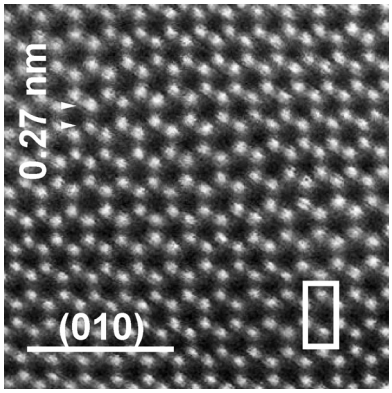

Figure IV- 106: HAADF-STEM micrograph of high purity Li_2MnO_3 showing the structure of the $Li_{1/3}Mn_{2/3}$ planes.

Figure IV- 107 presents a typical high resolution electron micrograph (HREM) image of an area of the sample containing stacking faults. The image is projected along the $[110]_M$ zone axis, the same as in Figure IV- 105. Stacking faults along the plane normal to the hexagonal closed packed TM planes are present within the basic monoclinic matrix.While most of the material shows the P-type pattern Figure IV- 105(a) typical for the monoclinic structure in this projection, there are R-type Figure IV-105(b) stacking meshes extending over only a few atomic distances.

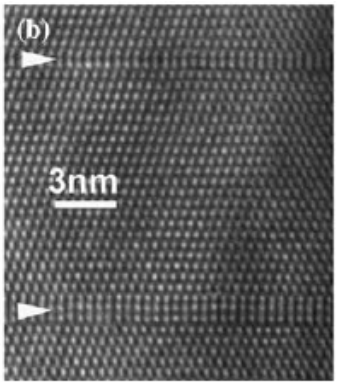

Figure IV- 107: HREM micrograph of high purity Li_2MnO_3 showing stacking faults corresponding to local rotations of the monoclinic lattice about the $Li_{1/3}Mn_{2/3}$ plane stacking direction.

Figure IV- 108 shows a HAADF image on an as-prepared $Li_{1.2}Co_{0.4}Mn_{0.4}O_2$ sample; the image shows a Li-Mn-Mn-Li sequence, which indicates the presence of Li_2MnO_3–like areas in **the sample.**

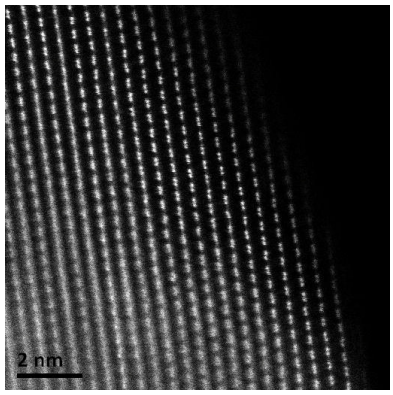

Figure IV- 108: $Li_{1.2}Co_{0.4}Mn_{0.4}O_2$ HAADF image showing Li-TM-TM contrast akin to earlier Figures **Figure IV- 105**(a) and (c)

Conclusions and Future Directions

We have successfully imaged the structure of Li_2MnO_3 with atomic resolution, providing a comparison benchmark to screen for and map segregation of Li_2MnO_3 in $Li_{1+a}(TM_{1-x}Mn_x)_{1-a}O_2$ compounds. Our continuing studies include the following:

- Examination of as-prepared $Li_{1.2}Co_{0.4}Mn_{0.4}O_2$. Initial data reveal the coexistence of nanosized regions with Li_2MnO_3- and $LiCoO_2$-like structures.
- Examination of $Li_{1.2}Co_{0.4}Mn_{0.4}O_2$ during and after electrochemical cycling. Initial data show significant structural rearrangements that affect oxide performance.
- Studies on $Li_{1+x}(Ni_aCo_bMn_c)_{1-x}O_2$ and $Li_{1.2}Co_{0.4}Mn_{0.4}O_2$ compounds. Initial data show that the transition metal type has a strong effect on the local atomic structure.

FY 2010 Publications/Presentations

1. "Layered Oxide electrode Materials for Li-ion Cells" *Adv. Mater. 22 (2010) 1122*
2. "Structural Study of Li_2MnO_3 by Electron Microscopy" *J. Mater. Sci. 44 (2009) 5579*
3. *"XAFS and TEM Studies of Layered Lithium-Manganese Oxide Based Cathode Materials for Lithium-Ion Technologies".* Presentation at the Gordon Conference on Solid State Studies in Ceramics (2010).
4. 2010 DOE Annual Peer Review Meeting Presentation
5. *"Microscopy and Spectroscopy of Lithium-bearing Mn-based layered oxides",* 15th International Meeting on Lithium Batteries (2010).

IV.C.1.4 Electrochemistry Diagnostics of Baseline and New Materials (LBNL)

Robert Kostecki, Frank McLarnon

Environmental Energy Technologies Division
Lawrence Berkely National Laboratory
1 Cyclotron Road, MS 90-3026D
Berkeley, CA 94720
Phone: (510) 486-4636; Fax: (510) 486-4260
E-mail: frmclarnon@lbl.gov

Start Date: October 1, 2009
Projected End Date: September 30, 2010

Objectives

- Diagnostic evaluation of ABR program chemistries
  - Carry out post-test characterization of components from ABR test cells
  - Understand factors that can enhance the stability of SEI layers
  - Establish and investigate degradation mechanisms of PHEV cells
- Develop strategies to minimize irreversible cell capacity losses
  - Fabricate anodes that reduce the charge required to form stable SEI layers
  - Investigate surface treatment regimens to reduce side reactions.
  - Establish direct correlations between electrodes' interfacial chemistry, morphology, topology, interfacial phenomena, and degradation modes of Li-ion cell.

Technical Barriers

- EV and PHEV battery durability and safety, as well as the need for efficient cell-formation processes, are the major barriers addressed by LBNL diagnostic work
- The primary LBNL role in the ABR program is to carry out specific diagnostic evaluations to determine the changes in cell components that accompany Li-ion cell power fade, capacity fade, and/or failure
- LBNL also seeks to identify electrode and electrolyte processes that are significantly influenced by various cell-formation protocols

Technical Targets

- Cycle life: 5000 (deep) and 300,000 (shallow) cycles (40 mile).
- Available energy: 96 Wh/kg (40 mile).
- Calendar life: 15 years.

Accomplishments

- Completed study of graphite anode structural degradation
- Identified approaches to anode stabilization
- Identified candidate anode and cathode fade mechanisms in Gen-3 cells

✧ ✧ ✧ ✧ ✧

Introduction

A primary aim of this project is to develop and use advanced diagnostic techniques to characterize basic physico-chemical properties of electrode active and passive components in ABR program cells that are being developed for use in PHEV and EV applications. The focus of this task is to correlate fundamental processes that occur in Li-ion batteries with the system electrochemical performance. The diagnostic results are used to determine cell failure mechanisms, anticipate the system lifetime as well as to suggest new approaches to design more-stable materials, composites and electrodes.

Approach

- Strategies to minimize irreversible capacity losses
  - Synthesis and diagnostic evaluation of C/Me composites and surface-modified carbons
  - Investigation of reactive impurities in anodes
- Diagnostic evaluation of ABR program lithium-ion cell chemistries
  - Carry out post-test diagnostic evaluation of components from ABR test cells and model thin-film cells
    - Spectroscopic, microscopic, X-ray, chromatographic, and related techniques
  - Understand factors that can enhance the stability of SEI layers
    - Use results to suggest approaches to stabilize interfaces
  - Establish and investigate degradation mechanisms of PHEV cells

Results

The objective of this work is to investigate the origin of the surface structural disordering in graphite, and the relationship between the amount of surface structural damage, cycling conditions, and the electrochemical performance of graphitic anodes in Li-ion battery systems. We previously reported that graphitic anodes suffer severe surface structural disordering upon prolonged cycling in rechargeable lithium-ion batteries. This deleterious effect is intensified at high charging rates and elevated temperatures as evidenced in the Raman spectra of graphite anodes sampled from aged/cycled lithium-ion cells, which show an increased intensity of the carbon D-band (ca. 1350 cm^{-1}) (ID) with respect to the G-band (ca. 1580 cm^{-1}) (IG).

Representative Raman ID/IG ratio surface maps obtained from (a) pristine MAG-10 electrode and (b) MAG-10 electrode cycled between 1 and 0.18V are shown in Figure IV- 109. The ID/IG ratios were derived from each individual Raman spectra recorded in the mapping area at 0.7 µm spatial resolution. Dark areas on the map correspond to highly graphitic carbon with low ID/IG ratios, whereas light areas represent disordered graphite with elevated ID/IG ratios. The fresh anode displays a fairly uniform graphitic structure with some local disorder. The increased prevalence of light areas at the surface of the cycled graphitic anode indicates an increased extent of local graphite structural degradation. Some severe local structural disorder is observed in the cycled anode with only a few local areas which retained the original graphitic structure. This Raman surface map of the cycled anode shows clearly that graphite structural degradation proceeds in a highly non-uniform manner.

Lithium-ion intercalation and transport in graphene crystallites involves a series of basic surface and bulk phenomena. Theoretical (and experimental) studies indicate that Li^+ ions tend to form stronger bonds with carbon edge atoms than in between grapheme layers and electron transfer rates on edge-plane graphite are ca. 1×10^5 times higher than basal-plane graphite. Thus, the surface concentration of Li^+ in graphite during intercalation/deintercalation processes is always higher than in the bulk. The resulting concentration gradient between the fully occupied surface sites and the bulk induces a significant local stress and lattice deformation in the graphene layers in the vicinity of their edges.

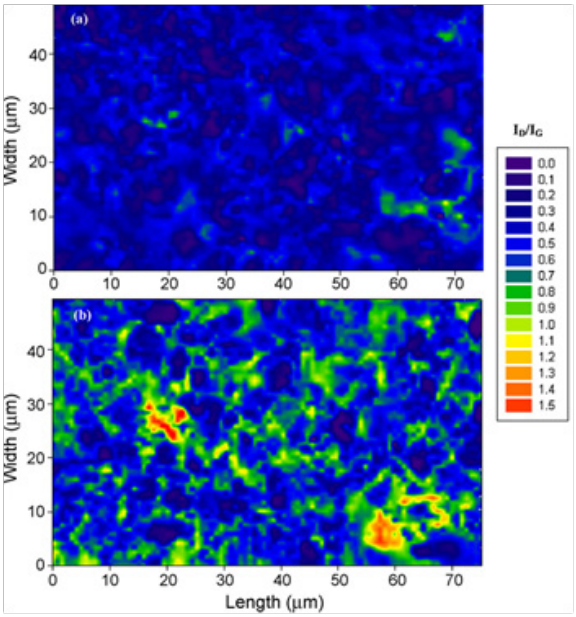

Figure IV- 109: Surface Raman maps of the ID/IG ratio from 48µm×74µm area at ca. 0.7µm resolution of (a) pristine graphite electrode, and (b) electrode cycled between 1 and 0.18V vs. Li/Li^+.

One can expect structural stress associated with intercalating and deintercalating a graphite electrode during early phases of the Li^+ intercalation (i.e., formation of stage-4 and stage-3 compounds), and final steps of deintercalation processes (i.e., complete delithiation of Li_xC). The Li^+ surface-bulk concentration gradient and the induced stress in the graphite lattice gradually diminish during the formation of Li^+-rich stage-3 or stage-2 not to mention stage-1 compounds. Therefore the observed amount of crystalline disorder generated during charge/discharge cycling between more concentrated stages ($x > 0.1$) is significantly lower than during cycling between dilute stages ($x < 0.1$). These results point at the origin of one of the graphite degradation modes in Li-ion batteries, which may have serious implications for the battery's electrochemical performance, calendar and cycle-life (Figure IV- 110). It appears that shallow cycling of graphitic anodes (i.e., between dilute Li_xC stages and pristine graphite) should be avoided in order to minimize the surface structural damage, the SEI layer reformation processes, impedance rise and loss of cyclable lithium in the battery. Therefore, complete discharge of commercial lithium-ion batteries should be avoided so that graphite anodes do not experience the transition between a dilute Li_xC and pure graphite upon charge.

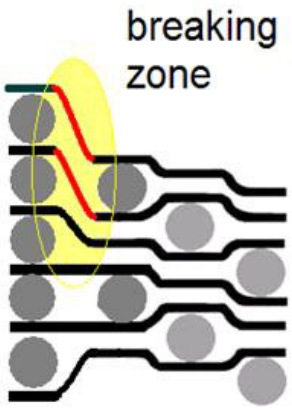

Figure IV- 110: Schematic diagram of structural stress induced into grapite upon Li+ intercalation

The electrochemical-impedance spectroscopy results indicate a buildup of significant mass-transfer and charge-transfer barriers across the SEI layer at the surface of graphite particles during long-term cycling. This impedance behavior pattern corresponds exactly to the extent of surface carbon disordering observed by the Raman measurements. This is in concert with our earlier studies, which have shown that the surface disordering of the graphite upon cycling results in the continuous reformation of SEI, leading to a thicker SEI layer, and consequently, higher interfacial resistance.

Chemical grafting of the edge-carbon sites to weaken the strength of C_{edge}-Li^+ bonds and/or using electrolyte additives to help quickly reform the SEI at the damaged sites may be considered as strategies to minimize the observed surface structural disordering and reduce its detrimental effects on the anode and the Li-ion system. However, our preliminary attempts to synthesize graphites with edges sites terminated with fluorine atoms yielded materials which did not exhibit improved properties in terms of long-term structural stability or diminished irreversible capacity loss during formation cycles.

Our second objective was to probe and characterize degradation modes in Gen-3 composite cathodes from cycled cells. *Ex situ* Raman and XRD measurements revealed non-uniform state of charge of the active $Li_xNi_{1/3}Co_{1/3}Mn_{1/3}O_2$ material in the tested cathodes at the end of long-term cycling experiments. We postulate that the degradation of electrochemical properties of $LiNi_{1/3}Co_{1/3}Mn_{1/3}O_2$ composite cathodesis is quite similar to the mechanism observed in the Gen-2 $LiNi_{0.8}Co_{0.15}Al_{0.05}O_2$ cathodes and cycling/aging is mainly due to deterioration of electronic contact within the composite cathodes.

Carbon additive rearrangement, formation of surface films, as well as poor intrinsic electronic properties of oxide active material powder contribute to the observed loss of electronic conductance and constitute a common degradation mode for composite Li-ion cathodes. A simple theoretical model based on a distributed network confirms that a local increase of the contact resistance between composite electrode particles can alter distribution of the conductive paths, and consequently, lead to a significant shift of the low-frequency intercept in the impedance spectra with a minimal effect on the position of the high-frequency intercept. These local effects may be responsible for non-uniform local kinetic behavior of individual oxide particles and the overall degradation of electrochemical performance of the electrode.

Conclusions and Future Directions

- Carbon disordering increases anode surface reactivity and causes SEI layer reformation, which shifts the cathode to a higher SOC and accelerates cathode degradation
  - Li^+ concentration gradient between occupied surface sites and bulk induces local stress
  - Surface-bulk Li^+ concentration gradients diminish during formation of Li^+-rich stages 1-3
  - Complete delithiation of graphitic anodes accelerates structural disordering and must be avoided to increase Li-ion cell lifetimes
  - Chemical grafting of fluorine onto graphite edges did not improve anode performance
- Diagnostic analyses of a Gen-3 cathodes showed degradation characteristics similar to Gen-2 cathodes
  - Contact resistances between primary particles and conductive carbon matrix, loss of available Li, and/or electrolyte starvation are likely cell fade mechanisms
- Studies of SEI layer formation/stabilization
  - Continue search for anodes that display smaller irreversible capacity losses and improved coulombic efficiency during cycling
    - Reduce the irreversible charge required to form stable SEI layers
    - Investigate pretreatment regimens to reduce side reactions
- Diagnostics of ABR program cell components
  - Carry out post-test characterization of components from ABR cells
    - Examine electrode composition, structure, and surface films
    - Understand factors that can enhance the stability of SEI layers
- Establish and investigate degradation mechanisms of PHEV cells
- Compare degradation mechanisms in ATD vs. ABR cells

FY 2010 Publications/Presentations

1. Vijay A. Sethuraman, Laurence J. Hardwick, Venkat Srinivasan, and Robert Kostecki, "Surface structural disordering in graphite upon lithium intercalation/deintercalation", *Journal of Power Sources* **195** (2010) 3655–3660

2. Frank McLarnon and Robert Kostecki, "Studies of the Mechanism of Graphite Structural Degradation in Li-ion Cell Anodes", The 50th Battery Symposium in Japan, International Session on Battery Technology for the Next 50 Years, November 30 – December 2, 2009, Kyoto, Japan.

IV.C.1.5 Investigate Mechanical Fatigue in Cycled Electrodes (ORNL)

Claus Daniel

Oak Ridge National Laboratory (ORNL)
1 Bethel Valley Rd.
P.O. Box 2008, MS-6083
Oak Ridge, TN 37831-6083
Phone: (865) 241-9521; Fax: (865) 241-5531
E-mail: danielc@ornl.gov

Collaborators:
Nancy Dudney, ORNL
Edgar Lara-Curzio, ORNL
Andrew Payzant, ORNL
Yan Wu, General Motors
Yue Qi, General Motors
Steve Harris, General Motors

Start Date:	January, 2009
Projected End Date:	September 2013

Objectives

- Develop cost effective *in situ* characterization tools for the validation of degradation mechanisms
- Develop an understanding of degradation mechanisms and the role of mechanical degradation of battery materials in capacity fade

Technical Barriers

The primary technical barriers are a lack of development tools to support lifetime predictions and of quality control procedures for plug-in hybrid electric vehicle batteries with 10 years of life that meet or exceed all performance goals.

- Identification of degradation mechanisms during formation cycling

Technical Targets

- Develop techniques to evaluate and understand quality and expected life of active electrode materials in experimental and real battery cells.
- Develop a formation cycle analysis tool.

Accomplishments

- Developed a laboratory-scale methodology for using acoustic emission (AE) and X-ray diffraction (XRD) for monitoring degradation in lithium-ion batteries (LIBs).
- *in situ* AE-XRD uses safe, inexpensive components that can be tailored to work with either anode or cathode materials, making the design useful in a wide variety of situations.
- Lattice strain in silicon was measured and correlated well with the observed AE activity.
- Lattice strain in Li(NiMnCo)O_2 (NMC) cathodes was monitored *in situ* for the first time with a standard diffractometer. The strain behavior also was monitored further into the cycling life of the cell than has been previously reported.

✧ ✧ ✧ ✧ ✧

Introduction

Electrode materials for LIBs undergo many changes as they are cycled, including lattice strain and particle fracture. The role of mechanical degradation in overall LIB performance is not thoroughly understood but is likely to play an important role in the development of next-generation active materials and cell design. However, the progress of work in this area is limited by current characterization techniques. A novel *in situ* technique that combines AE and XRD has been developed and tested on both anode and cathode materials.

Approach

AE has been used to detect, sort, and classify mechanical events such as particle fracture inside cycling LIBs [1]. In order to directly correlate the observed fracture events with strain in the active materials, special *in situ* methods of XRD can be used. A novel beryllium-free *in situ* AE-XRD cell has been devised which uses a metalized Mylar window to allow X-ray penetration during cycling in standard coin cell hardware. Figure IV- 111 shows the design of this cell, and Figure IV- 112 shows a general experimental setup. This technique provides a safe, inexpensive alternative to current *in situ* XRD methods. It also provides data for a depth of understanding which before was possible only with special miniature cells and very short synchrotron beam time. The new cell allows for extended beam time in inexpensive laboratory-scale diffractometers. Mylar disks sputtered with copper can be used in direct contact with anode materials, and disks sputtered with aluminum can be used in contact with cathode materials. Studies using this combined technique will allow for further fundamental understanding of material degradation mechanisms and how they are correlated with capacity fade and cell failure.

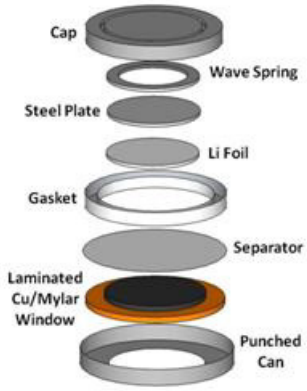

Figure IV- 111: Schematic view of the *in situ* AE-XRD cell design used to study LIBs during cycling.

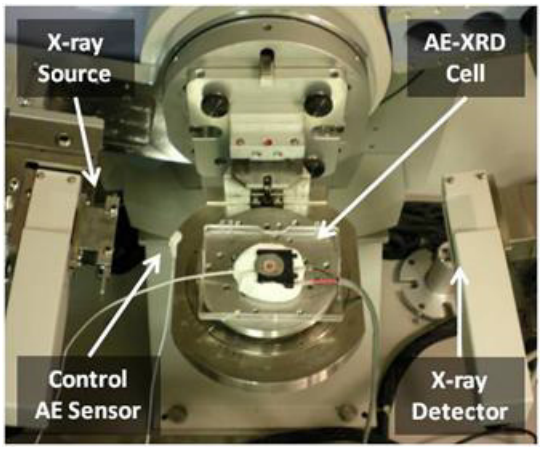

Figure IV- 112: *in situ* AE-XRD experimental setup showing the cell connected to an AE sensor and current leads and sitting in the X-ray beam path

Results

A study of silicon anodes was performed using the new characterization method; a plot of cumulative AE and voltage is shown in Figure IV- 113. These data correlated very well with previously reported results of AE from unmodified coin cells containing silicon electrodes. By performing Rietveld fits of XRD scans, the lattice strain in the crystalline region of silicon particles was determined (see Figure IV- 114). The periods of highest AE activity overlap perfectly with major inflection points in the calculated strain. This directly shows the strain release occurring in the particles as they fracture.

When the technique was applied to NMC materials, a very clear picture of lattice strain was achieved (Figure IV- 115). These results show very clearly the decrease in the "c" parameter during the voltage plateau, which correlates to cation rearrangement in the material. Results similar to those seen in the charge stage have been reported from synchrotron experiments, but this is the first time that ordinary laboratory XRD has successfully measured them. Additionally, this is the first attempt to look at lattice changes past the first charge stage.

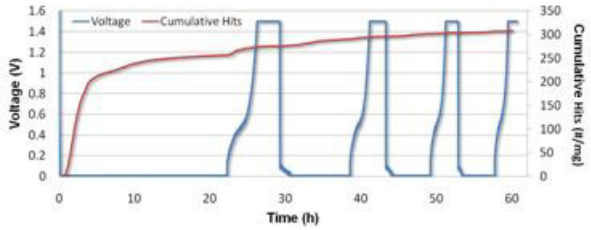

Figure IV- 113: Cumulative AE and cycling voltage of *in situ* AE-XRD cell containing a composite silicon electrode.

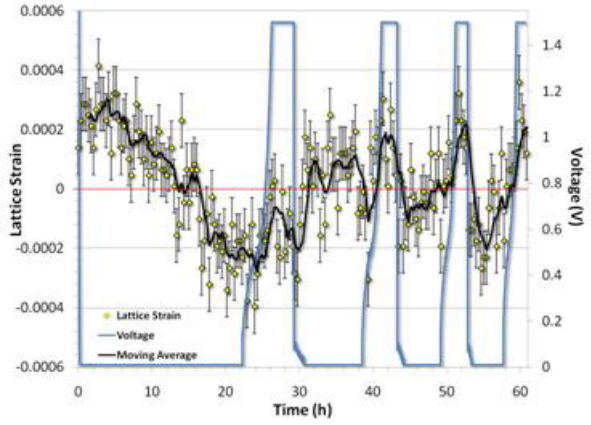

Figure IV- 114: Lattice strain in the crystalline region of silicon particles and voltage as a function of time.

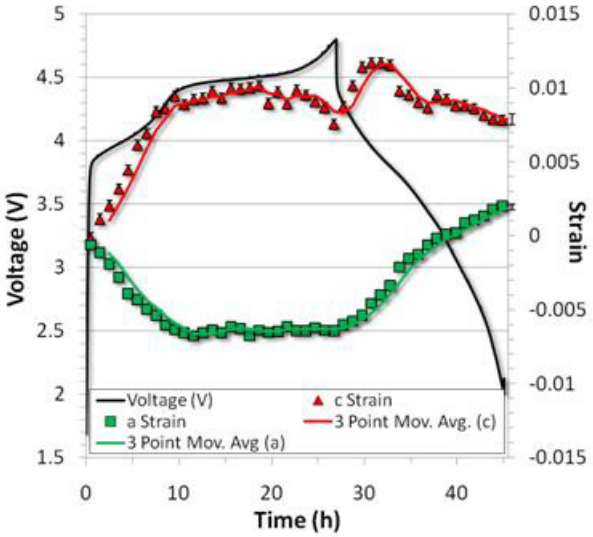

Figure IV- 115: a and c lattice strains in NMC materials cycled in an *in situ* AE-XRD cell.

Conclusions and Future Directions

The developed *in situ* cell will be used to improve understanding of degradation mechanisms in cathode materials. In the next step, the understanding developed will be used in large-scale battery cells from U.S. manufacturers during formation cycling. Formation cycling is the key aspect of forming materials within the cell and obtaining the maximum performance from cells. It also provides insight into mechanical events during the formation of those materials. This information will be used to understand how mechanical response to formation cycling can be used as an early detection tool.

FY 2010 Publications/Presentations

Publications

1. "Understanding the Degradation of Silicon Electrodes for Lithium-ion Batteries Using Acoustic Emission", K. Rhodes, N. Dudney, E. Lara-Curzio, C. Daniel, J. Electrochem. Soc., IN PRESS
2. "A study of lithium-ion intercalation induced fracture of silicon particles used as anode material in Li-ion battery", S. Kalnaus, K. Rhodes, C. Daniel, Eng. Fract. Mech., IN REVIEW
3. "A Novel Lithium-ion Battery Cell for *in situ* Acoustic Emission and XRD", K. Rhodes, C. Daniel, Rev. Scientific Inst., IN PREPARATION
4. "Monitoring Lattice Strain and Fracture of Silicon Particles In Lithium-ion Batteries", K. Rhodes, M. Kirkham, R. Meisner, C. Daniel, J. Electrochem. Soc., IN PREPARATION

Posters

1. "Combining Acoustic Emission and XRD for *in situ* Characterization of Lithium-ion Batteries", K. Rhodes, M. Kirkham, R. Meisner, A. Payzant, C. Daniel, SPM for Energy Application Workshop - Oak Ridge, TN, Sept. 15-17, 2010
2. " *in situ* Acoustic Emission Spectroscopy Combined with Stress Analysis", K. Rhodes, S. Kalnaus, C. Daniel, N. Dudney, E. Lara-Curzio, Beyond Lithium-ion: Computational Perspectives, Chicago, IL, May 31-June 1, 2010
3. "Monitoring Electrode Degradation in Lithium-ion Batteries by Acoustic Emission", K. Rhodes, C. Daniel, E. Lara-Curzio, N. Dudney, TMS '10 - Seattle, WA, Feb. 14-18, 2010

Presentations

1. "Combined *in situ* Acoustic Emission and XRD Analysis of Lithium-ion Battery Materials", K. Rhodes, C. Daniel, E. Lara-Curzio, N. Dudney, 218th ECS - Las Vegas, NV, Oct. 10-15, 2010
2. "Degradation Mechanisms in Batteries", C. Daniel, K. Rhodes, S. Kalnaus, National Academy of Engineering, Frontiers of Engineering Symposium, Armonk, NY, Sept. 23-25, 2010
3. "Probing mechanical degradation in energy storage applications", C. Daniel, K. Rhodes, S. Kalnaus, International Workshop on SPM for Energy Applications, Oak Ridge, TN, Sept. 15-17, 2010
4. "Acoustic Emission from Silicon Electrodes in Cycling Lithium-ion Cells", K. Rhodes, C. Daniel, E. Lara-Curzio, N. Dudney, 217th ECS - Vancouver, BC, April 22-25, 2010
5. "Application of Acoustic Emission for Characterization of Lithium-ion Batteries", K. Rhodes, C. Daniel, E. Lara-Curzio, N. Dudney, TMS '10 - Seattle, WA , Feb. 14-18, 2010
6. "Development of a Combined *in situ* AE-XRD Technique for Advanced Characterization of Lithium-ion Batteries", K. Rhodes, C. Daniel, E. Lara-Curzio, N. Dudney, UT Materials Science and Engineering Graduate Seminar - Knoxville, TN

IV.C.1.6 Mechanistic, Molecular, and Thermodynamic Modeling/Diagnostics in support of ABR Cell Performance and Aging Studies (INL)

Kevin L. Gering, PhD

Idaho National Laboratory
2525 N. Fremont Ave.
Idaho Falls, ID 83415-2209
Phone: (208) 526-4173; Fax: (208) 526-0690
E-mail: kevin.gering@inl.gov

Collaborators:
David K. Jamison, INL
Christopher J. Michelbacher, INL
Sergiy V. Sazhin, INL
Matthieu Dubarry, HNEI
Bor Yann Liaw, HNEI

Start Date: April, 2008
Projected End Date: ongoing

Objectives

- Establish a platform of Developmental and Applied Diagnostic Testing (DADT) geared toward specific issues of cell performance and aging in vehicular applications (e.g., HEV, PHEV).
- Employ DADT to examine mechanistic contributions to cell aging and path dependence (PD) thereof, to support technology improvements and better management.
- Develop advanced modeling tools that will complement DADT, based on fundamental principles of molecular interactions, chemical physics, reaction kinetics, and thermodynamics.
- Develop/optimize an operational protocol to manage and minimize the aging process (chemistry-specific, but with generalized approach).

Technical Barriers

Long-term usage of lithium-ion batteries in vehicle applications represents a significant warranty commitment. Yet, there is insufficient knowledge regarding prolonged aging processes in such batteries, particularly in cases of strong path dependence of performance degradation. And, modeling tools that describe first-principles or physics-level phenomena over multiple domains (and their impact on aging) have generally not kept pace with Li-ion technology worldwide.

Batteries employed in HEV, PHEV, or EV applications will undergo thousands of thermal cycles during their service life, the severity of which depends on the onboard thermal management scheme and the local climate. Yet, there is much to be learned about how a particular cell chemistry and the physical design of a cell responds to repeated thermal cycling or other unique operational aspects of vehicle applications. If indeed a strong path-dependent correlation exists between thermal cycling and aging rates, this will have a sobering consequence toward meeting battery warranties for HEV, PHEV, and EV systems, since in many such cases battery life is studied through a series of isothermal studies. Seeing this need, this work aims to standardize a testing methodology and modeling techniques for looking squarely at the issue of aging path dependence.

Technical Targets

- Perform well-designed DADT that looks at specific issues of aging PD as it relates to PHEV applications, using a Li-ion chemistry that is a reasonable candidate (here, Sanyo 'Y' cells). For example, we will quantify the impact of thermal cycling on cell aging.
- Monitor aging trends for several months to establish mature trends of key metrics (capacity loss, conductance loss, etc.) that can be evaluated through advanced modeling tools that perform mechanistic analyses.
- Develop and validate computer modeling and simulation tools that yield accurate interpretation of aging and performance data in terms of meaningful physical and chemical quantities. Demonstrate INL diagnostic/predictive modeling capabilities through software that integrates key modules regarding cell performance over life.
- Develop and demonstrate DADT tools that enable materials-level investigations of cell performance.

Accomplishments

Using seventy (70) Sanyo Y 18650 cells split between INL and HNEI:

- Initial characterization of cells was accomplished, which allowed us to set more precise conditions for the path dependence studies.
- Path Dependence Studies 1 and 2 recently commenced at INL (Sept/Dec 2009), producing early

aging trends to date. These studies will continue for at least 12-18 months or until adequate performance loss is seen to elucidate mature trends.

- Incremental capacity analysis (ICA) has been performed on the target cells, revealing key information regarding cell chemistry and design (HNEI). ICA data will be valuable information toward aging mechanisms of materials.
- Key computational methods have been developed and benchmarked on Gen2 and other Li-ion cell performance and aging data. A framework has been formulated to adapt such tools to PD scenarios and will be applied to our DADT data. These methods cover:
  - Capacity loss over aging,
  - Cell conductance loss over aging,
  - Kinetic performance over multiple domains,
  - Incremental capacity analysis,
  - Equivalent circuit analysis,
  - Other diagnostic data.

✧ ✧ ✧ ✧ ✧

Introduction

As domestic and worldwide vehicle designs go more toward electric-drive platforms based on advanced batteries (Li-ion), there is a commensurate need for a rational foundation for understanding how battery usage conditions affect the aging rates and the effective service life of batteries. A study was recently initiated by the INL to investigate issues tied to aging path dependence of cells used for PHEV-type duty cycling. The INL has a long and proven history of testing a variety of electrochemical systems for DOE, and has produced numerous testing manuals as well as strategic modeling capabilities that address key factors in electrolyte performance and aging of electrochemical cells, and enable diagnostic analysis, performance predictions, and intelligent control.

We leverage complimentary capabilities between INL and Hawaii Natural Energy Institute (HNEI) to achieve synergy toward programmatic goals. This collective effort allows us to answer fundamental questions on aging processes, path dependence thereof, and how to mitigate performance limitations over life. Recent references document or relate to this work [1-3].

Approach

This work aims to bridge the gap between ideal laboratory test conditions and PHEV field conditions by isolating the predominant aging factors of Li-ion cells in PHEV service, which would include, for example, the nature and frequency of duty cycles, as well as the frequency and severity of thermal cycles. Through DADT, these factors are studied in controlled and repeatable laboratory conditions to facilitate mechanistic evaluation of aging processes and path dependence thereof. Collaboration between INL and HNEI provides a synergistic basis due to the complementary histories of INL and HNEI in battery testing, research, and modeling.

Modeling tools developed and employed are those that promote diagnostic analysis over multiple domains, looking at aging mechanisms and key performance issues (Figure IV- 116). Model parameters represent physical, chemical, electrochemical, or molecular quantities. Thermodynamic principles and quantities are incorporated where appropriate. These tools are supported by a suite of Diagnostic Testing, naturally lend themselves to PD scenarios, and some have intellectual property status.

There are two studies being performed that look at PD issues. The first considers constant-power pulses of various magnitudes, using a time-average cumulative discharge energy that is equal for all scenarios. This study seeks to answer the question *Is there an aging path dependence due to severity and randomness of power pulses?* The second study combines cell cycling (PHEV protocol, CD+CS) and thermal cycling to answer the question *Is there an aging path dependence due to cells operating under ambient temperature ramping?* Such thermal cycling will occur thousands of times during the projected life of a HEV/PHEV battery pack. The main parameters are (1) the magnitude and frequency of the thermal cycling, looking at isothermal, mild, and severe scenarios, and (2) frequency of duty cycle (Figure IV- 117). This is a valuable study in transitioning between idealized lab data and actual PHEV field data, and the temperature and cycling parameters can be tailored for specific regional targets.

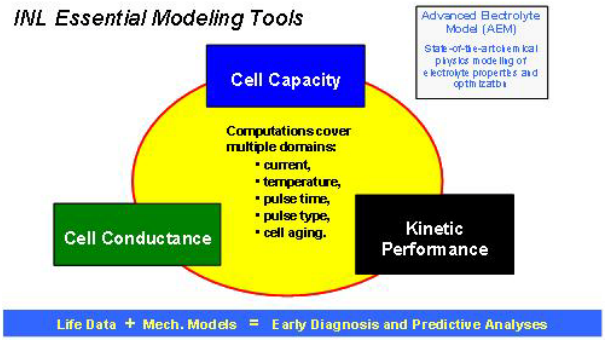

Figure IV- 116: INL Essential Modeling Tools

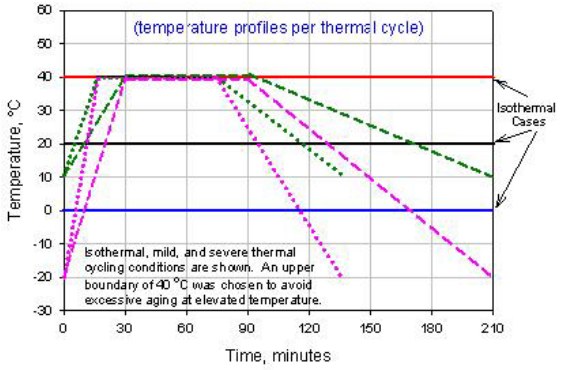

Figure IV- 117: Temperature Profiles per Thermal Cycle

Path Dependence (PD) of Cell Aging. The extent and rate of cell aging over time depends on specific operational conditions (stress factors) encountered over the timeline. Path dependence asserts that the *sequence* of aging conditions (as well as the nature of conditions) has a direct influence on the rate of aging and net aging along the timeline (think "batch reactor"). A change in aging conditions can accelerate or decelerate degradation mechanisms, and can initiate new ones. Principles of reaction kinetics and thermodynamics are key to understanding the aging process along the path. Cell aging should be simultaneously judged from several metrics, including loss of capacity, rise in impedance, loss of power, self discharge, etc., where each require a standard basis. INL aging models are easily adaptable to PD scenarios.

Modeling Aging Cells as Batch Reactors. Contributions from chemical kinetics and thermodynamics to cell degradation processes determine the effective rate and extent that cells age, affecting losses in capacity, power, general performance, and ancillary quantities over service life of electrochemical cells (Figure IV- 118). Sigmoidal expressions are well suited to describe these processes within a batch reactor scenario, e.g., for capacity loss at aging condition i (Ψ_i) we have:

$$\Psi_i = \sum_j 2M_j \left[\frac{1}{2} - \frac{1}{1+\exp\left(a_j t^{b_j}\right)} \right]_i$$

a_j : rate constant attributable to mechanism j,

b_j : related to the order of reaction for mechanism j,

M_j : theoretical maximum limit of capacity loss under mechanism j considering the thermodynamic limit of degradation under j for a batch system.

These mathematical expressions are self-consistent, properly bounded, adaptive, relevant to cell environments, and easily lend themselves to a comprehensive degradation rate analysis of performance data. This basis enables rendering of the constituent (mechanistic) sources of performance loss.

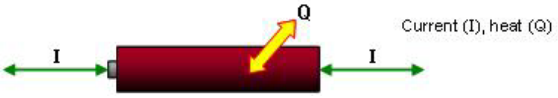

Figure IV- 118: Electrochemical cell modeling parameters

Results

FY 2010 was a pivotal year in establishing DADT protocols for PHEV-relevant conditions, and for mobilizing computational tools for evaluating aging mechanisms and related path dependence. Our data now covers early detailed analysis of the chosen test cells (Sanyo Y) as well as emerging performance data over aging, which includes pulse-per-day (PPD) and monthly reference performance test (RPT) data. Early results such as ICA and EIS are useful for establishing beginning of life (BOL) values and providing initial estimates of parameters for aging models. More extensive data over time is needed to surmise probable degradation mechanisms regarding capacity, impedance, etc. Examples of modeling capabilities are given in Figure IV-119 and Figure IV- 120, which show conductance and capacity losses, respectively, for Gen2 cells aged under HEV cycle-life conditions at 25 °C. The sigmoidal-based model results show very high fidelity to the data, and similar techniques will be used for the mature data sets produced by this PD work.

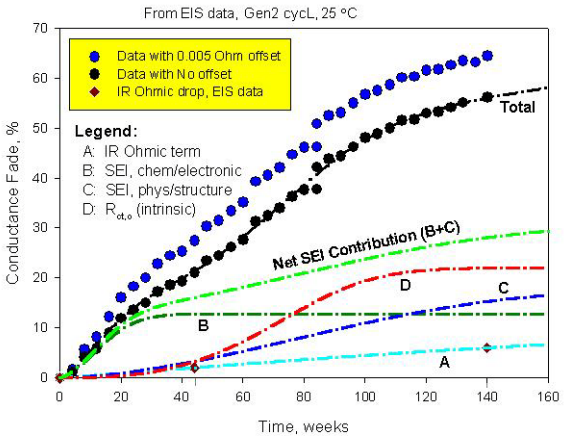

Figure IV- 119: Conductance fade profile over time

Figure IV- 121 shows examples of interim results for PPD discharge impedances, considering various test conditions of thermal cycling. While early trends are starting to emerge, more mature trends will allow better resolution of aging characteristics. A wealth of additional test data exists and will be presented in the future.

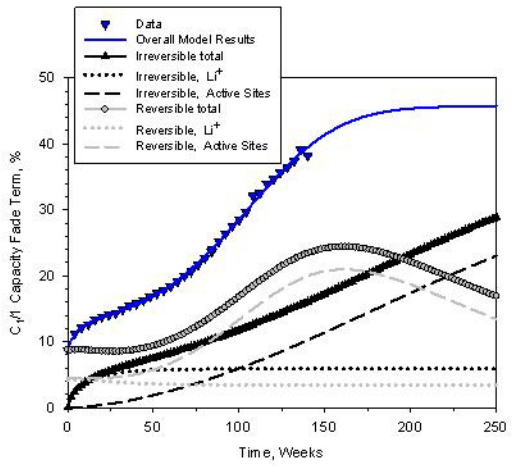

Figure IV- 120: Capacity fade profile over time

Conclusions and Future Directions

INL and HNEI have developed key DADT tools used to test, diagnose, model and predict performance and aging of electrochemical cells. Within the context of cell aging under PHEV protocols, these tools are targeting mechanisms of cell degradation, related path dependence, and chief causes and conditions of performance loss. The immediate benefits of this work are (1) to provide more realistic and accurate life predictions by accounting for the influence of thermal cycling effects and related path dependence on aging mechanisms, and (2) provide a basis for improving battery development, design, and management. These capabilities can accelerate domestic battery testing and development.

Thermal cycling should be considered as a standard aging condition for batteries intended for vehicle applications (HEV, PHEV, EV), and could be useful as an accelerated aging condition. Future path dependence studies could involve other duty-cycles (e.g., FUDS, DST), other temperature parameters defined for a particular city or region, and other Li-ion cell chemistries.

FY 2010 Publications/Presentations

1. K. L. Gering, “Diagnostic Testing and Analysis Toward Understanding Aging Mechanisms and Related Path Dependence”, 2010 DOE-VTP Annual Merit Review Presentation, Project ES096.
2. K. L. Gering, S. V. Sazhin, D. K. Jamison, C. J. Michelbacher, M. Dubarry, M. Cugnet and B. Liaw, "Path Dependence of Aging in Commercial Li-Ion Cells Chosen for PHEV Duty Cycle Protocols", 217th Meeting of the Electrochemical Society, Vancouver, BC, Canada (April 26-30).
3. K. L. Gering, S. V. Sazhin, D. K. Jamison; C. J. Michelbacher; B. Y. Liaw, M. Dubarry, and M. Cugnet, "Investigation of Path Dependence in Commercial Li-ion Cells Chosen for PHEV Duty Cycle Protocols", accepted by Journal of Power Sources under Special Edition IBA Meeting 2010. Publication in Progress.

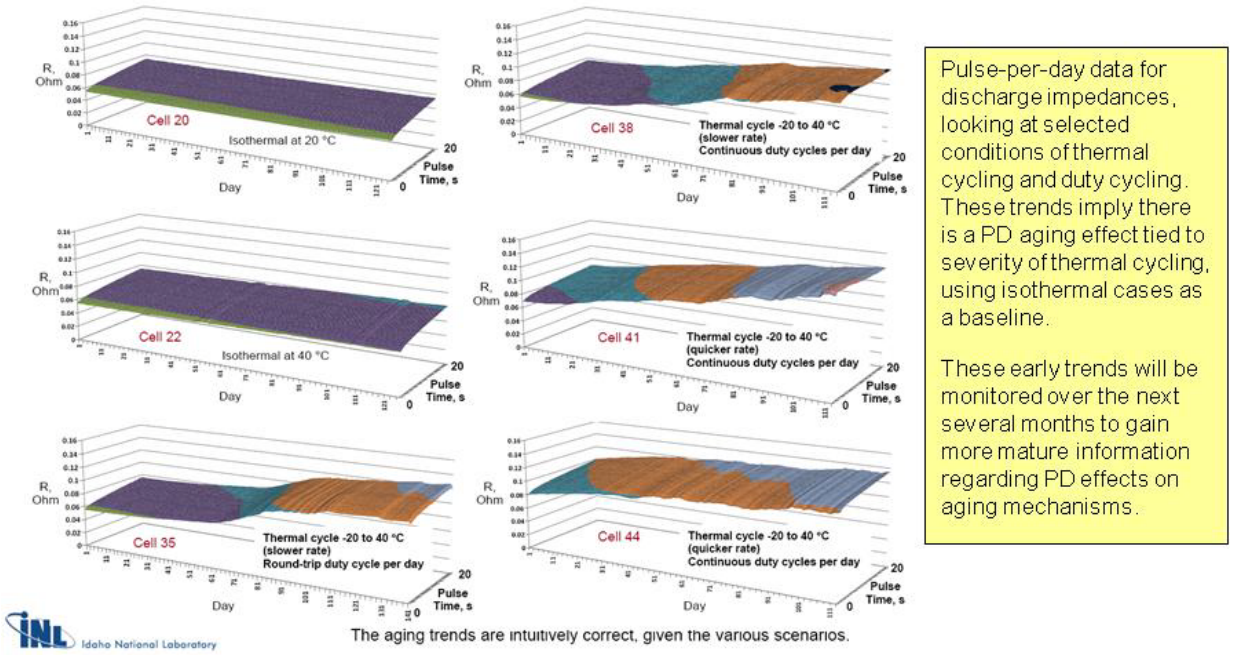

Figure IV- 121: Interim results from PPD discharge impedances

IV.C.2 Cell Fabrication and Testing

IV.C.2.1 Fabricate PHEV Cells for Testing & Diagnostics (ANL)

Andrew N. Jansen

Argonne National Laboratory (ANL)
9700 South Cass Avenue
Argonne, IL 60439-4837
Phone: (630) 252-4956; Fax: (630) 972-4461
E-mail: jansen@anl.gov

Collaborators:
Dennis Dees, ANL
Bryant Polzin, ANL
Wenquan Lu, ANL
Sun-Ho Kang, ANL
Paul Nelson, ANL
Chris Joyce, ANL
Johnson Controls-SAFT
Mobius Power
Media-Tech
A-Pro

Start Date: October, 2008
Projected End Date: September, 2014

Objectives

- Several new battery chemistries are being proposed for PHEV batteries that must be evaluated in cell formats larger than a few mAh. The main objective of this task is to obtain trial cells for calendar and cycle life studies in pouch cell or rigid cell (e.g. 18650) formats.
- Electrode designs must be developed that are appropriate for PHEV batteries.
- Argonne will develop the capability to fabricate in-house trial cells in its new cell fabrication facility.

Technical Barriers

- Newly developed battery materials for PHEVs need to be tested in limited batch size before larger scale industrial commitment.
- Validation tests are needed in cell formats with at least 0.4 Ah in capacity.

Technical Targets

- Produce graphite and NCA electrodes of varying thickness and test performance to prepare for advanced chemistry cell builds.
- Use thickness performance data to design PHEV battery.
- Place order with qualified vendors to make electrodes and pouch/18650 cells for ABR.
- Distribute vendor cells to ABR researchers for testing and diagnostics.
- Design and install facility for making 18650 and pouch cells at Argonne.

Accomplishments

- Made cathode and anode electrodes of varying thickness to determine influence of electrode thickness on impedance and active material utilization.
- Determined optimum PHEV battery parameters using Argonne's Battery Design Model with baseline electrode results as input.
- Obtained baseline PHEV electrodes and 18650 cells from contracted vendors.
- Distributed PHEV electrodes and 18650 cells to national labs in the ABR program for testing and diagnostic studies.
- Completed installation of new dry room that will be used to fabricate lithium-ion prototype cells.
- Installed 18650 and pouch cell making equipment in new dry room with necessary safety modifications and approvals.
- Ordered electrode coating and hot roll press equipment from vendor.

✧ ✧ ✧ ✧ ✧

Introduction

Cell builds are generally based on materials from the vendor screening subtask or from novel materials

developed in the ABR and BATT programs. The previous ATD program required cells designed for HEV applications, which used thin electrodes. The ABR program has little experience with thicker electrodes that are now required for PHEV applications. The performance of these thicker electrodes will be determined and verified in a sample cell build using NCA and Mag-10 graphite. These were the baseline materials known as Gen2 in the ATD program and their use now will enable a direct comparison between HEV and PHEV applications. This build is being conducted to prepare for a near term build (early CY 2011) of cells using advanced anode and cathode materials. Once the influence of electrode thickness has been established, the many novel high-energy materials being developed world wide will be explored in new cell builds.

Historically, cell builds have been carried out through subcontracts with battery developers to produce flexible or rigid cells per program directions. This approach has often resulted in delays due to lack of sufficient material quantities for the larger coating equipment or due to the battery developer's internal priorities taking precedence. Thus, it was decided that Argonne should develop its own in-house cell making capability. Note that this capability will also permit a design of experiment approach in the cell build area. New additives, electrolyte mixtures, and electrode constructions can be made to investigate fade mechanisms and other issues.

Approach

Promising new exploratory materials are often developed in small coin cells, which may or may not scale up well in large PHEV battery designs. For this reason, pouch cells or rigid cells such as 18650s in the capacity range of 0.4 to 2 Ah will be used to evaluate new materials.

It is anticipated that pouch cells will be used for initial evaluations of long-term exploratory materials. Pouch cells are an efficient method of determining the stability of a cell system during calendar and cycle life aging. If the chemistry is not stable, it is likely that gassing will occur inside the cell. This will result in the pouch cell bulging or rupturing if the gassing is significant. More established materials and chemistries (or those that pass the pouch cell evaluation) will be used in rigid cells (*e.g.* 18650s).

Concurrent to the fabrication of PHEV cells by industrial vendors, Argonne will develop the capability to fabricate pouch and 18650 cells. Key to this is the installation of a cell fabrication facility in Argonne's new dry room. Electrode-making equipment will be installed based on arrival of purchased equipment. Once in-house cells are deemed to be reliable, the developer subcontracts will be reduced and eventually eliminated.

Results

PHEV Baseline Cell Build. In FY09, single-sided negative and positive electrodes were made with varying thicknesses using Argonne's mini-coater. A relationship between total material loading and calendered thickness was established. Half cell studies were performed to establish specific capacity of the active materials as a function of total material loading. Investigations were also performed to assess the impact of material loading density on HPPC impedance. It was determined that the move to thicker electrodes for PHEV batteries should not pose a significant challenge regarding electrode impedance, as long as the electrolyte is able to support the higher current densities. A rate study was also performed with appropriately matched electrodes to show that cells with thicker electrodes deliver less capacity at discharge rates above 1C. As a result, it was decided that the positive electrode should not exceed 100 µm material thickness (~27 mg/cm²) for PHEV use.

Electrodes were then contracted to be fabricated by a battery developer based on the above results regarding performance as a function of electrode thickness. Some difficulty in obtaining good adhesion occurred during the making of the thicker negative electrodes using Mag-10 graphite and PVdF binder. It was necessary to reduce the thickness of the negative electrode and switch to an aqueous based binder. This then required a reduction of the positive electrode thickness to maintain a negative to positive ratio near 1.1. The final composition of these electrodes (hot calendered to ~33%) is given Table IV- 7.

Table IV- 7: Final composition of electrodes for the PHEV cell build

Anode	HEV (Gen 2)	PHEV - baseline
Composition	92% Mag-10 Graphite 8% PVDF Binder	95% Mag-10 Graphite 2.5% CMC Binder 2.5% SBR Binder
Electrode Thickness*, µm	34	79
Foil Thickness, µm	18 (Cu)	10 (Cu)
Electrode Loading*, mg/cm²	5.06	10.6
C/5 Capacity, mAh/cm²	1.44	3.02
Cathode	**HEV (Gen 2)**	**PHEV - baseline**
Composition	84% $LiNi_{0.8}Co_{0.15}Al_{0.05}O_2$ 8% PVDF Binder 4% Acetylene Black Carbon 4% SFG-6 Graphite	84% $LiNi_{0.8}Co_{0.15}Al_{0.05}O_2$ 8% PVDF Binder 4% Super P Carbon 4% SFG-6 Graphite
Electrode Thickness*, µm	36	65
Foil Thickness, µm	30 (Al)	22 (Al)
Electrode Loading*, mg/cm²	8.88	18.9
C/5 Capacity, mAh/cm²	1.23	2.54

In FY10, another battery developer was contracted to make 18650 cells from these electrodes. It was decided to add an additional variable to this study (in addition to the

thickness study) by incorporating an SEI forming additive into the electrolyte. The lack of an SEI additive in the ATD Gen2 cells was considered a shortcoming of that study. Thus, 30 PHEV baseline cells were made with no additive in the electrolyte (1.2 M $LiPF_6$ in EC:EMC (3:7w)), and another 30 cells were made with 1.5 wt % vinylene carbonate (VC). These cells were delivered to Argonne in January of 2010 (Figure IV- 122).

Figure IV- 122: PHEV baseline 18650 cells.

An evaluation plan was developed that involves tests for both HEV and PHEV cells. The HEV tests and reference performance tests (RPTs) are similar to those done with the previous ATD Gen 2 cells so that direct comparisons can be made between the two cell designs. These cells are now being tested in two batches of 12 cells each at ANL and INL, and an additional four cells were sent to SNL for thermal abuse testing.

Cell Fabrication Facility. A new dry room was installed by Scientific Climate Systems that will maintain ≤100 PPM moisture (-42°C dew point) for an area of ~500 ft^2, with 6 persons, and 750 standard cubic feet per minute (SCFM) exhaust capability. The dry room became operational in August 2009.

Two vendors were located that deal with manufacturing of pilot scale Li-ion cell making equipment. The decision was made to purchase the Li-ion pouch cell making equipment from Media Tech and to use the XX3450 cell format (34 mm wide by 50 mm high). This equipment includes: pouch stamper, electrode punch, winder/stacker (Figure IV- 123), grid trimmer, ultrasonic welder, tab area sealer, side area sealer, and electrolyte-filling vacuum chamber (Figure IV- 124).

Media Tech was also selected to make the lithium-ion 18650 cell making equipment. This equipment includes: electrode slitter, winder, groover, electrolyte filler, resistance welder, and crimper (Figure IV- 125). Both sets of cell making equipment were received in the spring of 2010. Training was provided by Media Tech engineers soon after. Modifications were made to enhance the function and safety of all equipment during the installation process. A safety review process was conducted with approval to operate the pouch and 18650 cell making equipment granted in August of 2010.

The electrode coater and hot roll press equipment was contracted to A-Pro, with an expected delivery date of October and November, respectively. Installation, training, and safety approval to operate are expected to be finalized in December of 2010.

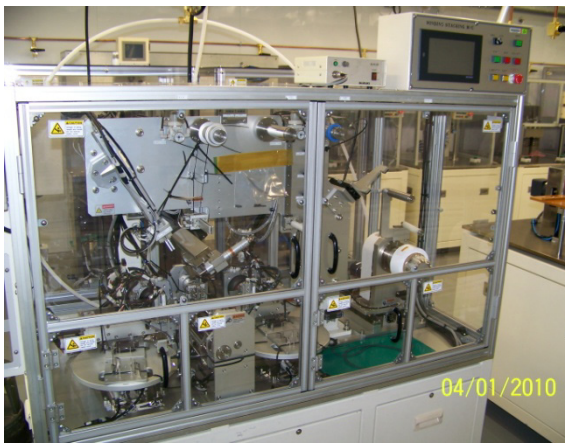

Figure IV- 123: Winder/stacker used to assemble lithium-ion pouch cells in Argonne's cell fabrication facility.

Figure IV- 124: Electrolyte-filling vacuum chamber and heat sealer for lithium-ion pouch cell fabrication at Argonne.

Figure IV- 125: 18650 cell making equipment in Argonne's cell fabrication facility.

Conclusions and Future Directions

The influence of electrode thickness on electrochemical performance is not expected to be a major concern for discharges less than a 1C rate, but problems in electrode fabrication and handling may arise for electrodes thicker than 100 microns each side. Adhesion of the electrode slurry to the current collecting foils will be critical to the success of the cell fabrication facility.

Future work will include the installation of the coater and hot press and completion of training from A-Pro engineers. Modifications are likely needed to enhance the safety of the coater and press, upon which, approval to operate this equipment will be obtained.

Once the coater and press are fully functional, the first priority will be to fabricate PHEV baseline electrodes and cells in-house and compare against the baseline cells made by vendors for the ABR program as a means of proofing the new equipment and operation. Once a reasonable amount of confidence is reached, cell fabrication will begin with exploratory high-energy materials. This approach will minimize the waste of precious, limited-quantity, novel materials that have yet to be scaled up in production.

FY 2010 Publications/Presentations

1. Oral presentation at the DOE Vehicles Technology Program 2010 Annual Merit Review Meeting.

IV.C.2.2 Baseline PHEV Cell Life Testing (ANL, INL)

Ira Bloom
Argonne National Laboratory (ANL)
9700 South Cass Avenue
Argonne, IL 60439-4837
Phone: (630) 252-4516; Fax: (630) 972-4520
E-mail: ira.bloom@anl.gov

Co-Principal Investigators:
Jon Christophersen/Kevin Gering
Idaho National Laboratory (INL)
P.O. Box 1625
Idaho Falls, ID 83415
Phone: (208) 526-4280; Fax: (208) 526-0690
E-mail: jon.christophersen@inl.gov

Collaborators:
John K. Basco (ANL)
Chinh D. Ho (INL)

Start Date: October 2008
Projected End Date: September 2011

Objectives

- The objective of this work is to provide aged cells with well-documented histories for diagnostic studies.
- The effects of electrode thickness, electrode coatings, and electrolyte additives on cell performance and life will be determined.

Technical Barriers

The primary technical barrier is the development of a safe, cost-effective PHEV battery with a 40 mile all electric range that meets or exceeds all performance goals.

- Identification of cell degradation mechanisms.

Technical Targets

- Establish the impact of PHEV-type cycles on aging relative to HEV-type cycles
- Establish a PHEV cell aging baseline for use in comparing advanced cell chemistries

Accomplishments

- Test plan for protocol comparison developed
- Calendar life testing started

Introduction

A newly-developed battery testing manual for plug-in hybrid applications (PHEV) has just been released.[18] While the new manual contains procedures which are similar to those found in the more-established manual for hybrid electric vehicle (HEV) battery testing,[19] there are a number of significant changes and new test procedures. We recognize that the magnitude and type of aging mechanisms might differ between HEV and PHEV test conditions, and we are particularly interested in how these mechanisms impact execution of the PHEV duty cycles later in cell life. To determine the impact of these changes on battery aging characteristics, a well-understood and characterized cell chemistry is being used to test the procedures. The essential question to be answered is what additional stresses are placed on the battery in the PHEV application? Additionally, the effects of electrode thickness and electrode coatings on cell performance and life will be determined. It is thought that there should be no difference in life when the electrodes in the cells are thicker and that the coatings should extend cell life.

Approach

The approach for this work is to use cells made for the PHEV application and to test them using both sets of aging and characterization protocols in calendar and cycle life tests. A baseline for cell aging will be obtained byperforming cell aging experiments at 45°C and 60% SOC using the HEV protocols and changes in performance will be characterized by reference performance tests (RPTs) at regular time intervals. After the baseline is obtained, comparison of protocols will begin.

The distribution of cells to be tested is given in Table IV- 8. The cells were made by Leyden Energy (labeled "LE" in Table IV- 8) and by EcoPro (labeled "EC" in Table IV- 8). The cell chemistry consists of a $LiNi_{0.8}Co_{0.15}Al_{0.05}O_2$ cathode, a MAG-10 anode and a mixed, organic carbonate electrolyte. The base ANL and LE electrolytes are compositionally equivalent, but came from different sources. The composition of both electrolytes is 1.2 M $LiPF_6$ in EC/EMC (3:7 by wt).

The first round of testing repeats some of what was done with the Gen2 cells in the ATD program. Here, the

[18] Battery Test Manual for Plug-in Hybrid Electric Vehicles, ID/EXT 07-12536
[19] FreedomCAR Battery Test Manual For Power-Assist Hybrid Electric Vehicles, DOE/ID-11069, October 2003.

cells labeled PH1C, PH1D, PH1E and PH1F will be subjected to HEV testing protocols. The initial characterization and subsequent RPTs will be performed at 25°C after 28 days of testing. The RPTs consist of C/1 and C/25 capacity measurements, the hybrid pulse-power characterization test at the low current value (HPPC-L) test and electrochemical impedance spectroscopy (EIS) characterization.

Table IV- 8: Cell distribution

ABRT label[1]	Cell designation	Calendar life at 45°C and 60%SOC[2]	PHEV combined cycling[3]			PHEV Deep CD cycling[4]	HEV cycle at 45°C and 60% SOC[2]
			30°C	45°C	55°C		
PH1A[5]	EC-B	5 cells	6	6	6	5	
PH1B[5]	EC-C	5	6	6	6	5	
PH1C	LE-360-A	3		3			3
PH1D	LE-360-B	4		4			4
PH1E	LE-362-A	3		3			3
PH1F	LE-362-B	2		2			2

Notes:

1. PH1A=bare cathode; PH1B=Alumina-coated cathode; PH1C=ANL electrolyte; PH1D=ANL electrolyte + VC; PH1E=LE electrolyte; PH1F=LE electrolyte + VC
2. Calendar life at 45°C and 60% SOC and the HEV cycling are being performed to compare to the earlier Gen2 results. The SOC will be defined by C/25 voltage at 40% DOD.
3. A PHEV combined cycle is defined as removing the scaled 3.4-kWh of energy using the charge-depleting profile, followed by 50 charge-sustaining profiles.
4. PHEV deep charge-depleting cycling is defined as discharging the battery using the CD profile until 15% SOC, as defined by initial C/1 discharge voltage measurements.
5. These cells will not be tested with the others. They will be held until after channels have opened up after the other cells are taken off test.

Results

Calendar Life. The cells initially were characterized at 25°C using C/1 and C/25 capacity measurements, the HPPC-L test and EIS. The initial, average values of the capacities and the area-specific impedances (ASI) are given in Table IV- 9. The average, initial value of the Gen2 baseline cells was about 27 Ωcm^2. The ASI values shown in Table IV- 9 are higher than those observed in the Gen2 baseline cells. The difference is due to thicker electrodes in the PHEV cells and slight differences in cell construction.

Table IV- 9: Initial values from cells used in the calendar life test.

ABR Label	C/1 capacity, Ah	C/25 capacity, Ah	ASI at 60% SOC, Ωcm^2
PH1C	1.43	1.65	51.53
PH1D	1.46	1.65	52.50
PH1E	1.42	1.49	56.59
PH1F	1.45	1.66	52.65

Of key interest is how the performances of the cells change with time relative to the Gen 2 cells. Plots of the RPT data from eight weeks of calendar testing are shown below. The least-squares fits to the Gen2 data for selected measurements are also included in the figures and are shown as solid curves. Since the initial data from the PHEV cells and those from the Gen2 cells were different, normalized data are used in the figures to facilitate the comparison.

As the cells age, their performance characteristics change with time. Figure IV- 126 shows that the ASI of the PHEV cells increases. Comparing the PHEV data to that from Gen2 shows that the initial rate of ASI increase tends to be slower. Additionally, the VC additive in the PH1D and PH1F cells further slows the rate ASI increase.

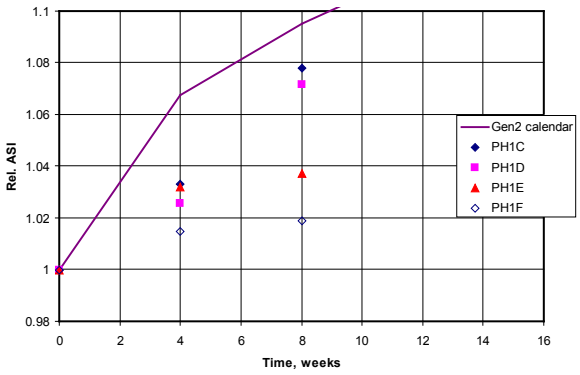

Figure IV- 126: Relative ASI vs. calendar time.

Figure IV- 127 and Figure IV- 128 show that the capacity of the cells tends to decrease, as expected with time. In both figures, the rate of capacity fade is less than that displayed by the Gen2 curve. However, there is no clear difference as yet between the cells which contain VC and those which do not regarding capacity fade.

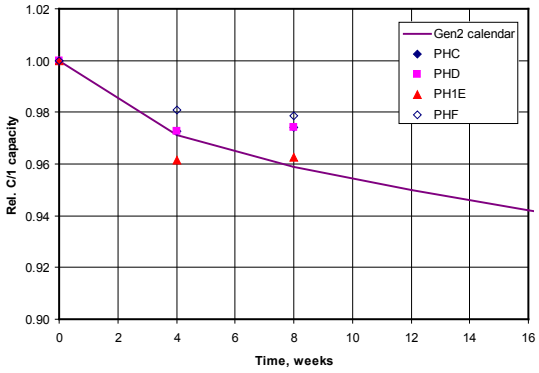

Figure IV- 127: Relative C/1 capacity vs. calendar time.

EIS data were obtained during each RPT. A plot of EIS data from a PH1C cells is shown in Figure IV- 129. This plot shows that the curves tend to shift to the left with time, similar to what is seen in Gen2 baseline cells (Figure IV- 130). Comparing the real-axis intercepts of the data from the PH1 cell with those from the Gen2 baseline cell shows that there was no change in overall curve shape.

The real-axis intercept in the PH1C cell increase about 20% and there is no discernable change in that in the Gen2 cell. The width of the interfacial arc does not change markedly with time in either case.

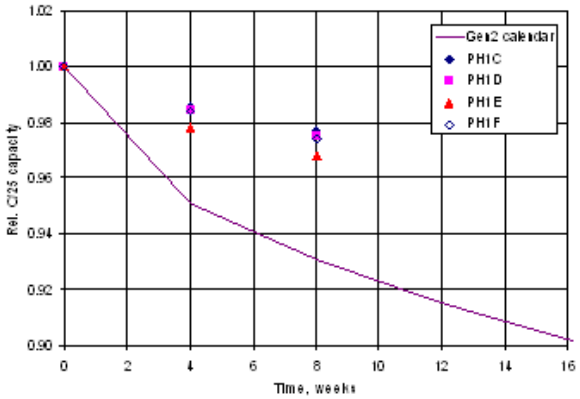

Figure IV- 128: Relative C/25 capacity vs. calendar time.

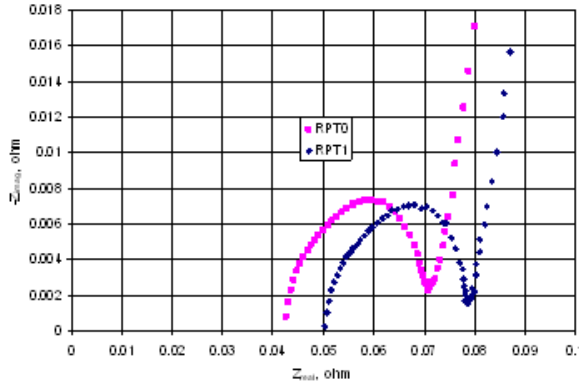

Figure IV- 129: EIS from a PH1C cell.

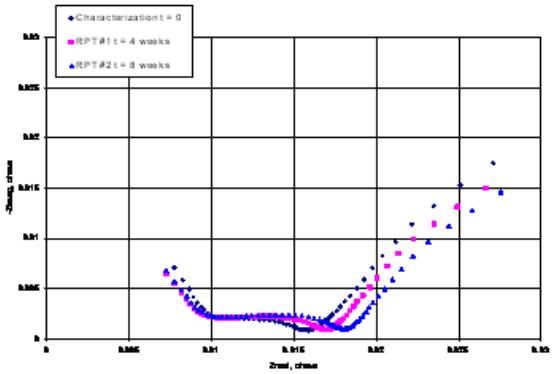

Figure IV- 130: EIS from a Gen2 baseline cell.

Conclusions and Future Directions

Cycle-life testing will commence October 2010, which will give another crucial metric by which to compare to previous Gen2 data. Based on the results above, it is too early to conclude how the performance of the cells in either the calendar or cycle life changes with age. Thus, more testing is needed. Once this step has reached a certain level, then the next step, protocol comparison can begin.

FY 2010 Publications/Presentations

None

IV.D Abuse Tolerance Studies

IV.D.1 Abuse Diagnostics

IV.D.1.1 Diagnostic Studies supporting Improve Abuse Tolerance (BNL)

Xiao-Qing Yang, Kyung-Wan Nam (PIs)
Hung-Sui Lee
Xiaojian Wang

Brookhaven National Laboratory
Upton, NY 11973-5000
Phone: (631) 344-3663; Fax: (631) 344-5815
E-mail: xyang@bnl.gov

Start Date: October 1, 2009
Projected End Date: September 30, 2011

Objectives

- Develop new diagnostic techniques with ability to distinguish bulk and surface processes, to monitor the degradation processes, to determine the effects of structural changes of electrode materials, the interfacial phenomena, and electrolyte decomposition on the cell capacity and power, as well as on the abuse tolerance.
- Using diagnostic techniques to evaluate and screen the new materials, material processing and modification procedures which are aimed to improve the performance, calendar and cycle life, and the abuse tolerance of lithium batteries for HEVs, PHEVs, and EVs.

Technical Barriers

- Li-ion and Li-metal batteries with long calendar and cycle life
- Li-ion and Li-metal batteries with superior abuse tolerance
- To reduce the production cost of PHEV batteries

Technical Targets

- To develop new *in situ* diagnostic techniques with surface and bulk sensitivity for studying the thermal stability of various cathode materials.
- To establish and investigate the thermal decomposition mechanisms of various cathode materials.
- To provide valuable information about how to design thermally stable cathode materials for HEV and PHEV applications.

Accomplishments

- Completed *in situ* hard and soft X-ray absorption spectroscopy (XAS) study on charged $Li_xNi_{0.8}Co_{0.15}Al_{0.05}O_2$ (Gen2) and $LiNi_{1/3}Co_{1/3}Mn_{1/3}O_2$ (Gen3) cathode materials during heating.
- Developed a new *in situ* diagnostic tool using high resolution TEM (HR-TEM) during heating of charged cathode materials to study the thermal decomposition mechanism with high location specification and special resolution.
- Completed *in situ* HR-TEM study of overcharged $Li_{0.27}Ni_{0.8}Co_{0.15}Al_{0.05}O_2$ (Gen2) cathode material during heating and discovered the unstable rock salt phase formed at room temperature due to the overcharge condition.
- Identified thermal decomposition mechanisms of charged Gen2 and Gen3 cathode materials and provided ideas how to improve the thermal stability of layered cathode materials.
- Completed *in situ* XRD studies of new Cr and F doped $LiMn_{1-x}Cr_xO_{4-y}F_y$ spinel in collaboration with Argonne National Lab.

✧ ✧ ✧ ✧ ✧

Introduction

Achieving the DOE goals of power for HEV, PHEV, and EV batteries for HEV, PHEV, and EV require in-depth understanding of how to improve rate, capacity and long-term cycling performance. These understandings will provide guidance on discovery of new materials and new mechanisms. This project has been working on these issues by developing new diagnostic tools to investigate battery materials both *in* and *ex situ*, and then apply them towards

understand relationships between structure and function for new materials development.

Approach

- A combination of time resolved X-ray diffraction (TR-XRD), *in situ soft and hard* X-ray absorption (XAS), *in situ* transmission electron microscopy (TEM) techniques are applied during sample heating to study the thermal stability of the electrode materials.
- *In situ* XRD, soft and hard XAS studies of new electrode materials are carried out during charge-discharge cycling to understand the power and energy density fading mechanisms. These studies are expected to increase understanding of factors affecting the calendar and cycle life of Li-ion batteries.
- The characterization efforts will include contributions resulting from extended collaboration with other US and international academic institutions and US industrial partners

Results

In situ X-ray absorption and time-resolved XRD studies of Gen2 and Gen3 cathode materials during heating

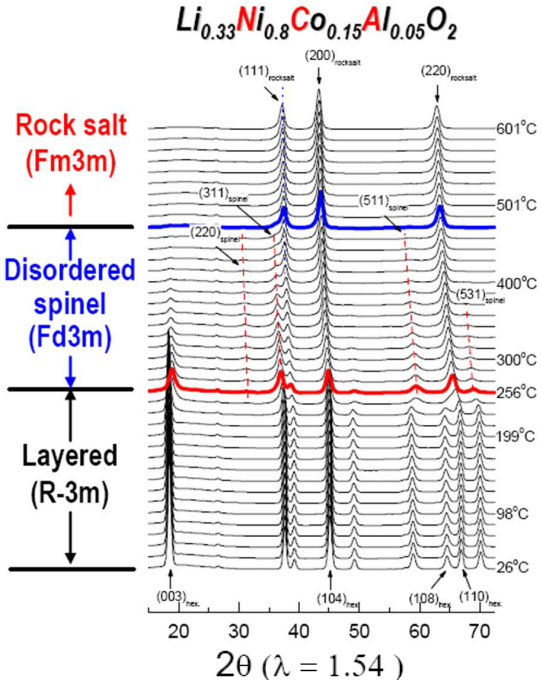

Figure IV- 131: TR-XRD of charged $Li_{0.33}Ni_{0.8}Co_{0.15}Al_{0.05}O_2$ (Gen2) during heating

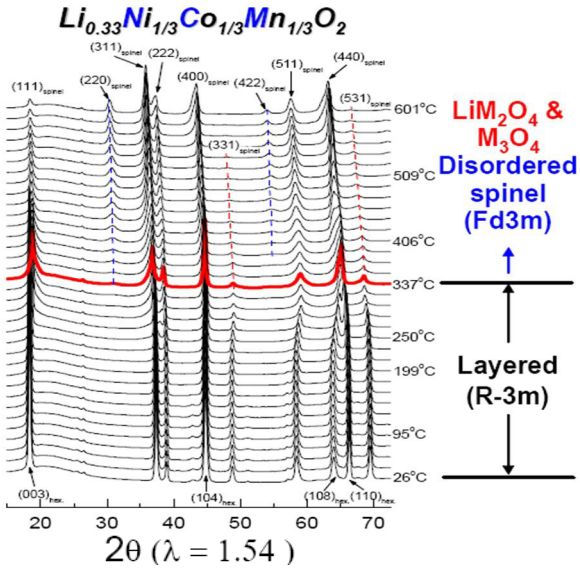

Figure IV- 132: TR-XRD of charged $Li_{0.33}Ni_{1/3}Co_{1/3}Mn_{1/3}O_2$ (Gen3) during heating

As shown from Figure IV- 131 and Figure IV- 132, the time resolved XRD resilts of overcharged Gen2 and Gen3 cathode materials have different phase transition behavior during heating. For the Gen3 material, the phase transition from layered to spinel starts at higher temperature than the Gen2(337°C vs 256°C) and stays in the spinel structures ($LiMn_2O_4$ and M_2O_4 types) in a much wider temperature range up to 600°C. In contrast, the Gen2 material transformed to the rock salt structure at a temperature as low as 500°C

As shown in Figure IV- 133 and Figure IV- 134, the Ni K-edge showed the most significant shift to lower energy during heating indicating the reduction of oxidation state. The reduction of Ni ions starts at much lower temperatures than the Gen3 material

The evolution of the transmission diffraction patterns as a function of increasing temperature are compared in Figure IV- 135 and Figure IV- 136, where Figure IV- 135 showing the uncoated Gen2 electrode and Figure IV- 136 the coated Gen2 electrode. The lack of any rock salt structural diffraction pattern and thus the higher temperature stability of the disordered spinel when protected by a ZrO_2 surface coating is seen in Figure IV-136 and not in Figure IV- 135.

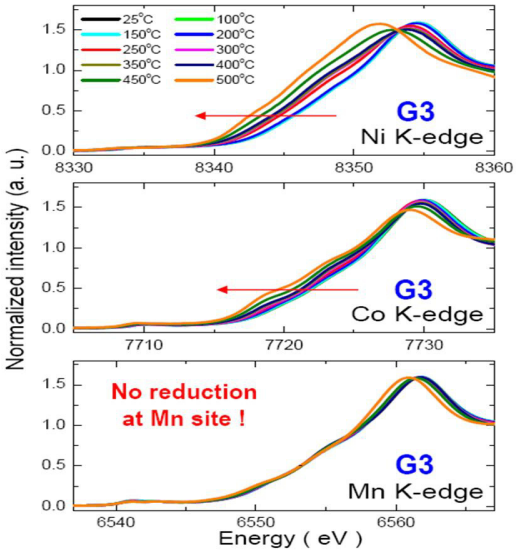

Figure IV- 133: *In situ* XAS spectra of charged $Li_{0.33}Ni_{0.8}Co_{0.15}Al_{0.05}O_2$ (Gen2) and $Li_{0.33}Ni_{1/3}Co_{1/3}Mn_{1/3}O_2$ (Gen3) during heating

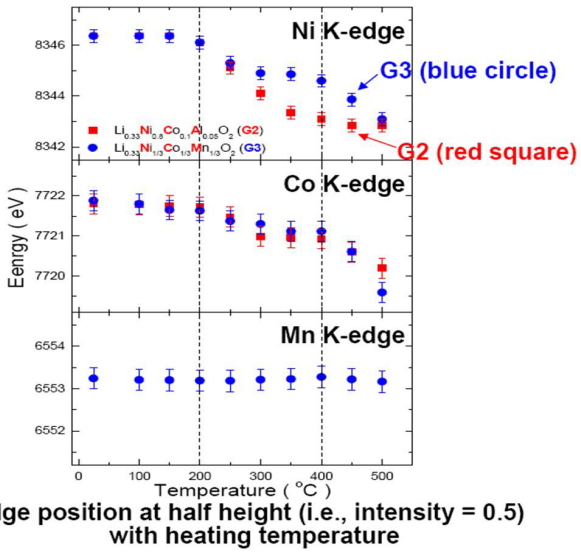

Figure IV- 134: Edge position changes with heating temperature of Gen2 and Gen3 cathode materials

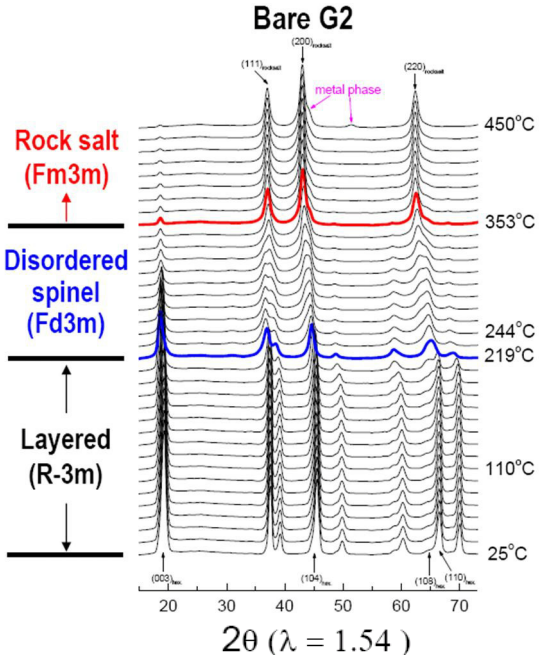

Figure IV- 135: TR-XRD of bare overcharged $Li_{0.33}Ni_{0.8}Co_{0.15}Al_{0.05}O_2$ (Gen2) during heating

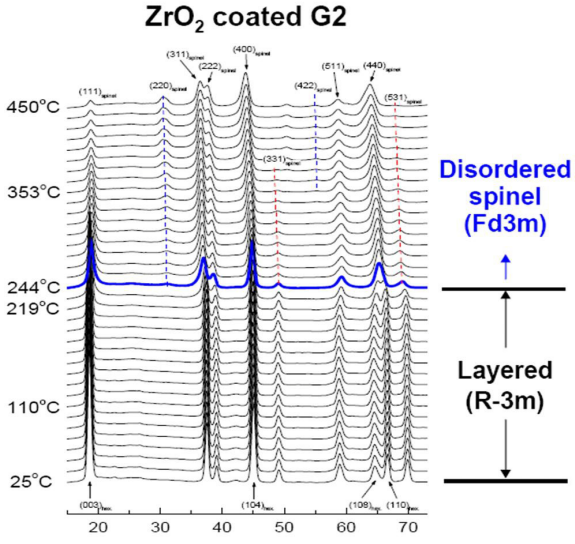

Figure IV- 136: TR-XRD of ZrO_2 coated overcharged $Li_{0.33}Ni_{0.8}Co_{0.15}Al_{0.05}O_2$ (Gen2) during heating

The thermal evolution of coated and uncoated G2 electrodes can also be studied by x-ray absorption spectroscopy, as shown for surface-sensitive partial electron yield spectra in Figure IV- 137 and bulk-sensitive fluorescence yield spectra in Figure IV- 138. Both figures

(at the surface and in the bulk) clearly show that the ZrO_2 surface coating suppressed the transition from Ni^{4+} to Ni^{2+} during heating.

Additional comments on the results appear in Figure IV- 139, Figure IV- 140, Figure IV- 141, Figure IV- 142, and Figure IV- 143. It is seen through them tha at 100°C, the spinel and rock-salt structures are seen growing into the bulk from the surface and edge of the particle. At 200°C, the spinel and rock-salt phases continues to grow larger and larger at the expense of the layered structure. At 300°C, the spinel and rock-salt phases become the dominating phases. At 400°C, the majority of the particles are composed of rock-salt crystallites.

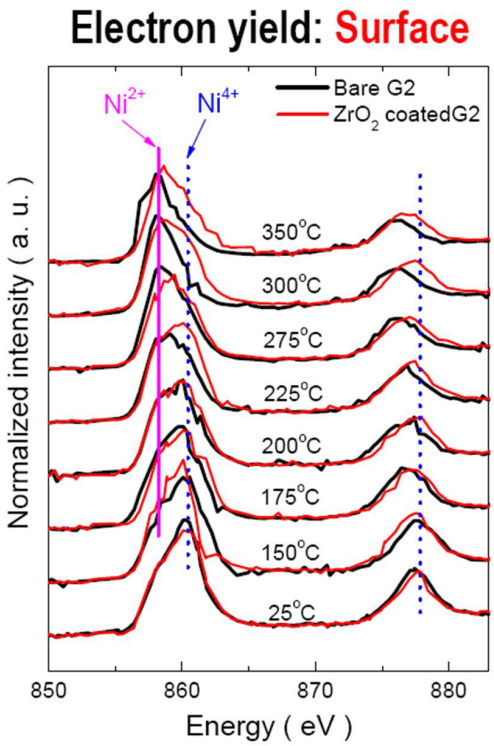

Figure IV- 137: *in situ* soft XAS results of bare overcharged $Li_{0.33}Ni_{0.8}Co_{0.15}Al_{0.05}O_2$ (Gen2) by PEY mode (surface) during heating

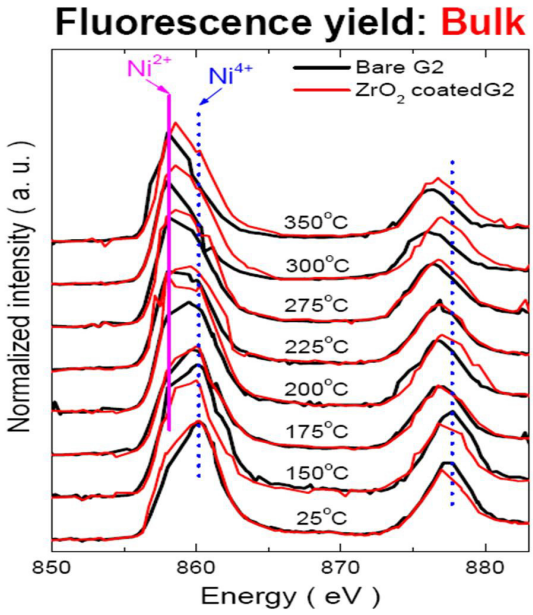

Figure IV- 138: *In situ* soft XAS results of ZrO_2 coated overcharged $Li_{0.33}Ni_{0.8}Co_{0.15}Al_{0.05}O_2$ (Gen2) by FY mode (bulk) during heating

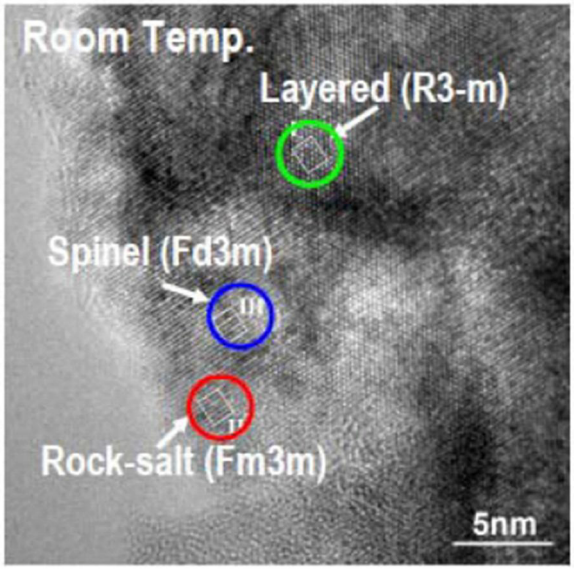

Figure IV- 139: The HRTEM image of overcharged Gen2 cathode particle at room temperature. The spinel and rock-salt structures observed only at high temperatures by XRD were observed at the surface and edge of the particle at room temperature

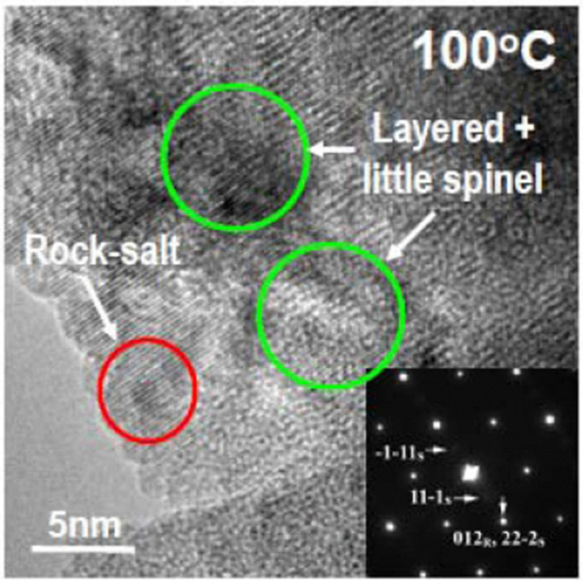

Figure IV- 140: The *in situ* HRTEM image of overcharged G2 cathode particle at 100°C. The Spinel and rock-salt structures were growing into the bolk from the surface and edge of the particle.

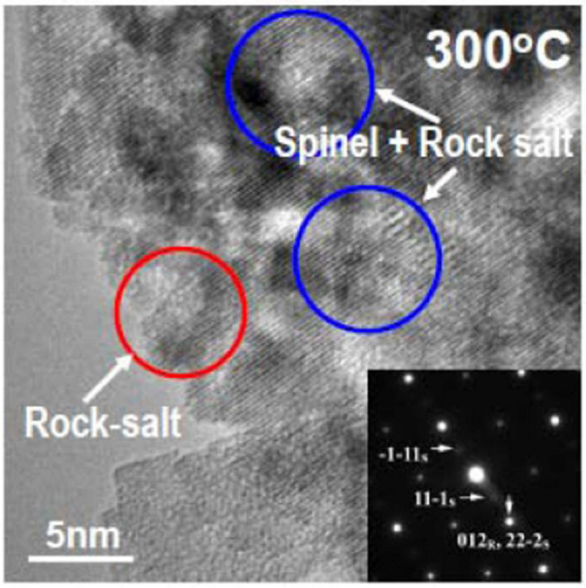

Figure IV- 142: The *in situ* HRTEM image of overcharged G2 cathode particle at 300°C. The Spinel and rock-salt phases became the dominating phases.

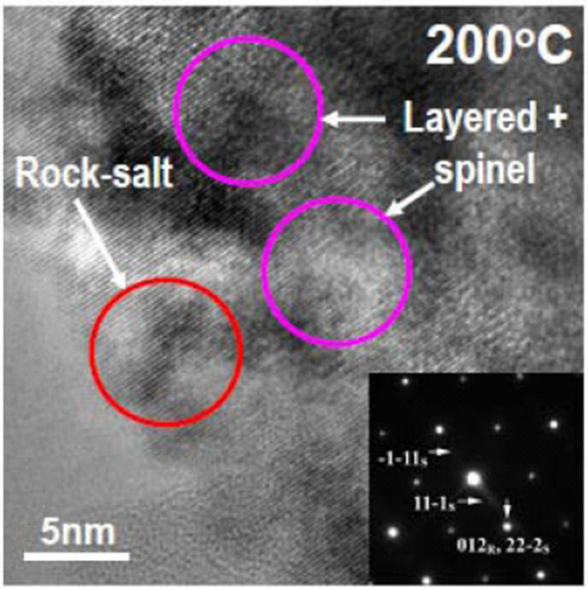

Figure IV- 141: The *in situ* HRTEM image of overcharged G2 cathode particle at 200°C. The Spinel and rock-salt phases continued to grow larger and larger with raising temperature in the expense of layeed structure.

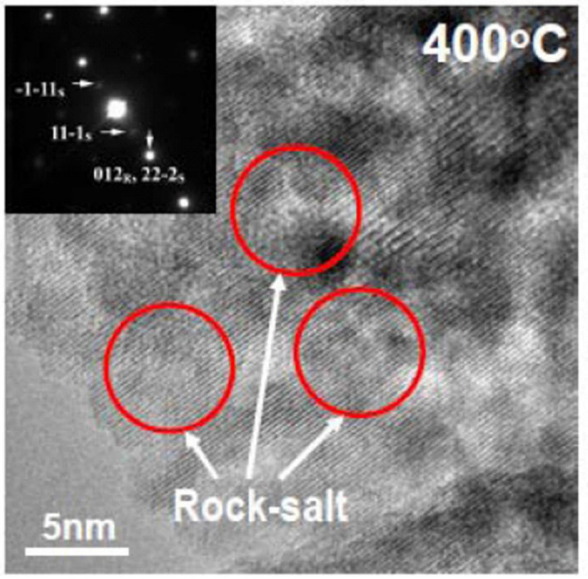

Figure IV- 143: The *in situ* HRTEM image of overcharged G2 cathode particle at 400°C. The majority of the particle changed into the rock-salt phases.

Conclusions and Future Directions

- The overcharged $Li_{1-x}Ni_{0.8}Co_{0.15}Al_{0.05}O_2$ particle at room temperature has core-shell structure with the rhombohedral structure in the core, the spinel structure in the shell and the rock-salt structure at the surface. By heating the sample in the microscope, the

spinel phase propagates toward the core of the particle while the rock-salt phase grows at the shell of the spinel phase. This result agrees quite well with the previous *in situ* soft XAS result during heating which showed that the thermal decomposition occurs at the surface much earlier than in the bulk.

- Combined *in situ* TEM and hard & soft XAS study during thermal decomposition (i.e., heating) clearly shows where and how the new structure nucleated and propagated with high location specification and special resolution as well as the structural changes at the surface and in the bulk in an elemental selective way. This *in situ* study provides new insight into the thermal decomposition mechanism of charged cathode materials and valuable information how to design thermally stable cathode materials of lithium-ion battery for the vehicle applications.
- *In situ* XRD, TR-XRD, hard and soft XAS study of $LiNi_xCo_yMn_zO_2$ (x + y + z = 1) cathode materials are useful in identifying the effect of Ni, Co, and Mn composition on the thermal stability, capacity and power fading during heating and/or charge-discharge cycling.
- In the future, these new techniques will be applied to various electrode materials to probe the structural changes at the surface and in the bulk simultaneously. These changes will be correlated to understand the fundamental aspects of the safety-related thermal run away of lithium-ion cells.
- New collaborative research relationships with US and International international academic research institutions will be expanded and US industrial partners will be established.

FY 2010 Publications/Presentations

1. 2010 DOE Annual Peer Review Meeting Presentation.
2. Kyung-Wan Nam, Won-Sub Yoon, Karim Zaghib, Kyung-Yoon Chung, and Xiao-Qing Yang, "The phase transition behaviors of $Li_{1-x}Mn_{0.5}Fe_{0.5}PO_4$ during lithium extraction studied by *in situ* X-ray absorption and diffraction techniques", *Electrochemistry Communications*, Vol. 11, Iss. 10, pp 2023-2026 (2009).
3. O. Haas, U.F. Vogt, C. Soltmann, A. Braun, W.-S. Yoon, X.Q. Yang, T. Graule, "The Fe K-edge X-Ray Absorption Characteristics of $La_{1-x}Sr_xFeO_{3-\delta}$ Prepared by Solid State Reaction Materials", Material Research Bulletin Vol. 44 (2009), pp. 1397-1404
4. X.J. Wang, H.S. Lee, H. Li, X.Q. Yang. X.J. Huang, "The Effects of Substituting Groups in Cyclic Carbonates for Stable SEI Formation on Graphite Anode of Lithium Batteries" Electrochemistry Communications Vol. 12, Iss. 3, pp 386-389 (2010)
5. Xiao-Qing Yang, K-Wan Nam, L. Wu, Y. Zhou, X. Wang, H.S. Lee, O. Haas, and Y. Zhu, Hong Li, Xuejie Huang, and Liquan Chen, "Using Synchrotron Based *in situ* X-ray Techniques and TEM to Study Electrode Materials for Lithium Batteries" **Invited**, presented at AVS 56th International Symposium & Exhibition, San Jose, California, USA, November 8-13, 2009
6. K-W Nam, X. Q. Yang, X.J. Wang, Y.N. Zhou, H.S. Lee, L.J. Wu and Y. Zhu, "Comparative Studies between Surface and Bulk Structural Changes during Heating and cycling for Layer-structured and Olivine–structured Cathode Materials" , presented the 15th International Meeting of Lithium Batteries (IMLB-15), *June 27 to July 2nd, 2010, Montreal, Canada*, **Invited.**
7. X. Q. Yang, "Application of synchrotron based *in situ* X-ray techniques to the study of lithium-ion batteries for HEV,PHEV, and EV" , presented the "U.S. – China Electric Vehicle and Battery Technology Workshop", Argonne National Lab., Argonne, Illinois, USA, August 30 to September 1st, 2010, **Invited.**

IV.D.1.2 Internal Short Circuit Test Development (SNL)

Christopher J. Orendorff
Sandia National Laboratories
PO. Box 5800, MS-0614
Albuquerque, NM 87185-0614
Phone: (505) 844-5879; Fax: (505) 844-6972
E-mail: corendo@sandia.gov

Start Date: October 1, 2009
Projected End Date: September 30, 2010

Objectives

- Develop an "on-demand" internal short circuit (ISC) approach using an external trigger that does not involve mechanical perturbation or deformation of the cell (crushing, pressing, pinching, etc.).
- Demonstrate the utility of this approach in Li-ion cells (18650 or larger format)
- Evaluate other techniques to trigger internal short circuits

Technical Barriers

There are a number of technical barriers to developing an "on-demand" ISC trigger including:

- Simulating an ISC in cells independent of cell chemistry, design, or geometry
- Demonstrating "normal" cell behavior (capacity, cycling, etc.) while the trigger is "off" (e.g. identifying a trigger that is electrochemically inert)
- Utility of studying the four primary ISC scenarios (current collector-current collector, current collector-anode, current collector-cathode, anode-cathode)
- Positioning the ISC at different locations in a cell

Technical Targets

- Identify candidate techniques (defects and triggers) that can be used to cause an "on-demand" ISC
- Demonstrate the utility of these ISC techniques in test platforms (foil electrodes) and in 18650 cells
- Identify the challenges of each technique and potential solutions to be explored next FY.

Accomplishments

- Used the metal alloy defect to trigger internal shorts in 18650 cells
- Demonstrated differences in shorts between active materials and shorts between current collectors
- Performed preliminary investigations of the internal heater approach to initiating internal shorts.

✧ ✧ ✧ ✧ ✧

Introduction

There is significant interest in better understanding and mitigating field failure modes of Li-ion batteries; especially for internal short circuit field failure in cells related to the transportation industry. To date, there is no suitable, widespread laboratory test for an internal short circuit. Moreover, a better understanding of the role and performance of the separator under these conditions could facilitate mitigation of ISCs.

Approach

Current test approaches for internal short circuits (ISCs) all include some degree of battery package deformation. These include the blunt rod test (conductive and insulated blunt nail press tests), the Battery Association of Japan (BAJ) ISC test (blunt nail press on a millimeter-sized defect placed in the cell), and the ISC pinch test by Motorola and ORNL (crush test between two blunt pressure points). Our approach is to generate an ISC in a cell without employing any cell package deformation while maintaining the ability to control the cell state-of-charge during the test. This approach includes deploying a defect into a cell and triggering that defect by some external stimulus. This FY we have focused our efforts on our low melting point metal alloy defect particles and have demonstrated the ability to trigger an internal short circuit in an 18650 cell using this approach. We have also evaluated other techniques to trigger internal short circuits, including the approach developed at Saft,[1] employing an internal heater wire to trigger an internal short and a runaway event.

Results

ISC Test Method Development. The primary focus this FY has been on developing an ISC test using metal alloy defects in cells. In this approach, cells are built with the alloy defects insulated and physically separated from the electrodes to preserve "normal" function of the cell when the trigger is "off". The internal short is triggered in the cell when the alloy undergoes the solid-liquid phase transistion and the liquid alloy breeches the insulation and makes electrical contact with both electrodes. This has been demonstrated in a proof-of-concept experiment by monitoring the AC impedance between two copper foil

electrodes wound in an 18650 configuration and separated by a polyethylene (PE) separator with the alloy defect, shown in Figure IV- 144. Here, the temperature is measured in the core of three foil roll samples and the alloy melting temperature is ~60°C. In all three samples, once the alloy melts, it leaks through the separator, triggering an ISC with a final impedance value of <100 mΩ. These results demonstrate the proof-of-concept of using these defects to triggering shorts in electrochemical system.

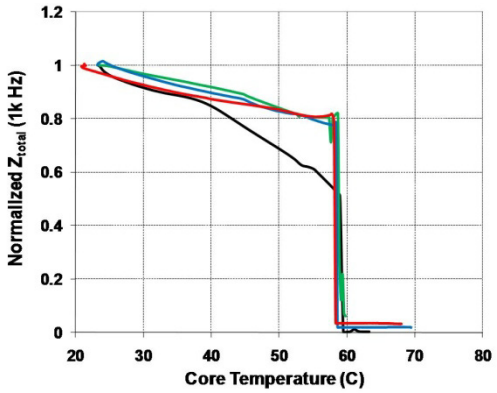

Figure IV- 144: Normalized AC impedance of a separator sheet rolled between two copper foil electrodes. Each of the four traces represents replicate samples. The electrodes are shorted together using a Bi/Sn/In alloy with a melting temperature of 60°C.

This approach has been used to trigger shorts in actual Li-ion cells, as well. 2032 coin cells were built with Li nickel manganese cobalt oxide (NMC) cathodes, graphitic carbon anodes, and metal alloy defect particles (m.p. ~60°C) insulated between the electrodes. Four cells were built with the alloy defect between the active materials on the electrodes and one cell was built with the alloy between the aluminum and copper current collectors. Cells were formation cycled and charged to a final voltage between 4.0 and 4.3 V. Figure IV- 145 shows a plot of cell voltage as a function of temperature for all five 2032 coin cells with alloy particles defects. All of the cells tested shorted at a cell skin temperature between 60-65°C, which is consistent with an alloy melting temperature of 60°C. It is interesting to note, however, the differences in the severity of the observed short. The four cells (black, gray, red and navy traces) built to short between the carbon and NMC active materials only shorted to 2.5 to 3.2 V, suggesting a soft or intermediate short. The fifth cell (blue trace), shorted between the aluminum and copper current collectors and the voltage dropped to < 1.5 V. This suggests a significant difference in behavior between the two different short conditions (anode-cathode vs. current collector-current collector) and is consistent with observations made in the literature.[2] This preliminary observation will be confirmed in additional experiments in coin cells and the differences in thermal behavior of each type of short will be evaluated in 18650 cells.

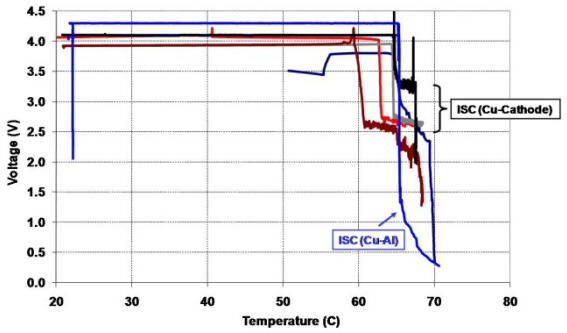

Figure IV- 145: Cell voltage as a function of temperature for NMC coin cells that are shorted using a Bi/Sn/In alloy with a melting temperature of 60°C. The red, black, gray, and navy traces are cells built with the alloy between the anode and cathode and the blue trace is for a cell built with the alloy between the two current collectors.

ISCs in 18650 cells. 18650 cells with the same metal alloy defects as in the 2032 coin cells have also been built at the Sandia cell prototyping lab. 18650 cells were built with the alloy defects that were completely isolated from the cell electrodes and the cells functioned just as "normal" Li-ion cells. Figure IV- 146 shows cycling behavior of an 18650 cell with the alloy defect at C/5 (200 mA).

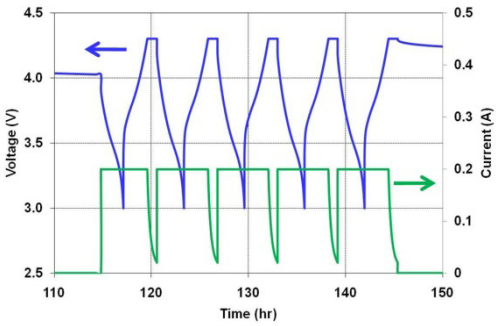

Figure IV- 146: Ambient temperature charge/discharge cycling of an NMC 18650 cell with a metal alloy defect showing "normal" cell behavior.

To trigger the internal short, cells are heated to > 60°C to melt the alloy. Figure IV- 147 shows a plot of voltage as a function of temperature for an 18650 cell with an alloy defect. The cell OCV holds constant at 4.3 V until the skin temperature reaches 68°C, where the cell voltage drops/recovers and then drops/recovers to 4.0 V again at 73°C. It is important to note that this observed soft short occurs at cell skin temperatures that are 8-13°C higher than the melting point of the alloy. However, there can be a 10-15°C difference in temperature from the inner core to the cell skin, suggesting that the internal cell temperature where the short occurred is likely to be at the alloy melting temperature of ~60°C. Attempts to cycle the cell post-ISC test shows a clear change in cell state of health with clear indications of internal shorting and is shown in Figure IV-148.

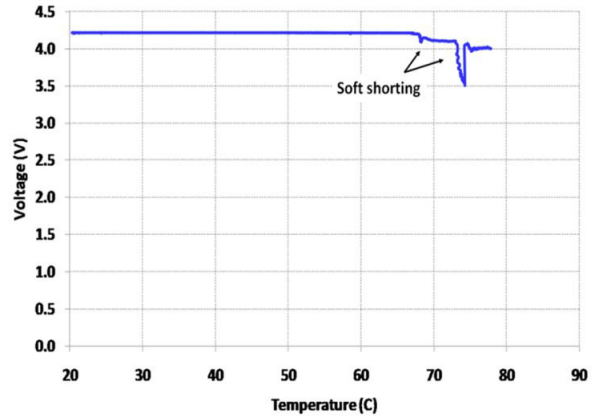

Figure IV- 147: Cell OCV as a function of temperature for an NMC 18650 cell that develops a short circuit as a result of a metal alloy trigger at 68°C.

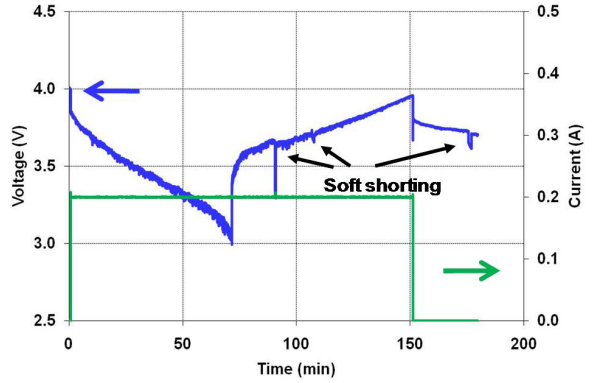

Figure IV- 148: Ambient temperature charge/discharge cycling of an NMC 18650 cell post-ISC triggering clearly showing evidence of soft shorting.

There are clear differences in the response of coin and 18650 cells to the same ISC trigger. Since this approach is based on the ability of a liquid metal to flow and make contact with both electrodes, it is highly dependant on the pressure exerted on the alloy to force flow and electrical contact. The coin cells are built with an internal spring to ensure good contact between the negative cap and copper current collector, which exerts some defined load on the electrode stack (and the alloy defect in these experiments). While the load on an alloy defect in an 18650 cell is dictated by the tension set on the winder, which could be widely variable and much more dynamic (changes upon introduction of electrolyte, charge/discharge cycling, etc.). Clearly, additional work is needed to optimize the effectiveness of the defect trigger for the different cell formats.

Internal heater short circuit test (Saft). Saft has recently proposed using an internal heater to trigger an internal short circuit in spiral wound Li-ion cells. In this experiment, cells are wound with a tungsten heater wire between the separator and electrodes. The leads of the heater are drawn through the header, out of the cell and the cell is sealed with epoxy. Figure IV- 149 shows an X-ray image of a typical 18650 cell with an internal heater.

Figure IV- 149: X-ray image of an 18650 cell with an internal heater.

The cells were tested by applying a constant current to the heater wire through an external power supply and the cell voltage and temperature were monitored during the experiment. Representative data are shown in Figure IV-150. Current is applied at time = 0, and the cell skin temperature begins to increase after ~1 min. The cell skin temperature continues to increase to 100°C without any change is cell voltage. At 100°C, the cell voltage increases, which is likely due to some increase in internal impedance (electrolyte solvent boiling or oxidation at the electrode interface). At 115°C, the cell shorts and the voltage drops < 2 V.

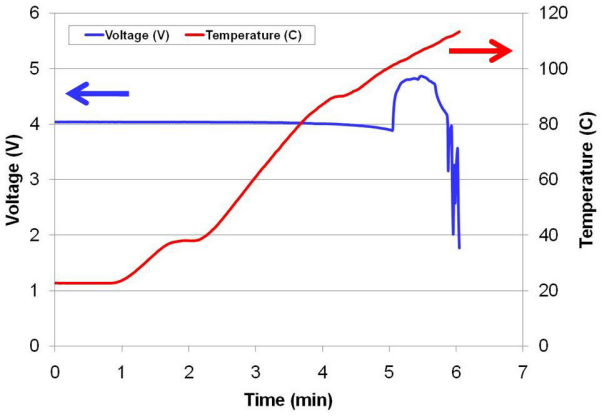

Figure IV- 150: Internal short circuit of an 18650 cell with an internal heater at 115°C.

The amount of time required to initiate an internal short is somewhat surprising because of the temperature of the heated wire; which glows red hot with applied current.

One might expect the hot wire to instantly melt the separator (m.p. ~135°C) and directly short the electrodes. Without more data, it is difficult to interpret a mechanism of cell failure. One possibility is that the melted separator coates the heater wire and prevents direct contact with the electrodes. Moreover, the heat generated by the wire could be absorbed and distributed through the cell heat capacity (~0.9 J/g-C) during the course of the experiment and the effective heating is not as localized as anticipated. This preliminary data set suggests this approach could be a viable option to trigger an internal short circuit. However, it should be noted that this approach may not be representative of cell field failure since the internal shorting is triggered at elevated cell exterior temperatures (> 110°C).

Conclusions and Future Directions

These results represent significant progress toward the development of an "on-demand" internal short circuit trigger. The use of metal alloy defect particles to initiate an internal short has been shown as a viable approach not only for small coin cells, but also for 18650 cells. Work will continue to engineer this approach to give reproducible hard internal shorts for cylindrical and prismatic cells (> 2 Ah). Thermal response to internal shorting will also be evaluated for the various types of shorts (impedance of the short, location in the cell, etc.) to develop a more complete understanding of cell behavior under field failure. Work on the internal heater and other new approaches will also continue to determine their attributes as potential test methods for internal short circuits.

References

1. S. Bourlot et al. "Investigation of ageing mechanism of high power Li-ioncells used for hybrid electric vehicles (HEVs)"International Meeting on Lithium Batteries, Montreal, Canada July 2010.
2. S. Santhanagopalan, R. Ramadass, J. Zhang J. Power Sources, 194 (2009) 550-557.

FY 2010 Publications/Presentations

1. 2010 DOE Annual Merit Review
2. C. J. Orendorff and E. P. Roth, "Triggering Internal Short Circuits in Lithium-ion Batteries" International Meeting on Lithium Batteries, Montreal, Canada July 2010.
3. E. P. Roth and C. J. Orendorff, "A Review of Critical Safety Issues in Li+ Batteries" International Battery Association/Pacific Power Sources Symposium, Waikoloa, HI, January 2010.

IV.D.2 Abuse Mitigation

IV.D.2.1 Develop & Evaluate Materials & Additives that Enhance Thermal & Overcharge Abuse (ANL)

Khalil Amine & Zonghai Chen

Argonne National Laboratory
9700 South Cass Avenue
Argonne, IL 60439-4837
Phone: (630) 252-3838; Fax: (630) 972-4451
E-mail: amine@anl.gov

Collaborators:
Yang ren, Argonne National Laboratory
Christopher J. Orendorff, Sandia National Laboratories
Hitachi Chemical Inc.
ECPRO Co. Ltd.
EnerDel

Start Date: October, 2008
Projected End Date: September, 2010

Objectives

- Determine the role of cell materials/components on the abuse tolerance of lithium-ion cells.
- Identify and develop more stable materials that will lead to more inherently abuse-tolerant cell chemistries.
- Secure sufficient quantities of these advanced materials (and electrodes) to supply them to Sandia National Laboratories (SNL) for validation and quantification of the safety benefits in 18650 cells.

Technical Barriers

- Determine role of the solid-electrolyte interface (SEI) layer on carbon anodes in cell safety.
- Determine role of cathode in cell safety.
- Provide overcharge protection of lithium-ion batteries.

Technical Targets

- Understand the response of the SEI layer to thermal abuse.
- Develop functional additives that enhance the stability of the SEI layer.
- Understand the response of cathode materials to thermal abuse.
- Develop functional protection strategies to enhance the thermal stability of batteries.
- Benchmark and develop advanced redox shuttles to improve the overcharge tolerance of lithium-ion batteries.

Accomplishments

- SEI formation on different carbon anodes
  - Material investigated: MCMB-1028, three types of surface modified graphite (from Hitachi) and hard carbon
  - 18650 cells using $LiFePO_4$ and different carbons were secured and sent to SNL for accelerating rate calorimetry (ARC).
  - Differential scanning calorimetry (DSC) data (ANL) and ARC data (SNL) agreed that the type of carbon anode can significantly affect the safety of lithiated carbon.
- Electrolyte additive for stable SEI layer
  - Three electrolyte additives were identified to provide a stable SEI on graphite and hence to improve the safety of lithium-ion cells.
  - Better capacity retention was shown with the electrolyte additives.
  - SNL is quantifying the effect of the additive LiDFOB at the 18650 cell level.
- Role of $LiPF_6$ on the thermal reactivity of cathodes
  - The reaction of delithiated nickel-manganese-cobalt oxide with electrolyte components was studied with DSC.
  - $LiPF_6$ was investigated against pure solvents, $LiBF_4$, LiTFSI, and $Li_2B_{12}F_{12}$.
  - $LiPF_6$ has a negative impact on cathode safety by reducing the onset temperature from ~310^{o}C to about ~230^{o}C.
- Enhancement of overcharge abuse

- Three new aromatic redox shuttles with a redox potential of 4.17, 4.2, and 4.85 V vs. Li+/Li were synthesized at ANL.
- Their overcharge protection functionality was confirmed in coin cells.

✧ ✧ ✧ ✧ ✧

Introduction

The safety of lithium-ion batteries, along with cost, is the major technical barrier for their application in hybrid electric vehicles and plug-in hybrid electric vehicles. Understanding the mechanism of thermal runaway reactions is a key to developing advanced technologies that improve the abuse tolerance and mitigate the safety hazard of lithium-ion batteries.

Approach

The following approaches are being taken to tackle the safety issue of lithium-ion batteries:

- Understanding the impact of the graphite surface on the safety of the lithium-ion cell.
- Exploring new functional electrolyte additives that form a stable passivation film at the carbon surface, which can lead to the reduction of the overall heat generated from the SEI breakdown.
- Exploring new redox-shuttle materials to (a) improve the overcharge protection of lithium batteries and (b) achieve automatic capacity balancing of battery packs.
- Quantifying the role of the additives and surface area of carbon on 18650-type cells in collaboration with SNL.

Results

The following documents the progress on (1) understanding the root cause of battery safety data and (2) improving the thermal abuse tolerance and overcharge protection of lithium-ion cells over the past year.

Thermal Stability of Lithiated Graphite. It is well known that the lithium-ion cell is sensitive to thermal abuse. A lithium-ion cell stored in a 160-180°C oven (UL hotbox test) will generally undergo thermal runaway. Figure IV- 151 shows the DSC profile of different cell components in a lithium-ion cell to identify the bottleneck chemical reaction that triggers the thermal runaway at such a low temperature (160-180°C). Figure IV- 151 clearly shows that only two components have a thermal event below 200°C. The shutdown and melting of the separator occurs in two steps, at 130°C and 160°C, respectively (Figure IV- 151(d). However, the melting/shutdown of the separator is an endothermic reaction and cannot be responsible for the thermal runaway. The only exothermic reaction below 200°C is the continuous decomposition/formation of the SEI layer on the surface of graphite, as shown in Figure 1c. This reaction is believed to heat the cell to higher temperature and trigger other major exothermal reactions. To confirm this speculation, five different carbons, whose physical parameters are listed in Table IV- 10, were investigated using DSC and ARC.

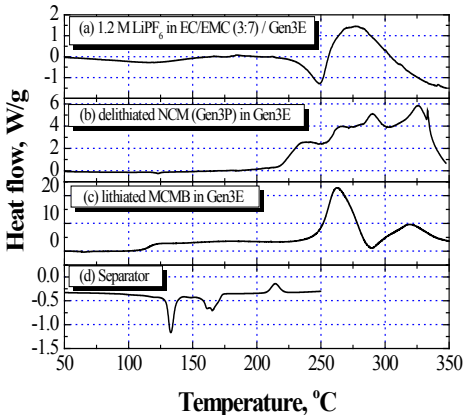

Figure IV- 151: DSC profile of different cell components showing that the SEI decomposition is the bottleneck for battery safety.

Table IV- 10: Physical and chemical properties of carbon anodes

	MCMB-1028	SMG-N-7b	SMG-N-20	SMG-Ns-15f	HC
Description	MCMB	Surface modified	Nature graphite	Surface modified	Hard carbon
D50 dia. (μm)	11.8	11.1	19.5	21.6	-
BET surface area (m^2/g)	2.01	5.0	5.1	0.7	-
Activ. Energy, E_a (kJ/mol)	53.54	88.08	92.66	78.46	87.34

Figure IV- 152 shows the DSC profiles from the reactions between lithiated carbon and the non-aqueous electrolyte of 1.2 M $LiPF_6$ in ethylene carbonate-ethyl methyl carbonate (EC/EMC) at 3:7 ratio by weight. Clearly, MCMB-1028 has the lowest onset temperature for the SEI decomposition, while the onset temperature for hard carbon is the highest. In other words, the thermal stability of hard carbon is better than surface modified graphite (SMG) and even better than mesocarbon microbeads (MCMB). Meanwhile, the activation energies of SEI decomposition with different carbons were also measured and are listed in Table IV- 10. It can be seen that SMG-N-20 has the highest activation energy and relatively high onset temperature (Figure IV- 152). Thus, we expect

that SMG-N-20 is safer than SMG-N-7b and SMG-Ns-15f, although it has the highest specific surface area. To confirm this, we collaborated with SNL to run an ARC experiment on 18650 cells using different carbon anodes and a $LiFePO_4$ cathode (to minimize the impact of the cathode). The ARC data confirmed that SMG-N-20 is safer than SMG-N7f and SMG-Ns-15f. Those data will be reported independently by SNL.

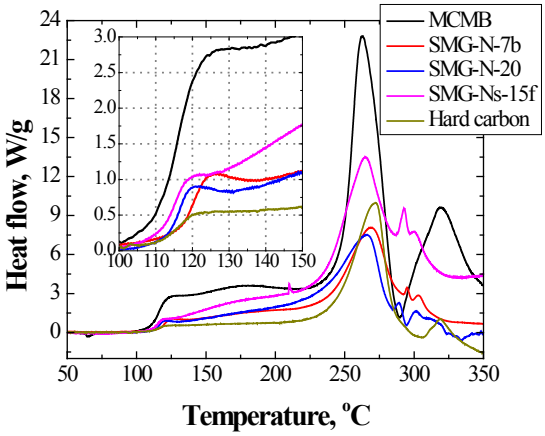

Figure IV- 152: DSC profiles of different lithiated carbons with non-aqueous electrolyte.

Overcharge Protection of Lithium-Ion Cells. Overcharge of lithium-ion batteries can lead to the failure of a battery pack or a fire hazard. A "redox shuttle" is an electrolyte additive that provides an intrinsic mechanism that enhances the overcharge tolerance of lithium-ion batteries. Moreover, the redox shuttle in lithium-ion batteries can provide automatic balancing for the battery pack.

Figure IV- 153 shows the charge and discharge capacity of a $Li_{1.1}[Mn_{1/3}Ni_{1/3}Co_{1/3}]_{0.9}O_2$/C cell using an electrolyte of 0.4 M $Li_2B_{12}F_9H_3$ in EC/EMC (3:7, by weight) with 5.0 wt% 2-(pentafluorophenyl)-tetrafluoro-1,3,2-benzodioxaborole and 1.0 wt% lithium difluoro(oxalato)borate. The cell was tested with a constant current of C/3 (0.5 mA). For each cycle, the cell was charged for 3.2 mAh, and the initial discharge capacity of the cell was about 1.5 mAh. This means that the cell was overcharged by about 100% of its reversible capacity each cycle. Figure IV- 153 shows that the overcharge protection mechanism was fully functional up to 450 cycles.

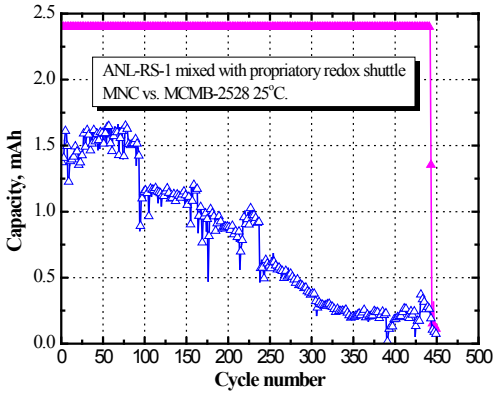

Figure IV- 153: Charge (red) and discharge (blue) capacity of a $Li_{1.1}[Mn_{1/3}Ni_{1/3}Co_{1/3}]_{0.9}O_2$/C lithium-ion cell during the overcharge test using $Li_2B_{12}F_9H_3$ based electrolyte containing 5 wt% 2-(pentafluorophenyl)-tetrafluoro-1,3,2-benzodioxaborole and 1 wt% lithium difluoro(oxalato)borate.

Figure IV- 154 shows the cyclic voltammogram of a new redox shuttle synthesized at ANL and tested in a Pt/Li/Li three-electrode electrochemical cell. The background electrolyte was 1.2 M $LiPF_6$ in EC/EMC (3:7 by weight). Figure IV- 154 shows that ANL-RS-3 has a redox potential at 4.85 V, which is high enough for overcharge protection of high-voltage, high-energy cathode materials like $Li_{1+x}(Ni_{0.25}Mn_{0.75})O_2$ and $Li_{1+x}(Ni_{0.5}Mn_{1.5})O_4$.

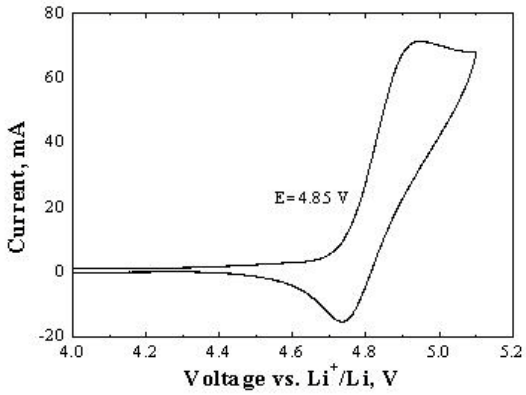

Figure IV- 154: Cyclic voltammogram of a newly synthesized redox shuttle tested in Pt/Li/Li three-electrode electrochemical cell. The structure of the redox shuttle is shown as an inet.

Figure IV- 155 shows the voltage profile of an MCMB/$Li_{1.2}Ni_{0.15}Co_{0.1}Mn_{0.55}O_2$ lithium-ion cell during overcharge test. The electrolyte used is 1.2 M $LiPF_6$ in EC/EMC (3:7 by weight) with 5.0 wt% redox shuttle. For each cycle of the test, the cell was charged for 4.0 mAh with a constant current of C/10, which is amost three times of the reversible capacity of the cell, or to impose 200% overcharge on each cycle. Figure IV- 155 shows a clear voltage plateau at about 4.7 V, which is very difficult for redox shuttle to be stable at such high oxidation condition.

The charge/discharge capacity of this cell is shown in Figure IV- 156. This preliminary data demonstrates that the development of redox shuttles for overcharge protection of high voltage cathode materials is possible. More effort will be devoted to understanding the mechanism and improving the stability of redox shuttles at such a high working potential.

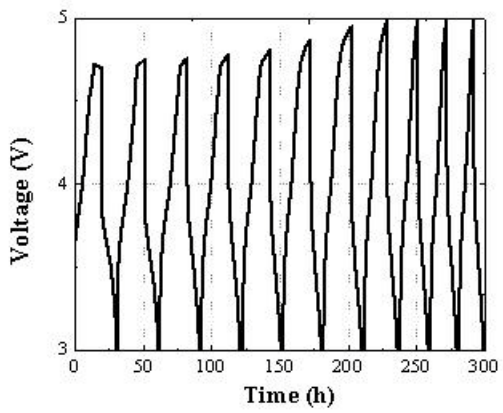

Figure IV- 155: Voltage profile of an MCMB/$Li_{1.2}Ni_{0.15}Co_{0.1}Mn_{0.55}O_2$ lithium-ion cell during overcharge test.

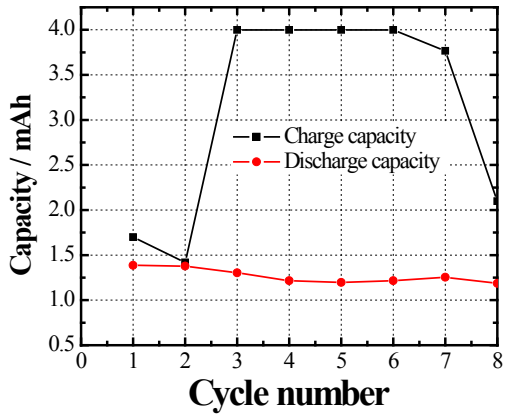

Figure IV- 156: Charge/discharge capacity of an MCMB/$Li_{1.2}Ni_{0.15}Co_{0.1}Mn_{0.55}O_2$ lithium-ion cell during overcharge test.

FY 2010 Publications/Presentations

1. 2010 DOE Annual Peer Review Meeting Presentation.
2. Wei Weng, Zhengcheng Zhang, Paul C. Redfern, Larry A. Curtiss, and Khalil Amine, J. Power Sources, in press (2010).
3. Zhengcheng Zhang, Lu Zhang, John A. Schlueter, Paul C. Redfern, Larry A.Curtiss, and Khalil Amine, J. Power Sources, 195(15): 4957-4962 (2010).
4. Yan Qin, Zonghai Chen, K. Amine, H. S. Lee, and X.-Q. Yang, J. Phys. Chem. C, 114:15202-15206 (2010).
5. Zonghai Chen, Yan Qin, Khalil Amine, and Y.-K. Sun, J. Mater. Chem., 20:7606-7612 (2010).
6. Yan Qin, Zonghai Chen, Wenquan Lu, and Khalil Amine, J. Power Sources, 195: 6888-6892 (2010).
7. Zonghai Chen, J. Liu, A. N. Jansen, G. Girish Kumar, Bill Casteel, and K. Amine, Electrochem. Solid State Lett., 13(4): A39-A43 (2010).
8. Y. Qin, Zonghai Chen, J. Liu, and K. Amine, Electrochem. Solid State Lett., 13(2): A11-A14 (2010).
9. Lu Zhang, Zhengcheng Zhang, Khalil Amine, and Zonghai Chen, patent applied for (ANL-IN-09-84).
10. Zhengcheng Zhang, Lu Zhang, and Khalil Amine, patent applied for (ANL-IN-09-82).

IV.D.2.2 Impact of Materials on Abuse Response (SNL)

Christopher J. Orendorff and E. Peter Roth
Sandia National Laboratories
P. O. Box 5800, Mail Stop 0614
Albuquerque, NM 87185-0614
Phone: (505) 844-5879; Fax: (505) 844-6972
E-mail: corendo@sandia.gov

Start Date: October 1, 2009
Projected End Date: September 30, 2010

Objectives

- Elucidate degradation mechanisms in lithium-ion cells that lead to gas evolution and heat-generating products
- Develop and evaluate advanced materials (or materials combinations) that will lead to more abuse tolerant lithium-ion cells and battery systems
- Build 18650 cells in the SNL fabrication facility for full cell level evaluation of new materials

Technical Barriers

- There are several technical barriers to achieving the goals stated above including:
- Develop lithium-ion cells that are intrinsically abuse tolerant and do not lead to high order catastrophic failures
- Mitigate the gas evolution decomposition products and the inherent flammability of liquid electrolytes

Technical Targets

- Quantify the thermal runaway response of materials at the full (18650) cell level
- Determine the effect of additives on cell thermal stability and abuse performance
- Evaluate the thermal response of candidate active materials
- Identify materials that could be used to reduce gas generation during cell thermal decomposition

Accomplishments

- Quantitative demonstration of improved cell thermal response in 18650 cells using more thermally stable graphite anodes
- Demonstrated a 15°C stabilization of the onset temperature to thermal runaway in full cells with VC electrolyte additives attributed to stabilization of the anode SEI
- Demonstrated that the use of AlF_3-coated NMC cathodes has a significant impact on the kinetics and enthalpy of thermal runaway compared to uncoated NMC cathodes in 18650 cells
- Demonstrated dramatic improvements in the thermal stability and reduced gas generation using LiF/ABA (anion binding agent) electrolytes in cells
- Used the SNL cell fabrication facility to evaluate the effects of new materials on the thermal stability and abuse response in 18650 cells.

Introduction

As lithium-ion battery technologies mature, the size and energy of these systems comtinues to increase (> 50 kWh for EVs); making safety and reliability of these high energy systems increasingly important. While most materials advances for lithium-ion chemistries are directed torward improving cell performance (capacity, energy, cycle life, etc.), there are a variety of materials improvements that can be made to improve lithium-ion battery safety. Issues including energetic thermal runaway, electrolyte decomposition and flammability, anode SEI stability, and cell-level abuse tolerance continue to be critical safety concerns. This report highlights work with our collaborators to develop advanced materials to improve lithium-ion battery safety and abuse tolerance and to perform cell-level characterization of new materials.

Approach

The effect of materials (electrolytes, additives, anodes, and cathodes) on the thermal response of full cells is determined using several techniques. One of the most useful and quantitative techniques is accelerating rate calorimetry (ARC). The ARCs at SNL are fitted with uniquely designed high pressure fixtures to measure quantitative heat flow and gas generation under ideal adiabatic conditions during full cell runaway. Cells were fabricated using a variety of active materials, electrolytes, and additives in the SNL cell prototyping facility. Coated electrodes are either provided by our collaborators or coated from bulk powder. The in-house prototyping capabiltity gives us the versatility to target candidate materials, perform full cell evaluation, and correlate cell response to fundamental materials properties.

Results

Anode Stability in Hitachi $LiFePO_4$ cells. $LiFePO_4$ cells were built by Hitachi with several different anode materials in 1.2 M $LiPF_6$ EC:EMC (3:7) electrolyte in order to evaluate the effect of anode reactivity on the onset of thermal runaway in collaboration with Argonne National Laboratory (ANL). The themal runaway response of these cells is largely determined by the anode material since the $LiFePO_4$ cathodes do not release oxygen at high temperatures as seen in other Li-ion cell chemistries. Cells were also constructed with 2% VC (vinylene chloride) additive to quantitate the effect of SEI stabilization on these anode materials and determine the effect on overall thermal stability of 18650 cells. Anode type, surface area, and activation energy (E_a, determined by DSC) are shown in Table IV- 11 (from ANL).

Table IV- 11: Anode description for 2% VC cells

Anode	Type	BET(m^2/g)	E_a (kJ/mol)
SMG-N-7b	Surface modified	5.0	88.08
SMG-N-20	Natural graphite	5.1	92.66
SMG-Ns-15f	Surface modified	0.7	78.46

Accelerating rate calorimetry was used to determine the thermal response of the Hitachi cells with the different anode materials. ARC profiles (heating rate vs. temperature) for three cells with the VC additive (labled VC2) are shown in Figure IV- 157. The thermal response of the N-20 and N-7b cells were very comparable (heating rates ~0.2 C/min), while the Ns-15f cell was measureably more reactive (~10 ˚C lower onset temperatures, 0.75 C/min heating rate and a broadened runaway peak). These cell results were consistent with the materials properties shown in Table IV- 11, where cells with the largest runaway response (Ns-15f) had the anode with the smallest activation energy. The two cells with comparable behavior had anodes with comparable activation energies (N-7b and N-20, Table IV- 11), both of which were greater than that for Ns-15f.

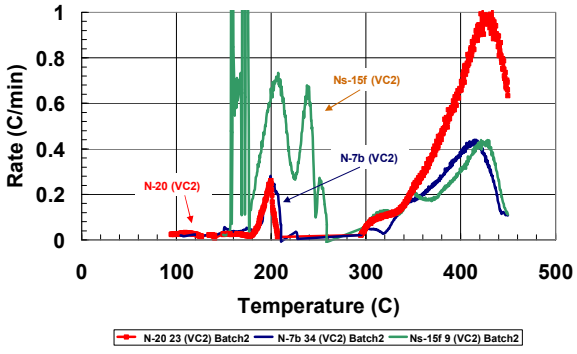

Figure IV- 157: ARC profiles for Hitachi $LiFePO_4$ cells with N-7b, N-20, and Ns-15f anode materials.

Anode SEI stabilization in full cells was also studied using ARC on cells with VC additives. 2% VC was added to the Hitachi cell electrolyte with each anode type. ARC experiments were performed to determine if any stabilization in the anode SEI could be elucidated in full cells and if the degree of stabilization was different for each type of anode material. ARC results for the cells with N-20 and Ns-15f anodes showed no significant improvement in anode stability with the addition of VC (no change in onset temperature or runaway enthalpy). Cells with N-7b anodes (high surface area and surface modified) showed a ~20 ˚C increase in the onset temperature of thermal runaway with the addition of VC as shown in Figure IV- 158 for three of the N-7b cells. Cells with VC (VC2, red and green traces) had onset temperatures of 180-185 ˚C, while the cell without VC (VC0, blue trace) showed an onset of 160 ˚C. This suggests some measureable improvement of SEI stability on this surface modified carbon anode (N-7b) and that this surface modification approach in combination with VC additives could improve the overall stability of the negative electrode under abuse conditions.

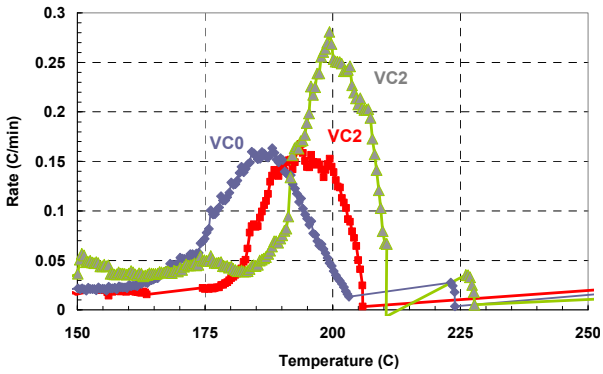

Figure IV- 158: ARC profiles for three Hitachi $LiFePO_4$/N-7b cells: two cells with VC (VC2, red and green trace) and one cell without VC (VC0, blue trace).

Thermal Stability of AlF_3-coated NMC cathodes. ANL has developed inert coatings for cathode materials in order to improve their inherent safety by reducing the high-temperature oxidation reactions of the cathode with the electrolyte which can lead to energetic thermal runaway.. One such material is AlF_3-coated $Li_{1.1}(Ni_{1/3}Mn_{1/3}Co_{1/3})_{0.9}O_2$ (AlF_3 NMC), where the surface of the NMC cathode particles were modified with ~10 nm of crystalline AlF_3. Preliminary work at ANL used DSC to determine that the AlF_3 NMC materials have improved thermal stability, with onset decomposition temperatures of 260 ˚C for AlF_3 NMC compared to ~240 ˚C for uncoated NMC. The objective of the cell-level experiments was to determine the impact of this stabilized NMC on the thermal response of a full cell.

ARC experiments were performed on 18650 baseline NMC cells and AlF_3 NMC cells built at SNL using coated

electrodes provided by ANL. Figure 3 shows ARC profiles for a representative NMC cell (red trace) and three AlF_3 NMC cells (blue, navy and green traces) tested under the same adiabatic ARC conditions. The onset runaway temperatures for the NMC and AlF_3 NMC cell chemistries were 235 and 245˚C, respectively. The maximum normalized heating rate for the NMC cell was 180°C/min-Ah compared to 2 to 65˚C/min -Ah for the AlF_3 NMC cells. Moreover, the relative runaway enthalpy of the AlF_3 NMC cell was ~40% less than for the NMC cell (indicated by the width of the runaway peak in Figure IV- 159). These data suggest a significant improvement in the thermal stability of the coated NMC cathode cells compared to those that are uncoated. It is interesting to note the wide variability in the thermal response of the AlF_3 NMC cells. This is likely due to the known heterogeneity of the AlF_3 coating at the surface of the NMC particles, which could give rise to variability in material thermal stability in full cells (i.e. oxygen release, electrolyte/cathode interfacial reactivity, etc.).

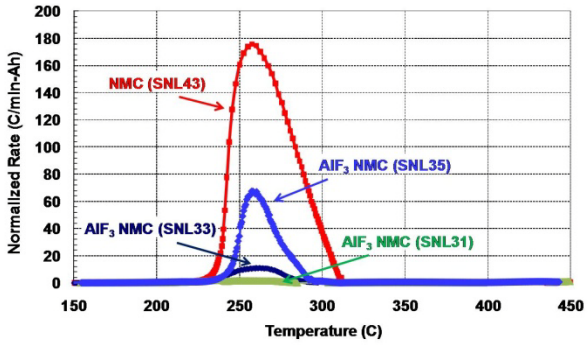

Figure IV- 159: ARC profiles for NMC (red trace) and AlF_3-coated NMC cells (blue, navy, and green traces).

During the ARC experiment, gas pressure is measured in a pressure tight fixture (to 3,000 psi) and is used to calculate total gas volume at standard temperature and pressure (STP). STP gas volumes from representative NMC and AlF_3 NMC cell\ARC experiments are shown in Figure IV- 160. Despite the significant differences observed in the cell thermal responses (Figure IV- 159), the total gas volume evolution profiles were very similar. Both cells exhibited the same gas generation profile to 300˚C, showed the same large gas volume change at the end of peak runaway (300 and 320˚C, respectively), and had approximately the same total gas volume at the end of the experiment (~1,800 mL at 450˚C). One might expect the lower heating rates and a decrease in the runaway enthalpy observed for the coated NMC cells (Figure IV- 159) to be attributed to less exothermic heat from electrolyte oxidation at the passivated AlF_3 interface which would also produce less total gas decomposition products. However, since the gas volumes (and total moles of gas) are equivelant for the coated and uncoated cathodes, that mechanism may not be correct. These results are consistent with previous measurements of several cell cathode materials which showed that gas evolution is largely determined by the volume of electrolyte which undergoes catalytic decomposition at high temperatures. Additional experiments at the materials and cell level will have to be performed in order to elucidate the degradation mechanism leading to the runaway enthalpy changes and how that impacts gas generation for the coated and uncoated NMC cathode materials.

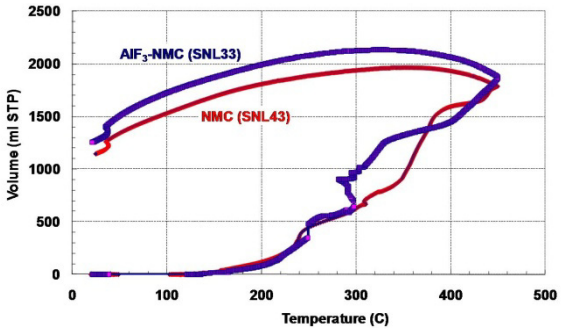

Figure IV- 160: Total STP gas volume as a function of temperature during an ARC experiment for NMC (red trace) and AlF_3-NMC (navy trace) 18650 cells. Gas evolution shown during heating, themal runaway and cooldown.

LiF/ABA electrolyte. Lithium hexafluorophosphate ($LiPF_6$)/carbonate solvents are the most common liquid electrolyte systems because of their good conductivity (10 mS/cm) and voltage stability (to 4.5V vs. Li). However, $LiPF_6$ does have some shortcomings in terms of its thermal stability and decomposition products (e.g. HF, PF_5, POF_3) which can react to degrade other cell components and produce large volumes of decomposition gases (up to 2,500 mL for a 1 Ah 18650 cell). The use of lithium fluoride (LiF) electrolyte salt has been considered as an alternative to $LiPF_6$ because of its unmatched thermal stability, but early generation anion binding agents (ABAs, used to improve LiF solubility) were large molecules that were inapplicable to lithium-ion cell systems (large molecular weights, low rate capability, low conductivity, voltage instability, etc.). In collaboration with Binrad Industries (specialty chemical company) we have developed LiF/ABA salts to impart improved thermal stability in lithium-ion cells and to eliminate some of the shortcomings of using $LiPF_6$ salts. Figure IV- 161 shows the discharge capacity of NMC cells with LiF-ABA/EC:EMC and $LiPF_6$/EC:EMC electrolytes. The capacity of the LiF-ABA cell is only ~10% less than for the $LiPF_6$/ABA cell. This difference in measured capacity is attributed to differences in salt concentrations (1.0 M LiF/ABA and 1.2 M $LiPF_6$) and electrolyte conductivities (1.9 mS/cm for 1.0 M LiF/ABA and 9.1 mS/cm for 1.2 M $LiPF_6$).

While there is some trade-off in performance compared to using $LiPF_6$, the benefits of using LiF/ABA

are a significant improvement in material thermal stability and a reduction in gas decomposition products. ARC bomb results show a 150°C onset for decomposition and gas generation from $LiPF_6$ EC:EMC (3:7), while the LiF/ABA gas generation temperature is 240°C; a 90°C improvement in thermal stability. Moreover, in 18650 cells a 40% reduction in the total volume of decomposition gas at STP was measured in ARC experiments, shown in Figure IV-162. Work will continue in FY11 on studying the thermal behavior, performance, and degradation mechanisms of this and other LiF/ABA electrolyte systems.

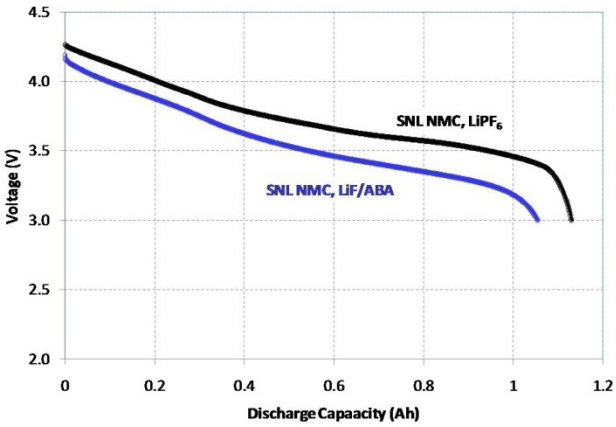

Figure IV- 161: Discharge capacity of NMC cells with 1.2 M $LiPF_6$ EC:EMC (3:7) (black trace) and 1.0 M LiF/ABA EC:EMC (3:7) (blue trace) electrolytes.

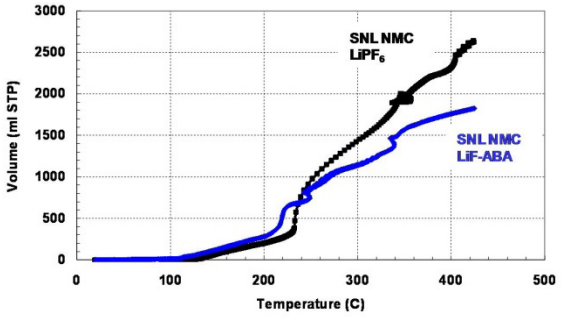

Figure IV- 162: STP gas volume during an ARC experiment for NMC cells with 1.2 M $LiPF_6$ EC:EMC (3:7) (black trace) and 1.0 M LiF/ABA EC:EMC (3:7) (blue trace) electrolytes.

SNL Cell Fabrication Facility. The SNL cell prototyping facility is fully equipped with three 18650 cell winders (in two separate dry rooms), prototype-scale electrode coater, electrode slitter, semi-automatic tabber, and an electrolyte filling station to support the ABR program cell thermal characterization and abuse tolerance evaluation work. In the past, the facility has been used to build cells using coated electrodes provided by our collaborators. In 2010, the facility was enhanced to coat electrodes under this program, primarily focusing on commercially available NMC cathode and Conoco Phillips anode materials. 18650 cell building at SNL has been critical to the success of the work described in this report (AlF_3-NMC studies, LiF/ABA cell evaluation) as well as our internal short circuit test development effort (IV.D.1.2) and our abuse testing work (V.D.2) within the Energy Storage Program.

Figure IV- 163 shows discharge capacity curves for representative NMC cells with capacities ranging from 1.05 to 1.17 Ah; where the electrodes were coated and cells were built solely using SNL facilities. These results are completely consistent with commercially supplied electrodes and cells. Figure IV- 164 shows ARC profiles for a 0.94 Ah $Li_{1.1}(Ni_{1/3}Mn_{1/3}Co_{1/3})_{0.9}O_2$ (Gen3) cell (electrodes provided by a commercial manufacturer and cells built at SNL) and a 1.04 Ah $LiNi_{0.4}Mn_{0.3}Co_{0.3}O_2$ cell (electrodes coated and cell built at SNL). The ARC profiles for each cell are characteristic for cells of this chemistry and are consistent with observations made on commercial cells. The greater heating rates and peak width (enthalpy) for the $LiNi_{0.4}Mn_{0.3}Co_{0.3}O_2$ cell is attributed to higher cell capacity, higher cell voltage, and more Ni in the cathode material.

Conclusions and Future Directions

This work demonstrates how specific advances in a variety of materials areas (anode, cathode, and electrolyte) can have a profound impact on cell-level safety and thermal characteristics. Work will continue in this area to evaluate cell-level abuse response using these and new materials. Future work in this area will focus on thermal characterization of coated cathode materials (Al_2O_3-NCA in collaboration with ANL), continued characterization of our LiF/ABA electrolytes, and studying the stability of new electrolytes and cell additives. In addition, we will begin to study the effects of cell age on thermal behavior and abuse response in collaboration with INL.

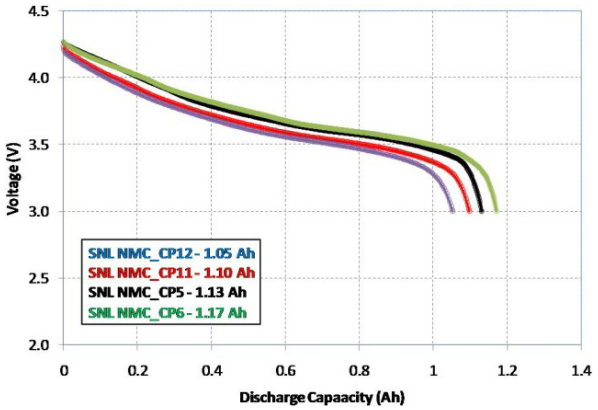

Figure IV- 163: Discharge capacity of a 2.0 Ah NMC cell where the electrodes were coated and the cell was built at SNL

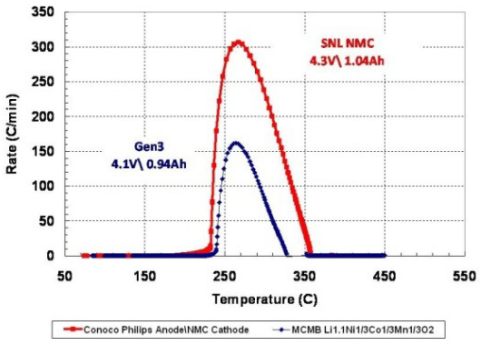

Figure IV- 164: ARC profiles for a 1.04 Ah $LiNi_{0.4}Mn_{0.3}Co_{0.3}O_2$ cell at 4.3 V (red trace) and a 0.94 Ah $Li_{1.1}(Ni_{1/3}Mn_{1/3}Co_{1/3})_{0.9}O_2$ (Gen3) cell at 4.1 V (blue trace).

FY 2010 Publications/Presentations

1. E. P. Roth and C. J. Orendorff, "A Review of Critical Safety Issues in Li^+ Batteries" International Battery Association/Pacific Power Sources Symposium, Waikoloa, HI, January 2010
2. 2010 DOE Annual Merit Review Presentation.

IV.D.2.3 Overcharge Protection for PHEV Cells (LBNL)

Thomas Richardson
Guoying Chen

Environmental Energy Technologies Division
Lawrence Berkeley National Laboratory
Berkeley, CA 94720
Phone: (510) 486-8619; Fax: (510) 486-8619
E-mail: TJRichardson@lbl.gov
GChen@lbl.gov

Start Date: October 1, 2009
Projected End Date: September 30, 2011

Objectives

- Develop and implement a long-lasting mechanism that provides inexpensive, reversible and high-rate overcharge protection for high-energy lithium-ion batteries intended for PHEV applications.

Technical Barriers

- Abuse tolerance
- Safety
- Poor cycle life

Technical Targets

- Improved rate capability and cycle life of overcharge-protected Li-ion cells.

Accomplishments

- Demonstrated improved rate and low-temperature performance by placing the polymer protection parallel to the electrode assembly.
- Showed increased sustainable current density in composite membranes with oriented polymer nanofibers.

✧ ✧ ✧ ✧ ✧

Introduction

The term "overcharge" is used to describe a variety of conditions, including simple charging at normal rates beyond rated capacity, overvoltage excursions for short or long periods, charging at a rate too high for one electrode (commonly the anode) without exceeding the maximum voltage, and other more complex scenarios. While overcharging is still a major safety issue for lithium batteries it is a serious lifetime issue as well. Even very slight overcharging reduces the discharge capacity of a cell, which can result in overdischarging, increased impedance, local heating, etc. Battery packs for consumer electronics are protected both by electronic controls and by internal shutdown mechanisms such as melting separators and disconnects acting in response to pressure or temperature excursions. In a multicell stack capable of delivering several hundred volts, permanently shutting down a cell reduces the usable capacity of the stack and puts added strain on the remaining cells in parallel with it. Complex re-routing of current around overcharged cells is impractical in these stacks. Internal protection mechanisms are needed that maintain a cell's potential and discharge capacity and can provide protection without adding substantially to the size, weight or volume of the stack.

The most familiar self-actuating internal mechanism is the redox shuttle additive (usually a neutral molecule). These generally have sharp onset potentials that can be chosen to be at a desired level just above the normal cathode charge cut-off potential. They have limited current-carrying abilities, however, because their operation depends upon diffusion of both the neutral and oxidized form of the additive (generally a radical cation). Each species must make a complete trip across the separator for each electron shuttled. The electroactive polymer approach, developed at LBNL, protects cells by forming a completely reversible resistive shunt between the current collectors during overcharging, thus maintaining the cell potential and the full discharge capacity. When overcharging ceases, the polymer reverts to its non-conducting state and the cell operates normally. Since the overcharge current is carried electronically rather than by diffusing solutes, much higher current densities can be achieved than with redox shuttles.

Approach

The approach is to use electroactive polymers as self-actuating and reversible overcharge protection agents. The redox window and electronic conductivity of the polymer will be tuned to match the battery chemistry for non-interfering cell operation. Rate capability and cycle life of the protection will be maximized through the optimization of polymer composite morphology and cell configuration.

Results

Cell Configurations. When impregnated in a battery separator and placed between the electrodes, electroactive polymers have been shown to provide overcharge

protection for lithium-ion batteries with various chemistries. The rate performance of the protected cell with the "sandwich" configuration, however, was found to be affected by the reduced porosity of the composite separator. Figure IV- 165(a) shows a $Li_{1.05}Mn_{1.95}O_4$ - Li cell protected by poly(9,9-dioctylfluorene) (PFO) and poly(3-butylthiophene) (P3BT) bilayer composite separators. The cell was charged and discharged at current densities of 0.06 (C/6), 0.50 (1.3C), 0.63 (1.7C), 0.75 (2C) and 1.0 mA/cm^2 (2.7C). Significant polarization and large decrease in discharge capacity were observed at higher rates. At a current density of 1.0 mA/cm^2 (2.7 C), the cell voltage increased to 4.6 V. A steady state potential could not be maintained above 1.0 mA/cm^2.

To decrease the internal resistance of the protected cell, a parallel configuration with the electroactive polymers placed outside of the active electrode area was adapted. The performance of thus protected $Li_{1.05}Mn_{1.95}O_4$ - Li cell at charge/discharge current densities of 0.25 (C/1.5), 0.375 (C), 0.50 (1.3C), 0.75 (2C), 1.0 (2.7C) and 1.125 mA/cm^2 (3C) is shown in Figure IV- 165(b). The cell was able to reach and maintain a steady state potential at the charging current of 1.125 mA/cm^2. Compared with the "sandwich" configuration, there is a slower increase in steady-state potential with rate, and the cell was able to maintain at 3C overcharging at 4.3 V. The voltage profile also indicates lower internal resistance, and the discharge capacity remained nearly unchanged with the increasing current density.

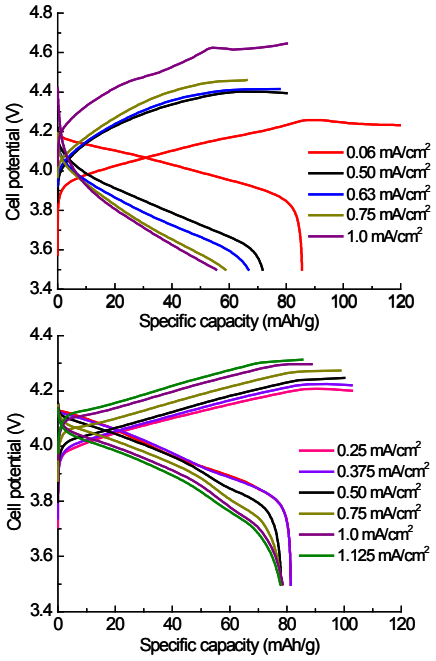

Figure IV- 165: Rate performance of an overcharge-protected $Li_{1.05}Mn_{1.95}O_4$ - Li cell with a) "sandwich" configuration and b) parallel configuration.

The parallel configuration also improves the low-temperature performance. At C/6 rate, a steady state potential was reached at each temperature from 25°C to -20°C (Figure IV- 166). Although, as in the case of protection with the "sandwich" configuration, the capacity gradually decreased with decreasing temperature, the change was less significant. The greatest capacity reduction occurred at -20°C, where the cell resistance increased drastically due to the increase in electrolyte viscosity. The onset protection potential increased with decreasing temperature, and the cell was protected at 4.5 V at -20°C.

The modified configuration may be easier to implant in a larger sized battery cell such as the 18650 cells. Unlike the "Swagelok"-type cell, these cells typically have unused current collector areas for tabs. A smaller, denser and more conductive internal shunt may be introduced between the two electrodes in this area to minimize the impact on the electrode assembly.

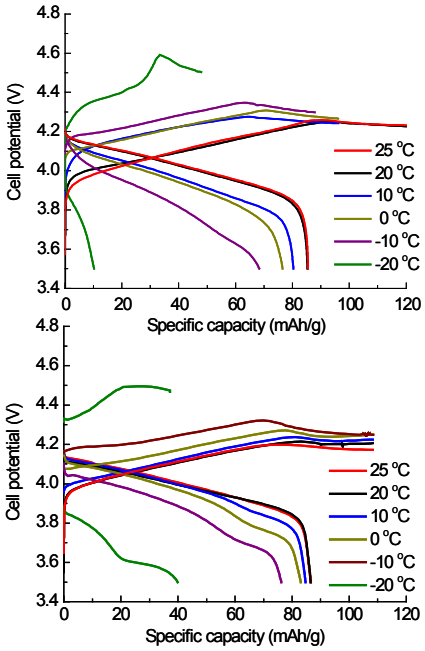

Figure IV- 166: Low-temperature performance of an overcharge-protected $Li_{1.05}Mn_{1.95}O_4$ - Li cell with a) "sandwich" configuration and b) parallel configuration.

Polymer Morphologies. The effectiveness of the overcharge protection was found to be dependant on polymer morphology. Previous art of solution impregnation has led to low utilization of the polymer and poor connection of conductive paths within the composite separators. In an effort to improve efficiency, arrays of oriented polymer nanofibers were prepared by electrodepositing the polymer into the regular nanosized channels of the porous alumina membrane (AAO template). The polymer deposit was shown to be

composed of uniform nanofibers that extend the full thickness of the template, allowing each polymer fiber to provide an overcharge current path upon oxidation. Figure IV- 167 compares the current carrying capability of the P3BT composites prepared by the solution impregnation and electrodeposition methods. It is evident that the utilization in the nanofiber composite was much higher, as up to 4 times improvement in sustainable current density was achieved.

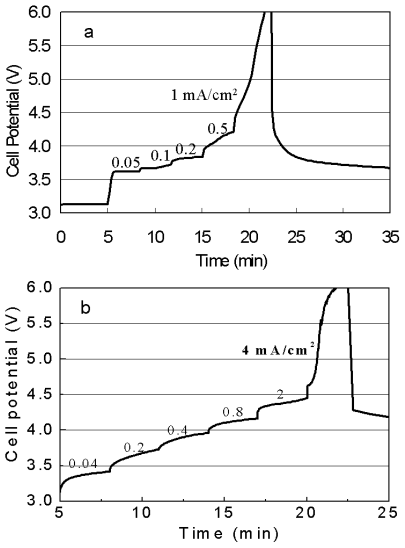

Figure IV- 167: Potential profiles across P3BT composites prepared by a) solution impregnation in Celgard separator and b) electrodeposition in AAO template.

Conclusions and Future Directions

Composite separators with electroactive polymer nanofibers will be prepared and evaluated for their rate capability and cycle life in Li-ion battery cells. Approaches to prepare various polymer morphologies will be further explored. Other high-voltage electroactive polymers will be investigated for their suitability for overcharge protection in PHEV batteries.

FY 2010 Publications/Presentations

1. 2010 DOE Annual Peer Review Meeting Presentation.
2. G. Chen and T. J. Richardson, "Overcharge Protection for 4 V Lithium Batteries at High Rates and Low Temperatures," *Journal of the Electrochemical Society*, **157**, A735 (2010).
3. T. J. Richardson, Book Chapter: "Overcharge Protection Shuttles for Lithium-ion Batteries," in Encyclopedia of Electrochemical Power Sources, Juergen Garche (Ed.), Vol. 5, pp. 404–408, Elsevier, Amsterdam (2009). ISBN: 978-0-444-52093-7.

IV.E Applied Research Facilities

IV.E.1 Battery Materials Pilot Production Facility

IV.E.1.1 Process Development and Scale up of Advanced Cathode Materials (ANL)

Gregory K. Krumdick

Argonne National Laboratory
9700 South Cass Avenue
Argonne, IL 60439-4837
Phone: (630) 252-3952; Fax: (630) 252-1342
E-mail: gkrumdick@anl.gov

Collaborators:
Kaname Takeya, Argonne
Illias Belharouak, Argonne

Start Date: June, 2010
Projected End Date: September, 2010

Objectives

The objective of this work is to develop a flexible pilot-scale system capable of producing 1-10 kg of high energy cathode materials, which is 5-10 times the amount that can currently be produced at the bench-scale. The pilot-scale system will be designed to facilitate further scaling to the next level in Argonne's Materials Engineering Facility (MEF), currently under construction.

Technical Barriers

Processes for the production of next-generation high-energy cathode materials have been developed only at the bench scale. Sufficient quantity of material cannot be generated for prototype testing, which is required prior to scaling the process to the next level. Therefore, pilot-scale facilities are required for battery materials scale-up research and development.

Technical Targets

- Establish a lab for scaling up cathode materials.
- Establish an analytical lab equipped for cathode materials characterization and product quality assurance.

Accomplishments

- A cathode materials scale-up lab has been established. A flexible pilot-scale cathode-material processing system capable of producing 1-10 kg batches has been designed and process equipment has been ordered.
- A cathode materials analytical lab has been established. Analytical equipment has been ordered and preparation of standard operating procedures has begun.

✧ ✧ ✧ ✧ ✧

Introduction

Researchers in the battery materials programs across the DOE complex refer to scale up as synthesis of battery materials in gram quantities, and with time consuming, multiple small-scale runs. There is a need to develop scale-up processes for battery materials (primarily lithium-ion based batteries) to the kilogram and tens-of-kilograms quantities at DOE labs to support the transition of these technologies to industry. Currently, there is no systematic engineering research capability or program across the DOE complex or in industry to identify and resolve constraints to the development of cost-effective process technology for the high-volume manufacture of these advanced materials.

Approach

Next generation cathode materials have been developed at the bench scale by a number of researchers focusing on developing advanced lithium-ion battery materials. Process engineers will work with these researchers to gain an understanding of the materials and bench-scale processes used to make these materials, and then scale up and optimize the processes to produce larger quantities of battery materials. Standard chemical engineering unit operations will be utilized to develop flexible systems that will enable scaling of a wide range of next generation high-energy cathode materials. Initial work will be based on NMC-based processes, but may

include lithium-rich technologies and layered-layered and layered-spinel classes of cathode materials.

Results

This project began in June, 2010; results will be presented at the 2011 Annual Merit Review and in the FY 2011 annual progress report.

IV.E.1.2 Process Development and Scale up of Organic Electrolyte Components (ANL)

Gregory K. Krumdick

Argonne National Laboratory
9700 South Cass Avenue
Argonne, IL 60439-4837
Phone: (630) 252-3952; Fax (630) 252-1342
E-mail: gkrumdick@anl.gov

Collaborators:
Krzysztof Pupek, ANL
Trevor Dzwiniel, ANL
Zhengcheng Zhang, ANL

Start Date: June, 2010
Projected End Date: September, 2010

Objectives

The objective of the work is to develop a flexible pilot-scale system capable of producing 1-10 kg of electrolyte or electrolyte additives, which is 5-10 times the amount that can currently be produced at the bench-scale. The pilot-scale system will be designed to facilitate further scaling to the next level in Argonne's Materials Engineering Facility (MEF), currently under construction.

Technical Barriers

Advanced electrolytes and additives have been synthesized in small batches using 1-5L vessels, which produce approximately 200mL of material. The bench-scale processes are labor-intensive and time-consuming. Sufficient quantity of material cannot be generated for prototype testing, which is required prior to scaling the process to the next level. Therefore, pilot-scale facilities are required for battery materials scale-up research and development.

Technical Targets

- Establish a lab for scaling up electrolytes and additive materials.
- Establish an analytical lab equipped for electrolytes and additives characterization and product quality assurance.

Accomplishments

- An electrolyte and additives scale-up lab has been established. A flexible pilot-scale electrolyte and additives processing system capable of producing 1-10 kg batches has been designed and process equipment has been ordered.
- An electrolyte and additives analytical lab has been established. Analytical equipment has been ordered and preparation of standard operating procedures has begun.

Introduction

Researchers in the battery materials programs across the DOE complex refer to scale up as synthesis of battery materials in gram quantities, and with time consuming, multiple small-scale runs. There is a need to develop scale-up processes for battery materials (primarily lithium-ion based batteries) to the kilogram and tens-of-kilograms quantities at DOE labs to support the transition of these technologies to industry. Currently, there is no systematic engineering research capability or program across the DOE complex or in industry to identify and resolve constraints to the development of cost-effective process technology for the high-volume manufacture of these advanced materials.

Approach

Advanced electrolytes and additives have been developed at the bench scale by a number of researchers focusing on developing advanced lithium-ion battery materials. Process engineers will work with these researchers to gain an understanding of the materials and bench-scale processes used to make these materials, and then scale up and optimize the processes to produce larger quantities of battery materials. Standard chemical engineering unit operations will be utilized to develop flexible systems that will be enable scaling of a wide range of next generation electrolytes and additives. Initial work will be based on redox shuttle chemistries.

Results

This project began in June, 2010; results will be presented at the 2011 Annual Merit Review and in the FY 2011 annual progress report.

V

FOCUSED FUNDAMENTAL RESEARCH

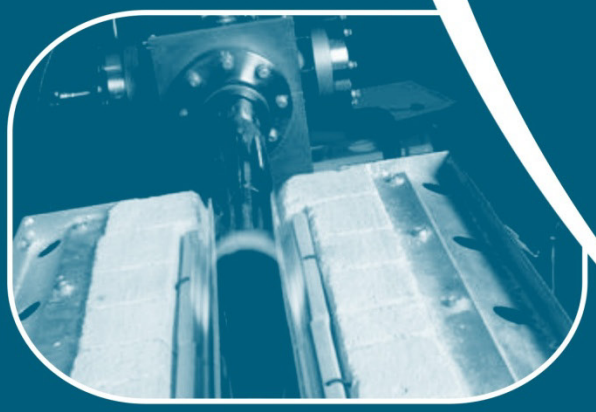

A. Introduction

B. Cathode Development

C. Anode Development

D. Electrolyte Development

E. Cell Analysis and Modeling

F. Energy Frontiers Research Centers

G. Integrated Lab-Industry Research Program

V. FOCUSED FUNDAMENTAL RESEARCH

V.A Introduction

The focused fundamental research program, also called the Batteries for Advanced Transportation Technologies (BATT) program, conducts research and analysis on new materials for high-performance, next generation, rechargeable batteries to facilitate their use in HEVs, PHEVs, and EVs. The effort in FY 2010 accelerated the increased emphasis on high energy materials for PHEV and EV applications.

Background and Program Context

The BATT Program addresses the fundamental problems of chemical and mechanical instabilities that have impeded the development of automotive batteries with acceptable cost, performance, life, and safety. The aim is to identify and better understand cell and material performance and lifetime limitations before initiating battery scale-up and development. Emphasis is placed on the synthesis of components into cells with determination of failure modes while continuing with materials synthesis and evaluation, advanced diagnostics, and improved model development. Battery chemistries are monitored continuously with timely substitution of more promising components. This is done consistent with advice from researchers within the BATT Program as well as outside experts and also includes consultations with automotive companies and DOE. Ongoing monitoring of world-wide battery R&D activities also gets factored into setting the direction of the BATT Program. The Program not only supports research for incremental improvements to existing materials, but also high-risk "leap-frog" technologies that might have a tremendous impact in the marketplace. An overview of the activities and focus of the program is shown in Figure V- 1.

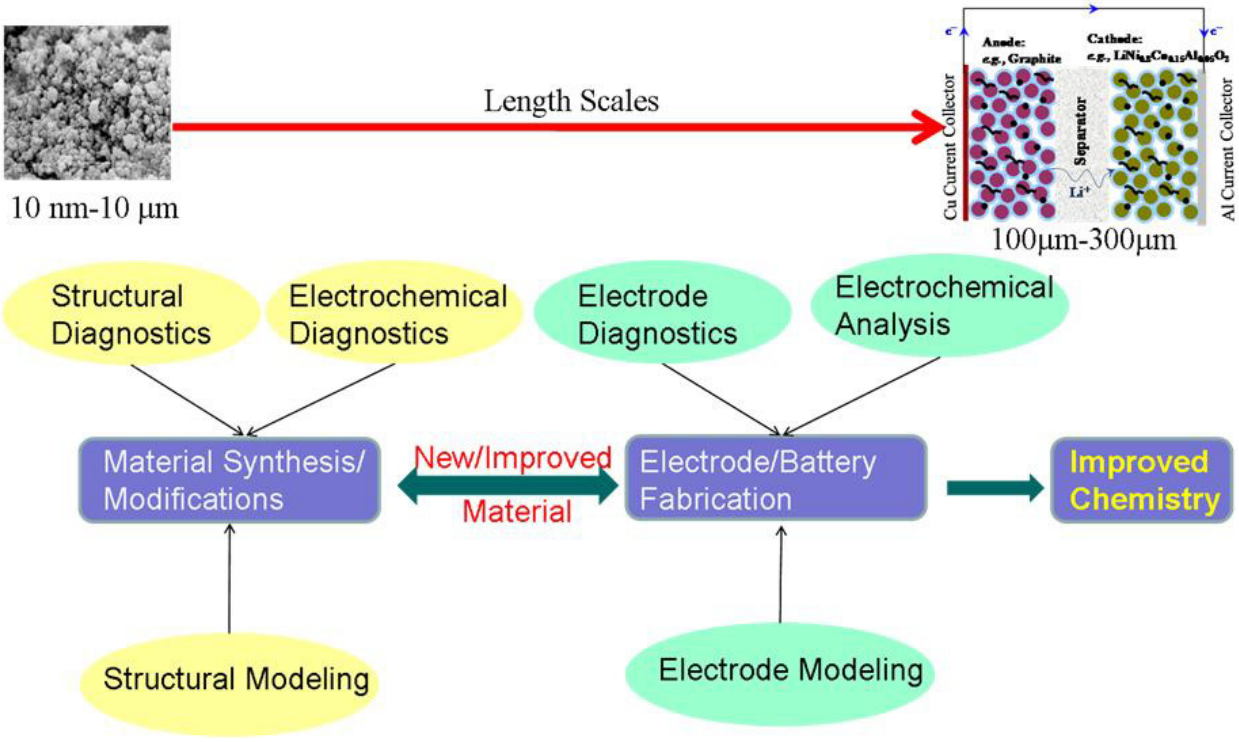

Figure V- 1: BATT Overview

The work is administered by the Lawrence Berkeley National Laboratory (LBNL) and involves principal researchers from LBNL, five additional laboratories, fourteen universities, and two commercial companies. It is organized into four areas:

- New Cathode Systems, Performance and Limitations
- New Anode Materials

- Novel Electrolytes and their Characterization
- Li-ion Modeling, Diagnostics, and Cell Analysis

This section summarizes the research activities of this program in FY 2010. The website for the BATT Program is found at http://berc.lbl.gov/BATT/BATT.html. Brief descriptions of each research area are as follows.

The ***New Cathode Materials*** task aims to find improved cathode materials that offer significant improvements in volumetric and specific energy and/or power over current state of the art materials, like $LiCoO_2$. The investigation into phosphate systems includes studies of capacity and power, lower cost synthesis methods, and the impact of processing steps on performance. Work on layered systems includes the $LiNi_{1/3}Mn_{1/3}Co_{1/3}O_2$ (called NMC) cathode material that can be used to produce either a high-energy cell that can be engineered to provide good power. Finally, the work into Mn spinel materials aims to understand the failure and degradation modes using various material doping, cell cycling, and advanced diagnostics. This work also includes the composite, high voltage, high-energy cathode materials that promise a significant increase in both capacity and voltage over current materials. This work aims to understand the failure and degradation modes in NMC and other such systems using cell builds, cell cycling, advanced diagnostics, and modeling.

The ***New Anode Materials*** task involves eight new projects selected following the anode solicitation in 2009. These projects aim to find improved anode materials that offer at least twice the volumetric and specific energy of graphite. Researchers are investigating several methods for stabilizing Si and Sn composite negative electrodes, including the use of Cu foam current collectors, investigation of Si clathrate materials, the use of atomic layer deposition to stabilize alloy electrodes, and a number of Si/carbon nanocomposite materials. Although no significant effort has been undertaken on these new projects, abstracts of planned work is provided in the anode section below.

The ***Novel Electrolyte Materials*** task continues projects that began in 2009 following a BATT solicitation posted in 2008. These five research efforts focus on expanding the temperature range of cells, additives to stabilize the negative and positive interfaces, development of new overcharge shuttles to further stabilize Li-ion cells, new ionic liquids to enable higher voltage windows, and first principles modeling to understand and eventually to construct a more stable SEI.

The ***Modeling, Diagnostics, and Cell Analysis*** tasks involve the use of advanced diagnostics techniques, such as FTIR, X-ray absorption fine structure (XAFS), X-ray diffraction (XRD), nuclear magnetic resonance (NMR) and other techniques to investigate interfacial and other properties in Li-ion batteries. Several modeling approaches are used to understand cell and fundamental material properties, including *ab-initio* calculations, macroscopic cell calculations, and finite element simulations. Finally, standard cell making and testing techniques are developed and applied to provide a common evaluation process for new materials.

V.B Cathode Development

V.B.1 First Principles Calculations and NMR Spectroscopy of Electrode Materials (MIT, SUNY)

Clare P. Grey
Chemistry Department
Stony Brook University
Phone: (631) 632-9548; Fax: (631) 632-5731
E-mail: cgrey@notes.cc.sunysb.edu

Co-PI: Gerbrand Ceder, MIT

Start Date: May 2006
Projected End Date: February 2010

Objectives

- Determine the effect of structure on stability and rate capability of cathodes and anodes.
- Explore relationships between electrochemistry and particle size and shape.
- Understand and predict reactivity of anode and cathode electrode materials with electrolytes.
- Develop new materials.

Technical Barriers

Low rate capabilities, high cost, poor stability of electrode materials, low energy density.

Technical Targets

- Specific power 300 W/kg, 15 year life, <20% capacity fade. Low cost.

Accomplishments

- Development of an *in situ* NMR methodology to monitor and quantify Li dendrite formation in lithium-metal batteries.
- Identified the local structures that give rise to the different processes seen on cycling the anode material silicon (with NMR and PDF methods).
- Used NMR methods to investigate the structure of new phosphocarbonates and oxysulfides.
- Computed binary phase diagrams and voltage curves of $Li_x(Fe_yMn_{1-y})PO_4$.
- Developed formalism to study Li transport as a function of particle size, explaining enhanced rate capability of nanoparticles.
- Developed the capability to predict thermal stability in the charged state, showing that Li_xMnPO_4 is less stable than Li_xFePO_4.
- Conducted high-throughput computational study evaluating the correlation between electrode voltage and oxidation strength at the charged state.

✧ ✧ ✧ ✧ ✧

Introduction

Achieving DOE goals in this field require both an understanding of how current materials function – with a view to improving rate, capacity and long term cycling performance – and the discovery of new materials and new mechanisms by which these materials function. This joint theoretical and experimental program attacks these issues by developing new experimental (and theoretical) tools to investigate battery materials both *in* and *ex situ*, and then applies these to understand relationships between structure and function. One aim is to use these findings to optimize material function and/or develop new materials.

Approach

Use solid state NMR and diffraction/TEM to characterize local and long range structure as a function of particle size, sample preparation method, state of charge and number of charge cycles (cathodes). Use electrochemistry to correlate particle size with rate performance. Continue to develop the use of *in situ* NMR methods to identify structural changes and reactivity in oxides and intermetallics. Use first principles calculations (density functional theory) to identify redox-active metals, relative stability of different structures, the effect of structure and particle size on cell voltages and rate capability, and to identify promising cathode materials for BATT applications.

Results

***In situ* NMR Observation of the Formation of Metallic Lithium Microstructures.** Lithium metal has

the highest volumetric and gravimetric energy density of all negative electrode materials in a lithium-ion rechargeable battery. However, the formation of lithium dendrites and/or "moss" on the metal electrode surface can lead to short circuits, following several electrochemical charge-discharge cycles, particularly at high rates, rendering this class of batteries potentially unsafe. Building on prior BATT work, we have developed an *in situ* NMR spectroscopic approach, to provide time-resolved, quantitative information about the nature of the metallic lithium deposited on lithium metal electrodes, without having to disassemble the battery. The method relies of the finite ability of radio frequency (rf) waves – used to excite the Li nuclei – to penetrate bulk Li metal. The so-called "skin-depth" – i.e., the penetration depth can be readily calculated and in the magnetic field used in our studies corresponds to approximately 15 µm. We have shown that we can exploit this phenomenon to differentiate between bulk and dendritic lithium, to monitor the growth of micron-sized (dendritic/mossy Li) and to determine whether this Li participates in the electrochemistry.[5]

In Figure V- 2, we show that the change in the intensity of the NMR signal can be explained only if the majority of the Li is deposited as micron sized deposits on charging of a $LiCoO_2$-Li cell. Furthermore, this micron-sized Li is consumed during the subsequent discharge. Similar phenomena were observed on cycling Li-Si cells. In collaboration with A. S. Best and A.F. Hollenkamp (CSIRO, Australia), we used this methodology to explore dendrite growth in symmetric cells, containing Li electrodes only. In this system, since the mass of Li metal is essentially constant on cycling, it is very simple to measure the fraction of mossy Li, since this follows directly from the increase in the Li metal signal. The approach was used to explore the effect of different electrolytes and additives on the extent of dendrite growth.

Structural Model for the Lithiation of Silicon. Lithium-ion batteries (LIBs) containing silicon negative electrodes have been the subject of much recent investigation, because of the extremely large gravimetric and volumetric capacities of silicon. In recent work, we have completed our *ex situ* ^{7}Li NMR studies and pair distribution function (PDF) analysis of X-ray data to investigate the changes in short range order that occur during the initial charge and discharge cycles of Silicon. In particular, we have identified some of the local structures that are responsible for the distinct electrochemical signatures that are seen in the electrochemical profiles. Lithiation of crystalline silicon, on the 1st discharge, starts and progresses with bond breakage of the Si matrix to form both lithiated isolated silicon anions and lithiated silicon clusters, surrounded by Li+ ions. Once all the bulk crystalline Si is consumed and total amorphization is achieved, the remaining Si clusters are broken to form predominantly fully lithiated isolated silicon environments. Key to this mechanism is (i) the difficulty associated with Si-Si bond rupture, thus it is kinetically more favorable to lithiate silicon clusters and form isolated Si ions, or smaller clusters, than to break up the Si framework. (ii) Since a distribution of different Si clusters and anions are formed, the (more thermodynamically stable) crystalline phase expected based on Li:Si ratio of the amorphous component, does not readily nucleate, since this would involve Si-Si bond

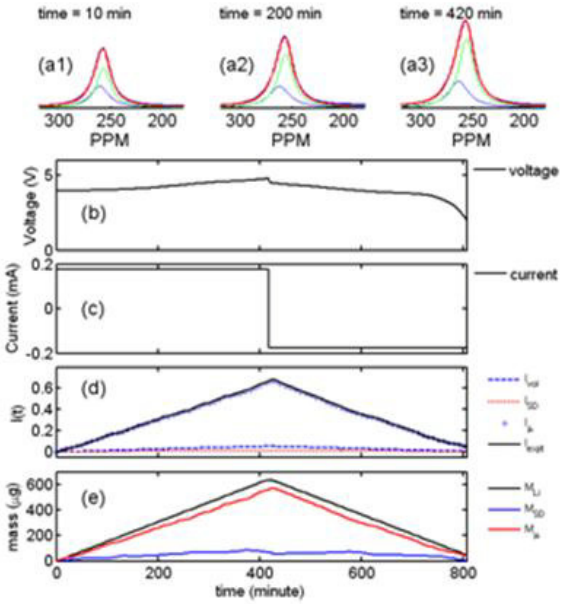

Figure V- 2: ^{7}Li NMR spectra of metallic lithium (a 1-3), as a function of time in a $LiCoO_2$ cell, for one charge-discharge cycle. Measured voltage and the applied current (C/10 rate) are plotted in (b) and (c). The measured Li metal intensity ($I_{exp}(t)$) is shown as a solid black line in (d), where the signal (S(t)) has been normalized to the signal at t=0, to give $I_{exp}(t) = [S(t)-S(t=0)]/S(t = 0))$. Theoretical values of I(t), calculated under various assumptions are shown for comparison: (i) no skin depth issues $I_{vol}(t)$ (blue dashed line), (ii) all of lithium is smoothly deposited $I_{SD}(t)$ (red dotted line), (iii) all of lithium deposited/stripped forms micro-structure $I_{\mu}(t)$ (blue circles; equation 16). Only $I_{\mu}(t)$ provides a good fit to the experimental data, the small deviation being due to a small amount of smoothly deposited lithium. $I_{exp}(t)$, in combination with total mass of Li deposited or stripped $M_{Li}(t)$ (extracted from the electrochemistry), can be used to calculate the mass of deposited Li, $M_{SD}(t)$ and Li microstructures $M_{\mu}(t)$, taking into account of the skin-depth problem (e).

breakage and rearrangement of the clusters. Only when essentially all of the Si clusters are broken up < 50 mV is it possible to nucleate a crystalline phase comprising isolated Si ions. The mechanism for delithiation to form the fully lithiated phase progresses from a small number of nuclei, which are either formed on delithiation or which may still be present in the fully discharged phase. These nuclei grow directly to form the amorphous (delithiated) Si phase

without (significant) formation of any intermediate structures or compositions with multiple small clusters. The amorphous Si phase formed on the top of charge contains Si tetrahedra, but no or little order beyond the silicon 2nd coordination shell (Figure V- 3).

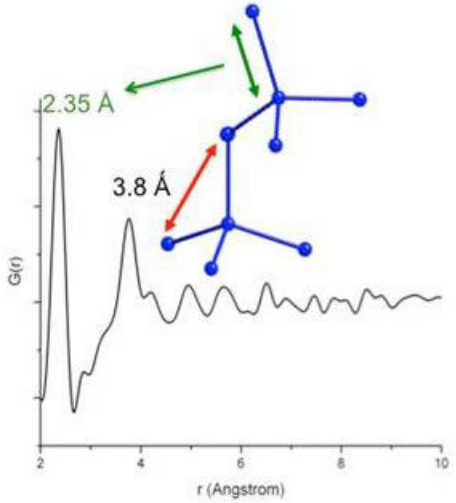

Figure V- 3: The pair distribution function (PDF) (G(r)) of silicon following 1 cycle, obtained from diffraction data. The 1st two dominant correspond to directly bound Si and Si within a tetrahedra.

The amorphous silicon matrix is much more open, so that the whole matrix can now be partially lithiated at the end of the higher voltage process (i.e., with a much lower overpotential than required to break the crystalline framework), partially breaking down the Si network. The lower electrochemical process is associated a breakage of the remaining smaller lithiated silicon clusters, and it again ends with recrystallization of fully lithiated phase. If a partially delithiated phase, and one that still contains Si clusters, is delithiated, these clusters appear to serve a nucleation sites, allowing the system to retrace a similar electrochemical pathway to that seen on discharge. In contrast, if lithiation proceeds to form $Li_{15}Si_5$, i.e., the phase with isolated anions, there are few Si nucleation sites, and delithiation proceeds via the growth of only a few Si clusters to form larger Si domains and eventually the amorphous Si phase. The results suggest that it is important to control the potential windows over which the material is cycled to optimize both the numbers and type of clusters that are formed and that this may affect the reversibility and rate performance of this system.

Materials discovery. A new iron phosphocarbonate that emerged from our theoretical screening of a wide variety of materials, has been sucessfully synthesized, and its electrochemical properties tested. Structural characterization, including time-resolved powder diffraction and NMR spectrosopy has been carried out to evaluate limitations to performance.

Olivines: Mixed Olivines, Nano-size Effects and Thermal Stability. We investigated several aspects of the olivine systems. Phase diagrams and voltage curves of the mixed olivine system $Li(Fe,Mn)PO_4$ system were computed from first-principles. It was shown, in good agreement with experiment, that disordered transition metal cation substitution dilutes phase-separating interactions and stabilizes a low-temperature solid-solution (SS) phase (Figure V- 4). Additionally, computed voltage curves show an increase in the $Fe^{2+/3+}$ phase transition voltages with increasing Mn content, in good agreement with experiments, attributed to increased energy arising from unfavorable Li^{+}–Fe^{3+} interactions in the intermediate solid-solution phase. The reverse trend is seen on the $Mn^{2+/3+}$ couple.

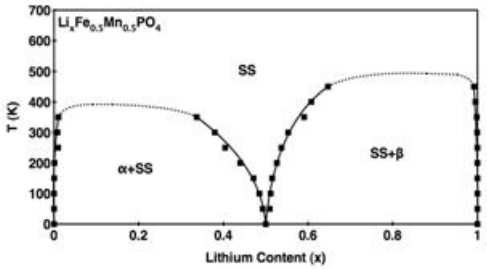

Figure V- 4: Calculated phase diagram of $Li_xFe_{0.5}Mn_{0.5}PO_4$

We have investigated the effect of point defects, specifically Li-Fe antisites, on Li transport. Since Li transport in $LiFePO_4$ occurs primarily through fast diffusion in 1D along the [010] direction, immobile Li-Fe antisites act to impede Li migration, and when two such defects occupy the same channel, the capacity between is trapped (Figure V- 5). This effect scales with particle size, since in the small-particle limit trapped capacity tends to zero and fast 1D diffusion can be accessed, and in the large particle limit, no unblocked capacity is accessible. We have computed the migration barrier to circumvent such point defect obstructions and recalculated the diffusion constants as a function of defect concentration, to good agreement with experiments, conclusively explaining why it is difficult to make large-particle size LFP high rate.

A study comparing the relative thermal stabilities of the olivines (in the charged state) was conducted, focusing on the $LiFePO_4$ and $LiMnPO_4$ systems. Using the computed phase diagrams of the Li-Fe-M-O systems (M= Fe, Mn) to determine the temperature of decomposition resulting in O_2 evolution, it was concluded that $MnPO_4$ is inherently less stable than $FePO_4$ as is also observed experimentally. It was determined that not only does $MnPO_4$ decompose at lower temperature than $FePO_4$, it also evolves more O_2 (Figure V- 6).

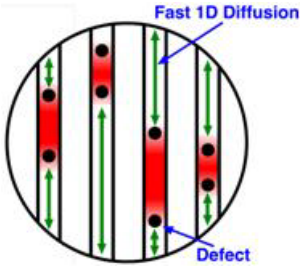

Figure V- 5: Schematic illustration of immobile point defects obstructing fast 1D Li diffusion.

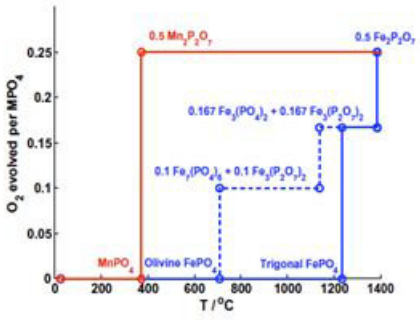

Figure V- 6: O_2 evolved versus temperature for delithiated MPO_4 (M = Fe, Mn)

New Materials. Using a high-throughput computational environment in which we can evaluate many relevant electrode properties of existing and new materials, we have performed a study comparing voltage to thermal stability on several thousand compounds (Figure V- 7). A general trend emerges showing that higher voltage compounds predominantly exhibit worse thermal stability. Nevertheless, there are new polyanion structures (such as silicates and borates) that buck this trend and offer a better tradeoff between voltage and thermal stability.

Conclusions and Future Directions

In conclusion, we have developed a novel NMR method to quantify Li dendrite growth on negative electrode materials. The method was used to explore the effect of additives and different electrolytes on dendrite formation. Future directions include a study of Li dendrite formation as a function of current and rate.

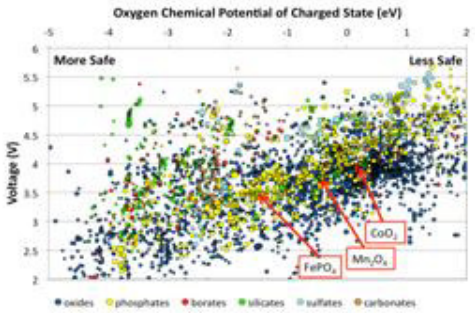

Figure V- 7: Voltage vs. thermal stability for thousands of compounds (calculated).

We have completed our study of structures that form on lithiating silicon. The results provide insight into the source of the large hysteresis in the electrochemical profile of this system. We will now use this structural studies to determine whether we can identify methods to minimize this hysteresis.

In the olivines, we have gained further insight into the phase behavior and electrochemical properties of mixed olivine systems, determined the cause and relative scale of improvement in Li diffusion kinetics by nano-sizing $LiFePO_4$ particles, and computed the relative thermal stabilities of $LiMnPO_4$ and $LiFePO_4$. In the area of new materials, we have used a high-throughput materials screening infrastructure to compute the voltage and thermal stability of thousands of compounds, resulting in the identification of new polyanion structures that potentially optimize both.

FY 2010 Publications/Presentations

1. Presentation to the 2009 DOE Annual Peer Review Meeting.
2. "Investigation of the Structural Changes in $Li[Ni_yMn_yCo_{(1-2y)}]O_2$ (y = 0.05) upon Electrochemical Lithium Deintercalation", D. Zeng, J. Cabana, W-S Yoon and C.P. Grey, *Chem. Mater.*, 22, (3), 1209-1219, (2010).
3. "High rate performance of lithium manganese nitride and oxynitride as negative electrodes in lithium batteries", J. Cabana, C.M. Ionica-Bousquet, C.P. Grey and M. R. Palacín, *Electrochem. Commun.,* 12, 315-318, (2010).
4. "MAS NMR Study of the Metastable Solid Solutions Found in the $LiFePO_4/FePO_4$ System", J. Cabana, K. Shirakawa, G.Y. Chen, T. J. Richardson, and C.P. Grey. *Chem. Mater.,* 22, (3), 1249-1262, (2010).
5. "*In situ* NMR Observation of the Formation of Metallic Lithium Microstructures in Lithium Batteries", R. Bhattacharyya, B. Key, H. Chen, A.S. Best, A.F. Hollenkamp, and C.P. Grey, *Nature Materials*, 9, 504-520 (2010).

6. "Chemically modified $Ba_6Mn_{24}O_{48}$ tunnel manganite as a lithium insertion host," E. Pomerantseva, T. Kulova, D. Zeng, A.M. Skundin, C.P. Grey, E.A. Goodilin, and Y.D. Tretyakov, *Solid State Ionics,* 181, (21-22), 1002-1008, (2010).
7. "Structural complexity of layered-spinel composite electrodes for Li-ion batteries". J. Cabana, C.S. Johnson, X.Q. Yang, K.Y. Chung, W.S. Yoon, S.H. Kang, M.M. Thackeray and C.P. Grey. *J. Materials Research*, 25, (8), 1601-1616, (2010).
8. "Thermodynamic and Kinetic Properties of the Li-graphite System from First-Principles Calculations". K. Persson, Y. Hinuma, Y.S. Meng, A. Van der Van, G. Ceder, *Phys. Rev. B*, 82, 125416 (2010).
9. "Lithium Diffusion in Graphitic Carbon, K. Persson, V.A. Sethuraman, L.J. Hardwick, Y. Hinuma, Y.S. Meng, A. van der Ven, V. Srinivasan, R. Kostecki, G. Ceder". *J. Phys. Chem. Lett*., 1, 1176-1180 (2010).
10. "Thermal Stabilities of Delithiated Olivine MP04 (M=Fe, Mn) Cathodes Investigated Using First Principles Calculations". S.P. Ong, A. Jain, G. Hautier, B.W. Kang, G. Ceder, *Electrochemistry Communications* (2010).
11. "Opportunities and Challenges for First-Principles Materials Design and Applications to Li Battery Materials". G. Ceder, *MRS Bulletin*, 35, pp. 693-701 (2010).
12. "High Rate Micron-Sized Ordered $LiNi_{0.5}Mn_{1.5}O_4$". X Ma, B. Kang, G. Ceder, *Journal of The Electrochemical Society* 157 (8). pp. A925 - A931 (2010).
13. "Particle Size Dependence of the Ionic Diffusivity". Malik R, Burch D, Bazant M, et al. *Nano Letters,* 10, 4123-4127 (2010)
14. "Hybrid density functional calculations of redox potentials and formation energies of transition metal compounds". Chevrier VL, Ong SP, Armiento R, et al. , *Physical Review B* 82 (075122). (2010)
15. "Electrochemical Performance of $LiMnPO_4$ Synthesized with Off-Stoichiometry". Kang B, Ceder G, *J. Electrochem. Soc.*, 157, A808-A811 (2010)

V.B.2 Cell Analysis, High-energy Density Cathodes and Anodes (LBNL)

Thomas Richardson
Environmental Energy Technologies Division
Lawrence Berkeley National Laboratory
Berkeley, CA 94720
Phone: (510) 486-8619; Fax: (510) 486-8609
E-mail: TJRichardson@lbl.gov

Start Date: October 1, 2004
Projected End Date: September 30, 2011

Objectives

- Synthesize and evaluate new electrode materials with improved energy density.
- Investigate the relationship of structure, morphology and performance of cathode and anode materials.
- Explore kinetic barriers, and utilize the knowledge gained to design and develop electrodes with improved energy density, rate performance and stability.

Technical Barriers

- Low energy density
- Poor cycle life

Technical Targets

- Available energy: 11.6 kWh
- Cycle life: 5,000cycles

Accomplishments

- Partial prelithiation of graphite, silicon, aluminum and tin with lithium nitride reduces the initial open circuit voltage and the first charge capacity loss. In the case of Si, good reversibility is maintained even in the absence of a binder.
- Cobalt phosphates derived from sodium cobalt phosphate were found to be stable, but had low capacities for lithium intercalation. Lithium copper phosphates, prepared here for the first time, were found to decompose to lithium copper oxides and lithium phosphate on cycling.
- A microdiffraction technique was developed for visualization of the charge distribution in cycled electrodes. This will allow comparison with and improvement of models that up to now could only be validated indirectly.

✧ ✧ ✧ ✧ ✧

Introduction

EV and PHEV batteries will have to have higher energy densities with good power capability, long cycle lives, and a high margin of safety. Advances in both anode and cathode chemistries are needed to achieve these goals. In addition, improving the design and construction of electrodes and reducing irreversible capacity losses are key routes to maximizing the utilization of theoretical capacities.

Approach

High energy density anodes. The very large irreversible capacity losses normally associated with intermetallic anodes may be reduced by preparing the active materials in a fully or partially pre-lithiated state. The lithium nitride metathesis route, for example: $4Li_3N + 7Si = Li_{12}Si_7 + 2N_2$, can be used to prepare fully or partially lithiated silicon or tin. The level of pre-lithiation can be limited to that required to reduce surface oxides and to form an initial SEI layer, or it can allow the active particles to undergo volume expansion before electrode fabrication. The reactions can be carried out in the presence of carbon black so that subsequent mixing is unnecessary. The method will also be investigated for the preparation of other lithium intermetallics. These anode materials will be evaluated in half-cells and complete cells with metal oxide and/or phosphate cathodes.

High energy density cathodes. We are investigating non-olivine phosphate cathode materials that may have Li intercalation potentials near the desired value of 4 V, but with less interphase strain than is found in olivines such as $LiMnPO_4$, possibly with single-phase behavior and better conductivity. Because only $LiMPO_4$ olivines are formed by direct synthesis from Li^+, metal (M), and phosphate precursors, alternative $LiMPO_4$ structures are created using other cations such as Na^+, K^+, or NH_4^+, which are then exchanged for Li. In the case of NH_4+, this may be achieved by "reactive exchange" with LiOH to release NH_3 (g).

Cell Analysis. The quality of porous composite electrodes is a subject of great interest. We have previously shown that a significant fraction of the active material in cathode laminates is poorly connected to the foil current collector due to defects arising during electrode fabrication and cell assembly. We use X-ray diffraction, electronic and electrochemical testing,

vibrational spectroscopies, synchrotron imaging, and analytical techniques to investigate the causes and potential solutions to the problem.

Results

High energy density anodes. Lithium nitride metathesis has proved to be useful in preparing partially lithiated anode materials, including graphite, silicon, aluminum and tin (Figure V- 8). The open circuit voltage of a prelithiated anode is much lower than that of the untreated material, substantially reducing the lithium lost during the first charge. The reactions can be carried out in the presence of carbon black so that subsequent mixing is unnecessary. In the case of Si (Figure V- 9), good reversibility is maintained even in the absence of a binder. We are currently testing various binders and solvents for stability during mixing and electrode fabrication.

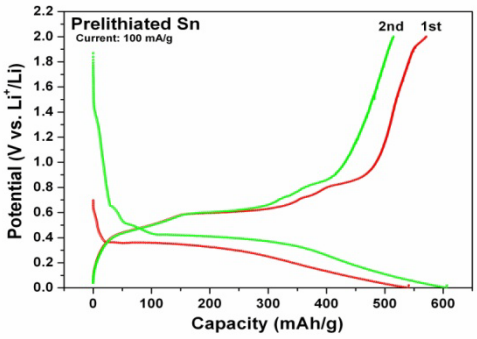

Figure V- 8: First two cycles of pre-lithiated Sn electrode.

High energy density cathodes. We have investigated a series of non-olivine phosphates of cobalt, copper, and manganese in hope of finding alternative cathode materials with desirable potentials, but with less interphase strain, possibly with single-phase behavior and high conductivity. Two examples, α-$NaCoPO_4$ and $NaCuPO_4$ are shown in Figure V- 11(a) and Figure V- 11 (b), respectively. The corresponding lithium compounds were prepared by ion exchange using nonaqueous solvents or molten salt mixtures.

The electrochemical performance of these materials has been disappointing. Cobalt phosphates derived by different ion exchange methods from sodium cobalt phosphate were stable, but had low lithium extraction capacities. Two types of lithium copper phosphate were prepared, one by ion exchange and one by solid state reaction in a manner similar to that recently reported by Amine et al. but with a different (thus far undetermined) structure. Both lithium copper phosphates decomposed to lithium copper oxides and lithium phosphate on cycling.

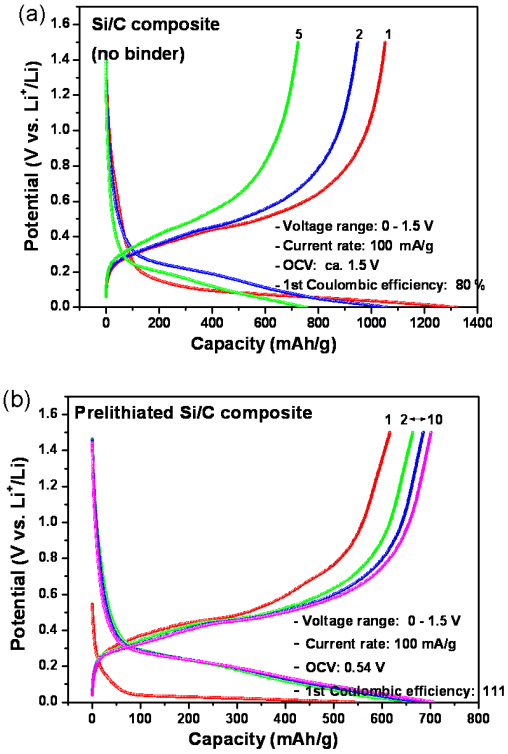

Figure V- 9: Comparison of irreversible capacities and cycling stability of (a) untreated and (b) pre-lithiated Si/C electrodes.

To address potential safety issues that may arise with the use of intermetallic anodes, we prepared a Si electrode (70% Si, 15% CB, 15% PVdF) and measured DSC curves for the active material at various states of charge (Figure V- 10) in the presence of 1M $LiPF_6$ in EC/DEC. The data show only minor reactivity below 250°C, most likely due to protective SEI formation. While this is good news from a safety perspective, it highlights the need to understand the role of the SEI in capacity fading and first cycle lithium losses.

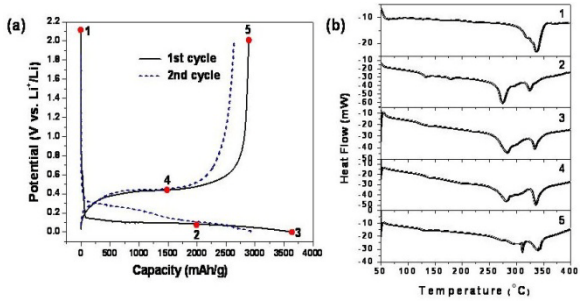

Figure V- 10: (a) Charge-discharge curves for Si electrode; (b) DSC traces at points marked in (a).

Cell Analysis. The distribution of current and charge within composite electrodes has been an active area of interest for many years. While numerous models have been developed, they have had to be refined by comparison of electrochemical behaviors rather than by direct

measurements at the electrode level. In collaboration with the operators of the microdiffraction beamline 12.3.2 at the Advanced Light Source, we have developed a technique for visualization of the charge distribution in cycled lithium iron phosphate electrodes. We take advantage of the two-phase nature of the redox reaction (which results in "freezing" of the charge distribution at a given state of charge or discharge), and obtain phase ratios equivalent to state of charge at different locations both in-plane and in cross section.

The charge distributions normal to the current collector in 50 µm thick Swagelok-cell electrodes charged at low and high rates are shown in Figure V- 12. The observed distribution at high rate is consistent with electrolyte polarization within the electrode. A simulation by V. Srinivasan of LBNL using a porous electrode model including electrolyte transport properties, thickness, porosity, and tortuosity somewhat overestimates the effect, most likely due to the presence of larger pores in the electrode.

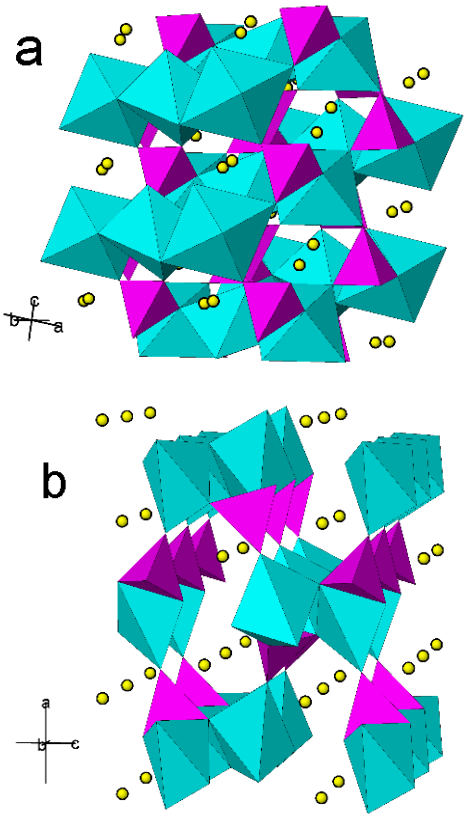

Figure V- 11: Crystal structures of (a) α-$NaCoPO_4$; (b) $NaCuPO_4$.

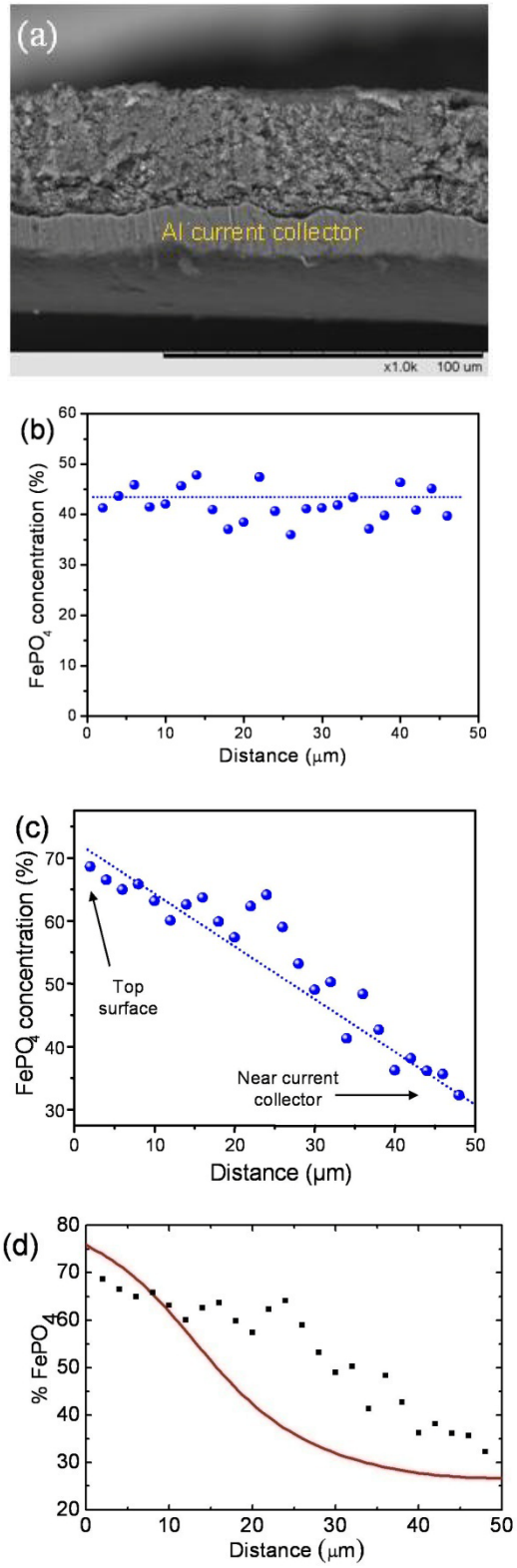

Figure V- 12: (a) Electrode cross section; state of charge distribution following charging to 50 % SOC at: (b) C/8, (c) 18 C; and (d) simulated charge distribution at 20 C (V. Srinivasan).

The in-plane charge distribution in a pouch cell electrode charged at 12 C is shown in Figure V- 13. Here, the effect of the potential drop due to electronic resistance in the 25 µm aluminum current collector is evident. In addition, poorly connected regions have not participated in the charging, due either to a loss of contact with the current collector or inadequate wetting by the electrolyte.

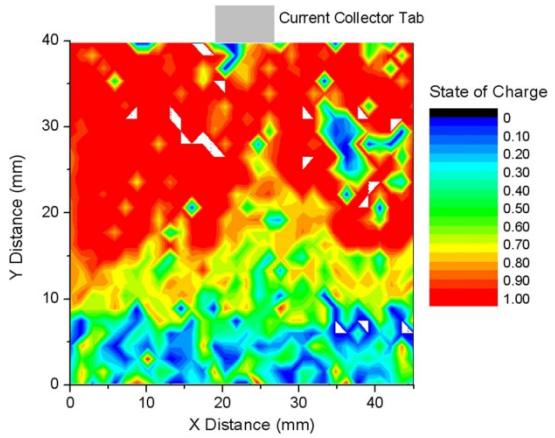

Figure V- 13: State of charge distribution in the plane of an electrode following charging to 50 % SOC at 12 C.

These results represent the first such experimental visualization of charge distribution in cycled electrodes, and offer the possibility of refining models as well as analyzing and optimizing electrode architecture to maximize active material utilization and minimize aging due to over exercising of some parts of electrodes.

Conclusions and Future Directions

Anodes. We have shown that the very large irreversible capacity losses normally associated with silicon and tin intermetallic anodes may be reduced or eliminated, and their performance improved, by preparing the active materials in a fully or partially pre-lithiated state through metathesis reactions with lithium nitride. The reactivity of these highly reduced powders toward binders and solvents has thus far hampered fabrication of high-quality electrodes for testing in full cells. We have initiated a collaboration with Gao Liu of LBNL to develop electrode recipes incorporating Liu's electroactive polymer binder, which becomes electronically conducting when intercalated with lithium. This combination should be ideally suited to our needs, and will allow us test prelithiated Si and Sn powders in cells with metal oxide or phosphate cathodes.

Cathodes. While a small number of high capacity and high voltage cathode materials have become the focus of research on routes to increased energy density in lithium-ion batteries, these have not yet been commercialized due to excessive irreversible capacity losses and/or electrolyte instability. It has proved difficult to translate the high stability if $LiFePO_4$ to higher voltage olivines, and non-olivine polyanion cathode materials that may have optimum Li intercalation potentials, but with less interphase strain and better conductivity have not been identified. We will expand the scope of our search for alternative cathodes to include mixed phosphate-borates with somewhat higher theoretical capacities and redox potentials above 4.2 V.

Cell Analysis. Our *ex situ* method for mapping the distribution of charge both in and normal to the cathode current collector plane enables a wide array of new experiments as well as the ability to evaluate the charge homogeneity in commercial cells. We plan to extend the technique to *in situ* cells, and to study the effects of tab placement and anode characteristics on cathode charge distribution. We will continue to collaborate with Venkat Srinivasan to improve the accuracy of our measurements and the utility of his models.

FY 2010 Publications/Presentations

1. "Study of Metastable Solid Solution Phases in the $LiFePO_4/FePO_4$ System by Solid State MAS NMR," J. Cabana, J. Shirakawa, G. Chen, T. J. Richardson and C. P. Grey, *Chemistry of Materials*, **22** (2010) 1249-1262.
2. "Visualization of Charge Distribution in a Lithium Battery Electrode," J. Liu, M. Kunz, K. Chen, N. Tamura, and T. J. Richardson, *J. Phys. Chem. Lett.*, **1** (2010) 2120-2123.
3. "Continuity and Performance in Composite Electrodes," G. Chen and T. J. Richardson, *Journal of Power Sources*, **195** (2010) 5387-5390.
4. "Materials and Design Considerations for Safe High Performance Lithium Batteries," presented by T. J. Richardson at the *15th International Meeting on Lithium Batteries*, Montréal, Canada, June 29, 2010.
5. "Visualization of Charge Distribution in Lithium Battery Electrodes," presented by T. J. Richardson at the *61st Annual Meeting of the International Society of Electrochemistry*, Nice, France, September 28, 2010.
6. 2010 DOE Annual Peer Review Meeting, Washington, DC, June, 2010.

V.B.3 Olivines and Substituted Layered Materials (LBNL)

Marca M. Doeff

Lawrence Berkeley National Laboratory
M/S 62R0100
Berkeley, CA 94720
Phone: (510) 486-5821 Fax: (510) 486-4881
E-mail: mmdoeff@lbl.gov

Start Date: Oct. 1, 2009
End Date: Sept. 30, 2010

Objectives

- Synthesize and electrochemically characterize $Li[Ni_{0.45}Co_{0.1-y}Al_yMn_{0.45}]O_2$ series for use as cathode materials
- Develop spray pyrolysis method for synthesis of cathode materials, including polyanionic compounds

Technical Barriers

The cathode is one of the most expensive components in Li-ion cells. Reducing cobalt content in layered NMCs lowers raw materials costs, but can adversely impact rate capability. Multi-step processing used during synthesis of high-performance olivine/carbon composites adds to cost. The use of organic solvents during synthesis is environmentally undesirable.

Technical Targets

- Reduce cobalt content in NMCs by substitution with low-cost metals such as Al or Ti, without impacting electrochemical performance.
- Design a spray pyrolysis system and demonstrate the synthesis of high performance electrode materials made by aqueous processing

Accomplishments

- Synthesized and characterized a series of $Li[Ni_{0.45}Co_{0.1-y}Al_yMn_{0.45}]O_2$ compounds for use as cathode materials. Demonstrated that the y=0.05 material outperforms the baseline material during cycling.
- Initiated *in situ* and *ex situ* XANES and X-ray diffraction experiments at the Stanford Synchroton Radiation Lightsource (SSRL) designed to better understand structure and functioning of NMC electrodes. (with J. Cabana, LBNL and A. Mehta, SSRL)
- Collaborated with A. Deb of U. of Michigan on XAS experiments on NMC materials, performed at the Advanced Photon Source (APS, Argonne National Lab).
- Produced a high performance $LiFePO_4$/C composite by spray pyrolysis, and demonstrated successful synthesis of $LiMnPO_4$/C composites and $LiNi_{0.5}Mn_{1.5}O_4$. (with T. Richardson, LBNL)

✧ ✧ ✧ ✧ ✧

Introduction

Achieving the DOE cost targets for Li-ion batteries for vehicular applications requires reducing the cost of the cathode materials. Significant savings can be realized by decreasing the Co content, which is the most expensive metal in NMC (lithium nickel manganese cobalt oxides) cathodes. However, materials with very low cobalt content exhibit poor power performance and the increased nickel content may adversely affect the thermal abuse tolerance. Our previous work shows that some formulations in which Al or Ti partially substitute for Co have superior electrochemical properties to the baseline NMC materials. In particular, several compositions demonstrate improved cycling characteristics and better rate performances in lithium half-cells. Work this year was directed towards extending composition ranges and developing experimental techniques designed to better understand the origins of this effect.

Carbon coating of particles is frequently used to improve electrochemical performance of olivines and other polyanionic compounds. $LiMnPO_4$ requires solvothermal synthesis followed by grinding with carbon. The multi-step processing and use of an organic solvent increases cost and is environmentally undesirable. We have been developing synthetic techniques designed to simplify synthesis of polyanionic compounds and reduce processing costs. Spray pyrolysis is a continuous processing method that is easily scalable, uses aqueous precursor solutions, and results in uniform spherical particles of controllable size. Either pure phases or carbon composites can be produced in one step, depending on the nature of the precursor solutions, and no exotic equipment is required. This year, we demonstrated that high-performance olivine/carbon composites could be synthesized using spray pyrolysis.

Approach

Materials are synthesized, assessed for phase purity, and physically characterized using X-ray powder diffraction (XRD), scanning electron microscopy (SEM), ICP and other relevant techniques. Composite electrodes are tested in half-cell configurations and compared to baseline materials. Post-mortem analyses are carried out, in conjunction with members of the BATT diagnostics team. In some cases, charged, discharged, or cycled electrodes are studied at SSRL by X-ray diffraction to understand structural changes that occur during electrochemical processes. Pouch cells with lithium anodes and composite cathodes are assembled and cycled in the relevant SSRL beamline for *in situ* XAS and X-ray diffraction experiments.

Figure V- 14 is a schematic of one of the spray pyrolysis setups used in our laboratory to produce powders. Several modifications of the equipment are used depending upon the nature of the desired product.

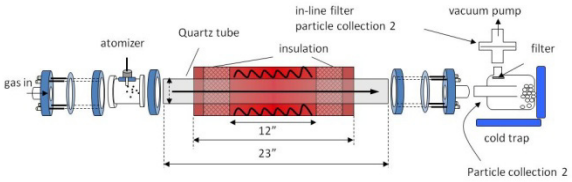

Figure V- 14: Schematic of one of the spray pyrolysis setups used to produce cathode materials.

Results

Substituted NMCs. A series of $Li[Ni_{0.45}Co_{0.1-y}Al_yMn_{0.45}]O_2$ compounds were prepared and characterized by XRD, ICP, and SEM. It was possible to fully substitute Al for Co (y=0.1) in this system, and substitution had no effect on the particle size or morphology. Al substitution at low levels (y≤0.05) did not decrease the practical capacity delivered between 4.3-2.0V upon discharge (Figure V- 15), nor did it adversely affect rate capability.

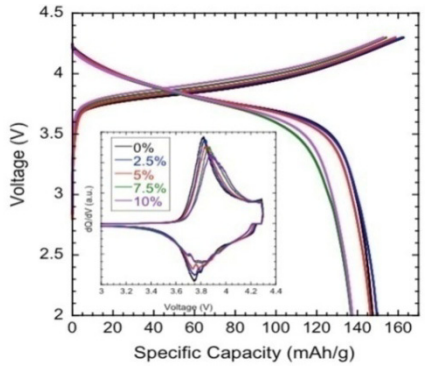

Figure V- 15: $Li/Li[Ni_{0.45}Co_{0.1-y}Al_yMn_{0.45}]O_2$ (y=0, 0.025, 0.05, 0.075, and 0.1) cells charged and discharged at 0.1 mA/cm² between 4.3 and 2.0V. The inset shows dQ/dV plots derived from the data.

The capacity retention of cycled cells with $Li[Ni_{0.45}Al_{0.05}Co_{0.05}Mn_{0.45}]O_2$ electrodes is superior to that of those containing $Li[Ni_{0.45}Co_{0.1}Mn_{0.45}]O_2$ (Figure V- 16). *in situ* XRD experiments on cells containing these two electrode materials carried out at SSRL show that volume changes during cell charge are less severe for the Al-substituted electrode than for the baseline material. In particular the c-axis undergoes relatively less change as charge progresses (Figure V- 17), which may be the origin of the improved cycling behavior.

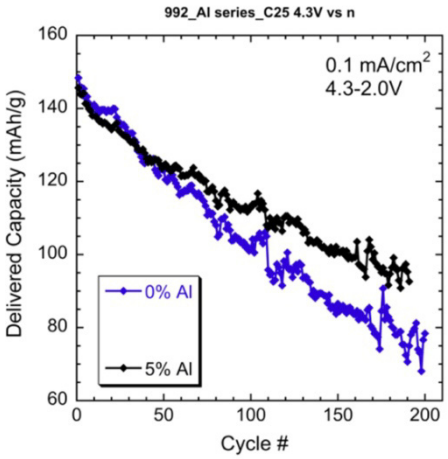

Figure V- 16: Discharge capacity as a function of cycle number for $Li/Li[Ni_{0.45}Co_{0.1}Mn_{0.45}]O_2$ and $Li/Li[Ni_{0.45}Al_{0.05}Co_{0.05}Mn_{0.45}]O_2$ cells discharged at 0.1 mA/cm².

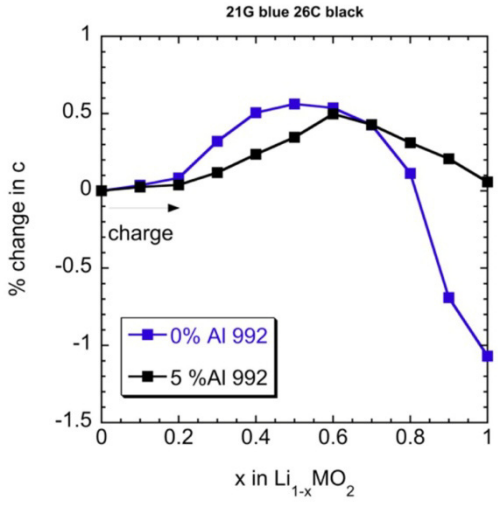

Figure V- 17: Relative changes in c-axis parameters as a function of state-of-charge in $Li_{1-x}[Ni_{0.45}Co_{0.1}Mn_{0.45}]O_2$ and $Li_{1-x}[Ni_{0.45}Al_{0.05}Co_{0.05}Mn_{0.45}]O_2$ electrode materials.

Similar improvements in cycling behavior have also been observed in other Al substituted NMC materials (e.g., $Li[Ni_{0.4}Co_{0.15}Al_{0.05}Mn_{0.4}]O_2$) compared to baseline materials. An *in situ* EXAFS study of a cell containing this

material undergoing charge and discharge shows that changes in metal-oxygen bondlengths are entirely reversible (not shown). Both Ni and Co undergo redox throughout the charge and discharge process, although not all of the Co is utilized.

Ti-substitution for Co in NMC is more complex than that of Al substitution, as charge compensation must occur. (Ti^{4+} substitutes for Co^{3+}). It is also somewhat difficult to control stoichiometry due to the instability of the $TiO(NO_3)_2$ used during solution synthesis (mixed hydroxide method or glycine nitrate combustion). Our results indicate that small amounts of Ti (<10%) can, however, be substituted for Co, but larger amounts result in the production of a spinel impurity, which lowers the discharge capacity. In phase-pure materials, small amounts of Ti substitution enhance both discharge capacity and cycling behavior (Figure V- 18 and Figure V- 19).

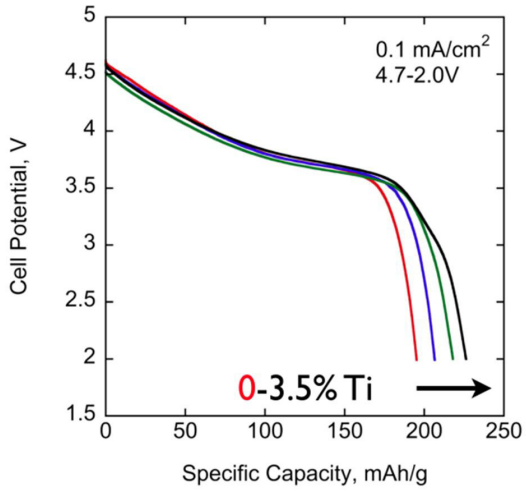

Figure V- 18: Discharge profiles of lithium cells containing $Li[Ni_{0.33}Co_{0.33-y}Ti_yMn_{0.33}]O_2$ compounds, discharged at 0.1 mA/cm² between 4.7 and 2.0V.

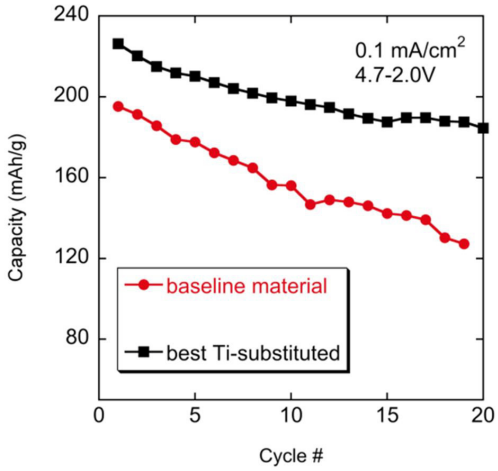

Figure V- 19: Capacity as a function of cycle number for $Li/Li[Ni_{0.33}Co_{0.33}Mn_{0.33}]O_2$ and $Li/Li[Ni_{0.33}Co_{0.3}Ti_{0.03}Mn_{0.33}]O_2$ cells cycled between 4.7 and 2.0 V at 0.1 mA/cm².

The origin of these effects is currently unknown. It is possible that the aliovalent substitution improves the electronic conductivity of the as-made materials (plausible if Mn^{3+} compensates for the substituting Ti^{4+}, resulting in mixed valencies). However, modest improvement in capacity is also observed when small amounts of both Mg^{2+} and Ti^{4+} are substituted for Co^{3+} or when Ti is partially substituted for Mn (more than a few percent has a deleterious effect).

Spray pyrolysis. A $LiFePO_4$/C composite was made in one step using spray pyrolysis. The product consisted of nanoporous spherical particles approximately 10 μm in diameter (Figure V- 20). Energy dispersive X-ray spectroscopy (EDS) indicates that carbon is uniformly deposited throughout the particles and a high resolution transmission electron micrograph (HR-TEM) of a fractured particle, shows a thin layer of amorphous carbon on an internal surface (Figure V- 21).

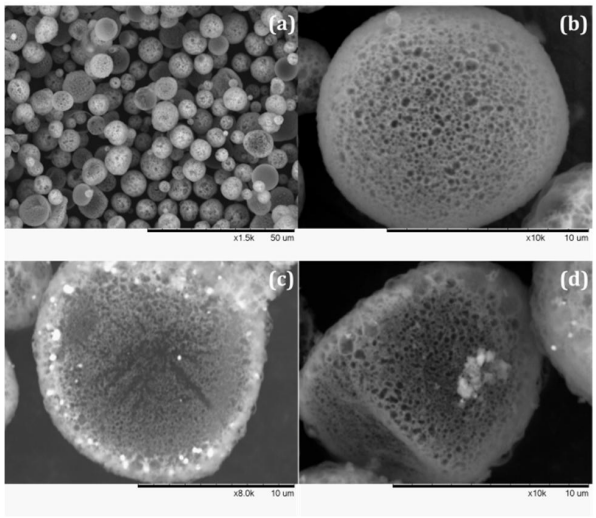

Figure V- 20: SEM images of a) nanoporous $LiFePO_4$/C spheres; b) a single 3D nanoporous $LiFePO_4$/C sphere; c, d) broken 3D nanoporous $LiFePO_4$/C spheres, showing the 3D nanoporous microstructure.

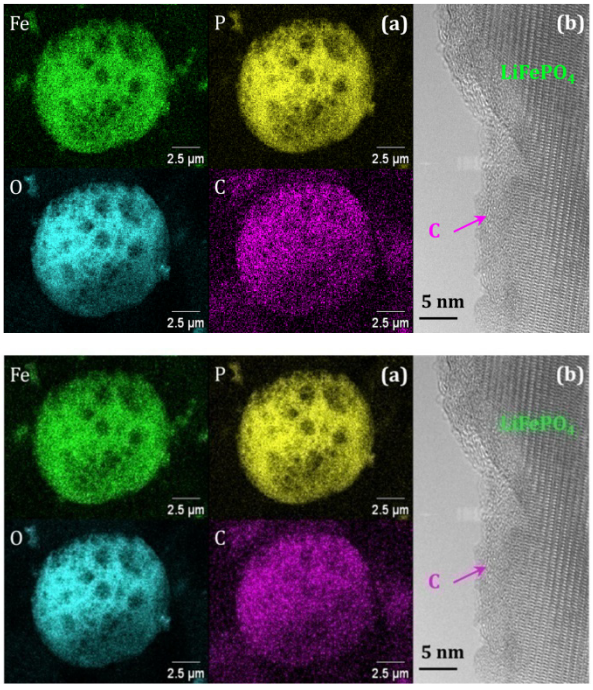

Figure V- 21: a) EDS maps of Fe, P, O, and C on single $LiFePO_4$/C spheres and b) HR-TEM image of a fractured surface, showing the carbon coating.

The rate capability (Figure V- 22) and cycling behavior of this material was extremely good.

$LiMnPO_4$/C and $LiNi_{0.5}Mn_{1.5}O_4$ samples have also been produced by spray pyrolysis and are undergoing evaluation in our laboratory.

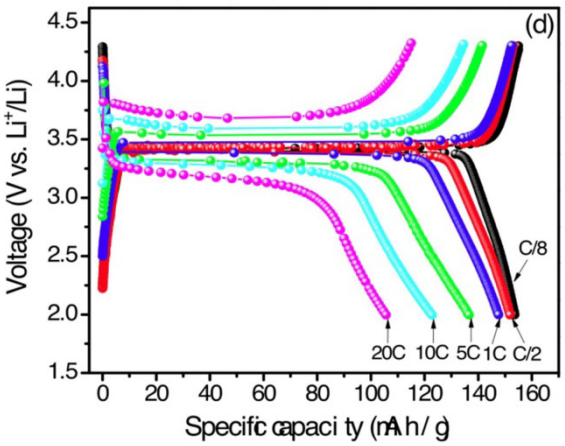

Figure V- 22: Rate capability of $LiFePO_4$/C sample produced by spray pyrolysis.

Conclusions and Future Directions

Although 5% Al substitution improved the rate behavior in the $Li[Ni_{0.4}Co_{0.2-y}Al_yMn_{0.4}]O_2$ system, this effect was not observed in the $Li[Ni_{0.45}Co_{0.1-y}Al_yMn_{0.45}]O_2$ compounds studied this year. However, partial Al-substitution for Co appears to improve the cycling behavior of NMCs in general, as observed in both of these systems. Synchrotron experiments carried out at SSRL and APS indicate that bondlength changes are very reversible for $Li_x[Ni_{0.4}Co_{0.15}Al_{0.05}Mn_{0.4}]O_2$ and that the c lattice parameter undergoes smaller changes during charge for $Li_x[Ni_{0.45}Co_{0.05}Al_{0.05}Mn_{0.45}]O_2$ than in $Li_x[Ni_{0.45}Co_{0.1}Mn_{0.45}]O_2$. Further work at SSRL will be directed towards understanding the origin of the capacity fading seen in NMC systems, using these two electrode materials. Some *in situ* and *ex situ* XAS and/or X-ray diffraction experiments may also be carried out on Ti-substituted NMCs to understand the mechanism of charge compensation and the increased capacity that is observed. The electronic conductivities of Ti-substituted NMCs will be measured by AC impedance and/or DC four point probe methods in the coming year. The Ti-substitution results suggest that it may be possible to increase the capacity of NMC materials by 10-15% without resorting to complicated composite materials which require formation cycles.

We were able to produce a very high performance $LiFePO_4$/C electrode material using a simple, potentially low-cost spray pyrolysis method. This technique produces uniform spherical particles, which could be easily processed into composite electrodes. We have also successfully synthesized $LiMnPO_4$/C and $LiNi_{0.5}Mn_{1.5}O_4$ samples, which we will characterize. We plan to expand this synthesis method to other materials that may benefit from carbon coating and currently do not perform well

(polyanionic compounds such as borates, other types of phosphates and silicates).

FY 2010 Publications/Presentations

1. 2010 DOE Annual Peer Review Meeting Presentation, June 2010.
2. "Combustion Synthesis of Nanoparticulate $LiMg_xMn_{1-x}PO_4$ (x=0, 0.1, 0.2) Carbon Composites" Marca M. Doeff, Jiajun Chen, Thomas E. Conry, Ruigang Wang, James Wilcox, and Albert Aumentado, **J. Mater. Res.**, 25, 1460 (2010).
3. "The Impact of Aluminum and Iron Substitution on the Structure and Electrochemistry of $Li[Ni_{0.4}Co_{0.2-y}M_yMn_{0.4}]O_2$ Materials" James D. Wilcox, Efrain E. Rodriguez, and Marca M. Doeff, **J. Electrochem. Soc.**, 156, A1011 (2009).
4. "Improved Layered Mixed Transition Metal Oxides for Li-ion Batteries" Marca M. Doeff, Thomas Conry, and James Wilcox, SPIE Energy Harvesting and Storage: Materials, Devices, and Applications, Proceedings of SPIE, SPIE Defense, Security, and Sensing, Vol. 7683, 768309-2, 5-9 April 2010, Orlando, FL (invited)
5. "Layered Mixed Transition Metal Oxide Materials for Li-ion Battery Cathodes" Thomas E. Conry and Marca M. Doeff, Materials Research Society, April 2010, San Francisco, CA.
6. " Advanced Li-ion Battery Cathode Materials for Vehicle Technologies" American Chemical Society, Electrochemistry and Battery Applications symposium, August 2010, Boston, MA, Paper 355. (invited)
7. "Substitution of Ti, Fe, and Al for Co in $Li[Ni_xM_yCo_{1-y}Mn_z]O_2$ Systems" International Battery Association Pacific Power Source Symposium 2010, January 2010, Waikoloa, HI. (invited)
8. "Nanostructured Cathodes for Li Ion Batteries" Berkeley Lab Women Scientists Council, Lawrence Berkeley National Laboratory, Oct. 23, 2009, Berkeley, CA. (invited)

V.B.4 Stabilized Spinels and Nano Olivines (University of Texas)

Arumugam Manthiram
University of Texas at Austin
Materials Science and Engineering Program
Austin, TX 78712
Phone: (512) 471-1791; Fax: (512) 471-7681
E-mail: rmanth@mail.utexas.edu

Start Date: April 1, 2004
Projected End Date: May 31, 2011

Objectives

- Develop high-performance cathodes for lithium-ion batteries and a fundamental understanding of their structure-composition-performance relationships.
- Develop low-cost spinel manganese oxide compositions exhibiting high power capability and long cycle life at elevated temperatures.
- Develop novel chemical synthesis and manufacturing processes for polyanion-containing cathodes such as olivine phosphates and silicates with controlled size and nano-morphologies.

Technical Barriers

This project addresses the following technical barriers of the lithium-ion battery technology, especially focusing on the cathode materials:

- Battery cost
- Cycle life
- Energy and power densities

Technical Targets

- Long cycle life for 4 V and 5 V spinel cathodes
- Low manufacturing cost for polyanion (e.g., olivine) cathodes
- Increased energy and power with spinel and polyanion cathodes

Accomplishments

- Fundamental understanding of the factors that control the electrochemical performances of cation-substituted 4 V spinels, which can serve as a guide for the design of high-performance 4 V spinel cathodes
- Oxyfluoride spinel cathodes offer better thermal stability than the oxide counterparts
- Segregation of certain cations like Fe^{3+} to the surface during the synthesis of cation-substituted 5 V spinels offers a robust, stable cathode-electrolyte interface, resulting in good cycle life and rate capability despite the high operating voltage and offering a new low-cost approach to develop surface-stabilized, high-voltage cathodes
- The redox energy of the lower-voltage couple increases while that of the higher-voltage couple decreases in olivine solid solutions $LiFe_{1-y}M_yPO_4$ (M = Mn or Co) compared to that in the unsubstituted $LiMPO_4$
- Synthesis of phosphate and silicate cathodes by a novel microwave-assisted solvothermal process
- Synthesis of nano-engineered alloy, carbon-decorated Fe_3O_4 nanowire, and graphene anodes with high capacities and long cycle life, but these results are not presented below due to limited space.

✧ ✧ ✧ ✧ ✧

Introduction

Achieving the DOE targets for vehicle applications will require development of low-cost, better-performing cathode and anode materials with high energy and power densities. Accordingly, this project focuses on improving the performance and/or lowering the manufacturing cost of 4 V and 5 V spinel and polyanion cathode systems. Both the spinel and the polyanion-containing nano olivine phosphate cathodes are known to offer high rate capability and are heavily pursued for vehicle applications. Also, novel synthesis approaches for Li_2MSiO_4 (M = Mn and Fe) nano silicate cathodes are pursued. These materials have the potential to reversibly extract/insert two lithium-ions per formula unit and thereby increase the energy density. In addition, the project has focused on high-capacity anodes, but the results are not presented here.

Approach

To meet the DOE performance and cost targets for vehicle applications, our approach is to develop a firm scientific understanding of the factors that control/influence the electrochemical performances of the spinel oxide and polyanion-containing cathodes and utilize the knowledge gained to design and develop high performance cathode compositions. In this regard, cationic and anionic substitutions in the 4 V and 5 V spinels, surface modifications with self-surface segregation of certain cations during the synthesis process, and novel low-cost synthesis approaches for nano olivine and silicate cathodes are being pursued. The materials synthesized by conventional solid-state, high-energy ball milling, or

solution-based synthesis approaches are characterized by a variety of chemical and physical techniques: wet-chemical analysis by inductively coupled plasma (ICP) analysis, X-ray diffraction (XRD), scanning electron microscopy (SEM), transmission electron microscopy (TEM), thermal analysis, Fourier transform infrared (FTIR) spectroscopy, Raman spectroscopy, and X-ray photoelectron spectroscopy (XPS). The electrochemical performances are evaluated in coin cells with charge-discharge, cyclability, rate capability, and impedance spectroscopic measurements. Based on the chemical, structural, morphological, and electrochemical data collected with the synthesized samples, an in-depth structure-property-performance relationship is established. The understanding gained is utilized to refine the compositions and develop new materials.

Results

Stabilized 5 V Spinel Cathodes. Spinel $LiMn_{1.5}Ni_{0.5}O_4$ with the $Ni^{2+/4+}$ couple and an operating voltage of 4.8 V versus Li/Li^+ is appealing for vehicle applications. The major issues with $LiMn_{1.5}Ni_{0.5}O_4$ are (i) chemical instability of $Ni^{3+/4+}$ in contact with the electrolytes, resulting in deterioration in cycle life and power capability and (ii) the formation of $Li_xNi_{1-x}O$ impurity during synthesis. We showed previously that the $Li_xNi_{1-x}O$ impurity can be eliminated by a substitution of other cations for Mn/Ni while the instability in contact with the electrolyte can be suppressed by chemical surface modification with materials like Al_2O_3 and $AlPO_4$. However, it may be difficult to obtain a uniform, robust chemical surface modification; it will also involve additional processing costs. Accordingly, we have pursued self-segregation of certain cations like Fe^{3+} to the surface (during the synthesis process) that can offer better chemical stability in contact with the electrolyte.

The cyclability data in Figure V- 23 reveal that $LiMn_{1.5}Ni_{0.42}Fe_{0.08}O_4$ exhibits 136 mAh/g with 100 % capacity retention in 100 cycles. Figure V- 24 compares the normalized discharge capacity at various C rates in reference to the value at C/6 rate. Clearly, the Fe-substituted samples show superior rate capability. The electrochemical impedance spectroscopic (EIS) data in Figure V- 25 reveal that the Fe-substituted samples exhibit lower surface resistance R_s and charge transfer resistance R_{ct} compared to $LiMn_{1.5}Ni_{0.5}O_4$, resulting in superior electrochemical performance.

In order to develop a better understanding of the lower R_s and R_{ct} values, we have examined the samples by XPS before and after sputtering for 5 min. The data reveal that while the relative concentrations of the elements in the bulk are close to the nominal values, the surface of the Fe-substituted samples has a higher concentration of Fe and a lower concentration of Ni compared to the bulk. The Fe enrichment on the surface alleviates electrolyte decomposition at high voltage and prevents the formation of thick SEI layer, resulting in lower R_s and R_{ct} and superior performance.

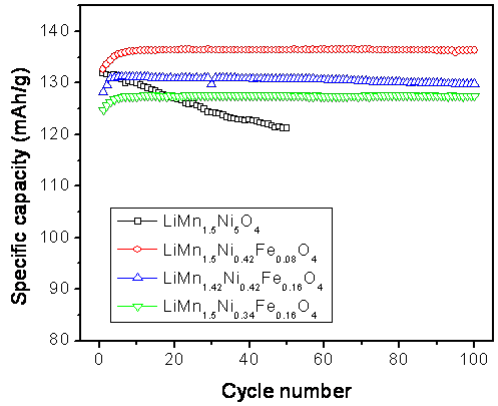

Figure V- 23: Cyclability of $LiMn_{1.5}Ni_{0.5}O_4$ and the Fe-substituted samples.

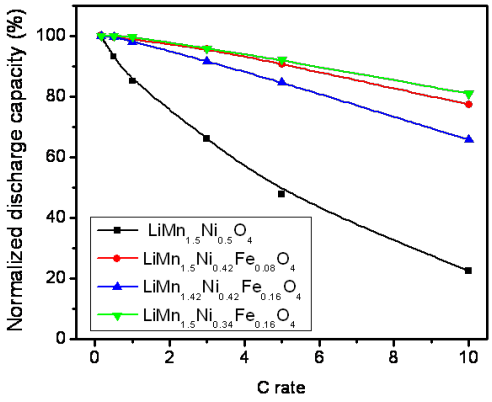

Figure V- 24: Comparison of the rate capabilities of $LiMn_{1.5}Ni_{0.5}O_4$ and the Fe-substituted samples.

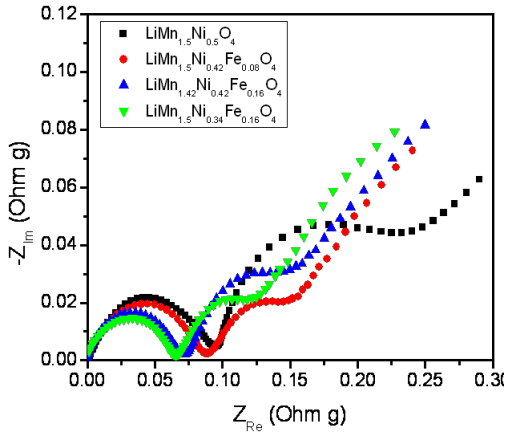

Figure V- 25: EIS plots of $LiMn_{1.5}Ni_{0.5}O_4$ and the Fe-substituted samples.

Nano Olivine Solid Solutions. Investigations of $LiFePO_4$ and $LiFe_{1-y}Mn_yPO_4$ solid solutions have shown several interesting observations such as a change in the reaction mechanism from a two-phase behavior to a single-phase behavior depending on the particle size, temperature, and doping. To develop further understanding, we have focused on a systematic investigation of the structure, electrochemical performance, redox potential, and reaction behavior of carbon-coated $LiM_{1-y}M_yPO_4$ (M = Mn, Fe, or Co) solid solutions synthesized by an efficient high-energy mechanical milling of the raw materials with super-p carbon, followed by heating in argon at 550°C for 6 hours. A comparison of the equilibrium redox potentials of the $M^{2+/3+}$ redox couples in the solid solutions reveals that the potential of the lower-voltage couple increases while the potential of the higher-voltage couple decreases in the $LiM_{1-y}M_yPO_4$ solid solution compared to that in the pristine $LiMPO_4$. Changes in the M-O covalence (inductive effect) play a role in shifting the redox potentials. For example, substitution of the less electropositive Co^{2+} for Fe^{2+} or Mn^{2+} in $LiFe_{1-y}Co_yPO_4$ and $LiMn_{1-y}Co_yPO_4$ decreases the Fe-O or Mn-O covalence and thereby lowers the $Fe^{2+/3+}$ or $Mn^{2+/3+}$ redox energy and increases the voltages of $Fe^{2+/3+}$ and $Mn^{2+/3+}$, while the substitution of more electropositive Fe^{2+} or Mn^{2+} for Co^{2+} increases the Co-O covalence and thereby raises the $Co^{2+/3+}$ redox energy and decreases the voltage of $Co^{2+/3+}$.

Nano Silicates. Li_2MSiO_4 (M = Mn and Fe) silicates offer the possibility of reversibly extracting/inserting two lithium-ions per formula unit with a theoretical capacity of ~ 330 mAh/g. However, only limited literature is available on this class of materials due to the difficulty in synthesizing phase-pure Li_2MSiO_4, and they suffer from poor electronic conductivity like the olivine phosphates. Accordingly, we extended the microwave-assisted solvothermal (MW-ST) approach developed in our laboratory to this class of materials, and nanostructured Li_2MSiO_4 have been obtained by the MW-ST process at 300°C for 20 min, followed by heating at 650°C for 6 h in argon atmosphere to obtain well-crystallized phases with carbon coating. XRD, SEM, and TEM data reveal the formation of carbon-coated single-phase Li_2MSiO_4 with an average particle size of ~ 20 nm.

As seen in Figure V- 26(a) and Figure V- 26(b), Li_2FeSiO_4/C and Li_2MnSiO_4/C deliver a first discharge capacity of, respectively, ~ 148 and 210 mAh/g at room temperature at C/20 rate, which increase to, respectively, 204 and 250 mAh/g at 55°C, demonstrating the ability to extract/insert more than one lithium. However, while the Li_2FeSiO_4/C exhibits a stable cycle life with 100% capacity retention at both room temperature and 55°C, Li_2MnSiO_4/C exhibits drastic capacity fade, especially at 55°C, and it retains only 50% of its initial capacity at room temperature and 15% of its initial capacity at 55°C after 20 cycles. The poor cyclability of Li_2MnSiO_4/C is due to the dynamic Jahn-Teller distortion of Mn^{3+} ions and manganese dissolution. In addition, while Li_2FeSiO_4 exhibits high rate performance and good thermal stability, Li_2MnSiO_4 shows poor rate performance and low thermal stability.

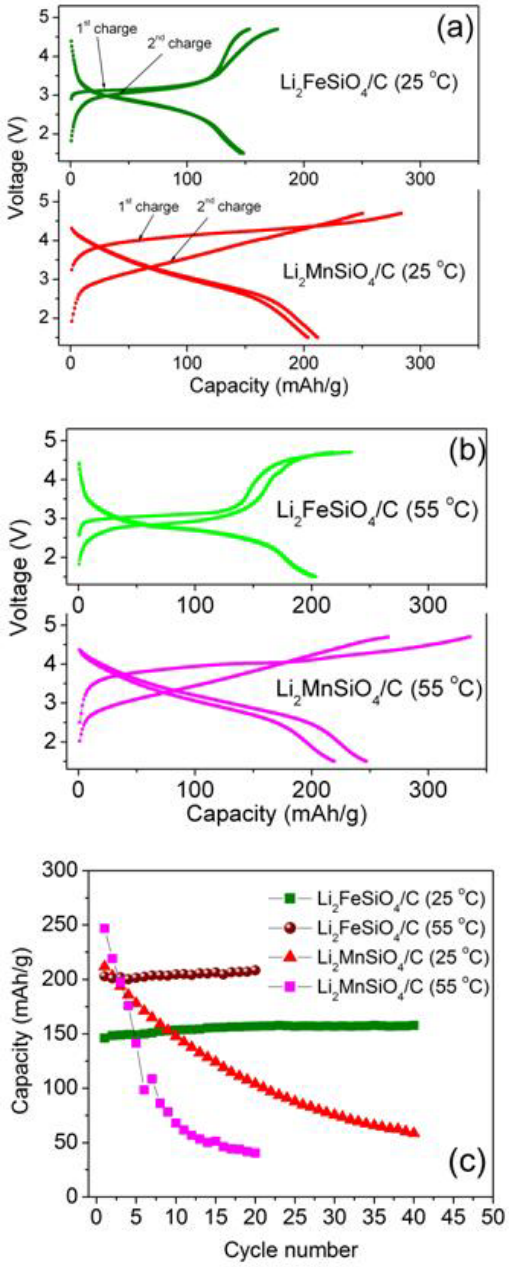

Figure V- 26: Charge-discharge profiles and cycle life of Li_2MSiO_4/C.

Conclusions and Future Directions

Self-segregation of certain cations to the surface during the synthesis process is found to be beneficial not only to overcome the chemical instability of the 5 V spinel cathodes in contact with the electrolyte but also to lower

the manufacturing cost. Intrigued by this observation, our future work will focus on an investigation of the self-surface segregation of a number of other cations with 4 V and 5 V spinels and their characterization by advanced techniques.

$LiM_{1-y}M_yPO_4$ (M = Mn, Fe, and Co) phosphates and Li_2MSiO_4 (M = Mn and Fe) silicates have been synthesized by high energy mechanical milling or novel microwave-assisted solvothermal approaches. Building on this, our future work will focus on the synthesis of carbon-coated nano $Li_2M_{1-y}M_ySiO_4$ (M = Mn, Fe, Co, and Ni) solid solutions and nanostructured Nasicon-type cathodes like $Li_3V_2(PO_4)_3$ and $Li_3Fe_2(PO_4)_3$. Based on advanced chemical, structural, and surface characterizations of the materials, an in-depth understanding of the structure-composition-performance relationships will be developed.

FY 2010 Publications/Presentations

Journal Articles

1. S. Yoon and A. Manthiram, "Superior Capacity Retention Sn-Ni-Fe-C Composite Anodes for Lithium-ion Batteries," *Electrochemical and Solid State Letters* **12**, A190-A193 (2009).
2. J. Liu and A. Manthiram, "Understanding the Improved Electrochemical Performances of Fe-substituted 5 V Spinel Cathode $LiMn_{1.5}Ni_{0.5}O_4$," *Journal of Physical Chemistry C* **113**, 15073-15079 (2009).
3. S. Yoon and A. Manthiram, "Sb-MO_x-C (M = Al, Ti, or Mo) Nanocomposite Anodes for Lithium-ion Batteries," *Chemistry of Materials* **21**, 3898-3904 (2009).
4. J. Liu and A. Manthiram, "Kinetics Study of the 5 V Spinel Cathode $LiMn_{1.5}Ni_{0.5}O_4$ before and after Surface Modifications," *Journal of the Electrochemical Society* **156**, A833-A838 (2009).
5. T. Muraliganth, A. Vadivel Murugan, and A. Manthiram, "Facile Synthesis of Carbon-decorated Single-crystalline Fe_3O_4 Nanowires and Their Application as High Performance Anode in Lithium-ion Batteries," *Chemical Communications* 7360-7362 (2009).
6. A. Vadivel Murugan, T. Muraliganth, and A. Manthiram, "Rapid, Facile Microwave-solvothermal Synthesis of Graphene Nanosheets and Their Polyaniline Nanocomposites for Energy Storage," *Chemistry of Materials* **21**, 5004-5006 (2009).
7. S. Yoon and A. Manthiram, "Nanoengineered Sn-TiC-C Anode for Lithium-ion Batteries," *Journal of Materials Chemistry* **20**, 236-239 (2010).
8. N. Kalaiselvi and A. Manthiram, "One-pot, Glycine-assisted Combustion Synthesis and Characterization of Nanoporous $LiFePO_4$/C Composite Cathodes for Lithium-ion Batteries," *Journal of Power Sources* **195**, 2894-2899 (2010).
9. J. Liu, W. Li, and A. Manthiram, "Dense Core-shell Structured SnO_2/C Composites as High Performance Anodes for Lithium-ion Batteries," *Chemical Communications* **46**, 1437-1439 (2010).
10. T. Muraliganth and A. Manthiram, "Understanding the Shifts in the Redox Potentials of Olivine $LiM_{1-y}M_yPO_4$ (M = Fe, Mn, Co, and Mg) Solid Solution Cathodes," *Journal of Physical Chemistry C* **114**, 15530-15540 (2010).
11. T. Muraliganth, K. R. Stroukoff, and A. Manthiram, "Microwave-Solvothermal Synthesis of Nanostructured Li_2MSiO_4/C (M = Mn and Fe) Cathodes for Lithium-Ion Batteries," *Chemistry of Materials,* DOI: 10.1021/cm102058.

Presentations

1. A. Manthiram, "High Energy Density Electrode Materials for Next Generation Lithium-ion Batteries," *IUPAC 5th International Symposium on Novel Materials and Synthesis,* Shanghai, China, October 18-23, 2009 (invited).
2. A. Manthiram, "Materials Challenges and Opportunities of Lithium-ion Battery Technology," *Materials Science and Technology 2009 (MS&T 2009) Conference,* Pittsburgh, PA, October 25-29, 2009 (invited).
3. A. Manthiram, "Understanding the Improvement in the Electrochemical Properties of Surface Modified 5 V Spinel Cathodes," *2009 Fall Meeting of the Materials Research Society,* Boston, MA, November 30- December 4, 2009.
4. A. Manthiram, "Spinel and Layered Oxyfluoride Cathodes for Lithium-ion Batteries," *Workshop on Fluorinated Materials & Energy Conversion (FMEC 2010),* Bordeaux, France, April 11-13, 2010 (invited).
5. A. Manthiram and S. Yoon, "Nanoengineered Sn-TiC-C and Sb-MO_x-C (M = Al, Ti, or Mo) Composite Anodes for Lithium-ion Batteries," *217th Meeting of the Electrochemical Society,* Vancouver, Canada, April 25-30, 2010.
6. A. Manthiram, "Nanomaterials for Lithium-Ion Batteries," *Workshop of Physics of Novel Energy Materials,* Institute for Complex Adaptive Matter, Beijing, China, May 29-June 3, 2010 (invited).
7. A. Manthiram, "Nanomaterials for Lithium-ion Batteries," *Workshop on Nanomaterials for Alternative Energy Applications*, University of British Columbia, Vancouver, Canada, June 20-23, 2010 (invited).
8. A. Manthiram, "Materials Challenges and Opportunities of Lithium-ion Battery Technology," *Fall 2010 American Chemical Society Meeting*, Boston, MA, August 22-26, 2010 (invited).

V.B.5 The Synthesis and Characterization of Substituted Olivines and Layered Manganese Oxides (SUNY)

M. Stanley Whittingham
SUNY at Binghamton
Vestal Parkway East
Binghamton, NY 13902-6000
Phone: (607) 777-4623; Fax: (607) 777-4623
E-mail: stanwhit@binghamton.edu

Start Date: June 1, 2007
Projected End Date: December 31, 2011

Objectives

- Find lower-cost and higher-capacity cathodes, exceeding 200 Ah/kg (lab experimental)
- Find high-rate PHEV compatible cathodes
- Both of the above are to be based on environmentally benign materials.

Technical Barriers

This project addresses the following technical barriers:

(A) Lower cost materials and processing

(B) Higher power materials

(C) Higher capacity materials

(D) Abuse-tolerant safer cathodes

Technical Targets

- Determine for PHEV and EV applications the optimum composition of $LiNi_yMn_yCo_{1-2y}O_2$.
- Evaluate phosphate structures with varying morphologies and dopants, containing Fe and/or Mn, and compare with optimum $LiFePO_4$.
- Identify materials that can undergo more than one electron per redox center.

Accomplishments

- Shown for the layered oxides that the composition $LiMn_{0.4}Ni_{0.4}Co_{0.2}O_2$ is as good electrochemically as $LiMn_{0.33}Ni_{0.33}Co_{0.33}O_2$.
  - Lower cobalt contents have higher surface area and lower cost
  - To achieve capacities over 200 Ah/kg in the layered oxides will require charging voltages over 4.4 volts at RT, or modification of metal content to reduce the voltage profile
  - Shown, in a collaborative work with NREL that the layered oxides have power capability.
- Substitution in $LiFePO_4$ shown to be advantageous:
  - Vanadium substitution leads to nanostructure
    - Needs lower conductive carbon level, leading to higher volumetric capacities
    - Vanadium appears to substitute on the Fe and P sites
  - Opens up opportunities for $LiMnPO_4$
- Scoping and literature survey underway on two-electron redox active intercalation materials
  - Identified iron pyrophosphates, $Li_2FeP_2O_7$ as a class of material where two lithium-ions may be cycled.
    - With present electrolytes only one lithium can be cycled below 4.5 volts.
    - Results of G. Ceder at MIT agree.
  - Vanadium oxides and phosphates are viable candidates for > 1 electron transfer.
- Technology transfer accomplished
  - Working with several local battery companies (Primet on nano-scissored material), and many ex-students now in battery companies
  - Students now have positions at BNL, NREL, and PNNL

✧ ✧ ✧ ✧ ✧

Introduction

Achieving the DOE energy and power targets for PHEV and EV batteries will require much higher capacity materials. To meet the DOE cost targets, we are looking at reducing high-cost components, and for power and energy targets at modifying the chemical composition and morphology of the cathode compounds.

Approach

Our cathode approach is to place emphasis on low cost materials, predominantly oxides and phosphates, both

pure and modified with other transition metals, using a range of practical synthesis approaches. These materials will be synthesized, and characterized both structurally, including defects and morphology, and for thermal and chemical stability. All will be evaluated electrochemically in a range of cell configurations.

For the modified layered dioxides, we are determining the role of each of the transition metals, with the goal of minimizing expensive components such as cobalt. To that end, we are studying the layered compositions, $LiNi_yMn_yCo_{1-2y}O_2$, with a close to stoichiometric Li to transition metal ratio and with values of y of 0.4 and 0.45 leading to a cobalt content of only 10%.

One major challenge facing the use of the olivine class of materials, such as $LiFePO_4$, is their low volumetric energy density, which is exaserbated by the probable need to use nanomaterials. Our approach is to form more dense powder structures, using low cost techniques by isovalent substitution on either the iron or phosphorus site. We are determining the role of the substituent cation on morphology and capacity. A second challenge is the apparent high cost of making high quality material. Earlier we developed the hydrothermal method as a low cost approach.

We are searching for new classes of materials that might react with more than one lithium-ion per redox center. Phosphates are one area for our search and vanadium containing materials another area.

Results

Layered Transition Metal Oxides. We have formed a range of transition metal oxides $LiNi_yMn_yCo_{1-2y}O_2$ to determine the optimum composition for both energy density and power density. The theoretical capacity was determined by measuring the open circuit voltages, on both lithium removal and lithium insertion. The material with y = 0.4 showed as good behavior as any other composition. The rate behavior of this compound was evaluated in collaboration with C. Ban and A. Dillon of NREL. The material was spread on a carbon nanotube mesh with no binder and no additional carbon. The results are shown in Figure V- 27.

The results clearly show that the layered materials can deliver high rates when the electrode is configured optimally.

Structural Modification of $LiFePO_4$. We have shown that vanadium can be substituted into the olivine lattice. Such substitution at the 5% level leads to enhanced rate capability. The material consists of micron size particles as shown in Figure V- 28; these in turn were found to be made of 50 nm crystallites. We have found that the vanadium causes a contraction of the crystalline lattice, but it is still not clear whether substitution on the iron or phosphorus site is more important. This study continues.

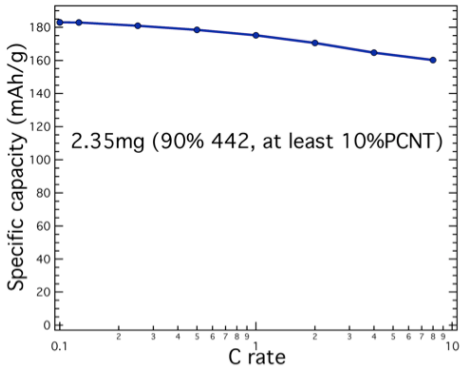

Figure V- 27: Capacity as a function of discharge rate for $LiNi_{0.4}Mn_{0.4}Co_{0.22}O_2$, on a carbon nanotube mesh grid.

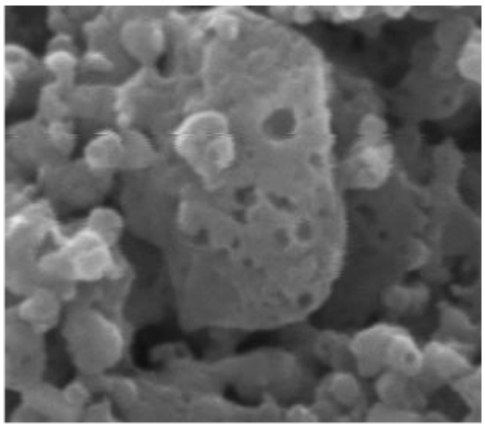

Figure V- 28: Morphology of $LiFePO_4$ substituted with 5 wt% V.

Higher Capacity Electrodes – Pyrophosphates. We have formed a series of pyrophosphates of general formula: $Li_2Mn_{1-y}Fe_yP_2O_7$. Ideally it should be possible to cycle both lithium-ions, leading to a capacity well in excess of 200 Ah/kg. This series of materials have been structurally characterized, and using TGA in oxygen shown to contain only Fe and Mn in the 2+ oxidation state, as shown in Figure V- 29. The weight gains are as expected for oxidation of ferrous to ferric; the manganese remains in the +2 oxidation state.

The electrochemical behavior of this Fe-Mn series is shown in Figure V- 30. The capacity of the iron material is 90 mAh/g, less than the calculated value of 110 mAh/g; this difference may be associated with both the very large particle size, > 1 μm, and iron residing on the lithium site. The latter is observed for the pure iron material, which also has a smaller than expected unit cell volume, based on the trends from the Fe content. The observed capacity is directly related to the iron content; suggesting that the manganese ion is not redox active in the voltage range studied.

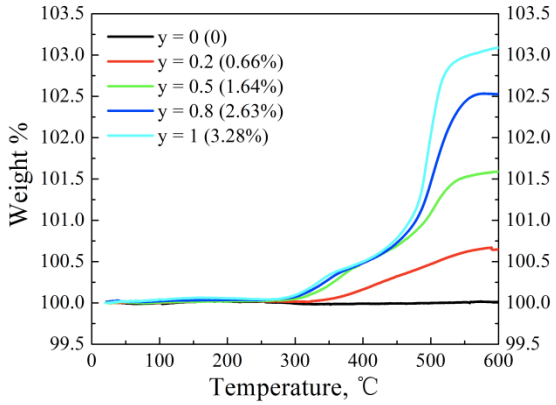

Figure V- 29: TGA in O_2 of $Li_2Mn_{1-y}Fe_yP_2O_7$.

Cyclic voltammogram studies suggest that further redox activity can be found at potentials over 5 V, but any quantitative studies are complicated by electrolyte breakdown.

We have initiated collaboration with the group of Gerd Ceder at MIT to calculate the potentials at which redox activity is to be expected. Initial studies are consistent with the experimental data and are giving assistance with guiding future experimental studies.

Studies are continuing on vanadium based oxides and phosphates, as vanadium offers the opportunity for a two electron redox process between V^{5+} and V^{3+}. We have formed novel vanadium oxides and mixed phases of lithium vanadium phosphate.

Conclusions and Future Directions

200 Ah/kg can be obtained from the layered oxides when charging in excess of 4.4 volts, but more stable electrolytes will be needed; alternatively the voltage profile will need to be reduced. Collaborative work with NREL showed $LiNi_{0.4}Mn_{0.4}Co_{0.2}O_2$ has an inherent high discharge rate. Future work will address what controls the voltage of the $LiMO_2$ materials. We have found the positive effect of substituents in $LiFePO_4$, and will determine the composition range of $LiFe_{1-y}V_yP_{1-z}V_zO_4$, and understand the role of substituents on reaction rate. We have identified several materials that can undergo more than one electron per redox active center, and characterized the behavior of an iron pyrophosphate class of material. We will build on our collaboration with the Ceder group at MIT to better understand attainable potentials in these materials and thus guide our program in finding 200 Ah/kg materials.

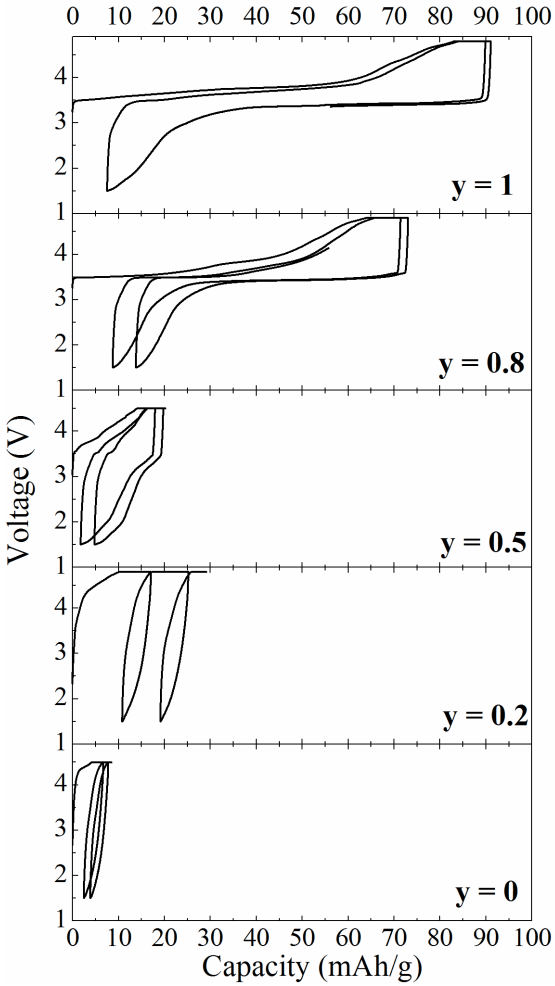

Figure V- 30: Cycling of $Li_2Mn_{1-y}Fe_yP_2O_7$.

FY 2010 Publications/Presentations

1. Presentation to the 2010 DOE Annual Peer Review Meeting, Washington, DC.
2. Jie Xiao, Natasha A. Chernova, and M. Stanley Whittingham, "Influence of Manganese Content on the Performance of $LiNi_{0.9-y}Mn_yCo_{0.1}O_2$ ($0.45 \leq y \leq 0.60$) as a Cathode Material for Li-Ion Batteries", Chem. Mater., 2010, 22: 1180-1185.
3. C. Ban, N. Chernova, M. S. Whittingham, "Electrospun Nano-Vanadium Pentoxide Cathode", Electrochem. Commun., 2009, 11: 522-525
4. Many invited presentations, incl.:
   a. National Academy, US Army Lab., Toyota Ann Arbor, Applied Materials in Santa Clara, AABC Orland, Vale
   b. Cornell, U. Michigan, Michigan State, Warsaw
   c. IMLB, MRS, ACS
   d. PNNL
   e. Local outreach

V.B.6 Low Cost SiO_x-Graphite and Olivine Materials (HQ)

Karim Zaghib

Hydro-Quebec IREQ.
1800 Lionel Boulet
Varennes, QC, Canada J3X 1S1
Phone: (450) 652-8019; Fax: (450) 652-8424
E-mail: Zaghib.Karim@ireq.ca

Subcontractor:
LBNL, Berkeley, CA

Start Date: March 1, 2010
Projected End Date: April 30, 2011

Objectives

- Synthesize and evaluate $LiMnPO_4$ with improved electrochemical characteristics.
- Replace graphite with an alternative anode that meets the requirement for low cost and high energy density.
- Continue developing new binders for the cathode and alternative anode to improve the properties of the SEI layer that forms.

Technical Barriers

Low energy and poor cycle/calendar life

Technical Targets

- Identify a suitable technique to produce $LiMnPO_4$ cathodes with acceptable reversible capacity.
- Develop an alternative anode based on SiO_x to replace graphite.
- Investigate the interface on SiO_x.

Accomplishments

- Different types of graphites were evaluated and their electrode films produced at Hydro-Quebec were sent to investigators in the BATT Program.
- Evaluated mixed SiO_x-graphite as an alternative anode material.
- The effect of the binder on performance of the alternative anode (first coulombic efficiency and reversible capacity) was evaluated.
- Different synthesis routes (solid state and hydrothermal and microwave) were investigated to produce $LiMnPO_4$ material.
- Completed study of a new graphite (OMAC from Osaka Gas) and compared its performance with SNG12 (HQ) in standard electrolyte 1M $LiPF_6$–EC/DEC with VC and VEC as additives. Also characterization of electrodes with water-dispersed binder was completed.

✧ ✧ ✧ ✧ ✧

Introduction

Achieving the DOE cost targets will require finding alternative low-cost materials, both for the anode and cathode. We are investigating the performance of Mn-based olivine cathodes and alloy anodes. In order to understand the capacity fade of the alloy due to the volume expansion, we are studying the stability of the SEI layers on this material.

Approach

Our approach is to develop a suitable method to synthesize Mn-phosphate–base materials with improved electrochemical performance and acceptable carbon content in the electrodes. The effect of particle size on the reversible capacity and cycle life will be investigated. Some new binders with different mechanical properties will be investigated and evaluated with the alternative anode material. All materials will be evaluated electrochemically and provided to other researchers in the BATT Program for evaluation. The coating processes will be optimized because the different physical properties of the new anode material and binders will influence the coating parameters.

Laminate cathode films and powders will be prepared and sent to investigators in the BATT Program for evaluation

Results

Alternative anode. The effect of SiO_x electrode density and type of carbon conductive matrix were investigated. The aim of this study is to determine the optimum electrode density because the porosity can have a significant influence on the anode performance. Three electrodes densities were considered; 1.0, 1.18 and 1.4 g/cc. Because of the large volume expansion, the electronic pathways between the particles can decrease. Thus, three type of carbon additives (Denka, Ketjen black and SuperP(Timcal)), having different physicochemical properties, were investigated.

The first cycle results at C/24 as a function of the electrode density with different carbons are shown in Figure V- 31. The highest reversible capacity was obtained with Ketjen black at low electrode density, but the

coulombic efficiency was only 69% in the first cycle (EC1). The highest EC1 and reversible capacity were obtained with SuperP. The data in Figure V- 31 show that the electrode should be pressed at an optimum density depending on the type of carbon additive. For the electrode containing Denka black as additive, higher electrode density (1.4g/cc) is preferable compared to Ketjen black and SuperP, which yielded better performance at 1.18g/cc.

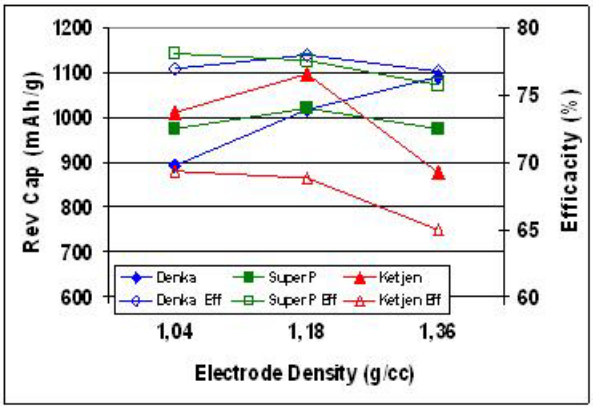

Figure V- 31: Reversible capacity and efficiency of Li/ SiOx:Gr cells in EC-DEC-LiPF$_6$.

At high rates, the anode performance (Figure V- 32) shows acceptable charge capacity of 600 mAh/g at 1C for the cells with Denka and SuperP, however higher capacity (750 mAh/g) is obtained with the cell using Ketjen black. A capacity of 690 mAh/g is observed with low fading at 8C. The high surface area carbon (Ketjen black) shows better performance at high rate but it has the lowest EC1.

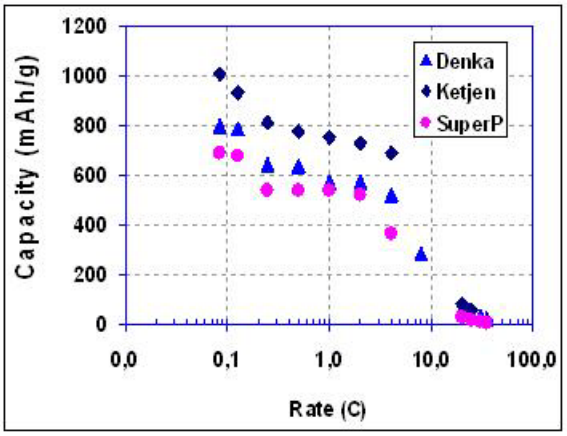

Figure V- 32: Ragone plot of Li/SiOx:Gr cells in EC-DEC-LiPF$_6$ with # carbons.

The cycle life was determined at C/12 with cut-off voltages on discharge of 5mV and 0mV, and 2.5V on charge. The reversible capacity after 30 cycles (see Figure V- 33) varies only slightly with the cut-off voltage. The cut-off voltage had a small effect on the capacity fade with cycling at C/12.

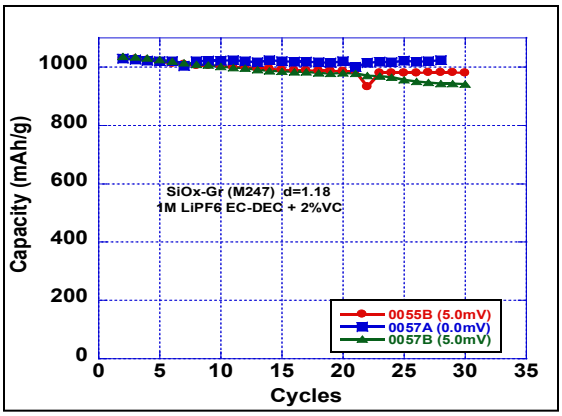

Figure V- 33: Reversible capacity and efficiency of Li/ SiOx:Gr cells in EC-DEC-LiPF$_6$.

We found that high rates affect the performance of the anode, as expected due to the high volume change of the particles. Therefore, improvements at high rates are needed; small particles or other anode compositions are necessary. Hence, other SiO_x anode compositions are under investigation. We began analysis of SiO_x anodes by *in situ* SEM. In the first trials, we will use solid polymer in the anodes due to solvent evaporation in the SEM chamber. We expect these experiments will help provide a better understand the cycling mechanism of this anode, and the failure mode associated with capacity fade at higher rates.

$LiMnPO_4$ cathode. Increasing the reversible capacity of $LiMnPO_4$ above 70mAh/g after wet milling to form nano-size particles is difficult. Therefore, we concentrated on the hydrothermal synthesis of Fe-substituted $LiMn_{(1-x)}Fe_xPO_4$.

The first result at C/24 (Figure V- 34) shows clearly an increase of the reversible capacity of Fe-doped $LiMnPO_4$ at room temperature. A stable 4V plateau was observed even with 80% Mn. The highest reversible capacity was found with the composition Mn:Fe (1:1). With a lower Fe content ($LiMn_{0.8}Fe_{0.2}$), 109mAh/g was obtained.

The electrochemical results for the Fe-substituted $LiMn_{(1-x)}Fe_xPO_4$ obtained by a hydrothermal method are presented in Figure V- 35. The highest reversible capacity at 25°C was obtained with the composition Mn:Fe (1:1). We repeated the experiments to confirm the results obtained at the ratio Mn:Fe (0.8:0.2) in Figure V- 34 Then, we determined the energy density as a function of the capacity of the Mn content in $LiMn_{(1-x)}Fe_xPO_4$. The highest energy density was found with the composition Mn:Fe (0.7:0.3), which yielded 576 mWh/g. The energy density was higher in the range where Mn varied from 0.5 to 0.8.

The particle size was determined by a particle size analyzer (Horiba); the d_{50} varied from 0.31µm to 1.86µm, respectively, for Mn concentration of 0.5 to 1.

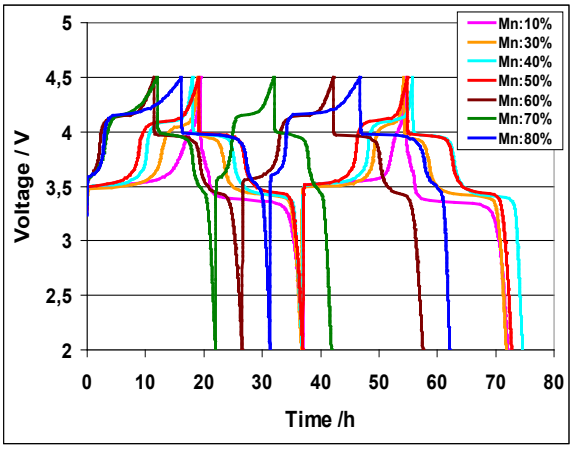

Figure V- 34: 1st cycles of Li/LiMnFePO$_4$ cells in EC-DEC 1M LiPF$_6$ at 25°C.

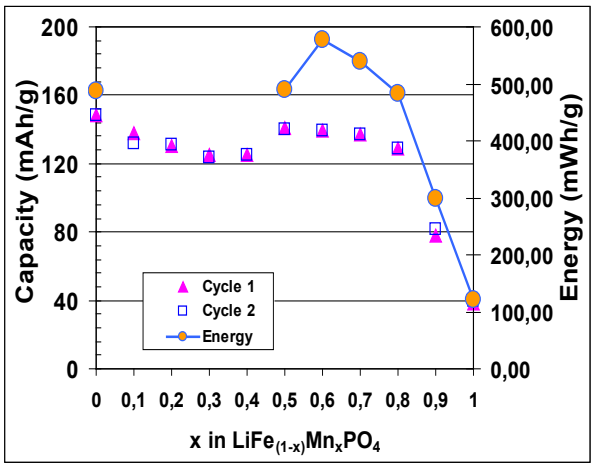

Figure V- 35: Reversible capacity and energy density of cycles 1 and 2 of Li/LiMnFePO$_4$ cells in EC-DEC 1M LiPF$_6$ at different ratios of Fe/Mn.

Conclusions and Future Directions

Improvements in the SiO_x anode performance at high rates are still needed; small particles or other anode compositions are necessary. Hence, other SiO_x anode compositions are under investigation.

We started to analyse SiO_x anodes by *in situ* SEM. In the first trials, solid polymers in the anodes will be used due to solvent evaporation in the SEM chamber. We expect these studies will improve our understanding of the cycling mechanism, and the failure mode associated with capacity fade at higher rates

Efforts will continue on improving the performance of substituted LiFeMnPO$_4$ olivine material at ambient temperature by reducing the particle size and optimizing the synthesis method.

FY 2010 Publications/Presentations

1. Presentation to the 2010 DOE Annual Peer Review Meeting.
2. Guerfi, P. Charest, M. Dontigny, P. Hovington, J. Trottier and K. Zaghib, " SiOx Material as High Capacity Anode for Li-Ion Batteries", IMLB meeting, Montreal-2010 abstracts # 45,
3. Guerfi, J.F. Labrecque, P. Charest, W. Zhu, M. Dontigny and K. Zaghib, "Nano-LiMnPO$_4$ Cathode Material Prepared by Combination Hydrothermal-Wet Mill Processes", IMLB meeting, Montreal-2010 abstracts # 399.
4. M. Mathieu, J-F. Labrecque, A. Guerfi, I. Rodrigues, C. Julien, A. Mauger and K. Zaghib, "LiMn$_y$Fe$_{1-y}$PO$_4$ Hydrothermal for Li-ion Batteries" IMLB meeting, Montreal-2010 abstracts #364.

V.B.7 The Role of Surface Chemistry on the Cycling and Rate Capability of Lithium Positive Electrode Materials (MIT)

Yang Shao-Horn

Mechanical Engineering and Materials Engineering
Massachusetts Institute of Technology, 3-344
77 Massachusetts Avenue
Cambridge, MA 02139
Phone: (617) 253-2259; Fax: (617) 258-7018
E-mail: shaohorn@mit.edu

Subcontractor:
A.N. Mansour, NSWCCD, West Bethesda, MD

Start Date: April 1, 2009
Projected End Date: March 31, 2010

Objectives

- Develop a fundamental understanding of processes associated with the interfacial instability between active materials and electrolyte.
- Design low cost positive electrodes with stable electrode-electrolyte interface with improved cycling performance and rate capability over wider operating temperatures.

Technical Barriers

This project addresses the following technical barriers in relation to positive electrode materials for lithium-ion batteries:

(A) High Cost

(B) Poor cycle life

(C) Poor calendar life

(D) Abuse tolerance

Technical Targets

- PHEV: Specific energy 56-96 Wh/kg; Specific power 316-750 W/kg; 15-year life (35°C); 3,000-5,000 cycles
- EV: Specific energy 200 Wh/kg; 1,000 cycles

Accomplishments

- As requested by one of the reviewers at the FY2009 Annual Merit Review, we developed a capability to transfer electrodes from an Ar-filled glove box to the test chamber of our XPS spectrometer without exposure to ambient conditions.
- Cycled $LiCoO_2$ and "$AlPO_4$" coated $LiCoO_2$ electrodes in lithium cells with 1 M of $LiPF_6$ in EC:DMC and characterized the surface chemistry by angle resolved XPS (ARXPS).
- Cycled $LiCoO_2$ and "$AlPO_4$" coated $LiCoO_2$ electrodes in lithium cells with 1 M of $LiClO_4$ in EC:DMC and characterized the surface chemistry by ARXPS.
- Cycled $LiNi_{0.5}Mn_{0.5}O_2$ electrodes in lithium cells with 1 M of $LiPF_6$ in EC:DMC and characterized the surface chemistry by ARXPS.
- Characterized the atomic structure of spinel-layered and layered-layered composite materials such as $Li_xNi_{0.25}Mn_{0.75}O_y$ by TEM (in collaboration with M.M. Thackeray).

✧ ✧ ✧ ✧ ✧

Introduction

Achieving a fundamental understanding of the role of coatings and synthesis conditions on the surface chemistry and structural integrity of positive electrode materials is necessary to design stable surfaces and structures for Li-ion batteries. The design of chemically and structurally-stable surfaces of Li storage materials is key to the development of low cost, high-energy, high-power, long-life, and thermally-stable Li rechargeable batteries.

Approach

- Probe the surface chemistry of positive electrode materials before and after cycling using surface-sensitive electron microscopy, angle resolved X-ray photoelectron spectroscopy and electron-yield X-ray adsorption spectroscopy.
- Study the bulk structure of positive electrode materials before and after cycling using synchrotron X-ray diffraction and transmission X-ray absorption spectroscopy.
- Correlate surface chemistry and bulk structure information with electrochemical performance characteristics such as capacity retention and rate capability to determine the origin of surface instability.

Results

Interfacial stability of "$AlPO_4$" Coated $LiCoO_2$. We have shown that "$AlPO_4$" coated $LiCoO_2$ materials have much improved capacity retention relative to uncoated $LiCoO_2$ when cycled in $LiPF_6$ based electrolyte and proposed a mechanism for the interfacial stability between electrolyte and electrode. In order to understand the role of electrolyte on interfacial stability of uncoated and coated $LiCoO_2$, we have cycled electrodes in lithium cells with $LiPF_6$ and $LiClO_4$ based electrolytes and analyzed the surface composition by ARXPS. ARXPS was used to examine the depth distribution of various species near the surface region without Ar-ion sputtering, which may alter the surface composition. As can be seen from Figure V- 36, capacity retention and extent of polarization are much better for the "$AlPO_4$" coated $LiCoO_2$ electrodes cycled in $LiPF_6$ than in $LiClO_4$.

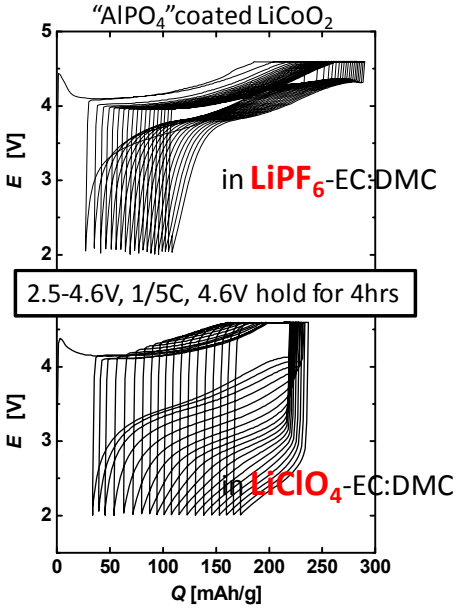

Figure V- 36: Voltage capacity profiles for "$AlPO_4$" coated $LiCoO_2$ electrodes cycled in lithium cells with $LiPF_6$ and $LiClO_4$ in EC:DMC

The cycled electrodes were characterized as is without washing by the solvent unless otherwise indicated by "W". All electrodes were mounted in an argon glove box and transferred to the test chamber of the XPS system without exposure to ambient conditions to avoid possible contamination from the atmosphere. The following general observations can be made from the XPS results: (i) the surface of electrodes cycled in $LiPF_6$ contained large amounts of the salt and its decomposition products, (ii) the amount of $LiPF_6$ was reduced in the case of electrodes washed by the EC:DMC solvent, and (iii) the surface of electrodes cycled in $LiClO_4$ contained a small amount of the salt as indicated by the small concentration of Cl. The O 1s ARXPS spectra (Figure V- 37) for pristine uncoated and "$AlPO_4$"-coated $LiCoO_2$ electrodes show that the double-peak structure of the O1s region changes considerably with the electron take off angle relative to the electrode plane, where the intensity of the lattice oxygen peak decreases relative to that of the surface oxygen peak with decrease in electron takeoff angle. The trend for the intensities of the O 1s peaks is consistent with the assignments that the low binding energy peak is characteristic of lattice oxygen while the high binding energy peak is consistent with oxygen containing surface species. This is in agreement with the presence of Li_3PO_4 on the surface of the coated electrode. The O 1s ARXPS spectra of bare electrodes cycled in $LiPF_6$ or $LiClO_4$ always shows a contribution from surface oxygen (as one would expect) but the lattice oxygen contribution emerges for takeoff angles at or above 30 degrees. However, the lattice oxygen contribution is absent in the O 1s ARXPS spectra of coated electrodes cycled in $LiPF_6$ or $LiClO_4$.

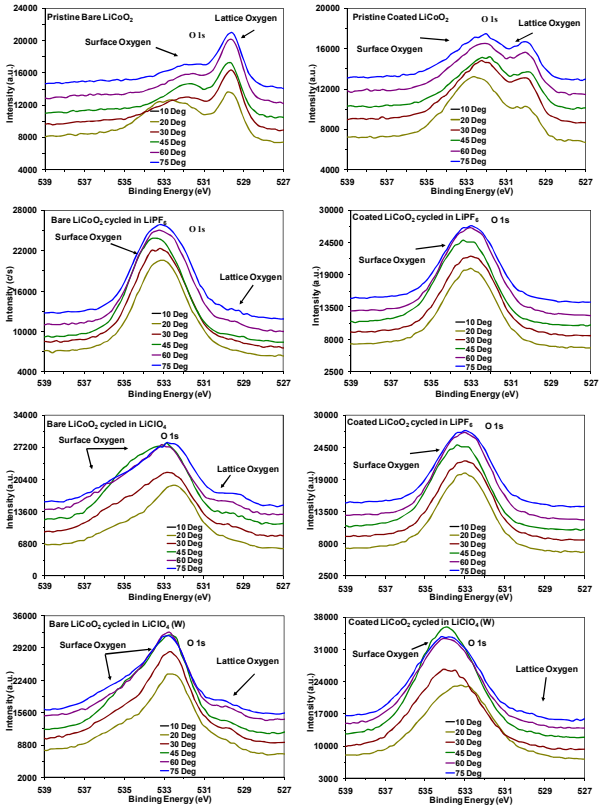

Figure V- 37: ARXPS of O 1s region for pristine bare and "$AlPO_4$" coated $LiCoO_2$ and after 20 cycles in $LiPF_6$ and $LiClO_4$ in EC:DMC. Electrodes were analyzed without washing by the solvent unless otherwise indicated by "(W)".

The ARXPS measurements of the Co 2p region for the coated $LiCoO_2$ electrodes cycled in $LiPF_6$ and $LiClO_4$ are unchanged within the maximum sampling depth of XPS (not shown), which corresponds to an electron take-

off angle of 75 degrees. However, the Co 2p binding energies for the $LiPF_6$ cycled electrode are somewhat higher than those for the $LiClO_4$ cycled electrode due to the formation of Co-oxyfluoride film in the case of $LiPF_6$ versus possibly Co-oxychloride film in the case of $LiClO_4$. Furthermore, Ar-depth profile analyses of the coated electrodes cycled in $LiPF_6$ and $LiClO_4$ (Figure V- 38) reveal the evolution of the Co 2p structure of the pristine $LiCoO_2$, which is shifted to lower binding energy after 2 and 0.5 minutes of sputtering, respectively, indicating a much thicker Co-O-F film than that of Co-O-Cl formed on the surfaces of the electrodes. The sputtering rate in these experiments was estimated to be 27 Å of SiO_2 per minute. This observation further confirms that the enhanced cycling stability in $LiPF_6$-based electrolyte is due to the formation of a Co-oxyfluoride film, which is thick enough to protect against attack by HF.

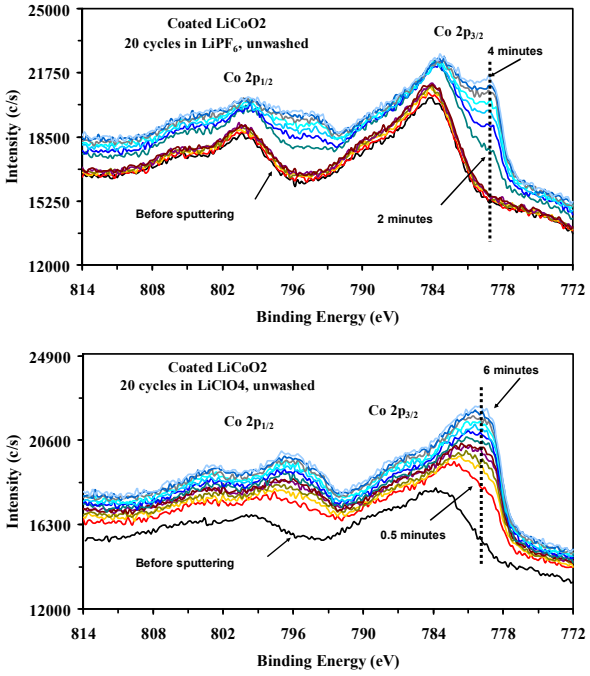

Figure V- 38: Depth profile spectra of the Co 2p region of coated $LiCoO_2$ electrodes after 20 cycles in $LiPF_6$ and $LiClO_4$.

High-energy and power $LiNi_{0.5}Mn_{0.5}O_2$ (LNMO). The active material was prepared by quenching from 1000°C followed by annealing in air at 700°C. The composite electrodes were cycled 20-times in lithium cells with 1M of $LiPF_6$ in EC:DMC between 2.0-4.6V with 4h hold at 4.6V at the C/5 rate. The electrodes were also transferred from the Ar-filled glove box to the test chamber of the XPS spectrometer without exposure to ambient conditions. They were characterized as well after washing with the solvent of the electrolyte to remove excess electrolyte and other species loosely attached to the surface. ARXPS measurements of annealed LNMO electrodes (Figure V- 39) cycled in $LiPF_6$ did not reveal changes in the Mn and Ni surface chemistry within the maximum sampling depth. The Ni and Mn $2p_{3/2}$ binding energies for the unwashed electrodes of 857-858 and 644eV, respectively, are significantly higher than those reported for powder material indicating that surface Ni and Mn are present in highly oxidized states after cycling in $LiPF_6$. Such high binding energy for Ni is close to that reported for $NiF_2{\cdot}4H_2O$ (857.3 eV) indicating the possible formation of Ni fluorides. This assignment can be supported by the Ni shake-up structure, the lack of lattice oxygen component in the O 1s spectrum, and the presence of a fluorine component which corresponds to the formation of metal fluorides.

It is to be noted that the Mn $2p_{3/2}$ region is slightly distorted by a weak signal from an X-ray induced Auger line of F but the extent of distortion can be significant since F is present in larger amount than Mn. This distortion manifests itself as a second structure on the high energy side of the Mn $2p_{3/2}$ peak. Nonetheless, the binding energy for Mn of ~644 eV is significantly higher than those reported for simple Mn oxides as well as fluorides (642.4 eV for both MnF_2 and MnF_3). Higher binding energies relative to those of simple oxides and fluorides have been reported for $MnSO_4$ (644.7 eV) and $KMnO_4$ (646.8 eV). Clearly the chemistry of surface Mn is complex and requires further examination.

On the other hand, the Ni and Mn $2p_{3/2}$ binding energies for the washed electrodes are significantly shifted relative to those for the unwashed electrodes. The Ni $2p_{3/2}$ binding energy of ~855 eV is consistent with those observed for Ni^{2+} in active material or NiO. The Mn $2p_{3/2}$ binding energy of ~642 eV is close to that of Mn^{4+} in active material but the presences of other forms of manganese oxides can't be ruled out. Clearly, the surfaces of unwashed electrodes contained surface Ni and Mn in highly oxidized species, which are loosely attached to the surface and was removed by rinsing the electrodes by the solvent.

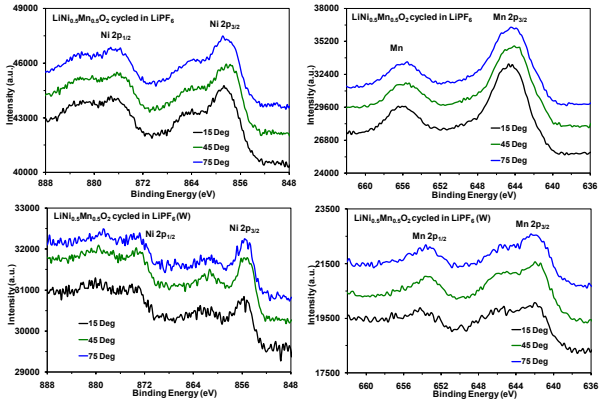

Figure V- 39: ARXPS of Ni and Mn 2p spectra for $LiNi_{0.5}Mn_{0.5}O_2$ electrodes cycled in $LiPF_6$ electrolyte before and after washing by the solvent.

TEM studies of $Li_xNi_{0.25}Mn_{0.75}O_2$ (collaboration with M.M. Thackeray, ANL). TEM was used to study the atomic structure of spinel-layered and layered-layered composite materials such as $Li_xNi_{0.25}Mn_{0.75}O_y$. Preliminary results of high-resolution transmission electron microscopy (TEM) and Fast-Fourier Transform (Figure V- 40) have shown direct evidence for intergrowth of spinel-like (with space group Fd-3m) and layered-like (space group C2/m of Li_2MnO_3) structures at the nanometer scale for $Li_{1.2}Ni_{0.25}Mn_{0.75}O_y$ prepared at 900°C). The streaks in the FFT of the layered structure indicated stacking disorder of transition metal layers similar to those reported recently for Li_2MnO_3 by Boulineau et al. (Chem. Mater. 2009). Cycled $Li_{1.2}Ni_{0.25}Mn_{0.75}O_y$ (900°C, 2.0-4.95 V, 50 cycles) had mostly the spinel Fd-3m structure. In addition, quite a few dislocations were observed in the high-resolution TEM images (shown in Figure V- 40 insert). These dislocations have a Burgers vector of $\mathbf{a}/2[111]_{spinel}$, which can be attributed to oxygen loss from the oxide structure during cycling to high voltages such as 4.95 V.

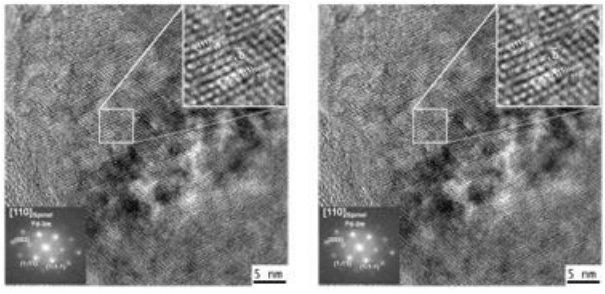

Figure V- 40: TEM micrographs of pristine and cycled $Li_{1.2}Ni_{0.25}Mn_{0.75}O_y$.

Conclusions and Future directions

We have used a number of analytical tools XPS, ARXP, XAS, XRD, TEM to examine the interfacial stability between electrode and electrolyte during cycling in lithium cells. The $LiCoO_2$ and "$AlPO_4$" coated $LiCoO_2$ were used as a model compound to identify the role of surface coating of active material on interfacial stability during cycling. These studies were extended to the high energy LNMO cathode material. The role of electrolyte on interfacial stability was also examined by cycling in $LiPF_6$ and $LiClO_4$ electrolytes. Our results showed that the coated $LiCoO_2$ had significantly better capacity retention during cycling in $LiPF_6$ electrolyte but not in $LiClO_4$. The formation of Co-Al-F-O oxyfluorides in the case of $LiPF_6$ but not in the case of $LiClO_4$ cycling was essential to provide the interfacial stability. TEM studies provided direct evidence for the integration of spinel and layered material in the as-prepared $Li_{1.2}Ni_{0.25}Mn_{0.75}O_y$.

Future directions include the continuation of using XPS and ARXPS to investigate the surface chemistry of high-energy electrode materials such as Li-rich $(Li_2O)_x.(MO_2)_y$ (where M = Mn, Co, Ni, etc.) layered compounds. It is known that some oxygen can be produced during the first charge, and we are particularly interested to understand how the surface chemistry during the first charge and the electrode surface reaches steady-state during cycling. Data will be collected at different voltages in the first charge and discharge, as a function of cycling and of lithium overstoichiometric content. Cycling and surface chemistry changes of high-voltage and high-energy $LiNi_{0.5}Mn_{1.5}O_4$ will be used as a reference. Lastly we will apply the fundamental understanding gained in this project to design stable surfaces of cycled high-energy cathodes such as $LiNi_xMn_xCo_{1-2x}O_2$ (NMC).

Furthermore, we are exploring the possibility of using hard X-rays at the National Synchrotron Light Source of Brookhaven National Laboratory to increase the depth of the region analyzed by XPS and ARXS. This will provide a nondestructive way of increasing the depth of the analyzed region. Furthermore, we would like to explore collaborations with Robert Kostecki (LBNL) in the area of FT-IR and Raman studies.

FY2010 Publications/Presentations:

Publications:

1. Lu, Y. C.; Xu, Z. C.; Gasteiger, H. A.; Chen, S.; Hamad-Schifferli, K.; Shao-Horn, Y., Platinum-Gold Nanoparticles: A Highly Active Bifunctional, Electrocatalyst for Rechargeable Lithium-Air Batteries. Journal of the American Chemical Society 132, (35), 12170-12171 (2010).

2. Y.C. Lu, H.A. Gasteiger, M.C. Parent, C. Vazrik, and Y. Shao-Horn, The Influence of Catalysts on Discharge and Charge Voltages of Rechargeable Li–Oxygen Batteries, Electrochem. Solid-State Lett., 13, A68-A72 (2010).

3. Y.C. Lu, H.A. Gasteiger, E. Crumlin, R. McGuire, and Y. Shao-Horn, Journal of The Electrochemical Society 157, (9), A1016-A1025 (2010).

4. N. Yabuuchi, Y.C. Lu, A. N. Mansour, T. Kawaguchi and Y. Shao-Horn, The Role of Surface Chemistry on the Electrochemical Reactivity of $LiNi_{0.5}Mn_{0.5}O_2$ in Lithium Cells, Electrochem. Solid-State Let., 13(11), A158-A161 (2010).

5. N. Yabuuchi, Y.C. Lu, A.N. Mansour, S. Chen and Y. Shao-Horn, The Influence of Heat-Treatment Temperature on the Cation Distribution of $LiNi_{0.5}Mn_{0.5}O_2$ and its Rate Capability in Lithium Rechargeable Batteries, submitted to J. Elechtrochem. Soc., under revision, (2010).

Presentations

1. Y.C. Lu, H.A. Gasteiger, and Y. Shao-Horn, "Catalysis studies and electrode design considerations for Lithium-air batteries" American Chemical Society, August 22, 2010, Boston, MA, USA.

2. Y.C. Lu, J.R. Harding, Y. Tsukada, H.A. Gasteiger, and Y. Shao-Horn, "Catalysis studies and electrode design considerations for Lithium-air batteries" American Chemical Society, August 24, 2010, Boston, MA, USA.

3. Y.C. Lu, H.A. Gasteiger, and Y. Shao-Horn, "Electrocatalytic Activity Studies of Select Metal Surfaces and Implications in Li-Air Batteries" 15th International Meeting on Lithium Batteries, July 2, 2010, Montréal, Canada.

4. Y.C. Lu, M. Parent, V. Chiloyan, and Y. Shao-Horn "The Influence of Catalysts on Discharge and Charge Voltages of Rechargeable Li-Oxygen Batteries" 15th International Meeting on Lithium Batteries, July 1, 2010, Montréal, Canada.

5. Y. Shao-Horn, Tajima Prize Award lecture "Oxygen Reduction Reaction Kinetics on Select Catalysts in Aqueous and Nonaqueous Solutions and Implications for Fuel Cells and Li-Air Batteries." 61st Annual Meeting of the International Society, September 29, 2010, Nice, France.

V.B.8 Characterization of New Cathode Materials using Synchrotron-based X-ray Techniques and the Studies of Li-Air Batteries (BNL)

Xiao-Qing Yang
Kyung-Wan Nam
Brookhaven National Laboratory
Upton, NY 11973-5000
Phone: (631) 344-3663; Fax: (631) 344-5815
E-mail: xyang@bnl.gov

Start Date: October 1, 2009
Projected End Date: September 30, 2011

Objectives

- Develop new diagnostic techniques with the ability to distinguish bulk and surface processes, to monitor the degradation processes, to determine the effects of structural changes of electrode materials, the interfacial phenomena, and electrolyte decomposition on the cell capacity and power fading, as well as on the abuse tolerance for safety characteristic related issues
- Use diagnostic techniques to evaluate and screen the new materials and components to improve the performance, calendar and cycling life, and the abuse tolerance of lithium batteries for HEV, PHEV, and EV.

Technical Barriers

- Li-ion and Li-metal batteries with long calendar and cycle life
- Li-ion and Li-metal batteries with superior abuse tolerance
- To reduce the production cost of a PHEV batteries

Technical Targets

- To determine the contributions of electrode materials changes, interfacial phenomena, and electrolyte decomposition to the cell capacity and power decline.
- To develop and apply synchrotron based *in situ* X-ray techniques to study materials in an environment that is close to the real operating conditions.
- To screen and study potentially low cost materials such as $LiFe_{1-x}Mn_xPO_4$.
- To carry out fundamental studies of high energy density Li-air batteries.
- To develop new diagnostic tools for battery studies.

Accomplishments

- Completed *in situ* X-ray absorption spectroscopy (XAS) and *in situ* XRD studies on $LiFe_{1-x}Mn_xPO_4$ cathode materials during charge-discharge cycling.
- Completed *in situ* hard XAS studies on high energy $Li_{1.2}Mn_{0.6}Ni_{0.2}O_2$ cathode material during charge-discharge cycling.
- Identified the effects of carbon structure for gas diffusion electrode (GDE) of Li-air-battery and synthesized new carbon materials with larger pore size, which significantly improved the discharge capacity of the cell.
- Developed novel surface modification of the carbon materials for GDE and obtained dramatic increase in the capacity of the Li-air cell using the surface modified carbon for GDE.

✧ ✧ ✧ ✧ ✧

Introduction

Achieving DOE goals for HEV, PHEV, and EV batteries will require fundamental understanding of how current materials function – including how to improving rate, capacity and long-term cycling performance as well as the guidance on discovery of new materials and new mechanisms. This project attacks these issues by developing new diagnostic tools to investigate battery materials both *in* and *ex situ*, and then applies these to explain the relationships between structure and function for new material development.

Approach

Perform *in situ* XAS and XRD studies of new electrode materials such as $LiFe_{1-x}M_xPO_4$ (M=Mn, Co, Ni) and $Li_{1.2}Mn_{0.6}Ni_{0.2}O_2$ – during electrochemical cycling to carry out the diagnostic studies to improve the energy density.

Use soft XAS studies of new electrode materials to distinguish the difference between the surface and the bulk.

Carry out *in situ* and *ex situ* transmission electron microscopy (TEM) and selected area electron diffraction (SAED) to study the structural changes of electrode materials with high location specification and spatial resolution.

Conduct electrochemical studies of GDEs for Li-air batteries. Construct and test Li-air batteries using organic electrolytes.

Design and synthesize new electrolyte system with the ability to dissolve Li_2O and Li_2O_2 for Li-air batteries.

Results

***In situ* X-ray absorption and diffraction studies of new olivine type $LiFe_{1-x}Mn_xPO_4$ cathode materials with nano-pore structure.** As shown in Figure V- 41 the new olivine type cathode materials have neso-porous structure, which contributed to the good capacity and rate capability demonstrated in Figure V- 42.

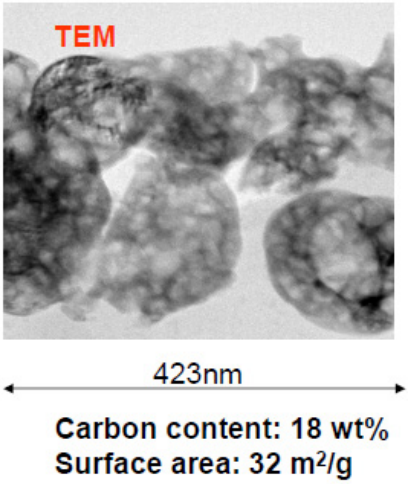

Figure V- 41: Carbon coated new olivine type $LiFe_{1-x}Mn_xPO_4$ cathode materials with nano-pore structure.synthesized by the Institute of Physics, Chinese Academy of Sciences.

As shown in Figure V- 43, Figure V- 44, Figure V- 45, and Figure V- 46, the two-phase coexistence regions of the $LiFe_{1-x}Mn_xPO_4$ cathode materials clearly co-relate with the transition part of the charge curves between the first (for Fe^{2+} to Fe^{3+}) and the second (Mn^{3+} to Mn^{3+}) plateaus.

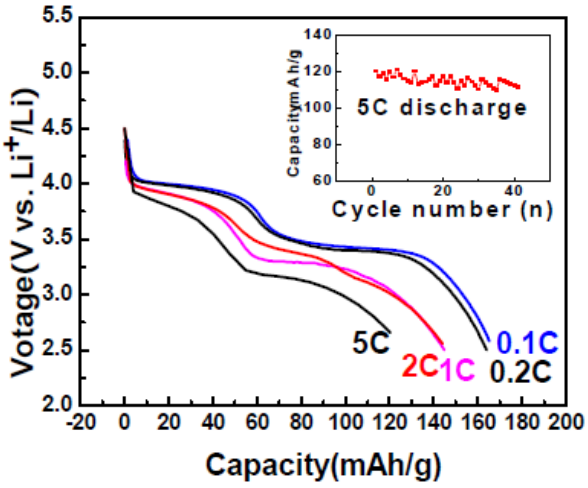

Figure V- 42: Rate capability of carbon coated new olivine type $LiFe_{1-x}Mn_xPO_4$ cathode materials with nano-pore structure.

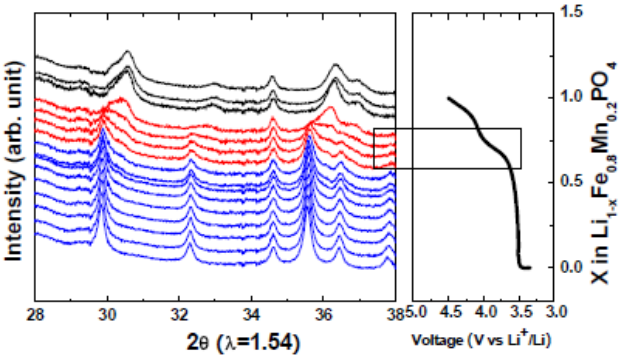

Figure V- 43: Charge and discharge curves and *in situ* XRD spectra of carbon coated $LiFe_{0.8}Mn_{0.2}PO_4$ sample during charge-discharge cycling.

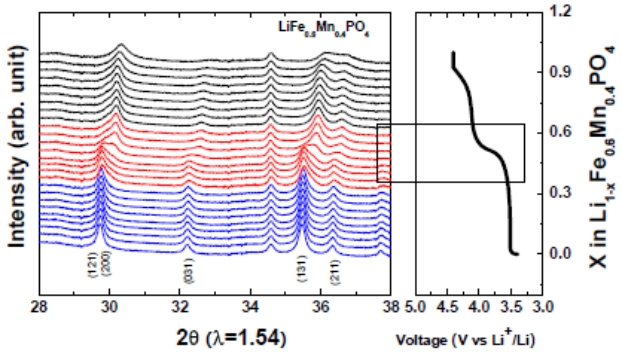

Figure V- 44: Charge and discharge curves and *in situ* XRD spectra of carbon coated $LiFe_{0.6}Mn_{0.4}PO_4$ sample during charge-discharge cycling.

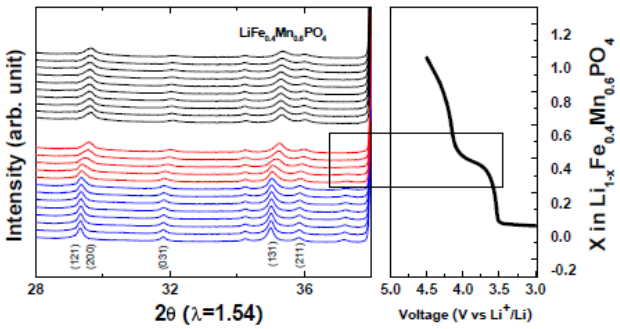

Figure V- 45: Charge and discharge curves and *in situ* XRD spectra of carbon-coated $LiFe_{0.4}Mn_{0.6}PO_4$ sample during charge-discharge cycling.

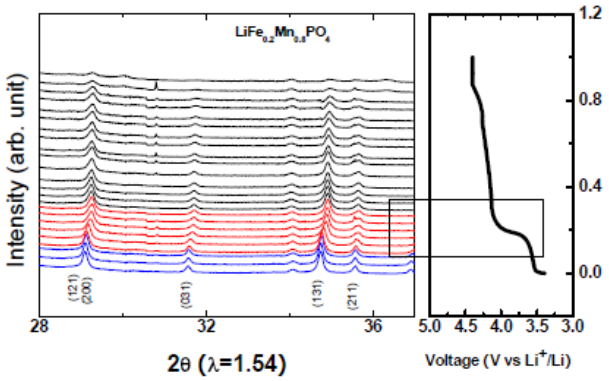

Figure V- 46: Charge and discharge curves and *in situ* XRD spectra of carbon coated $LiFe_{0.2}Mn_{0.8}PO_4$ sample during charge-discharge cycling.

***In situ* XAS study of high energy $Li_{1.2}Mn_{0.6}Ni_{0.2}O_2$ cathode during cycling in collaboration with Argonne National Lab.** As shown in Figure V- 47 and Figure V- 48, for the high energy $Li_{1.2}Mn_{0.6}Ni_{0.2}O_2$ cathode during first charge-discharge cycling, the Ni K-edge *in situ* XANES spectra have clear edge shift in a reversible manner, while the Mn K-edge spectra do not show entire edge shift at all.

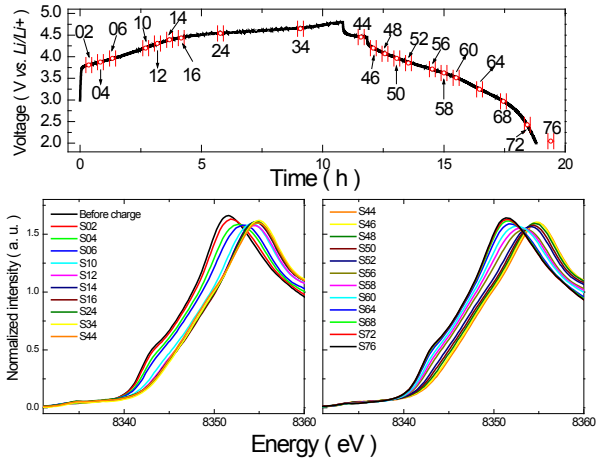

Figure V- 47: Charge and discharge curves and *in situ* XAS spectra at Ni K-edge of $Li_{1.2}Mn_{0.6}Ni_{0.2}O_2$ sample during charge-discharge cycling.

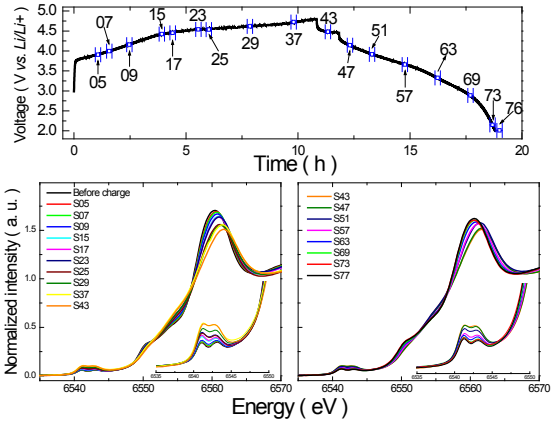

Figure V- 48: Charge and discharge curves and *in situ* XAS spectra of $Li_{1.2}Mn_{0.6}Ni_{0.2}O_2$ sample at Mn K-edge during charge-discharge cycling.

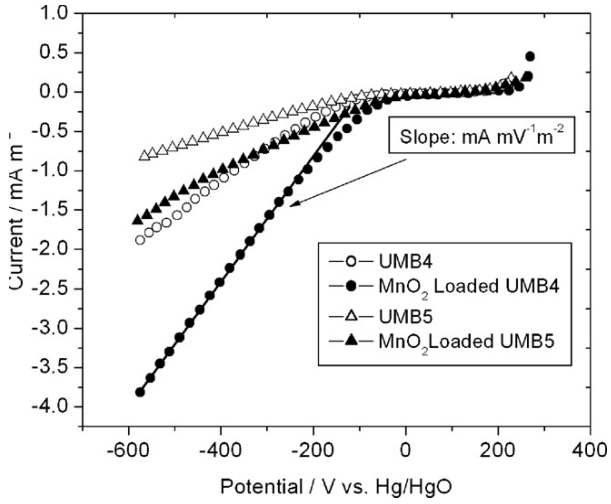

Figure V- 49: Potentiodynamic for O_2 reduction at pristine and MnO_2-loaded UMB4 and UMB5 activated carbon materials. Surface area of pores with size larger than 15Å was used to calculate the current density. Scan rate: $0.5mVs^{-1}$.

Figure V- 49 shows the potentiodynamic profiles taking into consideration the effective surface area. The surface area of the pores larger than 15Å was assumed as an effective surface for the ORR. Significant differences can be observed for the blank carbon electrodes and the MnO_2 loaded electrodes. The addition of a very small quantity of manganese in the form of permanganate appreciably lowered the electrode polarization over the whole current density **range.**

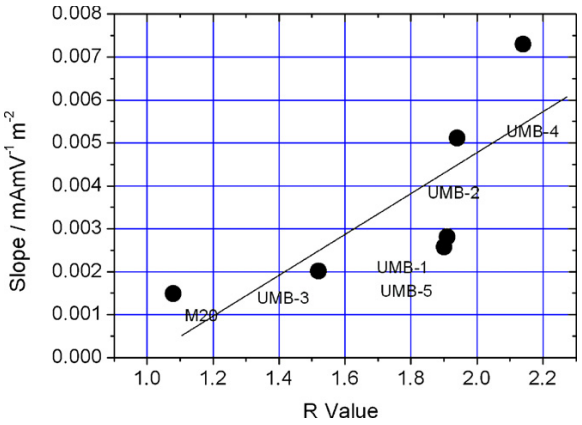

Figure V- 50: Catalytic activity (the slope of potentiodynamic reduction curves as shown in **Figure V- 49**) as a function of R value.

F**igure V- 50** shows the relationship of the "R value"[20] with the slope of the reduction curve (mAm^{-2} mV^{-1}). It is obvious that the specific catalytic activity of MnO_2-loaded carbon electrodes was significantly improved compared to that of the blank carbon electrodes.

Conclusions and Future Directions

In collaboration with Institute of Physics, Chinese Academy of Sciences, the nano-porous structured $LiFe_{1-x}Mn_xPO_4$ (x=0 , 0.2, 0.4, 0.6, 0.8) cathode material system are being studied by *in situ* XRD and XAS. The results of these systematic studies provide important information about the phase transition kinetics of this type of cathode materials.

In collaboration with ANL, $Li_{1.2}Ni_{0.6}Mn_{0.2}O_2$ high energy density cathode materials have been studied using *in situ* XAS. The results of these studies provide useful information for improving the energy density and cycleability of high energy density Li-ion batteries.

The effects of carbon structure for GDE for Li-air battery was investigated and new carbon materials with larger pore size have been synthesized, which significantly improved the discharge capacity of the Li-air cell.

We will complete soft and *in situ* hard XAS study of high energy $Li_{1.2}Mn_{0.6}Ni_{0.2}O_2$ cathode material and identify the charge compensation mechanisms (e.g., activation of Li_2MnO_3 like phase at voltages over ~4.5V and oxygen contribution) during prolonged cyclings.

Further develop surface and interface sensitive techniques, such as soft X-ray absorption, TEM, SAED, and electron energy loss spectroscopy (EELS) for diagnostic studies on surface-bulk differences and phase transition kinetics of electrode materials.

In collaboration with UMASS at Boston, continue on the efforts to develop a GDE for Li-air batteries using organic electrolytes. Start the preliminary studies of the rechargeable Li-air cells.

FY 2010 Publications/Presentations

1. 2010 DOE Annual Peer Review Meeting Presentation.
2. L. F. Li, H. S. Lee, H. Li, X. Q. Yang, and X. J. Huang, "A Pentrafluorophenylboron oxalate Additive in Nonaqueous Electrolytes for Lithium Batteries", *Electrochemistry Communications*, Vol. 11, Iss. 12, pp 2296-2299 (2009).
3. Chris Tran, Xiao-Qing Yang and Deyang Qu, "Investigation of the gas-diffusion-electrode used as lithium/air cathode in non-aqueous electrolyte and the

[20] The "R value" defines the relative content of the edge orientation against basal orientation in a non-graphitized carbon. The definition is the ratio of (002) peak height divided by the background signal. The higher the "R" value the more graphene layers stack on the top of each other; when "R" =1 then, all the graphene layers are randomly distributed as single layers.

importance of carbon material porosity", *Journal of Power Sources*, Vol. 195, pp 2057-2063 (2010).

4. Narah Ominde, Nick Bartlett , Xiao-Qing Yang and Deyang Qu, "Investigation of the Active Sites for Oxygen Reduction on MnO_2-loaded Carbon Electrodes", *Applied Catalysis B: Environmental*, submitted.
5. Narah Ominde, Nick Bartlett, Xiao-Qing Yang, and Deyang Qu, "Investigation of the oxygen reduction reaction on the carbon electrodes loaded with MnO_2 catalyst", Journal of Power Sources, Vol. 195 (13) (2010) 3984-39891
6. Yan Qin, Zonghai Chen, Khalil Amine, Hung-Sui . Lee, and Xiao-Qing Yang, "The Effects of Anion Receptors Used as Additives in Electrolyte on Electrochemical Performance for Lithium-ion Batteries", *The Journal of Physical Chemistry* , **accepted**
7. Jordi Cabana, Christopher S. Johnson, Xiao-Qing Yang, Kyung-Yoon Chung, Won-Sub Yoon, Sun-Ho Kang, Michael M. Thackeray, and Clare P. Grey, "Structural complexity of layered-spinel composite electrodes for Li-ion batteries", *J. Mater. Res.*, Vol. 25, No. 8, Aug 2010.
8. K-W Nam, X. Q. Yang, X.J. Wang, Y.N. Zhou, H.S. Lee, L.J. Wu and Y. Zhu, "Comparative Studies between Surface and Bulk Structural Changes during Heating and cycling for Layer-structured and Olivine–structured Cathode Materials" , presented the 15th International Meeting of Lithium Batteries (IMLB-15), *June 27 to July 2nd, 2010, Montreal, Canada*, **Invited.**

V.B.9 Layered Cathode Materials (ANL)

Michael Thackeray
Argonne National Laboratory
9700 South Cass Avenue
Argonne, IL 60439
Phone: (630) 252-9184 ; Fax: (630) 252-4176
E-mail: thackeray@anl.gov

Collaborators:
S.-H. Kang, R. Benedek, V. G. Pol, C. Johnson, J. T. Vaughey, M. Balasubramanian (ANL)
Y. Shao-Horn, C. Carlton (MIT)
V. Battaglia (LBNL)
Jose M. Calderon-Moreno (Romanian Academy)

Start Date: October 1, 2007
Projected End Date: September 30, 2011

Objectives

- Design high capacity, high-power and low cost cathodes for PHEVs and EVs.
- Improve the design, composition and performance of Mn-based cathodes.
- Explore new processing routes to prepare advanced electrodes with new architectural designs.
- Use atomic-scale modeling as a guide to identify, design and understand the structural features and electrochemical properties of cathode materials.

Technical Barriers

- Low energy density
- Poor low temperature operation
- Abuse tolerance limitations

Technical Targets (USABC - End of life)

- 97 Wh/kg, 383 W/kg (PHEV 40 mile requirement)
- Cycle life: 5000 cycles
- Calendar life: 15 years

Accomplishments

- Engineered and evaluated the electrochemical effects of protective coatings on composite electrode structures with a high Mn content.
- Modeled interfacial structures and dissolution phenomena of $LiMn_2O_4$ electrodes.
- Evaluated single-step, autogenic processes for synthesizing new or improved materials, cathode coatings and architectures.

✧ ✧ ✧ ✧ ✧

Introduction

Structurally integrated 'composite' electrode materials, such as 'layered-layered' $xLi_2M'O_3\bullet(1-x)LiMO_2$ and 'layered-spinel' $xLi_2M'O_3\bullet(1-x)LiM_2O_4$ systems in which M′ is predominantly Mn and M is predominantly Mn, Ni and Co, yield very high capacities approaching the theoretically-expected values (240-250 mAh/g) when discharged at relatively low rates. The rate and cycle life limitations of these materials have been attributed to structural degradation at the electrode surface when charged to high potentials.

Our research in FY2010 therefore focused predominantly on developing methods to improve surface coatings and the electrochemical properties of high capacity $xLi_2M'O_3\bullet(1-x)LiMO_2$ electrodes. In particular, work on Li-Ni-PO_4 coatings was extended to cover other phosphate-based materials. Our goal was to allow unrestricted access of lithium at the surface to the bulk of the electrode structure, thereby enhancing lithium-ion conductivity and the rate capability of the lithium-ion cell. In a second thrust, dry, autogenic reaction processes were explored for synthesizing and coating cathode materials with carbon in a single step, using $LiFePO_4$ as prototype system for the initial studies.

In a theoretical approach, atomic scale simulations using the VASP code[21] were performed to characterize the interface and atomic arrangement in $LiMn_2O_4$.

Approach

- Exploit the concept and optimize the performance of structurally-integrated, high-capacity electrodes, particularly 'layered-layered' $xLi_2MnO_3\bullet(1-x)LiMO_2$ (M=Mn, Ni, Co) electrodes.
- Design effective surface structures to protect the underlying metal oxide particles from the electrolyte and to their improve rate capability when charged at high potentials.

[21] Vienna Ab-initio Simulation Package (VASP) is a package for performing *ab-initio* quantum-mechanical molecular dynamics (MD) using pseudopotentials and a plane wave basis set.

- Explore autogenic (i.e., high pressure, solventless) reactions to synthesize cathode materials and surface structures with new architectural designs.
- Use first principles modeling to aid the design of bulk and surface cathode structures and to understand electrochemical phenomena.

Results

Surface-Protected $xLi_2MnO_3•(1-x)LiMO_2$ Electrodes. Studies of the effects of Li-Ni-PO_4 coatings on structurally-integrated electrode materials, $xLi_2MnO_3•(1-x)LiMO_2$, in which M is predominantly Mn, Ni and Co were continued. Solutions containing stoichiometric amounts of lithium, nickel and phosphate ions were used in accordance with the formula $Li_{3-2x}Ni_xPO_4$ for x=0, 0.25 and 0.75 such that a 2 mole percent coating was applied to mildly fluorinated $0.5Li_2MnO_3•0.5LiNi_{0.44}Co_{0.25}Mn_{0.31}O_2$ electrode particles. The resulting Li-Ni-PO_4-coated products were dried by heating at 550°C for 6 hours in air. The electrochemical properties of the coated electrodes were evaluated in lithium half cells at current rates between 15 mA/g (~C/10) and 150 mA/g (~C/1).

Cells with uncoated electrodes, while providing good electrochemical cycling stability, operated, on average, with 98.7% coulombic efficiency; the electrodes provided an average capacity of about 175 mAh/g at 150 mA/g (Figure V- 51(a)). By contrast, the charge/discharge reactions of $Li_{3-2x}Ni_xPO_4$-coated electrodes were 100% efficient, delivering superior electrode capacities of 184 and 193 mAh/g for x=0.25 and 0.75 at 150 mA/g, respectively, when cycled between 4.6 and 2.0 V (Figure V- 51(b) and Figure V- 51(c), respectively); the data for the cell containing the $Li_{3-2x}Ni_xPO_4$-coated electrode (x=0.75) indicate that, in terms of delivered capacity, the rate capability of $Li_{3-2x}Ni_xPO_4$-treated electrodes increases as a function of increasing Ni content, x. Li_3PO_4-coated electrodes (x=0) showed excellent coulombic efficiency but a relatively low capacity (164 mAh/g) at 150 mA/g.

TiO_2-C/$0.5Li_2MnO_3•0.5LiNi_{0.44}Mn_{0.31}Co_{0.25}O_2$ Cells. An electronically-interconnected, carbon-encapsulated anatase (TiO_2-C) nanoparticulate product can be fabricated by a dry, autogenic process. This process is extremely versatile in preparing a wide range of carbon-encapsulated electrode materials; these coated materials have implications, not only for protecting the surface of electrode structures from reactions with the electrolyte, but also for designing electrode architectures that can maintain good electrical connectivity between electrode particles at all times throughout charge and discharge. TiO_2 materials would be attractive alternative anodes to spinel $Li_4Ti_5O_{12}$ (theoretical capacity = 175 mAh/g) if they could be discharged to the rock salt composition $LiTiO_2$ (335 mAh/g). Lithium-ion cells were constriucted in which a high capacity cathode, $0.5Li_2MnO_3•0.5LiNi_{0.44}Mn_{0.31}Co_{0.25}O_2$ (ANL-NMC) was coupled with a carbon-encapsulated, nanoparticulate TiO_2-C anode. Two sets of electrodes with ANL-NMC loadings of 2.1 and 3.1 mg/cm^2 were prepared for cathode- and anode-limited cells using 100-μm and 125-μm blades; these electrodes are referred to as ANL-NMC100 and ANL-NMC125, respectively.

Electrochemical voltage–capacity plots of the first two formation cycles of a cathode-limited TiO_2-C/ANL-NMC100 cell, cycled between 3.25 and 0.05 V are shown in Figure V- 52(a); corresponding profiles for an anode-limited TiO_2-C/ANL-NMC125 cell, cycled between 3.5 and 0.05 V, are shown in Figure V- 52(b) for comparison. In general, the voltage profiles of both TiO_2-C/ANL-NMC cells are similar to $Li_4Ti_5O_{12}$/ANL-NMC cells (provided in an earlier report). Differences include: 1) the slightly lower operating voltage of TiO_2-C/ANL-NMC cells because the TiO_2-C anode provides a slightly higher redox potential (~1.8 V vs. Li^0) than a standard $Li_4Ti_5O_{12}$ spinel anode (1.55 V vs. Li^0); and 2) the end of charge of the anode-limited TiO_2-C/ANL-NMC125 cell is not as pronounced as it is in a corresponding $Li_4Ti_5O_{12}$/ANL-NMC125 cell, consistent with the sloping end-of-discharge of a reference Li/TiO_2-C cell (not shown). The relative cycling stability of the cathode-limited TiO_2-C/ANL-NMC100 and anode-limited TiO_2-C/ANL-NMC125 cells is shown in Figure V- 52(c). Despite offering a higher rechargeable anode capacity (~200 mAh/g) compared to $Li_4Ti_5O_{12}$, cells with nanoparticulate TiO_2-C anodes exhibit a steady capacity fade, which is attributed to the instability of the lithiated Li_xTiO_2 (anatase) structure at high lithium loadings (x>0.5).

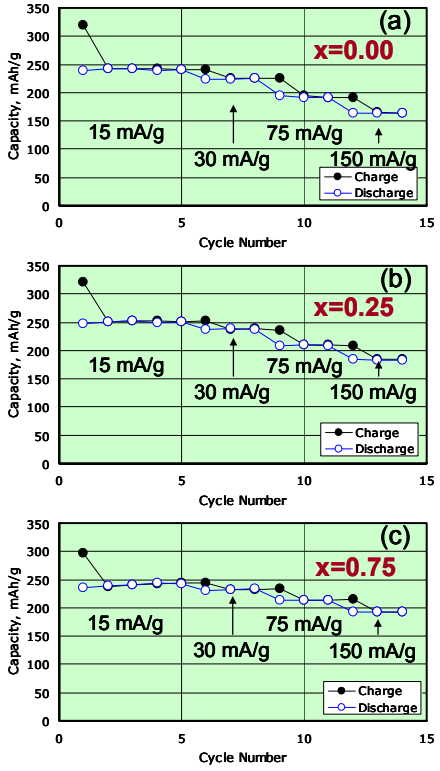

Figure V- 51: Electrochemical data of uncoated and $Li_{3-2x}Ni_xPO_4$-coated $0.5Li_2MnO_3 \bullet 0.5LiNi_{0.44}Co_{0.25}Mn_{0.31}O_2$ electrodes

Autogenic reactions to produce $LiFePO_4$. Autogenic reactions were also explored to synthesize carbon-coated $LiFePO_4$. Despite the apparent single-phase character of a nano-sized product synthesized from a FeC_2O_4 precursor, the olivine electrode displays very poor electrochemical behavior (<20 mAh/g) at a 0.08 mA/g rate.

However, significantly improved electrochemical behavior was obtained from single-phase, nano-sized $LiFePO_4$ particles from $FePO_4$ and glucose precursors, the carbon-coated product delivering 100-120 mAh/g at a 0.08 mA/g rate. The results demonstrate the difficulty in synthesizing $LiFePO_4$ electrode materials reliably with the autogenic technique.

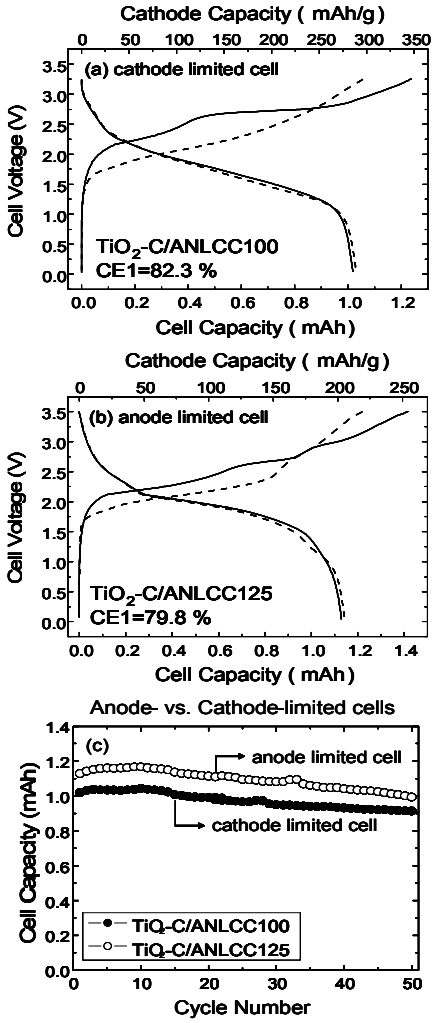

Figure V- 52: Initial two cycles of: (a) cathode-limited TiO_2-C/ANL-NMC100, 3.25-0.05 V, (b) anode-limited TiO_2-C/ANL-NMC125, 3.5-0.05 V, and (c) cycling performance of anode- vs. cathode-limited cells.

Simulation of the Surface Structure of $LiMn_2O_4$. The determination of surface atomic structure of electrode materials is a prerequisite to modeling their chemical and electrochemical reactions (e.g., at the electrode-electrolyte interface), or the interfacial structure between a coating (or SEI) and its active substrate. First principles simulations with the VASP code were performed on the low-index surfaces of the cathode material, $LiMn_2O_4$. Slab geometries were considered, with termination-layer vacancies introduced to suppress the electric dipole moment perpendicular to the surface for these polar ("Tasker type III") orientations, and to maintain stoichiometry. First-principles molecular dynamics simulations revealed an energetically favorable reconstruction of the Mn-terminated (111) surface, in which a stoichiometric mixed Li-Mn-O surface layer forms, with Mn coordinated in square planar units (Figure V- 53). Despite the resultant lowering of the (111) surface

energy, the (100) orientation is found to have the lowest energy among low index orientations, followed by (110), in agreement with the ordering predicted in simulations for the prototype spinel, $MgAl_2O_4$. Other conclusions drawn from this study were:

- Surface reconstruction of (111) minimizes under-coordination of surface Mn, O,
- Surface Mn ions are reduced,
- Despite under-coordination of flat surfaces (terraces), dissolution may require additional defects, such as non-bridging O.

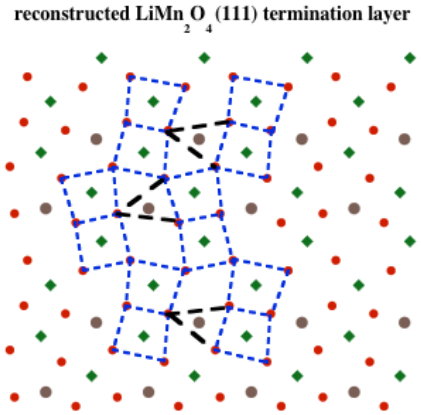

Figure V- 53: Simulated layer termination atomic arrangement of a reconstructed (111) surface in which the Mn ions (green squares) are coordinated in distorted square planar complexes, with mutual edge and corner sharing. The Li-ions (black circles) are three-fold coordinated. (Red dots are oxygen.)

Conclusions and Future Directions

Conclusions

- Further progress was made to stabilize the surface, and improve the rate capability and cycle life of high-capacity $xLi_2MnO_3\bullet(1\text{-}x)LiMO_2$ electrodes (M=Mn, Ni, Co) when charged to >4.5 V.
- $xLi_2MnO_3\bullet(1\text{-}x)LiMO_2$ electrode materials have the attention of industry – collaborations are in place with materials manufacturers worldwide.
- $Li_{3-2x}Ni_xPO_4$ coatings ($0<x\leq1$) improve the rate capability (200 mAh/g at C/1) and cycling efficiency (~100%) at room temperature; charged, coated electrodes generate less heat when reacted with electrolyte at elevated temperature.
- Autogenic reactions have been used to prepare carbon-coated electrodes in a single step – this versatile technique holds promise for fabricating advanced electrode materials (cathodes and anodes) with modified morphologies and electrochemical properties.
- Simulation of Mn- and MnO terminated surface structures of $LiMn_2O_4$ has provided insight into atomic coordination and Mn oxidation state that impact solubility.

Future Work

- Continue to exploit and optimize $xLi_2MnO_3\bullet(1\text{-}x)LiMO_2$ electrodes (composition and performance) with the particular goal of reaching or exceeding the energy and power goals required for 40-mile PHEVs and EVs.
- Focus on surface studies: phosphates and fluorides – use complementary experimental and theoretical approaches to improve the surface stability, rate capability and cycle life of high capacity Mn-rich oxide electrodes at high potentials.
- Exploit highly versatile, autogenic synthesis technique to fabricate and evaluate novel electrode materials and coating architectures, e.g., high capacity TiO_2 anodes coupled to high capacity Mn-based cathodes for safe Li-ion cells.
- Pursue interactions with energy storage EFRCs.
- Investigate novel cathode materials (optionally carbon coated in one processing step) and architectures.

FY 2010 Publications/Patents/Presentations

Publications

1. S.-H. Kang and M. M. Thackeray, *Enhancing the Rate Capability of High Capacity $xLi_2MnO_3\bullet(1\text{-}x)LiMO_2$ (M=Mn, Ni, Co) Electrodes*, Electrochem. Comm. **11**, 748 (2009).
2. S.-H. Kang, V. G. Pol, I. Belharouak and M. M. Thackeray, *A Comparison of $Li_4Ti_5O_{12}$- and Carbon-Encapsulated Anatase TiO_2 Anodes in Lithium-Ion cells with High Capacity $xLi_2MnO_3\bullet(1\text{-}x)LiMO_2$ (M=Ni,Co,Mn) Cathodes*, J. Electrochem. Soc. **157**, A267 (2010).
3. R. Benedek, M. M. Thackeray and A. van de Walle, *Pourbaix-like Phase Diagram for Lithium Manganese Spinels in Acid*, J. Mater. Chem., **20**, 369 (2010).

Patents

4. M. M. Thackeray, Sun-Ho Kang and C. S. Johnson, *Manganese Oxide Composite Electrodes for Lithium Batteries*, US Patent 7,635,536 (22 December 2009).

Presentations

5. S.-H. Kang, C. M. Lopez-Rivera, J. T. Vaughey, D. Shin, C. Wolverton and M. M. Thackeray, *Improved Rate Capability of High-Capacity $xLi_2MnO_3\bullet(1\text{-}x)LiMO_2$ Electrodes by Li-Ni-PO_4 Surface Treatment*, 216th ECS Meeting, Vienna, Austria, 4-9 October (2009).

6. M. M. Thackeray, C. S. Johnson, S.-H. Kang, H. H. Kung, V. G. Pol, L. Trahey and J. T. Vaughey, *Designing Advanced Anode and Cathode Materials for Lithium-Ion Batteries*, Materials Research Society Fall Meeting, Boston, 30 November – 4 December (2009).
7. M. M. Thackeray, M. Balasubramanian, C. S. Johnson, S.-H. Kang, S. Pol, V. G. Pol, L. Trahey, J. T. Vaughey, D. Shin and C. Wolverton, *Advances in the Design of Anode and Cathode Materials for Lithium Batteries*, 27th International Battery Seminar and Exhibit, Fort Lauderdale, Florida, 15-18 March (2010).
8. S.-H. Kang, *Advanced Nano-Composite Lithium Metal Oxide Electrodes for High Energy Lithium-Ion Batteries*, The 7th US-Korea Forum on Nanotechnology: Nanomaterials and Systems for Nano Energy, Seoul, Korea, 5-6 April, 2010.
9. S.-H. Kang, *Advanced Lithium Metal Oxide Electrode Materials with Integrated Structure for Lithium-Ion Batteries*, ICAM Workshop of Physics of Novel Energy Materials, Chinese Academy of Science, Beijing, China, 31 May - 3 June, 2010.
10. Presentation to the 2010 DOE Annual Peer Review Meeting, Washington D.C. 7-11 June 2010.

V.B.10 Development of High Energy Cathode (PNNL)

Ji-Guang Zhang and Jun Liu
Pacific Northwest National Laboratory
902 Battelle Blvd., Mail Stop K3-59
Richland, WA 99352
Phone: (509) 372-6515; (509) 375-4443
E-mail: jiguang.zhang@pnl.gov; jun.liu@pnl.gov

Objectives

- Develop high-energy cathode materials with improved safety
- Develop low-cost synthesis routes for high-capacity and environmentally-benign cathode materials.

Technical Barriers

This project addresses the following technical barriers:

- High cost of cathode materials
- Limited energy density and cyclability
- Safety

Technical Targets

- Synthesize and characterize olivine-structured $LiMnPO_4$ cathode materials and investigate non-stoichiometric Li_xMnPO_4 ($0.5 \leq x \leq 1.2$)
- Prepare and evaluate high-voltage Li_2CoPO_4F
- Synthesize renewable organic cathode materials with 2e- transfer per redox center.

Accomplishments

- Preferred growth of Li_xMnPO_4 nanoplates without agglomeration was achieved using a single-step, solid-state reaction. The reversible capacity of this material is high, amounting to ~168 mAh/g, and its cyclability is stable. The influence of the lithium (Li) content on the electrochemical performances of Li_xMnPO_4 ($0.5 \leq x \leq 1.2$) was investigated.
- A novel cathode material, Li_2CoPO_4F, was synthesized and characterized. Its operational voltage is ~5 V with 1 mole of reversible Li^+ ions intercalating/de-intercalating in the Li_2CoPO_4F.
- Anthraquinone polymer was prepared successfully and investigated as a high-capacity cathode material (with a reversible capacity of >200 mAh/g).

✧ ✧ ✧ ✧ ✧

Introduction

Li-ion batteries with high energy densities are required to reach DOE's goal on early commercialization of electrical vehicles, including hybrid electric vehicles and plug-in hybrid electric vehicles. To increase the energy of a cathode, the voltage or/and capacity of the material needs to be increased. During FY 2010, we investigated cathode materials with high operational voltages (e.g., $LiMnPO_4$) and renewable organic cathode materials with high capacities. Environmentally friendly materials and low cost synthesis approaches have been intentionally explored during our efforts.

Approach

- Synthesize high-performance $LiMnPO_4$ and high-voltage Li_2CoPO_4F using solid-state reactions
- Optimize the Li contents in non-stoichiometric $LiMnPO_4$ to improve electrochemical performance
- Characterize proposed cathode materials using X-ray diffraction (XRD), high-resolution transmission electron microscopy (HRTEM), and electrochemical evaluations.
- Prepare renewable organic cathode materials through polycondensation.
- Investigate the effect of electrolytes on the long-term cyclability and rate performance of organic cathodes.

Results

$LiMnPO_4$ Cathode Materials. The synthesis of $LiMnPO_4$ (Figure V- 54) in molten hydrocarbon has been optimized. Oleic acid was used as a surfactant and paraffin acted as a nonpolar solvent that facilitated thermodynamically preferred crystal growth without agglomeration. Figure V- 55 (a,b,e) shows field-emission scanning electron microscope (FESEM) images of uniformly dispersed $LiMnPO_4$ nanoplatelets synthesized using a molten hydrocarbon process. The $LiMnPO_4$ nanoplatelet is ~50-nm thick with plates extending as long as 1~3 µm. From the HRTEM and FESEM images in Figure V- 55, these $LiMnPO_4$ cathodes exhibit a porous structure with many nanorods aligned in the preferred orientation. We believe that the initially formed $LiMnPO_4$ nanorods re-aligned during high-temperature heat treatment by reducing certain planes of the $LiMnPO_4$ crystallites. The porous nature of the nanoplates and their

high specific surface area of 37.3 m^2/g facilitate uniform carbon coating and reduce polarization.

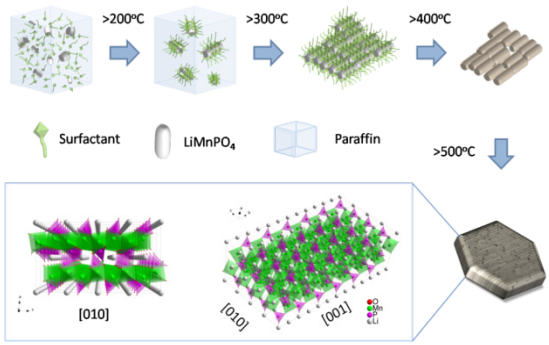

Figure V- 54: Synthesis of $LiMnPO_4$ in a molten hydrocarbon

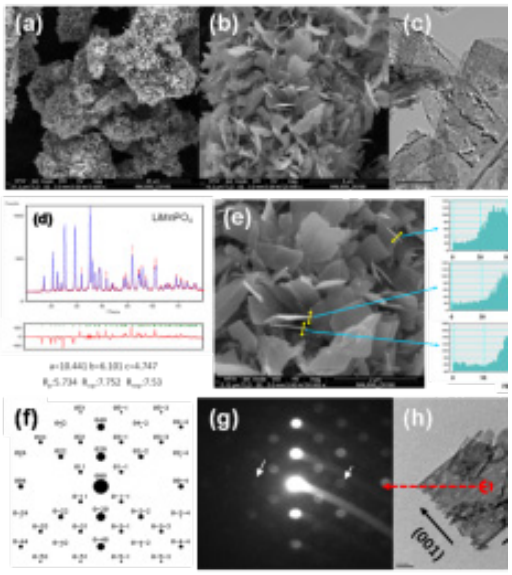

Figure V- 55: (a,b,e) FESEM and (c,h) HRTEM images of $LiMnPO_4$ nanoplates, (d) Rietveld refinement of $LiMnPO_4$, (f) simulated diffraction pattern parallel to [100], (g) nanobeam diffraction pattern, and (h) orientation of $LiMnPO_4$ grown using a molten hydrocarbon process

Figure V- 56(a) and Figure V- 56(b) show the rate performances of a $LiMnPO_4$/C cathode at various discharge rates ranging from C/50 to 10C. The voltage profiles clearly show a flat redox potential around 4.1 V compared to Li/Li and indicate that the charge/discharge reaction proceeds via a first-order phase transition between $LiMnPO_4$ and $MnPO_4$. A specific capacity of 168 mAh/g, which is close to the theoretical capacity, was achieved at the C/50 rate. At the 1C and 2C rates, capacity retention is 120 mAh/g and 100 mAh/g, respectively. The Ragone plot in Figure V- 56(c) indicates that the discharge power density of the $LiMnPO_4$ is close to that of $LiFePO_4$ when fully charged at C/25. At a low power (<30 W/kg), the energy density of $LiMnPO_4$ becomes comparable or higher than that of $LiFePO_4$.

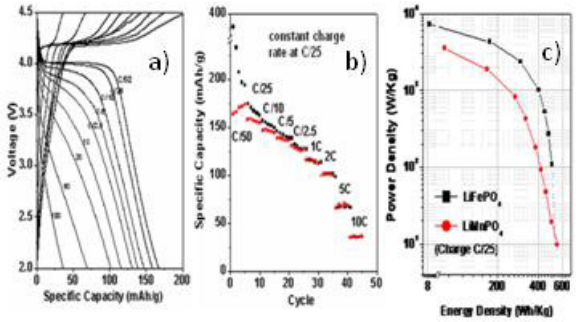

Figure V- 56: a) Voltage profiles of $LiMnPO_4$ at various discharge C rates; b) rate performances of $LiMnPO_4$; c) Ragone plot comparison of $LiMnPO_4$ to $LiFePO_4$. All the cells were constantly charged at C/25.

Non-Stoichiometric Li_xMnPO_4 ($0.5 \leq x \leq 1.2$). To investigate the effects of Li content on the performance of $LiMnPO_4$, a precipitation method was designed to prepare Li_xMnPO_4 ($0.5 \leq x \leq 1.2$).

Figure V- 57(a) shows that a single phase does exist between $Li_{0.8}MnPO_4$ and $LiMnPO_4$, while Li_3PO_4 begins to form when $x > 1$. When $x = 0.5$ the main impurity exists as $Mn_2P_2O_7$. The Li/Mn ratio matches well with the ICP results shown in . At a slow rate of C/50 (see Table V- 1), the initial discharge capacity increases from 73 mAh/g to 155 mAh/g as the Li content increases, indicating that Li content does affect the reversible capacities especially for $x > 1$ in Li_xMnPO_4. However, at a C/20 rate, there is no difference in the initial discharge capacity for $x \geq 1.0$ samples (120 mAh/g). Interestingly, the reversible capacities of $x \leq 1.0$ samples continue to increase during cycling as shown in Figure V- 57(b). Because the Li source is sufficient (Li metal as the anode) in all the tests, the increasing reversible capacity suggests that tetrahydral Li sites in $Li_{0.8}MnPO_4$ and $Li_{0.5}MnPO_4$ are being activated during the cycling. This phenomenon provides ideas for further improving the utilization rate and cyclability of the $LiMnPO_4$ cathode. $Li_{1.1}MnPO_4$ exhibits the most stable cycling behavior, probably because of surface modification by Li_3PO_4.

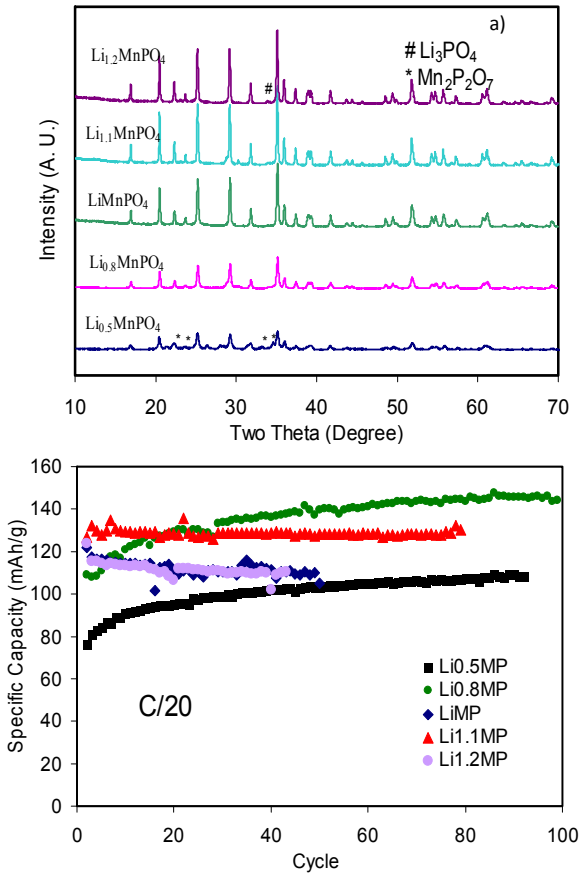

Figure V- 57: a) XRD patterns and b) cycling performances of Li_xMnPO_4 ($0.5 \leq x \leq 1.2$)

Table V- 1: ICP results and initial discharge capacities at C/50 for Li_xMnPO_4 ($0.5 \leq x \leq 1.2$)

	Li (mole)	Mn (mole)	First discharge capacities at C/50 (mAh/g)
$Li_{0.5}MnPO_4$	0.492	1	73
$Li_{0.8}MnPO_4$	0.774	1	113
$LiMnPO_4$	0.997	1	135
$Li_{1.1}MnPO_4$	1.078	1	146
$Li_{1.2}MnPO_4$	1.198	1	155

High-Voltage Li_2CoPO_4F. Another high-voltage cathode, Li_2CoPO_4F, was synthesized using a solid-state reaction. Discharge capacity increases with increasing cut-off voltages. A reversible capacity of 102 mAh/g was obtained between 2.0 V and 5.5 V as shown in Figure V-58(a). However, only up to one mole of Li^+ ions are reversibly extracted/ intercalated between 2.0 V to 5.5V. A second Li^+ ion cannot be removed electrochemically before decomposition of the electrolyte at 5.5 V. Stable cycling lasts for about 20 cycles as shown in Figure V-58(b). Although good structural stability upon de-lithiation and lithiation was observed from XRD patterns, appropriate electrolytes or electrolyte additives need to be identified for high-voltage cathode materials to reduce the electrolyte decomposition and improve interface stability.

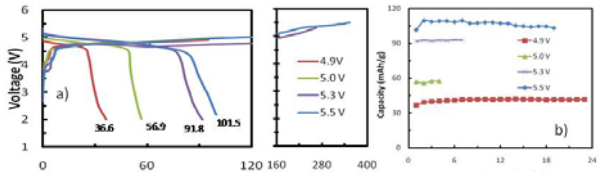

Figure V- 58: a) Voltage profiles and b) *cyclability* of Li_2CoPO_4F

Organic Cathode. In FY 2010, we investigated a novel organic cathode based on poly(anthraquinonyl sulfide) (PAQS). This renewable cathode was prepared using a simple poly-condensation that has been used commercially to synthesize poly(p-phenylene sulfide). Figure V- 59 shows the electrochemical reaction mechanism for this organic cathode during charge and discharge processes. PAQS is different from traditional intercalation cathode materials in that it allows 2e transfer that leads to a high theoretical capacity of 225 mAh/g. The electrochemically active site is O instead of S on the ring; therefore, the polysulfide dissolution issue encountered in Li/S batteries can be avoided.

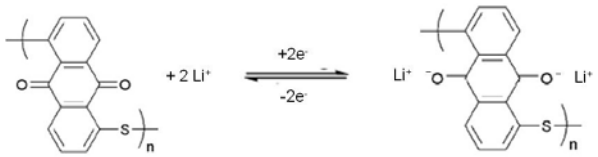

Figure V- 59: Electrochemical reactions of PAQS as a cathode material during charge and discharge processes

Figure V- 60 shows the electrochemical performances of the PAQS organic cathode. The reversible capacity of the material is 200 mAh/g, which approaches its theoretical value. As shown as Figure V- 60(a), the operational voltage is 2.0 V, which can be further tuned by adjusting the functional groups on the rings. Figure V- 60 (b) reveals that the cyclability of PAQS is related closely to the electrolyte composition. Increased initial capacity and reduced polarization are observed when using Li bis(trifluoromethylsulfonyl)imide in 1,3dioxolane/1,2-dimethoxyethane as the electrolyte. Relatively stable cycling was obtained with 80% capacity retention after 100 cycles.

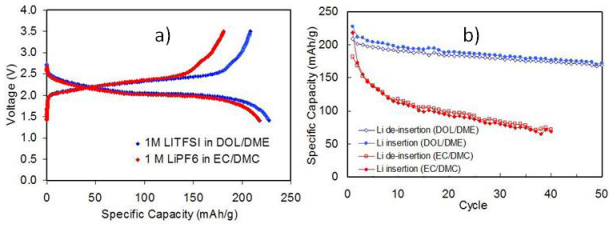

Figure V- 60: a) Voltage profiles of PAQS and b) cycling stability of PAQS in different electrolytes. Current density: 50 mA/g.

Conclusions and Future Directions

$LiMnPO_4$ was successfully synthesized using different approaches. The best $LiMnPO_4$ developed at PNNL demonstrated a capacity of 168 mAh/g at a C/25 rate, which is close to its theoretical value. Non-stoichiometric Li_xMnPO_4 ($0.5 \leq x \leq 1.2$) was investigated to determine the effect of Li content on the performance. At the C/50 rate, the initial discharge capacity increases with increasing Li content. However, at the C/20 rate, the differences in capacity of Li_xMnPO_4 ($0.5 \leq x \leq 1.2$) samples was negligible, probably because of the sluggish electron transfer that becomes the limiting step. When x is <1.0, the reversible capacity increases upon cycling. This behavior may relate to the activation of $LiMnPO_4$.

The high-voltage Li_2CoPO_4F cathode exhibits a discharge plateau at ~5.0 V. Stable cycling at up to 20 cycles has been observed. However, the expected extraction of the second Li^+ ion from Li_2CoPO_4F cathode still has not been realized because of electrolyte decomposition at high voltages (~5.5 V). New electrolyte and electrolyte additives that are stable at ~5.5V will be developed to further increase cathode capacity and stabilize long-term cycling.

A renewable organic cathode, PAQS, was prepared through a simple polycondensation reaction. A high capacity of 200 mAh/g was achieved with relatively stable cycling. In future work, the operational voltage of this organic cathode will be tuned by connecting it with different functional groups while the cyclability will be improved further by optimizing the electrolyte and the binders.

FY 2010 Publications/Presentations

1. D. Choi, D. Wang, I.-T. Bae, J. Xiao, Z. Nie, W. Wang, V. V. Viswanathan, Y. J. Lee, J-G. Zhang, G. L. Graff, Z. Yang, and J. Liu, "$LiMnPO_4$ Nanoplate Grown via Solid-State Reaction in Molten Hydrocarbon for Li-Ion Battery Cathode", *Nano Lett.*, **10,** (2010)2799.
2. J. Xiao, W. Xu, D. Choi, and J. Zhang, "Synthesis of Lithium Manganese Phosphate by a Novel Precipitation Method", *J. Electrochem. Soc.*, **157,** (2010)A142.
3. Facile synthesized nanorod structured vanadium pentoxide for high-rate lithium batteries, Anqiang Pan, Ji-Guang Zhang, Zimin Nie, Guozhong Cao, Bruce W. Arey, Guosheng Li, Shu-quan Liang, and Jun Liu, Journal of Materials Chemistry, DOI:10.1039/c0jm01306d.
4. "Synthesis and Characterization of $LiMnPO_4$ by a Novel Precipitation Method". J. Xiao, N. Chernova, W. Xu, M. Stanley Whittingham and J-G. Zhang, presented in 2009 MRS Fall meeting, 2009, Boston, Massachusetts.
5. "Novel Cathode Material Li_2CoPO_4F for Lithium-ion Batteries". D. Wang, J. Xiao, W. Xu, D. Choi, and J-G. Zhang, poster in 2009 MRS Fall meeting, 2009, Boston, Massachusetts.

V.B.11 High-Energy Cathodes - Performance and Safety of Olivines and Layered Oxides (LBNL)

Guoying Chen
Environmental Energy Technologies Division
Lawrence Berkeley National Laboratory
Berkeley, CA 94720
Phone: (510) 486-5843
E-mail: gchen@lbl.gov

Start Date: October 2009
Projected End Date: September 2011

Objectives

- Investigate phase transition mechanisms, explore kinetic barriers, and evaluate stability of high-energy cathode materials.
- Establish direct correlations between structure, composition, morphology, performance, and stability.
- Provide guidelines to design and develop electrode materials with improved energy density, rate capability, and safety, especially with regard to thermal stability.

Technical Barriers

- Low energy density
- Low power density
- Poor cycle life
- Safety

Technical Targets

- PHEV40: 96 Wh/kg, 750 W/kg, 5,000 cycles.
- EV: 200 Wh/kg, 1,000 cycles.

Accomplishments

- Demonstrated improved energy density, rate capability, physical and thermal stabilities of Mg substituted $LiMnPO_4$.
- Identified the optimal level of Mg substitution in $LiMnPO_4$.
- Developed an approach to prepare high-quality layered oxide crystals.
- Revealed the structural and performance effects of excess Li in layered $LiNi_{0.33}Mn_{0.33}Co_{0.33}O_2$: it promotes the formation of superlattice structure and decreases the volume change during Li extraction and insertion; it delays the onset of phase transition from O3 to P3 structure and increases energy density.
- Demonstrated the morphological damages during Li extraction and provided direct evidence for the reported poor cycle life of the overlithiated oxides.

Introduction

Achieving the DOE targets for Li-ion batteries for vehicular applications requires the use of electrode materials that offer high-energy density and high stability. This project focuses on phosphate olivines and layered oxides, two of the most promising cathode materials to meet these targets.

$LiMnPO_4$ has the potential to offer higher energy density than $LiFePO_4$, but it suffers poor kinetics during electrochemical charging and discharging. Our recent findings on thermal instability of delithiated manganese phosphate revealed further obstacles for $LiMnPO_4$ to be used in commercial high energy lithium-ion batteries. Significant improvements on both kinetics and stability are necessary.

Layered $Li_{1+x}M_{1-x}O_2$ (M=Mn, Ni and Co) can deliver high capacity over 200 mAh/g. It has been shown that crystal structure and cation ordering scheme, which are highly sensitive to chemical composition and synthesis conditions, are key to the performance and stability of the oxides. The relationships, however, are poorly understood, as studies were often carried out on aggregated particles where non-uniformity is common. The Li and Mn rich oxides also suffer poor rate and poor cycle life after charging through the activation plateau at 4.5 V. Further improvement in performance and stability of the oxide cathodes demands more in-depth understanding of the materials.

Approach

Prepare well-formed crystals with various structure, composition, size and morphology using wet chemistry synthesis routes, such as solvothermal and molten salt reactions. Characterize their physical properties and investigate their solid state chemistry using advanced spectroscopic, spectromicroscopic, scanning calorimetry and electron microscopic techniques. Optimize synthesis and processing conditions, improve performance and

safety of the cathode materials based on the structural and mechanistic understandings.

Results

Olivine Phosphates. The presence of Mg^{2+} was previously shown to improve kinetics and physical stability of the $LiMnPO_4$ crystals during chemical and electrochemical delithiation. Best performance was found in the sample with 20% substitution. When heated in an inert atmosphere, chemically delithiated phosphates, $Li_xMg_xMn_{1-x}PO_4$ (x=0, 0.1, 0.2, 0.3, 0.4, 0.5), decompose and release O_2, as evidenced by the XRD patterns in Figure V- 61(a). The reaction path, however, is largely influenced by the amount of Mg in the crystal structure. For the unsubstituted phosphate (x=0), it releases 0.25 mol of O_2 per mol of the phosphate to form $Mn_2P_2O_7$, starting around 150°C (equation 1). For 50% Mg substitution (x=0.5), the reaction proceeds through an alternative path that releases 0.125 mol of O_2 per mol of the phosphate and forms $Mn_3(PO_4)_2$ (equation 2). With the intermediate x value, both $Mn_2P_2O_7$ and $Mn_3(PO_4)_2$ were detected in the heat-treated samples. The ratio between the products decreases with the increase of x.

$$2Li_xMg_xMn_{1-x}PO_4 \rightarrow xLiMgPO_4+(1-x)Mn_2P_2O_7+0.5(1-x)O_2 \quad [1]$$

$$3Li_xMg_xMn_{1-x}PO_4 \rightarrow 3xLiMgPO_4+(1-x)Mn_3(PO_4)_2+ 0.5(1-x)P_2O_5+0.75(1-x)O_2 \quad [2]$$

Oxygen released from the electrode material is known to react with the solvents in lithium-ion battery cells. The combustion heat of the oxidation process can be measured by differential scanning calorimetry (DSC). In the presence of 1M $LiPF_6$ in PC and EC (44:56 by mole ratio), the amount of heat decreased monotonically as the Mg content increased from 0 to 0.5, as shown in the DSC profiles of the $Li_xMg_xMn_{1-x}PO_4$ series in Figure V- 61(b). The total heat evolved from $Li_xMg_xMn_{1-x}PO_4$ (x=0.5) was 505 J/g, whereas the unsubstituted phosphate produced 884 J/g. The peak temperature of the exothermal reaction also gradually shifted from 256 (x=0) to 269°C (x=0.5), consistent with the increased thermal stability with increasing amount of Mg-substitution in the phosphates.

The heat evolved and the Mn content in the phosphates follow a linear relationship, as shown in Figure V- 61(c). As Mg is electrochemically and chemically inactive, it is evident that both theoretical capacity and the released oxygen are in proportion to the Mn content in the phosphates. This approach, therefore, entails a compromise between the energy density and the stability of the cathode material.

Layered Oxides. A molten salt method has been adapted to prepare well-formed oxide crystals. The approach provides a liquid reaction media that enables atomic level mixing of the reactants and allows for homogeneous nucleation and growth of crystals in the flux. Synthesis conditions can be varied to produce a range of crystal sizes and morphologies. For example, the shape of $Li_{1.14}(Ni_{0.33}Mn_{0.33}Co_{0.33})_{0.86}O_2$ crystals evolved from plates to octahedrons when the salt to metal precursors ratio (denoted as R) was increased from 4 to 40 (Figure V- 62).

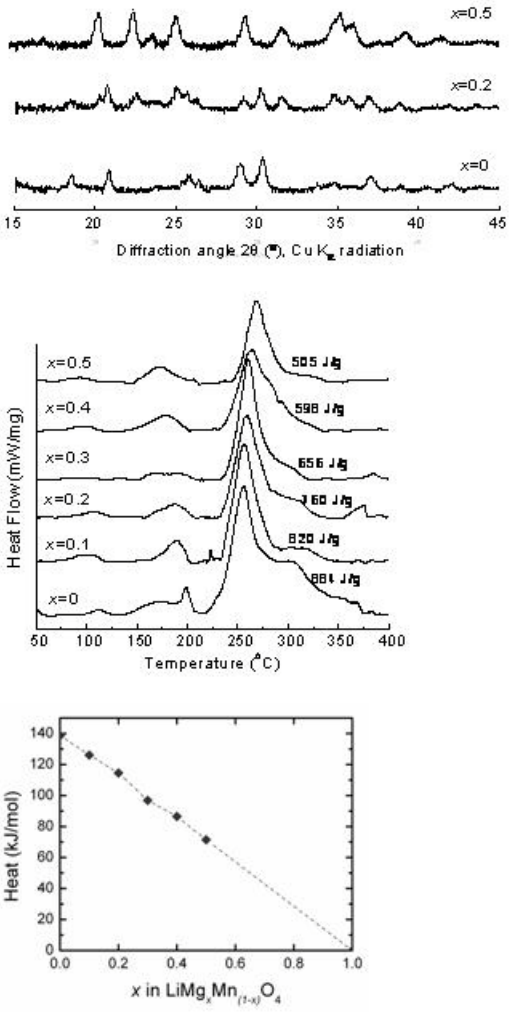

Figure V- 61: a) XRD patterns of heat-treated $Li_xMg_xMn_{1-x}PO_4$ crystals, b) DSC profiles of $Li_xMg_xMn_{1-x}PO_4$ in the presence of the electrolyte, and c) the relationship between the heat evolved and the Mn content in the phosphates.

Discrete, plate-shaped $Li_{1+x}(Ni_{0.33}Mn_{0.33}Co_{0.33})_{1-x}O_2$ crystals (x=0 and 0.14, by ICP analysis) were prepared to investigate the effect of initial Li content on structure, stability and performance. For x=0, the oxide showed an ordered rock salt α-$NaFeO_2$-type structure (space group R-3m), with alternating layers of transition metal and lithium-ions. There was no superlattice reflection on the electron diffraction patterns (Figure V- 63(a)). For x=0.14, all

examined crystals had electron diffraction patterns with strong superlattice reflections. The patterns matched well with the ones simulated from $P3_112$ space group, demonstrating the formation of an in-plane [$\sqrt{3} \times \sqrt{3}$] R30° -type superlattice that lowers the symmetry from *R*-3*m* to $P3_112$. On the XRD patterns (Figure V- 63(b), additional peaks between 20° and 26° (2θ) existed in the sample with x=0.14 but not in *x*=0, consistent with the presence of in-plane cation ordering in the "Li-excess" sample. The overlithiated crystals also showed better lamellar structure, as indicated by the larger separation between the (006)/(012) and (018)/(110) doublets.

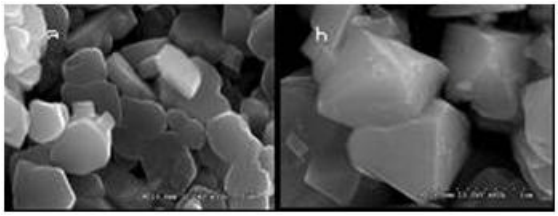

Figure V- 62: SEM images of $Li_{1.14}(Ni_{0.33}Mn_{0.33}Co_{0.33})_{0.86}$ crystals synthesized at 850°C in a 0.88$LiNO_3$-0.12LiCl eutectic mixture, a) R=4 and b) R=40.

a)

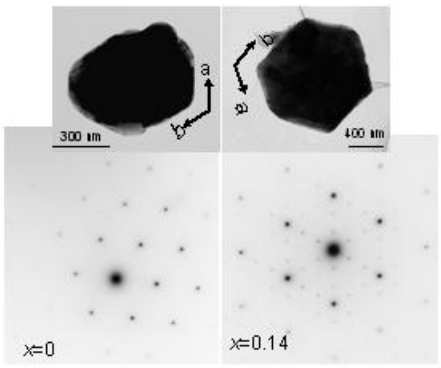

b)

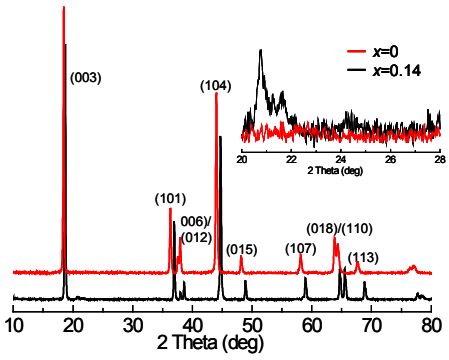

Figure V- 63: a) TEM and [001] zone axis electron diffraction patterns, and b) XRD patterns of $Li_{1+x}(Ni_{1/3}Mn_{1/3}Co_{1/3})_{1-x}O_2$ (*x*=0 and 0.14).

To investigate kinetic performance, the crystals were then chemically delithiated by NO_2BF_4 in acetonitrile ($E_{NO2^+/NO2} \approx 5.1$ V vs. Li/Li^+). The reaction proceeded according to equation 3, where *y* is larger than *z* to accommodate the kinetic hindrance during the Li extraction process. The relationship between the amount of oxidant used and the residual Li in the sample is shown in Figure V- 64(a).

$$Li_{1+x}(Ni_{0.33}Mn_{0.33}Co_{0.33})_{1-x}O_2 + yNO_2BF_4 \rightarrow Li_{1+x-z}(Ni_{0.33}Mn_{0.33}Co_{0.33})_{1-x}O_2 + zNO_2 + zLiBF_4 \quad [3]$$

Figure V- 64(b) shows the changes in cell dimension for the sample with *x*=0.14. In the *a* direction, the lattice first shrank, with the largest decrease of 0.8% occurring at Li content of 0.36, and then stabilized. In the *c* direction, it expanded 1.7% and then shrank nearly the same amount. The overall cell volume remained nearly constant after extracting 0.78 mol of Li per mol of the oxide. It then decreased, and was reduced by 1.6% upon the extraction of 1.02 mol of Li, at a total Li content of 0.09.

Delithiation caused continuous decrease in phase crystallinity (Figure V- 64(b)). The oxide crystals disintegrated after the removal of a large amount of Li, as demonstrated by the morphological changes in the SEM images (Figure V- 65). This is likely due to the phase transition as well as oxygen evolution accompanying the deep extraction of Li from the structure. TEM and electron diffraction studies showed that the in-plane $\sqrt{3}a_{hex} \times \sqrt{3}a_{hex}$ ordering in the fresh crystals disappears upon chemical delithiation to Li content of 0.76.

When the fresh "Li-stoichiometric" oxide crystals (*x*=0) were chemically delithiated, the unit cell shrank first and then expanded in the *a* direction, while it expanded first and then shrank in the *c* direction (Figure V- 66). Delithiation caused a continuous decrease in both crystalline domain size and cell volume, with the latter reduced by 5.4% at the Li content of 0.08.

The transformation from the initial O3 (with a space group of *R*-3*m*) to P3 structure (with a space group of *R*3*m*) occurred in both samples during delithiation. For *x*=0.14, the phase transition began at Li content of 0.12, after the extraction of 1.02 mol Li. For *x*=0, on the other hand, it occurred at a much higher Li content. Significant amount of P3 phase formed after removing only 0.77 mol of Li per mol of the oxide. The extractable Li in the "Li-stoichiometric" oxide, therefore, is at least 25% less compared to the overlithiated sample.

Conclusions and Future Directions

Mg substitution in $LiMnPO_4$ was found to improve kinetics and physical stability of the crystals during chemical and electrochemical delithiation, as well as the thermal stability of the delithiated phase. The inactivity of Mg intrinsically limits the applicability of this approach.

Future work will be directed toward binary and ternary Mn olivine crystals containing Mg, Fe, Co and Ni. The kinetic and thermal properties of the substituted $LiMnPO_4$ will be investigated.

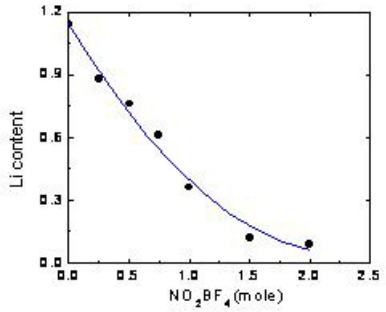

a)

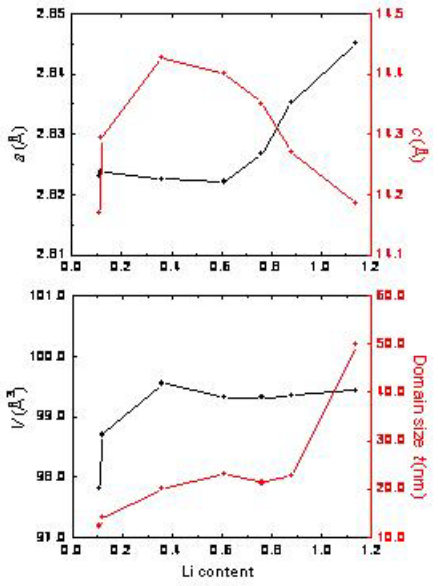

b)

Figure V- 64: a) relationship between the amount of NO_2BF_4 used and the residual Li in the delithiated $Li_{1.14}(Ni_{0.33}Mn_{0.33}Co_{0.33})_{0.86}O_2$ crystals and b) Lattice parameters and crystallite size of the crystals.

The use of oxide crystals for property evaluation and mechanistic studies was found fruitful. Future work will focus on the Li and Mn rich layered oxides that are currently being pursued as one of the most promising cathode materials for PHEV and EV batteries. To this end, detailed understandings on structural, performance and stability effects of Li content and metal ratios are planned. Synthesis conditions will be explored to produce desired oxide characteristics for optimum performance and safety in lithium batteries.

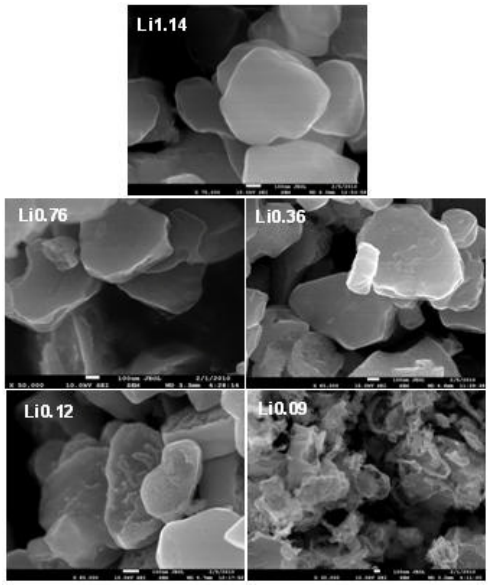

Figure V- 65: SEM images of fresh and delithiated $Li_{1.14}(Ni_{0.33}Mn_{0.33}Co_{0.33})_{0.86}O_2$ crystals.

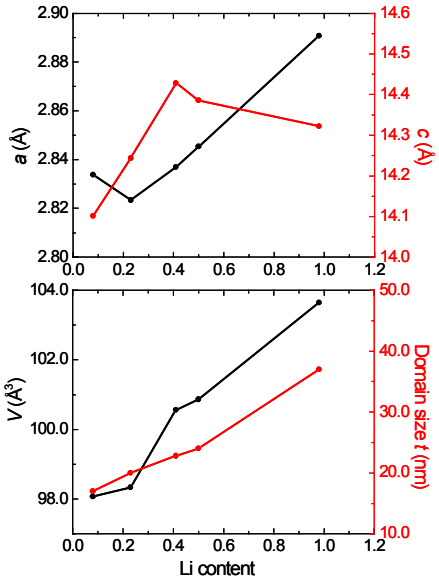

Figure V- 66: Lattice parameters and crystallite size of delithiated $LiNi_{0.33}Mn_{0.33}Co_{0.33}O_2$ crystals.

FY 2010 Publications/Presentations

1. "Solid Solution Phases in the Olivine-Type $LiMnPO_4/MnPO_4$ System," G. Chen and T. J. Richardson, *Journal of the Electrochemical Society*, **156**, A756 (2009).
2. "Thermal Instability of Olivine-type $LiMnPO_4$ Cathodes," G. Chen and T. J. Richardson, *Journal of Power Sources*, **195**, 1221 (2010).
3. "Continuity and Performance in Composite Electrodes," G. Chen and T. J. Richardson, *Journal of Power Sources*, **195**, 5387 (2010).

4. "MAS NMR Study of the Metastable Solid Solutions Found in the $LiFePO_4/FePO_4$ System," J. Cabana, J. Shirakawa, G. Chen, T. J. Richardson, and C. P. Grey, C*hemistry of Materials*, **22**, 1249 (2010).

5. "Performance and Safety of Olivines and Layered Oxides," presented at the 2010 DOE Hydrogen Program and Vehicle Technologies Program Annual Merit Review and Peer Evaluation Meeting, Washington, DC, June 08, 2010.

V.C Anode Development

V.C.1 Nanoscale Composite Hetero-structures: Novel High Capacity Reversible Anodes for Lithium-ion Batteries (University of Pittsburgh)

Prashant N. Kumta

Swanson School of Engineering,
Departments of Bioengineering, Chemical and Petroleum Engineering, Mechanical Engineering and Materials Science,
University of Pittsburgh, Pittsburgh, PA 15261
Phone: (412)-648-0223 ; Fax: (412) 624-8069
E-mail: pkumta@pitt.edu

Start Date: September 1, 2007
Projected End Date: December 31, 2010

Objectives

- Identify new alternative anode materials to replace synthetic graphite that will provide higher gravimetric and volumetric energy density.
- Similar or lower irreversible loss in comparison to synthetic graphite.
- Similar or better cyclability and calendar life in comparison to synthetic graphite.
- Investigate nano-structured (nc-Si) and amorphous Si (a-Si) based composite or hybrid structured anode.
- Improve the specific capacity, available energy density, rate capability and cycle life of nano-structured and amorphous Si based anode materials.

Technical Barriers

The important technical barriers of alternative anodes for lithium-ion batteries to be used in electrical vehicles or hybrid electrical vehicles are following:

(A) Low energy density

(B) Large first cycle irreversible loss

(C) Poor cycle life

(D) Poor rate capability

(E) Inadequate coulombic efficiencies

Technical Targets

- Synthesize nano-structured and amorphous Si based anodes using cost effective processing techniques.
- Achieve stable reversible capacity in excess of ~1,000mAh/g.
- Improve the rate capability.
- Characterize the nano-scale hetero-structures for structure and composition using electron microscopy techniques such as SEM, TEM and HREM.
- Reduce first cycle irreversible loss to less than ~20%.
- Investigate the origin and characterize the solid electrolyte interphase (SEI) layer.

Accomplishments

- Synthesized nanostructured or amorphous Si by thermal cracking of Si based precursor.
- Synthesized nanocrystalline Si and carbon nanotube (CNT) hybrid nanostructures by cost effective two step liquid injection CVD processes
- Optimized the processing parameters to achieve desirable microstructure of Si/CNT hybrid structure which shows high specific capacity along with excellent cyclability.
- The controlled hybrid structures of Si/CNT exhibit specific capacity in excess of ~2,000mAh/g with excellent stability and rate capability.
- Synthesized amorphous Si and graphite nanocomposite (a-Si/C) by thermal cracking of Si based precursors followed by high energy mechanical milling.
- The a-Si/C nano-composite shows excellent cyclability (0.1-0.2% loss per cycle) with specific capacity higher than ~1000mAh/g.
- The novel a-Si/C composite and nc-Si/CNT hybrid nanostructures exhibit less than 20% first cycle irreversible loss.

✧ ✧ ✧ ✧ ✧

Introduction

Achieving the DOE-BATT technical targets will require improving the cycling stability, irreversible loss, coulombic efficiency and rate capability of Si based anodes. Hence it is essential to synthesize Si based composites using economical processes exhibiting excellent mechanical properties to endure the large cycling induced volumetric stresses of Li-Si alloys. In 2008, we conducted a systematic investigation of the electrochemical properties of high energy mechanical

milling (HEMM) derived Si/C based composite anodes. These HEMM derived composite anodes synthesized using polymer additives displayed a reversible capacity ~700mAh/g or higher with a 0.01-0.03% capacity fade per cycle. Scale-up efforts to generate these novel composites are currently in progress; while efforts to further improve the capacities of these systems are also on-going. In addition, collaborative efforts to understand the SEI layers have been initiated with Dr. Kostecki and Dr. Battaglia at LBNL. Although Si/C based composites exhibiting capacity in excess of ~1000mAh/g have been generated, the system is commercially unsuitable due to capacity fade of above 0.3% per cycle. In order to improve the stability of Si/C based composite anodes, carbon nanotubes (CNTs) have been selected over graphite as a matrix. In this regard, a detailed structural investigation as well as electrochemical results on Si/CNT hybrid structures has been reported in 2009. CNT possess some unparalleled properties such as large aspect ratio, excellent electronic conductivity, structural flexibility, and tortuosity. Exploitation of these unique CNT attributes combined with its nano-scale dimensions will enable the generation of a nano-scale conductive network improving the electrical contact between the active Si particles. The Si/CNT hybrid structures exhibit high reversible capacity (~2,000mAh/g) up to 30 cycles while also displaying excellent cyclability with a fade in capacity ~0.1-0.2% capacity loss per cycle and low irreversible loss (~20%).

The microstructural studies revealed that the 10nm *nc*-Si particles are deposited on the CNT surface at defined spacing. However, a detailed structural investigation is needed to understand the improved cyclability of the *nc*-Si/CNT structure. In the present report, a detailed investigation conducted on the interfacial structure between *nc*-Si and CNT is presented. In addition, long term cyclability of the *nc*-Si/CNT (100 cycles) was investigated to explore its possible utilization in future applications.

The two step CVD process to synthesize CNT followed by deposition of *nc*-Si on CNT, though promising, requires optimization that is currently ongoing. Additionally, the low density CNT/Si hybrid structure makes slurry preparation tenuous using the typical 8-10% binder content normaly used in commercial electrodes. Use of high binder (~40-50 wt.%) contents during slurry preparation of CNT/Si structures increases the weight and volume of the electrode. Therefore, efforts were also focused at synthesizing *nc*-Si or *a*-Si based hybrid structure onto graphite instead of CNT using thermal cracking of Si precursors followed by high energy mechanical milling-a process simpler than the two step CVD. This will result in improved strength and final nanocomposite density.

Approach

To meet the technical targets, our approach is to explore inexpensive Si and C based composite or hybrid nano-structured electrodes exhibiting 1) an electrochemical potential a few hundred mV above the potential of metallic Li, and 2) a capacity of at least ~1,000mAh/g or greater. To achieve these goals, we focused on exploring novel low cost approaches to generate nano-scale hetero-structures comprising nano-structured Si or amorphous Si and a variety of carbons forms derived from graphitic carbon as well as CNT. A detailed study of these Si/C based composite anodes has already been recently presented at the 2009 DOE annual review.

In 2009 as well as 2010, a cost effective simple two-step CVD processes has been employed to synthesize hybrid Si/CNT nano-structures. The multi-wall carbon nanotubes (MWNT) were first synthesized on quartz using a solvent and catalyst sources, respectively. Deposition of Si on CNTs has been achieved by cracking the Si precursor in the temperature range of 723K-1,023K. Under the experimental conditions used, the CNTs grow perpendicular to quartz covered with Si nano-clusters deposited directly on CNT at defined spacing. On the other hand, *a*-Si/Gr nanocomposite has been synthesized using HEMM of *nc*-Si or *a*-Si, obtained by thermal decomposition of Si based precursor, with graphite in the presence of polyacrylonitrile (PAN). The milled powder was thermally treated at 773 and 1,073K for 6h in order to decompose the PAN to form the PAN based carbon, which is expected to anchor the graphite to *a*-Si and improve its interfacial strength.

These promising systems were tested in half cells using metallic lithium as both counter and reference electrodes. Rate capability, long term cyclability, including origin and state of the SEI layers were investigated.

Results

Detailed micro-structural study of Si/CNT hybrid nanostructure synthesized by CVD techniques. It is evident from high resolution TEM image (Figure V- 67(a)) that a distinct interfacial layer is formed between the CNT and the *nc*-Si particle. The composition of the interfacial layer has been studied by electron-energy-loss spectroscopy (EELS) measurements on the CNT, Si nanoparticle, and the interface. EELS spectra collected at the CNT, shown in Figure V- 67(b), demonstrate two peaks, 298eV and 325eV, both of which are attributed to the energy loss peaks of the π bonds and σ bonds of the carbon. On the other hand, the EELS spectra collected at the center of the Si particle matches well with that of $L_{2,3}$ edges for pure Si, which start at ca 100eV, followed by a broadened region. It is evident for Figure V- 67(c) that the EELS spectra acquired from the interfacial region between the Si particle and CNT corresponds to that of an

amorphous carbon. This clearly indicates the presence of an amorphous carbon interlayer serving to tether the Si nanodroplets to the underlying CNT. The anchoring of the Si nanoclusters to the underlying CNTs by the amorphous carbon interface layer is likely a key factor contributing to maintaining the Si clusters in contact with the CNTS during the first 20 cycles.

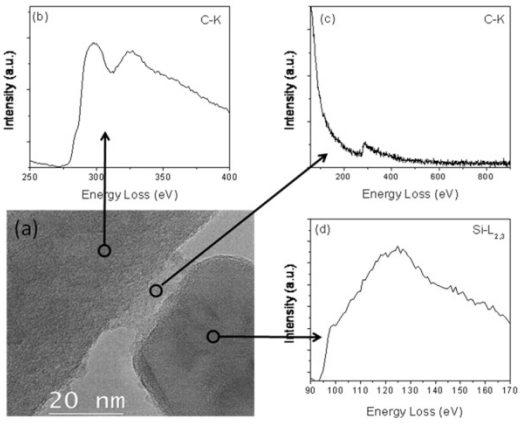

Figure V- 67: (a) HR-TEM image of nc-Si/CNT. EELS spectra of (b) CNT, (c) interface and (d) Si.

The cycling data of the Si/CNT nanostructures up to 100 cycles (Figure V- 68) however, indicate a rapid fade in capacity from cycles 25 to 50 (~1.3% fade per cycle between cycles 25 and 50) where the capacity drops to ~ 1250 mAh/g, and then gradually stabilizes to ~1,000mAh/g (~0.4% of fading rate from cycle 50 to 100). The reasons contributing to this drop in capacity are at present unknown but could relate to a number of factors such as: (1) weakening of the Si-CNT interface during long term cycling leading to detachment of the Si nanodroplets from the CNT, or (2) fragmentation of the Si nanodroplets attached to the CNT after the initial 20 cycles. Further detailed investigation into the causes contributing to the capacity fade observed during prolonged cycles beyond the initial 25 cycles is warranted and is currently under way. The two step CVD process to synthesize CNT followed by deposition of *nc*-Si on CNT, though promising, requires optimization that is currently in progress.

Synthesis of *a*-Si/C nanocomposite by thermal decomposition of Si precursor followed by HEMM. In 2009 reports, the excellent electrochemical performance of *a*-Si and C nanocomposite thin films deposited on Cu foil using rf magnetron sputtering was reported. The *a*-Si/C thin film showed high reversible specific capacity with low irreversible loss (~20%) and excellent cyclability up to 100 cycles with a fade in capacity ~0.03% loss per cycle. In order to study the rate capability, the *a*-Si/C thin film composite anode was discharged/charged at varying rates from C/2 to 3.6C. The variation of specific capacity and coulombic efficiency with cycle number for different C rates, plotted in Figure V- 69, demonstrated the expected reduction in reversible capacity with increasing C rates. The capacity retained at the discharge/charge rate of 3.57C is ~4,600mAh/cm^3 which is ~75% of the capacity at C/2. These data indicated that the *a*-Si/C nanocomposite could lead to promising anode materials for use in Li-ion batteries and may be a suitable candidate for high discharge/charge rate applications such as in plug-in hybrids.

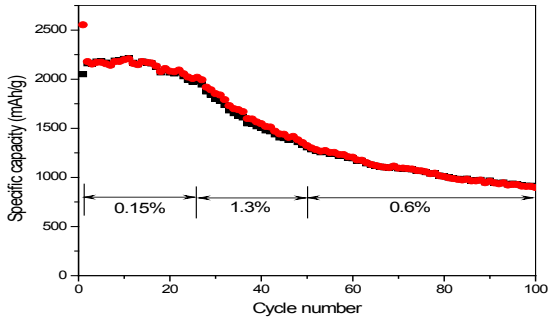

Figure V- 68: Discharge/charge capacity plot of *nc*-Si/CNT.

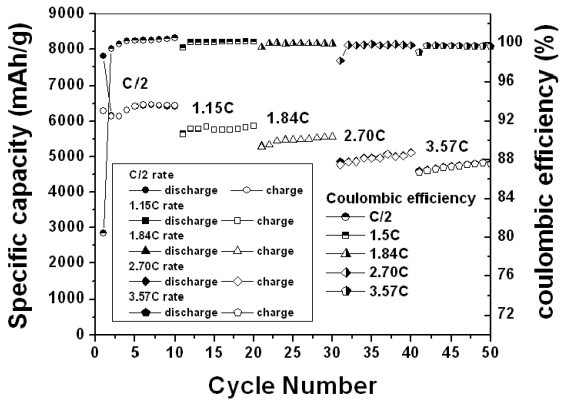

Figure V- 69: Variation of specific capacity and coulombic efficiency *vs.* cycle number of *a*-Si/C thin film anode.

In order to exploit the *a*-Si/C nano-structural features of thin films for high energy application, a low cost large scale manufacturing process of nanostructured *a*-Si/C needs to be developed. Therefore, efforts were focused on synthesizing nanostructured *a*-Si/C architectures using thermal cracking of Si precursors deposited onto graphite followed by HEMM with PAN and excess graphite. The as-deposited *a*-Si on graphite alone shows an impressive 1st cycle discharge and 1st cycle charge capacity of ~2,400 and ~2,150mAh/g, respectively, with a promising irreversible loss ~12% when cycled at ~C/7 rate. However, a rapid fade in capacity (1-2% fade in capacity per cycle) is observed for the *a*-Si deposited on graphite powder. In order to improve the cyclability of *a*-Si/Gr, the nanocomposite was mechanically milled with excess

graphite in the presence of PAN. The milled powder was thermally treated at 773K and 1,073K for 6 hours in order to decompose the PAN to form PAN based carbon, which was expected to anchor the graphite to *a*-Si and improve its interfacial strength. The XRD patterns of mechanically milled *a*-Si/Gr and the heat treated powder, provided in Figure V- 70, clearly shows the retention of *a*-Si up to 773K and transforming to nanocrystalline Si when further heated to 1073K. The specific capacity vs. cycle number of *a*-Si/C nanocomposite synthesized at 773K, shown in Figure V- 71, shows a 1st cycle discharge capacity ~1,400mAh/g and 1st cycle charge capacity ~1,000mAh/g cycled at C/3 rate. The *a*-Si/C nanocomposite shows excellent capacity retention (0.1% capacity loss per cycle) up to 50 cycles. A detailed analysis of the electrochemical results as well as detailed structural investigation of the *a*-Si/C will be presented in future reports.

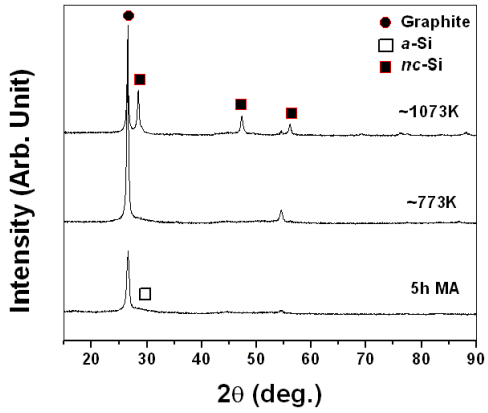

Figure V- 70: XRD patterns of *a*-Si/Gr nanocomposite after 5h of MA and after thermal treatment at 773K and 1073K.

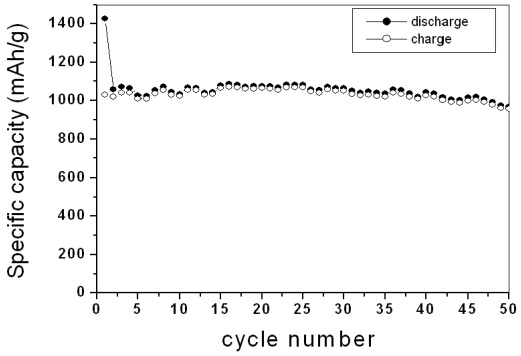

Figure V- 71: variation od specific capacity vs. cycle numbers of *a*-Si/C composite cycled at C/3 rate.

Conclusions and Future Directions

Amorphous or nanocrystalline Si has been successfully synthesized by thermal cracking of Si based precursors. The above synthesis process has been used to synthesize hybrid Si/CNT composite as well as *a*-Si/Gr composite. The *nc*-Si/CNT composite structure is synthesized using a simple cost effective CVD process in which the CNTs are first synthesized vertically aligned on quartz with defined spacing between each individual CNT. Subsequently, Si nano-particles are homogeneously deposited on CNT. The CNT functions as a flexible mechanical support for strain release offering an efficient conducting channel while the nano-structured Si provide the high capacity. It is demonstrated that the hybrid Si/CNTs exhibit high reversible capacity of ~2,000mAh/g with very little fade in capacity ~0.3% per cycle over 25 cycles. On the other hand, the *a*-Si/Gr nanocomposite is synthesized using HEMM of *nc*-Si or *a*-Si and graphite with PAN followed by thermal treatment at 773K. The *a*-Si/Gr composite shows a high reversible capacity ~1,000mAh/g and excellent capacity retention up to 50 cycles with an irreversible loss ~25%. The proposed approach affords a very facile strategy for the fabrication of next generation anodes exhibiting high energy density and cycle life.

Future work will be dedicated to improve the structural stability of Si/CNT hybrid structures above 25 cycles. In addition, detail structural investigation and electrochemical properties of *a*-Si/C will be studied in future. In this direction a hybrid nano-structure consisting of Si nanowire or nanotube along with CNT will be synthesized directly on copper substrates by the CVD approach to improve the mechanical properties and the electronic conductivity of the hybrid structures. In addition, scale up activities using *a*-Si/C composite and Si/CNT hybrid structures will be initiated and performed.

FY 2010 Publications/Presentations

1. W. Wang and P. N. Kumta, "Hybrid Silicon/Carbon Nanotube Heterostructures: Novel Reversible High Capacity Lithium battery anodes", ACS Nano, 4 (2010) 2233-2241.
2. W. Wang and P. N. Kumta, "Vertically Aligned Silicon/Carbon Nanotube (VASCNT) Arrays: Hierarchical Anodes for Lithium-ion Battery" Small (2010) under review.
3. R. Teki, M. K. Datta, R. Krishnan, T. C. Parker, T. M. Lu, P. N. Kumta and N. Koratkar, "Nanostructured Silicon anodes for lithium-ion rechargeable batteries" Small, 5 (2009) 2236-2242..
4. M. K. Datta and P. N. Kumta, "Thin film a-Si/C composite anode for lithium-ion batteries" (submitted to Electrochim. Acta.)
5. Presentation at the 2009 DOE Annual Peer Review Meeting.

6. P.N.Kumta, "Nanostructured Electrochemically Active Materials — Panacea to the Energy Storage Gridlock", IISc, India, July 13, 2009 (Invited).
7. P.N. Kumta, M. Datta, W. Wang, "Nanostructured Materials and Heterostructures: Prospects for New Anodes in Li-Ion Batteries", MS&T 2009, Pittsburgh (invited).

V.C.2 Interfacial Processes - Diagnostics (LBNL)

Robert Kostecki

Environmental Energy Technologies Division
Lawrence Berkely National Laboratory
1 Cyclotron Road, MS 90-3026D
Berkeley, CA 94720
Phone: (510) 486-6002; Fax: (510) 486-5454
E-mail: r_kostecki@lbl.gov

Start Date:October 1, 2009
Projected End Date: September 30, 2010

Objectives

- Establish direct correlations between BATT baseline electrodes' interfacial chemistry, morphology, topology, interfacial phenomena, and degradation modes of Li-ion cell.
- Evaluate and improve the capacity and cycle life limitations of intermetallic anodes.
- Determine physico-chemical properties of the SEI i.e., chemical composition, reactions kinetics, morphology, ionic/electronic conductivity etc.
- Investigate electrocatalytic behavior of intermetallic anodes in organic electrolytes
- Characterize degradation modes, improve SEI long-term stability in high-energy Li-ion systems
- Evaluate the effect of surface composition and architecture on electrochemical behavior of the electrode
- Provide remedies to interface instability e.g., new alloys and/or structures, electrolyte additives, co-deposition of other metals etc.

Technical Barriers

- This project addresses the following technical barriers facing the battery technology development effort in the DOE Office of Vehicle Technologies:
- Inadequate Li-ion battery energy (related to cost)
- Poor lithium battery calendar/cycle lifetime for PHEV and EV applications
- Electrode impedance that limits power density
- Need for new advanced battery materials with acceptable specific energy, durability, costs, and safety characteristics

Technical Targets

- Cycle life: 5,000 (deep) and 300,000 (shallow) cycles (40 miles).
- Available energy: 96 Wh/kg (40 miles).
- Calendar life: 15 years.

Accomplishments

- The mechanism of Li+ transport in aluminum was revealed and quantified.
- Higher rate of lithium diffusion in thicker membranes originates from the structural damage to Al matrix.
- Mixed electrolyte/solid solution transport mechanism and shorter diffusion length in Li_xAl phases contribute to this effect.
- Full assessment of interfacial processes on Sn electrode was completed.
- *In situ* studies revealed that an effective SEI layer never forms on polycrystalline Sn in EC-DEC $LiPF_6$ electrolytes.
- The mechanisms of interfacial processes were determined and characterized.
- Effective strategies to suppress unwanted surface reactions on Sn electrodes were proposed.
- Bulk and surface characterization of a $LiMnPO_4$ electrode was completed.
- $LiMnPO_4$ chemical instability upon delithiation was observed and characterized.
- Formation of surface films on $LiMnPO_4$ upon charging was observed and characterized.

✧ ✧ ✧ ✧ ✧

Introduction

A primary aim of this project is to develop and use advanced diagnostic techniques to characterize basic physico-chemical properties of electrode active and passive components that are being developed for use in PHEV and EV applications. The focus of this task is to correlate fundamental interfacial processes that occur in Li-ion batteries with the system electrochemical performance. The diagnostic evaluation of composite and model electrodes are used to determine cell failure mechanisms, anticipate the system lifetime as well as to suggest new approaches to design more-stable materials, composites and electrodes.

Approach

The main focus of this research project involves the development and application of new instrumental techniques and novel enabling methodologies to understand the mechanism of operation of Li-ion battery systems. Powerful and adequate analytic tools must be developed and used to characterize materials and active and passive cell components. *in situ* enhanced spectroscopic and microscopic techniques as well as standard post-test analyses are applied to investigate the morphology, topology, structure, and composition changes of electrode materials that accompany cell cycling.

This project employs the following specific research approaches:

1. Adopt and improve and use an electrochemical cell of the Devanathan-Stachurski type to study mass and charge transfer mechanism in intermetallic anodes.
   - Develop a time-dependent mass transport model to validate the observed experimental behavior and determine Li transport parameters in aluminum.
   - Characterize surface processes in aluminum anodes
2. Apply *in situ* and *ex situ* Raman and FTIR spectroscopy, spectroscopic ellipsometry, AFM, SEM, HRTEM, and electrochemical techniques to detect and characterize surface processes at intermetallic anodes.
   - Use model Sn electrodes to detect and monitor early stages of the SEI formation in various electrolytes.
   - Determine the nature and kinetics of surface phenomena and their implications for long–term electrochemical performance of the intermetallic anodes in high-energy Li-ion systems.
3. Apply *in situ* and *ex situ* Raman and FTIR spectroscopy, and electrochemical techniques to detect and characterize chemical and structural changes in $LiMnPO_4$, and interfacial processes on composite $LiMnPO_4$ cathodes (HPL).
   - Develop an experimental procedure for surface carbon removal through an O_2-plasma etching process to allow microRaman probing of $LiMnPO_4$ composite cathodes.
   - Design and construct a spectro-electrochemical cell for *in situ* FTIR-attenuated total reflectance (ATR) microscopy measurements.

Results

Our first objective was to apply a Devanathan-Stachurski type cell to investigate lithium diffusion through ultra thin-layer (<20 nm) Al and Sn metallic anodes. In this configuration, one side of the membrane is cathodically polarized (A-side) to serve as an entry surface for Li whereas the other side is held at potentials at which Li_xMe (B-side) delithiates. Li diffusion is measured from the time delay between the cathodic polarization at the A-side and the anodic current response at the B-side of the membrane.

Figure V- 72 shows the typical anodic current-time responses observed in compartment B after potentiostatic polarization of the Al membranes in compartment A. The time delays for 25, 100 and 250 µm thick Al membranes were 1535, 11797, and 42340 s, respectively. The corresponding calculated diffusion coefficients (D) are in relatively good agreement with previously reported D values for Li in Al, which vary between 5 and 50 x 10-10 $cm^2\ s^{-1}$, but surprisingly, D tends to increase with increasing thickness. This can be explained by the formation of cracks and crevices during the course of alloying with Li. The apparent higher rate of Li diffusion in thicker membranes originates from the mixed electrolyte/solid solution transport mechanism.

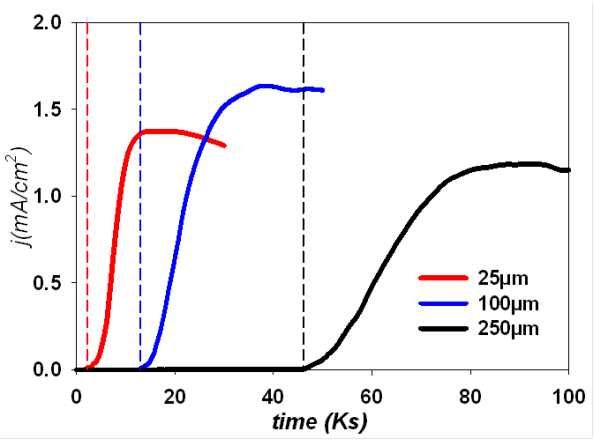

Figure V- 72: Anodic current-time responses observed in compartment B for different Al thicknesses.

A systematic investigation of surface and bulk phenomena of model $LiMnPO_4$ cathodes through spectroscopic observation during charge-discharge processes was carried out. Transmission FTIR spectra of a composite $LiMnPO_4$ electrode show three primary peaks in the 900-1,100 cm-1 range assigned as PO_4^{3-} vibrations. These peaks become broader after charging the electrode and shift down in energy. The broadening can be attributed to the increase in disorder of the delithiated active material, $MnPO_4$, due to the Jahn-Teller effect of Mn^{3+} in a high-spin, octahedral environment.

FTIR-ATR spectra of the surface of a composite $LiMnPO_4$ electrode at different stages of charging (C/20 rate) shows gradual changes in the phosphate vibrations. The changes in the primary phosphate peak positions indicate conversion to $MnPO_4$. After 149 mAh/g of charge, analysis of the phosphate region suggests other products are present on the electrode surface in addition to

$MnPO_4$. There is evidence of a surface film formation from decomposed electrolyte.

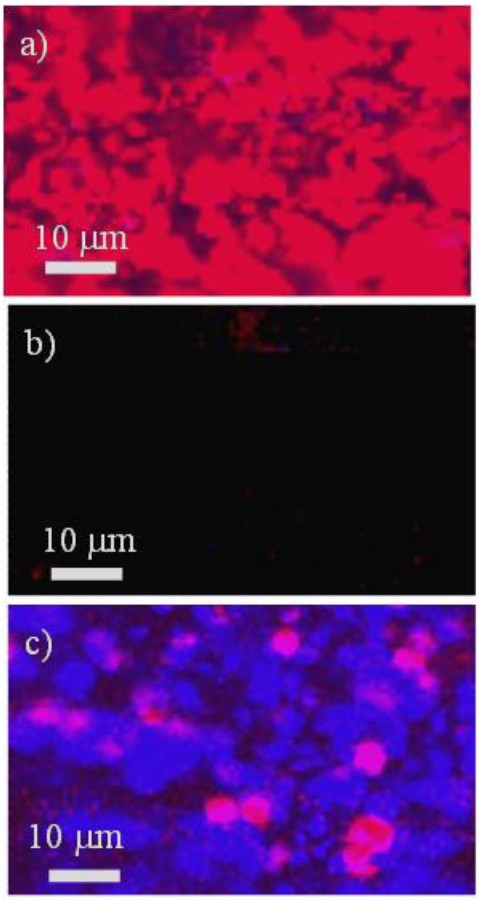

Figure V- 73: Raman images of a $LiMnPO_4$ electrode displaying areas with strong $LiMnPO_4$ (red) and $Li_4P_2O_7$ (blue) peak intensities a) after an O_2 plasma etch, b) followed by a full charge, and c) full discharge.

Raman images indicate the $LiMnPO_4$ active material is exposed over the majority of the etched electrode area (Figure V- 73(a)). After electrochemically charging the electrode (181 $mAhg^{-1}$), the PO_4 Raman bands mostly disappear without the formation of any new peaks (Figure V- 73(b)). This is consistent with the formation of $MnPO_4$ since we do not observe any distinct Raman features for chemically delithiated $LiMnPO_4$ powder samples. However, it is contrary to the spectral behavior observed for $LiFePO_4$, suggesting a slightly different reaction mechanism. After discharging the electrode (129 $mAhg^{-1}$), $LiMnPO_4$ reappears in some areas of the electrode, but most spectra are dominated by a set of new peaks at 390, 545, 708, 1036, and 1090 cm^{-1}, assigned to $Li_4P_2O_7$ (Figure V- 73(c)). This indicates that Li_xMnPO_4 is not chemically stable in the presence of electrolyte and undergoes transformation to $Li_4P_2O_7$ upon lithiation during discharge process. These reactions likely can be responsible for a significant reduction in the performance of $LiMnPO_4$ cathodes. Thus the long-term cycleability of $LiMnPO_4$ cathodes depends on the uniform carbon coating that impedes the decomposition process of Li_xMnPO_4 upon lithiation.

Conclusions and Future Directions

- Careful micro- and nano-design and advanced manufacturing methods of intermetallic materials is required to improve their rate performance and stability in Li-ion battery applications
  - Observed anomalies in the thickness dependence of the permeation rate of Li in Al suggest a more complicated transport mechanism.The amount of mechanical stress is higher in thicker electrodes, which leads to more structural damage.
  - The apparent higher rate of lithium diffusion in thicker membranes originates from the mixed electrolyte/solid solution transport mechanism
- It is critical for the long-term electrochemical performance of intermetallic anodes to suppress unwanted surface reactions. Coordinated electrode and electrolyte design must be carried out to achieve interfacial stability of Sn anodes in Li-ion battery applications.
  - *in situ* studies revealed that the nature and kinetics of surface reactions are strongly dependent on the electrode and electrolyte.
  - Effective SEI layer never forms at the surface of polycrystalline Sn in EC-DEC $LiPF_6$ electrolytes
  - Sn interface instability in organic carbonate electrolytes can be remedied by careful optimization of the electrolyte composition and use of additives that (re)produce a stable SEI layer.
- Instability of delithiated Li_xMnPO_4 likely precludes this material from achieving commercial viability without developing routes for stabilizing the active material.
  - Li_xMnPO_4 is unstable vs. $LiPF_6$: organic carbonate electrolytes.
  - $MnPO_4$ forms early during charging but then tends to undergo chemical and structural changes to convert to $Li_4P_2O_7$ after the full cycle of Li extraction and insertion is completed.
  - Surface film forms at the exposed Li_xMnPO_4 active material. No surface film was detected on carbon black additive.
- Continue studies of mass and charge transfer mechanisms at the electrode-electrolyte interface
  - Develop multi-task spectro-electrochemical cell of the Devanathan-Stachurski type to study *in situ* and model kinetics of Li intercalation and

diffusion through anode and cathode materials (V. Srinivasan)

- Carry out quantitative measurements of the mass and charge transfer across electrode/electrolyte interfaces.

- Design and apply *in situ* and *ex situ* experimental methodologies to detect and characterize surface processes in Li-ion intermetallic anodes
  - Fundamental *in situ* spectroscopic ellipsometry in conjunction with AFM and FTIR/Raman surface analysis studies of the SEI layer formation on model monocrystal Sn and Si electrodes will be carried out
  - Cooperate with the BATT Interfacial Studies Group to investigate the effect of material structure, morphology, topology on formation of the SEI layer
  - Investigate correlations between properties of the SEI layer and long-term electrochemical performance of Li-ion electrodes
- Diagnostic evaluation of detrimental phenomena in high-voltage (>4.3V) cathodes
  - Apply *in situ* and *ex situ* Raman and FTIR spectroscopy to detect and characterize surface and bulk processes in high voltage cathodes
  - Evaluate the effect of electrode passive additives and impurities on the electrochemical performance and long-term stability of the composite cathodes.

FY 2010 Publications/Presentations

1. Kristin Persson, Vijay A. Sethuraman Laurence J. Hardwick, Yoyo Hinuma, Ying Shirley Meng, Anton van der Ven, Venkat Srinivasan, Robert Kostecki, and Gerbrand Ceder, "Lithium Diffusion in Graphitic Carbon: Supporting Information" Journal of Physical Chemistry Letters, 1 (2010) 1176
2. Marek Marcinek, Laurence J. Hardwick, Grazyna Z. Zukowska, Robert Kostecki, Microwave plasma chemical vapor deposition of graphitic carbon thin films", Carbon, 48 (2010) 1552
3. Vijay A. Sethuraman, Laurence J. Hardwick, Venkat Srinivasan, Robert Kostecki, "Surface structural disordering in graphite upon lithium intercalation/deintercalation", Journal of Power Sources 195 (2010) 3655
4. Elad Pollak, Ivan T. Lucas, Robert Kostecki, "A study of lithium transport in aluminum membranes", Electrochemistry Communications 12 (2010) 198
5. Ivan T. Lucas, Elad Pollak, Robert Kostecki, *in situ* AFM studies of SEI formation at a Sn electrode", Electrochemistry Communications 11 (2009) 2157
6. Robert Kostecki, Ivan T. Lucas, Elad Pollak, „ *in situ* Studies of Interfacial Processes on a Sn Anode", International Battery Association Meeting Pacific Power Source Symposium 2010, January 11-15, 2010, Waikoloa, Hawaii, USA, (Invited talk)
7. Elad Pollak, Ivan.T. Lucas and Robert Kostecki, "A Study of Lithium Transport in Aluminum Membranes", Electrochemistry Gordon Research Seminar (GRS), January 9-10, 2010, Ventura CA, USA.
8. Frank McLarnon and Robert Kostecki, „Studies of the Mechanism of Graphite Structural Degradation in Li-ion Cell Anodes", The 50th Battery Symposium in Japan, International Session on Battery Technology for the Next 50 Years, November 30 – December 2, 2009, Kyoto, Japan. (Invited talk)
9. Marie Kerlau, Jinglei Lei Marek Marcinek, Frank McLarnon and Robert Kostecki, "Studies of Local Interfacial Phenomena in Li-ion Batteries", The 50th Battery Symposium in Japan, International Session on Battery Technology for the Next 50 Years, November 30 – December 2, 2009, Kyoto, Japan. (Invited talk)
10. Robert Kostecki, Ivan T. Lucas, Elad Pollak, „Interfacial studies of intermetallic anodes for Li-ion batteries", The 2nd International conference on Advanced Lithium Battery for Automobile Applications", November 25 – 28, 2009, National Center of Sciences, Tokyo, Japan. (Invited talk)
11. L.J. Hardwick, V.A. Sethuraman V. Srinivasan, and R. Kostecki, "Studies of the Mechanism of Lithium Diffusion in Graphitic Anodes", 216th ECS Meeting, October 4-9 2009, Vienna, Austria.
12. Marek Marcinek, Wioletta Wosko, Emilia Dudek, and Robert Kostecki, „Manufacturing of lithium-ion batteries anodes by microwave plasma assisted technique", 4th Int'l. Conf. on Polymer Batteries and Fuel Cells (PBFC 2009), August 2-6, 2009, Yokohama, Japan
13. L.J. Hardwick, V. A. Sethuraman, V.Srinivasan, and R. Kostecki, "A Study of the Mechanism of Lithium Transport in Graphite", LiBD-4, 2009 – Electrode materials, Arcachon, France 20-25 September 2005
14. R. Kostecki, I. T. Lucas, E. Pollak, „ *in situ* Studies of Interfacial Processes on Sn Anodes in Organic Electrolytes", The 60th Annual Meeting of the International Society of Electrochemistry, August 16-21, 2009 Beijing, China
15. I. T. Lucas, E. Pollak and R. Kostecki, „ *in situ* Studies of SEI Formation on Sn Anodes", 215th ECS Meeting in San Francisco, May 27, 2009
16. Kostecki, Robert; Majumdar, Arunava; Kim, Dong-Kwon; Duan, Chuanhua; Huang, Baoling , "Battery with Amphoteric Ion Exchange Layers ", Invention Disclosure IB-2719.

V.C.3 Nanostructured Metal Oxide Anodes (NREL)

Anne C. Dillon
National Renewable Energy Laboratory
1617 Cole Blvd.
Golden, Colorado 80401
Phone: (303) 384-6607; Fax: (303) 384-6655
E-mail: anne.dillon@nrel.gov

Subcontractor:
University of Colorado, Boulder, CO

Start Date: October 2007
Projected End Date: September 2010

Objectives

- Explore viable routes towards stabilizing metal oxide nanostructures such that durable high-rate capability is achieved.
- Develop simple fabrication methods for inexpensive iron oxide nano-structures (volume expansion≥100%) and demonstrate durable high capacity at high rate.
- Expand mechanistic knowledge as to why high-rate capability may be achieved for routes reported here: atomic layer deposition (ALD) coatings and employing carbon single-wall nanotubes (SWNTs) at 5 wt.% loading to replace conventional binder and conductive additives.

Technical Barriers

Many high capacity materials suffer from rapid capacity fade during cycling, especially at high-rate, due to volume expansion and subsequent structural changes that lead to a loss in electrical conductivity. Unless these issues are addressed, it will be difficult to develop materials suitable for next-generation electric vehicles. It is also important to rely on inexpensive, abundant materials and to implement scalable industrial processes for materials / electrode fabrication.

Technical Targets

- Demonstrate methods to stabilize high capacity materials at high rate such that the 40-mile PHEV targets and/or EV targets may be met.
- Obtain mechanistic understanding of how high capcity materials are stabilized such that the methods may be employed for a variety of technologies.

Accomplishments

- ALD coatings on composite MoO_3 electrodes fabricated with acetylene black (AB) and polyvinylidene fluoride (PVdF) enabled durable capacity of 900 mAh/g at C/2 and 600 mAh/g at 5C.
- Nano-scratch and indentation tests of ALD Al_2O_3 coated and uncoated electrodes demonstrated ~8Å ALD coatings enable significantly better adhesion of composite electrodes to the copper current collector.
- Paired the ALD coated MoO_3 anode with the ANL Li-excess ($0.5Li_2MnO_3 \bullet LiMn_{0.31}Ni_{0.44}Co_{0.25}O_2$) cathode and demonstrated a high capacity full cell (~ 150 mAh/g) with the Li-excess cathode compensating for the first irreversible capacity loss in the MoO_3.
- Developed a simple hydrothermal technique for the fabrication of iron oxide nanoparticles, as Fe is more abundant and less expensive than Mo.
- Developed a binder-free technology where 5 wt.% SWNTs served as both the conductive additive and a flexible net for Fe_3O_4, enabling stable high capacities of 1,000 mAh/g at 1C (~2,000 mAh cm-3), 800 mAh g-1 at 5C and ~600 mAh g-1 at 10C.
- Demonstrated a similar binder-free technology for the SUNY Binghamton $LiNi_{0.4}Mn_{0.4}Co_{0.2}O_2$ cathode enabling durable high capacity of ~ 130 mAh g-1 at 5C and ~120 mAh g-1 at 10C, for over 500 cycles.
- X-ray diffraction (XRD), tranmission electron microscopy (TEM) and Raman sectroscopy were employed to show that significant charge transfer, indicative of a chemical bond between the SWNTs and active materials, enables the high rate capability.

✧ ✧ ✧ ✧ ✧

Introduction

In our early work we demonstrated that thin film MoO_3 nanoparticle electrodes (~2 µm thick) have a stable reversible capacity of ~630 mAh/g at C/2. When fabricating more conventional electrodes (~15 µm thick) with a conductive additive and binder, an improved reversible capacity of ~1,000 mAh/g was achieved but unfortunately, the rate-capability was significantly decreased with stable cyling occurring at C/10. This year, in order to achieve high-rate capability for the thicker electrodes we applied a thin atomic layer deposition (ALD) coating of Al_2O_3 to allow for the high volume expansion and prevent mechanical degradation. Nano-scratch and indentation studies were employed to show

that ALD coatings enabled significantly better adheshion to the copper current collector. Also the ALD coated electrode was paired with the ANL Li-excess cathode material to form a high capacity full cell and to compensate for the first cycle irreversible capacity loss in the MoO_3 electrode.

More recently, we have focused our work on iron oxide nanostructures, as iron is an inexpensive, abundant and non-toxic material. Furthermore, we have synthesized binder-free, high-rate electrodes. The electrodes contain Fe_3O_4 nanorods as the active material and 5 wt.% SWNTs as the conductive additive. A stable capacity of ~1000 mAh/g (~2,000 mAh/cm^3) at C rate was demonstrated with high-rate capability of 800 mAh/g at 5C for 100 cycles and 600 mAh/g at 10C. These same techniques were employed to enable the SUNY Binghamton $LiNi_{0.4}Mn_{0.4}Co_{0.2}O_2$ cathode to have capacities of ~ 130 mAh g^{-1} at 5C and nearly 120 mAh g^{-1} at 10C, both for over 500 cycles. Various characterization techniques indicated the remarkable rate capability was observed because the SWNTs may actually bind to the active metal oxide materials.

Approach

NREL employed two different methods to enable high volume expansion materials (≥ 100%) to cycle reversibly at high rate. Although both materials suffer from high hysteresis in the voltage charge/discharge profiles (~ 1V), making them impractical for vehicular applications, the methods employed here are suitable for a variety of materials that could enable PHEV and EV technologies.

Results

MoO_3 Electrodes. Last year, we reported that MoO_3:PVdF:AB (70:20:10) electrodes exhibited nearly the theoretical capcity of 1000 mAh/g at C/10. (The MoO_3 nanoparticles are made from a scalable hot wire chemical vaporization (HWCVD) technique). This year we employed ALD to coat the fully fabricated electrodes with thin layers of Al_2O_3 (Å-level control) in order to demonstrate significantly improved rate capability. Self-limiting ALD is performed using trimethylaluminum (TMA) and H_2O precursors. Unlike wet-chemical techniques, ALD precursors can easily traverse tortuous paths within porous structures, providing a uniform coating on all exposed surfaces. Likewise, by using a rotary reactor, uniform growth can also be achieved on individual particles. One ALD cycle consists of TMA exposure, a purge, and H_2O exposure. Each complete deposition cycle of ALD grows ~1-2 Å of Al_2O_3 on porous surfaces and powders. Figure V- 74(a) compares the cycling performance of a bare MoO_3 electrode with a fully fabricated electrode coated with ~ 8 Å of Al_2O_3 and an electrode fabricated from MoO_3 nanoparticles that were coated prior to electrode assembly. Note that for the coated fully fabricated electrode a reversible capacity of 900 mAh/g was achieved at C/2. The uncoated electrode exhibits capacity fade after only 15 cycles. The elctrode

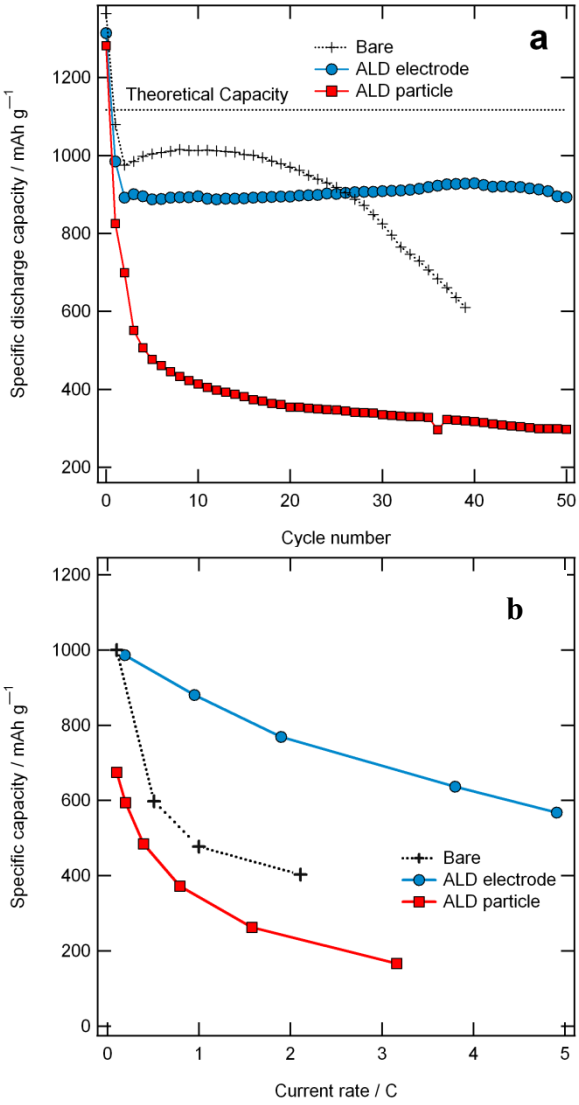

Figure V- 74: Electrochemical performance of 70:20:10, MoO_3:PVdF:AB electrodes: bare, coated with ~ 8Å ALD Al_2O_3 and MoO_3 particles coated prior to electrode fabrication for a) cycling stability and b) rate capability.

fashioned from pre-coated MoO_3 particles shows immediate capacity fade presumably due to the loss of electrical conductivity, since the particles are completely surrounded by the insulating alumina. This demonstrates the importance of full elctrode coating by a simple process such as ALD that is suitable for roll-to-roll processing. We also note that the capacity decrease for the coated electrode is consistent with the loss expected for the thin coating on these ~ 20 nm-sized MoO_3 particles showing that Å level control will be required for all nanoparticle electrodes. Figure V- 74(b) compares the rate capability of

the aforementioned electrodes demonstrating that the coated composite electrode has a capacity of ~ 600 mAh/g at 5C.

Upon stabilizing the high volume expansion MoO_3 anodes with the thin ALD coatings we then collaborated with ANL to build a full cell wit the ANL Li-excess cathode and the ALD coated anode. Importantly, we demonstrated that the excess Li in the ANL cathode could be used to compensate for the first cycle irreversible capacity loss in the MoO_3 anode, eliminating the need for pre-lithiation that is not suitable for industrial processes. It was also shown that the Al_2O_3-coating on the MoO_3 electrode increased the capacity retention of the full cell by ~33% after 20 cycles (Figure V- 75).

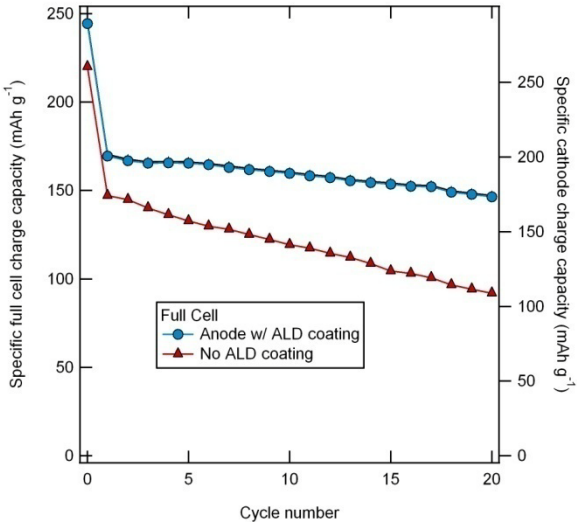

Figure V- 75: Cycling performance of ANL Li-excess and Al_2O_3-coated MoO_3 full cell, with a capacity of ~ 160 mAh/g.

Finally the mechanical properties of MoO_3 composite anodes coated with Al_2O_3 by atomic layer deposition were examined using nano-indentation and scratching. Figure V- 76 displays *in situ* microscope images of a) the uncoated and b) the coated electrodes following a scratch test in which 80 mN of force was applied to the surface of each electrode. The copper current collector was completely exposed with a scratch length of only 250 µm in the uncoated electrode. This corresponds to complete displacement of the 15µm thick electrode. The coated electrode remained virtually undamaged.

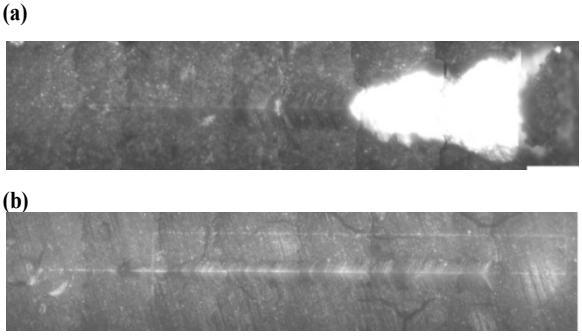

Figure V- 76: Optical images of damage caused by nanoscratching with a load of 80 mN for a) bare and b) 4-Al_2O_3 ALD coated MoO_3 composite electrodes.

Thus, significant improvement in adhesion to the current collector for the ALD coated MoO_3 is observed. This improved adhesion enables enhanced electrical conductivity for these high capacity / high volume expansion materials, suggesting the potential of these coatings for high-energy density Li-ion batteries.

Fe_2O_3 Electrodes. In order to employ abundant, less expensive materials we also synthesized FeOOH nanorods with an inexpensive hydrothermal technique. The nanorods were then suspended with only 5 wt.% of laser-generated, purified SWNTs and vacuum filtration enabled transfer of the composite to the copper current collector. Upon heating to 450°C in Ar, carbothermal reduction caused the FeOOH to be converted to Fe_2O_3 (hematite) The SWNTs were well dispersed and created a flexible net enabling both excellent electronic conductivity and allowing for the high volume expansion of the metal oxides upon Li^+ insertion. Figure V- 77(a) displays a colorized scanning electron microscopy (SEM) image of the SWNTs suspended in the nanotube net. Futhermore, a stable high capacity of 1,000 mAh/g was demonstrated at 1C and importantly durable high rate capability was achieved with a capacity of ~ 800 mAh/g for deep charge/discharge cycles without any voltage holds as shown in Figure V- 77(b). Also a capacity of 600 mAh/g was achieved at 10 C.

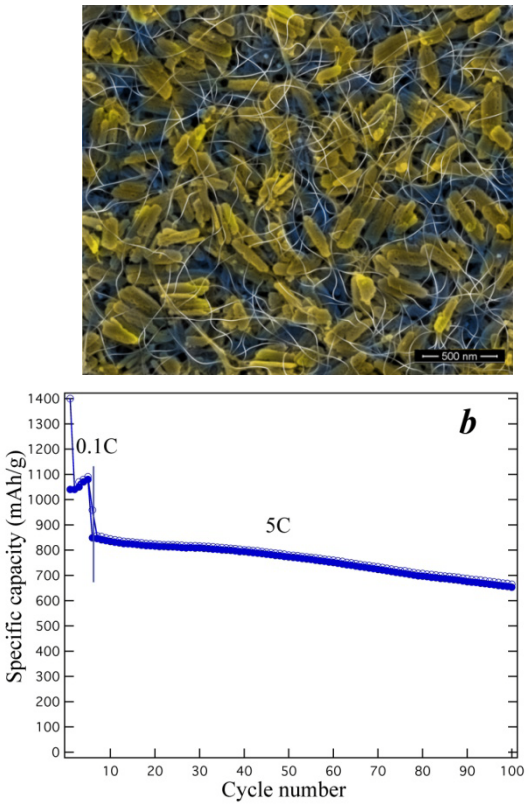

Figure V- 77: a) Colorized SEM image of Fe_2O_3 nanoparticles (yellow/blue) suspended in an SWNT net (white) and b) durable high-rate capability.

$LiNi_{0.4}Mn_{0.4}Co_{0.2}O_2$ Electrodes. The method described above was also demonstrated for cathodes consisting of 5 wt.% carbon SWNTs and $LiNi_{0.4}Mn_{0.4}Co_{0.2}O_2$ (NMCCNT). Figure V- 78(a) displays a TEM image of the NMCCNT composite revealing that a bundle of SWNTs (~8 nm thick) does not simply cross, but rather precisely follows the entire surface of the individual nanoparticles. This suggests a possible chemical-interaction between the SWNTs and the particle surface that would not be obtained with simple mixing. More importantly, the SWNTs enabled enhanced electrical conductivity and also prevented degradation such that high rate capability was demonstrated.

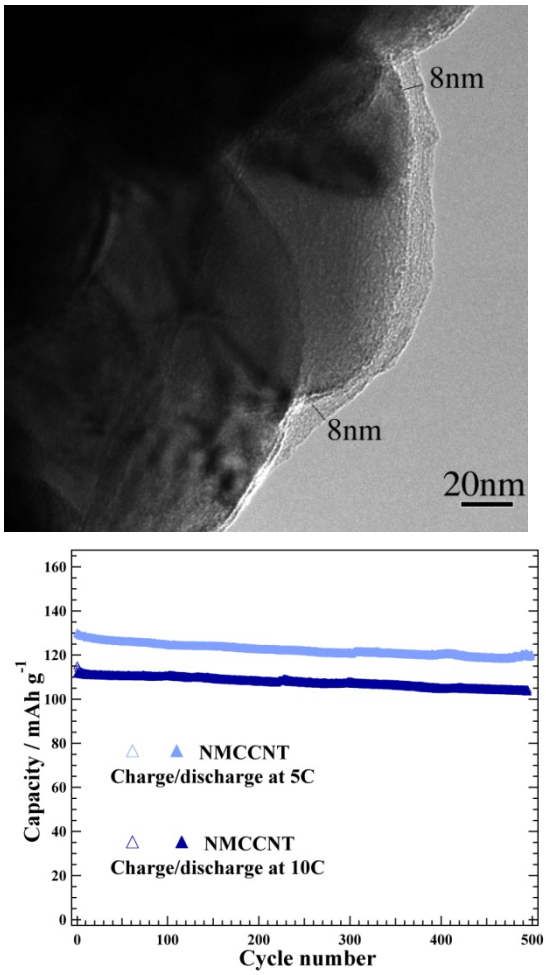

Figure V- 78: a) TEM image of SWNTs conformally following $LiNi_{0.4}Mn_{0.4}Co_{0.2}O_2$ particles b) NMCCNT rate capability.

As shown in Figure V- 78(b) the NMCSWNT electrodes exhibited remarkable rate capability of ~ 130 mAh g^{-1} at 5C and ~120 mAh g^{-1} at 10C, for over 500 cycles, with Li-metal as the counter electrode. At this high rate, 500 cycles is actually at the limit of Li-metal degradation. When fashioned into a conventional electrode with conductive additive and binder the same $LiNi_{0.4}Mn_{0.4}Co_{0.2}O_2$ capacity was only 50 mAh/g at C rate and found to be negligible at 5C.

In addition to the TEM data in Figure V- 78(a) that indicates a strong interaction between the $LiNi_{0.4}Mn_{0.4}Co_{0.2}O_2$ and SWNTs, *in situ* high temperature XRD measuearments performed at ORNL revealed a slight increase in the lattice parameters for the NMCSWNT composite during the heat treatment to fabricate the electrode. The increase in the lattice parameters also suggests that some degree of charge transfer occurs between the SWNTs, and the metal oxide material. The lattice perameters for $LiNi_{0.4}Mn_{0.4}Co_{0.2}O_2$ annealed without the SWNTs were not significantly altered. Finally, Raman spectra were obtained of the purified laser-

generated SWNTs employed prior to and during the fabrication and subsequent electrochemical cycling of the NMCSWNT electrode. The Raman spectra of the C-C stretching vibrations occur between 1,500-1,600 cm^{-1}. Notably, a pronounced shift in the Raman lines was observed in the electrode after annealing. This clearly demonstrates that significant charge transfer occurs and that a chemical bond may be formed. We believe that it is the surface-interaction that further enhances the electronic conductivity of the NMCSWNT electrode. The SWNT signal remains nearly identical after electrochemical cycling confirming the SWNTs are undamaged.

Conclusions and Future Directions

NREL has developed two methods to enable durable high rate capability for high volume expansion and low conductivity materials: (1) ALD coatings that may be deposited with Å-level control and (2) a method to employ 5 wt.% SWNTs that replaces other conductive additives and binders. The methods have been demonstrated for a variety of materials, including commercial materials not discussed here. In future work we will employ the scalable (HWCVD) process to produce amorphous or nanoparticle silicon and will employ ALD coatings to improve the irreversible capacity loss and stabilize the high volume expansion materials in convetional thick electrodes. ALD coatings will also be demonstrated for roll-to-roll processing.

FY 2010 Publications

1. L.A. Riley et al. J. Power Sources 195 (2010) 588.
2. Y.S. Jung et al. J. Electrochem. Soc 157 (20100 A75.
3. L.A. Riley et. al. *ChemPhysChem* 10 (2010) 2124.
4. C. Ban et. al. *Advanced Materials* 22 (2010) E145.
5. Y. S. Jung et al. *Advanced Materials* 22 (2010) 2172.
6. A.C. Dillon *Chemical Reviews* (available on line).
7. L.A. Riley et. al *Applied Physics Letters* (submitted).
8. C. Ban et. al. *Advanced Materials* (submitted).
9. L.A. Riley et. al. *Electrochem. and Solid-State Letters* (submitted).

V.C.4 Search for New Anode Materials (University of Texas)

John B. Goodenough

Texas Materials Institute

ETC 9.102, University of Texas at Austin
Austin, TX 78712
Phone: (512) 471-1646; Fax: (512) 471-7681
E-mail: jgoodenough@mail.utexas.edu

Start Date: October 30, 2009
Projected End Date: September 30, 2011

Objectives

- To design a high-rate insertion anode host giving a voltage 1.0< V <1.6 V vs. Li.
- To explore a new cell design using a solid electrolyte that would allow use of a lithium anode.

Technical Barriers

A carbon or carbon-buffered anode forms an SEI layer that (a) consumes Li irreversibly from the cathode on the first charge, thereby lowering the cell capacity, which is limited by the cathode capacity, and (b) limits the rate of charge before Li^o is plated out on the surface of the anode. The SEI layers forms on any anode having a voltage $V <$ 1.0 V *vs.* Li^o.

Technical Targets

- Identification of a Li insertion host capable of high rates of charge/discharge with a voltage in the window 1.0 < V <1.5 V vs. Li.
- Construction of a test cell to determine the feasibility of a cell having lithium and an organic liquid electrolyte on the anode side of a solid-electrolyte separator and an aqueous cathode on the other side.

Accomplishments

- Identified $TiNb_2O_7$ as a Li-insertion host allowing rapid charge/discharge in the voltage range 1.0 < V < 1.6 V having a capacity of 280 mAh/g at 0.1 C.
- Designed, built, and tested an open-cathode $Li/Fe(NO_3)_3$ test cell that demonstrated the feasibility of the concept and an efficiency superior to that of the Li/Air cell.
- Showed that the commercial $Li_{1.3}Ti_{1.7}Al_{0.3}(PO_4)_3$ solid electrolyte containing Ti(IV) is subject to reduction not only on contact with lithium, but also in the acidic solution of $Fe(NO_3)_3$.
- Designed a closed-cathode test cell and showed the importance of the change in pH of the aqueous cathode with change in the Fe^{3+}/Fe^{2+} ratio. FeO(OH) was shown to precipitate on the solid electrolyte with pH > 2.0. The precipitate not only decreased the active redox couple, it also increased the resistance of the solid electrolyte.

Introduction

Application of the Li-ion battery to the electrical-vehicle (EV) market suffers from two principal technical obstacles that contribute to cost and safety concerns: (1) rate of safe recharge without costly management of the cells of the battery and (2) a limited capacity of a Li-insertion cathode host, which increases the number of cells required for a given power and EV range between recharges. Any anode that gives a voltage $V < 1.0$ V *vs.* Li^o needs to form a passivating solid-electrolyte interface (SEI) layer that conducts Li^+ ions but not electrons. This layer consumes lithium irreversibly from the cathode on the initial charge, and the lithium solid solution range in the cathode is what limits the capacity of a battery cell.

Approach

We have targeted two approaches:

(1) Identification of a Li-insertion anode host giving a voltage $1.0 < V < 1.5$ V *vs.* Li^o since the spinel $Li_4Ti_5O_{12}$ with a $V \approx 1.5$ V *vs.* Li^o is known to provide for fast recharge without plating out of Li^o on its surface, but it has a low capacity.

(2) Use of a new battery strategy in which a solid-electrolyte separator with an organic liquid electrolyte on the anode side has a liquid cathode of high capacity on the other side. Since the solid electrolyte blocks dendrite penetration to the cathode, elemental lithium can be used as the anode.

Results

We have investigated the Ti(III)/Ti(II) and V(III)/V(II) redox couples in sulfides and the Nb(V)/Nb(IV) couple in oxides in the search for a Li-insertion anode host. We found a flat V=1.0 V for $Li_{1+x}VS_2$ (0<x<1), but this system formed an SEI layer. We then identified the $TiNb_2O_7$ host of Figure V- 79, which allows a fast charge without formation of an SEI layer in the voltage range $1.0V < V < 1.6$ V and has a capacity greater than that of the spinel $Li_4Ti_5O_{12}$.

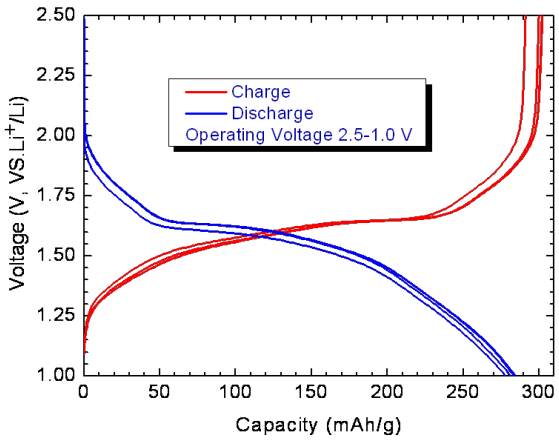

Figure V- 79: Performance of $TiNb_2O_7$ versus Li^+/Li with 1M $LiPF_6$/EC +DMC (1:1) half cell

To investigate the feasibility of our new cell design strategy, we investigated a $Li/Fe(NO_3)_3$ cell. This test cell, Figure V- 80, used a commercially available $Li_{1.3}Ti_{1.7}Al_{0.3}(PO_4)_3$ electrolyte having the NASICON framework. First we investigated a pure aqueous cathode having the reaction

$Li^+ + H_2O + e^- \rightarrow LiOH + 1/2H_2$: 2.2V at discharge
$LiOH - e^- \rightarrow Li^+ + 1/2H_2O + 1/4O_2$: 4.2V at charge

and then $Fe(NO_3)_3$ in water

$Li^+ + Fe(NO_3)_3 + e^- \rightarrow LiNO_3 + Fe(NO_3)_2$: 3.8V at discharge
$LiNO_3 + Fe(NO_3)_2 - e^- \rightarrow Li^+ + Fe(NO_3)_3$: 4.2 V at charge

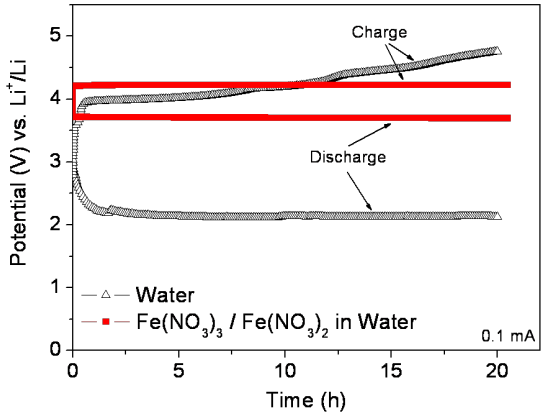

Figure V- 80: The first discharge and charge curves for the pure distilled water and Fe^{3+} / Fe^{2+} redox couples dissolved in water

The voltage difference between discharge and charge of the $Li/Fe(NO_3)_3$ cell could be decreased by increasing the mole content of $Fe(NO_3)_3$ in water and the surface area of the current collector. Although this test showed the feasibility of the concept, the test encountered instability of the solid electrolyte in the presence of a current. The instability was shown to be due to an attack on the Ti(IV) by the acidic cathode.

We subsequently investigated a closed-cathode cell and found that, due to the change in pH with Fe^{3+}/Fe^{2+} ratio, FeO(OH) precipitated on the solid electrolyte with pH > 2.0, Figure V- 81. The precipitate not only decreased the active redox couple, it also increased the resistance of the solid electrolyte. The results clearly highlight the need to identify and fabricate a better solid electrolyte.

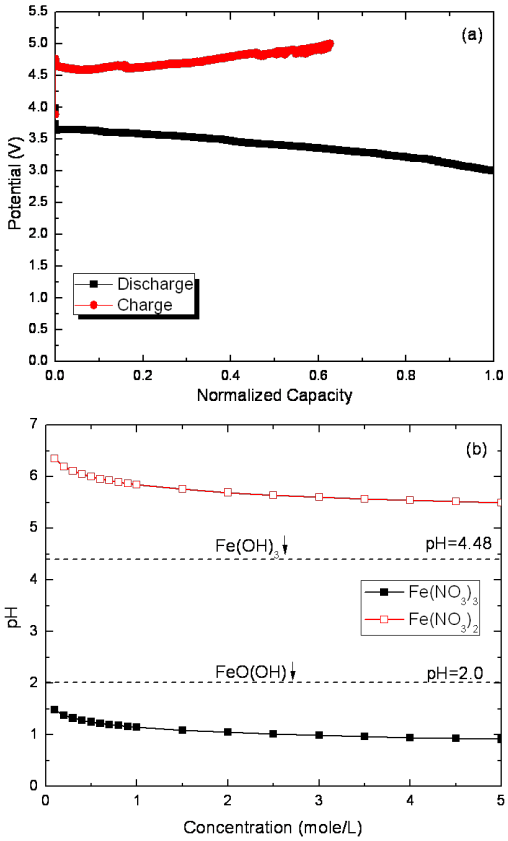

Figure V- 81: (a) Discharge/charge curves of $Li/Fe(NO_3)_3$ within a closed-cathode cell; (b) Hydrolysis of the $Fe(NO_3)_3$ and $Fe(NO_3)_2$ in aqueous solution.

Conclusions and Future Directions

Although we have identified a new, viable Li-insertion host anode that will allow a fast charge, we conclude that an alternative-cell strategy is required if the twin objectives of high voltage with large capacity is to be realized. We have shown that the aqueous cathode can give a large voltage with a better efficiency than the Li/Air cell. However an alternative solid electrolyte and its design need to be developed for long bench and cycle life as well as higher rate capabilities. Since the new strategy would allow for a Na-ion as well as a Li-ion battery, we are pursuing the development and design of better solid electrolytes. Meanwhile, to test the concept further with

the existing commercial solid electrolyte, we are using different redox couples stable in alkaline.

FY 2010 Publications/Presentations

1. Y. Kim and J.B. Goodenough, "Challenges for rechargeable Li Batteries", Chem. Mater 22, 587-603 (2010).
2. J.-T. Han and J.B. Goodenough "A Niobium-oxide anode for lithium-ion batteries" (submitted).
3. J.B. Goodenough and Youngsik Kim, "Challenges for rechargeable batteries" (submitted).
4. J.B. Goodenough "Challenges for rechargeable batteries' IMLB conference, Montréal, Canada, 28 may-1 July (2010).
5. Presentation to the 2010 DOE Annual Peer Review Meeting.

V.C.5 Intermetallic Anodes (ANL)

Michael Thackeray, Jack Vaughey

Argonne National Laboratory (ANL)
9700 South Cass Avenue
Argonne, IL 60439
Phone: (630) 252-9184 ; Fax: (630) 252-4176
E-mail: thackeray@anl.gov

Collaborators:
L. Trahey, ANL
V. Pol, ANL
N. Dietz Rago, ANL
A. N. Jansen, ANL
C. D. Joyce, ANL
C. Lopez Rivera, ANL
H. H. Kung, Northwestern University
Jose M. Calderon-Moreno, Romanian Academy

Start Date: October 1, 2006
Projected End Date: September 30, 2010

Objectives

- Design high capacity metal, semi-metal, intermetallic or metal oxide anodes that provide electrochemical couples to meet the 40-mile range of PHEVs
- Exploit electrochemical deposition reactions to improve the design and performance of tin-based intermetallic electrodes
- Explore autogenic reactions to design new or improved anode materials and architectures

Technical Barriers

- Low energy
- Poor low temperature operation
- Abuse tolerance limitations

Technical Targets

USABC - End of life

- 97 Wh/kg, 383 W/kg (PHEV 40 mile requirement)
- Cycle life: 5,000 cycles
- Calendar life: 15 years

Accomplishments

- Prepared metal and intermetallic electrode architectures by electrodeposition and determined their electrochemical properties in lithium cells.
- Exploited autogenic processes for synthesizing and simultaneously coating Sn oxides with carbon and evaluate their electrochemical properties.
- The synthesis and evaluation of an amorphous TiO_2 anode was successfully accomplished.
- Interactions with the EFRC – Center for Electrical Energy Storage - *Tailored Interfaces* (Argonne-Northwestern University-University of Illinois (Urbana-Champaign) were initiated.

✧ ✧ ✧ ✧ ✧

Introduction

The search for an alternative anode to replace graphite in lithium-ion batteries has been underway for many years. Several types of materials have been investigated, notably: i) metals, ii) metalloids, iii) intermetallic compounds, and iv) metal oxides. Metals (e.g., Sn), metalloids (e.g., Si) and intermetallic compounds (e.g., Cu_6Sn_5) are of particular interest because they offer significantly higher theoretical volumetric and gravimetric capacities compared to graphite (372 mAh/g and 818 mAh/ml, respectively), and because they react with lithium several hundred millivolts above the potential of metallic lithium. However, these materials have densely packed structures and therefore expand considerably on reaction with lithium.

A major objective of our research is to design three-dimensional, microporous copper architectures that can 1) act as a current collector and substrate for copper-based intermetallic electrodes, such as Cu_6Sn_5, and 2) provide a sufficiently large void volume to accommodate the volumetric expansion during reaction with lithium. As a result of our success in FY2009 in obtaining a reversible capacity of >600 mAh/g from Cu_6Sn_5/Sn films electrodeposited onto a copper foam substrate, we have maintained this approach to fabricate multi-component intermetallic systems. We focused our attention on Cu, Sn and Sb compositions that can react with lithium to form an array of ternary (or higher order) compounds, thereby offering the possibility of minimizing Li diffusion distances within the anode during electrochemical charge and discharge reactions.

In FY2010, the possibility of exploiting autogenic reactions to fabricate carbon-coated anode materials was also explored. These reactions typically involve the decomposition of a dry, organometallic precursor material in a high-pressure cell under inert conditions at elevated temperature. Focus was placed, in particular, on carbon-coated tin oxide electrodes.

A new titanium dioxide precursor was also developed that upon annealing converts to an amorphous electrochemically active phase. These amorphous TiO_2 electrodes were developed with the goal of finding a higher capacity metal oxide anode to the lithium titanate spinel, $Li_4Ti_5O_{12}$.

Approach

- Search for inexpensive anode materials that provide an electrochemical potential at least a few hundred mV above the potential of metallic Li.
- Focus predominantly on Sn-based systems as well as composite metal oxides.
- Design new electrode architectures by electrodeposition techniques in which a Cu foam provides an electronically connected substrate onto which electrochemically active metals can be deposited.
- Explore autogenic reactions to fabricate anode materials and architectures in a single step with an initial focus on metal oxides such as SnO_2 and SnO that are either coated with carbon or embedded in a carbon matrix.

Results

Electrodeposition reactions. Electrodeposition reactions of Cu, Sn and Sb on 2-dimensional (2-D) copper foil and three-dimensional (3-D) porous Cu foam substrates were undertaken to fabricate multi-component intermetallic electrodes; in principle, it was envisaged that the latter electrode design would provide superior void volume to accommodate the volumetric expansion during reactions with lithium. In addition, the advantage of electrodeposited electrodes was the possibility of tailoring the amount of active Sn and Sb in the electrode to maintain the average operating voltage of the cell well above the potential of metallic lithium, thereby reducing the safety hazards of lithium-ion cells. Moreover, it was anticipated that the interaction between the various elements in the electrode and the ability to form binary, ternary and higher order compounds, might enable the metal constituents to act as structural binding agents, thereby maintaining electronic connectivity between individual particles during repeated charge and discharge without the use of conventional binders.

Our initial investigations of multi-component electrodes were undertaken on Cu_6Sn_5-Sn and Cu_2Sb-Sb films electrodeposited sequentially on copper foil substrates. Cu_6Sn_5-Sn films were deposited from an aqueous solution containing 0.2 M $SnCl_2$ and 0.02 M $CuCl_2$ in ~10 vol. % HCl, whereas the Cu_2Sb-Sb films were deposited from a 0.04 M $CuCl_2$ and 0.02 M $SbCl_3$ solution, also in ~10 vol. % HCl. The electrode films were annealed at about 150°C in an argon-filled glove box for about 100 hours.

X-ray diffraction pattern of the annealed electrode (Figure V- 82) showed that the multi-component electrode was comprised of Cu_6Sn_5, Cu_2Sb, and Sn, with minor amounts of SnSb and possibly 'Cu_4Sn'. The voltage profiles of the initial discharge/charge cycle of lithium half cells with an as-grown, electrodeposited Cu_6Sn_5-Sn/Cu_2Sb-Sb electrode and an annealed electrode are shown in Figure V- 83. The data demonstrate that the annealing process provides a higher capacity electrode during the initial cycles. The capacity vs. cycle number plots (inset), however, show that although the annealed electrode provides superior capacity during the early cycles, the unannealed electrode shows steadier cycling; after 30 cycles, both unannealed and annealed electrodes deliver approximately 250 mAh/g.

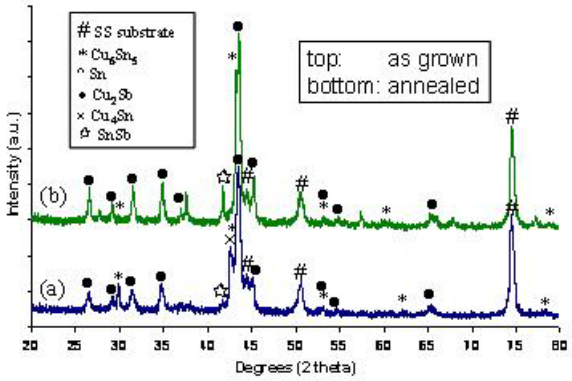

Figure V- 82: X-ray diffraction pattern of a Cu-Sn-Sb multi-component electrode.

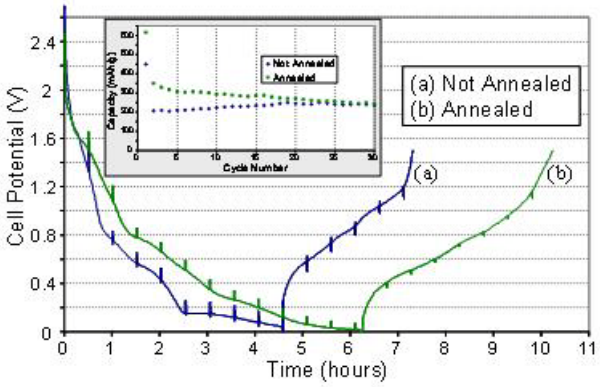

Figure V- 83: The electrochemical properties of a Cu-Sn-Sb multi-component electrode.

In order to understand electrode design rules and the perceived advantages of 3-D over 2-D architectures undergoing electrochemical transformations, 2-D thin film Cu_2Sb electrodes, electrodeposited onto copper foil, were compared with 3-D architectures obtained by

electrodepositing Cu_2Sb onto microporous copper foam substrates. Although Cu_2Sb is not a commercially attractive material, it is a good model system to use because it can be deposited pure without side reaction products, which simplifies the electrochemical, structural and morphological analyses and comparison of 2-D and 3-D electrodes and current collectors.

Electrodepositions were performed with 2 different galvanic square wave (GSW) procedures, both of which yielded 2.2 mg of Cu_2Sb on Cu foil and Cu foam substrates, resulting in 4 comparable sets of data. GSW-1, which consisted of a 30-sec pulse of 10 mA followed by a 10-sec rest, repeated 20 times, produced a nobular, cauliflower-like morphology of Cu_2Sb (Figure V- 84(a)). GSW-2, which consisted of a much shorter 1-sec pulse of 10 mA followed by a 10 sec pulse of 1 mA, repeated 300 times, produced a flat morphology (Figure V- 84(b)).

Figure V- 85 shows plots of the relative cycling performance and stability of 2-D and 3-D Cu_2Sb electrodes in lithium electrochemical cells, all of which were cycled at a current of 0.08 mA between 0 and 1.5 V vs. lithium metal counter electrodes in a Gen 2 electrolyte

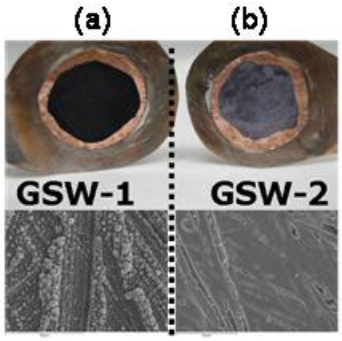

Figure V- 84: Cu_2Sb electrodes deposited on Cu foil under various conditions.

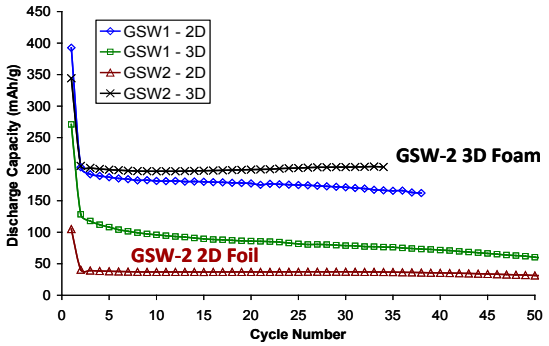

Figure V- 85: Electrochemical performance of 2-D and 3-D Cu_2Sb electrodes deposited under various conditions

(1.2 M $LiPF_6$ in EC:EMC (3:7)). The results demonstrate how the electrodeposition parameters and the resulting electrode morphology influence capacity and stability. Superior electrochemical capacity and cycling stability were obtained from 3-D electrodes deposited on Cu foam using the short pulse, GSW-2, method; 2-D electrodes, produced by the same protocol, initially provided similar capacity but showed inferior cycling stability. The worst performance was observed from 2-D electrodes (on Cu foil) that were prepared under the longer pulse, GSW-1, conditions. Results were reproduced in triplicate.

Carbon-coated SnO_2 Electrodes. Carbon-coated SnO_2 electrodes (SnO_2-C) were prepared by the autogenic decomposition of tin ethoxide according to the reaction.

$$Sn(OC_2H_5)_2 \xrightarrow[100\ psi]{600\ ^oC} Sn_{(s)} + C_{(s)} + \text{gaseous products}\uparrow$$

a typical HRTEM image of which is shown in Figure V-86.

The image in Figure V- 86 illustrates that the SnO_2 particles are approximately 10-20 nm in cross section, and that each nanoparticle is encapsulated by a carbon layer, a few nanometers thick. The electrochemical data of lithium half cells, shown in Figure V- 87(a) and Figure V-87(b), demonstrate that the first-cycle irreversible capacity loss is reduced by the carbon coating and that these electrodes provide an initial capacity of ~800 mAh/g.

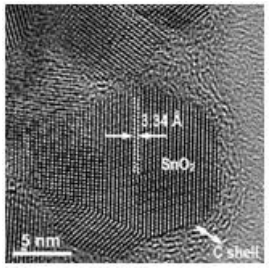

Figure V- 86: HRTEM image of a carbon-coated SnO_2 nanoparticle produced by an autogenic reaction

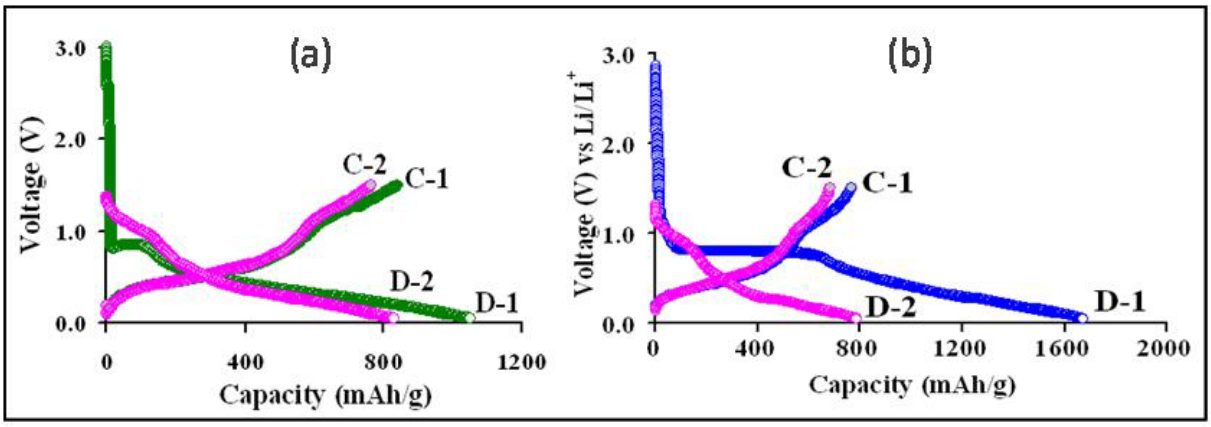

Figure V- 87: Electrochemical profiles of the first two cycles of a lithium cell with (a) C-coated SnO_2 electrode, and (b) SnO_2 electrode after burning off the carbon coating.

The autogenic process is extremely versatile and can be used to prepare a wide variety of C-protected nanoparticulate materials. The approach has excellent potential for preparing new anodes and cathode materials and architectures for lithium-ion cells.

Progress was also made in fabricating an amorphous TiO_2 product, the capacity of which significantly supercedes that of the lithium titanate spinel, $Li_4Ti_5O_{12}$. Lithium half cells containing an amorphous TiO_2 counter electrode were cycled between 4.0 and 0.6 V to determine the full voltage range over which capacity could be delivered. Essentially all the capacity was delivered during charge and discharge between 2.0 and 0.6 V. Continuously sloping voltage profiles were consistent with the behavior expected for an amorphous electrode. Allowing for the calculated mass of residual carbon in the electrodes, reversible electrochemical capacities of 350-400 mAh/g (TiO_2) were obtained for the first twenty cycles, i.e., slightly greater than the value expected for the insertion of 1 Li per TiO_2. These data have been published and can be found in the paper by C. D. Joyce et al. – see list of publications, patents and presentations. This material is being patented.

Conclusions and Future Directions

- A comparison of the electrochemical performance of 2-D vs. 3-D electrodes prepared by electrodeposition was made:
  a) Cu_2Sb was used as a model system.
  b) Deposition parameters and electrode morphology influence capacity and cycling stability.
  c) Short (1-sec) pulse protocol provides smoother 2D films and smaller Cu_2Sb particles on 3D Cu-foam than long pulse protocol.
  d) 3-D electrodes (short pulse) provide best capacity and cycling stability.
- Electrodeposited 3-D composite Cu-Sn-Sb electrodes outperform traditional laminated electrodes. This result provides the motivation to continue studies of electrodeposited Sn electrodes.
- Autogenic reactions are extremely versatile and can be used to prepare C-protected nanoparticulate materials with enhanced electrochemical properties. The approach has implications for preparing new electrode materials and architectures (both anodes and cathodes).
- An amorphous TiO_2 product was synthesized and evaluated; it has the potential of significantly superceding the capacity of the lithium titanate spinel, $Li4Ti_5O_{12}$.
- This project formally concludes on 30 September 2010. However, aspects of the project that relate to the preparation and characterization of electrodeposited intermetallic electrodes will be continued in FY2011 as outlined in the successful BATT proposal entitled "*Three-Dimensional Anode Architectures and Materials*".

FY2010 Publications/Patents/Presentations

1. D. Joyce, T. McIntyre, S. Simmons, H. LaDuca, J, G. Breitzer, C. M. Lopez, A. N. Jansen, and J. T. Vaughey, *Synthesis and electrochemical evaluation of an amorphous titanium dioxide derived from a solid state precursor*, J. Power Sources, **195**, 2064 (2010).
2. M. M. Thackeray, L. Trahey and J. T. Vaughey, US Patent Application 20100035153, 11 February, 2010
3. Presentation to the DOE Annual Peer Review Meeting, Washington D.C., 7-11 June 2010.

4. L. Trahey, J. T. Vaughey, H. H. Kung and M. M. Thackeray, *A Resistance Study on Electrodeposited Intermetallic Anodes for Li-ion batteries,* ACS Meeting, San Francisco, March 21-25 (2010).
5. M. M. Thackeray, C. S. Johnson, S.-H. Kang, H. H. Kung, V. G. Pol, L. Trahey and J. T. Vaughey, *Designing Advanced Anode and Cathode Materials for Lithium-Ion Batteries*, Materials Research Society Fall Meeting, Boston, November 30 – December 4 (2009) (Invited).
6. L. Trahey, J. T. Vaughey, H. H. Kung and M. M. Thackeray, *Composite Intermetallic Anodes with 3-D Architectures made by Electrodeposition*, 216th ECS Meeting, Vienna, Austria, 4-9 October (2009).

V.C.6 Nano-structured Materials as Anodes (SUNY)

M. Stanley Whittingham

SUNY at Binghamton
Vestal Parkway East
Binghamton, NY 13902-6000
Phone: (607) 777-4623; Fax: (607) 777-4623
E-mail: stanwhit@binghamton.edu

Start Date: June 1, 2007

Project End Date: December 31, 2010

Objectives

- Replace the presently used carbon anodes:
  - With safer materials that will be compatible with lower-cost layered oxide and phosphate cathodes and the associated electrolyte.
  - With materials having higher volumetric energy densities, twice that of carbon (1.6 Ah/cc and 0.5 Ah/g)

Technical Barriers

This project addresses the following technical barriers facing the use of lithium-ion batteries in PHEV and all-electric vehicles:

(A) Materials and manufacturing cost of lithium-ion batteries

(B) Safety of lithium-ion batteries

(C) Volumetric capacity limitations of lithium-ion batteries

Technical Targets

- Determine the limitations, besides cost, of the Sn-Co-C nanostructured anode.
- Identify the structural and surface changes of Sn anodes during cycling, while working collaboratively with LBNL (R. Kostecki)
- Explore nano-size Sn/Si alloys and metal oxides to identify their cycling characteristics.
- Explore Co-free alloys to identify lithium active stable phases.

Accomplishments

- Shown that bulk tin, in the form of foil, whether shallow or deep cycled, loses capacity at all depths of discharge.
  - SEI film is not protective, and increases continuously in resistance
- Shown that amorphous nano-size tin does not lose capacity whether shallow or deep cycled.
  - Shows high rates for lithium release
  - Shown that this material is charge-limited, that is lithium insertion is slow
- Technology transfer accomplished.
  - Working with several local battery companies, and many ex-students now in battery companies
  - Students now have positions at BNL, NREL, and PNNL. Electrospinning technique transferred to NREL.

Introduction

Achieving the DOE cost and energy/power density targets will require improved anode materials that have higher volumetric energy densities than carbon, and have lower cost production methods. At the same time the material must have higher lithium diffusion rates than carbon and preferably be at a slightly higher potential to improve the safety.

Approach

Explore, synthesize, characterize and develop inexpensive materials that:

- Have a potential around 500 mV above pure Li
- Have double the volumetric capacity of carbon
- Have a higher gravimetric capacity than carbon
- Emphasize nanostructures
  - Tin nanostructures
  - Compare with silicon based nanostructures
  - Keep aware of oxide-based anodes
    - We showed that Mn_3O_4 cycles well.

Results

Amorphous Nano-Sized Tin. We have continued our understanding of the capabilities of the amorphous tin anode developed by SONY. We have previously shown that this material cycles well, holding its capacity at all depths of discharge in contrast to crystalline tin. These results are a clear indication that tin at the nano-size and in amorphous form can be cycled repetitively without

capacity loss, and gives clear direction for future work on tin-based systems.

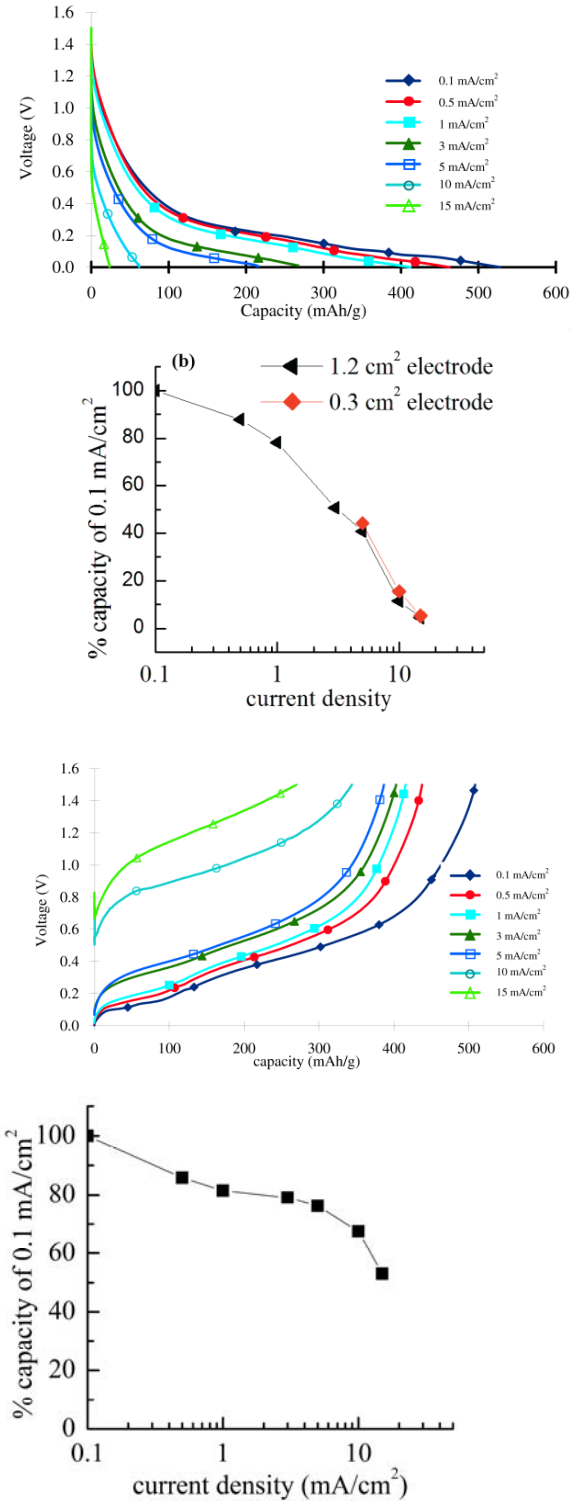

Figure V- 88: Lithium insertion and delivery rates from the Sn-Co amorphous material (top to bottom is a-d in discussion).

We set-out to determine the rate-capability on both lithium insertion and removal. The results are shown in Figure V- 88.

Figure V- 88(a) shows the lithium insertion curve, which is the charging of the battery using this material as an anode. Figure V- 88(b) shows the capacity as a percentage of the capacity at 0.1 mA/cm^2; for each data point, the lithium was first removed at the low rate of 0.1 mA/cm^2. It can be immediately seen that at the high rates used, the capacity falls off very rapidly. At a rate of 2 mA/cm^2 50% of the capacity is lost. In contrast, the capacity on lithium removal is maintained even at high rates; for example, around 70% of the capacity is retained at 10 mA/cm^2 (2.5C rate), see Figure V- 88(c) and Figure V- 88(d). Thus, this anode material can sustain high discharge rates (lithium delivery), and probably meets the technical needs of PHEV and EV. It is more limited on charging and in this respect is comparable to carbon anodes, and might create problems with the fast charging needs of HEV batteries.

Bulk Tin Foil Anodes. In contrast to nano-amorphous tin, bulk tin foil loses capacity after about 10 to 12 deep cycles (or equivalent shallow cycles). This is due to a resistance build-up caused by the continuous formation of the SEI layer as the tin expands and contracts on reaction with the lithium. Robert Kostecki at LBNL has shown that the SEI layer formed on tin in the carbonate electrolytes in non-protective.

Other Anode Materials. We continue to explore other potential anode materials containing aluminum, silicon and tin. We found, as shown in Figure V- 89, that aluminum-based anodes behave much better than pure aluminum in carbonate electrolytes. The latter materials rapidly lose capacity from the first cycle.

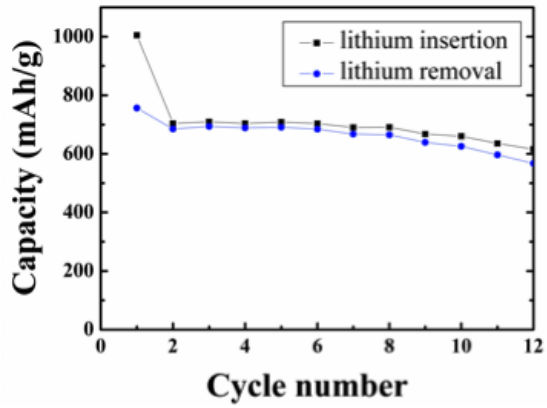

Figure V- 89: Cycling capacity of an Al-M-C material at 0.5 mA/cm^2.

Mixed aluminum-silicon anodes were found to cycle, but with less than 100% efficiency, lost capacity. This is in contrast to tin which cycles with 100% efficiency when

nano-sized. The results for an aluminum-silicon alloy with different lower voltage cut-offs are shown in Figure V- 90.

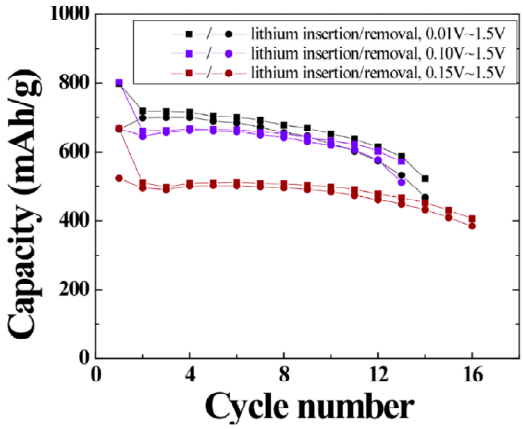

Figure V- 90: Cycling capacity of an Al-Si alloy at 0.5 mA/cm^2.

Figure V- 91 shows the behavior of silicon formed by ball-milling and a high-temperature anneal. The capacity shows a continuous fade.

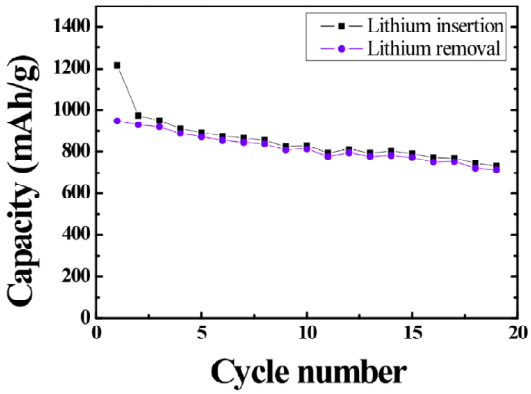

Figure V- 91: Cycling capacity of a Si-C material at 0.5 mA/cm^2.

In contrast to the fade observed in Figure V- 91, no fade is observed, when the silicon is capacity controlled. Figure V- 92 shows data when the cell was charged to 1.5 volts but only discharged to 600 or 700 mAh/g. No capacity fade is observed, but the efficiency was still only around 98-99%.

Conclusions and Future Directions

A clear result from our study of understanding the cycling behavior of tin anode materials is that nano/amorphous materials work, and that bulk materials with their high expansion on lithium reaction do not and are therefore unsuitable for batteries. Our future work will therefore emphasize tin nanostructures. We will synthesize nano-tin by a range of techniques, such as solvothermal, electrospinning and mechanochemical. These nanoparticles will be protected from reaction with the electrolyte by a surface coating. If the above approaches are successful, we will substitute part of the tin to raise the redox potential and thus the safety.

Silicon appears to cycle well if the capacity is restricted, and some effort will continue on silicon containing materials, but the challenge of round-cycle efficiency must be resolved.

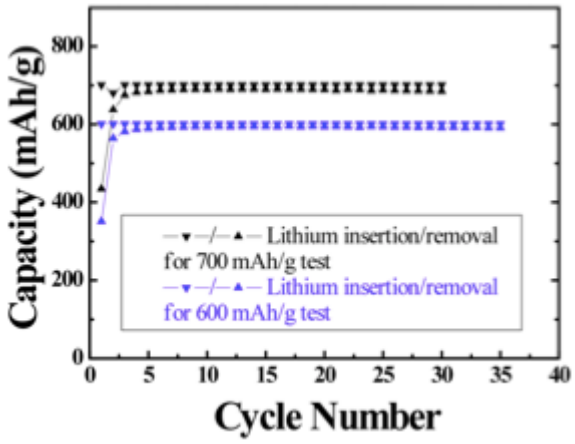

Figure V- 92: Cycling capacity of a Si-C material at 0.5 mA/cm^2.

FY 2010 Publications/Presentations

1. Presentation to the 2010 DOE Annual Peer Review Meeting.
2. Natasha A. Chernova, Megan Roppolo, Anne Dillon and M. Stanley Whittingham, “Layered vanadium and molybdenum oxides: batteries and electrochromics”, J. Mater. Chem., 2009, 19: 2526-2552.
3. Many invited presentations, incl.:
   - National Academy, US Army Lab., Toyota Ann Arbor, Applied Materials in Santa Clara, AABC Orland, Vale
   - Cornell, U. Michigan, Michigan State, Warsaw
   - IMLB, MRS, ACS
   - PNNL, BNL
   - Local outreach

V.C.7 Development of High Capacity Anodes (PNNL)

Ji-Guang Zhang and Jun Liu
Pacific Northwest National Laboratory
902 Battelle Blvd., Mail Stop K3-59
Richland, WA 99352
Phone: (509) 372-651; (509) 375-4443
E-mail: jiguang.zhang@pnl.gov; jun.liu@pnl.gov

Start: Date: October 1, 2009
Projected End Date: December 31, 2010

Objectives

- Develop novel anodes with high capacities and good rate capabilities
- Develop a low-cost synthesis route for high-capacity and stable silicon (Si) and SnO_2 based anode.

Technical Barriers

- Energy density, stability, and cost.

Technical Targets

- Synthesize nanocomposite materials with improved capacity and stability
- Increase power of new anode materials.

Accomplishments

- Developed a multiphase, self-assembly approach using graphene as fundamental building blocks to construct controlled graphene nanocomposites with active metal oxide or Si materials. Highly stable hybrid anodes of TiO_2/graphene and SnO_2/graphene were prepared. The electrodes were made without using binders or other additives. TiO_2/graphene anodes have the best rate capability reported and excellent cycling stability. An anode of a porous Si/graphene nanocomposite with high capacity and good stability was obtained using a similar method.
- Identified carbon additives that significantly affect the cycling stability of micron-sized porous Si. The cyclability of micron-sized Si is significantly improved by using Ketjenblack as the carbon additive. A new binder also was used to stabilize the Si anode.
- Developed a macroporous copper (Cu)/SnO_2 composite anode using a novel method based on slurry blending, tape casting, sintering, and reduction of metal oxides. The composite anodes show better discharge capacity and cycle life than the SnO_2 electrode prepared from conventional tape-casting method on Cu foil.

Introduction

Si and SnO_2 are good high-capacity anode materials for lithium (Li)-ion batteries, but usually show rapid capacity fading during charge/discharge cycles because of the large volume expansion and phase transformation upon lithiation and de-lithiation. The low conductivity and poor stability of such materials usually require the addition of conductive phases to enhance electron transport and electrical contact of the active materials in the electrode of a Li-ion battery. For example, high capacity exists in SnO_2/C composites, but capacity fading is still significant. Good capacity retention could be obtained only when a much larger amount of carbon (above 60 wt %) was added to the material. To increase the capacity of the anode, a novel anode material needs to be developed, with a capacity more than double that of state-of-the-art graphite anodes.

Approach

We developed novel metal oxides- and Si/graphene nanocomposites by ternary self-assembly of metal cation/carbon-coated Si, surfactants, and graphene sheets. The surfactants not only assist the dispersion of graphene in aqueous media but also link the metal ions or Si to graphene sheets, resulting in self-assembly of metal oxides/Si and graphene into composite nanostructures. Small anionic surfactant molecules are used in the synthesis of metal oxide-graphene composites. The hydrophobic parts of the anionic surfactants adsorb onto the graphene sheets to ensure their dispersion, while the anionic heads of the surfactants bind to the metal cations to ensure the assembly. Subsequently, the metal oxides are crystallized on graphene sheets, producing a new class of nanocomposites. In the Si/graphene composite, a polymer anionic surfactant is used to suspend graphene and carbon coated Si. The surfactant molecules bind to graphene sheets and the carbon coated porous Si leading to the self-assembly of Si/graphene composite. The polymer surfactants subsequently are graphitized by high-temperature annealing to form conducting frames between graphene sheets and carbon-coated Si nanoparticles.

In another effort, we developed a novel method to prepare macroporous copper (Cu)/SnO_2 composite anodes. This method is based on slurry blending, tape casting, and reduction of metal oxides. Porous Cu/SnO_2 composite anodes were prepared by mixing micro-sized powders of CuO and nano-sized powders of SnO_2 with certain amounts of graphite and binder, and dispersing the mixture in organic solvent to form slurries. After tape casting, the free standing film was calcined in air, reduced in pure hydrogen atmosphere, and then sintered in a pure argon atmosphere.

Results

TiO_2/graphene nanocomposites. The self-assembly process for TiO_2/graphene composites is shown in Figure V- 93. The surfactants are bridging agents that not only suspend graphene in solution but also direct the crystallization of metal oxides on graphene sheets, forming nanocomposites. The nanocomposite electrodes are free standing paper electrodes fabricated without using any binder or additives.

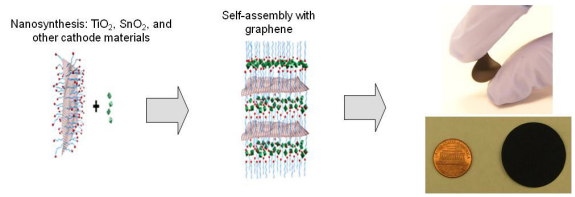

Figure V- 93: Self-assembly process for TiO_2/graphene composites

The synthesized TiO_2/graphene nanocomposites with only 2.5 wt% graphene have the best reported rate performance, and they also have excellent cycling stability. Figure V- 94 shows the charge/discharge profile, rate performance, and cycling stability of TiO_2/ graphene composites. The voltage range shown in Figure V- 94(a) is 1 V to 3 V; a good range in which to avoid the formation of SEI layers. Therefore, the first cycle capacity lost can be minimized. Figure V- 94(b) shows the capacities of TiO_2/ graphene composites at different charge/discharge rates. At a high charge/discharge rate of 30C, the capacity of anatase TiO_2/graphene is more than three times higher than the material that does not include graphene. The TiO_2/graphene composite also has excellent cycling stability. Figure V- 94(c) shows a stable capacity of 170 mAh/g for more than 100 cycles at a 1C rate.

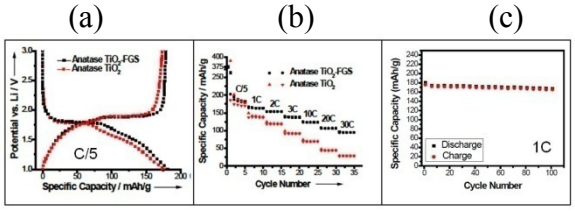

Figure V- 94: (a) Charge/discharge profile of anatase TiO_2 and anatase TiO_2/graphene composite. (b) Rate performance of anatase TiO_2 and anatase TiO_2/graphene composite. (c) Cycling stability of anatase TiO_2 and anatase TiO_2/graphene composite at 1C rate.

Si/Graphene Nanocomposites. The Si/graphene nanocomposite was prepared using a method similar to the one used for the TiO_2/graphene nanocomposites, but Si nanoparticles and a polymer anionic surfactant were used. Figure V- 95 is the schematic structure of the Si/graphene composite. The Si particles in Si/graphene composites are closely spaced within the same layer but separated by multiple graphene sheets to form a robust, free-standing electrode paper. In this design, the graphene matrix helps accommodate the repeated volume expansion and contraction during cycling, and maintains good electronic contact with Si.

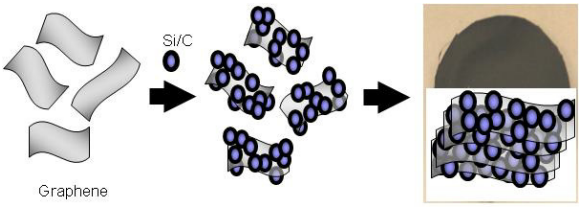

Figure V- 95: Formation process for porous Si/graphene composites

The structure of the Si/graphene nanocomposites was characterized by transmission electron microscopy (TEM). Figure V- 96 shows the TEM image of porous Si and the cross-sectional TEM image of the Si/graphene composite. As shown in Figure V- 96(a), the porous Si powder has a large particle size of about 4 µm, with deeply etched surface exhibiting a porous structure. The selected area diffraction pattern (see inset in Figure V- 96(a)) shows the (111) orientation of Si. The cross-sectional TEM image of the Si/graphene composite shows the undulated wrinkles of graphene stacks around the big Si particle (Figure V- 96(b)).

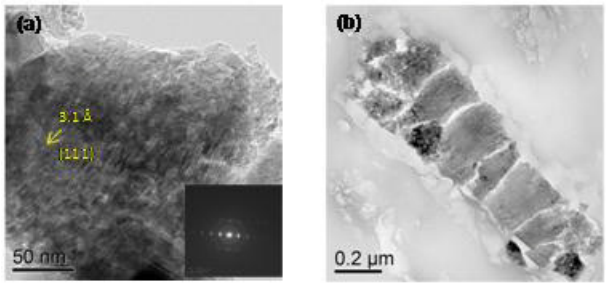

Figure V- 96: TEM images of (a) porous Si particles with selected area electron diffraction pattern (insert). (b) Cross-sectional image of porous Si/graphene nanocomposite.

The electrochemical performances of porous Si/graphene composite are shown in Figure V- 97. The first discharge plateau between 0.34 V and 0.1 V in the Si/graphene paper is a combined effect from the graphene and graphite restacked from the graphene sheets. The reversible capacity increases gradually and then becomes stable after the first few cycles. In the early stages of testing, the dense monolithic Si/graphene electrode is not fully wetted by the electrolyte; thus, the active material is not fully utilized. With further cycling, the contact between the electrode and electrolyte is improved when Li^+ ions continuously diffuse in and out from the composite structure. After activation in the initial cycles, an electrochemical kinetic equilibrium is reached, and the Coulombic efficiency stays at ~98% during subsequent cycles. Compared with the original porous Si, a significant improvement of cycling stability is achieved in the Si/graphene nanocomposite. After 30 cycles, the Si/graphene electrode still delivers a high capacity of 2,343 mAh/g Si. Even considering the weight of the total anode (which has a Si:carbon:binder ratio of 1:2:0), the capacity of the anode is still 781mAh/g, which is more than twice that of graphite anode. Therefore, the existence of graphene layers effectively alleviates the macroscopic mechanical stress arising from the continuous volume expansions and reductions of the Si particles. The whole electrode integrity is preserved, leading to good cyclability.

Carbon additive selection and binder "P"[22]. Further investigation indicates that conductive carbon plays a critical role in the performance of Si-based anodes. Micron-sized Si particles with nanopore structures have been investigated as an anode material for Li-ion batteries. The porous structure of Si helps to accommodate the large volume variations that occur during Li-insertion/extraction processes. To improve the electronic integrity of the Si-based anode, a two-step process was used. First, chemical vapor deposition (CVD) was used to enhance the electronic conductivity of individual Si particles by depositing a uniform carbon coating on both the exterior surfaces and within the pores. Next, the electronic contact among Si particles is improved by adding Ketjenblack (KB) carbon, which exhibits an elastic, chain-like structure that maintains a stable electronic contact among Si particles during cycling. Using this approach, an anode with a reversible capacity of more than 1600 mAh/g (based on the weight of Si) after 30 cycles was obtained as shown in Figure V- 98. Even considering the weight of the total anode (which has a Si:carbon:binder ratio of 6:3:1), the capacity of the anode is still 960 mAh/g, which is about three times more than that of graphite anode.

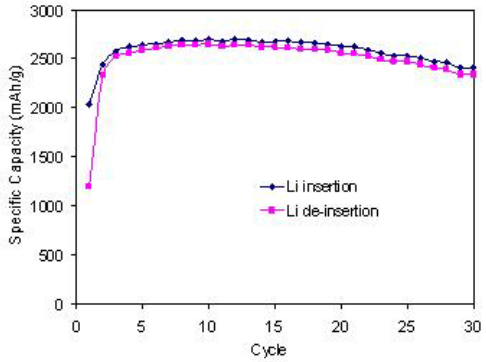

Figure V- 97: Cycling stability of porous Si/graphene hybrid electrode at 0.1C rate

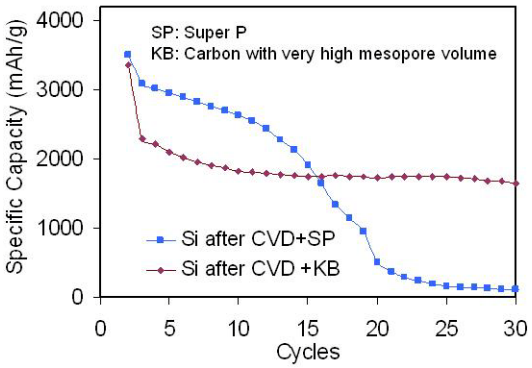

Figure V- 98: Cycling stability of micron-sized Si with different carbon additives

The combination of the nanopore structure, CVD-coated carbon on the Si surface, and the elastic carbon (KB) among the Si particles provides a cost-effective approach to using the large micron-sized Si particles in Li-ion batteries. Figure V- 98 also shows that a Si-based anode using KB carbon exhibits a much more stable capacity retention that those of using super P as conductive carbon additive. The volume of KB expands in the

[22] A proprietary binder developed by PNNL.

electrolyte and some of Si particles may be absorbed into the pores of the KB, resulting in stable contact between Si particles and conductive carbon, which in turn lead to improved cyclability.

We also investigated the affect of different binders and cycling protocols. Samples with a PNNL-developed binder P showed improved performance when compared to samples with PVdF or CMC binders. When binder P was used, the capacity fading rate is reasonably small, and the reversible capacity stays at ~1,000 mAh/g at a high current density of 400 mA/g (see Figure V- 99). At shallow cycling (0.17 V to 0.9 V) conditions, there was only 0.7% capacity loss per cycle after the first two formation cycles. Therefore, using binder P as a substitute to the regular PVdF binder is a simple and economical way to improve Si cycling.

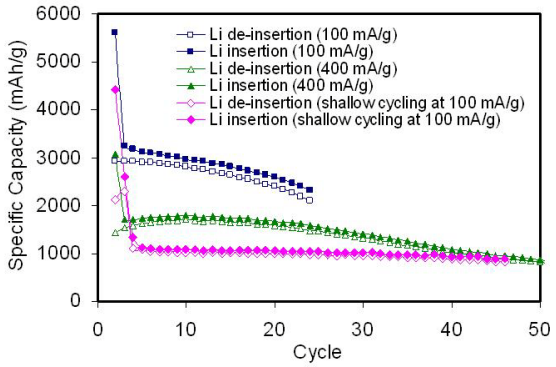

Figure V- 99: Si cycling stability at high current density (400 mA/g) and shallow (0.17 V to 0.9 V) cycling conditions

Macroporous Cu/SnO_2 Composite Anode. The surface morphology and porous structure of the porous Cu/SnO_2 composite anodes with Cu:SnO_2 weight ratios of 8:2 were measured by scanning electron microscopy (SEM). Figure V- 100(a) shows the uniformity of the composite morphology. In Figure V- 100(b), the smaller particles are nano-sized SnO_2, and the larger particles are Cu formed from the reduction of micro-sized CuO particles. As the SnO_2 content increases in the original CuO/SnO_2 mixtures, more small SnO_2 particles cover the Cu particles.

The capacity and cycling ability of these composite anode sheets were shown in Figure V- 101. The porous composite Cu/SnO_2 anodes show much higher capacity and better cycling stability than the nano-sized SnO_2 powder coated on Cu foil, which was prepared using a conventional tape casting method.

Conclusions and Future Directions

The SnO_2/graphene nanocomposite material showed significantly improved stability. Further improvements will be sought by optimizing the size and surface properties of graphene. For Si-based anodes, we will focus on the following three aspects: 1) optimizing the composition of Si/graphene to balance the high capacity and cyclability; 2) optimizing the size and morphology of Si and graphene in the Si/graphene composite to increase the utilization rate of Si; and 3) optimizing binder P and new additives to further improve cycling stability.

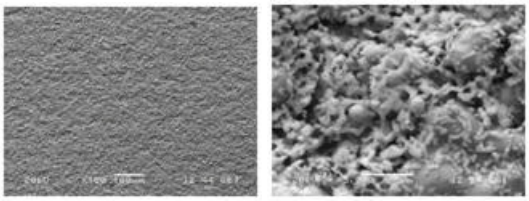

Figure V- 100: SEM images of the surface structure of porous Cu/SnO_2 composite anode sheets with Cu:SnO_2 weight ratios of 8:2

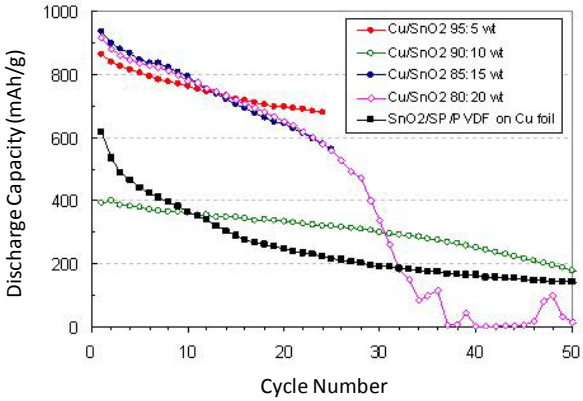

Figure V- 101: Battery cycling performance of macroporous Cu/SnO_2 composite anode sheets with Cu/SnO_2 at weight ratios of 95:5, 9:1, 85:15, and 8:2, along with a comparison of nano-sized SnO_2 powder coated on Cu foil.

FY 2010 Selected Publications/Presentations

1. "Ternary Self-Assembly of Ordered Metal Oxide-Graphene Nanocomposites for Electrochemical Energy Storage". Donghai Wang, Rong Kou, Daiwon Choi, Zhenguo Yang, Zimin Nie, Juan Li, Laxmikant V. Saraf, Ji-Guang Zhang, Gordon L. Graff, Jun Liu, Michael A. Pope, Ilhan A. Aksay, ACS Nano, 4(3),1587–1595 (2010).
2. "Vapor Induced Solid-Liquid-Solid Process for Silicon-Based Nanowire Growth". Ji-Guang Zhang, Jun Liu, Donghai Wang, Daiwon Choi, Leonard S. Fifield, Chongmin Wang, Gordon Xia, Zimin Nie, Zhenguo Yang, Larry R Pederson, and Gordon Graff, Journal of Power Sources, 195, 1691–1697 (2010).
3. "Crystal and Electronic Structure of Lithiated Nanosized Rutile TiO_2 by Electron Diffraction and Electron Energy-loss Spectroscopy". Chongmin

Wang, Zhenguo Yang, S. Thevuthasan, Jun Liu, Don R. Baer, Daiwon Choi, Donghai Wang, Ji-Guang Zhang, L.V. Saraf, Zimin Nie. Applied Physics Letters, 94(23), Art. No.: 233116 (2009).

4. An Approach to Make Macroporous Metal Sheets as Current Collectors for Lithium-Ion Batteries, Wu Xu, Nathan L. Canfield, Deyu Wang, Jie Xiao, Zimin Nie, Xiaohong S. Li, Wendy D. Bennett, Charles C. Bonham, and Ji-Guang Zhang, *Journal of The Electrochemical Society,* 157 (7) A765-A769 (2010).
5. Si_6H_{12}/Polymer Inks for Electrospinning a-Si Nanowire Lithium-ion Battery Anodes, Douglas L. Schulz, Justin Hoey, Jeremiah Smith, Arumugasamy Elangovan, Xiangfa Wu, Iskander Akhatov, Scott Payne, Jayma Moore, Philip Boudjouk, Larry Pederson, Jie Xiao, and Ji-Guang Zhang, Electrochem. Solid-State Lett., Volume 13, Issue 10, pp. A143-A145 (2010).
6. "Stabilization of Silicon Anode for Li-Ion Batteries," Jie Xiao, Wu Xu, Deyu Wang, Daiwon Choi, Wei Wang, Xiaolin Li, Gordon L. Graff, Jun Liu, and Ji-Guang Zhang, J. Electrochem. Soc., Volume 157, Issue 10, pp. A1047-A1051 (2010).

V.C.8 Advanced Binder for Electrode Materials (LBNL)

Gao Liu
Enviornmental Energy Technologies Division
Lawrence Berkeley National Laboratory
Berkeley, CA 94720
Phone: (510) 486-7207; Fax: (510) 486-8619
E-mail: gliu@lbl.gov

Start Date: October 2010
Projected End Date: September 2012

Objectives

- Develop new conductive polymer binder materials to enable the use of Si alloys as lithium-ion negative electrodes. Si has the highest lithium-ion storage capacity at 4,200 mAh/g. However, major issues prevent Si from being used as negative electrode material in lithium-ion cells, including limited life and low coulombic efficiency. The goal of this project is to develop negative electrode binder materials to improve the cycling performance of the Si-based electrode, and to ensure that it is compatable with current lithium-ion manufacturing process.

Technical Barriers

This project addresses the following technical barriers from the Energy Storage section of the Vehicle Technologies Program Multi-year Research, Development and Demonstration Plan:

- Calendar and cycle life
- Energy density
- Cost

Technical Targets

Relavent USABC goals

- EV
  - $150/kWh
  - 230 Wh/dm^3
  - 1,000, 80% capacity, discharge cycles
  - 10-year system life
- PHEV 40-mile
  - $300/kWh
  - 193 Wh/dm^3
  - 5,000 charge depleting cycles
  - 15-year system life

Accomplishments

- Synthesized a class of conductive polymer binders for Si materials.
- These binders are compatible with current lithium-ion electrode slurry casting process.
- These binders were tested with commercial Si particles in the lithium-ion cell, and showed significant improvement in cycling capacity and cycle life performance.
- Developed processes to compensate for the first cycle irreversible capacity loss for the Si electrode.

✧ ✧ ✧ ✧ ✧

Introduction

Achieving the DOE energy, cycle life and cost targets for PHEV batteries will require materials of higher capacity and/or voltage and improved coulombic efficiency. High capacity Si-based anode material has the potential to fulfill the energy density requirements for EV/HEV applications. However, full capacity cycling of Si results in significant capacity fade due to a large volume change during Li insertion and removal. Decreasing the particle size to nanometer scale can be an effective means of accommodating the volume change; however, the repeated volume change during cycling can also lead to repositioning of the particles in the electrode matrix and result in particle dislocation from the conductive matrix. This dislocation of particles causes the rapid fade of the electrode capacity during cycling. In order to address this issue,we developed a new class of electric conductive binder materials, which provide improved binding force to the Si surface to help maintain good electronic connectivity throughout the electrode. Then, Si/conductive polymer composite electrodes were developed and tested. This new electrode can be fabricated with the current lithium-ion manufacturing processes. The electrodes made with these binders have significantly improved the cycling capability of Si.

Approach

Use functional polymer design and synthesis to develop new conductive polymers with proper electronic properties, strong adhesion and improved flexibility to provide electric pathways in the electrode, and to accommodate the large volume change of the Si alloy active material during lithium insertion and removal. The rational design of binder is assisted with advanced

diagnostic techniques such as XAS at the Advanced Light Sources and with advanced molecular computation at National Energy Reseearch Secientific Computing Center – both are DOE national user facilities.

Results

Materials Synthesis. We have synthesized a class of electrically conductive polymer binder. These polymers are very effective as both binder and conductive matrix for Si based anode materials.

Electrode Fabrication and Morphology. A commercial Si material was used to fabricate anode electrode with the conductive binders. The Si material is NOT carbon coated. A standard slurry making process was used to fabricate all the composite Si/conductive binder electrodes.

Morphology of the Si Composite Electrode. The commercial Si particles are shown in the TEM image in Figure V- 102(a). The Si particles are nanosized with a bimodal distribution of particles size. No pretreament process was required for this Si sample. Using a simple slurry mixing, casting and drying process, a composite porous electrode was fabricated. The morphology of the porous electrode is similar to a lithium-ion electrode, as shown in the SEM image in Figure V- 102(b).

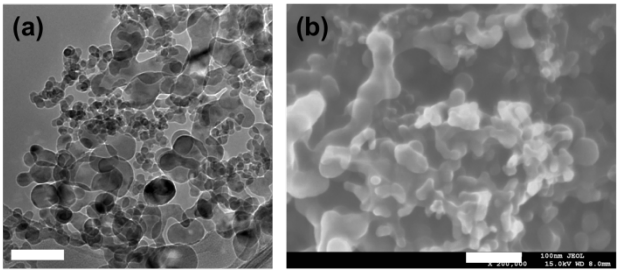

Figure V- 102: a. TEM image of commercial Si nanoparticles. b. SEM image of the surface of the composite Si/conductive polymer electrode.

Doping of the Conductive Polymer. Doping of the conductive polymer will happen during the operation of the Si/conductive polymer composite electrode. The doping process improves the electronic conductivity of the polymer matrix. The conductive polymers were combined with acetylene black conductive additive to form a composite electrode. The lithium-ion doping was studied by charging and discharging the conductive polymer electrode. The first cathodic doping is largely irreversible followed by very reversible oxidation and reduction processes as shown in Figure V- 103. Appreciable amount of lithium is consumed by the polymer during the first cathodic process.

Cycling Stability of the Si/Conductive Polymer Electrode. The Si/conductive polymer electrode was assembled into a test cell with lithium metal as a counter electrode. Full capacity cycling was performed on this electrode between a lower cut-off voltage at 0.01 V and upper cut-off voltage of 1 V. First cycle coulombic efficiency is around 65%. Part of the lithium consumption is due to the irreversible doping of the conductive binder. The electrode maintains a capacity over 2000 mAh/g during the first 100 cycles tested as shown in Figure V-104. The coulombic efficiency was over 99% for the fortieth cycles and beyond.

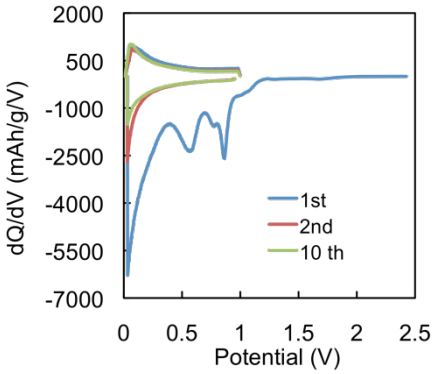

Figure V- 103: The lithium-ion doping process of the conductive polymer.

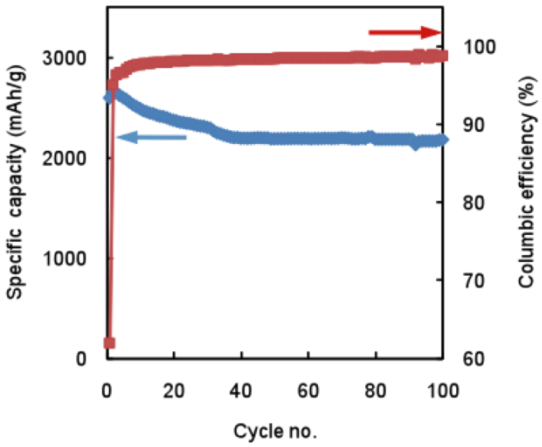

Figure V- 104: Cycling performance of the Si.conductive polymer composite electrode.

Compensation of the First Cycle Irreversible Capacity. Si-based electrodes tend to have high first cycle irreversible capacity loss. The Si/conductive polymer electrode has higher irreversible capacity, due to the irreversible doping of the conductive binders during the first lithiation. We used Stablized Lithium Metal Powder (SLMP) as anode additive to improve the first cycle efficiency of the Si/conductive polymer electrode. The first cycle efficiency can be systematically adjusted from 60%

to 100% as showed in Figure V- 105 without compromising cycling capabilities.

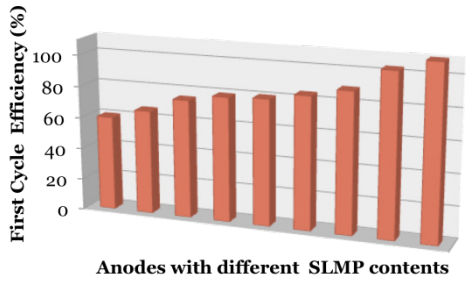

Figure V- 105: Improve 1st cycle coulombic efficiency by SLMP doping of the Si/conductive polymer anodes.

Conclusions and Future Directions

We have successfully developed a class of conductive polymer binder that is suitable for Si anode. Initial tests have demonstrated the effectiveness to accomondate Si volume change, provide electric conduction within the electrode, and the stability during cycling. In the future we will develop electrode that has high Si material loading and high capacity per unit area to meet the EV/PHEV energy density goals. We are now poised to combine the conductive polymer binder with other functionalities and additives to further stabilized the Si surface, minimize side reactions and increase coulombic efficiency. Other high capacity alloy materials such as Sn, face the same volume expansion challenges as Si does. We will explore the application of these binders in a Sn anode system to improve its the cycling capability.

FY 2010 Publications/Presentations

1. Provisional U.S. patent application IB-2643P "Electrically Conductive Polymer Binder for Lithium-ion Battery Electrode" Gao Liu, Shidi Xun, Vince Battaglia and Honghe Zheng. Filed in 2009.
2. Gao Liu, Shidi Xun, Honghe Zheng, Xiangyun Song, and Vince Battaglia "New Binder Marterials for Si Electrode" 216th Electrochemical Society Meeting *Abstract No. 663* Vienna, Austria, October 2009.
3. Shidi Xun, Honghe Zheng, Xiangyun Song, Vince Battalgia and Gao Liu "Electrochemical Properties of Si nanocomposite anode for Lithium-ion Battery" The American Chemical Society National Meeting San Francisco, CA, March 2010.
4. Gao Liu "Polymer Composite Development and Optimization for Lithium-ion Electrode Design" ME-EETD Seminar Series at UC Berkeley, February 2010. (Invited Lecture)
5. Gao Liu "Lithium-ion Composite Electrode Design for Energy and Power Applications*"* Institute of Physics of Chinese Academy of Sciences in Beijing, China, May 2010. (Invited Lecture)
6. Gao Liu " Challenges in Energy Storage" Tsinghua University in China, June 2010. (Invited lecture)

V.C.9 Executive Summaries of New Anode Projects for FY 2010 (Various)

Venkat Srinivasan
Enviornmental Energy Technologies Division
Lawrence Berkeley National Laboratory
Berkeley, CA 94720
Phone: (510) 495-2679; Fax: (510) 486-4260
E-mail: vsrinivasan@lbl.gov

Introduction

The FY 2010 Batteries for Advanced Transportation Technologies (BATT) Request for Proposals on the "Synthesis and Characterization of Novel Anode Materials and Structures for Use in Lithium Batteries" has resulted in new projects that can help accelerate the application of such batteries in plug-in hybrid electric vehicles and electric vehicles. These projects focus on developing next-generation anodes to increase the energy and decrease the cost of lithium batteries while maintaining safety and cycle life.

Approach

The BATT program received 88 white papers and encouraged 28 applicants to submit full proposals. A selection committee composed of leading lithium battery experts reviewed each proposal and recommended eight for funding. The BATT Program announced the funding of eight new R&D projects on lithium battery anodes.

Results

The awardees include two national laboratories, five universities, and one private non-profit research institute and are listed below, along with a brief description of their projects. The total requested funds are $8.54 million over four years.

Argonne National Laboratory (Michael Thackeray, Jack Vaughey, Lynn Trahey): Three-Dimensional Anode Architectures and Materials. This project will design high surface-area metal foam architectures as substrates for metal or intermetallic anodes. These new architectures will be superior to conventional laminated electrodes due to the enhanced stability derived from direct chemical bonding of the active materials to the current collector. The goal is to design anodes that will deliver a reversible capacity of at least 500 mAh/g with a lifetime of at least 500 cycles.

Binghamton University (Stanley Whittingham): Metal-Based High-Capacity Li-Ion Anodes. This project will synthesize nano-sized metal-based anodes, with most emphasis being placed on nano-tin. Additionally, other electroactive species will be incorporated so that greater lithium insertion rates can be obtained for safe and faster charging. The goal is to develop anodes with volumetric energy densities that approach double those of current carbon anodes, while still maintaining at least 400 mAh/g.

Drexel University (Yury Gogotsi, Michel Barsoum): New Layered Nanolaminates for Use in Lithium Battery Anodes. This project will explore a new class of materials combining the laminate structure of graphite with silicon, tin and other elements that can provide a higher lithium uptake per atom and lead to an improved capacity. The goal is to offer combined advantages of graphite and silicon anodes with a higher capacity than graphite and less expansion, longer cycle life, and a lower cost than silicon nanoparticles.

National Renewable Energy Laboratory and the University of Colorado (Anne Dillon, Steven George, Se-Hee Lee): Atomic Layer Deposition for Stabilization of Amorphous Silicon Anodes. This project will use atomic layer deposition to coat amorphous-silicon anodes with an artificial solid electrolyte interphase layer to help minimize degradation upon volume expansion of the silicon during charging. In addition, flexible organic coatings will be deposited via molecular layer deposition to accommodate this volume change. The goal is to produce an anode with unprecedented high capacity and high rate that is capable of thousands of cycles.

Pennsylvania State University (Donghai Wang, Michael Hickner): Synthesis and Characterization of Polymer-Coated Layered SiO_x-Graphene Nanocomposite Anodes. This project will synthesize anodes targeted to reach specific capacity of more than 1,500 mAh/g with minimal capacity fading in 500 cycles at 1C rates. The layered structure of graphene sheets and SiO_x nanoparticles can accommodate volume change or phase transformation of the SiO_x materials by providing good electric contact between highly conductive graphene layers during charge/discharge processes, leading to enhanced cycling stability. An elastic binder polymer with Li-ion conductivity will be used to further accommodate volume change.

Southwest Research Institute (Kwai S. Chan, Michael Miller, Wuwei Liang): Synthesis and Characterization of Silicon Clathrates for Anode Applications in Lithium-Ion Batteries. This project aims to synthesize silicon clathrate anodes that are designed to exhibit a volume expansion of only 9%, compared with 300% for the lithiation of crystalline

silicon. Because of the small volume changes during lithiation, silicon clathrate anodes have the potential for high specific energy density, while avoiding capacity fading and improving battery life.

Stanford University (Yi Cui): Wiring Up Silicon Nanoparticles for High-Performance Lithium-Ion Battery Anodes. This project will explore a hierarchical porous electrode concept to wire up silicon nanoparticles, which can be synthesized at low cost and in large scale. In addition, this project will investigate strategies to limit electrolyte penetration into the silicon nanoparticle anode and will modify the nanoparticle surface to obtain a stable solid electrolyte interphase layer for long-term cycling.

University of Pittsburgh (Prashant Kumta): Nanoscale Heterostructures and Thermoplastic Resin Binders: Novel Li-Ion Anode Systems. This project will use cost-effective methods to synthesize amorphous silicon and Li-Si alloys and carbon- and boron-based heterostructures. In addition, this project will explore thermoplastic resin binders with chemical, physical, and electrochemical attributes superior to the currently used poly-vinylidene fluoride for keeping silicon particles in contact and preventing electrode cracking during cycling. The project goals include reversible capacities exceeding 2,000 mAh/g and high rate capability.

V.D Electrolyte Development

V.D.1 Polymer Electrolytes for Advanced Lithium Batteries (University of CA, Berkeley)

Nitash P. Balsara
201 C Gilman Hall
Department of Chemical and Biomolecular Engineering
University of California
Berkeley, CA 94720
Phone: (510) 642-8973; Fax: (510) 643-4778
E-mail: nbalsara@berkeley.edu

Start Date: October 2008
Projected End Date: December 2011

Objectives

- Synthesis and characterization of self-assembled block copolymer electrolytes for stabilizing lithium metal anodes.
- Development of electronically and ionically conducting polymer binders.
- Development of self-assembled polymer separators.

Technical Barriers

Current lithium-ion cells use polymers for two applications: they serve as a binder to hold the active materials in place and as a porous separator to hold the liquid electrolyte and keep the electrodes physically separated. The cost of the porous separators is large due to the delicate processing steps that are used in manufacturing. Defects in the separator can cause catastrophic failures. The binder is essentially an inactive component, while electron and ion transport are mediated by separate components - carbon and liquid electrolyte that floods the pores of a porous electrode, respectively. Cell energy and power performance deteriorate if the active materials loses contact with charge transporting components. Lithium metal electrodes are not used in rechargeable batteries due to dendrite growth.

Technical Targets

- Enable the use of a lithium metal electrode stabilized by a block copolymer electrolyte.
- Synthesize and characterize self-assembled porous battery separators.
- Synthesize and characterize electronically and ionically conductive polymer binders.

Accomplishments

- Measured both conductivity and salt diffusion coefficient in block copolymer electrolytes.
- Completed the synthesis and characterization of a series of self-assembled battery separators.
- Completed the synthesis and characterization of the first polymer binder that conducts both electrons and ions.

✧ ✧ ✧ ✧ ✧

Introduction

The objective of this work is to comprehensively examine the role that polymers can play in the development of advanced lithium batteries - specifically addressing issues of safety, cycle life, and cost. Replacing conventional liquid electrolytes with a solid block copolymer enables the use of a lithium metal anode, which improves the energy density of the battery. The block copolymer comprises a hard non-conducting block that suppresses the formation of lithium dendrites while a soft block enables rapid transport of lithium-ions. In more recent work, we have replaced the hard non-conducting block with an electronically conducting block to serve as a polymer binder. Preliminary characterization data reveal the presence of both electron and ion transport capabilities in these materials. Finally, nanoporous separators have been synthesized by block copolymer self-assembly. These materials provide insight into the morphology-conductivity relationship in porous separators. The processing routes to create these separators may be more cost-effective and environmentally friendly than those used currently.

Approach

Sequential polymerization is used to synthesize the block copolymers for all of the projects. Physical characterization includes determination of morphology by X-ray scattering and electron microscopy, and electrochemical characterizations are performed using either blocking or non-blocking electrodes. Equipment for

cycling cells as a function of temperature and for making pouch cells with a solid electrolyte is now available.

Results

Materials. We have synthesized three different kinds of block copolymers: polystyrene-polyethyleneoxide (PS-PEO) copolymers for stabilizing the lithium metal electrode, polyphenelyene vinylene-polyethylene oxide (PPV-PEO) copolymers for electronically and ionically conducting binders, and polystyrene-polyethylene-polystyrene (PS-PE-PS) copolymers to make self-assembled porous separators.

Block Copolymer Electrolyte Characterization. The restricted diffusion approach was used to determine the effect of block copolymer morphology on the diffusion coefficient of LiTFSI salt. The results are shown in Figure V- 106. The surprising result is that the diffusion coefficient increases with increasing molecular weight of the PS-PEO block copolymer. The increase in diffusion coefficient mirrors the increase in conductivity with molecular weight as shown in Figure V- 106. One thus expects that cell polarization due to the development of concentration gradients to be lower in cells with high molecular weight block copolymers. Since dendrite formation is also suppressed by increasing the block copolymer molecular weight, this result has significant practical implications.

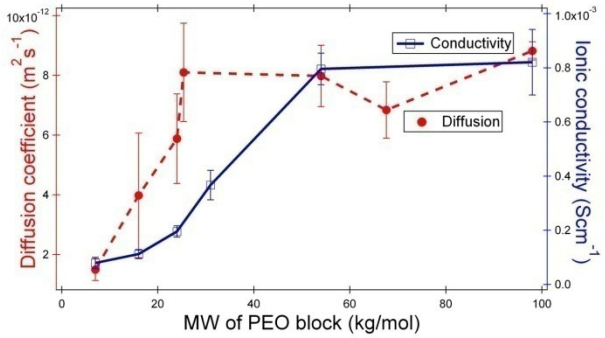

Figure V- 106: Salt diffusion coefficient and conductivity of symmetric PS-PEO block copolymers as a function of the molecular weight of the PEO block at 90°C.

Conducting Binder. We have successfully synthesized electronically conducting block (polypheneylene vinylene doped with iodine) and an ionically conducting block (polyethylene oxide doped with LiTFSi salt). Figure V- 107 shows frequency-dependent impedance spectra of one such PPV-PEO block copolymer, before and after adding a lithium salt. In the absence of the lithium salt, only the electronically conducting pathways participate in charge transport as evidenced by one Nyquist semi-circle. The addition of lithium salt results in two charge transport mechanisms evidenced by the two lobes. Experiments to prove that the lobes represent electron and ion transport are underway.

Self-assembled Separators. Nanoporous separators were created by synthesizing PS-PE-PS triblock copolymers, mixing the copolymer with PS homopolymer, and extracting the homopolymer by using a selective solvent for the PS chains. This results in a porous polyethylene film wherein the pores are lined with PS. The fact that PS is more polar than PE resolves wetting issues and capillarity-related effects, which, in turn may enable the use of membranes with smaller pores than conventional porous polyolefin separators. In Figure V-108 we compare the qualitative conductivities of three PS-PE-PS membranes filled with a 1 M $LiPF_6$ in EC/DEC (1:1 vol.). It is evident that increasing the pore size from 10 to 25 nm has a effect on the efficacy of the separator.

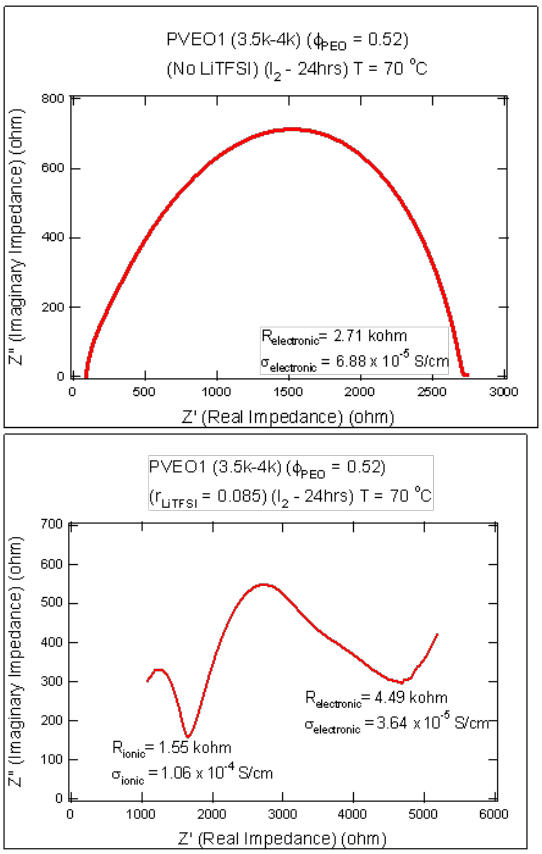

Figure V- 107: Impedance measurements on iodine doped polyphenylene vinylene- polyethylene oxide block copolymer. Top: No lithium salt. Bottom: With lithium salt.

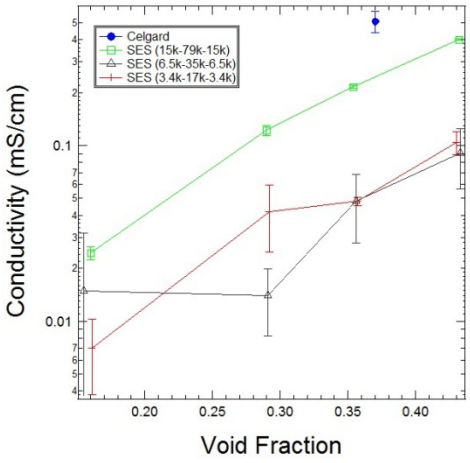

Figure V- 108: Conductivity of PS-PE-PS and conventional Celgard separators as a function of void fraction. The caption shows the molecular weights of the blocks in kg/mol. The average pore width increases with molecular weight: 11, 22, and 25 nm and is nearly independent of void fraction.

Conclusions and Future Directions

We have established a broad program with the potential to fundamentally alter the way polymers are used in rechargeable lithium batteries. The first project within this program was to develop block copolymer electrolytes to stabilize the lithium metal anode. We have determined conductivity and diffusion coefficients as a function of block copolymer morphology. In the future we will determine the lithium transference number and salt activity coefficients and thereby complete the characterization of this class of electrolytes. This will conclude our work on characterization of block copolymer electrolytes against lithium metal electrodes. We are now poised to combine the newly synthesized binder with active cathode particles and study the ability of the binder to transport electrons and ions to the reaction sites. We will complete our study of porous separators by characterizing a wider array of morphologies to understand the underpinnings of ion transport in these systems.

FY 2010 Publications/Presentations

1. "Comparing the Effect of Adding Imidazolium and Lithium Salts on the Thermodynamics of Block Copolymer Electrolytes", N.S. Wanakule, J.M. Virgili, A.A. Teran, N.P. Balsara, Z.-G., Wang, *Macromolecules*, accepted, 2010.
2. "Ionic Conductivity of Block Copolymer Electrolytes in the Vicinity of Order-Disorder and Order-Order Transitions", N.S. Wanakule, A. Panday, S.A. Mullin, E. Glann, A. Hexamer, N.P. Balsara, vol. 42, pg. 5642-5651, *Macromolecules,* 2009.
3. "Effect of Molecular Weight and Salt Concentration on Conductivity of Block Copolymer Electrolytes", A. Panday, S. Mullin, E.D. Gomez, N.S. Wanakule, V.L. Chen, A. Hexemer, J. Pople, and N.P. Balsara, vol. 42, pg. 4632-4637, *Macromolecules,* 2009.
4. Invited Lecture, "Solid-State Batteries with Lithium Metal Electrodes", Symposium on "Scalable Energy Storage Beyond Li-ion: Materials Perspective", Oak Ridge National Laboratory, Oak Ridge, Tennessee, October 7, 2010.
5. Invited Lecture, "Dry Block Copolymer Electrolytes for Lithium Batteries", International Meeting on Lithium Batteries, Montreal, Canada, June 30, 2010.
6. Invited Lecture, "Ion Transport in Block Copolymers", Gordon Research Conference, Polymer Physics, Mount Holyoke, Massachusetts, June 29, 2010.
7. Materials Research Lecture, "Batteries, Fuel Cells, and a Start-up", Department of Chemical Engineering, California Institute of Technology, Pasadena, California, May 6, 2010.
8. Departmental Seminar, "Batteries, Fuel Cells, and a Start-up", Department of Chemical Engineering, University of Illinois, Urbana, Illinois, May 5, 2010.

V.D.2 Interfacial Behavior of Electrolytes (LBNL)

John B. Kerr
Lawrence Berkeley National Laboratory,
MS 62R0203, 1 Cvclotron Road,
Berkeley, CA 94720
Phone: (510) 486-6279; Fax: (510) 486-4995
E-mail: jbkerr@lbl.gov

Start Date: October 1, 2008
Projected End Date: September 30, 2012

Objectives

FY09

- Determine the role of electrolyte structure upon the intrinsic electrochemical kinetics and how it contributes to the interfacial impedance.
- Determine how bulk and electrode reactions of electrolytes contribute to impedance growth and lead to battery failure.

FY10

- Demonstrate whether single-ion conductor polyelectrolytes (gel and dry polymer) prevent concentration polarization in composite cathodes and facilitate thicker electrodes.
- Determine whether single-ion conductor polyelectrolytes (gels and dry polymers) are beneficial for large volume-expansion anodes.

Technical Barriers

This project addresses the following technical barriers

- Poor cycle and calendar life.
- Low power and energy densities.
- High manufacturing cost.
- Safety

Technical Targets

- Determine the contribution to the interfacial impedance of the salt structure in terms of reactivity versus intrinsic electrode kinetics.
- Determine the contribution to the interfacial impedance of the solvent structure in terms of reactivity versus intrinsic electrode kinetics.
- Determine the contribution to the interfacial impedance of the physical properties of the electrolyte – liquid vs. gel. vs. solid polymer electrolyte.
- Develop analytical methods for determining side reaction products and chemical characterization of the SEI layer.

Accomplishments

- Prepared and tested three new lithium fluoroboromalonate salts which clearly demonstrate the effect of anion structure on interfacial impedance.
- Prepared and tested new single ion conductor polyelectrolytes based on fluoroboromalonate anions.
- Prepared new single ion conductor materials based on fluoroalkylsulfonylimide anions which appear stable to 5 Volts or higher.
- The new salts appear to have interesting and potentially beneficial effects in conventional lithium-ion cells when used as additives.

✧ ✧ ✧ ✧ ✧

Introduction

The choice of electrolyte used in lithium-ion batteries presents significant challenges. The material has to transport lithium-ions from one electrode to the other with minimum resistance and facilitate the transfer of charge across the interfaces with a minimum of irreversible electrochemical and chemical reactions that reduce capacity and shorten lifetime. Since it is desirable for the electrodes to possess high energy this requirement represents a major challenge for the design of electrolytes. The presence of large resistances within the battery results in heat generation which imposes further stress upon the electrolyte and hence it is important not only for power and energy density but also for lifetime to minimize the impedances within the cell.

The impedances presented by the electrolyte are the bulk ohmic resistance (conductivity), concentration polarization (transport properties) and interfacial impedance (intrinsic electrochemical kinetics of charge transfer at the electrodes). Most of the attention of electrolyte researchers over the years has focused upon the ohmic resistance (conductivity) of the bulk electrolyte yet this impedance is usually smaller than that due to concentration polarization (especially in composite electrodes) and much smaller than that of the interface.

Interfacial impedance is a critical barrier to the deployment of lithium-ion batteries in traction vehicles.

Single-ion polyelectrolyte lithium conductors possess the solution for many of the problems with present electrolytes. They can be used with no liquid electrolyte thereby reducing the safety problem. They can be prepared and deployed in ways that avoid many of the reactivity issues both in the bulk of the electrolytes and at the interfaces. Because they possess a unity transference number, there is no concentration polarization through the composite electrodes. Thus, provided the conductivity is in excess of 10^{-4} S/cm, the single ion conductors (SIC) can facilitate the use of thicker composite electrodes thereby leading to higher energy and power densities. In past years, this group has demonstrated that SIC materials, both dry and as gels, possess the bulk transport properties required. However, the interfacial behavior of these materials has exhibited disastrously high impedances rendering the SIC materials unusable. It is imperative that the source of this impedance be elucidated and reduced to manageable values and hence the whole goal of the work is to elucidate the mechanisms that lead to interfacial impedance so that this critical factor may be minimized.

There is considerable continuing discussion in the literature about the effect of the solid electrolyte interphase (SEI) upon the interfacial impedance of lithium-ion battery electrodes. Growth of the impedance is one mode of failure that limits the calendar and cycle life of lithium-ion batteries. From studies of a variety of electrolytes ranging from single ion polyelectrolyte lithium-ion conductors through binary salt polymer electrolytes, polymer gels, ionic liquids and liquid electrolytes it has been noted that the properties of the electrolyte have a significant impact on the apparent intrinsic rates of electrode reactions quite apart from their reactions to form side products that may form the SEI layer. To separate out these effects we have attempted to study a variety of electrolytes that can allow the separation of the effect of side reactions from that of intrinsic kinetics. Needless to say, the effects of trace impurities and intrinsic instabilities in both the electrolytes and the electrodes can have a major impact upon the interfacial behavior and considerable effort is still required to properly characterize the materials for reproducible results.

Approach

A physical organic chemistry approach is taken to electrolyte design, where the molecular structure is varied to provide insight into the processes that may affect the performance of the battery. These processes include transport properties, electrochemical kinetics, electrode side-reactions, thermal stability of the bulk material and interfacial behavior. The work involves use of model compounds as well as synthesis of new materials to test hypotheses which may explain battery behavior. Examples include:

- Different solvents and salts, including polymer gels and solid polymer electrolytes.
- Electrode materials with different reaction potentials.
- Single-ion conductor polyelectrolytes (dry polymers and gels) as separators and binders in composite electrodes.
- Functionalized surfaces for electrode components.

To accomplish this work requires collaboration with other groups in BATT.

- Surface analysis groups to identify side reaction products and reactive intermediates by combination of spectroscopy and product distribution analysis.
- Sharing data and materials with other electrolyte developers.
- MD and electrochemical systems modeling groups to provide experimental data.
- Deliver promising materials to cell testing group.

Results

Previous work from this group has reported upon the tethering of borate ester anions derived from malonic acid which allows the anion to be fixed to the polymer to form a network polymer that is cross-linked through the anion (see Figure V- 109). The cross-linking results in a higher glass transition temperature and lower mobility of the chains with the bound anions. Intuitively, it is expected that anions which are bound to the side chains but do not cross-link the polymer will have more mobility and hence higher conductivity. This expectation has been confirmed with polymers that contain fluoroalkylsulfonate and sulfonylimide anions, which possess high conductivities. During the past year we have prepared new borate ester anions which may be less expensive and provide insight into the effect of anion structure on the bulk and interfacial behavior.

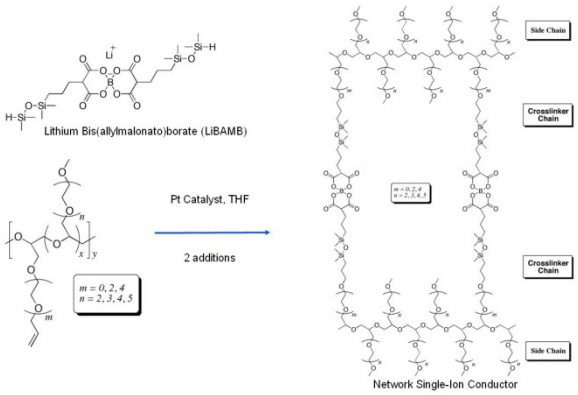

Figure V- 109: Preparation of Network Single ion Conductor.

Preparation and testing of new salts. Figure V- 110 shows the structures of new salts that have been synthesized and tested. The hydrosilated salt is used to attach the anion to the polymer as illustrated in Figure V-109 and this anion provides a material that is not cross-linked.

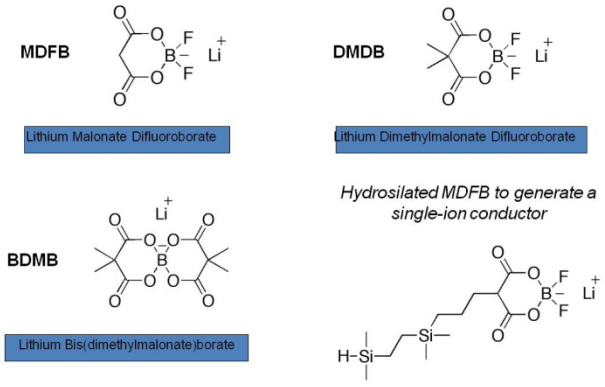

Figure V- 110: New salts synthesized and tested in FY10.

The conductivities of these salts in PEO as a function of temperature are shown in Figure V- 111 where the conductivity of LiTFSI is shown for comparison. The boron anions are all somewhat lower in conductivity but not so much as to be unusable. Figure V- 112 shows the exchange current densities obtained from the impedance measurements as a function of temperature of these salts at lithium metal electrodes with PEO as the solvent. Again the LiTFSI is higher but only by an order of magnitude. More importantly the slopes of the lines vary indicating changes is the activation energy required for charge transfer. This can be seen for BDMB and DMDB which do not have an acidic proton (MDFB) or an easily reducible C-F bond (TFSI) and may indicate that these anions react less with the electrode. In any case a clear effect of anion structure on interfacial behavior is demonstrated.

The borate salts show acceptable conductivity in liquid solvents as can be seen from Figure V- 113 but even more interesting is the effect on interfacial impedance and stability where the BDMB and DMDB salts appear to have a beneficial effect.

Figure V- 114 shows the improvement in cycling obtained with the LiDMMDFB salt versus the LiMDFB in Li-ion cells using cobalt oxide cathodes and MCMB anodes.

The full cell cycling results shown in Figure V- 114 reinforce the effects of the anion structure. The dimethyl anion has no acidic proton to react with the electrodes and hence shows better stability. Voltage stability experiments conducted by means of chronopotentiometry shows that these anions are stable to 5 volts versus lithium.

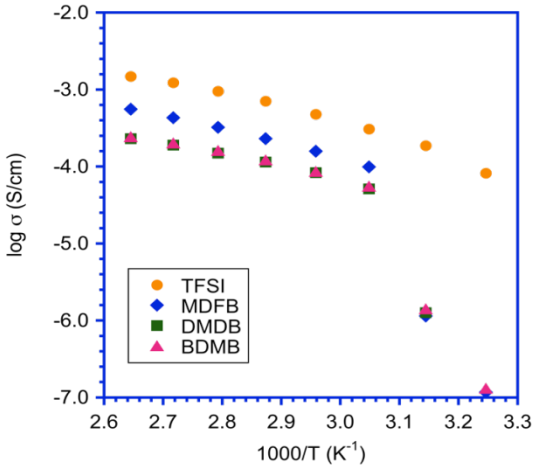

Figure V- 111: Conductivities of Li slats in PEIO as a function of temperature.

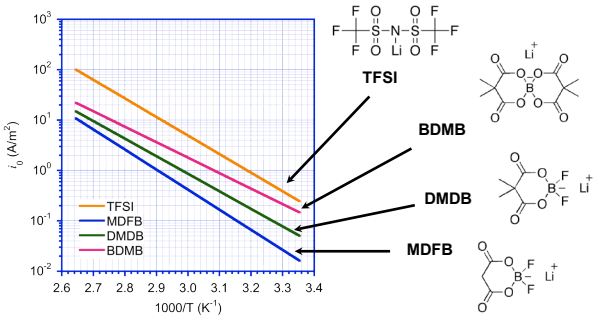

Figure V- 112: Exchange current densities for lithium salts in PEO as a function of temperature.

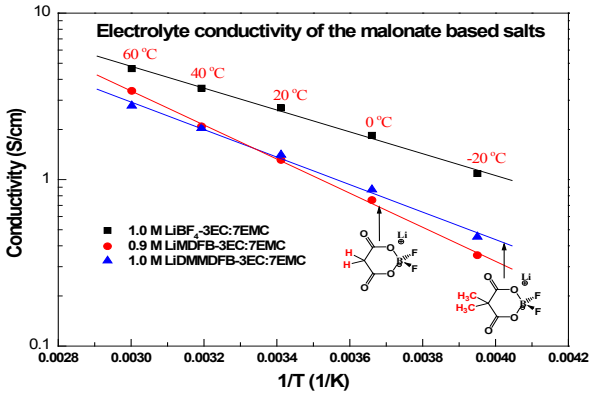

Figure V- 113: Conductivity of Borate salts in liquid solvents.

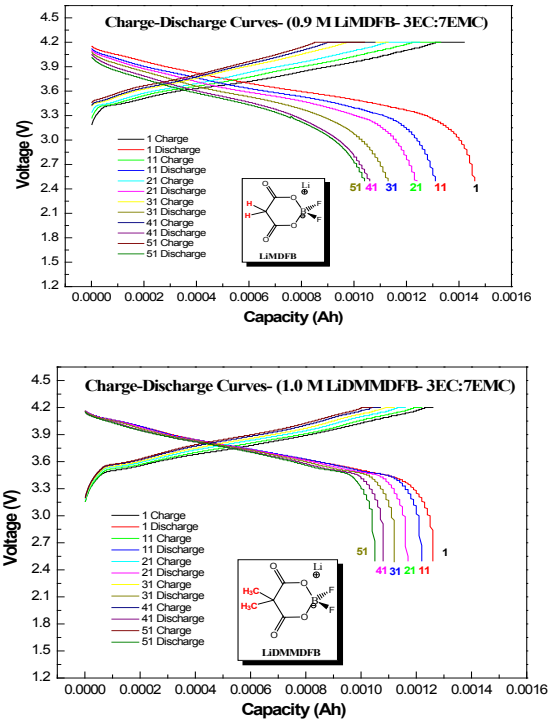

Figure V- 114: Comparison of cycling behavior of two lithium salts in EC/EMC solvents in full cells ($LiNi_{0.8}Co_{0.2}O_2$:MCMB).

The anions have been attached to polymers and the resulting materials tested for conductivity, interfacial impedance and cycling at lithium metal. The conductivities are in the range of 10^{-5}-10^{-6} S/cm between 85 and 25°C and the exchange current densities at lithium metal are about two orders of magnitude lower that the binary salt systems. Cycling at lithium metal shows a small amount of diffusional behavior which indicates the presence of impurities in the material. These materials are being purified and examined as binders for composite electrodes in lithium-ion cells

FY 2010 Publications/Presentations

1. Poster Presentation to the 2010 DOE Annual Peer Review Meeting. ES39.
2. "Polyelectrolyte Membranes Containing Lithium Malonate Difluoroborate for Lithium-ion Systems," Peter F. Driscoll, Li Yang, Hanjun Zhang and John B. Kerr, ECS Fall Meeting 2010, Las Vegas, NV
3. "Lithium Malonate Borate Based Salts and Their Performance," Li Yang , Hanjun Zhang , Peter F. Driscoll , John B. Kerr and Brett Lucht, ECS Fall Meeting 2010, Las Vegas, NV

V.D.3 Molecular Dynamics Simulation Studies of Electrolytes and Electrolyte/Electrode Interfaces (University of Utah)

Grant D. Smith and Oleg Borodin
122 S. Central Campus Drive, Rm. 304
University of Utah
Salt Lake City, UT 84112
E-mail: gsmith2@gibbon.mse.utah.edu

Start Date: February 2008
Projected End Date: December 2011

Objectives

- Use molecular simulations to predict the chemical composition and structure of SEI layers and to understand the role of additives in the formation of SEI layers
- Gain molecular level understanding of Li^+ transport mechanisms in SEI layers
- Gain molecular level understanding of Li^+ transport mechanisms in liquid and ionic liquid electrolytes comprised of new salts and solvents in collaboration with experimental BATT projects
- Gain molecular level understanding of Li^+ intercalation/deintercalation into/from representative anode and cathode materials
- Understand double layer structure, capacitance and transport at the anode and cathode interface as a function of potential and temperature
- Provide guidance for design of electrolytes with improved lithium transport, reduced interfacial resistance and/or improved electrochemical stability

Technical Barriers

- Poor low-temperature operations
- Poor transport through SEI layers
- High interfacial transport resistance

Technical Targets

- Develop a cell to meet the 40-mile PHEV goals.

Accomplishments

- Improved understanding of the outer SEI formation via single electron reduction of ethylene carbonate
- Improved understanding of the structure, dynamics and desolvation energetics of the graphite/electrolyte interface
- Predicted transport properties of novel electrolytes utilizing cyano-containing salts
- Predicted the influence of fluorination on the properties of sulfolane solvents

Introduction

The interfaces between electrodes and the bulk electrolyte in secondary lithium batteries are complex. Often in direct contact with the anode is the solid electrolyte interphase (SEI) comprised of species formed primarily by the electrochemical decomposition of the electrolyte, salt, and additives. The SEI layer in turn is in contact with the electrolyte (solvent + salt) whose structure and dynamics are likely strongly perturbed by the presence of the interfaces. Electrode/electrolyte interfaces influence cell performance in numerous ways. For example, the SEI layer, particularly at the anode but perhaps also at the cathode, stabilizes the electrode against solvent intercalation/dissolution and stabilizes the electrolyte against electrochemical decomposition but can result in high interfacial transport resistance, particularly at lower temperatures. Formation of SEI layers with good transport properties, good mechanical properties and electrochemical stability is of paramount importance.

Approach

Our approach to simulation of bulk electrolytes, SEI layers, and electrode/electrolyte interfaces is three-pronged. First, where possible and appropriate, we utilize quantum-chemistry based force fields and non-reactive simulation methods. These studies include bulk electrolytes, model SEI layers and electrode/electrolyte interfaces. Second, we utilize an electroactive interface model to study electrolyte structure and charge transfer processes at electrode/electrolyte interfaces where control of electrode potential is paramount. Finally, to investigate chemical pathways of SEI formation we utilized atomistic MD simulations with ReaxFF, a reactive force field developed by Adri van Duin and William Goddard at Caltech. This simulation method combines accuracy in modeling reaction energies and barriers with capability to

simulate systems large enough and over sufficiently long time to capture the diffusive properties of molecules necessary to adequately capture important chemical and structural reorganization during SEI formation. The ReaxFF is an empirical potential which is parameterized to reproduce results from quantum chemistry calculations.

Results

EC reduction and VC reactions. MD simulations using ReaxFF show that linear (open) ethylene carbonate (EC) radicals in the bulk electrolyte recombine to form exclusively lithium butylene dicarbonates shown below on the left. No ethylene dicarbonates (higher energy compounds) have been observed in our simulations. MD simulations using ReaxFF also show that linear and cyclic EC radicals in bulk electrolyte recombine to form the ester-containing compound shown below on the right. Finally, MD simulations using ReaxFF of EC radicals in bulk vinilyne carbonate (VC) show formation of poly(VC) compounds initiated by open and closed EC radicals (Figure V- 115).

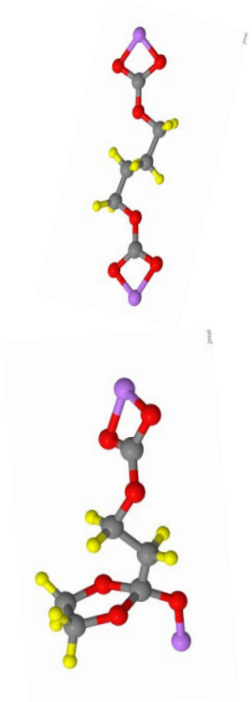

Figure V- 115: SEI components from the reduction of EC and VC as predicted by ReaxFF MD simulations.

Graphite/electrolyte structure and dynamics. Molecular dynamics simulations with our electroactive interface model (controlled electrode potential) allow us to study the influence of electrode potential on the structure, capacitance, and transport properties of the electrolyte at the electrode/electrolyte interface. A snapshot of a graphite/electrolyte/graphite system simulated over a range of potentials is shown in Figure V- 116.

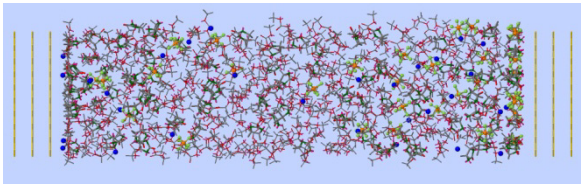

Figure V- 116: Snapshot of a simulation of an EC/DMC/$LiPF_6$ electrolyte between graphite electrodes at high potential difference between the electrodes.

Simulations reveal that the structure, differential capacitance and molecular dynamics at the electrode/electrolyte interface depend strongly upon electrode potential. For example, the ratio of EC molecules to DMC molecules at the interface increases dramatically with increasing electode potential.

Novel salt MD simulations. Polarizable force field has been developed for lithium (fluorosulfonyl)imide LiFSI and dicyano-1,2,3-triazolate (LiDCTA) salts. MD simulations were performed on the EC:DMC (1:1)/LiFSI 0.85 M electrolyte as a function of temperature. Ion conductivity for EC:DMC (1:1)/LiFSI 0.85 M predicted from MD simulations was found in excellent agreement with experimental data as shown in Figure V- 117. High degree of the LiFSI salt dissociation in EC:DMC (1:1) was observed: 38% of the Li^+ cations did not have oxygen atoms from FSI^- anions in its first coordination shell, while the dynamic degree of ion dissociation ad was found between 47% and 52 %, which is slightly higher than the values of 34%-44% observed from MD simulations for EC:DMC(1:1) 1 M $LiPF_6$ at 298 K - 363 K temperature range. At 298 K, the Li^+ coordination shell (<2.8 Å) consisted of 2.0 carbonyl oxygens from DMC, 1.5 carbonyl oxygens from EC and 0.9 oxygen atoms from FSI^- anions.

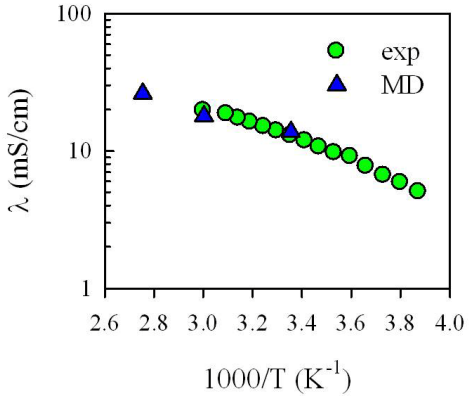

Figure V- 117: Conductivity of EC:DMC/LiFSI electrolytes from MD simulations and experiments. *Abouimrane et al. J. Power Sources 2009, 189, 693.*

MD simulations were also performed on γ-butyrolactone GBL/LiDCTA 0.6 M electrolyte. The

conductivity of GBL/LiDCTA 0.6 M at 298 K was found to be ~4.5 mS/cm, which is significantly lower than the conductivity for GBL-based electrolytes with $LiPF_6$ and LiTFSI salts (~10 mS/cm 298 K). Lower conductivity of GBL/LiDCTA 0.6 M compared to GBL/$LiPF_6$ 0.6 M was attributed to the two times slower ion diffusion and lower degree of ion dissociation in GBL/LiDCTA compared to GBL/$LiPF_6$.

Novel solvent simulations. Influence of complete and partial fluorination of sulfolane on the structural and transport properties of sulfolane/LiTFSI electrolytes was investigated in QC calculations and MD simulations. It was found that complete fluorination of sulfolane (sulfolane → sulfolane$_{F8}$) reduced the binding energy from 53.7 kcal/mol for sulfolane/Li^+ to 29.5 kcal/mol for sulfolane$_{F8}$/Li^+ as calculated at MP2/cc-pvTz level, while sulfolane with four fluorines (sulfolane$_{F4}$) yielded sulfolane$_{F4}$/Li^+ binding energy of -40.8 kcal/mol, which is similar to the DMC/Li^+ binding energy.

MD simulations of sulfolane$_{F8}$ doped with LiTFSI salt at solvent:Li=20 salt concentration showed complete salt aggregation, while MD simulations of sulfolane$_{F4}$/LiTFSI at solvent:Li=20 indicated a small degree of LiTFSI dissociation (<5%) and conductivity less than 1 mS/cm.

Conclusions and Future Direction

- Quantum chemistry (gas phase) and ReaxFF (condensed phase) simulations have revealed the importance of the cyclic EC radical in the formation of compounds believed to be important in the outer SEI.
- Introduction of vinylene carbonate to the electrolyte leads to the formation of poly(vinylene carbonate) initiated by both cyclic and linear EC radicals.
- The dynamics of the electrolyte near the $LiFePO_4$ interfacial are found to be dramatically slower than in the bulk or at the interface with graphite, but exhibit temperature dependence similar to the bulk (not shown in this report).
- Completely fluorinated sulfolane-based solvents are not promising candidates as electrolytes for operations with high voltage cathodes because of salt aggregation.
- LiDCTA salt has an inferior conductivity to $LiPF_6$ and LiTFSI in GBL solvents at 0.6 M salt concentration at room temperature.
- EC:DMC/LiFSI 0.8 M electrolytes show higher conductivity than EC:DMC/$LiPF_6$ 1 M. A slightly higher fraction of DMC than EC was found in the first coordination shell of the Li^+ cations for the mixed EC:DMC (1:1)/Lisalt electrolytes.
- EC/DMC/$LiPF_6$ electrolyte at the interface with graphite was found to exhibit a complex multilayer structure that depends strongly on electrode potential. The dependence of the interfacial (electrode) capacitance on potential correlates qualitatively but not quantitatively with the structure of the first interfacial electrolyte layer.
- Utilized ReaxFF simulations to predict the structure and transport properties of SEI layers for relevant model chemistries with emphasis on the role of additives (particularly VC).
- The free energy profile/interfacial impedance for Li^+ intercalation/deintercalation into $LiFePO_4$ and graphite electrodes was determined as a function of temperature and electrode potential.
- Explore the structure, transport, and stability of electrolytes comprised of new salts and solvents in collaboration with BATT investigators.
- Perform whole-cell (anode/electrolyte/cathode) simulations with controlled electrode potential using relevant model chemistries.
- Investigate oxidation mechanisms at the $LiFePO_4$ cathode.

FY 2010 Publications/Presentations

1. Borodin, O.; Gorecki, W.; Smith, G. D.; Armand, M. "Molecular dynamics simulation and pulsed-field gradient NMR studies of bis(fluorosulfonyl)imide and bis(trifluoromethanesulfonyl)imide-based ionic liquids" J. Phys. Chem. B 2010, 114, 6786–6798.
2. Didden, D.; Heuer, A.; Borodin, O. "Understanding the lithium transport within a Rouse-based model for a PEO/LiTFSI polymer electrolyte" *Macromolecules* **2010**, *43*, 2028–2036.
3. Vatamanu, J.; Borodin, O.; Smith, G. D. "Molecular Dynamics Simulations of Atomically Flat and Nanoporous Electrodes with a Molten Salt Electrolyte" *Chem. Phys. Phys. Chem.* **2010,** *12,* 170 - 182
4. Smith, G. D.; Borodin, O.; Salvy, R.; Rees, R.; Hollenkamp, A. F. "A Molecular Dynamics Simulation Study of $LiFePO_4$/Electrolyte Interfaces: Structure and Li^+ Transport in Carbonate and Ionic Liquid Electrolytes" *Chem. Phys. Phys. Chem.* **2009**, *11*, 9884 – 9897.
5. Grant D. Smith and Oleg Borodin "Molecular dynamics simulation studies of electrolytes and electrolyte/electrode interfaces" 2010 DOE Annual Peer Review Meeting Presentation.
6. (invited) Grant D. Smith and Oleg Borodin "Ionic Liquids as Electrolytes in Lithium Battery Applications: Insights from Molecular Dynamics Simulations" Gordon Research Conference on Electrochemistry, Venture, CA January 2010
7. (invited) Grant D. Smith and Oleg Borodin "Lithium-ion Transport in Polymer Electrolytes: Insights from

Molecular Simulations" Materials Research Society Meeting, San Francisco, CA April 2010
8. (invited) Grant D. Smith and Oleg Borodin "Lithium-ion Transport in Polymer Electrolytes: Insights from Molecular Simulations" Institute for Physics, Martin Luther University, Halle, Germany CA August 2010
9. (invited) Grant D. Smith "Multiscale Modeling of Electrolytes for Battery and Capacitor Applications" Army Multiscale Multidisciplinary Modeling of Electronic Materials Materials Workshop, VA September 2010
10. (invited) O. Borodin, J. Vatamanu, G. Smith "Structure and Ion Transport in Ionic Liquids and Liquid Electrolytes from Molecular Dynamics Simulations", 217th ECS Meeting, 2010, April 25-30, Vancouver, Canada
11. (invited) O. Borodin "Ion Transport and Structural Properties of Polymeric Electrolytes and Ionic Liquids from Molecular Dynamics Simulations", O. Borodin American Physical Society March Meeting, Portland, Oregon, March 15-19, 2010 (http://meetings.aps.org/Meeting/MAR10/Event/123562)
12. O. Borodin, Grant Smith, Dmitry Bedrov, Adri van Duin, Wladimir Gorecki, Michel Armand "Insight into Electrolyte Structure, Transport and Reduction Pathways from Molecular Dynamics Simulations", The 15th International Meeting on Lithium Batteries, 2010, June 27- July 2, Montréal, Canada
13. L. Cao, J. Vatamanu, O. Borodin, and G. Smith, Molecular Dynamics Simulation Study of the Structure, Capacitance and Li^+ Transport Properties of the $LiFePO_4$/Electrolyte Interface 218th ECS Meeting 2010, Oct. 10-15, Las Vegas, Nevada
14. O. Borodin, G. Smith, and I. Halalay "Comparison of Properties of Trialkyl Phosphate-Based and Cyclic Carbonate-Based Electrolytes from Molecular Dynamics Simulations", 218th ECS Meeting 2010, Oct. 10-15, Las Vegas, Nevada
15. D. Bedrov, G. Smith, and A. Van Duin A Quantum Chemistry and Reactive (ReaxFF) Molecular Dynamics Simulations Study of Mechanisms of SEI Formation in Lithium-Ion Batteries 218th ECS Meeting 2010, Oct. 10-15, Las Vegas, Nevada
16. Borodin, O.; Smith, G. "Interfacial Structure and Interfacial Resistance of EC:DMC/$LiPF_6$ and Ionic Liquid Electrolytes at Graphite and $LiFePO_4$" 216th ECS Meeting - Vienna, Austria, 2009

V.D.4 Bi-functional Electrolytes for Lithium-ion Batteries (CWRU)

Daniel Scherson and John Protasiewicz
Department of Chemistry
Case Western Reserve University
Cleveland, OH 44106
Phone: (216) 368-5186
E-mail: dxs16@po.cwru.edu

Start Date: October 1, 2009
Projected End Date: September 30, 2013

Objectives

- Design, synthesize, and characterize the physical and electrochemical properties of functionalized Li salt anions containing phosphorous and boron moieties known to impart materials with flame retardant properties (Flame Retardant Ions or FRIONS) and thus improve device safety.
- Gain insight into the overall chemical and electrochemical behavior of these novel bifunctional electrolytes toward Li-ion charged anodes using a combination of electrochemical and *in situ* spectroscopic techniques.
- Develop structure-function relationships that will guide further search of optimized FRIONS and other species that contribute to enhanced abuse tolerance.

Technical Barriers

This project addresses the abuse tolerance barriers from the BATT program

Technical Targets

- Demonstrate superior abuse characteristics compared to a baseline cell: Conoco Philips CPG-8 Graphite/1 M $LiPF_6$+EC:DEC (1:2)/Toda High-energy layered (NMC)

Accomplishments

- Synthesized first generation of Flame Retardant Ions (FRIONs)
- Completed characterization of first FRION including preliminary charge-discharge curves in coin cells
- Completed construction of an *in situ* attenuated total reflection Fourier transform infrared spectroscopy (ATR-FTIR) cell

✧ ✧ ✧ ✧ ✧

Introduction

The main objectives of this project are to develop rational guidelines for the design and synthesis of new classes of Li-based salts endowed with flame retardant properties while displaying fast ion transport characteristics. In addition to these key attributes, such *bifunctional electrolytes* should be weakly coordinating and of low molecular weight, exhibit low toxicity, promote formation of low impedance solid electrolyte interfaces (SEI) and be relatively inexpensive.

Approach

The tactic being implemented in our research group seeks to impart lithium-ion batteries with enhanced safety features by incorporating flame retardant and overcharge protection chemical groups to anionic species that display good transport properties and optimum SEI properties. These new materials are expected to either substitute for currently used electrolyte salts or be introduced as additives in conventional formulations. Systematic studies of compounds of this type will provide guidelines for the search of materials displaying optimized characteristics. Also to be thoroughly investigated is the structure of the solid electrolyte interfaces formed in these new media via a combination of electrochemical and *in situ* ATR-FTIR using a cell equipped with a diamond window optimally designed to avoid problems associated with impurities.

Results

Synthesis – The synthesis of the FRION $(THF)Li(C_2O_4)(O_2PPh_2)_2$, **1**, was accomplished by the dehydration reaction of diphenyl- phosphinic acid (Ph_2PO_2H) and oxalic acid ($C_2H_2O_4$) with boric acid (H_3BO_3) and deprotonation by lithium hydroxide (LiOH, see Scheme 1 – in Figure V- 118) yielding only about 50% conversion to the desired lithium salt. Addition of three additional equivalents of LiOH to the reaction mixture, however, resulted in complete conversion to an undesired side product $(Ph_2PO_2H)Li(O_2PPh_2)$, **2** (not shown). Attempts to limit the amount of **2** produced were made by synthesizing **1** from H_3BO_3, Ph_2PO_2H, $C_2H_2O_4$, and lithium diphenylphosphinide. Ph_2PO_2Li. In this case, complete consumption of Ph_2PO_2H was observed and only 25% of **2** was produced. Furthermore, when two equivalents of Ph_2PO_2H and LiOH were used, 40% of unreacted Ph_2PO_2H with about 10% of **2** was observed.

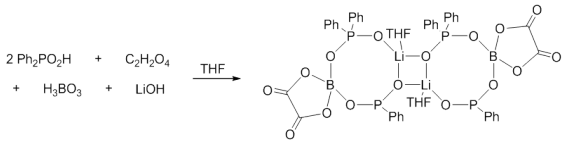

Figure V- 118: Scheme 1. Synthesis of $(THF)Li(C_2O_4)(O_2PPh_2)_2$, 1.

The ratio of electrolyte to side product was dependent upon reaction temperature, time, and ratios of starting materials. **1** was isolated from unreacted Ph_2PO_2H and side product in 20% yield through recrystallization as colorless, hygroscopic crystals. The ^1H NMR spectrum of **1** displayed upfield shifts for the aromatic resonances as well as the 1.5 equivalents of tetrahydrofuran. The ^{11}B and ^{31}P NMR spectra displayed single resonances at 7.99 and 20.9 ppm, respectively. Due to the nature of ^1H and ^{31}P NMR resonances, it was postulated that both phosphinic acid moieties were in similar chemical environments in solution. The melting point of **1** had a range of 161-166 °C due to the slow loss of THF (*vide infra*). Crystals of **1** grown from THF were analyzed by X-ray diffraction, and the results are presented in Figure V- 119. The overall solid state structure of **1** is that of a dimer associated by P-O•••Li interactions (Figure V- 119, lower). The lithium atoms are tetrahedrally coordinated by four oxygen atoms, from three different phosphinic acid molecules and a coordinated THF molecule. The boron atoms also adopt a tetrahedral geometry comprised of four oxygen atoms from two different Ph_2PO_2H molecules and a k^2-*O,O*-oxalato substituent (Figure V- 119, upper).

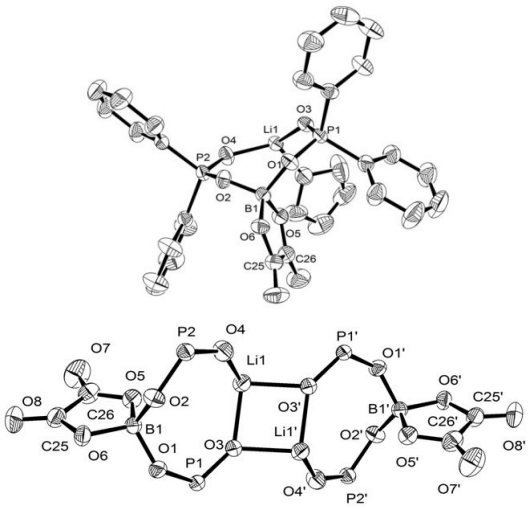

Figure V- 119: ORTEP diagrams of 1 showing monomer (upper figure, THF and hydrogen atoms omitted for clarity) and dimeric association (lower figure, hydrogen atoms, phenyl rings, and THF omitted for clarity.

Thermal Stability. In order to assess the thermal stability of **1**, thermogravimetric analysis (TGA) was performed on the lithium salt using a TGA experiments were performed on a Perkin Elmer DSC 7 (Figure V-120). A list of thermal events including the temperature at which these were observed and the proposed assignments are given in Table V- 2. Furthermore, a 0.015 M solution of **1** in propylene carbonate was held at 70°C for 2 weeks in a sealed NMR tube and monitored periodically via ^{31}P NMR spectroscopy. No visible decomposition was discernable after 1 week

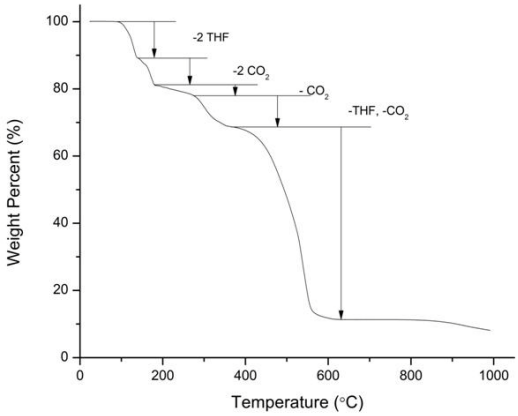

Figure V- 120: TGA analysis of solid 1.

Table V- 2: **Thermal Events, Temperature, and Mass Loss Assignments based on the data in Figure V- 120**

Event	T (°C)	Mass Loss Assignment
1	94.5	2 THF
2	155.4	2 CO_2
3	249.5	CO_2
4	343.6	THF & CO_2

Coin Cell Data. The effects of FRION **1** on the performance of 2032-type coin cells incorporating a $LiCoO_2$ cathode and a graphite anode in 1M $LiPF_6$ in EC:EMC (3:7 vol) + 1.5 wt% VC electrolyte are shown in Figure V- 121 which compares data collected at 1 mA between 4.2 and 2.75 V at a C/5 rate before (left) and after (right) addition of 2% 1 to the formulation. Based on the results obtained, the presence of **1** does not adversely affect the operation of the cell.

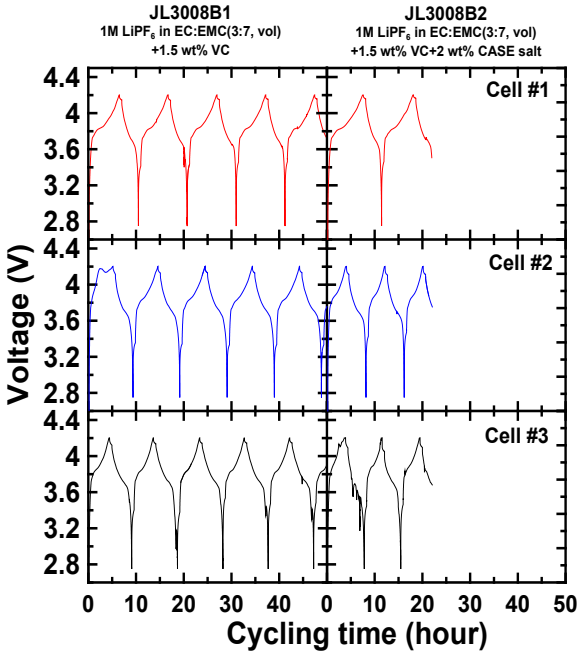

Figure V- 121: Charge/Discharge Curves with and without 1 in a 2032-type coin cell (see test for details. The cells were filled directly from septum type electrolyte container without using a glove box.

Spectroscopic Studies

Attenuated Total Reflection FTIR. A photograph of the cell for *in situ* ATR-FTIR measurements designed and constructed in our laboratory is shown in Figure V-122. The cell is made out of propylene and incorporates unique features that help mitigate problems associated with impurities. The upper knob allows for a nickel rod electrode isolated from the atmosphere to move along the vertical axis, z, whereas the left knob makes it possible to translate a stainless steel rod along an axis normal to z which houses at its end a piece of Li foil. Once the cell is filled with electrolyte, the nickel rod is lifted and the Li foil placed directly beneath and at a very small distance from the flat end of the Ni electrode. Application of a current between the Li and Ni electrodes allows for a film of pure Li to be deposited on the flat surface of the Ni rod. Once the deposition is completed, the Li foil is retrieved and the Ni rod is lowered and pressed directly against the diamond window for spectroscopic examination.

Conclusions and Future Directions

The first FRION in a series of lithium anions containing phosphorus moieties has been successfully synthesized and isolated. Preliminary examination of **1** in coin cell batteries has shown no deleterious effects upon battery performance. Further electrochemical and flammability testing of **1** are currently being undertaken.

Continuing work will include the synthesis of lower molecular weight variants of **1** as well as the development of other possible FRIONS as well as their electrochemical characterization.

The newly constructed cell for *in situ* ATR-FTIR measurements will be extensively used to characterize SEI layers in various electrolytes incorporating FRIONS synthesized under this program.

Figure V- 122: Photograph of the cell for *in situ* ATR-FTIR measurements.

FY 2010 Publications/Presentations

1. Shaffer, A. R., Deligonul, N., Scherson, D. A., and Protasiewicz. J. D. **A Hybrid Lithium Oxalate-Phosphinate Salt**. *Inorg. Chem.* Accepted.

V.D.5 Advanced Electrolyte and Electrolyte Additives (ANL)

Khalil Amine

Chemical Sciences and Engineering Division
Argonne National Laboratory
Argonne, IL 60439
Phone: (630) 252-3838; Fax: (630) 252-4672
E-mail: amine@anl.gov

Start Date: Jan 1, 2010
Projected End Date: December 30, 2014

Objectives

- Develop advanced quantum chemical models to predict functional additives that form a stable Solid Electrolyte Interface (SEI) on carbon anodes and for overcharge protection.
- Expand the model to predict how additives interact with the surface of anode and cathode during the initial charging.
- Synthesize suitable additives predicted by the modeling, characterize them and carry out extensive cycle and calendar life test.

Technical Barriers

This project addresses the following technical barriers in lithium-ion battery technology

(a) Cycle/calendar life

(b) Abuse tolerance

Technical Targets

- New additives that form stable film formation on anodes and cathodes
- Increased cycle life
- Improved safety

Accomplishments

- An improved quantum chemical model is being used in the calculation of reduction and oxidation potentials of potential additive molecules and shuttle molecules. The model uses improved basis sets and an improved continuum model for the solvation effects.
- Screened over 100 candidates as potential additives to form a protective film on anodes based on reduction potentials
- Further screened the 100 candidates for formation decomposition pathways involving lithium carbonates
- Initiated synthesis and testing of new candidate additives that are likely to form protective films.
- Investigated lithium carbonate reactions on graphite surfaces to understand film growth..
- Polymerization products resulting from reduction of bis(oxalate)borate salts were investigated to help understand new experimental results.

✧ ✧ ✧ ✧ ✧

Introduction

The stabilization of the interface of lithium-ion batteries is needed to prevent detrimental decomposition of the electrodes. We are investigating functional electrolyte additives that can be added to the electrolyte and that can either polymerize or be reduced at voltages higher than 1.1 V during the initial formation charging to prevent any conventional passivation film from forming first at the anode. In the case of the cathode, the additive must be oxidized at voltages above 4V to allow for stable film formation at the interface of the cathode. These additives must form a thin and uniform film made of one stable single component that protects the interface of both electrodes. We are also investigating new additives for overcharge protection.

Approach

We are using a joint theoretical/experimental approach for design and discovery of new electrolytic additives that react in a preferential manner to prevent detrimental decomposition of cell components. We use quantum chemical screening to predict oxidation and reduction potentials and decomposition pathways that form desirable coatings and to find stable additives for overcharge protection. We are using density functional studies of graphite surface reactions to determine mechanisms for protective film formation from additives. Synthesis of the new additives and testing of them is done to determine the cycle life of the batteries. Investigation of the SEI is done to determine structure and formation through both and experiment and theory.

Results

Screening and testing of reduction potentials of additives. Over 100 candidate additives have been screened for their reduction and oxidation potentials using our improved quantum chemical model for calculation of these quantities using higher levels of theory and a better

solvation model. Approximately 60 of these species have reduction potentials greater than 1 eV relative to a lithium electrode and, thus, are good candidates for further investigation for formation of good SEIs The candidates that have met the reduction potential screening criteria have been the subject of further screening for specific decomposition pathways.

Screening of additives for decomposition. We have used accurate quantum chemical methods to compute decomposition pathways for a direct two-electron reduction of the carbonate. The first step involves reduction of the carbonate. The second step involves ring opening upon addition of the electron. The third step involves further reduction and addition of two lithium cations to form lithium carbonate. The first step involves various other intermediate steps. The ring opening step plays a key role in the overall reaction mechanism as the other steps involved are generally downhill. We have focused on calculating the barrier for opening of the ring as a key descriptor for the additive candidates. In the screening based on this descriptor we have found 12 candidates that have small or no barrier for the ring opening. The candidate species have various bonding arrangements of R groups on the C2 of the five membered ring. These 12 candidate additives will be considered in experimental studies as possible additives.

Interaction of electrolyte decomposition products on graphite surface. In our studies of the adsorption of electrolyte decomposition products on a graphite anode we are using density functional calculations. The graphite model being used represents the edge surface of graphite. Both hydrogen terminated surfaces with no defects and hydrogen terminated surfaces with defects (*i.e.,* missing hydrogen atoms from the C-H bonds) have been considered. We have investigated the adsorption energies and structure of Li_2CO_3 monomers, dimers, and trimers resulting from decomposition of additives such as vinyl ethylene carbonate at different sites. Full geometry optimizations using density functional theory are carried out to determine the structures at the interface. An important finding of this work is that the nucleation of a Li_2CO_3 film likely occurs at the defect sites (Figure V-123). The calculated binding energies of the monomers, dimers, and trimers at the defect sites are much larger than at non-defect sites. It is also found that the clusters tend to grow outward from the surface initially based on the calculations of up to three Li_2CO_3 units. The vibrational frequencies of the Li_2CO_3 growth species on the graphite edge surface have been calculated and are being used to help identify peaks in FTIR spectra.

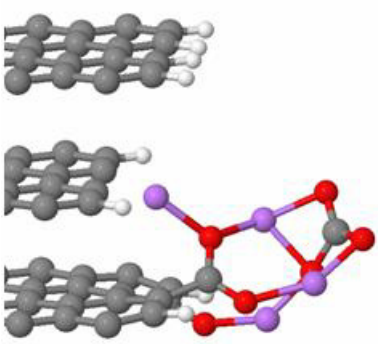

Figure V- 123: Structure of adsorbed Li_2CO_3 dimer at graphite defect site.

Poylmerization of bis(oxalate)borate We have investigated possible polymerization products resulting from reduction of bis(oxalato)borate based salts that are believed to form passivation layers. The calculations indicate that the modification of lithium bis(oxalato)borate (LiBOB) can have a dramatic effect on the structure of the polymer formed. Whereas LiBOB forms a three dimensional structure when we calculate the structure of the tetramer, the lithium oxalyldifluoroborate (LiDFOB) forms a linear type structure (Figure V- 124). The calculations suggest that the fluorine termination of LiDFOB prevents 3-D growth during polymerization. This is consistent with experimental measurements that show a much lower impedance for the films grown from LiDFOB compared to LiBOB.

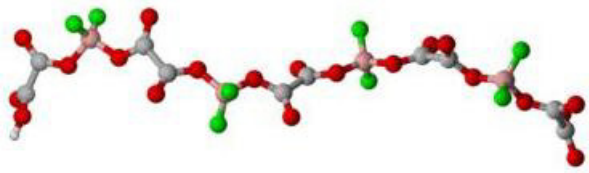

Figure V- 124: Calculated structure of the tetramer of LiDFOB.

Conclusions and Future Directions

Stabilization of the interfaces of lithium-ion batteries is needed to prevent detrimental decomposition of the electrodes. We have screened over 100 candidate materials for reduction potentials. In addition, selected electrolyte decomposition products are being investigated. In future work, the most promising candidate electrolyte additives will be studied experimentally. We will continue to screen further candidates based on experimental feedback and investigate other decomposition pathways. We will also be investigating new additives for overcharge protection

Our calculations on graphite surface reactions are being used to determine mechanisms for protective film formation from the electrolyte additives and providing vibrational properties to help in the characterization of the experiment. The determination of the film components is important for designing new additives.

In future work we will be using density functional calculations to help understand the properties of shuttle molecules for overcharge protection being studied experimentally and using this information to help design new shuttle molecules.

Publications/Presentations

1. Poster presentation at the DOE Vehicle 2010 Annual Merit Review Meeting.
2. Lithium Carbonate Interactions with Graphite Surfaces at 'Beyond Lithium-Ion: Computational Perspectives' May 2010.

V.D.6 Inexpensive, Nonfluorinated (or Partially Fluorinated) Anions for Lithium Salts and Ionic Liquids for Lithium Battery Electrolytes (NCSU)

Wesley Henderson
Ionic Liquids & Electrolytes for Energy Technologies (ILEET) Laboratory
Department of Chemical & Biomolecular Engineering
North Carolina State University
911 Partners Way, Campus Box 7905
Raleigh, NC 27695
Phone: (919) 513-2917; Fax: (919) 515-3465
E-mail: wesley_henderson@ncsu.edu

Collaborators: Michel Armand, Peter Fedkiw (co-PIs)

Start Date: April 1, 2009
Projected End Date: March 31, 2012

Objectives

- Develop new anions as replacements for PF_6- or as additives for electrolytes
- Establish characterization methods for electrolyte solvent-lithium salt and ionic liquid-lithium salt mixtures to aid in understanding structure-property relationships and optimization of cell performance

Technical Barriers

This project addresses the following technical barriers from the VT Research & Development plan regarding electrolytes:

- Improved cell performance, calendar life and abuse tolerance
- Improved low temperature performance
- Reduced cost

Technical Targets

- Obtain electrolyte salt materials that can operate in the potential range (4-5 V vs. Li/Li^+) enabling the use of high-voltage cathode materials
- Develop electrolyte materials which enable cell operation in the temperature range -30 to 55°C or higher
- Impove cycle life and safety

Accomplishments

- Characterized the phase behavior of $LiBF_2O_x$ (or LiODFB) with carbonate and sulfone solvents for comparison with $LiBF_4$ and LiBOB
- Synthesized and characterized ionic liquids with the dicyanotriazolate (DCTA-) anion
- Optimized the synthesis procedure for a new partially fluorinated cyanocarbanion

✧ ✧ ✧ ✧ ✧

Introduction

Electrolyte materials are a key component in terms of both the cost and performance (power, safety, lifetime) of a battery. The properties of salts (either lithium salts or ionic liquids) containing new anions are being explored to determine their utility for lithium battery applications.

Approach

To explore new anions for alternative salts to $LiPF_6$, ionic liquids and electrolyte additives, two classes of nonfluorinated (or partially fluorinated) anions were synthesized and characterized: 1) chelated and non-chelated organoborate anions (related to bis(oxalate) borate or BOB^-), and 2) Hückle-type anions in which the charge is stabilized on a 5-member azole ring and noncyclic cyanocarbanions. The physical properties of these new anions, incorporated in both lithium salts and ionic liquids, are being examined including the thermal phase behavior (phase diagrams); thermal, chemical and electrochemical stability; transport properties; interfacial properties; molecular interactions and cell performance. These salts will be compared with current salts of interest such as $LiBF_4$, $LiPF_6$ and LiBOB and ionic liquids based upon the bis(trifluoromethanesulfonyl)imide anion.

Results

Characterization of Solvent-LiBOB, -$LiBF_2Ox$ and -$LiBF_4$ Mixtures. New lithium organoborate salts which have been prepared have proven to be highly insoluble in common aprotic solvents (Figure V- 125).

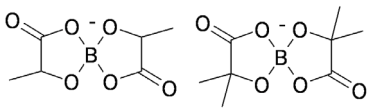

Figure V- 125: Sample organoborate salt structure

To more fully understand the link between anion structure and salt solubility, characterization of the thermal phase behavior and solvate structures of LiBOB and $LiBF_4$ in aprotic solvents has been performed. This work indicates that LiBOB is extensively aggregated, even in dilute solutions, in contrast with $LiBF_4$. For example, when dilute $(EC)_n$-LiBOB mixtures are stored at ambient temperature, an $(EC)_{3/2}$:LiBOB solvate crystallizes from solution (Figure V- 126). This is a highly aggregated structure in which each Li^+ cation is coordinated by 4 anions (by 5 oxygens) and one EC molecule. One EC molecule (for every 2 Li^+) is uncoordinated and occupies 'holes' in the structure. The anion coordination is the same as that found in crystalline LiBOB. Although lithium difluoro(oxolato)-borate ($LiBF_2Ox$ or LiODFB) is less soluble than $LiBF_4$, it is much more soluble than LiBOB. Initial evidence suggests that the anion fluorine atoms interact to a much lesser extent with Li^+ cations than the carbonyl oxygens. The crystal structure of $LiBF_2O_x$ was determined (Figure V- 127). In this structure, the oxylate portion of the anion is coordinated to 3 Li^+ cations and each fluorine is coordinated to a single Li^+ cation. In solvate structures such as $(DMC)_{3/2}$:$LiBF_2Ox$ (Figure V-128), however, the fluorines remain uncoordinated despite the limited number of solvent molecules available for cation coordination. Thus, the BOB^- anion, with two oxylate moieties, can readily form cross-linked structures through multiple bonds with different Li^+ cations (promoting aggregation), whereas the $BF_2O_x^-$ anion does not. It is expected that this difference in coordination may also be found in the SEI layers generated by these different anions, perhaps explaining the notable differences in their respective impedance properties. This work is being extended to other partially fluorinated organoborate anions to continue to examine how anion structure affects solubility and electrolyte properties.

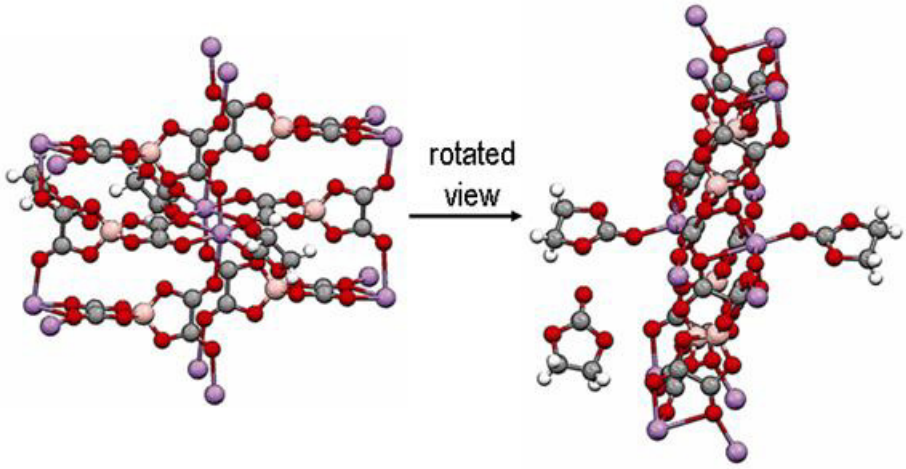

Figure V- 126: :Portion of crystal structure of the $(EC)_{3/2}$:LiBOB solvate (Li: purple, B: tan, O: red)

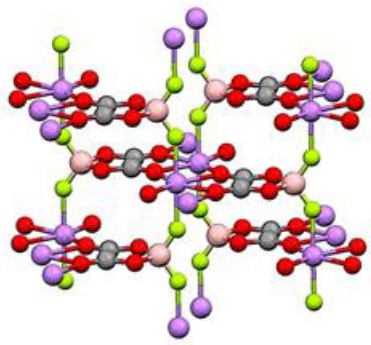

Figure V- 127: Crystal structure of $LiBF_2Ox$ (Li: purple, B: tan, O: red, F: green)

Salt Synthesis. Lithium dicyanotriazolate (LiDCTA) has been prepared and characterized (Figure V- 129). This salt is highly aggregated in dilute aprotic solvents. Work will continue to complete the characterization of this salt, but this will now be used as a reference for the properties of other cyanocarbanions. LiDCTA may still be useful as an additive to electrolytes and electrochemical characterization is being performed with this in mind. Work has, however, begin to shift to other cyanocarbanions. The preparation of LiDCTA requires a sublimation purification step which is time-consuming. This has limited the amount of salt that can be produced. Other synthesis/purification techniques are being employed to facilitate the scaling-up of salt synthesis for

both lithium salts and ionic liquids, with an emphasis on reducing the production steps and using inexpensive reagents.

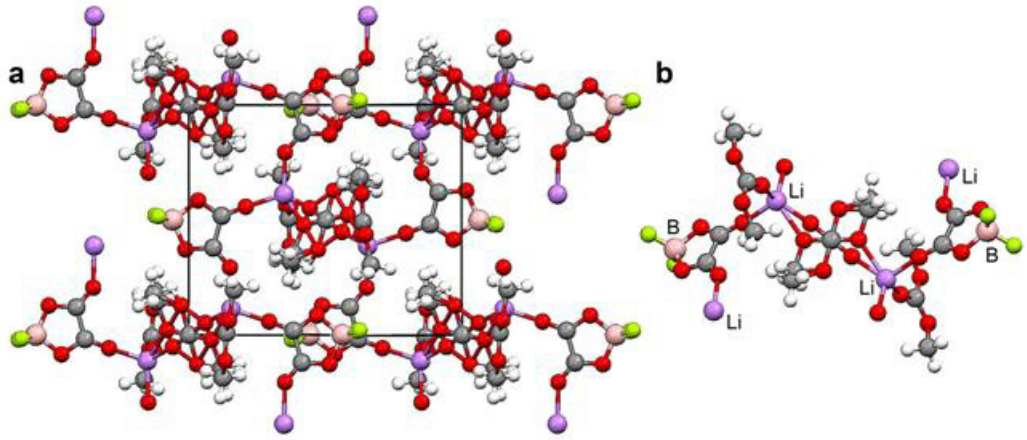

Figure V- 128: Crystal structure of the $(DMC)_{3/2}$:$LiBF_2O_x$ solvate (Li: purple, B: tan, O: red, F: green): (a) unit cell and (b) Li+ and anion coordination - note that the central DMC molecule in (b) is disordered over two positions

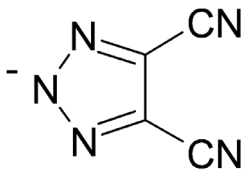

Figure V- 129: Lithium dicyanotriazolate (LiDCTA) structure

ILs with Cyanocarbanions. Ionic liquids (ILs) have been prepared with various cations and the $DCTA^-$ anion (as well as $N(CN)_2^-$ and $C(CN)_3^-$) (Figure V- 130). These salts have some of the lowest viscosities known for aprotic ILs. Why this is so is not yet known. Unfortunately, as noted above, the preparation of $DCTA^-$ is time-consuming making it difficult to prepare large quantities of ILs. A shift in focus is therefore occurring to other anions for which it is anticipated that large batches of ILs may be synthesized for testing and characterization. The latter will include the characterization of the thermal (phase behavior, stability), transport (conductivity, viscosity, diffusion coefficients) and electrochemical (stability) properties. This information may aid in further clarifying the interactions found for the related lithium salts in aprotic solvents. These ILs and their properties with lithium salts will be compared with ILs based upon bis(trifluoromethanesulfonyl)imide ($TFSI^-$) which are currently the most prevalent for IL-based electrolytes for lithium batteries. Specific comparisons will be made with *N*-methyl-*N*-pentylpyrrolidinium IL ($PY_{15}TFSI$) mixtures with LiTFSI for which extensive characterization has been performed.

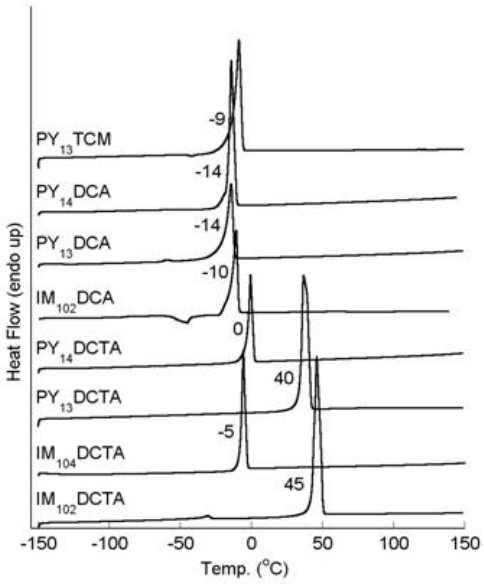

Figure V- 130: DSC heating traces of the crystallized ionic liquids (5°C/min).

Conclusions and Future Directions

Electrolyte characterization will continue to gain insight into salt structure-property relationships and the link between this and cell performance. Additional partially fluorinated organoborate and cyanocarbanions anions will be tested in carbonate, ester, sulfone and dinitrile solvents.

FY 2010 Publications/Presentations

1. 2010 DOE Annual Peer Review Meeting Presentation
2. Allen, J. L.; Boyle, P.; Henderson, W. A. "Crystal Structure and Physical Properties of Lithium Difluoro(oxalato)borate (LiDFOB)" 218th ECS Meeting - Las Vegas, NV, 2010

V.D.7 Development of Electrolytes for Lithium-ion Batteries (URI)

Brett L. Lucht
University of Rhode Island
Department of Chemistry
51 Lower College Rd., Pastore
Phone: (401) 874-5071; Fax: (401) 874-5072
E-mail: blucht@chm.uri.edu

Start Date: April 1, 2009
Projected End Date: March 31, 2014

Objectives

- Develop novel electrolytes for lithium-ion batteries based on $LiPF_4(C_2O_4)$ and investigate the novel electrolytes in test cells.
- Develop additives that allow for formation of protective coatings on the cathode, i.e., a cathode SEI, and enhance electrochemical stability above 4.3 V.
- Improve the thermal stability and calendar life of lithium-ion batteries via improvements of the electrolyte

Technical Barriers

This project addresses the following technical barriers from the OVT Research, Development Plan regarding electrolytes.

(A) Improve cell performance, life and cost

(B) Improve calendar Life

(C) Expand survival temperature range

Technical Targets

- Calendar life: 35°C for 15 yrs
- Survival Temp Range: -46 to 66°C
- Unassisted Operating Temperature Range, -30 to +52°C

Accomplishments

- Investigated the performance of the novel salt, $LiPF_4(C_2O_4)$, as electrolyte. Conducted accelerated aging experiments on $LiPF_4(C_2O_4)$ electrolytes compared to $LiPF_6$ electrolytes in graphite/$LiNi_xCo_{1-2x}Mn_xO_2$
- Developed novel cathode film forming additives that improved the performance of high voltage (>4.5 V vs Li) cathode materials.
- Investigated cell performance of $LiPF_4(C_2O_4)$ compared to $LiPF_6$ in small cells with different chemistries including EC/EMC electrolytes with graphite/$LiMn_2O_4$ and graphite/$LiFePO_4$ and $LiNi_xCo_{1-2x}Mn_xO_2$ cells with PC electrolytes.
- Developed a commercially viable synthesis method for $LiPF_4(C_2O_4)$.

Introduction

While commercial lithium-ion batteries (LIB) perform well for most home electronic applications, currently available LIB technology does not satisfy some of the performance goals for PHEVs. In particular, currently available LIB technology does not meet the 15 year calendar life requirement set by the United States Advanced Battery Consortium (USABC).

The most extensively used LIB electrolytes are composed of $LiPF_6$ dissolved in organic carbonates. However, $LiPF_6$ based electrolytes have poor thermal stability and performance when cycled to high voltage (> 4.5 V vs Li). Significant energy fading occurs after several years at room temperature and over only a few months at the survival temperature of 66°C required by the USABC. While there are several different factors that limit the thermal stability, calendar life and voltage window of LIBs, the reactions of the electrolyte with the surface of the electrode materials are frequently reported to be the most important.

Approach

Develop novel electrolytes for lithium-ion batteries to improve performance and lifetime. Investigate properties of $LiPF_4C_2O_4$/carbonate electrolytes under accelerated aging conditions and in the presence of multiple cell chemistries, in EC/EMC with graphite/$LiMn_2O_4$ and graphite/$LiFePO_4$ and with graphite/$LiNi_xCo_{1-2x}Mn_xO_2$ in the presence of propylene carbonate (PC). Develop commercially viable low-cost synthetic method for production of $LiPF_4(C_2O_4)$. Investigate cathode film forming additives which will allow the use of cathodes above 4.5 V. Investigate the surface of cycled cathodes and anodes with novel electrolytes or electrolyte / additive combinations to develop a mechanistic understanding of SEI formation and degradation. Use the mechanistic information to design superior electrolytes and additives for lithium-ion batteries.

Results

Investigation of $LiPF_4(C_2O_4)$ Electrolyte Under Accelerated Aging Conditions. Accelerated aging experiments were conducted on cells containing $LiPF_4(C_2O_4)$ and $LiPF_6$ electrolytes. While the thermal stability of crystalline $LiPF_4(C_2O_4)$ is comparable to crystalline $LiPF_6$, the thermal stability of $LiPF_4(C_2O_4)$/carbonate electrolytes is much better than $LiPF_6$/carbonate electrolytes (Figure V- 131). Incorporation of $LiPF_4(C_2O_4)$ electrolytes into lithium-ion cells provides better capacity retention after storage at elevated temperature than comparable cells containing $LiPF_6$ electrolytes. *Ex situ* surface analysis of the electrodes, both cathode and anode, after storage at elevated temperature and cycling suggest differences in structure of the electrode surface films generated in $LiPF_4(C_2O_4)$ electrolytes and $LiPF_6$ electrolytes. The anode SEI from the cell containing $LiPF_4(C_2O_4)$ contains a high concentration of oxalate containing species and LiF. The cathode surface film is thinner for the cell containing $LiPF_4(C_2O_4)$ and contains oxalate species but little LiF. The presence of oxalate species on the electrodes results in slower growth of electrode surface films on both the cathode and the anode and is a likely source for the improved performance after storage at elevated temperature.

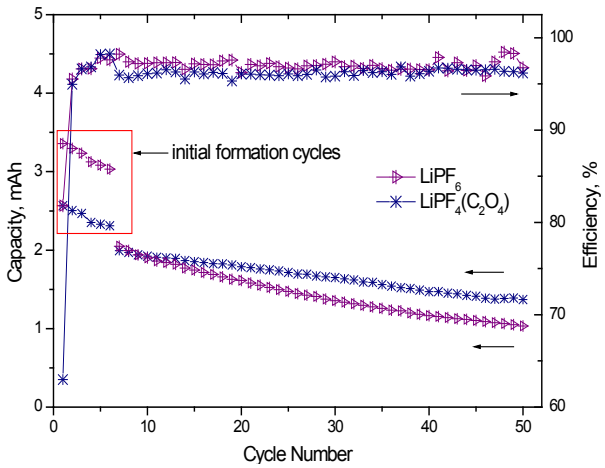

Figure V- 131: Cycling performance of lithium-ion batteries (MCMC/$LiNi_{0.8}Co_{0.2}O_2$) before (initial formation cycles) and after thermal storage at 65˚C for 2 weeks with 1 M $LiPF_6$ and 1 M $LiPF_4(C_2O_4)$ electrolytes.

Development of Novel Cathode Film Forming Additives. In order to better understand the reactions of the cathode surface with electrolyte at high voltage, we have conducted a detailed analysis of the surface of $LiMn_{0.5}Ni_{1.5}O_2$ cathodes stored at various (4.0 – 5.3 V vs Li) potentials for one week. The surfaces of the electrodes were analyzed by XPS and IR-ATR (Figure V- 132). At low potential (< 4.7 V vs Li) there is little reaction with the surface and peaks characteristic of the EPDM (ethylene propylene diene Monomer (M-class) rubber) binder are observable. Storage at high voltage (> 4.7 V vs Li) results in oxidation of the electrolyte and generation of polyethylene carbonate (PEC) on the surface.

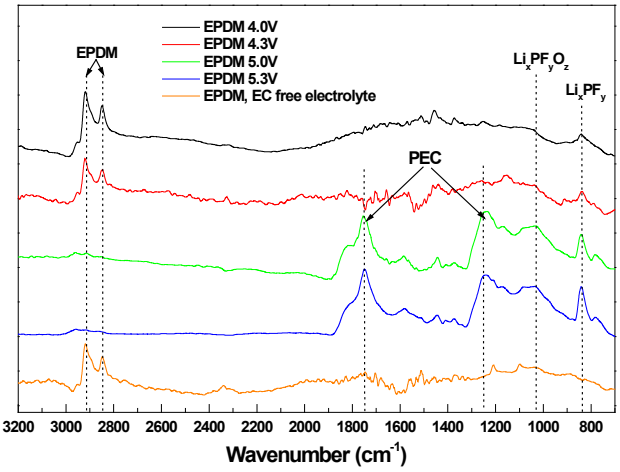

Figure V- 132: FTIR-ATR spectra of cathodes stored at different potentials with EPDM as the binder.

We have investigated novel additives for lithium-ion battery electrolytes that improve the cycling performance at high voltage (4.9 V vs Li). Common electrolytes used in lithium-ion batteries such as $LiPF_6$ in 3:7 EC/EMC have poor electrochemical stability in the presence of cathode materials cycled to high voltages (>4.5 V). Additives including 2,5-dihydrofuran (2,5-DHF) and GBL can sacrificially react with the surface of cathode materials to form passivation layers which inhibit further oxidation of the electrolyte. Incorporation of low concentrations of 2,5-DHF or GBL improves the capacity retention of $Li/Li_{1.17}Mn_{0.58}Ni_{0.25}O_2$ cells upon cycling to 4.9 V vs Li. Surface analysis of the cathodes after cycling by XPS and IR suggest that 2,5-DHF and GBL modify the structure of the cathode SEI and inhibit the generation of polyethylene carbonate. The presence of electrolyte additives leads to cathode passivation which inhibits electrolyte oxidation and improves capacity retention (Figure V- 133)

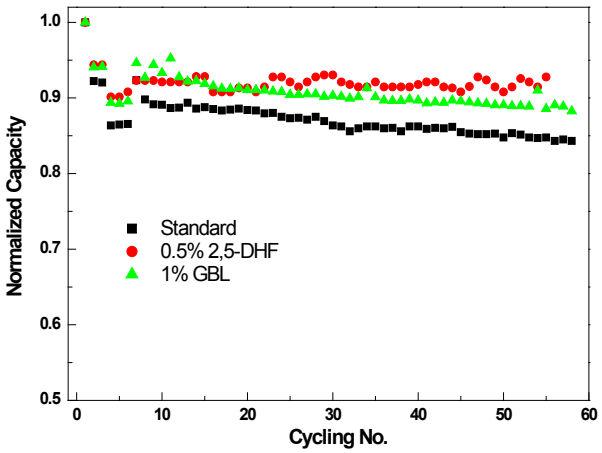

Figure V- 133: Capacity retention of the Li/$Li_{1.17}Mn_{0.58}Ni_{0.25}O_2$ cells cycled from 2.0 to 4.9 V containing 1 M $LIPF_6$ in 1:1:1 EC/DEC/DMC with and without additives.

Investigation of $LiPF_4(C_2O_4)$ with Different Cell Chemistries. Initial cycling has been conducted with $LiPF_4(C_2O_4)$/PC electrolyte. The cycling of the cells with the $LiPF_4(C_2O_4)$/PC electrolyte is comparable to the standard $LiPF_6$ electrolyte and much better than the $LiPF_6$/PC electrolyte (Figure V- 134). Surface analysis suggests that the performance differences are related to an inhibition of graphite exfoliation in the presence of $LiPF_4(C_2O_4)$. We suggest that this is due to the formation of a more stable anode SEI.

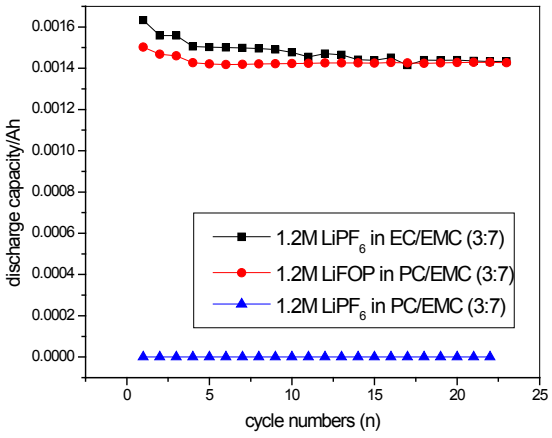

Figure V- 134: Cycling performance of graphite/ $LiNi_{1/3}Co_{1/3}Mn_{1/3}O_2$ cells with PC electrolytes.

Initial cycling has also been conducted with $LiPF_4(C_2O_4)$/EC/EMC electrolytes with graphite/$LiMn_2O_4$ and graphite/$LiFePO_4$ coin cells. The $LiPF_4(C_2O_4)$ electrolyte cycles well in both systems. The discharge capacity of graphite/$LiFePO_4$ cells is very similar for $LiPF_4(C_2O_4)$ and $LiPF_6$ electrolytes (Figure V- 135). Interestingly, in the graphite/$LiFePO_4$ cells there is a very small difference in the initial irreversible capacity for $LiPF_4(C_2O_4)$ compared to $LiPF_6$. Surface analysis of the electrodes suggests that the electrode surfaces are very similar. However, the discharge capacity is slightly lower for graphite/$LiMn_2O_4$ cells containing $LiPF_4(C_2O_4)$ when compared to $LiPF_6$.

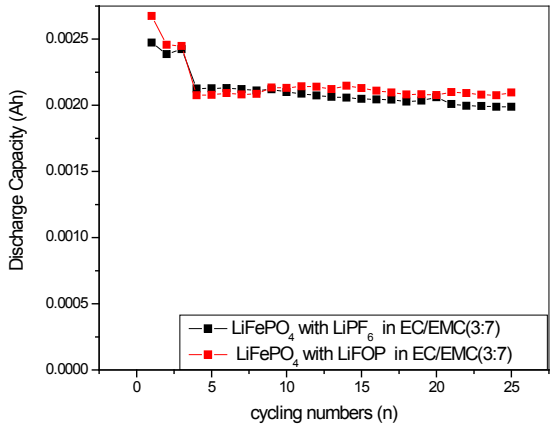

Figure V- 135: RT cycling performance of coin cells made of $LiFePO_4$ cathode with different electrolytes.

Development of a Commercially Viable Synthesis of $LiPF_4(C_2O_4)$. We have developed a superior method for the preparation of $LiPF_4(C_2O_4)$ which provides significantly higher yields. Initial analysis suggests that this synthetic method has commercial viability. We currently working with industrial partners to scale up the process.

Conclusions and Future Directions

We have developed cathode film forming additives that improve the cycling performance of graphite/$LiNi_xCo_{1-2x}Mn_xO_2$ cells cycled to high voltage (4.8 V vs Li). We expanded our investigation of the novel salt $LiPF_4(C_2O_4)$ by testing in coin cells under accelerated aging conditions with graphite/ $LiNi_xCo_{1-2x}Mn_xO_2$ cells, and RT cycling of graphite/$LiMn_2O_4$ and graphite/$LiFePO_4$, and graphite/ $LiNi_xCo_{1-2x}Mn_xO_2$ cells containing PC. We also developed a commercially viable synthesis of $LiPF_4(C_2O_4)$.

Our future work will include investigation of additional cathode film forming additives for high voltage cathodes. We will also investigate the low temperature (-30°C) performance of $LiPF_4(C_2O_4)$/PC electrolytes before and after accelerated aging. We will develop an understanding of the source of initial capacity fade during formation cycling with $LiPF_4(C_2O_4)$ electrolytes. Finally,

we will investigate novel electrolytes to improve performance of Si-based alloy anodes.

FY 2010 Publications/Presentations

1. L. Yang and B. L. Lucht, *Electrochem. & Solid State Lett*., **2009**,*12*, A229-A231.
2. M. Xu, A. Xiao, W. Li, and B. L. Lucht, *J. Electrochem. Soc.,* **2010**, *157*, A115-A120.
3. L. Yang, A. Xiao, B. L. Lucht *J. Mol. Liquids,* **2010**, *154*, 131-133**.**
4. M. Xu, L. Zhou, L. Xing, W. Li, L. Lucht *Electrochim. Acta*, **2010**, *55*, 6743-6748.
5. Li Yang, Boris Ravdel, and Brett L. Lucht, *Electrochem.& Solid State Lett.*, **2010**, *13*, A95-A97.
6. Lithium Mobile Power Conference, Boston, MA, November, 2009.
7. DOE Vehicle Technologies Program Review Meeting, Washington, DC, June 2010.
8. International Meeting on Lithium Batteries, Montreal, QC, June 2010.
9. Abstracts of Papers, 240th ACS National Meeting, Boston, MA, United States, August 22-26, 2010 (2010), PMSE-81.
10. Abstracts of Papers, 240th ACS National Meeting, Boston, MA, United States, August 22-26, 2010 (2010), INOR-213.
11. Abstracts of Papers, 240th ACS National Meeting, Boston, MA, United States, August 22-26, 2010 (2010), INOR-105.

V.E Cell Analysis and Modeling

V.E.1 Electrode Fabrication and Failure Analysis (LBNL)

Vince Battaglia
M.S.70R0108B
1 Cyclotron Road
Berkeley, CA 94720
Phone: (510) 486-7172; Fax: (510) 486-4260
E-mail: vsbattaglia@lbl.gov

Start Date: October 2008
Projected End Date: September 2012

Objectives

- Fabricate high-quality electrodes capable of approaching USABC performance targets.
- Evaluate failure modes of cells and delineate between material failures and electrode failures.

Technical Barriers

- The challenge to getting more electrified vehicles on the road is reducing the cost, which translates, technically, to improving the energy density and the life.

Technical Targets

Develop a cell to meet the 40-mile PHEV goals:

- Optimize the energy density of an electrode using standard active materials to meet the 207 Wh/l energy density target.
- Optimize the construction of the electrodes to meet the 5000 cycle requirement.

Accomplishments

- The order in which materials are combined results in slurries of different viscosities despite having the same composition.
- The viscosity is believed to be directly related to the degree of mixing. A higher viscosity indicates better mixing.
- Electrodes made with slurries of the higher viscosities cycled longer than electrodes made from slurries of the lower viscosities.
- Electrode failure appears to be due to stress fracturing of the electrode.
- We made graphite/NMC cells with $LiPF_6$ in EC:DEC that delivered 500 cycles with 20% loss of capacity when charged to 4.3 V.
- Higher charge voltages resulted in premature cell failure. This failure appears to be a result of cathode oxidation/dissolution, followed by SEI attack of the anode.
- The same cells, but with an electrolyte from Diakin, cycled 1000 cycles with a cut-off voltage of 4.4 V.
- Other electrochemical tests suggested that a protective film was formed on the cathode in the Diakin electrolyte.
- As such, we performed some high-voltage cycles on some cells (to 4.6 V) and then reduced the voltage to 4.4 V and found a further improvement in cycle life.

✧ ✧ ✧ ✧ ✧

Introduction

If one makes an electrode of a new material and receives in return poor electrochemical performance, is there something wrong with the material or something wrong with the electrode? This is the key question that is addressed with every change in chemistry that we face.

Energy density is a critical factor where improvements could lead to batteries of lower cost. The indiscriminant addition of the non-active constituents such as binder and conductive carbon to an electrode can lead to low capacity density and hence low energy density. What is the right level of these support materials? Does it matter how they are combined, or cast, or calendered? We seek to make cells that are both highly cycleable and of high energy density and to understand from a fundamental view point why changes in processing results in changes in performance.

As our cell manufacturing improves and our electrodes become more cycleable, we continue to question why the cells' capacity or power declines with cycling. Again, is this a result of poor electrode or material quality.

Two major efforts were reported on at this year's Annual Merit Review: 1) The effect of mixing order on electrode performance, and 2) The effect on cycling performance by switching to a new, high-voltage electrolyte.

Approach

Whether we are improving on electrode performance or evaluating a new material, the process requires identifying the failure modes. If there is excessive internal impedance or the electrodes show cracks after cycling, we make adjustments to our fabrication process. If it is believed to be a chemistry problem, we try to measure it, measure its rate, and identify the underlying source. Tools used to date to examine electrode preparation include a surface area analyzer, a particle size analyzer, an SEM, a rheometer for assessing degree of mixing, SEM for finding cracks, and a strain gauge for measuring elasticity and ultimate strength of our laminates. Tools used to evaluate cells include an electrochemical impedance analyzer, battery testers for 128 cells, potentiostats, and a new 3-electrode coin cell configuration. Tools used for assessing chemistry issues include a technique for capturing dissolved ions, an inductively coupled plasma optical emission spectrometry (ICP-OES) for measuring the concentration of dissolved species, and a technique for measuring the valence of dissolved species.

Results

Mixing Order. Our basic electrode design consists of three components: PVdF binder, Denka black conductive carbon, and active material (MCMB graphite). As shown previously, the optimum ratio of conductive carbon to PVdF falls between 1:5 and 1:1. A smaller ratio results in poor conductivity and a higher ratio results in poor lamination strength. The ratio of active material to inactive material is typically between 90:10 and 94:6. Now that our formulation has been established and supported with independent analysis, we turned to determining if the order in which these materials were mixed together made a difference with regard to electrode character and electrochemical performance.

To test the effect of mixing order, two slurries of identical composition were prepared. In slurry 1, which we also refer to as the solids method, graphite and conductive carbon were added to NMP and mixed together with an homogenizer. Once thoroughly mixed, PVdF binder was added and the solution was mixed some more. In slurry 2, which is also referred to as the glue method, the conductive carbon and the binder were mixed in NMP, again using the homogenizer. Once thoroughly mixed, the graphite active material was added and all four components were mixed some more. Once we obtained these two main samples, we created three more samples by combining the two in different ratios: 1:2, 1:1, and 2:1. This led to five samples overall.

Once we had our five samples, each was tested for its rheological properties. Samples were placed in the rheometer, which then measured viscosity as a function of shear rate. Results of the tests are provided in Figure V-136.

The slurries differ in viscosity monotonically, with the sample where the graphite and carbon were mixed together first having the highest viscosity and the sample where the carbon and PVdF binder were mixed together first having the lowest viscosity.

We believe that a proper interpretation of this data is that an increase in viscosity is consistent with a more thoroughly mixed solution. The rational behind this argument is that poorly mixed solutions have regions of low viscosity and high viscosity and the regions of low viscosity allow for slippage in the rheometer analogous to a low resistor in parallel with a high resistor.

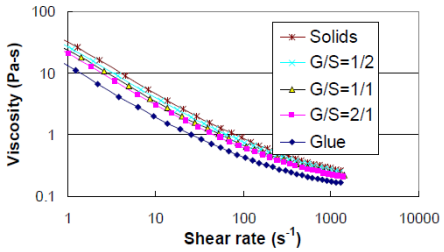

Figure V- 136: Measure of viscosity of five slurries of identical composition but differing by order in which the constituents were combined.

Thus, the slurry formed by mixing the carbon and the graphite together first is more thoroughly mixed than when the carbon is first mixed with the polymer. The reason we believe this occurs is due to the high surface area of the conductive carbon. If the polymer forms a thin coating on carbon, then when they are mixed together, much of the polymer is taken up by the carbon. When the low surface area graphite is then added to the mix, the polymer is not able to free itself from the carbon and therefore the three components are not of equally intimate contact.

After measuring the viscosity, electrodes were cast. SEMs of electrodes of the all solids process and the all glue process are provided in Figure V- 137.

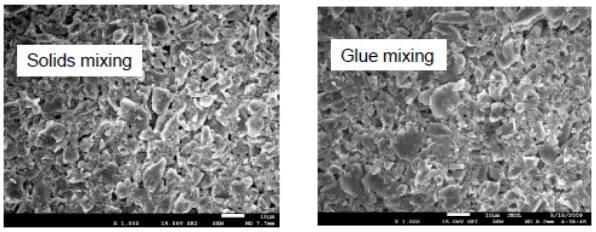

Figure V- 137: SEMs of an electrode made from the solids process and the glue process.

We were unable to detect any discernable differences of these electrodes on a 40 micron scale. Small difference could be detected at higher magnification but were difficult to quantify.

Laminates of these slurries were also subjected to stress testing. Laminates were made on glass plates, carefully peeled off, and put in a strain gauge. The gauge stretched the electrodes until they broke, measuring the force required and the distance of stretching. Results of this test are provided in Figure V- 138. One sees that as one moves from the glue mix to the solids mix, the Young's modulus *i.e.* stiffness of the electrode, decreases. As the stiffness decreases, the Ultimate strain increases, meaning that the laminate stretches further before breaking. If graphite expands and contracts by 13% during full charge and discharge, this would result in a strain of 0.13/3 = 0.043 in any one direction, which is close to the Ultimate Strain of the glue process electrodes.

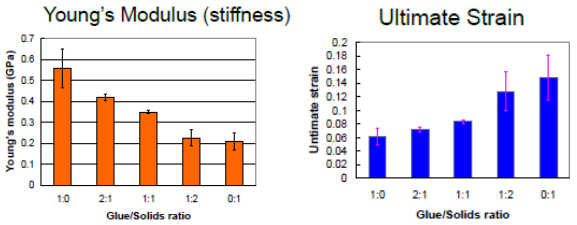

Figure V- 138: Young's modulus and Ultimate Strain before breaking of five laminates from starting materials combined five different ways.

Finally, electrodes were cycled between 3.5 and 4.3 volts. The results of those tests are provided in Figure V-139.

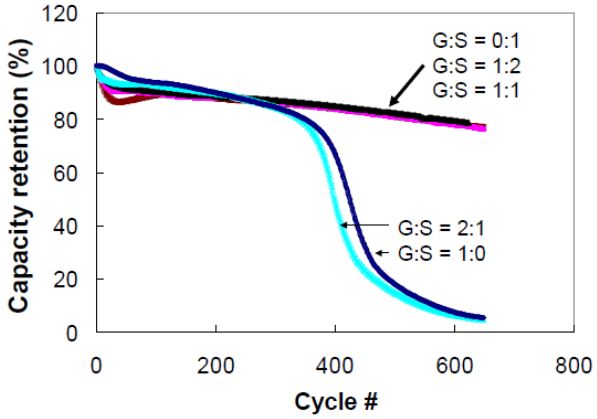

Figure V- 139: Cycling results, of cycling at a C/1 discharge and C/2 charge rate in coin cells against an NCM cathode, of anodes of differing processing steps.

One can see that electrodes consisting of slurries mainly from the glue process were more susceptible to cell failure than those produced mainly from the solids process. After 650 cycles, the cells were disassembled. SEMs of the anodes from the glue process and the solids process are provided in Figure V- 140. The electrodes from the glue process show extensive cracking; electrodes from the solids process look much like it did before cycling.

High-Voltage Electrolyte. In the summer of 2009, we received four different samples of potentially high-voltage electrolytes (HVE) from Diakin (Japan). The electrolytes contained 1M $LiPF_6$ in EC, DEC, FEC, and an unknown substance referred to as D2 in differing proportions. All four samples have since been tested and all four provided similar results. We will go through the results of one of those samples presented in comparison to the baseline electrolyte (BLE) of 1M $LiPF_6$ in EC:DEC 1:2.

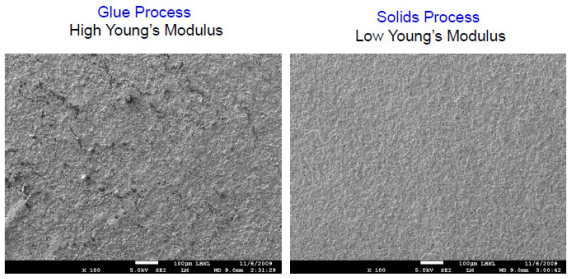

Figure V- 140: SEMs of the anodes after cycling. On the left is an electrode from the glue process and on the right is an electrode from the solids process.

Coin cells of Graphite/NCM were assembled with the BLE and the HVE and cycled between 3.5 and 4.1, 4.2, 4.3, 4.4, 4.5, and 4.6 V. The results of the testing are provided in Figure V- 141. As one can see, cells cycled with the BLE to 4.4 V cycled for 450 cycles before catastrophically failing, whereas, cells cycled with the HVE to 4.5 V cycled to 1000 cycles without catastrophe. Cells in the BLE showed minimal loss of capacity to 500 cycles when cycled to 4.3 V; cells in the HVE showed minimal loss of capacity to 1000 cycles when cycled to 4.4 V. We believe that this clearly demonstrates that Diakin has made a change of significance that resulted in an improvement of high-voltage cycling by 100 mV.

The electrolytes were put through additional electrochemical tests. A particular property of interest was the rate of the side reaction at the cathode and whether this rate changes as a function of upper voltage limit. Figure V-142 shows the average rate of the side reaction for 10 cycles for cutoff voltages of 4.1 to 4.7 V in increments of 0.1 V. As one might expect, the capacity shift per cycle increased with voltage, although it appeared to level off for the BLE between 4.2 and 4.4 V. This leveling off may be a result of a change in oxidation mechanism and/or the formation of a passivation film on the cathode. This graph immediately suggests that the HVE is less reactive than the BLE.

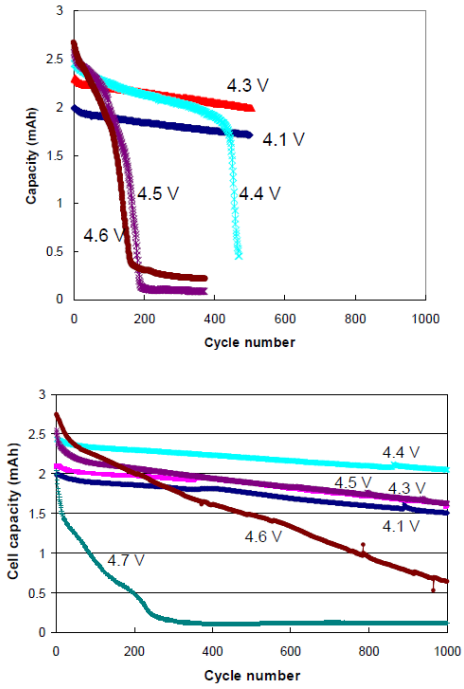

Figure V- 141: Cycling results of Graphite/NCM cells with the baseline electrolyte (left) and the high-voltage electrolyte (right).

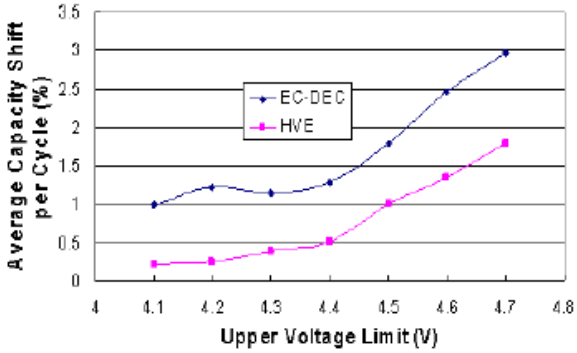

Figure V- 142: The average shift in capacity per cycle as a result of the side reactions with the baseline electrolyte and the high voltage electrolyte when stepping up in voltage.

In addition to stepping up the voltage from 4.1 V, we also investigated stepping down the voltage from 4.7 V, in 100 mV increments. The results of this test are provided in Figure V- 143. The interesting results in this experiment are that, for the HVE, after the first cycles at 4.7 V, the rate of capacity shift per cycle is cut in half for the remaining cut-off voltages. The same is true for the BLE down to about 4.4V, after which the side reaction returns to the rate seen in the forward voltage stepping. We believe that this is the result of a protective film formed from the HVE at high voltages. To test this theory, we made two full cells, both with HVE, except one was cycled seven times at 4.6 V and the other was cycled seven times at 4.4 V. After these initial cycles, both cells were fully cycled between 3.5 and 4.4 V. The result is presented in Figure V- 144.

From this figure it appears that the first few formation cycles resulted in improved long-term cycleability.

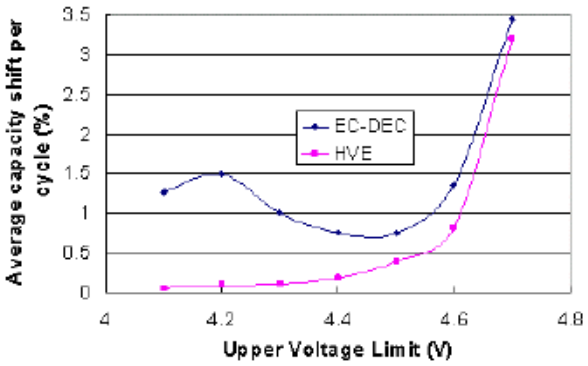

Figure V- 143: The average shift in capacity per cycle as a result of the side reactions with the baseline electrolyte and the high voltage electrolyte when stepping down in voltage.

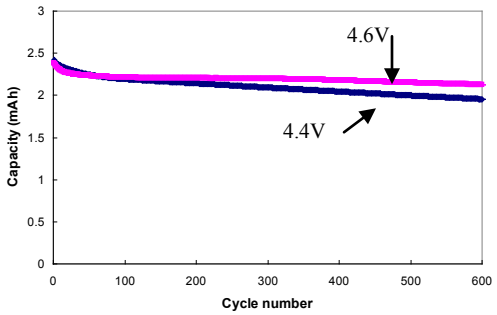

Figure V- 144: Long-term cycling of full cells with HVE to an upper cut-off voltage of 4.4V. One of the cells was first cycled to 4.6 V for seven cycles.

Conclusions and Future Directions

This year we investigated the effect of mixing order on electrode performance and found that the order matters. Apparently mixing the binder with the high surface area conductive additive ties up the binder preventing it from freely mixing with the active material when added subsequently. The differences can not be detected on the micron scale but long term cycling reveals cracks in electrodes where the active material is not first mixed with the conductive additive before adding the binder.

We also investigated a new, high-voltage electrolyte from Daikin. The electrolyte demonstrated a reduction in the side reaction with the cathode and good cycling to a cut-off voltage of 4.4 V. It is believed that a protective film is formed by the new electrolyte at high voltages, > 4.6 V, which results in improved long-term cycling when the cut-off potential is reduced to 4.4 V. The baseline

electrolyte also shows a passivation effect as the cut-off voltage was increased, but the film formed here did not have much effect when the cell voltage was reduced.

Future work will investigate other electrode processing parameters such as calendaring temperature and coating rates. We will also measure performance characteristics of the high-voltage cathode $LiNi_{1/2}Mn_{3/2}O_4$.

FY 2010 Publications/Presentations

1. 2009 DOE Annual Peer Review Meeting Presentation.
2. Honghe Zheng, Gao Liu, Xiangyun Song, Paul Ridgway, Shidi Xun, Vincent S. Battaglia, "Cathode performance as a function of inactive material and void volumes**,"** *J. Elec. Soc*., **157**, A1060 (2010).

V.E.2 Modeling—Thermo-electrochemistry, Capacity Degradation and Mechanics with SEI Layer (University of Michigan)

Ann Marie Sastry
University of Michigan
2350 Hayward St.
Ann Arbor, MI 48109
Phone: (734) 998-0006; Fax: (734) 998-0028
E-mail: amsastry@umich.edu

Start Date: October 1, 2008
Projected End Date: September 30, 2011

Objectives

- Develop multiscale/multiphysics finite element (FE) modeling considering thermal effects, self-assembly, its effect on cathode structure, and the effect in turn on cathode dissolution as the main effect in capacity degradation.
- Develop SEI layer formation model and perform parametric studies for SEI layer formation.
- Validate the SEI layer formation model through *ex situ* experimental techniques.

Technical Barriers

- Inadequate power and life in systems for PHEVs

Technical Targets

- Available energy: 56 Wh/kg (10 mile) and 96 Wh/kg (40 mile)
- 10 s discharge power: 750 W/kg (10 mile) and 316 W/kg (40 mile)
- Cycle life: 5,000 cycles
- Calendar life: 15 years

Accomplishments

- Development of multiphysics FE model for thermo-electrochemistry.
- Demonstration of the differences in temporal trends of reaction current density and heat generation between pseudo-2D modeling and 3D microscopic modeling.
- Development of an SEI growth process via phase field method.
- TEM observation of SEI layer formed on the surface of $LiMn_2O_4$ particles.

✧ ✧ ✧ ✧ ✧

Introduction

Capacity degradation of Li-ion batteries involves many mechanisms: active material dissolution, particle fractures, SEI layer evolution, etc. This capacity degradation becomes severe as temperature increases within cells. In order to accurately predict capacity degradation, these mechanisms need to be modeled with thermo-electrochemistry in simulating Li-ion battery performance. During FY2009, multiscale electrochemical modeling was proposed via surrogate-based scale bridging and stochastic 3D packing of active particles. As an extension, multiscale thermo-electrochemistry modeling can capture the microstructural effects on the performance prediction of Li-ion batteries. Multiscale modeling enables us to investigate the microstructural effect of particle aggregation on cathode structure and its dissolution. Also, capacity degradation of Li-ion battery anodic and graphitic materials can be directly related to the properties of the SEI layer including composition, internal structure, and mechanical strength. Fundamental understanding of SEI layer property variation can inform lifetime prediction of Li-ion battery cells.

Approach

Multiphysics finite element models of cells are developed in order to evaluate heat generation and temperature increase via a stochastic approach for 3D microstructure generation. The multiscale modeling of thermo-electrochemistry will be extended with microstructure reconstruction via self assembly. The formation and morphology changes in SEI films during the first electrochemical intercalation of Li-ions into electrodes are modeled as a precipitation process including a nucleation phase and phase growth involving the precipitation of new phases. The precipitation process, including a nucleation phase and phase growth, is governed by the interfacial energy differences between each of the species. By evaluating the parameters, we will explore the SEI growth phenomena. The formation and the structure of SEI layers are complex. We utilize experimental techniques such as TEM (transmission electron microscopy) and AFM (atomic force microscopy) to measure the properties of SEI layers depending on cycling, charge/discharge rate and temperature. SEI layers

will be characterized and the SEI formation model will be validated by *ex situ* experimental techniques with the leverage of ORNL (Oak Ridge National Laboratory).

Results

Multiphysics FE model. A voxel mesh of packed ellipsoids has been generated for the FE-mesh generation. As a result of thermal effects, the increase in temperature results in an increased Li-ion flux at the SEI in the microscale model as shown in Figure V- 145. The additional closure term for scale-bridging between macroscale and microscale is shown as heat generation at the SEI in Figure V- 146.

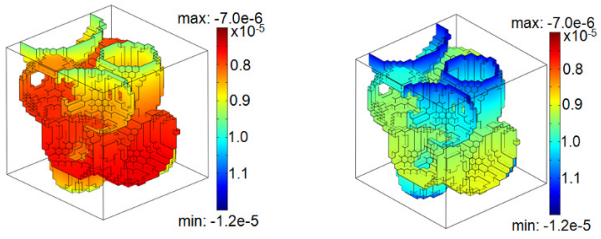

(a) (b)

Figure V- 145: Reaction current density via (a) electrochemical model and (b) thermo-electrochemical model.

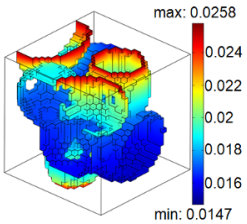

Figure V- 146: Heat generation via thermo-electrochemical model.

Three dimensional microscopic simulations have further investigated closure terms (i.e., reaction current density and heat generation). When the representative volume element is placed at the middle of the cathode, the temporal variations of reaction current density and heat generation from the pseudo-2D thermo-electrochemical model and 3D microscopic model are compared. As shown in Figure V- 147, the reaction current density and heat generation in the 3D model show different temporal trends from the pseudo-2D model.

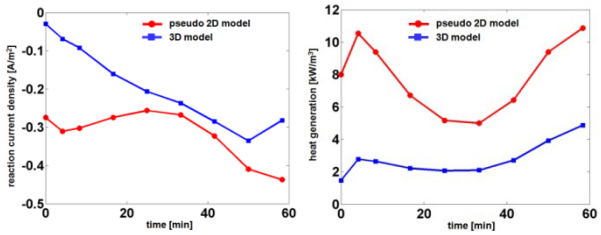

(a) (b)

Figure V- 147: Time history of (a) reaction current density and (b) heat generation via thermo-electrochemical model.

SEI Formation Modeling. It has been experimentally observed that the SEI is composed of two distinct layers: a thin inorganic compound layer and a thick porous organic compound layer. A three dimensional phase field model is proposed to account for the two-layer structure of the SEI. Here we integrate the chemical energy and interfacial energy between each of the species. A phase field model integrating the chemical energy and interfacial energy is developed to account for the SEI growth process. Figure V- 148 shows the schematic representation of SEI layer formation and the results of the phase field model. Depending on the surface energies between each of the species the final equilibrium angle varies.

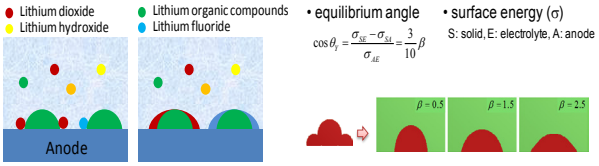

Figure V- 148: SEI layer formation via phase field model

Measurement of SEI Properties. A TEM image of a 3 to 4 nm SEI layer formed on a $LiMn_2O_4$ particle after cycling is shown in Figure V- 149. Surface morphology and modulus mapping of a $LiCoO_2$ thin film electrode (before cycling) are shown in Figure V- 150(a) and (b). The RMS roughness of the $LiCoO_2$ thin film annealed at 700°C (Figure V- 150(a)) was 11.5 nm. The mean value of Young's modulus of the $LiCoO_2$ thin film annealed at 700°C (Figure V- 150(b)) was 1.94 ± 0.71 GPa. Systematic investigation of the SEI layer microstructure and its relation to battery performance will be implemented with the collaboration of ORNL.

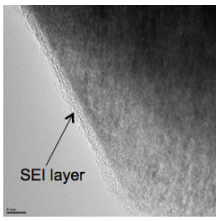

Figure V- 149: TEM image of $LiMn_2O_4$

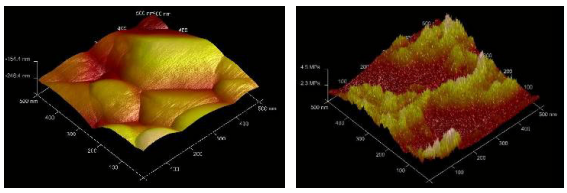

(a) (b)

Figure V- 150: (a) Surface morphology and (b) modulus mapping of $LiCoO_2$.

Conclusions and Future Directions

Mutiphysics modeling of thermo-electrochemistry has quantified differences in predicted electrochemical characteristics from the pseudo-2D model. Microscopic simulations have revealed the local distribution of reaction current density and heat generation and have demonstrated the 3D microstructural effect. Integration of thermal and kinetic effects has allowed the extension of modeling to many particle geometries and consideration of many types of packing architectures. The multiscale FE model for multiphysics simulations using self-assembly will be further developed and combined with the dissolution and SEI layer model. From the preliminary study of SEI layers using TEM and AFM, it was confirmed that SEI layers formed on the surface of $LiMn_2O_4$ particles and the modulus of composite electrode surface was varied as a function of tip position.

The formation and evolution of SEI layers during the initial electrochemical intercalation of lithium into electrodes has been modeled as a precipitation process including a nucleation phase, followed by a growth phase involving the precipitation for new phases on previously formed nuclei. This process is a result of the competition between Gibbs free energy and interfacial energies. These key parameters for different electrochemical systems and the effect of the parameter changes on SEI layer formation will be further investigated. Microstructure and chemical elements of SEI layers will be characterized using IR, Raman, SEM and TEM at ORNL, in connection with the SEI layer formation model. Also, subsequent cycling properties of Li-ion batteries will be correlated with the SEI layer formation model.

FY 2010 Publications/Presentations

1. 2010 DOE Annual Peer Review Meeting Presentation.
2. Seo J.H., Zhang X. and Sastry A.M., “Multiphysics Optimization of Battery Cells and Cell Materials: From Single Particles to packs”, International Battery Association Meeting & Packfic Power Source Symposium 2010, Waikoloa, Hawaii, Jan. 11-15, 2010
3. Sastry A.M., “Scale-Bridging Simulations and Experiments of Electrode Materials in Energetic Batteries”, Symposium on Research Opportunities in Electrochemical Energy Storage Beyond Lithium-ion: Computational Perspectives, Argonne, IL, May 03-04, 2010
4. Seo J.H., Less G., Park M., Zhang X., Chung M.D., Park J. and Sastry A.M., “State of the Art in Computational Multiphysics/Multiscale Modeling in Lithium-ion Batteries”, Invited presentation, 2010 ASME International Mechanical Engineering Congress and Exposition, Vancouver, BC, Canada, Nov. 12-18, 2010

V.E.3 Intercalation Kinetics and Ion Mobility in Electrode Materials (ORNL)

Claus Daniel

Oak Ridge National Laboratory
One Bethel Valley Road
P.O. Box 2008, MS-6083
Oak Ridge, TN 37831-6083
Phone: (865) 241-9521; Fax: (865) 241-5531
E-mail: danielc@ornl.gov

Collaborators:

Ann Marie Sastry, University of Michigan
Nina Balke, ORNL
Nancy Dudney, ORNL
Hongbin Bei, ORNL

Start Date: September 2009
Projected End Date: September 2013

Objectives

- Develop fundamental understanding of deformation processes and stress generation during lithium (Li) intercalation (deintercalation) from active cathode material via experimental work on focused ion beam (FIB) micromachined samples.
- Develop and validate coupled kinetic, thermal, and mechanical model based on the experimental results.
- Understand the role of defects, texture, and mechanical damage in Li-ion kinetics in intercalation compounds.

✧ ✧ ✧ ✧ ✧

Introduction

It is commonly accepted that Li-ion battery life is limited as a result of the degradation of electrode materials with repeated charging/discharging. One of the degradation mechanisms is related to development of internal stresses in electrode particles because of repeated Li insertion and removal, which ultimately leads to cracks in and the fracture of particles. The current project targets the fundamental understanding, description through mathematical modeling, and controlled experimental validation of internal stress generation and morphology change of electrode particles in a Li-ion battery. While the intercalation/deintercalation process induces the displacements, changing the overall dimension of the specimen, Li diffusion should be investigated on the single grain level. The second integral part of the project looks into texture and defect-dependent Li-ion mobility, which is the underlying process for diffusion-strain coupling.

Approach

The experiments are performed on model systems represented by micro-level specimens of electrode material. In this way, the modeling work is done on preselected geometries of specimens to validate the constitutive approach. Different cathode materials are investigated, including $LiCoO_2$, $LiMn_2O_4$, $Li_4Ti_5O_{12}$.

The specific distribution of tasks is as follows. Thin film battery systems with thicknesses suitable for FIB machining are synthesized at ORNL. Subsequent micro-machining of electrode samples is done at ORNL using dual beam FIB/scanning electron microscopy (SEM). Micro-samples are tested in a half-cell setup at the University of Michigan. The setup is equipped with an atomic force microscope (AFM) with a tip serving as a current collector, which allows for simultaneous cycling and investigation of morphology changes in the specimen. The experimental results will be used to validate the proposed coupled kinetic, thermal, and mechanical model.

In addition, electrochemical strain microscopy (ESM), recently developed at ORNL, was applied to study Li-ion concentration gradients in thin film $LiCoO_2$ electrodes. The method is based on strain-bias coupling used for detection of local electrochemical activity.

Results

PVD preparation of thin film systems. Thin film samples of a lithium cobalt oxide cathode were prepared by radio frequency magnetron sputtering of a cold pressed and sintered $LiCoO_2$ target. Layers were deposited on an Al_2O_3 substrate. A $LiCoO_2$ cathode was deposited over a thin layer of gold as a current collector. Annealing was done at 700 and 800°C. The lower temperature provides a fine grain size specifically suitable for FIB milling, and the higher temperature provides larger crystals for ESM analysis (Figure V- 151).

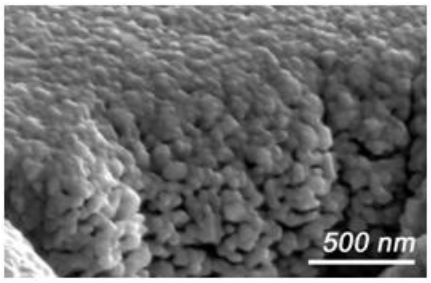

(a)

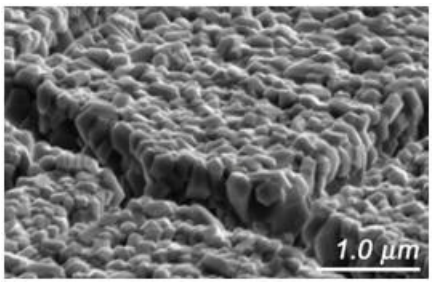

(b)

Figure V- 151: Thin film $LiCoO_2$ cathode annealed at (a) 700°C and (b) 800°C.

Micromachined electrodes. Samples were fabricated using a Hitachi NB5000 dual beam FIB/SEM. Runs with decreasing apertures were applied, with the final run having a current of 0.07 nA in order to remove the layer of gallium implantation. An SEM image of the milled samples is shown in Figure V- 152.

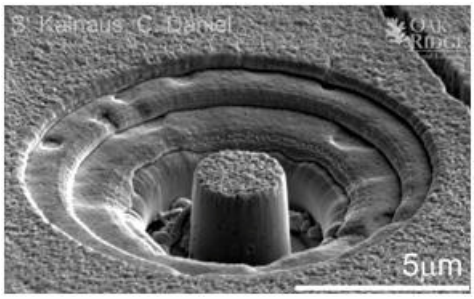

Figure V- 152: FIB machined pillar.

***In situ* AFM.** A Veeco electrochemical AFM (Veeco Instruments, Inc.) with a Z-direction noise level of less than 0.035 nm was used in the experiments. The system was equipped with a wet cell for *in situ* mapping of the electrode sample. A nonconductive silicon nitride AFM tip with a radius of 10 nm was used for scans in contact mode. A Bio-Logic VMP3 (Bio-Logic USA, LLC) potentiostat with current ranging from 1 nA to 400 mA was used for cycling. The height change of the pillars was measured as a function of applied voltage (Figure V- 153).

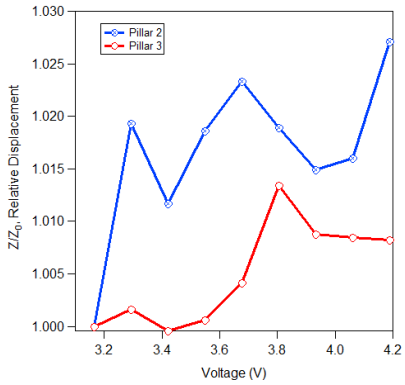

Figure V- 153: Relative vertical displacement of FIB micro-machined cylinders.

Modeling. The finite element method was applied for numerical solution of differential equations incorporated into the model. The pillar was simulated as rigidly attached at the bottom surface, and the flux of ions was allowed as a boundary condition along the remaining surfaces. Figure V- 154 depicts the results, showing the vertical displacement of the pillar as the voltage increases following the CV (0.05 mV/s) scan.

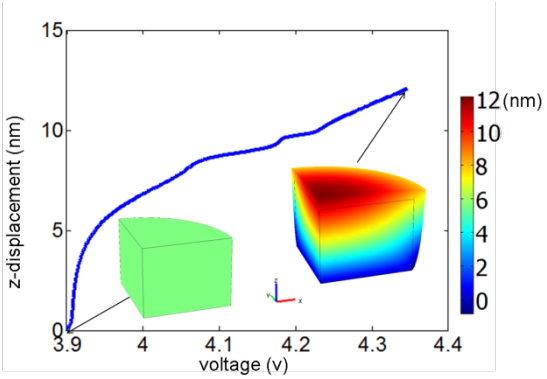

Figure V- 154: FEM modeling of $LiCoO_2$ micro-pillar.

Electrochemical strain microscopy. ESM was applied to 800°C annealed $LiCoO_2$ thin-film samples to map the strain induced by Li concentration gradients. A high–frequency, low-voltage pulse was applied via the AFM tip, which redistributed Li in the tip vicinity, causing local displacements in the grains. The results (Figure V- 155) show the significant dependence of electrochemical activity on the crystallographic features of the sample. Bias-induced strain amplitude (Figure V- 155(a)) and a corresponding hysteresis loop area (Figure V- 155(b)) are functions of the location of the pulse application. The technique is very promising for revealing preferential locations for Li-ion diffusion in a cathode material.

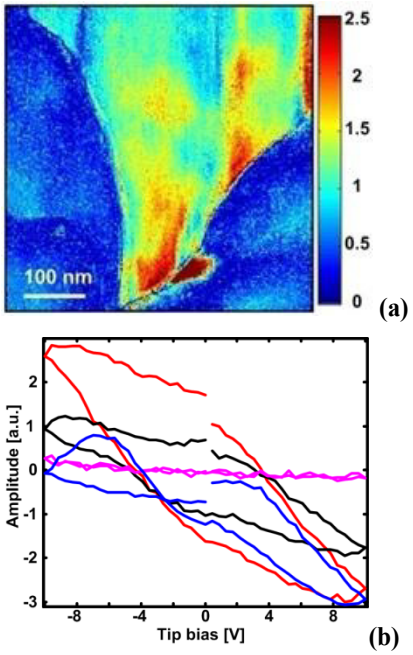

Figure V- 155: ESM of $LiCoO_2$ grains: (a) amplitude; (b) hysteresis loops at different locations

Micro-pillar compression. The effect of mechanical damage on the form of compressive pre-straining was investigated using nanoindentation techniques. At the preliminary stage, several FIB micromachined cylinders (Figure V- 152) were compressed in an MTS Nanoindenter XP system using a flat tip indenter 20 µm in diameter. The results allowed for a preliminary estimate of Young's modulus, which was determined to be close to 30 GPa. In further investigation, the effect of precompression on electrochemical strain will be determined by using AFM scans of the pillars. Additionally, work is under way to introduce damage to the thin films using a spherical tip indenter for further investigation of damage to local ion mobility by ESM.

Conclusions and Future Directions

The diffusion-stress coupling model shows the capability to predict strains in electrode micromachined specimens. The model awaits improvement based on the experimental data obtained from electrochemical cycling of electrode samples. Work will continue on application of the developed technique to other cathode materials.

The newly developed ESM technique is a powerful and promising method for investigation of Li mobility within the electrode as a function of defects, grain boundaries, introduced damage (slip lines), and state of charge. At present, the work has been done in ambient air, when the ions are moving within the material as a result of a locally applied pulse. At the next stage, it is proposed that the experiments will be performed in an electrolyte in order to study Li-ion transport across a solid/electrolyte interface. Future focus is proposed to develop an understanding of microstructural features for low state of charge power enhancements with guidance on future materials processing routes to maintain those microstructures in large scale batteries.

FY2010 Publications

1. "Investigation of Lithium Insertion/Extraction Induced Morphology Changes in Micromachined Specimens of Li-Ion Battery Cathode Material", S. Kalnaus, J. Park, M. Park, A. Sastry, N. Dudney, C. Daniel, 218th ECS Meeting, Las Vegas, NV, Oct. 10-15, 2010
2. "Lithium-ion intercalation induced stress and fracture of active electrode material", S. Kalnaus, K. Rhodes, C. Daniel, MRS Fall Meeting, Boston, MA, Nov. 29-Dec. 3, 2010

Acknowledgment

Dual-beam FIB and electron microscopy were performed at the Shared Research Equipment Collaborative Research Center at ORNL, sponsored by the Scientific User Facilities Division, Office of Basic Energy Science.

V.E.4 Investigations of Electrode Interface and Architecture (LBNL)

Venkat Srinivasan
Lawrence Berkeley National Lab
M.S.70R0108B
1 Cyclotron Road
Berkeley, CA 94720
Phone: (510) 495-2679
E-mail: vsrinivasan@lbl.gov

Start Date: October 2009
End Date: September 2010

Objectives

- Use a mathematical model to understand behavior of $LiFePO_4$ cathodes at high rates.
- Examine the implications of a flat potential in an electrode with different particle sizes.
- Develop a model for a silicon anode to capture effects within the particle as well as across the porous electrode.
- Develop a mechanical degradation model incorporating both active material as well as binder failure.

Technical Barriers

While the $LiFePO_4$ material has been successfully commercialized, numerous issues are not well understood even after a decade of research. Specifically, (i) it is not clear why some materials possess extreme high rate capability while other materials do not, and (ii) no clear understanding exists on how multiple particle sizes can impact the performance of this system.

Silicon anodes suffer from poor cycle life caused by cracking of particles due to the large volume change along with amorphous to crystalline phase transitions. Moreover, it has been shown that the design of the electrode is critical in ensuring better life. Quantifying these issues is critical in enabling the use of this anode.

While many models exist that predict conditions under which electrode particles can crack due to stress buildup, experimental data suggests that failure sometimes occurs at the binder and/or at the binder/particle interface. Present day models do not describe this observation.

Technical Targets

- Develop and use a mathematical model to predict rate capability of $LiFePO_4$
- Develop a model for silicon anodes
- Develop a mechanical degradation model incorporating both particles and binder.

Accomplishments

- Identified the limitation when operating $LiFePO_4$ at high rates and showed that lithium transport in the solid phase limits utilization.
- Showed that in a flat potential system like $LiFePO_4$ the small particles can have a significantly different SOC compared to the large particles and can lead to path-dependent behavior.
- Showed that optimal design of silicon anodes, both in choice of particle size and in thickness and porosity of the porous electrode, is critical in minimizing phase transformation.
- Showed that failure of electrodes can occur both because of the particles and the binder and that accounting for the binder is critical in accurate predictions of failure modes.

Introduction

In order to successfully commercialize PHEVs and EVs, safe, low cost, high-energy batteries are needed that have long lifetimes. New electrode materials that promise to increase the energy density, along with new designs that ensure high packing density are essential for this.

While numerous new materials have been proposed, they are plagued by various problems. While materials like $LiFePO_4$ promise very good safety and long life, the low packing density, caused by the use of nanoparticles, decreases the cell-level energy density. Similarly, while materials like silicon have the ability to increase the energy density, the large volume change makes it susceptible to cracking on cycling. Finally, mechanical breakdown of the electrodes, especially when cycling over a wide SOC range, needs to be controlled.

Mathematical models provide a unique approach to not only study the ability of new materials to be used in real-world operation but also in understanding failure.

Approach

Develop mathematical models for candidate Li-ion chemistries to quantify their ability to meet DOE/USABC performance and life goals for use in PHEV and EV applications. This is accomplished by developing

performance and life models for candidate materials and designing experiments to estimate thermodynamic, kinetic and transport properties. These properties are then used to test theoretical predictions and provide guidance to material-synthesis and cell-development researchers. Overall, the approach is to connect fundamental material properties to practical performance requirements.

Results

Modeling $LiFePO_4$ Electrodes. In order to understand why some $LiFePO_4$ materials have extremely high rates, a mathematical model was developed that accounts for diffusion in the solid particles *via* Fick's law. While transport and phase change in this chemistry has been a subject of intense controversy, the study was designed to understand the interplay between transport in the electrode *vs.* that in the electrolyte.

Simulation results are shown in Figure V- 156 where the model is compared to baseline data (blue symbols and line) and to the high rate data reported by Gerd Ceder's group (red symbols and line). The particle size, porosity, and thickness of the two electrodes are different and accounted for in the model. However, the fit to the high rate data was achieved by increasing the solid phase diffusion compared to the baseline data. This could either indicate an average particle size that is different from that reported or due to a different transport property (due to, say, defects).

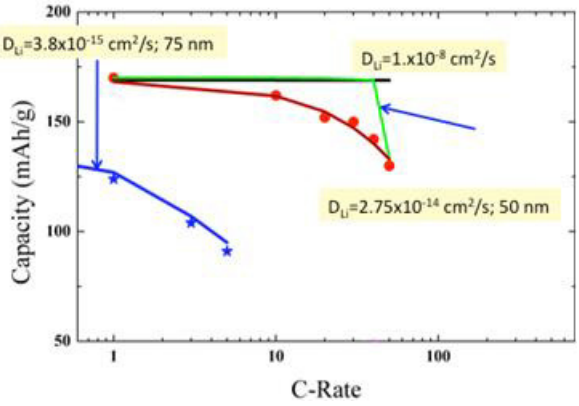

Figure V- 156: Model experimental comparison for base-line (Srinivasan and Newman) and high-rate (Kang and Cedar) data

Simulations were also conducted by assuming fast solid phase transport to see if electrolyte transport could account for the drop in utilization. Two simulations are shown, one using a typically brugemman-type expression (black line) and a second where the tortuosity was increased to fit the 50 C data (Green line). Results show that while its possible to get good fit at 50 C, the gradual drop in utilization is not predicted using electrolyte transport losses. The simulation results allude to the fact that $LiFePO_4$ is limited *via* transport in the solid phase and that the diffusion coefficient is on the order of 10^{-14} to 10^{-15} cm^2/s. Model results also suggest that a particle size distribution could be important in predicting the behavior of this electrode.

In order to study the effect of particle size distribution, the model was modified to include a second particle. The methodology for this inclusion is similar to inclusion of a second reaction (*e,g.,* side reaction). Figure V- 157 shows simulations of the state of discharge (SOD) of an electrode at the electrode/separator interface that illustrates one unique attribute of a two-particle system. Here the small particle can be highly lithated while the large particle is highly delithated. In a typical battery electrode where the potential is slopey, lithiation of the small particle will result in a change in the potential. As the potential of the small and large particles cannot be different, the large particles starts to lithiate to "catch up" with the small particle. However, in a flat potential system like $LiFePO_4$ as the potential is invariant, this internal mechanism to equilibrate the concentration does not exist. Hence a large disparity between the two particles can occur.

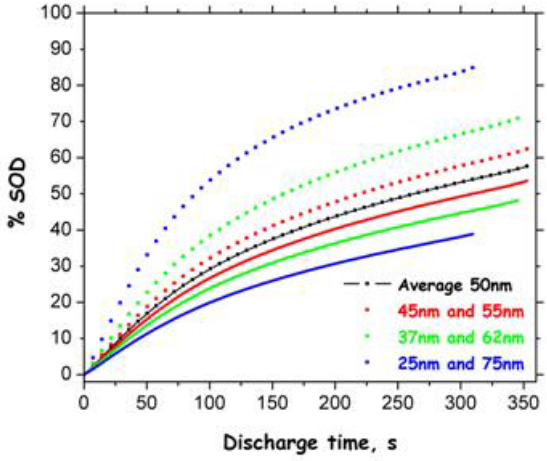

Figure V- 157: Extent of % State-of-Discharge disparity between small and large particles at the porous electrode/separator interface as a function of particle size distributions with an average particle size being 50 nm for a discharge process at 5C rate

Further studies have shown that this disparity can lead to a case where an electrode charged to 50% SOC from a fully-discharged state will have a different distribution of concentration between the two particles compared to an electrode discharged to 50% SOC from a fully charged state. This specific path dependent behavior is a unique feature of a flat potential system.

Modeling silicon anodes. A single-particle model that accounts for the solid-phase mass transport in silicon, volume change during lithiation/de-lithiation,

thermodynamics, and reaction kinetics was developed. This model has been used to predict the maximum capacity that can be achieved during charge before the formation of $Li_{15}Si_4$, which is a crystalline phase that has an effect on the life of the anode. Figure V- 158 shows this for cells cycled to partial and full capacities of Si. The rate capability of a cell cycled to 1000 mAh/g is better than the other two cases considered. This is due to larger crystalline-Si region that translates into a smaller diffusion length in the shell region. The figure shows the ability of the mathematical model to aid in the design of the material both from a performance and a life standpoint.

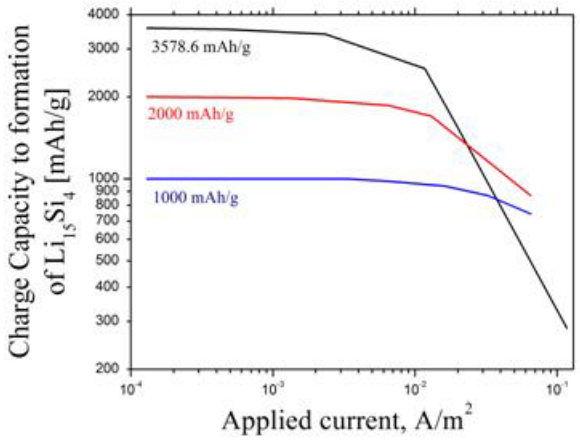

Figure V- 158: Maximum charge capacity that can be obtained before formation of $Li_{15}Si_4$ at different applied current densities for cells cycled to 1,000; 2,000; and 3,578.6 mAh/g

While the above shows results for a single particle, porous electrode effects are important to consider due to the distributed reaction. Therefore, a porous electrode model was developed by extending the single-particle model and by utilizing porous electrode theory, concentrated solution theory and change in volume with cycling. The electrode dimensions are assumed not to change due to volume expansion as the volume expands into the pores of the electrode with the header space occupied with electrolyte. The anode design is based on matching to a NCA cathode of 80 µm thickness and 35% porosity at 3.6 mAh/cm^2 loading. Figure V- 159 shows the importance of liquid phase transport limitation for the cell cycled to 1,000 mAh/g while the solid-phase transport limitation is almost negligible compared the other two cases. In the cells cycled to 2,000 and 3,000 mAh/g, the solid-phase limitation has an effect on the rate capability as evidenced from the slope between 1C and 7C before the final fall where the liquid phase limitation also adds up to the transport losses. The model allows for effective design of the porous electrode to achieve performance requirements for PHEVs. In addition, life limitations, arising from reaction distributions across the electrode, are also captured.

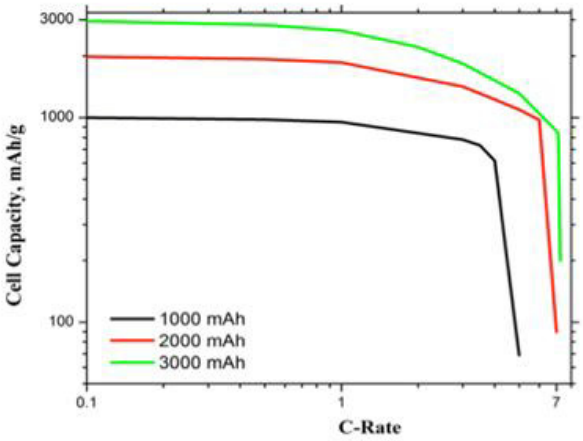

Figure V- 159: Rate capability of cells cycled to 1000, 2000, and 3000 mAh/g with the capacity matched to a NCA cathode of 180 mAh/g capacity, 80 µm thick, 35% porosity, and 3.6 mAh/g loading

Mechanical Degradation of Electrodes. In this fiscal year, we have developed a mathematical model to understand the mechanical degradation in electrodes talking into consideration the active material as well as the binder. The model takes into consideration concentration variations across the particle and the volume change on cycling. In addition, different mechanical failure modes *i.e.*, tensile/compressive failure in the active material/binder are considered. Figure V- 160 shows the stress generated in the active material (graphite) and binder (PVdF) at the end of discharge for different rates of discharge. The simulations were conducted with properties reported in the literature for the active material and the binder. This methodology will also aid in our understanding of mechanical failure in the next-generation electrodes like Si and help in tailoring the components and design for a mechanically durable porous composite electrodes.

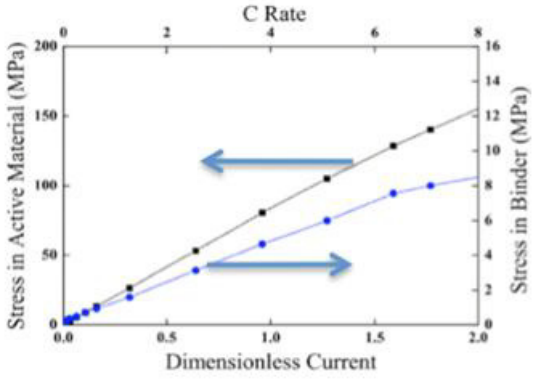

Figure V- 160: Stress in graphite and PVdF binder at the end of discharge as a function of rate of discharge.

We also looked into the effect of different discharge protocols on the mechanical durability of battery electrodes. One such scenario considered involved discharging a graphite electrode to 50% SOC. After the system reached its equilibrium state, the electrode was discharged to its full capacity. The stress in the active material obtained using this protocol was found to be less than that obtained for a complete discharge. The decrease in the stress expressed as percentage is plotted as a function of different rates of discharge in Figure V- 161. The figure argues for the need to incorporate the effect of the binder in predicting mechanical breakdown of electrodes. Further, the change in stress with cycling protocol suggests that smart cycling of batteries may provide a means of decreasing mechanical degradation effects.

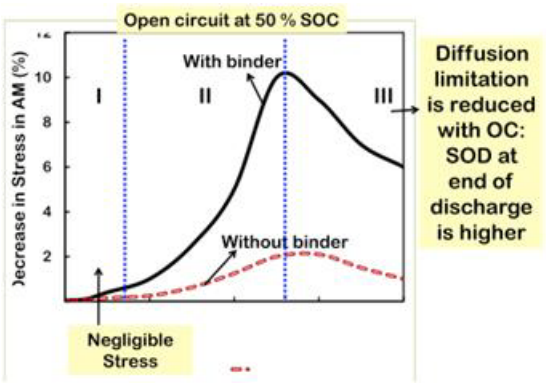

Figure V- 161: Decrease in stress in graphite with and without open circuit.

Conclusions and Future Directions

In this fiscal year we have used a mathematical model for the $LiFePO_4$ electrode in order to understand the high rate behavior of this system and the impact of having multiple particle sizes. The simulation results allude to the fact that $LiFePO_4$ is limited *via* transport in the solid phase and that the diffusion coefficient is on the order of 10^{-14} to 10^{-15} cm^2/s. Multiple particles sizes were shown to lead to a significant disparity in the amount of lithium intercalation/deintercalation in the large and small particles due to the flat equilibrium potential.

A model was developed for silicon anodes that takes into consideration complexities in both the solid and the porous-electrode scale. Results suggest that design of the material as well as the electrode is critical in understanding performance and life of this chemistry.

A mechanical degradation model was developed that showed the importance of taking into consideration the failure of the binder. The binder was seen to change the stress state of the electrode under certain cycling conditions.

Future work will focus on expanding these studies by comparing them to experimental data, and extending the models to predict degradation in next generation-battery materials.

FY 2010 Publications/Presentations

1. 2009 DOE Annual Peer Review Meeting Presentation.
2. "Resource constraints on battery energy storage potential for grid and transportation applications", *J. Power Sources*, accepted.
3. " *in situ* measurements of stress-potential coupling in lithiated silicon", *J. Electrochem. Soc.*, accepted
4. "Increased cycling efficiency and rate capability of copper-coated silicon anodes in Lithium-ion batteries", *J. Power Sources*, accepted and available online
5. "Lithium diffusion in graphitic carbon", *J. Phys. Chem. Lett.*, **1**, 1176 (2010)
6. "Surface structural disordering in graphite upon lithium intercalation/deintercalation", *J. Power Sources*, **195**, 3655 (2010)
7. " *in situ* measurements of stress evolution in silicon thin films during electrochemical lithiation and delithiation", , *J. Power Sources*, **195**, 5062 (2010)
8. " *in situ* Stress Measurements in Silicon Anodes for Lithium-Ion Batteries", Presented at the 218th ECS Meeting - Las Vegas, NV
9. "Investigations on Silicon Composite Electrodes for Lithium-Ion Batteries", Presented at the 218th ECS Meeting - Las Vegas, NV
10. "Mechanical Degradation in Lithium-Ion Battery Electrodes", Presented at the 218th ECS Meeting - Las Vegas, NV
11. "On the High Rate Capability of $LiFePO_4$", Presented at the 218th ECS Meeting - Las Vegas, NV.

V.E.5 Analysis and Simulation of Electrochemical Energy Systems (LBNL)

John Newman
Lawrence Berkeley National Laboratory
306 Gilman Hall
University of California, Berkeley
Berkeley, CA 94720
Phone: (510) 642-4063; Fax: (510) 642-4778
E-mail: newman@newman.cchem.berkeley.edu

Start Date: October 1, 2009
Projected End Date: September 30, 2010

Objectives

- Develop experimental methods for measuring transport, thermodynamic, and kinetic properties.
- Model electrochemical systems to optimize performance, identify limiting factors, and mitigate failure mechanisms.

Technical Barriers

This project addresses the following technical barriers from the USABC:

(A) Capacity and power fade

(B) Safety and overcharge protection

Technical Targets

This project contributes to the USABC requirements of end of life energy storage systems for PHEVs and EVs:

- 300,000 shallow discharge cycles
- 15 year calendar life

Accomplishments

- Began work on a two-dimensional model of lithium redistribution in lithium-metal batteries over long time scales.
- Developed experimental procedures for reproducibly forming a film of reduction products on a glassy carbon electrode
- Built models to describe both formation of surface films and reduction of ferrocene, a model redox shuttle, through the film

✧ ✧ ✧ ✧ ✧

Introduction

In FY10, we worked on two projects. In the first, we began a collaboration with Bosch to develop a realistic two-dimensional model of anodic lithium redistribution in a lithium-metal/CoO_2 battery. This research project operates under the assumption that dendrite formation can be prevented through the use of a polymer separator or ceramic protective layer and will look into the possibility that anodic lithium redistribution along the negative current collector could play a significant role in reducing both the lifetime and safety of lithium-metal batteries. Such a study helps identify limitations of current systems and suggest mitigation mechanisms. We also continued our experimental work on SEI formation reactions and the interaction of the SEI with redox shuttles. Our novel method of SEI characterization contributes to understanding passivation in nonaqueous electrolytes, which is in turn critical to battery performance and lifetime.

Approach

1. Develop two-dimensional model in COMSOL to describe long-term lithium redistribution on cycling, including effects of current density distribution, heat and pressure. The two dimensions are along the length of an unwound cell sandwich (50 cm) and through the thickness of the cell sandwich (200 μm). All of the current is passed through the positive and negative tabs at the corners of the cell sandwich.
2. Utilize classical electrochemistry experiments to understand the fundamental growth kinetics of the SEI, as well as how it interacts with a redox shuttle. Measure shuttle reduction kinetics in the presence and absence of passivating films to determine the relative transport and kinetic inhibitions to reaction.

Results

Shape Changes in Lithium Electrodes. Preliminary simulation results are shown in Figure V- 162 and Figure V-163. The lithium-metal battery model was cycled at three different rates beginning with a discharge, followed by a rest period of half an hour, and completed by a charge at the same rate and duration as the discharge. All rate calculations were based on the positive electrode. The three charge rates were 0.05, 0.1, and a 0.5 C-. All cycles were run to a time corresponding with a 25 percent depth of discharge.

Figure V- 162 shows the initial dimensionless current density for the 0.1 C-rate along the negative electrode/separator interface. The dimensionless reaction rate is calculated by dividing the local reaction rate by the maximum reaction rate. Here an asymmetric current distribution can be clearly seen with the minimum current occurring at about 0.75 in the X direction, along the current collector (closer to the positive tab) at approximately 88 percent of the maximum current. The tendency for the current to pass through the left side of the battery, nearest the negative tab, is due to the resistance of the negative current collector (which, in this case, is lithium) being roughly four times higher than that of the positive current collector. From Figure V- 162, it can be concluded that initial current distribution is dominated by the geometry and resistances of the battery.

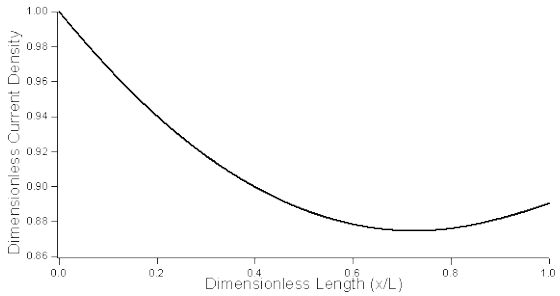

Figure V- 162: Dimensionless current density along the anode/separator interface at the beginning of discharge at a 0.1 C-Rate

Figure V- 163 shows the dimensionless shape change in the negative electrode after one full cycle to 25 percent depth of discharge. The dimensionless shape change is calculated by dividing the local value for the amount that the lithium moved after a full cycle, relative to its starting position, by the average amount that the lithium was depleted after the discharge.

From Figure V- 163, it can be seen that the rate plays a significant role on the amount of lithium movement that occurs and that even at moderate rates of discharge and charge (0.5 C), significant movement (1.9%) can occur even after one cycle. The dashed line labeled 'Resistance Model' corresponds to the dimensionless change in the lithium metal after one full cycle of a simplified resistance model with a moving boundary at the negative electrode/separator interface. It is seen here that after one cycle of the resistance model, the lithium returns to its original position. The slight deviation (~1.2×10^{-3} percent) can be attributed to numerical error. The lack of movement in the resistance model signifies that the shape change observed is due to underlying physical phenomena. More work will be done in order to understand these pehnomena.

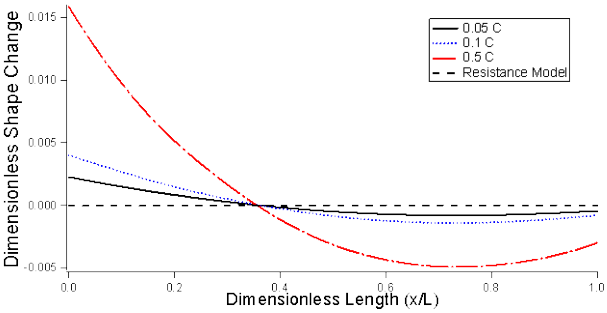

Figure V- 163: Dimensionless change in the lithium metal interface after a full cycle (discharge then charge) at various rates and a 25% depth of discharge. The dimensionless difference is calculated by dividing the change in the position of the Li after a full cycle by the average change in position after half of the cycle.

Interactions between Redox Shuttles and the SEI. We have devoted substantial time and effort to developing reproducible methods for studying reduction kinetics of nonaqueous electrolytes. The collapsing I-t curves for potentiostatic holds at 0.6 V in Figure V- 164 demonstrate our success in this endeavor. As time increases, the current decreases, showing that reduction products are passivating the surface. We are presently developing physics-based models that explain the shape of this curve and relate the current to properties such as film resistivity and solvent diffusion, as well as expanding the measurements to look at different voltages.

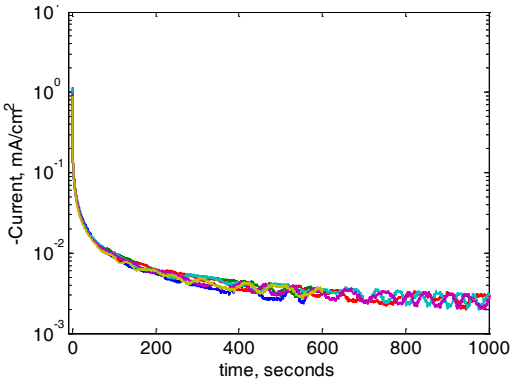

Figure V- 164: Current vs. time for the reduction of 1.0 M $LiPF_6$ in EC:DEC. The decreased current with time shows that products are passivating the surface, while collapsing curves for different trials show reproducibility.

In the absence of passivating films, the reduction of ferrocenium is reversible. Figure V- 165 shows the effect of passivating films on the reduction of ferrocenium. The markers show the Koutecky-Levich intercept i_K, or the current that would be measured if transport resistance from the bulk solution to the surface was negligible. The three curves show that as the electrode is passivated for 10, 30, and 60 minutes, ferrocenium current is increasingly blocked. The solid lines show model fits. Data are

described using only three parameters: a Tafel slope, an exchange current density, and a limiting current. Both the limiting current and the exchange current density decrease with increased passivation. More work is required to explain why this trend occurs.

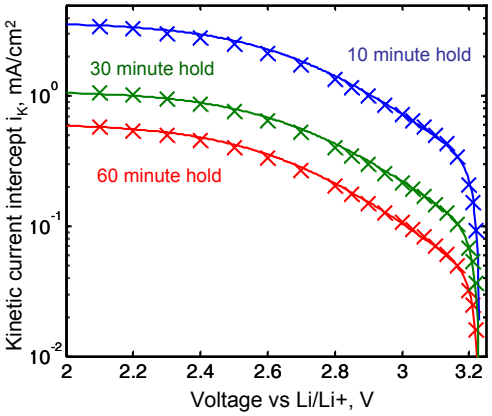

Figure V- 165: Kinetic current i_K versus voltage for electrode after 10, 30, and 60 minute holds at 0.6 V. Increased film formation time reduces the amount of ferrocene reduction for the same overpotential.

Conclusions and Future Directions

Shape Changes in Lithium Electrodes. From the current model it has been seen that significant shape changes could occur after one cycle at moderate discharge and charge rates. Future work includes modeling higher rates as well as multiple cycles and cycling at greater depths of discharge. Heat and pressure effects will also be included in the model. Experiments will also be conducted in order to validate the model. Ultimately this model will be used to predict the extent of redistribution in a lithium-metal battery, understand how this phenomenon impacts the lifetime of the battery, and how to design and optimize the battery to achieve greater than 1000 cycles without compromising safety.

Interactions between Redox Shuttles and the SEI. Rotating Disk Electrode studies on the reduction of ferrocene will continue. Our current task is to develop a physics-based mechanism that describes observations and provides quantitative measurements as a basis for comparison between shuttles. Qualitative observations have also shown that rotating the electrode during formation produces a film with significantly different behavior. We plan to investigate this phenomenon further, undertaking non-electrochemical characterization if necessary. Finally, we plan to return to our original plan of varying the redox shuttle to compare relative transport and kinetic resistances to reduction.

FY 2010 Publications/Presentations

1. Presentation to the 2009 DOE Annual Peer Review Meeting, May 2010

2. M. Tang and J. Newman, *ECS Meeting Abstracts*, **1002**, 451 (2010).

V.E.6 Carbon Fiber and Foam Current Collectors (ORNL)

Nancy J. Dudney
Oak Ridge National Laboratory
Material Science and Technology Division
Building 4500S MS6124
PO Box 2008
Oak Ridge, TN 37831-6030
Phone: (865) 576-4874
E-mail: dudneynj@ornl.gov

Start Date: July, 2007
Projected End Date: September 30, 2010

Objectives

- Investigate the use of highly-conductive graphite as the current collector and skeleton for Li-ion battery cathodes.

Technical Barriers

This project addresses the following technical barriers for development of plug in hybrid electric vehicle technologies:

(A) Cycle and calendar life (5,000 cycles for PHEV; 300,000 cycles HEV; 15 year life)

(B) Abuse tolerance

(C) Much higher energy density (40 mile system: 11.6 kWh; 120 kg; 80 liter)

Technical Targets

- Cathode composites with a state of the art specific energy and volumetric energy density when fabricated in dual sided prismatic cell.
- Cathode sheets up to 1mm thick with larger capacity per area to reduce the volume and mass associated with inactive cell components.
- Full utilization of the active cathode material and 100-1,000 cycles with little capacity fade from the cathode.
- Thermal stability and heat conduction that surpasses current cathode structures

Accomplishments

- The theoretical specific capacity was realized using a carbon fiber current collector calcined at 700°C with commercial $LiFePO_4$ powders and just 5 wt.% additional carbon.
- Composite fabricated with loose fibers provides good power performance with ~50% capacity at 10C.
- Composites fabricated with loose fibers were stronger, more durable, and less porous.
- Better than 99.3% capacity was retained at 100 deep discharge cycles.
- Carbon-bonding by annealed mesophase pitch improved the thermal diffusivity two-fold versus conventional bonding with PVdF and carbon black.
- The heat capacity of $LiFePO_4$ was measured to 500°C.

✧ ✧ ✧ ✧ ✧

Introduction

Cycling performance for PHEV batteries is extremely demanding. Although the multiple degradation processes have not been fully characterized, it is clear that the organic binders, carbon additives, and aluminum foil used in typical electrode sheets are not innocent materials, but contribute to degradation through corrosion, side reactions, or lost connectivity. Also, degradation is promoted by local variations in the current density and temperature, and perhaps also flaws introduced by pressing the electrode compact. Composites with well distributed and highly conductive carbon fibers acting as the support and current collector are expected to improve the cycling and thermal performance of the cathode. A higher energy density and lower materials cost for the battery is anticipated as the cathode thicknesses and energy per unit area is increased.

Approach

A variety of highly conductive commercial carbon fibers, veils, and papers have been infiltrated or coated with a slurry of $LiFePO_4$ particles with ~5 wt.% added aromatic resin pitch. The carbon structures provide at least 20-fold higher surface area for this current collector relative to the foot print. While carbon-bonded carbon papers and foams were investigated earlier, recent studies utilized lower cost, loose carbon fibers of comparable 5-10 µm diameter. Intimate and robust bonding with the active cathode particles is achieved by heat treatment at 700ºC, rather than by pressing or calendaring, resulting in a carbon bonded composite, such as that shown schematically in Figure V- 166. Composites were prepared with two different $LiFePO_4$ powders, one synthesized in-house and a carbon-coated powder obtained from HydroQuebec (HQ), the latter being finer and more uniform in size and shape. The cathodes are tested at

ORNL and LBNL in lithium half cells in coin cell and prismatic constructions using standard $LiPF_6$ carbonate electrolytes. Microstructure was characterized by SEM and X-ray tomography. Thermal properties were measured for the fiber composite electrodes and also for thin pressed pellets of $LiFePO_4$ *without* carbon fibers in order to directly assess the thermal transport with 5 wt.% carbon binder versus the usual 15-20 wt.% mixture of PVdF binder plus carbon black. Thermal diffusivity through the pellets was measured using a pulsed Xenon lamp or laser technique and heat capacity of pure $LiFePO_4$ and electrode composites was measured by high temperature differential scanning calorimetry (DSC).

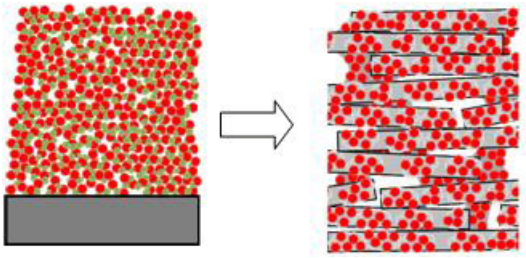

Figure V- 166: Replacement of standard particle coating on a metal foil (left) with a composite of particles carbon-bonded to highly conductive carbon fibers (right). Active cathode is red, organic binder green, and carbon fibers and binder, gray.

Results

Electrochemical characterization. Figure V- 167 is a Ragone plot showing the improved performance for cathodes with the commercial $LiFePO_4$ powder from HQ compared with sol gel prepared powder. The values are normalized for the total weight of $LiFePO_4$ plus carbon fibers and binder. The capacity per gram $LiFePO_4$ is near theoretical even for the 0.4mm thick cathode at low rates. These composites cycled well with little capacity fade for 100 or more cycles, and ultimately failed due to lithium dendrite formation. Unfortunately, composites from both powders had a poor volumetric energy density, with porosity of 60-70%. Attempts to apply multiple slurry coatings to the Toray paper proved ineffective for filling the interior porosity.

Subsequent composites were fabricated by molding the $LiFePO_4$ powder slurry with various loose commercial carbon fibers. These composites have higher density and strength that those prepared with Toray papers which are easily chipped. Cycling performance of the $LiFePO_4$ – fiber composites is outstanding. Figure V- 168 shows a cycle rate test up to 50C. The specific capacity at low rates is near theoretical. (Note the capacity is normalized to the $LiFePO_4$ weight.) Approximately 50% of the capacity is obtained at a 10C discharge rate. Returning to a C/5 shows that there was no significant capacity fade. Continuous cycling at 1C or C/5 shows that more than 99% of the initial capacity is retained at 100 cycles. By periodically replacing the anode with a new lithium foil, the cycle life tests are being extended beyond ~100 cycles.

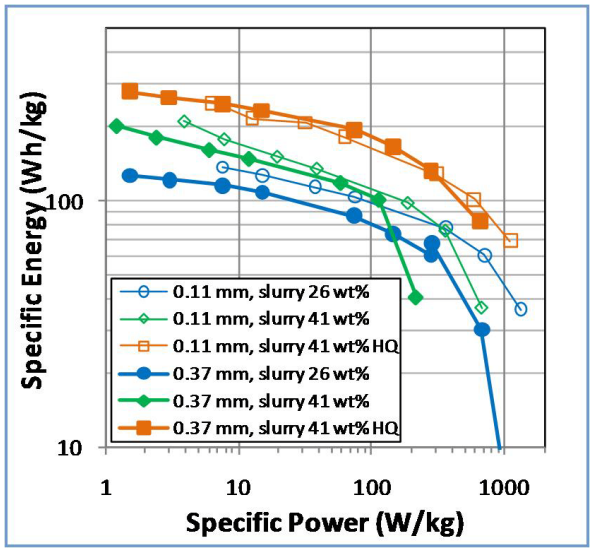

Figure V- 167: Specific energy and power performance of $LiFePO_4$ cathodes prepared with Toray carbon papers of 0.11 and 0.37 mm thickness. Values are normalized for the total cathode weight, including the fibers. The solids loading of the slurry and the source of $LiFePO_4$ powder are given in the legend.

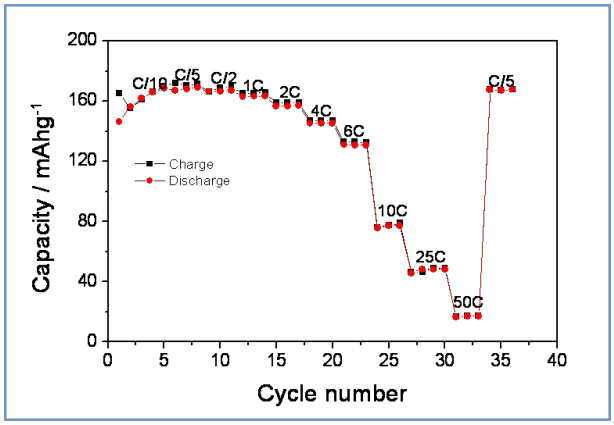

Figure V- 168: Rate performance from C/10 to 50C for a composite prepared of $LiFePO_4$(HQ) with loose carbon fibers and 5wt% carbon from mesophase pitch. Capacity is normalized to weight of the $LiFePO_4$ alone.

Thermal characterization. Although the electrochemical performance is impressive, the unique benefit from this cathode composite structure may be in improved thermal conductivity and thermal stability. Last year we reported thermal diffusivity of composites with fibers, which was very high and dominated by the fibers. Results in Figure V- 169 compare the thermal diffusivity measured using a pulsed Xenon lamp or laser through thin (~0.4mm) pellets without fibers. The porosities (~40

vol.%) are comparable for pellets annealed with the carbon pitch and pellets pressed with equal weights of PVdF and carbon black. The thermal diffusivity of all samples was rather low, but clearly 5% carbonized pitch binder gives a 2-fold higher diffusivity. The heat capacities for pure $LiFePO_4$ and the composites were also measured, to 500°C, for the binder-free samples. The heat capacity of $LiFePO_4$ powders shows non-Debye behavior at 300-400°C that warrants further investigation.

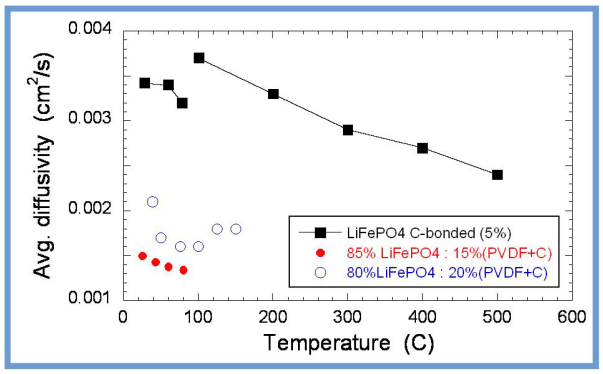

Figure V- 169: Thermal diffusivity measured through thin pellets with compositions shown in the legend.

Conclusions and Future Directions

Composites of $LiFePO_4$ and conductive carbon fibers formed by thermal processing have been shown to have promising cycle life, capacity utilization, and power performance. The structure and performance has been improved by using uniform submicron $LiFePO_4$ particles and loose carbon fibers that are both flexible and low cost.

Thermal properties, including the diffusivity and heat capacity, have been measured for composites and for pure $LiFePO_4$. Bonding the particles by heat treating with carbon pitch significantly improves the diffusivity.

This program will be completed soon. Pouch cells will be assembled and tested at LBNL with V. Battaglia. Additional thermal property analysis will include DSC studies of the full electrode in the presence of the liquid electrolyte. An improvement in the high temperature stability due to the carbon-pitch binder and carbon fiber current collector is anticipated. Two additional literature publications are in preparation in addition to a final report.

FY 2010 Publications/Presentations

1. Presentation to the 2010 DOE Annual Peer Review Meeting.
2. Two presentations to be presented by Surendra Martha, Jagjit Nanda, et.al. at Materials Research Society, Boston, November 2010: *Thermal and electrochemical behavior of high energy density carbon fiber paper (CFP)-$LiFePO_4$ positive electrodes;* and *Coating positive electrode materials on loose carbon fibers for Lithium batteries.*
3. K. Kercher, J. O. Kiggans, and N.J. Dudney, "Carbon Fiber Paper Cathodes for Lithium-ion Batteries," J. Electrochem. Soc., Vol.157, no.12 (2010) A1323-1327.

Acknowledgment

Parts of this research were performed at DOE user facilities including the High Temperature Materials Laboratory and at the Shared Research Equipment (SHaRE) user facility for electron microscopy.

V.E.7 Positive and Negative Electrodes: Novel and Optimized Materials (LBNL)

Jordi Cabana
Lawrence Berkeley National Laboratory
1 Cyclotron Rd. MS62R0203
Berkeley, CA 94720-8168
e-mail: jcabana@lbl.gov
Phone: 510-486-7097, Fax: 510-486-7303

Start Date: September 2009
Projected End Date: August 2011

Objectives

- Understand the relationship between particle size-shape and electrode performance.
- Understand the chemical and physical phenomena behind the reactivity of negative electrode materials based on metal oxides.
- Design new materials that yield high capacities at high voltages.
- Develop new and engineered materials that can fulfill the energy/power density, cycle life and safety requirements and goals of USABC.

Technical Barriers

- Low energy-density, poor cycle life, safety.

Technical Targets

- PHEV: 96 Wh/kg, 5000 cycles;
- EV: 200 Wh/kg; 1000 cycles..

Accomplishments

- The performance of $LiNi_{1/2}Mn_{3/2}O_4$ made using solvothermal routes has been evaluated and compared to a benchmark sample made from hydroxide precursors. The results suggest that nanostructuring is not necessary to achieve good cycle life at high rates.
- The chemical and physical phenomena behind the good initial reversibility but poor extended cycle life of NiO has been studied by XAS, NMR and TEM. The results show evidence of the formation of Li_2O and Ni, but also the possible formation of intermediates.
- Nanometric Sn-based alloys with narrow particle sizes (<10 nm) and shapes have been prepared.

✧ ✧ ✧ ✧ ✧

Introduction

Finding Li-ion battery electrode materials that can bring about increases in energy is a critical need if the social impact of their use in electric vehicles is to meet expectations. In order to fulfill this goal, the following strategies can be envisaged: i) raising the voltage of the battery by using electrodes that react at very high and very low potentials, respectively, and/or ii) improving the storage capacity by switching to alternative electrode materials that can exchange a larger amount of electrons/Li^+ ions. Yet these changes cannot come with a penalty in terms of safety and cycle life, which implies that the mechanisms of their reaction with lithium need to be well understood in order to locate possible sources of failure.

Spinel-type $LiNi_{0.5}Mn_{1.5}O_4$ is a promising candidate for the positive electrode because lithium is extracted at very high potentials (around 4.7 V vs. Li^+/Li^0), concomitant to the oxidation of Ni^{2+} to Ni^{4+}. While very high rate capability has been reported in nanometric samples, its use also entails the possibility of electrolyte decomposition on the surface of the particles at these high voltages.

A second alternative is to use materials that react with lithium through a conversion reaction. For instance, different transition metal oxides (M_xO_y, where M=Mn-Cu) have emerged as attractive negative electrode candidates because they can store as much as twice the amount of charge per unit of mass as carbon electrodes. Unfortunately, these electrodes suffer from three major drawbacks: i) the strong structural re-organization that takes place due to large volume changes results in unsatisfactory cycling performance, ii) an unacceptable round-trip energy efficiency due to the large voltage hysteresis that is observed between the discharge and charge steps, iii) a virtually ubiquitous large Coulombic inefficiency observed in the first cycle. The origins of these issues remain to be fully ascertained.

Finally, alloy-based anode electrodes, such as tin and tin-transition metal alloys, are also considered promising candidates to replace carbon. Although the large volume expansions occurring during cycling can lead to severe capacity losses, a battery that contains a tin-based electrode was put into the market by SONY. Nanoscaling

is believed to be critical for the good performance of these electrodes, but, despite the efforts by several research groups, its actual role is still to be fully unraveled. In addition, these materials are often prepared by methods that do not allow for a careful tailoring of the microstructure. In this project, we aim at gaining further understanding of the effect of both particle size and morphology, and the presence of a transition metal which does not alloy with lithium.

Approach

We performed a systematic study of $LiNi_{0.5}Mn_{1.5}O_4$ made with very different, controlled microstructure and compared the performance at different rates. To this end, we used simple synthetic routes such as co-precipitation and hydrothermal.

In order to understand the mechanism of conversion in NiO electrodes, short range characterization techniques are required because of the extensive electrochemical grinding that occurs during cycling. We combined XAS, TEM and NMR to obtain a clear picture.

In order to fully tailor the nanostructure (particle size, dispersion and morphology) of tin alloys, a solution method based on the use of an organic solvent, a reducing agent and a capping agent was employed. The synthesis is performed at low temperature to maximize control.

Results

Efforts were directed toward the tailoring of the micro/nanostructure of $LiNi_{0.5}Mn_{1.5}O_4$, the objective being to compare the effect of such nanostructure on its electrochemical performance. In one route, two precursors, MnO_2 and $MnCO_3$, made hydrothermally were used as starting materials, then mixed with $LiNO_3$ and $Ni(NO_3)_2$ before calcination at 750°C. The result is $LiNi_{0.5}Mn_{1.5}O_4$ that largely preserved the shape of the manganese sources (Figure V- 170). Two types of particles were obtained, namely, ~1 µm highly nanostructured cuboids (ex-$MnCO_3$), ~ 1 µm long, 150 nm wide (ex-MnO_2). The second route consisted of the co-precipitation of $Ni_{1/4}Mn_{3/4}(OH)_2$, followed by calcination with $LiOH{\cdot}H_2O$ at 900ºC. This route produces micron-size particles with very well defined octahedral morphology (Figure V- 170).

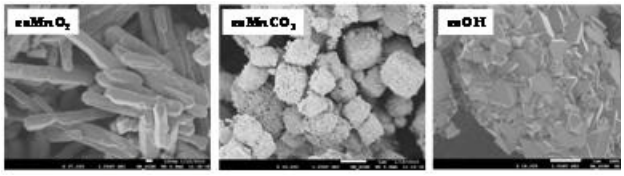

Figure V- 170: SEM pictures of $LiNi_{0.5}Mn_{1.5}O_4$ made from MnO_2, $MnCO_3$ and hydroxide precursors.

The performance of the three samples at a high C-rate was compared (Figure V- 171). Despite the nanostructured character of ex-MnO_2 and ex-$MnCO_3$, the sample labeled BM, made using the hydroxide method, shows better performance, with excellent retention after as many as 150 cycles, and a capacity of 115 mAh/g. These results strongly suggest that nanostructuring $LiNi_{0.5}Mn_{1.5}O_4$ is not necessary to improve performance, especially since smaller sizes will lead to increased surface area and, therefore, more potential for electrolyte decomposition.

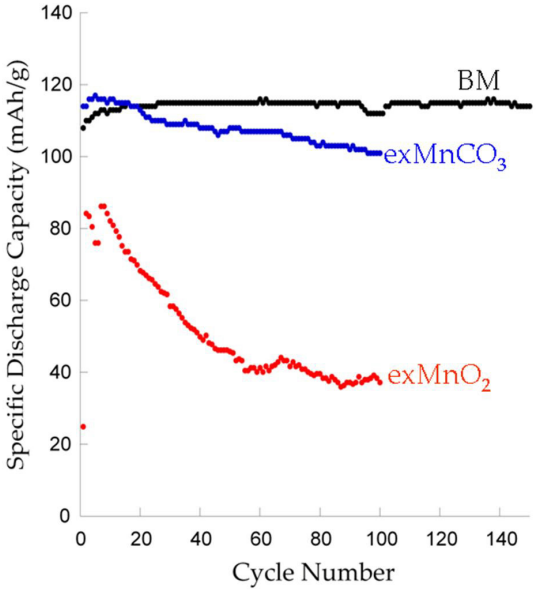

Figure V- 171: Electrochemical performance of $LiNi_{0.5}Mn_{1.5}O_4$ samples cycled in Li batteries at C rate (BM=exOH).

The NMR results of samples of NiO at different states of charge and discharge are shown in Figure V- 172. Quite surprisingly, the signals suggest the existence of species that contain Li-O-Ni bonds during the conversion reaction. This is not consistent with the theoretical reaction, which involves the direct reduction of NiO to form Ni and Li_2O, which has no such bonds. The oxidation state of Ni in NiO does not allow any topotactic intercalation of Li. These results were also compared to our study of the reaction using a combination of electron diffraction and O K and Ni L edge X-ray absorption spectroscopy. While the reduced state seems to be clearly formed by a mixture of Ni and Li_2O, anomalous O K edge signals were observed at intermediate states that are consistent with the formation of different species, as suggested by NMR. Further work is needed to fully understand these unexpected signals, and will continue during FY2011.

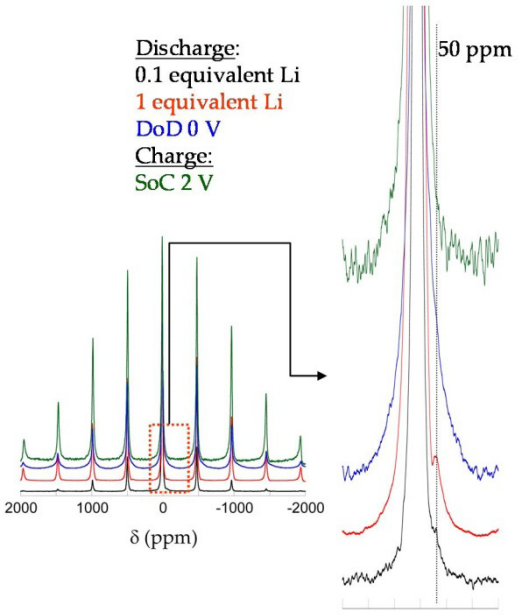

Figure V- 172: ^{6}Li MAS-NMR spectra of NiO electrodes at different states of charge and discharge.

Finally, the synthesis of Sn nanoparticles was performed at 70ºC in 1-octadecene (ODE) using oleylamine as a capping agent, $Li(C_2H_6)_3BH$ (1.0 M in THF) as a reducing agent and anhydrous $SnCl_2$ as a tin source. Figure V- 173 shows representative TEM images for a batch of Sn nanoparticles made using this method. Very high quality samples were obtained, with the particles having a spherical shape and a diameter of less than 10 nm, monodispersed and non-aggregated. Testing of these nanoparticles will start during FY2011.

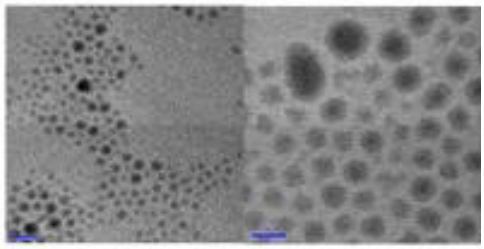

Figure V- 173: Representative TEM images for Sn nanoparticles.

Conclusions and Future Directions

We have explored different methods of synthesis tailored at overcoming the barriers of positive and negative electrodes for high energy density Li-ion batteries. Our work with $LiNi_{0.5}Mn_{1.5}O_4$ shows that reducing the particle size is not necessary to get good cycling stability, even at high rates. In addition, we have investigated the conversion reaction mechanism of NiO with Li. The TEM, NMR and XAS results suggest that, although the final products are Ni and Li_2O, intermediate phases with different characteristics are formed.

For FY2011, we will continue our work on $LiNi_{0.5}Mn_{1.5}O_4$ by addressing the issue with poor Coulombic efficiency due to excessive side reactions. We will evaluate samples made using different annealing treatments and test them with inorganic solid powder as additives. We will continue refining our synthesis of Sn nanoparticles and test them as electrode materials. Finally, we will continue our efforts toward understanding the conversion reaction in order to explain the origins of the poor roundtrip energy efficiency.

FY 2010 Publications/Presentations

1. 2010 DOE Annual Peer Review Meeting Presentation.
2. *"Toward High Energy Density Li-ion Batteries: Understanding the Key Parameters for Performing Electrode Materials"*, Presentation at the NCEM and Molecular Foundry Users' Meeting, October 1st 2010.

V.E.8 Modeling - Predicting and Understanding New Li-ion Materials Using Ab Initio Atomistic Computational Methods (LBNL)

Kristin Persson
Environmental Energy Technologies Division
Lawrence Berkeley National Laboratory
1 Cyclotron Rd, MS 70R0108B
Berkeley, CA 94720
Phone: (510) 486-7218
E-mail: kapersson@lbl.gov

Start Date: September 2008
Projected End Date: September 2011

Objectives

- Predict new chemistries and crystal structures for improved electrodes as defined by the goals of USABC.
- Understand rate-limiting behavior in current electrode materials in order to target and design optimal diffusion properties in new materials.

Technical Barriers

Investigating the rate-limiting properties of electrode materials from a computational standpoint is a major challenge. We have chosen to break down the problem into two pieces: a) a bulk investigation and b) a surface investigation. We have focused on establishing factors influencing the electronic and the ionic (Li) conductivity of the layered $Ni_{1/3}Mn_{1/3}Co_{1/3-x}Al_xO_2$ cathode material and the graphitic anode material. One of the barriers to overcome was to accurately model the Li-graphite system, which exhibits competing forces which are not well characterized in standard density functional theory. We overcame this technical barrier by rigorous bench marking against experimental results and the inclusion of 'non-traditional' approaches.

The layered $Ni_{1/3}Mn_{1/3}Co_{1/3-x}Al_xO_2$ cathode material displays cation disorder in the transition metal layer, which cannot be described completely from a first principles perspective. We addressed this barrier by looking at local effects of the Al substitution, which allowed us to draw conclusions.

Technical Targets

- Understand the bulk rate limiting bottlenecks in the carbon anode.
- Investigate the electronic state of the cathode material $Ni_{1/3}Mn_{1/3}Co_{1/3-x}Al_xO_2$ and as a function of Al content.
- Evaluate Li mobility in $Ni_{1/3}Mn_{1/3}Co_{1/3-x}Al_xO_2$ as a function of Li and Al content.

Accomplishments

- For the first time, very fast selective bulk Li diffusivity in graphitic carbons was established by our computations and verified experimentally by Kostecki's group.
- Li diffusion in the layered $Ni_{1/3}Mn_{1/3}Co_{1/3-x}Al_xO_2$ as a function of Al content was investigated as a function of Al content. It was found that Li diffusion is facilitated at high charge, as the valence state of Al is lower than for a Co equivalent. However, for low state of charge, the stiffness of the Al-O bond was found to increase the local Li diffusion barrier.

Introduction

There is increasing evidence that many of the performance limiting processes present in electrode materials are highly complex reactions occurring on the atomic level. We are studying these processes using first-principles density-functional theory modeling. By understanding the underlying reasons for the electrode materials' performance we can suggest improvements or design schemes directed at the root cause of the process. For cathodes, we have chosen to work with layered $Ni_{1/3}Mn_{1/3}Co_{1/3-x}Al_xO_2$ to understand the impact of Al substitution on the rate capability of the material. Al is substituted for Co to decrease the cost and increase the thermal stability of the material. However, the substitution may also have detrimental effects on the electronic as well as the ionic conductivity.

For anode materials, we have undertaken a rigorous study of the thermodynamics and kinetics of the Li-graphite system from first principles. At low temperatures, the graphitic anode suffers from poor rate capability and until now, there has been no concensus regarding the inherent bulk Li diffusivity of carbonerous materials. Our study, which was recently published jointly with the Kostecki group in the Journal of Physical Chemistry Letters, showed the potential of excellent inherent diffusivity of Li in graphite, assuming rational design of electrode architechture.

Approach

We use atomistic modeling to study the relevant thermodynamic and kinetic processes. The calculations are performed exclusively on the Lawrencium cluster at LBNL In the case of layered $Ni_{1/3}Mn_{1/3}Co_{1/3-x}Al_xO_2$ we have used first-principles zero-temperature calculations to establish the electronic state of the material and the Li diffusion activation barriers as a function of state of charge as well as Al content.

For the investigation on the Li-graphite system we have used density-functional theory to describe the low temperature characteristics of the material, and statistical mechanics to calculate the phase diagram and the Li chemical diffusivity.

Results

Cathode: $Ni_{1/3}Mn_{1/3}Co_{1/3-x}Al_xO_2$. We have concluded a comprehensive study of the electronic state as well as the Li mobility as a function of Al content and state of charge. The results indicate that the electronic conductivity decreases as Al content is increased. However, Al substitution also lowers local Li migration barriers at low Li concentration, which will facilitate Li migration through the Li layer. In contrast, at high Li concentration, i.e. discharge, the local Li migration barriers close to an Al is higher than for Co. However, since the amount of Al is relatively small, there will always be percolation paths away from the higher Li migration barriers.

We also find that Al substitution increases the Li slab space (see Figure V- 174), due to the tighter Al-O bond in the transition metal layer. Although the increase of the Li slab space is less than what is observed in experiments, and it is less significant than the effect of Li content, it will improve Li diffusivity, Figure V- 175. Thus, in conclusion, Al substitution is likely to improve Li diffusion overall in the layered material through a combined effect of increased Li slab space as well as lower local Li migration barriers at high charge.

Anode: Graphite. By carefully benchmarking the calculated Li-graphite voltage profile as well as the phase diagram against experimental results, we found it necessary to include van der Waals forces into our model for the Li-graphite system. Going further, we calculated the Li mobility barriers as a function of Li content and found that, at low Li content, the barriers are extremely sensitive to graphite interlayer distance. In contrast, at high Li content, the barriers are determined by Li-Li repulsive interactions, which are relatively insensitive to the interlayer distance. The barriers were then used in kinetic Monte Carlo simulations to derive the Li chemical diffusivity as a function of the state of charge, Figure V-176. This resulted in the important discovery that inherent Li diffusion in bulk graphite is very fast, which was confirmed by the Kostecki group. As an example of the potential impact of this discovery we can, assuming a design which efficiently utilizes the fast in-plane lithium diffusivity of 10^{-7} cm^2s^{-1}, expect natural graphite (MCMB) with typical crystalline domain sizes around 45 nm to be intercalated/deintercalated in less than 0.2 ms.

Conclusions and Future Directions

We have found that Li diffusivity in graphite can be extremely fast given a design that maximally utilizes the in-plane diffusion. In layered $Ni_{1/3}Mn_{1/3}Co_{1/3-x}Al_xO_2$ we have determined that Li diffusion is likely to be overall improved with Al substitution, although the effect is small at the low Al content considered.

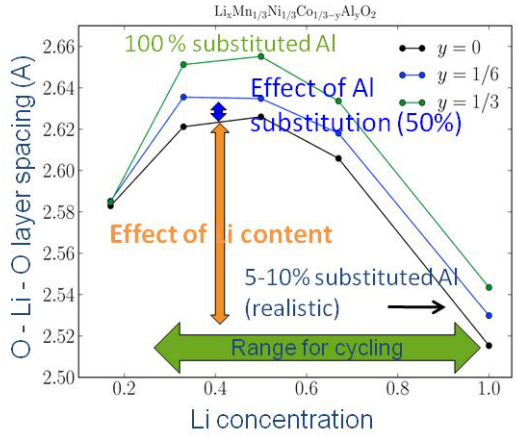

Figure V- 174: Li slab space as a function of state of charge in $Ni_{1/3}Mn_{1/3}Co_{1/3-x}Al_xO_2$.

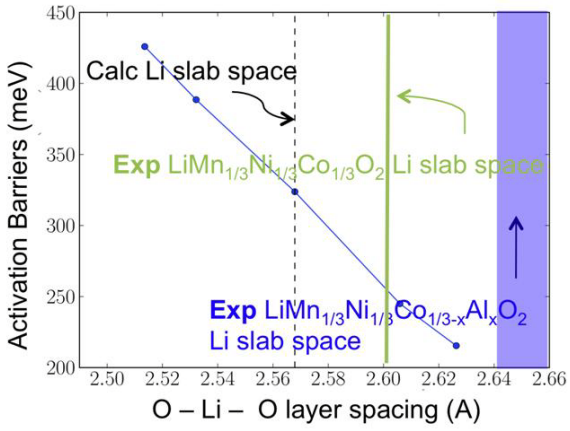

Figure V- 175: Li mobility barriers in $Ni_{1/3}Mn_{1/3}Co_{1/3-x}Al_xO_2$ as a function of Li slab space.

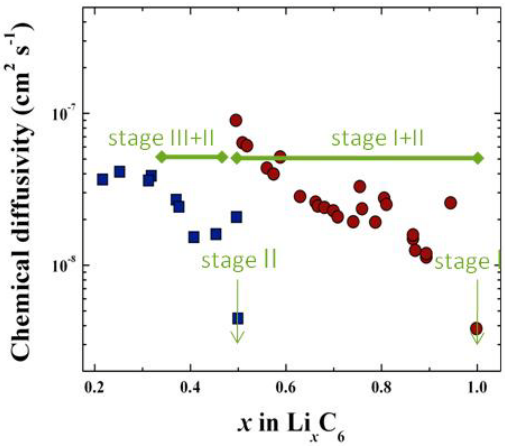

Figure V- 176: Li chemical diffusivity as a function of Li content in graphite, from first-principles calculations and kinetic Monte Carlo simulations.

Having established the inherent bulk properties of layered $Ni_{1/3}Mn_{1/3}Co_{1/3-x}Al_xO_2$ and graphite with respect to Li diffusion and electronic state, we are planning to expand our investigation to surface properties. Both the electronic state as a function of surface absorbates and defects as well as surface Li kinetics will be explored.

FY 2010 Publications/Presentations

1. K. Persson, Y. Hinuma, Y. S. Meng, A. Van der Ven, and G. Ceder. *Thermodynamic and Kinetic Properties of the Li – Graphite System from First-Principles Calculations*, Phys Rev B 82, 125416, 2010.
2. K. Persson, V. A. Sethuraman, L. J. Hardwick, Y. Hinuma, Y. Shirley Meng, A. van der Ven, V. Srinivasan, R. Kostecki, and G. Ceder, J Phys. Chem. Lett. **1** (8), 1176-1180, 2010.
3. Doe R.E., Persson K.A., Hautier G., and Ceder G., *First Principles Study of the Li−Bi−F Phase Diagram and Bismuth Fluoride Conversion Reactions with Lithium*, Electrochemical Solid State Letters. 12 (7), A125-A128, 2009.
4. Doe R.E., Persson K.A., Meng Y.S., Ceder G., *First-Principles Investigation of the Li-Fe-F Phase Diagram and Equilibrium and Nonequilibrium Conversion Reactions of Iron Fluorides with Lithium*, Chemical Materials 20 (16), 5274 – 5283, 2008.
5. Bi L., Taussig, A.R., Kim H.S., Wang L., Dionne G.F., Bono D., Persson K., Ceder G., and Ross C.A., *Structural, magnetic, and optical properties of $BiFeO_3$ and Bi_2FeMnO_6 epitaxial thin films: An experimental and first-principles study*, Physical Review B 78(10), 104106, 2008.
6. 2009 DOE Annual Peer Review Meeting Presentation.
7. *First Principles Calculations of Li Migration in Li Battery Electrode Materials,* MRS in San Francisco 2010 (Invited)
8. *Predicting Solid - Aqueous Equilbria for Materials Design*, TMS Hume-Rothery Symposium Seattle 2010 (Invited)
9. *Conversion Reaction Hysteresis Mechanism in Li-ion Batteries*, LiBD Arcachon 2009 (Contributed)
10. *Predicting Solid-Aqueous Equilibria for Optimized Energy Storage Materials*, MRS Cancun 2009 (Invited)
11. *Bottle Necks on the Graphite Anode*, ECS Hawaii 2008 (Contributed)

V.F Energy Frontier Research Centers

V.F.1 Energy Frontier Research Center at ANL

M. M. Thackeray[#], M. Balasubramanian[*]

Argonne National Laboratory
9700 South Cass Avenue
Argonne, IL 60439
[#]Phone: (630) 252-9184; Fax: (630) 252-4176
E-mail: thackeray@anl.gov
[*]Phone: (630) 252-0593; Fax: (630) 252-0580
E-mail: mali@aps.anl.gov

Collaborators:

J. Croy, N. Karan, D. Kim, S.-H. Kang (ANL)

Start Date: April 1, 2010
Projected End Date: September 30, 2011

Objective

- To undertake surface studies of technologically-significant high-capacity cathode materials emanating from the BATT program, such as integrated 'layered-layered' $xLi_2MnO_3 \bullet (1-x)LiMO_2$ and 'layered-spinel LiM_2O_4 structures (M=Mn, Ni, Co), that will complement the fundamental EFRC-related research activities at Argonne National Laboratory, Northwestern University, and the University of Illinois at Urbana Champaign on electrode-electrolyte interfaces.

Technical Barriers

- Low energy density
- Poor low temperature operation
- Abuse tolerance limitations

Technical Targets

USABC - End of life

- 97 Wh/kg, 383 W/kg (PHEV 40 mile requirement)
- Cycle life: 5000 cycles
- Calendar life: 15 years

Accomplishments

- This is a new project.
- Successfully advertized a post-doctoral position – screened and interviewed several candidates.
- Prepared surface-treated, high capacity lithium metal oxide cathodes.
- Initiated structural studies of lithium metal oxide cathode surfaces using X-ray absorption spectroscopy at Argonne's Advanced Photon Source (APS).

✧ ✧ ✧ ✧ ✧

Introduction

Bulk and interfacial electrochemical processes are of fundamental scientific interest as well as of technological importance. The performance of energy storage and power supply systems is largely dependent on these processes, which can occur at an electrode-electrolyte interface or in the bulk of the electrode. In this project, structural features, ionic transport phenomena and charge-transfer reactions at the electrode/electrolyte interface of lithium battery electrode materials, notably high potential metal oxide cathodes, will be studied. The electrode materials will be selected specifically from those being investigated in the BATT program and on their potential for making significant advances in electrochemical performance; the studies will complement the activities of the Energy Frontier Research Center, *Electrical Energy Storage – Tailored Interfaces* led by Argonne National Laboratory, with Northwestern University and the University of Illinois, Urbana-Champaign as partners.

Of particular importance to the project is Argonne's recent research in the BATT program on electrodes with integrated 'composite' structures, which has highlighted the possibility of designing new, high-potential and high capacity electrodes with Li_2MnO_3 as a stabilizing component. It has been demonstrated, in particular, that it is possible to integrate Li_2MnO_3 with layered $LiMO_2$- or spinel LiM_2O_4 components (e.g., M=Mn, Ni, Co) at the atomic level, and that these composite materials can provide an exceptionally high capacity (240-250 mAh/g), which is significantly higher than the capacity offered by layered $LiCoO_2$, spinel $LiMn_2O_4$ and olivine $LiFePO_4$ electrodes. These manganese-rich composite materials have extremely complex structures which are surprisingly stable when delithiated at high potentials (~5V). Despite the enhanced stability of these electrode materials, it is still necessary to passivate the electrode surface to prevent

electrode/electrolyte reactions from occurring, and to improve lithium-ion transport at the surface, thereby enhancing the power capability of the lithium-ion cell. In this respect, several coating techniques and passivating agents, such as metal oxides (Al_2O_3, ZrO_2), fluorides (AlF_3) and phosphates ($AlPO_4$) have been shown to improve surface stability and rate capability of the electrode, but little is known about surface structures, or the mechanisms by which lithium-ion transport occurs at the electrode surface. Knowledge gained from these studies will guide us in improving the composition and structure of electrode surfaces and advancing the overall performance of the electrodes to meet DOE's 40-mile PHEV battery requirements.

Approach

Analytical techniques for probing the structure-electrochemical property relationships of lithium battery electrode materials, notably at electrode surfaces, include neutron scattering, X-ray absorption, scattering and photoelectron spectroscopy, nuclear magnetic resonance, Raman spectroscopy, Fourier transform infrared spectroscopy, and electron microscopy. In this project, analytical efforts will focus predominantly on X-ray spectroscopic techniques, including "*in situ*" experiments, and high-resolution electron microscopy. Major facilities are available at Argonne to conduct these experiments, notably at the Advanced Photon Source (APS) and the Electron Microscopy Center (EMC).

Coated cathode materials with integrated composite structures in which the coating will contain specific 3d/4d transition metals, not present in the core structure, will be synthesized; and their electrochemical properties will be compared against uncoated electrodes. Coatings will be applied by various techniques, for example, from solution by standard sol-gel methods or by atomic layer deposition (ALD). A suite of "*in situ*" synchrotron hard X-ray spectroscopic techniques including X-ray absorption spectroscopy (XAS), resonant and non-resonant X-ray emission spectroscopy (XES) and X-ray Raman scattering (XRS) will be used to monitor the interfacial reactions at the electrode-electrolyte interface. The important traits of these spectroscopic techniques, specifically the element specific nature and the sensitivity to dilute constituents, will allow us to monitor the changes in the electronic and atomic structures of the coatings during charge-discharge cycling. We envision that these studies will provide key information at the molecular level on the structure of the coatings, the mechanism of lithium-transport at the electrode-electrolyte interface and further provide insights into degradation mechanisms during repeated cycling. Another aspect that will be investigated is the effect of the coating on the bulk structure of the composite material itself, particularly on deintercalation at high voltages during first charge. Our recent XAS studies of uncoated composite materials have shown convincing evidence of oxygen loss during first charge at high voltages. In coated samples, the exact oxygen loss mechanism and the possible condensation of the bulk structure might be significantly different and a detailed understanding of the local structure of the bulk might provide key insights on the structure-property relationship of the coated composites. The knowledge gained from both the bulk and interface using X-ray spectroscopic methods will feed into the design of improved electrodes to meet the 40-mile PHEV goals. In addition, studies of well defined electrode surfaces will be undertaken using spectroscopic and microbeam methods. Such studies utilize the property of total external reflection of X-rays at small incident angles, which minimizes the contribution from the bulk of the material and provides interface sensitivity without sacrificing the *in situ* capability of hard X-rays. These proposed spectroscopic investigations nicely complement the X-ray based scattering approaches, which are currently an integral part of Argonne's EFRC effort.

Results

For the initial studies, several parent 'layered-layered' $xLi_2MnO_3\bullet(1\text{-}x)LiMO_2$ materials and surface treated products were selected and successfully synthesized and characterized by X-ray diffraction. These included 1) $0.5Li_2MnO_3\bullet(1\text{-}x)LiCoO_2$, that can be represented alternatively as $Li_{1.2}Co_{0.4}Mn_{0.4}O_2$, treated by sol-gel methods with various Li-Ni-PO_4 compositions and $0.5Li_2MnO_3\bullet(1\text{-}x)LiNiO_2$, represented alternatively by $Li_{1.2}Ni_{0.4}Mn_{0.4}O_2$, treated with various Li-Co-PO_4 compositions. High quality XAS data of the former sample have been collected to determine the electronic and atomic structure of Ni in the as-synthesized samples. The real part of the Fourier transform of the Ni EXAFS data and a preliminary fit to the data are shown in Figure V-177. Detailed analyses of these data are currently being undertaken.

Conclusions and Future Directions

This project has been underway for approximately 6 months. Further beam time to characterize surface structures of the composite electrodes at the APS has been scheduled for December 2010 and February-April 2011. These data will be collected *in situ* to determine the effect of surface coatings on electrochemical performance. Targeted materials include those described above as well as the Gen-2 electrode $LiNi_{0.8}Co_{0.15}Al_{0.05}O_2$, coated with various Li-Mn-PO_4 compositions.

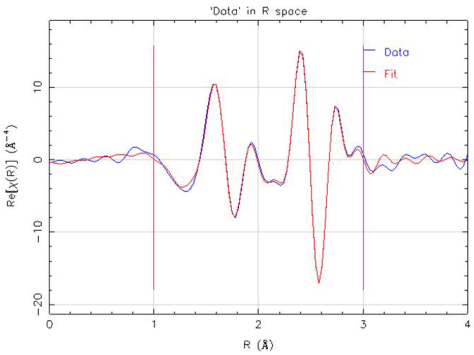

Figure V- 177: Real part of Ni EXAFS data and a preliminary fit to the data of a Ni-coated electrode structure.

Complementary techniques, as outlined in the 'Approach' section, will be used to gain further insight into the structural and electrochemical properties of these materials.

FY2010 Publications/Patents/Presentations

None to date.

V.F.2 Emerging Frontiers in Research Center – Novel *in situ* Diagnostics Tools for Li-ion Battery Electrodes (LBNL)

Robert Kostecki, Jordi Cabana

Environmental Energy Technologies Division
Lawrence Berkely National Laboratory
1 Cyclotron Road, MS 90-3026D
Berkeley, CA 94720
Phone: (510) 486-6002; Fax: (510) 486-5454
E-mail: r_kostecki@lbl.gov

Start Date: March 2009
Projected End Date: September 2010

Objectives

- Start a new sub-program devoted to the development of two synchrotron-based diagnostics tools, Transmission X-ray Microscopy (TXM) and X-ray Raman Spectroscopy (XRS).
- Apply TXM to study the porosity of cycled NiO electrodes and observe their phase transformations.

Technical Barriers

- Better understanding of the fundamental processes that occur in Li-ion batteries is essential for progress toward better performance. There is a need for new diagnostics techniques with high sensitivity and that cover wide time and dimension scales to probe phenomena at surfaces and interfaces, and the evolution of the phase transitions and boundaries upon electrode operation. Given the importance of kinetics and transient phenomena that occur in batteries, the development of these new techniques must run concurrent to the development of setups that enable the performance of experiments in real time.

Technical Targets

- Hire a postdoctoral researcher and start the sub-program.
- Prepare successful proposals to Stanford Synchrotron Radiation Lightsource (SSRL) to gain access to TXM and XRS beamlines.
- Obtain 3D images with chemical resolution of cycled NiO electrodes using TXM.

Accomplishments

- A postdoctoral researcher has been hired and will join LBNL October 15th 2010.
- Two proposals for beamlines 6-2a and 6-2c were successfully submitted to SSRL. Access has been gained to beamlines equipped for the TXM and XRS experiments.
- The first 3D TXM images of cycled NiO electrodes have been produced.

✧ ✧ ✧ ✧ ✧

Introduction

Advanced synchrotron-based techniques will enable us to probe processes occurring on increasingly shorter timescales and, through their enhanced sensitivity, to study increasingly more subtle changes. The high energy of the beam allows collection of data from whole battery ensembles. Here we propose to expand our technical capabilities through the use of the facilities at the Stanford Synchrotron Radiation Light source (SSRL). Two related techniques that we intend to use are X-ray absorption spectroscopy (XAS) and X-ray Raman spectroscopy (XRS).

XRS, employing hard X-rays, provides information on the bulk electronic structure of a given element, even light ones such as Li or C, at long penetration lengths without the need of ultrahigh vacuum. XRS, however is based on a different X-ray scattering phenomenon (inelastic Raman scattering), which allows access to the same information as soft XAS, but uses penetrating radiation. While improvements in XRS sensitivity are still needed, XRS is a technique that can already be employed to follow local structural changes in battery components that have not previously been accessible.

TXM is an imaging tool that provides information on the microstructure of materials. The spatial resolution is generally poorer than that for TEM, but recent advances make it possible to achieve a resolution of 30 nm, a length scale that is relevant to many battery features. TXM does not require elaborate sample preparation or exposure to high vacuum, and X-rays are less damaging to the sample than an electron beam. Both 2D and 3D images can be collected by turning the sample with respect to the beam, so that tomographic reconstructions are generated. In

addition, TXM can be coupled with XAS to obtain spatially resolved chemical speciation. We envision a series of *in situ* TXM experiments to image the dynamics of phase transformations and movement of phase boundaries. Such information is of critical value in the study of materials for Li-ion batteries as their operation is based on redox reactions that result in electronic structure changes of the phases involved.

Because these techniques do not require ultrahigh vacuum, it is possible to design a setup with liquid electrodes for *in situ* analysis of operating cells. Examples of proposed experiments include measurements of structural changes in carbonaceous materials upon cation and anion intercalation, and monitoring changes of physicochemical properties of SEI layer during formation and aging.

Approach

TXM and XRS are synchrotron-based techniques, and, therefore, are only available in User Facilities, such as SSRL. The success of this program relies on keeping active proposals in SSRL to have continued access to the corresponding beamlines. Together with the hiring of a postdoctoral researcher, this has been the focus of the first months of work.

Preliminary TXM work with cycled NiO has started. Measurements were performed at the wiggler beamline 6-2 at SSRL using an Xradia transmission X-ray microscope (TXM). The TXM is equipped with optics optimized for photon energies ranging from ~5 to 14 keV, provides a spatial resolution as high as 30 nm and a single flat field of view of 15 or 30 μm^2, depending on the chosen magnification. XANES images were collected from 8,250 to 8,600 eV, in 154 steps with varying energy intervals across the Ni K-edge, with zone plate adjustment to maintain focus and reference image collection at each energy level. The presence of the two chemical phases present (NiO and Ni) was confirmed by fitting the XANES data to spectra (collected with the same method) of pure NiO, pure Ni wire and Ni nanoparticles. Tomography was acquired at 13 distinct energy points, identified from the 2D XANES to have significantly different absorption values for NiO and Ni. The (fully automated) measurement of 3D XANES was accomplished within 18 hours. The tri-color maps containing red (NiO), and green (Ni) from the 2D chemical images obtained at each angle were reconstructed and rendered using the AVIZO Fire software package.

Results

Figure V- 178 illustrates the experimental procedure followed for XANES microscopy in a TXM beamline. A series of single images is recorded upon sweeping the photon energy across the X-ray absorption edge of the element of interest (in this case, Ni). The intensity change of each pixel as a function of energy provides XANES spectra which can be fit with known reference compounds using a least squares method. The resulting ratio of the two phases for each pixel is expressed in a red (NiO) to green (Ni) scale RGB image that represents a 2D chemical phase map. The blue pixels in these maps highlight areas where both phases coexist, and is highest for states with a 1:1 NiO:Ni ratio. The collection of 2D chemical maps at different sample-beam angles allows tomographic reconstruction with 3D chemical speciation.

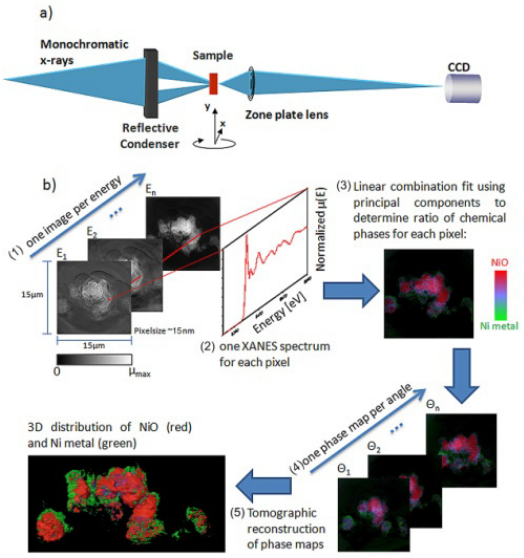

Figure V- 178: Microscope setup and principles of data processing for 3D XANES microscopy.

NiO reacts with lithium through a conversion reaction to produce Ni and Li_2O. The result is a very large capacity, above 700 mAh/g, that makes it attractive for use as negative electrode in Li-ion batteries. An example of 3D XANES tomography for a sample of NiO that was reduced halfway is shown in Figure V- 179. The measurement was performed for a large particle agglomerate and two smaller ones. A comparison of the different sized particles provides insight into the conversion of NiO to Ni during the discharge process: the smallest particle converts homogeneously, the transformation of the larger particles being concentrated around the edges. These images reveal that conversion to Ni can also happen through cracks that go through the interior of the grain. This process breaks down large NiO grains. We proved that pores between and within particles/agglomerates are large enough for the electrolyte to penetrate, and highlights the critical role of porosity in the battery electrode.

Porosity in the cycled electrodes is very complex and, due to the likely existence of pores smaller than the limit of resolution, the analysis of porosity in the hierarchical structures is challenging, Figure V- 180. Nonetheless,

qualitative information on particle size, morphology and relative porosity can be obtained by comparing tomographic reconstructions of samples.

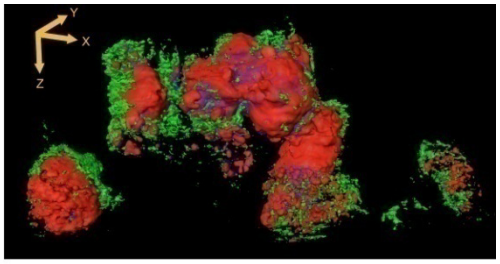

Figure V- 179: Reconstructed 3D XANES tomography data of a sample of NiO reduced halfway.

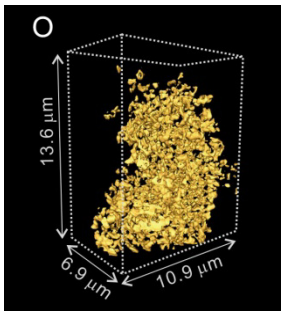

Figure V- 180: Tomography of a fully cycled NiO electrode.

Conclusions and Future Directions

XANES microscopy is a unique tool that can produce high quality images at 30 nm resolution with both chemical and morphological information. Because 2D and 3D images can be produced in a few minutes or hours, respectively, a path forward will be to extend this 3D characterization technique to other active materials and to build an *in situ* setup for evaluation of electrodes in operation using configurations relevant to the battery industry. We expect this work to accelerate in the coming months thanks to the support of the new postdoctoral researcher joining our group. This person will also start studying lithium intercalation in graphite electrodes using XRS, for which we expect to have promising results next year.

FY 2010 Publications/Presentations

1. 2010 DOE Annual Peer Review Meeting Presentation.
2. "Chemically-resolved 2D and 3D nanoimaging of hierarchical high capacity battery electrodes using transmission X-ray microscopy", F. Meirer, J. Cabana, Y. Liu, A. Mehta, J. C. Andrews, and P. Pianetta, *Submitted for publication*

V.G Integrated Lab-Industry Research Program (ANL, LBNL)

Jordi Cabana[1], John T. Vaughey[2], Jeff Chamberlain[2], Venkat Srinivasan[1]

[1]Environmental Energy Technologies Division
Lawrence Berkeley National Laboratory
1 Cyclotron Rd. MS62R0203
Berkeley, CA 94720-8168
E-mail: jcabana@lbl.gov

[2]Chemical Sciences and Engineering Division
9700 S Cass Ave
Argonne National Laboratory
Lemont, IL 60439
E-mail: vaughey@anl.gov

Collaborators:
Dennis Dees
David Schroeder
Brian Ingram
Daniel Abraham
Vince Battaglia
Gao Liu
Marca Doeff
Tom Richardson
Guoying Chen
Robert Kostecki
John Kerr

Objectives

- To overcome the well known problems with the metallic lithium electrode - stability, safety, and cycling efficiency - that continue to block its implementation into advanced lithium batteries for PHEVs and EVs.
- Characterize the morphological evolution of the lithium electrode on cycling. Study the effects of outside variables, e.g. pressure, on its cycling stability.
- Develop and characterize coating technologies that will withstand the lithium cell environment
- Develop a ceramic electrolyte system that is stable to lithium metal under cycling conditions.

Technical Barriers

This project addresses the following technical barriers from the Energy Storage section of the DOE Vehicle Technologies Program Multi-Year Research, Development and Demonstration Plan:

(A) 40 mile range for PHEVs

(B) Abuse tolerance

(C) Cell life

Technical Targets

- Synthesize, design and characterize ceramic electrolytes that may come in contact with the surface of a lithium electrode.
- Utilize characterization tools available at the National Electron Microscopy Center and Center for Nanoscale Materials to investigate the changes in morphology that occur on cycling for a lithium metal anode.
- Characterize the interfaces created in a lithium metal - ceramic electrolyte cell to determine failure mechanisms and breakdown products.

Accomplishments

- Initiated study of ceramic electrolytes with and without transition metals and their stability in an electrochemical cell utilizing lithium metal.
- Designed a standard test fixture to evaluate ceramic plate electrolytes.
- Identified and created joint institution research teams between ANL and LBNL to overcome several of the problems associated with lithium metal anodes.

✧ ✧ ✧ ✧ ✧

Introduction

Achieving the DOE 40 mile range target for PHEVs will require significant advancements in energy storage technology. The main focus of this project will be to devise new methods to understand and stabilize lithium metal anodes in a lithium battery. Previous literature work has focused on the electrolyte reactivity and electrodeposition problems and the effects of these issues on long term cycling stability. We have initiated a project to utilize recent advances in ceramic electrolyte materials, polymer science, and materials characterization to stabilize the interface of lithium metal in an electrochemical cell. With the advantages of lithium metal including significant increases in anode capacity, increased options for cathode materials, and a factor of four reduction in coating volume, new approaches to stabilizing this class of anodes would be a benefit to researchers seeking next generation energy storage systems.

Approach

To meet the DOE targets, we will investigate the morphological changes associated with lithium electrodeposition and look for strategies to prevent

deleterious contact between the metal electrode and the liquid electrolytes. Initial effort has been focused on using a ceramic membrane made from a variety of known ceramic lithium-ion conductors. Typical materials to be investigated will be divided in two categories. The first corresponds to well-known conductors containing transition metals, namely, $Li_{1+x}(Ti,Al)_2(PO_4)_3$ (LATP), $(Li,La)TiO_3$ (LLTO), and related materials. The second corresponds to compounds that do not contain transition metals; examples of the compositions to be studied are the crystalline and glassy phases in the Li_2O-P_2O_5-SiO_2-B_2O_3 phase diagram. The study will assess common failure mechanisms of these materials against lithium metal anodes, the interfacial material formed, and the conduction limitations they add to the system.

We are studying methods to establish a stable, dense, and uniform lithium/electrolyte interface exhibiting good electrochemical performance.

- Analyze the failure mechanisms of various Li-ion conducting ceramic materials in the presence of a Li-metal electrode.
- Develop a standard test fixture that incorporates a ceramic membrane to allow for reliable evaluation of various electrochemical couples and materials.
- Evaluate the effect of pressure on the formation of dendrites.
- Use some of the latest microscopic and spectroscopic characterization equipment to characterize the lithium/electrolyte interface.

Results

- To date we have been able to scale-up the synthesis of the two initially identified ceramic lithium-ion conductors, LATP and LLTO.
- We have started the synthesis of phases in the Li_2O-P_2O_5-SiO_2-B_2O_3 phase diagram. Good quality, dense $Li_{4-x}Si_{1-x}P_xO_4$ solid solutions have already been obtained.
- We have performed initial lithium metal stability studies and indentified the voltage where lithium conduction competes with titanium reduction. For both materials it is approximately 1.2 V vs Li.
- We have designed a standard test fixture for the ceramic plates to evaluate their performance under appropriate and realistic test conditions.

FY 2010 Publications/Presentations

New Program.

Appendix A: American Recovery and Reinvestment Act (ARRA) Awards

RECOVERY ACT AWARDS FOR ELECTRIC DRIVE VEHICLE BATTERY AND COMPONENT MANUFACTURING INITIATIVE			
Applicant	**DOE Award (Dollars in Millions)**	**Project Locations**	**Technology**
Cell, Battery, and Materials Manufacturing Facilities			
Johnson Controls, Inc.	$299.2	Holland, MI Lebanon, OR (Entek)	Production of nickel-cobalt-metal battery cells and packs, as well as production of battery separators (by partner Entek) for hybrid and electric vehicles.
A123 Systems, Inc.	$249.1	Romulus, MI Brownstown, MI	Manufacturing of nano-iron phosphate cathode powder and electrode coatings; fabrication of battery cells and modules; and assembly of complete battery pack systems for hybrid and electric vehicles.
KD ABG MI, LLC (Dow Kokam)	$161	Midland, MI	Production of manganese oxide cathode / graphite lithium-ion batteries for hybrid and electric vehicles.
Compact Power, Inc. (on behalf of LG Chem, Ltd.)	$151.4	St. Clair, MI Pontiac, MI Holland, MI	Production of lithium-ion polymer battery cells for the GM Volt using a manganese-based cathode material and a proprietary separator.
EnerDel, Inc.	$118.5	Indianapolis, IN	Production of lithium-ion cells and packs for hybrid and electric vehicles. Primary lithium chemistries include: manganese spinel cathode and lithium titanate anode for high power applications, as well as manganese spinel cathode and amorphous carbon for high energy applications.
General Motors Corporation	$105.9	Brownstown, MI	Production of high-volume battery packs for the GM Volt. Cells will be from LG Chem, Ltd. and other cell providers to be named.
Saft America, Inc.	$95.5	Jacksonville, FL	Production of lithium-ion cells, modules, and battery packs for industrial and agricultural vehicles and defense application markets. Primary lithium chemistries include nickel-cobalt-metal and iron phosphate.
Exide Technologies with Axion Power International	$34.3	Bristol, TN Columbus, GA	Production of advanced lead-acid batteries, using lead-carbon electrodes for micro and mild hybrid applications.
East Penn Manufacturing Co.	$32.5	Lyon Station, PA	Production of the UltraBattery (lead-acid battery with a carbon supercapacitor combination) for micro and mild hybrid applications.
Advanced Battery Supplier Manufacturing Facilities			
Celgard, LLC, a subsidiary of Polypore	$49.2	Charlotte, NC Aiken, SC	Production of polymer separator material for lithium-ion batteries.
Toda America, Inc.	$35	Goose Creek, SC	Production of nickel-cobalt-metal cathode material for lithium-ion batteries.
Chemetall Foote Corp.	$28.4	Silver Peak, NV Kings Mtn., NC	Production of battery-grade lithium carbonate and lithium hydroxide.
Honeywell International Inc.	$27.3	Buffalo, NY Metropolis, IL	Production of electrolyte salt (lithium hexafluorophosphate ($LiPF_6$)) for lithium-ion batteries.
BASF Catalysts, LLC	$24.6	Elyria, OH	Production of nickel-cobalt-metal cathode material for lithium-ion batteries.
EnerG2, Inc.	$21	Albany, OR	Production of high energy density nano-carbon for ultracapacitors.
Novolyte Technologies, Inc.	$20.6	Zachary, LA	Production of electrolytes for lithium-ion batteries.

RECOVERY ACT AWARDS FOR ELECTRIC DRIVE VEHICLE BATTERY AND COMPONENT MANUFACTURING INITIATIVE			
Applicant	**DOE Award (Dollars in Millions)**	**Project Locations**	**Technology**
FutureFuel Chemical Company	$12.6	Batesville, AR	Production of high-temperature graphitized precursor anode material for lithium-ion batteries.
Pyrotek, Inc.	$11.3	Sanborn, NY	Production of carbon powder anode material for lithium-ion batteries.
H&T Waterbury DBA Bouffard Metal Goods	$5	Waterbury, CT	Manufacturing of precision aluminum casings for cylindrical cells.
Advanced Lithium-Ion Battery Recycling Facilities			
TOXCO Incorporated	$9.5	Lancaster, OH	Hydrothermal recycling of lithium-ion batteries.

Appendix B: List of Contributors and Research Collaborators

Contributor/Collaborator (Affiliation)	Annual Progress Report Section(s)
Yasuhiro Abe (Toda America, Inc.)	II.C.2
Ali Abouimrane (ANL)	IV.B.3.5, IV.B.2.1, IV.B.3.1, IV.B.4.2
Kristin Abkemeier (New West Technologies)	III.F
Daniel Abraham (ANL)	IV.B.1.2, IV.C.1.1, V.G, IV.B.4.1, IV.C.1.2, IV.C.1.3
Mohamed Alamgir (LG Chem,MI/Compact Power, Inc.)	III.A.1.2
Jan L. Allen (ARL)	IV.B.4.3
S. Allu (ORNL)	III.E.2
Khalil Amine (ANL)	IV.B.3.5, IV.B.1.1, IV.B.2.1, IV.B.2.4, IV.B.3.1, IV.B.3.2, IV.B.4.2, IV.D.2.1, V.D.5
Michel Armand (NCSU)	V.D.6
Renata Arsenault (USABC)	III.A.1.1
Clair Ashton (INL)	III.D.3
William A. Averill (SNL)	II.E.6, III.D.4
M. Balasubramanian (ANL)	IV.B.3.3, IV.C.1.3, IV.B.3.4, V.B.9, V.F.1
Nitash P. Balsara (UCB)	V.D.1
Nina Balke (ORNL)	V.E.3
J. Bareño (ANL)	IV.C.1.2, IV.C.1.3
James A. Barnes (DOE, NSWC)	III.F
Brian Barnett (TIAX LLC)	III.C.1
John Basco (ANL)	III.D.1
Vince Battaglia (LBNL)	V.B.9, V.G, IV.B.1.3, V.E.1
Hongbin Bei (ORNL)	V.E.3
Illias Belharouak (ANL)	IV.B.2.1, IV.B.2.4, IV.B.3.2, IV.B.3.5, IV.B.3.1, II.E.1, IV.E.1.1
Jeffrey R. Belt (INL)	III.D.3
R. Benedek (ANL)	V.B.9
Taylor Bennett (INL)	III.D.3
D. Bernholdt (ORNL)	III.E.2
A. Best (CSIRO, Australia)	IV.B.4.1
Ira Bloom (ANL)	II.E.3, III.D.1, IV.C.2.2
Oleg Borodin (University of Utah)	V.D.3
Casey Butler (EnerDel)	II.B.3
Jordi Cabana (LBNL)	V.E.7, V.F.2, V.G
Jose M. Calderon-Moreno (Romanian Academy)	V.C.5
Chris Carlton (MIT)	V.B.9, IV.B.3.4
Gerbrand Ceder (MIT)	V.B.1
Jeff Chamberlain (ANL)	V.G
Zonghai Chen (ANL)	IV.B.4.2, IV.D.2.1
Guoying Chen (LBNL)	V.G, IV.D.2.3, V.B.11
Zonghai Chen, ANL	II.E.1
G. Cheng (ANL)	IV.B.4.1, IV.C.1.2
Jon Christophersen (INL)	IV.C.2.2, III.D.2
Andy Chu (A123Systems)	II.A.2
J. Croy (ANL)	V.F.1
Brian Cunningham (DOE)	III.B.13
Steven Dallek (Spectrum Technology Group)	III.A.2.2
Damien Dambournet (ANL)	IV.B.3.5, IV.B.2.1, IV.B.2.4
Claus Daniel (ORNL)	IV.C.1.5, V.E.3
Dennis Dees (ANL)	IV.C.1.2, IV.B.1.1, IV.B.1.2, IV.B.2.2, IV.C.2.1, V.G, II.E.1, IV.B.2.3, IV.C.1.1
Peter J. Denoncourt (Saft America, Inc.)	II.B.5

Contributor/Collaborator (Affiliation)	Annual Progress Report Section(s)
John B. Deppe (Deppe Associates)	All
Joe DiCarlo (BASF)	II.C.5
N. Dietz-Rago (ANL)	V.C.5
Anne C. Dillon (NREL)	V.C.3
Marca Doeff (LBNL)	V.G, V.B.3
Matthieu Dubarry (HNEI)	IV.C.1.6
Nancy Dudney (ORNL)	IV.C.1.5, V.E.3, V.E.6
Tien Q. Duong (DOE)	V
Trevor Dzwiniel (ANL)	IV.E.1.2
Kevin Eberman (3M)	III.B.4
Ron Elder (USABC)	III.A.1.3
Ron Elder (USABC)	III.A.2.1
Eric Ellerman (Johnson Controls, Inc.)	II.A.1
W. Elwasif (ORNL)	III.E.2
Scott Engstrom (Johnson Controls-Saft, Inc.)	III.A.1.1
Kee Eun (LG Chem, Michigan, Inc.)	II.B.2
Jiang Fan (American Lithium Energy Corp)	III.B.9
Peter Faguy (DOE)	IV
Peter Fedkiw (NCSU)	V.D.6, III.B.9
Robert P. Flicker (East Penn Manufacturing Co., Inc.)	II.A.4
Linda Gaines (ANL)	III.C.6
Kevin Gallagher (ANL)	IV.C.1.1
Jamie P. Gardner (3M)	III.B.3
Kevin Gellagher (ANL)	IV.B.3.4
Kevin Gering (INL)	IV.C.1.1, IV.C.2.2, IV.B.4.5, IV.C.1.6
Stephen Goguen (DOE)	III.E.1, III.E.2
Jeff Gonder (NREL)	III.C.7
John B. Goodenough (University of Texas at Austin)	V.C.4
Clare P. Grey (Stony Brook University)	V.B.1
John Groves (Chemetall Foote Corp.)	II.C.3
Ion Halalay (USABC)	III.B.2
Steve Harris (General Motors)	IV.C.1.5
Wesley Henderson (North Carolina State University)	V.D.6
Gary Henriksen (ANL)	IV.B.1.1
Chinh Ho (INL)	IV.C.2.2, III.D.3
David Howell (DOE)	All
Alex Q. Huang (North Carolina State University)	III.B.9
Adam J. Hunt (EnerDel)	III.B.10
Brian Ingram (ANL)	V.G
Michael J Sekedat (Pyrotek Incorporated)	II.C.9
Christopher J. Michelbacher (INL)	IV.C.1.6
Andrew Jansen (ANL)	IV.C.1.2, V.C.5, IV.B.1.1, IV.C.1.1, IV.B.2.2, IV.C.2.1, IV.B.1.2
Andrew Jansen, ANL	II.E.1
Thomas Jiang, NSWC	III.A.2.2
C. Johnson (ANL)	V.B.9
Christopher Johnson (NETL)	II.A.1, II.C.7, III.B.4, III.B.5, III.B.7, III.B.10, III.B.11, II.C.3, II.B.3
Christopher S. Johnson (ANL)	IV.B.3.3
T. Richard Jow (ARL)	IV.B.4.3
Chris Joyce (ANL)	V.C.5, IV.B.2.2, IV.C.2.1
John K. Basco (ANL)	IV.C.2.2
Mason K. Harrup (INL)	IV.B.4.5

Contributor/Collaborator (Affiliation)	Annual Progress Report Section(s)
David K. Jamison (INL)	IV.C.1.6
Sun-Ho Kang (ANL)	IV.B.3.3, IV.C.1.3, V.B.9, V.F.1, IV.B.1.1, IV.B.1.2, IV.B.3.4, IV.C.1.1, IV.C.2.1
Sun-Ho Kang (ANL)	II.E.1
N. Karan (ANL)	V.F.1
John Kerr (LBNL)	V.D.2, V.G
Matt Keyser (NREL)	II.E.5, III.E.3
Saad A. Khan (North Carolina State University)	III.B.9
Donghan Kim (ANL)	IV.B.3.4
D. Kim (ANL)	V.F.1
Gi-Heon Kim (NREL)	III.E.3, III.E.4
Gary Koenig (ANL)	IV.B.3.2
Robert Kostecki (LBNL)	IV.C.1.4, V.C.2, V.F.2, V.G
Gregory Krumdick (ANL)	IV.E.1.2, IV.E.1.1, II.E.2
Bob Kuhlke (Exide Technologies)	II.A.3
B. J. Kumar (Energetics, Inc.)	All
Prashant N. Kumta (University of Pittsburgh)	V.C.1
H. H. Kung (Northwestern University)	V.C.5
Edgar Lara-Curzio(ORNL)	IV.C.1.5
Hung-Sui Lee (BNL)	IV.D.1.1
Bor Yann Liaw (HNEI)	IV.C.1.6
Nathan Liu (ANL)	IV.B.1.1, IV.B.1.2
Gao Liu (LBNL)	V.C.8, V.G
Jun Liu (PNNL)	V.B.10, V.C.7
Carmen Lopez (ANL)	IV.B.2.3
Wenquan Lu (ANL)	II.E.1, IV.B.1.1, IV.B.1.2, IV.C.1.1, IV.C.2.1
B. Lucht (University of Rhode Island)	IV.B.4.1, IV.C.1.2, V.D.7
Eric Luebbe (EnerG2, Inc.)	II.C.6
A.N. Mansour (NSWC)	V.B.7
Arumugam Manthiram (University of Texas at Austin)	V.B.4
Gary McChesney (FutureFuel Chemical Company)	II.C.8
Frank McLarnon (LBNL)	IV.C.1.4
Yuriy Mikhaylik (Sion Power)	III.B.6
James F. Miller (ANL)	All
Bruce W. Mixer (NETL)	II.D.1, III.B.8, III.B.9, II.C.1, II.C.4, II.A.3
Dan Moffa (HTTM, LLC, H&T, Trans-Matic)	II.C.10
Hector Morales (Electricore, Inc., Toxco)	II.D.1
John Morrison (Montana Tech)	III.D.2
William Morrison (Qualtech Systems, Inc.)	III.D.2
Chet Motloch (ETEC)	III.D.2
P. Mukherjee (ORNL)	III.E.2
Timothy C. Murphy (INL)	II.E.4
Kyung-Wan Nam (BNL)	IV.D.1.1, V.B.8
Paul Nelson (ANL)	IV.B.2.2, IV.C.2.1
Jeremy Neubauer (NREL)	III.C.4, III.C.5
John Newman (LBNL)	V.E.5
Ralph Nine (NETL)	III.B.12, II.A.2, II.B.1
Michael O'Keefe (NREL)	III.C.4
Brian O'Leary (Honeywell International, Inc.)	II.C.4
Christopher J. Orendorff (SNL)	II.E.6, III.D.4, IV.D.1.2, IV.D.2.1, IV.D.2.2
Amy Paik (USABC)	III.B.1
S. Pannala (ORNL)	III.E.2
Andrew Payzant (ORNL)	IV.C.1.5

Contributor/Collaborator (Affiliation)	Annual Progress Report Section(s)
Richard W. Pekala (ENTEK Membranes, LLC)	III.B.2
Kristin Persson (LBNL)	V.E.8
Ahmad Pesaran (NREL)	II.E.5, III.C.4, III.C.7, III.E.1
I. Petrov (University of Illinois at Urbana-Champaign)	IV.C.1.2, IV.C.1.3
John Pham (Kokam/Dow)	II.B.1
Leslie Pinnell (A123Systems)	III.A.1.3, III.A.2.1
S. V. Pol (ANL)	IV.B.3.3
V. Pol (ANL)	V.B.9, V.C.5
Bryant Polzin (ANL)	IV.C.2.1, II.E.1
Panos Prezas (ANL)	III.D.1
John Protasiewicz (Case Western Reserve University)	V.D.4
Krzysztof Pupek (ANL)	IV.E.1.2
Yue Qi (General Motors)	IV.C.1.5
Yan Qin (ANL)	IV.B.4.2
Deyang Qu (University of Massachusetts, Boston)	III.A.2.2
Jane Rempel (TIAX LLC)	III.C.1
Yang Ren (ANL)	IV.D.2.1
Thomas Richardson (LBNL)	IV.D.2.3, V.B.2, V.G
Adrienne Riggi (NETL)	III.B.6
C. Lopez Rivera (ANL)	V.C.5
Harry W. Rollins (INL)	IV.B.4.5
E. Peter Roth (SNL)	III.D.4, IV.D.2.2
Gerry Rumierz (Celgard)	II.C.1
Terri Sacco (A123Systems)	III.A.2.1
Danilo J. Santini (ANL)	III.C.2
Ann Marie Sastry (University of Michigan)	V.E.2, V.E.3
Sergiy V. Sazhin (INL)	IV.B.4.5, IV.C.1.6
Daniel Scherson (Case Western Reserve University)	V.D.4
David Schroeder (ANL)	V.G
Yang Shao-Horn (MIT)	V.B.9, IV.B.3.4, V.B.7
Dileep Singh (ANL)	IV.B.2.2
Marshall C. Smart (JPL)	IV.B.4.4
Grant D. Smith (University of Utah)	V.D.3
Kandler Smith (NREL)	III.C.3
Patricia H. Smith (NSWC)	III.A.2.2
Venkat Srinivasan (LBNL)	V.C.9, V.E.4, V.G
Suresh Sriramulu (TIAX, LLC)	III.B.11
Fred F. Stewart (INL)	IV.B.4.5
Kristoffer Stokes (Celgard, LLC)	III.B.1
Richard Stringfellow (TIAX, LLC)	III.B.11
Y. K. Sun (Hanyang University)	IV.B.3.1, IV.B.3.2
John Tabacchi (NETL)	II.A.4, II.C.5, II.C.6, II.C.8, II.C.10, II.C.9
Kaname Takeya (ANL)	IV.E.1.1
Harshad Tataria (USABC)	III.A.1.2
Samuel Taylor (NETL)	II.B.2, II.B.4, II.B.5, II.C.2
Michael Thackeray (ANL)	IV.B.3.3, V.F.1, IV.B.3.4, V.B.9, V.C.5
Anthony M Thurston (BASF)	III.B.7
Adam Timmons (USABC)	III.B.3
L. Trahey (ANL)	V.C.5
Thanh Tran, NSWC	III.A.2.2
S. Trask (ANL)	IV.B.4.1, IV.C.1.2
Linda M. Trumm (General Motors)	II.B.4
John A. Turner (ORNL)	III.E.2

Contributor/Collaborator (Affiliation)	Annual Progress Report Section(s)
Jack Vaughey (ANL)	V.B.9, IV.B.2.2, V.C.5, IV.B.2.3, V.G, II.E.1
David P. Ventola (A123Systems)	III.B.12
Arthur von Cresce (ARL)	IV.B.4.3
Lee Walker (ANL)	III.D.1
Xiaojian Wang (BNL)	IV.D.1.1
J.G. Wen (University of Illinois at Urbana-Champaign)	IV.C.1.3
M. Stanley Whittingham (SUNY at Binghamton)	V.B.5, V.C.6
Ralph Wise (Novolyte)	II.C.7
Huiming Wu (ANL)	IV.B.3.1
Yan Wu (General Motors)	IV.C.1.5
Kang Xu (ARL)	IV.B.4.3
Marina Yakovleva (FMC Corporation)	III.B.5
Xiao-Qing Yang (BNL)	IV.B.3.1, IV.D.1.1, V.B.8
Karim Zaghib (Hydro-Quebec IREQ)	V.B.6
Aruna Zhamu (Angstron Materials)	III.B.8
Zhengcheng Zhang (ANL)	IV.B.4.2, IV.B.4.2, IV.E.1.2
Xiangwu Zhang (North Carolina State University)	III.B.9, III.B.9
Ji-Guang Zhang (PNNL)	V.B.10, V.C.7
Linda Zhong (Maxwell Technologies)	III.A.2.2

Appendix C: Acronyms

AABC	Advanced Automotive Batteries Conference
AAO	Anodized aluminum oxide
AATCC	American Association of Textile Chemists and Colorists
AB	Acetylene black
ABR	Applied Battery Research for Transportation
AC	Alternating Current
ACS	American Chemical Society
ADEME	Agence de l'Environnement et de la Maîtrise de l'Énergie (The French Environment and Energy Management Agency)
AE	Available energy
AEM	Analytical electron microscopy
AER	All electric range
AE-XRD	Acoustic emission (AE) and X-ray diffraction
AFM	Atomic force microscopy
AGM	Absorbed Glass Mat
ALD	Atomic layer deposition
AMR	Annual Merit Review
ANL	Argonne National Laboratory
APS	Advanced Photon Source
ARC	Accelerated rate calorimetry
ARL	Army Research Laboratory
ARPA-E	Advanced Research Projects Agency - Energy
ARRA	American Recovery & Reinvestment Act
ARXPS	Angle resolved X-ray photoelectron spectroscopy
ARXS	Angle resolved X-ray spectroscopy
ASCR	(DOE Office of) Advanced Scientific Computing Research
ASI	Area-specific impedance
ASME	American Society of Mechanical Engineers
ATD	Advanced Technology Development
ATR	Attenuated total reflection
AVS	American Vacuum Society
BAJ	Battery Institute of Japan
BATT	Batteries for Advanced Transportation Technologies
BBAR	boron based anion receptors
BCF	Binder and carbon free
BDB	2-(pentafluorophenyl)¬tetrafluoro-1,3,2-benzodioxaborole
BDMB	Lithium Bis(dimethylmalonate)borate
BET	Brunauer, Emmett, and Teller surface area
BEV	Battery electric vehicle
BLE	Baseline electrolyte
BM	Bending magnet beamline
BMS	Battery management system
BNL	Brookhaven National Laboratory
BOB-	bis(oxalate) borate
BOL	Beginning of life
BOM	Battery ownership model
BS	Butyl sulfone
BSF	Battery scaling factor
CAE	Computer-aided engineering
CAEBAT	Computer-aided engineering of batteries
CB	Carbon black
CD	Charge depleting
CDC	Charge-depleting cycles

CERC	Clean Energy Research Center
CERDEC	(U.S. Army) Communications-Electronics Research, Development, and Engineering Center
CGM	Concentration gradient material
CGR	Continuous stirring reactor
CIA	Central Intelligence Agency
CID	Current interrupt device
CMC	Sodium Carboxy Methyl Cellulose
CNF	Carbon nano-fibers
CNF-NGP	Carbon nano-fibers - nano-graphene platelets
CNT	Carbon nano-tubes
COGS	Cost of goods sold
COP	ConocoPhillips
CPI	Compact Power Inc.
CS	Charge-sustaining
CT	(X-ray) Computed tomography
CTQ	Critical to quality (metrics)
CV	Cyclic voltammogram
CVD	Chemical vapor deposition
CWRU	Case Western Reserve University
CY	Calendar year
DADT	Developmental and applied diagnostic testing
DC	Direct current
DCAA	Defense Contract Audit Agency
DCTA-	dicyanotriazolate-
DDB	2,5-di-tert-butyl-1,4-dimethoxybenzene
DEC	Diethyl carbonate
DFT	Density function theory
DMC	Dimethyl carbonate
DMDB	Lithium Dimethylmalonate Difluoroborate
DMF	Dimethylformamide
DOD	Depth-of-discharge
DOE	Department of Energy
DOH	Degree of hybridization
DOT	Department of Transportation
DPA	Destructive physical analysis
DSC	Differential scanning calorimetry
DST	Dynamic stress test
DVP&R	Design, validation, plan, and report
EA	Environmental assessment
EC	Ethylene carbonate
ECS	Electrochemical Society
EDS	Energy dispersive spectroscopy
EDV	Electric Drive Vehicle
EELS	Electron energy loss spectroscopy
EERE	(DOE Office of) Energy Efficiency and Renewable Energy
EES	Electrochemical energy storage
EFRC	Energy Frontier Research Center
EIA	Energy Information Administration
EIS	Electrochemical Impedance Spectroscopy
EMC	Electron Microscopy Center
EMD	Electrolytic manganese dioxide
EMS	Ethyl methyl sulfone
EOL	End of life
EPA	Environmental Protection agency
EPDM	Ethylene propylene diene Monomer (M-class)

EPRI	Electric Power Research Institute
ER	Electrical resistance
EREV	Extended range electric vehicle
ES	Electro-spinning (method)
ESM	Electrochemical strain microscopy
ESS	Energy storage system
EUCAR	European Council for Automotive Research and Development
EV	Electric vehicle
EVI	Electric Vehicle Initiative
EVM	Earned value management
EVMS	Earned value management system
EVS	Electric Vehicle Symposium
EXAFS	Extended X-ray absorption fine structure
FE	Finite element
FEC	fluoro ethylene carbonate
FEM	Finite Element Model
FESEM	Field-emission scanning electron microscope
FFCC	FutureFuel Chemical Company
FFT	Fast Fourier Transforms
FIB	Focused Ion Beam
FMEC	Fluorinated Materials & Energy Conversion
FOA	Federal opportunity announcement
FONSI	Finding of No Significant Impact
FRION	Flame-retardant ion
FRIONS	Flame-retardant ions
FS	1-Fluoro-2-(methylsulfonyl)benzene
FSI	(fluorosulfonyl)-imide
FTE	Full-time employee
FTIR	Fourier transform infrared
FUDS	Federal Urban Driving Schedule
FY	Fiscal year
GBL	Gamma butyrolactone
GC	Gas chromatography
GDE	Gas-diffusion-electrodes
GHG	Green house gases
GM	General Motors
GMS	Global Manufacturing Systems
HAADF	High Angle Annular Dark Field
HAADF-STEM	High Angle Annular Dark Field STEM (Tomography)
HCSD	Harmonic Compensated Synchronous Detection
HEMM	High energy mechanical milling
HEV	Hybrid electric vehicle
HF	Hydrofluoric acid
HPG	High power graphite
HPL	High Power Lithium
HPPC	Hybrid pulse power characterization
HQ	Hydro-Québec
HR	High resolution transmission electron microscopy
HREM	High resolution electron micrograph
HRTEM	High resolution transmission electron microscopy
HR-TEM	High resolution transmission electron microscopy
HTMI	High temperature melt integrity
HVE	High voltage electrolyte
HVM	High volume manufacturing

HWCVD	Hot wire chemical vaporization deposition
IA	Implementing Agreement - hybrid electric vehicles
IA-HEV	Implementing Agreement - hybrid electric vehicles
IAPG	Interagency Advanced Power Group
IBA	International Battery Materials Association
ICA	Incremental capacity analysis
ICL	Irreversible capacity loss
ICP	Inductively coupled plasma
ICP-OES	Inductively coupled plasma optical emission spectrometry
ID	Intensity of the carbon D-band
ID/IG	Ratio of integrated intensities of the D and G peaks
IEA	International Energy Agency
IEEE	Institute of Electrical and Electronics Engineers
IG	Intensity of the carbon G-band
IMLB	International Meeting on Lithium Batteries
INL	Idaho National Laboratory
IPA	Isopropyl alcohol
IPS	Integrated Plasma Simulation
IR	Infra-red
IR-ATR	Infra-red - attenuated total reflection
ISC	Internal short circuit
ISO	International Organization for Standardization
JCI	Johnson Controls, Incorporated
JCS	Johnson Controls - Saft
JPL	Jet Propulsion Laboratory
KB	Ketjenblack (carbon)
LATP	14 $Li_2O{\cdot}9Al_2O_3{\cdot}38TiO_2{\cdot}39P_2O_5$ (lithiated glass ceramic)
LBNL	Lawrence Berkeley National Laboratory
LCC	Linear cyclic carbonate
LCO	Lithium cobalt oxide
LCPM	Levelized cost per mile
LCR	Inductance, capacitance, and resistance
LE	Leyden Energy
LEESS	Lower-energy energy storage systems
LFCO	$Li_yFe_{1-x}Co_xO_4$
LFO	Li_5FeO_4
LFP	Li iron phosphate
LFP-G	Li iron phosphate - graphite
LGC	LG Chem
LGC/LGCMI	LG Chem/LG Chem, Michigan
LGCMI	LG Chem, Michigan
LIB	Lithium-ion battery
LL-NCM	Layered-layered nickel-cobalt-manganese
LLNL	Lawrence Livermore National Laboratory
LL-NMC/LTO	Layered-layered nickel-cobalt-manganese/lithium titanate
LLTO	$(Li,La)TiO_3$
LMO	Lithium manganese oxide
LMO-G	Lithium manganese oxide - graphite
LNCA	$LiNiCoAlO_2$
LNCM	$LiNiCoMnO_2$
LNMO	$LiNi_{0.5}Mn_{0.5}O_2$
LTFOP	Lithium tetrafluoro(oxalate) phosphate
LTFSI	Lithium trifluoromethanesulfonimide (salt)

LTO	Lithium titanate, $Li_4Ti_5O_{12}$
LTOP	Lithium tris(oxalato) phosphate
LVO	Lithium vanadium oxide (LiV_3O_8)
MAS-NMR	Magic Angle Spinning Nuclear Magnetic Resonance
MB	Methyl butyrate
MCMB	Mesocarbon micro beads
MDFB	Lithium Malonate Difluoroborate
MEF	Materials Engineering Facility
MIT	Massachusetts Institute of Technology
MP	Methyl propionate
MRS	Materials Research Society
MS	Mass spectroscopy
MSMD	Multi-scale, multi-dimensional
MT	Metric ton
MWNT	Multi-wall carbon nanotubes
MW-ST	Microwave-solvothermal
NAS	National Academy of Sciences
NASA	National Aeronautics and Space Administration
NASICON	Sodium Super Ionic Conductor
NCA	$LiNi_{0.8}Co_{0.15}Al_{0.05}O_2$
NCM	$Li_{1+w}[Ni_xCo_yMn_z]_{1-w}O_2$
NCSU	North Carolina State University
NEPA	National Energy Policy Act
NETL	National Energy Technology Laboratory
NGP	Nano-graphene platelets
NHTS	National Household Travel Survey
NMC	$LiNi_{1/3}Co_{1/3}Mn_{1/3}O_2$
NMCCNT	$LiNi_{0.4}Mn_{0.4}Co_{0.2}O_2$
NMC-G	$Li_{1.05}(Ni_{4/9}Mn_{4/9}Co_{1/9})_{0.95}O_2$/graphite
NMCSWNT	$LiNi_{0.4}Mn_{0.4}Co_{0.2}O_2$ Cathode with Single-Walled Carbon Nanotubes
NMP	N-methylpyrrolidone
NMR	Nuclear magnetic resonance
NNSA	National Nuclear Security Administration
NREL	National Renewable Energy Laboratory
NRO	National Reconnaissance Office
NSWC	Naval Surface Warfare Center
OAS	Open architecture software
OCV	Open circuit voltage
ODE	1-octadecene
OECD	Organization for Economic Cooperation and Development
OEM	Original equipment manufacturer
ONR	Office of Naval Research
ORM	Operational risk management
ORNL	Oak Ridge National Laboratory
ORR	Oxygen reduction reaction
ORTEP	Oak Ridge Thermal Ellipsoid Plot Program
OSHA	Occupational Safety and Health Administration
OVT	Office of Vehicle Technologies
PA-HEV	Power assist - hybrid electric vehicle
PAN	Polyacrylonitrile
PAN/DMF	Polyacrylonitrile/dimethylformamide
PAQS	Poly(anthraquinonyl sulfide)
PC	Propylene carbonate

PD	Path dependence
PDF	Pair distribution function
PE	Polyethylene
PEC	Polyethylene carbonate
PEO	Polyethyleneoxide
PEY	Partial electron yield
PFMEA	Process failure modes and effects analysis
PFO	Poly(9,9-dioctylfluorene)
PHEV	Plug-in hybrid electric vehicle
PNNL	Pacific Northwest National Laboratory
PPAP	Production Part Approval Process
PPD	Pulse per day
PPM	Parts per million
PPSS	Pacific Power Sources Symposium
PPV-PEO	Polyphenelyene vinylene-polyethylene oxide
PSAT	Powertrain System Analysis Toolkit
PS-PEO	Polystyrene-polyethyleneoxide
PS-PE-PS	Polystyrene-polyethylene-polystyrene
PTA	Post-test analysis
PTC	positive temperature coefficient (device)
PVD	Physical Vapor Deposition
RE	Reference electrode
RF	Radio frequency
RFP	Request for proposals
RGB	Red-green-blue
RMS	Root mean square
RPT	Reference performance test
RT	Room temperature
SAE	Society of Automotive Engineers
SAED	Selected area electrode diffraction
SBIR	Small Business Innovation Research
SBIR/STTR	Small Business Innovative Research/Small Business Technology Transfer
SBSM	Smart battery status monitor
SCFM	Standard cubic feet per minute.
SD	Sodium dodecanoate ($CH_3(CH_2)_{10}COONa$)
SEI	Solid electrolyte interphase
SEM	Scanning electron microscopy
SENB	Single Edged Notched Bend
SIC	Single ion conducting
SL	Sulfolane
SLMP	Stabilized lithium metal powder
SMG	Surface modified graphite
SNL	Sandia National Laboratories
SOA	State of the art
SOC	State of charge
SOD	State of discharge
SOH	State of health
SOPO	Statement of Project Objectives
SOW	Statement of Work
SRS	Safety Reinforcing Separator
SS	Solid solution
SSRL	Stanford Synchroton Radiation Lightsource
STP	Standard temperature and pressure
STTR	Small Business Technology Transfer Program
SUNY	State University of New York

SWIM	Simulation of RF Wave Interactions with Magnetohydrodynamics
SWNT	Single-walled nanotube
TACOM	(U. S. Army) Tank-Automotive Command
TEM	Transmission electron microscopy
TFC	tetrafluorocatechol
TFSI	bis(trifluoromethanesulfonyl)imide
TGA	Thermal gravimetric analysis
TLVT	Technology life verification test
TM	Transition metal
TMA	Thermomechanical Analysis
TMS	Tetramethylene sulfone
TRB	Transportation Research Board
TR-XRD	time-resolved X-ray diffraction
TXM	Transmission X-ray Microscopy
UL	Underwriters Laboratory
UMASS	University of Massachusetts
URI	University of Rhode Island
US, USA	United States of America
USABC	United States Advanced Battery Consortium
VASP	Vienna Ab-initio Simulation Package
VC	Vinylene carbonate
VEC	Vinyl ethylene carbonate
VG-CNF/CNT	vapor-grown carbon nanofibers/carbon nanotubes
VMT	Vehicle miles travelled
VRLA	Valve Regulated Lead-Acid
XAFS	X-ray absorption fine structure
XANES	X-ray absorption near edge structure
XAS	X-ray absorption spectroscopy
XES	X-ray emission spectroscopy
XPS	X-ray photoelectron spectroscopy
XRD	X-ray diffraction
XRS	X-ray Raman scattering

This document highlights work sponsored by agencies of the U.S. Government. Neither the U.S. Government nor any agency thereof, nor any of their employees, makes any warranty, express or implied, or assumes any legal liability or responsibility for the accuracy, completeness, or usefulness of any information, apparatus, product, or process disclosed, or represents that its use would not infringe privately owned rights. Reference herein to any specific commercial product, process, or service by trade name, trademark, manufacturer, or otherwise does not necessarily constitute or imply its endorsement, recommendation, or favoring by the U.S. Government or any agency thereof. The views and opinions of authors expressed herein do not necessarily state or reflect those of the U.S. Government or any agency thereof.

For more information
1-877-EERE-INFO (1.877.337.3463)
eere.energy.gov

DOE/EE-0382 January 2011